



MONASH University

Novel inhibitors of *Leishmania donovani* for the treatment of Visceral Leishmaniasis

Nicole Kate McNamara

Bachelor of Pharmaceutical Sciences Advanced with Honours

A thesis submitted for the degree of *Doctor of Philosophy* at

Monash University in 2021

Monash Institute of Pharmaceutical Sciences

Department of Medicinal Chemistry

The Faculty of Pharmacy and Pharmaceutical Sciences

Monash University

Copyright notice

Notice 1

© Nicole Kate McNamara (2021).

Under the Copyright Act 1968, this thesis may not be extracted, copied, or reproduced without the written consent from the author.

Notice 2

© Nicole Kate McNamara (2021).

I certify that I have made all reasonable efforts to secure copyright permissions for third-party content included in this thesis and have not knowingly added copyright content to my work without the owner's permission.

Table of Contents

Copyright notice.....	2
Table of Contents	3
Abstract.....	7
Declaration of Originality	9
Acknowledgements.....	10
Abbreviations, acronyms and chemical formulae	12
Chapter 1: Introduction.....	15
1.01 Leishmaniasis.....	15
1.02 Transmission and Life cycle of <i>Leishmania spp.</i>	15
1.03 Clinical Manifestations of leishmaniasis	17
1.04 Prevention	20
1.05 Current treatment	20
1.06 Leishmaniasis Drug Discovery and Development Pipeline.....	26
1.07 Target based drug discovery and phenotypic screening based drug discovery.....	45
1.08 High-throughput screen by GSK in relation to thesis scope ⁸⁸	46
1.09 Selected compounds for hit-to-lead SAR exploration	48
1.10 Hypothesis.....	55
1.11 Objectives	55
1.12 SAR rationale.....	56
1.13 Parameters for early hit-to-lead compounds	57
1.14 Conclusion from literature	60
1.15 Chapter 1 References	61
Chapter 2: Hit-to-lead optimization of the phenyl imidazole carboxamide scaffold (Scaffold 1).....	76
2.01 Introduction and objectives.....	76
2.02 Analogue Series 1: Primary LHS investigation	77
2.03 Analogue Series 1: Primary LHS investigation with analogues synthesized using alternate synthetic routes	90
2.03.1 Analogues derived from hydroxybenzoic acids.....	90
2.03.2 Analogues derived from piperidine carboxylic acids.....	92
2.04 Analogue Series 2: Initial RHS change investigation (brief exploration).....	93
2.05 Initial biological testing with <i>in vitro</i> free-living promastigote assay	93
2.06: Analogue Series 3: Amide and Core change studies	96
2.06.1 Core Investigation: Acyl Ureas.....	97
2.06.2 Core Investigation: Pyridine Replacement.....	99
2.06.3 Core Investigation: Isoxazole core.....	101
2.06.4 Core Investigation: Fused Imidazopyridine Core	102

2.06.5 Core Investigation: Benzimidazole Core	104
2.07: Axenic promastigote assay to intracellular amastigote assay	105
2.08 Initial biological testing with amastigote intramacrophage imaging assay performed by GRIDD	108
2.09 Series 1-2 library biological reassessment with intramacrophage amastigote assay performed by Bio21	116
2.09.1 Intramacrophage assay comparison between independent groups.....	117
2.09.2 Biological results and comparison of key analogues of Series 1-2.....	120
2.10 Combined biological results of Analogue Series 3	125
2.11 Further assessment of key analogues	128
2.11.1 Physicochemical and Metabolic analysis of initial leads and key analogues.....	128
2.11.2 Initial Cell Health studies.....	131
2.12 Summary of lead compounds of Chapter 2 and how further SAR studies were shaped, to be described in Chapter 3	134
2.13 Chapter 2 Experimental	137
2.14 Chapter 2 References	189
Chapter 3: Further SAR studies and optimization of the phenyl imidazole carboxamide scaffold (Scaffold 1)	198
3.01 Introduction and objectives	198
3.02 Analogue Series 4: Additive SAR studies influenced by initial GRIDD biological results ...	200
3.03 Parallel investigation surrounding pyridine pyrazole LHS hit 2.002.....	203
3.04 Analogue Series 5: <i>N</i> -alkyl and <i>N</i> -aryl modifications on the imidazole core	204
3.05 Analogue Series 6: Further exploration of the substituents around the RHS phenyl ring	207
3.06 Analogue Series 7: Further exploration around the imidazole core.....	210
3.07 Initial biological assessment of a small set of analogues using luminescence expressing <i>L. donovani</i> in a Luciferase Assay (UNC)	211
3.07.1 Initial set of biological results reported by UNC for a small subset of analogues	213
3.07.2 Physicochemical and Metabolic analysis of Oxazole analogue 3.131	214
3.08 Analogue Series 8: Additive SAR study combining LHS changes with oxazole core	216
3.09 Challenges with GRIDD retesting of key compounds of Analogue Series 1-2	217
3.10 Brief outline of <i>L. donovani</i> intramacrophage assay performed by IPK and summary of all intramacrophage assays used throughout Scaffold 1 analysis	223
3.11 Overcoming challenges around conflicting biological results associated with various analogues developed around Scaffold 1: Setting guidelines to interpret biological activity and develop a more reliable SAR profile	228
3.12 Complete biological re-evaluation of Analogue Series 1-2 library.....	230
3.12.1 Analogue Series 1-2 library retesting: Initial key compounds outlined in Figure 3.01 ...	231
3.12.2 Biological analysis of the remaining library of Series 1-2.....	234
3.12.3 Summary of the confirmed biological results around Analogue Series 1-2.....	240

3.13 Complete biological analysis of Analogue Series 3 (structural changes to the amide and imidazole core).....	242
3.14 Complete biological analysis of Analogue Series 4 (additive SAR studies)	246
3.15 Complete biological analysis of Analogue Series 5 (<i>N</i> -alkyl and <i>N</i> -aryl modifications on the imidazole core).....	251
3.16 Complete biological analysis of Analogue Series 6 (Further exploration of the substituents around the RHS phenyl ring)	257
3.17 Complete biological analysis of Analogue Series 7-8 (Further exploration around the imidazole core and additive SAR study combining LHS changes with oxazole core).....	264
3.18: Summary of Analogue Series 1-8	268
3.19: Analogue Series 9: continued SAR investigation around hit 2.002.....	272
3.20 Physicochemical and metabolic evaluation of several early lead compounds of Scaffold 1 ..	276
3.21 Further studies with lead compounds.....	279
3.22 Conclusion and Future work	280
3.23 Chapter 3 Experimental	284
3.24 Chapter 3 References	337
Chapter 4: Exploration of new scaffolds for parallel hit-to-lead investigations	342
4.01 New Compound Class Investigation.....	342
4.02 Scaffold 2 Exploration	343
4.03 Scaffold 2 Biological results	349
4.04 Scaffold 3 Exploration	351
4.05 Scaffold 3 Biological Results.....	354
4.06 Scaffold 4 Exploration	354
4.07 Scaffold 4 Biological Results.....	358
4.08 Scaffold 5 Exploration	360
4.09 Scaffold 5 Biological Results.....	363
4.10 Summary and Future work.....	365
4.11 Chapter 4 Experimental	369
4.12 Chapter 4 References	391
Chapter 5: Final Scaffold, <i>N</i> -(3-carbamoylphenyl)-2-(phenoxyethyl)benzamide exploration	397
5.01 Properties of hit 5.001	397
5.02 Targeting the benzamide ring	400
5.02.1 Optimization of the nitro reduction step (Step i of Scheme 5.01).....	400
5.02.2 Optimization of the amide bond formation step	404
5.02.3 Continued synthesis of analogues targeting the benzamide ring, terminal amide and chloro modifications.....	411
5.03 Biological results of analogues targeting benzamide modifications	413
5.03.1 Biological results and SAR discussion around analogues with terminal amide substitution	413

5.03.2 Biological results and SAR discussion around analogues 4-chloro substitution	415
5.03.4 Biological results and SAR discussion around analogues repositioning the chloro substituent	417
5.03.5 Biological results and SAR discussion around analogues repositioning both the terminal amide and chloro substituents	419
5.04 Targeting the ether linkage	421
5.05 Biological results of analogues modifying the ether linkage	423
5.06 Additions to the phenoxy ring.....	426
5.06.1 Synthesis for phenoxymethyl modified analogues.....	427
5.06.2 Refined synthetic pathway for phenoxymethyl modified analogues	432
5.07 Biological results of analogues modifying the phenoxy ring.....	433
5.08 Summary of final scaffold	436
5.09 Physicochemical and metabolic assessment of lead compounds	438
5.10 Further studies with lead compound	441
5.11 Future work	442
5.12 Chapter 5 Experimental	444
5.13 Chapter 5 Reference.....	480
Epilogue	488
Appendix.....	493
Chapter 1 Appendix	493
Chapter 2 Appendix	494
Chapter 3 Appendix	519
Chapter 4 Appendix	521
Chapter 5 Appendix	522

Abstract

Leishmaniasis is one of the world's largest parasitic endemics caused by the protozoan parasite *Leishmania*. It is estimated that more than 12 million people are infected worldwide and is currently listed by the World Health Organization as a neglected tropical disease. During the most severe manifestation, visceral leishmaniasis, the parasitic infection can spread to visceral organs, causing fatality if left untreated. This disease generally affects poorer communities and is associated with weak immunity and unsanitary conditions. Current treatments remain unsuitable to the field, as they are costly, involve complex therapeutic regimens, and are not efficacious against all parasite sub-species. Building resistance also remains a major concern. Consequently, new treatments better suited to the target population are urgently required.

A high-throughput screen of 1.8 million compounds against *Leishmania donovani* was undertaken by GlaxoSmithKline, which identified a large number of new hit compound classes. This thesis describes the synthesis and structure-activity relationships around five different compound classes.

Chapter 1 provides background information regarding the disease and a comprehensive literature review to outlining the current drug discovery pipeline for leishmaniasis, with a focus on visceral leishmaniasis. Project objectives and hypothesis are then outlined.

Chapter 2 describes the phenyl imidazole carboxamide scaffold (Scaffold 1) and the initial SAR studies that were conducted. A large increase in antileishmanial potency was achieved, where sub micromolar levels were initially reported. However, conflicting biological results emerged between our independent biological collaborators, creating challenges towards interpreting SAR. This was resolved during the discussions within Chapter 3, involving extensive collaborative efforts involving biological reassessments of our initial library of analogues. Chapter 3 also details the continued SAR studies and additive SAR studies around Scaffold 1, describing the vast library of analogues synthesized. Thanks to the large medicinal chemistry efforts made around this compound class, a reliable SAR profile was developed. New, desirable early lead compounds were achieved, demonstrating great improvements to antileishmanial activity and physicochemical properties, namely solubility and *in vitro* metabolic stability.

Chapter 4 entails the resynthesis and brief exploration around the remaining chosen compound classes, namely the phenyl pyrazinyl methanone hit (Scaffold 2), the phenyl thiadiazolebenzamide hit (Scaffold 3), the benzimidazole quinoline carbohydrazide hit (Scaffold 4) and the *N*-(3-carbamoylphenyl)-2-(phoxymethyl)benzamide hit (Scaffold 5). Surprisingly, the hits and surrounding analogues pertaining to Scaffolds 2 and 3 were confirmed to exhibit poor antileishmanial activity, suggesting the original hits to be false positives. However, the hits of Scaffolds 4 and 5 exhibited strong inhibition of *L. donovani*. Described in Chapter 5, further SAR studies around Scaffold 5 were continued due to their

highly optimizable structure. Many analogues were synthesized probing various structural attributes around the chemical space of Scaffold 5, forming another reliable SAR profile. New lead compounds with strong antileishmanial activity were also successfully identified.

Chapters 3-5 also concludes the remarks around their relevant compound classes and provides suggestions for future work. A summation of our various achievements detailed throughout this thesis are also listed within the epilogue. The reliable SAR profiles achieved within this project, along with the new early lead *L. donovani* inhibitors will help guide future SAR studies around these promising compound classes. The synthesis and results of this work has been detailed herein.

Declaration of Originality

This thesis is an original work of my research and contains no material which has been accepted for the award of any other degree or diploma at any university or equivalent institution and that, to the best of my knowledge and belief, this thesis contains no material previously published or written by another person, except where due reference is made in the text of the thesis.

Nicole McNamara

April 2021

Acknowledgements

Firstly, I would like to thank my principal supervisor, Professor Jonathan Baell for his continued support in guiding my education and growth as a Medicinal Chemist. Thank you for your patience, encouragement. You have taught me invaluable skills which I will be able to use throughout the next stage of my career. I have truly enjoyed my time here in the Baell lab.

This research was supported by an Australian Government Research Training Program (RTP) Scholarship and the Australia-India Strategic Research Fund (AISRF). Our “Eliminating Visceral Leishmaniasis” initiative had become a very large collaborative effort. I would like to thank the members of the “Leish team”, firstly from the Baell lab; Dr Swapna Varghese and Rebecca Zheng, and from the Indian Institute of Chemical Biology; Dr Dipyaman Ganguly, Dr Arindam Talukdar and the IICB team. Many thanks to each of you for your input in this project over the last few years. Many thanks are also extended to Dr Silvia Teguh, who spent a fair amount of time taking care of compound logistics and helped co-ordinate the large collaborative efforts within the “Leish Team”. It has truly been a pleasure working with you all.

Next and very importantly, I would like to thank my co-supervisor and “Leish team” collaborator Professor Malcolm McConville as well as Dr Eleanor Saunders of the Bio21 Institute of Molecular Science and Biotechnology. Thank you for all your hard work and patience, testing each of the seemingly endless number of compounds we sent your way. Thank you for also letting me join in on the fun and welcoming me into your lab. I have learnt so much from the both of you, and thoroughly enjoyed my time learning about the biological side of things.

To our biological collaborators at the University of North Carolina, who also performed biological assays against *L. donovani*; Professor Kristy Ainslie, Dr Devika Varma, Dr Monica Johnson and Dr M. Shamim Hasan Zahid, thank you for all your hard work. Special thanks to Devika for all the one-on-one calls to address all my queries, despite the difficulties with differing time zones, you were always so kind and helpful.

To our biological collaborators at the Institut Pasteur Korea, who also performed biological assays against *L. donovani*, as well as mitotoxicity studies and *in vivo* proof of concept studies; David Shum, Dr Joo Hwan No and their teams. We were consistently impressed by your professionalism and collegiality. Collaborative efforts felt so seamless with you and your team, to whom we are truly grateful.

I’d also like to thank Professor Vicky Avery, Dr Bilal Zulfiqar and their team for performing some of the biological assays against *L. donovani* during the early stages of this project.

To Dr Jason Dang, thank you for everything you have done for me throughout my PhD. Thank you for your guidance on spectroscopy and patience towards the endless number of HRMS samples I've submitted. I will certainly miss having a laugh with you in the LCMS room.

To my past supervisor Dr Jitendra Harjani, you have provided me with valuable knowledge and insights. Thanks to your guidance, you have helped me grow significantly and improve as a chemist. I have always been able to count on you, regardless of where you are in the world. I would also like to extend my gratitude to the past and present chemistry post docs of the Baell lab who I have yet to mention; Dr Nghi Ngyugen, Dr. Daniel Priebbenow, Dr Aaron DeBono, Dr Girdhar Deora, Dr Prashant Mujumdar, Dr Mnaza Noreen, Dr Ramesh Mudududdla, Dr Mitch Mathiew, Dr Yi Sing Gee, Dr Jiexiang Yin, Dr Yuji Nakano, and "fresh postdocs" Dr Andrew Tang, Dr Lisa Barbaro, Dr Noel Pitcher, Dr Julia Beveridge, Dr Alfred Wong, Dr Cathy Xie as well as current students during my time who I have yet to mention; Yayao Zhou, Heba Abd-Ellah Ali and Eric Tran. It has been truly a wonderful and memorable experience working with you all. To Heba, I will also miss being your fumehood neighbour and working alongside you every day.

To my close friends- the office ladies and our usual visitors; Dr Amanpreet Kaur, Sally Sun, Dr Thuy Le and Dr Jephtah Odiba, as well as honorary Baell lab member and my dearest friend; Corey "Ghost of Parkville" Ma, thank you all for keeping me entertained and sane throughout the past few years and listening to all of my woes. I cannot imagine getting through this without you all and will sincerely miss seeing you all every day in the tiny office.

To my dad, thank you for your love, encouragement, and support over the last eight years of university life. I would not have gotten this far if not for your financial and emotional support and I am so grateful for everything you have done for me. I would also like to extend this sentiment to my mum, whose dream is this PhD, and my brother Ryan, I thank you for your continued love and support. Even though not all you know what it is that I do every day, your encouragement has made this thesis possible. I would also like to thank my second parents; Ammi and Thathi for your love, warmth, support, and encouragement toward my studies.

Finally, to my sweet partner Shehan, thank you for being there with me at every step of this journey. Your constant love, understanding, extreme patience and strong emotional support has enabled me to reach this far. You have always showed enormous faith in me and encouraged me to believe in my abilities to reach my potential. Thank you for everything you have done for me, I am forever grateful.

Abbreviations, acronyms and chemical formulae

Å	Ångström
ACN	Acetonitrile
ADMET	Absorption, distribution, metabolism, excretion, and toxicity
AmB	Amphotericin B
aq.	Aqueous
ATP	Adenosine triphosphate
BBB	Blood brain barrier
b.i.d	Twice a day
Bio21	The Bio21 Institute of Molecular Science and Biotechnology
BnBr	Benzyl bromide
Bnz	Benzyl
br s	Broad singlet
Bu	Butyl
CanL	Canine leishmaniasis
CC ₅₀	Half maximal cytotoxic concentration
CDC	Centers for Disease Control and Prevention
CDCO	Centre for Drug Candidate Optimisation
CDCl ₃	Deuterated chloroform
CDM	Chemically defined media
CL	Cutaneous leishmaniasis
Cl _{int}	Intrinsic clearance
CnBr	Cyanogen bromide
CO ₂	Carbon dioxide
(COCl) ₂	Oxalyl chloride
cPen	Cyclopentane
d	Doublet
dd	Doublet of doublets
Da	Dalton
DCE	Dichloroethane
DCL	Diffuse cutaneous leishmaniasis
DCM	Dichloromethane
DIPEA	N,N-Diisopropylethylamine
DMAP	4-Dimethylaminopyridine
DMF	Dimethylformamide
DMSO	Dimethyl sulfoxide
DNDi	Drugs for Neglected Diseases Initiative
Dt	Doublet of triplets
DsRed2	Discosoma sp. red fluorescent protein variant
EDCI	1-Ethyl-3-(3-dimethylaminopropyl)carbodiimide
E _H	Hepatic extraction
equiv.	Equivalents
Et	Ethyl
Et ₃ N	Triethylamine
EtOH	Ethanol
Et ₃ SiH	Triethylsilane

FBS	Fetal bovine serum
FCS	Fetal calf serum
Fe	Iron
FeCl ₃ .6H ₂ O	Iron _(III) Chloride Hexahydrate
FLINT	Fluorescent intensity
FRB	Free rotatable bond
GRIDD	Griffith Institute for Drug Discovery
GSK	GlaxoSmithKline
h	Hours
H ₂	Hydrogen
H ₂ O	Water
H ₂ SO ₄	Sulfuric acid
HAT	Human African trypanosomiasis
HBA	Hydrogen bond acceptor
HBD	Hydrogen bond donor
HBTU	<i>O</i> -(Benzotriazol-1-yl)- <i>N,N,N',N'</i> -tetramethyluronium hexafluorophosphate
HCl	Hydrochloric acid
HCS	High content screening
HepG2	Hepatoma G2, human liver cancer cell line
HOAt	1-Hydroxy-7-azabenzotriazole
HOBt	Hydroxybenzotriazole
HPLC	High-performance liquid chromatography
HTS	High-throughput screening
IC ₅₀	Half maximal inhibitory concentration
IFI	Inhibitory frequency index
intramacrophage	Intracellular assay using macrophage host cells
IPK	Institut Pasteur Korea
iPr	Isopropyl
K ₂ CO ₃	Potassium carbonate
KI	Potassium iodide
<i>L. donovani</i>	<i>Leishmania donovani</i>
<i>L. infantum</i>	<i>Leishmania infantum</i>
<i>L. mexicana</i>	<i>Leishmania mexicana</i>
LCMS	Liquid chromatography–mass spectrometry
LHS	Left-hand side
LiPE	Lipophilic efficiency
LUC	Firefly luciferase gene
m	Multiplet
M	Molar
m/z	Mass-to-charge ratio
MAC	Intramacrophage assay
MCL	Mucocutaneous leishmaniasis
Me	Methyl
MeI	Methyl iodide
MeNH ₂	Methylamine
MeOH	Methanol
MIL	Miltefosine

Min	Minutes
MOI	Multiplicity of infection
MTT	3-(4,5-dimethylthiazol-2-yl)-2,5-diphenyltetrazolium bromide
MW	Molecular weight
NaBH ₄	Sodium borohydride
Na ₂ CO ₃	Sodium carbonate
NaHSO ₄	Sodium bisulfate
NaOH	Sodium hydroxide
NCE	New chemical entity
NH ₄ Cl	Ammonium chloride
NH ₄ OH	Ammonium hydroxide
NMM	N-Methylmorpholine
NMR	Nuclear Magnetic resonance
NTD	Neglected tropical disease
NW	New world
OW	Old world
Pd-C	Palladium on carbon
Pd(PPh ₃) ₄	Tetrakis(triphenylphosphine)palladium(0)
Ph	Phenyl
PKDL	Post kala-azar dermal leishmaniasis
PMA	Phorbol 12-myristate-13-acetate
PO	Oral
POCl ₃	Phosphoryl chloride
Pr	Propyl
PSA	Polar surface area
Pt-C	Platinum on carbon
PyBOP	Benzotriazol-1-yloxy)tripyrrolidinophosphonium hexafluorophosphate
RHS	Right-hand side
rt	Room temperature
s	singlet
SAR	Structure activity relationship
SDM	Semi-defined media
SI	Selectivity index
s.i.d	Once a day
SSG	Sodium stibogluconate
t	triplet
T _{1/2}	Half-life
T. brucei	Trypanosoma brucei
t-BuLi	Tert-butyllithium
T. cruzi	Trypanosoma cruzi
THF	Tetrahydrofuran
THP-1	Human monocytic cell line derived from an acute monocytic leukemia patient
TLC	Thin layer chromatography
TPP	Target product profile
UNC	University of North Carolina
VL	Visceral leishmaniasis
WHO	World health organization

Chapter 1: Introduction

1.01 Leishmaniasis

Leishmaniasis is a vector-borne disease caused by the protozoan parasite *Leishmania*. The disease was named after Doctor William Leishman for his identification of one of the earlier strains of *Leishmania* published in 1903, which would allow for the independent discovery by both Leishman and Captain Charles Donovan of the species complex *Leishmania donovani*, the causative agent of *kala-azar*, an early term to describe what is now known as visceral leishmaniasis, the most serious of the three main forms of leishmaniasis.^{1, 2}

Despite its official discovery over a century ago, leishmaniasis remains one of the world's largest parasitic endemics and most costly neglected tropical diseases (NTD) affecting 98 countries and territories across 5 continents. The majority of those affected reside in poorer rural and suburban areas of Africa, Asia and Latin America and the Mediterranean region.^{3, 4} It is estimated that more than 12 million people are infected worldwide, representing a threat for 350 million people living at risk in endemic areas. It is estimated at least 700,000 to 1.2 million new cases occur annually contributing to 20,000-40,000 deaths per annum.³⁻⁶ The disease affects some of the poorest people on earth and can also be associated with malnutrition, a weak immune system, poor housing and poor sanitary conditions. Leishmaniasis is also linked to environmental changes such as deforestation, urbanization and irrigation schemes.⁶

The kinetoplastid causative agent leishmaniasis belongs to the Trypanosomatidae family, which also hosts the parasites *Trypanosoma brucei* and *Trypanosoma cruzi*, responsible for human African trypanosomiasis (HAT) and Chagas disease respectively. *Leishmania* is most commonly transmitted through female phlebotomine sandfly vectors.⁷

1.02 Transmission and Life cycle of *Leishmania* spp.

Leishmania parasites are heteroxenous, whose life cycle involves a vertebrate and an invertebrate, summarized in **Figure 1.01**. Transmission of the *Leishmania* parasite to humans and other arboreal and terrestrial mammals occurs mostly through the blood sucking flies of the *Psychodidae* family, subfamily *Phlebotominae*.⁸ Vectoral transmission of the parasite begins when the infected female insect takes a blood meal and regurgitates infective promastigotes from their proboscis into the new host. Once they reach the puncture wound, promastigotes invade macrophages and other types of mononuclear phagocytic cells through phagocytosis. In these cells promastigotes transform into amastigotes, the intracellular form which proliferate using longitudinal binary fission in the phagolysosome of the macrophage.⁹ This process will ultimately rupture the host cell and free the daughter cell protozoans to enter the bloodstream and invade other macrophages. In cases of visceral leishmaniasis this infection

can spread to the host's mononuclear phagocyte system, progressing to visceral organs, particularly the spleen and liver. The free amastigotes can infect another sandfly vector after it is ingested during a blood meal. These ingested amastigotes transform back into promastigotes, develop in the gut and migrate to the proboscis.^{9, 10} Though less common, transmission can also occur without the vector. This is accomplished through blood transfusions from infected donors and contaminated needles (needle sharing).¹¹⁻¹³ Congenital transmission and infection from laboratory accidents has also been reported though these cases are also rare.^{14, 15}

Animal reservoirs are important for the life cycle maintenance of *Leishmania* species. There are two main reservoir sources of human leishmaniasis, zoonotic and anthroponotic, where the reservoir hosts are wild/domestic animals and humans respectively.¹¹ Canines are the main domestic reservoir of the parasite in endemic areas, particularly in the Mediterranean where seroprevalence of canine Leishmaniasis is greater than 30 %.^{16, 17} *Leishmania infantum*, another causative species of Visceral leishmaniasis is the main agent responsible for Old World (Eastern Hemisphere) and New World (Western Hemisphere) Canine leishmaniasis (CanL). A high proportion of the infected dogs are asymptomatic, which allows for the spread within the canine population to remain unnoticed, further contributing to reservoir maintenance.¹⁷

The epidemiology of leishmaniasis is dictated by a number of factors, including the parasite and sandfly species, local environment and host reservoir and the nutrition and immunodeficiency of the patient.⁶

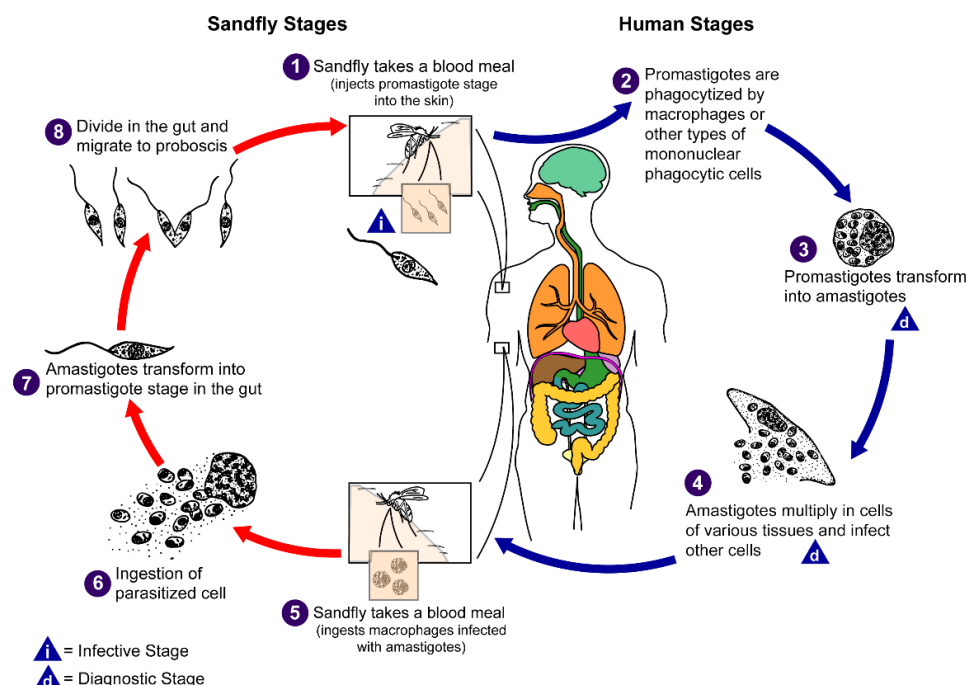


Figure 1.01: Visual summary of *Leishmania* spp. transmission and life cycle reproduced from the Centers for Disease Control and Prevention (CDC). Content provided by CDC/Alexander J da Silva and Melanie Moser.⁹

1.03 Clinical Manifestations of leishmaniasis

Over 20 *Leishmania* species are known to be transmitted to humans via sandfly vectors, broadly known as *Leishmania spp.* There are three main forms of leishmaniasis in humans caused by these various species, namely cutaneous (the most common), mucocutaneous and visceral, also known as kala-azar, black fever and Dum Dum fever and is the most serious form of the disease. For all three forms, the infection can range from asymptomatic to severe.¹⁸

- **Cutaneous leishmaniasis (CL)** is the most common manifestation of the disease which causes skin lesions on exposed parts of the body leaving lifelong unsightly scars. Infected macrophages are found primarily at the site of the infection and around the lesions. These lesions can heal by themselves within 12 months, but secondary infections are possible. Approximately 95% of cases occur in the central Asia region, the Americas, the Mediterranean basin and the Middle East. An estimated 600,000 to 1 million new cases occur annually. The main etiological agents affecting the Old World listed by the CDC and World Health Organization (WHO) include the *L. tropica* species complex (*L. tropica major*, *L. tropica minor*) as well as *L. aethiopica*, *L. infantum* and *L. donovani*. The species *L. infantum* and *L. donovani* are also the causative agents of visceral leishmaniasis. The main species affecting the New World includes *L. infantum* (also known as *L. chagasi*), the *L. mexicana* species complex (*L. mexicana*, *L. amazonensis*, *L. venezuelensis*) and the *Viannia* subgenus (*L.[V.]braziliensis*, *L.[V.] guyanensis*, *L.[V.] panamensis*, and *L. [V.] peruviana*).^{6, 8, 11, 18-20} A non-exhaustive list summarizing the main etiological agents affecting humans in all manifestations is depicted in **Table 1.01**.

- **Diffuse cutaneous leishmaniasis** is characterised by disseminated cutaneous macules, papules, plaques or nodules or skin diffuse infiltration. This causes unusual growths on the limbs and face resembling lepromatous leprosy. Generally, no ulceration occurs. Unlike other forms of CL, this manifestation does not heal spontaneous and relapses after treatment are common. This occurs in both the Old and New World.²⁰

Treatments for cutaneous leishmaniasis can depend on the species and the geographical area in which infection was acquired. Old World CL is not life threatening and can be treated locally with Paromomycin (compound **1.05**, section **1.05 Current Treatment**) ointments to accelerate cure and reduce scarring. Local therapy is favourable due to ease of application and limited toxicity. Other criteria favouring local treatment can include small single lesions, lack of risk of mucocutaneous development and *L. mexicana* lesions. Other options include thermotherapy, intralesional pentavalent antimonials (compounds **1.01-1.02**) and cryotherapy with liquid nitrogen. These methods are more costly, and application requires a skilled health-care

professional. Cryotherapy particularly is unsuited to the field as liquid nitrogen is not readily available and requires heavy equipment. Systemic therapies (see section **1.05 Current Treatment**) are reserved for more complex cases. New World CL requires systemic therapies, in order to speed up the healing process and to prevent dissemination to oral-nasal mucosa, causing mucocutaneous leishmaniasis.^{18, 20}

- **Mucocutaneous leishmaniasis (MCL)** occurs mainly in South America and usually starts to manifest within several years of the original cutaneous lesions if they have been treated suboptimally or not at all. This results in the dissemination of parasites from the skin and site of infection to the naso-oropharyngeal mucosa. Unusual nasal symptoms such as bleeding or stuffiness occur initially. If the disease does progress, partial or total destruction of mucosal membranes of the mouth, throat and nose can occur. The disfiguring appearance of the disease can often lead to social stigma and rejection by the community. Mucocutaneous leishmaniasis is unlikely to heal spontaneously and secondary bacterial infections are common with intercurrent pneumonia being a common cause of death. This disease manifestation is caused by the *Viannia* subgenus, particularly *L. [V.] braziliensis*. It also can be caused by *L. amazonensis*.^{8, 11, 18, 19} Mucosal lesions are very rare in the Old World region and do not correctly come under the term “mucocutaneous leishmaniasis”. WHO reports that patients in the Indian subcontinent and Sudan with visceral or PKDL leishmaniasis or a coinfection with HIV may develop lesions in the mouth, nose or on the genital mucosa. Buccal mucosa or larynx lesions caused by *L. infantum*, *L. major* and *L. tropica* may be present in elderly or minorly immunosuppressed patients.²⁰
- **Visceral leishmaniasis (VL)** is highly endemic in the Indian subcontinent, Brazil and in East Africa with an estimated 50,000 to 90,000 new cases of VL annually occurring worldwide. It is ranked second in mortality and fourth in morbidity amongst the neglected diseases.^{6, 21} VL is mainly caused by the species *L. donovani* and *L. infantum* and affects internal organs, particularly the spleen, liver and bone marrow. It is distinguished by weight loss, irregular bouts of fever, and lack of appetite which can last for weeks to months. It can also lead to an enlarged spleen and liver, pancytopenia and a high protein level and low albumin level. As the disease progresses, the skin becomes very dry and dark, hence the name kala azar, meaning “black fever”. If left untreated VL is typically fatal within 2 years, either directly from the disease or indirectly from complications, such as secondary bacterial infection or haemorrhage. Asymptomatic infection can also manifest years to decades after exposure in immunocompromised patients for other medical reasons (HIV/AIDS).^{8, 18, 20} Leishmania-HIV coinfecting patients have a high chance of developing the fully manifested disease, high relapse

and mortality rates.²⁰ Treatments for VL are discussed in depth below (section **1.05 Current Treatment**). The focus of this thesis will be towards this manifestation.

- **VL/HIV-1 co-infection** has been reported from 35 endemic countries and serves as a major challenge for control of VL. In endemic regions of East Africa, up to 40% of VL patients are co-infected with HIV.^{22, 23} The two diseases are reported as mutually reinforcing as HIV- infected patients are very susceptible to VL, whilst VL accelerates the virus progression into AIDS.^{20, 23} Current treatment options are not ideal and the risk of treatment failure for VL is high, and results in low cure rates, increased drug toxicity and high mortality rates.^{20, 22, 23}
- **Post-kala-azar dermal leishmaniasis (PKDL)** is an intermediate disease state before complete recovery of VL. It is most common in East Africa and the Indian subcontinent and may occur 6 to 12 months after treating the initial kala-azar. It is characterized by a macular, papular or nodular skin rash around persisting parasites. Systemic parasites are absent, though reinfection after VL may be considered. These patients are thought to be reservoirs for further transmission.^{6, 20,}

24

Table 1.01 Summary of the main etiological agents responsible for leishmaniasis in humans^{8, 11, 20}

<i>Leishmania spp.</i>	New/Old World classification	Manifestation	Distribution
<i>L. aethiopica</i>	OW	CL, DCL	East Africa
<i>L. amazonensis</i>	NW	CL, DCL, MCL	South America
<i>L. donovani</i>	OW	CL, VL, PKDL	Central Africa, South Asia, Middle East, Indian subcontinent, China
<i>L. infantum</i>	OW, NW	VL, CL	Africa, Mediterranean, Southeast Europe, Middle East, Central Asia, Central and South America
<i>L. major</i>	OW	CL	Central and North Africa, Middle East, Central Asia
<i>L. mexicana</i>	NW	CL, DCL	North America, South America
<i>L. tropica</i>	OW	CL, VL	Central and North Africa, Middle East, Central Asia, Indian subcontinent
<i>L. venezuelensis</i>	NW	CL, MCL	South America
<i>Viannia braziliensis</i>	NW	CL, MCL	South America
<i>Viannia guyanensis</i>	NW	CL, MCL	South America
<i>Viannia panamensis</i>	NW	CL, MCL	Central and South America
<i>Viannia peruviana</i>	NW	CL, MCL	South America

CL= cutaneous leishmaniasis; DCL= diffuse cutaneous leishmaniasis; MCL= mucocutaneous leishmaniasis; VL= visceral leishmaniasis; PKDL= post-kala-azar dermal leishmaniasis; NW= New world; OW= Old World.

1.04 Prevention

There are no vaccines or medications to prevent any form of leishmaniasis in humans and therefore the primary method of prevention is vector control. The large reservoir of *Leishmania spp.* in both wild and domestic animals in endemic countries means the parasite will be difficult to completely eradicate. Therefore, elimination of transmission and improved health care access for those infected are the best methods of control. Recommended approaches to prevention and control include the spraying of houses with insecticides, improvement of house structure, the use of bed-nets, safe hygiene practices.^{6, 18} Prophylactic measures are also in place to control infection within domestic reservoirs. Current preventative measures used for the control of Canine leishmaniasis (CanL) includes topical insecticides effective against sandflies. These contain synthetic pyrethroids, in the form of “spot-on” treatments and/or impregnated collars. Vaccinations for CanL are also commercially available, though their efficacy is only reported at 68-71%. These vaccines are not recommended for human use.²⁵

Health education in endemic communities is required to increase awareness and understanding of the disease etiology and transmission, vectors and control measures. This has an essential role to play in environmental management, prevention and disease elimination.²⁶ Blood screening and leukoreduction are also a recommended precaution in order to avoid infection through transfusion or to provide early diagnosis of newborns of infected mothers.^{27, 28}

1.05 Current treatment

Early and effective treatment in one of the keys of the leishmaniasis strategy. There are several chemotherapeutic options available for leishmaniasis infection are depicted in **Figure 1.02** and summarized in **Table 1.02**. Each of these compounds are included in the 21st WHO Model List of Essential Medicine for leishmaniasis treatments.²⁹

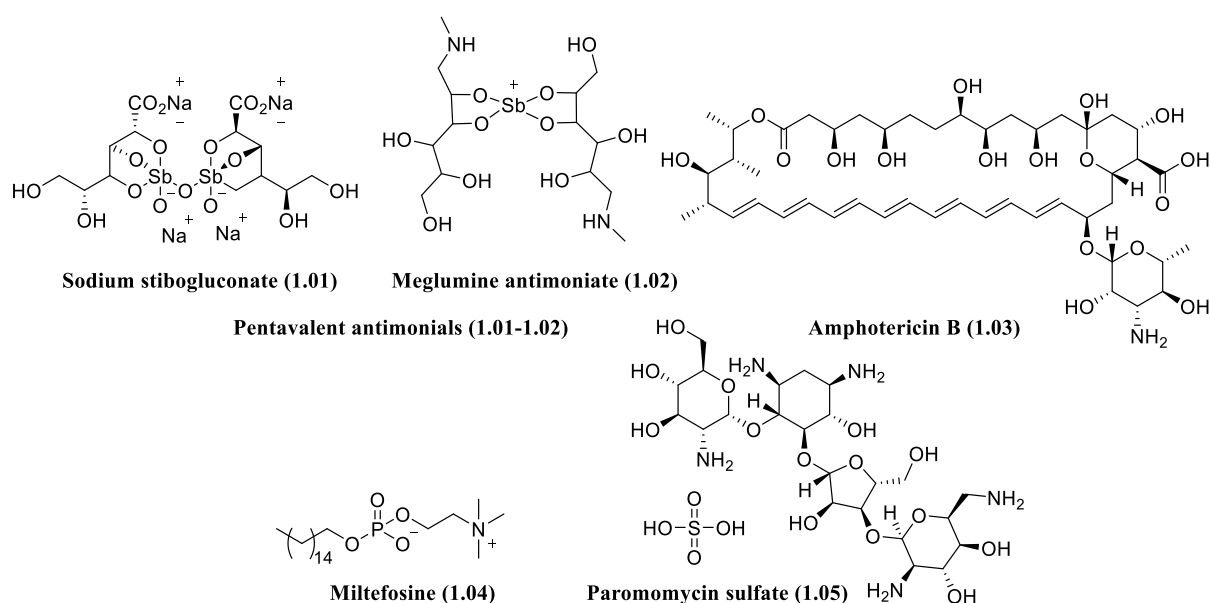


Figure 1.02: Main current therapeutics options for visceral leishmaniasis

Table 1.02: Summary of the main current therapeutic options for visceral leishmaniasis^{20, 30-32}

Drug	Administration, dosing regimen and efficacy*	Resistance	Toxicity	Price**
Pentavalent antimonials (1.01-1.02)	IV, IM, IL 30 days, 20 mg/kg/day; 35–95% (depending on area, resistance in India)	Common (>60% in Bihar, India)	Cardiotoxicity, pancreatitis, nephrotoxicity, hepatotoxicity, painful injection	\$50–70
Amphotericin B (1.03)	IV 30 days, 0.75-1 mg/kg (15 mg/kg total dose); >90%	Cases reported, though uncommon. Reports in non-endemic areas of resistance. ³³⁻³⁶	Severe nephrotoxicity, hypokalaemia, infusion related reactions High fever	~\$100
Liposomal amphotericin B (1.03)	IV 5–20 mg/kg total dose, 4–10 doses over 10–20 days; >95% India, variable response in Africa		Rigors and chills during infusion, Nephrotoxicity,	~\$280
Miltefosine (1.04)	PO 28 days, 1.5-2.5 mg/day; >90% (India), 60-93% (Africa), >42% (Brazil)	Resistance building (field strains reported, particularly in the Indian subcontinent) ³⁷⁻³⁹ Natural resistance reported in <i>L.infantum</i> (South America) ⁴⁰	Gastrointestinal, nephrotoxicity, hepatotoxicity, teratogenicity	~\$70
Paromomycin sulphate (1.05)	IM (VL) or topical (CL) 21 days, 15 mg/kg/day or 17 days, 20 mg/kg/day 93-95% (India) 46–85% (Africa, depending on dose)	Laboratory strains ³⁹	Severe nephrotoxicity, ototoxicity, hepatotoxicity, painful injections	~\$10

IV = intravenous administration; IM = intramuscular administration; IL = intralymphatic administration; PO = oral administration.

*Definitive cure at 6 months, ** per course, USD

Pentavalent antimonials (1.01-1.02) have been used for many decades as the first line drug of choice for cutaneous (New World), mucocutaneous, visceral leishmaniasis and VL-HIV co-infection as well as severe cases of post kala-azar dermal leishmaniasis.^{20, 23} Their suggested mechanism of action involves pentavalent antimony, Sb(V) entering the host cells, crossing the phagolysosomal membrane and is converted into trivalent antimony, Sb(III) which acts against amastigotes. They induce an efflux of intracellular thiols, compromising the cell thiol redox potential which inhibits trypanothione reductase (TR), an essential enzyme exclusive to parasites and crucial for their survival.^{30, 41} Pentavalent antimonials require injectable administration and can require patients to be hospitalized and monitored

due to the high cardio-, nephro- and hepatotoxicity associated with the treatment as well as pain at the injection site.^{28, 30} Drug resistance is a major concern, especially in the state of Bihar, India and Nepal. The World Health organization has reported unresponsiveness to pentavalent antimonials as high as 60% in these regions. Pentavalent antimonials are no longer recommended as a main monotherapy in Bihar due to the high percentage of treatment failure.^{20, 42-44}

Amphotericin B deoxycholate (AmB, 1.03) is a systemic antifungal repurposed as a potent antileishmanial drug. It is suggested that the drug complexes with membrane sterols such as ergosterol, which open pores and results in a loss of the permeability barrier to small metabolites, altering ion balance, leading to cell death.^{30, 45} Due to building resistance against antimonials, AmB is used as an alternative for MCL, VL, VL-HIV co-infection and PKDL. However, it is highly toxic and this treatment requires repeated IV administration to be delivered slowly and carefully.^{23, 30}

Lipid formulations of AmB have been developed in order to improve its pharmacokinetic properties and bioavailability. The liposomal version has an increased level of efficacy, reduced toxicity and better half-life. However, its poor stability at high temperatures, IV administration route and high cost, even for short courses make it less accessible for the poorer rural communities who are most impacted by this disease.^{30, 46} Though uncommon, reports of resistance to AmB have occurred in non-endemic areas. Resistance is thought to be species dependent and is reported to emerge uncommonly and slowly in isolates from patients treated with AmB. In such cases, increased dosage or combination therapy has been employed.^{33, 34, 36}

Miltefosine (MIL, 1.04) was the first effective oral drug for all forms of leishmaniasis. The exact mechanism of action is not well understood, though it has been reported to decrease oxygen consumption rate and ATP levels of *Leishmania* by inhibiting mitochondrial cytochrome c oxidase. This impairs mitochondrial function, lipid metabolism and ultimately causes parasite cell apoptosis.^{38, 39, 47} It was also shown to act at the host cell level stimulating the production of inducible nitric oxide synthetase 2, catalyzing nitric oxide generation which kills the parasite within the macrophage.^{30, 48} Recently Pinto-Martinez *et al.* reported Miltefosine to alter calcium levels disrupting parasite Ca^{+2} homeostasis and regulation. The drug is suggested to act on sphingosine-activated plasma membrane Ca^{+2} channels and directly affect acidocalcisomes, which in combination cause a large and abrupt increase in intracellular Ca^{+2} concentration. Both mechanisms are parasite specific and impair calcium function causing cell death.⁴⁷ In relation to lipid metabolism alteration, MIL has been reported to interfere with phosphatidylcholine and phosphatidylethanolamine synthesis, phospholipids used as components for the plasma membrane of the parasite. Transport of choline precursors are inhibited by MIL, causing the accumulation of intracellular choline and therefore affecting phospholipid synthesis.³⁸ MIL has reported teratogenicity issues, making it less than ideal.³⁰ Gastrointestinal side effects including vomiting and/or diarrhea are common side effects observed in every clinical trial for MIL.⁴⁹

Toxicities to the liver and kidneys are also associated with MIL.⁴⁹ The long half-life (approximately 150 hours) also poses major concerns, as it can lead to subtherapeutic levels remaining for some weeks after standard treatment course and may facilitate the emergence of resistance.^{38, 39, 50} Furthermore, the efficacy of MIL has decreased in the last decade. In India, 7% of patients with VL on directly observed treatment have reported to relapse within 6 months.^{47, 51, 52} In Nepal, the relapse rate has increased to 20% for patients within 12 months on a self-administration regimen.^{47, 51, 53} Both countries report a high failure rate in children, though this thought to be partly attributed to a drug underexposure at the recommended dose.^{38, 51, 54} Most recently, the natural resistance in *L. infantum* isolates were reported after the completion of a phase II, open-label, dose escalation study of oral MIL in children and adults.⁴⁰ This study was aimed to investigate the efficacy and safety of MIL in Brazilian VL patients. MIL had not been used in Brazil before these studies. After a 6-month follow up the cure rate observed was a mere 42% in patients following a treatment regimen of 28 days and 68% with treatment extended to 42 days. Carnielli *et al.* observed MIL susceptibility of clinical isolates *in vitro* correlated to the clinical response. Further genomic analysis showed a positive correlation between susceptibility to MIL and the presence of the MIL sensitivity locus (MSL), a locus in chromosome 31 of the parasite. Isolates without this locus were reported less susceptible to the drug, and the authors suggest screening for the presence of MSL as a prognostic marker by polymerase chain reaction (PCR) could be used in clinical practice to predict MIL efficacy.⁴⁰ Further studies are required to investigate the distribution of MSL in *L. infantum* populations throughout Brazil as their absence is directly correlated to the natural resistance of this species.^{38, 40}

Paromomycin (1.05) is an aminocyclitol glycoside antibiotic repurposed as an antileishmanial. It is used as a topical treatment for CL and an intravenous treatment for VL. Its mechanism of action remains unclear. Reports suggest that cationic paromomycin associates with leishmanial glycocalyx and lipophosphoglycan, which are negatively charged major components of the parasite cell surface. This impairs the mitochondrial membrane potential, inhibiting protein synthesis and leads to respiratory dysfunction.^{30, 55, 56} Membrane fluidity and lipid metabolism are also altered. Other reports suggest paromomycin binds to the 30S ribosomal subunit interfering with the initiation of protein synthesis at the start of mRNA codon. This leads to the accumulation of abnormal initiation complex and the misreading of mRNA template. Incorrect amino acids are incorporated into growing polypeptide chains.^{56, 57} Paromomycin is associated with nephrotoxicity, ototoxicity and hepatotoxicity and is painful to administer.^{56, 58, 59} The 2015 Phase III studies in the Indian subcontinent assessing paromomycin efficacy in VL patients reported final cure rates of 95%.^{28, 60} However, under the same dosing regimen, previous outcomes obtained from East Africa reported only an 80% average cure rate. This value was significantly lower than the 94% cure rates obtained using the current treatment of sodium stibogluconate (SSG).^{28, 61} After approval and the more widespread use of paromomycin, laboratory-derived resistant isolates have been created though current resistance in the field remains

unclear.³⁹ Paromomycin is now recommended to be used in combination with other antileishmanial agents to boost efficacy and slow resistance.²⁰

Alternative drugs

The following lists commercially available medications that the CDC suggests may have merit for treating selected cases of leishmaniasis, but the FDA-approved indications do not include this disease.¹⁸

Pentamidine (1.06) was used as a second-line drug against antimony-resistant VL treatment. It is available in the form of two salts, pentamidine isethionate (Pentam 300) and pentamidine dimethane sulphonate (Lomidine).⁶² This intramuscular drug is associated with high toxicity and persistent diabetes mellitus.^{18, 20, 63} Additionally, decreased efficacy in VL patients suggests building resistance. Consequently, the use of the drug as a single-agent therapy for VL has been abandoned in India. It is still in use as a single-agent therapeutic against CL and MCL.^{20, 62, 63}

Azoles (1.07-1.09) block ergosterol synthesis of *Leishmania* parasites and cause cell death. Ketoconazole, itraconazole and fluconazole have all been used as oral treatments for CL in several studies. Results of each drug were quite varied and found ineffective in certain regions and sub-species of *Leishmania*. Pentavalent antimonials remain more efficacious over these azole oral treatments.^{18, 58, 62}

Treatment for Canine leishmaniasis

Allopurinol (**1.10**) is the only drug recommended by WHO to treat CanL, though has limited use as an antileishmanial agent in humans.^{20, 64} The leishmanial enzyme hypoxanthine-guanine phosphoribosyl transferase is inhibited by allopurinol. This enzyme converts dephosphorylated purines to nucleoside monophosphates in the purine salvage pathway of the parasite. It is suggested that phosphorylated allopurinol is incorporated into nucleic acids causing protein translation disruption and selective parasite death.⁶⁴ Allopurinol is a long term treatment for CanL that has also been utilized in combination with pentavalent antimonials or miltefosine for one month, then allopurinol is continued alone. However, the medications used primarily for human disease are not endorsed by WHO to treat CanL, due to low leishmanicidal efficacy in this host and the concerns of promoting resistance.^{20, 64, 65} The structure of allopurinol, along with the alternative treatments for humans (**1.06-1.09**) are depicted below in **Figure 1.03**.

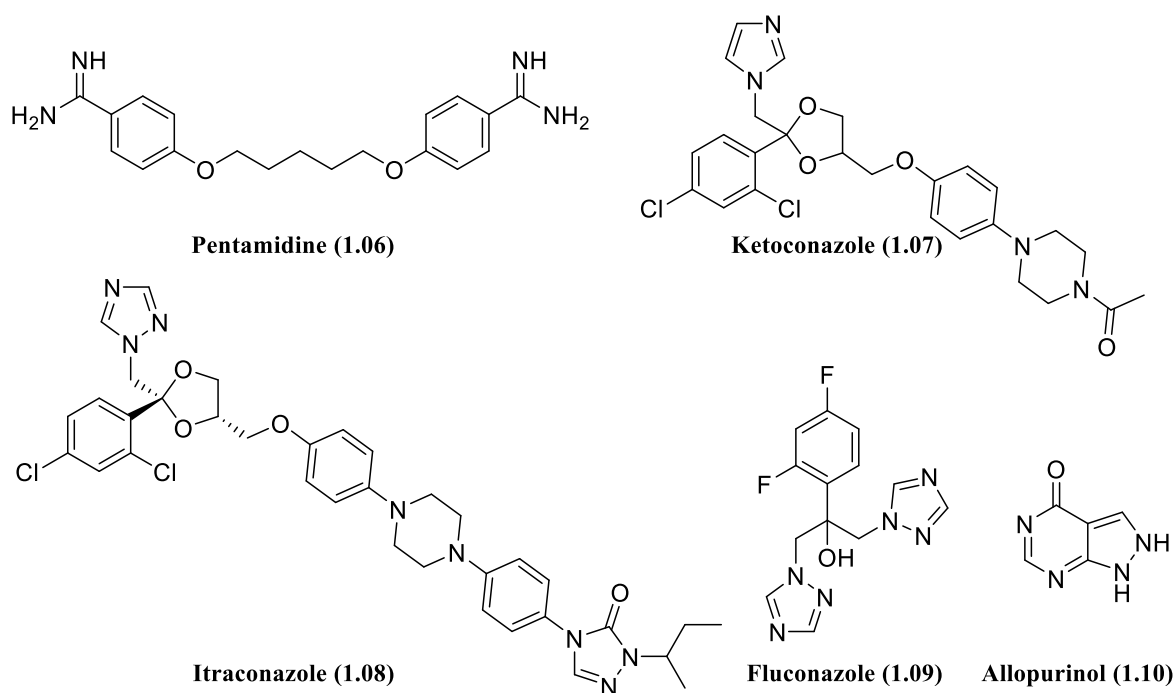


Figure 1.03: Alternative treatments less commonly used to treat leishmaniasis (1.06-1.09) and treatments for CanL (1.10)

Combination therapy

The main antileishmanial treatments summarized in **Table 1.02** can be used individually or in certain combinations. The use of combination therapy aims to improve efficacy in regions with emerging resistant or unresponsive strains. It also allows for shorter courses, reducing overall doses, toxic effects, cost, duration of hospitalization and overall improves patient compliance. The effective life of the available medicines are also prolonged.²⁰ Implemented combinations recommended by WHO for VL combination therapy in the Indian subcontinent are for a single dose of liposomal AmB together with MIL or a single dose of liposomal AmB with paromomycin or Mil co-administered with paromomycin. Phase III studies with each combination reported cure rates of at least 97%.^{20, 66} Other studies report a cure rate of 91.9% using lower doses of MIL with liposomal AmB.⁶⁷ For Sudan WHO recommends SSG plus paromomycin where initial an initial cure rate of 97% was also reported.^{20, 67} For East Africa, the top combination remains SSG plus paromomycin (91% initial cure rate), though WHO also recommends the less efficacious combinations (<90% cure rate) of a single dose of liposomal AmB followed by MIL, or AmB and SSG administered simultaneously.^{20, 38, 39, 67-69} Combination therapy is still being studied in trials to determine a shorter and more efficacious course in different regions (See section **1.06**).

Summary of Treatment Drawbacks and Socioeconomic factors

Despite the efforts to improve treatment with orally available options and combination therapies, all available drugs are still not ideal, and all share common drawbacks. Current treatments give rise to significant toxicities, require high dosing regimen as well as inadequate, and in some cases, painful modes of administration. Building resistance also possess a major concern. These issues have been discussed above per individual treatment as well highlighted in **Table 1.02**. Since leishmaniasis, particularly VL is most relevant to patients living in very poor and marginalized areas with inadequate healthcare, each of these drawbacks severely impedes access to treatment. Importantly, the high cost per treatment represents a significant barrier.^{20, 30} Despite the price reductions negotiated by WHO, these medications remain unaffordable to many of those affected. In poor regions such as Bihar, India, VL affects families living on less than \$1 USD per day and may need to sell assets or take loans with heavy interest to afford treatment. Poverty further worsens clinical outcomes as malnutrition and anemia increase disease severity. In return, leishmaniasis intensifies poverty. Even if households do not have to pay direct medical costs, they are heavily burdened with non-medical costs e.g transport, an income loss due to an absence from work or a loss of educational opportunities due to the disease or care-giving responsibilities.^{20, 70} Access to healthcare itself is limited in these regions where many cases experience a delay in diagnosis or receive none at all. This increases the risk of fatality, number of host reservoirs and the spread of infection.^{20, 70} The storage and delivery requirements call for specific equipment and skilled healthcare workers, both of which may not be available in these regions, further limiting access to healthcare. If medication is received, the regimen can be long, invasive and cause severe side effects.²⁰ These drawbacks commonly cause poor patient compliance and possibly premature course termination, contributing to building resistance. Overall, the current therapeutics remain unsuitable and unadaptable to the field.^{26, 30, 70} Therefore, new treatments and education that better accommodate the target population are required.

1.06 Leishmaniasis Drug Discovery and Development Pipeline

To be successful in the field and overcome the large list of difficulties associated with current treatments, the Drugs for Neglected diseases Initiative (DNDi) has published a “Target Product Profile” (TPP) for new chemical entities to treat VL (**Table 1.03**). This serves as a guideline to all groups designing and modifying new lead drug candidates. Top priorities for new candidates are safety, efficacy, quick and simple delivery (oral, 11 days maximum). A novel mechanism of action is preferred to overcome drug resistance. These candidates should be efficacious against at least *L. donovani* in the most endemic areas VL is rampant. To increase patient compliance decreased cost and side effects requiring monitoring is also sought after. New candidates should ideally be easy to manufacture and scale up to help reach an affordable price. Furthermore, long term stability and transport must be able to withstand the intended climate to be used in the field.^{28, 71}

Table 1.03: Target Product Profile for Visceral leishmaniasis New Chemical Entities recommended by DNDi⁷¹

	Optimal Target Profile	Minimal Target Profile
Target Label	VL and PKDL	VL
Species	All species	<i>L. donovani</i>
Distribution	All areas	Either India or Africa
Target Population	Immunocompetent and immunosuppressed	Immunocompetent
Clinical Efficacy	> 95%	> 90%
Resistance	Active against resistant strains	
Safety and Tolerability	No adverse effects requiring monitoring	1 monitoring visit in mid/end – point
Contraindications	None	Pregnancy/lactation
Interactions	None – Compatible for combination therapy	None for malaria, Tuberculosis, and HIV therapies
Formulation	PO / IM	PO/ IM
Treatment Regimen	1/day for 10 days PO/ 3 shots over 10 days	bid for <10 days PO; or <3 shots over 10 days
Stability	3 years in zone 4	Stable under conditions that can be reasonably achieved in the target region (> 2 years)
Cost	< \$10 / course	< \$80 / course

VL= Visceral leishmaniasis; PKDL= Post kala-azar dermal leishmaniasis; IM = intramuscular administration; PO = oral administration; zone 4= hot humid/tropical zone⁷²

The current VL pipeline contains various projects at different stages of the drug discovery (screening, hit-to-lead, lead optimization), translation (preclinical, Phase I, Phase IIa/proof of concept) and development platforms (Phase IIb/III, registration). The short-term strategy by DNDi for leishmaniasis treatment involves optimizing existing drugs and drug regimen to address immediate needs whilst in the long-term, new chemical entities (NCEs) are being developed and optimized into effective, affordable, oral treatments with short courses following the TTP in support of sustainable control the disease.⁷³ Noteworthy projects in the VL pipeline have been detailed below, however this is not an exhaustive list.

Combination therapy investigations

Drug combinations are replacing monotherapy as an effort to reduce the emergence of resistant strains. Finding complimentary or synergistic combinations without contradictions aims to also increase efficacy and speed up the approval process of new recommended antileishmanial courses since each compound in a known monotherapy by-passing the strenuous drug discovery process. Several notable clinical development phase studies for combination treatments by DNDi and partners are underway.⁷⁴ These include:

- A Phase III randomized and controlled non-inferiority trial of the combination regimen of MIL + paromomycin in Eastern Africa. This trial aims to compare the efficacy and safety of this

combination to the current standard VL treatment SSG + paromomycin. This investigation is based on the positive results of a similar study completed in South Asia and aims to find a safer oral replacement to pentavalent antimonials. This study began in early 2018 and will take place across 8 sites in Ethiopia, Kenya, Uganda and Sudan with an estimated total of 576 participants (children and adults). Completion of the trial and subsequent findings are currently pending at the time of writing this thesis.⁷⁴⁻⁷⁷ Clinical trial identifier: NCT03129646

- A similar Phase III study in India and Ethiopia, to compare the safety and efficacy of the combination regimen of MIL + liposomal AmB to liposomal AmB as a monotherapy in HIV/VL co-infected patients. This investigation is significant, as patients co-infected with HIV and VL commonly experience multiple relapses in VL, rarely achieving sustained control over the parasites. Trials in Ethiopia reported success in 2019 with the combination regimen. Results demonstrated a 67% cure rate in a 28-day regimen which increased to 88% when patients who were not cured received a second-round treatment to clear the parasite, with full treatment lasting 58 days.⁷⁸⁻⁸⁰ This extended combination treatment strategy is reported as the highest documented efficacy in HIV/VL patients, advocating this regimen as a first-line treatment strategy for HIV/VL patients in Eastern Africa.⁷⁹ Guidelines evaluating treatment recommendations are under review by WHO and their approval is currently pending at time of writing.⁷⁸ The results from matching the Phase III study in India are pending, though DNDi and partners expect complementary results to support this new treatment regimen for HIV/VL patients.^{78, 80} Clinical trial identifier Ethiopia: NCT02011958, India: CTRI/2015/05/005807
- An open label, randomized, parallel arm Phase II study of MIL + liposomal AmB and MIL + paromomycin using shorter courses in the Sudan for PKDL patients is underway. This study aims to determine the safety and efficacy of the two treatment regimens and understand the role of PKDL in VL transmission. Early treatment of PKDL could reduce the potential for patients to act as reservoir for VL infection and support elimination strategy of leishmaniasis.^{81, 82} The estimated study completion date is 2022.⁸² In India and Bangladesh, recruitment has been completed for a similar Phase II study comparing the safety and efficacy of the combination of liposomal AmB + MIL to liposomal AmB alone in patients with PKDL. DNDi states all patients have completed treatment and the 12-month follow up-visit. The 24-month follow up visits are planned for 2020 and are set to proceed, if not precluded by the COVID-19 situation.⁸³ Results for this study are also pending at time of writing. Previous infective studies in Asia confirmed PKDL patients act as a reservoir for ongoing infection. To assess infectivity in the long-term and treatment impact, the Phase II study protocol includes xenodiagnosis on patients after they have completed treatment. Similar infective studies in Sudan are also underway.⁸¹ Clinical trial identifier Sudan: NCT03399955, India/Bangladesh: CTRI/2017/04/008421

Monotherapy investigations

Despite the success of combination therapies thus far, new medications better suited to the field are still desperately needed. Long term solutions require a new barrage of appropriate oral combination treatment options to fight against resistance and phase out the standard intravenous and intramuscular treatments, pentavalent antimonials and paromomycin which require painful and repetitive administration.²⁸

Drug discovery for leishmaniasis still faces formidable challenges, being an NTD there is no lucrative market and therefore a lack of interest in developing antileishmanials. A lack of validated targets, poor translation of *in vitro* to *in vivo* models and a low hit rates for phenotypic screening (<0.1 %) further hinders the process.⁸⁴ These challenges may be due to physiological barriers distinctive to the parasite. The unique glycolipid-rich cell surface of amastigotes and their hidden location in the acidic phagosome compartments, parasitophorous vacuoles and enhanced oxidative stress in macrophages add a degree of difficulty to chemotherapy. Even after optimization, compounds developed from these cellularly active hits do not meet the TTP criteria.⁸⁴⁻⁸⁶ Furthermore, the two major forms, VL and CL, will likely require treatments with different pharmacokinetics and formulations since these manifestations have different sites of infection and their causative agents may possess different drug susceptibility.⁸⁷ With aims to overcome these barriers, recent decades have seen an expansion in drug discovery and development for neglected diseases. Academia is now supported by large contributions and collaborations with governmental, non-profit, the biotech/pharma sector and other organizations, in search of novel treatments for leishmaniasis. Some Big Pharma companies have shared their large libraries of compounds and facilities with academic groups. By doing so, the strenuous discovery and translation process may be accelerated, novel and repurposed compounds could reach clinical development faster.^{28, 73, 88}

One important example of a large BigPharma-non-profit collaborative effort is the NTD Booster program, described as a “global consortium of pharmaceutical companies” coordinated by DNDi to mine the vast and privileged compound libraries of the collaborative companies, and search for structural similarities to build a chemical series. Compounds are tested and the most potent are refined by repeating this process. This project has yielded several hit series undergoing optimization to be used as potential leads for leishmaniasis and Chagas disease.⁸⁹ Examples of disclosed compound series for *L. donovani* and *L. infantum* activity, elaborated by the booster projects are depicted in **Figure 1.04**. Each compound has potent and selective activity against the parasite and are currently under investigation at time of writing.⁸⁹

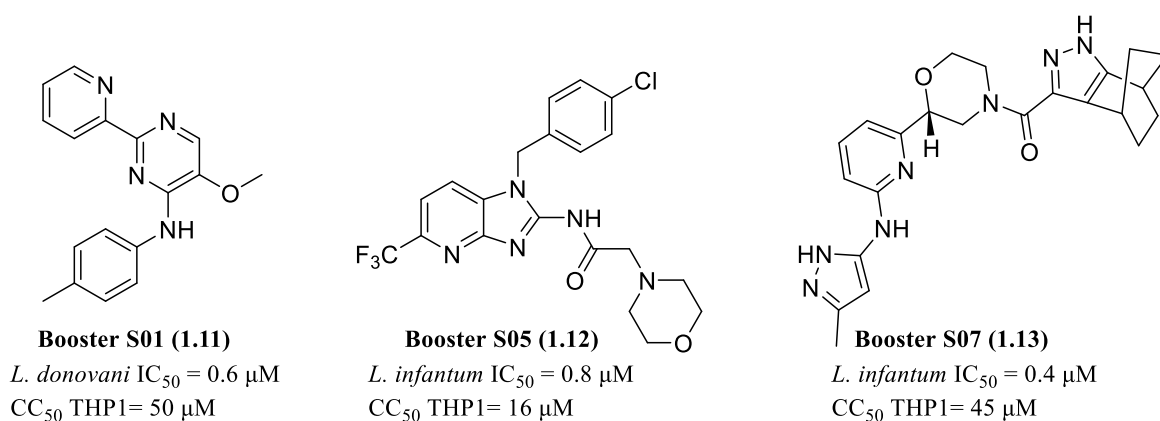


Figure 1.04: Examples of compound series investigated under the NTD Booster consortium^{83, 89}

Exploration into several notable compound classes have yielded encouraging progress in the discovery and translation phases. These have been described below. Review of the pipeline includes descriptions of the five new, significant classes of optimized lead, preclinical and/or clinical candidates belonging the following compound classes: benzoxaboroles, nitroimidazoles, aminopyrazoles, pyrazolopyrimidines and proteasome inhibitors.^{67, 74, 90, 91} These classes have been identified via high throughput screening and/or drug repurposing.^{28, 74} This review also includes other recent findings belonging to these related classes recent, significant failures as these compounds have helped shape new clinical and preclinical candidates. Short perspectives on a few additional significant compound classes within the pipeline have also been included as they may provide also further options for preclinical and clinical candidates for VL in the future,

Drug discovery based on drug repurposing

Drug repositioning or repurposing is a common theme to the current pipeline, as it has become an attractive approach towards candidate identification and has produced approved treatments. Current treatments for leishmaniasis are based on repurposed drugs, i.e Paromomycin (antibiotic), MIL (anticancer) and AmB (antifungal).⁹² It significantly reduces the development time and costs related to de novo hit-to-lead drug discovery, capitalizing on the fact that approved drugs and many abandoned compounds have undergone trials in humans or at least preclinical pharmacokinetic and safety assessments. Access to this data along with well documented chemical libraries pertaining to the compound of interest can accelerate further optimization of the chosen scaffold. New candidates against VL outlined below, have entered the translation phases of the pipeline as a result of drug-repurposing processes.^{28, 93, 94}

Benzoxaboroles

Benzoxaboroles are cyclic functionalities of boron which have previously reported to possess activity against bacteria, fungi and protozoans including *T. brucei* and *Plasmodium falciparum*.⁹⁵ Phenotypic

screening of a library of benzoxaboroles from Anacor Pharmaceuticals and further optimizations surrounding benzoxaborole 6-carboxamides gave rise to development of SCYX-7158/ acoziborole (**1.14**) currently in Phase III clinical trials for HAT.^{28, 91, 94-97} Investigations revealed this compound class to have broad antiprotozoal properties, resulting in studies for leishmaniasis and Chagas disease involving the benzoxazole 6-carboxamide scaffold.^{95, 97, 98} Of the antileishmanial developments, recent benzoxaborole optimization studies have reported compounds LSH001 (**1.15**) and LSH003 (**1.16**) as leads for CL treatment. Topically applied LSH001 (**1.15**) and orally dosed LSH003 (**1.16**) were reported to halt lesion growth and reduce *L. major* amastigote burden of BALB/c mouse skin and *in vivo* models for CL.^{28, 95}

For VL treatment, DNDi and Anacor have produced the 6-carboxamide benzoxaborole compound DNDI-6148 (**1.17**) as the current frontrunner of the oxaborole class. This candidate displayed potent activity against *L. infantum* and *L. donovani* intracellular amastigotes *in vitro* (IC₅₀= 0.63 µM and 2.29 µM respectively). DNDI-6148 was an improvement over the reference compound miltefosine (MIL) against *L. infantum* and was comparable against *L. donovani in vitro* (MIL IC₅₀= 3.50 µM and 1.80 µM respectively). DNDI-6148 was reported to achieve high levels of parasite burden reduction in hamster models using *L. donovani* and *L. infantum* (>90% reduction in the liver, spleen and bone marrow). This was achieved using a minimum oral dose of 25 mg/kg b.i.d, for 5 days. In comparison, the reference compound MIL achieved >97% reduction of parasite burden in this model, using a minimum dosage of 40 mg/kg s.i.d.^{28, 91} The mechanism of action for this compound is not yet known. It has shown to retain activity against strains resistant to current antileishmanials, therefore its mechanism of action is thought to be unique to current treatments.⁹⁰ Regulatory safety pharmacology and toxicology assessments were completed in 2017 and was approved in late 2019 for clinical trials. The Phase I multiple ascending dose study in healthy volunteers is currently ongoing at time of writing.^{74, 83, 97} Compounds DNDI-5421 and DNDI-5610 have been chosen as “backup” candidates for this class. Their chemical structure has yet to be released. In the same *in vivo* study described above, DNDI-5421 displayed similar efficacy in hamsters to DNDI-6148 (**1.17**) against *L. infantum* (parasite burden reduction >90 % in liver, spleen and bone marrow, 25mg/kg b.i.d).^{28, 91} Further development of these compounds remains on hold and will recommence if problems with DNDI-6148 (**1.17**) are encountered.⁷⁴

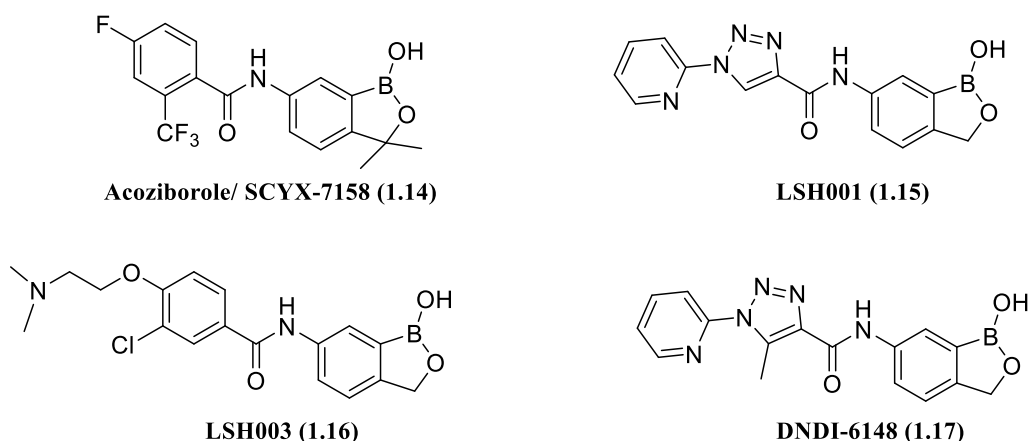


Figure 1.05 Structures of benzoxaborole compounds involved in the leishmaniasis pipeline^{28, 99}

Nitroimidazoles

Nitroaromatics are known pharmacologically active compounds and are used to treat various indications such as angina, insomnia and Parkinson's disease.^{28, 100} They are also used as anti-infective agents for tuberculosis and parasitic infections (HAT, Chagas disease).¹⁰⁰ Despite their association to potential mutagenicity and carcinogenicity issues due to metabolic activation of the nitro group, this compound class has been investigated by DNDi and partners for over 10 years.^{28, 90, 100} Fexinidazole (**1.18**) was originally developed as a broad-spectrum antimicrobial agent by Hoechst AG and was re-discovered by DNDi in a phenotypic screen of over 700 nitroheterocycles for antitrypanosomal activity. It is now the first orally available treatment effective against *T. brucei* (HAT).^{101, 102}

This compound has also demonstrated activity against *T. cruzi* and has undergone a phase II proof-of-concept study for adults with chronic intermediate Chagas disease (Clinical trial identifier: NCT03587766).¹⁰³ Fexinidazole (**1.18**) was reported to act as a prodrug, by using enzyme-mediated reduction via nitroreductases to generate cytotoxic metabolites that cause DNA, lipid and protein damage. The genome of *Leishmania* parasites contain a homologous nitroreductase gene so naturally the leishmanial activity of fexinidazole (**1.18**) was assessed.¹⁰⁴ Low micromolar potency was achieved against intracellular amastigotes *in vitro*, whilst stronger efficacy was demonstrated *in vivo*. Using VL BALB/c mouse models, 98% suppression of *L. donovani* parasite burden was achieved using fexinidazole (200 mg/kg s.i.d, 5 days).^{28, 105} Furthermore, the compound passed Phase I clinical trials in healthy volunteers given as a single dose or as repeated dose after 14 days. Beginning in 2013, a Phase II proof of concept trial (Clinical trial identifier: NCT01980199) was conducted in Sudan to assess safety and efficacy for VL in adult patients. All patients displayed clinical improvement during treatment and majority showed parasite clearance at the end of the course. However, at the 6 months follow up majority of patients experienced a relapse. This study was interrupted in 2014 as it failed to

conclusively exhibit efficacy in majority of patients. Clinical developed of fexinidazole (**1.18**) as a monotherapy for VL is now discontinued.^{28, 106}

Another example of nitroaromatic drug repurposing for VL drug discovery is the bicyclic nitroimidazopyran, PA-824/ Pretomanid (**1.19**), which was developed by TB alliance and is used to treat multi-drug resistant tuberculosis. Both enantiomers were investigated, though the *R* form reported superior potency against intracellular *L. donovani* amastigotes *in vitro*, using macrophages as host cells (intramacrophage assay, EC₅₀ = 0.9 µM).^{28, 107} The *in vivo* BALB/c model for VL exhibited >99% suppression of *L. donovani* parasite burden using a dosing regimen of 100 mg/kg b.i.d, orally for 5 days.^{28, 100, 107} Although this compound reported to have good ADMET properties for further investigation, it has not entered preclinical development. Despite this, PA-824 (**1.19**) helped guide the development of other compounds, some of which are now further in the pipeline.²⁸

Further interest in nitroaromatics originally designed for tuberculosis drug discovery lead to the contractual agreement between TB Alliance and DNDi. DNDi was granted access to a selected library of 72 nitroimidazoles for antileishmanial assessment, where phenotypic screening allowed for the identification of the preclinical candidate DNDI-VL-2098 (**1.20**). The racemate displayed high potency against *L. donovani* *in vitro* (IC₅₀= 0.03 µM) whilst the *R*-enantiomer displayed superior efficacy *in vivo* (>99% reduction in *L. donovani* parasite burden) using VL BALB/c mouse models with a minimum dose of 6.25 mg/kg s.i.d for 5 days. This was comparable to that of MIL (94% reduction in parasite burden).¹⁰⁸ Despite this high efficacy, development of this compound has been terminated due to adverse effects reported during toxicology studies.^{28, 109}

The fruit of extensive medicinal chemistry campaigning around bicyclic nitroimidazooxazoles for antitubercular activity resulted in delamanid/OP-67683 (**1.21**).¹¹⁰ It is now an orally available treatment for multi-resistant tuberculosis. Structural similarities of (*R*)-PA-824 (**1.19**) and DNDI-VL-2098 (**1.20**) to delamanid (**1.21**) encouraged the more recent investigations by the University of Dundee to repurpose this compound for VL.¹¹¹ The same trend in enantiomer potency was observed where the *R*-enantiomer proved to possess superior antileishmanial activity against *L. donovani* intracellular amastigotes (86 nM). Oral dosing of delamanid (**1.21**) in *L. donovani* infected BALB/c mice at 30 mg/kg b.i.d for 5-10 days exhibited 99.5% suppression of parasite burden, comparable to that of the reference drug MIL (98.8-99.8 % suppression at 30 mg/kg).¹¹¹ Wyllie *et al.* suggest the bicyclic nitro drugs delamanid (**1.21**), PA-824 (**1.19**) and DNDI-VL-2098 (**1.20**) undergo bioactivation by FMN dependant NADH oxidoreductase (NTR2), which is distinct from the reductive activation of fexinidazole (**1.18**) which involves mitochondrial oxygen-insensitive nitroreductase (NTR1).¹¹² Delamanid (**1.21**) was reported to have an unusual pharmacokinetic/pharmacodynamic relationship. Extended structure activity relationship (SAR) studies surrounding based on this scaffold along with the structures of PA-

824 (**1.19**) DNDI-VL-2098 (**1.20**) have been undertaken to improve upon this compound and has successfully yielded new candidates for VL.^{111, 113} DNDI-0690 (**1.22**) resulted from these intensive medical chemistry efforts defining a backup series after the serendipitous identification of DNDI-VL-2098. Scaffold hopping was applied to improve activity. The aim of scaffold hopping following Böhm *et al.* is to “discover structurally novel compounds” by altering the central core of a known active molecule. This technique can lead to compounds with chemically different core structures, still binding to the same receptor.²⁰¹ Using scaffold hopping and previous SAR provided the bicyclic nitroimidazooxazine functionality with attachment via the same inverted linker (CH₂OR) found in that of PA-824 and delamanid respectively. Aromatic side chains were moved from the 6 to 7-position to improve metabolism.¹¹³ The *R*-enantiomer displayed efficacy and selectivity *in vitro* for both intracellular *L. donovani* and *L. infantum*, using macrophage host cells (EC₅₀= 0.03 µM and 0.08 µM respectively).^{28, 113} The *in vivo* *L. infantum* infected hamster models for VL exhibited >96% reduction of parasite burden within the liver, spleen and bone marrow using a dosing regimen at 12.5 mg/kg orally, b.i.d over 5 days. This is comparable to the reference drug MIL, achieving >92% reduction of parasite burden with the liver and spleen and 89% inhibition within bone marrow, using a dosing regimen of 40 mg/kg s.i.d. Good bioavailability was reported.¹¹³ As with the aforementioned nitroaromatic compounds, it is believed that the nitro group of DNDI-0690 (**1.22**) also undergoes bioactivation by the nitroreductase enzyme NTR2.⁹⁰ This candidate has also shown potency *in vitro* and *in vivo* against CL models and further PK studies support this candidate for oral CL treatment.⁸⁷ A full preclinical toxicology and safety assessment was completed in 2017, no mutagenic problems have been reported. At time of writing, DNDI-0690 was reported to be recruitment stage of a Phase 1 single oral ascending dose study in healthy male volunteers, though the trial has been delayed due to the COVID-19 pandemic (Clinical trial identifier: NCT03929016).^{83, 114, 115}

Finally, DNDI-8219 (**1.23**) is a current “favourite” backup development candidate for Phase I studies for this series. After developing the successful 7-substituted-2-nitroimidazooxazine series, further extensive SAR investigations surrounding pretomanid analogues were assessed in a medium-throughput screen and the 6-substituted 2-nitroimidazooxine class was narrowed down and re-developed.^{28, 84} DNDI-8219 (**1.23**) (*R*-enantiomer) displayed consistent antileishmanial activity *in vitro* at low micromolar levels in VL and CL strains. The compound exhibited efficacy in the *in vivo* hamster model against *L. infantum*, with >97% parasite clearance in the liver, spleen and bone marrow. This was dosed at 25 mg/kg b.i.d. This was comparable to the reference drug MIL, which obtained >96% clearance in all target organs at 40 mg/kg s.i.d. Furthermore, improved solubility and PK profiles (in mouse, rat and hamster) as well as low hERG risk were established by Thompson *et al.*⁸⁴ The continuous development of the nitroimidazole compound class shows promise for in human trials and VL therapy development.

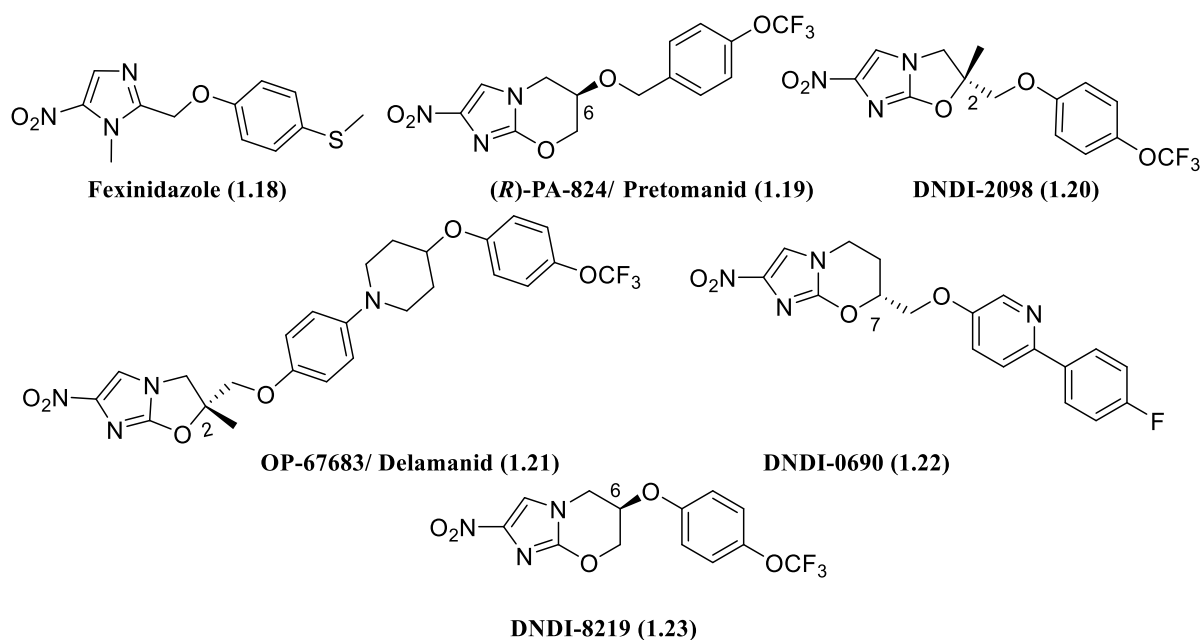


Figure 1.06: Structures of nitroimidazole compounds involved in the leishmaniasis pipeline²⁸

Protease inhibitors (PI)

The World health organization describes VL as an emerging opportunistic infection associated with HIV. A decline in VL in Europe was observed with the introduction of protease inhibitor based antiretroviral agents and has been somewhat connected with the effect of protease inhibitors on *Leishmania spp.*. However, this assumption is based on retrospective studies of observational data and true clinical significance has yet to be appropriately assessed.²² The fact that both the *Leishmania* parasite and HIV- 1 can infect the same target cells (namely, macrophages and dendritic cells) suggests the existence of complex interactions between both pathogens.¹¹⁶⁻¹¹⁸ Furthermore, Zhao *et al.* report the presence of *Leishmania* and HIV-1 within the same cellular microenvironment can lead to an enhancement of virus gene expression.¹¹⁹ Experimental and clinical studies confer that leishmaniasis causes an increase in the serum HIV-1 load and a more rapid progression to AIDs, reducing life expectancy.¹¹⁶ This resulted in investigations surrounding protease inhibitors used for HIV/AIDS treatment as possible candidates for leishmaniasis treatment. These are small molecules that inhibit HIV-1 replication by actively competing for the binding site of the viral protease enzyme.²² Over 10 years ago, protease inhibitors indinavir (**1.24**) and saquinavir (**1.25**) were assessed against *L. infantum* and *L. major*, displaying dose dependant leishmanicidal activity against promastigotes.²² Further studies with first-generation protease inhibitors nelfinavir (NVF, **1.26**), ritonavir (RTV, **1.27**) and saquinavir (**1.25**) were evaluated against *L. donovani* and *L. infantum*, where NFV was observed to consistently display inhibition against intracellular promastigotes and amastigotes (80-95% inhibition at NVF concentration of 25 $\mu\text{mol/L}$). During this study, Trudel *et al.* observed NFV was best at limiting intracellular growth of SbV-sensitive and resistant field isolates of *L. donovani*, suggesting resistance

to antimonials does not result in cross-resistance to protease inhibitors. Additionally coinfection of *Leishmania* with HIV-1 did not diminish the antileishmanial activity of the protease inhibitors.¹¹⁷ Since then, further studies with NVF demonstrated potency against various CL, VL and HIV-positive VL patient strains (>94% growth inhibition).¹²⁰ More recent studies with NVF found when administered in combination with MIL using an VL BALB/c mouse model (5 mg/kg for each drug, intraperitoneal infection, 15 days) an increased reduction of *L. infantum* parasite burden was observed. This combination reported an 89% and 84% reduction in the liver and spleen respectively, whilst NVF alone displayed a reduction of 61% and 64% in the liver and spleen respectively. The combination was also superior to MIL alone (77% and 76% reduction in parasite burden of the liver and spleen respectively). The authors state this synergistic combination may be useful in treatment of VL/HIV coinfection, though further dosing and safety assessments are required.¹¹⁶

As PIs were found to directly affect amastigotes *in vitro*, there is now an increased interest in developing combination therapy of protease inhibitors and antileishmanial agents for HIV/VL co-infected patients. Thus, various studies into the leishmanicidal potency (CL and VL) of an assortment of known PIs were conducted.²² This gave rise to Lopinavir (LPV, **1.28**) as an antileishmanial.^{22, 118} Most recently, LPV reached *in vivo* assessment against *L. infantum* infected BALB/c mice, both alone and in combination with MIL at various oral doses, b.i.d for 5 days. The minimum individual dose of 7.7 mg/kg MIL was able to completely suppress parasite burden. At 3.85 mg/kg, MIL was only able to reduce parasite burden by 46.7% in the liver and 67% in the spleen. Alone, LPV only at the highest dose tested (493.2 mg/kg) was able to somewhat reduce parasite burden (40% in liver, 52% in spleen). To assess concerns about possible drug association, in combination, LPV at doses of 493 mg/kg and 246.6 mg/kg did not exert any deleterious effect on MIL (7.7 mg/kg dose), which was still able to eliminate parasite burden. A lower dose of MIL (1.92 mg/kg) with the highest dose of LPV found parasite load of the liver and spleen showed parasite reduction of the liver and spleen at 44.5% and 77% respectively, suggesting the combined therapy is effective against *Leishmania*, allowing lower doses of MIL. This would provide a valuable strategy against increasing parasite resistance and lowering side effects of MIL. LPV was also shown to alter lipid composition of *L. amazonensis*, interfering with cholesterol homeostasis in parasites. As MIL impairs lipid metabolism, it is thought that this combination acts synergistically on different points of the same pathway.¹¹⁸ The mechanism of action of PIs in relation to leishmaniasis has not been completely elucidated and it is also thought that PIs also inhibit trypanosomatids aspartyl peptidases, a catalytic type of protease enzyme that uses a water molecule activated by aspartic acid residues for catalysis of their peptide substrates.^{118, 121, 122}

Authors of this study, Rebello *et al.* contest although this study may be more underwhelming than the previous combination study of NFV and MIL by Valdivieso *et al.*, it more closely represents the administration route for human patients, as oral administration was used, since MIL and HIV-PIs are

oral drugs. Furthermore, the contest previous study by Valdivieso *et al.* employed much higher treatment over 15 days vs the 5 days by Rebello *et al.* and question the more prominent combined effect of NFV and MIL.^{116, 118} Overall the continuous of protease inhibitors investigations have led to a new compound class demonstrating potency against *Leishmania spp.*. This may guide further studies and lead to a new therapeutic candidate for leishmaniasis or as a combination for co-infected VL/HIV patients. Furthermore, such combinations may allow for lower dosage therefore reducing toxicity and delay drug resistance increasing adaptability to the field.^{116, 118}

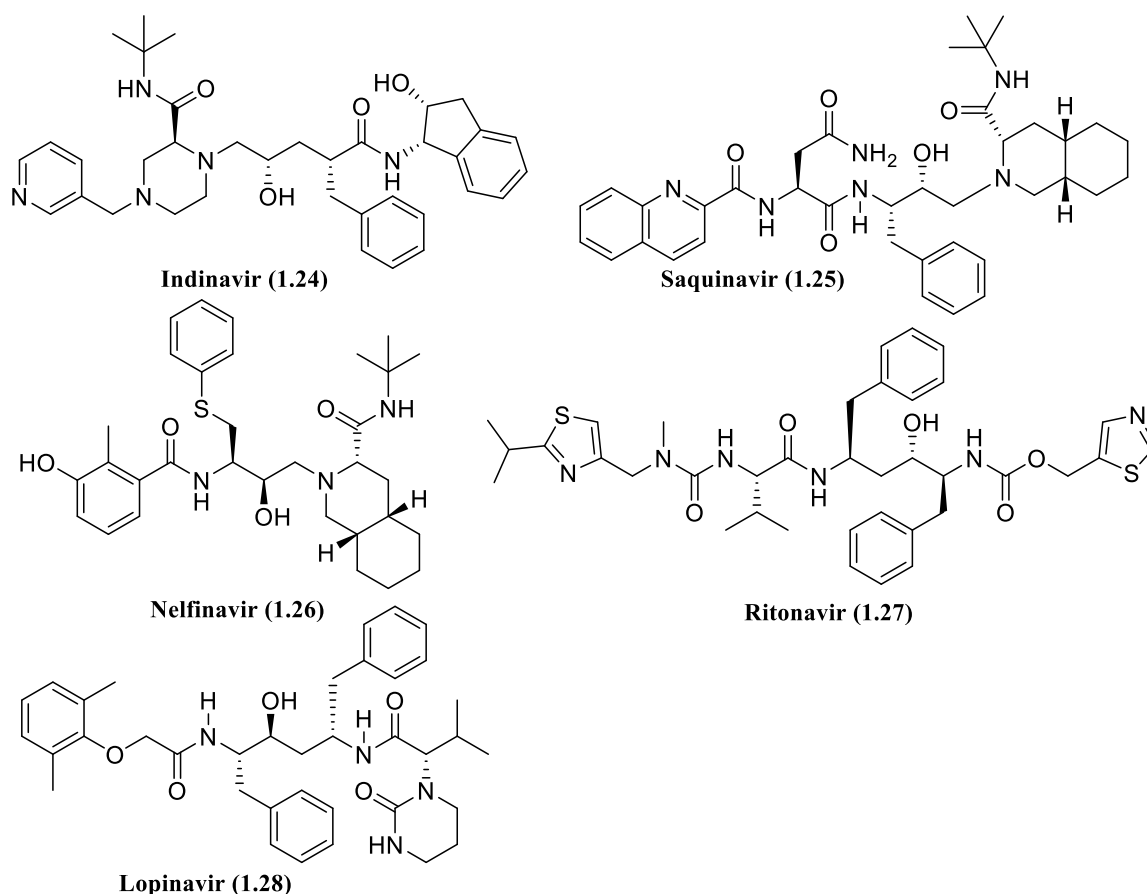


Figure 1.07: Structures of HIV-1 protease inhibitors involved in the leishmaniasis pipeline

Selective estrogen receptor modulators (SERM)

Tamoxifen (**1.29**) is a triphenylethylene derivative used as a selective estrogen receptor modulator (SERM) for breast cancer treatment. Tamoxifen has been proposed as antileishmanial candidate for visceral and cutaneous leishmaniasis. It was observed to display efficacy against cutaneous and visceral models for leishmaniasis *in vitro* and *in vivo*. Against *L. braziliensis* and *L. chagasi* intracellular amastigotes, using macrophage host cells (intramacrophage assay) tamoxifen demonstrated good activity ($IC_{50} = 1.9$ and $2.4 \mu M$).¹²³ Consistently low micromolar activity in other species for VL and CL models have been reported.¹²⁴ Miguel *et al.* report >95% reduction in parasite burden, using 20 mg/kg/day intraperitoneally for 15 days, in both the *L. braziliensis* infected BALB/c mouse model (CL) and *L. chagasi* infected golden hamster model (VL). This was shown to be as effective as drug reference

meglumine antimoniate.¹²³ However, further *in vivo* studies observed serious side effects to the male reproductive system.¹²⁵ Despite this, combination studies with current antileishmanial drugs were undertaken in CL models. The combination of AmB and tamoxifen *in vivo* have displayed superior efficacy to the sum of effects of each individual drug, suggestive of additive and possibly synergistic behaviour. Trinconi *et al.* indicate that tamoxifen does not hinder AmB activity and lower doses of combined drugs result in good clinical and parasitological responses.¹²⁶ Recently, tamoxifen was reported to alter sphingolipid metabolism of *Leishmania*, specifically inhibiting the biosynthesis of the anionic sphingolipid inositol phosphorylceramide, which is the most abundant sphingolipid in *Leishmania spp.* making up 5-10% of membrane total lipids. This may serve as an interesting target for therapeutic intervention as this sphingolipid is absent in mammalian cells.¹²⁷

Combination studies with tamoxifen and MIL also suggest a good clinical pairing, despite the absence of synergic interactions, good efficacy is observed in combination and this partnership can help hinder the building up of MIL resistant parasites.¹²⁸ Most recently tamoxifen was assessed in combined therapy with meglumine antimoniate during a pilot Phase II clinical trial for CL, undertaken in Brazil. Oral and topical routes of tamoxifen were employed at doses regularly used for breast cancer treatment. From this study, it was observed the co-administration resulted in higher cure rates in comparison to the standard antimonial treatment alone. However, the improvement was not to statistically significant level. The authors suggest higher doses could be investigated.¹²⁹ Since the initial repositioning efforts of tamoxifen, investigations around SERM scaffolds have been explored in pursuit of antileishmanial activity.

Raloxifene (**1.30**) is another example of a SERM assessed for antileishmanial activity, which demonstrated antileishmanial activity *in vitro* and *in vivo*.^{130, 131} Further probing around SERM scaffolds triphenylethylenes and benzothiophenes was undertaken, keeping in mind the potential safety concerns surrounding SERMS as leishmanial chemotherapy. Potent benzothiophenes (**1.31**) lacking the pharmacophore required for estrogen receptor activity have been identified as viable starting points for antileishmanial agents (VL and CL).¹²⁴ Overall the SERM based compound class may represent the possibility for new antileishmanials.

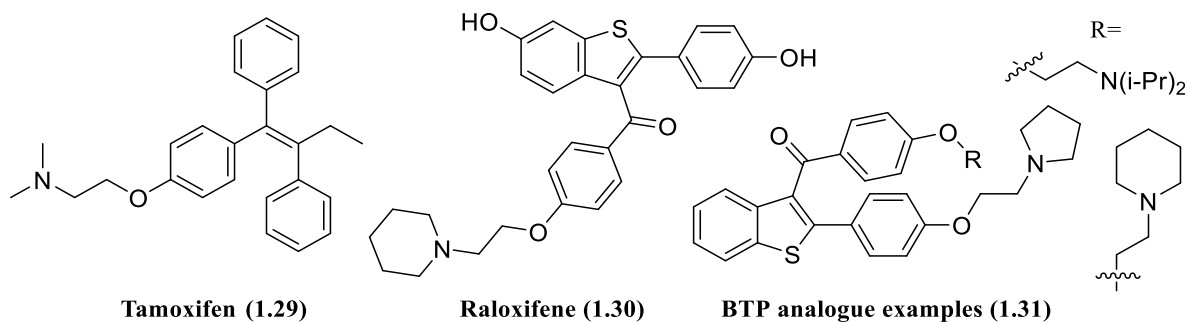


Figure 1.08: Structures of SERM based compounds involved in the leishmaniasis pipeline ¹²⁴

Despite the success and advantages of the use of drug repurposing, they are not without drawbacks. Compounds designed for a different human disease and initial therapeutic activity may cause undesirable side effects that need to be monitored, reduced or removed with further optimization.¹³² Repurposed compounds may not fit the TPP for NTDs and despite efficacy may remain unsuited to the field. As mentioned, current repurposed treatments remain expensive compounds which lack oral availability, poor stability to high temperatures or still require the need for long dosing regimens/hospitalization are matters that should be addressed during drug repositioning efforts to allow for accessible therapeutics.¹³²

Drug discovery based on high-throughput screening methods

Another common theme to the current leishmaniasis pipeline is the use of high throughput screening (HTS), particularly phenotypic HTS. Phenotypic or whole cell/organism HTS has become the classical approach to early drug discovery for leishmaniasis.¹³³ Further advancements in technology have led to a combination of HTS with high content imaging, whereby a number of established HTS methods utilizing high content imaging intracellular assays are now utilized for kinetoplastid drug discovery.^{85, 133-136} These methods employ automated image acquisition and analysis using automated microscopy, fluorescent detection and multi-parameter algorithms to quantify interactions of compounds in cell populations. Phenotypic changes such as cellular localization and proliferation can be monitored as well as assessing toxicity of host cell after exposure to compounds.^{85, 133, 137, 138} This process is considered robust, due to minimal human bias involved, as well as reproducible and time efficient. Disadvantages of high-throughput screening using intracellular imaging include the initial expenditure for specialised high-content screening equipment, in addition to ongoing maintenance and running costs, added to the need to have a level of technical expertise.⁸⁵ Despite this, phenotypic HTS methods have been employed successfully throughout the NTD pipeline to re-discover various known compounds previously discussed for drug repurposing as well as identifying NCE hits to be optimized in medical chemistry hit-to-lead campaigns.

Aminopyrazoles

The antileishmanial activity of the aminopyrazole hit **1.32** was identified during a high-throughput screen of a Pfizer small molecule diversity set against *L. donovani* amastigotes in THP-cell lines.^{28, 99, 139} Hit optimization gave rise to the early lead compound **1.33** by Mowbray *et al.*, which demonstrated good efficacy against *L. infantum* and *L. donovani* (IC₅₀ = 2.37 μ M and 1.31 μ M, respectively) as well as metabolic stability against liver microsomes.^{28, 139} Efficacy of the early lead compound **1.33** was assessed *in vivo* using hamster models infected with *L. infantum*. An oral dosing regimen at 50 mg/kg b.i.d for 5 days was used, resulting in reduction of parasite burden in the liver and spleen (92.7% and 95% respectively) without obvious signs of toxicity.^{28, 139} After proof of concept of this compound class *in vitro* and *in vivo*, further optimization was undertaken by Takeda Pharmaceutical Company Ltd and DNDi, producing the aminopyrazole preclinical candidate DNDI-5561 (**1.34**).¹⁴⁰ The mechanism of action of this compound is not yet known.⁹⁰ At the end of 2019, progress of the compound was terminated due to unfavourable safety results in preclinical studies.

Development of aminopyrazoles remains in the lead optimization phase of the pipeline.⁷⁴ Compounds DNDI-1044 (**1.35**) and DNDI-8012 (**1.36**) have been reported as possible lead candidates for the aminopyrazole series. These compounds were assessed alongside leads from the established oxaborole and nitroimidazole series. DNDI-8012 demonstrated efficacy *in vitro* against *L. donovani* and *L. infantum* (IC₅₀ = 0.39 μ M and 0.22 μ M respectively). Whilst DNDI-1044 displayed slightly better activity (0.26 μ M and 0.17 μ M respectively). Cytotoxicity of both compounds *in vitro* was not observed against MRC-5 cell lines (CC₅₀ > 200 μ M). The investigation leads also displayed a lack of cross resistance when assessment with current antileishmanials against various *L. infantum* field strains.⁹¹ In an early curative *L. infantum* hamster model DNDI-1044 was able to reduce parasite burden (> 95 %) in the liver, spleen and bone marrow using a minimum of 25 mg/kg b.i.d for 5 days. To reach the similar efficacy in the liver and spleen using the *L. donovani* model, a dosing regimen 50 mg/kg b.i.d for 5 days was required. DNDI-8012 also exhibited a comparable pattern in the *L. infantum* model, in which 50 mg/kg b.i.d for 5 days was also required to achieve over 95% parasite burden reduction in the liver and spleen. As a comparison a miltefosine reference dosing regimen of 40 mg/kg s.i.d for 5 days was used for early curative *L. donovani* and *L. infantum* hamster models. Over 97% reduction in parasite burden of the liver spleen and bone marrow was observed in both models. The authors suggest these leads could possibly be used in both mono- and combination therapies. Their cidal effects offer possibility in terms of lowered risk of drug resistance and shorter dosing regimens as per the requirements of DNDi's target product profile.^{28, 91}

These leads were also recently evaluated for CL treatment alongside aminopyrazole compound DNDI-1047 (structure yet to be disclosed). Van Bocxlaer *et al.* have recently recommended DNDI-1047 as a

lead for the aminopyrazole series for cutaneous treatment due to its ability to significantly reduce parasite burden and lesion size (no visible nodule). DNDI-1047 displayed excellent potency when applied topically and orally *in vivo* using BALB/c *L. major* mouse models for CL. Optimal dosing orally was found at a minimum of 12.5 mg/kg b.i.d for 10 days.^{28, 99} Though the status of this series remains under lead optimization phase, the efficacy against a wider range of *Leishmania spp.* suggests the aminopyrazoles to be promising candidates for VL and possible broad-spectrum treatment of leishmaniasis.

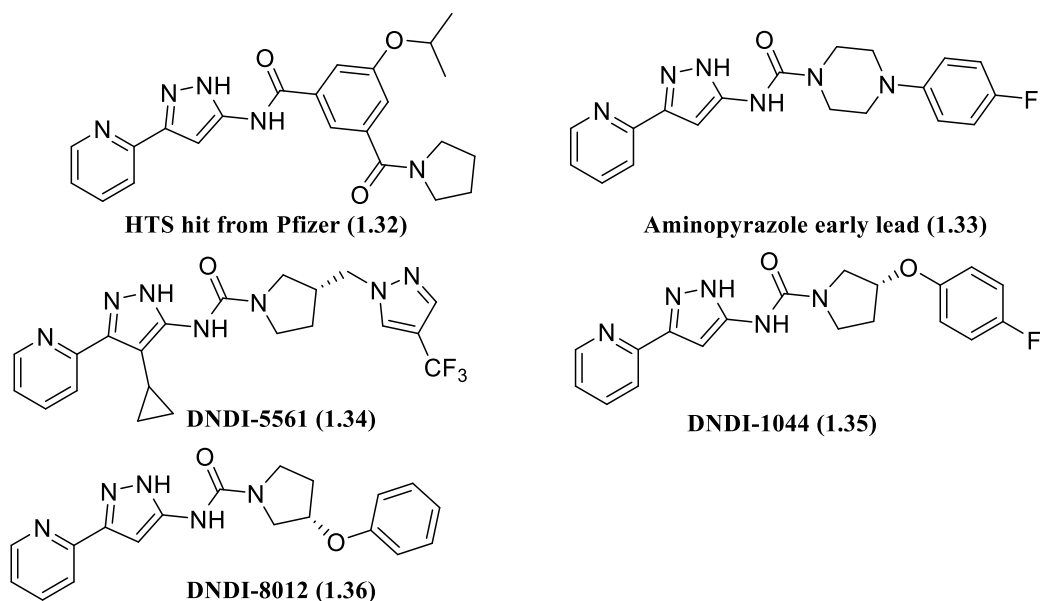


Figure 1.09: Structures of aminopyrazole compounds involved in the leishmaniasis pipeline^{99, 139, 141}

Pyrazolopyrimidines

The pyrazolopyrimidine compound class has previously been reported to possess diverse biological activity for application against various indications including anti-infectives, insecticides and kinase inhibition.¹⁴² As such they have become a scaffold of interest in various antiprotozoan investigations. A target-based high-throughput screen against *T. brucei* GSK3 kinase led to the identification of a diaminothiazole series (**1.37**).^{28, 143, 144} During explorations surrounding this series, Wyllie *et al.* report the antiparasitic activity observed was due to off-target activity.¹⁴⁴ Further probing, scaffold hoping and in-depth medicinal chemistry efforts by GlaxoSmithKline (GSK) and Dundee University led to the development of a novel pyrazolopyrimidine series against *L. donovani*.^{143, 144}

Current lead candidate GSK3186899/DDD853651 (**1.39**) displays good *in vitro* activity against *L. donovani* axenic and intracellular amastigotes within macrophage host cells (intramacrophage), with EC₅₀ values of 0.017 μ M and 1.4 μ M respectively. As a comparison, amphotericin B, miltefosine and paromomycin report intramacrophage EC₅₀ values of 0.07 μ M, 0.9 μ M and 6.6 μ M respectively.^{28, 144} Selectivity for parasites over THP-1 host cell lines was also observed (EC₅₀ > 50 μ M). Stability when incubated with liver microsomes and hepatocytes (mouse, rat, dog and human) and good oral

bioavailability in mice. Using an *in vivo* *L. donovani* mouse model, the compound significantly reduced parasite burden by 99% when dosed at 25 mg/mg b.i.d. for 10 days, orally.^{28, 144} Subsequent mode of action studies on this series have revealed Cdc-2-related kinase 12 (CRK12) inhibition as the primary mechanism of action. However, the complete function of this kinase has yet to be elucidated. Despite this, the deconvolution of a druggable target is still an impressive feat as currently there are so few chemically validated drug targets in *Leishmania* spp.^{28, 144} The candidate GSK3186899/DDD853651 has completed preclinical safety assessments. In 2019 this compound entered Phase 1 clinical trials to evaluate the safety, tolerability and PK profile in healthy subjects (Clinical trial identifier: NCT03874234). At time of writing, this study is currently suspended due to toxicity findings in a preclinical compound (not disclosed) with the same mechanism of action. This study is on hold so the developers, GSK can investigate the implications of these findings.^{74, 145}

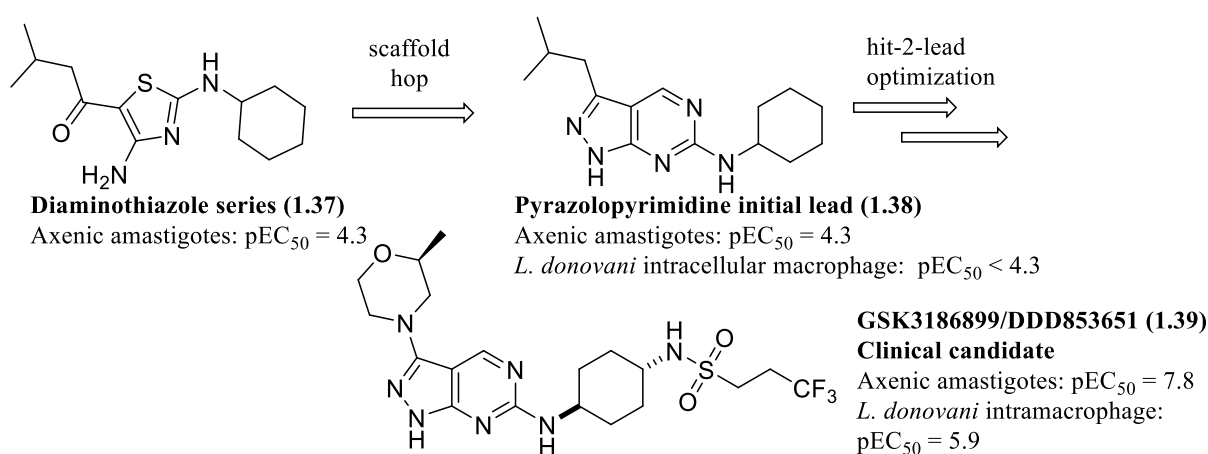


Figure 1.10: Optimization of pyrazolopyrimidine series involved in the leishmaniasis pipeline¹⁴³

Proteasome inhibitors

A massive high-throughput phenotypic screen of small molecules was carried out in 2016, by Novartis in collaboration with Wellcome Trust. A starting library of over 3 million compounds were screened against *L. donovani*, *T. cruzi* and *T. brucei*. This was followed by triaging of active compounds selective for parasites over mammalian cell lines (EC₅₀ < 10 µM, > fivefold selectivity). The azabenzoxazole hit GNF5343 (**1.40**) was identified in the *T. brucei* and *L. donovani* screens (EC₅₀ = 7.3 µM, intramacrophage *L. donovani*). An impressive optimization campaign of GNF5343 was reported to involve the design and synthesis of around 3000 compounds in order to improve bioavailability and efficacy against intracellular *L. donovani* parasites growth within host macrophages. This led to the identification of GNF6702 (**1.41**), which exhibited an EC₅₀ of 18 nM, a 400-fold increase of potency against intramacrophage *L. donovani* compared to the original hit. Oral dosing of *in vivo* *L. donovani* mouse models using a dosing regimen of 10 mg/kg b.i.d for 8 days with GNF6702 gave a 90% reduction of parasite burden in the liver, despite low bioavailability (F = 34%). This compound also displayed significant curative effects in *T. brucei* and *T. cruzi* models.^{28, 146}

Since this compound exhibited broad spectrum anti-kinetoplastid activity mechanistic studies were undertaken. Mechanistic studies revealed GNF6702 to act as an allosteric proteasome inhibitor selective to the kinetoplastids.¹⁴⁶ The $\beta 5$ subunit of the 20S proteasome was identified as the target, blocking chymotrypsin-like activity through noncompetitive mechanism.¹⁴⁶⁻¹⁴⁸ The $\beta 5$ subunit is an essential subunit which contributed to the complete assembly of the 20S proteasome complex.¹⁴⁹ Inhibition of proteasomes prevents the degradation of damaged and non-functional proteins, causing build up and eventual apoptosis.¹⁵⁰ This compound was not continued into clinical testing due to solubility limited oral absorption.¹⁵¹ Despite this, the elucidation of a pan-kinetoplastid druggable target is significant to the neglected disease drug discovery niche. Additionally, this series has led to the development of the analogue LXE-408 (**1.42**), which exhibited an EC₅₀ of 40 nM against *L. donovani* amastigotes within mouse macrophages and was found to reduce liver parasite burden by 95% in VL murine models. To determine the efficacy of this *in vivo* model, LXE-408 was administered orally at 1 mg/kg b.i.d..¹⁵¹ This compound is now a first in class compound undergoing clinical trials for oral treatment of VL. Novartis was responsible for completing Phase I studies and will now collaborate with DNDi to jointly develop this candidate as a new potential oral treatment for VL. DNDi will lead Phase II studies scheduled for early 2021 in India. Additional trials are planned to take place in East Africa.^{74, 152}

Researchers from GSK and the University of Dundee have also recently reported another proteasome inhibitor GSK3494245/ DDD1305143 (**1.44**) as a lead candidate for VL treatment. This compound was developed through SAR studies and scaffold hopping based on a hit (**1.43**) taken from a separate phenotypic screen. Interestingly, this starting compound is very close to the hit compound (**1.40**) in which Novartis used. The lead compound GSK3494245/ DDD1305143 (**1.46**) displayed efficacy *in vitro* (EC₅₀ = 1.6 μ M intramacrophage *L. donovani*) and *in vivo* (>95 % reduction of *L. donovani* in mouse model at 25 mg/kg b.i.d, 10 days). Mechanism studies around the imidazopyrimidine series discovered a novel binding site for chymotrypsin-like activity inhibition. The site lies between the $\beta 4$ and $\beta 5$ of the 20S proteasome. Wylie *et al.* report the exploitation of an induced cavity on one side by $\beta 4$ residues unique to protozoans.¹⁵³ This binding pocket differs from the binding site Khare *et al.* report for GNF6702.^{146, 153} At time of writing, this candidate is currently in the recruitment stage of a Phase I single ascending dose study (Clinical trials identifier: NCT04504435) to be developed as a treatment for VL.^{74, 154, 155} These proteasome inhibitors are a promising example of combining phenotypic drug discovery and subsequent target-based methods to achieve potent candidates and further understand their mode of action for translation and development stages.

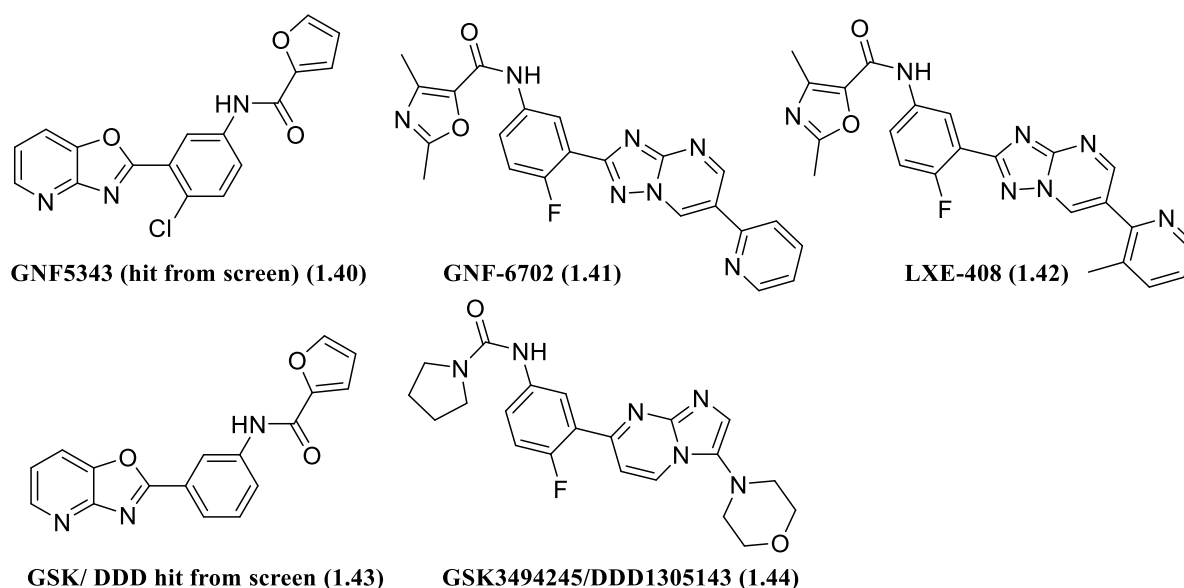


Figure 1.11: Structures of proteasome inhibitors involved in the leishmaniasis pipeline^{146, 151, 153}

A summary of the described the new compound classes previously detailed is depicted in **Table 1.04**. The continuous investigations of each class suggest the leishmaniasis pipeline may be closer to achieving a new efficacious therapeutic that may satisfy more of the TPP requirements than current therapeutics, thus more adaptable to the field.

Table 1.04: Summary of new notable compounds in the VL pipeline^{67, 74, 83, 84, 89, 94, 116, 118, 124, 129, 140, 152, 154, 155}

Compound series	Stage of development
Aminopyrazoles	Discovery (Lead optimization)
Benzoxaboroles DNDI-6148 (1.17)	Translation (Phase I Clinical trials) DNDI-5421 and DNDI-5610 lead optimization back ups
Nitroimidazoles DNDI-0690 (1.22)	Translation (Phase I Clinical trials)
Nitroimidazoles DNDI-8219 (1.23)	Discovery (Lead optimization last reported)
NTD Booster project	Discovery (Hit-to-lead optimization)
Protease inhibitors NVF (1.26) LPV (1.28)	Discovery (Combination studies with known treatments last reported)
Proteosome inhibitors LXE-408 (1.42)	Development (Phase II Clinical trials)
Proteosome inhibitors GSK3494245 / DDD1305143 (1.44)	Translation (preclinical)
Pyrazolopyrimidines GSK3186899/DDD853651 (1.39)	Translation (Phase I Clinical trials)
SERM based compounds Tamoxifen (1.29)	Development (completed pilot Phase II for CL, further status unknown)
SERM based compounds Benzothiophenes	Discovery (hit-to-lead optimization)

1.07 Target based drug discovery and phenotypic screening based drug discovery

Target based drug discovery and screening strategies are an example of another well-known method for discovering NCEs, involving screens against a defined target of interest, followed by subsequent optimization of identified active compounds for cellular activity against the enzyme/ pathway and improving selectivity.⁸⁵ To assist with target-based discovery, various open access virtual platforms such as the Tropical Disease Research (TDR) Targets database (hosted by WHO) are available to access chemogenomics resources and prioritize targets in complete genomes. These tools can examine of linkages between small molecules and genes (known and predicted) and give insight into whether certain target proteins could be druggable.¹⁵⁶

Other notable databases such as LmSmdB, for metabolic network simulation of *L. major* and LeishMicrosatDB, a search engine for microsatellite sequences in *Leishmania spp.* genomes, are also available to assist target-based discovery. Ferreira *et al.* states these advances have led to many protein structures from *Leishmania spp.* being registered in the Protein Data Bank, which have provided key insights into the parasite's "molecular machinery" and interspecies variability, vital information for broad-spectrum drug development.¹⁵⁷ However, current issues with confirming target effects of active compounds and the poor translation from biochemical to cellular activity and *in vivo* efficacy serve as major drawbacks. Poor permeability or ability to delivery activity under the acidic conditions of the macrophage parasitophorous vacuole in which intracellular amastigotes reside can contribute to the translational disconnect.^{85, 133, 138} Furthermore, due to the limited number of known and fully validated targets, this approach remains less applied in *Leishmania* drug discovery.¹³⁸ The advantage of preferred phenotypic HTS is the ability to demonstrate a direct impact on the parasite, determine potential off-target host cell toxicity and facilitates insights into compound cell permeability and stability within the unique host parasite environment. Kinetoplastids can harbour multiple proteins or pathways which would not have been identified though target-based screens. Notwithstanding the productivity of the phenotypic approach in NTD drug discovery, knowledge of molecular target or mode of action can be a key advantage for future optimization of compound leads, as well as identifying any existing target-specific liabilities.^{85, 133, 138} Target deconvolution can be employed on chosen lead series to elucidate molecular targets and assist in further synthetic optimization or scaffold hopping.

Development and comparison of *in vitro* assays has led to a more physiologically relevant and reliable model of phenotypic *in vitro* screening assays.^{28, 85, 158} Free living promastigotes have previously been used *in vitro* as they are easy to culture and handle, however they represent the insect-stage of the parasite lifecycle and have been noted to cause false positives. Freitas-Junior *et al.* report a mere 4% of compounds identified using *Leishmania* promastigotes translated into hits against intracellular amastigotes.^{30, 158} Furthermore, De Rycker *et al.* assessed the translation between axenic and intracellular amastigotes, reporting a lack of correlation between both platforms. Axenic amastigotes

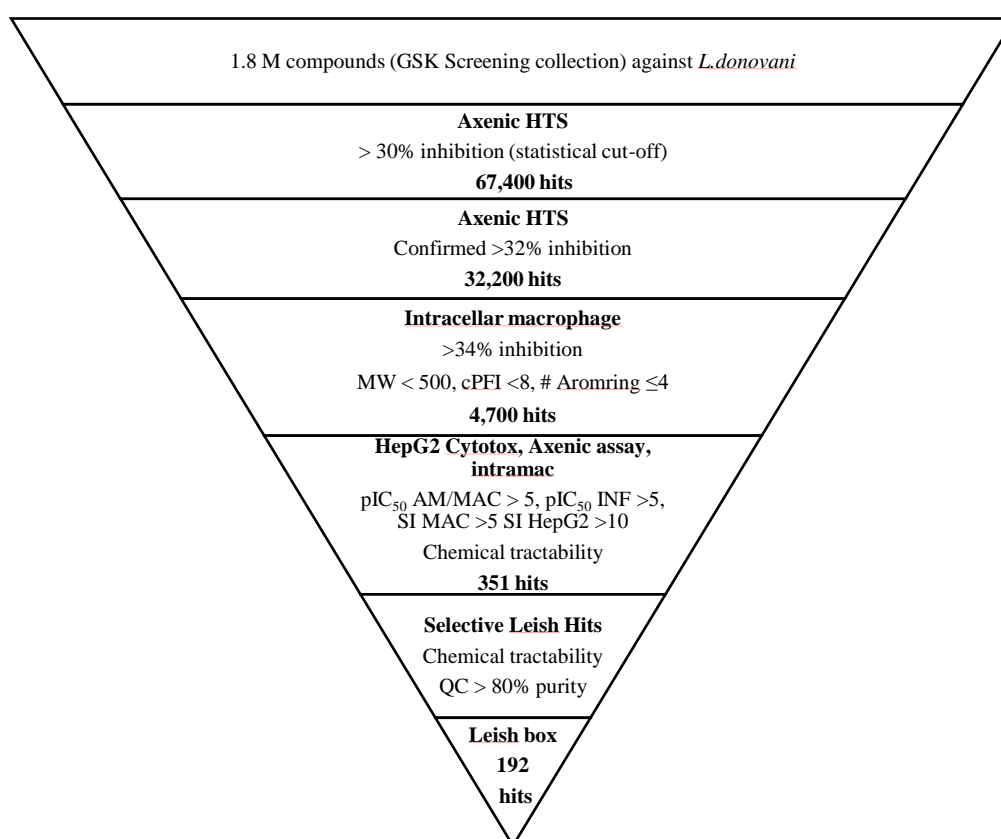
were found to be much more sensitive than the intracellular assay, likely due to the decreased number of barriers. The axenic amastigote platform has been utilized in various high throughput screening efforts, including those undertaken by GSK and Novartis. The former was used as a starting point for screening cascades using intracellular imaging assays, with macrophage host cells (intramacrophage assays).^{85, 88, 134} The intramacrophage amastigote assay is now considered the closest approximation to the clinically prevalent form of the disease.^{85, 134} As a result, HTS using high-content screening of intramacrophage amastigotes is considered the “gold standard” of *Leishmania* drug discovery.^{85, 138} Thus, majority of compound assessment in the scope of our project will be tested using the clinically relevant intramacrophage assays. A significant drawback to phenotypic drug discovery for leishmaniasis is the low compound hit rate, particularly in intracellular assays. This may be due to the intracellular environment which once again gives rise to physiological barriers reaching the acidic phagolysosomal environment in which the parasite resides.^{158, 159} Furthermore, since intracellular amastigotes replicate quite slowly, many of the intracellular assays may only report cytotoxic compounds, contributing to the low hit rate. This also causes further difficulty with the identification of weak or poorly selective hits that may be potentially valuable with optimization.¹³² However, these methods can by-pass the need for further cytotoxicity assessment and compound activity has been reported to translate into *in vivo* activity if PK properties are well optimized.^{132, 160}

1.08 High-throughput screen by GSK in relation to thesis scope⁸⁸

Despite the low hit rates, further efforts using phenotypic HTS have been undertaken in order to identify new compounds classes to be optimized as potential leads for leishmaniasis drug discovery.¹⁶¹ In search of new chemotypes GlaxoSmithKline (GSK) performed a high-throughput screen (HTS) of a diversity set of 1.8 million compounds against whole cell phenotypic assays for three related kinetoplastids: *Leishmania donovani*, *Trypanosoma cruzi* and *Trypanosoma brucei*. This resulted in a chemical box for each disease with approximately 200 compounds assembled. All data is open to the public to encourage research and drug discovery to combat these neglected diseases.⁸⁸

Growth inhibition was initially assessed in an *L. donovani* axenic amastigote assay as a primary screen. An average statistical cut-off of >30% was reported to yield 67,400 hits and an overall hit rate of 4%. This was further narrowed down to 32,200 hits upon assay repetition to confirm activity. These compounds were tested in an intracellular orthogonal assay of *L. donovani* infected THP-1 derived macrophage. The statistical cut off reviewing amastigotes per macrophage output was >34%. Physicochemical parameters to predict lead-likeness were used to further narrow down compounds. Compounds with high molecular weight, high calculated Property Forecast Index (cPFI= Chrom log $D_{pH7.4} + \#Ar$) >8 and compounds with more than 5 aromatic rings were filtered out as unlikely drug candidates (poor lead-likeness properties), leaving 4,700 hits.^{88, 162} Property forecast index is a measurement of drug “developability” used by GSK. A lower PFI (<7) is desirable as hydrophobicity

and number of aromatic rings affect compound solubility and ability to develop a compound further. A high PFI is correlated to increased clearance rates, protein binding, hERG issues and promiscuity, predicting possible unwanted interactions.¹⁶³ Compound activity was examined (pIC_{50}) in dose response experiments and cytotoxicity was assessed using HepG2 cell lines. Selectivity of hits for parasites over host cells (selectivity index) also helped narrow down this to 351 non cytotoxic antileishmanial hits. Hit compounds were triaged for lead-like properties, e.g following Lipinski's Rule of Five, more developability with a lower number of aromatic rings.¹⁶⁴⁻¹⁶⁶ The remaining hits were chemically clustered and filtered based on desirable physicochemical properties. No more than two members of the same class were selected for the chemical box to allow for chemical diversity. A final set of 192 compounds active against *L. donovani* were published. **Figure 1.12** summarizes the selection of hits. Database searches showed that 88% of compounds in all three boxes were not previously published. Additionally, these boxes don't contain any analogues used in current treatments for leishmaniasis, Chagas disease or sleeping sickness. Therefore, they represent a highly novel chemical diversity set for potential lead compounds in drug discovery for protozoan antiparasitic agents. The progression of the hit compounds identified through these various screens is ongoing, and the success will be determined over the coming years.⁸⁵



AM/MAC, ratio of amastigotes per macrophage as output from imaging assay; INF, percentage of infected host cell as output from imaging assay; SI MAC, selectivity index as ratio of IC_{50} versus macrophages over IC_{50} versus amastigotes; SI HepG2, selectivity index as ratio of IC_{50} versus HepG2 cells over IC_{50} versus amastigote

Figure 1.12: Triaging criteria for determining the *Leishmania* box⁸⁸

1.09 Selected compounds for hit-to-lead SAR exploration

For this project specifically, two compounds hits TCMDC-143315 (**1.45**) and TCMDC-143305 (**1.46**) were initially chosen, shown in **Figure 1.13**. An in-depth SAR investigation surrounding their chemical space is the focus of Chapters 2 and 3. As shown in **Table 1.05**, this compound class will act as an attractive starting point for medicinal chemistry optimization and are novel scaffolds in the literature. High potency and selectivity are shown for this class with $\text{pIC}_{50} \sim 6$ against *L. donovani* and low cytotoxicity in THP-1 host macrophages and HepG2 cell lines ($\text{pIC}_{50} = 4.3, 4.0$ respectively), showing that the compounds are 100-fold more selective for *L. donovani* over this mammalian cell line.

Sterol 14 α -demethylase (CYP51) inhibitors have known activity against kinetoplastids and was previously a commonly targeted mechanisms for kinetoplastid drug discovery. However, it was shown that inhibition of this target does not achieve complete clearance of parasitaemia. This was evidenced by potent azoles trialled as CYP51 inhibitors which reported clinical failure against *T. cruzi*. The re-emergence of parasites was observed in a significant number of patients after completing the dosing regimen.¹⁶⁷⁻¹⁷⁰ As a result it has now become more prudent within the anti-kinetoplastid drug discovery community, to employ CYP51 counter screens against phenotypic hits in order to avoid new starting points that are predominantly driven by CYP51 inhibition.¹⁶⁹ Therefore, part of our own selection criteria was to prioritise hits reported by Pena *et al* that did not appear to be acting via this inhibition pathway.⁸⁸

The compounds physicochemical properties are ideal for investigative hits. They possess a low molecular weight (< 500 Da) and suitable partition co-efficient values ($\text{Log P} < 5$). Less than 5 hydrogen bond donors and less than 10 hydrogen bond acceptors are present on these hits. These properties would allow for structural diversification, a balance of solubility and permeability, thus offering the possibility for oral availability, following Lipinski's Rule of Five.¹⁶⁵ This is reinforced by Veber's rule where our chosen compounds possess a relatively low polar surface area ($\leq 140 \text{ \AA}^2$), and number of rotatable bonds (≤ 10) as well as ideal "developability" with a lower number of aromatic rings where larger or more lipophilic functionalities may be added if required.^{166, 171} The target and mechanism of action is not yet known, as they were found through a phenotypic screen.

No previous SAR investigations for these systems have been published, leaving ample room for medicinal chemistry optimization, making these hits an attractive starting point. Previous work by GSK led to the synthesis of a small library containing around 30 active analogues surrounding TCMDC-143305 and 143115. Within this library, GSK observed a correlation between activity and host cell cytotoxicity across this chemical series. This information is currently un-published, and they are not at

liberty to disclose the data. GSK have indicated that cytotoxicity was observed *in vitro* with compounds displaying pIC_{50} (*L. donovani* in infected macrophages) > 5.2. They have specified there is not a structural moiety that can explain the cytotoxicity observed in the macrophage, HepG2 or both cell lines. This phenomenon is not observed in our initial hits TCMDC-143305 and 143115. Compound toxicity was assessed and Pena *et al.* reported our chosen hits to be non-cytotoxic towards HepG2 and THP-1 cell lines, whilst displaying high activity against parasites within THP-1 host macrophages.⁸⁸ Therefore, the first step in this investigation would focus on finding analogues that achieve lower host cell cytotoxicity whilst maintaining and improving activity.

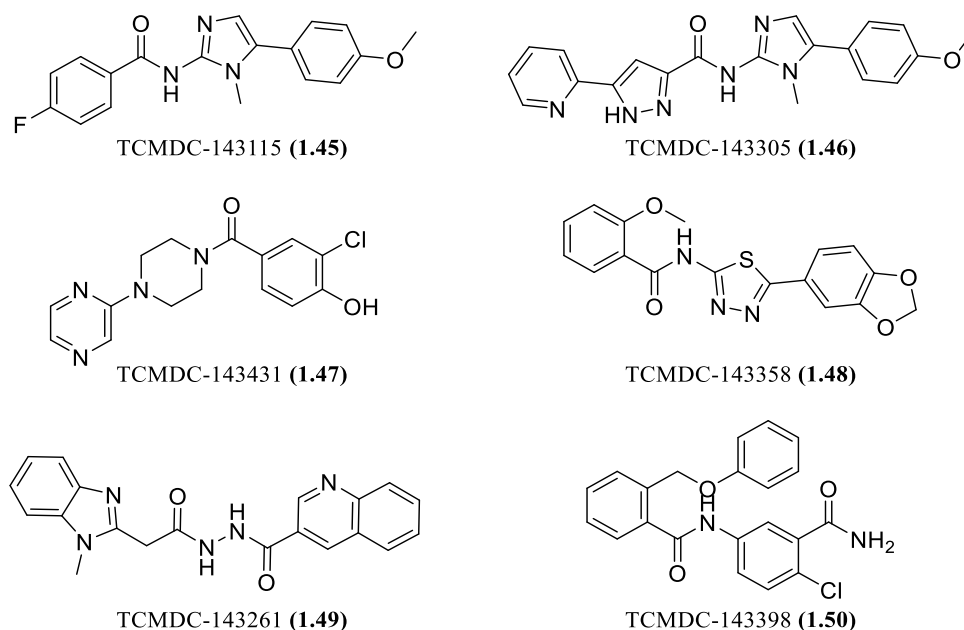


Figure 1.13: Hits selected from GSK HTS for hit-to-lead optimization studies⁸⁸

Table 1.05: Properties of selected hits from GSK HTS for hit-to-lead optimization studies⁸⁸

		TCMDC -143115 (1.45)	TCMDC -143305 (1.46)	TCMDC -143431 (1.47)	TCMDC -143358 (1.48)	TCMDC -143261 (1.49)	TCMDC -143398 (1.50)
Anti <i>L. donovani</i> activity	pIC_{50} <i>L. donovani</i> FLINT	5.5	5.4	6.5	6.4	5.2	5.1
	pIC_{50} <i>L. donovani</i> in infected macrophages	5.9	6.0	5.3	6.5	5.9	5.5
	pIC_{50} <i>L. donovani</i> imaging: Amastigotes/ Macrophages	6.3	6.1	5.5	7.1	6.1	5.8
CYP51 Inhibition	pIC_{50} CYP51	5.0	4.8	4.0	5.2	4.5	4.1
Cytotoxicity	pIC_{50} HepG2	4.0	4.0	4.0	4.0	4.0	4.0
	pIC_{50} <i>L. donovani</i> Imaging: THP-1	4.3	4.3	4.3	4.3	4.3	4.8

	Host Macrophages						
	Inhibitory frequency index (IFI)	4.8	3.7	0.96	2.2	1.8	2.4
Physico-chemical properties	cLog P	3.6	3.2	1.4	3.3	2.5	2.8
	Molecular weight (Da)	325	374	319	358	359	381
	Polar Surface Area (tPSA, Å ²)	56	98	70	69	90	81

Other compound classes were investigated in order to optimize different scaffolds with potentially unique mode of actions to that of Scaffold 1 (Compound **1.45** and **1.46**). Optimization on more than one scaffold could lead to combinatorial studies. Therefore, compounds **TCMDC-143431 (1.47)**, **TCMDC-143358 (1.48)**, **TCMDC-143261 (1.49)**, **TCMDC-143398 (1.50)** were also later selected from GSK's leishmaniasis box for exploration surrounding their chemical space and discussed in Chapter 4.

Based on biological results and synthetic ease, hit **TCMDC-143398 (1.50)** was further investigated and is the focus of Chapter 5. These hits were also chosen due to their moderate potency against *L. donovani*, low cytotoxicity against host cells and their drug-likeness, i.e. low molecular weight, acceptable Log P values, Hydrogen bonding ability. Little CYP51 inhibition was observed, once again allowing for the possibility of a novel mode of action. Additionally, superior efficacy displayed in the intracellular assay over the primary axenic fluorescent intensity assay (FLINT) was sought after. This suggests a compound to have the required ability to pass various membrane barriers to reach the target intracellular amastigote. The promiscuity of all hit chemotypes was also considered to avoid potential off-target effects. Measuring the Inhibitory frequency index (IFI) profiles of analogues across different target classes and assay technology can distinguish nonspecific nuisance effects from specific assay interference or genuine biological activity. Chakravorty *et al.* classify compound behaviour as follows,

- $0 < IFI \leq 1$: Specific active
- $1 < IFI \leq 2$: Moderately active
- $2 < IFI \leq 5$: Somewhat noisy
- $5 < IFI \leq 10$: Noisy
- $10 < IFI$: Very noisy

Chakravorty *et al.* also notes that there are existing drugs that exhibit noisy behaviour, some of which are antiparasitic or anticancer agents. Some also display specific potent activity against one or few

targets. Therefore, this criterion is not the sole indication of lead candidature.¹⁷² Finally, synthetic access and novelty of these systems makes these selected hits an attractive starting point, as no previous SAR investigations for these systems have been published or investigated by other groups according to GSK. This left an abundant opportunity for medicinal chemistry optimization.

Recent literature surrounding chemical classes

Whilst our hit compound structures are novel, wider substructure and similarity searches surrounding each scaffold were undertaken using Scifinder and Reaxys to understand the current usage and any possible utility these compound classes may be extended to. A few recent examples structurally close to our main scaffolds of interest (compounds **1.45**, **1.46** and **1.50**) are briefly highlighted below, however this is not an exhaustive list. The substructures used during each literature search are listed in the Appendix.

This the broad search found simplified chemotype of **1.45/1.46** to be employed in the therapeutic targeting of interleukin-1 receptor-associated kinase (IRAK) pathway, with focus of inhibition of IRAK4.¹⁷³ These kinases play a central role in inflammatory responses via the expression regulation of inflammatory genes in immune cells. These signals are crucial for the elimination of virus, bacteria and cancer cells.¹⁷⁴ Northwestern University report in their patent several compound structural identities to be assessed for anticancer activity (**Figure 1.14**). The structures of **1.51** and **1.52** are examples of the main IRAK-4 inhibitor scaffolds reported in this patent.¹⁷³ They share similar chemical space (particularly **1.53**) to our own hits TCMCD-143115 (**1.45**)/ TCMDC-143305(**1.46**) and it could be kept in mind that analogues explored in our own antiparasitic project could be investigated for anticancer properties.

Vaden *et al.* recently reported an update on their series derived from marine natural product naamidine A (**1.53**), though containing more complex substituents, the chemical space remains somewhat close to our own Scaffold 1 hits (Compound **1.45** and **1.46**). Their modified analogue, zinaamidole A (**1.54**) was reported as a natural product mimic and highly cancer selective zinc (Zn^{2+}) ionophore. They suggest the *N*²-acyl-2-aminoimidazole core to be a powerful chemotype for inducing cell death in cancer cells and simultaneous disruption of zinc homeostasis.^{175, 176} Structural similarities to zinaamidole A and related analogues further suggest our Scaffold 1 has the ability to be repurposed as an anticancer agent, though further modifications may be required to reach higher potency. Padmavathi *et al.* report a series of pyrrolyl (**1.55**) and the more relevant pyrazolyl (**1.56**)- imidazole, thiazole and oxazole analogues. These compounds, particularly the imidazole core analogues were shown to act as potent antimicrobial agents. Activity was demonstrated against various bacteria (*Pseudomonas aeruginosa*, *Klebsiella pneumoniae*) and fungi (*Penicillium chrysogenum*, *Aspergillus niger*).¹⁷⁷ Close similarities between

analogues by Padmavathi *et al.* and our own compound class once again suggest the possibility of repositioning compounds in future studies.

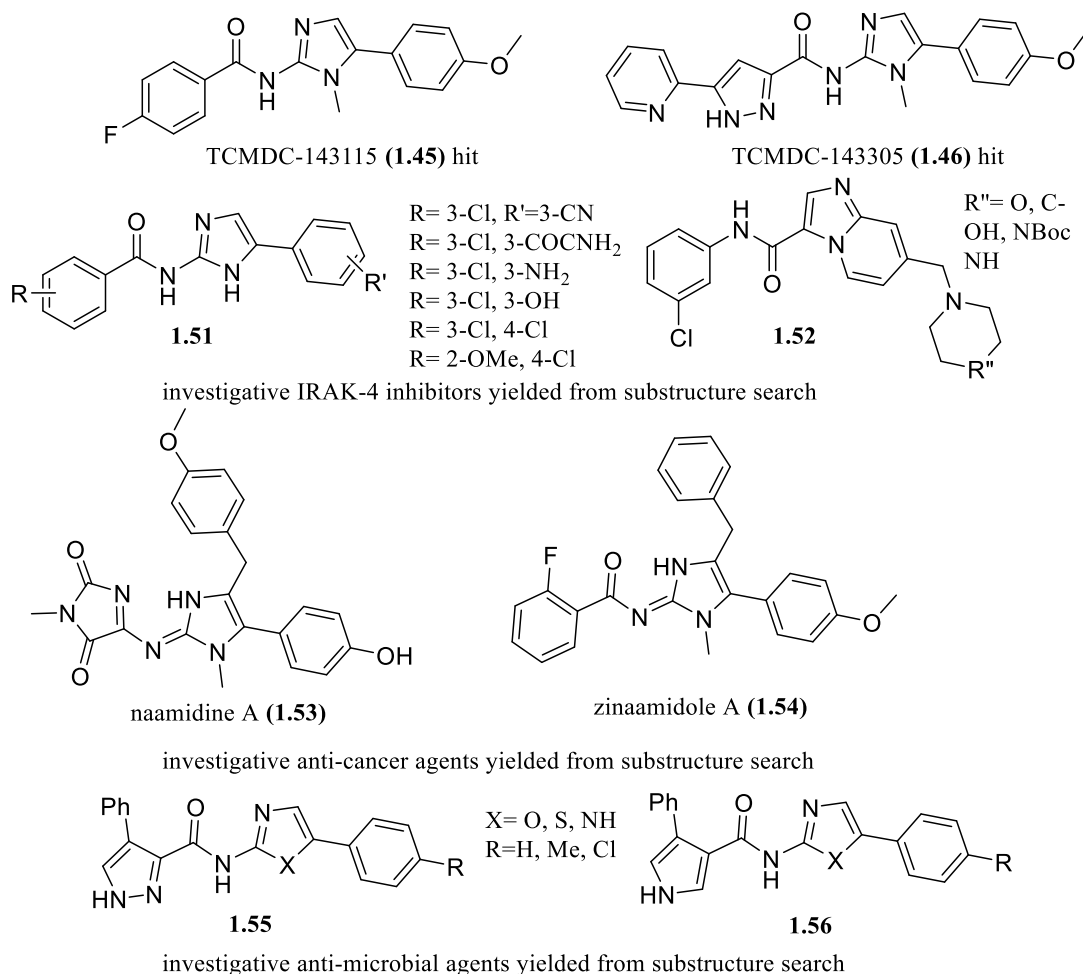


Figure 1.14: Substructure literature search examples surrounding Scaffold 1^{173, 175-177}

Broader scaffold searches of carboxamides for compound **1.50** found Vertex Pharmaceuticals have quite recently identified a number of potent and selective Nav 1.8 sodium channel blockers (**1.57**), characterized as the likely target of analgesia. These compounds share close chemical space to that of **1.50** hit and may lead to the development of a new pain management therapeutic. A few example analogues have been depicted below, though close to our hit, these analogues are more fully developed, possessing a greater number of functionalities.¹⁷⁸

Japan Tobacco Inc developed a series of analogues to be used as nociception opioid receptor antagonists to also be used for pain management (indicated for neuropathic and postoperative pain). Their lead candidate JTC-801 was terminated after Phase II clinical trial completion. Our hit compound **1.50** is closely related to their lead compound JTC-801 (**1.58**), though lacks the essential quinoline functionality the NOP antagonist possesses.¹⁷⁹ Further investigations of our hit **1.50** and subsequent analogues against appropriate assays for analgesic studies may be encouraged. It would be expected our

compounds would be at most weakly active and further modifications may be explored as future work for this scaffold.

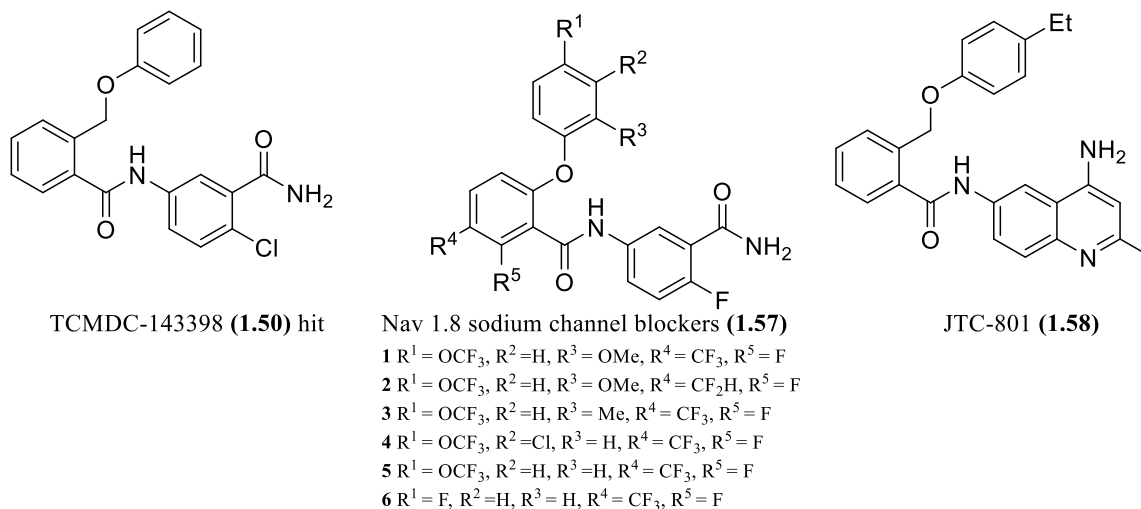


Figure 1.15: Substructure literature search examples surrounding chosen hit compound **1.50**^{178, 179}

Structurally similar compounds to our aforementioned hits **1.47**, **1.48** and **1.49** have been the subject of various recent SAR efforts (**Figure 1.16-1.18**) including but not limited to, optimizations of proline transporter (PROT) inhibitors for Alzheimer's disease (**1.59-1.60**) and negative allosteric modulators of metabotropic glutamate receptor 5 (mGluR5 NAM) for anxiety (**1.61**), in relation to compound **1.47** and FAK inhibitors for anticancer use (**1.62**), antitubercular (**1.63-1.64**) in relation to compound **1.48**. Singh *et al.* also report similar phenyl-1, 3, 4-thiadiazole carboxamide derivatives to possess some anti-inflammatory and antibacterial activity.¹⁸⁰⁻¹⁸⁴ Hydrazides with a similar chemical space to hit **1.49** have also been involved in SAR optimization campaigns for antituberculosis activity and as inhibitors of NF- κ B signalling for anti-inflammatory and anticancer treatments.^{185, 186} These scaffolds were not an on-going major focus, however versatility of these compound classes is suggested by the literature and may be explored in future projects and utilized for other systems.

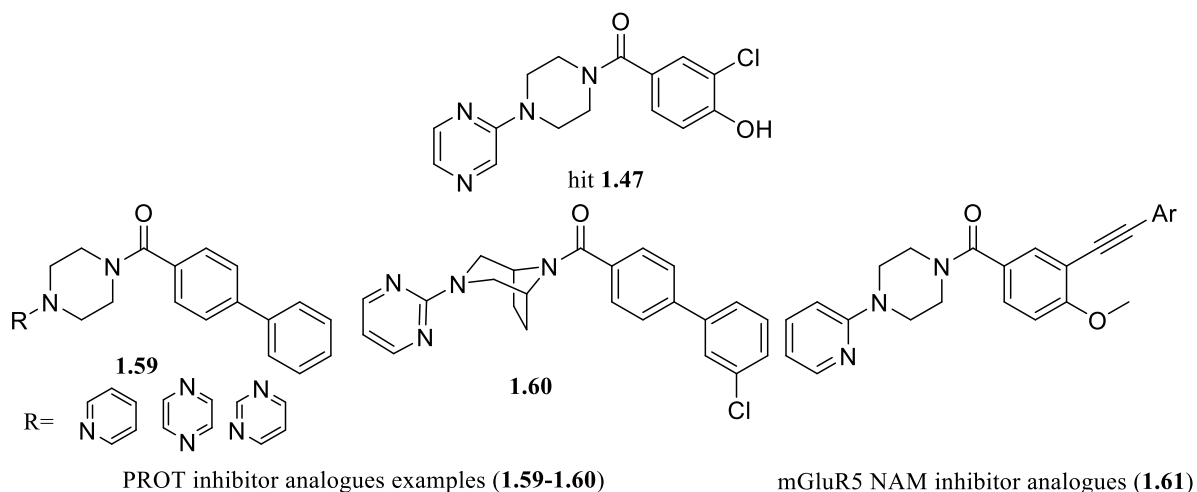


Figure 1.16: Examples of known compounds with structural similarities to hit 1.47 based on literature searches^{180, 181}

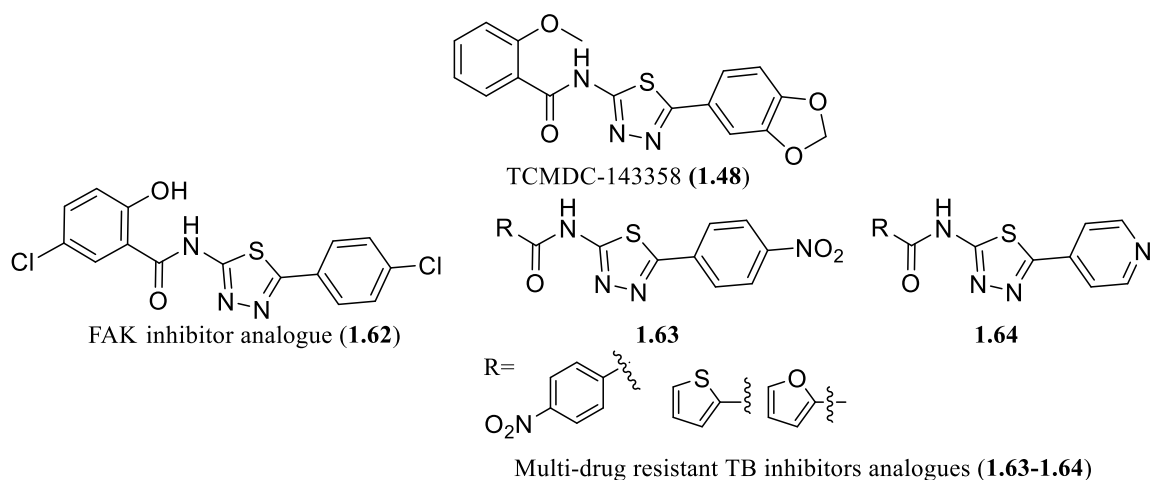


Figure 1.17: Examples of known compounds with structural similarities to hit 1.48 based on literature searches^{182, 183}

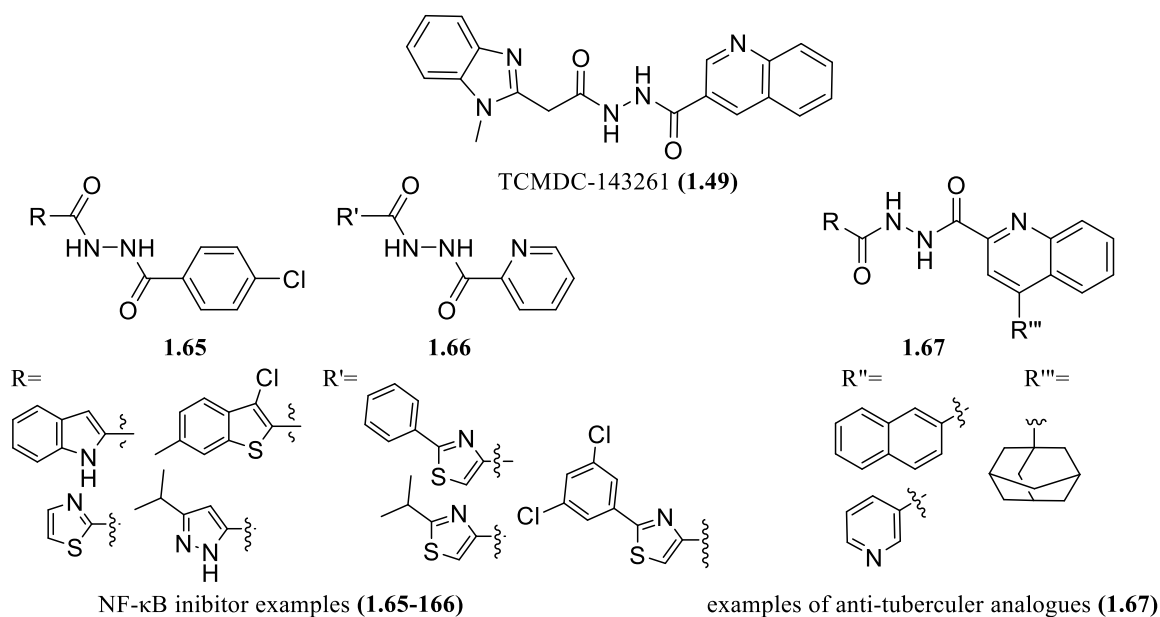


Figure 1.18: Examples of known compounds with structural similarities to hit 1.49 based on literature searches^{185, 186}

Extended screening was very recently undertaken by Lamotte *et al.* using majority of the aforementioned “GSK Leish-Box”. They describe a novel and clinically relevant *ex vivo* strategy to perform parallel, comparative phenotypic high content assays that combines primary murine macrophages and lesion derived *L. donovani* and *L. amazonensis* amastigotes and viability assays on promastigotes from both species, to distinguish stage and/or species-specific compounds. The use of both a viscerotropic (*L. donovani*) and a dermatropic (*L. amazonensis*) species, which are evolutionary distant parasites with distinct biological differences allowed for the identification of 5 compounds with potent broad spectrum antileishmanial activity. Lamotte *et al.* were able to characterize compounds into several categories. In relation to the intracellular macrophage assay these were listed as strong activity against *L. donovani*, weakly active against *L. donovani*, strongly active but toxic to host macrophages, highly toxic to host macrophages and inactive. Comparisons between assays and species further categorized each hit and ultimately a small list of 28 of their “best” compounds against both species was revealed.

Our chosen hits were not on this list and the status of the remaining compounds in the reassessed “GSK Leish-Box” remain unpublished. Though we are not privy to this newly ranked system we cannot underestimate our chosen hits.¹⁸⁷ As previously mentioned, compound hits for leishmaniasis are difficult to come by, though our chosen compounds may have weaker efficacy than initially thought, this is not such a bad thing as scaffold modification and optimization can transform a weaker starting point into a stronger candidate. Although broad-spectrum antileishmanial activity would indeed be a great value-add, at present our main and most accessible targets of interest are viscerotropic species, such as *L. donovani* inhibition. Further modification could also lead to a more broad-spectrum candidate.

1.10 Hypothesis

It is anticipated that synthesis of analogues based around at least of our chosen hit chemotypes namely, **1.45**, **1.46** and **1.50** will provide reasonable SAR, uncovering which substituents of the initial hit are favoured and which are best avoided, to facilitate the design and synthesis of a more active, selective early lead compounds. These primary SAR profiles and early lead compounds would be used to guide further optimizations in the future to reach an efficacious future drug candidate.

1.11 Objectives

During this hit-to-lead project, the aim was to synthesize novel compounds based on the hit compound class that maintain low cytotoxicity in human cells whilst improving their potency. This would enable us to investigate and demonstrate a first-generation SAR profile around novel scaffolds. Beyond this initial project, we aim for these initial studies to guide future SAR elaboration towards optimizing a lead compound with improvements in drug like characteristics, such as potency, metabolic stability and

low cytotoxicity that correlates to the ideals of the DNDi clinical target product profile. In accordance with the industry-agreed target product profile, our ultimate objective beyond the scope of this thesis, is to develop an orally available or injectable drug. This drug would display clinical efficacy greater than 95% with no adverse event that requires monitoring. This drug would be employed for all species of visceral leishmaniasis and post kala-azar dermal leishmaniasis.⁷¹

All newly synthesized compounds were assessed for antileishmanial activity via intracellular assays using *L. donovani*, within macrophage host cells (intramacrophage assays). Any compounds synthesized by another group member will be clearly indicated. The layout of each chapter is written in order of events to give the reader an understanding of our design rationale. The assays required for effective and clinically relevant assessment of *L. donovani* activity are complicated and expensive.

Difficulties arose with long waiting periods and technical issues pertaining to certain groups along as well as divergent activity between assays. Therefore, to quicken compound activity turn around and confirm activity, we were able to commence further collaboration with other groups globally. More than one intramacrophage assay was employed in order to confirm true activity, by independent groups. “True activity” in relation to the scope of this project, is defined here as when a compound displays convergent potent activity ($< 10 \mu\text{M}$) within the majority of independent assays employed to assess bioactivity. Guidelines to determining potent compounds of interest are outlined at length in Chapter 3. Descriptions of assay methodology and any pertaining issues are detailed in Chapters 2 and 3. These biological assays against intramacrophage *L. donovani* were undertaken by our collaborators at the McConville group, Bio21 Institute of Molecular Science and Biotechnology (Bio21), Department of Biochemistry and Pharmacology, University of Melbourne, the Avery group, Griffith Institute for Drug Discovery, Queensland University (GRIDD), the Ainslie group, University of North Carolina at Chapel Hill (UNC) and the No group, *Leishmania* Research Laboratory, Institut Pasteur Korea (IPK). Potential lead compounds/ compounds of interest underwent physicochemical and *in vitro* metabolic evaluation by the Centre for Drug Optimisation, Monash University (CDCO). Overall, the work described in this thesis was a large collaborative effort undertaken in the pursuit for better antileishmanials.

1.12 SAR rationale

Diverse sets of functional groups were explored to understand what properties are preferable for putative binding site/s interaction. Functional groups were chosen based on their steric, hydrophobic and electronic properties. Several key substituents with diverse effects used during this investigation have been highlighted in **Table 1.06**, however this not an exhaustive list. The **Π value** represents the hydrophobicity of a substituent, in other words, the ratio of the concentration of a substituted compound in a mixture between two phases, octanol phase and aqueous phase, in relation to the unsubstituted compound. The higher the **Π value**, the higher partitioning of a compound bearing that substituent to

the octanol phase. Correspondingly, the lower the **Π value** indicates higher partitioning to the aqueous phase. Hydrogen bonding ability is assessed with functionalities containing hydrogen bond donors, hydrogen bond acceptors, both or none. The molar refractivity (MR) value indicates the steric bulk of a functionality. A larger value is indicative of increasingly bulky groups. Finally, electronic effects of substituents are measured by σ values, where a positive value indicated electron withdrawing effect and a negative value indicated an electron donating effect.¹⁸⁸

Ring size, introduction of endocyclic heteroatoms, removing aromaticity will also be considered during substitutions of aryl rings. This will alter compound orientation, sterics, electronic and hydrophobicity properties as well changes in pi-pi stacking with the putative binding site/s. Modifications to rotatable bonds and altering aliphatic chain length to probe changes in flexibility and lipophilicity will be considered. As discussed, currently no SAR information surrounding our chosen hits has been reported nor have they gone biological target elucidation for *Leishmania*, leaving abundant room for medicinal chemistry modifications.

Table 1.06: Parameters used to probe steric, electronic, and hydrophobic properties of some key aryl substituents used for this study^{188, 189}

Substituent	Π^a	HBA ^b	HBD ^c	MR ^d	Electronics ^e	
					σ_m	σ_p
H	0	0	0	1.03	0	0
Br	0.86	0	0	8.88	0.39	0.23
Cl	0.71	0	0	6.03	0.37	0.23
F	0.14	1	0	0.92	0.34	0.06
OH	-0.67	1	1	2.85	0.12	-0.37
NO ₂	-1.23	1	0	7.36	0.71	0.78
NH ₂	-1.23	1	1	5.42	-0.16	-0.66
CF ₃	0.88	0	0	5.02	0.43	0.54
OCF ₃	1.04	1	0	7.86	0.38	0.35
CN	-0.57	1	0	6.33	0.56	0.66
CH ₃	0.56	0	0	5.65	-0.07	-0.17
OCH ₃	-0.02	1	0	7.87	0.12	-0.27
2-pyridyl	0.50	1	0	23.0	0.33	0.17

a= Calculated π value for hydrophobicity, b= Hydrogen-bonding acceptor, c= Hydrogen-bonding donor, d= Molar refractivity, e= Electronic effect, measured by sigma constant derived from different system, *m*: meta, *p*: para.

1.13 Parameters for early hit-to-lead compounds

The focus of this body of work was to explore and develop a primary SAR profile surrounding the novel scaffolds chosen. Beyond SAR elaborations, I also began to investigate the ADMET properties of the potential leads/compounds of interest, which underwent testing using relevant *in vitro* methods. These studies were undertaken to start to identify potential lead compounds. This may help guide future

studies, outside the scope of this project, around developing a more potent and metabolically stable lead-like compounds.

In order to help guide more early and intermediate stage lead compounds I have developed my own set of criteria. Additionally, this could ultimately allow for the design of a future candidate that delivers the objectives required in DNDi's clinical TPP.⁷¹ Multiple parameters have been listed in **Table 1.07** to guide optimization for our early leads and discuss the rationale behind each. However, new early lead compounds would not be required to strictly adhere to every parameter listed, this has been merely included as a suggested guide for early SAR lead-like qualities. A more comprehensive guideline with regards to pharmacokinetics, *in vivo* optimization and safety profiling would be detailed for future campaigns, if a more optimized lead is able to progress to these stages. At present, **Table 1.07** has been included to guide our early stage leads.

Table 1.07: Summary of criteria to guide early SAR hit-to-lead compounds¹⁹⁰

Parameter	Preferred range	Rationale
Activity	Ideal IC ₅₀ < 1 µM (intramacrophage) Acceptable <5 µM Activity confirmed in more than one independent assay	Must exhibit potent antileishmanial activity to be used effectively, though nanomolar range is optimistic, many current therapeutics do not reach this level of activity
Selectivity Index	Ideal SI >10 Acceptable >3	Must be selective for parasite over host cells to avoid high toxicity
cLogP	1-3 more ideal for developability 1-5 Acceptable	Maintains balance volume of distribution with moderate solubility and permeability. Oral bioavailability favourable. ¹⁹¹ Compounds at this LogP still have "developability" where various larger substituents can still be added if required
cLogD	1-3 more ideal for developability 1-5 Acceptable	Same as for cLogP. Use cLogD instead of cLogP if compound is significantly ionized at pH 7.4
tPSA (Å ²)	90-140 Å ²	<140 indicates acceptable oral absorption and membrane permeability. >90 preferred as blood brain barrier penetration is not required. ¹⁷¹
Lipophilic ligand efficacy (LipE/ LLE)	Lipophilic ligand efficiency = pIC ₅₀ - cLogP >3	Differentiates whether compound activity is based on true interaction with putative binding site/sites or is dependent of lipophilicity i.e an increase in lipophilicity of a

		compound has minor improvement in efficacy simply due to increase ability to permeate cell - measures efficiency of each part of the molecule. ¹⁹²
Water Solubility	Intermediate-high aqueous solubility >25µg/mL	Must be able to be solubilized for <i>in vitro</i> methods without crashing out of solution. Poor solubility also correlates to poor bioavailability. ¹⁹³
Intrinsic clearance CL_{int} (<i>in vitro</i>)	Intermediate- low (<40 µL/min/mg microsomal protein, human and mouse microsomes). ¹⁹⁴	Intrinsic clearance is the ability of the microsomal enzymes to metabolize compounds in the absence of protein binding or blood flow limitations. A high intrinsic clearance rate is not ideal, following the same rationale as above, high clearance may provide suboptimal response. ¹⁹⁵ The value of the <i>in vitro</i> CL_{int} assay is taken from the first order degradation rate constant ($CL_{int} = k$ (1/min) / mg/mL protein * 1000 uL/mL)
Microsome predicted hepatic extraction ratio (E_H)	E_H Intermediate (0.3-0.7) to low (< 0.3). ¹⁹⁶⁻¹⁹⁸	The ratio of hepatic clearance (predicted $CL_{int\ hepatic}$) to hepatic blood flow (Q, which is 20.7 mL/min/kg in humans). ^{197, 198}

Intrinsic clearance *in vitro* is the parameter used to assess compound metabolism. The value obtained from this assay does not require other factors or assumptions and is based on the real “raw” data of the *in vitro* assay. Conversion of the CL_{int} *in vitro* to CL_{int} *in vivo* is a common practise, though requires the use of scaling factors (i.e mg microsomal protein/g liver and g liver /kg body weight) which will differ for each species.

Factoring in compound binding to microsomal protein and to blood is also needed and such binding values may not be available. If available, the *in vivo* CL_{int} can be calculated along with the *in vivo* blood clearance and hepatic extraction ratio using the well stirred model of hepatic extraction in each species, according to the “*in vitro* $T_{1/2}$ ” approach described by Obach *et al.*¹⁹⁹ Predicted *in vivo* clearance values were not corrected for microsomal or plasma protein binding, and we cannot assume binding to microsomal proteins is equal to plasma protein binding. Therefore, it has been advised by our CDCO collaborators to focus on the *in vitro* intrinsic clearance measurement for both accuracy and cost effectiveness over the *in vivo* intrinsic clearance measurement. Ultimately, to get a realistic value for the predicted blood clearance and hepatic extraction ratio can require a lot more data than one typically

has in a university student medicinal chemistry project (microsome binding, plasma protein binding and blood to plasma ratio, equilibrium dialysis for binding values), particularly at commencement stages.²⁰⁰ However, for our preliminary studies, these *in vitro* methods and predictive tools will still provide great insight into the metabolic stability of our novel compounds. For convenience, the predicted microsomal hepatic extraction ratio (E_H) was consulted when available. Additionally, the microsomal half-life ($T_{1/2}$, min) was also measured and consulted as a useful metric to understand the elimination rate of our compounds within an *in vitro* system. As with the above measurements, this tool is also *in vitro* based and does not directly reflect *in vivo* models. This must also be measured using further studies as future work.

1.14 Conclusion from literature

The present literature review depicts that:

- Leishmaniasis remains a costly neglected tropical disease which particularly effects the world's poorest populations.
- The visceral manifestation of the disease is fatal within two years if left untreated.
- Current medications are unaffordable to a large majority of the afflicted and are riddled with other drawbacks, including toxicity, ill-suited to the field, inadequate modes of administration and building resistance.
- There is urgent need for new therapeutics with novel models of action
- Despite the efforts of various public-private partnerships, due to the physiological barriers of targeting the parasites, drug discovery efforts are currently experiencing low hit rates during large screens and high attrition rates of developed leads. Meanwhile the number of validated, druggable targets also remains low.

The aim of this research is to help contribute to the large and strenuous efforts of *Leishmania* drug discovery and development. This can be achieved by identifying and reassessing hit molecules discovered through screening campaigns. Even those starting with lower efficacy can still be utilized and subsequently modified towards optimizing lead compounds with improve potency and drug-likeness.

1.15 Chapter 1 References

1. Gibson ME. The identification of kala-azar and the discovery of *Leishmania Donovan*i. *Med Hist*. 1983;27(2):203-213.
2. Steverding D. The history of leishmaniasis. *Parasit Vectors*. 2017;10(1):82.
3. World Health Organization. Global Health Observatory data-Leishmaniasis [Internet]. [cited 2020 May 20]. Available from: <https://www.who.int/data/gho/data/themes/topics/gho-ntd-leishmaniasis>.
4. CDC. Leishmaniasis-Epidemiology & Risk Factors [Internet]. 2020 [cited 2020 May 3]. Available from: <https://www.cdc.gov/parasites/leishmaniasis/epi.html>.
5. Pan American Health Organization. Leishmaniasis factsheet [Internet]. 2017 [cited 2020 May 3]. Available from: <https://www.paho.org/hq/dmdocuments/2017/2017-cha-leishmaniasis-factsheet-work.pdf>.
6. World Health Organization. Leishmaniasis fact sheet [Internet]. 2020 [cited 2020 May 3]. Available from: <https://www.who.int/news-room/fact-sheets/detail/leishmaniasis>.
7. Filardy AA, Guimarães-Pinto K, Nunes MP, Zukeram K, Fliess L, Pereira L, et al. Human Kinetoplastid Protozoan Infections: Where Are We Going Next? *Front Immunol*. 2018;9:1493.
8. Akhoundi M, Kuhls K, Cannet A, Votýpka J, Marty P, Delaunay P, et al. A Historical Overview of the Classification, Evolution, and Dispersion of *Leishmania* Parasites and Sandflies. *PLoS Negl Trop Dis*. 2016;10(3):e0004349.
9. CDC. DPDx - Laboratory Identification of Parasites of Public Health Concern. Leishmaniasis [Internet]. 2017 [cited 2019 April 20]. Available from: <https://www.cdc.gov/dpdx/leishmaniasis/index.html>
10. McCall L-I, Zhang W-W, Matlashewski G. Determinants for the development of visceral leishmaniasis disease. *PLoS Pathog*. 2013;9(1):e1003053.
11. Bereket Alemayehu MA. Leishmaniasis: A Review on Parasite, Vector and Reservoir Host. *Health Sci J*. 2017;11(4): 519.
12. Dey A, Singh S. Transfusion transmitted leishmaniasis: A case report and review of literature. *Indian J Med Microbiol*. 2006; 24 (3): 165-170.
13. Cruz I, Morales MA, Noguer I, Rodriguez A, Alvar J. *Leishmania* in discarded syringes from intravenous drug users. *Lancet*. 2002;359(9312):1124-1125.
14. Herwaldt BL. Laboratory-Acquired Parasitic Infections from Accidental Exposures. *Clin Microbiol Rev*. 2001;14(4):659-688.
15. Meinecke CK, Schottelius J, Oskam L, Fleischer B. Congenital Transmission of Visceral Leishmaniasis (Kala Azar) From an Asymptomatic Mother to Her Child. *Pediatrics*. 1999;104(5):e65.
16. Velez R, Ballart C, Domenech E, Abras A, Fernández-Arévalo A, Gómez SA, et al. Seroprevalence of canine *Leishmania infantum* infection in the Mediterranean region and identification

- of risk factors: The example of North-Eastern and Pyrenean areas of Spain. *Prev Vet Med.* 2019;162:67-75.
17. Ferroglio E, Maroli M, Gastaldo S, Mignone W, Rossi L. Canine leishmaniasis, Italy. *Emerg Infect Dis.* 2005;11(10):1618-1620.
 18. CDC. Parasites- Leishmaniasis [Internet]. 2020 [cited 2020 May 3]. Available from: <https://www.cdc.gov/parasites/leishmaniasis/>.
 19. Parasite.org.au. Leishmania [Internet]. [cited 2020 May 3]. Available from: <http://parasite.org.au/para-site/text/leishmania-text.html>.
 20. World Health Organization. Control of the Leishmaniasis : Report of a meeting of the WHO Expert Committee on the Control of Leishmaniasis, Geneva, 22-26 March 2010. Geneva: World Health Organization technical report series. 2010(949): xii-xiii, 1-186.
 21. Balaña-Fouce R, Pérez Pertejo MY, Domínguez-Asenjo B, Gutiérrez-Corbo C, Reguera RM. Walking a tightrope: drug discovery in visceral leishmaniasis. *Drug Discov Today.* 2019; 24(5):1209-1216.
 22. van Griensven J, Diro E, Lopez-Velez R, Boelaert M, Lynen L, Zijlstra E, et al. HIV-1 protease inhibitors for treatment of visceral leishmaniasis in HIV-co-infected individuals. *Lancet Infect Dis.* 2013;13(3):251-259.
 23. Lindoso JAL, Moreira CHV, Cunha MA, Queiroz IT. Visceral leishmaniasis and HIV coinfection: current perspectives. *HIV AIDS (Auckl).* 2018;10:193-201.
 24. Zijlstra EE. The immunology of post-kala-azar dermal leishmaniasis (PKDL). *Parasit Vectors.* 2016;9(1):464.
 25. Ribeiro RR, Michalick MSM, da Silva ME, dos Santos CCP, Frézard FJG, da Silva SM. Canine Leishmaniasis: An Overview of the Current Status and Strategies for Control. *BioMed Res Int.* 2018;2018:3296893.
 26. Okwor I, Uzonna J. Social and Economic Burden of Human Leishmaniasis. *Am J Trop Med Hyg.* 2016;94(3):489-493.
 27. Mardani A. Prevention strategies of transfusion-transmitted parasitic infections (TTPIs): Strengths and challenges of current approaches, and evaluation of the strategies implemented in Iran. *Parasite Epidemiol Control.* 2020;9:e00141.
 28. Reguera RM P-PY, Gutiérrez-Corbo C, Domínguez-Asenjo B, Ordóñez C, García-Estrada C, et al. Current and promising novel drug candidates against visceral leishmaniasis. *Pure Appl Chem.* 2019;91(8):1385-404.
 29. World Health Organization. World Health Organization Model List of Essential Medicines, 21st List, 2019. Geneva: World Health Organization; 2019. Licence: CC BY-NC-SA 3.0 IGO.
 30. Freitas-Junior LH, Chatelain E, Kim HA, Siqueira-Neto JL. Visceral leishmaniasis treatment: What do we have, what do we need and how to deliver it? *Int J Parasitol Drugs Drug Resist.* 2012;2:11-9.

31. Mowbray CE. Chapter 2 Anti-leishmanial Drug Discovery: Past, Present and Future Perspectives. *Drug Discovery for Leishmaniasis: The Royal Society of Chemistry*; 2018. p. 24-36
32. de Menezes JPB, Guedes CES, Petersen ALdOA, Fraga DBM, Veras PST. Advances in Development of New Treatment for Leishmaniasis. *Biomed Res Int*. 2015;2015:815023.
33. Khodabandeh M, Rostami A, Borhani K, Gamble HR, Mohammadi M. Treatment of resistant visceral leishmaniasis with interferon gamma in combination with liposomal amphotericin B and allopurinol. *Parasitol Int*. 2019;72:101934.
34. Srivastava P, Prajapati VK, Rai M, Sundar S. Unusual Case of Resistance to Amphotericin B in Visceral Leishmaniasis in a Region in India Where Leishmaniasis Is Not Endemic. *J Clin Microbiol*. 2011;49(8):3088-3091.
35. Purkait B, Kumar A, Nandi N, Sardar AH, Das S, Kumar S, et al. Mechanism of Amphotericin B Resistance in Clinical Isolates of *Leishmania donovani*. *Antimicrob Agents Chemother*. 2012;56(2):1031-1041.
36. Kumar N, Sinha PK, Pandey K, Verma N, Lal CS, Ranjan A, et al. A rare case of Visceral leishmaniasis with multiple relapse and multi-drug unresponsive: successfully treated with combination therapy. *Int J Clin Pharm*. 2011;33(5):726.
37. Srivastava S, Mishra J, Gupta AK, Singh A, Shankar P, Singh S. Laboratory confirmed miltefosine resistant cases of visceral leishmaniasis from India. *Parasit Vectors*. 2017;10(1):49.
38. Reimão JQ, Pita Pedro DP, Coelho AC. The preclinical discovery and development of oral miltefosine for the treatment of visceral leishmaniasis: a case history. *Expert Opin Drug Discov*. 2020:1-12.
39. Ponte-Sucre A GF, Dujardin J-C, Barrett MP, López-Vélez R, García-Hernández R, et al. . Drug resistance and treatment failure in leishmaniasis: A 21st century challenge. *PLoS Negl Trop Dis* 2017;11(12):e0006052.
40. Carnielli JBT, Monti-Rocha R, Costa DL, Molina Sesana A, Pansini LNN, Segatto M, et al. Natural Resistance of *Leishmania infantum* to Miltefosine Contributes to the Low Efficacy in the Treatment of Visceral Leishmaniasis in Brazil. *Am J Trop Med Hyg*. 2019;101(4):789-794.
41. Tovar J, Wilkinson S, Mottram JC, Fairlamb AH. Evidence that trypanothione reductase is an essential enzyme in *Leishmania* by targeted replacement of the tryA gene locus. *Mol Microbiol*. 1998;29(2):653-660.
42. Chakravarty J, Sundar S. Drug resistance in leishmaniasis. *J Glob Infect Dis*. 2010;2(2):167-176.
43. Perry MR, Prajapati VK, Menten J, Raab A, Feldmann J, Chakraborti D, et al. Arsenic Exposure and Outcomes of Antimonial Treatment in Visceral Leishmaniasis Patients in Bihar, India: A Retrospective Cohort Study. *PLoS Negl Trop Dis*. 2015;9(3):e0003518.

44. Matlashewski G, Arana B, Kroeger A, Battacharya S, Sundar S, Das P, et al. Visceral leishmaniasis: elimination with existing interventions. *Lancet Infect Dis*. 2011;11(4):322-325.
45. Kumar Saha A, Mukherjee T, Bhaduri A. Mechanism of action of amphotericin B on *Leishmania donovani* promastigotes. *Mol Biochem Parasitol*. 1986;19(3):195-200.
46. Maltezou HC. Drug Resistance in Visceral Leishmaniasis. *J Biomed Biotechnol*. 2010;2010:617521.
47. Pinto-Martinez AK, Rodriguez-Durán J, Serrano-Martin X, Hernandez-Rodriguez V, Benaim G. Mechanism of Action of Miltefosine on *Leishmania donovani* Involves the Impairment of Acidocalcisome Function and the Activation of the Sphingosine-Dependent Plasma Membrane Ca(2+) Channel. *Antimicrob Agents Chemother*. 2017;62(1):e01614-17.
48. Wadhone P, Maiti M, Agarwal R, Kamat V, Martin S, Saha B. Miltefosine Promotes IFN- γ -Dominated Anti-Leishmanial Immune Response. *J Immunol*. 2009;182(11):7146-7154.
49. Dorlo TPC, Balasegaram M, Beijnen JH, de Vries PJ. Miltefosine: a review of its pharmacology and therapeutic efficacy in the treatment of leishmaniasis. *J Antimicrob Chemother*. 2012;67(11):2576-97.
50. Maltezou HC. Drug resistance in visceral leishmaniasis. *J Biomed Biotechnol*. 2010;2010:617521.
51. Sunyoto T, Potet J, Boelaert M. Why miltefosine-a life-saving drug for leishmaniasis-is unavailable to people who need it the most. *BMJ Glob Health*. 2018;3(3):e000709.
52. Sundar S, Singh A, Rai M, Prajapati VK, Singh AK, Ostyn B, et al. Efficacy of Miltefosine in the Treatment of Visceral Leishmaniasis in India After a Decade of Use. *Clin Infect Dis*. 2012;55(4):543-550.
53. Rijal S, Ostyn B, Uranw S, Rai K, Bhattarai NR, Dorlo TP, et al. Increasing failure of miltefosine in the treatment of Kala-azar in Nepal and the potential role of parasite drug resistance, reinfection, or noncompliance. *Clin Infect Dis*. 2013;56(11):1530-1538.
54. Ostyn B, Hasker E, Dorlo TPC, Rijal S, Sundar S, Dujardin J-C, et al. Failure of Miltefosine Treatment for Visceral Leishmaniasis in Children and Men in South-East Asia. *PLoS One*. 2014;9(6):e100220.
55. Jhingran A, Chawla B, Saxena S, Barrett MP, Madhubala R. Paromomycin: uptake and resistance in *Leishmania donovani*. *Mol Biochem Parasitol*. 2009;164(2):111-117.
56. Pund S, Joshi A. Chapter 23 - Nanoarchitectures for Neglected Tropical Protozoal Diseases: Challenges and State of the Art. In: Grumezescu AM, editor. *Nano- and Microscale Drug Delivery Systems*; Elsevier; 2017. p. 439-480.
57. Sundar S, Chakravarty J. Paromomycin in the treatment of leishmaniasis. *Expert Opin Investig Drugs*. 2008;17(5):787-794.
58. Piscopo TV, Mallia Azzopardi C. Leishmaniasis. *Postgrad Med J*. 2007;83(976):649-657.

59. Jamil KM, Haque R, Rahman R, Faiz MA, Bhuiyan ATMRH, Kumar A, et al. Effectiveness Study of Paromomycin IM Injection (PMIM) for the Treatment of Visceral Leishmaniasis (VL) in Bangladesh. *PLoS Negl Trop Dis*. 2015;9(10):e0004118.
60. Jamil KM, Haque R, Rahman R, Faiz MA, Bhuiyan ATRH, Kumar A, et al. Effectiveness study of paromomycin IM injection (PMIM) for the treatment of visceral leishmaniasis (VL) in Bangladesh. *PLoS Negl Trop Dis*. 2015;9(10):e0004118.
61. Musa A, Khalil E, Hailu A, Olobo J, Balasegaram M, Omollo R, et al. Sodium stibogluconate (SSG) & paromomycin combination compared to SSG for visceral leishmaniasis in East Africa: a randomised controlled trial. *PLoS Negl Trop Dis*. 2012;6(6):e1674.
62. Stark CG, Vidyashankar C. Leishmaniasis Treatment & Management: Approach Considerations, Pharmacotherapy, Management of Cutaneous Leishmaniasis. [Internet] *Emedicine.medscape.com*. 2020. [cited 2020 May 3]. Available from: <https://emedicine.medscape.com/article/220298-treatment>
63. Sundar S, Chakravarty J. An update on pharmacotherapy for leishmaniasis. *Expert Opin Pharmacother*. 2015;16(2):237-252.
64. Yasur-Landau D, Jaffe CL, David L, Baneth G. Allopurinol Resistance in *Leishmania infantum* from Dogs with Disease Relapse. *PLoS Negl Trop Dis*. 2016;10(1):e0004341.
65. Nascimento LFM, Miranda DFH, Moura LD, Pinho FA, Werneck GL, Khouri R, et al. Allopurinol therapy provides long term clinical improvement, but additional immunotherapy is required for sustained parasite clearance, in *L. infantum*-infected dogs. *Vaccine: X*. 2020;4:100048.
66. Sundar S, Sinha PK, Rai M, Verma DK, Nawin K, Alam S, et al. Comparison of short-course multidrug treatment with standard therapy for visceral leishmaniasis in India: an open-label, non-inferiority, randomised controlled trial. *Lancet*. 2011;377(9764):477-486.
67. Sundar S, Singh A. Chemotherapeutics of visceral leishmaniasis: present and future developments. *Parasitology*. 2018;145(4):481-489.
68. Wasunna M, Njenga S, Balasegaram M, Alexander N, Omollo R, Edwards T, et al. Efficacy and Safety of AmBisome in Combination with Sodium Stibogluconate or Miltefosine and Miltefosine Monotherapy for African Visceral Leishmaniasis: Phase II Randomized Trial. *PLoS Negl Trop Dis*. 2016;10(9):e0004880.
69. Sundar S, Singh A. Recent developments and future prospects in the treatment of visceral leishmaniasis. *Ther Adv Infect Dis*. 2016;3(3-4):98-109.
70. Alvar J, Yactayo S, Bern C. Leishmaniasis and poverty. *Trends Parasitol*. 2006;22(12):552-557.
71. DNDi. Target Product Profile for Visceral Leishmaniasis [Internet]. [cited 2019 April 20]. Available from: <https://dndi.org/diseases/visceral-leishmaniasis/target-product-profile/>

72. Siddharth Jadeja GpkaMBS. Adoption and Reasons for Withdrawal of ICH Q1F Guidelines. *J Young Pharm.* 2016;8(4):500-504.
73. DNDi. Towards a New Generation of Treatments for Leishmaniasis [Internet]. 2018. 1-20 Available from: https://dndi.org/wp-content/uploads/2018/12/DNDi_Leishmaniasis_2018.pdf
74. DNDi. 2019 R&D portfolio in review: Leishmaniasis [Internet]. 2020 [cited 2020 May 3]. Available from: <https://www.dndi.org/2020/media-centre/news-views-stories/news/leishmaniasis-rnd-portfolio-update/>.
75. DNDi. Clinical trial to find new treatment for visceral leishmaniasis begins in eastern Africa [Internet]. 2018 [cited 2020 May 3]. Available from: <https://www.dndi.org/2018/media-centre/press-releases/clinical-trial-find-new-treatment-visceral-leishmaniasis-begins-eastern-africa/>
76. U.S. National Library of Medicine. Miltefosine/Paromomycin Phase III Trial for Treatment of Primary Visceral Leishmaniasis (VL) Patients in Eastern Africa [Internet]. *Clinicaltrials.gov* 2019 [cited 2020 May 5]. Available from: <https://clinicaltrials.gov/ct2/show/NCT03129646>.
77. DNDi. Miltefosine + Paromomycin combination (Africa) [Internet]. 2020 [cited 2020 November 26]. Available from: <https://dndi.org/research-development/portfolio/miltefosine-paromomycin-combo/>.
78. DNDi. New Treatments for HIV/VL [Internet]. 2019 [cited 2020 May 3]. Available from: <https://www.dndi.org/diseases-projects/portfolio/hivvl/>.
79. Diro E, Blesson S, Edwards T, Ritmeijer K, Fikre H, Admassu H, et al. A randomized trial of AmBisome monotherapy and AmBisome and miltefosine combination to treat visceral leishmaniasis in HIV co-infected patients in Ethiopia. *PLoS Negl Trop Dis.* 2019;13(1):e0006988.
80. Clinical Trials Registry India. A randomized trial of AmBisome® single therapy and combination of AmBisome® and miltefosine for the treatment of Kala Azar in HIV positive patients in India [Internet]. 2017 [cited 2020 May 5] Available from: <http://www.ctri.nic.in/Clinicaltrials/pmaindet2.php?trialid=11735>.
81. DNDi. New Treatments for PKDL [Internet]. 2019 [cited 2020 May 5] Available from: <https://www.dndi.org/diseases-projects/portfolio/new-treatments-pkdl/>.
82. U.S. National Library of Medicine. Short Course Regimens for Treatment of PKDL (Sudan) [Internet]. *Clinicaltrials.gov* 2020 [cited 2020 May 5]. Available from: <https://clinicaltrials.gov/ct2/show/NCT03399955>.
83. DNDi. Status of DNDi clinical trials during the COVID-19 pandemic [Internet]. 2020 [cited 2020 May 26]. Available from: <https://www.dndi.org/2020/clinical-trials/status-dndi-clinical-trials-during-covid19-pandemic/>.
84. Thompson AM, O'Connor PD, Marshall AJ, Blaser A, Yardley V, Maes L, et al. Development of (6R)-2-Nitro-6-[4-(trifluoromethoxy)phenoxy]-6,7-dihydro-5H-imidazo[2,1-b][1,3]oxazine (DNDI-8219): A New Lead for Visceral Leishmaniasis. *J Med Chem.* 2018;61(6):2329-2352.

85. Zulfiqar B, Shelper TB, Avery VM. Leishmaniasis drug discovery: recent progress and challenges in assay development. *Drug Discov Today*. 2017;22(10):1516-1531.
86. Liévin-Le Moal V, Loiseau PM. Leishmania hijacking of the macrophage intracellular compartments. *FEBS J*. 2016;283(4):598-607.
87. Wijnant G-J, Croft SL, de la Flor R, Alavijeh M, Yardley V, Brailard S, et al. Pharmacokinetics and Pharmacodynamics of the Nitroimidazole DNDI-0690 in Mouse Models of Cutaneous Leishmaniasis. *Antimicrob Agents Chemother*. 2019;63(9):e00829-19.
88. Peña I, Pilar Manzano M, Cantizani J, Kessler A, Alonso-Padilla J, Bardera AI, et al. New Compound Sets Identified from High Throughput Phenotypic Screening Against Three Kinetoplastid Parasites: An Open Resource. *Sci Rep*. 2015;5:8771.
89. DNDi. NTD Drug Discovery Booster [Internet]. [cited 2020 May 5]. Available from: <https://www.dndi.org/diseases-projects/open-innovation/drug-discovery-booster/>.
90. Alves F, Bilbe G, Blesson S, Goyal V, Monnerat S, Mowbray C, et al. Recent Development of Visceral Leishmaniasis Treatments: Successes, Pitfalls, and Perspectives. *Clin Microbiol Rev*. 2018;31(4):e00048-18.
91. Van den Kerkhof M, Mabile D, Chatelain E, Mowbray CE, Brailard S, Hendrickx S, et al. In vitro and in vivo pharmacodynamics of three novel antileishmanial lead series. *Int J Parasitol Drugs Drug Resist* 2018;8(1):81-86.
92. Lamotte S, Aulner N, Späth GF, Prina E. Discovery of novel hit compounds with broad activity against visceral and cutaneous Leishmania species by comparative phenotypic screening. *Sci Rep*. 2019;9(1):438.
93. Astin JW, Keerthisinghe P, Du L, Sanderson LE, Crosier KE, Crosier PS, et al. Chapter 2 - Innate immune cells and bacterial infection in zebrafish. In: Detrich HW, Westerfield M, Zon LI, editors. *Methods in Cell Biology*. 138: Academic Press; 2017. p. 31-60.
94. DNDi. DNDi R&D Portfolio December 2019 [Internet]. 2019 [cited 2020 April 25]. Available from: <https://www.dndi.org/diseases-projects/portfolio/>.
95. Van Bocxlaer K, Gaukel E, Hauser D, Park SH, Schock S, Yardley V, et al. Topical Treatment for Cutaneous Leishmaniasis: Dermato-Pharmacokinetic Lead Optimization of Benzoxaboroles. *Antimicrob Agents Chemother*. 2018;62(5):e02419-17.
96. Jacobs RT, Nare B, Wring SA, Orr MD, Chen D, Sligar JM, et al. SCYX-7158, an Orally-Active Benzoxaborole for the Treatment of Stage 2 Human African Trypanosomiasis. *PLoS Negl Trop Dis*. 2011;5(6):e1151.
97. DNDi. DNDI-6148 [Internet]. 2019 [cited 2020 April 25]. [Available from: <https://www.dndi.org/diseases-projects/portfolio/dndi-6148/>].
98. Wall RJ, Rico E, Lukac I, Zuccotto F, Elg S, Gilbert IH, et al. Clinical and veterinary trypanocidal benzoxaboroles target CPSF3. *Proc Natl Acad Sci U S A*. 2018;115(38):9616-21.

99. Van Bocxlaer K, Caridha D, Black C, Vesely B, Leed S, Sciotti RJ, et al. Novel benzoxaborole, nitroimidazole and aminopyrazoles with activity against experimental cutaneous leishmaniasis. *Int J Parasitol Drugs Drug Resist*. 2019;11:129-138.
100. Patterson S, Wyllie S. Nitro drugs for the treatment of trypanosomatid diseases: past, present, and future prospects. *Trends Parasitol*. 2014;30(6):289-298.
101. Ferrins L, Rahmani R, Baell JB. Drug discovery and human African trypanosomiasis: a disease less neglected? *Future Med Chem*. 2013;5(15):1801-1841.
102. Buckner FS, Buchynskyy A, Nagendar P, Patrick DA, Gillespie JR, Herbst Z, et al. Phenotypic Drug Discovery for Human African Trypanosomiasis: A Powerful Approach. *Trop Med Infect Dis*. 2020;5(1)23.
103. DNDi. Fexinidazole for Chagas [Internet]. 2019 [cited 2020 May 20]. Available from: <https://www.dndi.org/diseases-projects/portfolio/fexinidazole-chagas/>.
104. Sundar S, Chakravarty J. Investigational drugs for visceral leishmaniasis. *Expert Opin Investig Drugs*. 2015;24(1):43-59.
105. Wyllie S, Patterson S, Stojanovski L, Simeons FRC, Norval S, Kime R, et al. The Anti-Trypanosome Drug Fexinidazole Shows Potential for Treating Visceral Leishmaniasis. *Sci Transl Med*. 2012;4(119):119re1.
106. DNDi. Fexinidazole/Miltefosine Combination (VL) [Internet]. 2016 [cited 2020 May 20]. Available from: <https://www.dndi.org/diseases-projects/portfolio/completed-projects/fexinidazole-vl/>.
107. Patterson S, Wyllie S, Stojanovski L, Perry MR, Simeons FRC, Norval S, et al. The R enantiomer of the antitubercular drug PA-824 as a potential oral treatment for visceral Leishmaniasis. *Antimicrob Agents Chemother*. 2013;57(10):4699-4706.
108. Gupta S, Yardley V, Vishwakarma P, Shivahare R, Sharma B, Launay D, et al. Nitroimidazoxazole compound DNDI-VL-2098: an orally effective preclinical drug candidate for the treatment of visceral leishmaniasis. *J Antimicrob Chemother* 2014;70(2):518-527.
109. Thompson AM, O'Connor PD, Blaser A, Yardley V, Maes L, Gupta S, et al. Repositioning Antitubercular 6-Nitro-2,3-dihydroimidazo[2,1-b][1,3]oxazoles for Neglected Tropical Diseases: Structure–Activity Studies on a Preclinical Candidate for Visceral Leishmaniasis. *J Med Chem*. 2016;59(6):2530-2550.
110. Sasaki H, Haraguchi Y, Itotani M, Kuroda H, Hashizume H, Tomishige T, et al. Synthesis and Antituberculosis Activity of a Novel Series of Optically Active 6-Nitro-2,3-dihydroimidazo[2,1-b]oxazoles. *J Med Chem*. 2006;49(26):7854-7860.
111. Patterson S, Wyllie S, Norval S, Stojanovski L, Simeons FR, Auer JL, et al. The anti-tubercular drug delamanid as a potential oral treatment for visceral leishmaniasis. *Elife*. 2016;5:e09744.
112. Wyllie S, Roberts AJ, Norval S, Patterson S, Foth BJ, Berriman M, et al. Activation of Bicyclic Nitro-drugs by a Novel Nitroreductase (NTR2) in *Leishmania*. *PLoS Pathog*. 2016;12(11):e1005971.

113. Thompson AM, O'Connor PD, Marshall AJ, Yardley V, Maes L, Gupta S, et al. 7-Substituted 2-Nitro-5,6-dihydroimidazo[2,1-b][1,3]oxazines: Novel Antitubercular Agents Lead to a New Preclinical Candidate for Visceral Leishmaniasis. *J Med Chem.* 2017;60(10):4212-4233.
114. DNDi. DNDI-0690 [Internet]. 2019 [cited 2020 May 5]. Available from: <https://www.dndi.org/diseases-projects/portfolio/dndi-0690/>.
115. U.S. National Library of Medicine. Single Oral Dose Escalation Study of DNDI-0690 in Healthy Male Subjects [Internet]. Clinicaltrials.gov 2019 [cited 2020 May 5]. Available from: <https://clinicaltrials.gov/ct2/show/NCT03929016?term=DNDI-0690&draw=2&rank=1#wrapper>.
116. Valdivieso E, Mejías F, Carrillo E, Sánchez C, Moreno J. Potentiation of the leishmanicidal activity of nelfinavir in combination with miltefosine or amphotericin B. *Int J Antimicrob Agents.* 2018;52(5):682-687.
117. Trudel N, Garg R, Messier N, Sundar S, Ouellette M, Tremblay MJ. Intracellular Survival of Leishmania Species That Cause Visceral Leishmaniasis Is Significantly Reduced by HIV-1 Protease Inhibitors. *J Infect Dis.* 2008;198(9):1292-1299.
118. Rebello KM, Andrade-Neto VV, Gomes CRB, de Souza MVN, Branquinha MH, Santos ALS, et al. Miltefosine-Lopinavir Combination Therapy Against Leishmania infantum Infection: In vitro and in vivo Approaches. *Front Cell Infect Microbiol.* 2019;9:229.
119. Zhao C, Papadopoulou B, Tremblay MJ. Leishmania infantum enhances human immunodeficiency virus type-1 replication in primary human macrophages through a complex cytokine network. *Clin Immunol.* 2004;113(1):81-88.
120. Santos LO, Vitória BS, Branquinha MH, Pedroso e Silva CM, Santos ALS, d'Avila-Levy CM. Nelfinavir is effective in inhibiting the multiplication and aspartic peptidase activity of Leishmania species, including strains obtained from HIV-positive patients. *J Antimicrob Chemother.* 2012;68(2):348-353.
121. InterPro. Aspartic peptidase, active site [Internet]. ebi.ac.uk. [cited 2020 May 20]. Available from: <https://www.ebi.ac.uk/interpro/entry/InterPro/IPR001969/#PUB00000522>.
122. Santos LO, Garcia-Gomes AS, Catanho M, Sodre CL, Santos ALS, Branquinha MH, et al. Aspartic peptidases of human pathogenic trypanosomatids: perspectives and trends for chemotherapy. *Curr Med Chem.* 2013;20(25):3116-3133.
123. Miguel DC, Zauli-Nascimento RC, Yokoyama-Yasunaka JKU, Katz S, Barbiéri CL, Uliana SRB. Tamoxifen as a potential antileishmanial agent: efficacy in the treatment of Leishmania braziliensis and Leishmania chagasi infections. *J Antimicrob Chemother.* 2008;63(2):365-368.
124. Bonano VI, Yokoyama-Yasunaka JKU, Miguel DC, Jones SA, Dodge JA, Uliana SRB. Discovery of Synthetic Leishmania Inhibitors by Screening of a 2-Arylbenzothiophene Library. *Chem Biol Drug Des* 2014;83(3):289-296.
125. Eissa MM, Amer EI, El Sawy SMF. Leishmania major: Activity of tamoxifen against experimental cutaneous leishmaniasis. *Exp Parasitol.* 2011;128(4):382-390.

126. Trinconi CT, Reimão JQ, Yokoyama-Yasunaka JKU, Miguel DC, Uliana SRB. Combination Therapy with Tamoxifen and Amphotericin B in Experimental Cutaneous Leishmaniasis. *Antimicrob Agents Chemother*. 2014;58(5):2608-2613.
127. Trinconi CT, Miguel DC, Silber AM, Brown C, Mina JGM, Denny PW, et al. Tamoxifen inhibits the biosynthesis of inositolphosphorylceramide in *Leishmania*. *Int J Parasitol Drugs Drug Resist*. 2018;8(3):475-487.
128. Trinconi CT, Reimão JQ, Coelho AC, Uliana SRB. Efficacy of tamoxifen and miltefosine combined therapy for cutaneous leishmaniasis in the murine model of infection with *Leishmania amazonensis*. *J Antimicrob Chemother*. 2016;71(5):1314-1322.
129. Machado PRL, Ribeiro CS, França-Costa J, Dourado MEF, Trinconi CT, Yokoyama-Yasunaka JKU, et al. Tamoxifen and meglumine antimoniate combined therapy in cutaneous leishmaniasis patients: a randomised trial. *Trop Med Int Health*. 2018;23(9):936-942.
130. Andrade-Neto VV, Cunha-Junior EF, Dos Santos Faioes V, Pereira TM, Silva RL, Leon LL, et al. Leishmaniasis treatment: update of possibilities for drug repurposing. *Frontiers in bioscience (Landmark edition)*. 2018;23:967-996.
131. Reimão JQ, Miguel DC, Taniwaki NN, Trinconi CT, Yokoyama-Yasunaka JKU, Uliana SRB. Antileishmanial activity of the estrogen receptor modulator raloxifene. *PLoS Negl Trop Dis*. 2014;8(5):e2842.
132. Field MC, Horn D, Fairlamb AH, Ferguson MAJ, Gray DW, Read KD, et al. Anti-trypanosomatid drug discovery: an ongoing challenge and a continuing need. *Nat Rev Microbiol*. 2017;15(4):217-31.
133. Roquero I, Cantizani J, Cotillo I, Manzano MP, Kessler A, Martín JJ, et al. Novel chemical starting points for drug discovery in leishmaniasis and Chagas disease. *Int J Parasitol Drugs Drug Resist*. 2019;10:58-68.
134. De Rycker M, Hallyburton I, Thomas J, Campbell L, Wyllie S, Joshi D, et al. Comparison of a High-Throughput High-Content Intracellular *Leishmania donovani* Assay with an Axenic Amastigote Assay. *Antimicrob Agents Chemother*. 2013;57(7):2913-2922.
135. Siqueira-Neto JL, Moon S, Jang J, Yang G, Lee C, Moon HK, et al. An Image-Based High-Content Screening Assay for Compounds Targeting Intracellular *Leishmania donovani* Amastigotes in Human Macrophages. *PLoS Negl Trop Dis*. 2012;6(6):e1671.
136. Dagley MJ, Saunders EC, Simpson KJ, McConville MJ. High-content assay for measuring intracellular growth of *Leishmania* in human macrophages. *Assay Drug Dev Technol*. 2015;13(7):389-401.
137. Charles River Laboratories. High Content Imaging [Internet]. criver.com [cited 2020 May20]. Available from: <https://www.criver.com/products-services/discovery-services/screening-and-profiling-assays/high-content-imaging?region=3701>.

138. Alcântara LM, Ferreira TCS, Gadelha FR, Miguel DC. Challenges in drug discovery targeting TriTryp diseases with an emphasis on leishmaniasis. *Int J Parasitol Drugs Drug Resist.* 2018;8(3):430-439.
139. Mowbray CE, Braillard S, Speed W, Glossop PA, Whitlock GA, Gibson KR, et al. Novel Amino-pyrazole Ureas with Potent In Vitro and In Vivo Antileishmanial Activity. *J Med Chem.* 2015;58(24):9615-9624.
140. DNDi. Aminopyrazoles [Internet]. 2019 [cited 2020 May 5]. Available from: <https://www.dndi.org/diseases-projects/portfolio/aminopyrazoles/>
141. DNDi. Visceral Leishmaniasis Strategy [Internet]. Kampala, 2018. [cited 2020 May 5] Available from: https://www.dndi.org/wp-content/uploads/2018/05/Alves_VLStrategy_LEAP2018.pdf
142. Atta KFM, Ibrahim TM, Farahat OOM, Al-Shargabi TQ, Marei MG, Bekhit AA, et al. Synthesis, modeling and biological evaluation of hybrids from pyrazolo[1,5c]pyrimidine as antileishmanial agents. *Future Med Chem.* 2017;9(16):1913-1929.
143. Thomas MG, De Rycker M, Ajakane M, Albrecht S, Álvarez-Pedraglio AI, Boesche M, et al. Identification of GSK3186899/DDD853651 as a Preclinical Development Candidate for the Treatment of Visceral Leishmaniasis. *J Med Chem.* 2019;62(3):1180-1202.
144. Wyllie S, Thomas M, Patterson S, Crouch S, De Rycker M, Lowe R, et al. Cyclin-dependent kinase 12 is a drug target for visceral leishmaniasis. *Nature.* 2018;560(7717):192-197.
145. U.S. National Library of Medicine. Safety, Tolerability and Pharmacokinetics (PKs) Investigation of GSK3186899 in Healthy Subjects [Internet] Clinicaltrials.gov 2020 [cited 2020 May 26]. Available from: <https://clinicaltrials.gov/ct2/show/NCT03874234?term=GSK-3186899&draw=2&rank=1>.
146. Khare S, Nagle AS, Biggart A, Lai YH, Liang F, Davis LC, et al. Proteasome inhibition for treatment of leishmaniasis, Chagas disease and sleeping sickness. *Nature.* 2016;537(7619):229-233.
147. Vermelho AB, Rodrigues GC, Supuran CT. Why hasn't there been more progress in new Chagas disease drug discovery? *Expert Opin Drug Discov.* 2020;15(2):145-158.
148. Rao SPS, Lakshminarayana SB, Jiricek J, Kaiser M, Ritchie R, Myburgh E, et al. Anti-Trypanosomal Proteasome Inhibitors Cure Hemolymphatic and Meningoencephalic Murine Infection Models of African Trypanosomiasis. *Trop Med Infect Dis.* 2020;5(1):28.
149. Kunjappu MJ, Hochstrasser M. Assembly of the 20S proteasome. *Biochim Biophys Acta.* 2014;1843(1):2-12.
150. Hoeller D, Dikic I. How the proteasome is degraded. *Proc Natl Acad Sci U S A.* 2016;113(47):13266-13268.
151. Nagle A, Biggart A, Be C, Srinivas H, Hein A, Caridha D, et al. Discovery and Characterization of Clinical Candidate LXE408 as a Kinetoplastid-Selective Proteasome Inhibitor for the Treatment of Leishmaniasis. *J Med Chem.* 2020;63(19):10773-10781.

152. DNDi. Novartis and DNDi to collaborate on the development of a new oral drug to treat visceral leishmaniasis [Internet]. 2020 [cited 2020 May 20]. Available from: <https://www.dndi.org/2020/media-centre/press-releases/novartis-dndi-collaborate-development-new-oral-drug-treat-visceral-leishmaniasis/>.
153. Wyllie S, Brand S, Thomas M, De Rycker M, Chung C-w, Pena I, et al. Preclinical candidate for the treatment of visceral leishmaniasis that acts through proteasome inhibition. *Proc Natl Acad Sci U S A*. 2019;116(19):9318-9323.
154. DNDi. GSK3186899/DDD853651 & GSK3494245/DDD1305143 [Internet]. 2019 [cited 2020 May 5]. Available from: <https://www.dndi.org/diseases-projects/portfolio/gsk3186899-ddd853651-gsk3494245-ddd1305143/>.
155. U.S. National Library of Medicine. Safety, Tolerability and Pharmacokinetics (PK) Investigation of GSK3494245 in Healthy Participants [Internet]. Clinicaltrials.gov 2020 [cited 2021 January 21]. Available from: <https://clinicaltrials.gov/ct2/show/NCT04504435>.
156. Manzano JI, Konstantinović J, Scaccabarozzi D, Perea A, Pavić A, Cavicchini L, et al. 4-Aminoquinoline-based compounds as antileishmanial agents that inhibit the energy metabolism of *Leishmania*. *Eur J Med Chem*. 2019;180:28-40.
157. Ferreira LLG, Andricopulo AD. Chemoinformatics Strategies for Leishmaniasis Drug Discovery. *Front Pharmacol*. 2018;9:1278.
158. Reguera RM, Calvo-Álvarez E, Álvarez-Velilla R, Balaña-Fouce R. Target-based vs. phenotypic screenings in *Leishmania* drug discovery: A marriage of convenience or a dialogue of the deaf? *Int J Parasitol Drugs Drug Resist*. 2014;4(3):355-357.
159. McConville MJ, de Souza D, Saunders E, Likic VA, Naderer T. Living in a phagolysosome; metabolism of *Leishmania* amastigotes. *Trends Parasitol*. 2007;23(8):368-375.
160. Don ROB, Ioset J-R. Screening strategies to identify new chemical diversity for drug development to treat kinetoplastid infections. *Parasitology*. 2014;141(1):140-146.
161. Martin J, Cantizani J, Peña I. Chapter 5 The Pursuit of Novel Anti-leishmanial Agents by High-throughput Screening (HTS) of Chemical Libraries. *Drug Discovery for Leishmaniasis: The Royal Society of Chemistry*; 2018. p. 77-100.
162. Leeson PD, Young RJ. Molecular Property Design: Does Everyone Get It? *ACS Med Chem Lett*. 2015;6(7):722-725.
163. Young RJ, Green DVS, Luscombe CN, Hill AP. Getting physical in drug discovery II: the impact of chromatographic hydrophobicity measurements and aromaticity. *Drug Discov Today*. 2011;16(17):822-830.
164. Hann MM, Oprea TI. Pursuing the leadlikeness concept in pharmaceutical research. *Curr Opin Chem Biol*. 2004;8(3):255-263.
165. Lipinski CA, Lombardo F, Dominy BW, Feeney PJ. Experimental and computational approaches to estimate solubility and permeability in drug discovery and development settings IPII of

original article: S0169-409X(96)00423-1. The article was originally published in *A Adv Drug Deliv Rev* 23 (1997) 3–25.1. *Adv Drug Deliv Rev*. 2001;46(1):3-26.

166. Ritchie TJ, Macdonald SJF. The impact of aromatic ring count on compound developability – are too many aromatic rings a liability in drug design? *Drug Discov Today*. 2009;14(21):1011-1020.

167. Hargrove TY, Wawrzak Z, Alexander PW, Chaplin JH, Keenan M, Charman SA, et al. Complexes of *Trypanosoma cruzi* sterol 14 α -demethylase (CYP51) with two pyridine-based drug candidates for Chagas disease: structural basis for pathogen selectivity. *J Biol Chem*. 2013;288(44):31602-31615.

168. Keenan M, Abbott MJ, Alexander PW, Armstrong T, Best WM, Berven B, et al. Analogues of Fenarimol Are Potent Inhibitors of *Trypanosoma cruzi* and Are Efficacious in a Murine Model of Chagas Disease. *J Med Chem*. 2012;55(9):4189-4204.

169. Riley J, Brand S, Voice M, Caballero I, Calvo D, Read KD. Development of a Fluorescence-based *Trypanosoma cruzi* CYP51 Inhibition Assay for Effective Compound Triaging in Drug Discovery Programmes for Chagas Disease. *PLoS Negl Trop Dis*. 2015;9(9):e0004014.

170. Thompson AM, O'Connor PD, Marshall AJ, Francisco AF, Kelly JM, Riley J, et al. Re-evaluating pretomanid analogues for Chagas disease: Hit-to-lead studies reveal both in vitro and in vivo trypanocidal efficacy. *Eur J Med Chem*. 2020;207:112849.

171. Veber DF, Johnson SR, Cheng H-Y, Smith BR, Ward KW, Kopple KD. Molecular Properties That Influence the Oral Bioavailability of Drug Candidates. *J Med Chem*. 2002;45(12):2615-2623.

172. Chakravorty SJ, Chan J, Greenwood MN, Popa-Burke I, Remlinger KS, Pickett SD, et al. Nuisance Compounds, PAINS Filters, and Dark Chemical Matter in the GSK HTS Collection. *SLAS Discov*. 2018;23(6):532-545.

173. Shilatifard A, Liang K, Smith ER. Therapeutic Targeting of Interleukin-1 Receptor-associated Kinase 4 (IRAK4) in cancers characterized by rearrangements in the mixed lineage leukemia gene (MLL-R). US 2017305901 A1, 2017.

174. Jain A, Kaczanowska S, Davila E. IL-1 Receptor-Associated Kinase Signaling and Its Role in Inflammation, Cancer Progression, and Therapy Resistance. *Front Immunol*. 2014;5:553.

175. Vaden RM, Guillen KP, Salvant JM, Santiago CB, Gibbons JB, Pathi SS, et al. A Cancer-Selective Zinc Ionophore Inspired by the Natural Product Naamidine A. *ACS Chem Biol*. 2019;14(1):106-117.

176. Looper RE, Vaden RM, Gibbons JB, Salvant JM, Edwards AV, Sigman MS et al. Compositions and Methods Comprising 2-(Acylamino)imidazoles. WO 2015143240 A2, 2015.

177. Padmavathi V, Prema kumari C, Venkatesh BC, Padmaja A. Synthesis and antimicrobial activity of amido linked pyrrolyl and pyrazolyl-oxazoles, thiazoles and imidazoles. *Eur J Med Chem*. 2011;46(11):5317-5326.

178. Ahmad N, Anderson C, Arumugam V, Asgian IL, Camp JL, Fanning LTD, Hadida Ruah SS et al. Carboxamides as Modulators of Sodium Channels. WO 2019014352 A1, 2019.
179. Zaveri NT. Nociceptin Opioid Receptor (NOP) as a Therapeutic Target: Progress in Translation from Preclinical Research to Clinical Utility. *J Med Chem*. 2016;59(15):7011-7028.
180. Zipp GG, Barbosa J, Green MA, Terranova KM, Fink C, Yu X-C, et al. Novel inhibitors of the high-affinity l-proline transporter as potential therapeutic agents for the treatment of cognitive disorders. *Bioorg Med Chem Lett*. 2014;24(16):3886-3890.
181. Gilbert AM, Bursavich MG, Lombardi S, Adedoyin A, Dwyer JM, Hughes Z, et al. 3-(Pyridin-2-yl-ethynyl)benzamide metabotropic glutamate receptor 5 negative allosteric modulators: Hit to lead studies. *Bioorg Med Chem Lett*. 2011;21(1):195-199.
182. Yang X-H, Xiang L, Li X, Zhao T-T, Zhang H, Zhou W-P, et al. Synthesis, biological evaluation, and molecular docking studies of 1,3,4-thiadiazol-2-amide derivatives as novel anticancer agents. *Bioorg Med Chem*. 2012;20(9):2789-2795.
183. Patel H, Jadhav H, Ansari I, Pawara R, Surana S. Pyridine and nitro-phenyl linked 1,3,4-thiadiazoles as MDR-TB inhibitors. *Eur J Med Chem*. 2019;167:1-9.
184. Singh AK, Lohani M, Singh UP. Synthesis, characterization and biological activity of some 1, 3, 4-thiadiazol derivatives. *Pak J Pharm Sci*. 2011;24(4):571-574.
185. Patel SR, Gangwal R, Sangamwar AT, Jain R. Synthesis, biological evaluation and 3D QSAR study of 2,4-disubstituted quinolines as anti-tuberculosis agents. *Eur J Med Chem*. 2015;93:511-522.
186. Zhang L, Shi L, Soars SM, Kamps J, Yin H. Discovery of Novel Small-Molecule Inhibitors of NF- κ B Signaling with Antiinflammatory and Anticancer Properties. *J Med Chem*. 2018;61(14):5881-5899.
187. Lamotte S, Aulner N, Späth GF, Prina E. Discovery of novel hit compounds with broad activity against visceral and cutaneous Leishmania species by comparative phenotypic screening. *Sci Rep*. 2019;9(1):438.
188. Corwin Hansch AL, David Hoekman. Exploring QSAR: Fundamentals and Applications in Chemistry and Biology. Washington DC: American Chemical Society; 1995.
189. Corwin H, Leo A, Hoekman D. Exploring QSAR: Hydrophobic, Electronic, and Steric Constants. Washington DC: American Chemical Society; 1995.
190. Baell JB. Optimization: Hit-to-Lead and Lead Optimization-Lecture 2020; June 26; Monash Institute of Pharmaceutical Sciences, Melbourne 2020.
191. Edward H Kerns LD. Drug-like Properties: Concepts, Structure Design and Methods: From ADME to Toxicity Optimization. 2008. 580 p.
192. Shultz MD. Setting expectations in molecular optimizations: Strengths and limitations of commonly used composite parameters. *Bioorg Med Chem Lett*. 2013;23(21):5980-5991.
193. Savjani KT, Gajjar AK, Savjani JK. Drug solubility: importance and enhancement techniques. *ISRN Pharm*. 2012;2012:195727.

194. Cyprotex. Microsomal stability assay [Internet]. 2020 [cited 2020 May 20]. Available from: <https://www.cyprotex.com/admepk/in-vitro-metabolism/microsomal-stability/>.
195. Laveé T & Funk C. 5.03 In Vivo Absorption, Distribution, Metabolism, and Excretion Studies in Discovery and Development. In: Taylor JB and Triggie DJ, editor. *Comprehensive Medicinal Chemistry II*, Volume 5. 2nd ed. Elsevier Science; 2007.
196. Taft DR. Chapter 9 - Drug Excretion. In: Hacker M, Messer W, Bachmann K, editors. *Pharmacology*. San Diego: Academic Press; 2009. p. 175-199.
197. Choi GW, Lee YB, Cho HY. Interpretation of Non-Clinical Data for Prediction of Human Pharmacokinetic Parameters: In Vitro-In Vivo Extrapolation and Allometric Scaling. *Pharmaceutics*. 2019;11(4):168
198. Lau YY, Krishna G, Yumibe NP, Grotz DE, Sapidou E, Norton L, et al. The use of in vitro metabolic stability for rapid selection of compounds in early discovery based on their expected hepatic extraction ratios. *Pharm Res*. 2002;19(11):1606-1610.
199. Obach RS. Prediction of human clearance of twenty-nine drugs from hepatic microsomal intrinsic clearance data: An examination of in vitro half-life approach and nonspecific binding to microsomes. *Drug Metab Dispos*. 1999;27(11):1350-1359.
200. Benet LZ, Liu S, Wolfe AR. The Universally Unrecognized Assumption in Predicting Drug Clearance and Organ Extraction Ratio. *Clin Pharmacol Ther*. 2018;103(3):521-525.
201. Böhm H-J, Flohr A, Stahl M. Scaffold hopping. *Drug Discovery Today: Technologies*. 2004;1(3):217-224.

Chapter 2: Hit-to-lead optimization of the phenyl imidazole carboxamide scaffold (Scaffold 1)

2.01 Introduction and objectives

As described in Chapter 1, the HTS by Pena *et al.* yielded a number of hits that could be progressed through to hit-to-lead medicinal chemistry optimization. From this screen, the *N*-(1-methyl-5-phenylimidazol-2-yl)carboxamide scaffold, Scaffold 1 was chosen as a compound class of interest.¹ The *N*-(1-methyl-5-phenylimidazol-2-yl)carboxamide hits compounds are depicted below in **Figure 2.01** and renamed here as **2.001** and **2.002** (previously **1.47**/TCMDC-143315 and **1.48**/TCMDC-143305, from Chapter 1 respectively). These compounds were chosen for their antileishmanial activity and selectivity for the parasite. Furthermore, higher antileishmanial activity was observed within the orthogonal intramacrophage assay (MAC) than within the primary fluorescent intensity assay (FLINT) readout. This seemed promising to us, as greater potency was observed within the more biologically relevant intramacrophage assay. This suggested that these hits may have a true ability to cross the various physiological barriers, including permeating the macrophage and phagolysosomal membranes, as well as survive within the harsh acidic phagolysosomal environment and cross the leishmanial barriers to exert their activity.

As discussed in Chapter 1, Section 1.09, both hits possess physicochemical properties that follow several guidelines for drug-likeness. Both compounds adhere to Lipinski's Rule of Five, displaying a low molecular weight (< 500 Da), appropriate Log P values (< 5) and a suitable number of hydrogen bond donors (< 5) and acceptors (< 10). In addition to the low molecular weight, the number of rotatable bonds (≤ 10) and low polar surface area (< 140 Å²) also follow Veber's rule, which is another predictive guide for drug-likeness.^{2,3} It should be noted, that these "rules" are merely predictive tools to help guide hit-to-lead optimization but do not guarantee drug-likeness of oral availability. Overall, the novel Scaffold 1 seemed to be a promising starting point with ample chemical space to explore.

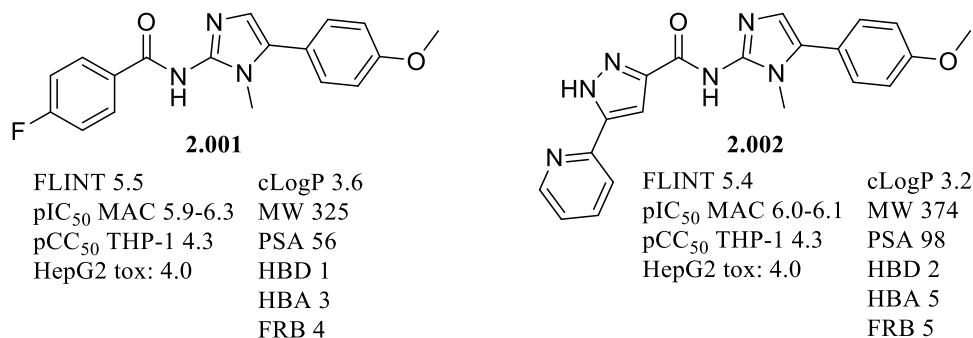


Figure 2.01: Scaffold 1 hits chosen from Pena *et al.* HTS¹

The overall aim for this chapter was to investigate the chemical space surrounding Scaffold 1 and begin to form a first-generation SAR profile. This included varying the left-hand side (LHS) substituents and ring, amide and imidazole core as well as altering the chemical space surrounding the right-hand side (RHS) ring in order to understand the structures required to improve activity and maintain low host cell cytotoxicity.

A large library of compounds was synthesized surrounding this scaffold and is described here in Chapter 2 and continued in Chapter 3. Long waiting periods between receiving and confirming biological results were a common occurrence during this project. Thus, we reached out to other independent groups for relevant biological testing against *L. donovani*. The methods of assessment surrounding intracellular *Leishmania* have proved expensive, complicated, and generally difficult to work with, as discussed previously in Chapter 1 and confirmed through personal communications with several of our independent biological collaborators. Further challenges arose when divergent activity of potential early lead compounds was reported between independent biological groups. This resulted in the need for a large number of compounds to undergo biological reassessment and initially made SAR interpretations somewhat difficult. To successfully overcome the challenges around conflicting biological results we have devised a set of guidelines to determine “true” activity and assist with SAR interpretation, detailed in Chapter 3. In order to understand our rationale during this hit-to-lead medicinal chemistry campaign, our results have been presented transparently and as much as possible, in the chronological order of events.

2.02 Analogue Series 1: Primary LHS investigation

As stated in Chapter 1, Section 1.09, a small library around our chosen hits **2.001** and **2.002** have previously been investigated by researchers at GSK. These analogues remain undisclosed, though correspondence with have provided us with observations, stating a correlation between activity and host cell cytotoxicity within this scaffold was detected. Therefore, in addition to the re-synthesis and biological confirmation of our chosen hits, our initial aims were to also quickly synthesize a diversity set of our own analogues. Due to synthetic ease, a probe surrounding the LHS ring was first targeted whilst keeping the shared core and RHS of Scaffold 1 constant. Quickly creating this library would determine whether low host cell cytotoxicity could be achieved in this portion of chemical space, whilst maintaining and/or improving activity. Furthermore, this would discern whether this compound class was worth pursuing, or if cytotoxicity would cause too great a risk. In which case, other compound classes would be investigated.

Compound **2.001** has a benzamide portion ideal for diversification through amide bond formation. A number of benzoic acids were commercially available and could be coupled with a derivative of the 1-methyl-5-phenyl-1*H*-imidazol-2-amine. The analogues shown in **Figure 2.02** were proposed to be used as an initial diversity set. They contain simple changes to the left-hand side (LHS), keeping the rest of

the compound the same. Changes focused on altering steric bulk, electronic and hydrophobic properties, enabling a better understanding of the favourable interactions in this chemical space. Other properties such as flexibility, orientation and aromaticity were also modified to get an insight into the structural attributes that modulate bioactivity. Focusing on this portion of the compound allowed for diverse library to be quickly formed, following the synthetic pathways depicted in both **Scheme 2.01** and **Scheme 2.03**.

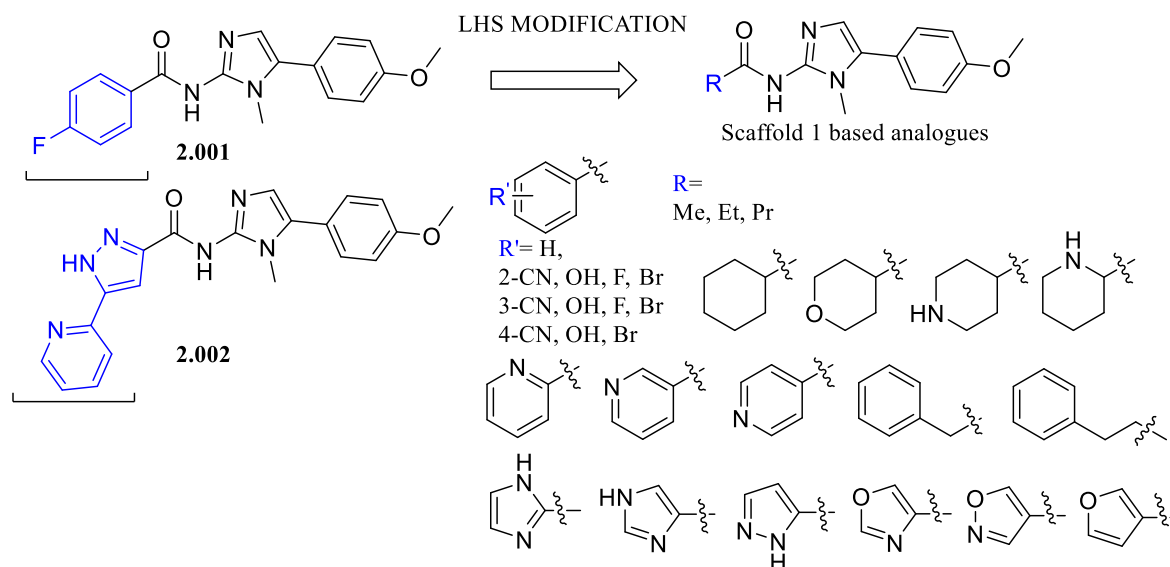
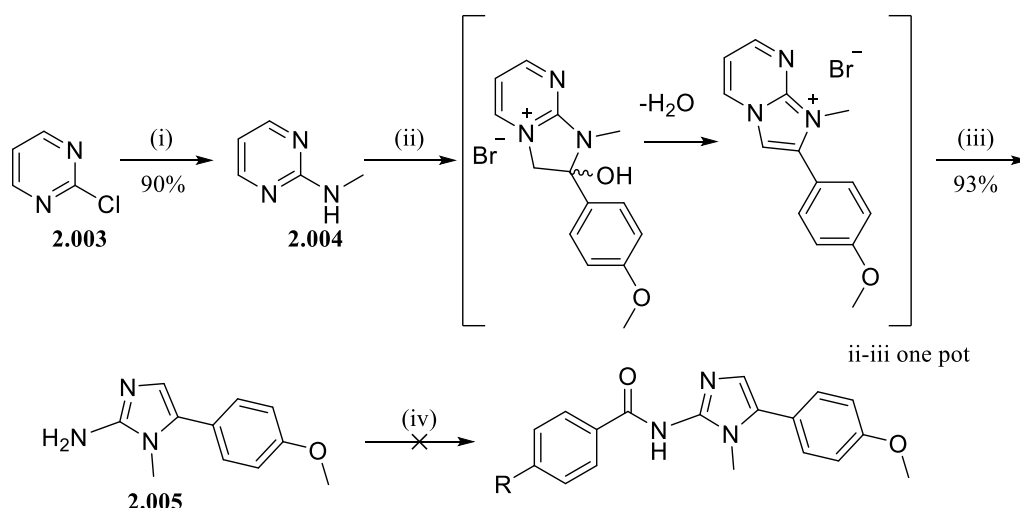


Figure 2.02: Diversity set for primary LHS investigation around Scaffold 1

The synthetic route shown in **Scheme 2.01** was first devised to obtain the analogues proposed in the above **Figure 2.02**.

Scheme 2.01: Attempted synthetic route for diversity set of compounds derived from 2.001/2.002



Reaction conditions i) methylamine, THF, 50 °C, ii) 2-bromo-1-(4-methoxyphenyl)ethan-1-one, ACN, 130 °C, microwave assisted, iii) hydrazine hydrate, 100 °C, microwave assisted, iv) Set of benzoic acids (**Table 2.01**), HOAt, EDCI, DCM, rt

The 2-chloropyrimidine **2.003** underwent nucleophilic substitution with methylamine to obtain *N*-methylpyrimidin-2-amine **2.004** as described by Chen *et al.*⁴ The *N*-methylpyrimidin-2-amine **2.004** is then employed in a one-pot, two step protocol developed by Ermolat'ev *et al.*⁵ This process involves the sequential formation of an imidazo[1, 2*a*]pyrimidinium salt with bromophenylethanones. This was followed by cleavage of the pyrimidine ring upon treatment with a strong nucleophile to give the phenyl-1*H*-imidazole-2-amine **2.005** in a one pot reaction.⁵

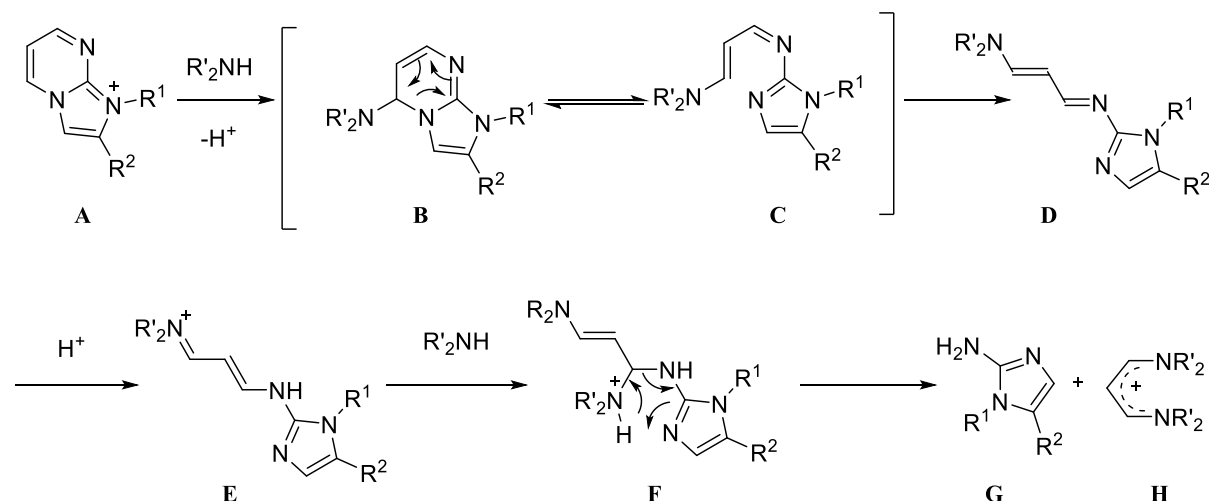


Figure 2.03 Proposed Mechanism by Ermolat'ev for the Ring Opening and Cleavage Reaction of Imidazo[1,2-*a*]pyrimidin-1-ium Salts with Amines

The suggested mechanism of the formation is further depicted above in detail which involves the formation of azabutadienes **D**.⁶ After initial fused ring formation and a loss of water, the imidazo[1,2-*a*]pyrimidin-1-ium salt **A** undergoes nucleophilic attack by a first amine molecule (hydrazine hydrate in this case) at the C-5 position. Rearrangement of intermediate **C** and isomerization of intermediate **C** result in the (*E,E*)- azabutadiene **D**. Protonation gives the azabutadiene **D**, which subsequently undergoes 1,4-addition with a second amine molecule to give the desired 2-aminoimidazole **G** with a diazabutadienium salt **H**. The secondary amine must be used in large excess for direct cleavage according to Ermolat'ev *et al.*⁶

The 5-phenyl-1*H*-imidazole-2-amine **2.005** was used to synthesize the corresponding *N*-(1-methyl-5-phenylimidazol-2-yl)carboxamide analogues with various carboxylic acids. However, the amide coupling using **2.005** proved to be challenging. A number of amide coupling conditions modified from the literature were trialled, but were not successful.⁷⁻¹² The amine was found to be quite unreactive under the conditions outlined above in **Scheme 2.01**, step iv, where the majority of the amine starting material **2.005** was observed to remain unreacted by LCMS analysis. A plausible explanation of the decreased reactivity of **2.005**, could be due to the electron delocalization. The lone pair of the amino group is delocalized onto the diazole ring, hence the amine group is less nucleophilic.¹³ As amide coupling was a key step in the synthesis of a number of benzamide analogues, optimizing this reaction

for reliability and yield was desirable. The various amide formation trials are summarized in **Table 2.01**.

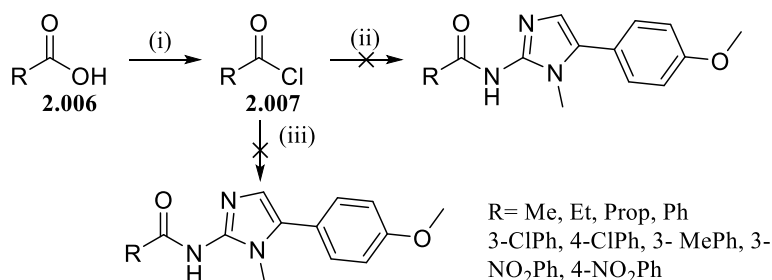
Table 2.01: Attempted amide coupling trials of Scheme 2.01 step iv

Carboxylic acid	Conditions ⁷⁻¹²	Outcome
4-Fluorobenzoic acid	HOAt, EDCI, DCM, rt	Low reactivity, the majority of amine starting material still present
	HOAt, EDCI, DMF, rt/ 80 °C	
	HOAt, EDCI, DCE, 80°C	
	HOAt, EDCI, DCM/THF (1:1), rt	
Benzoic acid	HOAt, EDCI, DCM/THF (1:1), rt	Both the amine starting material and diacylated present, low product selectivity
	HOBt, HBTU, NMM, DMF, rt	
	HOAt, DMAP, DIPEA, DMF, rt	
3-Cyanobenzoic acid	HOAt, EDCI, DCM/THF (1:1), rt/ 80°C	Low reactivity, the majority of amine starting material still present
4-Nitrobenzoic acid	HOAt, EDCI, DCM/THF (1:1), rt	
Butyric acid		

To boost solubility and reactivity of the starting materials, different solvents such as DCE, DMF and DCM/ THF (1:1) were trialled. The majority of amine starting material still remained unreacted, therefore these conditions were deemed unsuitable for this system. A variety of commercially available benzoic acids with both electron donating and withdrawing abilities were also trialled, but in all cases a majority of the amine starting material was still present. This proved that amine **2.005** was poor in reactivity under such conditions.

In parallel to the amide coupling with various carboxylic acids, acid chloride routes adapted from the literature were also trialled in an attempt to increase reactivity.¹⁴⁻¹⁷ This route is depicted in **Scheme 2.02**.

Scheme 2.02: Acid chlorides for the synthesis of amides derived from amine 2.005



Reaction conditions: i) oxalyl chloride, DCM, DMF (0.1 eq), 0°C-rt, ii) 5-(4-methoxyphenyl)-1-methyl-1H-imidazol-2-amine, Et₃N, DCM, 0°C-rt, iii) 5-(4-methoxyphenyl)-1-methyl-1H-imidazol-2-amine, pyridine, 0 °C-rt

Many of the acid chlorides (**2.007**) we aimed to employ in **Scheme 2.02** were not readily available, therefore conversion from the available carboxylic acids (**2.006**) to the acid chloride using oxalyl chloride was first required. After the successful formation of the acid halides (**2.007**), amide bond formation was undertaken. The outcomes of each amide bond formation trialled following step ii or iii of **Scheme 2.02** are described in **Table 2.02**.

Table 2.02: Amide formation trials with acid chlorides and their outcomes.

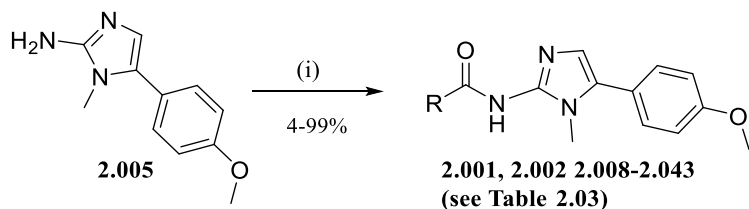
Trial #	Starting carboxylic acid/ acid chloride	Conditions (see Scheme 2.02)	Outcome
1	3-Chlorobenzoic acid	i, ii	Mono and bis- <i>N</i> -acylated amide products formed, indicated by LCMS analysis. Difficulties during purification steps occurred.
2	4-Chlorobenzoic acid	i, ii	Mono and bis- <i>N</i> -acylated products formed, indicated by LCMS analysis. Difficulties during purification steps occurred.
3	<i>m</i> -Toluic acid	i, ii	Mono and bis- <i>N</i> -acylated products formed, indicated by LCMS analysis. Difficulties during purification steps occurred.
4	4-Nitrobenzoic acid	i, ii	Desired monoacetylated product formed selectively, confirmed by LCMS analysis. Desired compound was obtained at 70 % yield.
5	Acetic acid	i, ii	Bis- <i>N</i> -acylated product formed only. Indicated by LCMS analysis.
6	Butyric acid	i, ii	
7	Benzoyl chloride	ii/ iii	Mono and bis- <i>N</i> -acylated products formed, indicated by LCMS analysis. Difficulties during purification steps occurred.
8	Propionyl chloride	iii	Bis- <i>N</i> -acylated product formed only. Indicated by LCMS analysis.
9	3-Nitrobenzoyl chloride	iii	Desired monoacetylated product formed selectively, confirmed by LCMS analysis. Desired compound was obtained at 60 % yield.

Indicated by LCMS analysis, Trials 4 and 9 proved to be successful under basic conditions, employing triethylamine (Et₃N) and pyridine respectively, to obtain the desired 4-nitrobenzamide (**2.013**, **Table 2.03**) and 3-nitrobenzamide (**2.019**, **Table 2.03**) analogues respectively. Despite the success observed in Trials 4 and 9, the amide bond formation step using the imidazole-2-amine **2.005** and acid chlorides summarized in **Scheme 2.02**, was found to be unreliable for this system and not suitable for all target analogues. The remaining trials listed in **Table 2.02**, found that the bis-*N*-acylated amide product had formed along with the desired mono-acylated product. This caused difficulties during the purification process with column chromatography. In Trials 5,6 and 8, only the diacylated product had formed. In hindsight, this was expected as these reactive acid chlorides employed within the aforementioned trials

possessed small aliphatic chains unincumbered by steric hindrance. This phenomenon has been reported in the literature, describing the formation of bis-acylated products from various aliphatic and aromatic acid halides.¹⁸⁻²² These conditions were set aside as parallel trials summarized in **Scheme 2.03** were found to be successful. However, if these conditions listed in **Scheme 2.02** were continued, de-acylation under basic conditions would have been attempted in order to achieve the desired mono-benzamide analogues.²²⁻²⁴

Fortunately, the amide coupling conditions trailed in **Scheme 2.03**, employing HBTU and DMAP were found to be successful when using a variety of readily available aliphatic and aromatic carboxylic acids with various hydrogen bonding ability and differing electronic, steric, and hydrophobic properties.¹¹ Success with this large array of carboxylic acids deemed this method appropriate for a majority of the analogues that we hoped to synthesize. Generally, the reactions following **Scheme 2.03** occurred cleanly and selectively, where the amine starting material (**2.005**) was consumed to form the desired amide bond and the desired analogues **2.001**, **2.008-2.041** were obtained successfully. Furthermore, bis-*N*-acylated product did not form, eliminating the previous purification issues outlined in **Table 2.02**. Step i of **Scheme 2.03** initially employed DMF as the solvent following Richter *et al.*, though was later substituted for ACN in order to improve yield.¹¹ The addition of the second base DMAP seems to have allowed for the reaction to be pushed further and allow for successful amide coupling to occur. Most of the target analogues were synthesized following **Scheme 2.03** and are summarized in **Table 2.03**. The formation of the desired analogues was confirmed with LCMS and ¹H NMR analysis.

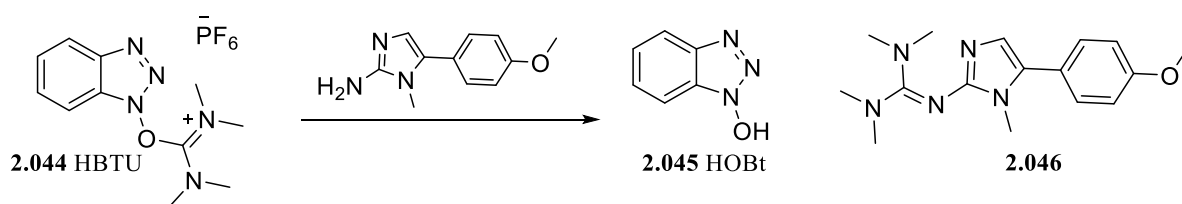
Scheme 2.03: Successful synthetic route for Scaffold 1 analogues



Reaction conditions: i) various carboxylic acids, HBTU, DIPEA, DMAP, ACN, rt (**2.001**, **2.008-2.041**) or PyBOP, DIPEA, DMAP, DMF, rt (**2.002**, **2.042-2.043**)

Our initial attempts to synthesize the amide analogues with pyrazole-pyridine (**2.002**) and imidazole (**2.042-2.043**) carboxylic acids in the presence of HBTU (**2.044**) were unsuccessful. LCMS analysis suggested that the guanidine-amine by-product (**2.046**) had formed instead of the desired analogues (**2.002**, **2.042-2.043**). This by-product was also formed during the synthesis of the pyrazole analogue **2.032**, in the presence of HBTU. However, in this case the desired product **2.032** was also formed and successfully separated from the guanidine by-product (**2.046**) during purification. This could be expected of uronium species coupling agents which are reported guanidylating agents.^{8, 25, 26} This side reaction (**Scheme 2.04**) is also reported to be particularly problematic when carboxyl activation is slow, which is likely the case here.²⁵

Scheme 2.04: Guanidine by-product formation using HBTU⁸



Identification of the guanidine-amine by-product (**2.046**) was established using LCMS analysis where the amine **2.005** was consumed and the guanidine by-product (**2.046**) was the main compound detected in place of our desired analogues (**2.002**, **2.042**, **2.043**). The desired products were also not apparent by ¹H NMR analysis. In another attempt to obtain analogue **2.043**, this reaction was investigated using an excess of the carboxylic acid starting material at higher temperatures (50 °C) in DMF. Under these altered conditions the desired compound **2.043** was apparent, though the undesired compound **2.046** had still formed as the main compound within the mixture. Here too, the reaction was monitored by LCMS analysis, and the mass detector was used to establish the reaction outcomes (**Figure 2.04**). A longer pre-activation period of the carboxylic acid starting material used in excess, may have likely encouraged increased synthesis of the desired product.²⁶ However, these methods were set aside, as a preferred set of conditions employing PyBOP were found successful.

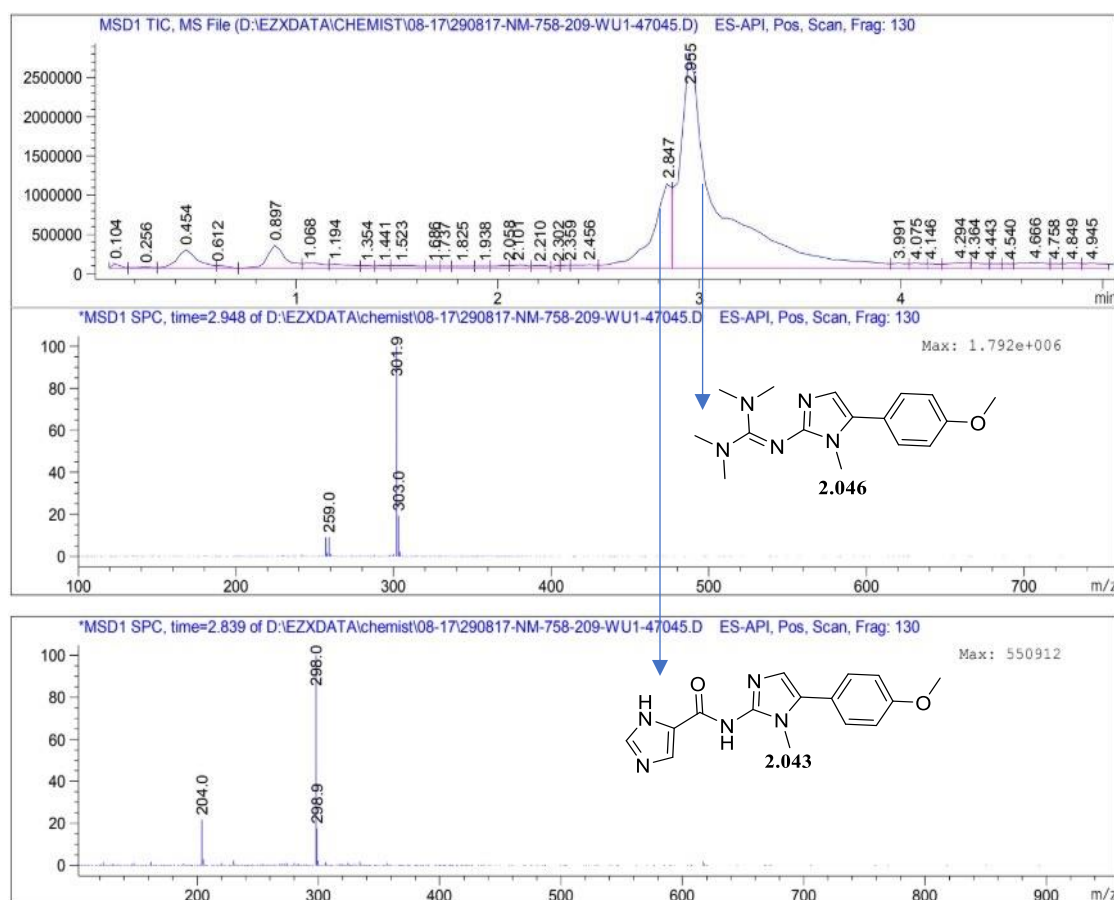


Figure 2.04: LCMS report of the guanidine-amine by-product (2.046) as the majority compound during amide coupling using imidazole carboxylic acid and HBTU (2.044) to obtain compound 2.043.

Upon consulting the literature, I found successful outcomes when the phosphonium species PyBOP was investigated as a replacement for HBTU.^{8, 25-31} The base and solvent were kept constant, as outlined in **Scheme 2.03**. This coupling agent was chosen as it does not cause guanidinylation and has been reported to allow cleaner reactions than uronium reagents.^{8, 25, 26} The coupling mechanism of PyBOP is described below in **Figure 2.05**. As I aimed to use this method for further analogue synthesis, ease in synthesis and purifications was sought after. The reaction mixtures indicated the formation of desired product by LCMS and ¹H NMR analysis.

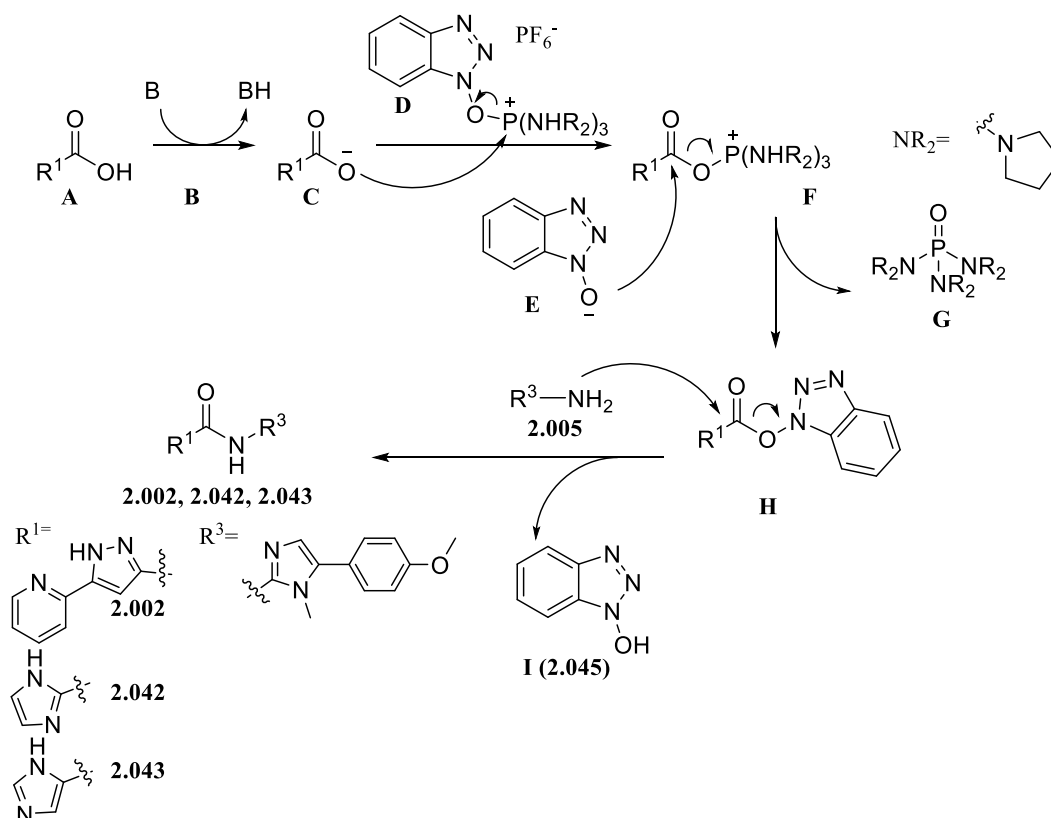
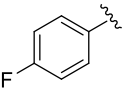
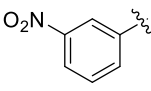
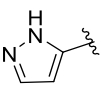
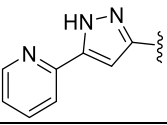
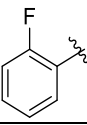
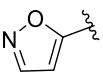
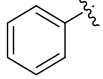
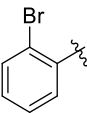
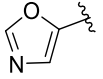
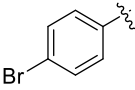
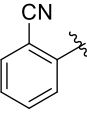
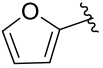
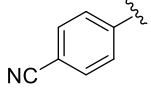
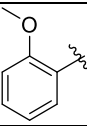
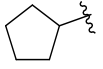
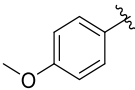
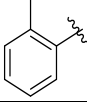
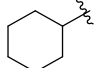
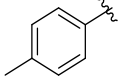
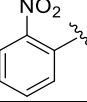
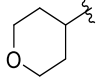
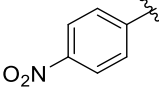
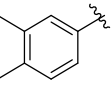
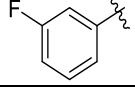
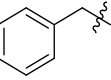
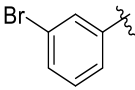
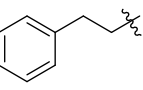
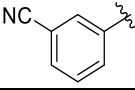
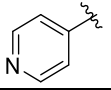
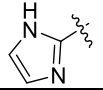
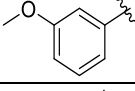
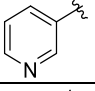
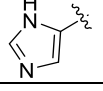
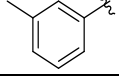
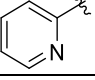


Figure 2.05: PyBOP coupling mechanism to form analogues 2.002, 2.042-2.043³²

To obtain the desired analogues **2.002, 2.042-2.043**, the relevant carboxylic acids underwent activation via the PyBOP coupling mechanism, depicted in **Figure 2.05**. This begins with the deprotonation of the carboxylic acid (**A**) by treatment with a base (**B**), allows for the resulting carboxylate anion (**C**) to attack the phosphorous atom of the phosphonium salt, which is the electrophilic centre of PyBOP (**D**). This substitution leads to the formation of intermediate **F**, where the deprotonated *N*-hydroxybenzotriazole (**OBt**, **E**) acts as the leaving group. The **OBt** molecule (**F**) in turn attacks the carbonyl carbon (**C=O**) of intermediate **F**, to form the *N*-hydroxybenzotriazole ester (**H**) whilst releasing a phosphoric triamide molecule (**G**). The ester intermediate (**H**) is now activated and can undergo amide coupling with the amine **2.005**, via nucleophilic attack on the ester carbonyl carbon (**C=O**) to form the desired analogues **2.002, 2.042-2.043**, with the release of HOBt (**2.045**).³² The mechanism of HBTU is more commonly known, though for the interest of the reader, it has been included in the Appendix.

In the presence of PyBOP, reasonable yields of the desired amide analogues **2.002**, **2.042-2.043** were obtained after separation using column chromatography. These compounds and their respective yields are listed below in **Table 2.03**, along with the overall diversity set of compounds that were successfully obtained following both conditions of **Scheme 2.03**.

Table 2.03: List of analogues synthesized using Scheme 2.03

I.D	R	Yield %	I.D	R	Yield %	I.D	R	Yield %
2.001		58	2.019		72	2.032		76
2.002		22	2.020		52	2.033		24
2.008		75	2.021		94	2.034		52
2.009		53	2.022		42	2.035		96
2.010		54	2.023		70	2.036		94
2.011		90	2.024		82	2.037		88
2.012		78	2.025		60	2.038		93
2.013		58	2.026		53	2.039	Me	4
2.014		53	2.027		90	2.040	Et	79
2.015		99	2.028		84	2.041	Pr	66
2.016		42	2.029		86	2.042		16
2.017		67	2.030		94	2.043		48
2.018		89	2.031		52			

The variety of analogues formed following **Scheme 2.03** endorses the generalizability of the working scheme. Generally, within this overall diversity set, the *ortho* substituted compounds gave lower yields in comparison to their *meta* and *para* counterparts, which can be attributed to steric hindrance. The cycloaliphatic series gave the highest yields overall. I believe that this may be in part because of the reactivity of their carboxylic acid starting material when activated. Most of the target analogues were obtained in a reasonable yield, with some exceptions. Nonetheless, the few target analogues that were acquired in low yield were not an issue, as each analogue still provided more than sufficient amounts of sample for biological assessment.

The diversity set summarized in **Table 2.03** was devised to begin to explore the chemical space surrounding the LHS of Scaffold 1 and gain some insight into the sorts of structural changes capable of altering bioactivity. Furthermore, this wide array of analogues would probe whether any host cell cytotoxicity was indeed present within this Scaffold, as warned by GSK.

Among the diversity set of **Table 2.03**, I prioritized the resynthesis and biological reassessment of the hits **2.001** and **2.002**. This was undertaken to confirm if the chosen hits actually possessed antileishmanial activity and selectivity towards the parasite. Furthermore, biological reassessment of the hit compounds would allow for a direct comparison to be made against all investigative analogues targeting this compound class, within the same assay conditions employed. The unsubstituted benzamide analogue (**2.008**) was devised as a direct analogue of **2.001**, exploring whether the *para*-fluoro substituent was required to maintain activity. Fluorine is a known monovalent isostere of the hydrogen atom, as they are similar in size and the fluorine substituent only slightly increases lipophilicity (refer to **Table 1.06**, Chapter 1 for substituent property comparison). The loss of the fluoro substituent in **2.008** would probe whether the loss of electronegativity and the ability to accept hydrogen bonds at this position correlated to a loss of antileishmanial activity.^{33, 34} Analogue **2.008** could also be used as another direct comparison to other substituted benzamides with varying properties. Repositioning the fluorine to the *meta* (**2.014**) and *ortho* (**2.020**) positions of the ring was also undertaken to probe if any potential interactions between the fluoro group and the putative binding site/s could still be maintained, or possibly even interact more strongly.

As many substituted benzoic acids were readily available to us, thus many analogues based around **2.001**, bearing varying substituents were devised. Briefly, the *para*-fluoro group was substituted with the bromo substituent (**2.009**), to probe whether a sterically larger, more hydrophobic halogen was preferred at this position. The electron withdrawing ability would remain consistent however this change would also help towards determining if hydrogen bond acceptors were required at this position. The bromo group was also substituted at the *meta* (**2.015**) and *ortho* (**2.021**) positions to investigate if this halogen was preferred at other positions of the ring. Electron donating groups were also explored within **Table 2.03** as well as later within Section 2.03. Here, this included substituting the methoxy

(**2.011, 2.017, 2.023**) and methyl (**2.012, 2.018, 2.024, 2.026**) groups around the phenyl ring to probe whether an electron rich ring was preferred within the putative binding site/s. Additionally the methoxy substituents would also maintain the ability to form hydrogen bonds with the putative binding site/s whilst methyl substitution would allow for a slight increase in lipophilicity around the scaffold. Strong electron withdrawing groups were substituted around the phenyl ring to determine whether a more electron poor aromatic ring was preferential. This included incorporating the cyano (**2.010, 2.016, 2.022**) and nitro (**2.013, 2.019, 2.025**) substituents around the ring, which also increased molar refractivity and hydrophilicity within this chemical space. Pyridine rings (**2.029-2.031**) were also introduced within this chemical space to gauge whether an electron poor ring was preferential. By positioning the heteroatom at each position of the ring, the heteroaromatic ring may take on different orientations, particularly if the heterocycle is engaged in potential pi-pi stacking with the putative binding site/s, where the preferred topology of the pyridine is when the nitrogen atom is directed away from the hypothetical aromatic ring of the putative binding pocket.³⁵

Analogues **2.027** and **2.028** were also devised to probe changes in orientation of the LHS ring, using a small increase in the number of carbons between the rigid amide functionality and aromatic ring. This would increase flexibility and the number of rotatable bonds within the scaffold. Analogue **2.032** was devised to investigate whether the pyridine of **2.002** was necessary to exert antileishmanial activity, or if the 5-membered pyrazole alone could maintain any required interactions with the putative binding site/s. The pyrazole ring, along with the analogues bearing an isoxazole (**2.033**), oxazole (**2.034**), imidazole (**2.042-2.043**) or furan (**2.035**) at the LHS of the scaffold were also acquired to investigate whether a smaller aromatic system could provide a better fit within the putative binding site/s. Altering the heteroatoms and their positions around the 5-membered aromatic ring was also studied using this group of analogues. This may provide insight into the atoms and arrangement required to form any potential interaction with the putative binding site/s, such as hydrogen bonding.

Finally, the diversity set also studied the replacement of the aromatic rings with aliphatic rings and chains within the LHS portion of the scaffold. Replacing the *para*-fluoro phenyl (**2.001**) and pyridine-pyrazole (**2.002**) aromatic systems with cycloalkanes (**2.036-2.038**) would significantly alter the chemical space around the LHS of the scaffold. This includes changing the hybridization state of the carbons within the ring, removing the planar system and the ability of the LHS system to form pi-pi interactions with the putative binding site/s. Such a change would help us determine if aromaticity was required at this portion of the chemical space. The substitution of small aliphatic chains (**2.039-2.041**) at the LHS position would further help probe if aromatic systems were required. This last set of analogues (**2.039-2.031**) allow for quite a dramatic change to the chemical space, significantly reducing lipophilicity and steric bulk around the LHS segment of the scaffold. These analogues were devised to gain an insight into whether the putative binding site/s would accommodate any sort structural change or if the larger aromatic systems were indeed required to hypothetically fit in a certain position and

potentially allow for certain interactions to occur. Overall, this diversity set indeed contained a range of different functionalities, probing electronics, sterics, hydrogen bonding ability as well as altering orientation, aromaticity and flexibility.

Compound structure and purity was confirmed with ^1H NMR, ^{13}C NMR, LCMS, HRMS and HPLC analysis. The characterization of all synthesized intermediate and final compounds has been listed in the Experimental Section. Additionally, key analogue NMR spectra examples have been included in the Experimental section as representatives for each series. The ^1H NMR spectrum of **2.001** is also depicted in **Figure 2.06**, which also serves as a key example for Compound Class 1. This figure features a zoomed in section of the aromatic region for the convenience of the reader.

Briefly, from **Figure 2.06**, each proton signal can be observed within the spectrum, excluding the N-H amide proton peak which has presumably broadened out and is not visible within chloroform and the conventional sweep width employed. Based on structurally close analogues (**2.011**, **2.024**, **2.027**, **2.028**, **2.031**), the N-H peak of hit **2.001** is expected as a downfield singlet at approximately 10.12-10.47 ppm (see Experimental section). Despite this absence, the presence of all C-H peaks is enough to confirm the success of the amide bond formation of **2.001** following **Scheme 2.03**. Furthermore, the loss of the NH_2 broad singlet of the starting amine **2.005**, reported at 5.40 ppm (see Experimental section) also signifies that amide bond formation has occurred.

Other notable signals within this spectrum include the most downfield multiplet centered at 8.31 ppm, which correlates to peak A. This set of equivalent protons are positioned *ortho* to the electron withdrawing carbonyl group of the amide, which causes a deshielding effect, shifting this set of protons downfield. Another notable aromatic peak is the multiplet centered at 7.00 ppm, correlating to peak D. The identical protons of peak D are shifted upfield due to their proximity to the electron donating O atom of the methoxy substituent. In addition, the signal at 6.67 ppm corresponds to the aromatic singlet of the imidazole (E). Finally, both singlets within the aliphatic region at 3.87 and 3.59 ppm correlate to the methyl group of the methoxy substituent (F) and *N*-methyl (G) of the imidazole ring respectively. The methyl of the methoxy group (F) is shifted more downfield as it is adjacent to a more electronegative atom. The complete assignment of the ^1H NMR and ^{13}C for **2.001** is outlined within the Experimental section.

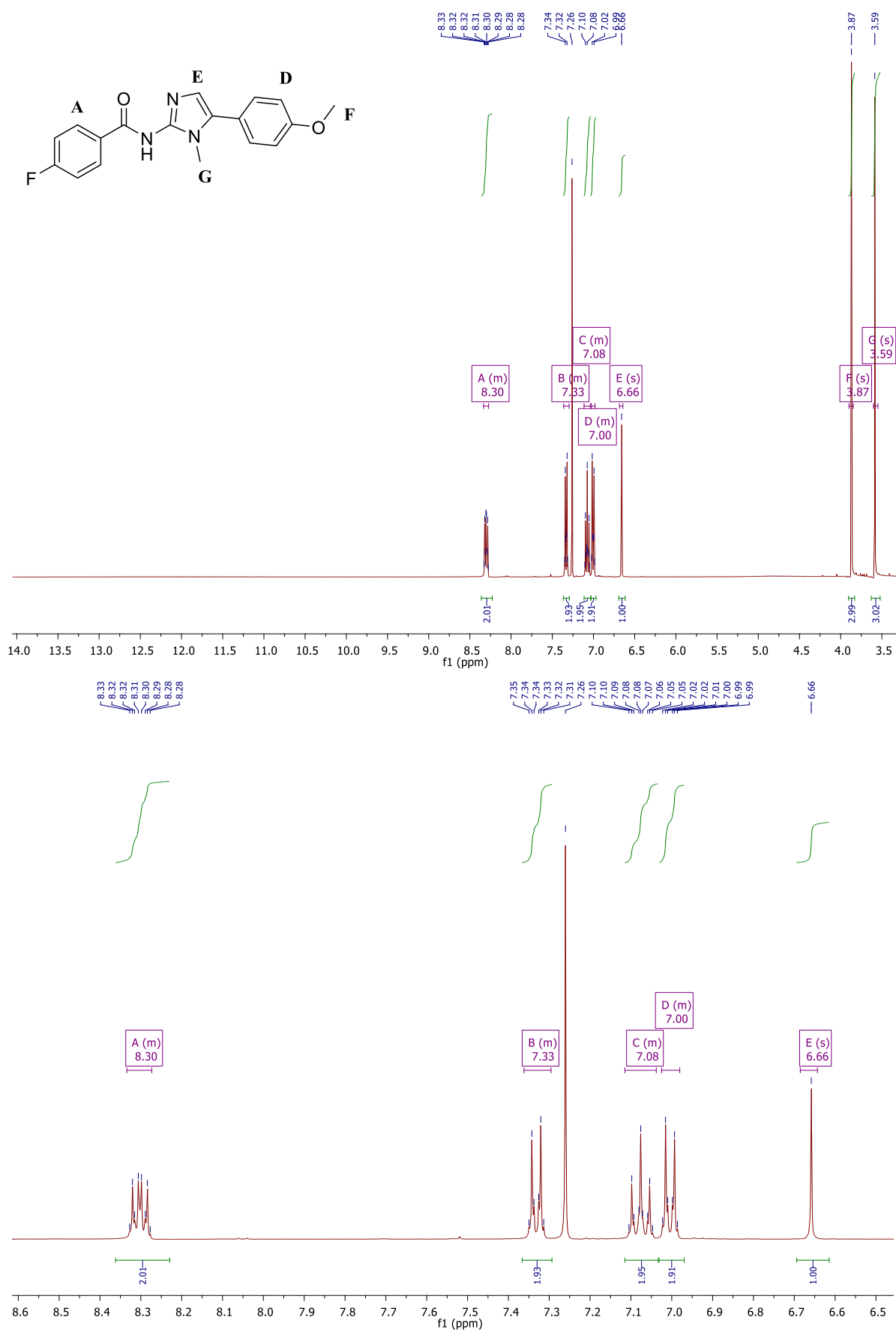


Figure 2.06: ¹H NMR spectrum confirming the successful formation of analogue 2.001. This analysis was undertaken using CDCl₃ as the solvent.

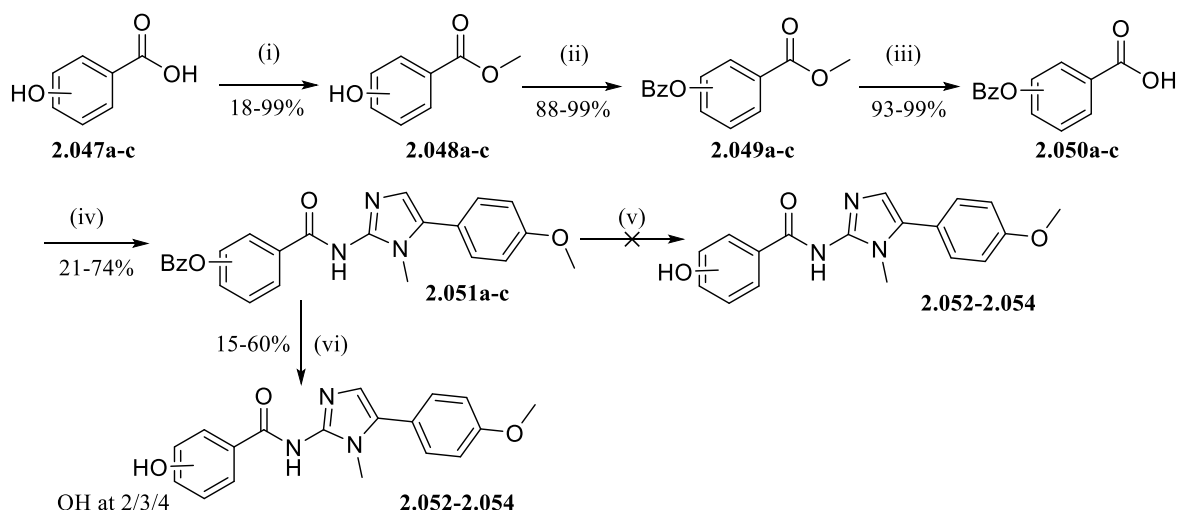
Throughout this scaffold exploration, an observation that was noted is that quaternary carbons were not always visible in ^{13}C NMR spectrum. It is known that ^{13}C sensitivity has lower sensitivity to ^1H NMR, therefore altering the sample amount used, number of scans and/or acquisition time was usually required. Though, at times this was either not an option or still was not enough to provide a distinct and/or visible peak.³⁶ This can be expected as quaternary carbons have long relaxation times, thus lower intensities and can “disappear” into the noise. Furthermore, in case of the quaternary carbons within the imidazole ring, the nitrogen atoms adjacent to these carbons may cause peak broadening due to quadrupolar relaxation of the ^{14}N nuclei (the majority isotope) making these signals harder to recognize.^{36, 37} Jacobsen *et al.* describes the nuclear quadrupole moment of ^{14}N to be due to the asymmetric distribution of positive charge in the nucleus. This leads to coupling between the electrostatic environment (bond configuration) around the nucleus and the magnetic properties of the nucleus. This causes rapid transitions among spin states of the spin-1 nucleus, broadening the ^{13}C peak directly bonded to the nitrogen.³⁶ Carbons adjacent to the nitrogens of the imidazole compound were particularly difficult to acquire. Restriction around the amide and imidazole ring likely contributed to their poor acquisition. Overall, difficulties in acquiring the quaternary carbons with some ^{13}C spectra was not a large issue as it did not hinder compound validation. Furthermore, this was not the only analysis tool relied upon for structure identification, but rather used as a corroborative tool for ^1H NMR and HRMS analysis, which were already sufficient for structure validation.

2.03 Analogue Series 1: Primary LHS investigation with analogues synthesized using alternate synthetic routes

2.03.1 Analogues derived from hydroxybenzoic acids

Analogues bearing phenol rings (**2.052-2.054**) at the LHS region of the chemical space were devised to study whether a hydroxy group was preferred over the *para*-fluoro of hit **2.001**. This change would investigate if an electron rich ring was preferred within the putative binding site/s and if the hydroxy substituent could potentially interact with the putative binding site/s as a hydrogen bond donator and/or acceptor in order to modulate bioactivity. Hydroxybenzoic acids were employed as starting materials to achieve these planned analogues.

Scheme 2.05: Synthetic scheme for phenol target analogues



Reaction conditions: i) H_2SO_4 , MeOH, reflux, ii) benzylbromide, K_2CO_3 , ACN, 60 °C, iii) NaOH, MeOH/ H_2O (1:2), 65 °C, iv) 5-(4-methoxyphenyl)-1-methyl-1*H*-imidazol-2-amine, DMAP, DIPEA, HBTU, ACN, rt, v) H_2 , Pd-C, MeOH, vi) Et_3SiH , Pd-C, 1,4-dioxane/ MeOH, rt.

Our attempts to directly use hydroxybenzoic acids **2.047** for amide couplings with amine **2.005**, following the reaction conditions outlined in **Scheme 2.03**, did not meet with any success. These reactions were monitored by LCMS analysis, which indicated only the presence of unreacted amine **2.005**. Similar reactions involving the amide coupling of hydroxybenzoic acids were reviewed, however upon further literature consultation an alternate pathway in which protecting groups was to be invoked.³⁸⁻⁴² The protection of the phenolic - OH was proposed in order to obtain the desired analogues, as shown in **Scheme 2.05**. This synthetic route began with the conversion of the hydroxybenzoic acids **2.047a-c** into the corresponding methyl esters **2.048a-c** using Fischer esterification.^{43, 44} The phenolic hydroxyl (- OH) group was protected as a benzyl ether (**2.049-c**) using BnBr in ACN and K_2CO_3 as a base.^{39, 40} The resulting intermediates **2.049a-c** were saponified using NaOH (aq) in MeOH to remove the methyl ester.⁴⁰ The benzyloxybenzoic acids **2.050a-c** were then coupled with amine **2.005** using the amide coupling conditions described in **Scheme 2.03**. This proved that phenolic - OH group protection was required for the success of amide coupling. In the final step, the *O*-debenzylation of amides **2.051a-c** was performed using transfer hydrogenolysis, employing Et_3SiH and Pd-C in order to successfully obtain analogues **2.052-2.054**.⁴⁵

Our initial attempts to achieve the phenolic - OH using deprotection by debenzylation involved the use of Pd-C and molecular hydrogen.³⁹ In general, this reaction proved to be slow as indicated by TLC and LCMS analysis. When the reaction was allowed to run for a longer period of time, the conversion of starting material was improved. However, when the reaction time was increased, a number of products were detected by both LCMS and TLC analysis. This implied that longer exposure of the starting material to Pd-C and H_2 resulted in a loss of product selectivity. The formation of the large number of products with Pd-C and H_2 may be due to the reduction of the imidazole ring, followed by subsequent,

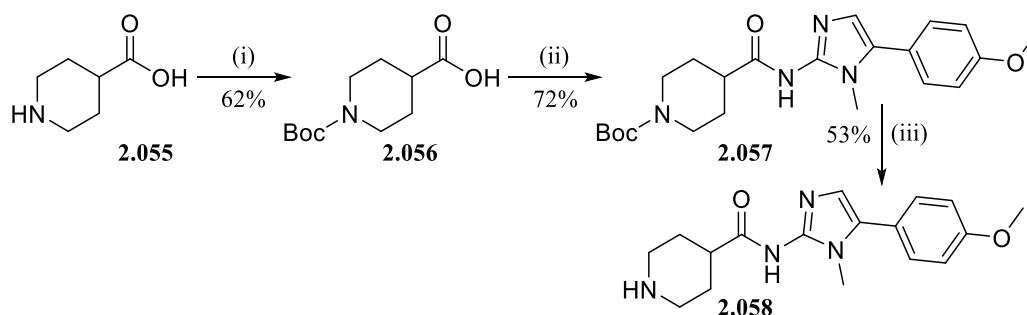
ongoing degradation of this system. However, this phenomenon was not further investigated as it was not pertinent to our primary objective of quickly obtaining a first-generation SAR library.

Product selectivity was improved using Et₃SiH and Pd-C. Better selectivity of the desired product could be because of the transfer hydrogenation mechanism employing Et₃SiH.⁴⁵ The debenzylation step using Et₃SiH was optimized with a focus on improving product selectivity. While optimizing this step, I made sure that the reaction conditions were adjusted so that the reaction time was not prolonged. This meant that a) exposure to the catalyst was not for longer periods of time, b) 1,4-dioxane was used as a cosolvent and fast stirring was employed and c) reactions were stopped even at low conversions to favour product selectivity over the yield. Following these modified conditions, analogues **2.052-2.054** were obtained exclusively.

2.03.2 Analogues derived from piperidine carboxylic acids

Similar to analogues **2.036-2.038**, the piperidine based analogue **2.058** was planned so that I could investigate whether an aromatic system was required within the LHS region of the chemical space, or if a cycloaliphatic could be tolerated within this space. Incorporating the N-H heteroatom onto the ring might also allow for hydrogen bond interactions could occur between the piperidine and the putative binding site. Our initial attempt to synthesize piperidine based analogue **2.058** using piperidine-4-carboxylic acid (**2.055**) directly following the method documented in **Scheme 2.03** did not meet with any success. The *N*-Boc protection strategy as outlined in **Scheme 2.06** was utilized. Piperidine-4-carboxylic acid **2.055** was *N*-Boc protected using Boc₂O in the presence of aqueous NaOH in 1,4-dioxane.⁴⁶ This process results in the formation of 1-*N*-Boc protected piperidine-4-carboxylic acid **2.056**, which readily coupled with amine **2.005** under the optimized conditions documented in **Scheme 2.03**. This proved that protection of the NH group was required for the success of amide coupling. In the last step *N*-Boc protection of **2.057** was removed using 4M HCl in 1,4-dioxane to successfully obtain analogue **2.058**.⁴⁶

Scheme 2.06: Synthesis of piperidine substituted analogue 2.058 using a Boc protecting group



Reaction conditions: i) Boc₂O, NaOH, 1,4-dioxane: water (1:1), ii) 5-(4-methoxyphenyl)-1-methyl-1*H*-imidazol-2-amine, DMAP, DIPEA, HBTU, ACN, iii) 4M HCl in 1,4-dioxane then NaOH, DCM

2.04 Analogue Series 2: Initial RHS change investigation (brief exploration)

A brief exploration around the RHS chemical space of Scaffold 1 was undertaken, by focusing on altering the *para*-methoxy group. To assess if the methoxy group was required at the *para*-position to maintain activity, the methoxy group was removed (**2.059**) and repositioned to the *meta* (**2.060**) and *ortho* (**2.061**) positions. These analogues would also study if a low host cell cytotoxicity could still be achieved when targeting this portion of the chemical space. Analogues **2.059-2.061** were synthesized following **Scheme 2.01**, employing differing bromophenylethanones in step ii/iii. This was followed by amide coupling utilizing the optimized conditions listed in **Scheme 2.03**. These analogues were obtained in reasonable yield over two steps, listed below in **Figure 2.07**.⁵ A more in-depth study surrounding the RHS compound space is continued within Chapter 3.

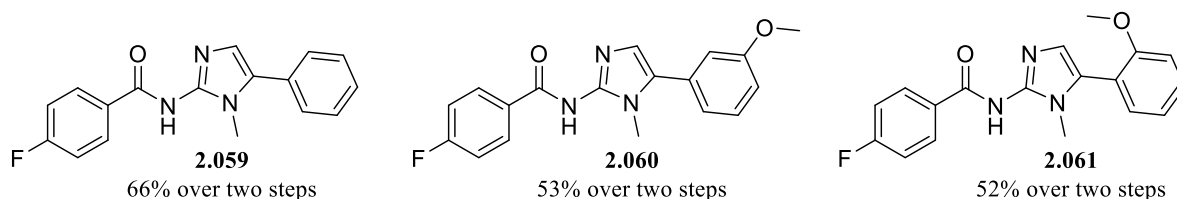


Figure 2.07: Analogues targeting the RHS chemical space of hit **2.001**

2.05 Initial biological testing with *in vitro* free-living promastigote assay

Analogues within the initial diversity set of compounds listed in Sections **2.02-2.04** of this chapter were biologically assessed by the McConville group of the Bio21 Institute of Molecular Science and Biotechnology (Bio21), Department of Biochemistry and Pharmacology, University of Melbourne. We were originally encouraged to investigate the biological activity of the first set of analogues using a novel combination assay being developed by the group at the time. This assay was designed to determine the potency of analogues against *L. mexicana* promastigotes in Shimony *et al.* modified completely defined media (CDM).⁴⁷⁻⁴⁹ This life-cycle stage and *Leishmania* species were routinely used by our collaborators at the time of assessment. This *in vitro* promastigote assay monitors parasite proliferation spectrophotometrically, using the SYBR green I fluorescence stain. This is a nucleic acid stain that binds and quantifies double-stranded DNA, measuring parasite cell number and identifying compounds with the ability to kill or inhibit promastigote growth within the media.⁴⁹⁻⁵¹

Miltefosine (**1.04**) is presented as the ‘gold standard’ antileishmanial and was used as a control for analogue comparison. During this time, this free-living promastigote assay was still being optimized and conditions still required modifications. The half maximal inhibitory concentration (IC₅₀) values determined using the SYBR Green 1 read out have been included below. Due to the large number of compounds requiring biological examination, compounds were not all assessed at the same time, i.e. different sets of compounds were assessed during different experiments following the same methodology. The axenic promastigote assay IC₅₀ values calculated for miltefosine reproducibility

usually fell between 6.0-8.0 μM , consistent with values previously reported and indicates limited experimental variability between assays. However, as recommended by our biological collaborators, for transparency, miltefosine controls are presented for each experiment.⁵²⁻⁵⁵

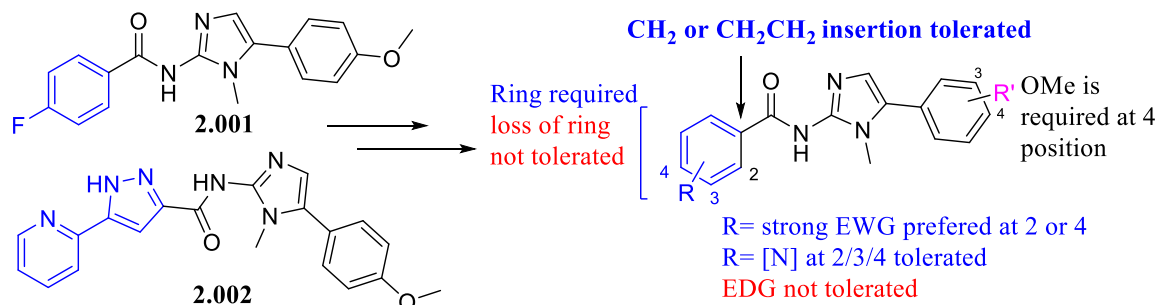


Figure 2.08: Summary of the SAR based on the initial free-living promastigote assay using SYBR Green 1

A representative set of analogues was first biologically assessed via these methods and an outline of their resulting SAR is depicted in **Figure 2.08** and **Table 2.04**. The SAR was shown to be dominated by sharp negative SAR. It was thought to give us a clear map on what specific structural requirements were needed to maintain activity and what is tolerated. Based on the biological results reported by Bio21, we initially thought electron withdrawing groups at the *ortho* (2-CN **2.022**, 2-NO₂ **2.025**) and *para* (4-CN **2.010**, 4-NO₂ **2.013**) positions were preferred. These compounds shaped a small additive SAR study outlined in **Figure 2.09**, combining the *ortho* electron withdrawing group with the *para*-fluoro of hit **2.001**. By doing so, we aimed to investigate whether the presence of the additional electron withdrawing substituents (2-CN, 2-NO₂) coupled with the original *para*-fluoro group would allow for any additional and preferential interactions to be made between the analogues and the putative binding site/s.

Continued biological studies employing this assay found that the pyridine ring replacement (**2.029-2.031**) and elongating chain length between the amide and LHS ring (**2.027-2.028**) seemed to have improved antileishmanial activity in comparison to the original hits **2.001**, **2.002**. Additional additive SAR studies were planned to involve these functionalities. From these initial *in vitro* studies, it seemed that the hit **2.002** was able to exert some activity against *L. mexicana*, though at a more modest value than initially reported. Later studies found the hit **2.001** also displayed activity (IC₅₀ = 7.3 μM), employing the more relevant *L. donovani* species whilst assessing *L. mexicana* (IC₅₀ = 19 μM) in parallel. As the hit **2.001** was found to have antileishmanial activity against *L. donovani*, our parasite of interest, SAR studies around Scaffold 1 were continued. These studies are described in Section 2.06 and involved synthesizing analogues based around **2.001**, targeting changes to the core. Further biological assessment employing the more relevant *L. donovani* was also planned for the remaining analogues within this series as well as compare activity between species. However, this did not proceed based on later biological reassessment with intracellular assays, as discussed below in Section 2.07. Biological assays examining

our investigative compounds against intracellular *L. donovani* amastigotes within host macrophages would later become our predominant method determining compound efficacy, cytotoxicity, and the resulting SAR profile. Therefore, the biological results around the *in vitro* free-living promastigote assay were not an overall large focus within this body of work.

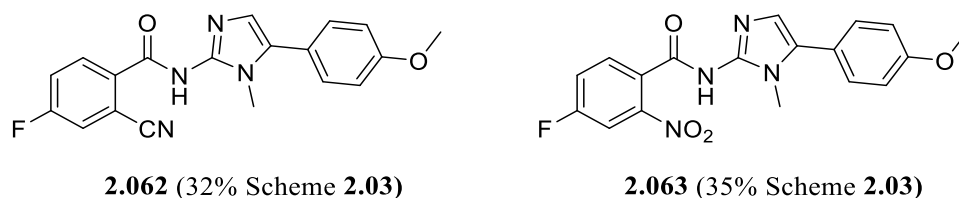


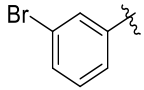
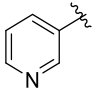
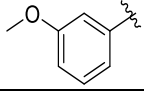
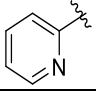
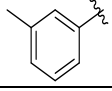
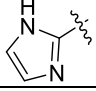
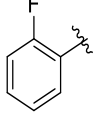
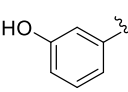
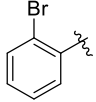
Figure 2.09: Initial additive SAR study based of biological results observed in free-living promastigote assay using SYBR Green 1. Further additive SAR studies were not pursued based off compound retesting in intracellular assays.

Table 2.04: Initial biological results of a number of Series 1 analogues against *L. mexicana* in the free-living promastigote assay using the SYBR Green 1 readout. Hit compounds highlighted in blue.

2.001, 2.002, 2.009-2.053

2.059-2.060

ID	R (LHS)	IC ₅₀ ^a (μM)	ID	R (LHS)	IC ₅₀ ^a (μM)	ID	R' (RHS)	IC ₅₀ ^a (μM)
2.001^b		7.3 ^{gh} , 19	2.022^{ed}		8.7 ± 5.4 ^e	2.059^c	H	58
2.002^{cd}		14 ± 3.9 ^e	2.023^{cd}		>100 ^{ef}	2.060^c	3-OMe	>100 ^f
2.009^c		>100 ^f	2.024^{ed}		>100 ^{ef}			
2.010^b		1.6	2.025^c		11			
2.011^c		>100 ^f	2.026^c		56			
2.012^c		62	2.027^c		2.3			
2.013^b		17	2.028^c		2.2			
2.014^c		>100 ^f	2.029^c		2.2			

2.015^{cd}		>100 ^{ef}	2.030^c		2.2
2.017^{cd}		>100 ^{ef}	2.031^c		2.0
2.018^b		88	2.042^c		66
2.020^{cd}		>100 ^{ef}	2.053^{cd}		>100 ^{ef}
2.021^c		66			

a = experiment performed against free-living *L. mexicana* promastigotes in duplicate wells in 1 experiment, n=1, using a top concentration of at 100 μ M (2 x serial dilution 10-point curve). IC₅₀ values for control and investigative compounds are based off the readout from SYBR Green 1 measurements.

b = control compounds for *L. mexicana* free-living promastigote assay. Average from experimental replicates; Miltefosine IC₅₀= 6.8 μ M

c = control compounds for *L. mexicana* free-living promastigote assay. Average from experimental replicates; Miltefosine IC₅₀= 7.8 \pm 0.52

d = control compounds for *L. mexicana* free-living promastigote assay. Average from experimental replicates; Miltefosine IC₅₀= 33 \pm 18 μ M

e = mean of two separate experiments

f = compound exhibited < 50% inhibition at the top concentration tested (100 μ M)

g = experiment performed against free-living *L. donovani* promastigotes in duplicate wells in 1 experiment, n=1, using a top concentration of at 100 μ M (2 x serial dilution 10-point curve). IC₅₀ values are based off the readout from SYBR Green 1 measurements.

h = control compounds for *L. donovani* free-living promastigote assay. Average from experimental replicates; Miltefosine IC₅₀= 6.3 \pm 1.1 μ M \pm standard deviation

2.06: Analogue Series 3: Amide and Core change studies

The hit **2.001** was able to demonstrate antileishmanial activity against *L. mexicana* and more so against the visceral disease relevant *L. donovani* parasites within the *in vitro* free-living promastigote assay. Hit **2.002** was also found to display antileishmanial activity. However, both hits were found to be less potent than originally reported. Nonetheless, since our initial hits seemed to have the potential for antileishmanial activity, it was decided that exploration surrounding the chemical space of Scaffold 1 would continue, studying one section of the scaffold was studied at a time, so that each structural change and any subsequent biological modulation could be compared to the original hits **2.001**, **2.002** as well as the other analogues within the series. We later aimed to combine the most potent attributes and functionalities, where appropriate during additive SAR studies.

To maximise our efforts as a team, **2.002** was assigned to another group member, investigating changes to the pyridine pyrazole functionality as well as the RHS chemical space of **2.002** (outlined in Chapter 3). This would be explored in parallel to the study around **2.001**. As a result, the SAR studies of this PhD medicinal chemistry project would focus on exploring the chemical space around **2.001**. At a later stage, continued exploration around hit **2.002** would continue within the scope of this PhD medicinal chemistry project and is also discussed within Chapter 3.

Further analogues based around the hit **2.001** were devised, targeting structural changes to the amide and the core, whilst keeping the rest of the structure constant. We aimed to investigate the necessity of the imidazole ring and the amide group in this chemical space. Modifications of the core functionalities may allow us to explore the changes to possible hydrogen bonding interactions within this region and examine the biological outcomes of altering the sterics and orientation around this chemical space. This set of analogues discussed here, within Section **2.06** would form Analogue Series 3. **Figure 2.10** serves as a visual summary of the structural modifications targeted within this series.

Additionally, the synthetic pathways utilized to obtain each of these analogues within this series are discussed below. Whilst the synthesis of Series 3 was underway, our initial library of analogues (Series 1-2) was also sent for further biological assessment in what is considered a more clinically relevant “gold standard” assay, intracellular *L. donovani* amastigote assays, using macrophages as host cells (intramacrophage assay).^{53, 55, 56} The methodology and biological outcomes involving these intramacrophage assays is discussed in Sections **2.08-2.09**. The analogues of Series 3 would also undergo biological evaluation using intramacrophage methods. The results of this biological analysis are outlined in Section **2.10**.

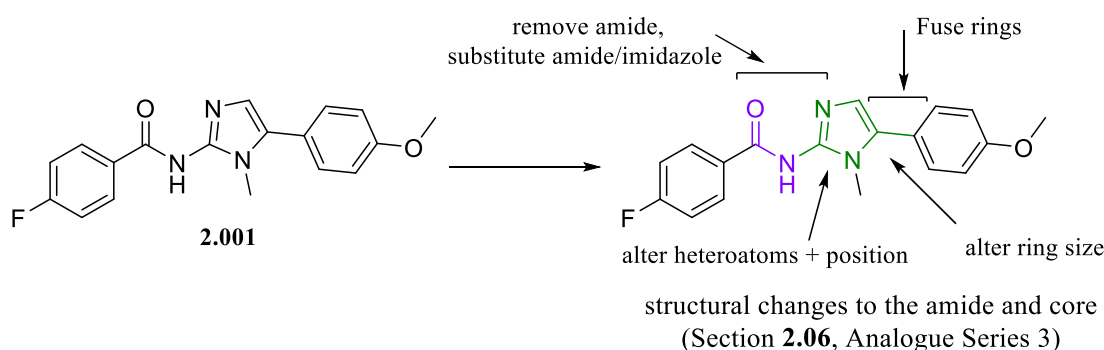


Figure 2.10: Summary of the investigative studies involving structural changes to **2.001** at the amide (purple) and imidazole core (green)

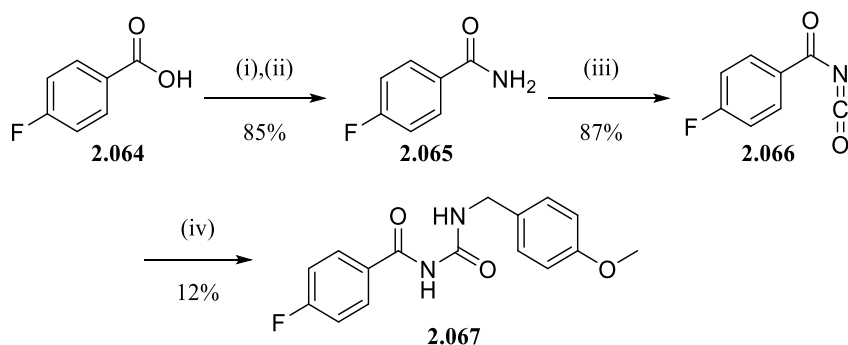
2.06.1 Core Investigation: Acyl Ureas

Replacing the amide-imidazole ring system with acyl ureas was briefly investigated using analogue compounds **2.067** and **2.070**. The aromatic ring was replaced for a smaller non-aromatic functionality that may form a pseudo ring through intramolecular hydrogen bonding interaction. This would allow us to devise whether the imidazole group was a requirement for this system, removing the ability of the core to partake in possible aromatic pi-pi interactions with the putative binding site/s. Additionally, these alterations would allow us to explore the hydrogen bonding capabilities of the urea within this chemical space. This structural change also introduced an additional rotatable bond to the scaffold, in the form of the methylene group linking the acyl urea and methoxy phenyl moieties together. These

overall structural changes may potentially alter the orientation of the scaffold, allowing us to investigate whether interactions between the compound and putative binding site/s could still be formed, or even improved.

The following synthetic routes were utilized to obtain compounds **2.067** and **2.070**, shown in **Schemes 2.07** and **2.08** respectively. To obtain compound **2.067**, following methods outlined by He *et al.*, *para*-fluorobenzoic acid **2.064** was transformed into an acid halide before subsequent formation of the terminal amide **2.065** using ammonium hydroxide in a one pot reaction. Compound **2.065** then reacted with oxalyl chloride to form the isocyanate **2.066** in good yield.⁵⁷ Finally the electrophilic isocyanate **2.066** reacted with the 4-methoxybenzylamine nucleophile to successfully form the desired acyl urea **2.067** following Librowski *et al.*⁵⁸

Scheme 2.07: Synthetic route for acyl urea analogue 2.067



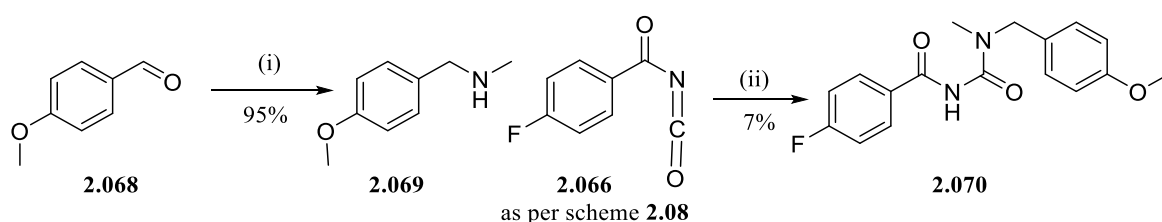
Reaction conditions i) oxalyl chloride, DCM, DMF, ii) NH_4OH , DCM, iii) oxalyl chloride, DCE 0°C , iv) 4-methoxybenzylamine, THF

In the case of compound **2.070**, **Scheme 2.08** depicts that *N*-(4-methoxybenzyl)formamide **2.068** underwent reductive amination using sodium borohydride to achieve 1-(4-methoxyphenyl)-*N*-methylmethanamine **2.069** as described by Park *et al.*⁵⁹ The isocyanate **2.066** and secondary amine **2.069** were then reacted successfully to form the selective *N*-methylated acyl urea **2.070**. The yield of this step was quite low. The 1-(4-methoxyphenyl)-*N*-methylmethanamine, a secondary amine, is a weaker base (lower calculated pK_a) and more sterically hindered than the benzylamine, thus making it a weaker nucleophile, and less willing to react. This most likely contributed to the lower reaction yield observed in **Scheme 2.08**, step ii.

Initial trials at this last stage using room temperature conditions, similar to that of the previous **Scheme 2.08**, Step iv, did not meet any success.^{60, 61} No reaction had occurred, as indicated by LCMS and TLC analysis, revealing only starting material to be present. This could be attributed to the decreased reactivity of the secondary amine, relative to the primary amine used to form compound **2.070**. Temperature was increased to push the reaction forward, though the same outcome occurred at 80°C . However, once the vessel was switched to a sealed tube the desired product was successfully formed,

despite the low yield obtained. As this synthetic route was not to be used routinely, the low yield was not an issue. Additionally, the amount of product obtained from this final step was more than enough to be used for biological testing. To improve the yield of both urea formations of **Schemes 2.07-2.08**, microwave irradiation at a higher temperature may improve the reaction in the future. Furthermore, anhydrous conditions should continue to be employed. Though amines are more nucleophilic and willing to react with the isocyanate than water, decreasing the amount of water within the reaction mixture will help avoid any side reactions occurring and increase product yield further.

Scheme 2.08: Synthetic route for acyl urea analogue 2.070



Reaction conditions i) methylamine, MeOH, NaBH₄, ii) 4-fluorobenzoyl isocyanate (obtained, following previous scheme 2.08 above) Et₃N, DMAP, DCE, 80°C

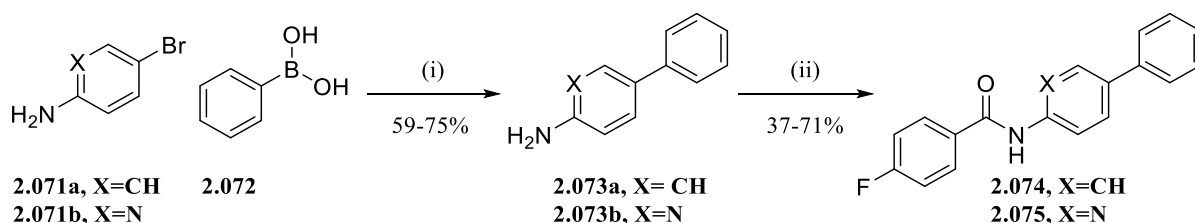
2.06.2 Core Investigation: Pyridine Replacement

Investigations around the chemical space of the imidazole core were continued, proposing a pyridine core as replacement. This would allow us to assess whether a 6 membered aromatic ring was preferential to a 5-membered aromatic ring within this chemical space. This change would also reduce the number of heteroatoms present within the core as well as potentially alter the orientation and fit within the putative binding site/s. Due to the change in sterics, position of the heteroatoms, and bond angles, the position and orientation of the adjacent methoxyphenyl group in relation to the core would be altered. If any pi-pi stacking was present between the original imidazole core and putative binding site, replacement with the sterically larger pyridine may further change the orientation of the scaffold so that the nitrogen atom of the pyridine is directed away from the hypothetical aromatic ring undergoing pi-pi interactions. This allows the topology of the system to achieve the lowest energy and optimal distance for binding interactions.³⁵

To achieve the devised analogues bearing a pyridine core, **Scheme 2.09** was proposed and initially trialled using 4-bromoaniline (**2.071a**) and 5-bromopyridin-2-amine (**2.071b**). These starting compounds would each undergo a Suzuki-Miyaura cross coupling with phenylboronic acid (**2.072**) to achieve aryl-aryl bond formation.^{4, 62, 63} Intermediates **2.073a-b** were obtained with relatively good yield and thus this method would be utilized for future analogues in this series. Intermediates **2.073a-b** underwent subsequent amide coupling employing the same conditions as employed in **Scheme 2.03**.¹¹ Coupling trials occurred with *para*-fluorobenzoic acid, successfully obtaining the desired analogues

2.074 and **2.075**. The analogue **2.075**, which bears the pyridine core was obtained in lower yield (37 %). This was not a concern as the yield was still adequate for obtaining a substantial amount of product for biological testing. The biphenyl based analogue **2.074** was obtained in good yield and was synthesized merely to confirm the success of this synthetic pathway. This analogue does not possess a pyridine core, though was still assessed for antileishmanial activity in case of any serendipitous activity.

Scheme 2.09: General synthetic route followed for analogues bearing a pyridine or phenyl ring core



Reaction conditions i) Pd(PPh₃)₄, Na₂CO₃, H₂O, DMF, 90 °C, ii) 4-fluorobenzoic acid, DMAP, DIPEA, HBTU, ACN, rt or 50 °C

Due to the relative synthetic ease of **Scheme 2.09**, analogues **2.076-2.085** (**Table 2.05**) were also synthesized following this synthetic pathway. The readily available starting materials and large interest in the SAR surrounding the chemical space of this scaffold allowed for several combinations within this series to be formed. These combinations included pairing *ortho*, *meta* and *para*-methoxy groups of the RHS phenyl ring with various pyridine cores, where the methoxyphenyl ring is positioned *ortho*, *meta* and *para* to the nitrogen atom of the pyridine core. These numerous combinations would allow for the potential discovery of any serendipitous antileishmanial activity.

During the synthesis trials of **Scheme 2.09**, the *para*-fluorophenylacetic acid starting material was also coupled to the biphenyl amine (**2.073a**), forming analogue **2.076**. Similar to analogue **2.074**, analogue **2.076** was synthesized to confirm the reliability of the devised synthetic pathway. This analogue would still undergo biological assessment as the increased carbon chain length between the phenyl and amide groups would allow us to explore the effects of increasing the flexibility of the system at this chemical space. Furthermore, this structural modification was supported by the antileishmanial activity of **2.027**, the *para*-fluorophenylacetamide LHS change of Analogue Series 1, observed in the previously described *in vitro* free-living promastigote assay.

Table 2.05: List of analogues synthesized using Scheme 2.09 and their related yields over two steps

I.D	Structure	Yield % (over 2 steps)	I.D	Structure	Yield % (over 2 steps)
2.074		65	2.080		52
2.075		56	2.081		67
2.076		56	2.082		39
2.077		47	2.083		77
2.078		84	2.084		59
2.079		57	2.085		81

Due to the somewhat low reactivity initially seen in part (ii) of **Scheme 2.09**, analogues that continued this series were heated to 50°C in an attempt to drive the reaction forward. In most cases the yield was observed to have improved, however generally lower yields remained for *ortho*-methoxy substituted compounds, which can be attributed to the steric hindrance and therefore their unwillingness to react. Using the synthetic route described in **Scheme 2.09**, 12 additional analogues have been successfully synthesized for biological testing. The biological results of this entire series (Series 3) are discussed in a later segment of this chapter, Section 2.10.

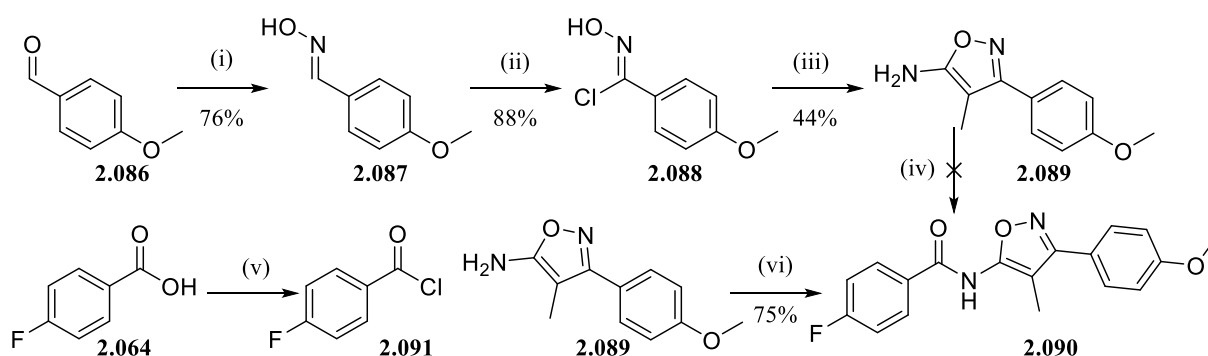
2.06.3 Core Investigation: Isoxazole core

Investigations around the necessity of the imidazole core of Scaffold 1 were continued using analogue **2.090**, which bears an isoxazole core in place of the imidazole ring. The aim this structural change was to keep the overall sterics within this chemical space constant, whilst altering the heteroatoms and their

position within the 5 membered aromatic ring. This change may alter any possible hydrogen bonding interactions between the core and putative binding site/s.

To obtain analogue **2.090**, **Scheme 2.10** was proposed. Following Schwarz *et al.* the starting benzaldehyde **2.086** was converted to the corresponding benzaldoxime compound **2.087** before chlorination with *N*-chlorosuccinimide to obtain the chlorooxime **2.088**.^{64, 65} The chlorooxime **2.088** would then undergo nucleophilic addition with a lithiated alkyl nitrile to obtain the oxazole amine **2.089** as described by Bourbeu *et al.*⁶⁶ Amide coupling was then trialled using the original conditions described in **Scheme 2.10**. However, no reaction occurred. The oxazole amine may have been more unreactive and less nucleophilic than the previous imidazoles (Analogue Series 1-2,) that usually underwent amide coupling following these conditions.¹¹ To remedy this, the *para*-fluorobenzoic acid **2.064** was made more reactive, by first converting it into an acid halide **2.091**, in which the methods were previously discussed in **Scheme 2.07**, step (i).⁵⁷ The acid chloride was then reacted immediately without purification with the oxazole amine to give the desired amide analogue **2.090** successfully.

Scheme 2.10: Synthetic route for isooxazole core analogue 2.090



Reaction conditions i) hydroxylamine, EtOH, H₂O, ii) NCS, DMF, iii) propionitrile, *t*-BuLi, THF, -78 °C, iv) 4-fluorobenzoic acid, HBTU, DMAP, DIPEA, ACN, v) oxalyl chloride, DCM, DMF, vi) Et₃N, THF

The synthetic steps employed to obtain compound **2.090** were mostly achieved in relatively high yield. Seeing as though this synthetic route would not be utilized often, no further optimization was necessary.

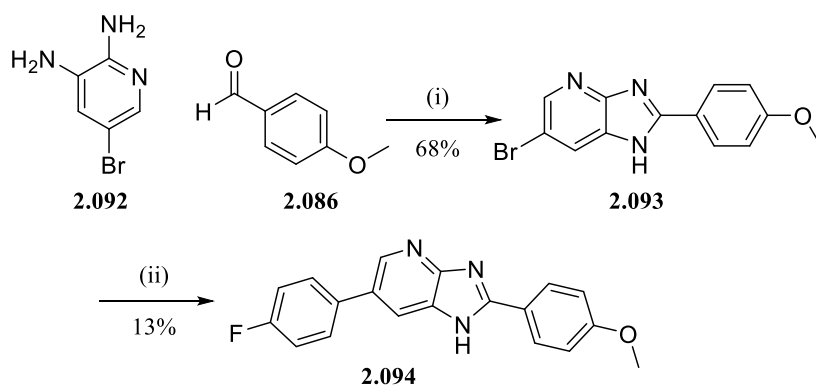
2.06.4 Core Investigation: Fused Imidazopyridine Core

The chemical space around the amide and core of Scaffold 1 were further explored to understand the structural requirements necessary to maintain potent antileishmanial activity and low host cell cytotoxicity. Analogue **2.094** was then devised, which removed the amide functionality of Scaffold 1 to examine whether the amide was critical to maintaining potency. In place of the amide, a pyridine ring was fused to the imidazole to take up the chemical space and maintain some rigidity within the core of the system. The removal of the amide functionality would probe if the loss of any potential hydrogen bonding interactions between the amide and the putative binding site/s correlated to the loss

of activity. The addition of the pyridine ring would increase lipophilicity and steric bulk to the scaffold, allowing us to explore if analogue **2.094** would still fit within the putative binding site/s and allow for any key interactions to be made. This would also gauge whether any extra lipophilic and/or pi-pi interactions could be made between the newly introduced aromatic ring and the putative binding site/s. The increased lipophilicity of **2.094** may also allow for an improved ability of the compound to permeate through the cell, and cross the various biological barriers, possibly leading to an increased ability to exert antileishmanial activity within the desired putative binding site/s.

The following synthetic route was proposed to obtain analogue **2.094**, shown in **Scheme 2.11**. Following the synthetic strategy proposed by Taha *et al.*, the synthetic route the synthetic route began with 5-bromopyridine-2,3-diamine **2.092** and 4-methoxybenzaldehyde **2.086**, which were cyclized to the fused imidazopyridine core intermediate **2.093**, before undergoing Suzuki coupling to give the desired analogue **2.094**.^{4, 62, 63, 67} Analogue **2.094** was obtained in low yield, following the conditions listed in step ii of **Scheme 2.11**. Optimization of the Suzuki coupling step was briefly undertaken in **Scheme 2.12** to improve product yield.

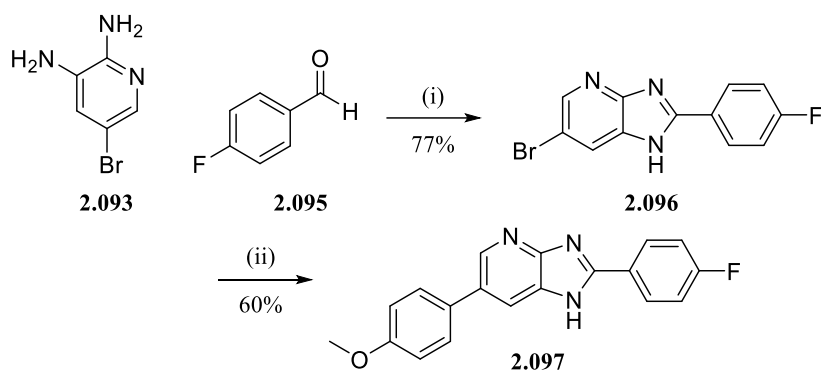
Scheme 2.11: Synthetic route for analogue 2.094.



Reaction conditions i) NaHSO₄, DMF, 130°C, ii) 4-fluorophenylboronic acid, Pd(PPh₃)₄, Na₂CO₃, DMF, H₂O, 90°C.

Due to the relative synthetic ease of **Scheme 2.11**, analogue **2.097** was also devised. This involved the pyridine ring fused to the opposite end of the imidazole ring, attached to the methoxy phenyl ring rather than the fluorophenyl group. By doing so, I would also be able to investigate if the sterics and orientation were more favourable with the pyridine in this position. The synthetic scheme, shown in **Scheme 2.12**, remained relatively the same as the previous. Due to the low yield of the Suzuki coupling for this system, observed in step ii of **Scheme 2.11**, we began to investigate using other catalysts for this step to optimize the reaction conditions and improve the product yield. Fortunately, the first catalyst that was trialled, dichlorobis(triphenylphosphine)palladium greatly improved the product yield therefore there was no need to continue trialling conditions.⁶⁸ No further synthetic optimizations were made as this synthetic route would not be employed regularly.

Scheme 2.12: Revised Synthetic route for analogue 2.097



Reaction conditions i) NaHSO₄, DMF, 130°C, ii) 4-methoxyphenylboronic acid, Pd(PPh₃)₂Cl₂, Na₂CO₃, DMF, H₂O, 90°C.

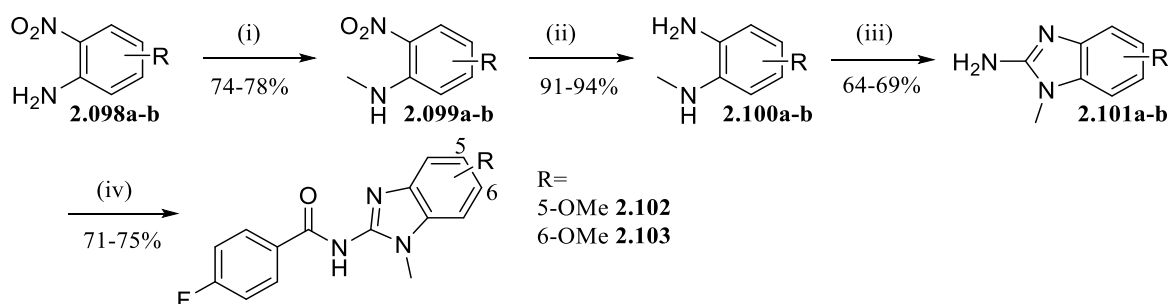
2.06.5 Core Investigation: Benzimidazole Core

A brief investigation surrounding the need for the space between the imidazole and adjoining RHS phenyl ring was explored. Like the previous analogues, we have prepared fused rings, this time in the form of benzimidazoles to ascertain whether this change in the RHS ring position and orientation was preferred. The RHS methoxy group was placed at the 5 and 6 positions of the benzamide ring to retain some similarity to the chemical space of hit **2.001**, aiming to minimise changes to the fused ring only. Though, positioning the methoxy substituents at the 5 and 6 positions would not be a perfect mimic of the RHS chemical space of hit **2.001**. The fused ring system would cause a change in position and orientation of the methoxyphenyl ring and therefore may also change the ability of the methoxy substituent to interact with the putative binding site/s.

To obtain the desired benzimidazole based analogues **2.102**, **2.103**, the synthetic pathway **Scheme 2.13** was devised. Firstly, the nitroaniline (**2.098**) was *N*-methylated using iodomethane to give the intermediate **2.099**, followed by the reduction of the nitro group by means of hydrogenation.⁶⁹ Compound **2.100** was then cyclized using cyanogen bromide to form the 2-aminobenzimidazole (**2.101**).⁷⁰ The amino building block can then undergo amide coupling with 4-fluorobenzoic acid to acquire analogues **2.102-2.103** in good yield.¹¹

This analogue set, along with the previously discussed analogues of Section **2.06** would form Analogue Series 3. As mentioned, each of these analogues underwent biological evaluation using *L. donovani* intramacrophage assays, to be discussed in Section **2.10**.

Scheme 2.13: Synthetic route for analogue 2.102-2.103



Reaction conditions i) MeI, NaH, DMF, 35°C, ii) Pd/C, H₂, MeOH, iii) CNBr, MeOH, H₂O, 60°C, iv) 4-fluorobenzoic acid, DMAP, DIPEA, HBTU, ACN

2.07: Axenic promastigote assay to intracellular amastigote assay

Various HTS in *Leishmania spp.* drug discovery with axenic amastigotes and promastigotes have been well described throughout the literature. These methods are still used in drug screening due to fact that they are inexpensive, straightforward assays, that are easily cultured in suspension. These assays allow for quick and easy screening against large libraries for identification of hit compounds. However, assays employing intracellular *Leishmania spp.* amastigotes, using cultured macrophages infected with the parasite (intramacrophage assays) are still considered the more clinically relevant investigative method, as discussed in Chapter 1, Section 1.07.^{52, 53, 71-74} Briefly, an intracellular assay which evaluates the ability of a compound to kill amastigotes within a macrophage much more closely reflects clinical representation, as it involves:

- The more relevant disease-causing stage of the parasite, the intracellular amastigotes
- Physiological barriers of and within the cell; compounds must be able to permeate at both neutral and acidic pH, in order to cross the macrophage, phagolysosome and *Leishmania* membrane. Even if a compound could kill intracellular amastigotes, it still needs to be able to reach them.⁵³
- A harsh environment; the acidic compartments within the cell in which amastigotes hide, thereby measuring the ability of a compound to exhibit activity at the target site. Microbicidal agents such as reactive oxygen species (ROS) can be present within this environment.
- Potential activity against the host macrophage itself; activity of a compound against the parasite and the host cell can be measured. Using fluorescent staining and high content imaging methods (discussed in Sections 2.08-2.09) the cytotoxicity of a compound against the host macrophage can be determined from the intramacrophage assay. This would help us accomplish one of the

initial goals stated in Section **2.01**, determining whether the diversity set of Scaffold 1 caused cytotoxicity against the host cells.

De Rycker *et al.* suggests the use of intracellular *Leishmania spp.* over the free-living parasites due to the higher false positive rates reported using axenic methods, where few compounds found active against axenic parasites translated into intracellular activity.^{53, 75} A few of the reasons that cause this lack of correlation include the differences in the accessibility to the host cell, rate of replication between free-living and intracellular parasites, and their localization.

- Investigative compounds may utilize the host macrophage within their mode of action, requiring the host cell to be present to illicit antileishmanial activity. Correspondence with our collaborators at Bio21 suggest compounds may target the macrophage directly, or indirectly, following host directed therapy, resulted in parasite clearance. Such a mechanism would not be observed within the free-living promastigote assay.
- Amastigote replication is significantly slower intracellularly when compared to the free-living parasite.^{53, 75} The rate of amastigote division *in vivo* is reported to be likely at a rate between intramacrophage and free-living assays. As such, neither are completely representative of the *in vivo* growth rate, and such an *in vitro* intracellular model which more closely replicates *in vivo* parasite growth rates has yet to be widely used.⁵³ Nonetheless, the difference in proliferative rates may correlate to a difference in drug sensitivity, where the replicating cells are more sensitive to inhibition. As reported in the literature, the high growth rate of the axenic amastigote assay may also identify both cyto-cidal and static compounds. Using this assay method, the ability of a compound to prevent parasite replication may be viewed as cidal, but in actuality may only be growth-slowing, or static, where the parasite burden has not been reduced completely.⁵³
- In regard to the environment of the parasite, the phagolysosome is likely a very different environment to the *in vitro* free-living promastigote assay media, rich in glucose, amino acids and vitamins. This is optimized to keep promastigotes alive and content, allowing for the proliferation of the parasite, short term. The proliferation of the promastigotes was key to measuring the ability of a compound completely reduce parasite burden and prevent further proliferation. The formulation of the modified CDM is listed in the Experimental section of this chapter. In contrast, nutrient limitations may occur in the harsher phagolysosome environment. The acidic pH of the parasitophorous vacuole in which the parasites localize, along presence of microbicidal agents such as reactive oxygen species (ROS) are other key differences to the assay environments. Through correspondence with our collaborators at Bio21, they suggest that the difference in nutrient levels, pH and presence of microbicidal agents may result in a

difference in parasite sensitivity toward the investigative compounds. Furthermore, since compounds must possess the ability to cross three biological membranes at both neutral and acidic pH, De Rycker *et al* states many compounds displaying potency against free-living *Leishmania*, may not be able to overcome these physiological barriers and reach the parasite intracellularly to exert their activity.⁵³

It should be noted that for these reasons, the intracellular assay may not identify potentially interesting compounds that could be optimized as new leads. However, for the purposes of our early hit-to-lead SAR campaign, the intramacrophage assay was the most biologically relevant *in vitro* method available to us.

Overall, the free-living promastigote assay did not necessarily reflect the physiological situation to the same degree as the intramacrophage assay. Despite this, it is still informative, more accessible and is significantly less time-consuming and less costly assays to employ.⁷⁶ We initially sought out to use the free-living promastigote assay, then employ the intracellular assays to confirm activity as previously undertaken in the literature.¹ However, this would become quite time consuming, add to cost and there were also concerns pertaining to the higher false positive rates associated with axenic assays.^{53, 77} Therefore, it was decided that the intracellular *L. donovani* amastigote assay (intramacrophage assay) would be used exclusively to assess antileishmanial activity. As discussed in Chapter 1, and further highlighted above, *Leishmania spp.* can be quite a difficult to target during the drug discovery process. Therefore, it was decided that a robust, routinely used, clinically relevant biological assessment was required. Several compounds which reported inactivity within the *in vitro* free-living promastigote assay were found to possess significant potency against *L. donovani* within the intramacrophage imaging assays undertaken by undertaken by the Avery group at the Griffith Institute for Drug Discovery (GRIDD) (Section **2.08**) and our collaborators at Bio21 (Section **2.09**). Therefore, the results derived from the promastigote assay were set aside in favour of intramacrophage imaging assays. The intramacrophage assays both assessed our compounds of interest against *L. donovani* amastigotes within THP-1 transformed macrophages, using high content screening. Though similar, these methods are not identical and the differences between assays is outlined in Section **2.09**. Despite the need for retesting, this was a good exercise for our group, as it further highlighted the complicated needs of *Leishmania* biological assays. These assessments are quite difficult to carry out, even at a high-throughput level and thus expensive to employ. Therefore, we also decided to focus our efforts on the currently relevant *L. donovani* species only.

2.08 Initial biological testing with amastigote intramacrophage imaging assay performed by GRIDD

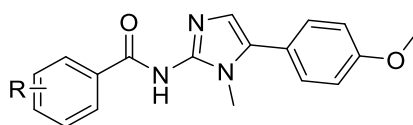
As mentioned, the analogues of Series 1-2 were retested against intracellular *L. donovani* amastigotes using the intramacrophage assay performed by GRIDD. The biological results are summarized below in **Tables 2.06-2.08** and were used to shape further investigations around the chemical space of Scaffold 1. This assay is routinely operated by our collaborators at GRIDD and was initially considered a robust “gold standard” assay for early antileishmanial assessment. This assay employs differentiated, non-dividing human acute monocytic leukemia cells (THP-1) host cells. The THP-1 host cells were transformed into macrophages via phorbol 12-myristate 13-acetate (PMA). Metacyclic promastigotes were used to infect transformed THP-1 macrophages at a multiplicity of infections (MOI) rate of 5:1 (parasite: host). The promastigotes were differentiated into amastigotes within the host cells. Therefore, compounds are added whilst the parasite is differentiating as it takes approximately 3-4 days to transform into an amastigote from a promastigote. The cells were treated with our test compounds for 96 h at a concentration range of 0.004-80 μM using a 14-point dose-response format to calculate the 50% inhibitory concentrations (IC_{50}) along with assessing the viability of the host THP-1 macrophages (CC_{50}). This intramacrophage imaging assay uses an Opera high-content imaging system. Healthy host cells were identified based on Cell Mask Deep Red cytoplasmic and SYBR green nuclear area and intensities. Intracellular parasites can be identified within the host cell cytoplasm using the SYBR green fluorescent staining and spot detection algorithms measuring the size and intensity used to define the *Leishmania* nucleus. An infected cell was defined as >3 parasites within the host cell cytoplasm. The complete method is outlined in the Experimental Section.⁷⁸ It was also noted that solubility issues occurred during this screen. In several cases, compounds displayed some activity ($>50\%$ inhibition) but were not able to reach a top plateau (usually $>90\%$ in the plateau of activity), therefore an IC_{50} or CC_{50} value was not able to be determined from the sub-efficacious curve. Where an IC_{50} or CC_{50} value could not be generated, the concentration which provides close to 50 % inhibition is reported. Therefore, **Tables 2.06-2.08, 2.10** and later studies within Chapter 3 report the biological results of several analogues as a percentage inhibition at certain concentrations where greater than 50 % activity was observed, though was not enough to achieve meaningful inhibition of the parasite. To get an absolute IC_{50} or CC_{50} value for these compounds, they must be tested at higher concentrations. For the purposes of our SAR studies, this was considered costly, time consuming and unnecessary, as our focus would be centred around analogues which demonstrated more obvious potency. The control compounds employed by GRIDD include amphotericin B and known *Leishmania* inhibitors VL-2098 (DNDI-VL-2098) and DNDI-1044, which were discussed in Chapter 1. Throughout this thesis, the GRIDD intramacrophage IC_{50} values calculated for amphotericin B, VL-2098 and DNDI-1044 reproducibility fell between 0.065-0.39 μM , 0.57-1.8 μM and 0.13-0.40 μM . These values are consistent with intracellular values reported within the literature and indicates that limited variability exists between

assays. For transparency, the controls are presented for each GRIDD experiment throughout this thesis.

52-54, 78-80

Compounds identified from the first few sets of results received are outlined in **Tables 2.06-2.08**. These compounds were later reassessed by the same assay described above, along with similar assays by independent groups. The assay methods undertaken by other independent groups is described later in Chapter 2 and 3. Divergent activity was later observed between our initial “best” compounds, changing the trajectory of our SAR hit-to-lead campaign. This is to be discussed later in this chapter (Sections **2.09**). Within this section (**2.08**) our initial SAR rationale based on these early sets of biological results are described below.

Table 2.06: Initial intramacrophage amastigote assay results for analogues with simple LHS substituent changes compared to hit 2.001 (blue)



I.D	R	IC ₅₀ ^{ab} (μM)	CC ₅₀ ^{ab} (μM)	I.D	R	IC ₅₀ ^{ab} (μM)	CC ₅₀ ^{ab} (μM)
2.001[†]	4-F	>80 ^f	>80 ^f	2.021[†]	2-Br	>80 ^f	>80 ^f
2.008[†]	H	>80 ^f	>80 ^f	2.022[†]	2-CN	>80 ^f	>80 ^f
2.009[†]	4-Br	2.1 ± 0.62	>80 ^f	2.023^c	2-OMe	57% at 80 μM*	>80 ^f
2.010[†]	4-CN	>80 ^f	>80 ^f	2.024[†]	2-Me	0.38 ± 0.040	>80 ^f
2.011[†]	4-OMe	>80 ^f	>80 ^f	2.025^{d†}	2-NO ₂	52% at 40 μM *	>80 ^f
2.012^{c†}	4-Me	2.3 ± 0.17	57% at 80 μM*	2.026[†]	3,4- Me	>80 ^f	64% at 80 μM*
2.013[†]	4-NO ₂	37 ± 0.62	27 ± 0.60	2.029[†]	4-[N]	>80 ^f	64% at 80 μM *
2.014[†]	3-F	>80 ^f	>80 ^f	2.030[†]	3-[N]	>80 ^f	>80 ^f
2.015[†]	3-Br	1.7 ± 0.10	>80 ^f	2.031[†]	2-[N]	>80 ^f	>80 ^f
2.016[†]	3-CN	>80 ^f	>80 ^f	2.052^{c†}	2-OH	56% at 20 μM*	34% at 80 μM*
2.017^{c†}	3-OMe	57% at 8 μM*	52% at 80 μM *	2.053^d	3-OH	>80 ^f	>80 ^f
2.018[†]	3-Me	0.45 ± 0.040	>80 ^f	2.054^c	4-OH	>80 ^f	>80 ^f
2.019^{d†}	3-NO ₂	>80 ^f	54% at 40 μM*	2.062^{e†}	2-CN, 4-F	>80 ^f	>80 ^f
2.020[†]	2-F	>80 ^c	>80 ^c	2.063^{d†}	2-NO ₂ , 4-F	>80 ^c	>80 ^c

a = anti *L. donovani* activity and toxicity measured in THP-1 transformed macrophage host cell lines using a top concentration of 80 μM (14-point curve). Experiment performed in duplicate wells. Values are means of two experiments, n=2.

b= control compounds for GRIDD *L. donovani* intramacrophage assay. Average from experimental replicates; Amphotericin B IC₅₀= 0.39 ± 0.0070 μM, CC₅₀= 1.5 ± 0.070 μM, VL-2098 IC₅₀= 1.8 ± 0.17 μM, CC₅₀> 80 μM, DNDI-1044 IC₅₀= 0.40 ± 0.014 μM, CC₅₀> 80 μM.

c= control compounds for GRIDD *L. donovani* intramacrophage assay. Average from experimental replicates; Amphotericin B IC₅₀= 0.076 ± 0.0020 μM, CC₅₀= 0.73 ± 0.18 μM, VL-2098 IC₅₀= 0.67 ± 0.21 μM, CC₅₀> 40 μM, DNDI-1044 IC₅₀= 0.13 ± 0.037 μM, CC₅₀> 40 μM.

d= control compounds for GRIDD *L. donovani* intramacrophage assay. Average from experimental replicates; Amphotericin B IC₅₀= 0.067 ± 0.0020 μM, CC₅₀= 0.94 ± 0.046 μM, VL-2098 IC₅₀= 0.57 ± 0.18 μM, CC₅₀> 40 μM, DNDI-1044 IC₅₀= 0.18 ± 0.040 μM, CC₅₀> 40 μM.

e= control compounds for GRIDD *L. donovani* intramacrophage assay. Average from experimental replicates; Amphotericin B IC₅₀= 0.065 ± 0.0060 μM, CC₅₀= 0.73 ± 0.0040 μM, VL-2098 IC₅₀= 0.64 ± 0.068 μM, CC₅₀> 40μM, DNDI-1044 IC₅₀= 0.21 ± 0.013 μM, CC₅₀> 40 μM. f= <50% activity at the top concentration tested (80 μM). Values are the means of two experiments
* CC₅₀ value is determined from a sub-efficacious curve. Solubility in the intermediate dilution in medium may have contributed to this effect observed.

† Out of solution in media reported between 800-20 μM

± standard deviation

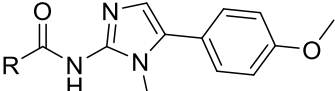
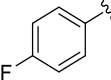
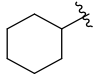
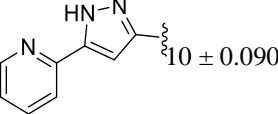
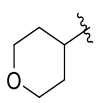
Depicted above, **Table 2.06** summarises the biological results of the hit **2.001** and the analogues devised to explore small substituent changes around the LHS ring of Scaffold 1. These analogues were based around hit **2.001** and the resulting structural changes can be compared directly. Contrary to the results obtained in the previous free-living promastigote assay (**Table 2.05**), strong electron withdrawing groups at the *ortho* (**2.022, 2.025**) and *para* (**2.010, 2.013**) positions were not favourable changes to the LHS chemical space and correlated to a loss in activity. Additionally, the pyridine replacements (**2.029-2.031**) which also displayed antileishmanial activity within the previous free-living promastigote assay were also found inactive within the intramacrophage assay. These compounds might be viewed as false positives, where the increased difficulty in reaching and exerting activity against the intracellular amastigote may have led to their inefficacy. Unsurprisingly, the initial additive SAR analogues **2.062-2.063**, which combined the *ortho*-EWG substituent with the *para*-fluoro, were also found inactive. Furthermore, solubility issues were associated with these compounds, where analogues were reported to partially crash out of solution during the assay. The inability to solubilize into the media and subsequently permeate the various cell barriers may have further contributed to compound inactivity. Additionally, repositioning the strong electron withdrawing groups to the *meta* position (**2.016, 3-CN** and **2.019, 3-NO₂**) also reported complete inactivity against *L. donovani*.

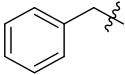
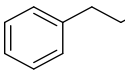
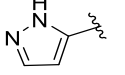
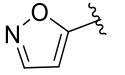
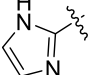
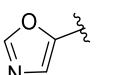
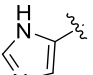
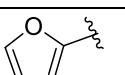
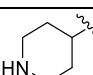
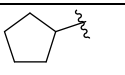
The hit **2.001** had also previously displayed antileishmanial activity against free-living promastigotes, though was observed here to be inactive within this intramacrophage assay. Solubility issues were once again reported and may be the reason for this unexpected result. However, compound **2.059**, a very close analogue to hit **2.001** gave very high potency (**Table 2.08**), which gave us reason to believe the scaffold based on **2.001** does indeed hold potential activity (see **Table 2.08** discussion below). The fluoro group was not tolerated in the *ortho* or *meta* position (**2.020** and **2.014** respectively). Interestingly, replacing the *para*-fluoro with the *para*-bromo (**2.009**) and *para*-methyl (**2.011**) substituents was preferred, where potent activity and selectivity against the parasite was reported for these analogues. Despite the solubility issues reported for these compounds, repositioning the bromo and methyl substituents around the LHS ring correlated to a large improvement in antileishmanial activity, where the *ortho* and *meta*-methyl substituted analogues reached sub-micromolar range (**2.018, 2.024** <0.5 μM). It seemed that these slightly larger and more hydrophobic, non-hydrogen bonding substituents were shown to be most favourable substituents within this chemical space, in comparison to **2.001**. This favourability excluded the *ortho*-bromo **2.021**, which was observed to cause a loss in antileishmanial activity. Surprisingly, the 3,4-methyl substituent **2.026** also correlated to a complete loss of activity, which may suggest

interactions between the putative binding site/s and mono-substituted phenyl groups were preferred. However, at this stage the exact reason for the inactivity of **2.026** was uncertain and the poor solubility reported may have also contributed to inactivity. The unsubstituted phenyl ring (**2.008**) also caused a loss in activity. Based on **Table 2.06**, it seemed that the unsubstituted phenyl ring could not maintain possible key interactions with the putative binding site/s and possibly required the addition of a larger, more hydrophobic substituent around the ring in order to exert antileishmanial activity. Finally, introducing the methoxy (**2.011**, **2.017**, **2.023**) and hydroxy substituents (**2.052-2.054**) around the phenyl ring correlated to poor inhibition of the parasite. This could suggest stronger electron donating groups and an electron rich ring may not be favoured within this chemical space. By comparing the methoxy (**2.011**, **2.017**, **2.023**) and hydroxy (**2.052-2.054**) substituted analogues to the newly found potent bromo (**2.009**, **2.015**) and methyl (**2.012**, **2.018**, **2.024**) substituted analogues, it seemed that the ability to form hydrogen bonding interactions with the putative binding site/s may not be required to maintain activity. It may be that key non-covalent, non-hydrogen bonding interactions such as Van der Waals (methyl), ionic, or dipole (halogens) interactions are present between the LHS moiety of Scaffold 1 and the putative binding site/s.

The analogues which were found highly potent within this assay (compounds **2.009**, **2.012**, **2.015**, **2.018**, **2.024**) did not display activity during the previous free-living promastigote assay. It may be possible that these compounds utilize macrophage or other intracellular components without harming them, within their mechanism of action. The same may be said of the most active compounds outlined below in **Table 2.07-2.08**. It is important to reiterate, our hits were obtained from a phenotypic screen and at time of writing we have yet to elucidate the mechanism of action of Scaffold 1. No significant host cell cytotoxicity was observed within this set of analogues. At most, only analogue **2.013** reported very mild cytotoxicity ($CC_{50} = 27 \mu M$) within this assay. Overall, it would seem this set of analogues did not exert host cell cytotoxicity.

Table 2.07: Initial intramacrophage amastigote assay results for analogues with LHS ring changes compared to hit 2.001 and 2.002 (blue)

							
I.D	R	IC ₅₀ ^{ab} (μM)	CC ₅₀ ^{ab} (μM)	I.D	R	IC ₅₀ ^{ab} (μM)	CC ₅₀ ^{ab} (μM)
2.001[†]		>80 ^e	>80 ^e	2.037[†]		1.6 ± 0.10	>80 ^e
2.002^c		10 ± 0.090	>80 ^e	2.038^{d†}		>80 ^e	>80 ^e

2.027		>80 ^e	>80 ^e	2.039^c	Me	48% at 80μM*	>80 ^e
2.028[†]		>80 ^e	>80 ^e	2.040^c	Et	68% at 40μM*	>80 ^e
2.032[†]		>80 ^e	>80 ^e	2.041^c	Pr	>80 ^e	>80 ^e
2.033[†]		>80 ^e	>80 ^e	2.042^c		5.3 ± 0.23	>80 ^e
2.034		>80 ^e	>80 ^e	2.043^c		>80 ^e	>80 ^e
2.035[†]		>80 ^e	>80 ^e	2.058^d		>80 ^e	>80 ^e
2.036[†]		97% at 80μM*	>80 ^e				

a = anti *L. donovani* activity and toxicity measured in THP-1 transformed macrophage host cell lines using a top concentration of 80 μM (14-point curve). Experiment performed in duplicate wells. Values are means of two experiments, n=2.

b= control compounds for GRIDD *L. donovani* intramacrophage assay. Average from experimental replicates; Amphotericin B IC₅₀= 0.39 ± 0.0070 μM, CC₅₀= 1.5 ± 0.070 μM, VL-2098 IC₅₀= 1.8 ± 0.17 μM, CC₅₀> 80μM, DNDI-1044 IC₅₀= 0.40 ± 0.014 μM, CC₅₀> 80 μM.

c= control compounds for GRIDD *L. donovani* intramacrophage assay. Average from experimental replicates; Amphotericin B IC₅₀= 0.076 ± 0.0020 μM, CC₅₀= 0.73 ± 0.18 μM, VL-2098 IC₅₀= 0.67 ± 0.21 μM, CC₅₀> 40μM, DNDI-1044 IC₅₀= 0.13 ± 0.037 μM, CC₅₀> 40 μM.

d= control compounds for GRIDD *L. donovani* intramacrophage assay. Average from experimental replicates; Amphotericin B IC₅₀= 0.067 ± 0.0020 μM, CC₅₀= 0.94 ± 0.046 μM, VL-2098 IC₅₀= 0.57 ± 0.18 μM, CC₅₀> 40μM, DNDI-1044 IC₅₀= 0.18 ± 0.040 μM, CC₅₀> 40 μM.

e= <50% activity at the top concentration tested (80 μM). Values are the means of two experiments

* CC₅₀ value is determined from a sub-efficacious curve. Solubility in the intermediate dilution in medium may have contributed to this effect observed.

[†] Out of solution in media reported between 800-20 μM

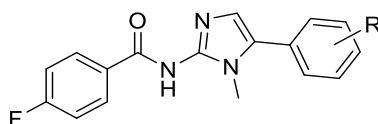
± standard deviation

The analogues listed above in **Table 2.07** were devised to compare structural changes of the entire LHS chemical space, based around hits **2.001-2.002**. The hit **2.002** was reported to display antileishmanial activity, though was found to be less potent than initially described by Pena *et al.*¹ In comparison to the pyridine pyrazole hit **2.002**, the analogue **2.032** which removed the pyridine ring and retained the pyrazole ring, reported a complete loss of antileishmanial activity. This suggested that the pyridine is required to maintain activity when a pyrazole was also present. Issues with solubility were reported and may have hindered the ability of the pyrrole analogue **2.032** to exert any antileishmanial activity. In comparison to compounds **2.002** and **2.032**, it seemed that the placement of the heteroatoms was highly important regarding the lone 5-membered rings. The 1*H*-imidazole-2-carboxamide (**2.042**) displayed improved potency when compared to both hits **2.001** and **2.002**. However, by moving the nitrogen to give the 1*H*-imidazole-5-carboxamide (**2.043**) a complete loss of activity was observed. It seemed that the orientation and placement of the heteroatoms within the 5 membered aromatic ring was imperative, where certain only arrangements of the heteroatoms allowed for antileishmanial activity. These certain arrangements may allow for the compound to undergo potentially specific and short-range hydrogen bonding interactions with the putative binding site/s. Furthermore, a lack of potency was observed in

the furan (**2.035**), isoxazole (**2.033**) and oxazole (**2.034**) based analogues. This inactivity may also be attributed to the heteroatoms incorporated within the 5 membered aromatic ring, as well as their arrangement. Interestingly, based on the greater potency observed from the cyclohexane-based analogue (**2.037**), it seemed that the specificity of the 5 membered aromatic ring may not be solely imperative to achieving antileishmanial activity. This structural modification removed the aromaticity within the LHS chemical space, thereby removing the planar arrangement capable of engaging in pi-pi interactions with the putative binding site/s.

At this stage, excluding **2.037**, analogues that had reported improved antileishmanial activity, all possessed aromatic systems. It was not clear why **2.037** gave such an improvement to potency when compared to hits **2.001**, **2.002**, though the improved activity of **2.037** suggested that that this portion of the chemical space may not be so particular in relation to possible binding interactions that may occur with the putative binding site/s. Despite this, the addition of a heteroatom (**2.038**, **2.058**) or decreasing the size of the aliphatic ring (**2.036**) was not tolerated within the putative binding site/s and reported complete inactivity. Furthermore, the removal of the cyclic system in place of a short aliphatic chain (**2.039-2.041**) was not tolerated. This suggested that some specificity was still required within this chemical space, where not all aliphatic functionalities were tolerated. Finally, analogues **2.027-2.028**, which extended the carbon-carbon chain between the amide and LHS aromatic ring, were found inactive against intracellular *L. donovani*. The increased number of rotatable bonds and flexibility of the scaffold was found unfavourable using the intramacrophage assay. Compounds **2.027-2.028** originally displayed activity against free-living promastigotes and may be considered here as false positives. The reported inactivity of **2.027-2.028** may be due to the increased degree of difficulty for analogues to reach and exert potency against intramacrophage amastigotes. No cytotoxicity was observed within this set of analogues against the host macrophage. The analogues surrounding Scaffold 1 are reported to be selective for the parasite only.

Table 2.08 Initial intramacrophage amastigote assay results for analogues with RHS ring changes compared to hit 2.001 (blue)



I.D	R	IC ₅₀ ^{ab} (μM)	CC ₅₀ ^{ab} (μM)
2.001 [†]	4-OMe	>80 ^d	>80 ^d
2.059 [†]	H	0.316±0.05	>80 ^d
2.060	3-OMe	>80 ^d	>80 ^d
2.061 ^c	2-OMe	>80 ^d	>80 ^d

a = anti *L. donovani* activity and toxicity measured in THP-1 transformed macrophage host cell lines using a top concentration of 80 μM (14-point curve). Experiment performed in duplicate wells. Values are means of two experiments, n=2.

b= control compounds for GRIDDD *L. donovani* intramacrophage assay. Average from experimental replicates; Amphotericin B IC₅₀= 0.39 ± 0.0070 μM, CC₅₀= 1.5 ± 0.070 μM, VL-2098 IC₅₀= 1.8 ± 0.17 μM, CC₅₀> 80μM, DNDI-1044 IC₅₀= 0.40 ± 0.014 μM, CC₅₀> 80 μM.

c= control compounds for GRIDD *L. donovani* intramacrophage assay. Average from experimental replicates; Amphotericin B IC₅₀= 0.076 ± 0.0020 μM, CC₅₀= 0.73 ± 0.18 μM, VL-2098 IC₅₀= 0.67 ± 0.21 μM, CC₅₀> 40μM, DNDI-1044 IC₅₀= 0.13 ± 0.037 μM, CC₅₀> 40 μM.

d= <50% activity at the top concentration tested (80 μM). Values are the means of two experiments

* CC₅₀ value is determined from a sub-efficacious curve. Solubility in the intermediate dilution in medium may have contributed to this effect observed.

† Out of solution in media reported between 800-20 μM

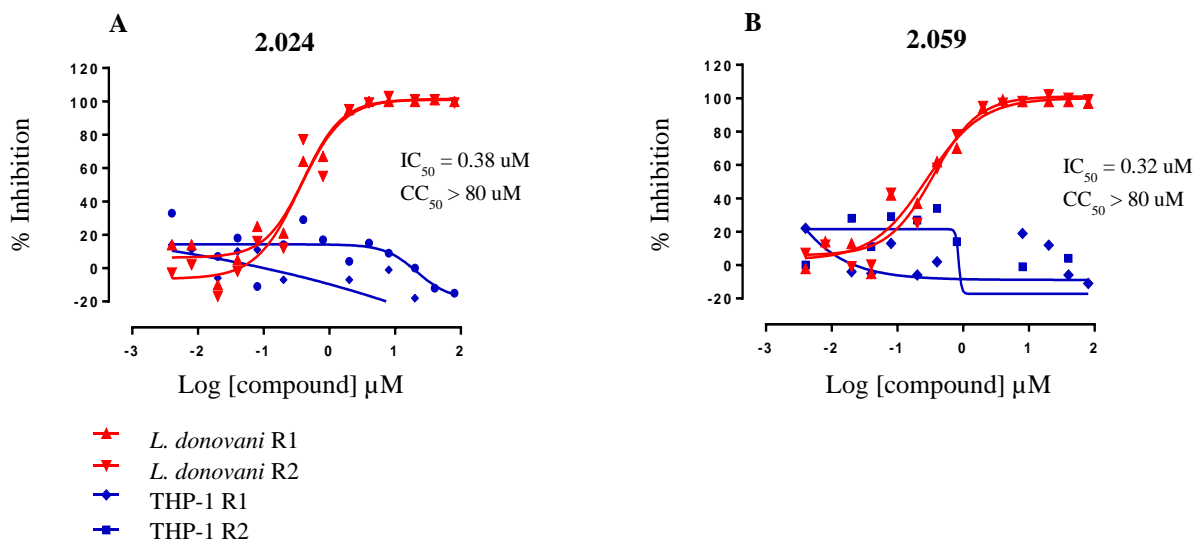
± standard deviation

The brief investigation around the RHS ring is outlined in **Table 2.08**. This study was undertaken to determine the necessity of the *para*-methoxy substituent. These analogues can be directly compared to hit **2.001** which also displayed poor activity within this assay. At the time, the antileishmanial activity and selectivity of compound **2.059** was encouraging. Of the initial diversity set (Series 1-2), analogue **2.059** displayed the highest potency against *L. donovani*. At this time, it was thought that the removal of the *para*-methoxy may have allowed for a better fit within the putative binding site/s, giving the improved activity. Excluding the removal of the RHS *para*-methoxy group, the chemical structure of analogue **2.059** is identical to that of the hit. Due to this, we initially thought the inactivity related to our hit **2.001** was related to the solubility issues reported, hampering the ability of **2.001** to exhibit the antileishmanial activity, originally reported by Pena *et al.*¹ Therefore, it was decided that exploring the chemical space of Scaffold 1, based around both **2.001** and **2.059** would continue. Further biological assessment was undertaken by Bio21 (Section **2.10**), and later by other independent labs (Chapter 3) to determine the true activity pertaining to this hit along with other key analogues. Moving the methoxy group to the *meta* (**2.060**) and *ortho* (**2.061**) position of the RHS ring were found to be unfavourable structural changes, reporting inactivity within the GRIDD intramacrophage assay. No cytotoxicity was observed within this small set of analogues against the host macrophages.

The dose response curves of key compounds **2.024** and **2.059** are depicted in **Figure 2.11**, which serves as a visual demonstration of the activity and selectivity of these compounds of interest against *L. donovani* within THP-1 macrophages. These curves are included here as key representatives of the subset of compounds found highly potent within the GRIDD intramacrophage assay. The red curve shown within **Figure 2.11a-b** was used to derive the IC₅₀ value of compound inhibition against *L. donovani*. From these curves, an increase in drug concentration (x axis) corresponds to an increase in percentage inhibition (y axis) and reduced parasite burden. A host cell was defined as infected if the host cell contained more than 3 parasites within the cytoplasm boundary. The measure of host cell viability is depicted in blue. Some noise was observed therefore a line of best fit was used.

From these curves, an increase in drug concentration (x axis) did not correlate to an increase in percentage inhibition (y axis) against the host cell. Each point of both graphs did not show any significant activity against the host cell, nor was it enough to allow for more than 50% activity to derive a CC₅₀ value even at the top concentration of analogue used. From this, it can be concluded that analogues **2.024** and **2.059** did not cause any significant cytotoxicity against the host cell, and only displayed activity against the target parasites. This experiment was undertaken in duplicate in wells per

experiment and was repeated a second time (i.e. n=2). The parasite inhibition and host cell cytotoxicity values (IC_{50} and CC_{50} respectively) are the mean of two experiments.



R1, replicate 1; R2, replicate 2

Figure 2.11a-b: Dose response curves of compounds 2.024 (a) and 2.059 (b) reported by GRIDD, the red curve measures the compound concentration (x axis) against % inhibition (y axis) of parasites to determine antileishmanial activity (IC_{50}), the blue curve measures compound concentration (x axis) against the viability of the THP-1 transformed macrophages (y axis) to determine the cytotoxicity against the host cell (CC_{50})

Based on the biological results of Analogue Series 1-2 assessed using the *L. donovani* intramacrophage assay performed by GRIDD, a few of our initial goals were thought to have been achieved. Namely, we obtained compounds that were reported to improve activity when compared to the initial hits **2.001**, **2.002**, whilst maintaining selectivity for the parasite. The diversity set of analogues that formed Series 1-2 also provided some insight into the structural changes required to maintain activity, and which changes to avoid. Finally, most compounds within Series 1-2 displayed no cytotoxicity issues against the host cells, where analogues devised around Scaffold 1 were shown to be selective for the parasite over the host cell. As mentioned, previous correspondence with GSK had stated that host cell cytotoxicity issues were observed within the undisclosed library of analogues they had synthesized around Scaffold 1. As we had not observed any such cytotoxicity, we could be confident with our decision to continue to explore the chemical space around Scaffold 1 to develop a new antileishmanial early lead compound.

From here, some of our most potent analogues identified from this assay were then incorporated into further SAR investigations around the rest of the scaffold. These potent analogues with varying functionalities included **2.059**, **2.024** and **2.037**, representing the loss of the RHS methoxy, *ortho*-methyl LHS substituent and cyclohexane LHS ring replacement respectively. A large portion of analogues were subsequently synthesized, though our focus changed after the biological re-assessment of Analogue Series 1-2 performed by our collaborators at Bio21 and Institut Pasteur Korea (Chapter 3).

The SAR studies and subsequent analogues that were shaped by these compounds of interest (including **2.059**, **2.024**, **2.037**) are described in Section **2.12**.

2.09 Series 1-2 library biological reassessment with intramacrophage amastigote assay performed by Bio21

A similar intramacrophage assay used to evaluate our investigative compounds against *L. donovani* amastigotes was employed by our collaborators at Bio21. This assay was used to confirm the biological activity of a representative subset of analogues within Series 1-2, including the initial hits **2.001**, **2.002** and key compounds of interest which previously reported high activity against intracellular *L. donovani* (**2.009**, **2.012**, **2.015**, **2.018**, **2.024**, **2.037**, **2.042**, **2.059**). The biological results of this subset of analogues are summarized in **Table 2.10**. Due to cost and manual efforts required for the screen, not all analogues of Series 1-2 were initially sent for biological reassessment. However, easier access to our collaborators at Bio21 allowed for their assay to become a primary method of biological assessment in later studies (Chapter 3).

This assay also employs differentiated, non-dividing human acute monocytic leukemia cells (THP-1) host cells. The THP-1 host cells were transformed into macrophages via phorbol 12-myristate 13-acetate (PMA). Axenic amastigotes stained with CellTracker Orange CMRA, were used to infect transformed THP-1 macrophages at a multiplicity of infections (MOI) rate of 10:1 (parasite: host). CellTracker Orange CMRA is a fluorescent dye ideal for monitoring movement or location.⁸¹ Infected cells were treated with our investigate compounds at a concentration range of 0.2-100 μ M using a 10-point dose-response format to calculate the 50% inhibitory concentrations (IC₅₀) along with assessing the viability of the host THP-1 macrophages (CC₅₀). After the addition of our investigative analogues, cells were incubated for 72 h. Cells were further stained with CellTracker Green CMFDA, a fluorescent dye also good for demonstrating viability.⁸² DAPI was also used to stain host and parasite nuclei. The intramacrophage imaging assay uses the Cellomics high-content imaging system. The CMRA stained objects are located within the region of interest defined by the cell masks of valid CMFDA stained objects. This identifies intracellular amastigotes within the host cell.⁵¹ The dose response curves also measure the percentage of cells containing 3 or more parasites within the host cell cytoplasm defined by the stains.

The Bio21 intramacrophage IC₅₀ values calculated for miltefosine and amphotericin B reproducibility usually fell between 0.39-0.78 μ M and 0.078-2.9 μ M respectively, throughout this thesis, which is consistent with intracellular values previously reported and indicates limited experimental variability between assays. Higher IC₅₀ values for miltefosine have also been reported, though remain consistent with the literature.⁵²⁻⁵⁵ As suggested by our collaborators, for transparency, miltefosine, amphotericin

B are presented for each Bio21 experiment throughout this thesis. The complete method is outlined in the Experimental section.⁵¹

2.09.1 Intramacrophage assay comparison between independent groups

Both GRIDD and Bio21 methodology has been developed for reproducibility and involve similar high-content screening (384 well) assays with automated image acquisition and analysis.^{51, 78} However, they are in no way identical. A summary and comparison of the conditions used for each assay is summarised in **Table 2.09**. Several notable differences have also been outlined below, where relevant we have also included our collaborator's reasoning for the use of certain conditions.

- **Parasite strain:** some strains may have an increased ability to divide in host cells over others.⁷⁶ The strain utilized by GRIDD, *L. donovani* MHOM/IN/80 is a WHO reference strain, commonly used for various studies reported in the literature.^{78, 83-85} The strain utilized by Bio21, *L. donovani* LRC-L52 is a relevant Indian isolate also notable within the literature.⁸⁶⁻⁸⁸
- **Parasite culture:** Both RPMI-1640 and M199, used by Bio21 and GRIDD respectively, are frequently used for promastigote cultivation.⁷⁶
- **Liquid handling:** Both methods involve automated liquid handling using various platforms. During the Bio21 assay, manual pipetting of the compounds into media occurred before automated dilution is performed, which involves efforts to further solubilize compounds. However, with larger high-throughput efforts in other assays, this may not always be an option. This may all affect the ability of a compound to be dissolved and remain soluble within the wells and thus may affect the ability to be absorbed and permeate membranes to exert any antileishmanial effects.
- **Parasite infection:** The Bio21 infection method involves THP-1 cell lines with amastigotes whilst GRIDD infected host cells with promastigotes which transform into the desired amastigotes intracellularly. A difference in using axenic amastigotes over promastigote infection is that they don't cause an oxidative burst when entering the macrophage. This burst can contribute to killing or sensitizing of the phagocytosed promastigotes which may enhance compound action. However, oxidative burst can be species and environment dependent. De Rycker *et al.* states as the disease dispersion occurs through amastigotes and, they may provide a better disease model.⁵³ Through correspondence with our collaborators at Bio21, they advocated for the use of amastigotes to induce infection as they are more clinically relevant, though more difficult to target, as these stage is more carefully calibrated to surviving within the host including becoming more metabolically inert. However, infection with promastigotes is quite commonly used throughout the literature due to the ease of infection protocols.^{76, 78, 89, 90} Through correspondence with our collaborators at GRIDD and Institut Pasteur Korea (see Chapter 3), they supported the use of promastigotes to induce infection is easier to maintain for

scale up methods to conduct larger scale screenings. They stated that promastigotes are motile form of the parasite and studies have indicated that stationary phase promastigote culture results in higher infection ratios because of the enrichment of metacyclic promastigotes in the culture media. Finally, our collaborators at GRIDD ensured us that this method of infection has provided their group with consistent data and minimal intracellular assay variability in terms of infectivity. From our perspective, both methods of infection have their own merit, though we cannot comment on which is superior as this requires a level of investigation and understanding outside the scope of this thesis.

- **Incubation length:** The incubation period of infected cells treated with our investigative compounds differs between the two assays (Bio21: 72 h, GRIDD: 96 h). Incubation periods of 72 and 96 hours are both common within the literature for this type of assay.^{1, 53, 78, 90} Correspondence with our collaborators at GRIDD stated the intention of the longer incubation period was to potentially help identify slow acting antileishmanial compounds. Our collaborators at Bio21 have stated that longer incubation periods are favourable, as amastigote replication is slow intracellularly, however it was not suitable for the CMRA fluorescent dye used, where weaker signals are observed after an extra 24 h.
- **Multiplicity of infection (MOI):** The MOI differs between the two independent assays, though both fit within acceptable ranges. Acceptable infections of amastigote/macrophage infection ratio are quite ranged in the literature and are dependent on several method parameters including, *Leishmania* species and stage type, host cell and length of infection. Infection ratios of 5-10:1, parasite to host are quite common though 20:1 has also been commonly used within the literature.^{51, 53, 78, 90-92} Comparative studies by Hendrickx *et al.* have previously recommended 10-15 parasites per cell (*L. infantum* study) though 5-10 has also been reported as acceptable. The amastigote quantification method may give variable infection ratios *in vitro*. Even after microscopic counting of viable stages before infection, fluctuations in infection ratios may occur. Hendrickx *et al.* states this is due to the unpredictability regarding intrinsic variation in parasite virulence and intracellular multiplication potential.⁷⁶ As the MOI ratio states, increasing the MOI increases the number of parasites per macrophage, increasing the percentage of cells infected with at least one parasite increases. Furthermore, in regard to the percentage of infected cells, low infection levels have been observed to yield unreliable IC₅₀ read-outs.⁷⁶
- **Compound concentration:** Both methodologies utilize a suitable concentration range to identify the antileishmanial potency (IC₅₀) and host cell cytotoxicity (CC₅₀) of our investigative compounds. If a known highly potent compound was under assessment, lower concentrations would be used to get a more accurate IC₅₀ value. In contrast, a weakly active compound would require higher concentrations to determine an accurate IC₅₀ value. As the investigative

compounds are novel and have yet to be assessed against *L. donovani*, the broad concentration range used in both methods is suitable to the needs of this early hit-to-lead project.

- **Imaging acquisition (read out):** The types of fluorescent stains and high-content imaging system also vary between methods. Though the stains should not affect viability or proliferation. Furthermore, the imaging system and should each be well-tuned for the type of acquisition and analysis used. However, fluorescent intensity is weakened if extended delays between fixation and image acquisition occurs.⁵¹

Table 2.09: Summary and comparison of methods between the intracellular *L. donovani* assays used

Method parameter	GRIDD ⁷⁸	Bio21 ⁵¹
Parasite Strain	<i>L. donovani</i> MHOM/IN/80	<i>L. donovani</i> LRC L52
Parasite culture	Promastigotes maintained in modified M199 Hanks salt medium, pH 6.8, supplemented with 10% FBS at 27°C.	Promastigotes RPMI 1640, pH 7.4, supplemented with 10% FCS at 27°C. Axenic amastigotes were obtained following the differentiation of stationary-phase promastigotes in fresh medium (RPMI: SDM-79, supplemented with 20% FCS at pH 5.5) for 4 days at 33°C
Host cell	THP-1	THP-1
Plate number of wells	384	384
THP-1 seeding concentration	12,500 cells/well	6 x10 ³ cells/well
THP-1 seeding media	RMPI supplemented with 10% FCS medium containing 25 ng/mL PMA	RMPI supplemented with 10% FCS, penicillin, and streptomycin medium. Addition of 50 ng/mL PMA for THP-1 differentiation
Liquid Handling	Automated: BioTek EL 405 liquid handling washer/ dispenser, Bravo liquid handling platform (drug/assay plate dilutions)	Automated: BioTek EL 406 liquid handling washer/ dispenser, Caliper Sciclone ALH 3000 workstation (drug/ assay plate dilutions)
Host cell incubation	24 h, 37°C in the presence of 5% CO ₂	24 h, 37°C in the presence of 5% CO ₂
Parasite infection	Metacyclic promastigote infection (differentiate intracellularly during the assay)	Axenic amastigote infection
Drug incubation period	96 h	72 h
MOI (parasite: host)	5:1	10:1
Drug concentration used	compounds ranged from 0.004 to 80 µM to formulate a 14-point concentration response curve.	compounds ranged from 0.195 to 100 µM to formulate a 10-point concentration response curve.
Readout	Fluorescence probe, acquire and analyse images	Fluorescence probe, acquire and analyse images
Staining	Cell Mask Deep Red, SYBR Green	CMRA, CMFDA, DAPI

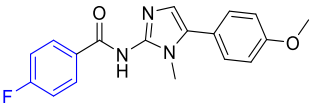
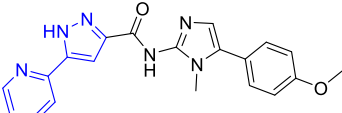
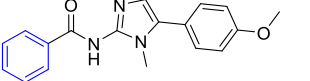
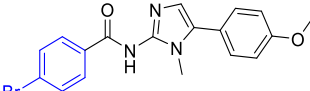
Imaging acquisition	Opera high-content imaging system	Cellomics Colocalization V4 BioApplication
Determine host cell toxicity	Same assay	Same assay

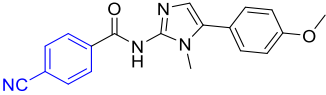
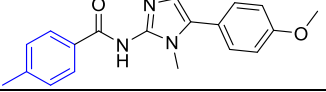
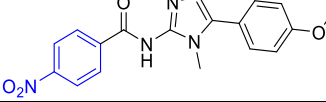
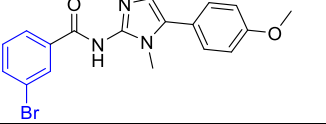
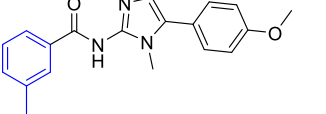
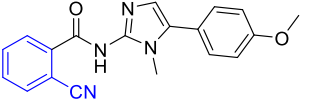
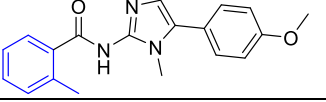
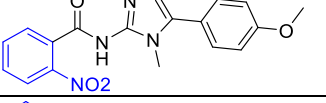
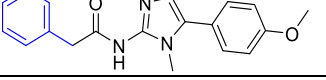
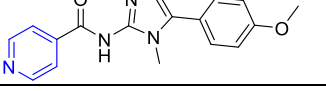
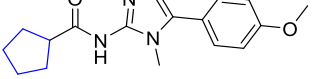
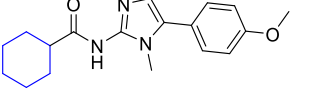
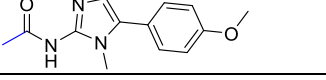
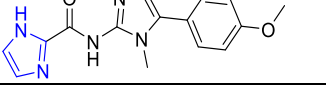
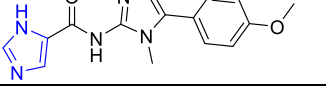
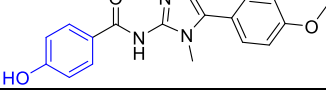
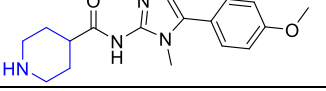
Requests for standardization, using similar conditions within *L. donovani* intracellular assays have been proposed in the literature, as these differences between methodologies may cause variations.⁷⁶ From a chemistry perspective, we do not have control over such things (since we do not perform such assays). Based on the differences between the independent assays outlined here, we also cannot predict how each varying condition could potentially alter biological outcomes, nor ultimately determine why certain investigative compounds may report conflicting results. This would require a more depth investigation, outside the scope of this PhD medicinal chemistry project. At this stage, we can merely acknowledge the differences that exist with the above **Table 2.09**. Furthermore, such a comparison is not commonly found within medicinal chemistry community. Lastly, as these *L. donovani* intramacrophage assays are in no way identical, one should not expect the results between them to completely mirror one another. To confirm if an analogue possessed true antileishmanial activity, convergent IC₅₀ values were required from both independent assays. For the purposes of this thesis, a compound would be considered potent if an IC₅₀ value of <10 µM was reported by both independent assays.

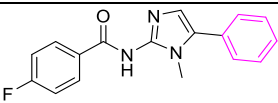
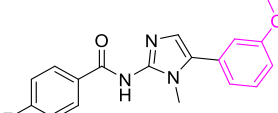
2.09.2 Biological results and comparison of key analogues of Series 1-2

The biological results of the key analogues re-examined by Bio21 are summarized in **Table 2.10**. For comparative ease, **Table 2.10** also lists the previous results obtained by the GRIDD intramacrophage assay (Section 2.09) for the same key analogues.

Table 2.10 Comparison of activity and toxicity values of key analogues between intramacrophage amastigote assays. Hit compounds are highlighted in blue.

I.D	Structure	GRIDD ^{ab}		Bio21 ^{fg}	
		IC ₅₀ (µM)	CC ₅₀ (µM)	IC ₅₀ (µM)	CC ₅₀ (µM)
2.001 [†]		>80 ^e	>80 ^e	12	>100
2.002 ^c		10 ± 0.090	>80 ^e	5.3	>100 ⁱ
2.008 [†]		>80 ^e	>80 ^e	28	>100 ⁱ
2.009 [†]		2.12 ± 0.62	>80 ^e	>100	>100 ⁱ

2.010[†]		>80 ^e	>80 ^e	>100 ⁱ	>100 ⁱ
2.012^{c†}		2.3 ± 0.17	57% at 80 μM*	19	>100
2.013^{†‡}		37 ± 0.62	27 ± 0.6	>100 ⁱ	>100 ⁱ
2.015^{th†}		1.7 ± 0.10	>80 ^e	>100	>100 ⁱ
2.018^{†‡}		0.45 ± 0.040	>80 ^e	>100	>100 ⁱ
2.022^{†‡§}		>80 ^e	>80 ^e	14	>100 ⁱ
2.024		0.38 ± 0.040	>80 ^e	65	>100 ⁱ
2.025^{d†‡‡}		52% at 40 μM*	>80 ^e	>100 ⁱ	>100 ⁱ
2.027[§]		>80 ^e	>80 ^e	25	>100 ⁱ
2.029[†]		>80 ^e	64% at 80μM *	44	>100 ⁱ
2.036[†]		97% at 80μM*	>80 ^e	83	>100 ⁱ
2.037^{†‡}		1.6 ± 0.10	>80 ^e	>100 ⁱ	>100 ⁱ
2.039^c		48% at 80μM*	>80 ^e	>100 ⁱ	>100 ⁱ
2.042^c		5.3 ± 0.23	>80 ^e	9.7	>100 ⁱ
2.043^{c†‡}		>80 ^e	>80 ^e	>100 ⁱ	>100 ⁱ
2.054^c		>80 ^e	>80 ^e	>100 ⁱ	>100 ⁱ
2.058^d		>80 ^e	>80 ^e	>100 ⁱ	>100 ⁱ

2.059 [†]		0.32 ± 0.050	>80 ^e	36	>100 ⁱ
2.060 ^{†‡}		>80 ^e	>80 ^e	>100 ⁱ	>100 ⁱ

a = anti *L. donovani* activity and toxicity measured in THP-1 transformed macrophage host cell lines using a top concentration of 80 µM (14-point curve). Experiment performed in duplicate wells. Values are means of two experiments, n=2.

b = control compounds for GRIDD *L. donovani* intramacrophage assay. Average from experimental replicates; Amphotericin B IC₅₀ = 0.39 ± 0.0070 µM, CC₅₀ = 1.5 ± 0.070 µM, VL-2098 IC₅₀ = 1.8 ± 0.17 µM, CC₅₀ > 80 µM, DNDI-1044 IC₅₀ = 0.40 ± 0.014 µM, CC₅₀ > 80 µM.

c = control compounds for GRIDD *L. donovani* intramacrophage assay. Average from experimental replicates; Amphotericin B IC₅₀ = 0.076 ± 0.0020 µM, CC₅₀ = 0.73 ± 0.18 µM, VL-2098 IC₅₀ = 0.67 ± 0.21 µM, CC₅₀ > 40 µM, DNDI-1044 IC₅₀ = 0.13 ± 0.037 µM, CC₅₀ > 40 µM.

d = control compounds for GRIDD *L. donovani* intramacrophage assay. Average from experimental replicates; Amphotericin B IC₅₀ = 0.067 ± 0.0020 µM, CC₅₀ = 0.94 ± 0.046 µM, VL-2098 IC₅₀ = 0.57 ± 0.18 µM, CC₅₀ > 40 µM, DNDI-1044 IC₅₀ = 0.18 ± 0.040 µM, CC₅₀ > 40 µM.

e = <50% activity at the top concentration tested (80 µM). Values are the means of two experiments

* CC₅₀ value is determined from a sub-efficacious curve. Solubility in the intermediate dilution in medium may have contributed to this effect observed.

[†] Out of solution in media reported between 800-20 µM during GRIDD assay

± standard deviation

f = anti *L. donovani* activity and toxicity measured in THP-1 transformed macrophage host cell lines using a top concentration of 100 µM (2x serial dilution 10-point curve). Experiment performed in duplicate wells in one experiment, n=1.

g = control compounds for Bio21 *L. donovani* intramacrophage assay. Miltefosine IC₅₀ = 11 µM CC₅₀ > 100 µM

h = control compounds for Bio21 *L. donovani* intramacrophage assay. Miltefosine IC₅₀ = 0.50 µM CC₅₀ = 40 µM, Amphotericin B IC₅₀ = 1.1 µM CC₅₀ = 66 µM

i = <50% activity at the top concentration tested (100 µM).

[‡] = poor solubility observed in DMSO stock (100mM) used for Bio21 assay

[§] = poor solubility observed in media up to 800 µM during Bio21 assay

From this table, it can be observed that most analogues that were found inactive by GRIDD were also confirmed inactive by Bio21, however a few exceptions were observed. This included the hit **2.001**, which reported moderate antileishmanial activity within the Bio21 assay only (IC₅₀ = 12 µM). The hit **2.001** was reported to have solubility issues during the GRIDD biological assessment. This hit was reported to have partially crashed out of solution by GRIDD and it is likely to have hindered the ability of hit **2.001** to completely permeate the various host cell barriers and target the parasite. This may account for the conflicting results reported for hit **2.001**, though this is merely a plausible suggestion and the exact cause remains unknown. Low antileishmanial activity was also observed in compounds **2.008**, **2.022** and **2.027** within the Bio21 assay alone. Interestingly, analogues **2.022** and **2.027** also exhibited activity within the free-living promastigote assay previously undertaken (Section 2.05). We had initially thought these compounds were false positives, as they did not exert activity within the GRIDD assay. Solubility issues particularly reported in **2.022** may possibly account for this discrepancy once again. Further biological assessment was undertaken to confirm the activity of **2.022** and is discussed in Chapter 3. Nevertheless, the activity reported for analogues **2.008**, **2.022** and **2.027** was not significant and did not merit further investigation.

It was encouraging to find compounds **2.002** (hit) and **2.042** displayed antileishmanial activity within both independent assays. Due to the convergent activity and low host cell cytotoxicity observed with **2.002** and **2.042**, these compounds became compounds of interest. These compounds were involved in later SAR studies with investigations around the RHS chemical space (Chapter 3), along with

physicochemical and metabolic studies (Chapter 2, Section 2.011). Analogue **2.012** also reported antileishmanial activity within both assays, though activity was observed to be largely weaker within the Bio21 assay in comparison to the GRIDD assay. The reason for this discrepancy remains unknown, however further biological assessment of **2.012** was undertaken to confirm the true level of parasite inhibition (discussed in Chapter 3).

Challenges arose when divergent activity was observed between the two assays in relation to our key potent compounds listed in **Table 2.10**. Compounds **2.009**, **2.012**, **2.015**, **2.018**, **2.024**, **2.037** and **2.059** had all previously displayed high activity and selectivity against *L. donovani*, observed using the GRIDD assay. Reassessment with the Bio21 intramacrophage assay found **2.059** and **2.024** to have low and extremely low parasitic inhibition respectively, while the rest of the aforementioned key compounds reported no inhibition. As stated, these assays are not identical, thus we aimed to use them as confirmatory tools and did not expect to find entirely concurrent values. Nevertheless, these greatly opposing reports were quite difficult to interpret and distinguish whether the divergence could be attributed to issues with compound solubility. Several key compounds were observed by both independent groups as poorly soluble within assay media during the experiment, thus a varying ability to remain in solution and allow for cell permeation may have contributed to the differing results. It was also uncertain as to whether the scaffold itself may utilize a slow acting mechanism of action. As amastigotes in the parasitophorous vacuole are difficult to reach, it could be possible that these slow acting compounds were able to exhibit activity more so, during the longer incubation period of the GRIDD assay. As neither group reported any highly potent activity (mid-low nanomolar range or less) it is also possible these compounds do not fit tightly within the putative target site/s or were not selective for one specific pathway. Overall, these are merely plausible suggestions and the exact cause of these conflicting biological results remains unknown.

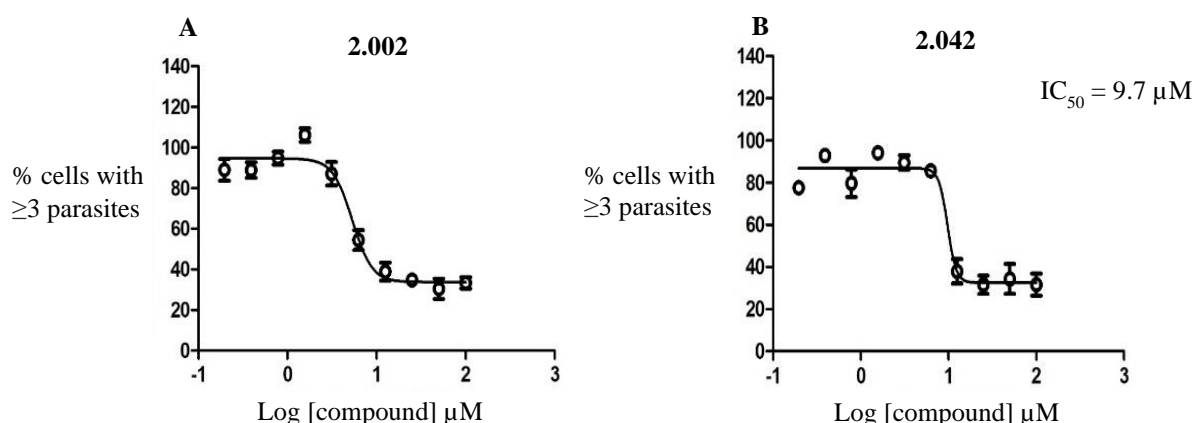


Figure 2.12a-b: Dose response curves of compounds **2.002** (a) and **2.042** (b) reported by Bio21, the compound concentration (x axis) is measured against the % of cells containing 3 or more amastigotes (y axis) to determine antileishmanial activity (IC_{50})

The dose response curves of key compounds **2.002** and **2.042**, generated from the Bio21 biological results are depicted in **Figure 2.12a** and **Figure 2.12b** respectively. These curves were used to derive the IC₅₀ value of the analogue, where increasing the drug concentration (x axis) is shown by **Figure 2.12a-b** to decrease the percentage of cells containing 3 or more parasites (y axis), thus decreasing parasite burden. Both **2.002** and **2.042** clearly have shown to significantly reduce the number of parasites within host cells. This experiment was undertaken in duplicate wells in one experiment (i.e. n = 1). Due to the high cost and long undertaking in terms of the manual requirements associated with this assay, the entire experiment was not repeated a second time. Only significant compounds would undergo retesting in repeated experiments to confirm activity.

After reviewing both sets of biological results, the complexity of intramacrophage assays with *L. donovani* was apparent. It was a possibility that the inhibition of *L. donovani* reported by our collaborators at GRIDD (Section **2.08**) may have overstated the actual level of potency our compounds were capable of exerting. The divergent results observed between our independent collaborators for many of the key compounds outlined in **Table 2.10** made interpreting SAR around Scaffold 1 quite challenging. Despite this, compounds **2.002** and **2.042** were still considered key compounds of interest as convergent activity was reported between both independent intramacrophage assays. No cytotoxicity was observed against the host cell, suggesting compounds **2.002** and **2.042** were selective for the parasite. This was encouraging as maintaining low cytotoxicity was an initial aim of this project, outlined above in Section **2.01**, as well as previously in Chapter 1. The ability to maintain low cytotoxicity would be monitored as further investigations around Scaffold 1 continued.

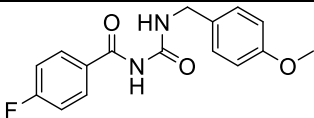
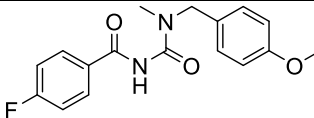
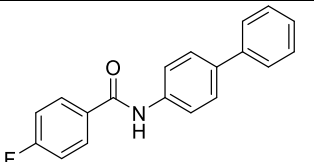
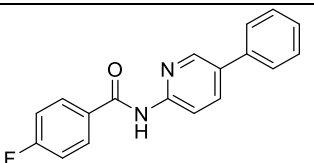
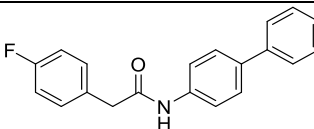
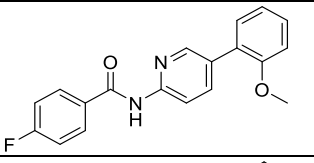
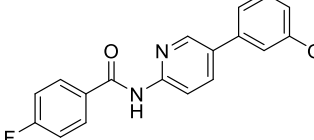
Due to the confusing nature of the combined data, the key analogues of Series 1-2 library (**Table 2.10**) were retested by both groups independently using the same respective methods. Due to the cost and large manual efforts required in drug plate preparation (before automated steps) of the Bio21 assay, we had originally planned to only assess several representative analogues per series using this assay. However, due to the vastly differing activities reported between groups, the remaining library of Series 1-2 (not previously assessed using the Bio21 methodology) would also be tested by Bio21. The complete biological re-examination of Analogue Series 1-2 required a large effort by our collaborators, due to the large number of compounds under analysis. This added to the already arduous undertaking that the complicated intramacrophage assay requires. Achieving this reassessment took more time than expected, due to temporary changes in personnel within their group. Additionally, technical issues arose with our GRIDD collaborators, causing further delays in the biological re-examination of our investigative compounds. By the time a decision was made to retest these key analogues and the remaining library of Series 1-2, further studies surrounding other portions of Scaffold 1 had already been completed based on the initial GRIDD biological studies. A “road map” of these analogues is summarized in Section **2.12** and described in detail in Chapter 3. Additionally, physicochemical and

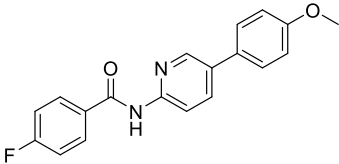
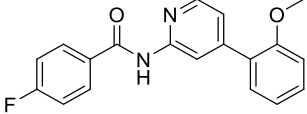
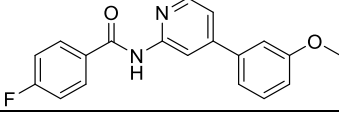
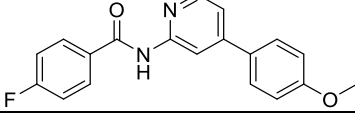
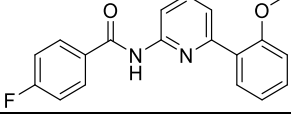
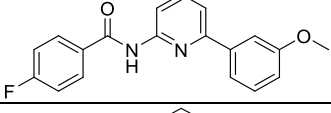
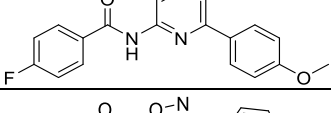
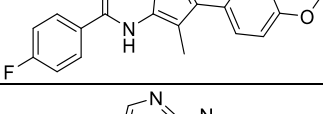
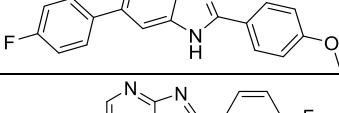
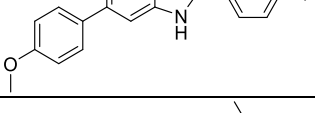
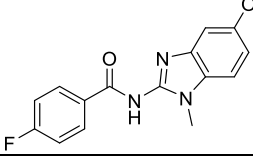
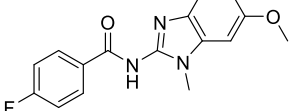
metabolic assessments had already been undertaken for key compounds identified first by GRIDD, outlined in Section 2.11.

2.10 Combined biological results of Analogue Series 3

The complete biological evaluation of Analogue Series 3, targeting core and amide structural modifications was completed before the re-examination of Analogue Series 1-2. This series was tested using both previously described intramacrophage assays against *L. donovani*, performed by our independent collaborators at Bio21 and GRIDD. As outlined in **Table 2.11**, the biological results regarding Series 3 were unanimous between the independent assays. Majority of the structural changes to the core and amide portions of chemical space were found unfavourable to Scaffold 1. Solubility issues were observed once again more so in the GRIDD assay than in the Bio21, nonetheless the results remained unanimous.

Table 2.11 Convergent biological results of Analogue Series 3 (Core and amide studies)

I.D	Structure	GRIDD ^a		Bio21 ^e	
		IC ₅₀ (μM)	CC ₅₀ (μM)	IC ₅₀ (μM)	CC ₅₀ (μM)
2.067 ^b		>80 ^d	>80 ^d	>50 ⁱ	>50 ⁱ
2.070		-	-	>50 ⁱ	>50 ⁱ
2.074 ^{cf†‡§}		>80 ^d	>80 ^d	>100 ⁱ	>100 ⁱ
2.075 ^{cg†}		52% at 80 μM*	82% at 80 μM*	>100 ⁱ	>100 ⁱ
2.076 ^{cf†§}		>80 ^d	>80 ^d	>100 ⁱ	>100
2.077 ^{cf†}		>80 ^d	73% at 80 μM*	>100 ⁱ	>100
2.078 ^{cf†§}		>80 ^d	>80 ^d	>100 ⁱ	>100

2.079 ^{cf†§}		>80 ^d	>80 ^d	>100 ⁱ	>100 ⁱ
2.080 ^{cg†}		54% at 80 μM*	58% at 80 μM*	>100 ⁱ	47.21
2.081 ^{cf†‡}		>80 ^d	>80 ^d	>100 ⁱ	>100
2.082 ^{cf†}		>80 ^d	>80 ^d	>100	>100
2.083 ^{ch†}		>80 ^d	>80 ^d	>100	>100
2.084 ^{ch}		>80 ^d	>80 ^d	>100	>100
2.085 ^{ch†}		>80 ^d	>80 ^d	>100	>100
2.090 ^{bf†}		>80 ^d	>80 ^d	>100 ⁱ	>100 ⁱ
2.094 ^{bf†‡}		>80 ^d	>80 ^d	>100 ⁱ	>100 ⁱ
2.097 ^{bf†‡}		>80 ^d	>80 ^d	>100 ⁱ	>100 ⁱ
2.102 ^{bf}		>80 ^d	>80 ^d	38.08	>100 ⁱ
2.103 ^{bf†}		>80 ^d	>80 ^d	43.50	>100 ⁱ

a = anti *L. donovani* activity and toxicity measured in THP-1 transformed macrophage host cell lines. Experiment performed in duplicate wells. Values are means of two experiments, n=2.

b= control compounds for *L. donovani* intramacrophage assay. Average from experimental replicates; Amphotericin B IC₅₀= 0.069 ± 0.0014 μM, CC₅₀= 0.94 ± 0.051 μM, VL-2098 IC₅₀= 0.72 ± 0.0021 μM, CC₅₀> 40μM, DNDI-1044 IC₅₀= 0.22 ± 0.028 μM, CC₅₀> 40 μM.

c= control compounds for *L. donovani* intramacrophage assay. Average from experimental replicates; Amphotericin B IC₅₀= 0.067 ± 0.0021 μM, CC₅₀= 0.94 ± 0.046 μM, VL-2098 IC₅₀= 0.57 ± 0.18 μM, CC₅₀> 40μM, DNDI-1044 IC₅₀= 0.18 ± 0.040 μM, CC₅₀> 40 μM.

d= <50% activity at the top concentration tested (80 μM). Values are the means of two experiments

* CC₅₀ value is determined from a sub-efficacious curve, with the maximum activity from 50-70%. Solubility in the intermediate dilution in medium may have contributed to this effect observed.

† Out of solution in media reported between 800-20 μM during GRIDD assay

± standard deviation

e= anti *L. donovani* activity and toxicity measured in THP-1 transformed macrophage host cell lines. Experiment performed in duplicate wells in one experiment, n=1.

f= control compounds for Bio21 *L. donovani* intramacrophage assay. Miltefosine IC₅₀= 11 µM CC₅₀> 100 µM

g= control compounds for *L. donovani* intramacrophage assay; Miltefosine IC₅₀ = 0.84 µM, CC₅₀ > 100 µM, Amphotericin B IC₅₀ = 1.9 µM, CC₅₀ = 65 µM

h= control compounds for *L. donovani* intramacrophage assay. Average from experimental replicates; Miltefosine IC₅₀ = 0.39 ± 0.55 µM, CC₅₀ > 20 µM, Amphotericin B IC₅₀ = 0.12 ± 0.055 µM, CC₅₀ = 6.0 ± 1.8 µM

i= <50% activity at the top concentration tested (100 µM).

j= compound was tested at a one-point concentration (50 µM), no activity was observed therefore was not retested using a 10-point system

‡= poor solubility observed in DMSO stock (100mM) used for Bio21 assay

§= poor solubility observed in media up to 800 µM during Bio21 assay

- not tested

Replacing the imidazole core with a 6 membered aromatic ring (**2.074-2.085**) was found unfavourable, as these compounds reported no inhibition of the parasite. This suggested that altering the ring size and orientation within this region of Scaffold 1 should be avoided. A lack of activity from these analogues was somewhat to be expected as they involved a larger set of changes around **2.001**, by replacing the imidazole with a pyridine or phenyl ring, there was an increase in steric bulk in this chemical space, a decreased number of heteroatoms, and change in position and orientation of the adjacent RHS ring along with the whole scaffold itself. Replacing the imidazole core with a pseudo-ring in the form of a urea (**2.067**, **2.070**) also reported a lack of antileishmanial activity. Furthermore, substituting the imidazole core with an isoxazole core (**2.090**) was also found to be an unfavourable structural change. The lack of antileishmanial activity reported for analogues **2.067**, **2.070** and **2.090** would suggest that keeping both the rigid 5 membered aromatic ring, along with the initial arrangement of heteroatoms is required to maintain activity. Loss of the amide functionality in place of a fused bi-heteroaromatic system (**2.094**, **2.097**) also correlated to a loss of activity. The structural modifications of **2.094**, **2.097** suggested that the overall change in orientation and lipophilicity caused by the fused bi-heteroaromatic system at the core position should be avoided. Additionally, this modification may have led to a potential loss of hydrogen bonding ability between the putative binding site/s and the original amide of Scaffold 1. Overall, it seemed this functionality may also be fundamental to maintain antileishmanial potency. Finally, the fused benzimidazole system (**2.102**, **2.103**) was found to give a complete loss of activity in the GRIDD assay. This change in shape and orientation at the RHS was found to be very weakly active within the Bio21 assay. The low antileishmanial activity observed was not significant enough to pursue. Overall, little to no host cell cytotoxicity was also observed within this series. A summary of requirements for antileishmanial activity (*L. donovani*) is depicted in **Figure 2.13**, as suggested by the both sets of biological results at this stage.

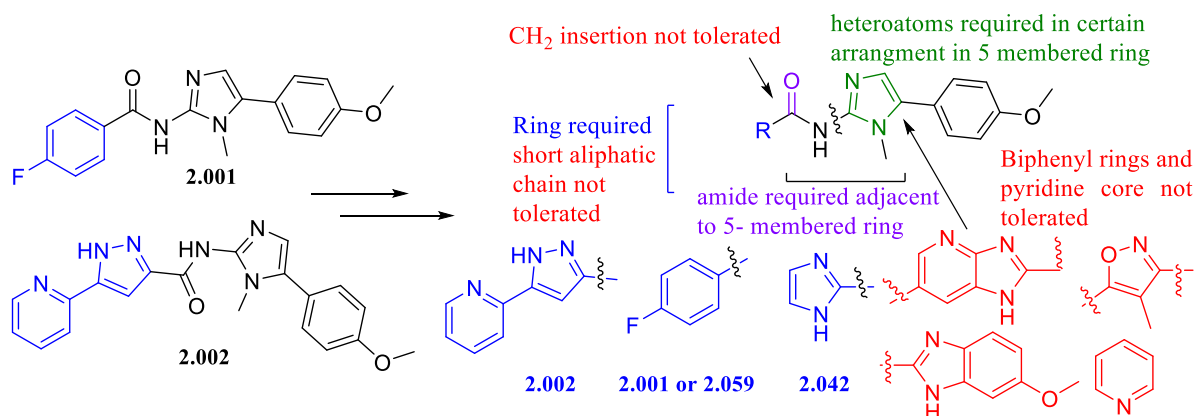


Figure 2.13: Summary of structural requirements for Scaffold 1 as outlined by the combined biological reports against *L. donovani*

During this entire campaign, compounds from Analogue Series 1-3, which we initially thought to be “lead-like” based on potency underwent further assessment by means of physicochemical and metabolic analysis, as well as cell health studies.

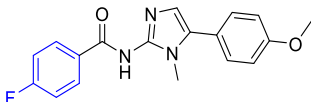
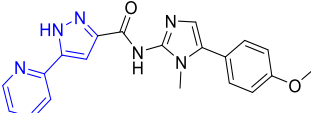
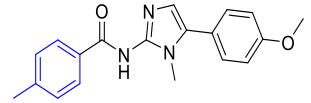
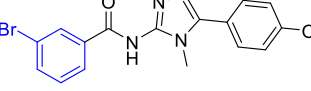
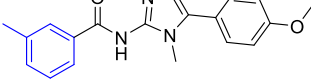
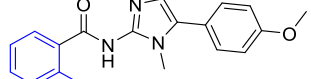
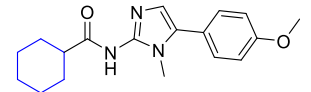
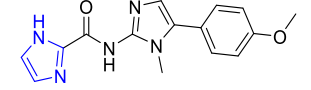
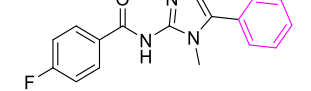
2.11 Further assessment of key analogues

2.11.1 Physicochemical and Metabolic analysis of initial leads and key analogues

The physicochemical and metabolic properties of the most active compounds featured in **Table 2.06-2.08, 2.10** were determined by the Centre for Drug Candidate Optimization (CDCO), to help assess the drug-likeness of these potential early lead compounds. Due to cost effectivity and time constraints, only compounds we believe to be lead-like in terms of antileishmanial activity and selectivity could be assessed. Along with the initial hits (**2.001, 2.002**), compounds **2.012 2.015, 2.018, 2.024, 2.037** and **2.059** were initially chosen and sent for assessment based on the first sets of biological testing by GRIDD. After the independent biological testing by Bio21, confirmed compounds **2.042** was also chosen. Various physicochemical and metabolic parameters were examined and are depicted below in **Tables 2.12** and **2.13** respectively. These properties would help assess if these compounds fit within the guidelines stated Chapter 1, Section **1.13** to help progress a new early lead antileishmanial compound. Outline in **Table 2.12**, all key compounds continued to follow Lipinski’s Rule of Five, with low molecular weights ranging between 295-386 gmol⁻¹ and moderate Log D values remaining below 5.² Compounds also maintain a PSA area less than 140 Å² following Veber’s Rule, another drug likeness predicative tool.³ Excluding the hit **2.002**, the PSA is quite low (<85 Å²), in order to avoid the BBB, modifications to increase PSA could be considered at a later stage, once a further realized lead was established. Aqueous solubility of most of the compounds was quite poor at pH 6.5, though displayed good activity at pH 2.0. In particular, the loss of the RHS methoxy group (**2.059**) showed superior solubility at pH 2.0 (>100 µg/mL). In comparison to the hits **2.001, 2.002**, the analogue **2.059** was

observed to improve overall solubility overall, suggested suggesting the loss of the RHS *para*-methoxy group was favourable in regard to improving solubility.

Table 2.12: Key physicochemical properties of selected analogues of Series 1-2

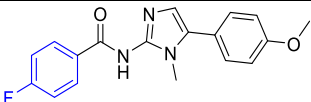
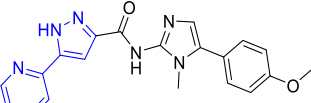
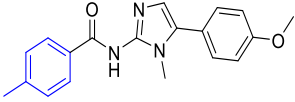
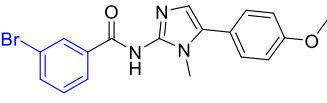
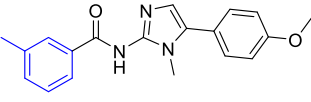
I.D/ Structure	Solubility (µg/mL) ^b							
	MW ^a	PSA (Å ²) ^a	FRB ^a	HBD ^a	HBA ^a	cLogD at pH 7.4 ^s	pH 2.0	pH 6.5
 2.001	325	56	4.0	1.0	3.0	3.4	12.5-25	<1.6
 2.002	374	98	5.0	2.0	5.0	2.7	50-100	3.1-6.3
 2.012	321	56	4.0	1.0	3.0	3.8	12.5-25	3.1-6.3
 2.015	386	56	4.0	1.0	3.0	4.0	25 - 50	<1.6
 2.018	321	56	4.0	1.0	3.0	3.8	25 - 50	1.6 - 3.1
 2.024	321	56	4.0	1.0	3.0	3.8	25 - 50	6.3 - 12.5
 2.037	313	56	4.0	1.0	3.0	3.5	25 - 50	12.5 - 25
 2.042	297	85	4.0	2.0	4.0	1.5	25-50	6.3-12.5
 2.059	295	47	3.0	1.0	2.0	3.6	>100	6.3 - 12.5

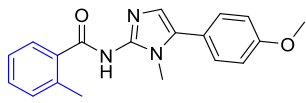
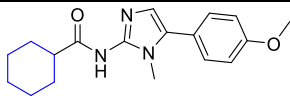
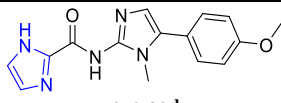
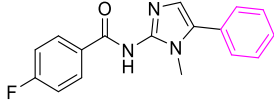
a= Calculated using ChemAxon JChem software, b=kinetic solubility determined by Nephelometry (Sol_{pH}).

Outlined in **Table 2.13**, the key compounds displayed improved stability within human microsomes, where reduced microsomal degradation relative to the original hits **2.001**, **2.002** was reported for several of the key analogues including **2.015**, **2.018**, **2.024**, **2.042** and **2.059**. A slight improvement in stability within human microsomes was also observed for **2.012**. The most improved compound within **Table**

2.13 was the imidazole based analogue **2.024**, which displayed minimal human microsomal degradation. This is also reflected in the longer microsomal half-life (>255 min), decreased intrinsic clearance *in vitro* ($Cl_{int\ in\ vitro} < 7\ \mu\text{L}/\text{min}/\text{mg protein}$) and decreased hepatic extraction ratio ($E_H < 0.22$). However, this improvement was observed in human microsomes alone, where rapid metabolism was indicated as high within mouse microsomes. Overall, most of the compounds listed in **Table 2.13** reported a large difference of microsomal stability between species. Despite the fact that we are aiming for human therapy, a large difference between species stability can complicate future *in vivo* studies, therefore developing analogues with more convergent stability between species is required. Compound **2.002**, and to a lesser extent compound **2.015** reported decreased microsomal degradation within mouse microsomes, compared to the rest of the analogue set listed in **Table 2.13**. The hit **2.002** was observed to possess superior metabolic stability within both species *in vitro* overall. The pyridine pyrazole LHS functionality may allow for this stability in mouse microsomes. It is not understood why we observed such a difference between species for majority of compounds. Distal part changes may be employed to alter the course of metabolism. These features were monitored during later SAR investigations, though to allow for cost and time efficiencies, an emphasis was placed on exclusive activity against *L. donovani*, where only our best leads were further assessed.

Table 2.13: Summary of metabolic properties of selected analogues of Series 1-2

I.D/ Structure	Species	T _{1/2} (min)	Cl _{int in vitro} ($\mu\text{L}/\text{min}/\text{mg protein}$)	Microsome- predicted E _H	Clearance classification ^a
 2.001	Human	59	30	0.54	Intermediate
	Mouse	4.0	396	0.89	High
 2.002	Human	56	31	0.55	Intermediate
	Mouse	89	19	0.29	Low
 2.012	Human	60	29	0.53	Intermediate
	Mouse	6.0	270	0.85	High
 2.015	Human	123	14	0.36	Intermediate
	Mouse	24	73	0.61	Intermediate
 2.018	Human	81	22	0.46	Intermediate
	Mouse	10	175	0.79	High

 2.024	Human	118	15	0.37	Intermediate
	Mouse	5.0	339	0.88	High
 2.037^{b, c}	Human	43	40	NA	NA
	Mouse	<2	>866	NA	NA
 2.042^d	Human	>255	<7	<0.22	Low
	Mouse	3.0	511	0.92	High
 2.059^c	Human	88	20	0.44	Intermediate
	Mouse	<2	>866	0.94	Very high

a = The E_H was used to classify compounds as low (<0.3), intermediate (0.3 - 0.7), high (0.7 - 0.95) or very high (>0.95) extraction compounds
b = Apparent non-NADPH mediated degradation (>30% degradation) was observed in metabolism control samples of human and mouse liver microsomes. A putative amide hydrolysis product with [MH⁺] of 204 was detected. Predicted *in vivo* clearance parameters are therefore not reported.

c = No measurable concentration of the parent compound was detected in mouse liver microsomes past the first time point (i.e. 2 minutes), hence, the clearance parameters could not be determined. Degradation half-life was considered to be < 2 minutes.

d = This compound showed minimal human microsomal degradation (<15%) over the course of the incubation.

NA- Not applicable

2.11.2 Initial Cell Health studies

Key compounds **2.015**, **2.018**, **2.024**, **2.037**, **2.059** and later **2.042**, underwent a series of cell health parameter tests by Cypotex. A cytotoxicity screening panel with high content screening was employed, using different toxicity markers to evaluate the effect of our investigative compounds against various cellular processes. This was undertaken using automated fluorescence imaging to analyse multiple cellular mechanisms simultaneously. Along with our investigative analogues, Rotenone and L-buthionine-sulfoximine were used as known toxic and non-toxic controls respectively. Cells were incubated with compounds at a range of concentrations to assess the amount required to cause a cellular response (see Experimental section). If compounds required very high concentrations to exert any sort of effect against the host cells, this would suggest the compounds were not inherently cytotoxic against the mammalian cell lines *in vitro*. Relevant dyes/antibodies were added to the cells after incubation and scanned using an automated imager to determine the cell health markers, following their proprietary assay methods. This was undertaken in HepG2 and HepaRG cell lines to assess the toxicity levels of our analogues against other types of mammalian cell lines and measure the effect on various cellular processes.^{93, 94} In addition to the toxicity assessment made in THP-1 macrophage host cells, this would help determine if our key compounds exhibited toxicity against other cell lines. Toxicity markers evaluated in this panel are listed as follows:

- Cell count: A decreasing number of cells per well specifies toxicity due to apoptosis, necrosis or necrosis, apoptosis or a decrease in cellular proliferation.

- Cellular ATP: Cellular ATP production is associated with metabolically active healthy cells, therefore a reduction in metabolically active cells is correlated to a decrease in cellular ATP levels.
- DNA structure: A rise in DNA structure can specify chromosomal instability and DNA fragmentation.
- Glutathione content: A rise in glutathione (GSH) content signifies an adaptive cellular response to oxidative stress. A reduction in GSH content can result from direct binding or production of reactive oxygen species (ROS).
- Mitochondrial mass: A reduction in mitochondrial mass specifies loss of total mitochondria and an increase suggests adaptive response to cellular energy demands or mitochondrial swelling.
- Mitochondrial membrane potential ($\Delta\psi_m$): A reduction in potential signifies mitochondrial toxicity and a loss of mitochondrial membrane
- An increase in mitochondrial membrane potential signifies an adaptive response to cellular energy demands and a possible role in apoptosis signalling,
- Nuclear size: An increase in nuclear area can signify G2 cell cycle arrest or necrosis. A decrease correlates to apoptosis.
- Oxidative stress: An increase in ROS indicates the formation of toxic superoxide intermediates, which is an early cytotoxic response.^{94, 95}

Table 2.14: Cell health summary of compounds in HepG2 cell lines

I.D	#	Most sensitive mechanism	↑↓	MEC (uM)	AC ₅₀ (uM)
2.015	8	Cellular ATP	↓	0.61	2.21
2.018	7	Cellular ATP	↓	0.64	2.41
2.059	8	Cell count	↓	0.77	24.9
2.024	6	Cellular ATP	↓	0.83	9.31
2.037	7	Cellular ATP	↓	5.68	33.0
2.042	4	Cell count	↓	3.40 (NS)	>100†(NS)

MEC: Minimum effective concentration that significantly crosses vehicle control threshold (see dose response curves listed in the Appendix).

AC₅₀: The concentration at which 50% maximum effect is observed for each cell health parameter.

†: An AC₅₀ was calculated, but is greater than the maximum surviving concentration.

↑↓: Direction of response.

NR: No response observed.

NS: Fit not statistically significant.

ER: Early response observed (the compound responded at the lowest concentration tested).

First Signal The cell health feature which responds at the lowest observed dose (marked by•).

Table 2.14 provides a summary of how each compound responded in HepG2 cell lines and indicates the most sensitive cellular mechanism responding to the analogue. The “#” also indicates how many of the mechanisms described above (8 total) were disrupted by the analogue and in most cases. Majority of analogues caused a decrease in cellular ATP (indicating a decrease in metabolically active cells) as well as effecting majority of the measured parameters. Analogue **2.042** was shown to be the most favourable (least cytotoxic) compound as it required the highest concentrations to exhibit any effects

against HepG2 cell lines. Analogues were also tested under the same conditions in HepaRG cell lines. Though all analogues showed very little to no response to each cell parameter. Cyprotex indicated the lack of response may be because HepaRG is a less sensitive, non-replicating cell lines in comparison to the more sensitive, replicating HepG2. The unknown mechanism of action of our analogues may require a feature in replicating cell lines to exhibit activity against the cell.

The dose response curves of each cell health parameter outlined above are listed in the Appendix section. The dose response curves measured the effects of increasing the compound concentration against the response of the particular cellular process being disrupted. In other words, the curves measured the host cell cytotoxicity levels that the compound induced within the toxicity marker being investigated. This would determine the amount of compound required to cause cytotoxicity to the cell via certain cellular functions. The corresponding data summaries for each compound within HepG2 and HepaRG cell lines are also listed in the Appendix. A representative data summary of **2.042** has been included in **Table 2.15** which further determined **2.042** to be the least cytotoxic, lead analogue amid this group, as it had affected the least amount cellular mechanisms and reported a higher minimum effective concentrations amongst all parameters. The dose response curves for each parameter of **2.042** have been included within the Appendix. From the table, compound **2.042** required high minimum concentrations to cause an effect in each cell health parameter. This suggests low inherit toxicity within this analogue and thus became a lead compound of interest. As a result, analogue **2.042** guided further SAR investigations around Scaffold 1, where the LHS imidazole ring was incorporated in later studies discussed in Chapter 3.

Table 2.15: Cell health summary of compound 2.042 in HepG2 cell lines

Compound	Cell health Parameter	↑↓	MEC (uM)	AC ₅₀ (uM)	First Signal	
					MEC	AC ₅₀
2.042	Cell count	↓	3.40 (NS)	>100†(NS)	•	
	Nuclear size		NR	NR		
	DNA structure	↑	44.0 (NS)	>100†(NS)		
	Mitochondrial mass	↑	NR	NR		
	Mitochondrial membrane potential	↑	70.7	>100†		
	Oxidative stress	↑	17.2	>100†		
	Glutathione content	↑	18.7	>100†		
	Cellular ATP	↓	61.0	99.2		•

MEC: Minimum effective concentration that significantly crosses vehicle control threshold.

AC₅₀: The concentration at which 50% maximum effect is observed for each cell health parameter.

†: An AC₅₀ was calculated, but is greater than the maximum surviving concentration.

↑↓: Direction of response.

NR: No response observed.

NS: Fit not statistically significant.

ER: Early response observed (the compound responded at the lowest concentration tested).

First Signal The cell health feature which responds at the lowest observed dose (marked by•).

It should be noted that later studies discussed in Chapter 3 found that these key analogues were significantly less active against *L. donovani* than initially reported. Therefore, these compounds were later no longer considered leads. The cell health studies described here would not be relied upon to guide further SAR, for this reason, the results of this study were not a large focus of this thesis, nor would it be discussed in further depth. Nonetheless, these cell health studies were a good exercise to undertake, as it showed that a variety of structural modifications to Scaffold 1 could maintain low host cell cytotoxicity against different types of mammalian cell lines *in vitro*. As mentioned, the full cytotoxicity panel, including all dose response curves generated for these studies in HepG2 and HepaRG is listed in the Appendix. Due to cost and later challenges with biological testing, further cell health parameter assessments could not be undertaken. This would be reserved for a more fully realized lead compound in the future.

2.12 Summary of lead compounds of Chapter 2 and how further SAR studies were shaped, to be described in Chapter 3

The most efficacious analogues to come from both intracellular studies have been summarized below in **Figure 2.14**. The initial hits reported by Pena *et al.* are positioned in Row 1, whilst the remaining compounds are presented in the order of biological data received from GRIDD in order to give an understanding of our timeline and SAR rationale.¹ Described more so in Chapter 3, Row 2 represents our “best” compounds from the first set of biological data received from GRIDD. From the set, compounds **2.059** and **2.037** were identified as leads/ compounds of interest. Compounds **2.001**, **2.059** and **2.037** shaped the studies altering the *N*-methyl chemical space of the imidazole ring core of Scaffold 1 (Chapter 3, Analogue Series 5). The synthesis and biological results are discussed in Chapter 3. As outlined, studies surrounding the chemical space of hit **2.001** were continued as we originally believed this scaffold still held potential for parasite inhibition, based on the high activity observed from the structurally similar **2.059**. We initially believed the poor solubility reported by GRIDD had contributed to the decreased inhibition observed for **2.001** in Section 2.08. Furthermore, efforts made by Bio21 later found hit **2.001** reported moderate activity when no solubility issues were reported. Therefore, we still believed an SAR exploration around **2.001** still held merit. Simple structural modifications around the chemical space of **2.001** continued, aiming to improve potency whilst maintaining low host cell cytotoxicity. Hit **2.002** would be studied in parallel by another group member, so we could achieve more in-depth study around Scaffold 1 overall. Upon receiving the next sets of biological data from GRIDD, we re-evaluated our lead compounds. The Row 3 compounds represent the “best” compounds of the later sets of biological data received. The *ortho*-methyl **2.024** gave an increased improvement to activity over the cyclohexane **2.037**. Therefore, further investigations around chemical space of Scaffold 1 involved were shaped by the compounds **2.001**, **2.059** and **2.024**. These compounds influenced the additional RHS investigations described in Chapter 3, Analogue Series 6.

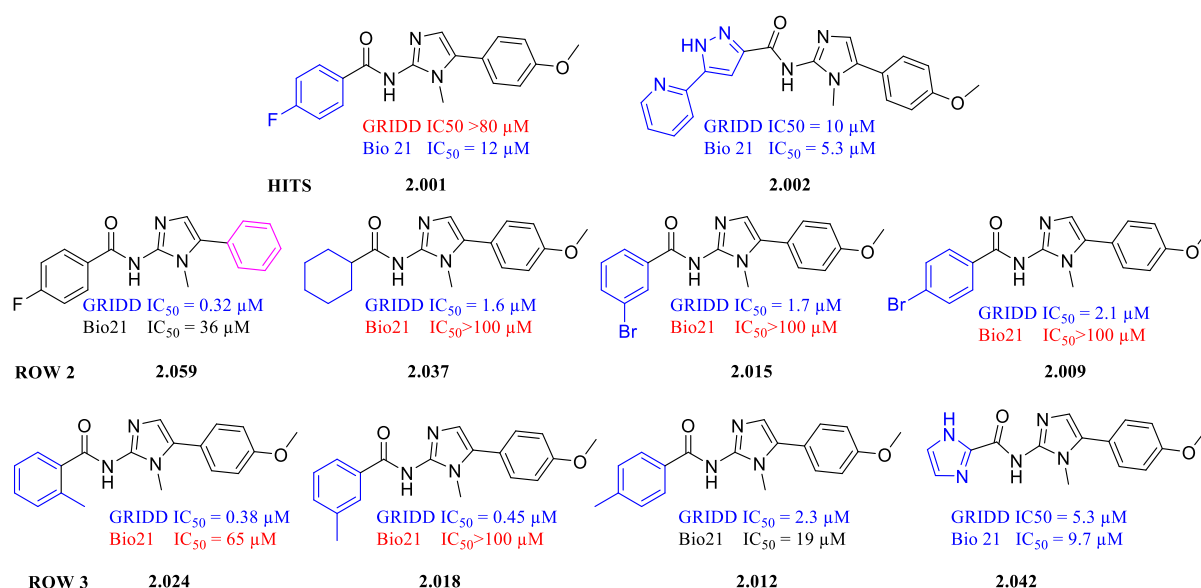


Figure 2.14: Summary of most potent analogues between both assays

During the biological assessment of key analogues against intracellular *L. donovani* performed by Bio21 (Section 2.09), compounds **2.042** and **2.002** reported consistent antileishmanial activity. Favourable stability in human microsomes and low toxicity within cell health studies suggested **2.042** to be a preferable lead. Studies from there on involved the LHS imidazole ring, which helped shape the continued RHS exploration of Scaffold 1, discussed in Chapter 3, Analogue Series 6. After initial parallel studies surrounding the chemical space of hit **2.002** were accomplished, the pyridine pyrazole hit was re-incorporated into this early hit-to-lead PhD project and would influence the SAR studies of Analogue Series 9, Chapter 3. Finally, an additive SAR study combining the bare RHS ring of **2.059** with the most active LHS ring functionalities summarized in **Figure 2.14** was also undertaken in an attempt to further improve activity. The synthesis and antileishmanial activity of each of these studies is described in Chapter 3. These collective studies are summarized below in **Figure 2.15** to help with visualization of our timeline, and further convey the lead compounds that influenced each study around the chemical space of Scaffold 1.

As several key analogues did not report convergent data between the independent biological assays employed, understanding the SAR profile of Scaffold 1 became challenging. Therefore, re-testing by both groups was commenced to confirm true antileishmanial activity and selectivity of the key compounds. This was a large undertaking and took some time. To prepare for any continued confusion, other independent collaborators were consulted at times to further evaluate any activity against *L. donovani*. From these efforts, we were confident that we could reach a better understanding of Scaffold 1 and determine which compounds were truly potent against the parasite.

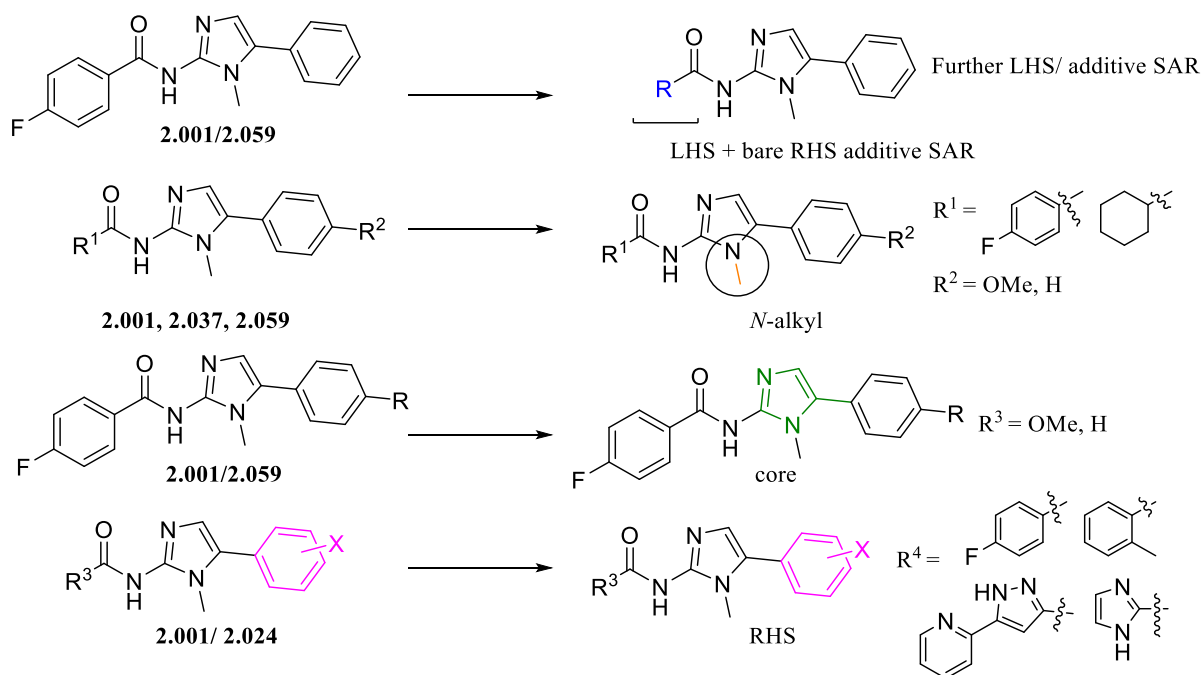


Figure 2.15: Studies around 2.001 and other leads at the LHS ring (red), imidazole core (blue), N-methyl (orange) and RHS ring (green) later discussed in detail in Chapter 3.

2.13 Chapter 2 Experimental

Biological Experimental

GRIDD methodology

GRIDD *L. Donovanii* intracellular amastigote assay

This assay was carried out as previously reported by Duffy *et al.*⁷⁸

Cell culture: *L. donovani* MHOM/IN/80 (ATCC 50212) promastigotes were maintained in modified M199 Hanks salt medium, pH 6.8, supplemented with 10% heat inactivated fetal bovine serum (FBS) at 27°C. Parasites were sub-cultured every 7 days at a concentration of 10⁵ cells/mL. THP-1 (ATCC TIB202) cells were maintained in RPMI medium and 10% FBS at 37°C and 5% CO₂. Cells were sub-cultured every 2-3 days to maintain cell density between 2 x 10⁵ and 1 x 10⁶ cells/mL.⁷⁸

Assay: THP-1 cells were seeded using a Bravo automated liquid handling platform (Agilent Technologies, Santa Clara, CA) into 384-well cell carrier imaging plates from Perkin-Elmer, Waltham, MA. Cells were seeded at a concentration of 12,500 cells/well in RPMI supplemented with 10% fetal calf serum (FCS) medium containing 25 ng/mL PMA in order to induce differentiation of the THP-1 cells. Assay plates were allowed to incubate at room temperature for 30 min for cells to adhere before being incubated at 37°C and 5% CO₂ for 24 h. After incubation, PMA was removed by discarding the medium within the wells and washing the plates three times in phosphate-buffered saline (PBS) on an EL405 plate washer (Biotek Instruments, Winooski, VT). After washing was complete, fresh RPMI and 10% FBS medium (40 µL) were added to the plates. Plates were incubated for 48 h at 37°C and 5% CO₂. The number of metacyclic promastigotes present in a 7-day old *L. donovani* DD8 promastigote culture was determined. Parasites were added to the plates containing transformed THP-1 cells 72 h after initial seeding. The multiplicity of infection used was 5:1 (parasite to host). The plates incubated at room temperature for 30 min. This was followed by subsequent incubation of the assay plates at 37°C and 5% CO₂ for 24 h. After incubation, the medium within wells were aspirated to remove the non-internalized parasites and plates were washed six times in PBS on an EL405 plate washer. Fresh RPMI with 10% FBS and 25 ng/mL PMA (45 µL) was subsequently added. The in-plate controls for experiments consisted of positive wells, containing a concentration range of 0.0002-4.0 µM amphotericin B, 0.002-40 µM VL2098 and 0.004-80 µM and negative wells containing 0.4% DMSO. Each test compound at 1 µL was diluted by the addition of 24 µL of RPMI medium without FCS. Portions of 5 µL of this dilution were dispensed using the Bravo liquid handler to the assay plates. The final assay concentrations for the investigational compounds ranged from 0.004-80 µM to formulate a 14-point concentration response curve for IC₅₀ confirmation. Plates were incubated for 96 h at 37°C and 5% CO₂. After incubation, plates were fixed with 4% paraformaldehyde and stained with SYBR green and CellMask Deep Red (Thermo-Fischer Scientific, Waltham, MA). Images were acquired on

an Opera high-content imaging system by Perkin-Elmer. Healthy host THP-1 macrophages were identified based on the CellMask Deep Red cytoplasmic area and SYBR green nuclear area and intensities. This helps separate nuclear and cell boundaries used to identify the region of the host cell and cytoplasm. Intracellular amastigotes were then identified within this region based on spot detection algorithms from the SBYR green staining, using size and intensity measurements to define the amastigote nucleus. This determined the number of parasites present within the THP-1 host macrophages. An infected cell was defined as a host cell contained more than 3 parasites within the cytoplasm boundary. Compound activity was determined based on the number of infected cells normalized to the positive and negative controls, Amphotericin B and DMSO respectively. Nonlinear sigmoidal dose-response curves with no constraints were plotted and IC₅₀ values were calculated using GraphPad Prism 6. The IC₅₀ values were calculated from two independent experiments.⁷⁸

Bio21 Methodology

Compound preparation

All compounds were resuspended in DMSO at 100 mM and, following extensive vortexing, were stored at – 20°C until use. For use, compounds were thawed at room temperature and vortexed or pulse sonicated (water bath, 20 sec) to aid resuspension.

Compound plate preparation

To prepared compound plates (384 well, v-bottom, Greiner 384 PP well plates Z642959), 25 µL of MCDM was dispensed (BioTek EL 406 washer/dispenser liquid handling robot) into all well except those to contain the highest concentration of compound. Dilutions of compounds (800 uM final) and controls (Miltefosine 800 µM final, amphotericin B 80 µM final, DMSO 1.6mM) controls were prepared in MCDM. These dilutions were manually added to the vacant wells of the compound plates (50 µL/well). A serial dilution was then undertaken (1:2, 10 points, transferring 25 µL) across the plate using the was performed using the Caliper Sciclone ALH 3000 workstation. Subsequently, 5 µL were transferred to the cell plates (*in vitro* or *intra* macrophage assays) resulting in a 1/8 dilution (miltefosine, starting 100 µM; amphotericin starting 10). The concentration range of the investigative compounds used was 0.195-100 µL.

Cells culture

Parasites: Parasite aliquots were stored at -80°C and thawed 2 weeks before use for infection. *Leishmania mexicana* (MNYC/BZ/62/M379) and *Leishmania donovani* parasites (LRC-L52) were maintained by twice weekly passages (twice weekly at 100-fold and 1000-fold dilution) of mid-log phage parasites into 10 mL of RPMI 1640 (hereafter RPMI, Life Technologies #11875-119)(pH 7.4)

medium or 10 ml of RPMI:SDM-79 (1:1 v/v, pH 7), respectively, supplemented with 10% heat-inactivated fetal calf serum (FCS, Sigma Aldrich) at 27°C.

Stationary-phase promastigotes were harvested 5 days after passaging (approximately *L. mexicana*; $\sim 2 \times 10^7$ cells/mL, *L. donovani*; $\sim 3 \times 10^7$ cells/mL). Axenic amastigotes were obtained following the differentiation of stationary-phase promastigotes in fresh medium (*L. mexicana*; RPMI, *L. donovani*, RPMI:SDM-79, 1:1 v/v) supplemented with 20% FCS at pH 5.5 for 4 days at an increased temperature (*L. mexicana*; 33 °C, *L. donovani* 37 °C).

Mammalian macrophage: THP-1 monocytes were cultured in RPMI supplemented with 10% FCS, penicillin and streptomycin, at 37 °C and 5% CO₂. Cells were maintained in at 2×10^5 – 1.2×10^6 cells/mL with regular passaging and fresh aliquots were thawed 1-2 weeks before the assay. THP-1 cells were differentiated to macrophage like cells via the addition of 50 ng/mL of PMA (P1585; Sigma-Aldrich).⁵¹

***In vitro* free-living promastigote assay**

Stationary phase promastigotes and amastigotes were resuspended (40,000 parasites/35 μ L) in modified CDM (MCDM) based upon formulations described by Shimony *et al* and Merlen *et al.* at pH 7 (promastigotes) or 5.5 (amastigotes), respectively.^{47, 48} and is described in **Table 1**. Duplicate cell plates were prepared using the BioTek EL 406 washer/dispenser liquid handling robot to dispense *L. donovani* onto a flat bottomed black walled 384 well plate (Corning, 3985BC) (35 μ L/well). 5 μ L of compound was then transferred from the compound plate using the Caliper Sciclone ALH 3000 workstation (see section XX). The cell plates were sealed with film (Veclocity 11 plate sealer) and at either 27 °C (promastigotes), 34 °C (*L. mexicana* amastigotes) or 37 °C (*L. donovani* amastigotes) for 72 h.

Table 1 MCDM formulation

Component	Concentration
NaCl	116 mM
Ca(NO ₃) ₂	0.423 mM
KCl	5.37 mM
MgSO ₄	0.406 mM
NaHCO ₃	23.8 mM
Na ₂ HPO ₄	0.836 mM
KH ₂ PO ₄	88.2 μ M
HEPES	20.1 mM
Sodium Acetate	0.12 mM
Tween 80	4 mg/L
2-(N-morpholino) ethanesulfonic acid (MES)	25 mM
Thymine	0.48 μ M
Adenine	10 μ M
L-Ascorbic Acid	0.06 μ M

d-biotin	1.50 μ M
p-Aminobenzoic	9 μ M
Folic acid	26 μ M
Nicotinic acid	0.04 μ M
Pyridoxine	5.4 μ M
Cyanocobalamin	4 μ M
Menadione	0.01 μ M
Cholesterol	0.1 μ M
Tocopherol	0.01 μ M
Retinyl-acetate	0.07 μ M
Calciferol	0.05 μ M
Biopterin	0.5 μ g/ml
Glutathione	3.6 μ M
Hydroxyproline	0.17 mM
Adenosine	108.6 μ M
guanosine	0.32 μ M
hypoxanthine	0.52 μ M
xanthine	0.5 μ M
uracil	0.62 μ M
MEM Vitamins (Gibco/Invitrogen 11120)	1x
Non Essential amino acids (GIBCO 11140)	3x
Essential amino acids (GIBCO 11130)	1x
Bovine serum albumin, (BSA	1% w/v
Hemin	5 μ g/ml

In vitro parasite proliferation/survival was determined using a modified CellTitreGlo® (CTG) assay (Promega, G9241). Briefly, the CTG lysis buffer was supplemented with SYBR Green I nucleic acid staining (Invitrogen, S7563 0.4 μ L/mL) and dispensed at 25 μ L/well (BioTek EL 406). Plates were gently rock for 10 min (dark), incubated at room temperature (dark, 5 min) before being read at excitation and emission wavelength bands centered at 485 and 530 nm, respectively (Cytation or Clariostar platforms).

Intramacrophage assay

This assay was carried out as previously reported with minor adjustments.⁵¹ Briefly, THP-1 monocytes were dispensed (BioTek EL 406 robotics) into a 384 well plate (Corning COSTAR, Catalogue number 3712) at 50 μ L/well (6×10^3 cells/well), in RPMI supplemented with 10% FCS and 50 ng/mL of PMA). Plates were briefly centrifuged and incubated at 37 °C with 5% CO₂ for 24 h.

The following day, axenic amastigotes were stained with CellTracker Orange CMRA (C34551; Life Technologies) as described previously⁵¹. Stained parasites were resuspended in RPMI supplemented with 10% FCS and dispensed (BioTek EL 406 robotics, 50 μ L/well) over now adherent macrophages following culture media aspiration (BioTek EL 406 robotics). Macrophages were infected at a multiple of infection of 10:1 (*L. donovani*) (parasite:host). Plates were briefly centrifuged and incubated at 37 °C with 5% CO₂. The following day, the infected macrophages were washed (removing non-

internalised parasites) with 1 x PBS (60 uL/well) and new media dispensed (35 uL/well, RPMI supplemented with 10% FCS, BioTek EL 406 robotics). Plates were briefly centrifuged and incubated at 37 °C with 5% CO₂. The following day, 5 uL of compound was then transferred from the compound plate using the Caliper Sciclone ALH 3000 workstation, the plates briefly centrifuged and incubated at 37 °C with 5% CO₂ for 72 hr.

After treatment, the infected macrophages were stained and imaged.⁵¹ Briefly, assay media was aspirated (BioTek EL 406 robotics) and 5 µM Cell Tracker Green CMFDA stain (CMFDA, 5-chloromethylfluorescein diacetate, C2925; Life Technologies, 5 uM) in RPMI was dispensed (25 µL/well) and incubated (30 min, 33 °C or 37 °C with 5% CO₂). Stain was aspirated and the infected macrophages cells incubated in RPMI supplemented with 10% FCS RPMI (50 uL/well, 37 °C with 5% CO₂, 40 min). The chase media was aspirated and the cells fixed (4% PFA, 10 mM EGTA in PBS without Ca²⁺ and Mg²⁺, 15 min at room temperature). The fixative solution was aspirated and host nuclei stained with DAPI (10236276001, Roche, 6 µL/mL in PBS, 25 µL/well, 10 min, room temperature). The final stain was aspirated, and the cells washed twice with PBS (50 uL). Plates were sealed using a thermal microplate sealer before being high content imaging was performed using the Cellomics Array Scan VTI platform. The imaging protocol based on the Cellomics Colocalization V4 BioApplication, was developed for two imaging parameters: separation of the host cells and detection of intracellular amastigotes. Autofocus was applied using the DAPI stain channel (Ch2), CellTracker Green CMFDA (Ch1) and CellTracker Orange CMRA (Ch3) with images acquired in sequence. The DAPI stain is used to observe nuclei as a complimentary stain to CellTracker Green CMFDA which stains the macrophage cytosol and provides a visible boundary of viable macrophages (host cell segmentation). CellTracker Orange CMRA stains the parasite cytosol. The Cellomics Colocalization V4 BioApplication, using size and intensity algorithms were used to count Ch3 (CMRA stained) objects indicating amastigotes within Ch1 CMFDA marked boundaries (i.e. the number of amastigotes in THP-1 macrophage cytosol). Several features were extracted (Table 2)

Table 2

Feature	Definition	Channel
Valid object count	Number of viable macrophages per well	1 (CMFDA)
MEAN_ROI_A_Target_II_ObjectCount	Average amastigotes per viable macrophage per well	3 (CMRA)
%_High_ROI_A_Target_II_ObjectCount	% of viable macrophages with 3 or more amastigotes	3 (CMRA)

Compound activity was expressed as a percent of the maximum (e.g. DMSO control) and minimal (Miltefosine/Amphotericin B controls). Nonlinear sigmoidal dose-response curves were plotted and IC₅₀ values were calculated using GraphPad Prism 6. The IC₅₀ values were calculated as the mean from duplicate wells in one experiment.⁵¹ Several compounds have been biologically assessed in multiple

experiments, and the average IC₅₀ and CC₅₀ value across all experiments was indicated within the main sections of this body of work.

Physicochemical and *in vitro* metabolic Experimental

Calculated physicochemical parameters using ChemAxon JChem software

A range of physicochemical properties evaluating likely oral absorption characteristics and drug-likeness were calculated using the ChemAxon chemistry cartridge via JChem for Excel software (version 16.4.11). A brief description of each parameter is provided below:

MW (< 500): Molecular Weight

PSA_{pH 7.4} (< 140 Å²): Polar surface area also inversely correlates with membrane permeability.

FRB (≤ 10): Number of freely rotating bonds represents the flexibility of a molecule's conformation.

HBD (< 5) & HBA (< 10): Number of hydrogen bond donors and acceptors gives an indication of the hydrogen bonding capacity, which is inversely related to membrane permeability.

cLogP/cLogD_{pH} (< 5): Calculated partition coefficients reflect the lipophilic character of the neutral structure, while distribution coefficients reflect the partitioning properties of the ionised molecule at a specific pH.

Kinetic Solubility Estimation using Nephelometry

Compound in DMSO was spiked into either pH 6.5 phosphate buffer or 0.01M HCl (approx. pH 2.0) with the final DMSO concentration being 1%. After 30 minutes had elapsed, samples were analysed via Nephelometry to determine a solubility range.⁹⁶

Distribution Coefficient Estimation using Chromatography

Partition coefficient values (Log D) of the test compounds were estimated at pH 7.4 by correlation of their chromatographic retention properties against the characteristics of a series of standard compounds with known partition coefficient values. The method employed is gradient HPLC based derivation of the method originally developed by Lombardo *et al.*⁹⁷

***In vitro* Metabolic Stability**

Incubation:

The metabolic stability assay was performed by incubating each test compound in liver microsomes at 37 °C and a protein concentration of 0.4 mg/mL. The metabolic reaction was initiated by the addition of an NADPH-regenerating system and quenched at various over a 60 min incubation period by the addition of ACN containing diazepam as internal standard. Control samples (containing no NADPH) were included (and quenched at 2, 30 and 60 min) to monitor for potential degradation in the absence of cofactor. The human liver microsomes used in this experiment were supplied by XenoTech, lot # 1410230. The mouse liver microsomes used in this experiment were supplied by XenoTech, lot #

1910002 (for our compounds tested in 2020) and lot #1510256 (for our compounds tested in 2018, 2019). Microsomal incubations were performed at a substrate concentration of 0.5-1 μM .

Data analysis:

Species scaling factors from Ring *et al.* were used to convert the *in vitro* CL_{int} ($\mu\text{L}/\text{min}/\text{mg}$) to an *in vivo* CL_{int} ($\text{mL}/\text{min}/\text{kg}$).⁹⁸ Hepatic blood clearance and the corresponding hepatic extraction ratio (E_{H}) were calculated using the well stirred model of hepatic extraction in each species, according to the "in vitro $T_{1/2}$ " approach described by Obach *et al.*⁹⁹ The E_{H} was then used to classify compounds as low (< 0.3), intermediate ($0.3 - 0.7$), high ($0.7 - 0.95$) or very high (> 0.95) extraction compounds. Predicted *in vivo* clearance values have not been corrected for microsomal or plasma protein binding. Species scaling calculations are based on two assumptions: 1) NADPH-dependent oxidative metabolism predominates over other metabolic routes (*i.e.* direct conjugative metabolism, reduction, hydrolysis, *etc.*), and; 2) rates of metabolism and enzyme activities *in vitro* are truly reflective of those that exist *in vivo*. If significant non-NADPH-mediated degradation is observed in microsome control samples, then assumption (1) is invalid and predicted clearance parameters are therefore not reported.

Cyprotex Cytotoxicity Screening Panel

HepaRG or HepG2 cells (100 μL per well) were plated on to a 96-well tissue culture treated black walled clear bottom polystyrene plates. These cells were dosed with the compound of interest at a range of concentrations: 0.04, 0.1, 0.4, 1, 4, 10, 40, 100 μM and incubated for 48 h, 3 replicates per concentration were performed. At the end of the incubation period, the relevant dye/ antibody for each cell health marker was added to the cells. The plates were scanned using an ArrayScan® (Thermo Scientific Celloomics) automated fluorescent cellular imager. Rotenone and L-buthionine-sulfoximine were used as known toxic and non-toxic control compounds respectively. DMSO (0.5%) was used as the vehicle control. An 8-point dose response curve up 50 μM / solubility limit is used. Minimum toxic concentration and dose response curves are generated.⁹³⁻⁹⁵

General Chemistry

All solvents and reagents were used directly from commercial suppliers unless otherwise stated. Analytical TLC was performed on silica gel 60/F254 pre-coated aluminium sheets (0.25 mm, Merck) and visualised under UV light (254 nm). Flash column chromatography was carried out with silica gel Kieselgel 60, (0,04-0,063 mm) (230–400 mesh, Carl Roth). Microwave reactions were performed on a CEM discovery fitted with an intellivent explorer unit. The temperature range of the unit is $-80\text{ }^{\circ}\text{C}$ to $300\text{ }^{\circ}\text{C}$, a pressure range of 0-27 bar, power range of 0-300 W and no pre-stirring was required. Melting points (m.p) were recorded using a Barnstead Electrothermal IA9100 Melting point apparatus. LCMS analysis was undertaken using the following instruments: Agilent 1260 LCMS SQ Pump: 1260 Infinity G1312B Binary pump Autosampler: 1260 Infinity G1367E 1260 HiP ALS Detector: 1290 Infinity

G4212A 1290 DAD Software: LC/MSD Chemstation Rev.B.04.03 SP2 coupled with MassHunter Easy Access Software LC conditions: Reverse Phase HPLC analysis Column: Raptor C18 2.7 μ m 50 X 3.0mm Column temperature: 35°C Injection Volume: 1 μ L- 2 μ L Solvent A: Water 0.1% Formic Acid Solvent B: Acetonitrile 0.1% Formic Acid Gradient: 5-100% B over 5.0 mins Detection: monitored at 254 nm and 214 nm MS conditions: Ion Source: Quadrupole Ion Mode: API-ES Drying gas temp: 350°C Capillary voltage (V): 3000 (positive) Capillary voltage (V): 3000 (negative) Scan Range: 100-1000 Step size: 0.1 sec Acquisition time: 5min. Gradient takes 2.5 minutes to get to 100% ACN; maintain until 3.8 minutes and back to the original 5% ACN in 5 mins. Agilent 1260 Infinity II LCMS SQ Pump: 1260 Infinity II G7111B Quat pump (DEAET02195) Autosampler: 1260 Infinity II G7129A 1260 Vialsampler (DEAEQ25558) Detector: 1260 Infinity II G7117C DAD HS (DEAEK04932) Software: OpenLab CDS Chemstation Rev C.01.10 (239) coupled with Masshunter WalkUp V.4.0 LC conditions: Reverse Phase HPLC analysis Column: Poroshell 120 EC-C18 3.0 X 50mm 2.7-Micron Column temperature: 35°C Injection Volume: 1 μ L- 2 μ L Solvent A: Water 0.1% Formic Acid Solvent B: Acetonitrile 0.1% Formic Acid Gradient: 5-100% B over 5.0 mins Detection: monitored at 254 nm and 214 nm MS conditions: Ion Source: Quadrupole Ion Mode: MM-ES-APCI Drying gas temp: 350°C Capillary voltage (V): 4000 (positive) Capillary voltage (V): 4000 (negative) Scan Range: 100-1000 Step size: 0.1 sec Acquisition time: 5min Gradient takes 2.0 minutes to get to 100% ACN; maintain until 4.5 minutes and back to the original 5% ACN in 5 mins.

HRMS analysis was undertaken using the following instruments: Agilent HRMS TOF Direct Injection All analyses were done on an Agilent 6224 TOF LC/MS Mass Spectrometer coupled to an Agilent 1290 Infinity (Agilent, Palo Alto, CA). All data were acquired, and reference mass corrected via a dual-spray electrospray ionisation (ESI) source. Each scan or data point on the Total Ion Chromatogram (TIC) is an average of 13,700 transients, producing a spectrum every second. Mass spectra were created by averaging the scans across each peak and background subtracted against the first 10 seconds of the TIC. Acquisition was performed using the Agilent Mass Hunter Data Acquisition software version B.05.00 Build 5.0.5042.2 and analysis was performed using Mass Hunter Qualitative Analysis version B.05.00 Build 5.0.519.13 Mass Spectrometer Conditions: Ionisation mode: Electrospray Ionisation Drying gas flow: 11 L/min; Nebuliser: 45 psi; Drying gas temperature: 325°C; Capillary Voltage (Vcap): 4000 V; Fragmentor: 160 V; Skimmer: 65 V; OCT RFV: 750 V; Scan range acquired: 100–1500 m/z Internal Reference ions: Positive Ion Mode = m/z = 121.050873 & 922.009798. Should chromatographic separation be performed, the Agilent Zorbax SB-C18 Rapid Resolution HT 2.1 x 50 mm, 1.8 μ m column would be used in the standard gradient method (5% to 100%) over 3.5 min at 0.5 mL/min. Solvent A = Aqueous 0.1% Formic Acid Solvent B = Acetonitrile/0.1% Formic Acid.

Purity was determined by HPLC analysis and was found to be \geq 95% for all compounds unless stated otherwise. Compound purity was analysed on an Agilent 1260 Infinity Analytical HPLC system with the following technical information: 1260 Degasser: G1322A (JPAAJ81416); 1260 Bin Pump: G1312B

(DEACB04606) ; 1260 HiP ALS: G1367E (DEACO03069); 1260 TCC: G1316A (DEACN16726); 1260 DAD: G4212B (DEAA304233) ; Column used: Zorbax Eclipse Plus C18 Rapid Resolution 4.6 X 100mm 3.5-Micron Solvent A: 99.9% water, 0.1% TFA, solvent B: 99.9% ACN, 0.1% TFA. Compounds were analysed using the following methods: gradient: a gradient of 5-100% solvent B in solvent A over 10 mins with the flow rate of 1 mL/min, hydrophobic: a gradient of 5-80% solvent B in solvent A over 0.6 min, then 80-100% of solvent B in solvent A over 9.4 mins; hydrophilic: a gradient of 5-25% of solvent B 8.5 mins, then 25-100% solvent B in solvent A over 1.5 mins.

All ^1H NMR, ^{13}C NMR and ^{19}F NMR of small molecules were performed on either of the following instruments: Avance III Nanobay 400 MHz Bruker spectrometer coupled to the BACS 60 automatic sample changer. The spectrometer is equipped with a 5 mm PABBO BB-1H/D Z- GRD probe. Bruker Avance III Nanobay 400 MHz NMR spectrometer coupled to the SampleXpress automatic sample changer. The spectrometer is equipped with a 5 mm PABBO BB/19F-1H/D Z- GRD probe. All spectra were processed in MestReNova. ^1H and ^{13}C NMR spectra were recorded at 400, 500 MHz or 100 MHz (as specified). ^{19}F NMR was recorded at 376 MHz. Chemical shifts (δ , ppm) are reported relative to the solvent peak (CDCl_3 : 7.26 [^1H], $\text{DMSO}-d_6$: 2.50 [^1H], MeOD : 4.87 [^1H]). If a compound structure is listed electronically, though without any reference or characterization data, we are regarding this as a new compound. Proton resonances are annotated as: chemical shift (ppm), multiplicity (bs broad singlet; s, singlet; d, doublet; t, triplet; q, quartet; m, multiplet), coupling constant (J , Hz), and number of protons. Exchangeable protons for some compounds were not observed in the NMR spectra.

General Procedures

General Procedure A Imidazole amine formation⁵

N-Methylpyrimidin-2-amine (290 mg, 2.70 mmol) and the appropriate phenylacetyl bromide (824 mg, 3.60 mmol) were dissolved in ACN (5 mL) and heated using microwave irradiation at 130 °C for 30 min. The reaction mixture was then cooled and hydrazine hydrate (0.65 mL) was added. The reaction mixture was heated using microwave irradiation at 100 °C for 5 minutes. The mixture was concentrated *in vacuo* then filtered with water via suction filtration to give the desired product (**2.005**). This procedure was also employed to obtain other imidazole amines such as **2.005b-d**.

General Procedure B Amide coupling¹¹

The appropriate phenyl imidazole-2-amine (0.980 mmol) and the appropriate carboxylic acid (0.980 mmol) were added to a solution of HBTU (0.980 mmol), DMAP (0.0980 mmol) and DIPEA (2.45 mmol) in ACN (3 mL). The reaction was left to stir at room temperature for 12 hours after which the reaction was reduced *in vacuo*. The reaction mixture was diluted with DCM and washed with citric acid/water followed by ammonia/water. The organic layer was dried with MgSO_4 , filtered and reduced *in vacuo*. The crude material was subsequently purified via column chromatography (EtOAc: Petroleum

spirits; 1:1). This procedure was also employed to obtain other amide compounds such as **2.001**, **2.008-2.041**. ¹H NMR spectra employing CDCl₃ generally show an absence of NH proton peaks as they have presumably broadened out and are not visible.

General Procedure C Alternative amide coupling¹¹

The appropriate phenyl imidazole-2-amine (0.980 mmol) and the appropriate carboxylic acid (0.980 mmol) were added to a solution of PyBOP (510 mg, 0.980 mmol), DMAP (12 mg, 0.0980 mmol) and DIPEA (0.42 mL, 2.45 mmol) in DMF (3 mL). The reaction was heated to 50 °C for 12 h after which the reaction was reduced *in vacuo*. The reaction mixture was diluted with EtOAc and washed with brine. The organic layer was dried with MgSO₄, filtered and reduced *in vacuo*. The crude material was subsequently purified by column chromatography (eluent CHCl₃ 94%, MeOH 5%, NH₄OH 1%) to give the desired product **2.042**. This procedure was also employed to obtain other amide compounds such as **2.002** and **2.043**. ¹H NMR spectra employing CDCl₃ generally show an absence of NH proton peaks as they have presumably broadened out and are not visible.

General Procedure D Fischer Esterification^{43, 44, 100}

To a solution of the appropriate hydroxybenzoic acid (5.00 g, 36.0 mmol) in MeOH (5 mL), 1 drop of H₂SO₄ was added. The reaction mixture was then heated to reflux for 12 h then reduced *in vacuo*. Upon reaction completion the pH was neutralized with base (NaOH 1M/ Na₂CO₃) to give a solid. The product was filtered and dried. If the compound does not solidify, the mixture is diluted with DCM and washed with brine. The organic layer was collected, dried over MgSO₄, filtered and reduced *in vacuo* to afford the desired product.

General Procedure E Benzylolation^{39, 40}

To a solution of the appropriate methyl benzyloxybenzoate (5.00 g, 33.0 mmol), benzyl bromide (4.3 mL, 36.0 mmol) in ACN (5 mL) was added potassium carbonate (9.10 g, 66.0 mmol). The reaction was heated to reflux over 12 h then reduced *in vacuo*. The crude material was diluted with EtOAc and washed with brine, dried with MgSO₄, filtered and concentrated *in vacuo* to afford the desired product.

General Procedure F Ester Hydrolysis⁴⁰

To a solution of the appropriate methyl benzyloxybenzoate (6.00 g, 25.0 mmol) in MeOH (5 mL) and water (10 mL) was added NaOH (4.90 g, 123 mmol). The reaction mixture was heated to 65°C for 3 h then reduced *in vacuo*. The mixture was acidified to pH 2 using 2N HCl. To the suspension EtOAc was added and washed with water. The organic layer was dried over MgSO₄, filtered and the solvent was removed *in vacuo* to afford the desired product.

General Procedure G Debenzylation⁴⁰

To a solution of the appropriate benzyloxy-*N*-(5-(4-methoxyphenyl)-1-methyl-1*H*-imidazol-2-yl)benzamide (297 mg, 0.720 mmol) and 10% palladium on carbon in MeOH (2 mL) and 1,4-dioxane (2 mL) was added triethylsilane (40 equiv.) dropwise. The reaction was allowed to stir for up to 6 h and was monitored by LCMS and TLC analysis. An additional total of 20 equiv. of triethylsilane was added throughout this time. Upon reaction completion the mixture was filtered through celite and the solvent was removed *in vacuo*. The crude product was subsequently purified via column chromatography (eluent EtOAc 20%: petroleum spirits 80%) to afford the desired product.

General Procedure H Suzuki Miyaura Coupling^{4, 63}

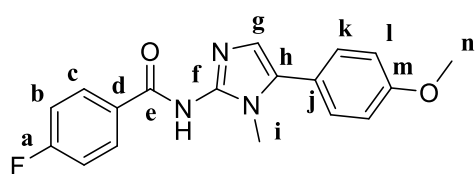
A mixture of the appropriate bromoaniline (396 mg, 2.00 mmol), the appropriate phenylboronic acid (365 mg, 3.00 mmol), Na₂CO₃ (362 mg, 3.00 mmol) and Pd(PPh₃)₄ (0.1 eq) in a solution of H₂O (3 mL) and DMF (3 mL) was heated to 90°C for 18 hours. The mixture cooled to room temperature then was filtered with MeOH through celite and concentrated *in vacuo*. The crude mixture was diluted with EtOAc, washed with brine, and the organic phase was collected and dried over MgSO₄, filtered and concentrated. The mixture was purified via column chromatography (eluent EtOAc 40% in petroleum spirits) to afford the desired product **2.071a**. This procedure was also used to form compound **2.071b**.

Synthesis

Analogue Series 1-2

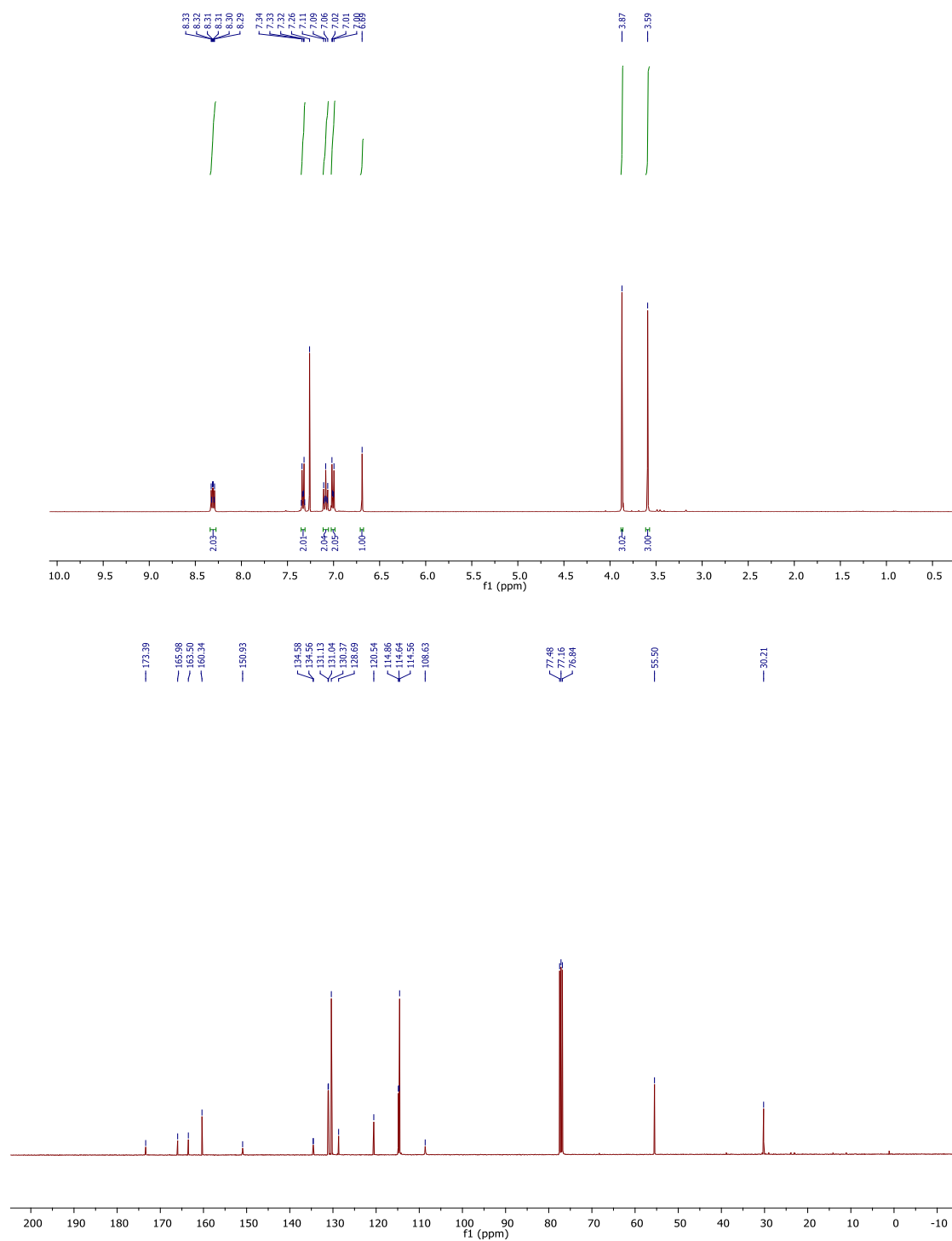
Example Spectra are included for compounds **2.001**, **2.002**, **2.008**, **2.009**, **2.030**

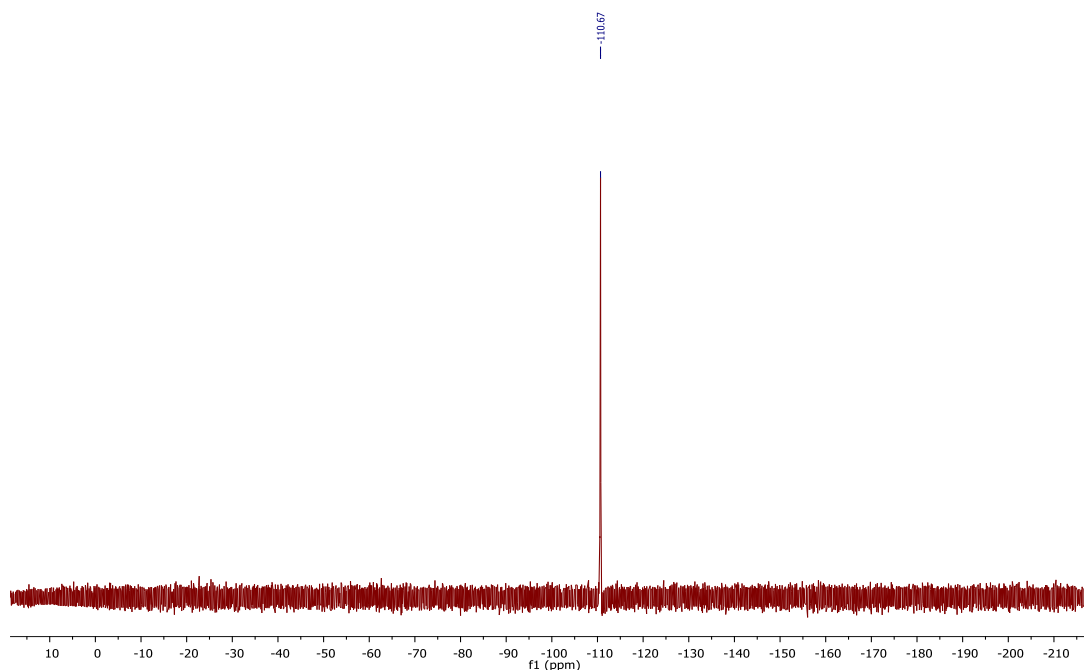
4-Fluoro-*N*-(5-(4-methoxyphenyl)-1-methyl-1*H*-imidazol-2-yl)benzamide (**2.001**)



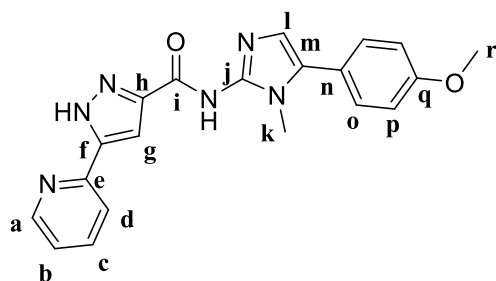
The title compound was prepared from 5-(4-methoxyphenyl)-1-methyl-1*H*-imidazol-2-amine (200 mg, 0.98 mmol) and 4-fluorobenzoic acid (137 mg, 0.980 mmol) in DMF (5 mL) according to General Procedure B (186 mg, 58%). HPLC - *t*_R 5.01 min > 99% purity at 254 nm; LRMS [M+H]⁺ 325.9 *m/z*; HRMS [M+H]⁺ 326.1299 *m/z*, found 326.1304 *m/z*; ¹H NMR (400 MHz, CDCl₃) δ_H 8.34 – 8.28 (m, 2H, H_c), 7.36 – 7.30 (m, 2H, H_k), 7.11 – 7.05 (m, 2H, H_b), 7.03 – 6.98 (m, 2H, H_l), 6.69 (s, 1H, H_g), 3.87 (s, 3H, H_n), 3.59 (s, 3H, H_i); ¹⁹F NMR (376 MHz, CDCl₃) δ -110.7; ¹³C NMR (101 MHz, CDCl₃) δ_C 173.4 (C_f), 164.7 (d, *J*_{C-F} = 249.6 Hz, C_a), 160.3 (C_e), 150.9 (C_h), 134.6 (d, *J*_{C-F} = 2.2 Hz, C_d), 131.1 (d, *J*_{C-F} = 8.8 Hz, 2C, C_c), 130.4 (2C, C_k), 128.7 (C_m), 120.5 (C_g), 114.8 (d, *J*_{C-F} = 21.5 Hz, 2C, C_b), 114.6 (2C, C_l), 108.6 (C_j), 55.5 (C_n), 30.2 (C_i). M.p 141.1-159.9°C.

Example spectra for Series 1-2: ^1H (400 MHz, CDCl_3), ^{13}C NMR (100 MHz, CDCl_3) and ^{19}F NMR (376 MHz, CDCl_3) spectrum of 4-Fluoro-*N*-(5-(4-methoxyphenyl)-1-methyl-1*H*-imidazol-2-yl)benzamide (2.001)





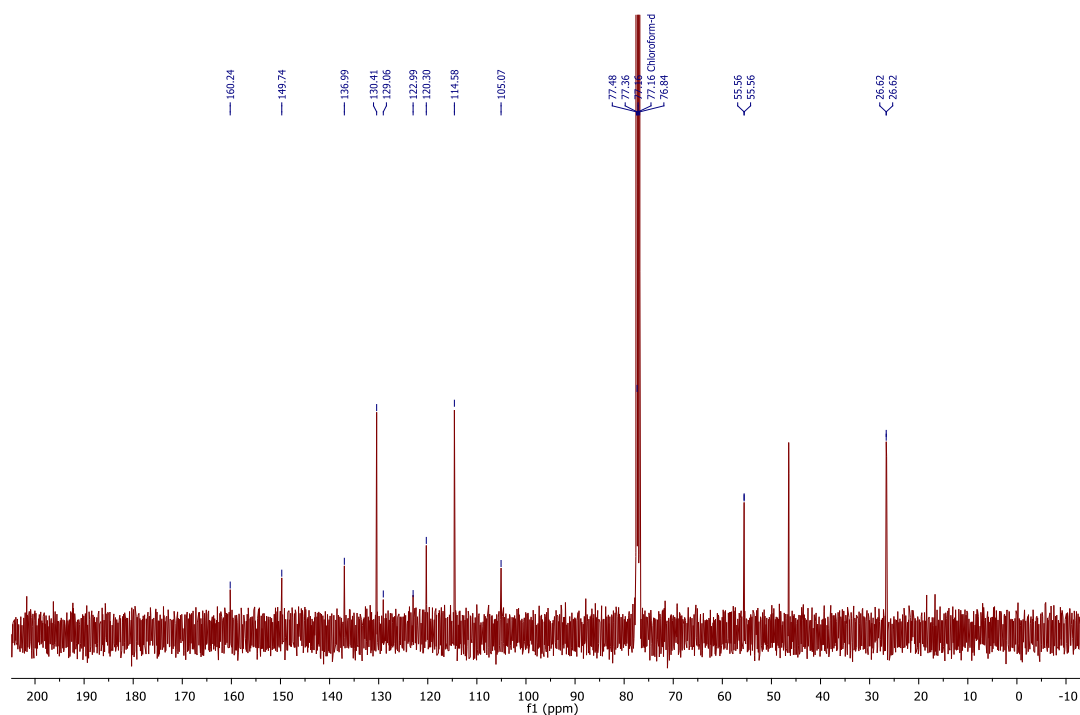
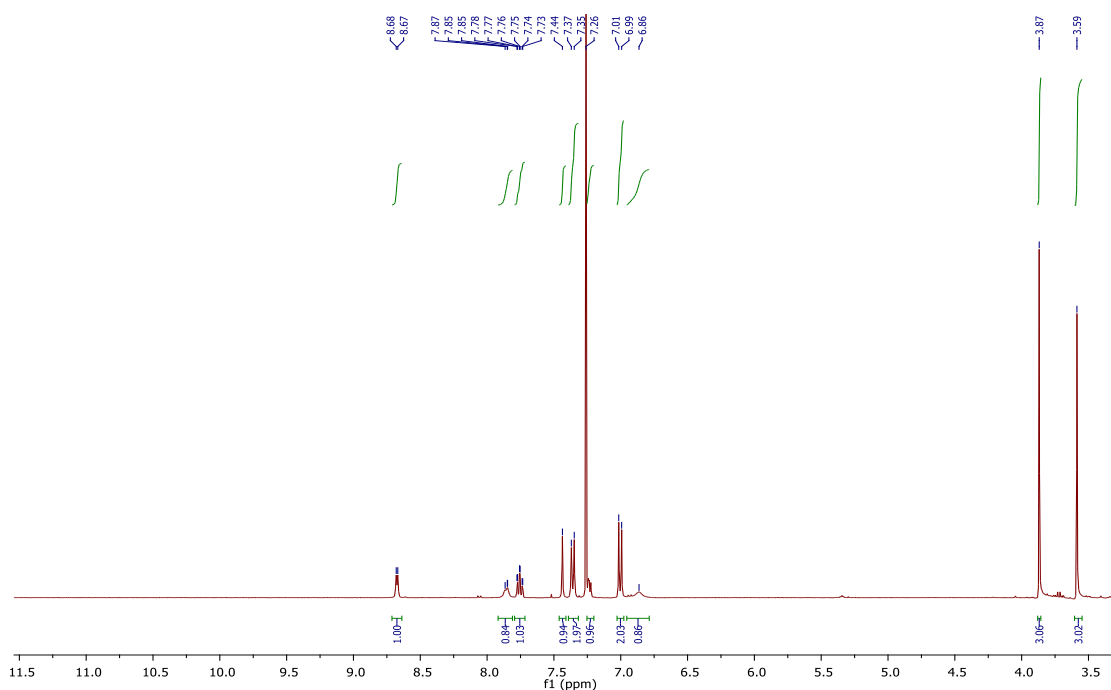
***N*-(5-(4-Methoxyphenyl)-1-methyl-1H-imidazol-2-yl)-5-(pyridin-2-yl)-1H-pyrazole-3-carboxamide (2.002)**



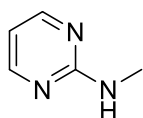
The title compound was prepared from 5-(4-methoxyphenyl)-1-methyl-1H-imidazol-2-amine (200 mg, 0.980 mmol) and 5-(pyridin-2-yl)-1H-pyrazole-3-carboxylic acid (187 mg, 0.98 mmol) according to General Procedure C (94.1 mg, 22%). HPLC - t_R 4.61 min > 99% purity at 254 nm; LRMS $[M+H]^+$ 374.9 m/z ; HRMS

$[M+H]^+$ 375.1564 m/z , found 374.1563 m/z ; 1H NMR (400 MHz, $CDCl_3$) δ 8.67 (d, J = 4.6 Hz, 1H, Ha), 7.90 – 7.81 (m, 1H, Hd), 7.75 (td, J = 7.7, 1.7 Hz, 1H, Hc), 7.44 (s, 1H Hg), 7.38 – 7.33 (m, 2H, Ho), 7.25 – 7.22 (m, 1H, Hb), 7.03 – 6.98 (m, 2H, Hp), 6.86 (bs, 1H, Hl), 3.87 (s, 3H, Hr), 3.59 (s, 3H, Hk); ^{13}C NMR (101 MHz, $CDCl_3$) δ_C 160.2 (Ci), 149.7 (Ca), 137.0 (Cc), 130.4 (2C, Co), 129.1 (Cb), 123.0 (Cd), 120.3 (Cg), 114.6 (2C, Cp), 105.1 (Cl), 55.6 (Cr), 26.6 (Ck). Aromatic quaternary carbons not available

Example spectra for Series 1-2: ^1H (400 MHz, CDCl_3) and ^{13}C NMR (100 MHz, CDCl_3) spectrum of *N*-(5-(4-methoxyphenyl)-1-methyl-1*H*-imidazol-2-yl)-5-(pyridin-2-yl)-1*H*-pyrazole-3-carboxamide (2.002)



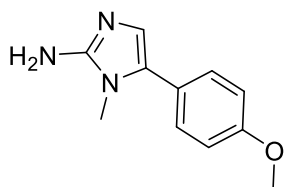
N-Methylpyrimidin-2-amine (2.003)⁶



To a solution of 2-chloropyrimidine (2 g, 17.5 mmol) in THF (25 mL) was added 40% methylamine (aq) (7.5 mL) at 0°C. The reaction mixture was then heated to reflux for 1 hour then saturated NaHCO_3 (aq) was added and extracted with ethyl acetate. The organic layer was washed with brine, dried using MgSO_4 and reduced *in vacuo* to give the known product as pale yellow crystals (1.72 g, 90%).⁴ LRMS $[\text{M}+\text{H}]^+$ 110.0 *m/z*; ^1H NMR (400 MHz, CDCl_3)

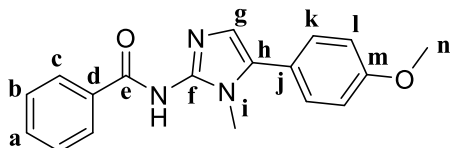
δ_{H} 8.21 (d, $J = 4.7$ Hz, 2H), 6.44 (t, $J = 4.8$ Hz, 1H), 5.46 (s, 1H), 2.92 (d, $J = 5.1$ Hz, 3H); ^{13}C NMR (101 MHz, CDCl_3) δ_{C} 163.1, 158.1, 110.4, 28.4. Acquired data is consistent with the literature.⁶

5-(4-Methoxyphenyl)-1-methyl-1*H*-imidazol-2-amine (2.005)



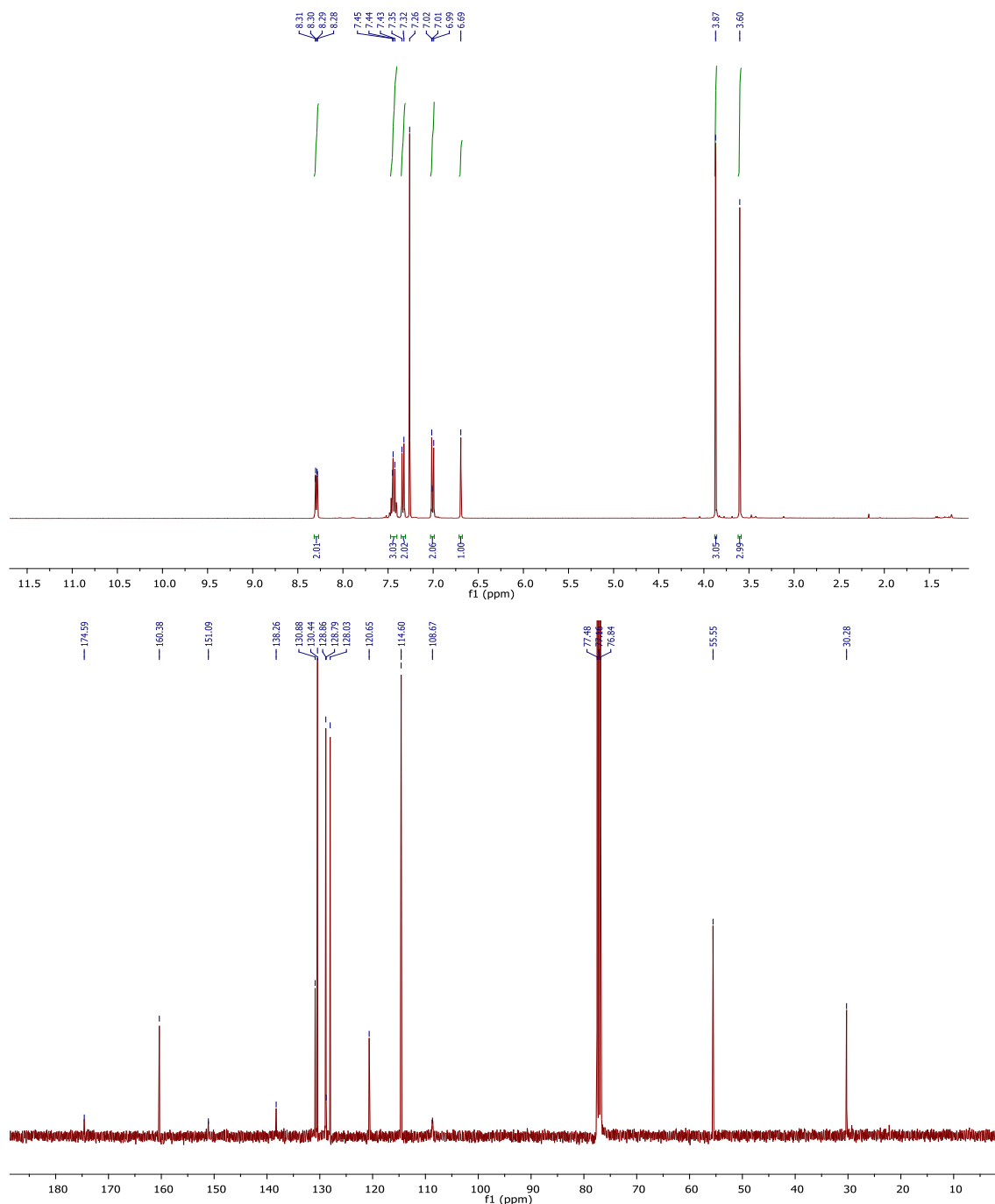
The title compound was prepared from 2-bromo-1-(4-methoxyphenyl)ethan-1-one (824 mg, 3.60 mmol) according to General Procedure A as an orange solid without further purification (496 mg, 93%). HPLC - t_{R} 4.04 min > 99% purity at 254 nm; LRMS $[\text{M}+\text{H}]^+$ 203.9 m/z ; ^1H NMR (400 MHz, $\text{DMSO}-d_6$) δ_{H} 7.31 – 7.24 (m, 2H), 7.00 – 6.92 (m, 2H), 6.43 (s, 1H), 5.40 (s, 2H), 3.77 (s, 3H), 3.30 (s, 3H); ^{13}C NMR (101 MHz, $\text{DMSO}-d_6$) δ_{C} 158.9, 150.6, 128.4, 127.5, 123.6, 121.7, 114.1, 55.1, 30.1.

N-(5-(4-Methoxyphenyl)-1-methyl-1*H*-imidazol-2-yl)benzamide (2.008)

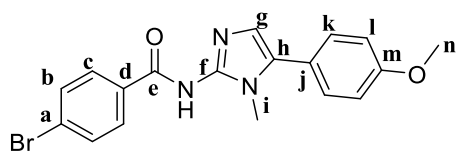


The title compound was prepared from 5-(4-methoxyphenyl)-1-methyl-1*H*-imidazol-2-amine (200 mg, 0.980 mmol) and benzoic acid (120 mg, 0.980 mmol) in DMF (5 mL) according to General Procedure B (224.1 mg, 75%). HPLC - t_{R} 5.01 min > 99% purity at 254 nm; LRMS $[\text{M}+\text{H}]^+$ 307.9 m/z ; HRMS $[\text{M}+\text{H}]^+$ 308.1394 m/z , found 308.1396 m/z ; ^1H NMR (400 MHz, CDCl_3) δ 8.31 – 8.28 (m, 2H, Hc), 7.47 – 7.40 (m, 3H, Ha, Hb), 7.36 – 7.31 (m, 2H, Hk), 7.07 – 6.95 (m, 2H, Hl), 6.69 (s, 1H, Hg), 3.87 (s, 3H, Hn), 3.60 (s, 3H, Hi); ^{13}C NMR (101 MHz, CDCl_3) δ_{C} 174.6 (Cf), 160.4 (Ce), 151.1 (Ch), 138.3 (Cd), 130.9 (Ca), 130.4 (2C, Ck/Cb/Cc), 128.9 (2C, Ck/Cb/Cc), 128.8 (Cm), 128.0 (2C, Ck/Cb/Cc), 120.7 (Cg), 114.6 (2C, Cl), 108.7 (Cj), 55.6 (Cn), 30.3 (Ci).

Example spectra for Series 1-2: ^1H (400 MHz, CDCl_3) and ^{13}C NMR (100 MHz, CDCl_3) spectrum of *N*-(5-(4-Methoxyphenyl)-1-methyl-1*H*-imidazol-2-yl)benzamide (2.008)



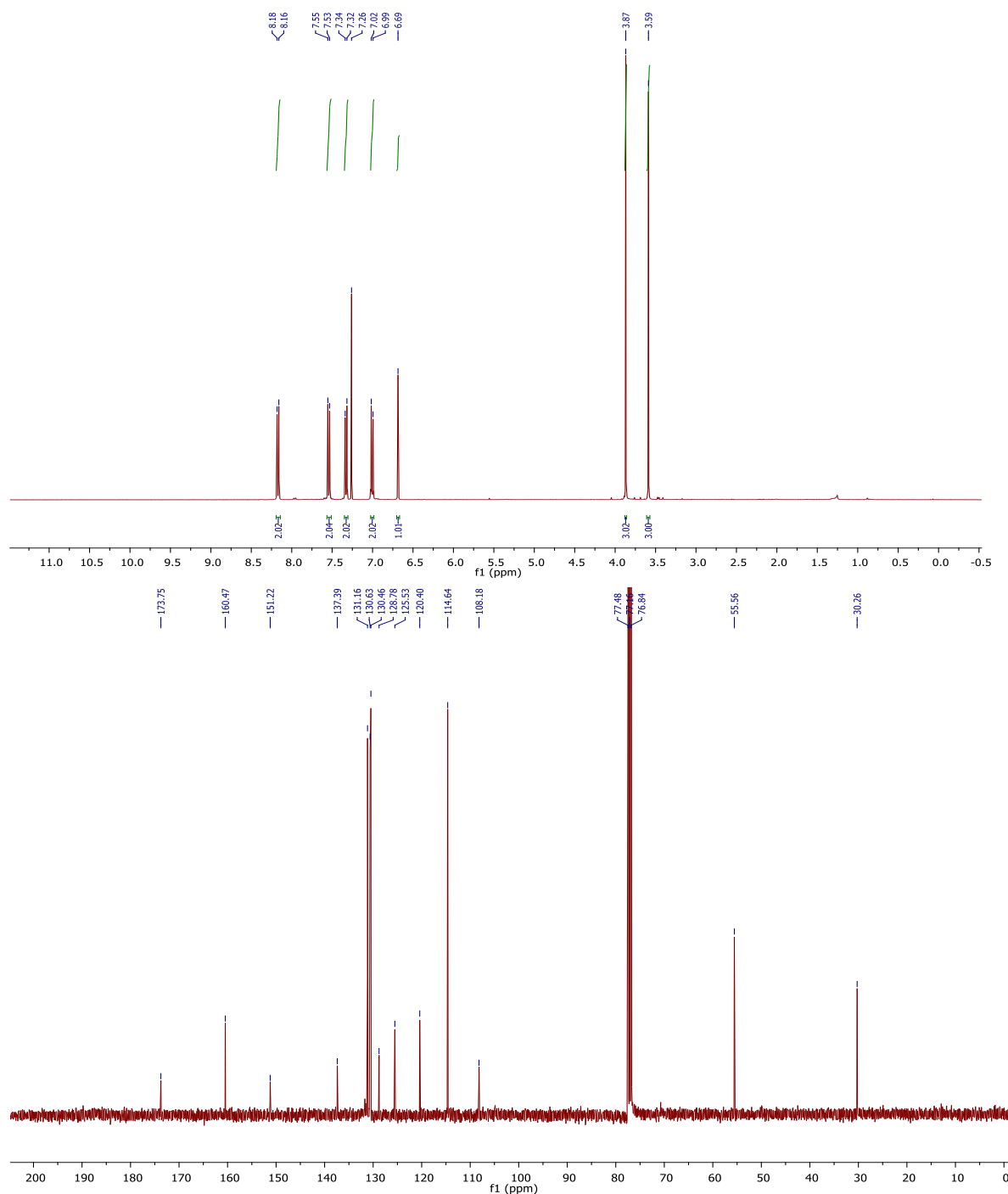
4-Bromo-*N*-(5-(4-methoxyphenyl)-1-methyl-1*H*-imidazol-2-yl)benzamide (2.009)



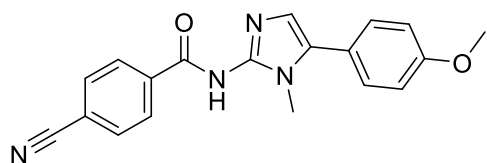
The title compound was prepared from 5-(4-methoxyphenyl)-1-methyl-1*H*-imidazol-2-amine (200 mg, 0.980 mmol) and 4-bromobenzoic acid (197 mg, 0.980 mmol) according to General Procedure B (202 mg, 53%). HPLC - t_R 5.52 min > 99% purity at 254 nm; LRMS $[\text{M}+\text{H}]^+$ 385.8 m/z ; HRMS $[\text{M}+\text{H}]^+$ 386.0499 m/z , found 386.0499 m/z ; ^1H NMR (400

MHz, CDCl₃) δ_{H} 8.19 – 8.15 (m, 2H, Hc), 7.56 – 7.53 (m, 2H, Hb), 7.35 – 7.31 (m, 2H, Hk), 7.02 – 6.99 (m, 2H, Hl), 6.69 (s, 1H, Hg), 3.87 (s, 3H, Hn), 3.59 (s, 3H, Hi); ¹³C NMR (101 MHz, CDCl₃) δ_{C} 173.8 (Cf), 160.5 (Ce), 151.2 (Ch), 137.4 (Cd/Cm), 131.2 (2C, Cb), 130.6 (2C, Cc/Ck), 130.5 (2C, Cc/Ck), 128.8 (Cd/Cm), 125.5 (Ca), 120.4 (Cg), 114.6 (2C, Cl), 108.2 (Cj), 55.6 (Cn), 30.3 (Ci).

Example spectra for Series 1-2: ¹H (400 MHz, CDCl₃) and ¹³C NMR (100 MHz, CDCl₃) spectrum of 4-Bromo-*N*-(5-(4-methoxyphenyl)-1-methyl-1*H*-imidazol-2-yl)benzamide (2.009)



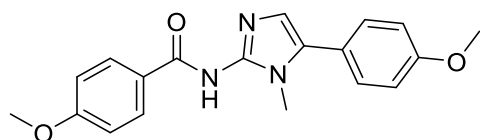
4-Cyano-*N*-(5-(4-methoxyphenyl)-1-methyl-1*H*-imidazol-2-yl)benzamide (2.010)



The title compound was prepared from 5-(4-methoxyphenyl)-1-methyl-1*H*-imidazol-2-amine (200 mg, 0.980 mmol) and 4-cyanobenzoic acid (144 mg, 0.980 mmol) according to General Procedure B (179 mg, 54%).

HPLC - t_R 4.99 min > 99% purity at 254 nm; LRMS $[M+H]^+$ 332.9 m/z ; HRMS $[M+H]^+$ 333.1346 m/z , found 333.1348 m/z ; 1H NMR (400 MHz, $CDCl_3$) δ_H 8.39 (d, J = 8.5 Hz, 2H), 7.71 (d, J = 8.4 Hz, 2H), 7.36 – 7.32 (m, 2H), 7.04 – 7.00 (m, 2H), 6.73 (s, 1H), 3.87 (s, 3H), 3.61 (s, 3H); ^{13}C NMR (101 MHz, $CDCl_3$) δ_C 172.9, 160.6, 151.3, 142.8, 131.9 (2C), 130.5 (2C), 129.4 (2C), 129.0, 120.1, 119.2, 114.7 (2C), 113.9, 107.9, 55.6, 30.2. M.p. 197.6–201.8°C.

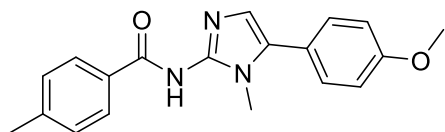
4-Methoxy-*N*-(5-(4-methoxyphenyl)-1-methyl-1*H*-imidazol-2-yl)benzamide (2.011)



The title compound was prepared from 5-(4-methoxyphenyl)-1-methyl-1*H*-imidazol-2-amine (200 mg, 0.980 mmol) and 4-methoxybenzoic acid (148 mg, 0.980 mmol) according to General Procedure B (296 mg, 90%).

HPLC - t_R 5.10 min > 99% purity at 254 nm; LRMS $[M+H]^+$ 337.9 m/z ; HRMS $[M+H]^+$ 338.1499 m/z , found 338.1500 m/z ; 1H NMR (400 MHz, $CDCl_3$) δ_H 8.25 (d, J = 8.8 Hz, 2H), 7.35 – 7.31 (m, 2H), 7.02 – 6.98 (m, 2H), 6.93 (d, J = 8.9 Hz, 2H), 6.65 (s, 1H), 3.86 (d, 6H, assumed 2x singlets 3H each with overlapping signals), 3.58 (s, 3H); 1H NMR (400 MHz, DMSO) δ_H 10.46 (bs, 1H), 8.06 (d, J = 5.1 Hz, 2H), 7.43 (d, J = 8.3 Hz, 2H), 7.05 – 6.96 (m, 4H), 6.88 (s, 1H), 3.80 (s, 3H), 3.79 (s, 3H), 3.44 (s, 3H); ^{13}C NMR (101 MHz, DMSO) δ_C 159.2, 130.1 (2C), 129.7 (2C), 114.4 (2C), 113.3 (2C), 55.3, 55.2, 30.5. Imidazole and aromatic quaternary carbons not visible.

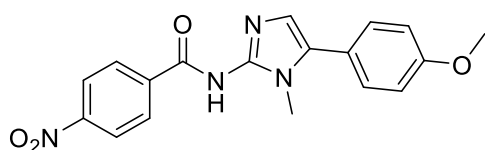
N-(5-(4-Methoxyphenyl)-1-methyl-1*H*-imidazol-2-yl)-4-methylbenzamide (2.012)



The title compound was prepared from 5-(4-methoxyphenyl)-1-methyl-1*H*-imidazol-2-amine (200 mg, 0.980 mmol) and 4-methylbenzoic acid (134 mg, 0.980 mmol) according to

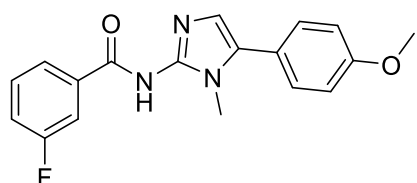
General Procedure B (217 mg, 78%). HPLC - t_R 5.24 min > 95% purity at 254 nm; LRMS $[M+H]^+$ 321.9 m/z ; HRMS $[M+H]^+$ 322.1550 m/z , found 322.1549 m/z ; 1H NMR (400 MHz, $CDCl_3$) δ_H 8.19 (d, J = 8.1 Hz, 2H), 7.35 – 7.31 (m, 2H), 7.23 (d, J = 7.9 Hz, 2H), 7.02 – 6.98 (m, 2H), 6.68 (s, 1H), 3.87 (s, 3H), 3.59 (s, 3H), 2.40 (s, 3H); ^{13}C NMR (101 MHz, $CDCl_3$) δ_C 160.4, 141.3, 130.5 (2C), 128.9 (2C), 128.8 (2C), 120.6, 114.6 (2C), 55.6, 30.5, 21.7. Aromatic quaternary carbons not observed

***N*-(5-(4-Methoxyphenyl)-1-methyl-1*H*-imidazol-2-yl)-4-nitrobenzamide (2.013)**



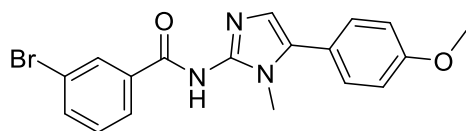
The title compound was prepared from 5-(4-methoxyphenyl)-1-methyl-1*H*-imidazol-2-amine (200 mg, 0.980 mmol) and 4-nitrobenzoic acid (163 mg, 0.980 mmol) in DMF (5 mL) according to General Procedure B (199 mg, 58%). HPLC - t_R 5.31 min > 99% purity at 254 nm; LRMS $[M+H]^+$ 352.9 m/z ; HRMS $[M+H]^+$ 353.1244 m/z , found 353.1251 m/z ; 1H NMR (400 MHz, $CDCl_3$) δ 8.42 (d, J = 8.9 Hz, 2H), 8.27 – 8.23 (m, 2H), 7.36 – 7.32 (m, 2H), 7.04 – 7.00 (m, 2H), 6.74 (s, 1H), 3.88 (s, 3H), 3.63 (s, 3H); ^{13}C NMR (101 MHz, $CDCl_3$) δ_C 172.5, 160.7, 151.1, 149.4, 144.4, 130.6 (2C), 129.8 (2C), 129.1, 123.2 (2C), 120.0, 114.7 (2C), 108.0, 55.6, 30.3. M.p. 212.4–228.8°C.

3-Fluoro-*N*-(5-(4-methoxyphenyl)-1-methyl-1*H*-imidazol-2-yl)benzamide (2.014)



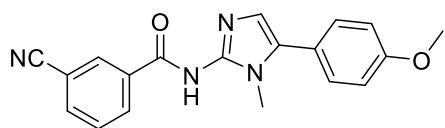
The title compound was prepared from 5-(4-methoxyphenyl)-1-methyl-1*H*-imidazol-2-amine (200 mg, 0.980 mmol) and 3-fluorobenzoic acid (137 mg, 0.980 mmol) according to General Procedure B (169 mg, 53%). HPLC - t_R 5.08 min > 99% purity at 254 nm; LRMS $[M+H]^+$ 325.9 m/z ; HRMS $[M+H]^+$ 326.1299 m/z , found 326.1287 m/z ; 1H NMR (400 MHz, $CDCl_3$) δ_H 8.11 – 8.06 (m, 1H), 8.02 – 7.97 (m, 1H), 7.42 – 7.31 (m, 3H), 7.17 – 7.12 (m, 1H), 7.04 – 6.97 (m, 2H), 6.69 (s, 1H), 3.87 (s, 3H), 3.60 (s, 3H); ^{13}C NMR (101 MHz, $CDCl_3$) δ_C 173.7, 162.9 (d, J_{C-F} = 244.5 Hz), 160.5, 151.3, 141.1, 130.5 (2C), 129.4 (d, J_{C-F} = 7.8 Hz), 128.8, 124.5 (d, J_{C-F} = 2.7 Hz), 120.4, 117.6 (d, J_{C-F} = 21.6 Hz), 115.8 (d, J_{C-F} = 22.2 Hz), 114.7 (2C), 108.0, 55.6, 30.2. M.p. 136.5–148.5°C.

3-Bromo-*N*-(5-(4-methoxyphenyl)-1-methyl-1*H*-imidazol-2-yl)benzamide (2.015)



The title compound was prepared from 5-(4-methoxyphenyl)-1-methyl-1*H*-imidazol-2-amine (200 mg, 0.980 mmol) and 3-bromobenzoic acid (197 mg, 0.980 mmol) according to General Procedure B (379 mg, 99%). HPLC - t_R 5.55 min > 99% purity at 254 nm; LRMS $[M+H]^+$ 385.7 m/z ; HRMS $[M+H]^+$ 386.0499 m/z , found 386.0499 m/z ; 1H NMR (400 MHz, $CDCl_3$) δ_H 8.44 (t, J = 1.7 Hz, 1H), 8.23 (d, J = 7.8 Hz, 1H), 7.60 – 7.56 (m, 1H), 7.36 – 7.28 (m, 3H), 7.03 – 6.99 (m, 2H), 6.72 (s, 1H), 3.87 (s, 3H), 3.61 (s, 3H); ^{13}C NMR (101 MHz, $CDCl_3$) δ_C 173.1, 160.4, 151.2, 140.7, 133.6, 132.0, 130.4 (2C), 129.6, 128.8, 127.4, 122.2, 120.4, 114.6 (2C), 108.2, 55.5, 30.3.

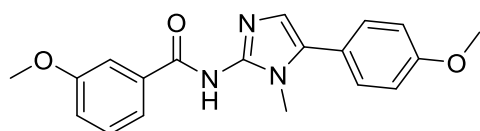
3-Cyano-*N*-(5-(4-methoxyphenyl)-1-methyl-1*H*-imidazol-2-yl)benzamide (2.016)



The title compound was prepared from 5-(4-methoxyphenyl)-1-methyl-1*H*-imidazol-2-amine (200 mg, 0.980 mmol) and 3-cyanobenzoic acid (144 mg, 0.980 mmol) according to General

Procedure B (138 mg, 42%). HPLC - t_R 5.01 min > 99% purity at 254 nm; LRMS $[M+H]^+$ 332.9 m/z ; HRMS $[M+H]^+$ 333.1346 m/z , found 333.1337 m/z ; 1H NMR (400 MHz, $CDCl_3$) δ_H 8.65 – 8.62 (m, 1H), 8.53 – 8.49 (m, 1H), 7.72 (dt, J = 7.6, 1.3 Hz, 1H), 7.55 – 7.51 (m, 1H), 7.36 – 7.32 (m, 2H), 7.04 – 7.00 (m, 2H), 6.71 (s, 1H), 3.88 (s, 3H), 3.62 (s, 3H); ^{13}C NMR (101 MHz, $CDCl_3$) δ_C 172.5, 160.6, 151.4, 139.9, 133.8, 133.1, 133.0, 130.51 (2C), 128.9, 128.9, 120.1, 119.2, 114.7 (2C), 112.1, 107.8, 55.6, 30.2.

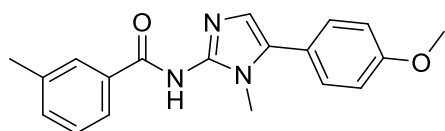
3-Methoxy-*N*-(5-(4-methoxyphenyl)-1-methyl-1*H*-imidazol-2-yl)benzamide (2.017)



The title compound was prepared from 5-(4-methoxyphenyl)-1-methyl-1*H*-imidazol-2-amine (200 mg, 0.980 mmol) and 3-methoxybenzoic acid (148 mg, 0.980

mmol) according to General Procedure B (220 mg, 67%). HPLC - t_R 5.09 min > 99% purity at 254 nm; LRMS $[M+H]^+$ 337.9 m/z ; HRMS $[M+H]^+$ 338.1499 m/z , found 338.1500 m/z ; 1H NMR (400 MHz, $CDCl_3$) δ_H 7.93 – 7.89 (m, 1H), 7.85-7.84 (m, 1H), 7.35 – 7.31 (m, 3H), 7.03 – 6.98 (m, 3H), 6.67 (s, 1H), 3.88 (s, 3H), 3.87 (s, 3H), 3.59 (s, 3H); ^{13}C NMR (101 MHz, $CDCl_3$) δ_C 174.2, 160.4, 159.6, 150.9, 139.8, 130.4 (2C), 129.0, 128.8, 121.4, 120.6, 117.3, 114.6 (2C), 113.5, 108.8, 55.5, 55.5, 30.3.

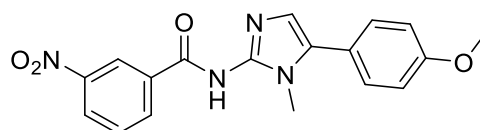
N-(5-(4-Methoxyphenyl)-1-methyl-1*H*-imidazol-2-yl)-3-methylbenzamide (2.018)



The title compound was prepared from 5-(4-methoxyphenyl)-1-methyl-1*H*-imidazol-2-amine (200 mg, 0.980 mmol) and 3-methylbenzoic acid (133 mg, 0.980 mmol) according to

General Procedure B (282 mg, 89%). HPLC - t_R 5.31 min > 99% purity at 254 nm; LRMS $[M+H]^+$ 321.9 m/z ; HRMS $[M+H]^+$ 322.155 m/z , found 322.1548 m/z ; 1H NMR (400 MHz, $CDCl_3$) δ_H 8.13 – 8.08 (m, 2H), 7.35 – 7.28 (m, 4H), 7.03 – 6.99 (m, 2H), 6.72 (s, 1H), 3.87 (s, 3H), 3.61 (s, 3H), 2.42 (s, 3H); ^{13}C NMR (101 MHz, $CDCl_3$) δ_C 174.5, 160.3, 150.8, 138.0, 137.6, 131.9, 130.4 (2C), 129.4, 128.9, 128.0, 126.0, 120.8, 114.6 (2C), 109.3, 55.5, 30.4, 21.6.

N-(5-(4-Methoxyphenyl)-1-methyl-1*H*-imidazol-2-yl)-3-nitrobenzamide (2.019)

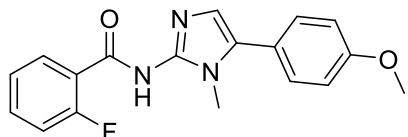


The title compound was prepared from 5-(4-methoxyphenyl)-1-methyl-1*H*-imidazol-2-amine (200 mg, 0.980 mmol) and 3-nitrobenzoic acid (164 mg, 0.980

mmol) according to General Procedure B (249 mg, 72%). HPLC - t_R 5.28 min > 99% purity at 254 nm; LRMS $[M+H]^+$ 352.9 m/z ; HRMS $[M+H]^+$ 353.1244 m/z , found 353.1244 m/z ; 1H NMR (400 MHz,

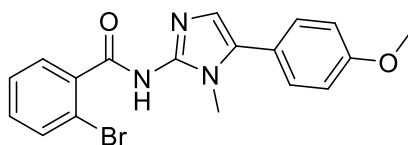
CDCl₃) δ_H 9.10 – 9.07 (m, 1H), 8.58 – 8.55 (m, 1H), 8.32 – 8.28 (m, 1H), 7.59 (t, J = 8.0 Hz, 1H), 7.36 – 7.33 (m, 2H), 7.04 – 7.00 (m, 2H), 6.76 (s, 1H), 3.88 (s, 3H), 3.64 (s, 3H); ¹³C NMR (101 MHz, CDCl₃, DEPT) δ_C 134.6, 130.4 (2C), 128.8, 125.1, 124.0, 114.6 (2C), 107.6, 55.5, 30.2. Quaternary carbons not visible. M.p 208.0-213.0°C.

2-Fluoro-*N*-(5-(4-methoxyphenyl)-1-methyl-1*H*-imidazol-2-yl)benzamide (2.020)



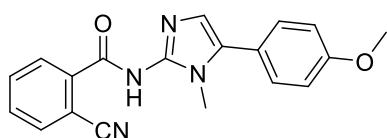
The title compound was prepared from 5-(4-methoxyphenyl)-1-methyl-1*H*-imidazol-2-amine (200 mg, 0.980 mmol) and 2-fluorobenzoic acid (137 mg, 0.980 mmol) according to General Procedure B (166 mg, 52%). HPLC - t_R 4.54 min > 99% purity at 254 nm; LRMS $[M+H]^+$ 325.9 m/z ; HRMS $[M+H]^+$ 326.1299 m/z , found 326.1285 m/z ; ¹H NMR (400 MHz, CDCl₃) δ_H 8.03 (td, J = 7.7, 1.8 Hz, 1H), 7.38 – 7.32 (m, 1H), 7.28 – 7.25 (m, 2H), 7.13 (td, J = 7.7, 1.0 Hz, 1H), 7.05 (ddd, J = 11.3, 8.3, 0.9 Hz, 1H), 6.96 – 6.91 (m, 2H), 6.68 (s, 1H), 3.80 (s, 3H), 3.50 (s, 3H); ¹³C NMR (101 MHz, CDCl₃) δ_C 171.2, 161.5 (d, J_{C-F} = 253.3 Hz), 160.2, 148.8, 132.2 (d, J_{C-F} = 8.8 Hz), 131.85 (d, J_{C-F} = 1.8 Hz), 130.4, 129.5, 126.1, 123.9 (d, J_{C-F} = 3.6 Hz), 120.8, 116.6 (d, J_{C-F} = 23.4 Hz), 114.5 (2C), 111.4, 55.5, 30.5. M.p. 150.5-159.3 °C

2-Bromo-*N*-(5-(4-methoxyphenyl)-1-methyl-1*H*-imidazol-2-yl)benzamide (2.021)

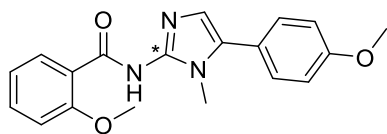


The title compound was prepared from 5-(4-methoxyphenyl)-1-methyl-1*H*-imidazol-2-amine (200 mg, 0.980 mmol) and 2-bromobenzoic acid (197 mg, 0.980 mmol) in DMF (5 mL) according to General Procedure B (320 mg, 94%). HPLC - t_R 5.12 min > 99% purity at 254 nm; LRMS $[M+H]^+$ 387.8 m/z ; HRMS $[M+H]^+$ 386.0499 m/z , found 386.0505 m/z ; ¹H NMR (400 MHz, CDCl₃) δ_H 7.74 (dd, J = 7.7, 1.7 Hz, 1H), 7.53 (dd, J = 8.0, 1.1 Hz, 1H), 7.28 – 7.23 (m, 3H), 7.16 – 7.11 (m, 1H), 6.95 – 6.92 (m, 2H), 3.80 (s, 3H), 3.49 (s, 3H); ¹³C NMR (101 MHz, CDCl₃) δ_C 175.3, 160.4, 150.1, 140.8, 133.7, 130.6, 130.5 (2C), 130.3, 129.1, 127.1, 120.7, 120.5, 114.6 (2C), 109.3, 55.6, 30.5.

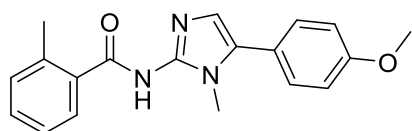
2-Cyano-*N*-(5-(4-methoxyphenyl)-1-methyl-1*H*-imidazol-2-yl)benzamide (2.022)



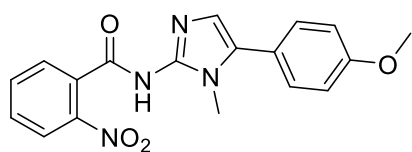
The title compound was prepared from 5-(4-methoxyphenyl)-1-methyl-1*H*-imidazol-2-amine (200 mg, 0.980 mmol) and 2-cyanobenzoic acid (144 mg, 0.980 mmol) according to General Procedure B (138 mg, 42%). HPLC - t_R 5.24 min > 99% purity at 254 nm; LRMS $[M+H]^+$ 332.9 m/z ; HRMS $[M+H]^+$ 333.1268 m/z , found 333.1243 m/z ; ¹H NMR (400 MHz, CDCl₃) δ_H 8.01 – 7.96 (m, 1H), 7.92 – 7.87 (m, 1H), 7.78 – 7.66 (m, 2H), 7.39 – 7.34 (m, 2H), 7.12 (s, 1H), 7.04 – 7.00 (m, 2H), 3.87 (s, 3H), 3.79 (s, 3H); ¹³C NMR (101 MHz, CDCl₃) δ_C 168.6, 159.8, 150.3, 137.2, 134.5, 133.2, 132.7, 132.0, 131.2, 130.0 (2C), 123.9, 123.8, 122.5, 122.1, 114.5 (2C), 55.5, 30.8.

2-Methoxy-*N*-(5-(4-methoxyphenyl)-1-methyl-1*H*-imidazol-2-yl)benzamide (2.023)

The title compound was prepared from 5-(4-methoxyphenyl)-1-methyl-1*H*-imidazol-2-amine (200 mg, 0.980 mmol) and 2-methoxybenzoic acid (148 mg, 0.980 mmol) according to General Procedure B (230.0 mg, 70%). HPLC - t_R 5.22 min > 99% purity at 254 nm; LRMS $[M+H]^+$ 337.9 m/z ; HRMS $[M+H]^+$ 338.1499 m/z , found 338.1499 m/z ; 1H NMR (401 MHz, $CDCl_3$) δ_H 8.26 (dd, J = 7.8, 1.6 Hz, 1H), 7.56 – 7.51 (m, 1H), 7.37 – 7.33 (m, 2H), 7.15 – 7.10 (m, 1H), 7.05 (d, J = 8.3 Hz, 1H), 7.00 – 6.95 (m, 2H), 6.94 (s, 1H), 4.03 (s, 3H), 3.85 (s, 3H), 3.52 (s, 3H); ^{13}C NMR (101 MHz, $CDCl_3$) δ_C 165.3, 159.6, 158.0, 140.5, 134.0, 132.7, 130.1 (2C), 123.2, 122.5, 121.6, 120.7, 114.3 (2C), 111.7, 56.3, 55.5, 31.9. Imidazole quaternary peak not visible*

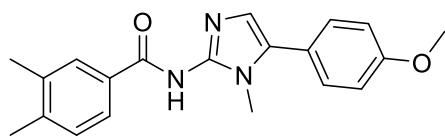
***N*-(5-(4-Methoxyphenyl)-1-methyl-1*H*-imidazol-2-yl)-2-methylbenzamide (2.024)**

The title compound was prepared from 5-(4-methoxyphenyl)-1-methyl-1*H*-imidazol-2-amine (200 mg, 0.980 mmol) and 2-methylbenzoic acid (133 mg, 0.980 mmol) according to General Procedure B (260 mg, 82%). HPLC - t_R 5.11 min > 99% purity at 254 nm; LRMS $[M+H]^+$ 322.0 m/z ; HRMS $[M+H]^+$ 322.1550 m/z , found 322.1548 m/z ; 1H NMR (400 MHz, $CDCl_3$) δ_H 7.84 (d, J = 7.7 Hz, 1H), 7.35 – 7.32 (m, 3H), 7.23 (d, J = 7.6 Hz, 2H), 7.03 – 6.99 (m, 2H), 6.77 (s, 1H), 3.87 (s, 3H), 3.58 (s, 3H), 2.60 (s, 3H); 1H NMR (400 MHz, DMSO) δ_H 10.47 (bs, 1H), 7.61 (bs, 1H), 7.39 (d, J = 8.5 Hz, 2H), 7.32 (d, J = 7.2 Hz, 1H), 7.25 (d, J = 7.4 Hz, 2H), 7.06 – 6.96 (m, 2H), 6.86 (s, 1H), 3.76 (s, 3H), 3.43 (s, 3H). LHS Methyl group not visible- eclipsed by solvent peak; ^{13}C NMR (101 MHz, DMSO) δ_C 159.4, 136.3, 132.0, 131.8, 131.1, 129.9 (2C), 126.7, 126.2, 125.9, 119.0, 114.7 (2C), 110.4, 55.5, 31.2, 21.4. Quaternary imidazole carbons not visible

***N*-(5-(4-Methoxyphenyl)-1-methyl-1*H*-imidazol-2-yl)-2-nitrobenzamide (2.025)**

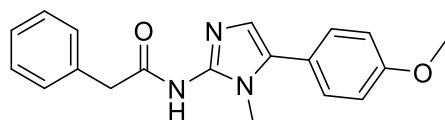
The title compound was prepared from 5-(4-methoxyphenyl)-1-methyl-1*H*-imidazol-2-amine (200 mg, 0.980 mmol) and 2-nitrobenzoic acid (164 mg, 0.980 mmol) according to General Procedure B (212 mg, 60%). HPLC - t_R 4.87 min > 99% purity at 254 nm; LRMS $[M+H]^+$ 352.8 m/z ; HRMS $[M+H]^+$ 353.1244 m/z , found 353.1243 m/z ; 1H NMR (400 MHz, $CDCl_3$) δ_H 7.94 (dd, J = 7.6, 1.1 Hz, 1H), 7.59 – 7.39 (m, 4H), 7.26 – 7.22 (m, 2H), 6.95 – 6.90 (m, 2H), 6.61 (s, 1H), 3.80 (s, 3H), 3.41 (s, 3H); ^{13}C NMR (101 MHz, $CDCl_3$) δ_C 172.4, 160.6, 155.1, 150.1, 140.7, 134.2, 131.5, 130.6 (2C), 130.0, 128.9, 123.0, 120.1, 114.7 (2C), 107.9, 55.6, 30.2.

***N*-(5-(4-Methoxyphenyl)-1-methyl-1*H*-imidazol-2-yl)-3,4-dimethylbenzamide (2.026)**



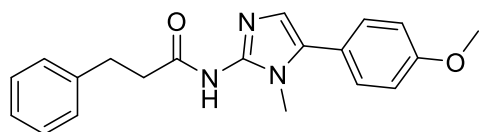
The title compound was prepared from 5-(4-methoxyphenyl)-1-methyl-1*H*-imidazol-2-amine (200 mg, 0.980 mmol) and 3,4-dimethylbenzoic acid (147 mg, 0.980 mmol) in DMF (5 mL) according to General Procedure B (178 mg, 53%). HPLC - t_R 5.59 min > 99% purity at 254 nm; LRMS $[M+H]^+$ 335.9 m/z ; HRMS $[M+H]^+$ 336.1707 m/z , found 336.1715 m/z ; 1H NMR (400 MHz, $CDCl_3$) δ_H 7.97 – 7.89 (m, 2H), 7.28 – 7.24 (m, 2H), 7.12 (d, J = 7.8 Hz, 1H), 6.95 – 6.92 (m, 2H), 6.64 (s, 1H), 3.80 (s, 3H), 3.53 (s, 3H), 2.26 (s, 3H), 2.24 (s, 3H); 1H NMR (400 MHz, $CDCl_3$) δ_H 8.04 – 7.98 (m, 2H), 7.35 – 7.31 (m, 2H), 7.19 (d, J = 7.8 Hz, 1H), 7.02 – 6.98 (m, 2H), 6.71 (s, 1H), 3.88 – 3.86 (m, 3H), 3.60 (s, 3H), 2.33 (s, 3H), 2.31 (s, 3H); ^{13}C NMR (101 MHz, $CDCl_3$) δ_C 173.2, 160.0, 149.0, 139.9, 136.1, 134.9, 130.2 (2C), 129.9, 129.4, 129.3, 126.3, 121.1, 114.4 (2C), 111.8, 55.4, 30.6, 19.9, 19.8.

***N*-(5-(4-Methoxyphenyl)-1-methyl-1*H*-imidazol-2-yl)-2-phenylacetamide (2.027)**

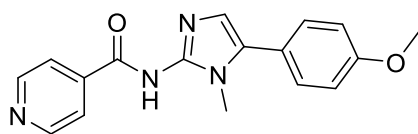


The title compound was prepared from 5-(4-methoxyphenyl)-1-methyl-1*H*-imidazol-2-amine (200 mg, 0.980 mmol) and 2-phenylacetic acid (134 mg, 0.980 mmol) according to General Procedure B (286 mg, 90%). HPLC - t_R 5.10 min > 99% purity at 254 nm; LRMS $[M+H]^+$ 321.9 m/z ; HRMS $[M+H]^+$ 322.1550 m/z , found 322.1548 m/z ; 1H NMR (400 MHz, $CDCl_3$) δ_H 7.31 – 7.19 (m, 5H), 7.19 – 7.11 (m, 2H), 6.88 (d, J = 8.5 Hz, 2H), 6.62 (s, 1H), 3.77 (s, 3H), 3.68 (s, 2H), 3.32 (s, 3H); 1H NMR (400 MHz, DMSO) δ_H 10.32 (s, 1H), 7.33 – 7.16 (m, 7H), 7.00 – 6.90 (m, 2H), 6.77 (s, 1H), 3.71 (s, 2H), 3.60 (s, 3H), 3.21 (s, 3H); ^{13}C NMR (101 MHz, DMSO) δ_C 171.2, 164.6, 158.9, 140.1, 135.6, 131.7, 129.3 (2C), 129.1 (2C), 128.3 (2C), 126.6, 122.1, 114.3 (2C), 55.2, 42.2, 31.0.

***N*-(5-(4-Methoxyphenyl)-1-methyl-1*H*-imidazol-2-yl)-3-phenylpropanamide (2.028)**

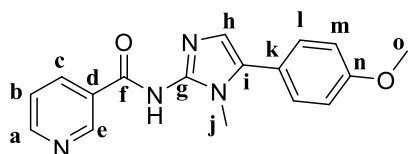


The title compound was prepared from 5-(4-methoxyphenyl)-1-methyl-1*H*-imidazol-2-amine (200 mg, 0.980 mmol) and hydrocinnamic acid (147 mg, 0.980 mmol) according to General Procedure B (282 mg, 84%). HPLC - t_R 5.40 min > 99% purity at 254 nm; LRMS $[M+H]^+$ 335.9 m/z ; HRMS $[M+H]^+$ 336.1707 m/z , found 336.1707 m/z ; 1H NMR (400 MHz, $CDCl_3$) δ_H 7.29 (dt, J = 5.5, 3.1 Hz, 5H), 7.23 – 7.13 (m, 2H), 7.00 – 6.96 (m, 2H), 6.76 (s, 1H), 3.86 (s, 3H), 3.40 (s, 3H), 3.08 – 3.03 (m, 2H (assumed t)), 2.85 – 2.80 (m, 2H); 1H NMR (400 MHz, DMSO) δ_H 10.12 (bs, 1H), 7.38 – 7.12 (m, 7H), 6.99 (d, J = 8.7 Hz, 2H), 6.81 (s, 1H), 3.75 (s, 3H), 3.20 (s, 3H), 2.89 (t, J = 7.2 Hz, 2H), 2.68 – 2.58 (m, 2H); ^{13}C NMR (101 MHz, DMSO) δ_C 172.3, 158.9, 140.9, 140.1, 131.8, 129.3 (2C), 128.3 (2C), 128.3 (2C), 126.0, 123.1, 122.3, 114.3 (2C), 55.2, 36.7, 31.0, 30.7.

N-(5-(4-Methoxyphenyl)-1-methyl-1H-imidazol-2-yl)isonicotinamide (2.029)

The title compound was prepared from 5-(4-methoxyphenyl)-1-methyl-1H-imidazol-2-amine (200 mg, 0.980 mmol) and isonicotinic acid (121 mg, 0.980 mmol) according to General

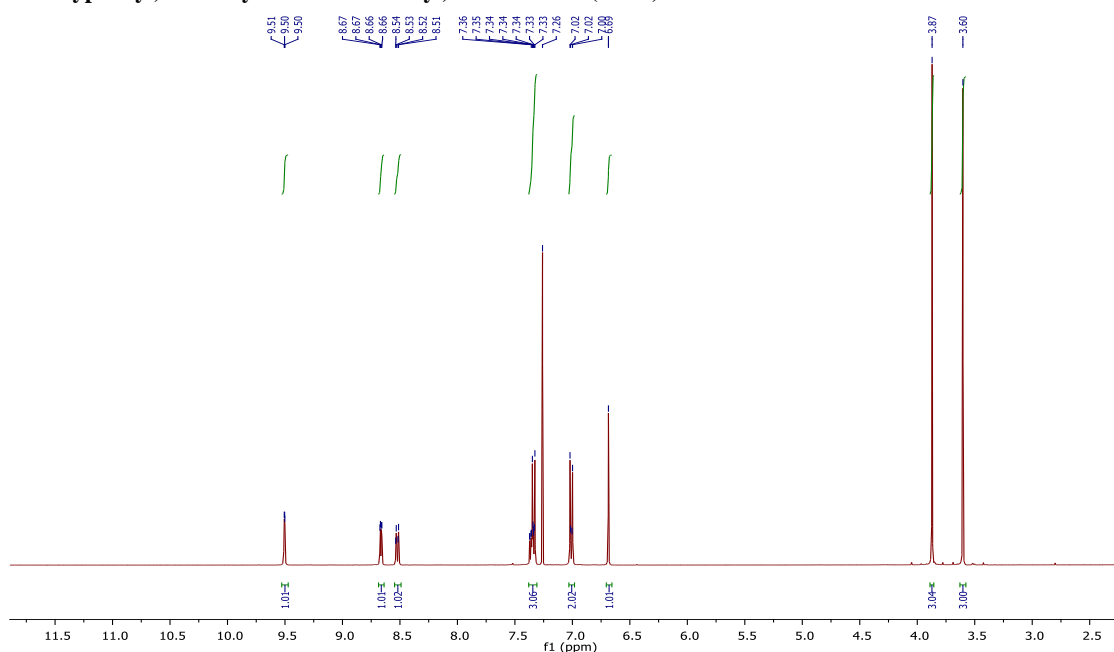
Procedure B (260 mg, 86%). HPLC - t_R 4.62 min > 99% purity at 254 nm; LRMS $[M+H]^+$ 308.9 m/z ; HRMS $[M+H]^+$ 309.1346 m/z , found 309.1348 m/z ; 1H NMR (400 MHz, $CDCl_3$) δ_H 8.64 (d, J = 5.9 Hz, 2H), 8.06 (dd, J = 4.5, 1.5 Hz, 2H), 7.29 – 7.25 (m, 2H), 6.97 – 6.93 (m, 2H), 6.64 (s, 1H), 3.81 (s, 3H), 3.54 (s, 3H); 1H NMR (400 MHz, MeOD) δ_H 8.63 (d, J = 5.9 Hz, 2H), 8.13 (d, J = 5.9 Hz, 2H), 7.49 – 7.39 (m, 2H), 7.12 – 7.02 (m, 2H), 6.93 (s, 1H), 3.86 (s, 3H), 3.61 (s, 3H); ^{13}C NMR (101 MHz, MeOD) δ_C 162.0, 150.3 (2C), 131.6 (2C), 124.2 (2C), 121.5, 115.5 (2C), 55.9, 30.8. Quaternary aromatic carbons not available.

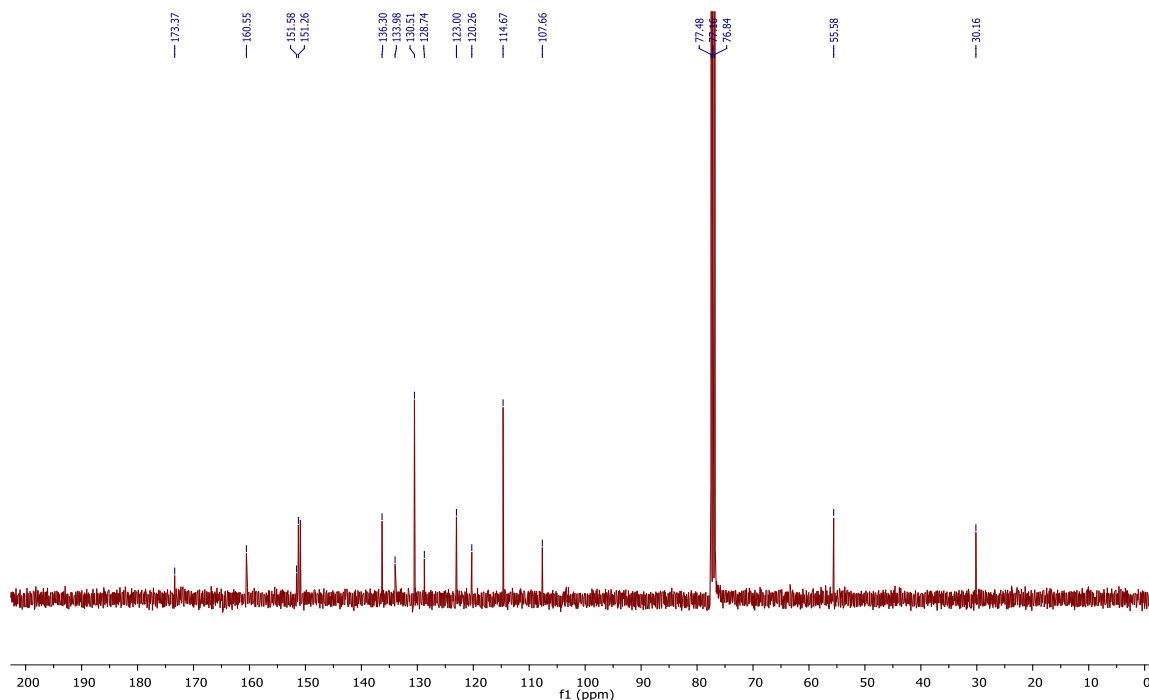
N-(5-(4-Methoxyphenyl)-1-methyl-1H-imidazol-2-yl)nicotinamide (2.030)

The title compound was prepared from 5-(4-methoxyphenyl)-1-methyl-1H-imidazol-2-amine (200 mg, 0.980 mmol) and nicotinic acid (121 mg, 0.980 mmol) according to General Procedure B (290

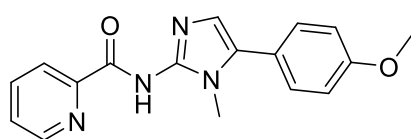
mg, 94%). HPLC - t_R 4.59 min > 99% purity at 254 nm; LRMS $[M+H]^+$ 308.9 m/z ; HRMS $[M+H]^+$ 309.1346 m/z , found 309.1348 m/z ; 1H NMR (400 MHz, $CDCl_3$) δ_H 9.51 – 9.50 (m, 1H, He), 8.67 (dd, J = 4.8, 1.7 Hz, 1H, Ha), 8.52 (dt, J = 7.9, 1.9 Hz, 1H, Hc), 7.38 – 7.32 (m, 3H, Hb, Hl), 7.03 – 6.99 (m, 2H, Hm), 6.69 (s, 1H, Hh), 3.87 (s, 3H, Ho), 3.60 (s, 3H, Hj); ^{13}C NMR (101 MHz, $CDCl_3$) δ_C 173.4 (Cg), 160.6 (Cf), 151.6 (Ci), 151.3 (Ce), 150.9 (Ca), 136.3 (Cc), 134.0 (Cd/Cn), 130.5 (2C, Cl), 128.8 (Cd/Cn), 123.0 (Cb), 120.3 (Ch), 114.7 (2C, Cm), 107.7 (Ck), 55.6 (Co), 30.2 (Cj).

Example spectra for Series 1-2: 1H (400 MHz, $CDCl_3$) and ^{13}C NMR (100 MHz, $CDCl_3$) spectrum of N-(5-(4-Methoxyphenyl)-1-methyl-1H-imidazol-2-yl)nicotinamide (2.030)





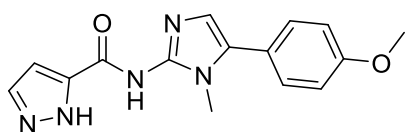
***N*-(5-(4-Methoxyphenyl)-1-methyl-1*H*-imidazol-2-yl)picolinamide (2.031)**



The title compound was prepared from 5-(4-methoxyphenyl)-1-methyl-1*H*-imidazol-2-amine (200 mg, 0.980 mmol) and picolinic (121 mg, 0.980 mmol) according to General Procedure B (157 mg, 52%). HPLC - t_R 4.79 min > 99% purity at 254 nm; LRMS [M+H]

$^+ 308.9 m/z$; HRMS [M+H] $^+ 309.1346 m/z$, found $309.1343 m/z$; 1H NMR (400 MHz, DMSO) δ_H 10.71 (s, 1H), 8.76 (d, $J = 3.3$ Hz, 1H), 8.23 – 8.03 (m, 2H), 7.67 (bs, 1H), 7.43 (d, $J = 8.6$ Hz, 2H), 7.09 – 7.04 (m, 1H), 6.95 (s, 1H), 3.82 (s, 3H), 3.44 (s, 3H); ^{13}C NMR (101 MHz, DMSO) δ_C 159.0, 148.7, 137.9, 129.4 (2C), 127.1, 122.7, 122.1, 114.4 (2C), 55.2, 31.0. Aromatic quaternary carbons not visible

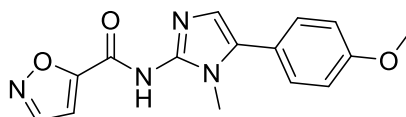
***N*-(5-(4-Methoxyphenyl)-1-methyl-1*H*-imidazol-2-yl)-1*H*-pyrazole-5-carboxamide (2.032)**



The title compound was prepared from 5-(4-methoxyphenyl)-1-methyl-1*H*-imidazol-2-amine (200 mg, 0.980 mmol) and 2*H*-pyrazole-3-carboxylic acid (110 mg, 0.980 mmol) according to

General Procedure B (223 mg, 76%). HPLC - t_R 4.26 min > 99% purity at 254 nm; LRMS [M+H] $^+ 297.9 m/z$; HRMS [M+H] $^+ 298.1299 m/z$, found $298.1296 m/z$; 1H NMR (400 MHz, CDCl₃) δ_H 7.68 (d, $J = 2.0$ Hz, 1H), 7.36 – 7.33 (m, 2H), 7.02 – 6.99 (m, 2H), 6.94 (d, $J = 1.9$ Hz, 1H), 6.90 (s, 1H), 3.87 (s, 3H), 3.58 (s, 3H).

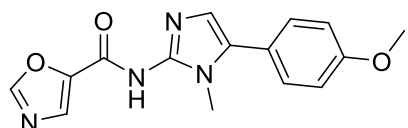
***N*-(5-(4-Methoxyphenyl)-1-methyl-1*H*-imidazol-2-yl)isoxazole-5-carboxamide (2.033)**



The title compound was prepared from 5-(4-methoxyphenyl)-1-methyl-1*H*-imidazol-2-amine (200 mg, 0.980 mmol) and

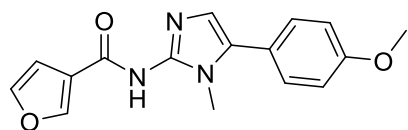
isoxazole-5-carboxylic acid (111 mg, 0.980 mmol) according to General Procedure B (70 mg, 24%). HPLC - t_R 4.73 min > 99% purity at 254 nm; LRMS $[M+H]^+$ 298.9 m/z ; HRMS $[M+H]^+$ 299.1139 m/z , found 299.1138 m/z ; 1H NMR (400 MHz, $CDCl_3$) δ 8.32 (d, J = 1.7 Hz, 1H), 7.35 – 7.32 (m, 2H), 7.08 – 7.01 (m, 3H), 6.82 (s, 1H), 3.88 (s, 3H), 3.62 (s, 3H); ^{13}C NMR (101 MHz, $CDCl_3$) δ_C 160.7, 150.7, 130.6, 129.4, 125.6, 119.8, 114.7 (2C), 108.5, 105.6, 55.6, 30.5. Imidazole quaternary carbons not visible.

***N*-(5-(4-Methoxyphenyl)-1-methyl-1*H*-imidazol-2-yl)oxazole-5-carboxamide (2.034)**



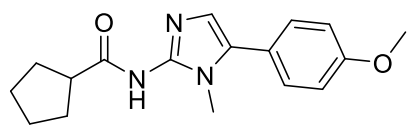
The title compound was prepared from 5-(4-methoxyphenyl)-1-methyl-1*H*-imidazol-2-amine (200 mg, 0.980 mmol) and oxazole-5-carboxylic acid (111 mg, 0.980 mmol) according to General Procedure B (152 mg, 52%). HPLC - t_R 4.33 min > 99% purity at 254 nm; LRMS $[M+H]^+$ 298.9 m/z ; HRMS $[M+H]^+$ 299.1139 m/z , found 299.1139 m/z ; 1H NMR (400 MHz, $CDCl_3$) δ 7.95 (s, 1H), 7.76 (s, 1H), 7.34 – 7.31 (m, 2H), 7.03 – 6.99 (m, 2H), 6.72 (s, 1H), 3.87 (s, 3H), 3.57 (s, 3H); ^{13}C NMR (101 MHz, $CDCl_3$) δ_C 165.5, 160.6, 151.9, 150.9, 150.1, 130.6 (2C), 129.8, 129.0, 120.0, 114.7 (2C), 108.1, 55.6, 30.3.

***N*-(5-(4-Methoxyphenyl)-1-methyl-1*H*-imidazol-2-yl)furan-3-carboxamide (2.035)**



The title compound was prepared from 5-(4-methoxyphenyl)-1-methyl-1*H*-imidazol-2-amine (200 mg, 0.980 mmol) and furan-2-carboxylic acid (110 mg, 0.980 mmol) according to General Procedure B (276 mg, 96%). HPLC - t_R 4.51 min > 99% purity at 254 nm; LRMS $[M+H]^+$ 297.9 m/z ; HRMS $[M+H]^+$ 298.1186 m/z , found 298.1183 m/z ; 1H NMR (400 MHz, $CDCl_3$) δ_H 8.08 (d, J = 0.8 Hz, 1H), 7.40 (t, J = 1.7 Hz, 1H), 7.33 – 7.30 (m, 2H), 7.02 – 6.98 (m, 2H), 6.87 (dd, J = 1.7, 0.5 Hz, 1H), 6.67 (s, 1H), 3.86 (s, 3H), 3.53 (s, 3H); ^{13}C NMR (101 MHz, $CDCl_3$) δ_C 171.0, 160.4, 150.5, 145.9, 143.2, 130.4 (2C), 128.8, 127.3, 120.6, 114.6 (2C), 110.3, 109.0, 55.6, 30.3.

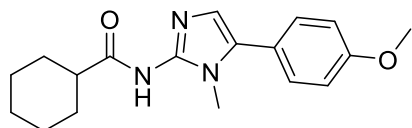
***N*-(5-(4-Methoxyphenyl)-1-methyl-1*H*-imidazol-2-yl)cyclopentanecarboxamide (2.036)**



The title compound was prepared from 5-(4-methoxyphenyl)-1-methyl-1*H*-imidazol-2-amine (200 mg, 0.980 mmol) and cyclopentanecarboxylic acid (0.110 mL, 0.980 mmol) according to General Procedure B (298 mg, 94%). HPLC - t_R 5.00 min > 99% purity at 254 nm; LRMS $[M+H]^+$ 300.0 m/z ; HRMS $[M+H]^+$ 300.1707 m/z , found 300.1704 m/z ; 1H NMR (400 MHz, $CDCl_3$) δ_H 7.33 – 7.29 (m, 2H), 7.00 – 6.95 (m, 2H), 6.81 (s, 1H), 3.85 (s, 3H), 3.47 (s, 3H), 2.01 – 1.58 (m, 9H); 1H NMR (400 MHz, DMSO) δ_H 9.96 (s, 1H), 7.29 (d, J = 8.4 Hz, 2H), 6.95 (d, J = 8.6 Hz, 2H), 6.76 (s, 1H), 3.78 – 3.68 (m, 3H), 3.25 (s, 3H), 2.79 – 2.71 (m, 1H), 1.83 – 1.46 (m, 8H); ^{13}C NMR (101 MHz,

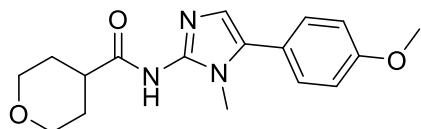
DMSO) δ_c 176.4, 164.8, 159.1, 140.4, 132.0, 129.5 (2C), 122.5, 114.5 (2C), 55.4, 44.3, 31.3, 30.1 (2C), 25.8 (2C).

***N*-(5-(4-Methoxyphenyl)-1-methyl-1*H*-imidazol-2-yl)cyclohexanecarboxamide (2.037)**



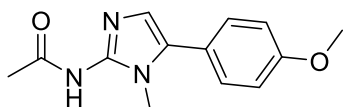
The title compound was prepared from 5-(4-methoxyphenyl)-1-methyl-1*H*-imidazol-2-amine (200 mg, 0.980 mmol) and cyclohexanecarboxylic acid (125 mg, 0.980 mmol) according to General Procedure B (272 mg, 88%). HPLC - t_R 5.39 min > 99% purity at 254 nm; LRMS $[M+H]^+$ 313.9 m/z ; HRMS $[M+H]^+$ 314.1863 m/z , found 314.1861 m/z ; 1H NMR (400 MHz, $CDCl_3$) δ_H 7.34 – 7.27 (m, 2H), 7.01 – 6.96 (m, 2H), 6.81 (s, 1H), 3.86 (s, 3H), 3.49 (s, 3H), 2.49 (tt, J = 11.7, 3.5 Hz, 1H), 2.01 – 1.95 (m, 2H), 1.84 – 1.77 (m, 2H), 1.72 – 1.67 (m, 1H), 1.58 – 1.48 (m, 2H), 1.37 – 1.21 (m, 3H); ^{13}C NMR (101 MHz, $CDCl_3$) δ_c 178.1, 159.7, 142.8, 132.2, 130.1 (2C), 122.2, 120.2, 114.4 (2C), 55.5, 45.6, 29.8 (2C), 25.9, 25.9 (2C). M.p. 200.1-208.4°C.

***N*-(5-(4-Methoxyphenyl)-1-methyl-1*H*-imidazol-2-yl)tetrahydro-2*H*-pyran-4-carboxamide (2.038)**



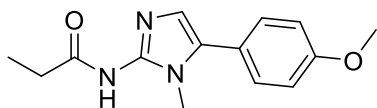
The title compound was prepared from 5-(4-methoxyphenyl)-1-methyl-1*H*-imidazol-2-amine (200 mg, 0.980 mmol) and tetrahydro-2*H*-pyran-4-carboxylic acid (127 mg, 0.980 mmol) according to General Procedure B (289 mg, 93%). HPLC - t_R 4.28 min > 99% purity at 254 nm; LRMS $[M+H]^+$ 315.9 m/z ; HRMS $[M+H]^+$ 316.1656 m/z , found 316.1654 m/z ; 1H NMR (400 MHz, $CDCl_3$) δ_H 7.32 – 7.28 (m, 2H), 7.00 – 6.95 (m, 2H), 6.70 (s, 1H), 4.03 (dt, J = 11.3, 3.4 Hz, 2H), 3.85 (s, 3H), 3.52 – 3.44 (m, 5H), 2.68 – 2.60 (m, 1H), 1.96 – 1.86 (m, 4H); ^{13}C NMR (101 MHz, $CDCl_3$, DEPT) δ_c 159.7, 129.8 (2C), 120.8, 114.1 (2C), 67.2 (2C), 55.1, 43.1, 30.5, 29.4 (2C). Aromatic quaternary carbons not visible.

***N*-(5-(4-Methoxyphenyl)-1-methyl-1*H*-imidazol-2-yl)acetamide (2.039)**



The title compound was prepared from 5-(4-methoxyphenyl)-1-methyl-1*H*-imidazol-2-amine (200 mg, 0.980 mmol) and acetic acid (0.06 mL, 0.980 mmol) according to General Procedure B. The crude material was purified via column chromatography (eluent: $CHCl_3$ 94%, MeOH 5%, NH_4OH 1%) to afford the product (10.5 mg, 4%). HPLC - t_R 3.86 min > 99% purity at 254 nm; LRMS $[M+H]^+$ 245.9 m/z ; HRMS $[M+H]^+$ 246.1237 m/z , found 246.1238 m/z ; 1H NMR (400 MHz, $CDCl_3$) δ_H 7.33 – 7.29 (m, 2H), 6.99 – 6.95 (m, 2H), 6.80 (s, 1H), 3.85 (s, 3H), 3.47 (s, 3H), 2.22 (s, 3H); ^{13}C NMR (101 MHz, $CDCl_3$) δ_c 159.9, 130.2 (2C), 121.8, 114.5 (2C), 55.5, 31.7, 21.0. Aromatic quaternary carbons not available.

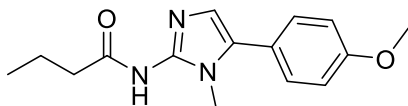
***N*-(5-(4-Methoxyphenyl)-1-methyl-1*H*-imidazol-2-yl)propionamide (2.040)**



The title compound was prepared from 5-(4-methoxyphenyl)-1-methyl-1*H*-imidazol-2-amine (200 mg, 0.980 mmol) and propionic acid (0.07 mL 0.980 mmol) according to General Procedure B. The

crude material was purified via column chromatography (eluent: CHCl₃ 94%, MeOH 5%, NH₄OH 1%) to afford the product (202 mg, 79%). HPLC - *t_R* 4.24 min > 99% purity at 254 nm; LRMS [M+H]⁺ 259.9 *m/z*; HRMS [M+H]⁺ 260.1394 *m/z*, found 260.1391 *m/z*; ¹H NMR (400 MHz, CDCl₃) δ_H 7.33 – 7.29 (m, 2H), 6.99 – 6.94 (m, 2H), 6.81 (s, 1H), 3.84 (s, 3H), 3.46 (s, 3H), 2.49 (q, *J* = 7.6 Hz, 2H), 1.23 (t, *J* = 7.6 Hz, 3H); ¹³C NMR (101 MHz, CDCl₃) δ_C 176.2, 159.7, 142.8, 132.2, 130.1 (2C), 122.3, 120.8, 114.4 (2C), 55.5, 32.0, 29.5, 9.9.

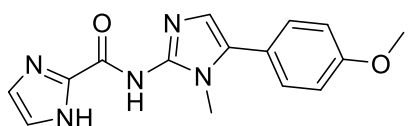
***N*-(5-(4-Methoxyphenyl)-1-methyl-1*H*-imidazol-2-yl)butyramide (2.041)**



The title compound was prepared from 5-(4-methoxyphenyl)-1-methyl-1*H*-imidazol-2-amine (200 mg, 0.980 mmol) and butyric acid (0.09 mL 0.980 mmol) according to General Procedure B.

The crude material was purified via column chromatography (eluent: CHCl₃ 94%, MeOH 5%, NH₄OH 1%) to afford the product (176 mg, 66%). HPLC - *t_R* 4.55 min > 99% purity at 254 nm; LRMS [M+H]⁺ 274.0 *m/z*; HRMS [M+H]⁺ 274.1550 *m/z*, found 274.1547 *m/z*; ¹H NMR (400 MHz, CDCl₃) δ_H 7.23 – 7.19 (m, 2H), 6.91 – 6.87 (m, 2H), 6.76 (s, 1H), 3.75 (s, 3H), 3.38 (s, 3H), 2.36 (t, *J* = 7.3 Hz, 2H), 1.71 – 1.61 (m, 2H), 0.92 (t, *J* = 7.4 Hz, 3H); ¹³C NMR (101 MHz, CDCl₃) δ_C 174.1, 160.0, 141.4, 132.5, 130.2 (2C), 120.9, 114.4 (2C), 110.8, 55.4, 32.8, 21.7, 18.8, 13.7.

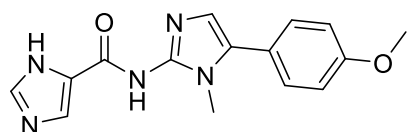
***N*-(5-(4-Methoxyphenyl)-1-methyl-1*H*-imidazol-2-yl)-1*H*-imidazole-2-carboxamide (2.042)**



The title compound was prepared from 5-(4-methoxyphenyl)-1-methyl-1*H*-imidazol-2-amine (200 mg, 0.980 mmol) and 1*H*-imidazole-2-carboxylic acid (110 mg, 0.980 mmol) according to

General Procedure C (45.3 mg, 16%). HPLC - *t_R* 4.50 min > 99% purity at 254 nm; LRMS [M+H]⁺ 297.9 *m/z*; HRMS [M+H]⁺ 298.1299 *m/z*, found 298.1299 *m/z*; ¹H NMR (400 MHz, CDCl₃) δ_H 7.31 – 7.27 (m, 2H), 7.17 (s, 2H), 6.99 – 6.93 (m, 2H), 6.74 (s, 1H), 3.84 (s, 3H), 3.54 (s, 3H); ¹³C NMR (101 MHz, CDCl₃) δ_C 160.3, 130.4 (2C), 129.9, 123.9, 120.5, 114.6 (2C), 55.6, 30.9. Aromatic quaternary carbons not available.

***N*-(5-(4-Methoxyphenyl)-1-methyl-1*H*-imidazol-2-yl)-1*H*-imidazole-5-carboxamide (2.043)**

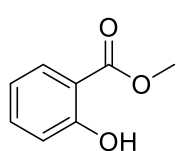


The title compound was prepared from 5-(4-methoxyphenyl)-1-methyl-1*H*-imidazol-2-amine (200 mg, 0.980 mmol) and 1*H*-imidazole-5-carboxylic acid (110 mg, 0.980 mmol) according to

General Procedure C (93.0 mg, 48%). HPLC - *t_R* 4.16 min > 99% purity at 254 nm; LRMS [M+H]⁺

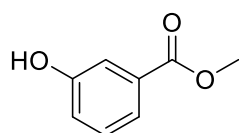
297.9 m/z ; HRMS $[M+H]^+$ 298.1299 m/z , 298.1299 m/z ; 1H NMR (400 MHz, $CDCl_3$) δ_H 7.75 (s, 1H), 7.67 (s, 1H), 7.33 – 7.30 (m, 2H), 7.00 – 6.96 (m, 2H), 6.76 (s, 1H), 3.85 (s, 3H), 3.53 (s, 3H); ^{13}C NMR (101 MHz, $CDCl_3$) δ_C 160.2, 136.0, 130.4 (2C), 130.1, 120.8, 114.6 (2C), 55.5, 30.8. Aromatic quaternary carbons not available.

Methyl 2-methoxybenzoate (2.048a)³⁹



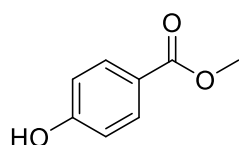
The known title compound was prepared from 2-hydroxybenzoic acid (5.00 g, 36.0 mmol) according to General Procedure D as a clear colourless oil (976 mg, 18%). HPLC - t_R 5.58 min > 99% purity at 254 nm; LRMS $[M+H]^+$ 153.0 m/z ; 1H NMR (400 MHz, $CDCl_3$) δ_H 10.76 (s, 1H), 7.83 (dd, J = 8.0, 1.7 Hz, 1H), 7.49 – 7.42 (m, 1H), 6.98 (dd, J = 8.4, 0.9 Hz, 1H), 6.90 – 6.86 (m, 1H), 3.95 (s, 3H); ^{13}C NMR (101 MHz, $CDCl_3$) δ_C 170.7, 161.7, 135.8, 130.0, 119.3, 117.7, 112.5, 52.4. Acquired data is consistent with the literature.³⁹

Methyl 3-hydroxybenzoate (2.048b)⁴³



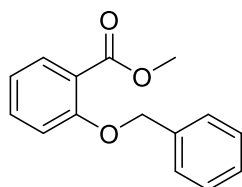
The known title compound was prepared from 3-hydroxybenzoic acid (5.00 g, 36.0 mmol) according to General Procedure D as a white solid (4.96 g, 91%). HPLC - t_R 4.43 min > 99% purity at 254 nm; LRMS $[M+H]^+$ 152.9 m/z ; 1H NMR (400 MHz, $CDCl_3$) δ_H 7.63 – 7.60 (m, 1H), 7.58 – 7.56 (m, 1H), 7.32 (t, J = 7.9 Hz, 1H), 7.08 – 7.04 (m, 1H), 5.49 (s, 1H), 3.92 (s, 3H); ^{13}C NMR (101 MHz, $CDCl_3$) δ_C 167.8, 156.2, 131.3, 129.9, 122.0, 120.6, 116.6, 52.6. Acquired data is consistent with the literature.⁴³

Methyl 4-hydroxybenzoate (2.048c)¹⁰¹



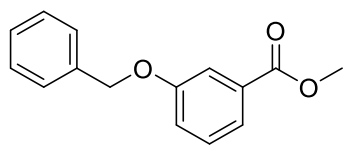
The known title compound was prepared from 4-hydroxybenzoic acid (5.00 g, 36.0 mmol) according to General Procedure D as a white solid (5.17 g, 94%). HPLC - t_R 4.18 min > 99% purity at 254 nm; LRMS $[M-H]^-$ 150.9 m/z ; 1H NMR (400 MHz, $CDCl_3$) δ_H 7.99 – 7.93 (m, 2H), 6.89 – 6.84 (m, 2H), 3.89 (s, 3H); ^{13}C NMR (101 MHz, $CDCl_3$) δ_C 167.5, 160.3, 132.1 (2C), 122.6, 115.4 (2C), 52.2. Acquired data is consistent with the literature.¹⁰¹

Methyl 2-(benzyloxy)benzoate (2.049a)³⁹



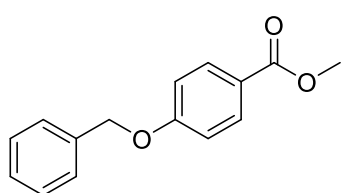
The known title compound was prepared from methyl-2-hydroxybenzoate (976 mg, 6.40 mmol) according to General Procedure E as a clear colourless oil (1.37 g, 88%). HPLC - t_R 6.69 min > 99% purity at 254 nm; LRMS $[M+H]^+$ 241.8 m/z ; 1H NMR (400 MHz, $CDCl_3$) δ_H 7.86 – 7.81 (m, 1H), 7.52 – 7.30 (m, 6H), 7.04 – 6.98 (m, 2H), 5.18 (s, 2H), 3.91 (s, 3H); ^{13}C NMR (101 MHz, $CDCl_3$) δ_C 166.9, 158.2, 136.9, 133.5, 131.9, 128.76 (2C), 127.9, 127.1 (2C), 121.0, 120.7, 114.1, 70.7, 52.1. Acquired data is consistent with the literature.³⁹

Methyl 3-(benzyloxy)benzoate (2.049b)¹⁰²



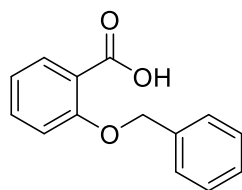
The known title compound was prepared from methyl-3-hydroxybenzoate (4.10 g, 27 mmol) according to General Procedure E as a white solid (5.60 g, 85%). HPLC - t_R 7.11 min > 99% purity at 254 nm; LRMS $[M+H]^+$ 242.9 m/z ; 1H NMR (400 MHz, $CDCl_3$) δ_H 7.68 – 7.63 (m, 2H), 7.47 – 7.30 (m, 6H), 7.19 – 7.15 (m, 1H), 5.11 (s, 2H), 3.92 (s, 3H); ^{13}C NMR (101 MHz, $CDCl_3$) δ_C 166.7, 158.7, 136.6, 131.5, 129.4, 128.5 (2C), 128.0, 127.4 (2C), 122.2, 120.0, 115.1, 70.0, 52.0. Acquired data is consistent with the literature.¹⁰²

Methyl 4-(benzyloxy)benzoate (2.049c)¹⁰³



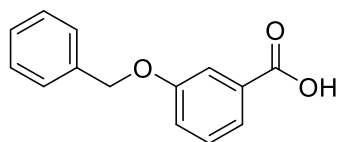
The known title compound was prepared from methyl-4-hydroxybenzoate (5.00 g, 33.0 mmol) according to General Procedure E as a white solid (7.9 g, 99%). HPLC - t_R 7.04 min > 99% purity at 254 nm; LRMS $[M+H]^+$ 242.9 m/z ; 1H NMR (400 MHz, $DMSO-d_6$) δ_H 7.95 – 7.89 (m, 2H), 7.50 – 7.31 (m, 5H), 7.19 – 7.07 (m, 2H), 5.20 (s, 2H), 3.82 (s, 3H); ^{13}C NMR (101 MHz, $DMSO$) δ_C 166.1, 162.4, 136.7, 131.4 (2C), 128.7 (2C), 128.2, 128.0 (2C), 122.3, 115.0 (2C), 69.8, 52.0. Acquired data is consistent with the literature.¹⁰³

2-(Benzyloxy)benzoic acid (2.050a)³⁹



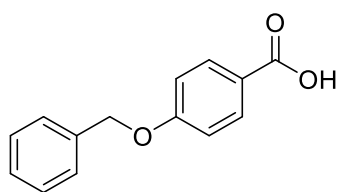
The known title compound was prepared from methyl 2-(benzyloxy)benzoate (1.17 g, 4.80 mmol) according to General Procedure F as a white solid. The product was used directly in the next step without further purification. (1.02 g, 93%). HPLC - t_R 5.76 min > 70 % purity at 254 nm; LRMS $[M+H]^+$ 229.0 m/z ; 1H NMR (400 MHz, $CDCl_3$) δ_H 10.72 (s, 1H), 8.22 (dd, J = 7.8, 1.8 Hz, 1H), 7.58 – 7.52 (m, 1H), 7.48 – 7.36 (m, 5H), 7.19 – 7.10 (m, 2H), 5.30 (s, 2H). Acquired data is consistent with the literature.³⁹

3-(Benzyloxy)benzoic acid (2.050b)¹⁰⁴



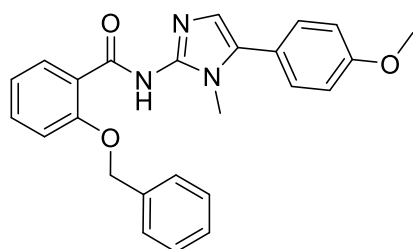
The known title compound was prepared from methyl 3-(benzyloxy)benzoate (5.20 g, 21.0 mmol) according to General Procedure F as a white solid (4.80 g, 99%). HPLC - t_R 6.04 min > 99% purity at 254 nm; LRMS $[M-H]^-$ 227.0 m/z ; 1H NMR (400 MHz, $CDCl_3$) δ_H 7.76 – 7.68 (m, 2H), 7.48 – 7.31 (m, 6H), 7.25 – 7.20 (m, 1H), 5.13 (s, 2H). Acquired data is consistent with the literature.¹⁰⁴

4-(Benzyloxy)benzoic acid (2.050c)¹⁰⁵



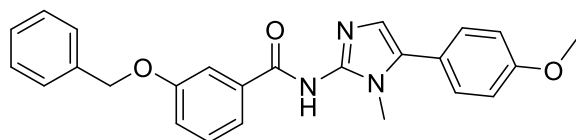
The known title compound was prepared from methyl 4-(benzyloxy)benzoate (6.00 g, 25.0 mmol) according to General Procedure F as a white solid (5.7 g, 99%). HPLC - t_R 6.06 min > 99% purity at 254 nm; LRMS $[M+H]^+$ 228.9 m/z ; 1H NMR (400 MHz, $CDCl_3$) δ_H 7.76 – 7.68 (m, 2H), 7.48 – 7.31 (m, 6H), 7.25 – 7.20 (m, 1H), 5.13 (s, 2H); 1H NMR (400 MHz, DMSO) δ_H 7.59 – 7.54 (m, 2H), 7.16 – 7.00 (m, 5H), 6.76 – 6.72 (m, 2H), 4.85 (s, 2H); ^{13}C NMR (101 MHz, DMSO) δ_C 167.7, 161.5, 136.8, 131.3 (2C), 128.6 (2C), 128.1, 127.9 (2C), 125.3, 114.5 (2C), 69.5. Acquired data is consistent with the literature.¹⁰⁵

2-(Benzyloxy)-*N*-(5-(4-methoxyphenyl)-1-methyl-1*H*-imidazol-2-yl)benzamide (2.051a)



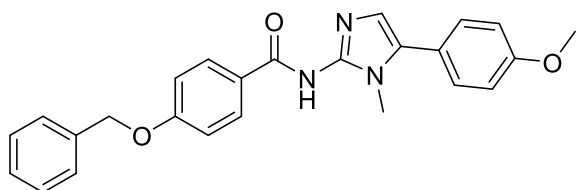
Using 5-(4-methoxyphenyl)-1-methyl-1*H*-imidazol-2-amine (1.00 g, 4.90 mmol) and 2-(benzyloxy)benzoic acid (1.10 g, 4.90 mmol), the title compound was prepared according to General Procedure B (894.9 mg, 44%). HPLC - t_R 6.29 min > 99% purity at 254 nm; LRMS $[M+H]^+$ 413.9 m/z ; 1H NMR (400 MHz, $CDCl_3$) δ_H 7.53 – 7.27 (m, 9H), 7.18 – 7.07 (m, 2H), 7.01 – 6.93 (m, 2H), 6.91 (s, 1H), 5.32 (s, 2H), 3.85 (s, 3H), 3.32 (s, 3H).

3-(Benzyloxy)-*N*-(5-(4-methoxyphenyl)-1-methyl-1*H*-imidazol-2-yl)benzamide (2.051b)



The title compound was prepared from 5-(4-methoxyphenyl)-1-methyl-1*H*-imidazol-2-amine (200 mg, 0.980 mmol) and 3-(benzyloxy)benzoic acid (223 mg, 0.980 mmol) according to General Procedure B as an orange solid (299 mg, 74%). HPLC - t_R 6.15 min > 99% purity at 254 nm; LRMS $[M+H]^+$ 413.9 m/z ; 1H NMR (400 MHz, $CDCl_3$) δ_H 7.98 – 7.89 (m, 2H), 7.50 – 7.44 (m, 2H), 7.42 – 7.29 (m, 7H), 7.03 – 6.89 (m, 2H), 6.68 (s, 1H), 5.15 (s, 2H), 3.87 (s, 3H), 3.58 (s, 3H); ^{13}C NMR (101 MHz, $CDCl_3$) δ_C 174.1, 160.3, 158.8, 150.9, 139.9, 137.3, 130.4 (2C), 129.0, 128.8, 128.7 (2C), 128.0, 127.7 (2C), 121.7, 120.7, 118.1, 114.7, 114.6 (2C), 108.9, 70.2, 55.5, 30.3.

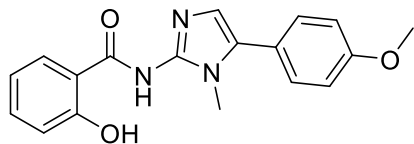
4-(Benzyloxy)-*N*-(5-(4-methoxyphenyl)-1-methyl-1*H*-imidazol-2-yl)benzamide (2.051c)



The title compound was prepared from 5-(4-methoxyphenyl)-1-methyl-1*H*-imidazol-2-amine (1.00 g, 4.90 mmol) and 4-(benzyloxy)benzoic acid (1.10 g, 4.90 mmol) according to General Procedure B as an orange solid (423 mg, 21%). HPLC - t_R 6.29 min > 99% purity at 254 nm; LRMS $[M+H]^+$ 413.9 m/z ; 1H NMR (400 MHz, $CDCl_3$) δ_H 7.95 – 7.88 (m, 2H), 7.48 – 7.29 (m, 9H), 7.02 –

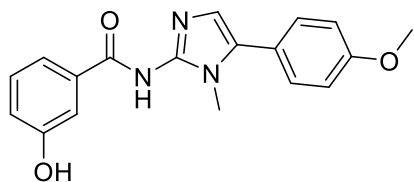
6.97 (m, 2H), 6.68 (s, 1H), 5.15 (s, 2H), 3.86 (s, 3H), 3.58 (s, 3H); ^{13}C NMR (101 MHz, CDCl_3) δ_{C} 160.4, 158.8, 130.7, 130.5 (2C), 130.4, 129.1, 128.7 (2C), 128.7 (2C), 128.0, 127.7 (2C), 127.7, 121.7, 118.1, 114.7 (2C), 114.6 (2C), 114.3, 70.3, 55.6, 30.3.

2-Hydroxy-*N*-(5-(4-methoxyphenyl)-1-methyl-1*H*-imidazol-2-yl)benzamide (2.052)



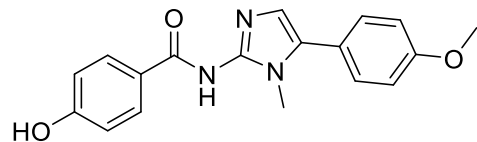
The title compound was prepared from 2-(benzyloxy)-*N*-(5-(4-methoxyphenyl)-1-methyl-1*H*-imidazol-2-yl)benzamide (870 mg, 2.10 mmol) according to General Procedure G (156 mg, 32%). HPLC - t_R 5.22 min > 95% purity at 254 nm; LRMS $[\text{M}+\text{H}]^+$ 323.9 m/z ; HRMS $[\text{M}+\text{H}]^+$ 324.1343 m/z , found 324.1346 m/z ; ^1H NMR (400 MHz, CDCl_3) δ_{H} 8.18 – 8.06 (m, 1H), 7.39 – 7.28 (m, 3H), 7.07 – 6.83 (m, 4H), 6.70 (s, 1H), 3.87 (s, 3H), 3.53 (s, 3H); ^1H NMR (400 MHz, DMSO) δ_{H} 14.21 (s, 1H), 12.43 (s, 1H), 7.95 (dd, J = 8.0, 1.6 Hz, 1H), 7.43 (d, J = 8.5 Hz, 2H), 7.31 – 7.23 (m, 1H), 7.01 (d, J = 8.6 Hz, 2H), 6.94 (s, 1H), 6.82 – 6.73 (m, 2H), 3.76 (s, 3H), 3.43 (s, 3H); ^{13}C NMR (101 MHz, DMSO) δ_{C} 171.7, 164.6, 160.6, 159.7, 147.4, 132.7, 130.3 (2C), 129.8, 128.0, 119.9, 119.8, 117.8, 116.7, 114.4 (2C), 55.3, 30.2.

3-Hydroxy-*N*-(5-(4-methoxyphenyl)-1-methyl-1*H*-imidazol-2-yl)benzamide (2.053)



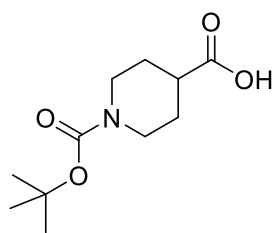
The title compound was prepared from 3-(benzyloxy)-*N*-(5-(4-methoxyphenyl)-1-methyl-1*H*-imidazol-2-yl)benzamide (500 mg, 1.20 mmol) according to General Procedure G (57.4 mg, 15%). HPLC - t_R 4.59 min > 99% purity at 254 nm; LRMS $[\text{M}+\text{H}]^+$ 323.9 m/z ; HRMS $[\text{M}+\text{H}]^+$ 324.1343 m/z , found 324.1343 m/z ; ^1H NMR (400 MHz, CDCl_3) δ_{H} 7.88 – 7.82 (m, 1H), 7.80 – 7.76 (m, 1H), 7.37 – 7.27 (m, 3H), 7.05 – 6.97 (m, 2H), 6.97 – 6.92 (m, 1H), 6.68 (s, 1H), 3.87 (s, 3H), 3.58 (s, 3H); ^{13}C NMR (101 MHz, CDCl_3 , DEPT) δ_{C} 155.7, 130.3, 129.2, 121.2, 120.4, 118.1, 115.5, 114.5, 55.4, 30.3. Aromatic quaternary carbons not visible.

4-Hydroxy-*N*-(5-(4-methoxyphenyl)-1-methyl-1*H*-imidazol-2-yl)benzamide (2.054)



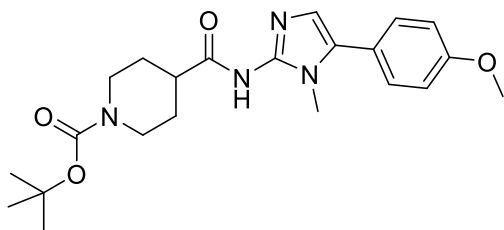
The title compound was prepared from 4-(benzyloxy)-*N*-(5-(4-methoxyphenyl)-1-methyl-1*H*-imidazol-2-yl)benzamide (297 mg, 0.720 mmol) according to General Procedure G (140 mg, 60%). HPLC - t_R 4.58 min > 99% purity at 254 nm; LRMS $[\text{M}+\text{H}]^+$ 323.9 m/z ; HRMS $[\text{M}+\text{H}]^+$ 324.1343 m/z , found 324.1345 m/z ; ^1H NMR (400 MHz, DMSO) δ_{H} 7.93 (d, J = 8.2 Hz, 2H), 7.48 – 7.38 (m, 2H), 7.09 – 7.00 (m, 2H), 6.88 (s, 1H), 6.82 – 6.78 (m, 2H), 3.80 (s, 3H), 3.43 (s, 3H); ^{13}C NMR (101 MHz, DMSO) δ_{C} 159.1, 130.2 (2C), 129.5 (2C), 114.9 (2C), 114.4 (2C), 55.2, 30.6. Imidazole and aromatic quaternary carbons not visible

1-(*tert*-Butoxycarbonyl)piperidine-4-carboxylic acid (2.056)^{46, 106}



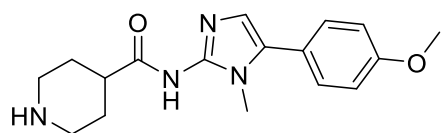
To a solution of piperidine-4-carboxylic acid (2.00 g, 15.5 mmol) in 1,4-dioxane (50 mL) and water (50 mL) di-*t*-butyl dicarbonate (3.40 g, 15.6 mmol) and NaOH (6.20 g, 155 mmol) were added. The mixture was allowed to stir for 12 h then concentrated *in vacuo*, diluted with EtOAc and acidified to pH 3 using HCl (2N). The solution was washed with water and the organic layer was dried over MgSO₄, filtered and concentrated *in vacuo* to afford the known title product as a white solid (2.23 g, 62%). ¹H NMR (400 MHz, MeOD) δ 4.04 – 3.89 (m, 2H), 2.99 – 2.79 (m, 2H), 2.48 (tt, *J* = 11.0, 3.9 Hz, 1H), 1.93 – 1.82 (m, 2H), 1.60 – 1.42 (m, 11H); ¹³C NMR (101 MHz, MeOD) δ_c 178.2, 156.5, 81.1, 44.2, 41.9 (2C), 29.2 (2C), 28.7 (3C). Acquired data is consistent with the literature.^{46, 106}

tert-Butyl-4-((5-(4-methoxyphenyl)-1-methyl-1*H*-imidazol-2-yl)carbamoyl)piperidine-1-carboxylate (2.057)



The title compound was prepared from 5-(4-methoxyphenyl)-1-methyl-1*H*-imidazol-2-amine (300 mg, 1.50 mmol) and 1-(*tert*-butoxycarbonyl)piperidine-4-carboxylic acid (338 mg, 1.47 mmol) according to General Procedure B (438 mg, 72%). HPLC - *t_R* 5.55 min > 99% purity at 254 nm; LRMS [M+H]⁺ 414.9 *m/z*; ¹H NMR (400 MHz, CDCl₃) δ_H 7.33 – 7.26 (m, 2H), 7.04 – 6.93 (m, 2H), 6.71 (s, 1H), 3.86 (s, 3H), 3.48 (s, 3H), 2.87 – 2.81 (m, 2H), 1.98 – 1.87 (m, 2H), 1.78 – 1.64 (m, 2H), 1.49 – 1.39 (m, 11H); ¹³C NMR (101 MHz, CDCl₃) δ_c 160.1, 155.0, 130.3 (2C), 121.2, 114.5 (2C), 79.5, 55.5, 44.4 (2C), 38.8, 31.2 (2C), 29.1, 28.6 (3C). Aromatic quaternary carbons not observed.

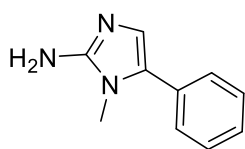
N-(5-(4-Methoxyphenyl)-1-methyl-1*H*-imidazol-2-yl)piperidine-4-carboxamide (2.058)



To 4M HCl in 1,4-dioxane (2 mL) was added *tert*-butyl 4-((5-(4-methoxyphenyl)-1-methyl-1*H*-imidazol-2-yl)carbamoyl)piperidine-1-carboxylate (400 mg, 0.960 mmol) and allowed to stir for 2 h. The reaction mixture was concentrated *in vacuo* then diluted with DCM and neutralized with 1M NaOH. Extracted with DCM, the organic layers were collected and dried over MgSO₄, filtered and concentrated *in vacuo* to afford the title compound without further purification.⁴⁶ HPLC - *t_R* 3.77 min > 97% purity at 254 nm; LRMS [M+H]⁺ 315.0 *m/z*; HRMS [M+H]⁺ 315.1816 *m/z*, found 315.1818 *m/z*; ¹H NMR (400 MHz, DMSO) δ_H 10.08 (bs, 1H), 7.38 (d, *J* = 8.5 Hz, 2H), 7.03 (d, *J* = 8.6 Hz, 2H), 6.85 (s, 1H), 3.91 – 3.76 (m, 3H), 3.74 – 3.42 (m, 4H), 3.22 – 3.00 (m, 2H), 2.01 – 1.77 (m, 2H), 1.74 – 1.50 (m, 2H), 1.50 – 1.13 (m, 2H); ¹H NMR (400 MHz, CDCl₃) δ_H 7.32 – 7.27 (m, 1H), 7.24 – 7.19 (m, 1H), 7.07 – 6.81 (m, 2H), 3.89 – 3.73 (m, 3H), 3.73 – 3.61 (m, 4H), 3.54 – 3.38

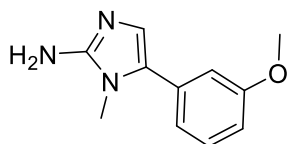
(m, 2H), 1.47 – 1.23 (m, 2H). Some aliphatic peaks eclipsed by water peak; ^{13}C NMR (101 MHz, CDCl_3) δ_{C} 130.4 (2C), 114.7 (2C), 55.8, 44.5 (2C), 39.0, 30.9, 30.1 (2C). Imidazole and quaternary carbons not visible.

1-Methyl-5-phenyl-1H-imidazol-2-amine (2.005b, precursor to 2.059)⁵



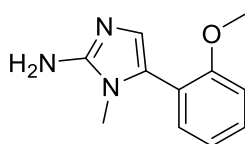
The known title compound was prepared from 2-bromo-1-phenylethan-1-one (716 mg, 3.60 mmol) according to General Procedure A as an orange solid without further purification (332 mg, 72%). HPLC - t_R 3.91 min > 99 % purity at 254 nm; LRMS $[\text{M}+\text{H}]^+$ 174.0 m/z ; ^1H NMR (400 MHz, $\text{DMSO}-d_6$) δ_{H} 7.42 – 7.34 (m, 4H), 7.27 – 7.22 (m, 1H), 6.56 (s, 1H), 5.51 (s, 2H), 3.34 (s, 3H); ^{13}C NMR (101 MHz, $\text{DMSO}-d_6$) δ_{C} 151.9, 131.6, 129.2 (2C), 128.3, 127.1 (2C), 126.5, 123.6, 30.9. Acquired data is consistent with the literature.⁵

5-(3-Methoxyphenyl)-1-methyl-1H-imidazol-2-amine (2.005c, precursor to 2.060)



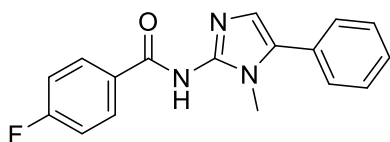
The title compound was prepared from 2-bromo-1-(3-methoxyphenyl)ethan-1-one (824.4 mg, 3.60 mmol) according to General Procedure A as an orange solid without further purification (484 mg, 88%). HPLC - t_R 4.17 min > 99% purity at 254 nm; LRMS $[\text{M}+\text{H}]^+$ 204.0 m/z ; ^1H NMR (400 MHz, CDCl_3) δ_{H} 7.34 – 7.27 (m, 1H), 6.93 – 6.88 (m, 1H), 6.87 – 6.83 (m, 2H), 6.69 (s, 1H), 3.81 (s, 3H), 3.41 (s, 3H); ^{13}C NMR (101 MHz, CDCl_3) δ_{C} 159.9, 149.6, 132.0, 129.9, 122.6, 120.3, 113.7, 112.7, 105.0, 55.4, 30.6.

5-(2-Methoxyphenyl)-1-methyl-1H-imidazol-2-amine (2.005d, precursor to 2.061)



The title compound was prepared from 2-bromo-1-(2-methoxyphenyl)ethan-1-one (824 mg, 3.60 mmol) according to General Procedure A to give the product as an orange solid (482 mg, 87%). The product was used directly in the next step without further purification or characterization. HPLC - t_R 4.35 min > 77% purity at 254 nm; LRMS $[\text{M}+\text{H}]^+$ 204.0 m/z .

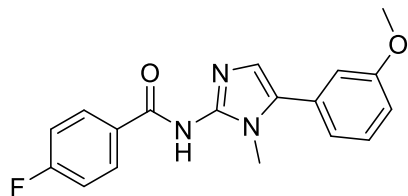
4-Fluoro-N-(1-methyl-5-phenyl-1H-imidazol-2-yl)benzamide (2.059)



The title compound was prepared from 1-methyl-5-phenyl-1H-imidazol-2-amine (220 mg, 1.26 mmol) and 4-fluorobenzoic acid (177 mg, 1.26 mmol) according to General Procedure B (215 mg, 58%). HPLC - t_R 4.88 min > 99% purity at 254 nm; LRMS $[\text{M}+\text{H}]^+$ 295.9 m/z ; HRMS $[\text{M}+\text{H}]^+$ 296.1194 m/z , found 296.1194 m/z ; ^1H NMR (400 MHz, CDCl_3) δ_{H} 8.34 – 8.28 (m, 2H), 7.52 – 7.40 (m, 5H), 7.12 – 7.05 (m, 2H), 6.75 (s, 1H), 3.63 (s, 3H); ^{13}C NMR (101 MHz, CDCl_3) δ_{C} 173.4, 164.8 (d, $J_{\text{C-F}}$ =

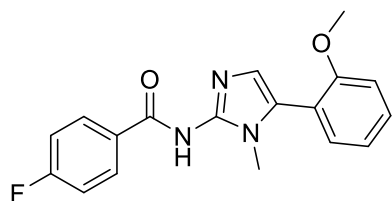
249.8 Hz), 151.1, 134.5 (d, J_{C-F} = 1.7 Hz), 131.1 (d, J_{C-F} = 8.8 Hz, 2C), 129.1 (2C), 129.1, 128.9, 128.8 (2C), 128.4, 114.8 (d, J_{C-F} = 21.5 Hz, 2C), 109.4, 30.4. M.p. 150.5-159.3°C.

4-Fluoro-*N*-(5-(3-methoxyphenyl)-1-methyl-1*H*-imidazol-2-yl)benzamide (2.060)



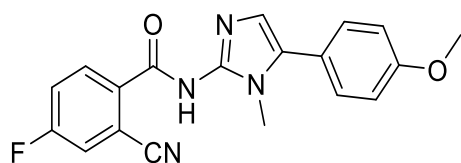
The title compound was prepared from 5-(3-methoxyphenyl)-1-methyl-1*H*-imidazol-2-amine (257 mg, 1.30 mmol) and 4-fluorobenzoic acid (177 mg, 1.30 mmol) according to General Procedure B (78.0 mg, 18%). HPLC - t_R 5.04 min > 99% purity at 254nm; LRMS $[M+H]^+$ 325.9 m/z ; HRMS $[M+H]^+$ 326.1299 m/z , found 326.1299 m/z ; 1H NMR (400 MHz, $CDCl_3$) δ_H 8.33 – 8.27 (m, 2H), 7.39 (t, J = 8.0 Hz, 1H), 7.11 – 7.04 (m, 2H), 7.01 – 6.97 (m, 2H), 6.94 – 6.92 (m, 1H), 6.73 (s, 1H), 3.86 (s, 3H), 3.62 (s, 3H); ^{13}C NMR (101 MHz, $CDCl_3$, DEPT) δ_C 173.9, 164.8 (d, J_{C-F} = 249.8 Hz), 160.1, 151.6, 134.6 (d, J_{C-F} = 2.1 Hz), 131.1 (d, J_{C-F} = 8.8 Hz, 2C), 130.3, 129.7, 128.7, 121.2, 114.8 (d, J = 21.5 Hz), 114.8, 114.4, 108.9, 55.5, 30.4.

4-Fluoro-*N*-(5-(2-methoxyphenyl)-1-methyl-1*H*-imidazol-2-yl)benzamide (2.061)



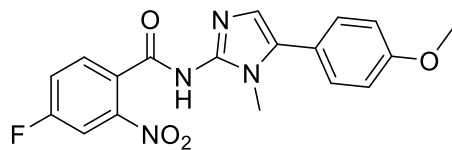
The title compound was prepared from 5-(2-methoxyphenyl)-1-methyl-1*H*-imidazol-2-amine (200 mg, 0.980 mmol) and 4-fluorobenzoic acid (137 mg, 0.980 mmol) according to General Procedure B (56.0 mg, 17%). HPLC - t_R 5.03 min > 99% purity at 254nm; LRMS $[M+H]^+$ 325.9 m/z ; HRMS $[M+H]^+$ 326.1300 m/z , found 326.1299 m/z ; 1H NMR (400 MHz, $CDCl_3$) δ_H 7.78 – 7.52 (m, 3H), 7.34 (bs, 1H), 7.25 – 7.09 (m, 3H), 7.05 – 6.95 (m, 2H), 3.98 (s, 3H), 3.60 (s, 3H); ^{13}C NMR (101 MHz, $CDCl_3$, DEPT) δ_C 170.6, 168.5, 167.4, 164.9, 164.3 (d, J_{C-F} = 251.7 Hz), 144.3, 132.9, 132.8, 131.9 (d, J_{C-F} = 3.5 Hz), 130.2 (d, J_{C-F} = 8.6 Hz), 128.2, 121.6, 116.3 (d, J_{C-F} = 22.0 Hz), 111.9, 56.1, 37.7.

2-Cyano-4-fluoro-*N*-(5-(4-methoxyphenyl)-1-methyl-1*H*-imidazol-2-yl)benzamide 2.062



The title compound was prepared from 5-(4-methoxyphenyl)-1-methyl-1*H*-imidazol-2-amine (200 mg, 1.00 mmol) and 2-cyano-4-fluorobenzoic acid (165 mg, 1.00 mmol) according to General Procedure B as a yellow solid (123 mg, 35%). HPLC - t_R 4.85 min > 95% purity at 254 nm; LRMS $[M+H]^+$ 351.9 m/z ; 1H NMR (400 MHz, $CDCl_3$) δ 8.05 – 7.97 (m, 1H), 7.67 (dd, J = 6.9, 2.2 Hz, 1H), 7.51 (td, J = 8.5, 2.3 Hz, 1H), 7.39 – 7.34 (m, 2H), 7.14 (s, 1H), 7.03 – 6.96 (m, 2H), 3.86 (s, 3H), 3.48 (s, 3H); ^{13}C NMR (101 MHz, $CDCl_3$) δ 166.9 (d, J_{C-F} = 259.0 Hz), 165.4, 165.2, 159.9, 134.7, 134.5 (d, J_{C-F} = 9.7 Hz), 132.9, 130.3 (2C), 127.5 (d, J = 2.8 Hz), 126.8 (d, J_{C-F} = 9.5 Hz), 126.3, 122.2 (d, J_{C-F} = 23.8 Hz), 121.8, 114.3 (2C), 112.0 (d, J_{C-F} = 24.8 Hz), 55.4, 31.2.

4-Fluoro-*N*-(5-(4-methoxyphenyl)-1-methyl-1*H*-imidazol-2-yl)-2-nitrobenzamide **2.063**



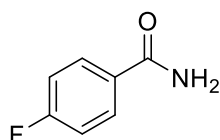
The title compound was prepared from 5-(4-methoxyphenyl)-1-methyl-1*H*-imidazol-2-amine (200 mg, 1.00 mmol) and 4-fluoro-2-nitrobenzoic acid (181 mg, 1.00 mmol) according to

General Procedure B as a yellow solid (116 mg, 32%). HPLC – t_R 4.99 min > 99% purity at 254 nm; LRMS $[M+H]^+$ 370.9 m/z ; HRMS $[M+H]^+$ 371.1150 m/z , found 371.1158 m/z ; 1H NMR (400 MHz, $CDCl_3$) δ_H 8.09 – 8.04 (m, 1H), 7.34 – 7.22 (m, 4H), 7.03 – 6.97 (m, 2H), 6.68 (s, 1H), 3.86 (s, 3H), 3.47 (s, 3H); ^{13}C NMR (101 MHz, $CDCl_3$) δ_C 167.2 (d, J_{C-F} = 694.3 Hz), 161.2, 160.5, 150.6 (d, J_{C-F} = 9.0 Hz), 150.1, 132.6 (d, J_{C-F} = 8.6 Hz), 130.4 (2C), 129.6 (d, J_{C-F} = 3.6 Hz), 128.9, 119.7, 118.2 (d, J_{C-F} = 21.1 Hz), 114.5 (2C), 110.6 (d, J_{C-F} = 26.7 Hz), 108.0, 55.4, 30.0.

Analogue series 3

Example Spectra are included for compounds **2.085**, **2.102**

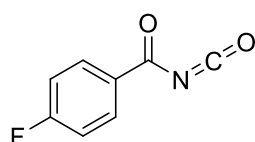
4-Fluorobenzamide (**2.065**)¹⁰⁷



The known title compound was prepared by adding oxalyl chloride (0.60 mL 5.70 mmol) to 4-fluorobenzoic acid (476 mg, 3.40 mmol) in DCM (10 mL) and DMF (0.010 mL). The solution was stirred at room temperature for 1h. The solution was

concentrated *in vacuo* and the acyl chloride intermediate was obtained. At 0°C THF (7 mL) and ammonium hydroxide (1.5 mL) was added and stirred for 1 h. After reaction completion, the solution was concentrated, extracted with DCM and washed with brine. The organic layers were collected, dried over $MgSO_4$, filtered and concentrated to give the desired product as a white solid. (400 mg, 85%).⁵⁷ HPLC – t_R 3.18 min > 99% purity at 254 nm; LRMS $[M+H]^+$ 140.0 m/z ; 1H NMR (400 MHz, MeOD) δ_H 7.98 – 7.89 (m, 2H), 7.24 – 7.14 (m, 2H); 1H NMR (400 MHz, DMSO) δ_H 7.97 (bs, 1H, NH), 7.95 – 7.89 (m, 2H), 7.37 (bs, 1H, NH), 7.29 – 7.18 (m, 2H) NH_2 split due to possible hyperconjugation with carbonyl; ^{13}C NMR (101 MHz, DMSO- d_6) δ_C 166.8, 163.9 (d, J_{C-F} = 248.3 Hz), 130.7, 130.1 (d, J_{C-F} = 9.0 Hz, 2C), 115.1 (d, J_{C-F} = 21.7 Hz, 2C). Acquired data is consistent with the literature.¹⁰⁷

4-Fluorobenzoyl isocyanate (**2.066**)⁵⁷

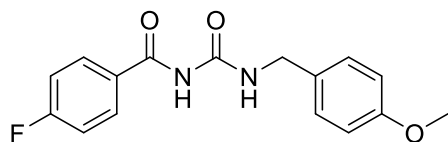


Oxalyl chloride (0.9 mL) was added to a mixture of 4-fluorobenzamide (696 mg, 5.00 mmol) in dichloroethane (3 mL) dropwise in ice bath over 10 min. Solution was left to stir over and heat to room temperature. After the solution became clear, the mixture was heated to 75°C and left to stir over 8 h. The

mixture was concentrated *in vacuo* and purified via column chromatography (eluent: Petroleum spirits 60 %/ EtOAc 40 %) to give the known title compounds as a white solid (677 mg, 82 %).⁵⁷ HPLC – t_R 6.00 min > 95% purity at 254 nm; 1H NMR (400 MHz, $CDCl_3$) δ_H 7.79 – 7.72 (m, 2H), 7.11 – 7.03 (m,

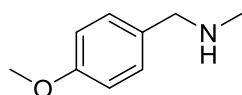
2H); ^1H NMR (400 MHz, DMSO) δ_{H} 8.10 – 8.01 (m, 1H), 7.99 – 7.89 (m, 1H), 7.47 – 7.38 (m, 1H), 7.35 – 7.25 (m, 1H); ^{13}C NMR (101 MHz, DMSO- d_6) δ_{C} 165.7, 165.0 (d, J = 251.8 Hz), 148.9, 131.0 (d, J = 9.6 Hz), 129.1, 116.0 (d, J = 22.2 Hz).

4-Fluoro-*N*-((4-methoxybenzyl)carbamoyl)benzamide (2.067)



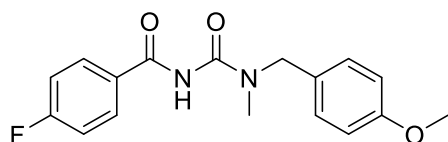
In dry THF (3 mL) was dissolved 4-methoxybenzyl amine (0.10 mL, 1 mmol) then 4-fluorobenzoyl isocyanate (180 mg, 1.00 mmol) was added. The mixture was allowed to stir over 16 h. The crude mixture was concentrated *in vacuo* and was purified via preparative HPLC (gradient: 30-100 %, eluent: ACN/TFA 0.1 %: H₂O/ TFA (0.1 %) and subsequently freeze dried to obtain the desired compound as a white solid (35 mg, 12 %). HPLC – t_{R} 5.984 min > 99 % purity at 254 nm; LRMS $[\text{M}-\text{H}]^-$ 301.0 m/z ; ^1H NMR (400 MHz, DMSO) δ_{H} 10.79 (s, 1H), 9.00 – 8.97 (m, 1H), 8.11 – 8.05 (m, 2H), 7.41 – 7.30 (m, 4H), 6.98 – 6.94 (m, 2H), 4.42 (d, J = 5.9 Hz, 2H), 3.79 (s, 3H); ^1H NMR (400 MHz, CDCl₃) δ_{H} 7.81 – 7.76 (m, 2H), 7.30 – 7.27 (m, 2H), 7.13 – 7.07 (m, 2H), 6.91 – 6.87 (m, 2H), 6.21 (bs, 1H), 4.57 (d, J = 5.5 Hz, 2H), 3.81 (s, 1H). Imide NH not visible, broadened out; ^{13}C NMR (101 MHz, CDCl₃) δ_{C} 167.3, 165.8 (d, J = 254.8 Hz), 159.2, 130.7 (d, J = 9.3 Hz), 130.2, 128.9, 128.7, 128.6, 116.0 (d, J = 22.1 Hz), 114.3, 55.5, 43.5.

1-(4-Methoxyphenyl)-*N*-methylmethanamine (2.069)¹⁰⁸



Methyl amine (0.30 mL, 6.50 mmol) and *p*-methoxybenzaldehyde (0.50 mL, 4.40 mmol) were dissolved in methanol (3 mL) and stirred at room temperature for 30min. Sodium borohydride (800 mg, 2.20 mmol) was added at 0°C and left to stir for 1 h. On reaction completion water was added and the crude mixture was concentrated *in vacuo*. The crude mixture was extracted with DCM and washed with brine. The organic layer was dried over MgSO₄, filtered and concentrated to obtain the known title compound a clear oil (0.50 mL, 88 %).⁵⁹ HPLC – t_{R} 2.82 > 90% purity at 254 nm; ^1H NMR (400 MHz, CDCl₃) δ_{H} 7.25 – 7.22 (m, 2H), 6.89 – 6.84 (m, 2H), 3.80 (s, 3H), 3.69 (s, 2H), 2.44 (s, 3H); ^{13}C NMR (101 MHz, CDCl₃) δ_{C} 158.9 (s), 132.1, 129.6 (2C), 114.0 (2C), 55.5, 55.4, 35.9. Acquired data is consistent with the literature.¹⁰⁸

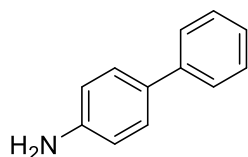
4-Fluoro-*N*-((4-methoxybenzyl)(methyl)carbamoyl)benzamide (2.070)



In a sealed tube was added 4-fluorobenzoyl isocyanate (200 mg, 1.20 mmol) to a solution of 4-methoxybenzyl amine (0.2 mL, 1 mmol), Et₃N (0.20 mL, 1.50 mmol) and DMAP (15.0 mg, 0.10 eq) in dichloroethane (3 mL). The mixture was heated to 80°C and left to stir for 12 h. The crude mixture was concentrated *in vacuo* and was purified via preparative HPLC (gradient: 5-100 %, eluent: ACN/TFA 0.1 %: H₂O/ TFA (0.1 %) and subsequently freeze dried to obtain the desired compound as a white solid (20.0 mg, 5 %). HPLC – t_{R} 5.464 min >

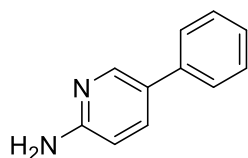
99 % purity at 254 nm; LRMS $[M-H]^-$ 314.9 m/z ; HRMS $[M+H]^+$ 317.1260 m/z , found 317.1296 m/z ; 1H NMR (400 MHz, $CDCl_3$) δ_H 7.86 (bs, 2H), 7.25 – 7.20 (m, 2H), 7.14 – 7.06 (m, 2H), 6.92 – 6.84 (m, 2H), 4.55 (s, 2H), 3.81 (s, 3H), 2.97 (s, 3H); ^{13}C NMR (101 MHz, $CDCl_3$) δ_C 165.6 (d, J_{C-F} = 254.1 Hz), 160.6, 159.4, 131.5 (2C), 129.9 (d, J_{C-F} = 9.0 Hz, 2C), 129.2, 122.4, 115.9 (dd, J_{C-F} = 22.0, 6.6 Hz, 2C), 114.6 (2C), 114.4, 55.4, 52.1., 31.6.

[1,1'-Biphenyl]-4-amine (2.073a)⁶³



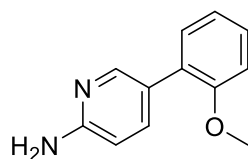
The known title compound was prepared from 4-bromoaniline (396 mg, 2.00 mmol) and phenylboronic acid (365 mg, 3.00 mmol) according to General Procedure A (299 mg, 59%) . HPLC – t_R 4.28 min > 99% purity at 254 nm; LRMS $[M+H]^+$ 170.0 m/z ; 1H NMR (400 MHz, $CDCl_3$) δ_H 7.48 – 7.44 (m, 2H), 7.36 – 7.29 (m, 4H), 7.21 – 7.15 (m, 1H), 6.70 – 6.65 (m, 2H), 3.63 (bs, 2H); ^{13}C NMR (101 MHz, $CDCl_3$) δ_C 146.0, 141.3, 131.8, 128.8 (2C), 128.1 (2C), 126.5 (2C), 126.4, 115.5 (2C). Acquired data is consistent with the literature.⁶³

5-Phenylpyridin-2-amine (2.073b)¹⁰⁹



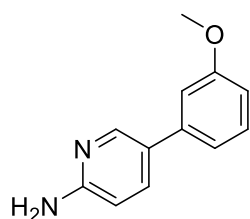
The known title compound was prepared from 2-amino-5-bromopyridine (398 mg, 2.00 mmol) and phenylboronic acid (362 mg, 3.00 mmol) according to General Procedure A (294 mg, 75%). HPLC – t_R 3.94 min > 99% purity at 254 nm; LRMS $[M+H]^+$ 171.0 m/z ; 1H NMR (400 MHz, $CDCl_3$) δ_H 8.32 (d, J = 2.1 Hz, 1H), 7.69 (dd, J = 8.5, 2.4 Hz, 1H), 7.52 – 7.49 (m, 2H), 7.45 – 7.40 (m, 2H), 7.34 – 7.29 (m, 1H), 6.60 (dd, J = 8.5, 0.5 Hz, 1H), 4.51 (bs, 2H); ^{13}C NMR (101 MHz, $CDCl_3$) δ_C 157.6, 146.1, 138.3, 136.9, 129.1 (2C), 127.6, 127.1, 126.4 (2C), 108.8. Acquired data is consistent with the literature.¹⁰⁹

5-(2-Methoxyphenyl)pyridin-2-amine (2.073c)¹¹⁰



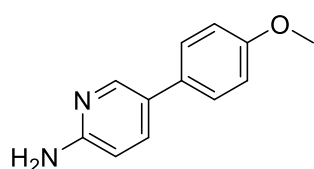
The title compound was prepared from 5-bromopyridin-2-amine (396 mg, 2.00 mmol) and 2-methoxyphenylboronic acid (454 mg, 3.00 mmol) according to General Procedure A to afford the crude product. The mixture was purified using column chromatography (eluent: MeOH 2% in DCM) to afford the known title product (301 mg, 65%). HPLC – t_R 4.19 min > 99% purity at 254 nm; LRMS $[M+H]^+$ 200.9 m/z ; 1H NMR (400 MHz, $CDCl_3$) δ_H 8.23 (dd, J = 2.3, 0.6 Hz, 1H), 7.69 – 7.66 (m, 1H), 7.33 – 7.26 (m, 2H), 7.04 – 6.96 (m, 2H), 6.56 (dd, J = 8.5, 0.7 Hz, 1H), 3.81 (s, 3H); ^{13}C NMR (101 MHz, $CDCl_3$) δ_C 157.1, 156.7, 147.8, 139.4, 130.3, 128.7, 127.6, 124.8, 121.1, 111.4, 108.1, 55.7. Acquired data is consistent with the literature.¹¹⁰

5-(3-Methoxyphenyl)pyridin-2-amine (2.073d)¹¹⁰



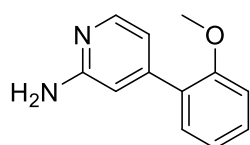
The known title compound was prepared from 5-bromopyridin-2-amine (396 mg, 2.00 mmol) and 3-methoxyphenylboronic acid (454 mg, 3.00 mmol) according to General Procedure A (322 mg, 70%). HPLC – t_R 4.16 min > 99% purity at 254 nm; LRMS $[M+H]^+$ 200.9 m/z ; 1H NMR (400 MHz, $CDCl_3$) δ_H 8.31 (dd, J = 2.4, 0.5 Hz, 1H), 7.68 – 7.64 (m, 2H), 7.34 (t, J = 7.9 Hz, 1H), 7.04 – 7.02 (m, 1H), 6.86 (ddd, J = 8.3, 2.5, 0.7 Hz, 1H), 6.57 (dd, J = 8.5, 0.7 Hz, 1H), 4.55 (bs, 2H), 3.85 (s, 3H); ^{13}C NMR (101 MHz, $CDCl_3$) δ_C 160.2, 157.8, 146.4, 139.9, 136.8, 130.1, 127.4, 118.9, 112.4, 112.3, 108.6, 55.4. Acquired data is consistent with the literature.¹¹⁰

5-(4-Methoxyphenyl)pyridin-2-amine (2.073e)¹¹¹



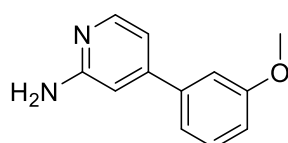
The known title compound was prepared from 5-bromopyridin-2-amine (396 mg, 2.00 mmol) and 4-methoxyphenylboronic acid (454 mg, 3.00 mmol) according to General Procedure A (382 mg, 83%). HPLC – t_R 4.12 min > 99% purity at 254 nm; LRMS $[M+H]^+$ 201.0 m/z ; 1H NMR (400 MHz, $CDCl_3$) δ_H 8.27 (d, J = 1.9 Hz, 1H), 7.65 – 7.61 (m, 1H), 7.44 – 7.40 (m, 2H), 6.98 – 6.94 (m, 2H), 6.57 (dd, J = 8.5, 0.6 Hz, 1H), 4.49 (bs, 2H), 3.84 (s, 3H); ^{13}C NMR (101 MHz, $CDCl_3$) δ_C 159.1, 157.2, 145.9, 136.5, 131.0, 127.5 (2C), 127.4, 114.5 (2C), 108.7, 55.5. Acquired data is consistent with the literature.¹¹¹

4-(2-Methoxyphenyl)pyridin-2-amine (2.073f)¹¹⁰



The title compound was prepared from 4-bromopyridin-2-amine (795mg, 4.60 mmol) and 2-methoxyphenylboronic acid (909 mg, 6.00 mmol) according to General Procedure A to afford the crude product. The mixture was purified using column chromatography (eluent: EtOAc 40% in Petroleum Spirits) to afford the known title product (614 mg, 66 %). HPLC – t_R 4.17 min > 96% purity at 254 nm; LRMS $[M+H]^+$ 201.0 m/z ; 1H NMR (400 MHz, $CDCl_3$) δ_H 8.06 (d, J = 5.3 Hz, 1H), 7.37 – 7.28 (m, 2H), 7.03 – 6.96 (m, 2H), 6.82 (dd, J = 5.4, 1.4 Hz, 1H), 6.67 (s, 1H), 3.80 (s, 3H); ^{13}C NMR (101 MHz, $CDCl_3$) δ_C 158.5, 156.6, 148.4, 147.4, 130.4, 129.9, 121.0, 115.5, 111.5, 109.3, 55.7. Acquired data is consistent with the literature.¹¹⁰

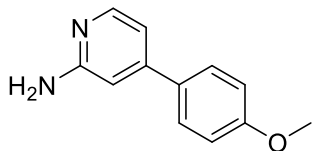
4-(3-Methoxyphenyl)pyridin-2-amine (2.073g)^{110, 112}



The title compound was prepared from 4-bromopyridin-2-amine (795mg, 4.60 mmol) and 3-methoxyphenylboronic acid (909 mg, 6.00 mmol) according to General Procedure A to afford the crude product. The mixture was purified using column chromatography (eluent: EtOAc 40% in Petroleum Spirits) to afford the known title product (835 mg, 90 %). HPLC – t_R 4.21 min > 99% purity at 254 nm; LRMS $[M+H]^+$ 201.0

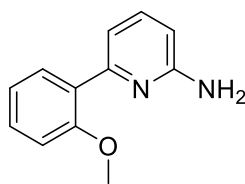
m/z ; ^1H NMR (400 MHz, CDCl_3) δ_{H} 8.10 (d, $J = 5.3$ Hz, 1H), 7.70 – 7.64 (m, 1H), 7.48 – 7.43 (m, 1H), 7.36 (t, $J = 8.0$ Hz, 1H), 7.11 – 7.09 (m, 1H), 6.87 (dd, $J = 5.4, 1.5$ Hz, 1H), 6.70 – 6.68 (m, $J = 1.4, 0.6$ Hz, 1H), 4.56 (bs, 2H), 3.86 (s, 3H); ^{13}C NMR (101 MHz, CDCl_3) δ_{C} 160.2, 159.0, 150.5, 148.5, 140.4, 130.1, 119.5, 114.3, 113.0, 112.8, 106.6, 55.5. Acquired data is consistent with the literature.^{110, 112}

4-(4-Methoxyphenyl)pyridin-2-amine (2.073h)¹¹²



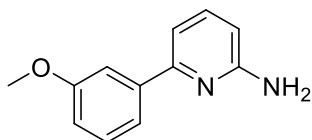
The title compound was prepared from 4-bromopyridin-2-amine (795mg, 4.60 mmol) and 4-methoxyphenylboronic acid (909 mg, 6.00 mmol) according to General Procedure A to afford the crude product. The mixture was purified using column chromatography (eluent: EtOAc 40% in Petroleum Spirits) to afford the known title product (346 mg, 37 %). HPLC – t_R 4.20 min > 95% purity at 254 nm; LRMS $[\text{M}+\text{H}]^+$ 200.9 m/z ; ^1H NMR (400 MHz, CDCl_3) δ_{H} 8.04 (dd, $J = 5.6, 0.6$ Hz, 1H), 7.58 – 7.52 (m, 2H), 7.01 – 6.96 (m, 2H), 6.88 (dd, $J = 5.6, 1.6$ Hz, 1H), 6.72 – 6.70 (m, 1H), 4.83 (s, 2H), 3.86 (s, 3H); ^{13}C NMR (101 MHz, CDCl_3) δ_{C} 160.7, 158.4, 150.9, 146.6, 130.7, 128.3 (2C), 114.6 (2C), 112.5, 106.2, 55.6. Acquired data is consistent with the literature.¹¹²

6-(2-Methoxyphenyl)pyridin-2-amine (2.073i)¹¹⁰



The title compound was prepared from 6-bromopyridin-2-amine (795mg, 4.60 mmol) and 2-methoxyphenylboronic acid (909 mg, 6.00 mmol) according to General Procedure A to afford the crude product. The mixture was purified using column chromatography (eluent: EtOAc 40% in Petroleum Spirits) to afford the known title product as an orange solid (920 mg, 99 %). HPLC – t_R 4.10 min > 99% purity at 254 nm; LRMS $[\text{M}+\text{H}]^+$ 201.0 m/z ; ^1H NMR (400 MHz, CDCl_3) δ_{H} 7.54 – 7.45 (m, 3H), 7.34 (t, $J = 7.9$ Hz, 1H), 7.07 (dd, $J = 7.5, 0.6$ Hz, 1H), 6.93 (ddd, $J = 8.2, 2.6, 0.9$ Hz, 1H), 6.43 (dd, $J = 8.1, 0.6$ Hz, 1H), 4.63 (s, 2H), 3.86 (s, 3H); ^{13}C NMR (101 MHz, CDCl_3) δ_{C} 160.0, 158.4, 155.9, 141.3, 138.4, 129.6, 119.4, 114.6, 112.2, 111.1, 107.4, 55.4. Acquired data is consistent with the literature.¹¹⁰

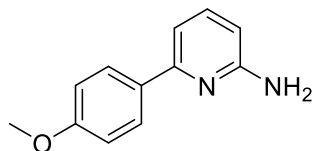
6-(3-Methoxyphenyl)pyridin-2-amine (2.073j)¹¹²



The title compound was prepared from 6-bromopyridin-2-amine (796mg, 4.60 mmol) and 3-methoxyphenylboronic acid (909 mg, 6.00 mmol) according to General Procedure A to afford the crude product. The mixture was purified using column chromatography (eluent: EtOAc 40% in Petroleum Spirits) to afford the known title product as an orange solid (920 mg, 99 %). HPLC – t_R 4.11 min > 90% purity at 254 nm; LRMS $[\text{M}+\text{H}]^+$ 201.0 m/z ; ^1H NMR (400 MHz, CDCl_3) δ_{H} 7.68 (dd, $J = 7.6, 1.8$ Hz, 1H), 7.49 – 7.43 (m, 1H), 7.36 – 7.31 (m, 1H), 7.13 (dd, $J = 7.5, 0.7$ Hz, 1H), 7.07 – 7.02 (m, 1H), 6.97 (dd, $J = 8.3, 0.7$ Hz, 1H), 6.43 (dd, $J = 8.1, 0.7$ Hz, 1H), 4.52 (bs, 2H), 3.84 (s, 3H); ^{13}C

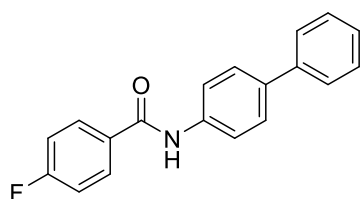
NMR (101 MHz, CDCl₃) δ_C 158.2, 157.1, 154.6, 137.6, 131.0, 129.6, 129.6, 121.0, 115.5, 111.6, 106.9, 55.8. Acquired data is consistent with the literature.¹¹²

6-(4-Methoxyphenyl)pyridin-2-amine (2.073k)¹¹²



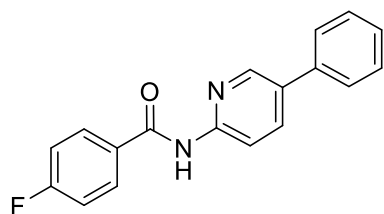
The title compound was prepared from 6-bromopyridin-2-amine (795mg, 4.60 mmol) and 4-methoxyphenylboronic acid (909 mg, 6.00 mmol) according to General Procedure A to afford the crude product. The mixture was purified using column chromatography (eluent: EtOAc 40% in Petroleum Spirits) to afford the known title product as an orange solid (920 mg, 99 %). HPLC – t_R 4.10min > 90% purity at 254 nm; LRMS $[M+H]^+$ 201.0 m/z ; ¹H NMR (400 MHz, CDCl₃) δ_H 7.91 – 7.86 (m, 2H), 7.45 (t, J = 7.8 Hz, 1H), 7.02 (d, J = 7.4 Hz, 1H), 6.99 – 6.94 (m, 2H), 6.41 – 6.36 (m, 1H), 4.60 (bs, 2H), 3.84 (s, 3H); ¹³C NMR (101 MHz, CDCl₃) δ_C 160.3, 158.3, 155.7, 138.5, 132.3, 128.2 (2C), 114.0 (2C), 110.3, 106.6, 55.3. Acquired data is consistent with the literature.¹¹²

N-([1,1'-Biphenyl]-4-yl)-4-fluorobenzamide (2.074)



The title compound was prepared from [1,1'-biphenyl]-4-amine (96.0 mg, 0.560 mmol) and 4-fluorobenzoic acid (78.0 mg, 0.560 mmol) according to General Procedure B (115mg, 71%). HPLC – t_R 6.94 min > 95% purity at 254 nm; LRMS $[M+H]^+$ 291.9 m/z ; HRMS $[M+H]^+$ 292.1132 m/z , found 2932.1136 m/z ; ¹H NMR (400 MHz, CDCl₃) δ_H 7.95 – 7.88 (m, 2H), 7.78 (bs, 1H), 7.73 – 7.69 (m, 2H), 7.64 – 7.57 (m, 4H), 7.47 – 7.41 (m, 2H), 7.37 – 7.31 (m, 1H), 7.22 – 7.15 (m, 2H); ¹H NMR (400 MHz, DMSO) δ_H 10.36 (s, 1H, NH), 8.09 – 8.04 (m, 2H), 7.90 – 7.84 (m, 2H), 7.71 – 7.66 (m, 4H), 7.49 – 7.44 (m, 2H), 7.42 – 7.32 (m, 3H); ¹³C NMR (101 MHz, DMSO) δ_C 164.4, 164.1 (d, J_{C-F} = 249.2 Hz), 139.7, 138.6, 135.3, 131.3 (d, J_{C-F} = 2.9 Hz), 130.4 (d, 2C, J_{C-F} = 9.0 Hz), 128.9 (2C), 127.1, 126.8 (2C), 126.3 (2C), 120.7 (2C), 115.3 (d, 2C, J_{C-F} = 21.8 Hz).

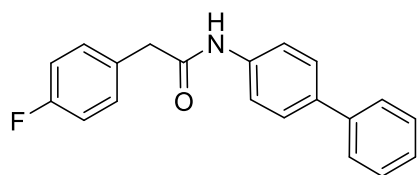
4-Fluoro-*N*-(5-phenylpyridin-2-yl)benzamide (2.075)



The title compound was prepared from 5-phenylpyridin-2-amine (167 mg, 1.00 mmol) and 4-fluorobenzoic acid (137 mmol, 1.00 mmol) according to General Procedure B (106 mg, 37%). HPLC – t_R 5.75 min > 95% purity at 254 nm; LRMS $[M+H]^+$ 292.9 m/z ; HRMS $[M+H]^+$ 293.1085 m/z , found 293.1086 m/z ; ¹H NMR (400 MHz, DMSO) δ_H 10.95 (s, 1H), 8.74 – 8.70 (m, 1H), 8.29 – 8.25 (m, 1H), 8.18 – 8.10 (m, 3H), 7.77 – 7.72 (m, 2H), 7.53 – 7.46 (m, 2H), 7.43 – 7.31 (m, 3H); ¹H NMR (400 MHz, CDCl₃) δ_H 8.49 – 8.43 (m, 2H), 8.05 – 7.92 (m, 3H), 7.58 – 7.53 (m, 2H), 7.50 – 7.44 (m, 2H), 7.21 – 7.14 (m, 2H), 7.09 – 7.02 (m, 1H); ¹³C NMR (101 MHz, CDCl₃) δ_C 165.4 (d, J_{C-F} = 201.5, 52.0 Hz), 164.8, 150.7, 146.0, 137.4,

137.2, 135.1, 130.6 (d, $J_{\text{C-F}} = 2.8$ Hz), 129.9 (d, 2C, $J_{\text{C-F}} = 9.1$ Hz), 129.2 (2C), 128.1, 126.9 (2C), 116.1 (d, 2C, $J_{\text{C-F}} = 22.0$ Hz), 114.1.

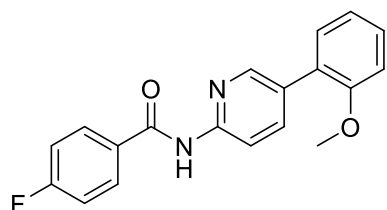
***N*-([1,1'-Biphenyl]-4-yl)-2-(4-fluorophenyl)acetamide (2.076)**



The title compound was prepared from [1,1'-biphenyl]-4-amine (167 mg, 1.00 mmol) and 4-fluorophenyl acetic acid (137, 1.00 mmol) according to General Procedure B (142 mg, 52%). HPLC – t_{R} 6.85 min > 99% purity at 254 nm; LRMS $[\text{M}+\text{H}]^+$ 305.9 m/z ;

HRMS $[\text{M}+\text{H}]^+$ 306.1289 m/z , found 306.1290 m/z ; ^1H NMR (400 MHz, CDCl_3) δ_{H} 7.57 – 7.48 (m, 5H), 7.46 – 7.38 (m, 2H), 7.36 – 7.29 (m, 3H), 7.14 – 7.06 (m, 3H), 3.74 (s, 2H); ^{13}C NMR (101 MHz, CDCl_3) δ_{C} 168.9, 140.5, 137.7, 136.9, 131.3 (d, $J_{\text{C-F}} = 8.1$ Hz, 2C), 130.3 (d, $J_{\text{C-F}} = 3.3$ Hz), 128.9 (2C), 127.7 (2C), 127.3, 127.0 (2C), 120.3, 116.3 (d, $J_{\text{C-F}} = 21.5$ Hz, 2C), 44.1. Quaternary C-F not visible.

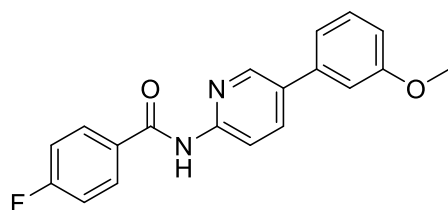
4-Fluoro-*N*-(5-(2-methoxyphenyl)pyridin-2-yl)benzamide (2.077)



The title compound was prepared from 5-(2-methoxyphenyl)pyridin-2-amine (197 mg, 1.00 mmol) and 4-fluorobenzoic acid (137 mg, 1.00 mmol) according to General Procedure B to afford the desired product (90 mg, 29 %). HPLC –

t_{R} 5.68 min > 95% purity at 254 nm; LRMS $[\text{M}+\text{H}]^+$ 322.8 m/z ; HRMS $[\text{M}+\text{H}]^+$ 323.1190 m/z , found 323.1182 m/z ; ^1H NMR (400 MHz, CDCl_3) δ_{H} 8.81 (s, 1H, NH), 8.48 – 8.40 (m, 2H, Hf), 8.01 – 7.96 (m, 3H), 7.40 – 7.30 (m, 2H, Hl), 7.22 – 7.17 (m, 2H), 7.09 – 6.99 (m, 2H, Hm), 3.84 (s, 3H); ^{13}C NMR (101 MHz, CDCl_3) δ_{C} 165.4 (d, $J_{\text{C-F}} = 253.5$ Hz), 164.7, 156.8, 150.0, 147.8, 139.9, 130.9, 130.6, 130.5, 129.9 (d, $J_{\text{C-F}} = 9.1$ Hz), 129.6, 126.6, 121.3, 116.1 (d, $J_{\text{C-F}} = 22.1$ Hz), 113.6, 111.5, 55.7.

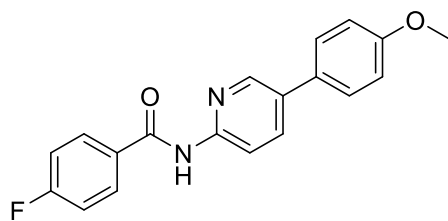
4-Fluoro-*N*-(5-(3-methoxyphenyl)pyridin-2-yl)benzamide (2.078)



The title compound was prepared from 5-(3-methoxyphenyl)pyridin-2-amine (300 mg, 1.50 mmol) and 4-fluorobenzoic acid (136 mg, 1.00 mmol) according to General Procedure B to afford the desired product (321 mg, 97%).

HPLC – t_{R} 5.89 min > 95% purity at 254 nm; LRMS $[\text{M}+\text{H}]^+$ 322.9 m/z ; HRMS $[\text{M}+\text{H}]^+$ 323.1190 m/z , found 323.1193 m/z ; ^1H NMR (400 MHz, DMSO) δ_{H} 10.97 (s, 1H), 8.74 (dd, $J = 2.5, 0.7$ Hz, 1H), 8.29 – 8.26 (m, 1H), 8.20 – 8.12 (m, 3H), 7.44 – 7.28 (m, 6H), 3.85 (s, 3H); ^{13}C NMR (101 MHz, DMSO) δ_{C} 164.9, 164.3 (d, $J_{\text{C-F}} = 249.6$ Hz), 159.9, 151.5, 145.8, 138.2, 136.2, 131.4, 130.8 (d, $J_{\text{C-F}} = 9.2$ Hz), 130.5 (d, $J_{\text{C-F}} = 2.9$ Hz), 130.1, 118.7, 115.3 (d, $J_{\text{C-F}} = 21.9$ Hz), 114.4, 113.4, 111.9, 55.2.

4-Fluoro-*N*-(5-(*p*-tolyl)pyridin-2-yl)benzamide (2.079)

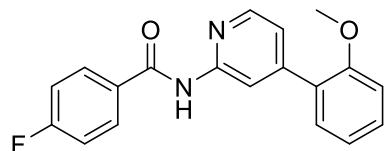


The title compound was prepared from 5-(4-methoxyphenyl)pyridin-2-amine (394 mg, 1.96 mmol) and 4-fluorobenzoic acid (274 mg, 1.96 mmol) according to General Procedure B to afford the desired product (179 mg, 28 %).

HPLC – t_R 5.68 min > 95% purity at 254 nm; LRMS $[M+H]^+$

322.9 m/z ; HRMS $[M+H]^+$ 323.1190 m/z , found 323.1197 m/z ; 1H NMR (400 MHz, $CDCl_3$) δ_H 8.97 (s, 1H), 8.47 – 8.38 (m, 2H), 8.02 – 7.95 (m, 2H), 7.52 – 7.46 (m, 2H), 7.20 – 7.15 (m, 2H), 7.03 – 6.97 (m, 2H), 3.86 (s, 3H); ^{13}C NMR (101 MHz, $CDCl_3$) δ_C 165.3 (d, J_{C-F} = 253.4 Hz), 164.7, 159.8, 150.2, 145.4, 136.8, 133.1, 130.6 (d, J_{C-F} = 3.1 Hz), 129.9 (d, J_{C-F} = 9.1 Hz, 2C), 129.8, 128.0 (2C), 116.1 (d, J_{C-F} = 22.0 Hz, 2C), 114.7 (2C), 114.3, 55.5. M.p. 148.8-153.7 °C.

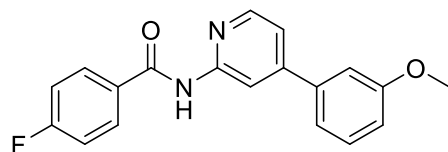
4-Fluoro-*N*-(4-(2-methoxyphenyl)pyridin-2-yl)benzamide (2.080)



The title compound was prepared from 4-(2-methoxyphenyl)pyridin-2-amine (360 mg, 1.80 mmol) and 4-fluorobenzoic acid (252 mg, 1.80 mmol) according to General

Procedure B to afford the desired product as a white solid (218 mg, 38 %). HPLC – t_R 5.45 min > 99% purity at 254 nm; LRMS $[M+H]^+$ 322.9 m/z ; HRMS $[M+H]^+$ 323.1190 m/z , found 323.1192 m/z ; 1H NMR (400 MHz, $CDCl_3$) δ_H 9.85 (s, 1H, NH), 8.51 (d, J = 1.1 Hz, 1H), 8.07 – 7.96 (m, 1H), 7.95 – 7.86 (m, 2H), 7.34 – 7.22 (m, 2H), 7.17 – 7.13 (m, 1H), 7.05 – 6.97 (m, 2H), 6.95 – 6.85 (m, 2H), 3.72 (s, 3H); ^{13}C NMR (101 MHz, $CDCl_3$) δ_C 165.5, 165.4 (d, J_{C-F} = 252.8 Hz), 157.0, 152.2, 149.9, 146.9, 132.8 (d, J_{C-F} = 9.3 Hz), 131.0, 130.7, 130.4 (d, J_{C-F} = 9.1 Hz), 128.0, 121.4, 121.4, 116.1 (d, J_{C-F} = 21.9 Hz), 115.7, 111.8, 56.0. M.p. 111.0-120.0 °C.

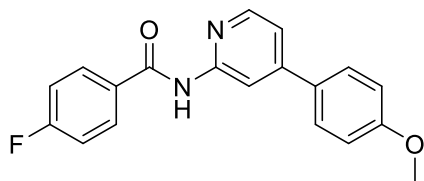
4-Fluoro-*N*-(4-(3-methoxyphenyl)pyridin-2-yl)benzamide (2.081)



The title compound was prepared from 4-(3-methoxyphenyl)pyridin-2-amine (400 mg, 2.00 mmol) and 4-fluorobenzoic acid (278 mg, 2.00 mmol) according to General

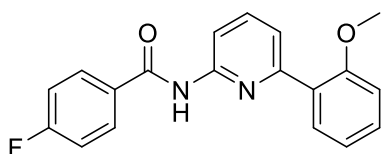
Procedure B to afford the desired product as a white solid (285 mg, 44 %). HPLC – t_R 5.49 min > 99% purity at 254 nm; LRMS $[M+H]^+$ 322.8 m/z ; HRMS $[M+H]^+$ 323.1190 m/z , found 323.119 m/z ; 1H NMR (400 MHz, $CDCl_3$) δ_H 9.56 (bs, 1H, NH), 8.57 (d, J = 1.1 Hz, 1H), 7.97 (d, J = 5.2 Hz, 1H), 7.90 – 7.84 (m, 2H), 7.27 (t, J = 7.9 Hz, 1H), 7.19 – 7.09 (m, 3H), 7.04 – 6.99 (m, 2H), 6.89 – 6.83 (m, 1H), 3.75 (s, 3H); ^{13}C NMR (101 MHz, $CDCl_3$) δ_C 165.2, 165.2 (d, J = 253.2 Hz), 160.2, 152.5, 151.1, 148.0, 139.6, 130.7, 130.1 (d, J_{C-F} = 3.1 Hz), 130.0 (d, J_{C-F} = 9.1 Hz, 2C), 119.7, 118.2, 115.9 (d, J_{C-F} = 22.0 Hz, 2C), 114.8, 112.9, 112.5, 55.4.

4-Fluoro-*N*-(4-(4-methoxyphenyl)pyridin-2-yl)benzamide (2.082)



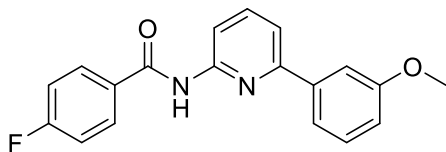
The title compound was prepared from 4-(3-methoxyphenyl)pyridin-2-amine (150 mg, 0.70 mmol) and 4-fluorobenzoic acid (104 mg, 0.70 mmol) according to General Procedure B to afford the desired product as a white solid (95 mg, 40 %). HPLC – t_R 5.43 min > 99% purity at 254 nm; LRMS $[M+H]^+$ 322.9 m/z ; HRMS $[M+H]^+$ 323.1190 m/z , found 323.1193 m/z ; 1H NMR (400 MHz, $CDCl_3$) δ 9.66 (s, 1H), 8.70 (d, J = 1.0 Hz, 1H), 8.24 (d, J = 5.1 Hz, 1H), 8.09 – 8.03 (m, 2H), 7.74 – 7.67 (m, 2H), 7.30 (dd, J = 5.3, 1.5 Hz, 1H), 7.23 – 7.13 (m, 2H), 7.04 – 6.99 (m, 2H), 3.87 (s, 3H); ^{13}C NMR (101 MHz, $CDCl_3$) δ_C 165.4 (d, J_{C-F} = 253.2 Hz), 165.2, 161.0, 152.3, 151.3, 147.2, 132.6, 130.2 (d, J_{C-F} = 9.1 Hz, 2C), 128.6 (2C), 117.7, 116.0 (d, J_{C-F} = 22.0 Hz, 2C), 114.7 (2C), 112.0, 55.6.

4-Fluoro-*N*-(6-(2-methoxyphenyl)pyridin-2-yl)benzamide (2.083)



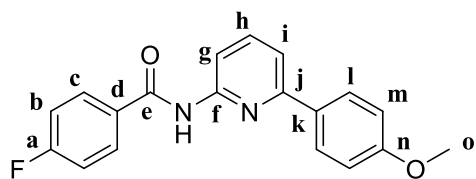
The title compound was prepared from 6-(2-methoxyphenyl)pyridin-2-amine (657 mg, 3.30 mmol) and 4-fluorobenzoic acid (460 mg, 3.30 mmol) according to General Procedure B to afford the desired product as a white solid (580 mg, 55 %). HPLC – t_R 5.72 min > 99% purity at 254 nm; LRMS $[M+H]^+$ 322.9 m/z ; HRMS $[M+H]^+$ 323.1190 m/z , found 323.1192 m/z ; 1H NMR (400 MHz, $CDCl_3$) δ_H 9.78 (s, 1H, NH), 8.20 (dd, J = 8.2, 0.7 Hz, 1H), 7.68 – 7.55 (m, 3H), 7.47 – 7.34 (m, 2H), 7.20 – 7.11 (m, 1H), 6.86 – 6.66 (m, 4H), 3.57 (s, 3H); ^{13}C NMR (101 MHz, $CDCl_3$) δ_C 165.2, 164.9 (d, J_{C-F} = 252.2 Hz), 156.9, 154.6, 151.6, 138.4, 130.9, 130.5 (d, J_{C-F} = 3.0 Hz), 130.2, 129.8 (d, J_{C-F} = 9.1 Hz, 2C), 128.0, 121.3, 120.7, 115.4 (d, J_{C-F} = 21.9 Hz, 2C), 112.5, 111.2, 55.2.

4-Fluoro-*N*-(6-(3-methoxyphenyl)pyridin-2-yl)benzamide (2.084)



The title compound was prepared from 6-(3-methoxyphenyl)pyridin-2-amine (494 mg, 2.50 mmol) and 4-fluorobenzoic acid (346 mg, 2.50 mmol) according to General Procedure B to afford the desired product as a white solid (141 mg, 18 %). HPLC – t_R 5.99 min > 96% purity at 254 nm; LRMS $[M+H]^+$ 322.9 m/z ; HRMS $[M+H]^+$ 323.1190 m/z , found 323.119 m/z ; 1H NMR (400 MHz, $CDCl_3$) δ_H 8.94 (s, 1H), 8.30 (dd, J = 8.2, 0.4 Hz, 1H), 7.91 – 7.85 (m, 1H), 7.81 (t, J = 8.0 Hz, 1H), 7.53 – 7.47 (m, 2H), 7.38 – 7.25 (m, 2H), 7.13 – 7.01 (m, 3H), 6.95 (ddd, J = 8.2, 2.6, 0.9 Hz, 1H), 3.82 (s, 3H); ^{13}C NMR (101 MHz, $CDCl_3$) δ_C 165.2 (d, J_{C-F} = 253.1 Hz), 164.9, 160.2, 155.9, 151.4, 139.4, 130.6 (d, J_{C-F} = 3.1 Hz), 129.9, 129.8 (d, J_{C-F} = 9.1 Hz), 129.7, 119.3, 117.0, 115.9 (d, J_{C-F} = 22.0 Hz), 115.2, 112.8, 112.3, 55.4.

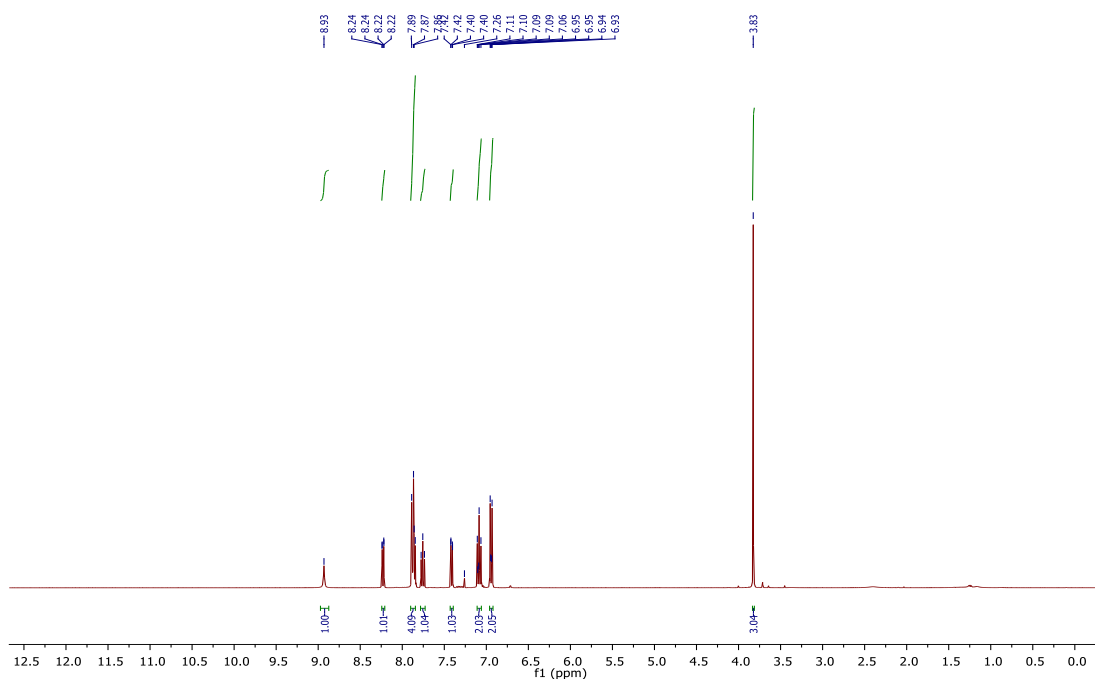
4-Fluoro-*N*-(6-(4-methoxyphenyl)pyridin-2-yl)benzamide (2.085)

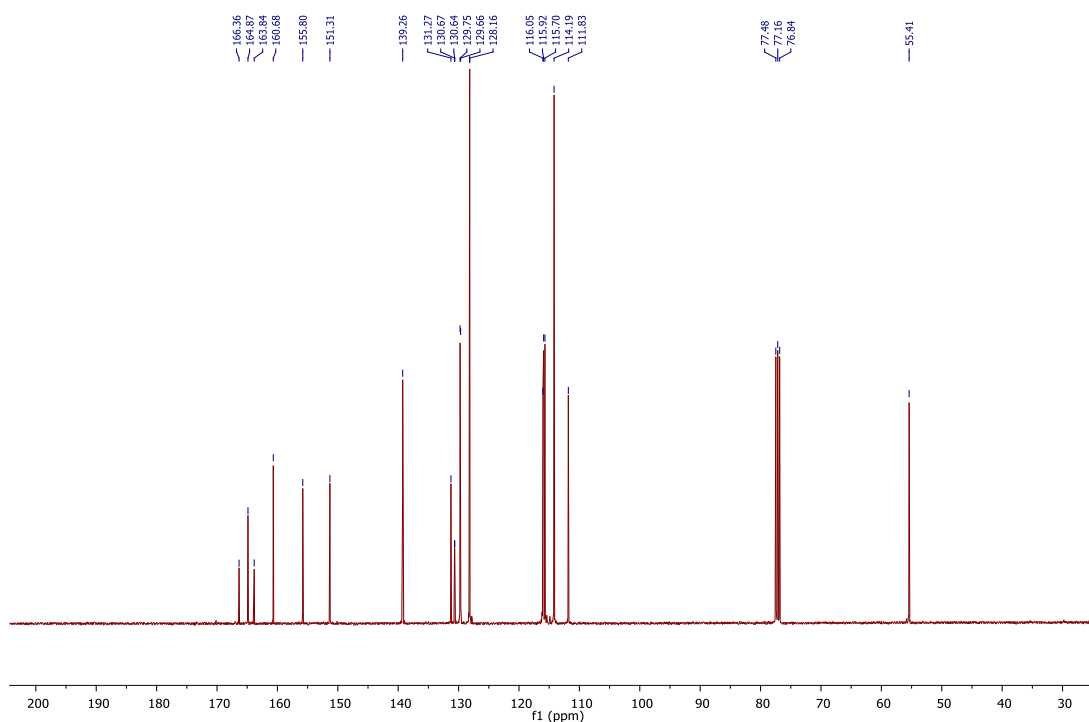


The title compound was prepared from 6-(4-methoxyphenyl)pyridin-2-amine (700 mg, 3.50 mmol) and 4-fluorobenzoic acid (490 mg, 3.50 mmol) according to General Procedure B to afford the desired product as a white

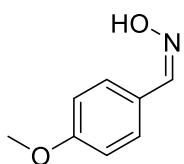
solid (700 mg, 62 %). HPLC – t_R 6.25 min > 99% purity at 254 nm; LRMS $[M+H]^+$ 322.9 m/z ; HRMS $[M+H]^+$ 323.1190 m/z , found 323.1191 m/z ; 1H NMR (400 MHz, $CDCl_3$) δ_H 8.93 (s, 1H, NH), 8.23 (dd, J = 8.2, 0.5 Hz, 1H, Hg), 7.90 – 7.84 (m, 4H, Hc,Hi), 7.76 (t, J = 8.0 Hz, 1H, Hh), 7.41 (dd, J = 7.7, 0.6 Hz, 1H, Hi), 7.11 – 7.06 (m, 2H, Hb), 6.97 – 6.92 (m, 2H, Hm), 3.83 (s, 3H, Ho); ^{13}C NMR (101 MHz, $CDCl_3$) δ_C 165.1 (d, J = 252.9 Hz, Ca), 164.9 (Ce), 160.7 (Cj), 155.9 (Cf), 151.3 (Cn), 139.3 (Ch), 131.3 (Ck), 130.7 (d, J_{C-F} = 3.1 Hz, Cd), 129.7 (d, J_{C-F} = 9.1 Hz, 2C, Cc), 128.2 (2C, Cl), 116.1 (Cg), 115.8 (d, J_{C-F} = 22.0 Hz, 2C, Cb), 114.2 (2C, Cm), 111.8 (Ci), 55.4 (Co).

Example spectra for Series 3 (pyridine core): 1H (400 MHz, $CDCl_3$) and ^{13}C NMR (100 MHz, $CDCl_3$) spectrum of 4-Fluoro-*N*-(6-(4-methoxyphenyl)pyridin-2-yl)benzamide (2.085)





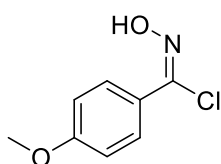
4-Methoxybenzaldehyde oxime (2.087)^{113, 114}



Hydroxylamine solution (1.80 mL) was added to 4-methoxybenzaldehyde (6 mL) in EtOH. The mixture stirred at room temperature for 12 h. On reaction completion the solution was concentration *in vacuo*, diluted with DCM and washed with brine.

^{64, 65}The organic layers were collected, dried with MgSO₄, filtered and concentrated to obtain the known title compound as yellow crystals (5.60 g, 74 %).^{64, 65} HPLC – *t_R* 4.33 min > 90% purity at 254 nm; LRMS [M+H]⁺ 152.0 *m/z*; ¹H NMR (400 MHz, DMSO) δ_H 10.94 (s, 1H), 8.05 (s, 1H), 7.53 – 7.49 (m, 2H), 6.98 – 6.93 (m, 2H), 3.76 (s, 3H); ¹³C NMR (101 MHz, DMSO) δ_C 160.1, 147.6, 127.8 (2C), 125.6, 114.2 (2C), 55.2. Acquired data is consistent with the literature.^{113, 114}

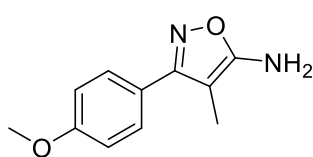
N-Hydroxy-4-methoxybenzimidoyl chloride (2.088)⁶⁵



N-Chlorosuccinimide (4.00 g, 30.0 mmol) was added to 4-methoxybenzaldehyde oxime (30.0 mmol) dissolved in DMF. The solution was heated to 40°C for 20 min to accelerate the reaction. The reaction stirred at room temperature for 12 h.

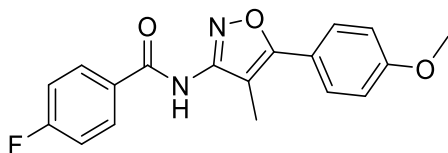
On reaction completion, ice water was added and extracted with ether. The organic layers were collected, dried over MgSO₄ and concentrated *in vacuo* to obtain the known desired compound as a clear oil (4.00 mL, 88 %).⁶⁴ Due to slow decomposition at room temperature, the compound was not further purified and was stored at 0°C until direct use in the next step. LRMS [M+H]⁺ 185.9 *m/z*.

3-(4-Methoxyphenyl)-4-methylisoxazol-5-amine (2.089)⁶⁶



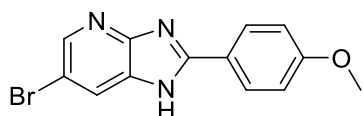
To a solution of propionitrile (0.50 mL, 7.70 mmol) in THF (15 mL) at -78°C, *tert* butyl lithium was added. The solution was stirred for 20 mins. *N*-hydroxy-4-methoxybenzimidoyl chloride (0.3 mL, 1.90 mmol) was added slowly over 10min in THF (2 mL) then stirred for 30 min. Ammonium chloride was added to the solution, diluted with EtOAc and washed with brine. The organic layers were collected, dried over MgSO₄, filtered and concentrated to give the known title compound as a white solid (170 mg, 44 %).⁶⁶ HPLC – *t_R* 4.85 min > 99% purity at 254 nm; LRMS [M+H]⁺ 205.0 *m/z*; ¹H NMR (400 MHz, DMSO) δ_H 7.55 – 7.51 (m, 2H), 7.05 – 7.01 (m, 2H), 6.42 (s, 2H), 3.81 (s, 3H), 1.87 (s, 3H); ¹H NMR (400 MHz, CDCl₃) δ_H 7.60 – 7.55 (m, 2H), 7.00 – 6.95 (m, 2H), 3.85 (s, 3H), 1.94 (s, 3H); ¹³C NMR (101 MHz, CDCl₃) δ_C 165.2, 163.1, 160.3, 129.3 (2C), 122.9, 114.2 (2C), 87.3, 55.5, 7.5. Acquired data is consistent with the literature.⁶⁶

4-Fluoro-*N*-(5-(4-methoxyphenyl)-4-methylisoxazol-3-yl)benzamide (2.090)



Oxalyl chloride (0.3 mL) was added to 4-fluorobenzoic acid (317 mg, 2.30 mmol) in DCM/DMF (10 mL/ 0.01 mL). The solution stirred for 2 h until the solution became clear and was subsequently concentrated *in vacuo*. The benzyl chloride was dissolved in THF (1 mL) and was added to a solution of 3-(4-methoxyphenyl)-4-methylisoxazol-5-amine (100 mg, 0.50 mmol), Et₃N (0.1 mL) in THF (3 mL) at 0°C. The solution was heated to room temperature and stirred for 16 h. Upon reaction completion the mixture was concentrated, diluted with EtOAc and washed with citric acid/ water then ammonia/water. The organic layers were collected, dried, filtered and concentrated. The mixture was further purified via column chromatography (eluent: Petroleum spirits, 60%/ EtOAc, 40%). The title product was obtained as a yellow solid (210 mg, 75 %). HPLC – *t_R* 6.19 min > 95% purity at 254 nm; LRMS [M+H]⁺ 326.9 *m/z*; HRMS [M+H]⁺ 327.1139 *m/z*, found 327.1139 *m/z*; ¹H NMR (400 MHz, CDCl₃) δ_H 8.02 (s, 1H), 7.96 – 7.92 (m, 2H), 7.65 – 7.60 (m, 2H), 7.23 – 7.17 (m, 2H), 7.03 – 6.98 (m, 2H), 3.87 (s, 3H), 2.11 (s, 3H); ¹³C NMR (101 MHz, CDCl₃) δ_C 166.7, 164.5, 164.5, 164.0, 159.5 (d, *J*_{C-F} = 269.5 Hz), 130.6 (d, *J*_{C-F} = 9.2 Hz, 2C), 129.4 (2C), 129.1 (d, *J*_{C-F} = 3.1 Hz), 121.8, 115.9 (d, *J*_{C-F} = 22.0 Hz, 2C), 114.3 (2C), 102.9, 55.4, 8.8.

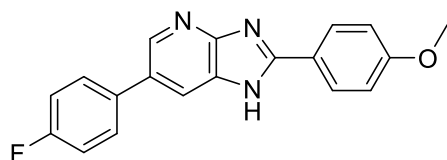
6-Bromo-2-(4-methoxyphenyl)-1*H*-imidazo[4,5-*b*]pyridine (2.093)⁶⁷



In order to obtain the title compound, 2,3-diamino-5-bromopyridine (500 mg, 2.70 mmol) 4-methoxybenzaldehyde (0.3 mL, 2.70 mmol) and sodium bisulfate (505 mg, 2.70 mmol) were dissolved in DMF (3 mL) and heated to reflux for 6 h. On reaction completion the solution was concentrated *in vacuo* and recrystallized from EtOH to obtain the known desired compound as a brown solid (550 mg, 68 %).⁶⁷

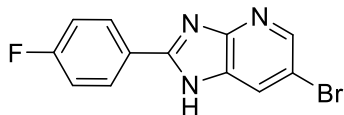
HPLC – t_R 4.69 > 99% purity at 254 nm; LRMS $[M+H]^+$ 305.8 m/z ; 1H NMR (400 MHz, MeOD) δ_H 8.45 – 8.38 (m, 1H), 8.14 – 8.08 (m, 2H), 7.95 – 7.85 (m, 1H), 7.18 – 7.08 (m, 2H), 3.91 (s, 3H); 1H NMR (400 MHz, DMSO) δ_H 13.59 (s, 1H), 8.44 – 8.06 (m, 4H), 7.17 – 7.08 (m, 2H), 3.84 (s, 3H); ^{13}C NMR (101 MHz, DMSO) δ_C 161.4, 154.2, 148.3, 143.2, 137.2, 128.6 (2C), 127.8, 121.6, 114.5 (2C), 112.7, 55.4. Acquired data is consistent with the literature.⁶⁷

6-(4-Fluorophenyl)-2-(4-methoxyphenyl)-1H-imidazo[4,5-b]pyridine (2.094)



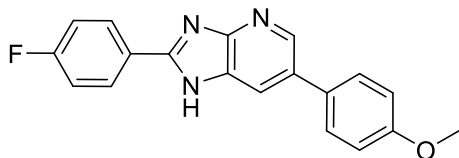
The title compound was prepared from 4-fluorophenylboronic acid (228 mg, 1.60 mmol) and 6-bromo-2-(4-methoxyphenyl)-1H-imidazo[4,5-b]pyridine (380 mg, 1.30 mmol) according to General Procedure A to afford the crude product. The mixture was purified using column chromatography (eluent: EtOAc 40% in Petroleum Spirits) to afford the title product as an orange solid (50 mg, 13 %). HPLC – t_R 5.19 min > 95% purity at 254 nm; LRMS $[M+H]^+$ 319.9 m/z ; HRMS $[M+H]^+$ 320.1194 m/z , found 320.1195 m/z ; 1H NMR (400 MHz, MeOD) δ_H 8.58 (bs, 2H), 8.16 – 8.12 (m, 2H), 7.76 – 7.71 (m, 2H), 7.29 – 7.24 (m, 2H), 7.17 – 7.13 (m, 2H), 3.92 (s, 3H); 1H NMR (400 MHz, DMSO) δ 13.34 (bs, 1H), 8.58 (d, $J = 2.1$ Hz, 1H), 8.23 – 8.19 (m, 2H), 8.16 (bs, 1H), 7.83 – 7.78 (m, 2H), 7.37 – 7.30 (m, 2H), 7.17 – 7.12 (m, 2H), 3.86 (s, 3H). assumed NH peak too broad/flattened out at 13.34 ppm; ^{13}C NMR (101 MHz, DMSO) δ_C 138.3, 129.0 (d, $J_{C-F} = 8.1$ Hz), 128.4, 122.2, 115.8 (d, $J_{C-F} = 21.4$ Hz), 114.5, 55.4. Quaternary carbons not visible.

6-Bromo-2-(4-fluorophenyl)-1H-imidazo[4,5-b]pyridine (2.096)⁶⁷



In order to obtain the title compound, 2,3-diamino-5-bromopyridine (500 mg, 2.70 mmol) 4-fluorobenzaldehyde (0.3 mL, 2.70 mmol) and sodium bisulfate (505 mg, 2.70 mmol) were dissolved in DMF (3 mL) and heated to reflux for 6 h. On reaction completion the solution was concentrated *in vacuo* and recrystallized from EtOH to obtain the known desired compound as a brown solid (600 mg, 77 %).⁶⁷ HPLC – t_R 4.98 > 99% purity at 254 nm; LRMS $[M+H]^+$ 293.8 m/z ; 1H NMR (400 MHz, DMSO) δ_H 13.76 (s, 1H), 8.46 – 8.11 (m, 4H), 7.69 – 7.14 (m, 2H); ^{13}C NMR (101 MHz, DMSO) δ_C 163.6 (d, $J_{C-F} = 249.0$ Hz), 153.1, 148.2, 143.8, 136.9, 129.3 (d, 2C, $J_{C-F} = 7.7$ Hz), 128.4, 125.8, 116.2 (d, 2C, $J_{C-F} = 22.1$ Hz), 112.9. Acquired data is consistent with the literature.⁶⁷

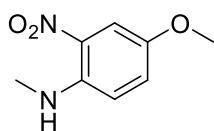
2-(4-Fluorophenyl)-6-(4-methoxyphenyl)-1H-imidazo[4,5-b]pyridine (2.097)



The title compound was prepared from 4-methoxyphenylboronic acid (100 mg, 0.66 mmol) and 6-bromo-2-(4-fluorophenyl)-1H-imidazo[4,5-b]pyridine (100 mg, 0.34 mmol) according to General Procedure A using dichlorobis(triphenylphosphine)palladium (0.10 eq) as the catalyst to afford the crude product. The

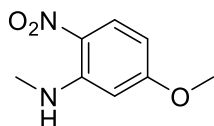
mixture was purified using column chromatography (eluent: EtOAc 40% in Petroleum Spirits) to afford the title product as a white solid (65 mg, 65 %). HPLC – t_R 5.18 min > 95% purity at 254 nm; LRMS $[M+H]^+$ 319.8 m/z ; HRMS $[M+H]^+$ 320.1194 m/z , found 320.1197 m/z ; 1H NMR (400 MHz, DMSO) δ_H 13.49 (bs, 1H), 8.61 (d, J = 1.5 Hz, 1H), 8.33 – 8.27 (m, 2H), 8.16 (bs, 1H), 7.73 – 7.68 (m, 2H), 7.47 – 7.41 (m, 2H), 7.09 – 7.05 (m, 2H), 3.82 (s, 3H).

4-Methoxy-*N*-methyl-2-nitroaniline (2.099a)^{69, 115}



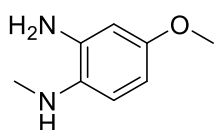
To a cooled solution of 4-methoxy-2-nitroaniline (1.0 g, 6.0 mmol) and DMF (10 mL), NaH (261 mg, 10.0 mmol) was added portion wise. The mixture was heated to room temperature and stirred for a further 10 minutes. Methyl iodide (1.5 eq) was added. The reaction was heated to 35°C and stirred for 90 min. Upon reaction completion, the reaction mixture was diluted with EtOAc and washed with brine. The organic layers were collected, dried over $MgSO_4$, filtered and concentrated to afford the known title compound as a yellow solid (1.04g, 95 %).⁶⁹ HPLC – t_R 5.32 min > 99% purity at 254 nm; LRMS $[M+H]^+$ 183.0 m/z ; 1H NMR (400 MHz, $CDCl_3$) δ_H 7.98 (bs, 1H), 7.62 – 7.59 (m, 1H), 7.19 – 7.15 (m, 1H), 6.84 – 6.80 (m, 1H), 3.79 (s, 3H), 3.01 (bs, 3H); ^{13}C NMR (101 MHz, $CDCl_3$) δ_C 149.7, 142.5, 131.0, 127.6, 114.9, 107.2, 56.0, 30.0. Acquired data is consistent with the literature.^{69, 115}

5-Methoxy-*N*-methyl-2-nitroaniline (2.099b)¹¹⁵



To a cooled solution of 5-methoxy-2-nitroaniline (1.0 g, 6.0 mmol) and DMF (10 mL), NaH (261 mg, 13.1 mmol) was added portion wise. The mixture was heated to room temperature and stirred for a further 10 minutes. Methyl iodide (1.5 eq) was added. The reaction was heated to 35°C and stirred for 90 min. Upon reaction completion, the reaction mixture was diluted with EtOAc and washed with brine. The organic layers were collected, dried over $MgSO_4$, filtered and concentrated to afford the known title compound as a yellow solid (1.08 g, 99 %).⁶⁹ HPLC – t_R 5.35 min > 99% purity at 254 nm; LRMS $[M+H]^+$ 183.0 m/z ; 1H NMR (400 MHz, $CDCl_3$) δ_H 8.27 (bs, 1H, NH), 8.11 (d, J = 9.5 Hz, 1H), 6.22 (dd, J = 9.5, 2.6 Hz, 1H), 6.11 (d, J = 2.6 Hz, 1H), 3.87 (s, 3H), 2.99 (s, 3H); ^{13}C NMR (101 MHz, $CDCl_3$) δ_C 166.2, 148.8, 129.3, 126.7, 104.6, 94.9, 55.8, 29.8. Acquired data is consistent with the literature.¹¹⁵

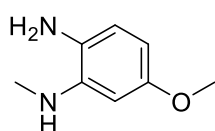
4-Methoxy-*N*¹-methylbenzene-1,2-diamine (2.100a)⁶⁹



To a degassed solution of 4-methoxy-*N*-methyl-2-nitroaniline (1.0 g, 5.5 mmol) in MeOH and THF (1:1) was added Pd/C (10% weight) and the reaction flask was further flushed with nitrogen 3 times before being placed under hydrogen gas for 12 h. Upon reaction completion the mixture was filtered through celite and concentrated *in vacuo* to afford the known title compound as an orange solid without further investigation (711 mg, 85 %).⁶⁹ HPLC – t_R 2.15 min > 99% purity at 254 nm; LRMS $[M+H]^+$ 153.0 m/z ; 1H NMR (400 MHz, $CDCl_3$)

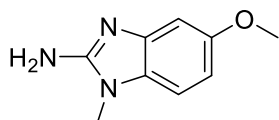
δ_{H} 6.62 (d, $J = 8.5$ Hz, 1H), 6.41 – 6.34 (m, 2H), 3.28 (bs, 3H), 2.82 (bs, 3H); ^{13}C NMR (101 MHz, CDCl_3) δ_{C} 153.8, 136.9, 132.3, 113.1, 104.0, 103.4, 55.7, 32.0. Acquired data is consistent with the literature.⁶⁹

5-Methoxy-*N*¹-methylbenzene-1,2-diamine (2.100b)¹¹⁵



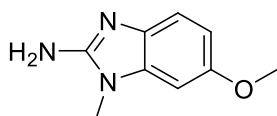
To a degassed solution of 5-methoxy-*N*-methyl-2-nitroaniline (300 mg, 1.6 mmol) in MeOH and THF (1:1) was added Pd/C (10% weight) and the reaction flask was further flushed with nitrogen 3 times before being placed under hydrogen gas for 12 h. Upon reaction completion the mixture was filtered through celite and concentrated *in vacuo* to afford the known title compound as an orange solid without further investigation (200 mg, 80 %).⁶⁹ HPLC – t_{R} 2.79 min > 99% purity at 254 nm; LRMS $[\text{M}+\text{H}]^+$ 153.0 m/z ; ^1H NMR (400 MHz, CDCl_3) δ_{H} 6.64 (d, $J = 8.2$ Hz, 1H), 6.25 (d, $J = 2.7$ Hz, 1H), 6.18 (dd, $J = 8.3, 2.7$ Hz, 1H), 3.76 (s, 3H), 2.84 (s, 3H); ^{13}C NMR (101 MHz, CDCl_3) δ 155.5, 141.5, 126.8, 117.8, 101.0, 98.1, 55.7, 30.9. Acquired data is consistent with the literature.¹¹⁵

5-Methoxy-1-methyl-1*H*-benzo[d]imidazol-2-amine (2.101a)¹¹⁶



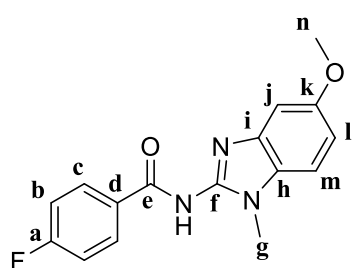
Cyanogen bromide (1.5 eq) was added to a solution of 4-methoxy-*N*¹-methylbenzene-1,2-diamine (500 mg, 3.3 mmol) in MeOH (5 mL). the solution was left to stir at room temp over 72 h. The solution was boiled to remove MeOH and basified with ammonia solution. The solution was filtered, concentrated and purified via recrystallization to obtain the known title compound (410 mg, 70 %).⁷⁰ HPLC – t_{R} 3.39 min > 99% purity at 254 nm; LRMS $[\text{M}+\text{H}]^+$ 178.0 m/z ; ^1H NMR (400 MHz, CDCl_3) δ 6.98 – 6.94 (m, 2H), 6.71 (dd, $J = 8.6, 2.3$ Hz, 1H), 3.82 (s, 3H), 3.55 (s, 3H); ^{13}C NMR (101 MHz, CDCl_3) δ_{C} 156.2, 153.6, 140.9, 128.8, 108.5, 108.1, 100.7, 56.1, 29.1.

6-Methoxy-1-methyl-1*H*-benzo[d]imidazol-2-amine (2.101b)¹¹⁷



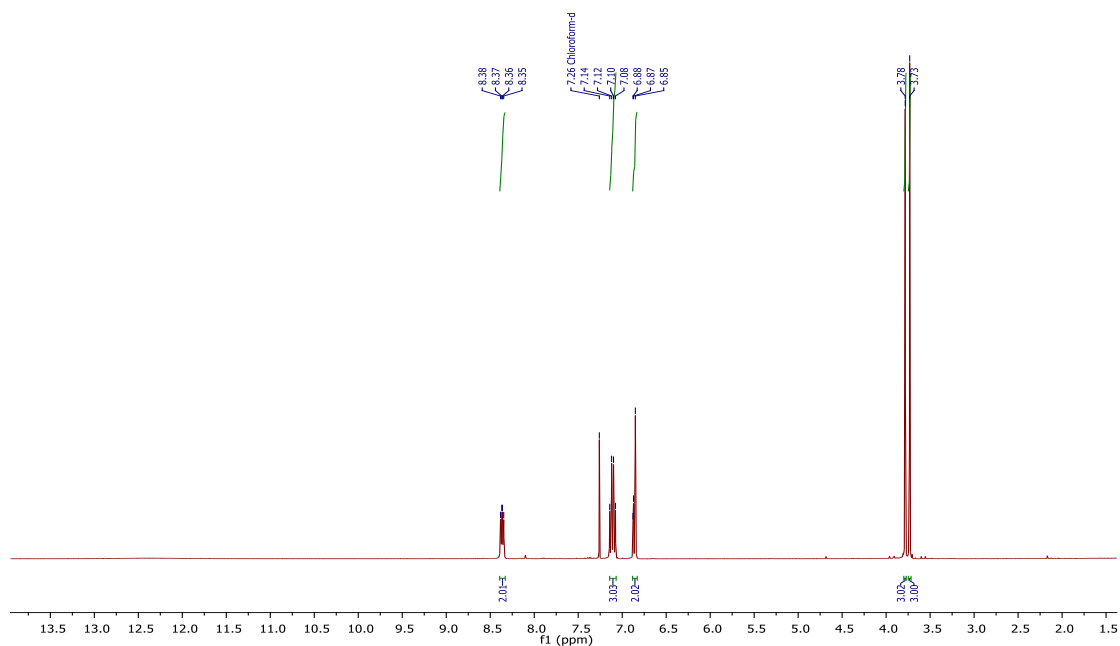
Cyanogen bromide (1.5 eq) was added to a solution of 5-methoxy-*N*¹-methylbenzene-1,2-diamine (250 mg, 1.6 mmol) in MeOH (5 mL). the solution was left to stir at room temp over 72 h. The solution was boiled to remove MeOH and basified with ammonia solution. The solution was filtered, concentrated and purified via recrystallization to obtain the known title compound (166 mg, 57 %).⁷⁰ HPLC – t_{R} 3.34 min > 99% purity at 254 nm; LRMS $[\text{M}+\text{H}]^+$ 178.0 m/z ; ^1H NMR (400 MHz, CDCl_3) δ_{H} 7.29 (d, $J = 8.6$ Hz, 1H), 6.74 (dd, $J = 8.6, 2.4$ Hz, 1H), 6.62 (d, $J = 2.4$ Hz, 1H), 3.84 (s, 3H), 3.50 (s, 3H); ^{13}C NMR (101 MHz, CDCl_3) δ_{C} 154.9, 153.2, 135.7, 135.3, 116.7, 108.8, 93.9, 56.2, 28.9.

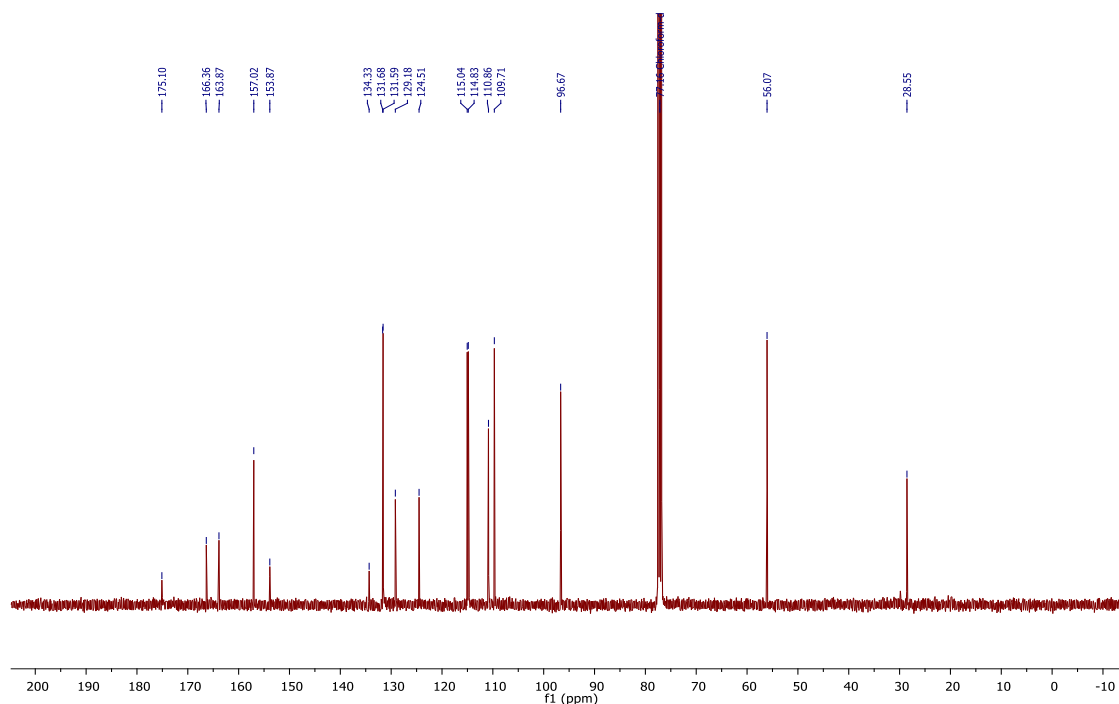
4-Fluoro-*N*-(5-methoxy-1-methyl-1*H*-benzo[*d*]imidazol-2-yl)benzamide (2.102)



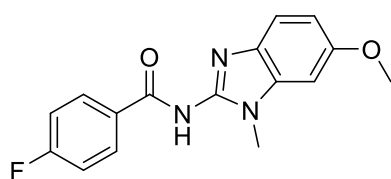
The title compound was prepared from 5-methoxy-1-methyl-1*H*-benzo[*d*]imidazol-2-amine (220 mg, 1.2 mmol) and 4-fluorobenzoic acid (133 mg, 0.95 mmol) according to General Procedure B to afford the desired product as a white solid (45 mg, 16 %). HPLC – t_R 4.92 min > 99% purity at 254 nm; LRMS $[M+H]^+$ 300.0 m/z ; HRMS $[M+H]^+$ 300.1143 m/z , found 300.1149 m/z ; 1H NMR (400 MHz, $CDCl_3$) δ_H 8.39 – 8.34 (m, 2H, Hc), 7.15 – 7.07 (m, 3H, Hj, Hl, Hm), 6.88 – 6.84 (m, 2H, Hb), 3.78 (s, 3H, Hn), 3.73 (s, 3H, Hg); ^{13}C NMR (101 MHz, $CDCl_3$) δ_C 175.1 (Cf), 165.1 (d, J_{C-F} = 250.7 Hz, Ca), 156.7 (Ce), 153.9 (Ch), 134.3 (Cd), 131.6 (d, J_{C-F} = 8.9 Hz, Cc), 129.2 (Ck), 124.5 (Ci), 114.9 (d, J_{C-F} = 21.5 Hz, Cb), 110.9 (Cl), 109.7 (Cm), 96.8 (Cj), 56.1 (Cn), 28.6 (Cg).

Example spectra for Series 3 (pyridine core): 1H (400 MHz, $CDCl_3$) and ^{13}C NMR (100 MHz, $CDCl_3$) spectrum of 4-fluoro-*N*-(5-methoxy-1-methyl-1*H*-benzo[*d*]imidazol-2-yl)benzamide (2.102)





4-Fluoro-*N*-(6-methoxy-1-methyl-1*H*-benzo[*d*]imidazol-2-yl)benzamide (2.103)



The title compound was prepared from 6-methoxy-1-methyl-1*H*-benzo[*d*]imidazol-2-amine (100 mg, 0.56 mmol) and 4-fluorobenzoic acid (80 mg, 0.57 mmol) according to General Procedure B to afford the desired product as a white solid (103 mg,

61 %). HPLC – t_R 4.93 min > 99% purity at 254 nm; LRMS $[M+H]^+$ 300.0 m/z ; HRMS $[M+H]^+$ 300.1143 m/z , found 300.1149 m/z ; 1H NMR (400 MHz, $CDCl_3$) δ_H 8.38 – 8.32 (m, 2H), 7.20 (d, J = 8.6 Hz, 1H), 7.13 – 7.06 (m, 2H), 6.82 (dd, J = 8.6, 2.3 Hz, 1H), 6.76 (d, J = 2.3 Hz, 1H), 3.87 (s, 3H), 3.72 (s, 3H); ^{13}C NMR (101 MHz, $CDCl_3$) δ_C 175.1, 165.0 (d, J_{C-F} = 250.6 Hz), 156.9, 154.2, 134.2 (d, J_{C-F} = 2.8 Hz), 131.5 (d, J_{C-F} = 8.9 Hz, 2C), 131.2, 122.3, 114.8 (d, J_{C-F} = 21.5 Hz, 2C), 111.8, 110.1, 94.9, 56.0, 28.3.

2.14 Chapter 2 References

1. Peña I, Pilar Manzano M, Cantizani J, Kessler A, Alonso-Padilla J, Bardera AI, et al. New Compound Sets Identified from High Throughput Phenotypic Screening Against Three Kinetoplastid Parasites: An Open Resource. *Sci Rep*. 2015;5:8771.
2. Lipinski CA, Lombardo F, Dominy BW, Feeney PJ. Experimental and computational approaches to estimate solubility and permeability in drug discovery and development settings1PII of original article: S0169-409X(96)00423-1. The article was originally published in *Adv Drug Deliv Rev* 23 (1997) 3–25.1. *Adv Drug Deliv Rev*. 2001;46(1):3-26.
3. Veber DF, Johnson SR, Cheng H-Y, Smith BR, Ward KW, Kopple KD. Molecular Properties That Influence the Oral Bioavailability of Drug Candidates. *J Med Chem*. 2002;45(12):2615-2623.
4. Chen M-H, Chuang S-H, Chen Y-J, Chang L-H, Li T-H, Chen C-H, et al. Novel tubulin inhibitors and methods of using the same. WO 2012092471 A2, 2012.
5. Ermolat'ev DS, Babaev EV, Van der Eycken EV. Efficient One-Pot, Two-Step, Microwave-Assisted Procedure for the Synthesis of Polysubstituted 2-Aminoimidazoles. *Org Lett*. 2006;8(25):5781-5784.
6. Ermolat'ev DS, Van der Eycken EV. A Divergent Synthesis of Substituted 2-Aminoimidazoles from 2-Aminopyrimidines. *J Org Chem*. 2008;73(17):6691-6697.
7. Le TG, Kundu A, Ghoshal A, Nguyen NH, Preston S, Jiao Y, et al. Structure–Activity Relationship Studies of Tolfenpyrad Reveal Subnanomolar Inhibitors of *Haemonchus contortus* Development. *J Med Chem*. 2019;62(2):1036-1053.
8. Montalbetti CAGN, Falque V. Amide bond formation and peptide coupling. *Tetrahedron*. 2005;61(46):10827-10852.
9. Takasugi H, Terasawa T, Inoue Y, Nakamura H, Nagayoshi A, Ohtake H, et al. Benzamide compounds as apo b secretion inhibitors. WO 2002028835 A1, 2002.
10. Valeur E, Bradley M. Amide bond formation: beyond the myth of coupling reagents. *Chem Soc Rev*. 2009;38(2):606-631.
11. Richter J, Bischof J, Zaja M, Kohlhof H, Othersen O, Vitt D, et al. Difluoro-dioxolo-benzoimidazol-benzamides As Potent Inhibitors of CK1 δ and ϵ with Nanomolar Inhibitory Activity on Cancer Cell Proliferation. *J Med Chem*. 2014;57(19):7933-7946.
12. Powers JP, Li S, Jaen JC, Liu J, Walker NPC, Wang Z, et al. Discovery and initial SAR of inhibitors of interleukin-1 receptor-associated kinase-4. *Bioorg Med Chem Lett*. 2006;16(11):2842-5.
13. Soderberg T. Organic Chemistry with a Biological Emphasis Volume I. University of Minnesota, Morris: Chemistry Publications. 1; 2019.

14. Ding J, Cao F-D, Geng Y-R, Tian Y, Li P, Li X-F, et al. Synthesis and in vitro anti-epileptic activities of novel [1,2,4]-triazolo[1,5-a]pyrimidin-7(4H)-one derivatives. *J Asian Nat Prod Res.* 2019;21(12):1190-1204.
15. Atkinson AJ, Wang J, Zhang Z, Gold A, Jung D, Zeng D, et al. Grafting of bioactive 2-aminoimidazole into active layer makes commercial RO/NF membranes anti-biofouling. *J Memb Sci.* 2018;556:85-97.
16. Buckman B, Nicholas JB, Serebryany V, Seiwert SD. Novel Inhibitors of Hepatitis C Virus Replication. WO 2012087976 A2, 2012.
17. Shilatifard A, Kaiwei L, Smith ER. Therapeutic targeting of interleukin-1 receptor-associated kinase 4 (IRAK4) in cancers characterized by rearrangements in the mixed lineage leukemia gene (MLL-r). US 20170305901 A1, 2017
18. Thompson QE. The Diacylation of Amides by Acyl Chloride—Pyridine Compounds. *J Am Chem Soc.* 1951;73(12):5841-5846.
19. Sonntag NOV. The Reactions of Aliphatic Acid Chlorides. *Chem Rev.* 1953;52(2):237-416.
20. LaLonde RT, Davis CB. Triamides prepared by the diacylation of amides. *J Org Chem.* 1970;35(3):771-774.
21. Bannard RAB. N,N-DIACETYLAMINES AS BY-PRODUCTS FROM THE ACETYLATION OF AMINES. *Can J Chem.* 1964;42(4):744-752.
22. Morningstar ML, Roth T, Farnsworth DW, Kroeger Smith M, Watson K, Buckheit RW, et al. Synthesis, Biological Activity, and Crystal Structure of Potent Nonnucleoside Inhibitors of HIV-1 Reverse Transcriptase That Retain Activity against Mutant Forms of the Enzyme. *J Med Chem.* 2007;50(17):4003-4015.
23. Michejda CJ, Morningstar M, Roth T. Substituted benzimidazoles as non-nucleoside inhibitors of reverse transcriptase. WO 1998037072 A1, 1998.
24. Mortlock AA, Keen NJ, Jung FH, Brewster AG. Quinazoline derivatives and their use as pharmaceuticals. WO 2001021596 A1, 2001.
25. Merck. Peptide Coupling Reagents Selection Guide [Internet]. 2020. [cited 2020 June 20]. Available from: <https://www.sigmaaldrich.com/technical-documents/articles/chemistry/peptide-coupling-reagents-selection-guide.html>.
26. Global Marketing, Bachem AG. Coupling Reagents [Internet]. Bachem, 2020 [Cited 2020 July 3]. Available from: https://www.bachem.com/fileadmin/user_upload/pdf/Monographs/Coupling_Reagents.pdf
27. Hangauer DG Jr, Marsilje TH, Milkiewicz KL. A Novel Method for Designing Protein Kinase Inhibitors. WO 2000042213 A1, 2000.
28. Schmuck C, Geiger L. Dipeptide Binding in Water by a de Novo Designed Guanidiniocarbonylpyrrole Receptor. *J Am Chem Soc.* 2004;126(29):8898-8899.

29. Al-Warhi TI, Al-Hazimi HMA, El-Faham A. Recent development in peptide coupling reagents. *J Saudi Chem Soc.* 2012;16(2):97-116.
30. Shimada M, Murata T, Fuchikami K, Tsujishita H, Omori N, Kato I, et al. Fused Azole-Pyrimidine Derivatives. WO 2004029055 A1, 2004.
31. Eis K, Ackerstaff J, Wagner S, Basting D, Golz S, Bender E, et al. Amido-substituted Azole Compounds. WO 2015150449 A2, 2015.
32. Moiola M, Memeo MG, Quadrelli P. Stapled Peptides—A Useful Improvement for Peptide-Based Drugs. *Molecules.* 2019;24(20):3654.
33. Meanwell NA. Synopsis of Some Recent Tactical Application of Bioisosteres in Drug Design. *J Med Chem.* 2011;54(8):2529-2591.
34. Meanwell NA. Fluorine and Fluorinated Motifs in the Design and Application of Bioisosteres for Drug Design. *J Med Chem.* 2018;61(14):5822-80.
35. Meanwell NA. Chapter Five - A Synopsis of the Properties and Applications of Heteroaromatic Rings in Medicinal Chemistry. In: Scriven EFV, Ramsden CA, editors. *Advances in Heterocyclic Chemistry.* 123: Academic Press; 2017. p. 245-361.
36. Jacobsen NE. *NMR Data Interpretation Explained: Understanding 1D and 2D NMR Spectra of Organic Compounds and Natural Products.* Hoboken, New Jersey: John Wiley & Sons; 2016.
37. Reich HJ. Hans Reich's Collection NMR Spectroscopy, Chem605 Structure Determination Using NMR. [Internet] 2020. University of Wisconsin. [cited 2020 July 10]. Available from: <https://www2.chem.wisc.edu/areas/reich/nmr/index.htm>.
38. Skála P, Macháček M, Vejsová M, Kubicová L, Kuneš J, Waisser K. Synthesis and antifungal evaluation of hydroxy-3-phenyl-2H-1,3-benzoxazine-2,4(3H)-diones and their thioanalogs. *J Heterocycl Chem.* 2009;46(5):873-880.
39. Huang S-T, Hsei IJ, Chen C. Synthesis and anticancer evaluation of bis(benzimidazoles), bis(benzoxazoles), and benzothiazoles. *Bioorg Med Chem.* 2006;14(17):6106-6119.
40. Albrecht BK, Audia JE, Cook A, Gagnon A, Harmange J-C, Naveschuk CG. Modulators of Methyl Modifying Enzymes, Compositions and Uses thereof. WO 2013075083 A1, 2013.
41. Wuts PGM. *Greene's Protective Groups in Organic Synthesis.* 5th ed. Somerset, United States: John Wiley & Sons, Incorporated; 2014.
42. Kahvedžić-Seljubać A, Nathwani S-M, Zisterer DM, Rozas I. Isouronium and N-hydroxyguanidinium derivatives as Cell growth inhibitors: A comparative study. *Eur J Med Chem.* 2016;117:269-282.
43. Segal M, Avinery R, Buzhor M, Shaharabani R, Harnoy AJ, Tirosh E, et al. Molecular Precision and Enzymatic Degradation: From Readily to Undegradable Polymeric Micelles by Minor Structural Changes. *J Am Chem Soc.* 2017;139(2):803-810.
44. Ramkumar SG, Rose KAA, Ramakrishnan S. Direct synthesis of terminally “clickable” linear and hyperbranched polyesters. *J Polym Sci A Polym Chem.* 2010;48(14):3200-3208.

45. Mandal PK, McMurray JS. Pd-C-Induced Catalytic Transfer Hydrogenation with Triethylsilane. *J Org Chem*. 2007;72(17):6599-6601.
46. Vicker N, Day JM, Bailey HV, Heaton W, Gonzalez AMR, Sharland CM, et al. Preparation of substituted aliphatic amines for use as anticancer or therapeutic agents inhibiting 17 β -hydroxysteroid dehydrogenase. WO 2007003934 A2, 2007
47. Shimony O, Jaffe CL. Rapid fluorescent assay for screening drugs on *Leishmania* amastigotes. *J Microbiol Methods* 2008;75(2):196-200.
48. Merlen T, Sereno D, Brajon N, Rostand F, Lemesre JL. *Leishmania* spp: completely defined medium without serum and macromolecules (CDM/LP) for the continuous in vitro cultivation of infective promastigote forms. *Am J Trop Med Hyg*. 1999;60(1):41-50.
49. Saunders E, McConville M. *Leishmania* drug screen checklist in vitro and in vivo. [Unpublished data]. The Bio21 Institute of Molecular Science and Biotechnology, Department of Biochemistry and Molecular Biology, The University of Melbourne; 2018
50. Smilkstein M, Sriwilaijaroen N, Kelly JX, Wilairat P, Riscoe M. Simple and Inexpensive Fluorescence-Based Technique for High-Throughput Antimalarial Drug Screening. *Antimicrob Agents Chemother*.. 2004;48(5):1803-1806.
51. Dagley JM, Saunders EC, Simpson KJ, J. McConville MJ. High-Content Assay for Measuring Intracellular Growth of *Leishmania* in Human Macrophages. *Assay Drug Dev Technol* 2015;13(7):389-401.
52. Paloque L, Vidal N, Casanova M, Dumètre A, Verhaeghe P, Parzy D, et al. A new, rapid and sensitive bioluminescence assay for drug screening on *Leishmania*. *J Microbiol Methods* 2013;95(3):320-323.
53. De Rycker M, Hallyburton I, Thomas J, Campbell L, Wyllie S, Joshi D, et al. Comparison of a High-Throughput High-Content Intracellular *Leishmania donovani* Assay with an Axenic Amastigote Assay. *Antimicrob Agents Chemother*. 2013;57(7):2913-2922.
54. Paape D, Bell AS, Heal WP, Hutton JA, Leatherbarrow RJ, Tate EW, et al. Using a Non-Image-Based Medium-Throughput Assay for Screening Compounds Targeting N-myristoylation in Intracellular *Leishmania* Amastigotes. *PLoS Negl Trop Dis*. 2014;8(12):e3363.
55. Saunders E, McConville M. 1 year milestones –Investigating the mode of action and antiparasite drugs. [Unpublished data] The Bio21 Institute of Molecular Science and Biotechnology, Department of Biochemistry and Molecular Biology, The University of Melbourne; 2018.
56. Alcântara LM, Ferreira TCS, Gadelha FR, Miguel DC. Challenges in drug discovery targeting TriTryp diseases with an emphasis on leishmaniasis. *Int J Parasitol Drugs Drug Resist*. 2018;8(3):430-439.
57. He H, Wang X, Shi L, Yin W, Yang Z, He H, et al. Synthesis, antitumor activity and mechanism of action of novel 1,3-thiazole derivatives containing hydrazide–hydrazone and carboxamide moiety. *Bioorg Med Chem Lett*. 2016;26(14):3263-3270.

58. Librowski T, Kubacka M, Meusel M, Scolari S, Müller CE, Gütschow M. Evaluation of anticonvulsant and analgesic effects of benzyl- and benzhydryl ureides. *Eur J Pharmacol.* 2007;559(2):138-149.
59. Park SY, Oh YJ, Lho Y, Jeong JH, Liu K-H, Song J, et al. Design, synthesis, and biological evaluation of a series of resorcinol-based N-benzyl benzamide derivatives as potent Hsp90 inhibitors. *Eur J Med Chem.* 2018;143:390-401.
60. Lim ZY, Wang H, Zhou Y. Acylurea Connected and Sulfonylurea Connected Hydroxamates. WO 2005040101 A1, 2005.
61. Wang H, Lim Z-Y, Zhou Y, Ng M, Lu T, Lee K, et al. Acylurea connected straight chain hydroxamates as novel histone deacetylase inhibitors: Synthesis, SAR, and in vivo antitumor activity. *Bioorg Med Chem Lett.* 2010;20(11):3314-3321.
62. Miyaura N, Suzuki A. Palladium-Catalyzed Cross-Coupling Reactions of Organoboron Compounds. *Chem Rev.* 1995;95(7):2457-2483.
63. Alacid E, Nájera C. First Cross-Coupling Reaction of Potassium Aryltrifluoroborates with Organic Chlorides in Aqueous Media Catalyzed by an Oxime-Derived Palladacycle. *Org Lett.* 2008;10(21):5011-5014.
64. Schwarz L, Girreser U, Clement B. Synthesis and Characterization of para-Substituted N,N'-Dihydroxybenzamidines and Their Derivatives as Model Compounds for a Class of Prodrugs. *European J Org Chem.* 2014;2014(9):1961-1975.
65. Azzali E, Machado D, Kaushik A, Vacondio F, Flisi S, Cabassi CS, et al. Substituted N-Phenyl-5-(2-(phenylamino)thiazol-4-yl)isoxazole-3-carboxamides Are Valuable Antitubercular Candidates that Evade Innate Efflux Machinery. *J Med Chem.* 2017;60(16):7108-7122.
66. Bourbeau MP, Rider JT. A Convenient Synthesis of 4-Alkyl-5-aminoisoxazoles. *Org Lett.* 2006;8(17):3679-3680.
67. Taha M, Ismail NH, Imran S, Ainaa I, Selvaraj M, baharudin Ms, et al. Synthesis of 2-phenyl-1H-imidazo[4,5-b]pyridine as type 2 diabetes inhibitors and molecular docking studies. *Med Chem Res.* 2017;26(5):916-28.
68. Klein M. Quinazoline derivatives as PI3 kinase inhibitors and their preparation. AU 2011323026 A1, 2012.
69. Buckman B, Nicholas JB, Beigelman L, Serebryany V, Stoycheva AD, Thrailkill T, et al. Cyclic Peptide Inhibitors of Hepatitis C Virus Replication. WO 2011038293 A1, 2011.
70. Swayze E, Seth P, Griffey R, Jefferson E. Benzimidazoles and analogs thereof as antivirals. US 20050124638 A1, 2005.
71. Shimony O, Jaffe CL. Rapid fluorescent assay for screening drugs on Leishmania amastigotes. *J Microbiol Methods.* 2008;75(2):196-200.

72. Campos-Salinas J, León-Guerrero D, González-Rey E, Delgado M, Castanys S, Pérez-Victoria JM, et al. ABCG2, a new ABC transporter implicated in phosphatidylserine exposure, is involved in the infectivity and pathogenicity of *Leishmania*. *PLoS Negl Trop Dis*. 2013;7(4):e2179.
73. Siqueira-Neto JL, Song O-R, Oh H, Sohn J-H, Yang G, Nam J, et al. Antileishmanial High-Throughput Drug Screening Reveals Drug Candidates with New Scaffolds. *PLoS Negl Trop Dis*. 2010;4(5):e675.
74. Fumarola L, Spinelli R, Brandonisio O. In vitro assays for evaluation of drug activity against *Leishmania* spp. *Res Microbiol*. 2004;155(4):224-230.
75. Jara M, Berg M, Caljon G, de Muylder G, Cuypers B, Castillo D, et al. Macromolecular biosynthetic parameters and metabolic profile in different life stages of *Leishmania braziliensis*: Amastigotes as a functionally less active stage. *PloS one*. 2017;12(7):e0180532.
76. Hendrickx S, Van Bockstal L, Caljon G, Maes L. In-depth comparison of cell-based methodological approaches to determine drug susceptibility of visceral *Leishmania* isolates. *PLoS Negl Trop Dis*. 2019;13(12):e0007885.
77. Freitas-Junior LH, Chatelain E, Kim HA, Siqueira-Neto JL. Visceral leishmaniasis treatment: What do we have, what do we need and how to deliver it? *Int J Parasitol Drugs Drug Resist*. 2012;2:11-9.
78. Duffy S, Sykes ML, Jones AJ, Shelper TB, Simpson M, Lang R, et al. Screening the Medicines for Malaria Venture Pathogen Box across Multiple Pathogens Reclassifies Starting Points for Open-Source Drug Discovery. *Antimicrob Agents Chemother*. 2017;61(9): e00379-17.
79. Van den Kerkhof M, Mabile D, Chatelain E, Mowbray CE, Braillard S, Hendrickx S, et al. In vitro and in vivo pharmacodynamics of three novel antileishmanial lead series. *Int J Parasitol Drugs Drug Resist*. 2018;8(1):81-86.
80. Gupta S, Yardley V, Vishwakarma P, Shivhare R, Sharma B, Launay D, et al. Nitroimidazo-oxazole compound DNDI-VL-2098: an orally effective preclinical drug candidate for the treatment of visceral leishmaniasis. *J Antimicrob Chemother*. 2014;70(2):518-527.
81. Thermo Fischer Scientific. CellTracker™ Orange CMRA Dye [Internet]. [Cited 2020 July 3]. Available from: <https://www.thermofisher.com/order/catalog/product/C34551#/C34551>.
82. Thermo Fischer Scientific. CellTracker™ Green CMFDA Dye [Internet]. [Cited 2020 July 3]. Available from: <https://www.thermofisher.com/order/catalog/product/C2925#/C2925>.
83. de Monbrison F, Mihoubi I, Picot S. Real-time PCR assay for the identification of cutaneous *Leishmania* parasite species in Constantine region of Algeria. *Acta Trop*. 2007;102(2):79-83.
84. Sunduru N, Nishi, Palne S, Chauhan PMS, Gupta S. Synthesis and antileishmanial activity of novel 2,4,6-trisubstituted pyrimidines and 1,3,5-triazines. *Eur J Med Chem*. 2009;44(6):2473-2481.
85. World Health Organization. Control of the Leishmaniases : Report of a meeting of the WHO Expert Committee on the Control of Leishmaniases, Geneva, 22-26 March 2010. Geneva: World Health Organization technical report series. 2010(949): xii-xiii, 1-186.

86. Jaffe CL, Bennett E, Grimaldi G, McMahon-Pratt D. Production and characterization of species-specific monoclonal antibodies against *Leishmania donovani* for immunodiagnosis. *J Immunol.* 1984;133(1):440-447.
87. Kelleher M, Moody SF, Mirabile P, Osborn AH, Bacic A, Handman E. Lipophosphoglycan blocks attachment of *Leishmania* major amastigotes to macrophages. *Infect Immun.* 1995;63(1):43-50.
88. Symons FM, Murray PJ, Ji H, Simpson RJ, Osborn AH, Cappai R, et al. Characterization of a polymorphic family of integral membrane proteins in promastigotes of different *Leishmania* species. *Mol Biochem Parasitol.* 1994;67(1):103-113.
89. Jain SK, Sahu R, Walker LA, Tekwani BL. A parasite rescue and transformation assay for antileishmanial screening against intracellular *Leishmania donovani* amastigotes in THP1 human acute monocytic leukemia cell line. *J Vis Exp.* 2012(70):4054.
90. Phan T-N, Baek K-H, Lee N, Byun SY, Shum D, No JH. In Vitro and in Vivo Activity of mTOR Kinase and PI3K Inhibitors Against *Leishmania donovani* and *Trypanosoma brucei*. *Molecules.* 2020;25(8):1980.
91. Verma JK, Rastogi R, Mukhopadhyay A. *Leishmania donovani* resides in modified early endosomes by upregulating Rab5a expression via the downregulation of miR-494. *PLoS Pathog.* 2017;13(6):e1006459.
92. Yang Z, Mosser DM, Zhang X. Activation of the MAPK, ERK, following *Leishmania amazonensis* infection of macrophages. *J Immunol.* 2007;178(2):1077-1085.
93. Cyprotex. High Content Toxicology: Cytotoxicity Screening Panel [Internet]. 2020 [cited 2020 July 23]. Available from: <https://www.cyprotex.com/toxicology/multiparametric/cytotoxicity-screening-panel>.
94. O'Brien P, Haskins JR. In Vitro Cytotoxicity Assessment. In: Taylor DL, Haskins JR, Giuliano KA, editors. *High Content Screening. Methods in molecular biology.* 356: Humana Press; 2007. p. 415-425.
95. Cyprotex. Mechanism of Drug Induced Toxicity Guide. [Internet] 2018. [cited 2020 July 23]. Available from: <https://www.cyprotex.com/guides/>
96. Bevan CD, Lloyd RS. A High-Throughput Screening Method for the Determination of Aqueous Drug Solubility Using Laser Nephelometry in Microtiter Plates. *Anal Chem.* 2000;72(8):1781-1787.
97. Lombardo F, Shalaeva MY, Tupper KA, Gao F. ElogDoct: A Tool for Lipophilicity Determination in Drug Discovery. 2. Basic and Neutral Compounds. *J Med Chem.* 2001;44(15):2490-2497.
98. Ring BJ, Chien JY, Adkison KK, Jones HM, Rowland M, Jones RD, et al. PhRMA CPCDC initiative on predictive models of human pharmacokinetics, part 3: Comparative assesement of prediction methods of human clearance. *J Pharm Sci.* 2011;100(10):4090-4110.

99. Obach RS. Prediction of human clearance of twenty-nine drugs from hepatic microsomal intrinsic clearance data: An examination of in vitro half-life approach and nonspecific binding to microsomes. *Drug Metab Dispos.* 1999;27(11):1350-1359.
100. Slaihim MM, Al-Suede FSR, Khairuddean M, Khadeer Ahamed MB, Shah Abdul Majid AM. Synthesis, characterisation of new derivatives with mono ring system of 1,2,4-triazole scaffold and their anticancer activities. *J Mol Struct.* 2019;1196:78-87.
101. Ding A, Zhang Y, Chen Y, Rios R, Hu J, Guo H. Visible light induced oxidative hydroxylation of boronic acids. *Tetrahedron Lett.* 2019;60(9):660-663.
102. Halbert SM, Thompson SK, Veber DF. Protease Inhibitors. WO 9959570 A1, 1999.
103. Orłowska E, Roller A, Wiesinger H, Pignitter M, Jirsa F, Krachler R, et al. Benzoic hydroxamate-based iron complexes as model compounds for humic substances: synthesis, characterization and algal growth experiments. *RSC Adv.* 2016;6(46):40238-49.
104. Stackhouse PJ, Wilson A, Lacey D, Hird M. Synthesis and properties of novel columnar liquid crystals based on symmetrical and non-symmetrical 1,3,5-trisubstituted benzene derivatives. *Liq Cryst.* 2010;37(9):1191-1203.
105. Wang L-Y, Tsai H-Y, Lin H-C. Novel Supramolecular Side-Chain Banana-Shaped Liquid Crystalline Polymers Containing Covalent- and Hydrogen-Bonded Bent Cores. *Macromolecules.* 2010;43(3):1277-1288.
106. Jansen K, Heirbaut L, Verkerk R, Cheng JD, Joossens J, Cos P, et al. Extended Structure–Activity Relationship and Pharmacokinetic Investigation of (4-Quinolinyloxy)glycyl-2-cyanopyrrolidine Inhibitors of Fibroblast Activation Protein (FAP). *J Med Chem.* 2014;57(7):3053-3074.
107. Li X-Q, Wang W-K, Han Y-X, Zhang C. One-Pot Synthesis of Symmetrical 1,3-Diarylsureas or Substituted Benzamides Directly from Benzylic Primary Alcohols and Effective Oxidation of Secondary Alcohols to Ketones Using Phenyliodine Diacetate in Combination with Sodium Azide. *Adv Synth Catal.* 2010;352(14-15):2588-2598.
108. Zishiri VK, Hunter R, Smith PJ, Taylor D, Summers R, Kirk K, et al. series of structurally simple chloroquine chemosensitizing dibemethin derivatives that inhibit A chloroquine transport by PfCRT. *Eur J Med Chem.* 2011;46(5):1729-1742.
109. Itoh T, Mase T. Direct synthesis of hetero-biaryl compounds containing an unprotected NH₂ group via Suzuki–Miyaura reaction. *Tetrahedron Lett.* 2005;46(20):3573-3577.
110. Bollenbach M, Salvat E, Daubeuf F, Wagner P, Yalcin I, Humo M, et al. Phenylpyridine-2-ylguanidines and rigid mimetics as novel inhibitors of TNF α overproduction: Beneficial action in models of neuropathic pain and of acute lung inflammation. *Eur J Med Chem.* 2018;147:163-182.
111. Hoshi T, Honma T, Mori A, Konishi M, Sato T, Hagiwara H, et al. An Active, General, and Long-Lived Palladium Catalyst for Cross-Couplings of Deactivated (Hetero)aryl Chlorides and Bromides with Arylboronic Acids. *J Org Chem.* 2013;78(22):11513-11524.

112. Calderone V, Minutolo F, Tuccinardi T, Testai L, Granchi C, Martelli A, et al. New Activators of SIRT1 Enzyme for the Treatment of Cardiovascular and Cardiometabolic pathologies. WO 2019162911 A1, 2019.
113. Puerto Galvis CE, Kouznetsov VV. An unexpected formation of the novel 7-oxa-2-azabicyclo[2.2.1]hept-5-ene skeleton during the reaction of furfurylamine with maleimides and their bioprospection using a zebrafish embryo model. *Org Biomol Chem*. 2013;11(3):407-411.
114. Augustine JK, Kumar R, Bombrun A, Mandal AB. An efficient catalytic method for the Beckmann rearrangement of ketoximes to amides and aldoximes to nitriles mediated by propylphosphonic anhydride (T3P®). *Tetrahedron Lett*. 2011;52(10):1074-1077.
115. Newsome JJ, Colucci MA, Hassani M, Beall HD, Moody CJ. Benzimidazole- and benzothiazole-quinones: excellent substrates for NAD(P)H:quinone oxidoreductase 1. *Org Biomol Chem*. 2007;5(22):3665-3673.
116. Bentzien J, Hickey ER, Kemper RA, Brewer ML, Dyekjær JD, East SP, et al. An in Silico Method for Predicting Ames Activities of Primary Aromatic Amines by Calculating the Stabilities of Nitrenium Ions. *J Chem Inf Model*. 2010;50(2):274-297.
117. Xie D, Li Q, Xue W, Liu H. Preparation of the benzimidazole compound and their application for the preventing and treating FAK-related diseases patent CN 108912095 (Chinese). 2018.

Chapter 3: Further SAR studies and optimization of the phenyl imidazole carboxamide scaffold (Scaffold 1)

3.01 Introduction and objectives

As described in Chapter 2, an early hit-to-lead study around the antileishmanial hits **2.001** and **2.002** (Scaffold 1) was commenced. The overall aims of this study were to begin to investigate the chemical space surrounding Scaffold 1 and start to form a first-generation SAR profile. This investigation included the synthesis and biological evaluation of a number of analogues, bearing structural modifications to the LHS and RHS chemical space (Analogues Series 1 and 2 respectively), as well as altering the amide functionality and imidazole core (Analogue Series 3). The antileishmanial properties of these analogues was assessed against intracellular *L. donovani* amastigotes, using macrophages as host cells (intramacrophage assay), performed by our collaborators at GRIDD.

The antileishmanial activity of the hit **2.002** was confirmed and new potential lead compounds were identified. The structure and antileishmanial activity of these compounds of interest are listed in **Figure 3.01**. The hit **2.001** was reported to have displayed solubility issues and was originally suggested by GRIDD to have possibly contributed to the poor antileishmanial activity observed. Interestingly, compound **2.059** was initially reported by GRIDD to display highly potent antileishmanial activity ($IC_{50} = 0.32 \mu M$). As this compound was structurally very similar to the hit **2.001**, we believed this scaffold still held the potential for parasite inhibition. Furthermore, re-examination of **2.001** using an independent *L. donovani* intramacrophage assay performed by our collaborators at Bio21, found that this hit exhibited moderate antileishmanial activity when no solubility issues were reported. The hit **2.002** was also reported to exhibit *L. donovani* inhibition within this assay. Therefore, we still believed an SAR exploration around both hits **2.001**, **2.002** of Scaffold 1 still held merit, and could provide new lead compounds with improved antileishmanial activity whilst maintaining low cytotoxicity in mammalian cell lines.

Our initial aims for this section was to continue to explore the remaining chemical space around Scaffold 1. During these studies, we also aimed to perform additive SAR studies, incorporating the structural attributes of the key analogues which had demonstrated high antileishmanial activity within the GRIDD intramacrophage assay (**Figure 3.01**). During these studies, we also aimed to maintain low mammalian cytotoxicity, intending to develop analogues which displayed selectivity for the parasite over the host macrophage. As discussed in Chapter 2, correspondence with GSK informed us that they had developed an undisclosed small library of analogues around chosen hits **2.001**, **2.002**. Further development around this library was discontinued by GSK, as they had observed that strong activity within these analogues correlated to increasing host cell cytotoxicity. Based on their informal warning,

we would continue to “keep an eye out” for this phenomenon during our continued exploration around Scaffold 1.

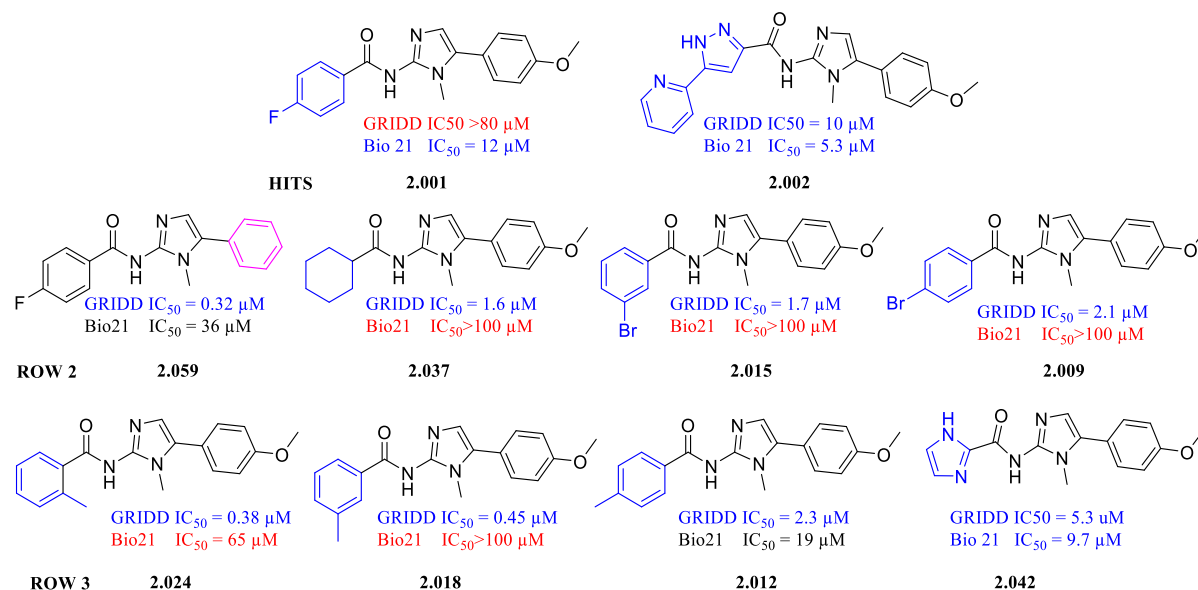


Figure 3.01: Summary of analogues which exhibited the strongest inhibition against *L. donovani* within either and/or both independent intramacrophage assays employed

The biological reassessment of the key analogues listed in **Figure 3.01**, performed by Bio21 also confirmed the antileishmanial activity of analogue **2.042**, which bears the imidazole ring replacement within the LHS region of Scaffold 1. This analogue would influence further SAR studies around Scaffold 1, which is described below in Section **3.05**. However, conflicting biological results were reported between the independent groups for the remaining compounds of interest, as summarized above in **Figure 3.01**. Consequently, SAR interpretation became a difficult task. By this stage of the project, due to the long waiting periods between receiving and/or confirming biological results, a larger library of analogues had already been synthesized. This library includes Analogue Series 4-7, discussed in later sections of this chapter, containing analogues influenced by the compounds of **Figure 3.01**, as they were originally reported by GRIDD to be highly potent against *L. donovani*.

To successfully overcome the challenges around the conflicting biological results and ensure further studies around this scaffold were guided by a reliable SAR profile, our objectives for this early hit-to-lead project were temporarily altered. The continued synthesis of analogues devised around Scaffold 1 was provisionally paused, to give priority towards determining the “true” antileishmanial activity and selectivity of each compound within our library of analogues. This involved the biological reassessment of the key analogues of Series 1-2, performed independently by our collaborators at GRIDD and Bio21. Furthermore, the biological examination of our entire library (Analogue Series 1-9) was undertaken by Bio21 and our new collaborators at the Institut Pasteur Korea (IPK). A large subset of analogues was also re-tested by our collaborators at the University of North Carolina at Chapel Hill (UNC). The

complete set of biological results is outlined in the latter half of this chapter. Each independent group employed clinically relevant *L. donovani* intramacrophage assays, also discussed in later sections of this chapter. The methodology of each assay is also described in the Experimental section. From these large efforts made by our collaborators, we were confident that we could achieve our aim of understanding the “true” antileishmanial activity of our compounds. To overcome any further issues with conflicting biological results, we have devised a set of guidelines to determine “true” activity and assist with SAR interpretation, detailed in Section 3.11.

The final objectives for this chapter included pivoting and focusing on a new set of lead compounds that were identified and confirmed during the large biological re-examination, performed by our independent collaborators. Our aims to develop compounds with improved antileishmanial activity and maintain low mammalian cytotoxicity were continued, using this new set of lead compounds to influence the structural changes, and continue to develop a primary SAR profile around Scaffold 1. The new early lead compounds chosen, would undergo physicochemical and metabolic assessment to determine drug-likeness. These new early lead compounds would also help set out the blueprints for future work around this scaffold, to achieve a more developed antileishmanial lead candidate, outside the scope of this thesis. To understand our rationale during this hit-to-lead medicinal chemistry campaign, our results have been presented transparently and as much as possible, in the chronological order of events.

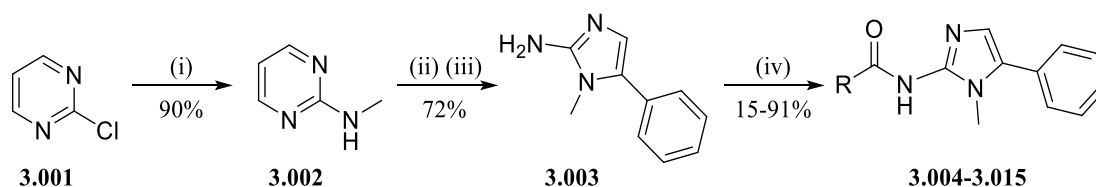
3.02 Analogue Series 4: Additive SAR studies influenced by initial GRIDD biological results

An additive SAR study was undertaken, combining the structural attributes of analogues which reported the strongest parasite inhibition, identified during the *L. donovani* intramacrophage screen performed by GRIDD. Analogue **2.059**, which bears an unsubstituted phenyl ring at the RHS of the scaffold, reported the highest antileishmanial activity overall (**Figure 3.01**). Therefore, the RHS unsubstituted phenyl ring was paired with the various LHS structural changes that had also previously reported strong parasite inhibition using the GRIDD intramacrophage assay. This included pairing the RHS unsubstituted phenyl ring with the pyridine pyrazole system (**3.004**), cyclohexane ring (**3.010**) imidazole ring (**3.011**) at the LHS. The RHS unsubstituted phenyl ring was also paired with the LHS phenyl ring bearing methyl and bromo substituents (**3.005-3.010**). These analogues were devised to probe whether these combined structural modifications would allow for a greater improvement in antileishmanial activity, possibly allowing for a more suitable fit within the putative binding site/s.

The synthetic pathway outlined in **Scheme 3.01** was utilized to obtain these analogues. This synthetic route had been previously optimized to obtain the structurally close analogues discussed in Chapter 2, Section 2.02 (**Scheme 2.01/2.03** of Chapter 2). Briefly, 2-chloropyrimidine **3.001** underwent

nucleophilic substitution with methylamine, to obtain *N*-methylpyrimidin-2-amine **3.002**.¹ This was followed by the formation of the phenyl-1*H*-imidazole-2-amine intermediate **3.003** as outlined by Ermolat'ev *et al.*, the suggested mechanism of this one-pot, two step protocol was also outlined in Chapter 2. Finally, subsequent amide coupling was undertaken to successfully obtain the analogues **3.004-3.015**.¹⁻⁴ Most of the analogues were obtained in a reasonable yield, with a small number of exceptions. However, the few target analogues that were acquired in low yield were not an issue, as each analogue still provided more than sufficient amounts of sample for the array of biological assessments we utilized. The structure and yield of each analogue of Series 4 is summarized below in **Table 3.01**. Additionally, the ¹H NMR and ¹³C NMR spectra of representative compounds for each analogue series, including Series 4, have been included within the Experimental section.

Scheme 3.01: Synthetic pathway for additive SAR analogues



Reaction conditions i) methylamine, THF, 50 °C, ii) 2-bromo-1-phenylethan-1-one, ACN, 130 °C, microwave assisted, iii) hydrazine hydrate, 100 °C, microwave assisted, iv) substituted benzoic acid, DIPEA, DMAP, HBTU, ACN, 50°C or substituted benzoic acid, DIPEA, DMAP, PyBOP, DMF, 25- 50°C

Table 3.01: Structure and yields of additive SAR analogues of Analogue Series 4

I.D	Structure	Yield % (step iv)	I.D	Structure	Yield % (step iv)
3.004		25	3.010		85
3.005		44	3.011		15
3.006		84	3.012		77
3.007		38	3.013		54
3.008		89	3.014		56
3.009		60	3.015		91

3.03 Parallel investigation surrounding pyridine pyrazole LHS hit 2.002

Continued studies around the chemical space of hit **2.002** were undertaken by a fellow group member, Dr Swapna Varghese. This study was undertaken in parallel to the exploration around the chemical space of hit **2.001** described within this chapter, roughly along the same timelines as the development of Analogue Series 4-7. The aim of studying the hits in parallel medicinal chemistry projects was to achieve a more in-depth SAR profile around Scaffold 1 overall.

The structural changes devised in this parallel study included modifications to the amide, imidazole core and adjoining *para*-methoxyphenyl ring, which were inspired by Mowbray *et al.*, who had developed a potent early lead antileishmanial candidate (**3.019**) which possessed a similar pyridine pyrazole system within the LHS chemical space. The early lead described by Mowbray *et al.* reported high antileishmanial activity against *L. donovani* amastigotes (intramacrophage, $IC_{50} = 1.31 \mu M$) and >90% efficacy against *L. infantum* in hamster models.⁵ These results had peaked our interest, hence structural changes to **2.002** were devised by Dr Varghese, which included substitution of the amide functionality with the urea, and the imidazole core was replaced with various piperazine (**3.020**, **3.021**) pyrrolidine (**3.022**, **3.023**) and piperidine (**3.024**) rings. The *para*-fluorophenyl ring of **3.019** was also incorporated to the RHS chemical space of analogues **3.020**, **3.021**. Finally, structural changes to the LHS chemical space of **2.002** were also devised, substituting the pyridine pyrazole with pyridine triazoles (**3.021**, **3.023**, **3.024**) and bipyridine rings (**3.020**). A cyclopropane ring was also added to the LHS chemical space (**3.022**), based on previous SAR studies reported by Mowbray *et al.* around structural similar pyridine pyrazole benzamides.⁵ Analogues synthesized for this parallel study have been denoted with “SV”. These compounds are depicted below in **Figure 3.03**.

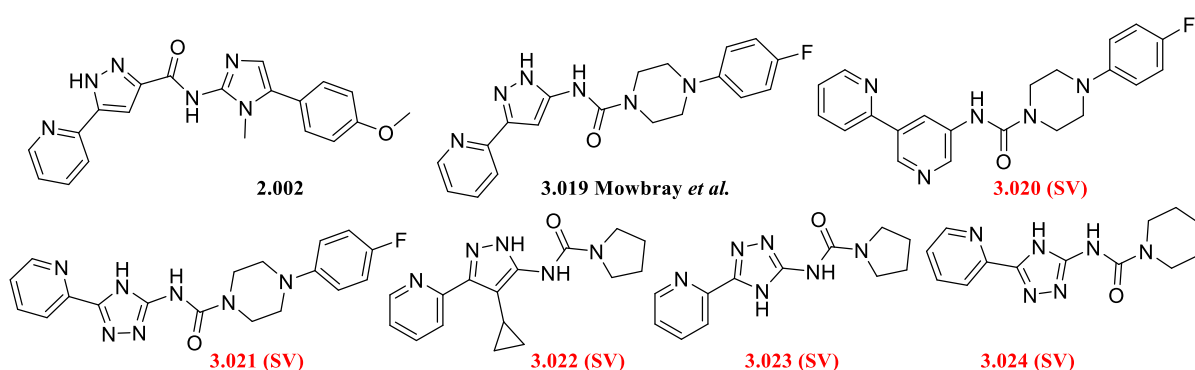


Figure 3.03: Structures of analogues devised in parallel studies around hit **2.002** by a fellow lab member

The biological activity of this parallel series was assessed using the *L. donovani* intramacrophage assay performed by Bio21. Despite the synthetic efforts, no parasite inhibition was observed within this entire series. Each analogue was reported to be completely inactive against *L. donovani*, though no cytotoxicity against the host macrophages was observed either. After these initial parallel studies

surrounding the chemical space of hit **2.002** were accomplished, the pyridine pyrazole hit **2.002** was re-assigned into this early hit-to-lead PhD project and would influence the SAR studies of Analogue Series 9 (Section **3.019**). This study focused on retaining the pyridine pyrazole LHS chemical space, while altering the RHS functionality.

3.04 Analogue Series 5: *N*-alkyl and *N*-aryl modifications on the imidazole core

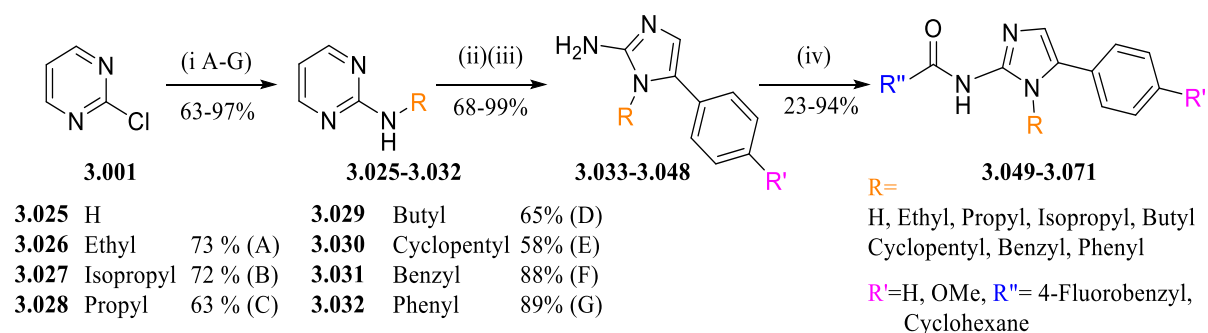
In parallel to the additive SAR study described in Section **3.02** (Analogue Series 4), investigations around the *N*-methyl group of the imidazole core within Scaffold 1 were undertaken as a part of this PhD medicinal chemistry project. Herein, we aimed to probe if the *N*-methyl group was required to maintain antileishmanial activity, and if larger aliphatic chains and rings could be substituted at this position. The *N*-methyl group was removed entirely (**3.049**, **3.057**) to probe whether the secondary amine of the imidazole ring was preferable within this chemical space. The loss of the *N*-methyl would alter the hydrogen bonding abilities of the amine, where the secondary amine could possibly interact with the putative binding site as a hydrogen bond donor or acceptor.⁶ The methyl chain was also extended to probe if larger carbon-carbon chains could increase the number of key interactions formed with the putative binding site/s and possibly deduce if a lipophilic pocket was present. To study the effects of increasing the carbon-carbon chain, ethyl to butyl chains were introduced at this region of the scaffold (**3.050-3.053**, **3.058-3.061**, **3.065-3.068**).

Aliphatic (**3.054**, **3.062**, **3.069**) and aromatic rings (**3.055-3.056**, **3.063-3.064**, **3.070-3.071**) were also substituted in place of the *N*-methyl group to determine if a large increase in lipophilicity and steric bulk within this region would allow for an improved fit within the putative binding site/s. Furthermore, introducing the benzyl and phenyl aromatic rings to this position would also probe if potential pi-pi interactions could be made between this region of the scaffold and the putative binding site/s. introduction of these more hydrophobic groups at one end of the ligand may even cause the parent compound to bind in a flipped orientation, which may be more beneficial to activity. During this investigation, analogues **3.049-3.056** retained the structure of hit **2.001**, whilst only the *N*-methyl group was altered. We decided to take the opportunity to expand our scope slightly and incorporate the structural attributes of **2.059** (unsubstituted RHS phenyl ring) and **2.037** (cyclohexane LHS ring), as they had initially reported to exert high antileishmanial activity within the intramacrophage assay performed by GRIDD (Chapter 2, Section **2.08**). These analogues were reported by GRIDD as the most potent analogues against *L. donovani*, at the time of developing Analogue Series 5. The synthetic ease and availability of starting reagent also encouraged the inclusion of these structures within analogues **3.057-3.071**. It should be noted that the analogues **2.024** and **2.018** were later found to exhibit stronger parasite inhibition than the cyclohexane LHS based analogue **2.037**, as outlined in Chapter 2. Analogue **2.024** and **2.018** possessed the *ortho* and *meta*-methyl substituents on the LHS phenyl ring of Scaffold 1 respectively. Nonetheless, the inclusion of the cyclohexane ring at the LHS chemical space of these

analogues was still relevant, due to the high antileishmanial activity and low host cell cytotoxicity reported by GRIDD.

To obtain these analogues, a modified version of the optimized pathway described in **Scheme 3.01** was developed. Following the literature, the nucleophilic substitution of step i required several different methods (A-G) to install the appropriate *N*-substituted group of interest.^{1, 7-10} These intermediates (**3.025-3.032**) would then form the desired amine building blocks (**3.032-3.048**) in moderate to high yield.³ This was followed by subsequent amide coupling to obtain the desired analogues (**3.049-3.071**).⁴ The analogue yield ranged broadly in the coupling step (step iv), with the lower yields attributed to the analogues possessing *N*-benzyl and *N*-phenyl rings. These large aromatic groups may cause some steric hindrance during the coupling stage, contributing to the lower yields. However, this was not an issue as each analogue still provided more than sufficient amounts of sample for the array of biological assessments we employed. A summary of the analogues synthesized for this series along with their related yield are listed in **Table 3.02** below.

Scheme 3.02: Synthetic route to achieve N-alkyl and aryl modified analogues of Series 5



Reaction conditions i A) ethylamine, EtOH, THF, reflux/ i B) isopropylamine, EtOH, 80 °C/ i C) propylamine, Et₃N, THF, 110 °C/ i D) butylamine, Et₃N, *n*-butanol, 110 °C/ i E) cyclopentylamine, K₂CO₃, *t*BuOH, THF, 150 °C, microwave assisted/ i F) aniline, acetic acid, dioxane, 110 °C/ i F) phenylmethanamine, acetic acid, dioxane, 110 °C, ii) 2-bromo-1-(4-methoxyphenyl)ethan-1-one/ 2-bromo-1-phenylethan-1-one, ACN, 130 °C, microwave assisted, iii) hydrazine hydrate, 100 °C, microwave assisted, iv) various benzoic acids, DIPEA, DMAP, HBTU, ACN, 50°C.

Table 3.02: Summary of analogues exploring the N-alkyl chain

I.D	Structure	Yield % (step iv)	I.D	Structure	Yield % (step iv)
3.049		60	3.061		94
3.050		65	3.062		41

3.051		68	3.063		36
3.052		48	3.064		23
3.053		79	3.065		77
3.054		68	3.066		57
3.055		50	3.067		53
3.056		40	3.068		90
3.057		50	3.069		66
3.058		93	3.070		20
3.059		48	3.071		39
3.060		55			

Exploration of the chemical space around Scaffold 1 was continued whilst awaiting the biological results of Analogue Series 5, and the biological re-examination of the remaining compound library (Analogue Series 1-2, LHS structural changes and brief RHS structural changes to Scaffold 1). During this time, we decided to move on and continue the exploration around the RHS chemical space of hit **2.001**.

3.05 Analogue Series 6: Further exploration of the substituents around the RHS phenyl ring

Exploration around the RHS chemical space of Scaffold 1 was resumed. Repositioning the *para*-methoxy substituent of hit **2.001** to the *meta* (**2.060**) and *ortho* (**2.061**) positions was previously found to cause a loss of antileishmanial activity, as discussed in Chapter 2 (Section **2.08**). Further studies around this chemical space would also incorporate simple changes to the RHS, keeping the rest of the structure the same as the hit **2.001**, and close analogue **2.059**. These changes focused on altering the hydrogen bonding ability, electron and hydrophobic properties around the RHS phenyl ring, to enable a better understanding of the favourable interactions in this chemical space with the putative binding site/s. The substitution of the chloro (**3.092**, **3.098**, **3.103**) and bromo groups (**3.093**, **3.099**, **3.014**) around the RHS phenyl ring would probe if a more lipophilic, electron withdrawing group was preferred around this ring in place of the *para*-methoxy group (**2.001**) or the unsubstituted RHS phenyl ring (**2.059**). The substitution of these halogens would also explore whether the loss of the ability to accept hydrogen bonds at this position correlated to a loss of antileishmanial activity. The substitution of the fluoro group (**3.094**, **3.100**, **3.105**) would retain the ability to accept hydrogen bonds and determine if a sterically smaller electronegative atom was preferred at this position. The introduction of the strong electron withdrawing groups, namely the cyano (**3.091**, **3.097**) and nitro groups (**3.096**, **3.102**, **3.017**) would also help determine if a more electron poor ring was preferred. These substituents would also investigate whether increase hydrophilicity was preferred.

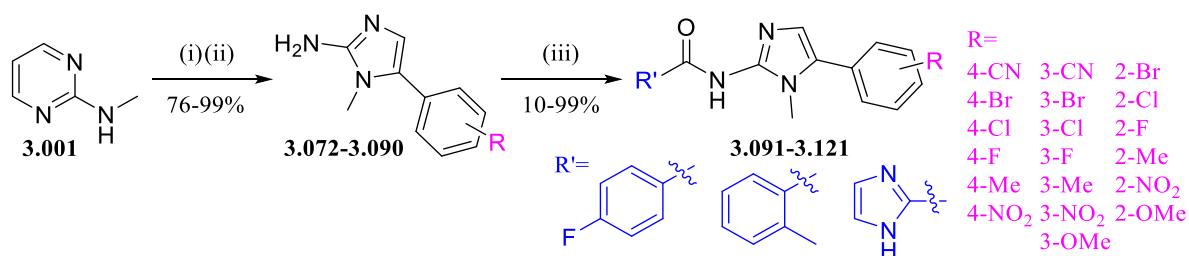
Finally, the electron donating methyl substituents (**3.095**, **3.101**, **3.106**) were also explored. Like the initial methoxy substituents (**2.001**) this would probe if an electron rich ring was preferred within the putative binding site/s, though the methyl groups would allow for an increase in lipophilicity and remove the ability to potentially form hydrogen bonding interactions with the putative binding site/s (refer to **Table 1.06**, Chapter 1 for substituent property comparison).

The scope of this investigation was extended to include analogues bearing structural changes to the LHS aromatic ring. This included pairing the variety of substituents around the RHS aromatic ring, with the *ortho*-methyl substituent at the LHS aromatic ring. This LHS modification was influenced by analogue **2.024**, which was initially reported by our collaborators at GRIDD to exhibit high antileishmanial activity. During this time, analogue **2.024** was considered one of the most potent compounds within our initial library (Analogue Series 1-2). Based on the high antileishmanial activity of **2.024** and synthetic ease, analogues **3.109-3.114** were devised. As discussed in Chapter 2, Section **2.09**, key analogues were reassessed by our collaborators at Bio21, and the LHS 1*H*-imidazole based analogue (**2.042**) was found to be consistently potent against *L. donovani* and selective for the parasite by both independent collaborators. Analogue **2.042** became a new lead compound, thus our focus within this series was redirected. This further influenced the analogues (**3.115-3.121**), which bear the imidazole

ring at the LHS position of the scaffold, paired with various substituents around the RHS aromatic ring (**3.115-3.121**). As this investigation had become quite large, we decided to decrease the scope, limiting substituents around the RHS ring to the cyano, chloro and methoxy groups. These functionalities were diverse enough to probe the different hydrogen bonding ability, electronic and hydrophobic properties preferred within this chemical space.

These analogues were obtained following **Scheme 3.03**, which employs the optimized conditions listed previously in **Scheme 3.01**. Various phenylethanones were utilized in step i/ii to form the amine intermediates **3.072-3.090** via microwave irradiation. This was followed by subsequent amide coupling to obtain the desired analogues **3.091-3.121**. The subsequent analogues synthesised following this route and their relevant reaction yield of step iii are highlighted in **Table 3.03**.

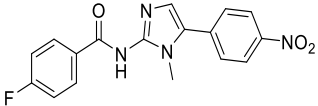
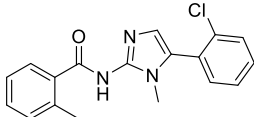
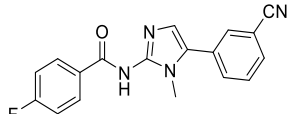
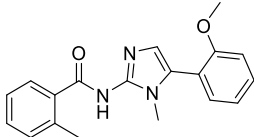
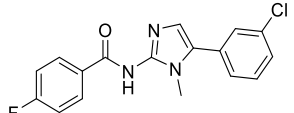
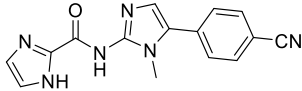
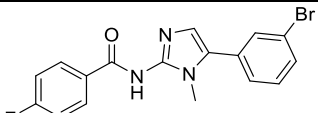
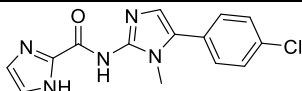
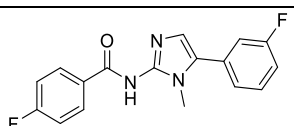
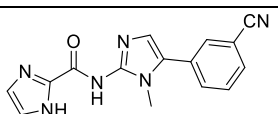
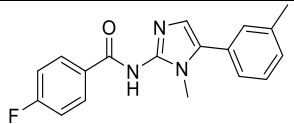
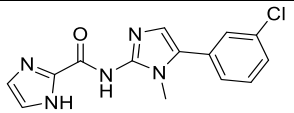
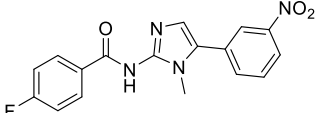
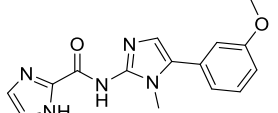
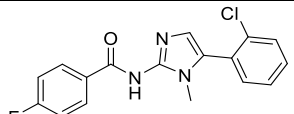
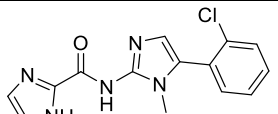
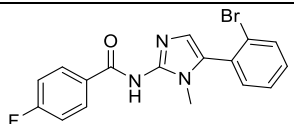
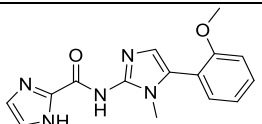
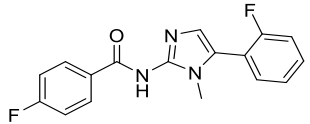
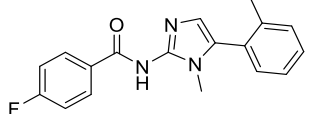
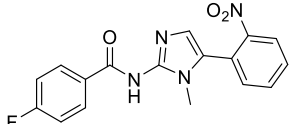
Scheme 3.03: Synthetic route to obtain analogues targeting structural changes to the RHS



Reaction conditions i) various phenylethanones, ACN, 130 °C, microwave assisted, ii) hydrazine hydrate, 100 °C, microwave assisted, iii) various carboxylic acids, DIPEA, DMAP, HBTU, ACN, 50°C or various carboxylic acids DIPEA, DMAP, PyBOP, DMF, 25- 50°C

Table 3.03: Analogues Series 6 continued investigation the RHS chemical space, structures and relevant yields

ID	Structure	Yield % (step iii)	ID	Structure	Yield % (step iii)
3.091		61	3.108		83
3.092		62	3.109		37
3.093		68	3.110		57
3.094		79	3.111		56
3.095		77	3.112		59

3.096		42	3.113		23
3.097		60	3.114		79
3.098		99	3.115		10
3.099		37	3.116		10
3.100		42	3.117		20
3.101		74	3.118		29
3.102		24	3.119		15
3.103		53	3.120		17
3.104		14	3.121		11
3.105		83			
3.106		24			
3.107		35			

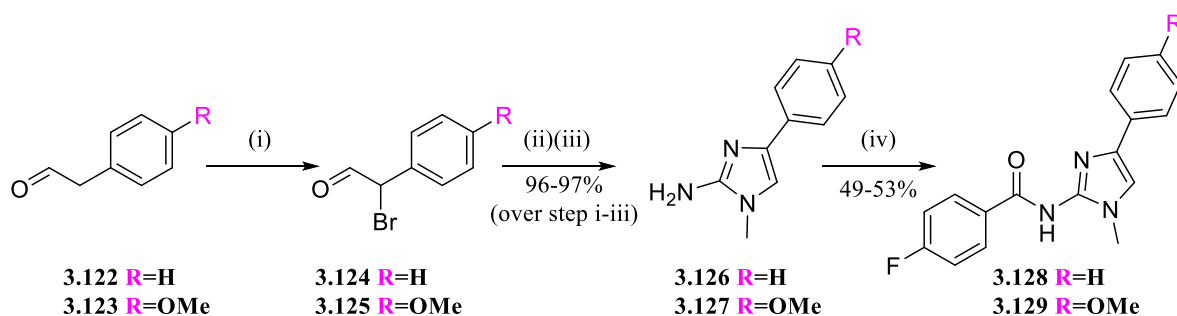
The yields of these analogues were similar to those generated in Chapter 2 for Analogue Series 1-2. Analogues bearing the imidazole ring at the LHS position of the scaffold gave lower product yields, possibly due to the unreactive nature of the imidazole ring. Overall, this was not an issue as sufficient amounts of product were obtained per analogue for biological testing. Due to reagent availability, not

every LHS substituent included in this study was paired with every RHS substitution. This was not necessary as this is only a general probe into the regions of the scaffold.

3.06 Analogue Series 7: Further exploration around the imidazole core

A brief study on shifting the RHS phenyl ring from the 5 to 4 position on the imidazole was explored. This was undertaken to alter the orientation of the overall scaffold and quickly probe which position could provide a better fit within the putative binding site/s. It should be noted that the substitution of the phenyl ring at the 4-position of the imidazole is more commonly reported within the literature. Though the original 5-phenyl-1*H*-imidazole core of Scaffold 1 also looks common, relative to the 4-substituted imidazole it is not.¹¹⁻¹⁴ Additionally, to target the more common 4-phenyl-1*H*-imidazole intermediates, different regiochemistry was required. This is depicted in **Scheme 3.04**, which begins with the bromination of the 2-phenylacetaldehyde derivatives (**3.122-3.123**).^{15, 16} These 2-bromo-2-phenylacetaldehyde intermediates (**3.124, 3.125**) immediately underwent microwave irradiation to form the 4-phenyl-1*H*-imidazol-2-amines (**3.126-3.127**).³ Subsequent amide coupling using the previously optimized conditions was then undertaken to afford the desired analogues (**3.128-3.129**).⁴ Analogue **3.129** was devised around the hit **2.001**, targeting the structural modification around the imidazole core, while the rest of the scaffold remained the same. Analogue **3.128** incorporated the unsubstituted phenyl RHS feature from influenced by our most potent analogue at the time (**2.059**).

Scheme 3.04: Synthetic pathway for 4-phenyl-1*H*-imidazol-2-yl benzamide analogue derivatives **3.128-3.129**

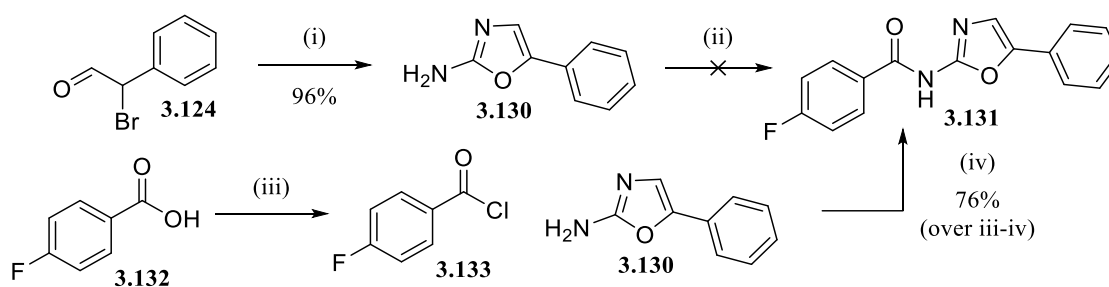


Reaction conditions i) bromine, 1,4-dioxane, 0°C ii) *N*-methylpyrimidin-2-amine, ACN, 150 °C, microwave assisted iii) hydrazine hydrate, 100 °C, microwave assisted iv) 4-fluorobenzoic acid, DIPEA, DMAP, HBTU, ACN, 50°C.

As the 2-bromo-2-phenylacetaldehyde intermediate (**3.124**) had been previously synthesized, it was opportunistic to repurpose it for other analogue studies, where relevant. Hence, **Scheme 3.05** was devised following the literature to utilize intermediate **3.124** as a starting reagent to form the oxazole core of analogue **3.131**. The 2-bromo-2-phenylacetaldehyde (**3.124**) underwent microwave irradiation of with urea to form the phenyloxazol-2-amine building block (**3.130**).^{17, 18} Amide coupling with 4-fluorobenzoic acid was then initially trialed as per the usual coupling conditions listed in **Schemes 3.01-3.03**, however, no reaction occurred. The oxazole ring may have been more unreactive under these conditions than that of the imidazole ring usually employed. To increase reactivity, the *para*-

fluorobenzoic acid **3.132** was converted to the acid halide **3.133** and subsequently reacted with the oxazole amine **3.130** to successfully give analogue **3.131**.¹⁹⁻²¹ Analogue **3.131** was derived from the hit **2.001** and lead compound **2.059**. This analogue was devised to explore whether the change in heteroatom and loss of *N*-methyl group of the original imidazole core would modulate bioactivity, and determine if any specific hydrogen bonding interactions existed between the core and putative bind site/s, while keeping the position of the heteroatoms around the 5-membered aromatic core the same.

Scheme 3.05: Synthetic pathway for oxazole core analogue 3.131



Reaction conditions i) urea, DMF, 160 °C, microwave assisted, ii) 4-fluorobenzoic acid, DIPEA, DMAP, HBTU, ACN, 50 °C, iii) DCM/ DMF (10:0.1), (COCl)₂, 0 °C- rt, iv) DIPEA, DCM, reflux

3.07 Initial biological assessment of a small set of analogues using luminescence expressing *L. donovani* in a Luciferase Assay (UNC)

The long waiting periods associated with receiving the biological results of our analogue library became a large issue within this PhD project as we could not continue to build an SAR profile around Scaffold 1 without reliable biological data. These waiting periods were prolonged due to key personnel changes within the Bio21 group. Additionally, as mentioned in Chapter 2, technical issues arose with our GRIDD collaborators, causing further delays in the biological re-examination of our investigative compounds. As it was uncertain when our growing library of analogues would be biologically evaluated against intracellular *L. donovani*, therefore collaborative efforts were established with the Ainslie group at the University of North Carolina (UNC). A small subset of analogues within our library, yet to be biologically evaluated, was sent to UNC to be assessed against intracellular *L. donovani* using macrophages as host cells.

To determine the antileishmanial activity, a low-throughput *in vitro* luciferase assay was employed. THP-1 monocytes were differentiated into macrophages using PMA. Fully differentiated macrophages were infected with stationary phase luminescence expressing *L. donovani* promastigotes (MOI 10: 1, parasite to host). The strain of *L. donovani* employed expresses firefly luciferase and a red fluorescent protein, LUC and DsRed2 (Ds-Red-lux).²² Promastigotes differentiated into amastigotes within the host cell during the assay. The cells were treated with our test compounds at a concentration range of 1.0-50 µM. Cells were incubated for 72 h. The Luciferase Assay System (Promega) was used to assess

leishmanial viability within the infected macrophages. The luciferase substrate was added to the assay plates and incubated at room temperature for 5 min. Parasite viability was then evaluated via the luminescence intensity, measured using a microplate reader. The IC₅₀ values of the compounds were calculated using a 4-point curve of relative luminescence units versus drug concentration. Compounds were tested in triplicate wells in one experiment.^{23, 24} The complete method is outlined in the Experimental Section.

The viability of the host cells (CC₅₀ value) was determined by dosing uninfected but differentiated THP-1 macrophages with test analogues using a 3-(4,5-dimethylthiazol-2-yl)-2,5-diphenyl-2*H*-tetrazolium bromide (MTT) assay. This is a colorimetric assay used to assess cell metabolic activity. This assay uses nicotinamide-adenine-dinucleotide (NAD(P)H) coenzymes from metabolically active cells which reduce tetrazolium salts to strongly coloured products. This reflects the number of viable cells present and is then quantified by absorbance.^{25, 26} The complete method is also outlined in the Experimental Section. The intramacrophage assay using luminescence expressing *L. donovani* and the MTT cell viability assay both utilize low-throughput systems, thus only key compounds of Scaffold 1 were sent for biological assessment. The complete evaluation of our entire library surrounding Scaffold 1 was not an option using these methods due to the large manual undertaking. The assays were performed in triplicate wells in one experiment (n=1) for the same reason, along with high cost. Key compounds are planned for duplicate testing as future work to minimise cost and manual efforts.

In comparison to the previously described assay methodologies operated by Bio21 and GRIDD, the luciferase assay performed by UNC entails a different readout method. As mentioned, UNC evaluates leishmanial viability within infected macrophages via the luminescence intensity of the assay plates. The assays performed by Bio21, GRIDD (and later collaborative group IPK, to be discussed in Section **3.10**), incorporated automated systems, high content screening (HCS) and imaging using fluorescent dyes to determine the number of amastigotes per macrophage. The UNC intramacrophage luciferase-based assay against *L. donovani* would be used as another complimentary investigative tool to determine anti-parasitic activity. This assay could be potentially used as a “tie-breaker” between the high content intramacrophage assays when divergent activity was reported. Additionally, UNC methods employ a separate MTT colorimetric assay to determine the cytotoxicity of the investigative compounds against uninfected but differentiated macrophage host cells. In contrast, the assays performed by Bio21, GRIDD and IPK (to be discussed, Section **3.10**) assess the parasite and host macrophage viability simultaneously, in other words, host cells are assessed while infected.

Through correspondence with our collaborators at UNC, they stated that the advantage of evaluating the cytotoxicity levels of our investigative compounds against uninfected host macrophages, is that it would directly measure the effect of the compound alone against the host cell. When evaluating the cytotoxicity of compounds within infected cells, it must be considered that the infection itself could

impact host cell survival. The host cell death may be quickened or may become more sensitive if they are already under stress due to parasite infection. However, measuring host cell viability using infected cells is the more clinically relevant method. Nonetheless, both types of assessment have merit, as gaining an understanding the cytotoxic effects on both infected and non-infected host macrophages is required to progress potential lead compounds through the leishmaniasis drug development pipeline.

3.07.1 Initial set of biological results reported by UNC for a small subset of analogues

As mentioned, due to the low-throughput nature of the luciferase assay performed by UNC, smaller batches of compounds were sent at a time for biological analysis. This system was mainly used for Scaffolds 2-5 (discussed in Chapters 4 and 5), which contained much smaller libraries of analogues and more straightforward SAR profiles. Our potential leads depicted above in **Figure 3.01** were sent along with analogues from each series as representatives. Several compounds had previously reported conflicting bioactivity, causing difficulties with developing an SAR profile around Scaffold 1, therefore these compounds would still undergo further validation using complimentary assays by our other collaborators to help confirm true antileishmanial activity.

The first few sets of sets of biological results derived from the *L. donovani* luciferase assay and MTT colorimetric assay performed by UNC are summarised in **Table 3.04**. Analogues **3.013** and **3.015**, which bear the *para* and *ortho*-chloro substituents on the LHS phenyl ring respectively, paired with the unsubstituted RHS phenyl ring, were observed to display potent antileishmanial activity ($IC_{50} < 10 \mu M$) and demonstrated selectivity for the parasite. Strangely, the *meta*-chloro substituent (**3.014**) caused a loss in antileishmanial activity. Repositioning the RHS phenyl ring from the 5-position on the imidazole core to the 4-position was found to be an unfavourable modification, evidenced by analogues **3.128-3.129** which displayed low parasite inhibition. This may suggest that the altered shape and orientation of analogues **3.128-3.129** gave a poor fit within the putative binding site/s and this type of structural modification should be avoided. Finally, replacing the imidazole core with the oxazole (**3.131**) was initially reported to exert very high antileishmanial activity ($< 1.0 \mu M$). This potential new lead analogue encouraged further synthesis incorporating the oxazole core, discussed below in Section **3.08**. Analogue **3.131** was later retested using a lower concentration range (0.1-10 μM) to get a more accurate IC_{50} value (6.5 μM). Though this compound was not as potent against *L. donovani* as originally reported, it was still found to possess antileishmanial activity and was still considered an interesting potential lead compound. Consequently, analogue **3.131** would also undergo physicochemical and metabolic studies.

Table 3.04: Preliminary biological results of various Scaffold 1 analogues using the Luciferase assay to measure antileishmanial activity and the colorimetric MTT assay to measure toxicity

ID	Structure	IC ₅₀ (μ M) ^a	CC ₅₀ (μ M) ^b	ID	Structure	IC ₅₀ (μ M) ^a	CC ₅₀ (μ M) ^b
3.013		7.3	>50 ^c	3.128		>10	>50 ^c
3.014		>50 ^c	>50 ^c	3.129		>10	26.5
3.015		9.9	>50 ^c	3.131		<1.0, 6.5 ^d	33.7

a= anti *L. donovani* activity measured in THP-1 transformed macrophage host cell lines using luminescent expressing *L. donovani*. Experiment performed in triplicate wells in one experiment, n=1 using a concentration range of 1-50 μ M. DMSO was used as sole control against which the percent *L. donovani* viability is calculated

b= host cell toxicity measured in MTT assay with uninfected macrophage host cells. Experiment performed in triplicate wells in one experiment, n=1 using a concentration range of 1-50 μ M. DMSO was used as sole control against which the percent cell viability is calculated

c= <50% activity at the top concentration tested (50 μ M)

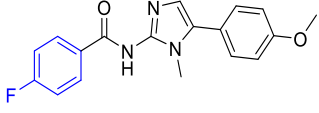
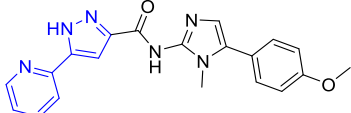
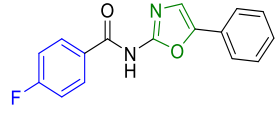
d= this compound was initially found active at a higher concentration and retested here, at lower concentration to achieve a more accurate IC₅₀ (concentration range: 0.1-10 μ M)

3.07.2 Physicochemical and Metabolic analysis of Oxazole analogue 3.131

The physicochemical parameters and *in vitro* metabolic stability of analogue **3.131** is outlined in **Table 3.05** and **Table 3.06** respectively. The physicochemical and metabolic properties of the hits **2.001** and **2.002** are also included to allow for direct comparison.

The physicochemical properties of **3.131** fit within the drug-likeness parameters as previously described in Chapter 1 and 2. Lipinski's Rule of Five was adhered to, as analogue **3.131** reported a low molecular weight, moderate Log D value (< 5) and an appropriate number of hydrogen bond donors (<5) and acceptors (<10).²⁷ Compound **3.131** also maintained a PSA less than 140 Å², and an appropriate number of rotatable bonds (< 10) following Veber's Rule, another drug likeness predicative tool. However, as previously mentioned in Chapter 2, future studies should aim to increase polar surface area (between 140 and 90 Å²) to avoid unneeded and potentially toxic BBB penetration.²⁸ Compared to the hit **2.001** a slight improvement in solubility was reported for **3.131** at pH 6.5 only. Overall, no significant improvement in solubility was observed from **3.131** in comparison to both the hits **2.001** and **2.002**.

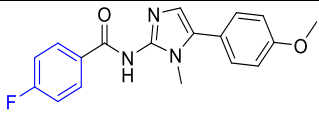
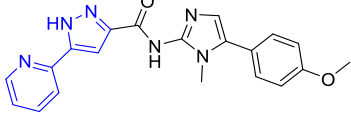
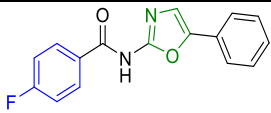
Table 3:05: Key physicochemical parameters of 3.131 compared to hits 2.001 and 2.001

ID/ Structure	Solubility (µg/mL) ^b							
	MW ^a	PSA (Å ²) ^a	FRB ^a	HBD ^a	HBA ^a	cLogD at pH 7.4 ^a	pH 2.0	pH 6.5
 2.001	325	56	4.0	1.0	3.0	3.4	12.5-25	<1.6
 2.002	374	98	5.0	2.0	5.0	2.7	50-100	3.1-6.3
 3.131	282	55	3.0	1.0	2.0	3.4	12.5-25	3.1-6.3

a= Calculated using ChemAxon JChem software, b=kinetic solubility determined by Nephelometry (Sol_{pH})

In comparison to the hits **2.001**, **2.002**, analogue **3.131** did not improve *in vitro* metabolic stability, where a faster rate of degradation was observed in human microsomes, as evidenced by the shorter half-life (19 min) and increased intrinsic clearance *in vitro* (Cl_{int in vitro} = 90 µL/min/ mg protein). In comparison to the hit **2.001**, a marginal improvement to metabolic stability in mouse microsomes was observed for **3.131**. However, overall rapid degradation was reported, suggesting the replacing the imidazole core with an oxazole may not be an ideal structural replacement in relation to microsomal stability *in vitro*. By this stage of the project, a small number of analogues bearing an oxazole core with structural changes to the LHS aromatic ring, had already been synthesized (discussed below, Section **3.08**). If strong antileishmanial activity was correlated to incorporating the oxazole core, further distal changes would be explored in the future to improve physicochemical and metabolic properties.

Table 3:06: Summary of metabolic properties of analogue 3.131 compared to hits 2.001 and 2.002

ID/ Structure	Species	T _{1/2} (min)	Cl _{int in vitro} (µL/min/ mg protein)	Microsome-predicted E _H	Clearance classification ^a
 2.001	Human	59	30	0.54	Intermediate
	Mouse	4.0	396	0.89	High
 2.002	Human	56	31	0.55	Intermediate
	Mouse	89	19	0.29	Low
 3.131	Human	19	90	NA	NA
	Mouse	5.0	352	NA	NA

3.131^{bc}

a = The E_H was used to classify compounds as low (< 0.3), intermediate (0.3 - 0.7), high (0.7 - 0.95) or very high (> 0.95) extraction compounds
b = Apparent non-NADPH mediated degradation (>30% degradation) was observed in human and mouse metabolism control samples. A putative amide hydrolysis product with [MH⁺] of 161 was detected. Predicted *in vivo* clearance parameters are therefore not reported for either species.

c = Calculated mouse metabolism parameters are based on the first 2 time-points (i.e. 2 & 5 minutes) due to rapid degradation and are therefore an estimate only.

NA = Not applicable

3.08 Analogue Series 8: Additive SAR study combining LHS changes with oxazole core

The high antileishmanial activity reported for analogue **3.131** (Section 3.07) encouraged the brief additive SAR study summarised in **Figure 3.04**. This study aimed to incorporate the oxazole ring at the core of the scaffold, and the unsubstituted phenyl ring at the RHS chemical space, influenced by the structure of lead compounds **3.131** and **2.059** respectively. These features would be paired with distal changes to the LHS chemical space. This included substituting the initial *para*-fluoro group possessed by the lead compound **3.131**, with the *para*-chloro (**3.134**) and *para*-methyl (**3.135**) substituents at the LHS phenyl ring of the scaffold. These functionalities were chosen as they had previously exhibited high antileishmanial activity within the intramacrophage assays performed by UNC (analogue **3.013**, Section 3.08) and GRIDD (analogue **2.012**, Chapter 2, Section 2.08) respectively. The cyclohexane ring was also incorporated within the LHS chemical space (**3.136**) during this additive SAR study. This structural change was included as it had also displayed high antileishmanial activity and selectivity for the parasite, as reported by GRIDD (**2.037**, Chapter 2, Section 2.08). Furthermore, we had an interest in pairing a broader range of functionalities at the LHS which had previously demonstrated potency against *L. donovani*. These analogues were obtained following the previously described **Scheme 3.05**, in moderate yields summarised below.

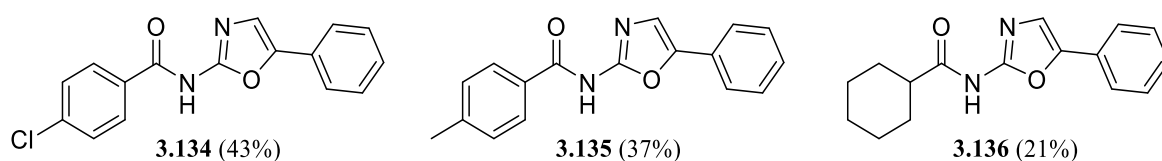


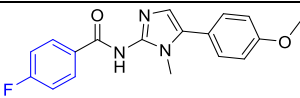
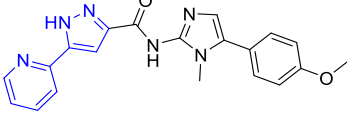
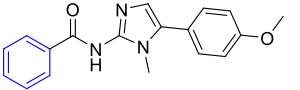
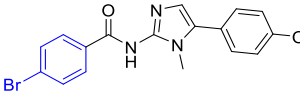
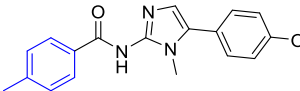
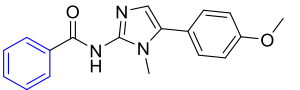
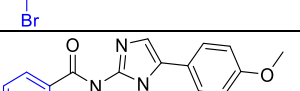
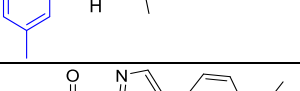
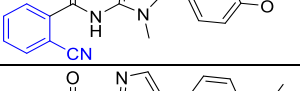
Figure 3.04: Structures of Analogue Series 8, pairing active LHS functionalities with oxazole core and unsubstituted RHS ring, and their relevant yields (step iv of Scheme 3.05)

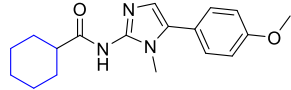
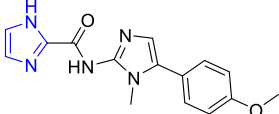
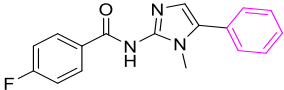
We had planned to continue this additive SAR study and incorporate other structural changes to the LHS chemical space, including the imidazole ring influenced by **2.042** and other functionalities that had previously reported high antileishmanial activity. However, no further synthesis for this series occurred. Synthesis of compounds around Scaffold 1 was paused once the re-testing of analogues was achieved.

3.09 Challenges with GRIDD retesting of key compounds of Analogue Series 1-2

As previously described, many of our key analogues from Series 1-2 (LHS structural changes and brief RHS changes respectively) displayed conflicting biological activity between independent *L. donovani* intramacrophage assays, previously highlighted in **Figure 3.01**. This made SAR interpretation challenging, therefore biological reassessment of these analogues was required, to gain a better insight into the true levels of parasite inhibition these analogues could exhibit. Both independent groups, Bio21 and GRIDD, performed this biological reassessment using their same respective high content screening (HCS) intramacrophage assays against *L. donovani*, as previously detailed in Chapter 2. The reassessment by GRIDD was accomplished first and the results are summarized in **Table 3.07**. The previous activity of these key compounds determined by GRIDD in the first few rounds of testing are also listed for comparative ease. Unexpectedly, the high antileishmanial activity previously reported was not confirmed during this re-examination, and conflicted biological results were obtained.

Table 3.07: Comparison of activity and cytotoxicity against *L. donovani* in THP-1 macrophages of key compounds of analogue series 1-2 in GRIDD assay reassessment. Hit compounds are highlighted in blue

I.D	Structure	GRIDD ^{ab}		GRIDD Retest ^{ae}	
		IC ₅₀ (μM)	CC ₅₀ (μM)	IC ₅₀ (μM)	CC ₅₀ (μM)
2.001		>80 ^{d†}	>80 ^{d†}	63% at 80 μM*	55% at 80 μM*
2.002		10 ± 0.090 ^c	>80 ^{cd}	-	-
2.008		>80 ^{d†}	>80 ^{d†}	>80 ^{d††}	>80 ^{d††}
2.009		2.1 ± 0.62 [†]	>80 ^{d†}	>80 ^{d†}	57% at 80 μM ^{*†}
2.012		2.3 ± 0.17 ^{c†}	57% at 80 μM ^{c*†}	62% at 10 μM ^{f*†}	52% at 40 μM ^{f*†}
2.015		1.7 ± 0.10 [†]	>80 ^{d†}	65% at 80 μM*	>80 ^d
2.018		0.45 ± 0.040 [†]	>80 ^{d†}	66% at 40 μM*	60% at 40 μM*
2.022		>80 ^{d†}	>80 ^{d†}	>40 ^{d††}	>40 ^{d††}
2.024		0.38 ± 0.040	>80 ^d	58% at 40 μM ^{*†}	>80 ^{d†}

2.037		$1.59 \pm 0.10^{\dagger}$	$>80^{\dagger}$	$>80^{\dagger}$	$>80^{\dagger}$
2.042		5.3 ± 0.23^c	$>80^{cd}$	57% at 20 μM^{f*}	$>80^{df}$
2.059		$0.32 \pm 0.050^{\dagger}$	$>80^{\dagger}$	64% at 20 μM^*	60% at 40 μM^*

a = anti *L. donovani* activity and toxicity measured in THP-1 transformed macrophage host cell lines using a top concentration of 80 μM (14-point curve). Experiment performed in duplicate wells. Values are means of two experiments, n=2.

b= control compounds for GRIDD *L. donovani* intramacrophage assay. Average from experimental replicates; Amphotericin B $\text{IC}_{50}= 0.39 \pm 0.0070 \mu\text{M}$, $\text{CC}_{50}= 1.5 \pm 0.070 \mu\text{M}$, VL-2098 $\text{IC}_{50}= 1.8 \pm 0.17 \mu\text{M}$, $\text{CC}_{50}> 80\mu\text{M}$, DNDI-1044 $\text{IC}_{50}= 0.40 \pm 0.014 \mu\text{M}$, $\text{CC}_{50}> 80 \mu\text{M}$.

c= control compounds for GRIDD *L. donovani* intramacrophage assay. Average from experimental replicates; Amphotericin B $\text{IC}_{50}= 0.076 \pm 0.0020 \mu\text{M}$, $\text{CC}_{50}= 0.73 \pm 0.18 \mu\text{M}$, VL-2098 $\text{IC}_{50}= 0.67 \pm 0.21 \mu\text{M}$, $\text{CC}_{50}> 40\mu\text{M}$, DNDI-1044 $\text{IC}_{50}= 0.13 \pm 0.037 \mu\text{M}$, $\text{CC}_{50}> 40 \mu\text{M}$.

d=<50% activity at the top concentration tested (80 μM). Values are the means of two experiments

e= control compounds for GRIDD *L. donovani* intramacrophage assay. Average from experimental replicates; Amphotericin B $\text{IC}_{50}= 0.069 \pm 0.0020 \mu\text{M}$, $\text{CC}_{50}= 0.94 \pm 0.044 \mu\text{M}$, VL-2098 $\text{IC}_{50}= 0.73 \pm 0.017 \mu\text{M}$, $\text{CC}_{50}> 40\mu\text{M}$, DNDI-1044 $\text{IC}_{50}= 0.22 \pm 0.039 \mu\text{M}$, $\text{CC}_{50}> 40 \mu\text{M}$.

f= control compounds for GRIDD *L. donovani* intramacrophage assay. Average from experimental replicates; Amphotericin B $\text{IC}_{50}= 0.065 \pm 0.0060 \mu\text{M}$, $\text{CC}_{50}= 0.73 \pm 0.0040 \mu\text{M}$, VL-2098 $\text{IC}_{50}= 0.64 \pm 0.068 \mu\text{M}$, $\text{CC}_{50}> 40\mu\text{M}$, DNDI-1044 $\text{IC}_{50}= 0.21 \pm 0.013 \mu\text{M}$, $\text{CC}_{50}> 40 \mu\text{M}$.

d= control compounds for GRIDD *L. donovani* intramacrophage assay. Average from experimental replicates; Amphotericin B $\text{IC}_{50}= 0.076 \pm 0.002 \mu\text{M}$, $\text{CC}_{50}= 0.73 \pm 0.18 \mu\text{M}$, VL-2098 $\text{IC}_{50}= 0.67 \pm 0.21 \mu\text{M}$, $\text{CC}_{50}> 80\mu\text{M}$, DNDI-1044 $\text{IC}_{50}= 0.13 \pm 0.037 \mu\text{M}$, $\text{CC}_{50}> 80 \mu\text{M}$.

* CC_{50} value is determined from a sub-efficacious curve

† Out of solution in media reported between 800-20 μM during GRIDD assay. Solubility in the intermediate dilution in medium may have contributed to a sub-efficacious curve

\pm standard deviation

From this biological reassessment, GRIDD could not generate and IC_{50} values for many of the analogues listed in **Table 3.07 (2.001, 2.012, 2.015, 2.018, 2.024, 2.042, 2.059)**. These compounds displayed some antileishmanial activity (> 50% inhibition) but were not able to reach a top plateau (usually > 90 % inhibition in the plateau of activity), thus an IC_{50} value was not able to be determined from the sub-efficacious curve these compounds provided. The biological results of these analogues were reported by GRIDD as percentage inhibitions at certain concentrations where greater than 50 % activity was observed, though were not enough to achieve meaningful inhibition of the parasite, following their methods. To obtain an absolute IC_{50} value following the methods performed by GRIDD, these analogues required testing at higher concentrations. For the purposes of this biological re-examination, this would be even more time consuming and unnecessary as we merely aimed to confirm whether the high antileishmanial activity initially reported could be replicated. Solubility issues were reported once again for **2.009, 2.012** and **2.024**, where these compounds were noted to drop out of solution in media very easily. This may have contributed to the poor parasite inhibition reported for these analogues, as an inability to remain in solution would cause a decreased ability to then permeate through the cell and exert antileishmanial effects. Solubility issues were also reported for analogue **2.037**, and our collaborators at GRIDD suggested that this may have contributed to the loss of antileishmanial activity observed. However, this seemed somewhat unlikely to us, as replacing the aryl system with the saturated cyclohexane ring at the LHS region of Scaffold 1 would have largely increased the likelihood of higher solubility, following Lovering *et al.*²⁹ Furthermore, previous physicochemical studies detailed in Chapter 2, Section **2.11**, reported **2.037** had demonstrated improved solubility, when compared to the

hit **2.001** as well as analogues **2.015**, **2.018**, **2.042**, each of which did not report solubility issues during the GRIDD biological reassessment. Albeit, compound **2.037** reported improved solubility at pH 2.0 and/or pH 6.5, which is more acidic than physiological pH. Overall, it is uncertain why analogue **2.037** was unable to replicate the high antileishmanial activity reported in the initial assay. This sentiment was also true of key analogues **2.015**, **2.018**, **2.042**, **2.059** which did not report solubility issues during the biological reassessment yet reported poor parasite inhibition. Correspondence with GRIDD stated the only technical difference between the assays was the plate washer used. The “old” plate washer used in the initial assays gave greater variability in cell loss than the “new” used to retest the key analogues. They have stated however that this was not significant enough to make this level of difference. It may be likely that a technical or human error may have occurred during the initial assays performed, and/or during the reassessment. Correspondence with our other independent collaborators have suggested it may be possible that simply the wrong compounds were initially tested, since complete divergence in antileishmanial activity is observed for most of these key compounds, particularly **2.009** and **2.037**. To further illustrate the conflicting activity between the GRIDD biological assays, representative dose response curves for several of the key compounds have been included below in **Figure 3.05a-n**. The initial dose-response curves are shown below on the LHS and their associated re-examination on the RHS. Each of the red curves shown within **Figure 3.05a-n** was used to derive the IC₅₀ value or percentage inhibition at certain concentrations, where compound was not able to reach > 90% inhibition against *L. donovani*. The blue curve measures host cell viability. The increase in drug concentration is depicted by the x-axis, and the increase in parasite inhibition (red curve) and increase in cytotoxicity against the host cell (blue) are both measured by the y axis as percentage inhibition. A host cell was defined as infected if the host cell contained more than 3 parasites within the cytoplasm boundary. Some noise was observed therefore a line of best fit was used. These experiments were undertaken in duplicate in wells per experiment and was repeated a second time (i.e. n=2).

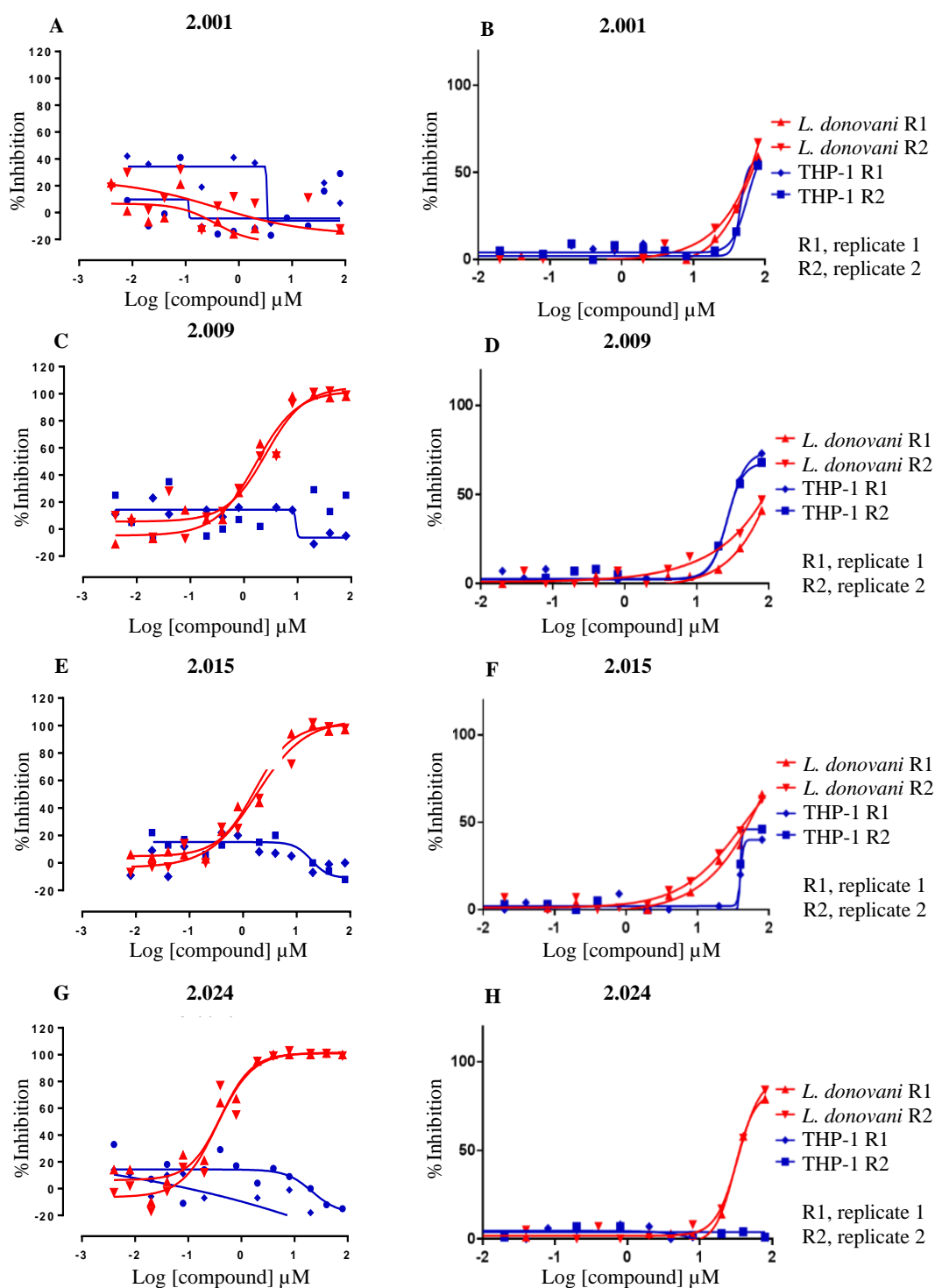


Figure 3.05a-b: Comparison of Dose response curves provided by GRIDD, the initial curve (A) and retested (B) of 2.001. Figure 3.05c-d: Comparison of Dose response curves provided by GRIDD, the initial curve (C) and retested (D) of 2.009. Figure 3.05e-f: Comparison of Dose response curves provided by GRIDD, the initial curve (E) and retested (F) of 2.015. Figure 3.05g-h: Comparison of Dose response curves provided by GRIDD, the initial curve (G) and retested (H) of 2.024. The red curves measures the compound concentration (x axis) against % inhibition (y axis) of parasites to determine antileishmanial activity (IC_{50}), the blue curve measures compound concentration (x axis) against the viability of the THP-1 transformed macrophages (y axis) to determine the cytotoxicity against the host cell (CC_{50}).

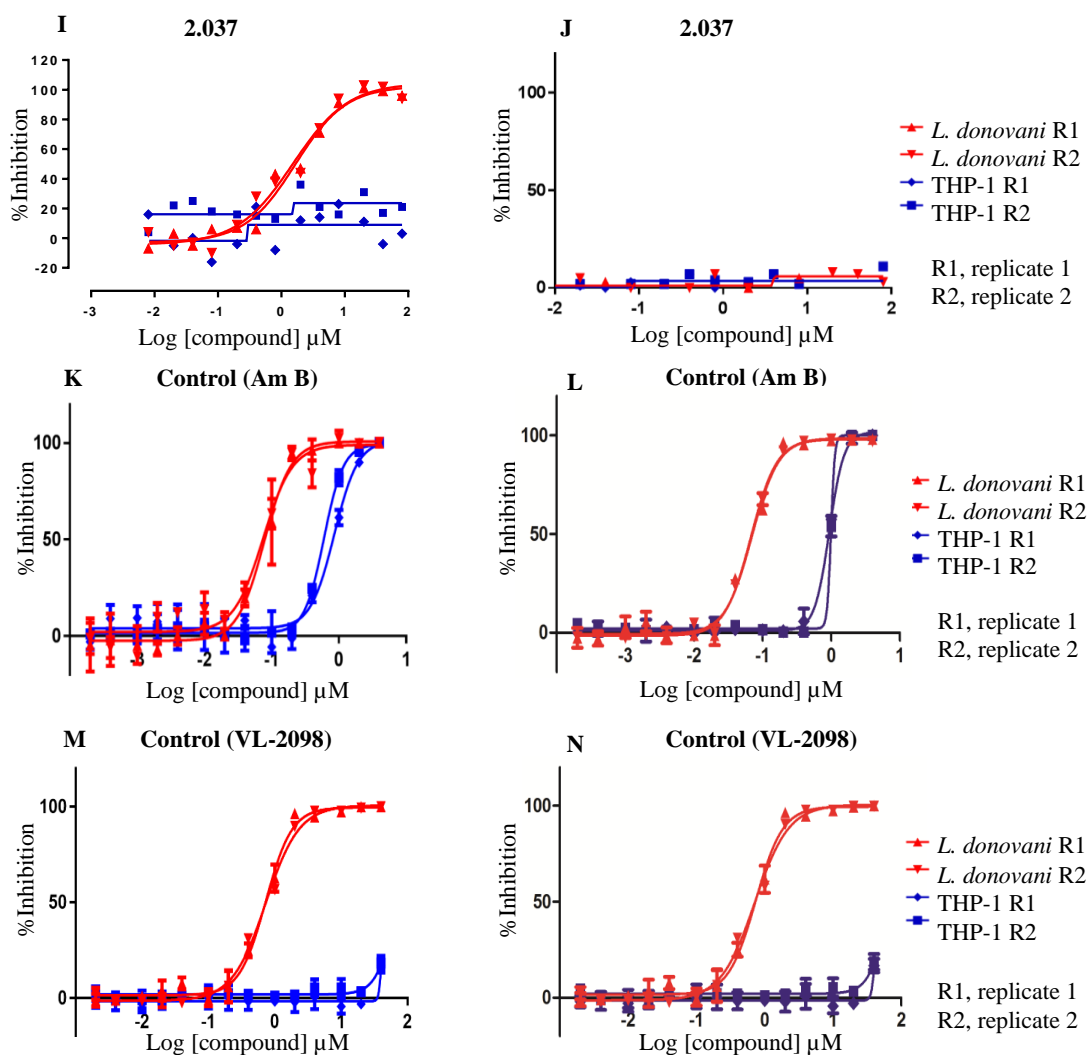


Figure 3.05i-j: Comparison of Dose response curves provided by GRIDD, the initial curve (I) and retested (J) of 2.037. Figure 3.05k-l: Comparison of Dose response curves provided by GRIDD, the initial curve (K) and retested (L) of Amphotericin B control compound. Figure 3.05m-n: Comparison of Dose response curves provided by GRIDD, the initial curve (M) and retested (N) of VL-2098 control compound. The red curves measures the compound concentration (x axis) against % inhibition (y axis) of parasites to determine antileishmanial activity (IC_{50}), the blue curve measures compound concentration (x axis) against the viability of the THP-1 transformed macrophages (y axis) to determine the cytotoxicity against the host cell (CC_{50}).

Based on the dose response curves for the compounds **2.009**, **2.015**, **2.024**, **2.037** strong antileishmanial activity was originally observed during the initial biological assessments of the compounds (LHS dose response curves, C, E, G, I respectively). However, this was not at all replicated during the biological re-evaluation of these analogues, demonstrated in the related dose response curves D, F, H, J (pictured at the RHS). During the biological reassessment performed by GRIDD, compounds **2.009**, **2.015**, **2.024** exhibited some antileishmanial activity, though at higher concentrations only, which is not ideal for a

lead candidate. Additionally, the antileishmanial activity was not significant enough to reach a top plateau (> 90% inhibition), thus IC₅₀ values were not able to be determined. This suggested that the initial highly potent values previously reported by GRIDD seemed to have overstated the antileishmanial potency exerted by the investigative compounds.

Compound **2.037** had previously reported strong antileishmanial activity as demonstrated in **Figure 3.05i**, and consequently had influenced further SAR studies around Scaffold 1. However, the biological re-evaluation of **2.037** by GRIDD found that the compound exhibited no inhibition against the parasite, as evidenced by the dose response curve in **Figure 3.05j**. This analogue was also found inactive within the initial intramacrophage assay performed by Bio21 (Chapter 2, Section **2.09**). It seemed the initial results by GRIDD may have provided a false positive and the cyclohexane structural change at the LHS of the chemical space was undesirable. Interestingly, during the initial biological assessment performed by GRIDD, the hit **2.001** reported both no inhibition of parasites and solubility issues. However, re-evaluation of hit **2.001** found that some antileishmanial activity, albeit sub-optimal activity was observed at higher concentrations. This is depicted below in **Figure 3.05a-b**. It seemed that the antileishmanial activity of hit **2.001** observed during the biological reassessment correlated to increased cytotoxicity against the host macrophage. This phenomenon was also observed for analogues **2.009** and **2.015** and may indicate that these compounds were not selective for the parasite over the host cell, or that it may employ and impact the macrophage within its mode of action, of which we are not yet privy to. Yet, it is strange that this increase in host cell cytotoxicity was not observed during the first rounds of testing. Nonetheless, the antileishmanial activity observed within these retested compounds was not significant enough to further influence additive SAR studies.

The GRIDD intramacrophage IC₅₀ values calculated for each of the positive controls employed; namely amphotericin B, VL-2098 and DNDI-1044 were consistent with the values previously reported. As previously mentioned, throughout this thesis the IC₅₀ values calculated for amphotericin B, VL-2098 and DNDI-1044 reproducibility fell between 0.065-0.39 μ M, 0.57-1.8 μ M and 0.13-0.40 μ M, suggested limited variability exists between the assays.³⁰⁻³⁴ The dose response curves of amphotericin B and VL-2098 are depicted in **Figures 3.05k-n**, which serves as a visual demonstration of the consistency achieved between the control compounds utilized within the initial assay and the biological reassessment of the compounds outlined **Figures 3.05a-n**. From these results, it would seem the assay itself had not failed. As stated, it is uncertain why such conflicting results were obtained between the initial intramacrophage assay and the retest both performed by GRIDD. We could not determine if the issue was derived from the scaffold itself. It may be that these key compounds of Scaffold 1 actually possess antileishmanial activity, though do not interact tightly with the putative binding site/s and/or do not interact in the exact same way or in the same orientation within the putative binding site/s. Another possibility to consider is that the scaffold may not be selective for one type of binding site and may act more promiscuously. Targeting *Leishmania spp.* is still considered quite difficult, due to its evasiveness

and its intracellular environment. There is evidence in the literature of previously reported potent compounds against *L. donovani*, or other visceral leishmaniasis causing species to have later been reported sub-optimal.³⁵

Overall, this suggests true activity against this parasite can be difficult to determine at times. However, we could not count out the possibility that a technical or human error had occurred during these biological assessments. Overall, we still do not have a solid understanding as to why these compounds continued to give such confusing non-confirmative biological results. To understand why these conflicting results were reported, a more in-depth analysis would be required around the GRIDD intramacrophage assay, which was outside the scope of this thesis. Instead, this group of key analogues was reassessed by other independent groups to further confirm any true activities within this scaffold, and further understand whether these deviating results are due to the assay performed or the scaffold itself. This is described in Section **3.12**.

The hit **2.002** was not retested, we had hoped to reassess this compound and continue biological assessments by GRIDD. Though, we had to cease our collaborative efforts regarding antileishmanial projects (at least for the time being) with GRIDD. This was due to arising technical issues and a need to slow down on routine *L. donovani* assays. This led to new collaborative efforts with other independent groups, namely the Ainslie group (UNC) and the No group at Institut Pasteur Korea (IPK). Return in personnel within our Bio21 collaborators led to timelier and more routine assay performance, therefore a pause with one of our collaborators was not an issue.

3.10 Brief outline of *L. donovani* intramacrophage assay performed by IPK and summary of all intramacrophage assays used throughout Scaffold 1 analysis

The somewhat confusing, divergent biological results obtained for key compounds of Scaffold 1 led to us further reaching out to other independent groups in search for answers. The biological assessment of our entire library of analogues around Scaffold 1 was continued by Bio21 using their intramacrophage assay against *L. donovani* amastigotes. The assay methods were detailed in Chapter 2, Section **2.09** and are also outlined within the Experimental Section. Time constraints and the need to reach a better understanding around our scaffold, led us to branching out our collaborative efforts to include the No group of the Institut Pasteur Korea (IPK). Interest in this group came about, as their HCS intramacrophage assay against *L. donovani* is validated, routinely used, and employs high-throughput methods. They would be able to handle the somewhat large number of analogues that we had accumulated within our library. Furthermore, this group is a part of the DNDi NTD booster initiative, discussed in Chapter 1, suggesting their work in this field is reliable.³⁶

The HCS intramacrophage assay performed by IPK was similar to the assay methodologies followed by Bio21 and GRIDD, though not identical. Consequently, complimentary but not identical results were

anticipated between the independent biological groups.³⁷⁻³⁹ This assay employs differentiated, non-dividing human acute monocytic leukemia cells (THP-1) host cells. The THP-1 host cells were transformed into macrophages via PMA. The cells were infected with *L. donovani* promastigotes (MOI 20:1, parasite to host). The promastigotes were differentiated into amastigotes within the host macrophage cells. Infected cells were treated with our investigative compounds at a concentration range of 0.2-100 μM using a 10-point dose-response format to calculate the 50% inhibitory concentrations (IC_{50}) along with assessing the viability of the host THP-1 macrophages (CC_{50}). After the addition of our investigative compounds, cells were incubated for 72 h. Amphotericin B and miltefosine were used as positive controls and DMSO (0.5% v/v) as the negative control. After incubation, assay plates were stained with DRAQ5, a far-red DNA stain for fluorescent cellular imaging applications.⁴⁰ Plates were read and imaged using an Operetta[®] automated microscope and further analysed using Columbus software to quantify parasite numbers, host cell numbers and infection ratios. Using DRAQ5, the larger size nucleus of the macrophages was detected first. Host cell boundary masking was performed, using the low-intensity signals from the cytosol (another application of DRAQ5). The small sized nucleus signal was detected with DRAQ5 were then used to identify the parasites within the mask area of the macrophage. The infection ratio was determined with the value of the number of infected macrophages, divided by the number of macrophages. The average number of parasites per macrophage was defined by the value of the number of parasites divided by the number of infected macrophages in the image acquired.³⁹

The IPK intramacrophage IC_{50} values calculated for the controls; miltefosine and amphotericin B reproducibility fell between 1.1-2.3 μM and 0.26-0.83 μM respectively, throughout this thesis. This is consistent with values previously reported and indicates limited experimental variability between assays.^{30-32, 41} For the sake of transparency, miltefosine, amphotericin B are presented for each IPK experiment throughout this thesis.

A summary of comparison of the conditions used for each HCS intramacrophage assay is outlined in **Table 3.08**, highlighting notable differences between each method. This table is derived from the comparison section of between GRIDD and Bio21 bioassays in Chapter 2, Section 2.09. Each method has been developed for reproducibility and involve similar high-content screening (384 well) assays with automated image acquisition and analysis.³⁷⁻³⁹ Several notable differences between the IPK intramacrophage assay and the previously described GRIDD and Bio21 assays are listed below.

- **Parasite strain and culture:** The strain utilized by IPK, *L. donovani* MHOM/SD/62/1S-CL2d is a relevant clinical isolate source from Sudan, commonly used within the literature.^{42, 43} M199 medium is also frequently used for promastigote cultivation.⁴⁴
- **Parasite infection:** Promastigotes are used to induce infection of host cells following the IPK methodology, the parasites would then differentiate into the clinically relevant amastigote stage

intracellularly during the assay. This differs from the methods followed by Bio21, which use axenic amastigotes to induce host cell infection. Using the promastigote stage of the parasite lifecycle to infect host macrophages is commonly used within literature.^{38, 39, 44, 45} Through correspondence with our collaborators at IPK, the use of promastigotes to induce infection is easier to maintain for scale up methods and can be used to conduct the larger scale screening undertaken at IPK. The differences between infection has been previously detailed in Chapter 2.

- **Drug incubation length:** A 72 h incubation period was employed by IPK and Bio21 and is also commonly used within the literature.^{31, 37} This incubation period differs from the GRIDD intramacrophage assay (96 h), however since we were relying less on the GRIDD assay for further biological testing, we would not focus on this difference further.
- **Multiplicity of infection (MOI):** The MOI differs between each assay, though all fit within acceptable ranges. As described in Chapter 2, Infection ratios of 5-10:1, parasite to host are quite common though 20:1 has also been commonly used within the literature.^{31, 37-39, 46, 47} Correspondence with our collaborators at IPK have stated they utilize a higher MOI (20 :1) in order to achieve a higher infection ratio, leading to good Z' for HTS.

Imaging acquisition: The staining protocol performed by IPK involves DRAQ5 to determine the sizes and cell parameters of both the parasite and host cells. As outlined in Chapter 2, the type of fluorescent stain used should not affect viability or proliferation. Furthermore, the imaging system used per independent group should each be well-tuned for the type of acquisition and analysis used.³⁹

The low throughput intramacrophage assay performed by our collaborators at UNC was also included in **Table 3.08**, to encompass all the *L. donovani* intramacrophage assays used to evaluate our investigative compounds throughout this thesis, for convenience to the reader. As stated in Section **3.07**, this assay involved measuring the viability of parasites via the luminescence intensity of the assay plates, using a microplate reader. This differs from the HCS intramacrophage assays employed by GRIDD, Bio21 and IPK, which involve staining assay plates with fluorescence probes and automated imaging and analysis. Due to the different readout methods used to determine *L. donovani* viability, the UNC method is placed separately within **Table 3.08**. As this is a validated method, it was used as a complimentary, parallel method to assess the true activities of our analogues.²³ Identical results were not expected between independent groups, though we did anticipate somewhat concurrent biological results. This is discussed further below in Section **3.11**. All biological methodologies are described in the Experimental Section.

As detailed in Chapter 2, Section **2.09**, based on the differences between the independent assays outlined here, we cannot predict how each varying condition could potentially alter biological outcomes. We also cannot determine why an investigative compound may report contradictory biological results. This

required a more depth investigation, outside the scope of this PhD medicinal chemistry project. At this stage, we can merely acknowledge the differences that exist with the above **Table 3.08**.

Table 3.08: Summary of methodology of all intracellular assays against *L. donovani* performed by all biological collaborators for Scaffold 1, including a comparison of the high through put fluorescent staining and imaging assays²³

37-39

Intracellular imaging assay against <i>L. donovani</i> (HCS, fluorescent staining)				Intracellular assay against luminescent <i>L. donovani</i> , low through put
Method parameter	GRIDD	Bio21	IPK	UNC
Strain	<i>L. donovani</i> MHOM/IN/80	<i>L. donovani</i> LRC L52	<i>L. donovani</i> MHOM/SD/62/1S-CL2d	<i>L. donovani</i> LV82 expressing firefly luciferase and a red fluorescent protein, LUC and DsRed2 promastigotes (Ds-Red-Lux) ²²
Parasite culture	Promastigotes maintained in modified M199 Hanks salt medium, pH 6.8, supplemented with 10% FBS at 27°C.	Promastigotes RPMI 1640, pH 7.4, supplemented with 10% FCS at 27°C. Axenic amastigotes were obtained following the differentiation of stationary-phase promastigotes in fresh medium (SDM-79, supplemented with 20% FCS at pH 5.5) for 4 days at 33°C	Promastigotes were cultured in modified M199 medium supplemented with 10% FBS serum, penicillin and streptomycin at 28°C.	Promastigotes maintained in modified M199 medium, supplemented with 10% FBS and antibiotic cocktail (penicillin, streptomycin) at 26°C.
Host cell	THP-1	THP-1	THP-1	THP-1
Plate number of wells	384	384	384	96
THP-1 seeding concentration	12,500 cells/well	6 x 10 ³ cells/well	0.8 x 10 ⁴ cells/well	2.5 x 10 ⁴ cells/ well
THP-1 seeding media	RMPI supplemented with 10% FCS medium containing 25 ng/mL PMA	RMPI supplemented with 10% FCS, penicillin and streptomycin medium. Addition of 50 ng/mL PMA for THP-1 differentiation	RMPI 1640 complete medium supplemented with 10% FBS, Addition of PMA for THP-1 differentiation	RMPI media + 1% P/S + 10% FBS + 0.05mM beta mercaptoethanol. Addition of PMA for THP-1 differentiation
Liquid Handling	Automated: BioTek EL 405 liquid handling	Automated: BioTek EL 406 liquid handling washer/	Automated: Thermo Fischer Scientific Multidrop Combi	Manual

	washer/ dispenser, Bravo liquid handler (drug/assay plate dilutions)	dispenser, Caliper Sciclone ALH 3000 workstation (drug/ assay plate dilutions)	Reagent Dispenser (assay plates). Apricot Personal Pipettor (drug plates and serial dilutions). Digilab HummingBird (Drug plate transferred to assay plate).	
Host cell incubation	24 h, 37°C in the presence of 5% CO ₂	24 h, 37°C in the presence of 5% CO ₂	48 h, 37°C in the presence of 5% CO ₂	72 h, 37°C in the presence of 5% CO ₂
Parasite infection	Promastigote infection (differentiate intracellularly during the assay)	Axenic Amastigote infection	Promastigote infection (differentiate intracellularly during the assay)	Promastigote infection (differentiate intracellularly during the assay)
Drug incubation period	96 h	72 h	72 h	72 h
MOI (parasite: host)	5:1	10:1	20:1	10:1
Drug concentration used	Compounds ranged from 0.004 to 80 µM to formulate a 14-point concentration response curve.	Compounds ranged from 0.195 to 100 µM to formulate a 10-point concentration response curve.	Compounds ranged from 0.195 to 100 µM to formulate a 10-point concentration response curve.	Compounds ranged from 1.0 to 50 µM for general screening. To obtain a more accurate A concentration range of 1-10 µM was used to determine more accurate IC ₅₀ value
Readout	Fluorescence probe, acquire and analyse images	Fluorescence probe, acquire and analyse images	Fluorescence probe, acquire and analyse images	Luminescence probe, Luciferase Assay System Promega, E1501, microplate reader
Probe/ Stain	Cell Mask Deep Red, SYBR Green	CMRA, CMFDA, DAPI	DRAQ5	Luciferase substrate (Luciferase Assay System Promega, E1501)
Acquisition	Opera high-content imaging system	Cellomics Colocalization V4 BioApplication	Operetta High Content Imaging System	Microplate reader (Synergy HT, Biotek)
Determine host cell toxicity	Same assay	Same assay	Same assay	MTT colorimetric assay

3.11 Overcoming challenges around conflicting biological results associated with various analogues developed around Scaffold 1: Setting guidelines to interpret biological activity and develop a more reliable SAR profile

As detailed in Sections 3.01 and 3.09, we had obtained conflicting biological data for key analogues of Scaffold 1. This caused difficulties around interpreting SAR for this compound class. To overcome these issues, broader guidelines were defined within this early hit-to-lead PhD project for considering “true” antileishmanial activity and selectivity. Compounds would undergo biological evaluation by at least Bio21 and IPK, using their HCS intramacrophage assays against *L. donovani*, to be performed more routinely.

Within Analogue Series 1-2 (LHS and brief RHS investigation of Scaffold 1), to be considered active, these analogues of interest should display activity within at least 2 out of 4 collective assays we employed overall (GRIDD, Bio21, IPK and UNC). Due to the low throughput nature of the luciferase assay, not every analogue within our compound library could be evaluated by our collaborators at UNC. This assay was used more as a confirmatory tool and/or tie breaker if the results of the HCS intracellular assays were conflicting. Though this assay involved differing readout methods to determine biological activity, similar antileishmanial activity was still anticipated between each assay, as a potent compound was expected to exhibit parasite inhibition regardless of the assay used. This approach would be extended to confirming the biological results of the rest of the analogue library. “True” antileishmanial activity would be considered, if a compound displayed convergent activity in 2 out of 2 bioassays (Bio21 and IPK) or 2 out of 3 bioassays employed (Bio21, IPK and UNC) where applicable.

Within Analogue Series 1-2, several analogues underwent biological testing using the same intramacrophage assay more than once (initial testing and retesting performed by the same biological group). If biological variability existed for an individual analogue between this same assay, in such cases we may also look to the other assays, using the remaining majority of results to help determine if correlating values and thus “true” potency was demonstrated.

It was also difficult to compare analogues to each other at times, and determine which structural change correlated to superior antileishmanial activity. This was due to the variable IC₅₀ values reported between each assay for one individual compound. To build an SAR profile using the large amounts of biological data we had amassed, overall values were used for this project (high antileishmanial activity with 2 out of 3 assays as above).

As mentioned throughout this chapter, the *L. donovani* intramacrophage assay performed by each of our collaborators were not identical to one another, therefore we did not expect the biological results to be identical. To overcome this potential variability, we aimed for compounds to display convergent

results that did not differ by a large amount. To help determine the “true” antileishmanial activity of compounds, the following guidelines were set for this early hit-to-lead project.

- A compound would be considered to have high antileishmanial activity for this early stage hit-to-lead campaign if IC₅₀ values < 10 µM were reported in 2 out of the 3 independent intramacrophage assays used, or 2 out of the 2 independent assays where appropriate. Compounds exhibiting IC₅₀ values around 10 µM would not normally be considered to possess “high” activity in later stage lead development projects, involving more optimized lead compounds, where sub-micromolar values are more deserving of this description. However, for the purposes of this early lead PhD project compounds exhibiting < 10 µM would be considered to possess high antileishmanial activity.
- A compound would be considered to have moderate antileishmanial activity for this early stage hit-to-lead campaign if IC₅₀ values between 10-20 µM were reported in 2 out of the 3 independent intramacrophage assays used.
- Compounds exhibiting <10 µM in one assay, whilst exhibiting more moderate activity in another were also considered compounds of interest, particularly if patterns arose within certain structural changes and functional groups.
- The IC₅₀ values for a certain compound with strong antileishmanial potency should not differ greatly (> 10 µM). Activities differing by a larger amount were expected for those with low activity against *L. donovani* (> 20 µM).

However, these guidelines were not treated as strict rules as many analogues within Scaffold 1 have proven somewhat difficult to interpret. Compounds would be treated in a case by case matter if such difficulties arose. Due to delays caused by the COVID-19 situation, a small set of compounds (Analogue Series 9 in particular) still require further confirmation using the “tie breaker” UNC assay. This was out of our control and due to time constraints would be undertaken in future projects. Despite this, using the “2 out of 3” approach devised here, we have developed a stronger SAR profile around Scaffold 1, to be discussed below.

Guidelines around cytotoxic behaviour were also defined, though were also not treated as strict rules. Structural changes causing extremely low selectivity (Selectivity index < 3) for the parasite over the host cell should be avoided. Low selectivity must be exhibited in 2 out of 3 independent assays to be considered cytotoxic against mammalian host cells. Where relevant, for convenience the SI values have been included within the tables of biological results (Section 3.14, 3.16, 3.17, 3.19) to help illustrate the host cell cytotoxicity and selectivity exerted by certain compounds. Though other factors such as reoccurring patterns or high antileishmanial activity would be taken into consideration when advocating for certain analogues. In the case of compounds found strongly potent against *L. donovani*, though also

highly cytotoxic against the mammalian host cell, exploring an isosteric replacement may be a future option.

Our collaborators at UNC also suggested that differences in CC₅₀ values may be observed between the uninfected MTT assay performed by UNC and the intramacrophage assay that simultaneously evaluates parasite inhibition and compound cytotoxicity within infected host macrophages, performed by GRIDDD, Bio21 and IPK. As outlined in Section 3.07, due to the presence of the parasite, infected host cells are subjected to larger stress levels. The infection itself could further impact host cell survival, thus may be more sensitive to our investigative compounds in comparison to the non-infected host cells. This factor would also need to be taken into consideration when assessing the host cell cytotoxicity of a compound across all assays performed.

Our final aim was to obtain analogues with clear antileishmanial potency (< 5 µM) in 2 out of 3 assays or 2 out of 2 bioassays, where appropriate, along with selectivity for the parasite over the host cell. We hoped to identify new early leads, gain an overall understanding of the scaffold to develop a reliable first-generation SAR profile. This would allow for the synthesis of a more developed lead in future studies with the ability to deliver reliable and unquestionable activity within this scaffold.

3.12 Complete biological re-evaluation of Analogue Series 1-2 library

The entire set of compounds within Analogue Series 1-3 (structural changes to the LHS, RHS and core of Scaffold 1 respectively) first described in Chapter 2, underwent complete biological reassessment against *L. donovani*. This was undertaken to resolve the challenges around the conflicting biological results previously reported (Section 3.09 and Chapter 2, Section 2.09) and continue to develop an SAR profile around Scaffold 1.

At this stage of the project, a large number of analogues had accumulated within our library. In an effort save on time, cost and the manual efforts required for the drug plate preparation protocol, our collaborators at Bio21 first performed the high throughput intramacrophage assay against *L. donovani* using a high one-point drug concentration (50 µM). This would allow us to quickly gauge which compounds possessed any anti-parasitic or cytotoxic properties that would most likely be exhibited at high concentrations during a serial dilution. This also quickly removed any compounds that observed complete inactivity at high drug concentrations and would allow us to narrow down the number of compounds that required further testing using the more costly and time consuming intramacrophage assay following the 10-point concentration response curve. Control compounds miltefosine and amphotericin B were also employed within the high one-point drug concentration HTS, strong antileishmanial activity was demonstrated by the control drugs, though an IC₅₀ value could not be generated, since only one concentration was used. Compounds that managed to display antileishmanial behaviour during the high one-point drug concentration intramacrophage HTS were further investigated

in the using the usual 10-point curve (100 μM top concentration) protocol to determine an accurate IC_{50} . Excluding the concentrations and serial dilutions used, both bioassays performed by Bio21 followed the same methodology previously described.

3.12.1 Analogue Series 1-2 library retesting: Initial key compounds outlined in Figure 3.01

The original key leads identified in Chapter 2 and summarized in **Figure 3.01** underwent complete reassessment using *L. donovani* intramacrophage assays performed by each of our past and current collaborators. The complete set of biological results are outlined in **Table 3.09**. The guidelines set in Section 3.11 were followed to help determine the antileishmanial activity of compounds with conflicting biological results between assays.

Both GRIDD assays (initial rounds of testing and the re-examination) were included to allow for a complete summary and visual comparative ease. However, caution was used when interpreting activity as both sets of GRIDD biological results often did not correlate with the results reported by the other independent groups within **Table 3.09** (excluding **2.002**, **2.042**). Each compound which exhibited high potency in the initial GRIDD intramacrophage assay, was followed by subsequent underwhelming antileishmanial activity or a complete loss of activity during the GRIDD biological reassessment. Any activity present was too low for an accurate IC_{50} value to be ascertained. Most compounds of **Table 3.09** reported low to moderate parasite inhibition by the remaining majority of independent collaborative groups, thus it appeared the initial GRIDD intramacrophage assay overstated antileishmanial activity, while the GRIDD biological reassessment may have understated the antileishmanial properties present. It is uncertain why the GRIDD biological data often did not correlate with the results reported by each of the other independent groups. Overall, evaluating our complete library of analogues with several independent labs was useful, as their combined results helped provide better insight into any true activity present. Solubility issues were not reported by UNC or IPK.

Table 3.09: Complete summary of biological results of key Analogues of Series 1-2, hit compounds are listed in blue

HCS intracellular assay against <i>L. donovani</i>											Luciferase /MTT assay	
I.D	GRIDD ^{ab}		GRIDD retest ^{ae}		Bio21 ^{gh}		Bio21 retest ^{gi}		IPK ^{op}		UNC ^{qr}	
	IC_{50} (μM)	CC_{50} (μM)	IC_{50} (μM)	CC_{50} (μM)	IC_{50} (μM)	CC_{50} (μM)	IC_{50} (μM)	CC_{50} (μM)	IC_{50} (μM)	CC_{50} (μM)	IC_{50} (μM)	CC_{50} (μM)
2.001	>80 ^{df}	>80 ^{df}	63% at 80 μM^*	55% at 80 μM^*	12	>100	>100	>100	28	>100	46	>50
2.002	10 \pm 0.090	>80 ^{cd}	-	-	5.3	>100 ⁿ	41 ^{js}	>100 ^{js}	3.7 ^s	>100	13	>50
2.008	>80 ^d	>80 ^d	>80 ^{df†}	>80 ^{df†}	28 [‡]	>100 ^{n‡}	>50 ^m	>50 ^m	15	>100	-	-
2.009	2.1 \pm 0.62 [†]	>80 ^{df}	>80 ^{df}	57% at 80 $\mu\text{M}^*†$	>100	>100 ⁿ	>100	>100	18	27	9.9	>50

2.012	2.3 ± 0.17 ^{c†}	57% at 80 μM ^{c*†}	62% at 10 μM ^f *†	52% at 40 μM ^f *†	19	>100	39 ^k	>100 ^{kn}	39	96	30	>50
2.015	1.7 ± 0.10 [†]	>80 ^{d†}	65% at 80 μM [*]	>80 ^d	>100 ⁱ	>100 ⁱⁿ	>100 ^l	>100 ^{ln}	17	28	13	>50
2.018	0.45 ± 0.040 [†]	>80 ^{d†}	66% at 40 μM [*]	60% at 40 μM [*]	>100 [‡]	>100 ^{n‡}	>100 ^{ln}	>100 ^{ln}	15	32	12	>50
2.024	0.38 ± 0.040	>80 ^d	58% at 40 μM ^{*†}	>80 ^{d†}	65	>100 ⁿ	>50 ^m	>50 ^m	27	>100	18	>50
2.037	1.6 ± 0.10 [†]	>80 ^{d†}	>80 ^{e†}	>80 ^{d†}	>100 ^{n‡}	>100 ^{n‡}	>50 ^m	>50 ^m	>100	>100	>50	>50
2.042	5.3 ± 0.23 ^c	>80 ^{cd}	57% at 20 μM ^f *	>80 ^{df}	9.7	>100 ⁿ	12 ^k	>100 ^{kn}	26	>100	34	>50
2.059	0.32 ± 0.050 [†]	>80 ^{d†}	64% at 20 μM [*]	60% at 40 μM [*]	36	>100 ⁿ	>100	>100	12	22	11	>50

a = anti *L. donovani* activity and toxicity measured in THP-1 transformed macrophage host cell lines using a top concentration of 80 μM (14-point curve). Experiment performed in duplicate wells. Values are means of two experiments, n=2.

b= control compounds for GRIDD *L. donovani* intramacrophage assay. Average from experimental replicates; Amphotericin B IC₅₀= 0.39 ± 0.0070 μM, CC₅₀= 1.5 ± 0.070 μM, VL-2098 IC₅₀= 1.8 ± 0.17 μM, CC₅₀> 80 μM, DNDI-1044 IC₅₀= 0.40 ± 0.014 μM, CC₅₀> 80 μM.

c= control compounds for GRIDD *L. donovani* intramacrophage assay. Average from experimental replicates; Amphotericin B IC₅₀= 0.076 ± 0.0020 μM, CC₅₀= 0.73 ± 0.18 μM, VL-2098 IC₅₀= 0.67 ± 0.21 μM, CC₅₀> 40 μM, DNDI-1044 IC₅₀= 0.13 ± 0.037 μM, CC₅₀> 40 μM.

d=<50% activity at the top concentration tested (80 μM). Values are the means of two experiments

e= control compounds for GRIDD *L. donovani* intramacrophage assay. Average from experimental replicates; Amphotericin B IC₅₀= 0.069 ± 0.0020 μM, CC₅₀= 0.94 ± 0.044 μM, VL-2098 IC₅₀= 0.73 ± 0.017 μM, CC₅₀> 40 μM, DNDI-1044 IC₅₀= 0.22 ± 0.039 μM, CC₅₀> 40 μM.

f= control compounds for GRIDD *L. donovani* intramacrophage assay. Average from experimental replicates; Amphotericin B IC₅₀= 0.065 ± 0.0060 μM, CC₅₀= 0.73 ± 0.0040 μM, VL-2098 IC₅₀= 0.64 ± 0.068 μM, CC₅₀> 40 μM, DNDI-1044 IC₅₀= 0.21 ± 0.013 μM, CC₅₀> 40 μM.

* CC₅₀ value is determined from a sub-efficacious curve

† Out of solution in media reported between 800-20 μM during GRIDD assay. Solubility in the intermediate dilution in medium may have contributed to a sub-efficacious curve

± standard deviation

g= anti *L. donovani* activity and toxicity measured in THP-1 transformed macrophage host cell lines using a top concentration of 100 μM (2x serial dilution 10-point curve). Experiment performed in duplicate wells in one experiment, n=1.

h= control compounds for Bio21 *L. donovani* intramacrophage assay. Miltefosine IC₅₀= 11 μM CC₅₀> 100 μM

i= control compounds for Bio21 *L. donovani* intramacrophage assay. Miltefosine IC₅₀= 0.50 μM CC₅₀= 40 μM, Amphotericin B IC₅₀= 1.1 μM CC₅₀= 66 μM

j= control compounds for Bio21 *L. donovani* intramacrophage assay. Average from experimental replicates; Miltefosine IC₅₀= 0.39 ± 0.55 μM, CC₅₀> 20 μM, Amphotericin B IC₅₀= 0.12 ± 0.055 μM, CC₅₀= 6.0 ± 1.8 μM

k= control compounds for Bio21 *L. donovani* intramacrophage assay. Miltefosine IC₅₀= 0.52 μM CC₅₀> 100 μM, Amphotericin B IC₅₀= 2.6 μM CC₅₀= 26 μM

l= control compounds for Bio21 *L. donovani* intramacrophage assay. Miltefosine IC₅₀= 0.75 μM CC₅₀= 91 μM, Amphotericin B IC₅₀= 0.29 μM CC₅₀= 83 μM

m= anti *L. donovani* activity and toxicity measured in THP-1 transformed macrophage host cell lines using a one-point concentration (50 μM) to assess any form of antileishmanial activity. Experiment performed in duplicate wells in one experiment, n=1.

n=<50% activity at the top concentration tested (100 μM).

‡= poor solubility observed in DMSO stock (100mM) used for Bio21 assay

§= poor solubility observed in media up to 800 μM during Bio21 assay

o= anti *L. donovani* activity and toxicity measured in THP-1 transformed macrophage host cell lines using a top concentration of 100 μM (2x serial dilution 10-point curve). Experiment performed in duplicate wells in one experiment, n=1.

p= control compounds for IPK intramacrophage *L. donovani* assay. Miltefosine IC₅₀= 1.7 μM, CC₅₀>100 μM, Amphotericin B IC₅₀= 0.83 μM, CC₅₀> 100 μM.

q= anti *L. donovani* activity measured in THP-1 transformed macrophage host cell lines using luminescent expressing *L. donovani*. Experiment performed in triplicate wells in one experiment, n=1 using a concentration range of 1-50 μM. DMSO was used as sole control against which the percent *L. donovani* viability is calculated

r= host cell toxicity measured in MTT assay with uninfected macrophage host cells. Experiment performed in triplicate wells in one

experiment, n=1 using a concentration range of 1-50 μ M. DMSO was used as sole control against which the percent cell viability is calculated

s = value is a mean of two experiments

- not tested

The hit **2.002** was found to have demonstrated consistent antileishmanial activity and low cytotoxicity against the host cells. High antileishmanial activity (IC_{50} value $\leq 10 \mu$ M) was reported by most of the independent biological groups. Additionally, this compound was still found to be moderately active ($IC_{50} = 13 \mu$ M) within the intramacrophage assay against luminescence expressing *L. donovani*, performed by UNC. Strangely, very low parasite inhibition was reported for **2.002** during the biological retest performed by Bio21. Correspondence with our collaborators at Bio21 suggested this lack of consistency was possibly due to solubility issues within the media during the experiment, as it was difficult to monitor. They also suggest a potential human error, such as a pipetting error, may have caused this lack of consistency. Further assessment of **2.002** would be undertaken in the future, outside the scope of this thesis to confirm the bioactivity **2.002** within the Bio21 intramacrophage assay. Due to the delays caused by COVID-19, hit **2.002** was not able to be re-evaluated further using the Bio21 intramacrophage assay within the time constraints of this project. Following the guidelines set in Section **3.11**, as most of the independent assays reported high antileishmanial activity, hit **2.002** remained a compound of interest. Based on the overall results, this compound was later allowed to return to this PhD project, as it was no longer being studied by fellow lab members and would guide further SAR studies described in Section **3.19**.

Analogue **2.037**, which contained the cyclohexane ring at the LHS chemical space of Scaffold 1, was found to be consistently inactive against *L. donovani* across all independent intramacrophage assays. This excluded the initial intramacrophage assay performed by GRIDD, in which it was likely a false positive. Consequently, further studies incorporating the cyclohexane structural modification to the LHS chemical space of Scaffold 1 were discontinued. The loss of aromaticity within this region of the scaffold was also confirmed to correlate to a loss of antileishmanial activity.

The remaining compounds of **Table 3.09** were more difficult to interpret, thus the guidelines set out in Section **3.11** were consulted. The hit **2.001** and analogue **2.008** were determined to be weakly active against *L. donovani* only. Moderate to low parasite inhibition was observed against *L. donovani* within the intramacrophage assays performed by Bio21 (initial intramacrophage assay only, no activity reported within the Bio21 re-test), IPK and UNC. In contrast, no significant antileishmanial activity was reported within either biological assays performed by GRIDD. From this range of results, it is likely that compounds **2.001** and **2.008** actually do possess some anti-parasitic abilities, though they may not provide strong interactions with any putative binding site/s. These compounds would not influence any further SAR studies. Low parasite inhibition was reported for the previous lead compounds **2.012** and **2.024** (*para* and *ortho*-methyl substituents on the LHS phenyl ring of Scaffold 1) by at least 2 out of 4 independent intramacrophage assays employed. It seemed these analogues also possessed the ability to

exert antileishmanial activity, though at much weaker inhibitory levels than initially reported. These analogues would also no longer be considered as key compounds, nor would they influence further additive SAR studies. Excluding the conflicting results reported by GRIDD, compounds **2.009** (LHS *para*-bromo substituent), **2.015** (LHS *meta*-bromo substituent), **2.018** (LHS *meta*-methyl substituent) and **2.059** (RHS unsubstituted phenyl ring) were found to exhibit more moderate antileishmanial activity (< 20 μ M) within 2 out of 3 of the remaining independent intramacrophage assays. Despite this, the level of parasite inhibition was not significant enough for compounds **2.009**, **2.015** and **2.018** to be considered as lead compounds, used to influence further SAR studies. Previous lead compound **2.042** (imidazole LHS) had also guided various SAR studies around Scaffold 1 (Section **3.05**). Biological re-evaluation of **2.042** reported somewhat convergent moderate to high antileishmanial activity between the initial GRIDD intramacrophage assay and both Bio21 biological assays. However, low anti-parasitic inhibition was observed in the remaining independent assays (> 20 μ M). From this range of results, it was also likely that **2.042** possessed more moderate antileishmanial properties, though they may not provide strong interactions with any putative binding site/s. This compound would still be considered a compound of interest, since correlating moderate to high antileishmanial activity was reported in 2 out of 4 independent bioassays.

Overall, our previous lead compounds were confirmed in **Table 3.09** to exert lower levels of parasite inhibition than initially thought. These compounds may have weaker binding affinities within the putative active site/s or may exert antileishmanial properties through more than one mode of action, of which we are not privy to. Issues with solubility may have also caused variability between the independent assays. As a result, it is still difficult to deduce at this stage whether these previous issues with conflicting bioactivities, particularly within the GRIDD assay, were caused by issues within the biological assay, due to the scaffold itself, a combination or another matter entirely. Thus, we are yet to have a complete answer to the large variability originally observed. This may be another question to address in later studies (future work).

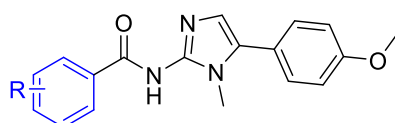
Despite the more moderate levels of parasite inhibition defined in **Table 3.09**, incorporating the structural changes based around these analogues in later studies (Series 4-8) was by no means a waste of time. On the contrary, we were able to achieve improved true lead like compounds in these later analogues, particularly influenced by the structural modifications of **2.042** and **2.059**, to be discussed below.

3.12.2 Biological analysis of the remaining library of Series 1-2

The remaining analogues of Analogue Series 1-2 were assessed by Bio21 and IPK to ensure any real antileishmanial activity was not overlooked. A select few were also assessed using the intramacrophage assay against luminescence expressing *L. donovani* performed by UNC. The biological results are listed in **Tables 3.10-3.12**, which include the initial assay by GRIDD. In most cases, the biological results

across all assays, including the initial GRIDD assay were unanimous. Solubility issues were generally not reported within the Bio21, IPK or UNC intramacrophage assays. The original hit **2.001** that influenced this SAR study has been included for comparative ease. Hit **2.001** has undergone more than one round of biological assessment performed by GRIDD and Bio21, thus for the sake of convenience, the IC₅₀ values that correlated somewhat more closely to the other independent groups have been included. This was also the case for **2.002** in later discussions. The complete set of biological results for analogues focusing on substituting various functionalities around the LHS phenyl ring of Scaffold 1 are highlighted in **Table 3.10**.

Table 3.10: Complete summary of biological results of remaining analogues of Series 1-2, focusing on LHS substituent changes based on hit **2.001** (blue)



HCS intracellular assay against <i>L. donovani</i>								Luciferase /MTT assay	
I.D	R	GRIDD ^{ab}		Bio21 ^{hi}		IPK ^{pq}		UNC ^{rs}	
		IC ₅₀ (μM)	CC ₅₀ (μM)	IC ₅₀ (μM)	CC ₅₀ (μM)	IC ₅₀ (μM)	CC ₅₀ (μM)	IC ₅₀ (μM)	CC ₅₀ (μM)
2.001^g	4-F	63% at 80 μM*	55% at 80 μM*	12	>100	28	>100	46	>50
2.010[†]	4-CN	>80 ^f	>80 ^f	>100 ^o	>100 ^o	>100	>100	-	-
2.011^{j†}	4-OMe	>80 ^f	>80 ^f	>100	>100	23	54	-	-
2.013^{†‡§}	4-NO ₂	37 ± 0.62	27 ± 0.60	>100 ^o	>100 ^o	>100	>100	-	-
2.014^{k†}	3-F	>80 ^f	>80 ^f	>100 ^o	>100 ^o	23	36	-	-
2.016^{k†}	3-CN	>80 ^f	>80 ^f	>100 ^o	>100 ^o	>100	>100	-	-
2.017^{ej†}	3-OMe	57% at 80 μM*	52% at 80 μM*	>100	>100	20	40	-	-
2.019^{dk†}	3-NO ₂	>80 ^f	54% at 40 μM*	>100	>100	>100	>100	-	-
2.020^{k†}	2-F	>80 ^f	>80 ^f	>100 ^o	>100 ^o	47	>100	-	-
2.021^{k†‡}	2-Br	>80 ^f	>80 ^f	>100	>100	12	>100	13	>50
2.022^{†‡§}	2-CN	>80 ^f	>80 ^f	14 ^o	>100 ^o	>100	>100	12	>50
2.023^{ej}	2-OMe	57% at 80 μM*	>80 ^f	33 ^g	>100 ^g	36	>100	-	-
2.025^{d†}	2-NO ₂	52% at 40 μM*	>80 ^f	>50 ^m	>50 ^m	24	>100	-	-
2.026^{k†}	3,4- Me	>80 ^f	64% at 80 μM*	>100	>100	10	22	-	-
2.029[†]	4-[N]	>80 ^f	64% at 80 μM*	44	>100 ^o	25	>100	-	-
2.030^{k†}	3-[N]	>80 ^f	>80 ^f	>100	>100 ^j	35	>100	-	-
2.031^{k†}	2-[N]	>80 ^f	>80 ^f	13	>100	20	>100	-	-
2.052^{cn†}	2-OH	56% at 20 μM*	34% at 80 μM*	0.39	>100	>100	>100	-	-
2.053^{dk}	3-OH	>80 ^f	>80 ^f	54	>100	87	>100	-	-
2.054^c	4-OH	>80 ^f	>80 ^f	>100 ^o	>100 ^o	>100	>100	-	-

2.062^{e†}	2-CN, 4-F	>80 ^f	>80 ^f	>50 ^m	>50 ^m	>100	>100	-	-
2.063^{d†}	2-NO ₂ , 4-F	>80 ^f	>80 ^f	>100 ^o	>100 ^o	19	>100	-	-

a = anti *L. donovani* activity and toxicity measured in THP-1 transformed macrophage host cell lines using a top concentration of 80 µM (14-point curve). Experiment performed in duplicate wells. Values are means of two experiments, n=2.

b= control compounds for GRIDD *L. donovani* intramacrophage assay. Average from experimental replicates; Amphotericin B IC₅₀= 0.39 ± 0.0070 µM, CC₅₀= 1.5 ± 0.070 µM, VL-2098 IC₅₀= 1.8 ± 0.17 µM, CC₅₀> 80µM, DNDI-1044 IC₅₀= 0.40 ± 0.014 µM, CC₅₀> 80 µM.

c= control compounds for GRIDD *L. donovani* intramacrophage assay. Average from experimental replicates; Amphotericin B IC₅₀= 0.076 ± 0.0020 µM, CC₅₀= 0.73 ± 0.18 µM, VL-2098 IC₅₀= 0.67 ± 0.21 µM, CC₅₀> 40µM, DNDI-1044 IC₅₀= 0.13 ± 0.037 µM, CC₅₀> 40 µM.

d= control compounds for GRIDD *L. donovani* intramacrophage assay. Average from experimental replicates; Amphotericin B IC₅₀= 0.067 ± 0.0020 µM, CC₅₀= 0.94 ± 0.046 µM, VL-2098 IC₅₀= 0.57 ± 0.18 µM, CC₅₀> 40µM, DNDI-1044 IC₅₀= 0.18 ± 0.040 µM, CC₅₀> 40 µM.

e= control compounds for GRIDD *L. donovani* intramacrophage assay. Average from experimental replicates; Amphotericin B IC₅₀= 0.065 ± 0.0060 µM, CC₅₀= 0.73 ± 0.0040 µM, VL-2098 IC₅₀= 0.64 ± 0.068 µM, CC₅₀> 40µM, DNDI-1044 IC₅₀= 0.21 ± 0.013 µM, CC₅₀> 40 µM.

f= <50% activity at the top concentration tested (80 µM). Values are the means of two experiments

g= control compounds for GRIDD *L. donovani* intramacrophage assay. Average from experimental replicates; Amphotericin B IC₅₀= 0.069 ± 0.0020 µM, CC₅₀= 0.94 ± 0.044 µM, VL-2098 IC₅₀= 0.73 ± 0.017 µM, CC₅₀> 40µM, DNDI-1044 IC₅₀= 0.22 ± 0.039 µM, CC₅₀> 40 µM.

* CC₅₀ value is determined from a sub-efficacious curve. Solubility in the intermediate dilution in medium may have contributed to this effect observed.

† Out of solution in media reported between 800-20 µM

± standard deviation

h= anti *L. donovani* activity and toxicity measured in THP-1 transformed macrophage host cell lines using a top concentration of 100 µM (2x serial dilution 10-point curve). Experiment performed in duplicate wells in one experiment, n=1.

i= control compounds for Bio21 *L. donovani* intramacrophage assay. Miltefosine IC₅₀= 11 µM CC₅₀> 100 µM

j= control compounds for Bio21 *L. donovani* intramacrophage assay. Miltefosine IC₅₀= 0.62 ± 0.19µM CC₅₀> 40 µM, Amphotericin B IC₅₀= 1.9 ± 0.72 µM CC₅₀>26 µM

k= control compounds for Bio21 *L. donovani* intramacrophage assay. Miltefosine IC₅₀= 0.50 µM CC₅₀= 40 µM, Amphotericin B IC₅₀= 1.1 µM CC₅₀= 66 µM

l= control compounds for Bio21 *L. donovani* intramacrophage assay. Miltefosine IC₅₀= 0.52 µM CC₅₀> 100 µM, Amphotericin B IC₅₀= 2.6 µM CC₅₀= 26 µM

m= anti *L. donovani* activity and toxicity measured in THP-1 transformed macrophage host cell lines using a one-point concentration (50 µM) to assess any form of antileishmanial activity. Experiment performed in duplicate wells in one experiment, n=1.

n= control compounds for Bio21 *L. donovani* intramacrophage assay. Miltefosine IC₅₀= 0.78 µM CC₅₀= 14 µM, Amphotericin B IC₅₀= 0.078 µM CC₅₀= 7.3 µM

o= <50% activity at the top concentration tested (100 µM).

p= anti *L. donovani* activity and toxicity measured in THP-1 transformed macrophage host cell lines using a top concentration of 100 µM (2x serial dilution 10-point curve)

q= control compounds for IPK intramacrophage *L. donovani* assay. Miltefosine IC₅₀= 1.7 µM, CC₅₀>100 µM, Amphotericin B IC₅₀= 0.83 µM, CC₅₀> 100 µM.

r= anti *L. donovani* activity measured in THP-1 transformed macrophage host cell lines using luminescent expressing *L. donovani*. Experiment performed in triplicate wells in one experiment, n=1 using a concentration range of 1-50 µM. DMSO was used as sole control against which the percent *L. donovani* viability is calculated

s= host cell toxicity measured in MTT assay with uninfected macrophage host cells. Experiment performed in triplicate wells in one experiment, n=1 using a concentration range of 1-50 µM. DMSO was used as sole control against which the percent cell viability is calculated ± standard deviation

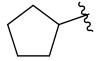
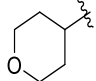
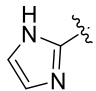
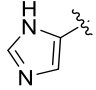
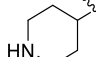
- not tested

From **Table 3.10**, most of the analogues were confirmed inactive against *L. donovani*. Substituting the *para*-fluoro group with electron donating groups capable of hydrogen bonding interactions (hydroxy, methoxy substituents) around the ring was found unfavourable. Analogues bearing electron donating functionalities at the *ortho*, *meta* or *para* positions generally reported poor antileishmanial activity unanimously. This excluded the *ortho*-hydroxy substituent **2.052**, which surprisingly displayed highly potent antileishmanial activity within the Bio21 intramacrophage assay alone. Following the guidelines outlined in Section **3.11**, this analogue was not considered to be a potential lead compound, as it did not report supporting antileishmanial activity in 2 out of the 3 independent assays employed and may have been a false positive. Stronger electron withdrawing groups (nitro, cyano substituents) at the *para* and *meta*-positions reported unanimously poor anti-parasitic inhibition (> 20 µM). Repositioning the fluoro

group to the *meta* (**2.014**) and *ortho* (**2.020**) positions was also unanimously reported to exhibit poor parasite inhibition. Substituting certain electron withdrawing functionalities, sterically larger than the fluoro group was found to provide some improvement to antileishmanial activity. Analogues bearing the *ortho*-bromo (**2.021**), *ortho*-cyano (**2.022**) were reported to exert moderate inhibition (< 20 μ M) against *L. donovani* in at least 2 out of 4 independent assays utilized. Incorporating the bromo substituent around the LHS phenyl ring has maintained moderate parasite inhibition, where the *para* (**2.009**) and *meta*-bromo (**2.015**) also displayed moderate antileishmanial activity (**Table 3.09**). This suggests this sterically larger halogen was preferable to the initial *para*-fluoro substituent (**2.001**) within the LHS chemical space of Scaffold 1. Introducing the nitrogen of the pyridine replacement at the 2-position (**2.031**) also provided moderate (< 20 μ M) parasite inhibition in 2 out of 3 assays, suggesting electron withdrawing ability at the 2-position maintained antileishmanial activity. Interestingly, **2.022** and **2.031** were found highly active within the initial free-living promastigote assay performed by Bio21 (Chapter 2, Section **2.05**). Though, as only limited antileishmanial activity was confirmed here, these compounds would not influence further additive SAR studies.

Table 3.11: Complete summary of biological results of remaining analogues of Series 1-2, focusing on LHS ring structural changes influenced by hit 2.001, 2.002 (blue)

HCS intracellular assay against <i>L. donovani</i>							
I.D	R	GRIDD ^{ab}		BIO21 ^{gi}		IPK ^{kl}	
		IC ₅₀ (μ M)	CC ₅₀ (μ M)	IC ₅₀ (μ M)	CC ₅₀ (μ M)	IC ₅₀ (μ M)	CC ₅₀ (μ M)
2.001^{eh}		63% at 80 μ M*	55% at 80 μ M*	12	>100	28	>100
2.002^{ch}		10 \pm 0.090	>80 ^f	5.3	>100 ^j	3.7 ^k	>100
2.008^h		>80 ^f	>80 ^f	28 [‡]	>100 ^{j‡}	15	>100
2.027		>80 ^f	>80 ^f	25	>100 ^j	37	>100
2.028[†]		>80 ^f	>80 ^f	22	>100	>100	>100
2.032[†]		>80 ^f	>80 ^f	>100 ^j	>100 ^j	>100	>100
2.033[†]		>80 ^f	>80 ^f	>100 ^j	>100 ^j	>100	>100
2.034		>80 ^f	>80 ^f	>100 ^j	>100 ^j	>100	>100
2.035[†]		>80 ^f	>80 ^f	23	>100 ^j	32	>100

2.036^{h†}		97% at 80 μM*	>80 ^f	83	>100 ^j	>100	>100
2.038^{d†}		>80 ^f	>80 ^f	>100	>100	>100	>100
2.039^{ch}	Me	48% at 80 μM*	>80 ^f	>100 ^j	>100 ^j	>100	>100
2.040^c	Et	68% at 40 μM*	>80 ^f	>100	>100	>100	>100
2.041^c	Pr	>80 ^f	>80 ^f	>100 ^j	>100 ^j	>100	>100
2.042^{chi}		5.3 ± 0.23	>80 ^f	11 ^m	>100 ^j	26	>100
2.043^{c‡§}		>80 ^f	>80 ^f	>100 ^j	>100 ^j	>100	>100
2.058^d		>80 ^f	>80 ^f	>100 ^j	>100 ^j	>100	>100

a = anti *L. donovani* activity and toxicity measured in THP-1 transformed macrophage host cell lines using a top concentration of 80 μM (14-point curve). Experiment performed in duplicate wells. Values are means of two experiments, n=2.

b= control compounds for GRIDD *L. donovani* intramacrophage assay. Average from experimental replicates; Amphotericin B IC₅₀= 0.39 ± 0.0070 μM, CC₅₀= 1.5 ± 0.070 μM, VL-2098 IC₅₀= 1.8 ± 0.17 μM, CC₅₀> 80 μM, DNDI-1044 IC₅₀= 0.40 ± 0.014 μM, CC₅₀> 80 μM.

c= control compounds for GRIDD *L. donovani* intramacrophage assay. Average from experimental replicates; Amphotericin B IC₅₀= 0.076 ± 0.0020 μM, CC₅₀= 0.73 ± 0.18 μM, VL-2098 IC₅₀= 0.67 ± 0.21 μM, CC₅₀> 40 μM, DNDI-1044 IC₅₀= 0.13 ± 0.037 μM, CC₅₀> 40 μM.

d= control compounds for GRIDD *L. donovani* intramacrophage assay. Average from experimental replicates; Amphotericin B IC₅₀= 0.067 ± 0.0020 μM, CC₅₀= 0.94 ± 0.046 μM, VL-2098 IC₅₀= 0.57 ± 0.18 μM, CC₅₀> 40 μM, DNDI-1044 IC₅₀= 0.18 ± 0.040 μM, CC₅₀> 40 μM.

e= control compounds for GRIDD *L. donovani* intramacrophage assay. Average from experimental replicates; Amphotericin B IC₅₀= 0.069 ± 0.0020 μM, CC₅₀= 0.94 ± 0.044 μM, VL-2098 IC₅₀= 0.73 ± 0.017 μM, CC₅₀> 40 μM, DNDI-1044 IC₅₀= 0.22 ± 0.039 μM, CC₅₀> 40 μM.

f=<50% activity at the top concentration tested (80 μM). Values are the means of two experiments

* CC₅₀ value is determined from a sub-efficacious curve. Solubility in the intermediate dilution in medium may have contributed to this effect observed.

† Out of solution in media reported between 800-20 μM during GRIDD assay

± standard deviation

g= anti *L. donovani* activity and toxicity measured in THP-1 transformed macrophage host cell lines using a top concentration of 100 μM (2x serial dilution 10-point curve). Experiment performed in duplicate wells in one experiment, n=1.

h= control compounds for Bio21 *L. donovani* intramacrophage assay. Miltefosine IC₅₀= 11 μM CC₅₀> 100 μM

i= control compounds for Bio21 *L. donovani* intramacrophage assay. Miltefosine IC₅₀= 0.67 ± 0.24 μM CC₅₀> 40 μM, Amphotericin B IC₅₀= 1.5 ± 0.55 μM CC₅₀= 66 ± 0.56 μM

j= <50% activity at the top concentration tested (100 μM).

k= anti *L. donovani* activity and toxicity measured in THP-1 transformed macrophage host cell lines using a top concentration of 100 μM (2x serial dilution 10-point curve)

l= control compounds for IPK intramacrophage *L. donovani* assay. Miltefosine IC₅₀= 1.7 μM, CC₅₀>100 μM, Amphotericin B IC₅₀= 0.83 μM, CC₅₀> 100 μM.

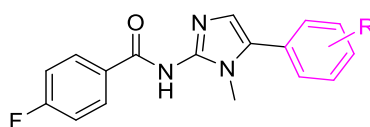
m = value is a mean of two experiments

‡= poor solubility observed in DMSO stock (100mM) used for Bio21 assay

Replacing the pyridine pyrazole (**2.002**) or *para*-fluorophenyl (**2.001**) aromatic rings with the structural modifications outlined in **Table 3.11** were overall unanimously found to cause a loss of antileishmanial activity. Analogues **2.027**, **2.028** which extended the carbon-carbon chain between the LHS aromatic ring and amide functionality were found to be unfavourable. Compared to analogue **2.008** (unsubstituted LHS phenyl ring without carbon chain extension), which was also included in **Table 3.12**, extending the chain further seemed to correlate to a decrease in antileishmanial activity within the IPK intramacrophage assay.

Overall, each independent assay reported poor parasite inhibition for analogues **2.027**, **2.028**, suggesting that increasing the number of rotatable bonds within this chemical space was not favourable and this structural modification should be avoided. The removal of the pyridine ring of **2.002** was also confirmed to be an undesirable structural modification to Scaffold 1. Poor parasite inhibition was unanimously reported for analogue **2.032**, which bears the pyrazole ring alone, suggesting when the pyrazole is present within this region of the chemical space, the pyridine ring is also required to maintain antileishmanial activity. As suggested in Chapter 2, it seemed that the heteroatoms and their placement within the 5-membered ring included within the LHS region of Scaffold 1 required some specificity, as the isoxazole (**2.033**), oxazole (**2.034**), furan (**2.035**) and the imidazole (1*H*-imidazole-5-carboxamide **2.043**) ring replacements all reported unanimously poor antileishmanial activity. In contrast, previous lead **2.042** (1*H*-imidazole-5-carboxamide) was the only single 5-membered heteroaromatic ring reported to maintain strong to moderate inhibition of *L. donovani* by 2 out of the 4 independent intramacrophage assays. It may be that possible specific hydrogen bonding interactions with the putative active site/s require certain heteroaromatic atoms of the 5-membered within the LHS region of the scaffold to be positioned in a precise way to maintain binding. Finally, replacement of the aromatic system within the LHS region of Scaffold 1 with aliphatic rings and chains unanimously caused a complete loss of antileishmanial activity. This suggested the loss of aromaticity and potential pi-pi bonding with the putative binding site/s was unfavourable. It seemed the rigid, planar orientation was required to maintain potency and removing an aromatic system from this portion of the chemical space should be avoided. This confirmation of results helped develop our SAR profile around Scaffold 1, as we could now confirm that the putative binding site/s were indeed somewhat selective and not all structural modifications were tolerated in this chemical space.

Table 3.12: Complete summary of biological results of remaining analogues of Series 1-2, focusing on RHS changes repositioning the para-methoxy group



HCS intracellular assay against <i>L. donovani</i>								Luciferase /MTT assay	
		GRIDD ^a		BIO21 ^f		IPK ^{kl}		UNC ^{mn}	
I.D	R	IC ₅₀ (μM)	CC ₅₀ (μM)	IC ₅₀ (μM)	CC ₅₀ (μM)	IC ₅₀ (μM)	CC ₅₀ (μM)	IC ₅₀ (μM)	CC ₅₀ (μM)
2.001^{eg}	4-OMe	63% at 80 μM*	55% at 80 μM*	12	>100	28	>100	46	>50
2.060^{bh}	3-OMe	>80 ^d	>80 ^d	>100 ^j	>100 ^j	12	>100	8.8	>50
2.061^{ci}	2-OMe	>80 ^d	>80 ^d	>100	>100	>100	>100	>50	>50

a = anti *L. donovani* activity and toxicity measured in THP-1 transformed macrophage host cell lines using a top concentration of 80 μM (14-point curve). Experiment performed in duplicate wells. Values are means of two experiments, n=2.

b= control compounds for GRIDD *L. donovani* intramacrophage assay. Average from experimental replicates; Amphotericin B IC₅₀= 0.39 ± 0.0070 μM, CC₅₀= 1.5 ± 0.070 μM, VL-2098 IC₅₀= 1.8 ± 0.17 μM, CC₅₀> 80μM, DNDI-1044 IC₅₀= 0.40 ± 0.014 μM, CC₅₀> 80 μM.

c= control compounds for GRIDD *L. donovani* intramacrophage assay. Average from experimental replicates; Amphotericin B IC₅₀= 0.076 ± 0.0020 μM, CC₅₀= 0.73 ± 0.18 μM, VL-2098 IC₅₀= 0.67 ± 0.21 μM, CC₅₀> 40μM, DNDI-1044 IC₅₀= 0.13 ± 0.037 μM, CC₅₀> 40 μM.

d= <50% activity at the top concentration tested (80 μM). Values are the means of two experiments

e= control compounds for GRIDD *L. donovani* intramacrophage assay. Average from experimental replicates; Amphotericin B IC₅₀= 0.069 ± 0.0020 μM, CC₅₀= 0.94 ± 0.044 μM, VL-2098 IC₅₀= 0.73 ± 0.017 μM, CC₅₀> 40μM, DNDI-1044 IC₅₀= 0.22 ± 0.039 μM, CC₅₀> 40 μM.

* CC₅₀ value is determined from a sub-efficacious curve. Solubility in the intermediate dilution in medium may have contributed to this effect observed.

† Out of solution in media reported between 800-20 μM

± standard deviation

f= anti *L. donovani* activity and toxicity measured in THP-1 transformed macrophage host cell lines using a top concentration of 100 μM (2x serial dilution 10-point curve). Experiment performed in duplicate wells in one experiment, n=1.

g= control compounds for Bio21 *L. donovani* intramacrophage assay. Miltefosine IC₅₀= 11 μM CC₅₀> 100 μM

h=control compounds for Bio21 *L. donovani* intramacrophage assay. Miltefosine IC₅₀= 0.75 μM CC₅₀= 91 μM, Amphotericin B IC₅₀= 0.29 μM CC₅₀= 83 μM

i= control compounds for Bio21 *L. donovani* intramacrophage assay. Miltefosine IC₅₀= 0.62 ± 0.19μM CC₅₀> 40 μM, Amphotericin B IC₅₀= 1.9 ± 0.72 μM CC₅₀>26 μM

j= <50% activity at the top concentration tested (100 μM).

‡= poor solubility observed in DMSO stock (100mM) used for Bio21 assay

k= anti *L. donovani* activity and toxicity measured in THP-1 transformed macrophage host cell lines using a top concentration of 100 μM (2x serial dilution 10-point curve)

l= control compounds for IPK intramacrophage *L. donovani* assay. Miltefosine IC₅₀= 1.7 μM, CC₅₀>100 μM, Amphotericin B IC₅₀= 0.83 μM, CC₅₀> 100 μM.

m= anti *L. donovani* activity measured in THP-1 transformed macrophage host cell lines using luminescent expressing *L. donovani*. Experiment performed in triplicate wells in one experiment, n=1 using a concentration range of 1-50 μM. DMSO was used as sole control against which the percent *L. donovani* viability is calculated

n= host cell toxicity measured in MTT assay with uninfected macrophage host cells. Experiment performed in triplicate wells in one experiment, n=1 using a concentration range of 1-50 μM. DMSO was used as sole control against which the percent cell viability is calculated

The results of Analogue Series 2, which briefly explored changes simple changes to the RHS phenyl ring of Scaffold 1 are outlined in **Table 3.12**. repositioning the *para*-methoxy group of the original hit **2.001** to the *ortho*-position (**2.061**) was confirmed by each independent intramacrophage assay to cause a complete loss of antileishmanial activity, thus this modification should be avoided. Repositioning the methoxy group to the *meta*-position (**2.060**) was found to improve antileishmanial activity in 2 out of 4 assays employed.

3.12.3 Summary of the confirmed biological results around Analogue Series 1-2

The complete biological reassessment of the entire Analogue Series 1-2 was a large undertaking. Thanks to the efforts of each of our biological collaborators, we were finally able to gain a better understanding of SAR around Scaffold 1. Depicted below, **Figure 3.06** summarizes the confirmed structural modifications that were reported to maintain or improve antileishmanial activity, along with those to be avoided. As highlighted, an aromatic system is required within the LHS region of Scaffold 1 to maintain antileishmanial activity. The pyridine pyrazole functionality of hit **2.002** was still the most preferred structure within this portion of the chemical space. The original *para*-fluoro benzyl hit (**2.001**) was overall reconfirmed to have low potency against *L. donovani*. Substituting the *para*-fluoro for an *ortho*-cyano (**2.022**), *ortho*-bromo (**2.021**) or 2-[N] of a pyridine ring (**2.031**) gave some improved activity in comparison to **2.001**. Additionally, reposition the bromo functionality at the *meta* and *para* positions (**2.015**, **2.009** respectively) also maintained activity, suggested this larger halogen with weaker electronegativity in comparison to the *para*-fluoro (**2.001**) is preferred around this ring. Replacing the *para*-fluoro with the *meta*-methyl substituent also provided moderate levels of parasite inhibition.

Stronger electron withdrawing groups at the *para* and *meta*-positions were confirmed to be undesirable modification. Replacing the *para*-fluoro of **2.001** with stronger electron donating groups around the ring was also found to be unfavourable, suggesting a more electron rich aromatic system was not favourable within the putative binding site/s. Elongating the carbon-carbon chain between the LHS aromatic ring and the amide functionality should also be avoided. Analogues **2.027**, **2.028** were confirmed to decrease anti-parasitic activity, suggesting increasing the number of rotatable bonds and flexibility within this region of the scaffold gave a poor fit within the putative binding site/s.

Within the LHS region of the chemical space, it was confirmed that removing the pyridine of **2.002**, leaving the pyrazole ring alone (**2.032**) caused a loss of antileishmanial activity, suggesting the pyridine ring was required to maintain potency when the pyrazole ring was present. Replacing the pyridine pyrazole system with other 5-membered aromatic rings revealed heteroatoms were required to be positioned in specific arrangements to maintain potency. This was evidenced by the poor parasite inhibition reported for analogues bearing the isoxazole (**2.033**), oxazole (**2.034**), furan (**2.035**) and 1,5-imidazole (1-*H*-imidazole-5-carboxamide, **2.043**). In contrast, the arrangement and orientation of 1,2-imidazole (1-*H*-imidazole-2-carboxamide, **2.042**) was confirmed to exert moderate to high bioactivity within 2 out of the 4 independent assays performed. The replacement of the aromatic system with an aliphatic ring (**2.036-2.038**, **2.058**) or chain (**2.039-2.041**) was confirmed to cause a complete loss of potency against *L. donovani*. This confirmed that the more rigid, planar aromatic system capable of forming pi-pi interactions with the putative binding site/s was required at this region of Scaffold 1.

Finally, retaining the original *para*-methoxy group on the RHS benzyl ring was shown to maintain antileishmanial activity. Repositioning this group to the *meta* position improved antileishmanial activity compared to **2.001**. Whilst moving this group to the *ortho* position gave a complete loss in activity and should be avoided. Removing the methoxy group all together also maintained moderate bioactivity, shown in previous lead **2.059**, suggesting that this group is not crucial to maintaining antileishmanial activity.

Low cytotoxicity was maintained within Analogue Series 1-2. Following the “2 out of 3” guidelines described in Section **3.11**, each analogue was selective for the parasite over the host cell. This fulfilled our early objective of maintaining low host cell cytotoxicity within this compound class.

From this SAR investigation, we have improved antileishmanial activity around hit **2.001**, but have not improved upon hit **2.002**. This was somewhat to be expected, as our efforts had focused around **2.001** and **2.059**. This was not an issue, as **2.002** was studied in a parallel project (Section **3.03**) was later returned to this PhD project. Studies surrounding **2.002**, undertaken within this PhD project are discussed in Section **3.19**. As previously stated, the SAR studies influenced by the previous lead compounds that are listed in **Table 3.09** were not wasteful. Although these previous leads were confirmed to exert weaker antileishmanial activity than initially reported, their inclusion into later

studies has given rise to more potent analogues which will be used to shape a more polished candidate in the future. This is discussed in later sections.

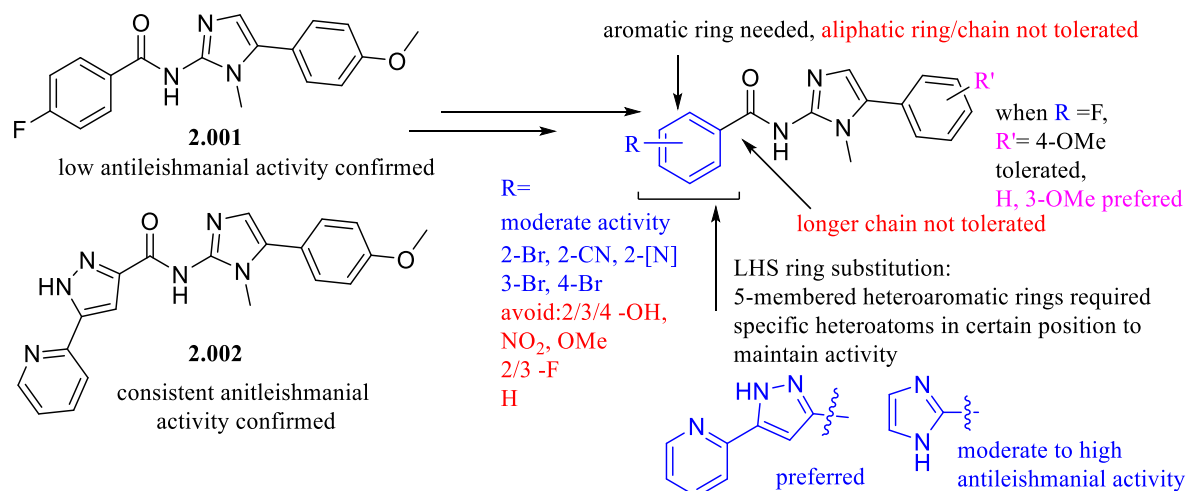


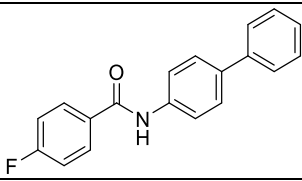
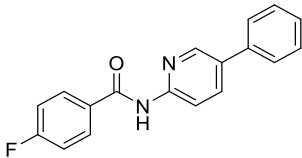
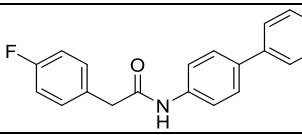
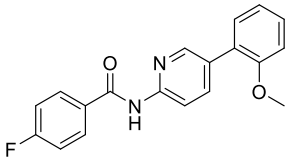
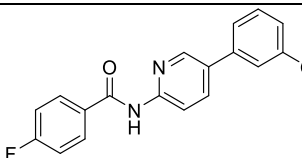
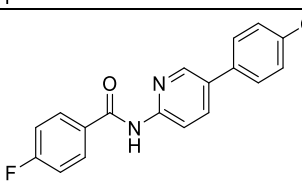
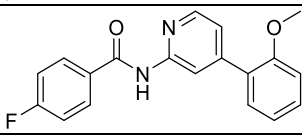
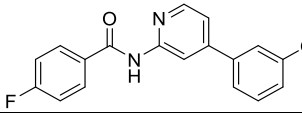
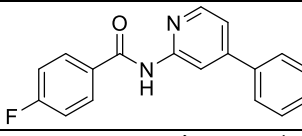
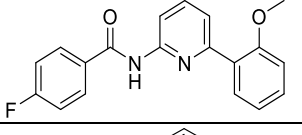
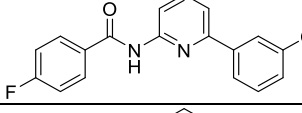
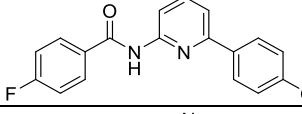
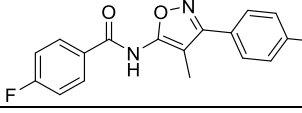
Figure 3.06: Summary of the SAR profile of Scaffold 1, derived from the confirmed biological results of Analogue Series 1-2

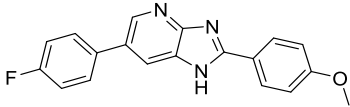
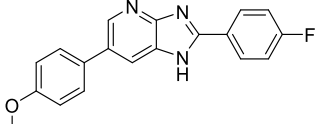
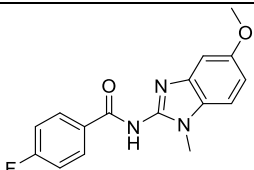
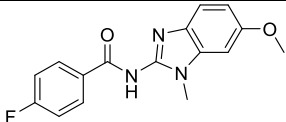
3.13 Complete biological analysis of Analogue Series 3 (structural changes to the amide and imidazole core)

Analogue Series 3 underwent further biological evaluation to confirm if any antileishmanial activity existed within this set of compounds. This series focused on structural changes to the amide functionality and imidazole core. These compounds were influenced by the hit **2.001** and previous lead **2.059**, therefore analogues within this series maintained the *para*-fluorophenyl ring within the LHS region of Scaffold 1. The complete set of biological results for Analogue Series 3 are summarized in **Table 3.13**.

Table 3.13: Complete summary of biological results of Series 3

HCS intracellular assay against <i>L. donovani</i>							
I.D	Structure	GRIDD ^a		Bio21 ^c		IPK ^{kl}	
		IC ₅₀ (μ M)	CC ₅₀ (μ M)	IC ₅₀ (μ M)	CC ₅₀ (μ M)	IC ₅₀ (μ M)	CC ₅₀ (μ M)
2.067^b		>80 ^d	>80 ^d	>50 ^j	>50 ^j	>100	>100
2.070		-	-	>50 ^j	>50 ^j	>100	>100

2.074 ^{cf†‡§}		>80 ^d	>80 ^d	>100 ⁱ	>100 ⁱ	>100	>100
2.075 ^{cg†}		52% at 80 μM*	82% at 80 μM*	>100 ⁱ	>100 ⁱ	>100	>100
2.076 ^{cf†§}		>80 ^d	>80 ^d	>100 ⁱ	>100	>100	>100
2.077 ^{cf†}		>80 ^d	73% at 80 μM*	>100	>100	>100	>100
2.078 ^{cf†§}		>80 ^d	>80 ^d	>100 ⁱ	>100	>100	>100
2.079 ^{cf†§}		>80 ^d	>80 ^d	>100 ⁱ	>100 ⁱ	>100	>100
2.080 ^{cg†}		54% at 80 μM*	58% at 80 μM*	50	47	39	>100
2.081 ^{cf†‡}		>80 ^d	>80 ^d	>100	>100	50	>100
2.082 ^{cf†}		>80 ^d	>80 ^d	>100	>100	51	>100
2.083 ^{ch†}		>80 ^d	>80 ^d	>100	>100	>100	>100
2.084 ^{ch}		>80 ^d	>80 ^d	>100	>100	>100	>100
2.085 ^{ch†}		>80 ^d	>80 ^d	>100	>100	>100	>100
2.090 ^{bf†}		>80 ^d	>80 ^d	>100 ⁱ	>100 ⁱ	>100	>100

2.094 ^{bf†‡}		>80 ^d	>80 ^d	>100 ⁱ	>100 ⁱ	21	>100
2.097 ^{bf†‡}		>80 ^d	>80 ^d	>100 ⁱ	>100 ⁱ	>100	>100
2.102 ^{bf}		>80 ^d	>80 ^d	38	>100 ⁱ	47	>100
2.103 ^{bf†}		>80 ^d	>80 ^d	44	>100 ⁱ	>100	>100

a = anti *L. donovani* activity and toxicity measured in THP-1 transformed macrophage host cell lines. Experiment performed in duplicate wells. Values are means of two experiments, n=2.

b= control compounds for *L. donovani* intramacrophage assay. Average from experimental replicates; Amphotericin B IC₅₀= 0.069 ± 0.0014 μM, CC₅₀= 0.94 ± 0.051 μM, VL-2098 IC₅₀= 0.72 ± 0.0021 μM, CC₅₀> 40μM, DNDI-1044 IC₅₀= 0.22 ± 0.028 μM, CC₅₀> 40 μM.

c= control compounds for *L. donovani* intramacrophage assay. Average from experimental replicates; Amphotericin B IC₅₀= 0.067 ± 0.0021 μM, CC₅₀= 0.94 ± 0.046 μM, VL-2098 IC₅₀= 0.57 ± 0.18 μM, CC₅₀> 40μM, DNDI-1044 IC₅₀= 0.18 ± 0.040 μM, CC₅₀> 40 μM.

d= <50% activity at the top concentration tested (80 μM). Values are the means of two experiments

* CC₅₀ value is determined from a sub-efficacious curve, with the maximum activity from 50-70%. Solubility in the intermediate dilution in medium may have contributed to this effect observed.

† Out of solution in media reported between 800-20 μM during GRIDD assay

± standard deviation

e = anti *L. donovani* activity and toxicity measured in THP-1 transformed macrophage host cell lines. Experiment performed in duplicate wells in one experiment, n=1.

f = control compounds for Bio21 *L. donovani* intramacrophage assay. Miltefosine IC₅₀= 11 μM CC₅₀> 100 μM

g = control compounds for Bio21 *L. donovani* intramacrophage assay; Miltefosine IC₅₀ = 0.84 μM, CC₅₀ > 100 μM, Amphotericin B IC₅₀ = 1.9 μM, CC₅₀ = 65 μM

h = control compounds for Bio21 *L. donovani* intramacrophage assay. Average from experimental replicates; Miltefosine IC₅₀ = 0.39 ± 0.55 μM, CC₅₀ > 20 μM, Amphotericin B IC₅₀ = 0.12 ± 0.055 μM, CC₅₀ = 6.0 ± 1.8 μM

i = <50% activity at the top concentration tested (100 μM).

= compound was tested at a one-point concentration (50 μM), no activity was observed therefore was not retested using a 10-point dilution curve to determine an IC₅₀ value.

‡= poor solubility observed in DMSO stock (100mM) used for Bio21 assay

§= poor solubility observed in media up to 800 μM during Bio21 assay

k = anti *L. donovani* activity and toxicity measured in THP-1 transformed macrophage host cell lines using a top concentration of 100 μM (2x serial dilution 10-point curve)

l = control compounds for IPK intramacrophage *L. donovani* assay. Miltefosine IC₅₀= 1.7 μM, CC₅₀ >100 μM, Amphotericin B IC₅₀= 0.83 μM, CC₅₀ > 100 μM.

- not tested

The previous biological results reported by our collaborators and GRIDD and Bio21 were corroborated by the additional results obtained from the intramacrophage assay against *L. donovani* performed by IPK. Most analogues within this series were unanimously confirmed as completely inactive, whilst the remaining few (**2.080**, **2.102**) were reported to have extremely poor inhibitory effects against the parasite.

Replacing the 5-membered imidazole core with the 6-membered pyridine or phenyl ring (**2.074-2.085**) were found to be undesirable structural modifications. This suggested that incorporating a sterically larger core, altering the heteroatoms and their placement along were unfavourable within the putative

binding site/s. Additionally, incorporating the 6-membered pyridine ring within this chemical space may have also altered potential pi-pi interactions with the putative binding site/s as well as overall orientation of the scaffold within the putative binding site/s.

Replacing the amide and imidazole core with the urea functionality to form a pseudo ring via intramolecular hydrogen bonding was also not tolerated within the putative binding site/s. Analogues **2.070**, **2.074** were confirmed to be completely inactive against *L. donovani*, which further suggests that both the 5-membered imidazole core and adjacent amide functionality were required to maintain the correct orientation and binding interactions within the putative active site/s. Altering the heteroatoms within the imidazole core caused a complete loss in antileishmanial activity, demonstrated by analogue **2.090**. The isoxazole core of **2.090** suggested that this arrangement of heteroatoms was unfavourable and may not allow for possible specific hydrogen bonding interactions to be made with the putative binding site/s. Moreover, the oxazole core of **3.131** (Section **3.07-3.08**, Section **3.17**), which retained the same heteroatom positions as the original imidazole core was found to exert high antileishmanial activity, further advocating that the arrangement of heteroatoms within the 5-membered aromatic core was key to maintaining antileishmanial activity.

Loss of the amide functionality in place of a fused bi-heteroaromatic system (**2.094**, **2.097**) also correlated to a loss of activity. The structural modifications of **2.094**, **2.097** suggested that the overall change in orientation, steric bulk and lipophilicity caused by the fused bi-heteroaromatic system at the core may have caused a poor fit within the putative binding site/s and should be avoided. This modification may have led to a potential loss of hydrogen bonding ability between the putative binding site/s and the original amide of Scaffold 1. Finally, the fused benzimidazole system (**2.102**, **2.103**) was found to cause poor parasite inhibition. This change in overall shape and orientation of the scaffold may have caused a poor fit within the putative binding site/s and should be avoided in future studies around Scaffold 1. A summary of each structural modification studied in Analogue Series 3 is summarised in **Figure 3.07**, which highlights all the modifications to the amide and imidazole core that should be avoided. This negative SAR is not a bad thing, as we have been given an insight into the sorts of structural modifications that are not tolerated within the putative binding site/s, and which structural attributes of Scaffold 1 are key to maintaining antileishmanial activity.

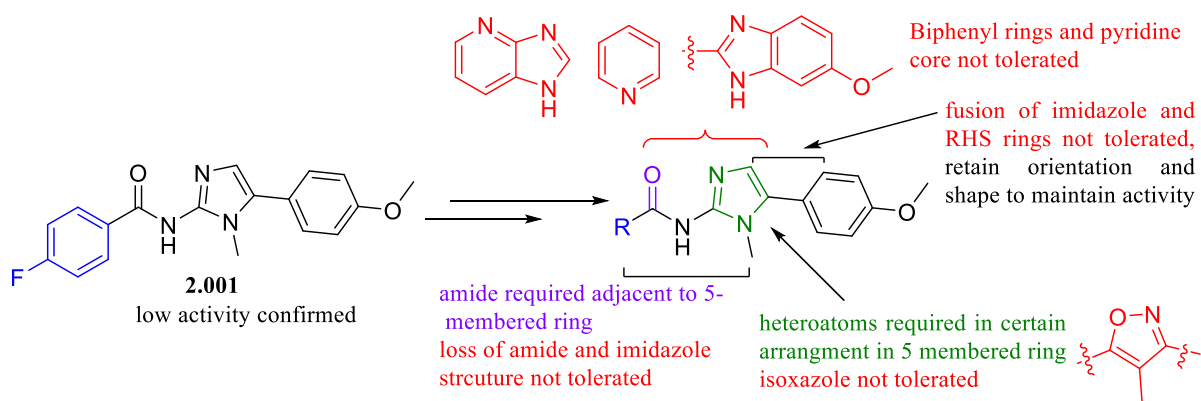


Figure 3.07: Summary of the SAR profile of Scaffold 1, derived from the confirmed biological results of Analogue Series 3

3.14 Complete biological analysis of Analogue Series 4 (additive SAR studies)

The rationale behind developing the compounds within Analogue Series 4 was to combine the structural attributes that were reported to exert the strongest inhibition against *L. donovani* within the intramacrophage assays initially performed by GRIDD and Bio21. This involved combining the unsubstituted RHS phenyl ring, influenced by previous lead compound **2.059**, with various LHS structural modifications influenced by other past key compounds described throughout this chapter, and summarized in **Figure 3.01**. Even though these past lead compounds were later confirmed to exert lower levels of parasite inhibition that initially reported, combining these structural modifications achieved an overall improvement to antileishmanial activity.

Variations in activity and/or cytotoxicity were reported between the independent assays for the same compound. This made interpreting SAR and generating comparisons between different analogues within this series challenging. In some instances, it was also difficult to determine which structural changes gave rise to superior potency. For example, when comparing the antileishmanial activities of analogues **3.005** and **3.013**, both compounds were reported to exert parasite inhibition overall. Compound **3.013** was found to exhibit superior potency within the Bio21 intramacrophage assay (**3.005** $IC_{50} = 37 \mu M$, **3.013** $IC_{50} = 12.48 \mu M$), whilst similar antileishmanial activity was reported within the intramacrophage assay reported by IPK (**3.005** $IC_{50} = 11 \mu M$, **3.013** $IC_{50} = 9.1 \mu M$). Finally, **3.005** reported superior parasite inhibition within the UNC intramacrophage assay against luminescence expressing *L. donovani* (**3.005** $IC_{50} = 4.9 \mu M$, **3.013** $IC_{50} = 7.3 \mu M$). As one assay was not superior to another, we could not favour one set of results from one specific collaborator. Therefore, we would continue to use a more holistic approach of looking across all sets of results, looking to see if correlating antileishmanial activity was reported in 2 out of 3 independent assays, following the guidelines outlined in Section 3.11. This would help simplify SAR analysis. Our focus for this series would be to simply determine which structural changes reported convergent high antileishmanial activity and allowed for

overall improvement to the initial hits **2.001**, **2.002**. These analogues would help shape further SAR studies in the future. The guidelines outlined in Section **3.11** would also help navigate whether parasite inhibition was caused by toxicity against both the parasite and host cell, where damage the macrophage caused parasite death, rather than selectivity for the parasite alone. Analogues with a selectivity index (SI) >3, reported within 2 out of the 3 independent assays were considered as “truly active”. Analogues reporting an SI <3 shows a window that is too narrow to be considered active. This was more pertinent to strong parasite inhibitors, exhibiting very clear antileishmanial activity (< 5 μ M). Once again, this would be used as a guide and not a strict rule.

From **Table 3.14**, it was encouraging to see that for Analogues Series 4 overall, no large continuous discrepancies between antileishmanial activity was reported by our independent collaborators. This may have meant there was no underlying issues within the assays themselves and/or the structural changes allowed for the scaffold to display more reliable solubility, permeability and possibly an improved fit within the putative binding site/s. This table also includes the Analogue Series 1 counterparts (analogues bearing the same LHS structural change, and RHS *para*-methoxy substituent) to allow for comparative ease. As these compounds underwent more than one round of biological assessment performed by Bio21, where convergent activity was observed, biological results were reported as an average value. For the sake of convivence, in the case of divergent activity reported between the Bio21 experiments, the IC₅₀ values that correlated somewhat more closely to the other independent groups have only been included.

Table 3.14: Complete summary of biological results of Series 4 and direct comparison of their related previous leads

HCS intracellular assay against <i>L. donovani</i>									Luciferase /MTT assay		
			Bio21 ^a			IPK ^{gh}			UNC ^{ik}		
I.D	R ¹	R ²	IC ₅₀ (μ M)	CC ₅₀ (μ M)	SI	IC ₅₀ (μ M)	CC ₅₀ (μ M)	SI	IC ₅₀ (μ M)	CC ₅₀ (μ M)	SI
2.001 _b	F-Ph	OMe	12	>100	>8.3	28	>100	>3.5	46	>50	>1.1
2.059 _b	F-Ph	H	36	>100 _m	>2.8	12	22	1.8	11	>50	>4.6
2.002 _b	2-(1 <i>H</i> -Pyrazol-5-yl)pyridine	OMe	5.3	>100 _m	>19	3.7 ^l	>100	>27	13	>50	>3.8
3.004 _{de}	2-(1 <i>H</i> -Pyrazol-5-yl)pyridine	H	0.68 ^l	>50	>74	6.0	>100	>17	23	>50	>2.2
2.009 _{bd}	4-Br-Ph	OMe	>100	>100 _m	>1.0	18	27	1.5	9.9	>50	>5.1
3.005 _c	4-Br-Ph	H	37	>100	>2.7	11	18	1.6	4.9	>50	>10

2.012 bc	4-Me-Ph	OMe	29 ^l	>100	>3.4	39	96	2.5	30	>50	>1.7
3.006 c	4-Me-Ph	H	2.4	>50	>20	14	22	1.6	9.0	>50	>5.6
2.015 de	3-Br-Ph	OMe	>100	>100	>1.0	17	28	1.6	13	>50	>3.8
3.007 c	3-Br-Ph	H	3.1	>50	>16	8.1	12	1.5	2.5	>50	>20
2.018 bd	3-Me-Ph	OMe	>100	>100 _m	>1.0	15	32	2.1	12	>50	>4.2
3.008 c	3-Me-Ph	H	3.5	>50	>14	13	22	1.7	8.7	>50	>5.7
2.024 b	2-Me-Ph	OMe	65	>100	>1.5	27	>100	>3.7	18	>50	>2.8
3.009 c	2-Me-Ph	H	57	>100 _m	>1.8	36	>100	>2.8	22	>50	>2.3
2.037 b	Cyclohexane	OMe	>100	>100	>1.0	>100	>100	>1.0	>50	>50	>1.0
3.010 c	Cyclohexane	H	46	>100 _m	>2.2	60	>100	>1.7	-	-	-
2.042 bc	1H-imidazole	OMe	11 ^l	>100 _m	>9.1	26	>100	>3.8	34	>50	>1.5
3.011 ce	1H-imidazole	H	6.4 ^l	>100 _m	>16	>100	>100	>1.0	>50	>50	>1.0
2.008 b	Ph	OMe	28	>100 _m	>3.6	15	>100	>6.7	-	-	-
3.012 c	Ph	H	4.5	>100	>22	10	36	3.6	20	>50	>2.5
3.016 fi	4-Cl-Ph	OMe	8.1	>100	12	26	75	2.9	-	-	-
3.013 c	4-Cl-Ph	H	12	>100	>8.3	9.1	19	2.1	7.3	>50	>6.8
3.017 fi	3-Cl-Ph	OMe	>10	>28	>2.8	19	>100	>5.3	-	-	-
3.014 c	3-Cl-Ph	H	8.5	>50	>5.9	6.0	11	1.8	>50	>50	>1.0
3.018 fi	2-Cl-Ph	OMe	13	>50	>3.8	17	>100	>5.9	-	-	-
3.015 c	2-Cl-Ph	H	8.1 ^l	>50	>6.2	21	66	3.1	9.9	>50	>5.1

a= anti *L. donovani* activity and toxicity measured in THP-1 transformed macrophage host cell lines using a top concentration of 100 μ M (2x serial dilution 10-point curve). Experiment performed in duplicate wells in one experiment, n=1.

b= control compounds for Bio21 *L. donovani* intramacrophage assay. Miltefosine IC₅₀= 11 μ M CC₅₀> 100 μ M

c= control compounds for Bio21 *L. donovani* intramacrophage assay. Miltefosine IC₅₀= 0.52 μ M CC₅₀> 100 μ M, Amphotericin B IC₅₀= 2.60 μ M CC₅₀= 26

d= control compounds for Bio21 *L. donovani* intramacrophage assay. Miltefosine IC₅₀= 0.47 μ M CC₅₀= 8.3 μ M, Amphotericin B IC₅₀= 0.69 μ M CC₅₀= 57

e= control compounds for Bio21 *L. donovani* intramacrophage assay. Miltefosine IC₅₀= 0.75 μ M CC₅₀= 91 μ M, Amphotericin B IC₅₀= 0.29 μ M CC₅₀= 83

f= control compounds for Bio21 *L. donovani* intramacrophage assay. Average from experimental replicates; Miltefosine IC₅₀= 0.39 \pm 0.55 μ M, CC₅₀> 20 μ M, Amphotericin B IC₅₀= 0.12 \pm 0.055 μ M, CC₅₀= 6.0 \pm 1.8 μ M

g= anti *L. donovani* activity and toxicity measured in THP-1 transformed macrophage host cell lines using a top concentration of 100 μ M (2x serial dilution 10-point curve)

h= control compounds for IPK intramacrophage *L. donovani* assay. Miltefosine IC₅₀= 1.7 μ M, CC₅₀>100 μ M, Amphotericin B IC₅₀= 0.83 μ M, CC₅₀> 100 μ M.

i = control compounds for IPK intramacrophage *L. donovani* assay. Miltefosine IC₅₀= 1.1 μ M, CC₅₀>100 μ M, Amphotericin B IC₅₀= 0.26 μ M, CC₅₀> 100 μ M.

j= anti *L. donovani* activity measured in THP-1 transformed macrophage host cell lines using luminescent expressing *L. donovani*. Experiment performed in triplicate wells in one experiment, n=1 using a concentration range of 1-50 μ M. DMSO was used as sole control against which the percent *L. donovani* viability is calculated

k= host cell toxicity measured in MTT assay with uninfected macrophage host cells. Experiment performed in triplicate wells in one experiment, n=1 using a concentration range of 1-50 μ M. DMSO was used as sole control against which the percent cell viability is calculated
l= values are a mean of two experiments, n=2
m = <50% activity at the top concentration tested (100 μ M).
- not tested

From **Table 3.14**, several patterns around Analogue Series 4 were observed. The loss of the RHS *para*-methoxy group often correlated to improved antileishmanial activity. This was evidenced by analogues **2.059** (*para*-fluoro substituent), **3.005** (*para*-bromo substituent), **3.006** (*para*-methyl substituent), **3.007** (*meta*-bromo substituent), **3.008** (*meta*-methyl substituent), **3.012** (unsubstituted LHS), **3.14** (*meta*-chloro substituent), **3.015** (*ortho*-chloro substituent), which displayed improved antileishmanial activity in comparison to their counterparts bearing the *para*-methoxy group within the RHS region of Scaffold 1. The loss of the RHS *para*-methoxy also often correlated to a loss of selectivity for *L. donovani*, more so within the intramacrophage assay performed by IPK. This was observed in several analogues, including **2.059**, **3.006**, **3.008**, **3.013**, **3.014**, which had reported moderate to high parasite inhibition within the IPK assay (< 20 μ M), though also reported low selectivity (SI < 3). In contrast, no host cell cytotoxicity was observed within the MTT colorimetric assay performed by UNC. As mentioned in Section **3.11**, the difference in CC₅₀ values was due to the difference in host cell infection. As the IPK intramacrophage assay evaluated antileishmanial activity and host cell cytotoxicity simultaneously within the same assay, host cells were required to be infected with *L. donovani*. This infection subjected host cells to increased stress levels that could impact host cell survival, and may become more sensitive to our investigative compounds, in comparison to the non-infected host cells employed in the MTT colorimetric assay performed by UNC.

Overall, low parasite selectivity (SI <3) was not reported within the Bio21 intramacrophage assay. This intramacrophage assay also measured cytotoxicity using infected host cells, whilst simultaneously assessing parasite inhibition. Following the guidelines described in Section **3.11**, these compounds were not cause for concern as each analogue had demonstrated selectivity (SI >3) for the parasite over the host cell in 2 out of 3 independent assays employed. Nonetheless, compound selectivity would be monitored closely in future work around analogues influenced by Series 4 compounds, particularly in the seemingly more sensitive IPK intramacrophage assay. It may be likely that the macrophages are employed in the mode of action within this series which may cause harm to the host cell whilst targeting the parasite. It may also be likely that these compounds do not fit tightly within specific putative binding site/s, and may be more promiscuous, causing varying cytotoxicity against the host cells. At this stage, we can only speculate, and this would also be investigated in future work, outside the scope of this project.

Analogue **3.007** (*meta*-bromo substituent) was one of the more significant compounds of Series 4, as higher, clear antileishmanial activity (< 5 μ M), along with parasite selectivity (SI > 3) was reported in

2 out of 3 independent assays employed. Analogue **3.007** was shown to improve parasite inhibition in 2 out of 3 independent assays, when compared to both hits **2.001**, **2.002** and structurally close analogue **2.015** (bearing the LHS *meta*-bromo substituent with RHS *para*-methoxy substituent). This suggested that the *para*-methoxy group within the RHS chemical space of Scaffold 1 was not required to exert antileishmanial activity. Additionally, the sterically larger, more lipophilic halogen seemed to be preferred over the initial *para*-fluoro of hit **2.001** and previous lead **2.059**.

As mentioned, the loss of the RHS *para*-methoxy group generally correlated to increased antileishmanial activity. When this structural modification was combined with substituents around the LHS ring of Scaffold 1 which possessed sterically larger, more lipophilic properties in comparison to the initial *para*-fluoro group of **2.001**, superior antileishmanial potency was observed over **2.001**, **2.059** as well as the respective counterparts retaining the RHS *para*-methoxy group. This was evidenced by analogues **3.006** (*para*-methyl substituent), **3.008** (*meta*-methyl substituent), **3.013** (*para*-chloro substituent), **3.014** (*meta*-chloro substituent), **3.015** (*ortho*-chloro substituent), which all reported high antileishmanial activity (< 10 μ M) within 2 out of 3 independent assays. Furthermore, **3.005** (*para*-bromo substituent) displayed moderate to high antileishmanial activity (\leq 11 μ M) within 2 out of 3 independent intramacrophage assays. This excluded analogue **3.009** (*ortho*-methyl substituent), which reported poor parasite inhibition. This may suggest that these more lipophilic, non-hydrogen bonding substituents were not tolerated at every position around the LHS aromatic ring of Scaffold 1. Interestingly, **3.012** which possessed the unsubstituted phenyl rings within the LHS and RHS regions of the chemical space, observed moderate to high antileishmanial activity (< 20 μ M) across all independent assays employed. This suggested that substitutions around the LHS and RHS phenyl rings of Scaffold 1 were not crucial to maintaining potency.

Removal of the *para*-methoxy group did not improve the antileishmanial activity **3.004** and **3.011** in comparison to their respective counterparts **2.002** and **2.042**. In the case of **3.004**, which bears the LHS pyridine pyrazole aromatic system influenced by hit **2.002**, high antileishmanial activity and clear selectivity for *L. donovani* was reported in at least 2 out of 3 independent assays. However, significant improvement to antileishmanial activity in comparison to **2.002** was only reported within the intramacrophage assay reported by Bio21. Since this strong level of parasite inhibition was not closely corroborated by the other independent assays, the level of parasite inhibition exerted by **3.004** remained uncertain. Nonetheless, high antileishmanial activity was observed overall. Even though parasite inhibition of **3.004** was not superior to the hit **2.002**, the loss of the RHS *para*-methoxy group did not correlate to a complete loss of potency, providing further evidence that this functionality was not crucial to maintaining key interactions with the putative binding site/s. A significant exception to this pattern was analogue **3.011** which bears an imidazole ring within the LHS region of the chemical space. In 2 out of 3 independent assays, the loss of the RHS *para*-methoxy group in **3.011** seemed to correlate with the direct loss of antileishmanial activity. High antileishmanial activity was only reported within the

Bio21 intramacrophage assay only ($IC_{50} = 6.4 \mu M$). In comparison, close analogue **2.042**, which retained the *para*-methoxy group within the RHS of the chemical space, was previously reported by Bio21 and GRIDD possess high antileishmanial activity (Section 3.12), though was only weakly active within the IPK and UNC intramacrophage assays. The variability pertaining to **3.011** and **2.042** may be due to weak binding within the putative binding site/s. It may be that these structures do possess some antileishmanial properties, though require further optimization to form stronger interactions with the putative binding site/s. Finally, as expected, the cyclohexane analogue **3.010** did not account for any significant antileishmanial activity, as its counterpart, **2.037** which retained the RHS *para*-methoxy group was confirmed as a false positive.

A summary of Analogue Series 4 is depicted below in **Figure 3.08**, where the loss of the RHS *para*-methoxy had in most causes improved activity compared to both hit **2.001**, previous lead **2.059** as well as the respective counterparts of Analogue Series 1, which retained the *para*-methoxy substituent within the RHS chemical space of Scaffold 1. The pyridine pyrazole LHS functionality was consistently active, with or without the *para*-methoxy. In comparison to the *para*-fluoro group of **2.001** and **2.059**, it seemed larger, more lipophilic, non-hydrogen bonding substituents were favoured, when combined with the loss of the RHS *para*-methoxy substituent of Scaffold 1. Additionally, no substitution at the LHS or RHS phenyl ring was required to maintain moderate levels of inhibition against *L. donovani*.

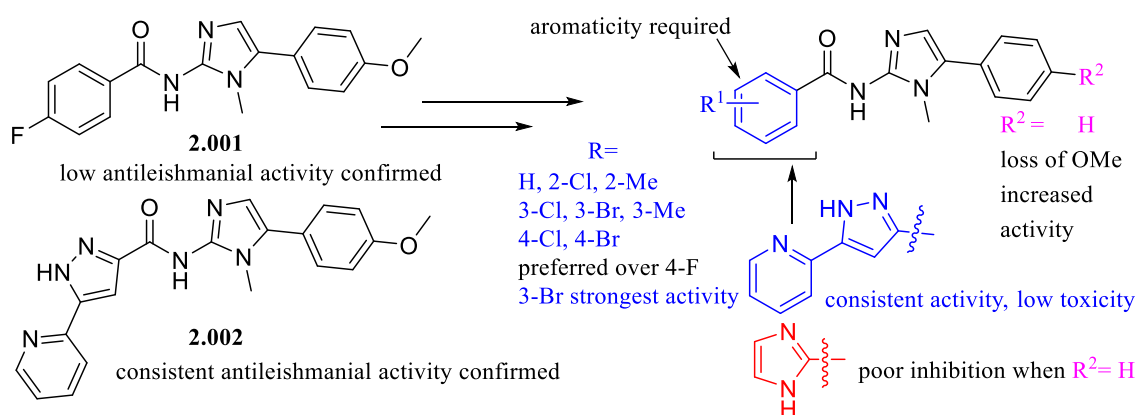


Figure 3.08: Summary of the SAR profile of Scaffold 1, derived from the confirmed biological results of Analogue Series 4

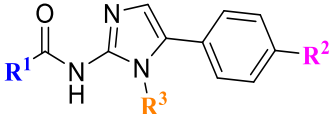
3.15 Complete biological analysis of Analogue Series 5 (*N*-alkyl and *N*-aryl modifications on the imidazole core)

This series was initially developed to determine whether the *N*-methyl of the imidazole core was crucial to maintaining antileishmanial activity. Further analogues were synthesized replacing the *N*-methyl with longer alkyl chains, as well as larger aliphatic and aromatic rings. This would determine if a large increase in lipophilicity and steric bulk within this region would allow for an improved fit within the

putative binding site/s and increase the number of key interactions formed with the putative binding site/s. This would also potentially deduce if this scaffold could interact with a potential lipophilic pocket within the putative binding site/s. Additionally, introducing aromaticity to this region of the chemical space would also probe if potential pi-pi interactions could be made between this region of the scaffold and the putative binding site/s. The structure of the remaining chemical space was influenced by hit **2.001** which bears the *para*-fluoro substituent on the LHS aromatic ring of the scaffold. Analogues **3.057-3.064** also possessed the unsubstituted phenyl ring within the RHS of the chemical space, influenced by previous lead **2.059**. Analogues **3.065-3.071** incorporated the cyclohexane ring within the LHS region of Scaffold 1, influenced by previous lead **2.037**. These structural modifications were incorporated as **2.059** and **2.037** were previously thought to be the most potent inhibitors of *L. donovani* at the time of synthesis. The complete set of biological results pertaining to these analogues are summarized in **Table 3.15**. Solubility issues were not reported for compounds within this series.

Variations in antileishmanial activity were observed between the independent intramacrophage assays against *L. donovani*. Higher potency was often reported by UNC in comparison to the remaining assays. It was uncertain why stronger inhibition was observed within this assay. Following the guidelines described in Section 3.11, compounds would need to display somewhat convergent activity (< 10 μ M) in at least 2 out of the 3 independent assays to be considered to have high antileishmanial activity.

Table 3.15: Complete summary of biological results of Series 5 and direct comparison of their related previous leads (blue)



I.D	R ¹	R ²	R ³	HCS intracellular assay against <i>L. donovani</i>						Luciferase /MTT assay		
				Bio21 ^{ac}			IPK ^{gh}			UNC ^{ij}		
				IC ₅₀ (μ M)	CC ₅₀ (μ M)	SI	IC ₅₀ (μ M)	CC ₅₀ (μ M)	SI	IC ₅₀ (μ M)	CC ₅₀ (μ M)	SI
2.001_b	4-F-Ph	OMe	Me	12	>100	>8.3	28	>100	>3.6	46	>50	>1.1
3.049	4-F-Ph	OMe	H	38	>100 ^f	>2.6	35	>100	>2.9	-	-	
3.050	4-F-Ph	OMe	Et	>100	>100 ^f	>1.0	27	48	1.8	-	-	
3.051	4-F-Ph	OMe	<i>i</i> Pr	>50 ^e	>50 ^e	>1.0	40	77	1.9	-	-	
3.052	4-F-Ph	OMe	Pr	18	>100	>5.6	7.0	14	2.0	2.3	41	18
3.053	4-F-Ph	OMe	Bu	>100 ^f	>100 ^f	>1.0	8.4	17	2.0	2.4	>50	>21
3.054	4-F-Ph	OMe	cPen	35	>100 ^f	>2.9	15	44	2.9	-	-	
3.055	4-F-Ph	OMe	Ph	6.1 ^d	8.8 ^d	1.4	5.7	>100	>18	1.1	26	24
3.056	4-F-Ph	OMe	Bnz	>100	>100 ^f	>1.0	36	>100	>2.8	3.6	>50	>14
2.059_b	4-F-Ph	H	Me	36	>100 ^f	>2.8	12	22	1.8	11	>50	>4.5

3.057	4-F-Ph	H	H	>50	>100 ^f	>2.0	46	>100	>2.2	-	-	
3.058	4-F-Ph	H	Et	9.0	>50	>5.6	8.5	12	1.4	23	>50	>2.2
3.059	4-F-Ph	H	<i>i</i> Pr	8.2	>50	>6.1	9.3	13	1.4	2.8	>50	>18
3.060	4-F-Ph	H	Pr	>100 ^f	>100 ^f	>1.0	7.7	15	1.9	2.1	>50	>24
3.061	4-F-Ph	H	Bu	6.2	>100 ^f	>16	12	23	1.9	2.2	>50	>23
3.062	4-F-Ph	H	cPen	6.7	13	1.9	10	12	1.2	2.9	50	17
3.063	4-F-Ph	H	Ph	30 ^k	>100 ^f	>3.3	7.0	17	2.4	2.7	26	9.6
3.064	4-F-Ph	H	Bnz	40	>100 ^f	>2.5	11	19	1.7	1.7	>50	>29
2.037 _b	cHex	OMe	Me	>100	>100	>1.0	>100	>100	>1.0	>50	>50	>1.0
3.065	cHex	OMe	Et	23	>100 ^f	>4.3	35	>100	>2.9	>10	>50	>5.0
3.066	cHex	OMe	<i>i</i> Pr	>100 ^f	>100 ^f	>1.0	23	53	2.3	>10	>50	>5.0
3.067	cHex	OMe	Pr	6.2	>50	>8.1	16	72	4.5	-	-	
3.068	cHex	OMe	Bu	>10	>40	>4.0	9.2	57	6.2	-	-	
3.069	cHex	OMe	cPen	46	>100 ^f	>2.2	11	34	3.1	-	-	
3.070	cHex	OMe	Ph	>50 ^e	>50 ^e	>1.0	44	>100	>2.3	-	-	
3.071	cHex	OMe	Bnz	>100 ^f	>100 ^f	>1.0	13	>100	>7.7	-	-	

cHex= cyclohexane, cPen= cyclopentane, Ph= phenyl, Bnz= benzyl

a= anti *L. donovani* activity and toxicity measured in THP-1 transformed macrophage host cell lines using a top concentration of 100 μ M (2x serial dilution 10-point curve). Experiment performed in duplicate wells in one experiment, n=1.

b= control compounds for Bio21 *L. donovani* intramacrophage assay. Miltefosine IC₅₀= 11 μ M CC₅₀> 100 μ M

c= control compounds for Bio21 *L. donovani* intramacrophage assay. Miltefosine IC₅₀= 0.50 \pm 0.02 μ M CC₅₀> 10 μ M, Amphotericin B IC₅₀= 1.5 \pm 0.80 μ M CC₅₀>26

d= control compounds for Bio21 *L. donovani* intramacrophage assay. Miltefosine IC₅₀= 0.78 μ M CC₅₀= 14 μ M, Amphotericin B IC₅₀= 0.078 μ M CC₅₀= 7.3 μ M

e= anti *L. donovani* activity and toxicity measured in THP-1 transformed macrophage host cell lines using a one-point concentration (50 μ M) to assess any form of antileishmanial activity. Experiment performed in duplicate wells in one experiment, n=1

f= <50% activity at the top concentration tested (100 μ M).

‡= poor solubility observed in DMSO stock (100mM) used for Bio21 assay

g= anti *L. donovani* activity and toxicity measured in THP-1 transformed macrophage host cell lines using a top concentration of 100 μ M (2x serial dilution 10-point curve)

h= control compounds for IPK intramacrophage *L. donovani* assay. Miltefosine IC₅₀= 1.7 μ M, CC₅₀>100 μ M, Amphotericin B IC₅₀= 0.83 μ M, CC₅₀> 100 μ M.

i= anti *L. donovani* activity measured in THP-1 transformed macrophage host cell lines using luminescent expressing *L. donovani*. Experiment performed in triplicate wells in one experiment, n=1 using a concentration range of 1-50 μ M. DMSO was used as sole control against which the percent *L. donovani* viability is calculated

j= host cell toxicity measured in MTT assay with uninfected macrophage host cells. Experiment performed in triplicate wells in one experiment, n=1 using a concentration range of 1-50 μ M. DMSO was used as sole control against which the percent cell viability is calculated

k= values are a mean of two experiments, n=2

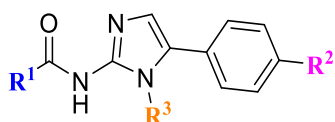
From **Table 3.15**, variations in host cell cytotoxicity were observed between the HCS intramacrophage assays performed by Bio21 and IPK and the MTT colorimetric assay performed by UNC. As previously outlined, this could be expected as the Bio21 and IPK methods assess host cell viability using infected macrophages, which may be more sensitive to our investigative compounds in comparison to the MTT colorimetric assay, which employs uninfected host macrophages. Structural modifications that significantly reduced selectivity for the parasite over the host cell (SI <3) in 2 out of 3 assays, such as **2.062** would be avoided in future studies, as such cytotoxicity levels would suggest any that antileishmanial activity that was observed may be induced by harming the host cell, followed by

subsequent harm to the internalized parasite, rather than targeting the parasite directly. Though analogue **2.062** did not display strong host cell cytotoxicity within the MTT assay performed by UNC, both clinically relevant intramacrophage assays had reported convergent CC₅₀ values and significant cell death. Additionally, the antileishmanial activity reported was not nearly significant enough (sub micromolar) to advocate for continued studies around analogue **2.062**.

Outlined in **Table 3.15**, the loss of the *N*-methyl group correlated to poor parasite inhibition, as evidenced by **3.049**, **3.057**, which possess the secondary amine within the imidazole ring. Replacing the *N*-methyl group with slightly longer carbon chains, namely ethyl and isopropyl groups, were not favourable when the *para*-methoxy substituent was present within the RHS region of Scaffold 1. Analogues **3.050**, **3.051** which possessed these structural changes may have not allowed for specific interactions with the putative binding site/s to occur. Analogues **3.065** (*N*-ethyl), **3.066** (*N*-isopropyl), which bear the cyclohexane ring at the LHS chemical space of Scaffold 1, exhibited unanimously poor inhibition (> 20 µM). This was to be expected, as these analogues were influenced by previous lead compound **2.037**, which has been confirmed as a false positive. However, when larger increases in lipophilicity were introduced at this position, in the form of longer aliphatic chains, aliphatic and aromatic rings, improved antileishmanial activity was generally observed, regardless of the structural modifications to the LHS and RHS regions of Scaffold 1. This increase in antileishmanial activity was likely due to the lipophilic effect, where structural changes that provide an increase in lipophilicity may have simply improved the ability of a compound to permeate the cell barriers and reach the target site to exert some form of potency, rather than contributing to a better fit or allowing for stronger interactions within the putative binding site/s.

To understand how beneficial these structural changes were to Scaffold 1, we would consider the balance of lipophilicity with antileishmanial potency. This was achieved by measuring the Lipophilic Efficiency (LiPE = pIC₅₀ – log P) of each analogue within Series 5, and is outlined in **Table 3.16**.^{48, 49} When the bioactivity is increased more so than the Log P, the LiPE is also improved, suggesting the structural change provides true merit. Compounds with LiPE above 5 are considered to be highly optimized.⁴⁸ Since we are at the early stages in our campaign, we are aiming to obtain a lead compound with improved LiPE of at least 3. This form of measurement is difficult to use when comparing compounds of vastly different sizes and potencies, as well as when a target may require very polar compounds.⁴⁹ Nevertheless, the use of this metric seems to be valid here, as all compounds did not vary largely in molecular weight and the antileishmanial activity examined here did not differ immensely, as all compounds exhibiting activity within the micromolar range. Though we have yet to discover our biological target of interest, potency has been achieved with analogues possessing moderate Log P values, suggesting the target binding site may not require compounds with largely increased polarity.

Table 3.16: Comparison of Log P, antileishmanial activity and LipE within Series 5



					HCS intracellular assay against <i>L. donovani</i>				Luciferase /MTT assay	
					Bio21 ^{ac}		IPK ^{gh}		UNC	
ID	R ¹	R ²	R ³	Log P [*]	IC ₅₀ (μM)	LipE ^k	IC ₅₀ (μM)	LipE ^k	IC ₅₀ (μM)	LipE ^k
2.001 ^b	4-F-Ph	OMe	Me	3.4	12	1.5	28	1.2	46	0.93
3.049	4-F-Ph	OMe	H	3.7	38	0.72	35	0.76	-	-
3.050	4-F-Ph	OMe	Et	3.8	>100	<0.20	27	0.77	-	-
3.051	4-F-Ph	OMe	<i>i</i> Pr	4.2	>50 ^e	<-0.10	40	0.20	-	-
3.052	4-F-Ph	OMe	Pr	4.3	18	0.44	7.0	0.85	2.3	1.3
3.053	4-F-Ph	OMe	Bu	4.7	>100 ^f	<-0.70	8.4	0.38	2.4	0.91
3.054	4-F-Ph	OMe	cPen	4.8	35	-0.34	15	0.023	-	-
3.055 ^d	4-F-Ph	OMe	Ph	5.1	6.1	0.10	5.7	0.14	1.1	0.86
3.056	4-F-Ph	OMe	Bnz	5.1	>100	<-1.1	36	-0.66	3.6	0.34
2.059 ^b	4-F-Ph	H	Me	3.6	36	0.84	12	1.3	11	1.4
3.057	4-F-Ph	H	H	3.8	50	0.50	46	0.54	-	-
3.058	4-F-Ph	H	Et	3.9	9.0	1.1	8.5	1.2	23	0.74
3.059	4-F-Ph	H	<i>i</i> Pr	4.3	8.2	0.79	9.3	0.73	2.8	1.3
3.060	4-F-Ph	H	Pr	4.4	>100 ^f	<-0.40	7.7	0.71	2.1	1.3
3.061	4-F-Ph	H	Bu	4.9	6.2	0.31	12	0.021	2.2	0.80
3.062	4-F-Ph	H	cPen	4.9	6.7	0.27	10	0.10	2.9	0.64
3.063	4-F-Ph	H	Ph	5.2	30 ^j	-0.68	7.9	-0.010	2.7	0.37
3.064	4-F-Ph	H	Bnz	5.3	40	-0.90	11	-0.34	1.7	0.47
2.037 ^b	cHex	OMe	Me	3.5	>100	<0.50	>100	<0.50	>50	<0.80
3.065	cHex	OMe	Et	3.9	23	0.74	35	0.56	>10	<1.1
3.066	cHex	OMe	<i>i</i> Pr	4.3	>100 ^f	<-0.3	23	0.34	10	0.70
3.067	cHex	OMe	Pr	4.4	6.2	0.81	16	0.40	-	-
3.068	cHex	OMe	Bu	4.9	5.6	0.35	9.2	0.14	-	-
3.069	cHex	OMe	cPen	4.9	46	-0.54	11	0.078	-	-
3.070	cHex	OMe	Ph	5.2	>50 ^e	<-0.90	44	-0.84	-	-
3.071	cHex	OMe	Bnz	5.3	>100 ^f	<-1.3	13	-0.41		

a= anti *L. donovani* activity and toxicity measured in THP-1 transformed macrophage host cell lines using a top concentration of 100 μM (2x serial dilution 10-point curve). Experiment performed in duplicate wells in one experiment, n=1.

b= control compounds for Bio21 *L. donovani* intramacrophage assay. Miltefosine IC₅₀= 11 μM CC₅₀> 100 μM

c= control compounds for Bio21 *L. donovani* intramacrophage assay. Miltefosine IC₅₀= 0.50 ± 0.02 μM CC₅₀ > 10 μM, Amphotericin B IC₅₀= 1.5 ± 0.80 μM CC₅₀>26

d= control compounds for Bio21 *L. donovani* intramacrophage assay. Miltefosine IC₅₀= 0.78 μM CC₅₀= 14 μM, Amphotericin B IC₅₀= 0.078 μM CC₅₀= 7.3 μM

e= anti *L. donovani* activity and toxicity measured in THP-1 transformed macrophage host cell lines using a one-point concentration (50 μM) to assess any form of antileishmanial activity. Experiment performed in duplicate wells in one experiment, n=1

f= <50% activity at the top concentration tested (100 μM).

‡= poor solubility observed in DMSO stock (100mM) used for Bio21 assay

g= anti *L. donovani* activity and toxicity measured in THP-1 transformed macrophage host cell lines using a top concentration of 100 μM (2x serial dilution 10-point curve)

h= control compounds for IPK intramacrophage *L. donovani* assay. Miltefosine IC₅₀= 1.7 μM, CC₅₀ >100 μM, Amphotericin B IC₅₀= 0.83 μM, CC₅₀ > 100 μM.

i= anti *L. donovani* activity measured in THP-1 transformed macrophage host cell lines using luminescent expressing *L. donovani*. Experiment performed in triplicate wells in one experiment, n=1 using a concentration range of 1-50 μ M. DMSO was used as sole control against which the percent *L. donovani* viability is calculated

j= values are a mean of two experiments, n=2

k= LiPE calculated from pIC₅₀ value minus the calculated log P

- not tested

*Partition co-efficient calculated using CDD Vault software

Ryckmans *et al.* suggests that changes that improve potency by tenfold may appear advantageous, though that change may be deceptive if the lipophilicity of said compound is increased by a similar amount (one Log P or Log D unit).⁴⁸ This seemed to be the case for many of the analogues found highly active (<10 μ M) in at least 2 out of the 3 independent bioassays. This included analogues bearing longer aliphatic chains, namely propyl (**3.052**), butyl (**3.053**, **3.062**, **3.068**) groups, cycloaliphatic substituents (**3.062**) and aromatic rings (**3.055**, **3.063**, **3.064**), which increased lipophilicity by at least one Log P unit in comparison to the original hit **2.001**, or previous lead compound **2.059** or **2.037** in which these analogues were derived from. If these structural modifications allowed for significant interactions with the putative binding site/s, a much larger surge in antileishmanial activity would have been detected. This is attested by the low LiPE values (<1.5) reported for each analogue within Series 5, calculated for each independent bioassay. These low LiPE values suggested that the improvement to antileishmanial activity observed within these analogues was simply due to the increased ability to permeate the cell and inner barriers, rather than an improved ability to interact with the putative binding site/s in a more meaningful manner.

Analogues **3.058** (*N*-ethyl), **3.059** (*N*-isopropyl), **3.060** (*N*-propyl) which bear the unsubstituted phenyl ring within the RHS chemical space of Scaffold 1, also reported high antileishmanial activity (< 10 μ M) within at least 2 out of the 3 independent intramacrophage assays. These analogues did not increase the overall lipophilicity of the scaffold by large amounts in comparison to **2.059** (less than one Log P). Analogues **3.059-3.060** did not provide any improvement in LiPE values in comparison to **2.059**, whilst the *N*-ethyl substitution (**3.058**) displayed a slight improvement to LiPE when evaluating the results from the Bio21 intramacrophage assay. In comparison to the related compound **2.059**, the LiPE of **3.058** remained unchanged following the biological results reported by IPK. Overall, this suggested that these structural changes did not provide significantly stronger binding interactions within the putative active site/s. However, since these modifications did not involve largely increasing lipophilicity, these small aliphatic groups could be introduced to future analogues to help increase antileishmanial activity, if required.

Not all compounds within this series were able to undergo biological evaluations performed by UNC, though this was not required. Despite the more potent antiparasitic behaviour observed within this assay, overall bioactivity still seemed to be due to lipophilic effect, where increasing the lipophilicity of the overall scaffold allowed for an improved ability to permeate cell barriers, rather than improving the ability to interact with the putative binding site/s more tightly. Thus, further exploration around these

larger lipophilic structural changes to this region of Scaffold 1 was not worthwhile. Furthermore, compounds that greatly increased the Log P (Log P > 4) gave less room for any further additions that may be required in future lead compounds. Striking a balance between Log P and molecular weight (<500 Da) is in our interest, to allow for easier optimization of lead candidates and to avoid poor solubility.⁴⁹ Large molecular weight is not an issue at this stage, though the larger analogues of Series 5 possess a Log P > 4. Higher Log P values have been reported to show an increased risk of adverse effects within animal safety studies.⁴⁸ Therefore, unless this boost in lipophilicity gave any true benefit to binding ability such structural changes would not be pursued.

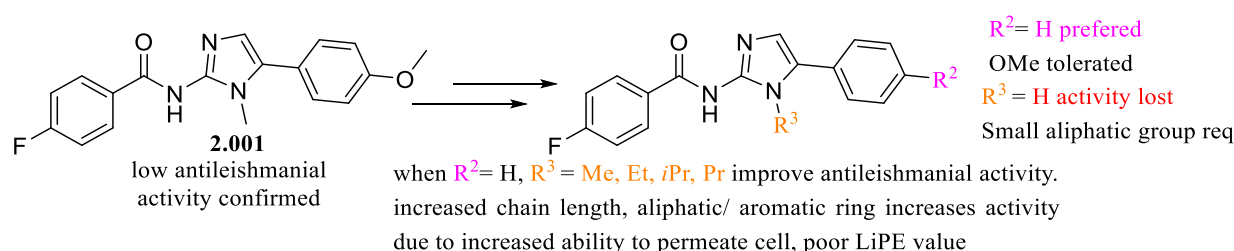


Figure 3.09: Summary of the SAR profile of Scaffold 1, derived from the confirmed biological results of Analogue Series 5

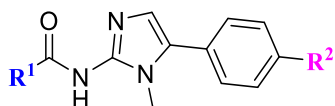
3.16 Complete biological analysis of Analogue Series 6 (Further exploration of the substituents around the RHS phenyl ring)

This series of analogues involved substituting small functional groups around the RHS aromatic ring of Scaffold 1. These functionalities possessed different hydrogen bonding abilities, electronic and hydrophobic properties to help determine if certain substituents were preferred within this region of the chemical space, in comparison to the initial *para*-methoxy group of **2.001**, or the unsubstituted phenyl ring of **2.059**. Structural changes to the LHS chemical space of Scaffold 1 were also included within this study, replacing the *para*-fluoro group with the *ortho*-methyl substituent influenced by previous lead **2.024**. The imidazole ring was also incorporated within the LHS region of Scaffold 1, influenced by previous lead **2.042**. The biological results of this series are summarized in **Table 3.17**. For comparative ease, the hit **2.001** and previous leads **2.024**, **2.042** have been included. Additionally, their respective counterparts **2.059** (LHS *para*-fluoro substituent), **3.009** (LHS *ortho*-methyl substituent) and **3.011** (LHS imidazole ring), which each bear the unsubstituted phenyl ring within the RHS region of the chemical space, were also included in **Table 3.17**.

Variations in cytotoxicity were also observed within this series between the HCS intramacrophage assays performed by Bio21 and IPK and the MTT colorimetric assay performed by UNC. Following the guidelines set in Section 3.11, each compound within this series reported higher selectivity for the

parasite over the host cell (SI >3) in at least 2 out of 3 independent bioassays. Thus, the *in vitro* cytotoxicity was not a large concern. Nonetheless, compound selectivity would be monitored closely in future work around analogues influenced by Series 6 compounds, particularly in the seemingly more sensitive IPK intramacrophage assay

Table 3.17: Summary of biological results for Analogue Series 6. Hit and previous leads outlined in blue.



			HCS intracellular assay against <i>L. donovani</i>						Luciferase /MTT assay		
			Bio21 ^{ac}			IPK ^{gh}			UNC ^{ij}		
ID	R ¹	R ²	IC ₅₀ (μM)	CC ₅₀ (μM)	SI	IC ₅₀ (μM)	CC ₅₀ (μM)	SI	IC ₅₀ (μM)	CC ₅₀ (μM)	SI
2.001 _b	4-F-Ph	4-OMe	12	>100 ^e	>8.3	28	>100	>3.5	46	>50	>1.1
2.059 _b	4-F-Ph	H	36	>100 ^e	>2.8	12	22	1.8	11	>50	>4.5
3.091 _f	4-F-Ph	4-CN	>50	>50	>1.0	>100	>100	>1.0	>50	>50	>1.0
3.092	4-F-Ph	4-Cl	4.9	37	7.6	15	32	2.1	6.2	>50	>8.1
3.093	4-F-Ph	4-Br	7.1	46	6.5	12	37	3.1	>50	>50	>1.0
3.094 _d	4-F-Ph	4-F	>100 ^e	>100 ^e	>1.0	16	82	5.1	17	>50	>2.9
3.095	4-F-Ph	4-Me	13	60	4.5	21	62	3.0	25	>50	>2.0
3.096 _f	4-F-Ph	4-NO ₂	>50	>50	>1.0	29	>100	>3.4	20	>50	>2.5
3.097	4-F-Ph	3-CN	16	>100	>6.3	>100	>100	>1.0	42	>50	>1.2
3.098	4-F-Ph	3-Cl	22	>50	>2.3	6.3	12	1.9	4.9	>50	>10
3.099	4-F-Ph	3-Br	5.4	>50	9.3	5.5	11	2.0	20	>50	>2.5
3.100	4-F-Ph	3-F	12	58	4.8	12	34	2.8	7.1	>50	>7.0
3.101	4-F-Ph	3-Me	79	>100 ^e	>1.3	7.1	14	2.0	>50	>50	>1.0
3.102 _f	4-F-Ph	3-NO ₂	>50	>50	>1.0	84	>100	>1.2	>50	>50	>1.0
3.103	4-F-Ph	2-Cl	15	>50	3.3	6.2	10	1.6	15	>50	>3.3
3.104 _d	4-F-Ph	2-Br	>100	>100	>1.0	>100	>100	>1.0	6.7	>50	>7.5
3.105 _d	4-F-Ph	2-F	>100 ^e	>100 ^e	>1.0	11	27	2.5	12	>50	>4.2
3.106	4-F-Ph	2-Me	3.9	>50	>13	17	47	2.8	27	>50	>1.9
3.107	4-F-Ph	2-NO ₂	9.8	31	3.2	34	>100	2.9	32	>50	>1.6
2.024 _b	2-Me-Ph	4-OMe	65	>100	>1.5	27	>100	>3.7	18	>50	>2.8
3.009	2-Me-Ph	H	57	>100 ^e	>1.8	36.	>100	>2.8	22	>50	>2.3
3.108 _f	2-Me-Ph	4-CN	>50	>50	>1.0	>100	>100	>1.0	-	-	
3.109	2-Me-Ph	4-Cl	8.1	59	7.3	27	>100	>3.7	27	>50	>1.9

3.110 f	2-Me-Ph	3-CN	>50	>50	>1.0	>100	>100	>1.0	-	-	
3.111	2-Me-Ph	3-Cl	2.1	18	8.6	11	27	2.5	2.7	>50	>19
3.112	2-Me-Ph	3-OMe	>100 ^e	>100 ^e	>1.0	18	40	2.2	-	-	
3.113	2-Me-Ph	2-Cl	11	>100	>9.1	45	>100	>2.2	-	-	
3.114	2-Me-Ph	2-OMe	8.4	>50	>6.0	22	>100	>4.5	-	-	
2.042 bc	1- <i>H</i> -imidazole	4-OMe	11 ^k	>100 ^e	>9.1	26	>100	>3.8	34	>50	>1.5
3.011 bd	1- <i>H</i> -imidazole	H	6.4 ^k	>100 ^e	>16	>100	>100	>1.0	>50	>50	>1.0
3.115	1- <i>H</i> -imidazole	4-CN	14	>100 ^e	>7.1	35	>100	>2.9	>50	>50	>1.0
3.116	1- <i>H</i> -imidazole	4-Cl	0.52	52	100	3.9	>100	>26	>50	>50	>1.0
3.117 f	1- <i>H</i> -imidazole	3-CN	>50	>50	>1.0	80	>100	>1.3	-	-	
3.118	1- <i>H</i> -imidazole	3-Cl	0.74	55	74	3.5	>100	>29	16	>50	>3.1
3.119	1- <i>H</i> -imidazole	3-OMe	8.1	>100 ^e	>12	20	>100	>5.0	>50	>50	>1.0
3.120	1- <i>H</i> -imidazole	2-Cl	5.2	>50	>9.6	25	>100	>4.0	-	-	
3.121 f	1- <i>H</i> -imidazole	2-OMe	>50	>50	>1.0	53	>100	>1.9	>50	>50	>1.0

a= anti *L. donovani* activity and toxicity measured in THP-1 transformed macrophage host cell lines using a top concentration of 100 μ M (2x serial dilution 10-point curve). Experiment performed in duplicate wells in one experiment, n=1.

b= control compounds for Bio21 *L. donovani* intramacrophage assay. Miltefosine IC₅₀= 11 μ M CC₅₀> 100 μ M

c= control compounds for Bio21 *L. donovani* intramacrophage assay. Average from experimental replicates; Miltefosine IC₅₀ = 0.50 \pm 0.026 μ M, CC₅₀ > 10 μ M, Amphotericin B IC₅₀ = 1.6 \pm 0.93 μ M, CC₅₀ > 26 μ M

d= control compounds for Bio21 *L. donovani* intramacrophage assay. Miltefosine IC₅₀= 0.75 μ M CC₅₀= 91 μ M, Amphotericin B IC₅₀= 0.29 μ M CC₅₀= 83 μ M

e= <50% activity at the top concentration tested (100 μ M).

f= anti *L. donovani* activity and toxicity measured in THP-1 transformed macrophage host cell lines using a one-point concentration (50 μ M) to assess any form of antileishmanial activity. Experiment performed in duplicate wells in one experiment, n =1

g= anti *L. donovani* activity and toxicity measured in THP-1 transformed macrophage host cell lines using a top concentration of 100 μ M (2x serial dilution 10-point curve)

h= control compounds for IPK intramacrophage *L. donovani* assay. Miltefosine IC₅₀= 1.7 μ M, CC₅₀ >100 μ M, Amphotericin B IC₅₀= 0.83 μ M, CC₅₀ > 100 μ M.

i= anti *L. donovani* activity measured in THP-1 transformed macrophage host cell lines using luminescent expressing *L. donovani*. Experiment performed in triplicate wells in one experiment, n=1 using a concentration range of 1-50 μ M. DMSO was used as sole control against which the percent *L. donovani* viability is calculated

j= host cell toxicity measured in MTT assay with uninfected macrophage host cells. Experiment performed in triplicate wells in one experiment, n=1 using a concentration range of 1-50 μ M. DMSO was used as sole control against which the percent cell viability is calculated

k= values are a mean of two experiments, n=2

- not tested

From **Table 3.17**, it was encouraging to find that consistent antileishmanial activity was often observed within this series, across each independent bioassay. From these results, several patterns around Analogue Series 6 emerged. More hydrophilic, stronger electron withdrawing functionalities, namely cyano and nitro substituents, were not well tolerated at any position around the RHS phenyl ring. This was evidenced by analogues **3.091** (*para*-cyano), **3.095** (*para*-nitro), **3.097** (*meta*-cyano), **3.102** (*meta*-nitro), **3.107** (*ortho*-nitro) which reported poor antileishmanial activity (> 20 μ M) in at least 2 out of 3 independent intramacrophage assays, against *L. donovani*. The structure of these analogues was derived

from **2.001** and **2.059**, excluding the change to the RHS region of the scaffold. Substitution of the cyano functionality within analogues **3.108**, **3.110** and **3.115**, **3.177** also caused poor parasite inhibition. These analogues possessed the LHS *ortho*-methyl substitution and imidazole ring replacement respectively. Overall, this suggested that increasing the hydrophilicity at this region of the chemical space was unfavourable. Hydrogen bonding ability also did not seem to be required within this region of the scaffold. In contrast, when analogues possessed the *para*-fluoro substituent within the phenyl ring of LHS region of the scaffold, incorporating halogens to the RHS phenyl ring was often found to improve antileishmanial activity. Substituting the fluoro group (**3.094**, **3.100**, **3.105**) at each position of the aromatic ring was found to improve antileishmanial activity in comparison to the initial hit **2.001**, exerting moderate activity ($< 20 \mu\text{M}$) within at least 2 out of the 3 independent bioassays. Introduction of the bromo substituent at the *para*-position (**3.093**) and the chloro substituent at the *ortho*-position (**3.103**) also exhibited moderate antileishmanial activity in at least 2 out of the 3 independent bioassays. High antileishmanial activity ($< 10 \mu\text{M}$) was reported for analogues bearing chloro substituents at the *para* (**3.092**) and *meta*-positions (**3.098**), as well as the bromo substituent at the *meta*-position (**3.099**).

From these results, it seemed that the sterically larger, more lipophilic halogens were favourable at the *meta* and *para* positions of the RHS aromatic ring. These halogens also possess electron withdrawing ability, though are not as strongly withdrawing as the nitro and cyano functionalities. This suggests the electron poor aromatic ring is actually tolerated, though more lipophilic functionalities are required to allow for favourable interactions with the putative binding site/s. It was interesting to discover that *meta* and *para*-bromo and chloro substituents were highly favourable within this region of the chemical space, as these substituents were also found favourable when placed at the LHS region of the chemical space. This was observed previously within Analogue Series 4, Section **3.14**, which comprised of compounds bearing the unsubstituted RHS phenyl ring. Within Analogue Series 4, the *meta*-bromo (**3.005**) and chloro (**3.013**) substituents, and the *para*-bromo (**3.007**), *para*-chloro (**3.014**) substituents of **Table 3.14** exhibited moderate to high antileishmanial activity. These results may suggest that possible pseudo-symmetry existed within the scaffold, where the opposing LHS and RHS regions of Scaffold 1 may have the ability to interact with a specific portion of the putative binding site/s.

Positioning the *meta* and *para*-chloro substituents at the RHS phenyl ring of Scaffold 1 seems to have been the most consistent improvement within this series. When these RHS structural modifications were paired with the *ortho*-methyl functionality (**3.111**) or the imidazole ring replacement (**3.116**, **3.118**) within the LHS region of the chemical space, very high, clear antileishmanial activity ($< 5 \mu\text{M}$) was displayed in at least 2 out of the 3 independent intramacrophage assays. Analogues **3.111**, **3.116** and **3.118** were also found to be selective for the parasite over the host cell ($\text{SI} > 3$) in at least 2 out of the 3 independent assays employed.

Due to the superior antileishmanial activity displayed, these analogues were identified here as our new early lead compounds. This was rather humorous as analogues **3.111**, and **3.116**, **3.118** were derived from previous leads **2.024** and **2.042** respectively. The previous leads **2.024** and **2.042** underwent several rounds of biological assessment to confirm only moderate to low parasite inhibition were exerted by these compounds. If it were not for the initial rounds of testing by GRIDD and Bio21 that suggested stronger antileishmanial behaviour within previous leads **2.024** and **2.042**, these structural changes may not have been pursued further and these new leads may not have been discovered. A summary of the results surrounding Analogue Series 6 is summarized below in **Figure 3.10**.

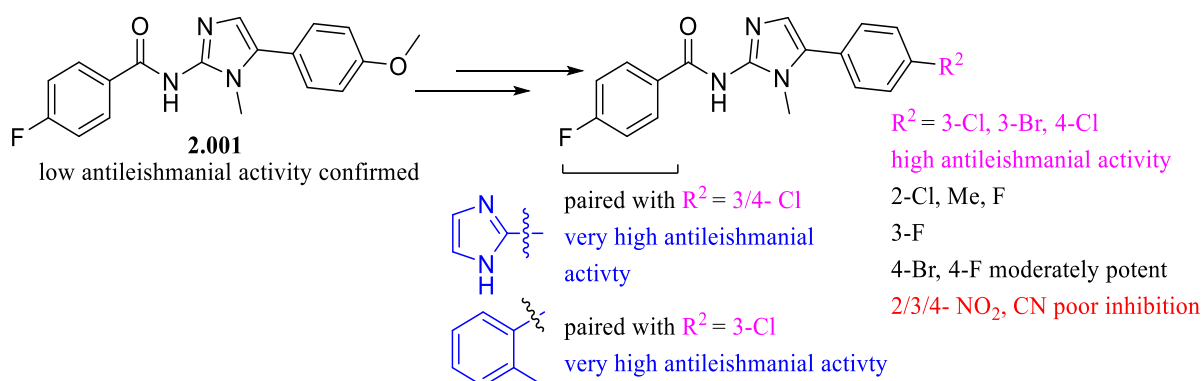


Figure 3.10: Summary of the SAR profile of Scaffold 1, derived from the confirmed biological results of Analogue Series 6

The dose response curves of **3.111** and **3.116** reported by Bio21 are depicted in **Figure 3.11a-b** and **Figure 3.12a-b** respectively. These curves serve as a visual demonstration of the activity and selectivity of **3.111** and **3.116** against *L. donovani* within THP-1 macrophages. These curves are used as representatives to depict the consistent potency of **3.111** and **3.116** reported by most of our collaborators. **Figure 3.11a** and **Figure 3.12a** were used to report the IC_{50} against *L. donovani* and depicts the reduction of parasite burden, where an increase in compound concentration correlated to a decrease in the percentage of infection within viable host macrophage cells. A host cell is considered infected when ≥ 3 parasites per host macrophage are detected. **Figure 3.11b** and **Figure 3.12b** was used to determine the CC_{50} and cytotoxicity against the THP-1 transformed host macrophages. Although **Figure 3.11b** displayed some cytotoxicity against the host macrophage, **3.111** was still more selective for the parasite over the host cell. From **Figure 3.12b**, cytotoxicity was only observed at high concentrations, also suggesting **3.116** was selective for the parasite over the host cell.

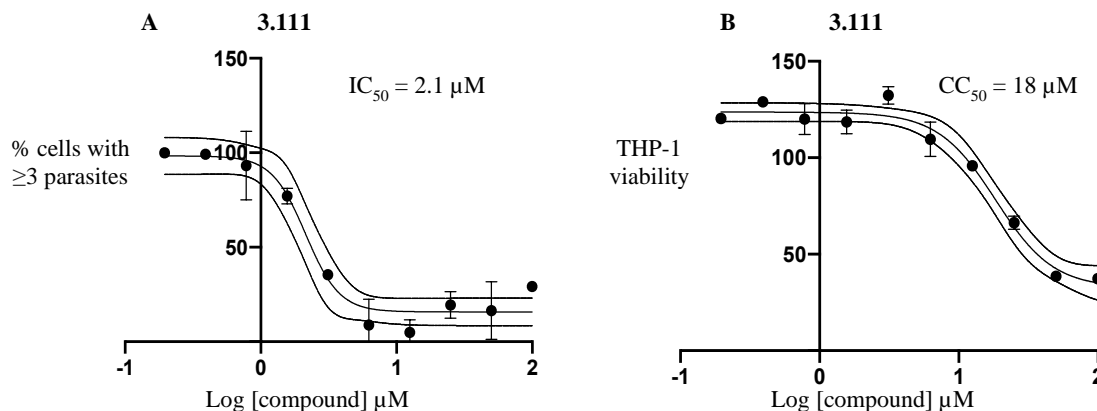


Figure 3.11a-b: Dose response curves of 3.111 reported by Bio21, a) measuring compound concentration (x axis) against % of infection within host macrophages (y axis) to determine the antileishmanial activity (IC_{50}) of 3.111, b) measuring compound concentration (x axis) against the viability of the THP-1 transformed macrophages (y axis) to determine the cytotoxicity against the host cell (CC_{50})

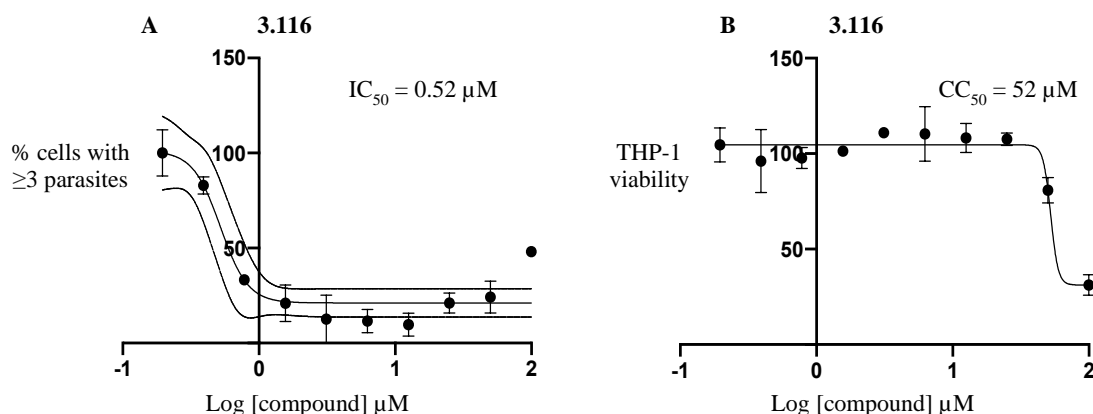


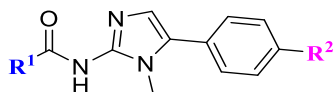
Figure 3.12a-b: Dose response curves of 3.116 reported by Bio21, a) measuring compound concentration (x axis) against % of infection within host macrophages (y axis) to determine the antileishmanial activity (IC_{50}) of 3.116, b) measuring compound concentration (x axis) against the viability of the THP-1 transformed macrophages (y axis) to determine the cytotoxicity against the host cell (CC_{50})

Measuring the LiPE of highly potent antileishmanial analogues from Series 6 in comparison to previous leads

Briefly, a comparison of lipophilic efficiency of the most potent analogues of Analogue Series 6 is summarized in **Table 3.18** to understand how beneficial the insertion of heavier hydrophobic atoms was to this chemical space. This was achieved by calculating the LiPE ($\text{LiPE} = \text{pIC}_{50} - \text{Log P}$) of each compound. As stated in Section 3.15, if the antileishmanial activity is increased more so than the Log P, the LiPE is also improved, suggesting the modification provides improved interactions with the

putative binding site/s. Compounds with LiPE above 5 are considered to be highly optimized.⁴⁸ Since we are at the early stages in our campaign, we are aiming to obtain a lead compound with improved LiPE of at least 3, within at least of 2 out the 3 independent bioassays.

Table 3.18: Comparison of lipophilic efficiency between Series 6 lead analogues (pink) and previous leads (blue)



I.D	Structure R ¹ R ²		Log P [*]	HCS intracellular assay against <i>L. donovani</i>				Luciferase /MTT assay	
				Bio21 ^a		IPK ^{gh}		UNC ^{ij}	
				IC ₅₀ (μM)	LipE ^l	IC ₅₀ (μM)	LipE ^l	IC ₅₀ (μM)	LipE ^l
2.001^b	4-F-Ph	OMe	3.4	12	1.5	28	1.2	46	0.93
2.024^b	2-Me-Ph	4-OMe	3.8	65	0.39	27	0.77	18	0.94
3.009^c	2-Me-Ph	H	3.9	57	0.34	36	0.54	22	0.76
3.111^c	2-Me-Ph	3-Cl	4.5	2.1	1.2	11	0.46	2.7	1.1
2.042^{bc}	1- <i>H</i> -imidazole	4-OMe	1.5	11 ^k	3.5	26	3.1	34	3.0
3.011^{bd}	1- <i>H</i> -imidazole	H	1.7	6.4 ^k	3.5	100	2.3	50	2.6
3.116^c	1- <i>H</i> -imidazole	4-Cl	2.3	0.52	4.0	3.9	3.1	50	2.0
3.118^c	1- <i>H</i> -imidazole	3-Cl	2.3	0.74	3.8	3.5	3.2	16	2.5

a= anti *L. donovani* activity and toxicity measured in THP-1 transformed macrophage host cell lines using a top concentration of 100 μM (2x serial dilution 10-point curve). Experiment performed in duplicate wells in one experiment, n=1.

b= control compounds for Bio21 *L. donovani* intramacrophage assay. Miltefosine IC₅₀= 11 μM CC₅₀> 100 μM c= control compounds for Bio21 *L. donovani* intramacrophage assay. Average from experimental replicates; Miltefosine IC₅₀ = 0.50 ± 0.026 μM, CC₅₀ > 10 μM, Amphotericin B IC₅₀ = 1.6 ± 0.93 μM, CC₅₀ > 26 μM

d= control compounds for Bio21 *L. donovani* intramacrophage assay. Miltefosine IC₅₀ = 0.75 μM CC₅₀ = 91 μM, Amphotericin B IC₅₀ = 0.29 μM CC₅₀ = 83

e= <50% activity at the top concentration tested (100 μM).

f= anti *L. donovani* activity and toxicity measured in THP-1 transformed macrophage host cell lines using a one-point concentration (50 μM) to assess any form of antileishmanial activity. Experiment performed in duplicate wells in one experiment, n =1

g= anti *L. donovani* activity and toxicity measured in THP-1 transformed macrophage host cell lines using a top concentration of 100 μM (2x serial dilution 10-point curve)

h= control compounds for IPK intramacrophage *L. donovani* assay. Miltefosine IC₅₀= 1.7 μM, CC₅₀ >100 μM, Amphotericin B IC₅₀= 0.83 μM, CC₅₀ > 100 μM.

i= anti *L. donovani* activity measured in THP-1 transformed macrophage host cell lines using luminescent expressing *L. donovani*. Experiment performed in triplicate wells in one experiment, n=1 using a concentration range of 1-50 μM. DMSO was used as sole control against which the percent *L. donovani* viability is calculated

j= host cell toxicity measured in MTT assay with uninfected macrophage host cells. Experiment performed in triplicate wells in one experiment, n=1 using a concentration range of 1-50 μM. DMSO was used as sole control against which the percent cell viability is calculated

k= values are a mean of two experiments, n=2

l= LipE calculated from pIC₅₀ value minus the calculated log P

*Partition co-efficient calculated using CDD Vault software

- not tested

In comparison to the original lead **2.024** (RHS *para*-methoxy group) and close analogue **3.009** (unsubstituted RHS phenyl ring), the introduction of the *meta*-chloro (**3.111**) was an improvement and effective use of chemical space. Analogue **3.111** was reported to exert superior antileishmanial activity over **2.024** and **3.009** by each independent collaborator. Improved LiPE values are also observed for **3.111** over **2.024** and **3.009** in 2 out of 3 assays employed. Overall, the LiPE values of **3.111** are still quite low (< 3), suggesting more tactical structural changes could be made, thus further optimization around this new lead is required.

New lead analogues **3.116** and **3.118** also displayed superior inhibitory properties in comparison to previous lead **2.042** (RHS *para*-methoxy group) and close analogue **3.011** (unsubstituted RHS phenyl ring). An increase in both Log P and potency is observed for **3.116** and **3.118**, though the increase in potency is far more evident, within the Bio21 and IPK assays. This is reflected by the increase in LiPE values of **3.116** and **3.118** over **2.042**, **3.011**. This suggests that substitution of the chloro functionalities was an efficient addition to this chemical space, and allowed for tighter binding within the putative binding site/s. Through the improvement to antileishmanial activity and LiPE values, we have accomplished our aims of achieving an early-lead compound, with a LiPE >3 that has been somewhat optimized to target *L. donovani*. However, further optimizations to develop a more lead-like candidate are still required in future studies around Scaffold 1.

3.17 Complete biological analysis of Analogue Series 7-8 (Further exploration around the imidazole core and additive SAR study combining LHS changes with oxazole core)

The small series of analogues influenced by hit **2.001** and previous lead **2.059**, were devised to further probe the structural requirements of the imidazole core needed to maintain antileishmanial activity. These structural changes included shifting the right-hand side phenyl ring from the 5 to 4 position on the imidazole core (**3.128**, **3.129**) and replacing the imidazole core with an oxazole core (**3.131**). Previous biological assessments by UNC reported that the oxazole core replacement (**3.131**) exerted high antileishmanial activity, encouraging further exploration involving the oxazole core. The *para*-fluoro substituent of **3.131** was substituted with the *para*-chloro (**3.134**) and methyl (**3.135**) substituents influenced by the analogues **2.012** and **3.013** respectively. The cyclohexane ring replacement (**3.136**) was also incorporated onto the LHS of the scaffold, influenced by previous lead compound **2.037**. These structural modifications to the LHS were included as they had reported strong inhibition of *Leishmania* at the time of synthesis (Section **3.07**, **3.08**). The complete set of biological results is listed below in **Table 3.19**.

Table 3.19: Complete summary of biological values of Analogue Series 7-8. Hit compounds and previous leads are outlined in blue

I.D	Structure	HCS intracellular assay against <i>L. donovani</i>						Luciferase /MTT assay		
		Bio21 ^{ac}			IPK ^{fg}			UNC ^{hi}		
		IC ₅₀ (μ M)	CC ₅₀ (μ M)	SI	IC ₅₀ (μ M)	CC ₅₀ (μ M)	SI	IC ₅₀ (μ M)	CC ₅₀ (μ M)	SI
2.001 ^b		12	>100 ^e	>8.3	28	>100	>3.6	46	>50	>1.1
2.059 ^b		36	>100 ^e	>2.8	12	22	1.8	11	>50	>4.5
3.128 ^d		>50	>50	>1.0	87	>100	>1.1	>10	>50 ^e	>5.0
3.129 ^d		>50	>50	>1.0	>100	>100	>1.0	>10	27	2.7
3.131		1.1	17	15	9.4	18	1.9	6.5	34	5.2
2.013 ^b		12	52	4.3	9.1	19	2.1	7.3	>50	>6.8
3.134		0.33	10	30	25	48	1.9	5.9	>50	>8.5
2.012 ^b		29 ^j	>100	>3.4	39	96	2.5	30	>50	>1.7
3.006		2.4	13	5.4	14	22	1.6	9.0	>50	>5.6
3.135		1.4 ^j	26 ^j	19	34	66	1.9	21	>50	>2.4
2.037 ^b		>100	>100	>1.0	>100	>100	>1.0	>50	>50	>1.0
3.010		46	>100 ^e	>2.2	60	>100	>1.7	-	-	-
3.136		>100 ^e	>100 ^e	>1.0	>100	>100	>1.0	>50	>50	>1.0

a= anti *L. donovani* activity and toxicity measured in THP-1 transformed macrophage host cell lines using a top concentration of 100 μ M (2x serial dilution 10-point curve). Experiment performed in duplicate wells in one experiment, n=1.

b= control compounds for Bio21 *L. donovani* intramacrophage assay. Miltefosine IC₅₀= 11 μ M CC₅₀> 100 μ M

c= control compounds for Bio21 *L. donovani* intramacrophage assay. Average from experimental replicates; Miltefosine IC₅₀ = 0.51 ± 0.024 μM, CC₅₀ > 100 μM, Amphotericin B IC₅₀ = 2.1 ± 0.70 μM, CC₅₀ > 26 μM

d= anti *L. donovani* activity and toxicity measured in THP-1 transformed macrophage host cell lines using a one-point concentration (50 μM) to assess any form of antileishmanial activity. Experiment performed in duplicate wells in one experiment, n =1

e= <50% activity at the top concentration tested (100 μM).

f= anti *L. donovani* activity and toxicity measured in THP-1 transformed macrophage host cell lines using a top concentration of 100 μM (2x serial dilution 10-point curve)

g= control compounds for IPK intramacrophage *L. donovani* assay. Miltefosine IC₅₀ = 1.7 μM, CC₅₀ >100 μM, Amphotericin B IC₅₀ = 0.83 μM, CC₅₀ > 100 μM.

h= anti *L. donovani* activity measured in THP-1 transformed macrophage host cell lines using luminescent expressing *L. donovani*. Experiment performed in triplicate wells in one experiment, n=1 using a concentration range of 1-50 μM. DMSO was used as sole control against which the percent *L. donovani* viability is calculated

i= host cell toxicity measured in MTT assay with uninfected macrophage host cells. Experiment performed in triplicate wells in one experiment, n=1 using a concentration range of 1-50 μM. DMSO was used as sole control against which the percent cell viability is calculated

j= values are a mean of two experiments, n=2

- not tested

From **Table 3.19**, it was observed that repositioning right-hand side phenyl ring from the 5 to 4 position on the imidazole core (**3.128**, **3.129**) was found cause inactivity against *L. donovani*. Each independent assay reported an overall loss of antileishmanial activity, in comparison to the hit **2.001** and previous lead **2.059**. This suggested that the change in overall shape and orientation of the scaffold was not favourable within the putative binding site/s, and this structural modification should be avoided in future studies. Following the guidelines outlined for this project in Section **3.11**, analogue **3.131** was found to exhibit high antileishmanial activity (<10 μM) in each independent assay. The structural modification of **3.131** involved replacing the imidazole core with the oxazole, whilst retaining the remaining chemical structure of **2.059**. In comparison to previous lead **2.059**, the improved antileishmanial activity of **3.131** suggested that the oxygen atom that replaced the *N*-methyl group may have allowed for more favourable hydrogen bonding interactions with the putative binding site/s. From **3.131** it seemed that that the *N*-methyl-1*H*-imidazole was not required to maintain potency, when an appropriate bioisosteric replacement was employed, which retained the heteroatoms in the same positions. This was further evidenced by previous analogue **2.090** (**Table 3.13**, Section **3.13**), which possessed the isoxazole core and was found completely inactive against *L. donovani*. Analogue **3.134** was the fruit of our additive SAR studies, combining the structural attributes that had confirmed stronger parasite inhibition, namely the LHS *para*-chloro substituent and RHS unsubstituted phenyl ring (Analogue Series 4, Section **3.02**, **3.14**) and the oxazole core replacement (Analogue Series 7, Section **3.07**, **3.08**). Analogue **3.134** exhibited superior antileishmanial activity when compared to **3.131** and **3.013**, in 2 out of 3 independent bioassays employed, suggesting these combined structural modifications allowed for improved interactions with the putative binding site/s. Future work around this series may combine the structural attributes of **3.131** and **3.134** with the lead compounds of Analogue Series 6, namely **3.111**, **3.116**, **3.118**. This would entail replacing the LHS *para*-chloro group with the *ortho*-methyl substituent or incorporate the imidazole ring at this position, as well as introducing *para* or *meta*-chloro substituents to the RHS phenyl ring, whilst maintaining the oxazole core. Increased cytotoxicity against the host cell was observed for **3.131** and **3.134**, predominantly within the Bio21 assay. It seemed that infected host macrophages were particularly sensitive to potent analogues containing the oxazole core. However, as

selectivity was maintained for the parasites over the host cells ($SI > 3$) in each bioassay employed, this was not a large issue. Nonetheless, future studies around the oxazole core would closely monitor cytotoxicity against the host cells. Substituting the *para*-fluoro group of **3.131** with the *para*-methyl reported high antileishmanial activity within the Bio21 assay alone. Poor inhibition ($>20 \mu\text{M}$) was observed in the remaining independent intramacrophage assays against *L. donovani*. It was uncertain why conflicting results were reported, and it was likely that compound **3.135** does possess some form of antileishmanial activity and may need distal changes to the scaffold to allow for more obvious parasite inhibition across each assay. This may be explored further in future studies. Finally, analogue **3.136** (LHS cyclohexane ring) reported complete inactivity against *L. donovani*. This was expected, as this LHS structural change was based on the previous lead **2.059**, now confirmed as a false positive. A summary of the results surrounding Analogue Series 7-9 is summarized below in **Figure 3.13**.

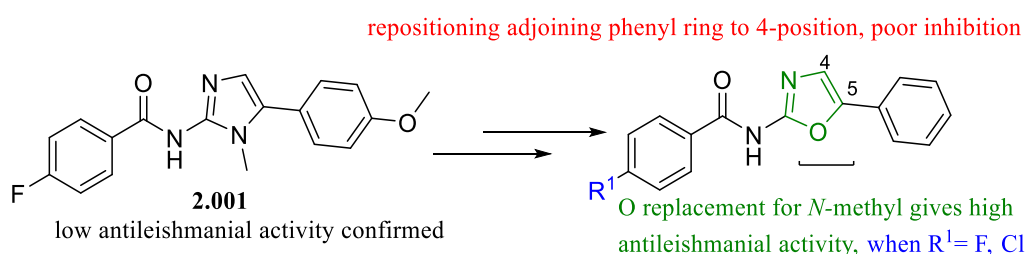


Figure 3.13: Summary of the SAR profile of Scaffold 1, derived from the confirmed biological results of Analogue Series 7-8

The dose response curves of **3.131** reported by Bio21 are depicted in **Figure 3.14a-b**, as a visual demonstration of the antileishmanial activity and selectivity exerted by **3.131**. Similar to the above **Figures 3.11-3.12**, here the **Figure 3.14a** is shown to decrease the percentage of infection within the host macrophage when the concentration of compound is increased slightly. Compound **3.131** is selective for the parasite, where cytotoxicity against the host cells is observed at higher concentrations only.

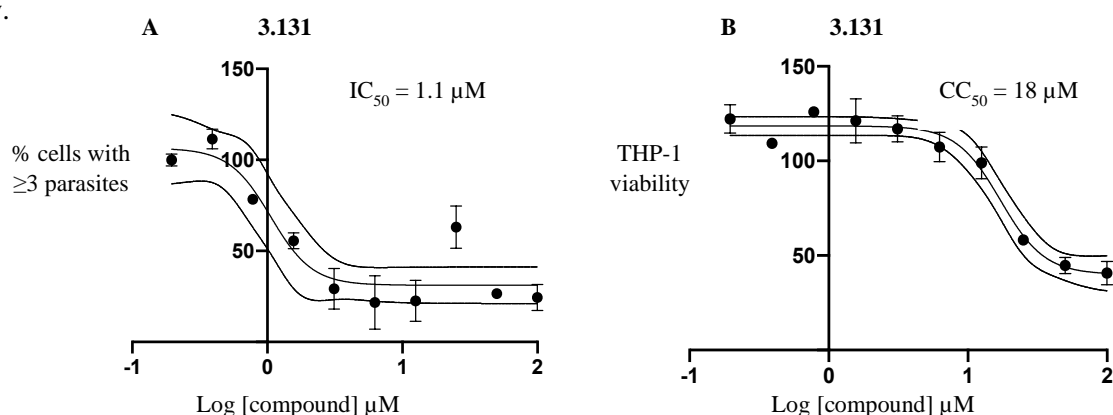


Figure 3.14a-b: Dose response curves of **3.131** reported by Bio21, a) measuring compound concentration (x axis) against % of infection within host macrophages (y axis) to determine the antileishmanial activity (IC₅₀) of **3.131**, b) measuring compound concentration (x axis) against the viability of the THP-1 transformed macrophages (y axis) to determine the cytotoxicity against the host cell (CC₅₀)

3.18: Summary of Analogue Series 1-8

A summary of our entire analogue library developed to investigate Scaffold 1 is summarized below in **Figure 3.15**. Studies around Scaffold 1 were mainly influenced by the chemical structure of the hit. **2.001**. The hit **2.002** and close analogue **3.004** (RHS unsubstituted phenyl ring) were confirmed to exhibit high antileishmanial activity by the majority of independent intramacrophage assays against *L. donovani* (Section 3.12, 3.14). However, the hit **2.002** was assigned to a parallel early hit-to-lead investigation, discussed in Section 3.03, thus, the focus of Chapters 2 and 3 are around the exploration and improvement of the chemical space surrounding hit **2.001**. Consequently, the summary here will reflect that. Hit **2.001** was confirmed to exhibit weaker efficacy against *L. donovani* than originally reported, despite this, the large optimization efforts described throughout Chapters 2 and 3 have indeed transformed this weaker starting point into early lead compounds which demonstrated strong inhibition against *L. donovani* and clear selectivity for the parasite over the host macrophage.

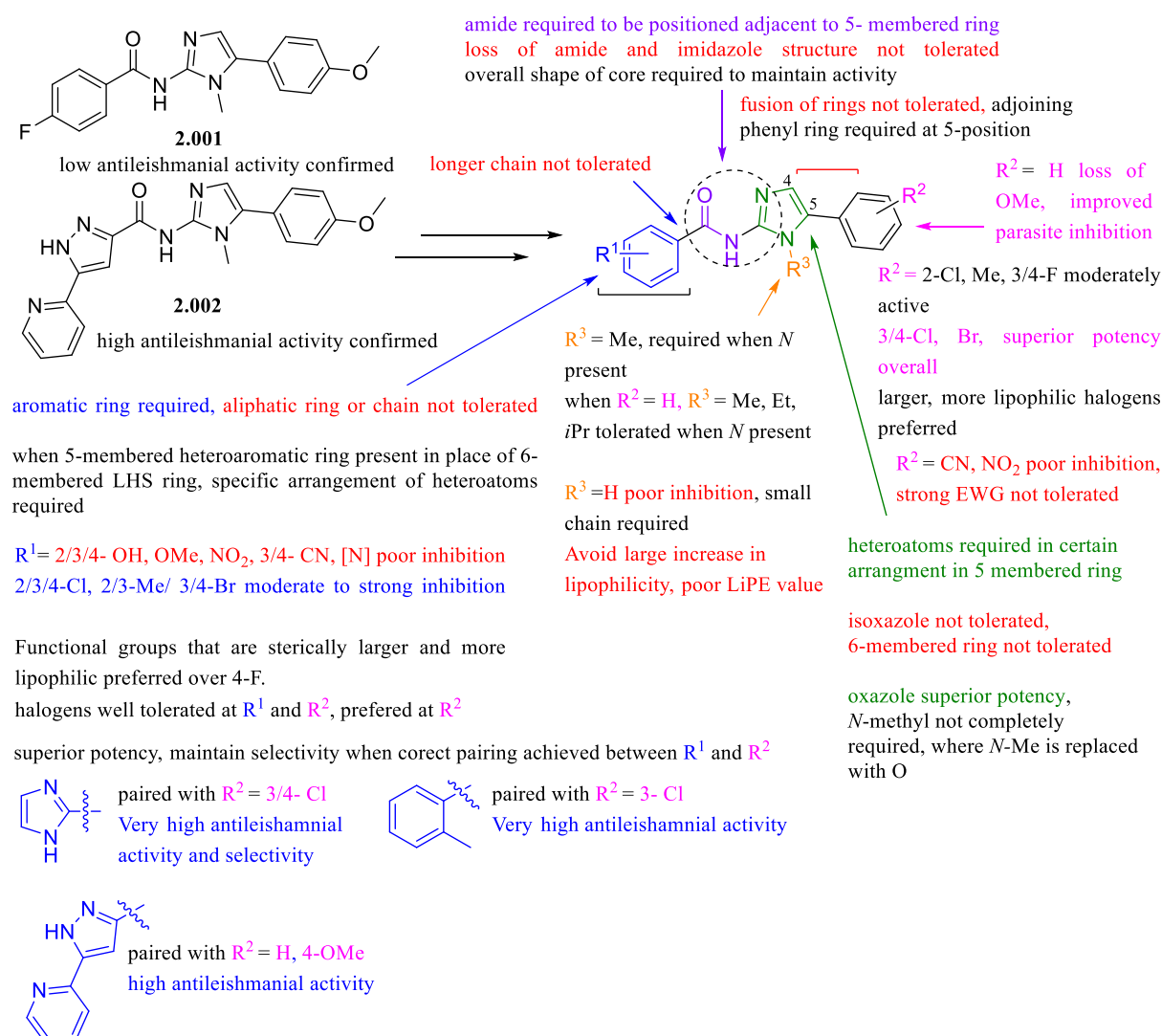


Figure 3.15: Complete SAR summary of Series 1-8 around Scaffold 1

The large set of analogues developed for Analogue Series 1 involved structural changes to the LHS region of Scaffold 1. The biological results outlined in Section 3.12 (Section 3.14 for chloro substituents) confirmed that substituting the original *para*-fluoro substituent of the hit **2.001** with hydrophilic, strong electron withdrawing groups (nitro, cyano) were not tolerated around the LHS ring. Electron donating groups, capable of forming hydrogen bond interactions (methoxy, hydroxy) were also unfavourable within this region of the chemical space. The more hydrophobic halogen functionalities with larger steric bulk (bromo, chloro) over than initial *para*-fluoro group were confirmed as the most favourable substitutions. The *para*-methyl substituent was also confirmed to exhibit improved antileishmanial activity over the *para*-fluoro group of **2.001**. However, when the *para*-methoxy functional group was retained at the RHS ring, these antileishmanial activity observed was often exerted moderate levels only (<20 μ M). Extending the carbon-carbon chain between the aromatic ring and amide functionality was also confirmed to display poor parasite inhibition. Thus, it was determined that the change in orientation and increased number of rotatable bonds was unfavourable. An aromatic system was required at this region of the chemical space, where aliphatic rings and chains caused a loss of antileishmanial activity. The loss the planar arrangement and ability to form pi-pi interactions with the putative binding site/s correlated to a loss of antileishmanial activity. Furthermore, when the pyridine pyrazole aromatic system of **2.002** was replaced with a sole 5-membered heteroaromatic ring, only certain heteroatom arrangements were tolerated, suggesting only specific heteroatoms in certain positions were required to maintain interactions with the putative binding site/s.

The small set of analogues encompassing Analogue Series 2, briefly explored the necessity of the *para*-methoxy functionality at the RHS region of Scaffold 1. The biological results outlined in Section 3.12 confirmed that repositioning the methoxy group to the *ortho*-position caused a loss of antileishmanial activity, whilst repositioning this functionality to the *meta*-position was confirmed to be more favourable than the initial hit **2.001**. Complete loss of the methoxy substituent (**2.059**) was also found to improve antileishmanial activity over the hit **2.001**, suggesting this functionality was not crucial to maintaining key interactions with the putative binding site/s. Further studies influenced by **2.059** allowed for greater improvement around Scaffold 1 in later studies (Analogue Series 4, Analogue Series 7-8).

The structural modifications explored within Analogue Series 3 targeted the imidazole core and amide functional group. The biological results described Chapter 2, and reconfirmed in Section 2.13, found that replacing the 5-membered imidazole core with the 6-membered pyridine core caused a complete loss of antileishmanial activity. Furthermore, removal of the amide and the 5-membered imidazole core was highly unfavourable. Replacing the amide and imidazole core with the urea functionality to form a pseudo ring via intramolecular hydrogen bonding interactions, was also not tolerated within the putative binding site/s. Replacing the imidazole core with an isoxazole caused a complete loss of antileishmanial activity, suggesting that a specific arrangement of heteroatoms was required within the 5-membered

heteroaromatic core to maintain key interactions with the putative binding site/s. Loss of the amide functionality in place of a fused bi-heteroaromatic system also correlated to a loss of activity. Overall, it was confirmed that the 5-membered imidazole core and adjacent amide functionality were required to maintain the correct orientation and binding interactions within the putative active site/s. Fusion of the imidazole core and adjacent *para*-methoxyphenyl ring to form the benzimidazole system was also confirmed to cause poor parasite inhibition. From this series, it was confirmed that the overall shape and orientation of the core should not be altered significantly in order to maintain potency.

The additive SAR undertaken in Analogue Series 4, combined the positive structural attributes of previous lead analogues defined in Chapter 2. This included combining various structural modifications around the LHS region of Scaffold 1, with the unsubstituted phenyl ring within the RHS region of the scaffold. Though these initial lead compounds were later confirmed to possess lower antileishmanial activity than initially reported in Chapter 2, the analogues developed within Series 4 provided superior potency over hit **2.001**, as outlined in Section 3.14. Loss of the RHS *para*-methoxy group often correlated to improved antileishmanial activity, when paired with substitutions at the LHS phenyl ring, incorporating sterically larger, more hydrophobic functionalities (chloro, bromo, methyl) in comparison to the original *para*-fluoro group of **2.001**. The *meta*-bromo LHS (**3.007**) was the standout lead within this series, as it was confirmed to be the strongest inhibitor of *L. donovani* within this series.

The compounds developed within Analogue Series 5 probed structural changes to the *N*-methyl group of the imidazole core. The biological results summarized in Section 3.15 confirmed that the loss of the aliphatic group correlated to a loss of antileishmanial activity, whilst small aliphatic groups were required at this position. Additionally, when the *para*-methoxy group was removed from the RHS phenyl ring, *N*-ethyl, *N*-isopropyl and *N*-propyl groups were tolerated within this chemical space. Introducing larger aliphatic chains and/or rings, as well as aromatic rings also improved potency. However, it seemed that this was achieved simply due to the scaffold's increased ability to permeate through the cell and inner barriers, due to the large increase in lipophilicity. This was made obvious by the calculating their respective lipophilic efficiencies, where low values were obtained. This advised that these structural changes and improved activities were not worth the large increase in lipophilicity and should therefore be avoided.

Analogue Series 6 involved a continued exploration around the RHS region of Scaffold 1. The biological results described in Section 3.16 confirmed that stronger electron withdrawing groups (cyano, nitro) were also not tolerated within this chemical space. The sterically larger, more hydrophobic halogens substituents (bromo, chloro) greatly improved antileishmanial activity over **2.001** and close analogue **2.059**, suggesting these functionalities allowed for improved interactions with the putative binding site/s. From this series, it was also determined that highly active leads were developed, when the correct pairing of the LHS and RHS phenyl ring substitutions was achieved. This

was most obvious within the new leads **3.111** and **3.116**, **3.118**, where the *ortho*-methyl phenyl and imidazole rings were incorporated within the LHS region of Scaffold 1 was paired with the *para* and *meta*-chloro substituents within the RHS region of Scaffold 1. The leads **3.116** and **3.118** also was found to improve LiPE values compared to hit **2.001**. The physicochemical and metabolic properties of **3.116** and **3.118** were also improved in comparison to hit **2.001**, which is discussed below in Section **3.20**.

Analogue Series 7 briefly continued probing the chemical space around the imidazole core. Outlined in Section **3.17**, it was confirmed that repositioning the adjoining phenyl ring from the 5-position to the 4-position caused a complete loss of antileishmanial activity. This confirmed that the overall shape of the scaffold should remain the same. Isosteric replacement of the imidazole core with an oxazole core was confirmed to exhibit superior antileishmanial activity over **2.001** and close analogue **2.059**, suggesting the *N*-methyl group of the imidazole ring was not required, so long as the same arrangement of heteroatoms was maintained. This high potency correlated to the oxazole core encouraged the development of Analogue Series 8, which paired the oxazole core replacement and unsubstituted RHS phenyl ring with various structural modifications around the LHS chemical space of Scaffold 1. From this study, it was confirmed that replacing original *para*-fluoro group of **2.001** with the *para*-chloro substituent further improved antileishmanial activity. Future work incorporating the oxazole core, with simultaneous structural changes to the LHS and RHS regions of Scaffold 1 is encouraged improve potency across all assays.

From the large medicinal chemistry efforts described within Chapters 2 and 3, our objectives have been achieved. A library of novel compounds exploring the chemical structure of hit **2.001** was developed and a first-generation SAR profile was accomplished. Though some variability exists between the biological assays of our independent collaborators, we were still able to overcome these difficulties and understand the structural requirements needed to maintain interactions with the putative binding site/s. This guided the optimization around Scaffold 1, achieving new lead compounds with superior antileishmanial activity. Furthermore, we were able to achieve our initial aims of maintaining low cytotoxicity against the host cell, confirming that increased potency did not directly correlate to increased cytotoxicity, which had been previously observed within the undisclosed analogue library around Scaffold 1, developed by GSK.

A visual summary of the new early lead compounds of interest are summarized in **Figure 3.16**. These leads were chosen as they accomplished our initial aims of achieving clear, superior antileishmanial activity and selectivity for the parasite over the host macrophage (<5 μ M, SI >3, reported in 2 out of the 3 independent intracellular assays). Additionally, new lead compounds **3.116** and **3.118** also displayed improved solubility and metabolic stability in comparison to the hit **2.001**, discussed below in Section **3.20**. These new leads also continue to follow the suggested rules of drug-likeness and oral bioavailability, where their respective physicochemical properties and *in vitro* metabolic stability fit

within the range of criteria for lead compounds outlined in **Table 1.07** of Chapter 1. After the large synthetic efforts and difficulties with biological assessment, development of these new leads was highly gratifying.

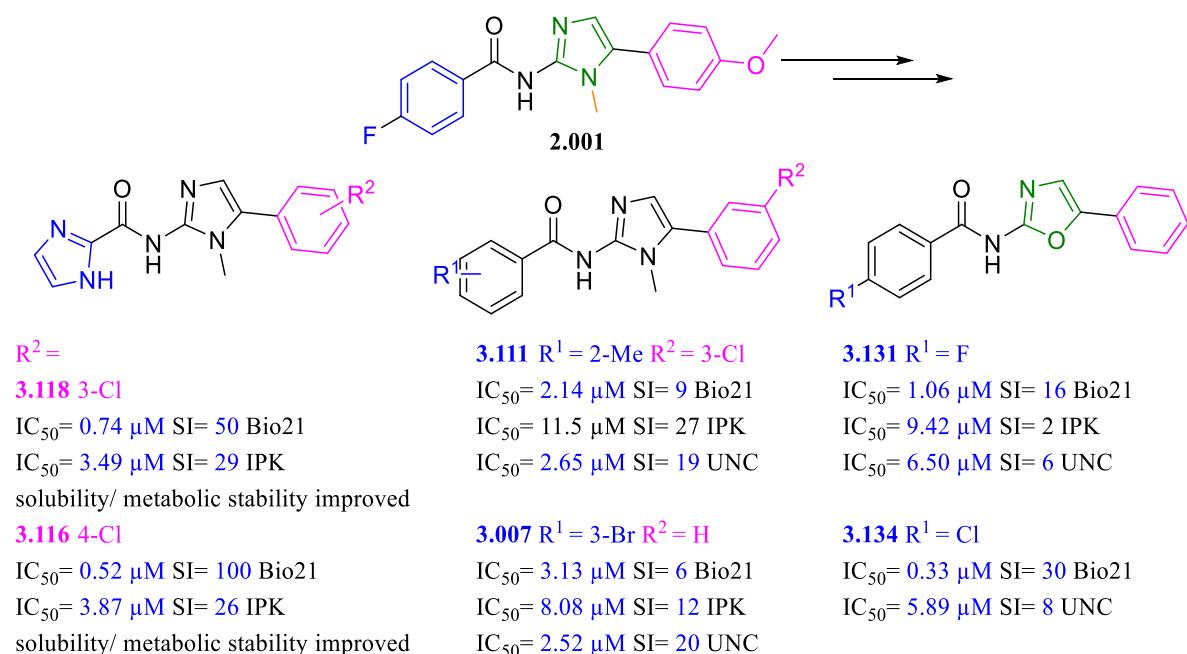


Figure 3.16: Summary of new leads and compounds of interest of Scaffold 1, based on hit **2.001**

3.19: Analogue Series 9: continued SAR investigation around hit **2.002**

From the extensive biological testing of our analogue library, the hit **2.002** and close analogue **3.004** (unsubstituted RHS phenyl ring) were confirmed to possess high antileishmanial activity. After the parallel studies around the hit **2.002** were completed, this chemical structure was returned to this PhD project. Thanks to the efforts by fellow colleagues, summarized in Section **3.03** we know that large structural changes to the imidazole core of the scaffold should be avoided and the overall shape and orientation may be key to maintaining activity.

The structural modifications within this study targeted the RHS chemical space of hit **2.002** and are summarized in **Table 3.17**. Unlike the previous alterations to hit **2.002**, during the parallel project described in Section **3.03**, changes here would focus on smaller, one step changes to understand exactly why biomodulation observed. This distal change was chosen at it would allow us to quickly obtain analogues with synthetic ease and probe which functional groups allowed for tighter binding within the putative active site/s.

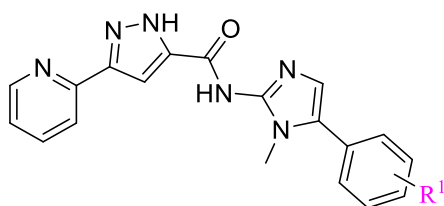
The established **Scheme 3.01** was employed to acquire these analogues. The amide coupling step of **Scheme 3.01** (Step iv) often provided the desired analogues at lower yields, listed in **Table 3.17**. This was observed previously with the hit **2.002**, and close analogue **3.004**, due to the unreactive pyrazole carboxylic acid employed during the amide coupling step (Step iv, **Scheme 3.01**). However, this was

not an issue as more than enough product was obtained for any extended *in vitro* experiments. Compound **3.139** was synthesized by fellow PhD candidate Rebecca Zheng, who would continue studies within this project.

The structural changes focused on altering the hydrogen bonding ability, steric, electron and hydrophobic properties around the RHS phenyl ring, whilst maintaining the pyridine pyrazole aromatic system within the LHS region of the scaffold, to enable a better understanding of the favourable interactions in this chemical space with the putative binding site/s. The methoxy group was repositioned to the *meta*-position (**3.146**) of the RHS aromatic ring could form stronger interactions with the putative binding site/s at this position. The substitution of bromo (**3.137**) and chloro (**3.138**, **3.142**, **3.147**) groups would investigate if a more lipophilic, electron withdrawing group was preferred around this ring in place of the *para*-methoxy group (**2.002**) or the unsubstituted RHS phenyl ring (**3.004**). The substitution of these halogens would also explore whether the loss of the ability to accept hydrogen bonds at this position correlated to a loss of antileishmanial activity. The introduction of the fluoro substituent (**3.139**, **3.143**, **3.148**) would determine if a sterically smaller electronegative atom was preferred at this position. Incorporating the fluoro group would also retain the ability to form potential hydrogen bond interactions with the putative binding site/s. Incorporating the cyano group (**3.140**, **3.144**) would determine if a more hydrophilic, stronger electron withdrawing group was preferred. Finally, the more hydrophobic, electron donating methyl substituents (**3.141**, **3.145**, **3.149**) were also explored. Like the initial methoxy substituent (**2.002**) this would probe if an electron rich ring was preferred within the putative binding site/s. Not all functional groups were substituted at every position (*ortho*, *meta* and *para*), as this was an initial probe to understand the needs of this portion of the chemical space, this was not needed.

The biological results of this series are summarized in **Table 3.20**. Due to delays caused by COVID-19, biological assessments performed by our collaborators at UNC are still pending. Most analogues reported convergent biological results, suggesting that the strong parasite inhibition observed within both bioassays was true. The often closely correlating antileishmanial activities between the independent groups was very encouraging, as explorations derived around the scaffold of **2.001** had often led to conflicting IC₅₀ or CC₅₀ values reported between the independent biological groups. From Analogue Series 9, an SAR profile was developed with greater ease, and the strong and consistent inhibition of *L. donovani* suggested the pyridine pyrazole hit **2.002** and subsequent analogues may allow for more significant binding interactions within the putative active site/s.

Table 3.20: Complete summary of biological values of Analogue Series 9, hit and previous lead outlined in blue



			HCS intracellular assay against <i>L. donovani</i>					
			Bio21 ^{ab}			IPK ^{fg}		
I.D	R ¹	Yield% (step iv Scheme 3.01)	IC ₅₀ (μM)	CC ₅₀ (μM)	SI	IC ₅₀ (μM)	CC ₅₀ (μM)	SI
2.002^{ch}	4-OMe	22	5.3	>100 ⁱ	>19	3.7 ^j	>100	>27
3.004^{deh}	H	25	0.68 ^j	46	68	6.0 ^j	>100	>17
3.137	4-Br	20	>15	>100	>6.7	1.5	>100	67
3.138	4-Cl	55	1.6	>100	>63	1.4	>100	>71
3.139^k	4-F	28	0.79	33	42	1.7	65	38
3.140	4-CN	25	7.7	>100	>13	7.1	81	11
3.141	4-Me	35	0.79	34	43	2.2	>100	>46
3.142	3-Cl	11	>100	>100	>1.0	>100	>100	1.0
3.143	3-F	24	27	>50	>1.9	3.5	66	19
3.144	3-CN	11	13	>100	>7.7	22	>100	>4.5
3.145	3-Me	30	1.5	>100	>67	1.2	59	49
3.146	3-OMe	32	1.1	21	19	2.4	>100	>42
3.147	2-Cl	20	1.8	30	17	4.5	>100	>22
3.148	2-F	15	8.9	>50	>5.6	1.8	33	18
3.149	2-Me	20	0.28	14	50	0.95	51	54

a= anti *L. donovani* activity and toxicity measured in THP-1 transformed macrophage host cell lines using a top concentration of 100 μM (2x serial dilution 10-point curve). Experiment performed in duplicate wells in one experiment, n=1.

b= control compounds for Bio21 *L. donovani* intramacrophage assay. Average from experimental replicates; Miltefosine IC₅₀ = 0.39 ± 0.55 μM, CC₅₀ > 20 μM, Amphotericin B IC₅₀ = 0.12 ± 0.055 μM, CC₅₀ = 6.0 ± 1.8 μM

c= control compounds for Bio21 *L. donovani* intramacrophage assay. Miltefosine IC₅₀= 11 μM CC₅₀> 100 μM

d= control compounds for Bio21 *L. donovani* intramacrophage assay. Miltefosine IC₅₀= 0.47 μM CC₅₀ = 8.3 μM, Amphotericin B IC₅₀= 0.69 μM CC₅₀ = 57

e= control compounds for Bio21 *L. donovani* intramacrophage assay. Miltefosine IC₅₀ = 0.75 μM CC₅₀ = 91 μM, Amphotericin B IC₅₀= 0.29 μM CC₅₀ = 83

f= anti *L. donovani* activity and toxicity measured in THP-1 transformed macrophage host cell lines using a top concentration of 100 μM (2x serial dilution 10-point curve)

g= control compounds for IPK intramacrophage *L. donovani* assay. Miltefosine IC₅₀= 1.1 μM, CC₅₀ >100 μM, Amphotericin B IC₅₀= 0.26 μM, CC₅₀ > 100 μM.

h= control compounds for IPK intramacrophage *L. donovani* assay. Miltefosine IC₅₀= 1.7 μM, CC₅₀ >100 μM, Amphotericin B IC₅₀= 0.83 μM, CC₅₀ > 100 μM.

i= <50% activity at the top concentration tested (100 μM).

j= values are a mean of two experiments, n=2

k= compound was synthesized by project member Rebecca Zheng

l = LipE calculated from pIC₅₀ value minus the calculated log P

* Log P values calculated from CDD vault software

- not tested

From **Table 3.20**, many of the substitutions to the RHS aromatic ring exhibited high antileishmanial activity within both independent intramacrophage assays against *L. donovani*. Repositioning the methoxy substituent to the *meta*-position (**3.146**) was confirmed to improve antileishmanial activity over the original *para*-methoxy group of hit **2.002**. The cyano substituents were the least preferable

functionality overall. Though the *para*-cyano (**3.140**) was able to maintain antileishmanial activity, anti-parasitic properties were not improved. Furthermore, repositioning the cyano group (**3.144**) to the *meta*-position decreased antileishmanial activity further. This suggested that a more hydrophilic functionality was not preferable within this region of the chemical space. The most preferable substitutions involved including the methyl functionality around the ring. This was most distinct at the *ortho*-position (**3.149**) which clearly displayed very high antileishmanial activity, along with selectivity for the parasite over the host cell. The addition of the halogens, particularly the chloro (**3.138**) and fluoro (**3.139**) at the *para*-positions also yielded strong inhibition of *L. donovani*. However, repositioning the chloro group to the *meta*-position (**3.142**) was the only substitution to have caused a complete loss of antileishmanial activity within this series. At this early stage of our hit-to-lead project it is uncertain why this modification would cause such a dramatic loss of potency, when the *ortho* (**3.147**) and *para* (**3.138**) chloro substituents provided high antileishmanial activity, as well as clear selectivity for the parasite. It was encouraging to find that the investigation of the RHS chemical space via small modifications seemed to provide the clearest antileishmanial activity within the entire library. Most functional groups either maintained or improved antileishmanial activity in comparison to the original hit **2.002**. Many of the analogues of **Table 3.20** would influence future studies around this scaffold, to further improve antileishmanial activity further. A summary of the SAR investigation around **2.002** is depicted in **Figure 3.17**, mainly focusing around Analogue Series 9. This summary also includes previous SAR findings, where the loss of the pyridine ring (**2.032**, Section 3.12) and amide and/or imidazole core substitutions (Sections 3.03, parallel studies) demonstrated a complete loss of antileishmanial activity. This was the final set of analogues synthesized around Scaffold 1 during this early hit-to-lead PhD project.

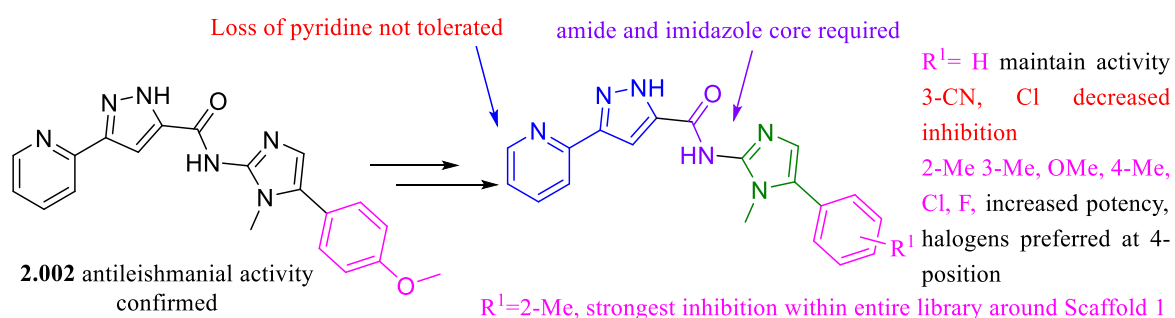


Figure 3.17: Summary of the SAR profile of Scaffold 1, derived from the confirmed biological results of Analogue Series 9

The dose response curves of **3.149** reported by Bio21 are depicted in **Figure 3.18a-b**, as a visual demonstration of the antileishmanial activity and selectivity exerted by **3.149**. Similar to the above **Figures 3.11-3.12**, **3.14**, here, **Figure 3.18a** is shown to significantly decrease the percentage of infection within the host macrophage when the concentration of compound is increased slightly, demonstrating strong parasite inhibition. Compound **3.149** is selective for the parasite, where

cytotoxicity against the host cells is observed, though much higher concentrations of the compound **3.149** are required to illicit this effect. This compound would help influence SAR studies the future.

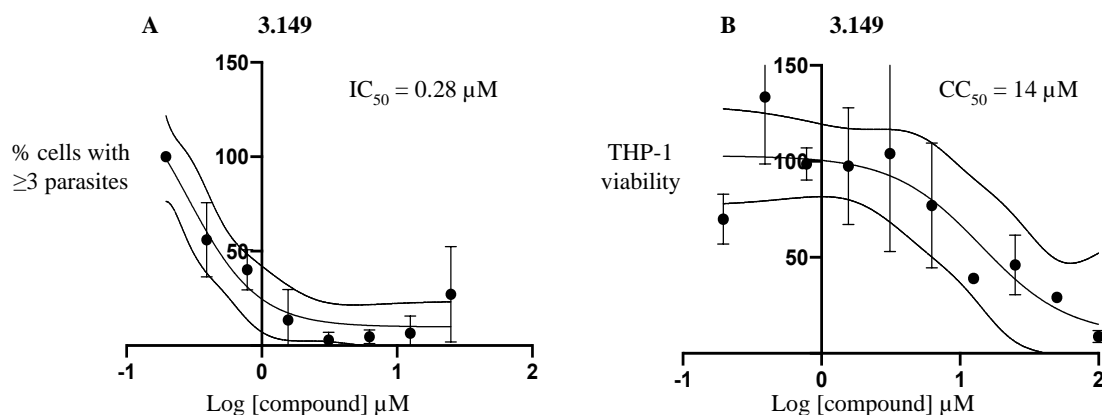


Figure 3.18a-b: Dose response curves of **3.149** reported by Bio21, a) measuring compound concentration (x axis) against % of infection within host macrophages (y axis) to determine the antileishmanial activity (IC_{50}) of **3.149**, b) measuring compound concentration (x axis) against the viability of the THP-1 transformed macrophages (y axis) to determine the cytotoxicity against the host cell (CC_{50})

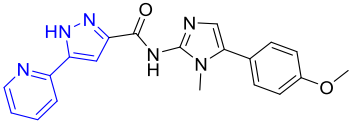
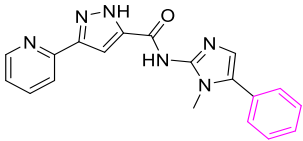
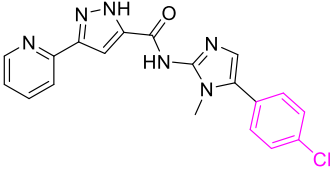
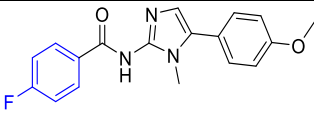
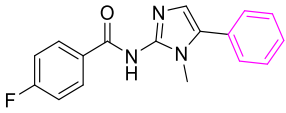
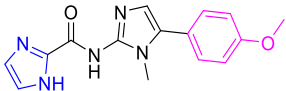
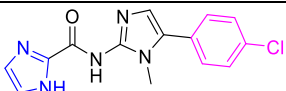
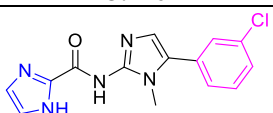
3.20 Physicochemical and metabolic evaluation of several early lead compounds of Scaffold 1

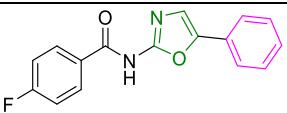
The physicochemical parameters and *in vitro* metabolic stability of several new lead compounds were measured to assess the drug-likeness of each compound of interest. This is outlined in **Table 3.21-3.22**, which also includes the physicochemical and metabolic properties of hits **2.001**, **2.002** and previous leads **2.042**, **2.059**, **3.004** for comparative ease. At this stage of our early hit-to-lead medicinal chemistry campaign, only a few representative lead analogues underwent drug-like assessment, allowing for cost efficiency. Other lead compounds such as **3.149** (LHS pyridine pyrazole aromatic system, RHS *ortho*-methyl substituent), may be assessed in the future, along with further developed analogues around Scaffold 1.

The physicochemical properties of our new compounds of interest, namely **3.116**, **3.118**, **3.131**, **3.138**, each fit within some of the guidelines for drug-likeness, outlined in Chapters 1 and 2. Each compound reported low molecular weights (< 500 Da), moderate Log D values (< 5), and an appropriate number of hydrogen bond donors (< 5) and acceptors (< 10), following Lipinski's Rule of Five.²⁷ Compound also adhered to Veber's Rule, another guideline for drug-likeness, as each compound maintained a PSA area less than 140 Å² and an appropriate number of rotatable bonds (< 10). However, as previously mentioned in Section 3.07, future studies should aim to increase polar surface area (between 140 and 90 Å²) to avoid unneeded and potentially toxic BBB penetration.²⁸ Compared to the hit **2.002** and close analogue **3.004**, the new related lead **3.138** did not improve solubility. Of these compounds, removing the substituents from the RHS phenyl ring allowed for superior solubility overall, as evidenced by **3.004**.

The new leads identified from Analogue Series 6, namely compounds **3.116**, **3.118**, both displayed some improvement to solubility over the previous lead **2.042**, of which they were derived from. The RHS *meta*-chloro (**3.118**) modification particularly displayed a larger improvement at both pH 2.0 and 6.5. These new leads also displayed superior solubility over the initial hit **2.001**. As mentioned in Section 3.07, replacing the imidazole core with the oxazole core (**3.131**) was not found able to significantly improve solubility in comparison to the previous lead and close analogue **2.059**.

Table 3.21: Key physicochemical parameters of several representative lead compounds, compared to hits 2.001, 2.002 and previous leads 2.042, 2.059 and 3.004

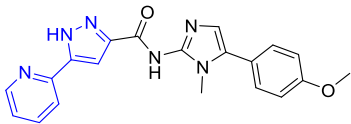
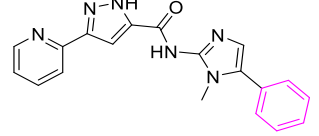
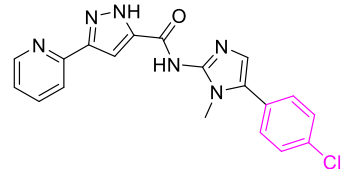
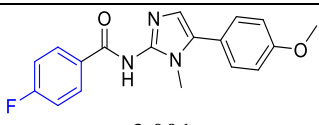
ID/ Structure	Solubility (µg/mL) ^b							
	MW ^a	PSA (Å ²) ^a	FRB ^a	HBD ^a	HBA ^a	cLogD at pH 7.4 ^a	pH 2.0	pH 6.5
 2.002 Hit	374	98	5.0	2.0	5.0	2.7	50-100	3.1-6.3
 3.004	344	89	4.0	2.0	4.0	2.8	>100	6.3 - 12.5
 3.138	379	89	4.0	2.0	4.0	3.4	50-100	3.1-6.3
 2.001 Hit	325	56	4.0	1.0	3.0	3.4	12.5-25	<1.6
 2.059 Previous lead	295	47	3.0	1.0	2.0	3.6	>100	6.3 - 12.5
 2.042 Previous lead	297	85	4.0	2.0	4.0	1.5	25-50	6.3-12.5
 3.116	302	76	3.0	2.0	3.0	2.3	25-50	25-50
 3.118	302	76	3.0	2.0	3.0	2.3	50-100	25-50

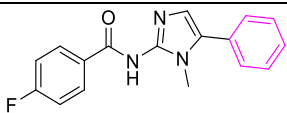
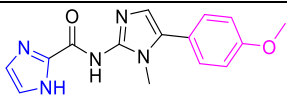
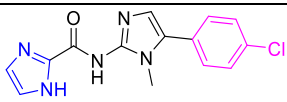
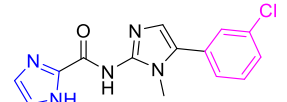
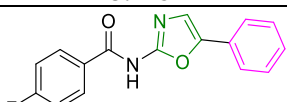
	282	55	3.0	1.0	2.0	3.4	12.5-25	3.1-6.3
3.131								

a= Calculated using ChemAxon JChem software, b=kinetic solubility determined by Nephelometry (Sol_{pH})

Compared to the hit **2.002** and close analogue **3.004**, the new lead compound **3.138** significantly improved *in vitro* metabolic stability in human microsomes. Similar stability was observed in mouse microsomes, between compounds **3.004** and **3.138**, though overall were a vast improvement over the hit **2.002**. Minimal microsomal degradation was observed for both human and mouse microsomes, evidenced by the increased half-life (>255 min in both human and mouse microsomes), decreased intrinsic clearance *in vitro* ($Cl_{int \text{ in vitro}} < 7.0 \text{ } \mu\text{L}/\text{min}/\text{mg protein}$) and decreased hepatic extraction ratio ($E_H < 0.13$). New lead compounds **3.116**, **3.118** displayed similar low microsomal degradation in human microsomes when compared to the related previous lead **2.042**. Replacing the RHS *para*-methoxy substituent with the *meta* and *para*-chloro groups also improved microsomal stability within mouse microsomes over compound **2.042**. Overall, these leads displayed superior *in vitro* microsomal stability in comparison to the original hit **2.001**. As mentioned in Section 3.07, replacing the imidazole core with an oxazole ring (**3.131**) caused poor microsomal stability and rapid degradation in comparison to the rest of the lead compounds of **Table 3.22**. Any future studies involving the oxazole core would need focus on improving metabolic stability.

Table 3.22: Summary of *in vitro* metabolic properties of several representative lead compounds, compared to hits 2.001, 2.002 and previous leads 2.042, 2.059 and 3.004

I.D/ Structure	Species	T _{1/2} (min)	Cl _{int in vitro} ($\mu\text{L}/\text{min}/\text{mg protein}$)	Microsome- predicted E _H	Clearance classification ^a
 2.002	Human	56	31	0.55	Intermediate
	Mouse	89	19	0.29	Low
 3.004^c	Human	72	24	0.49	Intermediate
	Mouse	>255	<7.0	<0.13	Low
 3.138^{cd}	Human	>255	<7.0	<0.22	Low
	Mouse	>255	<7.0	<0.13	Low
 2.001	Human	59	30	0.54	Intermediate
	Mouse	4.0	396	0.89	High

 2.059^b	Human	88	20	0.44	Intermediate
	Mouse	<2.0	>866	0.94	Very high
 2.042^d Previous lead	Human	>255	<7.0	<0.22	Low
	Mouse	3.0	511	0.92	High
 3.116^d	Human	>255	<7.0	<0.22	Low
	Mouse	43	41	0.47	Intermediate
 3.118^d	Human	229	8.0	0.23	Low
	Mouse	82	21	0.31	Intermediate
 3.131^{ef}	Human	19	90	NA	NA
	Mouse	5.0	352	NA	NA

a = The E_H was used to classify compounds as low (< 0.3), intermediate (0.3 - 0.7), high (0.7 - 0.95) or very high (> 0.95) extraction compounds
b = No measurable concentration of the parent compound was detected in mouse liver microsomes past the first time point (i.e. 2 minutes), hence, the clearance parameters could not be determined. Degradation half-life was considered to be < 2 minutes.

c = This compound showed minimal microsomal degradation (<15%) over the course of the incubation in mouse liver microsomes

d = This compound showed minimal microsomal degradation (<15%) over the course of the incubation in human liver microsomes

e = Apparent non-NADPH mediated degradation (>30% degradation) was observed in human and mouse metabolism control samples. A putative amide hydrolysis product with [MH⁺] of 161 was detected. Predicted *in vivo* clearance parameters are therefore not reported for either species.

f = Calculated mouse metabolism parameters are based on the first 2 time-points (i.e. 2 & 5 minutes) due to rapid degradation and are therefore an estimate only.

NA - Not applicable

Overall, it was encouraging to find that many of our new leads, namely **3.116**, **3.118**, **3.138** demonstrated improved physicochemical properties, particularly solubility along with improving *in vitro* metabolic stability within both microsomal species, in comparison to our initial hits. This satisfied our initial aims of developing new lead compounds which displayed superior antileishmanial activity, maintained drug-likeness and also improved *in vitro* metabolic stability, adhering to the criteria to guide early SAR lead compounds outlined in Chapter 1, **Table 1.07**. Considering the large number of analogues synthesized for this scaffold, achieving the objectives of refining not only antileishmanial properties, but also improving physicochemical and *in vitro* metabolic properties was very rewarding.

3.21 Further studies with lead compounds

Briefly, the lead compounds **3.116** and **3.118** underwent further toxicity assessment via cytotoxicity and mitotoxicity profiling, undertaken using the Crabtree effect assay by IPK. To gauge whether compounds exerted toxicity against mitochondria, they were assessed against HepG2 cells in both glucose and galactose media. Under glucose conditions, the cells utilize ATP from glycolysis whereas under galactose conditions, ATP is utilized from oxidative phosphorylation and is therefore

mitochondria dependant. The impact of the compounds, at increasing concentrations can be directly compared between conditions to determine whether mitotoxicity was observed.^{50, 51} No significant mitochondrial toxicity or cytotoxicity was observed for both compounds in HepG2 cells, which is encouraging for future optimization and development potential. The dose response curves and CC₅₀ values are listed within the Appendix. Further mitochondrial toxicity assessment will be required for the next generation of optimized analogues.

Based on the high antileishmanial activities displayed, and the amounts of product available, the new lead compounds **3.116** and **3.138** were also subjected to an *in vivo* proof of concept study using VL mouse models, with BALB/c mice infected with *L. donovani* amastigotes. This was undertaken by our collaborators at IPK following the methods described by Phan *et al.*³⁹ Compounds were dosed at 75 mg/kg, via bolus intraperitoneal injection, with the aim increasing the potential for an observable therapeutic window *in vivo*. Some problematic toxicity was observed, and compounds **3.116** and **3.138** were found to be lethal at this dose. Clearly, improvements in pharmacokinetic properties and potency would be necessary before resubmitting the next generation of optimized analogues for efficacy studies *in vivo*.

3.22 Conclusion and Future work

An extensive number of analogues were synthesized around a large portion of the chemical space of Scaffold 1, influenced by the starting hits **2.001** and **2.002**. Despite the challenges around biological testing, particularly related to the first few series of compounds biologically evaluated, we were able to define a set of parameters used to determine the true antileishmanial activities of each analogue. Consequently, we were able to successfully achieve our aims set out in Chapters 1 and 2, including establishing a reliable primary SAR profile around this compound class. This led to a better understanding around which structural components of Scaffold 1 were required to maintain antileishmanial activity, the sorts of functionalities to avoid at certain regions of the scaffold, and the types of substitutions which provided stronger interactions with the putative binding site/s. Consequently, we were able to develop and accomplish early lead compounds, which exhibited clear and superior antileishmanial activity over the initial lead compounds. The new lead compounds also maintained selectivity for the parasite over the host cell. This was a relief to us, as we had previously been cautioned by GSK through personal correspondence that their own proprietary library of analogues which were developed around our chosen hits had displayed a pattern of strong host cell cytotoxicity correlating with antileishmanial activity. This phenomenon was not largely observed within our library of analogues. Overall, the antileishmanial activity and selectivity of each new lead compounds fit within the preferred ranges of criteria suggested in Chapter 1, **Table 1.07** to guide early hit-to-lead compounds (Ideal IC₅₀ <1 μ M, SI >10 Acceptable <5 μ M, SI >3, in 2 out of the 3 independent bioassays employed).

These early lead compounds each maintained desired physicochemical properties, adhering to drug-likeness guidelines such as Lipinski's Rule of Five. This included maintain a low molecular weight, moderate Log P (<5), and an appropriate number of and an appropriate number of hydrogen bond donors (<5) and acceptors (<10).²⁷ Compound also adhered to Veber's Rule, maintaining a PSA area less than 140 Å² and an appropriate number of rotatable bonds (< 10).²⁸ Several new lead compounds displayed superior solubility and *in vitro* metabolic stability over the initial hits, as evidenced by **Table 3.21-3.22**. Many of the lead compounds accomplished the criteria for physicochemical properties, following guidelines for drug-likeness as well as achieving increased *in vitro* metabolic stability. The new leads demonstrated the desired intrinsic clearance rates (intermediate to low Cl_{int} values <40 µL/min/mg microsomal protein, human and mouse microsomes) and predicted hepatic extraction ratio (intermediate to low E_H values <0.7) for early lead compounds. This set of criteria was suggested to guide early SAR lead compounds and was outlined in Chapter 1, **Table 1.07**.

The lead compounds derived from Analogue Series 1-8 are listed in **Figure 3.19** and were originally devised to explore the chemical space around hit **2.001**. Each compound was chosen as an early SAR lead due to the strong inhibition of *L. donovani* displayed in at least 2 out of 3 independent intramacrophage assays employed. Clear selectivity for the parasite over the host macrophage was also reported in at least 2 out of 3 independent bioassays for each of these chosen leads. Leads, **3.116, 3.118** reported superior LiPE values (>3) over the hit **2.001**, suggesting each structural modification led to true improvements to binding interactions with the putative active site/s. These compounds also demonstrated superior solubility and microsomal stability over the original hit **2.001**. The future work around our newly established early lead compounds of interest is also outlined in **Figure 3.19**.

Future work would focus on further additive SAR studies, pairing the structural attributes that reported the strongest antileishmanial activity within our compound library. This would include involving the imidazole ring at the LHS region of the chemical space, an oxazole ring at the core and *meta* or *para*-chloro substituents at the RHS phenyl ring. Continued explorations pairing the imidazole within the LHS region of the chemical space with various RHS substituents, such as the methyl, bromo and fluoro groups would be trialled, as these functionalities have demonstrated some antileishmanial activity in previous analogues, bearing other substituents around the LHS chemical space of the scaffold (Section **3.16**). Pairing halogens at both opposing ends of the structure may also be interesting, to investigate if potential pseudosymmetry within the scaffold allowed for improved binding within the putative active site/s.

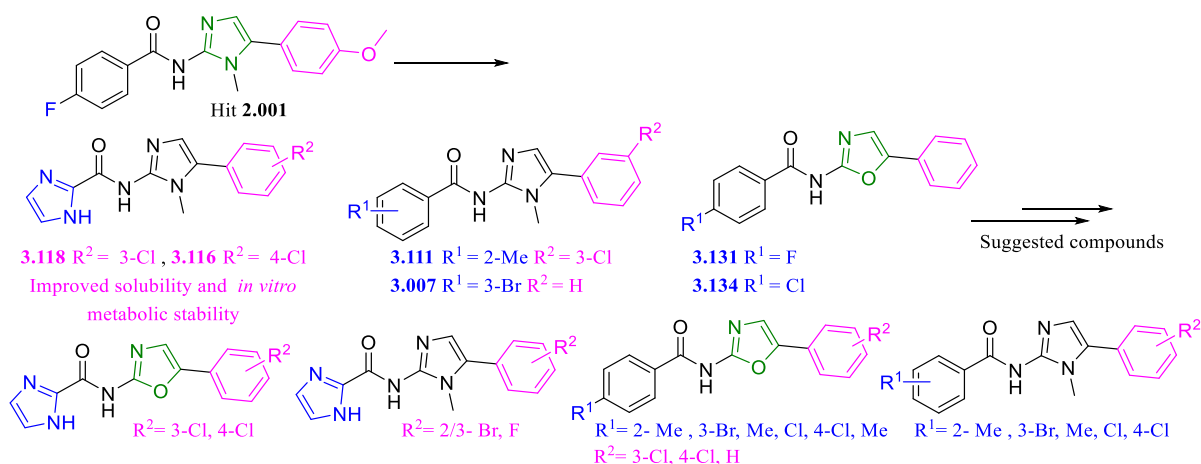


Figure 3.19: Summary of chosen early lead compounds of Scaffold 1 which were identified from Analogue Series 1-8, and the suggested structural changes to be trialled in future studies.

The lead compounds derived from Analogue Series 9 are listed in **Figure 3.20** and were originally devised to explore the chemical space around hit **2.002**. Each compound was chosen as an early SAR lead due very strong antileishmanial activity reported in 2 out of 2 independent intramacrophage assays employed ($\text{IC}_{50} < 2.5 \mu\text{M}$). Selectivity for the parasite over the host cell was reported for these chosen leads ($\text{SI} > 10$). The lead compound **3.138** also reported superior microsomal stability over the original hit **2.002**. These compounds also adhered to the guidelines for early lead SAR compounds suggested in Chapter 1, **Table 1.07**.

Future work surrounding the lead compounds derived from this series is outlined in **Figure 3.20**. Further studies around the chemical space are encouraged, continuing to explore different functionalities with varying chemical properties around the RHS phenyl ring of the scaffold. This would enable a better understanding of the substituents preferred at this position of the scaffold. Additive SAR studies, pairing the *ortho*-methyl group with *para*-substituents within the RHS phenyl ring are encouraged. These pairings may allow for an increased number of key interactions to form with the putative binding site/s. Larger substituents, such as the addition of phenyl rings around this chemical space may also be explored, to probe the fit within the putative binding site/s. Future work around the pyridine pyrazole aromatic system should also be studied further. Unlike the simultaneous larger changes listed in Section **3.03** undertaken in the parallel project, small one step changes around these heteroaromatic rings are encouraged to gain a better understanding around which structural modifications modulated bioactivity. Incorporation of the oxazole core in place of the imidazole would also be an interesting modification, aiming to improve potency whilst retaining the superior physicochemical and metabolic properties of **2.002** and **3.004**. The oxazole structural change has displayed strong antileishmanial activity within analogues derived from the hit **2.001**. Overall, the chemical structure derived from **2.002** seems to possess consistent and true activity against *L. donovani* and further optimization around these early lead compounds may indeed progress further towards drug-candidacy.

The new early lead compounds are also encouraged to undergo metabolomic studies with Bio21, to gain an understanding of the mode of action employed to exert antileishmanial activity. Despite previous difficulties with conflicting data around Scaffold 1, discussed throughout Chapters 2 and 3, it is evident that we have now successfully obtained new early lead compounds which possess clear antileishmanial activity and selectivity for the parasite over the host cells. As expressed above, development of this reliable primary SAR profile and early lead compounds have allowed us to accomplish each of our goals pertaining to Scaffold 1. Continued SAR investigations around the chemical space of these lead compounds may further guide the development of a more fully optimized, lead compound to be progressed through the pipeline as a potential novel treatment for visceral leishmaniasis.

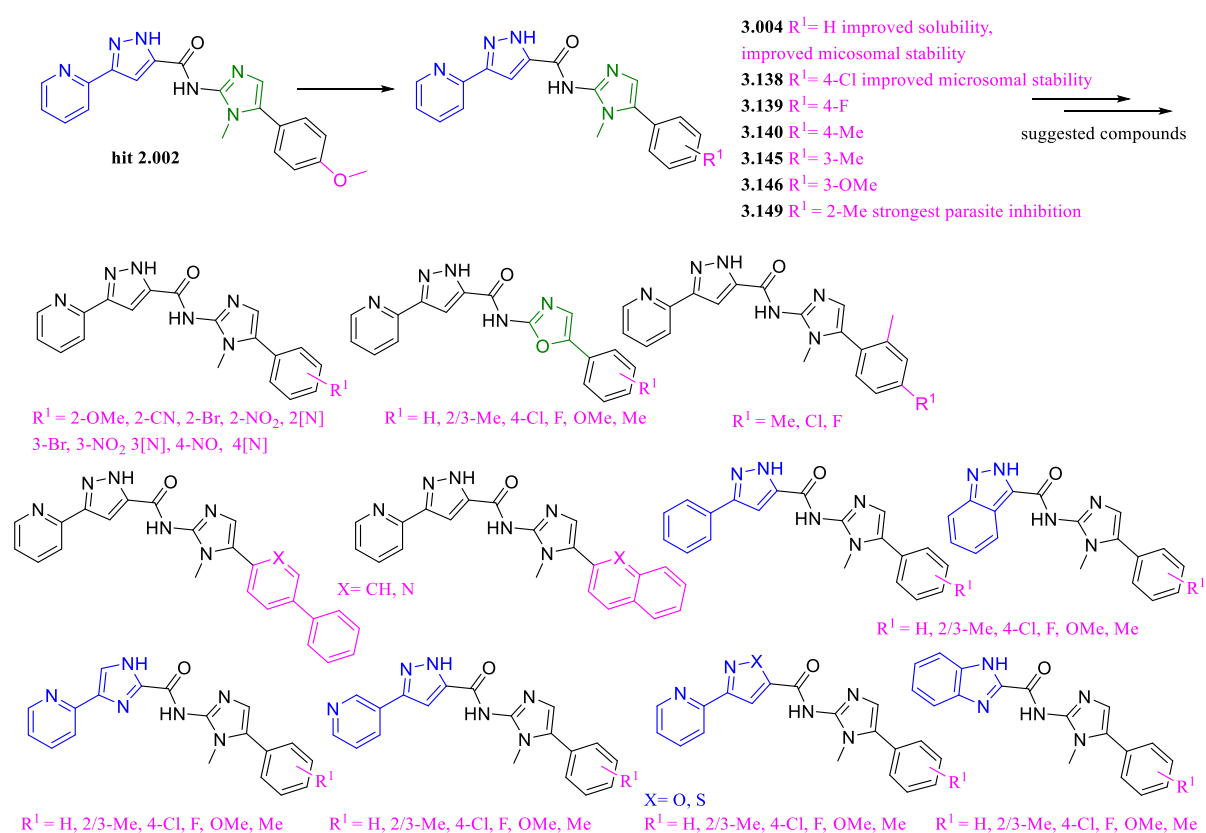


Figure 3.20: Summary of chosen early lead compounds of Scaffold 1 which were identified from Analogue Series 9, and the suggested structural changes to be trialled in future studies.

3.23 Chapter 3 Experimental

Biological methods

GRIDD *L. Donovanii* intracellular amastigote assay

This assay was carried out as previously reported by Duffy *et al.*³⁸ This assay was previously described in great detail, please refer to Chapter 2, Experimental Section.

Bio21 Methodology

Compound preparation

All compounds were resuspended in DMSO at 100 mM and, following extensive vortexing, were stored at – 20°C until use. For use, compounds were thawed at room temperature and vortexed or pulse sonicated (water bath, 20 sec) to aid resuspension.

Compound plate preparation

To prepared compound plates (384 well, v-bottom, Greiner 384 PP well plates Z642959), 25 µL of MCDM was dispensed (BioTek EL 406 washer/dispenser liquid handling robot) into all well except those to contain the highest concentration of compound. Dilutions of compounds (800 uM final) and controls (Miltefosine 800 µM final, amphotericin B 80 µM final, DMSO 1.6mM) controls were prepared in MCDM. These dilutions were manually added to the vacant wells of the compound plates (50 µL/well). A serial dilution was then undertaken (1:2, 10 points, transferring 25 µL) across the plate using the was performed using the Caliper Sciclone ALH 3000 workstation. Subsequently, 5 µL were transferred to the cell plates (*in vitro* or *intra* macrophage assays) resulting in a 1/8 dilution (miltefosine, starting 100 µM; amphotericin starting 10). The concentration range of the investigative compounds used was 0.195-100 µL.

Cells culture

Parasites: Parasite aliquots were stored at -80°C and thawed 2 weeks before use for infection. *Leishmania mexicana* (MNYC/BZ/62/M379) and *Leishmania donovani* parasites (LRC-L52) were maintained by twice weekly passages (twice weekly at 100-fold and 1000-fold dilution) of mid-log phase parasites into 10 mL of RPMI 1640 (hereafter RPMI, Life Technologies #11875-119)(pH 7.4) medium or 10 ml of RPMI:SDM-79 (1:1 v/v, pH 7), respectively, supplemented with 10% heat-inactivated fetal calf serum (FCS, Sigma Aldrich) at 27°C.

Stationary-phase promastigotes were harvested 5 days after passaging (approximately *L. mexicana*; ~2x10⁷ cells/mL, *L. donovani*; ~3x10⁷ cells/mL). Axenic amastigotes were obtained following the differentiation of stationary-phase promastigotes in fresh medium (*L. mexicana*; RPMI, *L. donovani*,

RPMI:SDM-79, 1:1 v/v) supplemented with 20% FCS at pH 5.5 for 4 days at an increased temperature (*L. mexicana*; 33 °C, *L. donovani* 37 °C).

Mammalian macrophage: THP-1 monocytes were cultured in RPMI supplemented with 10% FCS, penicillin and streptomycin, at 37 °C and 5% CO₂. Cells were maintained in at 2 x 10⁵ – 1.2 x 10⁶ cells/mL with regular passaging and fresh aliquots were thawed 1-2 weeks before the assay. THP-1 cells were differentiated to macrophage like cells via the addition of 50 ng/mL of PMA (P1585; Sigma-Aldrich).³⁷

Intramacrophage assay

This assay was carried out as previously reported with minor adjustments.³⁷ Briefly, THP-1 monocytes were dispensed (BioTek EL 406 robotics) into a 384 well plate (Corning COSTAR, Catalogue number 3712) at 50 uL/well (6 x10³ cells/well), in RPMI supplemented with 10% FCS and 50 ng/mL of PMA). Plates were briefly centrifuged and incubated at 37 °C with 5% CO₂ for 24 h.

The following day, axenic amastigotes were stained with CellTracker Orange CMRA (C34551; Life Technologies) as described previously³⁷. Stained parasites were resuspended in RPMI supplemented with 10% FCS and dispensed (BioTek EL 406 robotics, 50 uL/well) over now adherent macrophages following culture media aspiration (BioTek EL 406 robotics). Macrophages were infected at a multiple of infection of 10:1 (*L. donovani*) (parasite:host). Plates were briefly centrifuged and incubated at 37 °C with 5% CO₂. The following day, the infected macrophages were washed (removing non-internalised parasites) with 1 x PBS (60 uL/well) and new media dispensed (35 uL/well, RPMI supplemented with 10% FCS, BioTek EL 406 robotics). Plates were briefly centrifuged and incubated at 37 °C with 5% CO₂. The following day, 5 uL of compound was then transferred from the compound plate using the Caliper Sciclone ALH 3000 workstation, the plates briefly centrifuged and incubated at 37 °C with 5% CO₂ for 72 hr.

After treatment, the infected macrophages were stained and imaged.³⁷ Briefly, assay media was aspirated (BioTek EL 406 robotics) and 5 µM Cell Tracker Green CMFDA stain (CMFDA, 5-chloromethylfluorescein diacetate, C2925; Life Technologies, 5 uM) in RPMI was dispensed (25 µL/well) and incubated (30 min, 33 °C or 37 °C with 5% CO₂). Stain was aspirated and the infected macrophages cells incubated in RPMI supplemented with 10% FCS RPMI (50 uL/well, 37 °C with 5% CO₂, 40 min). The chase media was aspirated and the cells fixed (4% PFA, 10 mM EGTA in PBS without Ca²⁺ and Mg²⁺, 15 min at room temperature). The fixative solution was aspirated and host nuclei stained with DAPI (10236276001, Roche, 6 µL/mL in PBS, 25 µL/well, 10 min, room temperature). The final stain was aspirated, and the cells washed twice with PBS (50 uL). Plates were sealed using a thermal microplate sealer before being high content imaging was performed using the Cellomics Array Scan VTI platform. The imaging protocol based on the Cellomics Colocalization V4 BioApplication,

was developed for two imaging parameters: separation of the host cells and detection of intracellular amastigotes. Autofocus was applied using the DAPI stain channel (Ch2), CellTracker Green CMFDA (Ch1) and CellTracker Orange CMRA (Ch3) with images acquired in sequence. The DAPI stain is used to observe nuclei as a complimentary stain to CellTracker Green CMFDA which stains the macrophage cytosol and provides a visible boundary of viable macrophages (host cell segmentation). CellTracker Orange CMRA stains the parasite cytosol. The Cellomics Colocalization V4 BioApplication, using size and intensity algorithms were used to count Ch3 (CMRA stained) objects indicating amastigotes within Ch1 CMFDA marked boundaries (i.e. the number of amastigotes in THP-1 macrophage cytosol). Several features were extracted (Table 1)

Table 1

Feature	Definition	Channel
Valid object count	Number of viable macrophages per well	1 (CMFDA)
MEAN_ROI_A_Target_II_Object Count	Average amastigotes per viable macrophage per well	3 (CMRA)
%_High_ROI_A_Target_II_ObjectCount	% of viable macrophages with 3 or more amastigotes	3 (CMRA)

Compound activity was expressed as a percent of the maximum (e.g. DMSO control) and minimal (Miltefosine/Amphotericin B controls). Nonlinear sigmoidal dose-response curves were plotted and IC₅₀ values were calculated using GraphPad Prism 6. The IC₅₀ values were calculated as the mean from duplicate wells in one experiment.³⁷ Several compounds have been biologically assessed in multiple experiments, and the average IC₅₀ and CC₅₀ value across all experiments was indicated within the main sections of this body of work.

IPK Methodology

Parasite and cell culture along with the intracellular assay were performed according to Phan *et al.* with small modifications.³⁹

Parasite and Cell Cultures

L. donovani MHOM/SD/62/1S-CL2d parasites were cultured at the promastigote stage in M199 medium (Sigma-Aldrich, St Louis, MO, USA) with 40 mM HEPES, 0.1 mM adenine, 0.0001% biotin and 4.62 mM NaHCO₃ supplemented with 10% fetal bovine serum (FBS, Gibco, Carlsbad, CA, USA), 100 µ/mL penicillin (Gibco) and 100 µg/mL streptomycin (Gibco) at 28°C. The parasites were subcultured every 3 to 4 days. The parasites were maintained for 10 passages.

THP-1 cells (ATCC TIB) were cultured in RPMI 1640 medium containing 4.5 g/L glucose, 10 mM HEPES, 1 mM sodium pyruvate and 10% FBS. The cells were maintained in tissue culture flasks (Nunc A/S, Roskilde, Denmark) in an incubator at 37°C in the presence of 5% CO₂.³⁹

Screening of test compounds against Intracellular *Leishmania*

THP-1 human monocytic cells were treated with PMA to transform the cells into macrophage like cells. The PMA treated THP-1 cells were seeded into a 384-well culture plate (Greiner Bio-One, Kremsmünster, Austria) at 0.8×10^4 cells/well in RPMI 1640 complete medium supplemented with 10% FBS. The assay plate was incubated for 48 h at 37°C in the presence of 5% CO₂. After incubation, *L. donovani* promastigotes previously incubated with lectin for 30 min at 28°C, were added to the cells at a multiplicity of infection ratio of 20:1 (parasite to host). Infected THP-1 cells were treated with control compounds. The dose response of the positive control amphotericin B started from 4 µM; 2x dilution for a 20-point dose response curve. The positive control miltefosine started from 40 µM; 2x dilution for 20 points. The screening compounds were added, using a concentration range of 0.2-100 µM, starting at 100 µM, two-fold serial dilution, for 10 points in 0.5% DMSO (v/v). The negative control consisted of THP-1 macrophages with infected parasites with 0.5% DMSO. After 72 h incubation, cells that were infected and treated with test compound were washed with serum free RPMI 1640 medium. The assay plate was stained with 5 µM DRAQ5 and 4% PFA. Plates were read and imaged using an Operetta® automated microscope (PerkinElmer, Inc., Waltham, MA, USA). They were further analysed using Columbus™ (PerkinElmer, Inc., Waltham, MA, USA) software to quantify parasite numbers, host cell numbers and infection ratios. Large sized nucleus of host cells were detected first using DRAQ5 (Thermo Fisher, Rockford, IL, USA) signal. The host cell boundary masking was performed using the low-intensity signals from the cytosol (using DRAQ5). The small sized nucleus signal by DRAQ5 was used to identify the parasites within the mask area of the host cell. The infection ratio (IR) was determined with the value of the number of infected macrophages, divided by the number of macrophages. The average number of parasites per macrophage was defined by the value of the number of parasites divided by the number of infected macrophages in the image acquired.³⁹

UNC Methodology

Infecting THP-1 Macrophages with *Leishmania donovani* (Ds-Red-lux) and evaluating by Luciferase assay²⁴

Parasites: *L. donovani* LV82 expressing firefly luciferase and a red fluorescent protein, LUC and DsRed2 promastigotes (Ds-Red-Lux) promastigotes were provided by Dr. Abhay Satoskar, Department of Pathology, The Wexner Medical Centre, The Ohio State University. Ds-Red-lux *L. donovani* promastigotes were routinely cultured at 26 °C in M199 medium (Catalogue number 10-060, Corning) supplemented with, 7.6 mM hemin, 0.1, 10% (v/v) heat-inactivated fetal bovine serum (FBS) and antibiotic cocktail (50 U/ml penicillin, 50 µg/ml streptomycin).

Generation of the red-shifted lux *L. donovani* strain was undertaken based on the methods described by Lezama-Davila *et al.*²²

***In vitro* luciferase assay**

The assay and conditions were adapted from methods as previously described by Álvarez-Velilla et al. which employed *L. infantum* rather than *L. donovani* which was utilised within these studies.²³

***L. donovani* infection of host cells**

Luminescent *L. donovani* (Ds-Red-lux) stationary phase promastigotes were prepared for infection of THP-1 cells by performing a count via a hemacytometer. A 3 mL aliquot of the *L. donovani* parasites, was centrifuged for 3000 x g for 5 min to obtain a pellet. Media was removed and fresh RPMI media (10 mL) was added. For the cell count, 50 µL of cells was mixed with 25 µL of PBS and 25 µL 4% Formalin. The fixed cells were added to a hemocytometer to count the cells and determine the concentration needed for treatment.

THP-1 cells (ATCC) were differentiated into macrophages with a 72-hour treatment of PMA. Differentiated host cells were infected with stationary phase Ds-Red-lux *L. donovani* promastigotes (MOI 1:10, host to parasite) over 18 hours. The host cells were washed with serum free RPMI media (3x 50 µL) to remove unencapsulated, extracellular parasites. Infected host cells were treated with compounds or DMSO (1:400 dilution) vehicle in the control group for 72 h at 37 °C. Compound stocks were prepared in DMSO and diluted in THP-1 media at a concentration range of 1- 50 µM. An uninfected control group was also incorporated. THP-1 cells used in these experiments were limited to passage 10.

Firefly Luciferase assay:

The Luciferase Assay System (Promega) was used to assess leishmanial viability in infected macrophages. After treating *L. donovani* infected THP-1 cells (ATCC) with compounds over 72 hours, media was aspirated with a glass pipette. Cells were lysed with 20 µL/ well of 1x lysis buffer. (Lysis buffer, Promega). After 5 minutes of incubation at 37°C, 50 µL/well of the luciferase substrate (Promega kit 151A, thawed) was added to the assay plate and incubated at room temperature for 5 min. The luminescence intensity of the resulting of 50 µL of the resulting solution was measured in a 96-well white plate (Costar) using a microplate reader (Synergy HT, Biotek) (2 second integration). The IC₅₀ values of the compounds was calculated using a 4-point curve of relative luminescence units versus drug concentration. Compounds were tested in triplicate in one experiment, n=1. The curve fitting was performed on Excel and IC₅₀ was calculated using the equation that fit the data the best.

Cell viability analysis: MTT assay

The effect of test compounds on the viability of un-infected but differentiated THP-1 macrophages was assessed using the 3-(4,5-dimethylthiazol-2-yl)-2,5-diphenyl-2H-tetrazolium bromide (MTT) assay in triplicate per experiment. Cells were seeded into a 96-well (Costar) plates at 2.5 x 10⁴ cell/well. The

assay plates were cultured for 24 h at 37°C. The test compounds diluted in RPMI media were added to the plate at 1- 50 μ M and incubated over 24 hours at 37°C. Controls received DMSO vehicle (1:400 dilution), equivalent to that used in the drug treatment. At the end of the treatment, the medium was replaced with 200 μ L of 0.5 mg/ml of MTT in RPMI medium. Cells were subsequently incubated in at 37°C (5% CO₂) for an additional 1 h. Supernatants were removed from the wells and the reduced MTT dye was solubilized in isopropanol (200 μ L/ well). The absorbance at 570 nm was determined using a microplate reader (Biotek) to determine the viability of the host cells. The CC₅₀ value was calculated by plotting the relative cell viability versus drug concentration on Excel and obtaining the equation that best fit the curve. These assay conditions are similar to that reported by Chiu *et al*, as directed by our colleagues at UNC.²⁶

Physicochemical Experimental

Calculated physicochemical parameters using ChemAxon JChem software

A range of physicochemical properties evaluating likely oral absorption characteristics and drug-likeness were calculated using the ChemAxon chemistry cartridge via JChem for Excel software (version 16.4.11). A brief description of each parameter is provided below:

MW (< 500): Molecular Weight

PSA_{pH 7.4} (< 140 Å²): Polar surface area also inversely correlates with membrane permeability.

FRB (≤ 10): Number of freely rotating bonds represents the flexibility of a molecule's conformation.

HBD (< 5) & HBA (< 10): Number of hydrogen bond donors and acceptors gives an indication of the hydrogen bonding capacity, which is inversely related to membrane permeability.

cLogP/cLogD_{pH} (< 5): Calculated partition coefficients reflect the lipophilic character of the neutral structure, while distribution coefficients reflect the partitioning properties of the ionised molecule at a specific pH.

Kinetic Solubility Estimation using Nephelometry

Compound in DMSO was spiked into either pH 6.5 phosphate buffer or 0.01M HCl (approx. pH 2.0) with the final DMSO concentration being 1%. After 30 minutes had elapsed, samples were analysed via Nephelometry to determine a solubility range.⁵²

Distribution Coefficient Estimation using Chromatography

Partition coefficient values (LogD) of the test compounds were estimated at pH 7.4 by correlation of their chromatographic retention properties against the characteristics of a series of standard compounds with known partition coefficient values. The method employed is gradient HPLC based derivation of the method originally developed by Lombardo *et al*.⁵³

***In vitro* Metabolic Stability**

Incubation:

The metabolic stability assay was performed by incubating each test compound in liver microsomes at 37 °C and a protein concentration of 0.4 mg/mL. The metabolic reaction was initiated by the addition of an NADPH-regenerating system and quenched at various over a 60 min incubation period by the addition of ACN containing diazepam as internal standard. Control samples (containing no NADPH) were included (and quenched at 2, 30 and 60 min) to monitor for potential degradation in the absence of cofactor. The human liver microsomes used in this experiment were supplied by XenoTech, lot # 1410230. The mouse liver microsomes used in this experiment were supplied by XenoTech, lot # 1910002 (for our compounds tested in 2020) and lot #1510256 (for our compounds tested in 2018, 2019). Microsomal incubations were performed at a substrate concentration of 0.5-1 μ M.

Data analysis:

Species scaling factors from Ring *et al.* were used to convert the *in vitro* CL_{int} (μ L/min/mg) to an *in vivo* CL_{int} (mL/min/kg).⁵⁴ Hepatic blood clearance and the corresponding hepatic extraction ratio (E_H) were calculated using the well stirred model of hepatic extraction in each species, according to the "in vitro T_{1/2}" approach described by Obach *et al.*⁵⁵ The E_H was then used to classify compounds as low (< 0.3), intermediate (0.3 - 0.7), high (0.7 - 0.95) or very high (> 0.95) extraction compounds. Predicted *in vivo* clearance values have not been corrected for microsomal or plasma protein binding. Species scaling calculations are based on two assumptions: 1) NADPH-dependent oxidative metabolism predominates over other metabolic routes (*i.e.* direct conjugative metabolism, reduction, hydrolysis, *etc.*), and; 2) rates of metabolism and enzyme activities *in vitro* are truly reflective of those that exist *in vivo*. If significant non-NADPH-mediated degradation is observed in microsome control samples, then assumption (1) is invalid and predicted clearance parameters are therefore not reported.

General Chemistry

General chemistry, solvents and machines employed followed the same description detailed in Chapter 2, Experimental

Synthesis

General Procedures

General Procedure A Imidazole amine formation³

The appropriate *N*-alkylpyrimidin-2-amine (290 mg, 2.70 mmol) and the appropriate bromo phenylethanone (3.60 mmol) were dissolved in ACN (5 mL) and heated using microwave irradiation at 130 °C for 30 min. The reaction mixture was then cooled and hydrazine hydrate (0.65 mL) was added.

The reaction mixture was heated using microwave irradiation at 100 °C for 5 minutes. The mixture was concentrated *in vacuo* then filtered with water via suction filtration to give the desired product.

General Procedure B Amide coupling⁴

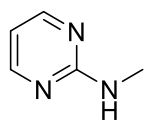
The appropriate phenyl imidazole-2-amine (0.980 mmol) and the appropriate carboxylic acid (0.980 mmol) were added to a solution of HBTU (0.980 mmol), DMAP (0.0980 mmol) and DIPEA (2.45 mmol) in ACN (3 mL). The reaction was left to stir at 50°C 12 hours after which the reaction was reduced *in vacuo*. The reaction mixture was diluted with DCM and washed with citric acid/water followed by ammonia/water. The organic layer was dried with MgSO₄, filtered and reduced *in vacuo*. The crude material was subsequently purified via column chromatography (EtOAc: Petroleum spirits; 1:1). ¹H NMR spectra employing CDCl₃ generally show an absence of NH proton peaks as they have presumably broadened out and are not visible.

General Procedure C Alternative amide coupling⁴

The appropriate phenyl imidazole-2-amine (0.980 mmol) and the appropriate carboxylic acid (0.980 mmol) were added to a solution of PyBOP (510 mg, 0.980 mmol), DMAP (12 mg, 0.0980 mmol) and DIPEA (0.42 mL, 2.45 mmol) in DMF (3 mL). The reaction was heated to 50 °C for 12 h after which the reaction was reduced *in vacuo*. The reaction mixture was diluted with EtOAc and washed with brine. The organic layer was dried with MgSO₄, filtered and reduced *in vacuo*. The crude material was subsequently purified by column chromatography (eluent CHCl₃ 94%, MeOH 5%, NH₄OH 1%) to give the desired product. ¹H NMR spectra employing CDCl₃ generally show an absence of NH proton peaks. This was not an issue as the presence of this peak has been confirmed in close analogues demonstrated in Analogue Series 1. Furthermore, the structure of each compound can be confirmed with the current panel of characterisation techniques employed here.

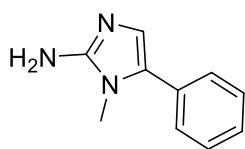
Analogue Series 4

N-methylpyrimidin-2-amine (3.002/ 2.004)²



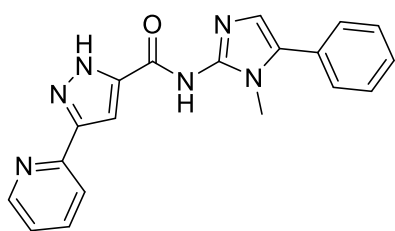
To a solution of 2-chloropyrimidine (2 g, 17.5 mmol) in THF (25 mL) was added 40% methylamine (aq) (7.5 mL) at 0°C. The reaction mixture was then heated to reflux for 1 hour then saturated NaHCO₃ (aq) was added and extracted with ethyl acetate. The organic layer was washed with brine, dried using MgSO₄ and reduced *in vacuo* to give the known product as pale yellow crystals (1.72 g, 90%).¹ HPLC - *t_R* 1.68 min > 95% purity at 254 nm; LRMS [M+H]⁺ 110.0 *m/z*; ¹H NMR (400 MHz, CDCl₃) δ_H 8.21 (d, *J* = 4.7 Hz, 2H), 6.44 (t, *J* = 4.8 Hz, 1H), 5.46 (s, 1H), 2.92 (d, *J* = 5.1 Hz, 3H); ¹³C NMR (101 MHz, CDCl₃) δ_C 163.1, 158.1, 110.4, 28.4. Acquired data is consistent with the literature.²

1-Methyl-5-phenyl-1*H*-imidazol-2-amine (3.003/2.005b, precursor to 2.059)³



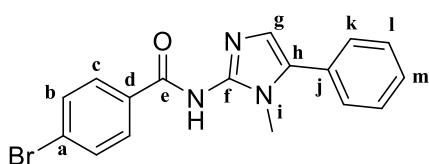
The known title compound was prepared from 2-bromo-1-phenylethan-1-one (716 mg, 3.60 mmol) according to General Procedure A as an orange solid without further purification (332 mg, 72%). HPLC - t_R 3.91 min > 99 % purity at 254 nm; LRMS $[M+H]^+$ 174.0 m/z ; 1H NMR (400 MHz, DMSO- d_6) δ_H 7.42 – 7.34 (m, 4H), 7.27 – 7.22 (m, 1H), 6.56 (s, 1H), 5.51 (s, 2H), 3.34 (s, 3H); ^{13}C NMR (101 MHz, DMSO- d_6) δ_C 151.9, 131.6, 129.2 (2C), 128.3, 127.1 (2C), 126.5, 123.6, 30.9. Acquired data is consistent with the literature.³

N-(1-Methyl-5-phenyl-1*H*-imidazol-2-yl)-3-(pyridin-2-yl)-1*H*-pyrazole-5-carboxamide (3.004)



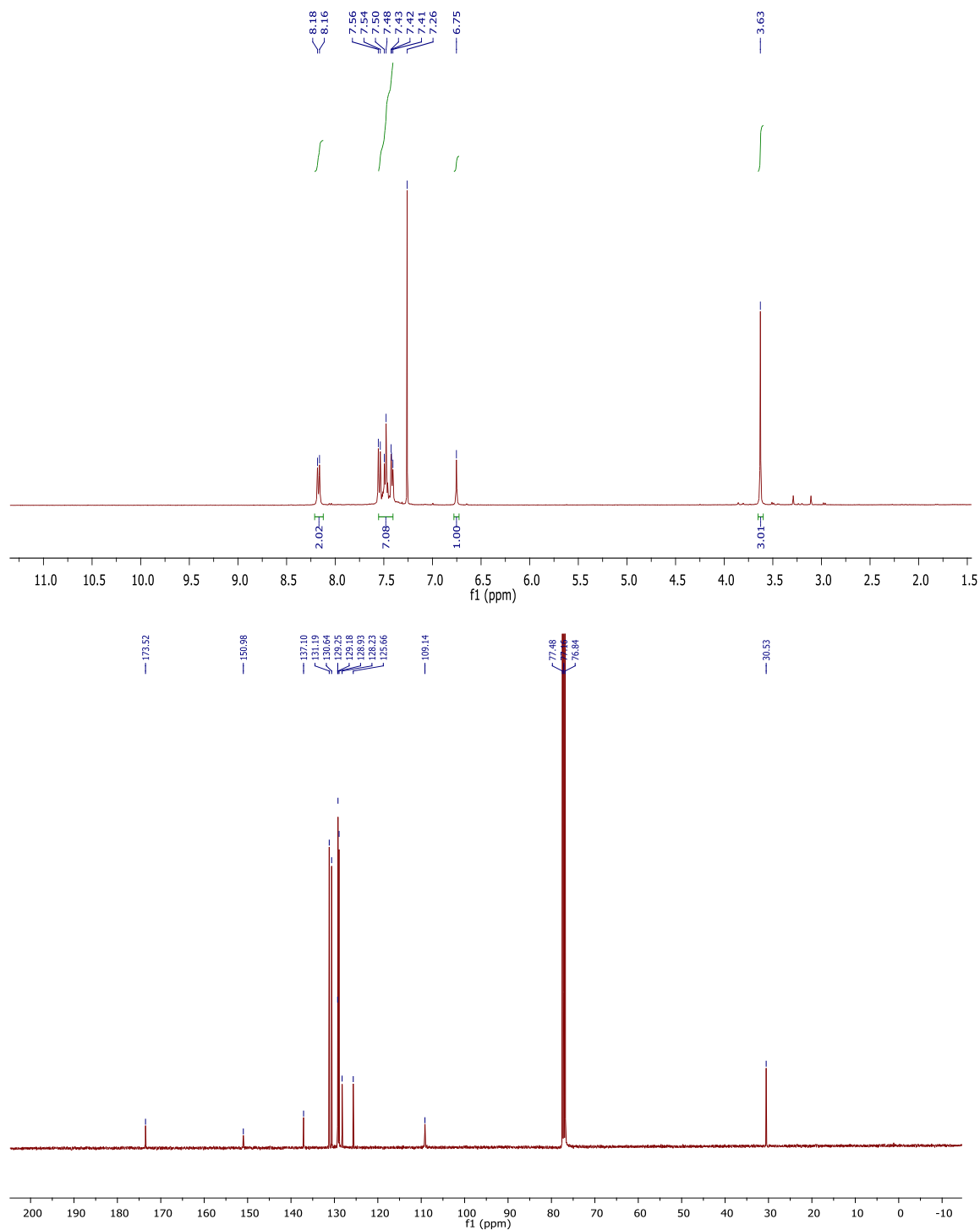
The title compound was prepared from 1-methyl-5-phenyl-1*H*-imidazol-2-amine (200 mg, 1.16 mmol) and 3-(pyridin-2-yl)-1*H*-pyrazole-5-carboxylic acid (218 mg, 1.00 mmol) according to General Procedure C as a white solid (100 mg, 25%). HPLC – t_R 4.36 min > 99% purity at 254 nm; LRMS $[M+H]^+$ 345.0 m/z ; HRMS $[M+H]^+$ 344.1380 m/z , 344.1369 found; 1H NMR (400 MHz, CDCl₃) δ_H 8.70 (d, J = 4.7 Hz, 1H), 7.86 – 7.74 (m, 2H), 7.52 – 7.40 (m, 6H), 7.28 – 7.26 (m, 1H), 7.25 – 7.24 (m, 1H), 7.04 (bs, 1H), 3.64 (s, 3H); ^{13}C NMR (101 MHz, CDCl₃) δ_C 148.9, 148.3, 137.9, 129.6, 129.4, 129.3, 129.3, 129.2 (2C), 129.1, 129.1 (2C), 128.1, 127.0, 123.3, 120.9, 109.9, 106.0, 32.4.

4-bromo-*N*-(1-methyl-5-phenyl-1*H*-imidazol-2-yl)benzamide (3.005)

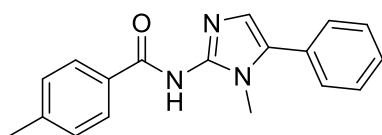


The title compound was prepared from 1-methyl-5-phenyl-1*H*-imidazol-2-amine (100 mg, 0.58 mmol) and 4-bromobenzoic acid (117 mg, 0.58 mmol) according to General Procedure B (91 mg, 44%). HPLC – t_R 5.18 min > 99% purity at 254 nm; LRMS $[M+H]^+$ 355.9 m/z ; HRMS $[M+H]^+$ 356.0393 m/z , 356.0399 found; 1H NMR (400 MHz, CDCl₃) δ_H 8.17 (d, J = 8.4 Hz, 2H, Hc), 7.60 – 7.33 (m, 7H, Hb, Hk, Hl, Hm), 6.75 (s, 1H, Hg), 3.63 (s, 3H, Hi); ^{13}C NMR (101 MHz, CDCl₃) δ_C 173.5 (Ce), 151.1 (Cf), 137.1 (Ch), 131.2 (2C, Cb), 130.6 (2C, Cc), 129.3 (Cm), 129.2 (2C, Cl), 128.9 (Ck), 128.2 (Ca), 125.7 (Cg), 109.1 (Cj), 30.5 (Ci). One aromatic quaternary carbon eclipsed by peak at 129.8, missing carbon is likely Cd.

Example spectra for Series 4 (additive SAR): ^1H NMR (400 MHz, CDCl_3) and ^{13}C NMR (100 MHz, CDCl_3) spectrum of 4-bromo-*N*-(1-methyl-5-phenyl-1*H*-imidazol-2-yl)benzamide (3.005)



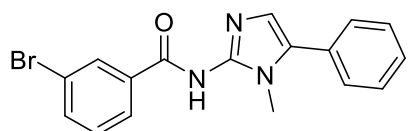
4-Methyl-*N*-(1-methyl-5-phenyl-1*H*-imidazol-2-yl)benzamide (3.006)



The title compound was prepared from 1-methyl-5-phenyl-1*H*-imidazol-2-amine (100 mg, 0.58 mmol) and 4-methylbenzoic acid (79 mg, 0.58 mmol) according to General Procedure B as a brown solid (142 mg, 84%). HPLC – t_R 4.94 min > 99% purity at 254 nm;

LRMS $[M+H]^+$ 292.0 m/z ; HRMS $[M+H]^+$ 292.1444 m/z , 292.145 found; 1H NMR (400 MHz, $CDCl_3$) δ_H 8.19 – 8.16 (m, 2H), 7.49 – 7.39 (m, 5H), 7.25 – 7.22 (m, 2H), 6.76 (s, 1H), 3.62 (s, 3H), 2.40 (s, 3H); ^{13}C NMR (101 MHz, $CDCl_3$) δ_C 173.2, 149.7, 143.4, 141.6, 134.4, 129.1 (2C), 128.9, 128.9 (2C), 128.9 (2C), 128.9 (2C), 128.8, 111.6, 31.0, 21.7.

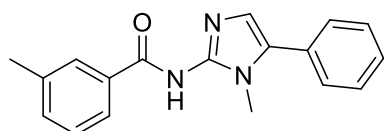
3-Bromo-*N*-(1-methyl-5-phenyl-1*H*-imidazol-2-yl)benzamide (3.007)



The title compound was prepared from 1-methyl-5-phenyl-1*H*-imidazol-2-amine (100 mg, 0.58 mmol) and 4-bromobenzoic acid (117 mg, 0.58 mmol) according to General Procedure B as an off-

white solid (73 mg, 38%). HPLC – t_R 5.13 min > 99% purity at 254 nm; LRMS $[M+H]^+$ 357.9 m/z ; HRMS $[M+H]^+$ 356.0393 m/z , 356.0398 found; 1H NMR (400 MHz, $CDCl_3$) δ_H 8.46 (t, J = 1.7 Hz, 1H), 8.24 – 8.20 (m, 1H), 7.58 – 7.55 (m, 1H), 7.49 – 7.39 (m, 5H), 7.30 – 7.26 (m, 1H), 6.74 (s, 1H), 3.63 (s, 3H); ^{13}C NMR (101 MHz, $CDCl_3$) δ_C 173.1, 151.3, 140.6, 133.6, 132.0, 129.6, 129.2, 129.1 (2C), 128.9, 128.9 (2C), 128.2, 127.4, 122.2, 108.9, 30.4.

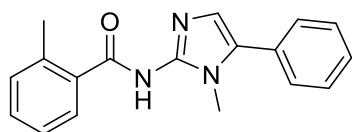
3-Methyl-*N*-(1-methyl-5-phenyl-1*H*-imidazol-2-yl)benzamide (3.008)



The title compound was prepared from 1-methyl-5-phenyl-1*H*-imidazol-2-amine (100 mg, 0.58 mmol) and 3-methylbenzoic acid (79 mg, 0.58 mmol) according to General Procedure B as a brown

solid (150 mg, 89%). HPLC – t_R 4.96 min > 99% purity at 254 nm; LRMS $[M+H]^+$ 292.0 m/z ; HRMS $[M+H]^+$ 291.1444 m/z , 291.1451 found; 1H NMR (400 MHz, $CDCl_3$) δ_H 8.10 – 8.07 (m, 2H), 7.50 – 7.40 (m, 5H), 7.35 – 7.27 (m, 2H), 6.80 (s, 1H), 3.62 (s, 3H), 2.41 (s, 3H); ^{13}C NMR (101 MHz, $CDCl_3$) δ_C 173.0, 149.3, 137.8, 137.0, 133.4, 132.0, 130.5, 129.4, 129.1, 128.9, 128.8, 128.1, 126.0, 112.2, 31.0, 21.5.

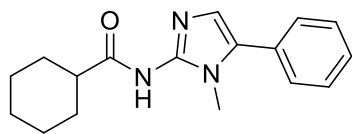
2-Methyl-*N*-(1-methyl-5-phenyl-1*H*-imidazol-2-yl)benzamide (3.009)



The title compound was prepared from 1-methyl-5-phenyl-1*H*-imidazol-2-amine (100 mg, 0.58 mmol) and 3-methylbenzoic acid (79 mg, 0.58 mmol) according to General Procedure B as a brown solid

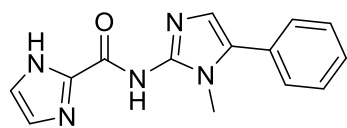
(102 mg, 60%). HPLC – t_R 4.75 min > 99% purity at 254 nm; LRMS $[M+H]^+$ 292.0 m/z ; HRMS $[M+H]^+$ 291.1444 m/z , 291.1449 found; 1H NMR (400 MHz, $CDCl_3$) δ_H 7.84 – 7.80 (m, 1H), 7.48 – 7.37 (m, 5H), 7.34 – 7.29 (m, 1H), 7.25 – 7.20 (m, 2H), 6.62 (s, 1H), 3.57 (s, 3H), 2.60 (s, 3H); ^{13}C NMR (101 MHz, $CDCl_3$) δ_C 174.6, 165.9, 147.3, 137.5, 137.3, 131.3, 130.6, 130.0, 129.0 (2C), 129.0, 128.7 (2C), 128.7, 125.6, 114.8, 31.4, 21.1.

***N*-(1-Methyl-5-phenyl-1*H*-imidazol-2-yl)cyclohexanecarboxamide (3.010)**



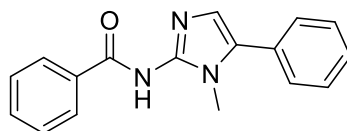
The title compound was prepared from 1-methyl-5-phenyl-1*H*-imidazol-2-amine (100 mg, 0.58 mmol) and cyclohexanecarboxylic acid (74 mg, 0.58 mmol) according to General Procedure B as an off-white solid (140 mg, 85%). HPLC – t_R 4.94 min > 99% purity at 254 nm; LRMS $[M+H]^+$ 284.1 m/z ; HRMS $[M+H]^+$ 284.1757 m/z , 284.1763 found; 1H NMR (400 MHz, $CDCl_3$) δ_H 7.48 – 7.37 (m, 5H), 6.90 (s, 1H), 3.50 (s, 3H), 2.53 – 2.42 (m, 1H), 1.97 (d, J = 11.9 Hz, 2H), 1.83 – 1.49 (m, 5H), 1.38 – 1.22 (m, 3H); ^{13}C NMR (101 MHz, $CDCl_3$) δ_C 178.4, 132.6, 130.0, 129.1, 129.1 (2C), 128.8, 128.7, 128.3, 45.6, 32.2, 29.7 (2C), 25.9, 25.7 (2C).

***N*-(1-Methyl-5-phenyl-1*H*-imidazol-2-yl)-1*H*-imidazole-2-carboxamide (3.011)**



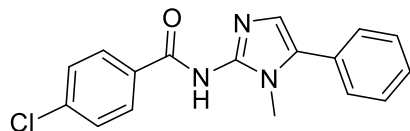
The title compound was prepared from 1-methyl-5-phenyl-1*H*-imidazol-2-amine (200 mg, 1.16 mmol) and 1*H*-imidazole-2-carboxylic acid (130 mg, 1.16 mmol) according to General Procedure B as a white solid (46 mg, 15 %). HPLC – t_R 4.23 min > 99% purity at 254 nm; LRMS $[M+H]^+$ 268.0 m/z ; HRMS $[M+H]^+$ 268.1193 m/z , 268.1190 found; 1H NMR (400 MHz, $CDCl_3$) δ_H 7.49 – 7.35 (m, 2H), 7.21 (s, 2H), 6.86 (s, 1H), 3.61 (s, 3H); ^{13}C NMR (101 MHz, $CDCl_3$) δ_C 128.9 (2C), 128.9, 128.8, 128.7 (2C), 128.1, 128.0, 31.2 Quaternary carbons not visible.

***N*-(1-Methyl-5-phenyl-1*H*-imidazol-2-yl)benzamide (3.012)**



The title compound was obtained using 1-methyl-5-phenyl-1*H*-imidazol-2-amine (260 mg, 1.5 mmol) and benzoic acid (183 mg, 1.5 eq) following General Procedure B, affording the title compound as an orange solid (322 mg, 77 %). HPLC – t_R 4.40 min > 99 % purity at 254 nm; LRMS $[M+H]^+$ 278.0 m/z ; HRMS $[M+H]^+$ 278.1288 m/z , found 278.1291 m/z ; 1H NMR (400 MHz, $CDCl_3$) δ 8.30 – 8.26 (m, 2H), 7.49 – 7.38 (m, 8H), 6.75 (s, 1H), 3.62 (s, 3H); ^{13}C NMR (101 MHz, $CDCl_3$) δ_C 173.9, 150.4, 137.8, 131.0, 129.2, 129.1 (2C), 128.9, 128.8 (2C), 128.8 (2C), 128.6, 128.0 (2C), 110.6, 30.6.

4-Chloro-*N*-(1-methyl-5-phenyl-1*H*-imidazol-2-yl)benzamide (3.013)

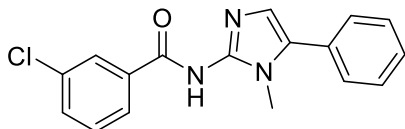


The title compound was obtained using 1-methyl-5-phenyl-1*H*-imidazol-2-amine (260 mg, 1.5 mmol) and 4-chlorobenzoic acid (233 mg, 1.5 mmol) following General Procedure B, affording the title compound as a yellow solid (250 mg, 54 %). HPLC – t_R 4.90 min > 99 % purity at 254 nm; LRMS $[M+H]^+$ 311.9 m/z ; HRMS $[M+H]^+$ 312.0898 m/z , found 312.0902 m/z ; 1H NMR (400 MHz, $CDCl_3$) δ_H 8.26 – 8.22 (m, 2H), 7.52 – 7.35 (m, 7H), 6.73 (s, 1H), 3.61 (s, 3H); 1H NMR (400 MHz, MeOD) δ_H 8.18 (d, J = 8.3 Hz, 2H), 7.58 – 7.48 (m, 7H), 7.03 (s, 1H), 3.65 (s, 3H); ^{13}C NMR (101 MHz, MeOD)

δ_c 131.3 (2C), 130.1 (2C), 130.0, 130.0 (2C), 129.4 (2C), 31.3. Imidazole and quaternary carbons not visible

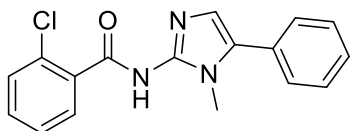
3-Chloro-*N*-(1-methyl-5-phenyl-1*H*-imidazol-2-yl)benzamide (3.014)

The title compound was obtained using 1-methyl-5-phenyl-1*H*-imidazol-2-amine (100 mg, 0.58 mmol) and 3-chlorobenzoic acid (90 mg, 0.58 mmol) following General Procedure B, to afford the title



compound as a pale yellow solid (100 mg, 56 %). HPLC – t_R 4.95 min > 99 % purity at 254 nm; LRMS $[M+H]^+$ 312.1 m/z ; HRMS $[M+H]^+$ 312.0898 m/z , found 312.0898 m/z ; 1H NMR (400 MHz, DMSO) δ_H 12.47 (bs, 1H, NH), 8.14 (s, 2H), 7.58 – 7.41 (m, 7H), 7.02 (s, 1H), 3.57 (s, 3H); ^{13}C NMR (101 MHz, DMSO) δ_c 133.0, 130.5 130.0, 129.1 (2C), 128.6, 128.5 (2C), 128.1, 127.1, 30.5. Quaternary carbons not visible.

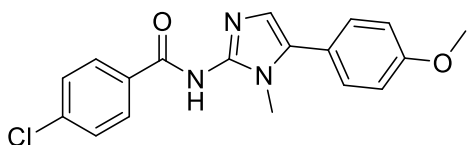
2-Chloro-*N*-(1-methyl-5-phenyl-1*H*-imidazol-2-yl)benzamide (3.015)



The title compound was obtained using 1-methyl-5-phenyl-1*H*-imidazol-2-amine (200 mg, 1.2 mmol) and 2-chlorobenzoic acid (180 mg, 1.2 mmol) following General Procedure B, to afford the title

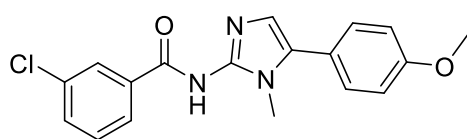
compound as a yellow solid (338 mg, 91 %). HPLC – t_R 4.59 min > 99 % purity at 254 nm; LRMS $[M+H]^+$ 312.1 m/z ; HRMS $[M+H]^+$ 312.0898 m/z , found 312.0902 m/z ; 1H NMR (400 MHz, MeOD) δ_H 7.68 (dd, J = 7.2, 1.7 Hz, 1H), 7.54 – 7.39 (m, 8H), 7.01 (s, 1H), 3.61 (s, 3H); 1H NMR (400 MHz, DMSO) δ_H 10.47 (bs, 1H), 7.49 (d, J = 6.7 Hz, 1H), 7.40 – 7.19 (m, 7H), 6.82 (s, 1H) N-Me eclipsed by solvent peak; ^{13}C NMR (101 MHz, DMSO) δ_c 131.0, 130.4, 130.0, 129.6, 129.1 (2C), 128.3 (2C), 127.2, 31.1. Quaternary carbons not visible. M.p. 144.5-147.0 °C.

4-Chloro-*N*-(5-(4-methoxyphenyl)-1-methyl-1*H*-imidazol-2-yl)benzamide 3.016



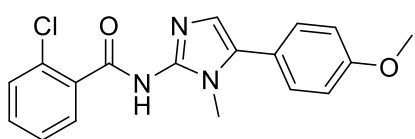
The title compound was obtained using 5-(4-methoxyphenyl)-1-methyl-1*H*-imidazol-2-amine (200 mg, 0.98 mmol) and 4-chlorobenzoic acid (156 mg, 1.0 mmol) following General Procedure B, to afford the title compound as a yellow solid (190 mg, 56 %). HPLC – t_R 4.69 min > 99 % purity at 254 nm; LRMS $[M+H]^+$ 342.1 m/z ; HRMS $[M+H]^+$ 342.1004 m/z , found 342.1012 m/z ; 1H NMR (400 MHz, MeOD) δ_H 8.16 (d, J = 8.4 Hz, 2H), 7.48 – 7.43 (m, 4H), 7.09 – 7.06 (m, 2H), 6.92 (s, 1H), 3.59 (s, 3H); ^{13}C NMR (101 MHz, MeOD) δ_c 161.8, 131.5 (2C), 131.3 (2C), 129.3 (2C), 122.0, 115.4 (2C), 55.9, 30.9. Aromatic quaternary carbons not visible.

3-Chloro-*N*-(5-(4-methoxyphenyl)-1-methyl-1*H*-imidazol-2-yl)benzamide 3.017



The title compound was obtained using 5-(4-methoxyphenyl)-1-methyl-1*H*-imidazol-2-amine (200 mg, 0.98) and 3-chlorobenzoic acid (156 mg, 1.0 mmol) following General Procedure B, to afford the title compound as a yellow solid (170 mg, 50 %). HPLC – t_R 4.72 min > 99 % purity at 254 nm; LRMS $[M+H]^+$ 342.1 m/z ; HRMS $[M+H]^+$ 342.1004 m/z , found 342.1012 m/z ; 1H NMR (400 MHz, MeOD) δ_H 8.20 – 8.16 (m, 1H), 8.13 – 8.09 (m, 1H), 7.54 – 7.42 (m, 4H), 7.10 – 7.06 (m, 2H), 6.93 (s, 1H), 3.88 (s, 3H), 3.61 (s, 3H).

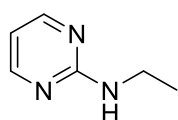
2-Chloro-*N*-(5-(4-methoxyphenyl)-1-methyl-1*H*-imidazol-2-yl)benzamide 3.018



The title compound was obtained using 5-(4-methoxyphenyl)-1-methyl-1*H*-imidazol-2-amine (200 mg, 0.98) and 2-chlorobenzoic acid (156 mg, 1.0 mmol) following General Procedure B, to afford the title compound as a yellow solid (195 mg, 57 %). HPLC – t_R 4.44 min > 99 % purity at 254 nm; LRMS $[M+H]^+$ 342.1 m/z ; HRMS $[M+H]^+$ 342.1004 m/z , found 342.1012 m/z ; 1H NMR (400 MHz, MeOD) δ_H 7.69 – 7.66 (m, 2H), 7.54 – 7.40 (m, 5H), 7.09 – 7.05 (m, 2H), 6.95 (s, 1H), 3.87 (s, 3H), 3.57 (s, 3H); ^{13}C NMR (101 MHz, MeOD) δ_C 161.7, 132.5, 132.3, 132.0, 131.5 (2C), 131.4, 131.1, 130.4, 128.0, 127.8, 122.2, 115.5 (2C), 55.9, 31.5. Imidazole quaternary carbons not visible.

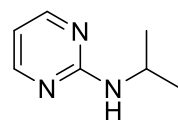
Analogue Series 5

N-Ethylpyrimidin-2-amine (3.026)²



A solution of 2-chloropyrimidine (600 mg, 5.00 mmol) in ethylamine 2M in THF (20 mL) was heated to reflux for 16 h. After cooling to room temperature, 1M HCl was added and washed with DCM. The aqueous layer was made basic with Na_2CO_3 and extracted with DCM. The organic layer was collected and dried with $MgSO_4$, filtered and concentrated *in vacuo* to give the desired known product as orange crystals (475 mg, 73%).¹ HPLC – t_R 2.00 min > 90% purity at 254 nm; LRMS $[M+H]^+$ 124.0 m/z ; 1H NMR (400 MHz, $CDCl_3$) δ_H 8.26 (d, J = 4.8 Hz, 1H), 6.50 (t, J = 4.8 Hz, 1H), 5.20 (s, 1H), 3.47 – 3.40 (m, 2H), 1.24 (t, J = 7.2 Hz, 3H); ^{13}C NMR (101 MHz, $CDCl_3$) δ_C 162.5, 158.1 (2C), 110.5, 36.4, 15.0. Acquired data is consistent with the literature.²

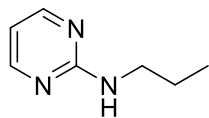
N-Isopropylpyrimidin-2-amine (3.027)²



The known title compound by dissolving 2-chloropyrimidine (10.00 mmol) and isopropylamine (20.00 mmol) in ethanol (15 mL) in a sealed tube. The mixture was heated to 80 °C for 16 h. The mixture was then cooled, concentrated *in vacuo*, diluted with EtOAc washed with brine. The organic layer was collected, dried with $MgSO_4$, filtered and concentrated *in vacuo* to an orange oil (0.94 mL, 72 %).⁹ HPLC – t_R 2.32 min > 85% purity at 254 nm;

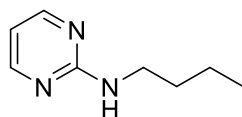
LRMS $[M+H]^+$ 138.1 m/z ; 1H NMR (400 MHz, $CDCl_3$) δ_H 8.21 (d, $J = 4.8$ Hz, 2H), 6.44 – 6.41 (m, 1H), 5.49 (bs, 1H), 4.15 – 4.01 (m, 1H), 1.19 (d, $J = 6.5$ Hz, 6H); ^{13}C NMR (101 MHz, $CDCl_3$) δ_C 161.9, 157.9 (2C), 110.0, 42.7, 22.9 (2C). Acquired data is consistent with the literature.²

***N*-Propylpyrimidin-2-amine (3.028)²**



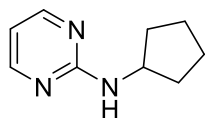
The known title compound was prepared by dissolving 2-chloropyrimidine (2.20 g, 19.20 mmol), propylamine (1.57 mL, 19.20 mmol) and triethylamine (6 mL) in THF (10 mL). The mixture was heated to 110°C for 16 h. Upon reaction completion the mixture was cooled and concentrated. The crude material was diluted with EtOAc and washed with brine. The organic layers were collected and dried with $MgSO_4$, filtered and concentrated *in vacuo*.⁷ The title compound was obtained as an orange oil. (1.65 g, 63 %). HPLC – t_R 2.42 min > 80% purity at 254 nm; LRMS $[M+H]^+$ 138.1 m/z ; 1H NMR (400 MHz, $CDCl_3$) δ_H 8.08 (d, $J = 4.4$ Hz, 2H), 6.32 – 6.21 (m, 2H), 3.23 – 3.16 (m, 2H), 1.50 – 1.40 (m, 2H), 0.83 – 0.75 (m, 3H); ^{13}C NMR (101 MHz, $CDCl_3$) δ_C 162.4, 157.7 (2C), 109.7, 43.0, 22.6, 11.3.²

***N*-Butylpyrimidin-2-amine (3.029)^{7, 56}**



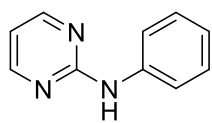
The known title compound was prepared by dissolving 2-chloropyrimidine (2.20 g, 19.20 mmol), butylamine (1.90 mL, 19.20 mmol) and triethylamine (6 mL) in *n*-butanol (40 mL). The mixture was heated to 110°C for 16 h. Upon reaction completion the mixture was cooled and concentrated. The crude material was diluted with EtOAc and washed with brine. The organic layers were collected and dried with $MgSO_4$, filtered and concentrated *in vacuo*.⁷ The title compound was obtained as an orange liquid. (1.88 g, 65 %). HPLC – t_R 3.20 min > 83% purity at 254 nm; LRMS $[M+H]^+$ 152.1 m/z ; 1H NMR (400 MHz, $CDCl_3$) δ_H 8.19 (d, $J = 4.5$ Hz, 2H), 6.43 – 6.38 (m, 1H), 5.78 (bs, 1H), 3.37 – 3.30 (m, 2H), 1.57 – 1.48 (m, 2H), 1.39 – 1.28 (m, 2H), 0.90 – 0.84 (m, 3H); ^{13}C NMR (101 MHz, $CDCl_3$) δ_C 162.6, 159.6, 158.0, 110.1, 41.2, 31.7, 20.2, 13.8 (2C).^{7, 56}

***N*-Cyclopentylpyrimidin-2-amine (3.030)³**



The known title compound was prepared by dissolving 2-chloropyrimidine (1.00 g, 8.81 mmol), cyclopentylamine (2.3 eq), K_2CO_3 (0.72 mg, 5.17 mmol) in *t*BuOH (4 mL) and THF (4 mL) and heated using microwave irradiation at 150 °C for 15 min. The mixture was concentrated *in vacuo* and diluted with DCM washed with brine and the organic layers were collected, dried with $MgSO_4$ and concentrated *in vacuo*.⁸ The title compound was obtained as a brown solid. (806.3 mg, 58 %). HPLC – t_R 3.25 min > 97% purity at 254 nm; LRMS $[M+H]^+$ 164.1 m/z ; 1H NMR (400 MHz, $CDCl_3$) δ_H 8.25 (d, $J = 4.8$ Hz, 2H), 6.47 (t, $J = 4.8$ Hz, 1H), 5.25 (bs, 1H), 4.29 – 4.20 (m, 1H), 2.08 – 1.99 (m, 2H), 1.77 – 1.57 (m, 4H), 1.51 – 1.40 (m, 2H); ^{13}C NMR (101 MHz, $CDCl_3$) δ_C 162.3, 158.1 (2C), 110.3, 53.0, 33.4 (2C), 23.8 (2C).

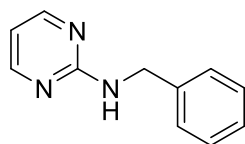
***N*-Phenylpyrimidin-2-amine (3.031)^{2,7}**



The known title compound was prepared by dissolving 2-chloropyrimidine (573 mg, 5.00 mmol), aniline (0.70 mL) and acetic acid (0.05 mL) in dioxane (5.00 mL).

The mixture was heated to 110°C for 16 h. Upon reaction completion the mixture was cooled and concentrated. The crude material was diluted with DCM and washed with brine. The organic layers were collected and dried with MgSO₄, filtered and concentrated *in vacuo*.⁷ The title compound was obtained as an orange solid. (755 mg, 88 %). HPLC – *t_R* 3.67 min > 99 % purity at 254 nm; LRMS [M+H]⁺ 172.0 *m/z*; ¹H NMR (400 MHz, CDCl₃) δ_H 8.43 (d, *J* = 4.9 Hz, 2H), 8.01 (bs, 1H), 7.65 – 7.61 (m, 2H), 7.38 – 7.33 (m, 2H), 7.10 – 7.06 (m, 1H), 6.75 (t, *J* = 4.9 Hz, 1H); ¹³C NMR (101 MHz, CDCl₃) δ_C 159.4, 157.8 (2C), 138.9, 129.1, 123.4, 120.1 (2C), 112.3. Acquired data is consistent with the literature.^{2,7}

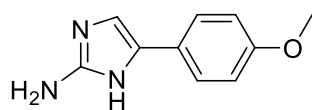
***N*-Benzylpyrimidin-2-amine (3.032)^{2,7}**



The known title compound was prepared by dissolving 2-chloropyrimidine (460 mg, 4.0 mmol), phenylmethanamine (0.12 mL) and triethylamine (0.28 mL) in EtOH (5.00 mL). The mixture was heated to 78°C for 16 h. Upon reaction completion the mixture was cooled and concentrated. The crude material was

diluted with EtOAc and washed with brine. The organic layers were collected and dried with MgSO₄, filtered and concentrated *in vacuo*.⁷ The title compound was obtained as a yellow solid. (330 mg, 89 %). HPLC – *t_R* 3.72 min > 85 % purity at 254 nm; LRMS [M+H]⁺ 186.0 *m/z*; ¹H NMR (400 MHz, CDCl₃) δ_H 8.58 (d, *J* = 4.8 Hz, 1H), 8.21 (d, *J* = 4.8 Hz, 2H), 7.30 – 7.17 (m, 4H), 6.48 (t, *J* = 4.8 Hz, 1H), 5.54 (bs, 1H), 4.58 (d, *J* = 5.9 Hz, 2H); ¹³C NMR (101 MHz, CDCl₃) δ_C 159.7, 158.2 (2C), 139.2, 128.7 (2C), 127.6 (2C), 127.4, 119.9, 111.0, 45.6.^{2,7}

5-(4-Methoxyphenyl)-1*H*-imidazol-2-amine (3.033)⁵⁷

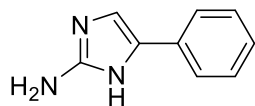


The known title compound was prepared from 2-Bromo-4'-methoxyacetophenone (150 mg, 0.66 mmol) and acetyl guanidine (200 mg, 1.98 mmol) in ACN. The mixture was reacted in the microwave and

was heated to 100°C for 15 min. Upon reaction completion the mixture was diluted with water, concentrated *in vacuo* and filtered with water to get a grey solid. The solid (200 mg) was put in a microwave vial and MeOH/H₂O (1:1) was added followed by H₂SO₄ (0.6 mL). The reaction mixture was heated in the microwave for 30 min at 100°C. Upon reaction completion the mixture was concentrated, diluted with water and made basic (pH 8) with Na₂CO₃. The solution was washed with EtOAc, the organic layers were collected, dried with MgSO₄, filtered and concentrated to give the title product as a purple solid. (290 mg, 72 %).^{3,11} HPLC *t_R* = 3.754 min >99% purity at 254nm; LRMS [M+H]⁺ 190.1 *m/z*; ¹H NMR (400 MHz, MeOD) δ_H 7.35 – 7.30 (m, 2H), 6.75 – 6.71 (m, 2H), 6.63 (s,

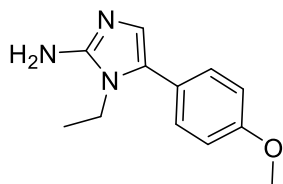
1H), 3.62 (s, 3H); ¹³C NMR (101 MHz, MeOD) δ_C 159.7, 151.4, 134.5, 127.3, 126.3 (2C), 115.0 (2C), 111.3, 55.7.

5-Phenyl-1*H*-imidazol-2-amine (3.034)^{11, 57}



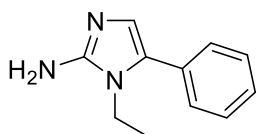
The known title compound was prepared from pyrimidin-2-amine (475mg, 5.00 mmol), 5-phenyl-1*H*-imidazol-2-amine (1,294 mg, 6.00 mmol) and DMAP (0.05 mmol) were added in ACN (10 mL) and heated using microwave irradiation at 80 °C for 45 min. The mixture was cooled and washed with acetone and ether and dried *in vacuo*. The crude mixture was dissolved in ACN and hydrazine hydrate (14 mmol) was added and heated using microwave irradiation at 100 °C for 10 min. The mixture was cooled and washed with water, filtered and dried. The crude material was subsequently purified via column chromatography (DCM, 94%: MeOH, 5%: NH₃OH, 1%). The compound was obtained as a yellow solid (100 mg, 13 %).¹⁰ HPLC – *t_R* 3.50 min > 99% purity at 254 nm; LRMS [M+H]⁺ 160.0 *m/z*.¹¹ ¹H NMR (400 MHz, CDCl₃) δ_H 7.54 – 7.48 (m, 2H), 7.32 – 7.27 (m, 2H), 7.20 – 7.15 (m, 1H); ¹³C NMR (101 MHz, CDCl₃) δ_C 164.3, 152.0, 132.8, 128.8 (2C), 126.5, 124.2 (2C), 111.7.

1-Ethyl-5-(4-methoxyphenyl)-1*H*-imidazol-2-amine (3.035)



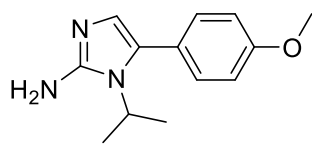
The title compound was prepared from 2-bromo-1-(4-methoxyphenyl)ethan-1-one (824 mg, 3.60 mmol) and *N*-ethylpyrimidin-2-amine (334 mg, 3.00 mmol) according to General Procedure A as an orange solid without further purification (588 mg, 99%). HPLC – *t_R* 4.34 min > 95% purity at 254 nm; LRMS [M+H]⁺ 217.9 *m/z*; ¹H NMR (400 MHz, CDCl₃) δ_H 7.20 – 7.17 (m, 2H), 6.89 – 6.85 (m, 2H), 6.53 (s, 1H), 3.71 (dd, *J* = 8.6, 5.9 Hz, 2H), 1.16 (t, *J* = 7.2 Hz, 3H); ¹³C NMR (101 MHz, CDCl₃) δ_C 159.3, 148.1, 130.1 (2C), 129.2, 123.3, 122.1, 114.3 (2C), 55.5, 38.0, 15.2.

1-Ethyl-5-phenyl-1*H*-imidazol-2-amine (3.036)³



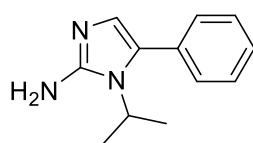
The known title compound was prepared from *N*-ethylpyrimidin-2-amine (372 mg, 3.00 mmol) and 2-bromo-1-phenylethan-1-one (806 mg, 4.05 mmol) according to General Procedure A as a brown solid (383 mg, 68 %). HPLC – *t_R* 4.07 min > 90% purity at 254 nm; LRMS [M+H]⁺ 188.1 *m/z*; ¹H NMR (400 MHz, CDCl₃) δ_H 7.40 – 7.29 (m, 5H), 6.66 (s, 1H), 4.42 (bs, 2H), 3.79 (q, *J* = 7.2 Hz, 2H), 1.22 (t, *J* = 7.2 Hz, 3H); ¹³C NMR (101 MHz, CDCl₃) δ_C 149.1, 131.1, 129.3, 128.7 (2C), 128.2 (2C), 127.3, 123.2, 38.0, 15.1. Acquired data is consistent with the literature.³

1-Isopropyl-5-(4-methoxyphenyl)-1*H*-imidazol-2-amine (3.037)



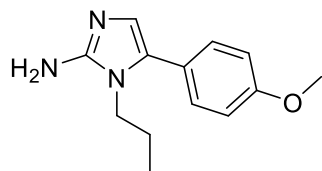
The title compound was prepared from *N*-isopropylpyrimidin-2-amine (0.40 mL, 3.00 mmol) and 2-bromo-1-(4-methoxyphenyl)ethan-1-one (927 mg, 4.05 mmol) according to General Procedure A as an orange solid (600 mg, 86%). HPLC – t_R 4.53 min > 90 % purity at 254 nm; LRMS $[M+H]^+$ 232.1 m/z ; 1H NMR (400 MHz, $CDCl_3$) δ_H 7.22 – 7.17 (m, 2H), 6.96 – 6.89 (m, 2H), 6.51 (s, 1H), 4.33 – 4.22 (m, 1H), 3.83 (s, 3H), 1.41 (d, J = 7.0 Hz, 6H); ^{13}C NMR (101 MHz, $CDCl_3$) δ_C 159.4, 148.0, 131.0 (2C), 129.6, 123.7, 122.3, 114.1 (2C), 55.5, 46.5, 21.3 (2C).

1-Isopropyl-5-phenyl-1*H*-imidazol-2-amine (3.038)⁵⁸



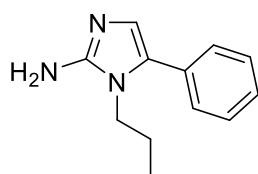
The known title compound was prepared from *N*-isopropylpyrimidin-2-amine (0.40 mL, 3.00 mmol) and 2-bromo-1-phenylethan-1-one (806 mg, 4.05 mmol) according to General Procedure A as a brown oil (600 mg, 99%). HPLC – t_R 4.39 min > 98% purity at 254 nm; LRMS $[M+H]^+$ 202.1 m/z ; 1H NMR (400 MHz, $CDCl_3$) δ_H 7.47 – 7.40 (m, 3H), 7.31 – 7.27 (m, 2H), 6.58 (s, 1H), 6.07 (bs, 2H, NH₂), 4.40 – 4.28 (m, 1H), 1.46 (d, J = 7.1 Hz, 6H); 1H NMR (400 MHz, MeOD) δ_H 7.50 – 7.33 (m, 5H), 6.52 (s, 1H), 4.45 – 4.35 (m, 1H), 1.46 (d, J = 7.1 Hz, 6H); ^{13}C NMR (101 MHz, MeOD) δ_C 130.7 (2C), 129.6 (2C), 129.0, 121.5, 40.1, 20.9 (2C). Quaternary carbons not visible.

5-(4-Methoxyphenyl)-1-propyl-1*H*-imidazol-2-amine (3.039)



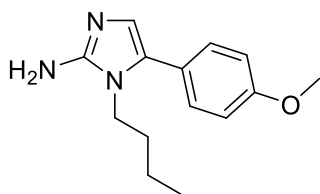
The title compound was prepared from *N*-propylpyrimidin-2-amine (0.39 mL, 3.00 mmol) and 2-bromo-1-(4-methoxyphenyl)ethan-1-one (927 mg, 4.05 mmol) according to General Procedure A as a brown oil (635 mg, 92 %). HPLC – t_R 4.63 min > 90% purity at 254 nm; LRMS $[M+H]^+$ 232.0 m/z ; 1H NMR (400 MHz, $CDCl_3$) δ_H 7.23 (d, J = 8.6 Hz, 1H), 6.93 (d, J = 8.7 Hz, 2H), 6.57 (bs, 1H), 3.83 (s, 3H), 3.72 – 3.66 (m, 2H), 1.64 – 1.54 (m, 2H), 0.80 (t, J = 7.3 Hz, 3H); ^{13}C NMR (101 MHz, $CDCl_3$) δ_C 159.5, 148.2, 130.3, 123.1, 120.9, 114.3, 113.8, 55.5, 44.8, 23.0, 11.2.

5-Phenyl-1-propyl-1*H*-imidazol-2-amine (3.040)



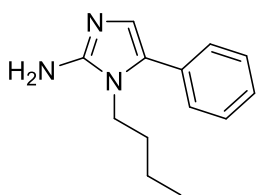
The title compound was prepared from *N*-propylpyrimidin-2-amine (0.39 mL, 3.00 mmol) and 2-bromo-1-phenylethan-1-one (806 mg, 4.05 mmol) according to General Procedure A as a brown oil (600 mg, 99 %). HPLC – t_R 4.46 min > 94 % purity at 254 nm; LRMS $[M+H]^+$ 202.0 m/z ; 1H NMR (400 MHz, $CDCl_3$) δ_H 7.43 – 7.36 (m, 2H), 7.34 – 7.29 (m, 3H), 6.66 (s, 1H), 4.14 (bs, 2H), 3.75 – 3.68 (m, 2H), 1.66 – 1.56 (m, 2H), 0.81 (t, J = 7.4 Hz, 3H); ^{13}C NMR (101 MHz, $CDCl_3$) δ_C 149.1, 131.2, 129.7, 128.8 (2C), 128.4 (2C), 127.4, 123.2, 44.9, 23.1, 11.1.

1-Butyl-5-(4-methoxyphenyl)-1*H*-imidazol-2-amine (3.041)



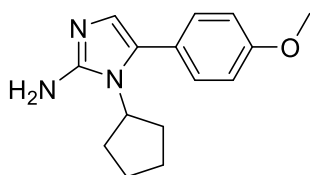
The title compound was prepared from *N*-butylpyrimidin-2-amine (0.46 mL, 3.00 mmol) and 2-bromo-1-(4-methoxyphenyl)ethan-1-one (927 mg, 4.05 mmol) according to General Procedure A as a brown solid (680 mg, 90 %). HPLC – t_R 5.03 min > 99 % purity at 254 nm; LRMS $[M+H]^+$ 246.1 m/z ; 1H NMR (400 MHz, $CDCl_3$) δ_H 7.24 – 7.20 (m, 2H), 6.94 – 6.90 (m, 2H), 6.56 (s, 1H), 3.83 (s, 3H), 3.74 – 3.69 (m, 2H), 1.58 – 1.49 (m, 2H), 1.23 – 1.14 (m, 2H), 0.80 (t, $J = 7.4$ Hz, 3H); ^{13}C NMR (101 MHz, $CDCl_3$) δ_C 159.3, 148.4, 130.2, 123.2, 121.3, 114.2, 104.9, 55.4, 42.9, 31.7, 19.9, 13.6.

1-Butyl-5-phenyl-1*H*-imidazol-2-amine (3.042)³



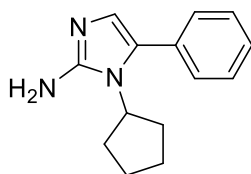
The known title compound was prepared from *N*-butylpyrimidin-2-amine (0.46 mL, 3.00 mmol) and 2-bromo-1-phenylethan-1-one (806 mg, 4.05 mmol) according to General Procedure A as a brown solid (606 mg, 94 %). HPLC – t_R 4.95 min > 95 % purity at 254 nm; LRMS $[M+H]^+$ 216.0 m/z ; 1H NMR (400 MHz, $CDCl_3$) δ_H 7.41 – 7.36 (m, 2H), 7.33 – 7.28 (m, 3H), 6.65 (s, 1H), 4.69 (bs, 2H), 3.78 – 3.73 (m, 2H), 1.60 – 1.52 (m, 2H), 1.24 – 1.15 (m, 2H), 0.80 (t, $J = 7.4$ Hz, 3H); ^{13}C NMR (101 MHz, $CDCl_3$) δ_C 149.2, 131.1, 129.5, 128.7 (2C), 128.3 (2C), 127.3, 122.7, 43.0, 31.7, 19.8, 13.5. Acquired data is consistent with the literature.³

1-Cyclopentyl-5-(4-methoxyphenyl)-1*H*-imidazol-2-amine (3.043)



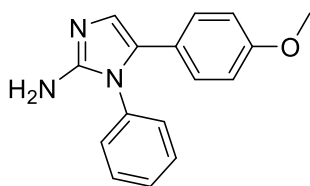
The title compound was prepared from *N*-cyclopentylpyrimidin-2-amine (492 mg, 3.00 mmol) and 2-bromo-1-(4-methoxyphenyl)ethan-1-one (927 mg, 4.05 mmol) according to General Procedure A as a brown solid (752 mg, 98 %). HPLC – t_R 5.06 min > 95% purity at 254 nm; LRMS $[M+H]^+$ 258.0 m/z ; 1H NMR (400 MHz, $CDCl_3$) δ_H 7.24 – 7.20 (m, 2H), 6.99 – 6.95 (m, 2H), 6.55 (s, 1H), 4.44 – 4.34 (m, 1H), 3.85 (s, 3H), 2.06 – 1.97 (m, 3H), 1.89 – 1.81 (m, 2H), 1.64 – 1.56 (m, 2H); ^{13}C NMR (101 MHz, $CDCl_3$) δ_C 160.7, 146.7, 131.5 (2C), 129.5, 120.1, 114.6 (2C), 112.2, 56.2, 55.6, 29.6, 25.0.

1-Cyclopentyl-5-phenyl-1*H*-imidazol-2-amine (3.044)³



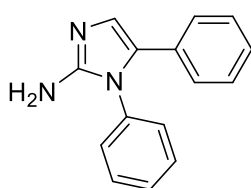
The known title compound was prepared from *N*-cyclopentylpyrimidin-2-amine (492 mg, 3.00 mmol) and 2-bromo-1-phenylethan-1-one (806 mg, 4.05 mmol) according to General Procedure A as a brown solid (668 mg, 98 %). HPLC – t_R min > 80 % purity at 254 nm; LRMS $[M+H]^+$ 228.1 m/z ; 1H NMR (400 MHz, $CDCl_3$) δ_H 7.50 – 7.46 (m, 3H), 7.31 – 7.27 (m, 2H), 6.54 (s, 1H), 4.47 – 4.24 (m, 1H), 2.05 – 1.90 (m, 2H), 1.92 – 1.79 (m, 2H), 1.75 – 1.60 (m, 2H), 1.61 – 1.42 (m, 2H).³

5-(4-Methoxyphenyl)-1-phenyl-1*H*-imidazol-2-amine (3.045)



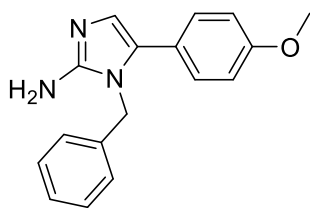
The title compound was prepared from *N*-phenylpyrimidin-2-amine (285 mg, 3.00 mmol) and 2-bromo-1-(4-methoxyphenyl)ethan-1-one (927 mg, 4.05 mmol) according to General Procedure A as an orange solid. (550 mg, 69 %). HPLC t_R = 4.748 min >85% purity at 254nm; LRMS $[M+H]^+$ 266.0 m/z ; 1H NMR (400 MHz, $CDCl_3$) δ_H 7.47 – 7.41 (m, 3H), 7.22 – 7.17 (m, 2H), 6.92 (d, J = 8.7 Hz, 2H), 6.76 – 6.71 (m, 3H), 2.80 (s, 3H); ^{13}C NMR (101 MHz, $CDCl_3$) δ_C 159.7, 148.0, 143.6, 133.1, 130.5 (2C), 130.1, 129.4 (2C), 129.2, 127.7 (2C), 114.2 (2C), 111.2, 55.3.

1,5-Diphenyl-1*H*-imidazol-2-amine (3.046)



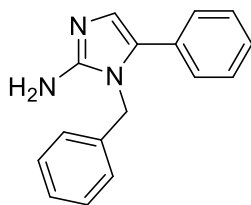
The title compound was prepared from *N*-phenylpyrimidin-2-amine (516 mg, 3.00 mmol) and 2-bromo-1-phenylethan-1-one (806 mg, 4.05 mmol) according to General Procedure A, though the condensation step requires 150°C for 25 min. The title compound was obtained as a brown solid (600 mg, 85 %). HPLC – t_R 4.69 min > 99 % purity at 254 nm; LRMS $[M+H]^+$ 236.0 m/z ; 1H NMR (400 MHz, $CDCl_3$) δ_H 7.45 – 7.39 (m, 3H), 7.25 – 7.22 (m, 2H), 7.17 – 7.10 (m, 3H), 7.03 – 6.99 (m, 2H), 6.88 (s, 1H).

1-Benzyl-5-(4-methoxyphenyl)-1*H*-imidazol-2-amine (3.047)



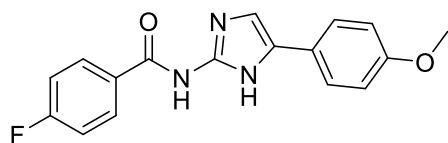
The title compound was prepared from *N*-benzylpyrimidin-2-amine (558 mg, 3.00 mmol) and 2-bromo-1-(4-methoxyphenyl)ethan-1-one (927 mg, 4.05 mmol) according to General Procedure A as a brown solid (808 mg, 97 %). HPLC – t_R 5.07 min > 95 % purity at 254 nm; LRMS $[M+H]^+$ 280.1 m/z ; 1H NMR (400 MHz, $CDCl_3$) δ_H 7.29 – 7.17 (m, 3H), 7.11 – 7.07 (m, 2H), 7.04 – 6.98 (m, 2H), 6.80 – 6.74 (m, 2H), 6.60 (s, 1H), 4.88 (s, 2H), 3.70 (s, 3H); ^{13}C NMR (101 MHz, $CDCl_3$) δ_C 159.3, 149.0, 136.5, 129.9, 129.8 (2C), 129.3 (2C), 127.9, 126.1 (2C), 122.8, 121.7, 114.3 (2C), 55.4, 46.5.

1-Benzyl-5-phenyl-1*H*-imidazol-2-amine (3.048)³



The known title compound was prepared from *N*-benzylpyrimidin-2-amine (558 mg, 3.00 mmol) and 2-bromo-1-phenylethan-1-one (806 mg, 4.05 mmol) according to General Procedure A as a brown solid (740 mg, 99 %). HPLC – t_R 4.99 min > 99 % purity at 254 nm; LRMS $[M+H]^+$ 250.0 m/z ; 1H NMR (400 MHz, $CDCl_3$) δ_H 7.35 – 7.21 (m, 8H), 7.08 (d, J = 7.2 Hz, 2H), 6.74 (s, 1H), 5.01 (s, 2H); ^{13}C NMR (101 MHz, $CDCl_3$) δ_C 149.7, 136.1, 130.0, 129.8, 129.2 (2C), 128.8 (2C), 128.1 (2C), 127.9, 127.6, 126.1 (2C), 121.0, 46.5. Acquired data is consistent with the literature.³

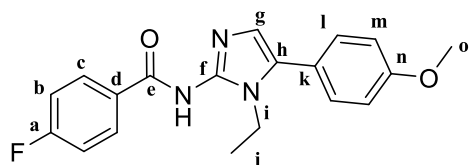
4-Fluoro-N-(5-(4-methoxyphenyl)-1H-imidazol-2-yl)benzamide (3.049)



The title compound was prepared from 4-fluorobenzoic acid (147 mg, 1.1 mmol) in DCM/DMF (10:0.1) stirring at 0 °C.

Oxalyl chloride (2 eq) was added dropwise at 0 °C and the mixture was heated to room temperature and left to stir for 4 h. The solution is concentrated *in vacuo* then diluted in DCM. This was added to a solution of 5-(4-methoxyphenyl)-1H-imidazol-2-amine (200 mg, 1.1 mmol) in DCM (3 mL) and DIPEA (3.71 eq). The mixture stirred at reflux for 18 h. Upon reaction completion the mixture was concentrated, diluted with EtOAc and washed with citric acid in H₂O, followed by NH₂OH in H₂O. The organic layers were collected, dried with MgSO₄ and concentrated. Column chromatography (EtOAc: Petroleum spirits; 1:1) was performed to afford the title compound (205 mg, 63 %). HPLC – *t_R* 5.16 min > 99 % purity at 254 nm; LRMS [M+H]⁺ 312.0 *m/z*; HRMS [M+H]⁺ 312.1143 *m/z*, found 312.1143 *m/z*; ¹H NMR (400 MHz, CDCl₃) δ_H 7.99 – 7.93 (m, 2H), 7.43 – 7.39 (m, 2H), 7.02 – 6.94 (m, 2H), 6.89 – 6.78 (m, 3H), 3.80 (s, 3H); ¹³C NMR (101 MHz, CDCl₃) δ_C 166.7, 165.4 (d, *J* = 253.5 Hz), 159.1, 143.9, 132.5 (d, *J* = 9.3 Hz), 130.7 (d, 2C, *J* = 9.1 Hz, 2C), 129.5 (d, *J* = 3.0 Hz), 126.2 (2C), 115.7 (d, *J* = 22.0 Hz, 2C), 114.4 (2C), 55.5. Imidazole quaternary carbons not visible; ¹³C NMR (101 MHz, DMSO) δ_C 166.5, 164.7, 164.3 (d, *J*_{C-F} = 249.7 Hz), 157.9, 141.8, 132.1 (d, *J*_{C-F} = 9.5 Hz), 130.7 (d, *J*_{C-F} = 9.2 Hz, 2C), 130.0 (d, *J*_{C-F} = 2.8 Hz), 125.4, 115.7, 115.37 (d, *J*_{C-F} = 21.8 Hz, 2C), 114.0 (2C), 55.0.

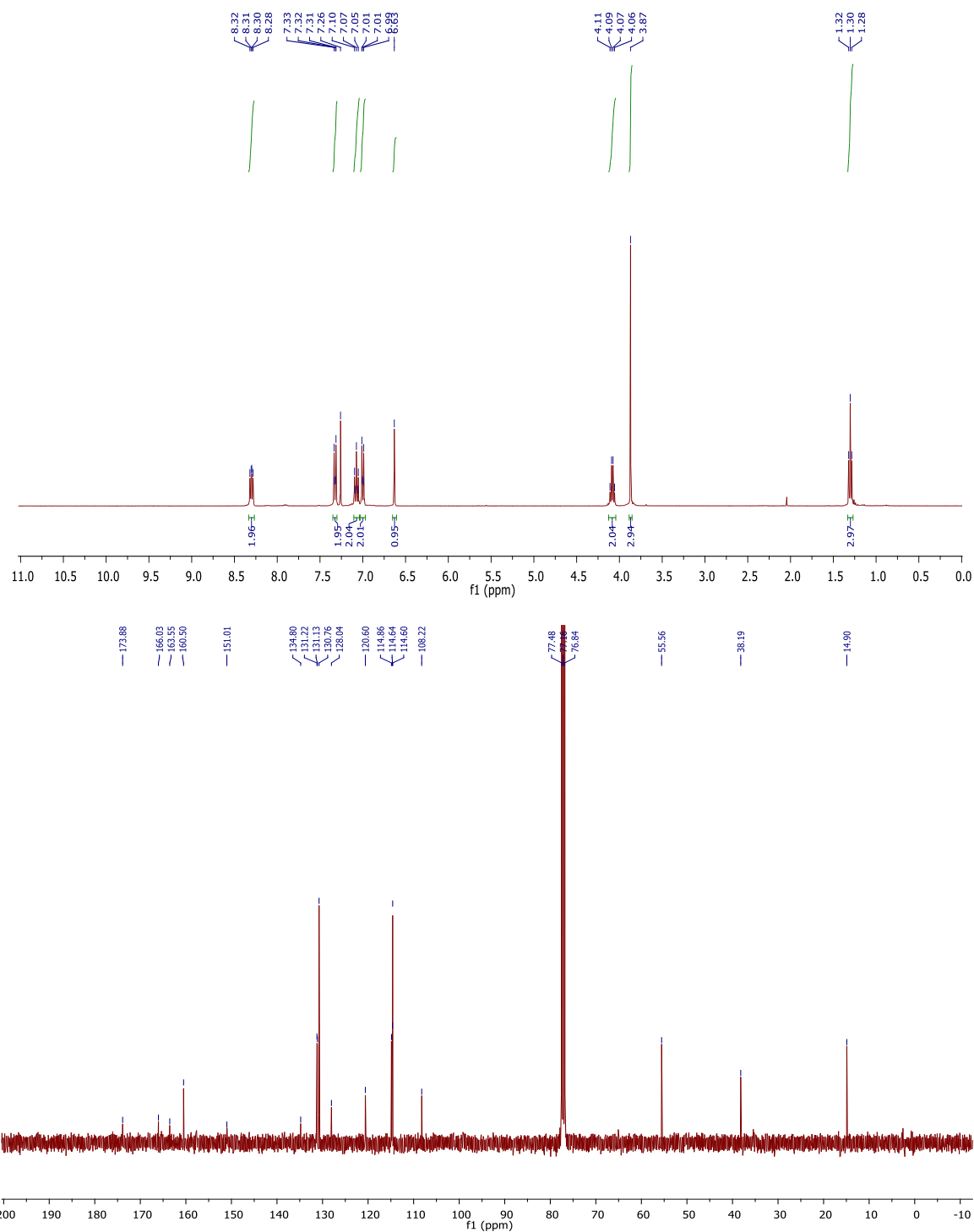
N-(1-Ethyl-5-(4-methoxyphenyl)-1H-imidazol-2-yl)-4-fluorobenzamide (3.050)



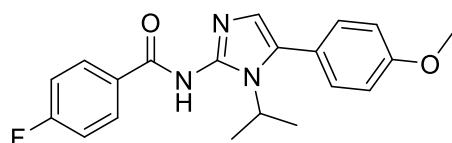
The title compound was prepared from 1-ethyl-5-(4-methoxyphenyl)-1H-imidazol-2-amine (213 mg, 1.00 mmol) and fluorobenzoic acid (137 mg, 1.00 mmol) according to General Procedure B (214 mg, 65%). HPLC – *t_R* 5.24 min

> 99% purity at 254 nm; LRMS [M+H]⁺ 339.9 *m/z*; HRMS [M+H]⁺ 340.1456 *m/z*, found 340.1456 *m/z*; ¹H NMR (400 MHz, CDCl₃) δ_H 8.33 – 8.27 (m, 2H, Hc), 7.34 – 7.30 (m, 2H, Hl), 7.10 – 7.04 (m, 2H, Hb), 7.02 – 6.98 (m, 2H, Hm), 6.63 (s, 1H, Hg), 4.08 (q, *J* = 7.2 Hz, 2H, Hi), 3.87 (s, 3H, Ho), 1.30 (t, *J* = 7.1 Hz, 3H, Hj); ¹³C NMR (101 MHz, CDCl₃) δ_C 173.9 (Cf), 164.8 (d, *J*_{C-F} = 249.6 Hz, Ca), 160.5 (Ce), 151.0 (Ch), 134.8 (d, *J*_{C-F} = 2.3 Hz, Cd), 131.2 (d, *J* = 8.7 Hz, 2C, Cc), 130.8 (2C, Cl), 128.0 (Cn), 120.6 (Cg), 114.8 (d, *J*_{C-F} = 21.5 Hz, 2C, Cb), 114.6 (2C, Cm), 108.2 (Ck), 55.6 (Co), 38.2 (Ci), 14.9 (Cj).

Example spectra for Series 5 (*N*-alkyl modification on imidazole core): ¹H (400 MHz, CDCl₃) and ¹³C NMR (100 MHz, CDCl₃) spectrum of *N*-(1-Ethyl-5-(4-methoxyphenyl)-1*H*-imidazol-2-yl)-4-fluorobenzamide (3.050)



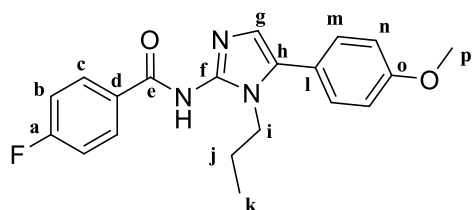
4-Fluoro-*N*-(1-isopropyl-5-(4-methoxyphenyl)-1*H*-imidazol-2-yl)benzamide (3.051)



The title compound was prepared from 1-isopropyl-5-(4-methoxyphenyl)-1*H*-imidazol-2-amine (200 mg, 0.87 mmol) and 4-fluorobenzoic acid (121 mg, 0.87 mmol) according to General Procedure B as an orange solid (209 mg, 68 %). HPLC – *t_R* 5.46 min > 99% purity at 254 nm; LRMS [M+H]⁺ 354.0 *m/z*; HRMS [M+H]⁺ 354.1612 *m/z*, found 354.1625 *m/z*; ¹H NMR (400 MHz,

CDCl₃) δ_{H} 8.30 – 8.26 (m, 2H), 7.30 – 7.27 (m, 2H), 7.10 – 7.05 (m, 2H), 7.01 – 6.97 (m, 2H), 6.57 (s, 1H), 4.43 (hept, $J = 6.9$ Hz, 1H), 3.87 (s, 3H), 1.64 (d, $J = 6.9$ Hz, 6H); ^{13}C NMR (101 MHz, CDCl₃) δ_{C} 173.3, 164.7 (d, $J_{\text{C-F}} = 249.3$ Hz), 160.5, 151.1, 135.2 (d, $J_{\text{C-F}} = 2.7$ Hz), 131.5 (2C), 131.1 (d, $J_{\text{C-F}} = 8.7$ Hz, 2C), 128.1, 121.0, 114.7 (d, $J_{\text{C-F}} = 21.5$ Hz, 2C), 114.4 (2C), 108.4, 55.5, 48.5, 20.9.

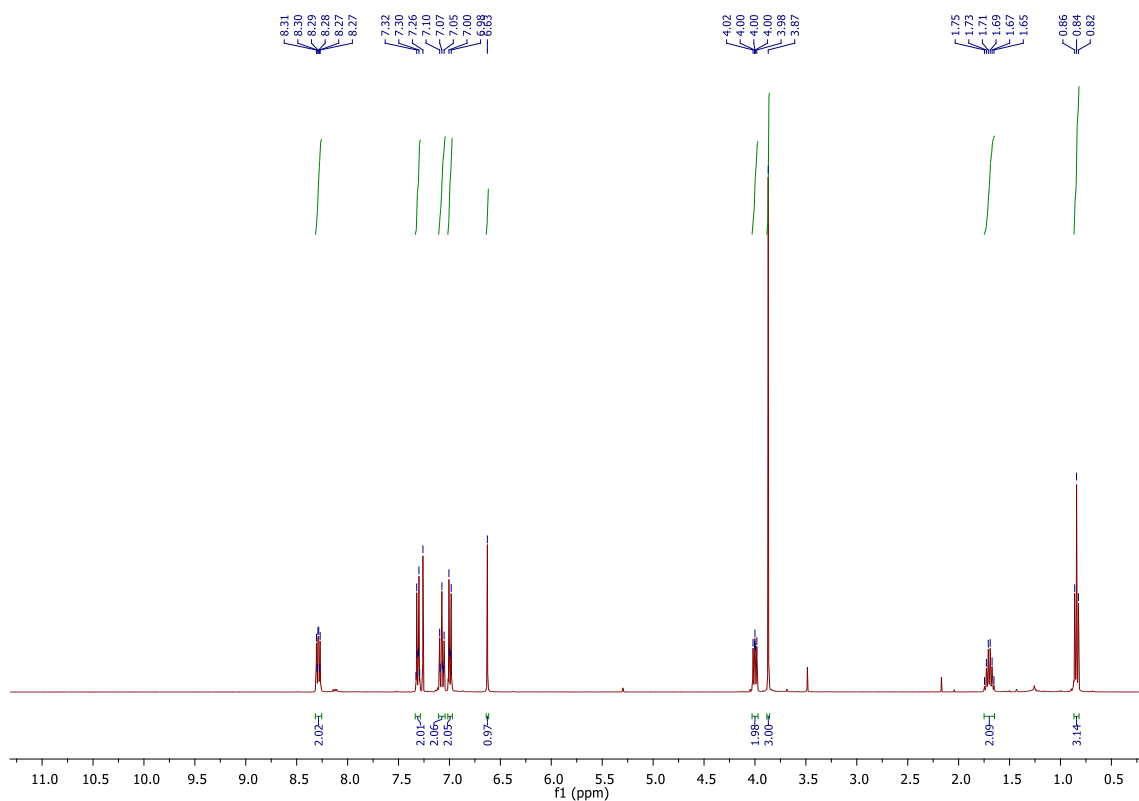
4-Fluoro-*N*-(5-(4-methoxyphenyl)-1-propyl-1*H*-imidazol-2-yl)benzamide (3.052)

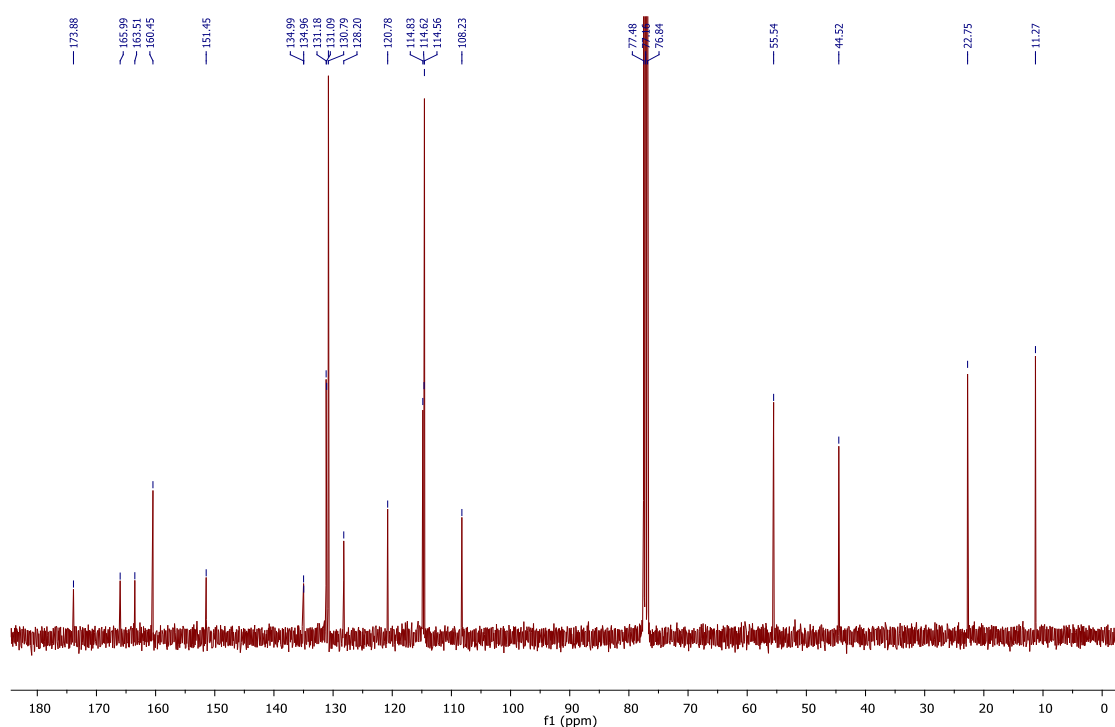


The title compound was prepared from 5-(4-methoxyphenyl)-1-propyl-1*H*-imidazol-2-amine (200 mg, 0.87 mmol) and 4-fluorobenzoic acid (121 mg, 0.87 mmol) according to General Procedure B as a red solid (147 mg, 48

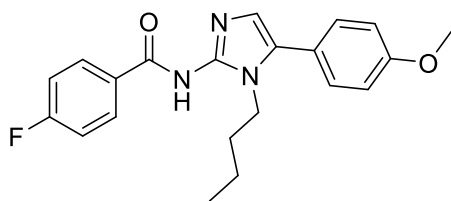
%). HPLC – t_{R} 5.47 min > 99 % purity at 254 nm; LRMS $[\text{M}+\text{H}]^+$ 354.0 m/z ; HRMS $[\text{M}+\text{H}]^+$ 354.1612 m/z , found 354.1621 m/z ; ^1H NMR (400 MHz, CDCl₃) δ_{H} 8.31 – 8.26 (m, 2H, Cc), 7.33 – 7.29 (m, 2H, Cm), 7.10 – 7.05 (m, 2H, Cb), 7.01 – 6.97 (m, 2H, Cn), 6.63 (s, 1H, Cg), 4.02 – 3.98 (m, 2H, Ci), 3.87 (s, 3H, Cp), 1.75 – 1.65 (m, 2H, Cj), 0.84 (t, $J = 7.4$ Hz, 3H, Ck); ^{13}C NMR (101 MHz, CDCl₃) δ_{C} 173.9 (Cf), 164.8 (d, $J_{\text{C-F}} = 249.4$ Hz, Ca), 160.5 (Ce), 151.5 (Ch), 135.0 (d, $J_{\text{C-F}} = 2.6$ Hz, Cd), 131.1 (d, $J_{\text{C-F}} = 8.7$ Hz, 2C, Cc), 130.8 (2C, Cm), 128.2 (Co), 120.8 (Cg), 114.7 (d, $J_{\text{C-F}} = 21.5$ Hz, 2C, Cb), 114.6 (2C, Cn), 108.2 (Cl), 55.5 (Cp), 44.5 (Ci), 22.8 (Cj), 11.3 (Ck).

Example spectra for Series 5 (*N*-alkyl modification on imidazole core): ^1H NMR (400 MHz, CDCl₃) and ^{13}C NMR (100 MHz, CDCl₃) spectrum of 4-Fluoro-*N*-(5-(4-methoxyphenyl)-1-propyl-1*H*-imidazol-2-yl)benzamide (3.052).





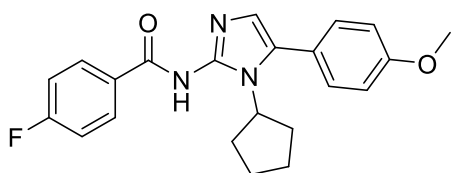
***N*-(1-Butyl-5-(4-methoxyphenyl)-1*H*-imidazol-2-yl)-4-fluorobenzamide (3.053)**



The title compound was prepared from 1-butyl-5-(4-methoxyphenyl)-1*H*-imidazol-2-amine (200 mg, 0.81 mmol) and 4-fluorobenzoic acid (114 mg, 0.81 mmol) according to General Procedure B as a brown solid (236 mg, 79 %). HPLC – t_R 5.82 min > 99 % purity at 254 nm; LRMS $[M+H]^+$ 368.0

m/z ; HRMS $[M+H]^+$ 368.1769 m/z , found 368.1772 m/z ; 1H NMR (400 MHz, $CDCl_3$) δ_H 8.32 – 8.27 (m, 2H), 7.29 (d, J = 8.5 Hz, 2H), 7.08 – 7.03 (m, 2H), 6.99 – 6.96 (m, 2H), 6.62 (s, 1H), 4.06 – 4.01 (m, 2H), 3.84 (s, 3H), 1.67 – 1.57 (m, 2H), 1.29 – 1.19 (m, 2H), 0.84 (t, J = 7.3 Hz, 3H); ^{13}C NMR (101 MHz, $CDCl_3$) δ_C 173.5, 164.7 (d, J_{C-F} = 249.4 Hz), 160.3, 151.0, 134.9 (d, J_{C-F} = 2.7 Hz), 131.1 (d, J_{C-F} = 8.7 Hz, 2C), 130.7 (2C), 128.1, 120.7, 114.6 (d, J_{C-F} = 21.5 Hz, 2C), 114.5 (2C), 108.6, 55.4, 42.6, 31.3, 19.8, 13.6.

***N*-(1-Cyclopentyl-5-(4-methoxyphenyl)-1*H*-imidazol-2-yl)-4-fluorobenzamide (3.054)**

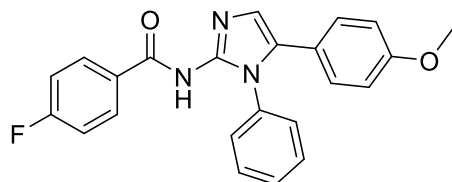


The title compound was prepared from 1-cyclopentyl-5-(4-methoxyphenyl)-1*H*-imidazol-2-amine (200 mg, 0.78 mmol) and 4-fluorobenzoic acid (108 mg, 0.78 mmol) according to General Procedure B as an off white solid (200 mg, 68 %).

HPLC – t_R 5.92 min > 99 % purity at 254 nm; LRMS $[M+H]^+$ 380.0 m/z ; HRMS $[M+H]^+$ 379.1691 m/z , found 379.1690 m/z ; 1H NMR (400 MHz, $CDCl_3$) δ_H 8.28 – 8.23 (m, 2H), 7.31 – 7.26 (m, 2H), 7.07 (t, J = 8.7 Hz, 2H), 7.01 – 6.96 (m, 2H), 6.58 (s, 1H), 4.42 (p, J = 8.9 Hz, 1H), 3.85 (s, 3H), 2.71 – 2.61

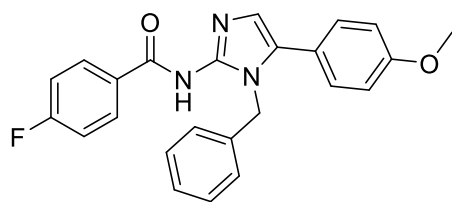
(m, 2H), 2.08 – 1.99 (m, 2H), 1.92 – 1.84 (m, 2H), 1.65 – 1.56 (m, 2H); ^{13}C NMR (101 MHz, CDCl_3) δ_{C} 173.3, 164.6 (d, $J_{\text{C-F}} = 249.2$ Hz), 160.4, 150.8, 135.3 (d, $J_{\text{C-F}} = 2.7$ Hz), 131.3 (2C), 131.0 (d, $J_{\text{C-F}} = 8.7$ Hz, 2C), 128.7, 120.9, 114.6 (d, $J_{\text{C-F}} = 21.4$ Hz, 2C), 114.4 (2C), 108.1, 56.8, 55.5, 30.1 (2C), 25.3 (2C). M.p. 180.0-188.3 °C.

4-Fluoro-*N*-(5-(4-methoxyphenyl)-1-phenyl-1*H*-imidazol-2-yl)benzamide (3.055)



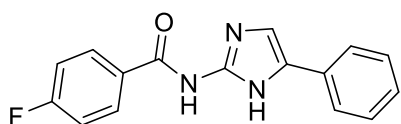
The title compound was prepared from 5-(4-methoxyphenyl)-1-phenyl-1*H*-imidazol-2-amine (200 mg, 0.75 mmol) and 4-fluorobenzoic acid (105 mg, 0.75 mmol) according to General Procedure B as a yellow solid (145 mg, 50 %). HPLC – t_{R} 5.55 min > 99 % purity at 254 nm; LRMS $[\text{M}+\text{H}]^+$ 388.0 m/z ; HRMS $[\text{M}+\text{H}]^+$ 388.1456 m/z , found 388.1463 m/z ; ^1H NMR (400 MHz, CDCl_3) δ_{H} 8.10 – 8.05 (m, 2H), 7.45 – 7.37 (m, 3H), 7.33 – 7.29 (m, 2H), 7.04 – 6.93 (m, 4H), 6.83 (s, 1H), 6.80 – 6.76 (m, 2H), 3.77 (s, 3H); ^{13}C NMR (101 MHz, CDCl_3) δ_{C} 173.8, 164.8 (d, $J_{\text{C-F}} = 249.9$ Hz), 159.8, 151.3, 134.9, 134.3, 131.2 (d, $J_{\text{C-F}} = 8.8$ Hz, 2C), 129.7 (2C), 129.0 (2C), 128.5, 128.4, 128.3 (2C), 120.6, 114.7 (d, $J_{\text{C-F}} = 21.5$ Hz, 2C), 114.2 (2C), 109.7, 55.4.

***N*-(1-Benzyl-5-(4-methoxyphenyl)-1*H*-imidazol-2-yl)-4-fluorobenzamide (3.056)**



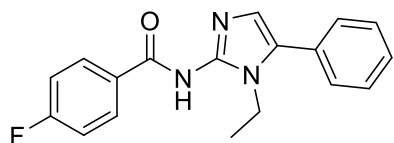
The title compound was prepared from 1-benzyl-5-(4-methoxyphenyl)-1*H*-imidazol-2-amine (200 mg, 0.71 mmol) and 4-fluorobenzoic acid (100 mg, 0.71 mmol) according to General Procedure B as a brown solid (112 mg, 40 %). HPLC – t_{R} 5.90 min > 99 % purity at 254 nm; LRMS $[\text{M}+\text{H}]^+$ 402.0 m/z ; HRMS $[\text{M}+\text{H}]^+$ 402.1612 m/z , found 402.1630 m/z ; ^1H NMR (400 MHz, CDCl_3) δ_{H} 8.21 – 8.16 (m, 2H), 7.19 – 7.14 (m, 3H), 7.07 – 7.02 (m, 4H), 6.99 – 6.92 (m, 2H), 6.84 – 6.79 (m, 2H), 6.58 (s, 1H), 5.15 (s, 2H), 3.75 (s, 3H); ^{13}C NMR (101 MHz, CDCl_3) δ_{C} 173.9, 164.8 (d, $J_{\text{C-F}} = 249.6$ Hz), 160.5, 151.7, 137.1, 134.8 (d, $J_{\text{C-F}} = 2.5$ Hz), 131.2 (d, $J_{\text{C-F}} = 8.8$ Hz, 2C), 131.1 (2C), 128.7 (2C), 128.4, 127.7, 127.5 (2C), 120.3, 114.7 (d, $J_{\text{C-F}} = 21.5$ Hz, 2C), 114.4 (2C), 108.7, 55.5, 46.3.

4-Fluoro-*N*-(5-phenyl-1*H*-imidazol-2-yl)benzamide (3.057)



The title compound was prepared from 5-phenyl-1*H*-imidazol-2-amine (80 mg, 0.50 mmol) and 4-fluorobenzoic acid (70 mg, 0.50 mmol) according to General Procedure B as a white solid (70 mg, 50 %). HPLC – t_{R} 5.10 min > 99% purity at 254 nm; LRMS $[\text{M}+\text{H}]^+$ 282.0 m/z ; HRMS $[\text{M}+\text{H}]^+$ 282.1037 m/z , 282.1029 found; ^1H NMR (400 MHz, CDCl_3) δ_{H} 8.04 – 7.97 (m, 2H), 7.52 – 7.48 (m, 2H), 7.37 – 7.28 (m, 2H), 7.23 – 6.98 (m, 4H); ^{13}C NMR (101 MHz, CDCl_3) δ_{C} 166.5, 165.5 (d, $J_{\text{C-F}} = 253.9$ Hz), 143.9, 130.7 (d, $J_{\text{C-F}} = 9.2$ Hz, 2C), 129.2 (d, $J_{\text{C-F}} = 3.0$ Hz), 128.9 (2C), 127.4, 124.8 (2C), 115.9 (d, $J_{\text{C-F}} = 22.0$ Hz, 2C), 115.6. Imidazole quaternary carbons not visible.

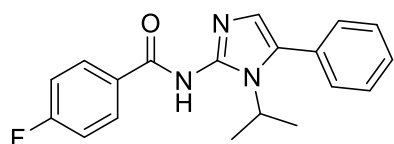
***N*-(1-Ethyl-5-phenyl-1*H*-imidazol-2-yl)cyclohexanecarboxamide (3.058)**



The title compound was prepared from 1-ethyl-5-phenyl-1*H*-imidazol-2-amine (100 mg, 0.53 mmol) and 4-fluorobenzoic acid (74 mg, 0.53 mmol) according to General Procedure B as a brown solid (152 mg, 93 %). HPLC – t_R 5.02 min > 99 % purity at 254 nm;

LRMS $[M+H]^+$ 310.0 m/z ; HRMS $[M+H]^+$ 310.1350 m/z , found 310.1356 m/z ; 1H NMR (400 MHz, $CDCl_3$) δ_H 8.35 – 8.29 (m, 2H), 7.50 – 7.38 (m, 5H), 7.10 – 7.03 (m, 2H), 6.68 (s, 1H), 4.11 (q, J = 7.1 Hz, 2H), 1.31 (t, J = 7.1 Hz, 3H); ^{13}C NMR (101 MHz, $CDCl_3$) δ_C 173.6, 164.7 (d, J_{C-F} = 249.5 Hz), 151.0, 134.9 (d, J_{C-F} = 2.7 Hz), 131.1 (d, J_{C-F} = 8.7 Hz, 2C), 129.2, 129.1 (2C), 129.1 (2C), 128.6, 128.1, 114.7 (d, J_{C-F} = 21.5 Hz, 2C), 109.1, 38.2, 14.8.

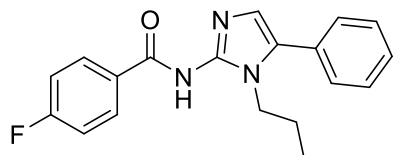
4-Fluoro-*N*-(1-isopropyl-5-phenyl-1*H*-imidazol-2-yl)benzamide (3.059)



The title compound was prepared from 1-isopropyl-5-phenyl-1*H*-imidazol-2-amine (200 mg, 1.00 mmol) and 4-fluorobenzoic acid (140 mg, 1.00 mmol) according to General Procedure B as a brown solid (156 mg, 48 %). HPLC – t_R 5.36 min > 99 % purity at 254 nm;

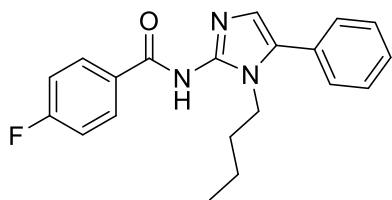
LRMS $[M+H]^+$ 324.0 m/z ; HRMS $[M+H]^+$ 324.1512 m/z , found 324.1507 m/z ; 1H NMR (400 MHz, $CDCl_3$) δ_H 8.32 – 8.27 (m, 2H), 7.49 – 7.45 (m, 3H), 7.38 – 7.35 (m, 2H), 7.11 – 7.05 (m, 2H), 6.62 (s, 1H), 4.45 (hept, J = 6.9 Hz, 1H), 1.67 (d, J = 6.9 Hz, 6H); ^{13}C NMR (101 MHz, $CDCl_3$) δ_C 173.4, 164.7 (d, J_{C-F} = 249.3 Hz), 151.4, 135.2 (d, J_{C-F} = 2.8 Hz), 131.0 (d, J_{C-F} = 8.7 Hz, 2C), 130.0 (2C), 129.3, 129.0 (2C), 128.9, 128.3, 114.7 (d, J_{C-F} = 21.4 Hz, 2C), 108.6, 48.6, 20.9 (2C).

4-Fluoro-*N*-(5-phenyl-1-propyl-1*H*-imidazol-2-yl)benzamide (3.060)



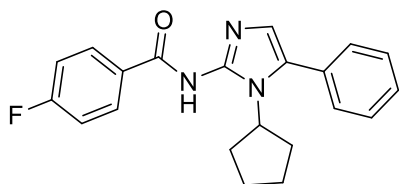
The title compound was prepared from 5-phenyl-1-propyl-1*H*-imidazol-2-amine (200 mg, 1.00 mmol) and 4-fluorobenzoic acid (140 mg, 1.00 mmol) according to General Procedure B as a brown solid (179 mg, 55 %). HPLC – t_R 5.37 min > 99 % purity at 254 nm; LRMS $[M+H]^+$ 324.0 m/z ; HRMS

$[M+H]^+$ 324.1513 m/z , found 324.1507 m/z ; 1H NMR (400 MHz, $CDCl_3$) δ_H 8.33 – 8.27 (m, 2H), 7.49 – 7.37 (m, 5H), 7.10 – 7.04 (m, 2H), 6.68 (s, 1H), 4.07 – 4.02 (m, 2H), 1.75 – 1.66 (m, 2H), 0.84 (t, J = 7.4 Hz, 3H); ^{13}C NMR (101 MHz, $CDCl_3$) δ_C 173.4, 164.6 (d, J_{C-F} = 249.4 Hz), 151.1, 134.9 (d, J_{C-F} = 2.7 Hz), 131.1 (d, J_{C-F} = 8.7 Hz, 2C), 129.1 (2C), 129.1, 129.0 (2C), 128.7, 128.3, 114.6 (d, J_{C-F} = 21.5 Hz, 2C), 109.2, 44.6, 22.7, 11.1.

***N*-(1-Butyl-5-phenyl-1*H*-imidazol-2-yl)-4-fluorobenzamide (3.061)**

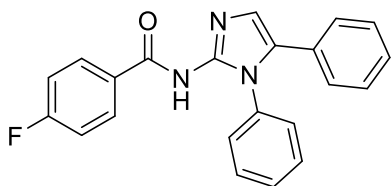
The title compound was prepared from 1-butyl-5-phenyl-1*H*-imidazol-2-amine (200 mg, 0.93 mmol) and 4-fluorobenzoic acid (130 mg, 0.93 mmol) according to General Procedure B as a brown solid (296 mg, 94 %). HPLC – t_R 5.75 min > 99 % purity at 254 nm;

LRMS $[M+H]^+$ 338.0 m/z ; HRMS $[M+H]^+$ 338.1663 m/z , found 338.1674 m/z ; 1H NMR (400 MHz, $CDCl_3$) δ_H 8.22 – 8.17 (m, 2H), 7.38 – 7.25 (m, 5H), 6.99 – 6.92 (m, 2H), 6.58 (s, 1H), 4.00 – 3.93 (m, 2H), 1.57 – 1.49 (m, 2H), 1.19 – 1.09 (m, 2H), 0.73 (t, J = 7.4 Hz, 3H); ^{13}C NMR (101 MHz, $CDCl_3$) δ_C 173.4, 164.6 (d, J_{C-F} = 249.7 Hz), 150.7, 134.7 (d, J_{C-F} = 2.6 Hz), 131.1 (d, 2C, J_{C-F} = 8.7 Hz), 129.1 (2C), 129.1, 129.0 (2C), 128.5, 128.4, 114.7 (d, 2C, J_{C-F} = 21.5 Hz), 109.4, 42.7, 31.3, 19.7, 13.5.

***N*-(1-Cyclopentyl-5-phenyl-1*H*-imidazol-2-yl)-4-fluorobenzamide (3.062)**

The title compound was prepared from 1-cyclopentyl-5-phenyl-1*H*-imidazol-2-amine (200 mg, 0.88 mmol) and 4-fluorobenzoic acid (123 mg, 0.88 mmol) according to General Procedure B as a brown solid (127 mg, 41 %) HPLC – t_R 5.90 min > 99 % purity at 254 nm; LRMS $[M+H]^+$ 350.0 m/z ; HRMS $[M+H]^+$ 350.1663 m/z , found 350.1677 m/z ;

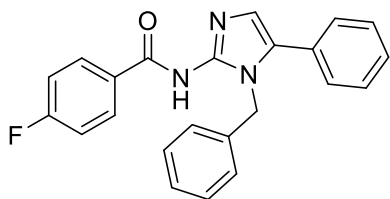
1H NMR (400 MHz, $CDCl_3$) δ_H 8.28 – 8.23 (m, 2H), 7.50 – 7.46 (m, 3H), 7.40 – 7.36 (m, 2H), 7.11 – 7.04 (m, 2H), 6.65 (s, 1H), 4.45 (p, J = 8.9 Hz, 1H), 2.74 – 2.63 (m, 2H), 2.11 – 2.00 (m, 2H), 1.96 – 1.87 (m, 2H), 1.67 – 1.55 (m, 2H); ^{13}C NMR (101 MHz, $CDCl_3$) δ_C 173.4, 164.7 (d, J_{C-F} = 249.5 Hz), 150.9, 135.2 (d, J_{C-F} = 2.8 Hz), 131.1 (d, J_{C-F} = 8.7 Hz, 2C), 129.9 (2C), 129.3, 129.1, 129.0 (2C), 128.9, 114.7 (d, J_{C-F} = 21.5 Hz, 2C), 108.6, 57.1, 30.2 (2C), 25.3S (2C).

***N*-(1,5-Diphenyl-1*H*-imidazol-2-yl)-4-fluorobenzamide (3.063)**

The title compound was prepared from 1,5-diphenyl-1*H*-imidazol-2-amine (200 mg, 0.85 mmol) and 4-fluorobenzoic acid (119 mg, 0.85 mmol) according to General Procedure B as a yellow solid (110 mg, 36%). HPLC – t_R 5.49 min > 99 % purity at 254 nm;

LRMS $[M+H]^+$ 358.0 m/z ; HRMS $[M+H]^+$ 358.135 m/z , found 358.156 m/z ; 1H NMR (400 MHz, $CDCl_3$) δ_H 8.04 – 7.99 (m, 2H), 7.38 – 7.32 (m, 3H), 7.26 – 7.22 (m, 2H), 7.21 – 7.15 (m, 3H), 7.04 – 7.00 (m, 2H), 6.95 – 6.87 (m, 2H), 6.84 (s, 1H); ^{13}C NMR (101 MHz, $CDCl_3$) δ_C 174.0, 164.9 (d, J_{C-F} = 250.0 Hz), 161.3, 151.6, 134.9, 134.2 (d, J_{C-F} = 2.9 Hz), 131.3 (d, J_{C-F} = 8.8 Hz, 2C), 129.0 (2C), 128.7 (2C), 128.5 (bs, 2C, two carbons overlapped), 128.3, 128.3 (2C), 128.3 (2C), 114.8 (d, J_{C-F} = 21.5 Hz, 2C).

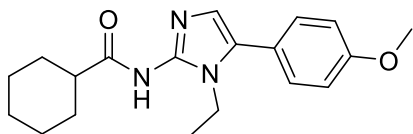
***N*-(1-Benzyl-5-phenyl-1*H*-imidazol-2-yl)-4-fluorobenzamide (3.064)**



The title compound was prepared from 1-benzyl-5-phenyl-1*H*-imidazol-2-amine (200 mg, 0.80 mmol) and 4-fluorobenzoic acid (112 mg, 0.80 mmol) according to General Procedure B as a brown solid (70 mg, 23 %) HPLC – t_R 5.86 min > 99 % purity at 254 nm; LRMS $[M+H]^+$ 372.0 m/z ; HRMS $[M+H]^+$ 372.1507 m/z , found

372.1523 m/z ; 1H NMR (400 MHz, $CDCl_3$) δ_H 8.30 – 8.22 (m, 2H), 7.43 – 7.38 (m, 3H), 7.26 – 7.22 (m, 4H), 7.12 – 7.02 (m, 5H), 6.74 (s, 1H), 5.28 (s, 2H); ^{13}C NMR (101 MHz, $CDCl_3$) δ_C 173.6, 164.8 (d, J_{C-F} = 249.9 Hz), 158.1, 151.4, 136.9, 134.5 (d, J = 2.7 Hz), 131.2 (d, 2C, J_{C-F} = 8.8 Hz), 129.5 (2C), 129.2, 128.9 (2C), 128.7 (2C), 127.8, 127.4 (2C), 114.8 (d, 2C, J_{C-F} = 21.5 Hz), 110.8, 109.7, 46.5.

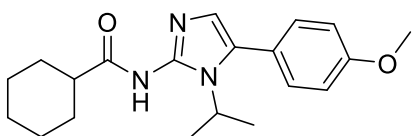
***N*-(1-Ethyl-5-(4-methoxyphenyl)-1*H*-imidazol-2-yl)cyclohexanecarboxamide (3.065)**



The title compound was prepared from 1-ethyl-5-(4-methoxyphenyl)-1*H*-imidazol-2-amine (200 mg, 0.92 mmol) and cyclohexanecarboxylic acid (117 mg, 0.92 mmol) according to

General Procedure B as a brown solid (233 mg, 77 %). HPLC – t_R 5.38 min > 99 % purity at 254 nm; LRMS $[M+H]^+$ 328.0 m/z ; HRMS $[M+H]^+$ 328.2020 m/z , found 328.2028 m/z ; 1H NMR (400 MHz, $CDCl_3$) δ_H 7.31 – 7.26 (m, 2H), 6.98 – 6.94 (m, 2H), 6.75 (s, 1H), 3.95 (q, J = 7.2 Hz, 2H), 3.84 (s, 3H), 2.47 – 2.39 (m, 1H), 1.97 – 1.89 (m, 2H), 1.80 – 1.74 (m, 2H), 1.69 – 1.62 (m, 1H), 1.58 – 1.46 (m, 2H), 1.35 – 1.21 (m, 3H), 1.17 – 1.10 (m, 3H); ^{13}C NMR (101 MHz, $CDCl_3$) δ_C 179.3, 165.8, 159.9, 142.0, 131.0, 130.5 (2C), 121.8, 114.3 (2C), 55.4, 39.0, 38.6, 29.7 (2C), 25.9, 25.7 (2C), 15.1.

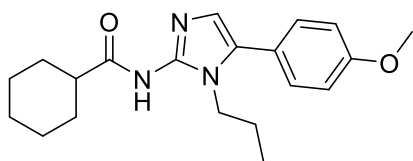
***N*-(1-Isopropyl-5-(4-methoxyphenyl)-1*H*-imidazol-2-yl)cyclohexanecarboxamide (3.066)**



The title compound was prepared from 1-isopropyl-5-(4-methoxyphenyl)-1*H*-imidazol-2-amine (200 mg, 0.87 mmol) and cyclohexanecarboxylic acid (111 mg, 0.87 mmol) according to

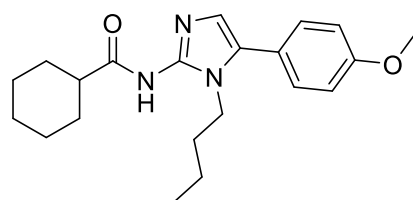
General Procedure B as a brown solid (170 mg, 57 %). HPLC – t_R 5.54 min > 95 % purity at 254 nm; LRMS $[M+H]^+$ 342.1 m/z ; HRMS $[M+H]^+$ 342.2176 m/z , found 342.2186 m/z ; 1H NMR (400 MHz, $CDCl_3$) δ_H 7.25 – 7.22 (m, 2H), 6.97 – 6.92 (m, 2H), 6.60 (bs, 1H), 4.38 – 4.27 (m, 1H), 3.84 (s, 3H), 2.36 – 2.28 (m, 1H), 2.00 – 1.92 (m, 2H), 1.80 – 1.74 (m, 2H), 1.69 – 1.62 (m, 1H), 1.56 – 1.48 (m, 2H), 1.45 (d, J = 6.9 Hz, 6H), 1.36 – 1.22 (m, 3H); ^{13}C NMR (101 MHz, $CDCl_3$) δ_C 180.8, 160.1, 131.6 (2C), 130.9, 127.5, 122.0, 114.9, 114.0 (2C), 55.3, 46.1, 38.5, 29.7 (2C), 25.8, 25.7 (2C), 21.6.

***N*-(5-(4-Methoxyphenyl)-1-propyl-1*H*-imidazol-2-yl)cyclohexanecarboxamide (3.067)**



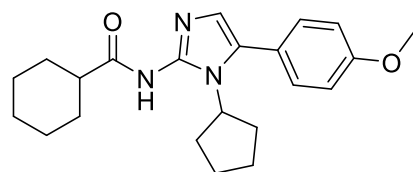
The title compound was prepared from 5-(4-methoxyphenyl)-1-propyl-1*H*-imidazol-2-amine (200 mg, 0.87 mmol) and cyclohexanecarboxylic acid (111 mg, 0.87 mmol) according to General Procedure B as a red solid (158 mg, 53 %). HPLC – t_R 5.67 min > 99 % purity at 254 nm; LRMS $[M+H]^+$ 342.1 m/z ; HRMS $[M+H]^+$ 342.2176 m/z , found 342.2181 m/z ; 1H NMR (400 MHz, MeOD) δ_H 7.40 – 7.36 (m, 2H), 7.09 – 7.04 (m, 2H), 6.91 (s, 1H), 3.93 – 3.83 (m, 5H), 2.57 – 2.47 (m, 1H), 2.02 – 1.72 (m, 5H), 1.62 – 1.29 (m, 7H), 0.75 (t, J = 7.4 Hz, 3H); ^{13}C NMR (101 MHz, MeOD) δ_C 179.8, 161.5, 140.2, 133.9, 131.5 (2C), 123.6, 123.2, 115.3 (2C), 55.8, 46.5, 38.9, 30.5 (2C), 26.8, 26.6 (2C), 24.2, 11.1.

***N*-(1-Butyl-5-(4-methoxyphenyl)-1*H*-imidazol-2-yl)cyclohexanecarboxamide (3.068)**



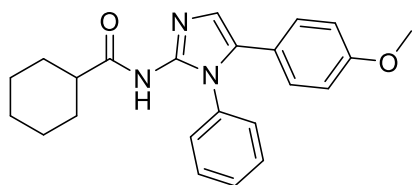
The title compound was prepared from 1-butyl-5-(4-methoxyphenyl)-1*H*-imidazol-2-amine (200 mg, 0.81 mmol) and cyclohexanecarboxylic acid (104 mg, 0.81 mmol) according to General Procedure B as a brown solid (258 mg, 90 %). HPLC – t_R 6.02 min > 99 % purity at 254 nm; LRMS $[M+H]^+$ 356.1 m/z ; HRMS $[M+H]^+$ 356.2333 m/z , found 356.234 m/z ; 1H NMR (400 MHz, $CDCl_3$) δ_H 7.23 – 7.19 (m, 2H), 6.91 – 6.87 (m, 2H), 6.69 (s, 1H), 3.83 – 3.76 (m, 5H), 2.37 – 2.28 (m, 1H), 1.90 – 1.82 (m, 2H), 1.77 – 1.70 (m, 2H), 1.65 – 1.58 (m, 1H), 1.50 – 1.35 (m, 4H), 1.30 – 1.14 (m, 3H), 1.08 – 1.00 (m, 2H), 0.69 (t, J = 7.3 Hz, 3H); ^{13}C NMR (101 MHz, $CDCl_3$) δ_C 178.7, 159.7, 140.0, 131.8, 130.2 (2C), 121.7, 121.1, 114.1 (2C), 55.1, 45.0, 43.5, 31.5, 29.3 (2C), 25.5, 25.4 (2C), 19.4, 13.1.

***N*-(1-Cyclopentyl-5-(4-methoxyphenyl)-1*H*-imidazol-2-yl)cyclohexanecarboxamide (3.069)**



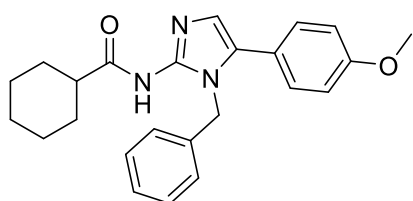
The title compound was prepared from 1-cyclopentyl-5-(4-methoxyphenyl)-1*H*-imidazol-2-amine (200 mg, 0.78 mmol) and cyclohexanecarboxylic acid (100 mg, 0.78 mmol) according to General Procedure B as an orange solid (188 mg, 66 %). HPLC – t_R 5.94 min > 99 % purity at 254 nm; LRMS $[M+H]^+$ 368.1 m/z ; HRMS $[M+H]^+$ 368.2333 m/z , found 368.2347 m/z ; 1H NMR (400 MHz, $CDCl_3$) δ_H 7.20 – 7.16 (m, 2H), 6.92 – 6.87 (m, 2H), 6.50 (s, 1H), 4.28 (p, J = 8.6 Hz, 1H), 3.79 (s, 3H), 2.38 – 2.21 (m, 3H), 1.92 – 1.86 (m, 2H), 1.86 – 1.68 (m, 6H), 1.62 – 1.57 (m, 1H), 1.49 – 1.38 (m, 4H), 1.30 – 1.16 (m, 3H); ^{13}C NMR (101 MHz, $CDCl_3$) δ_C 182.8, 160.0, 145.4, 133.5, 131.4 (2C), 129.9, 122.0, 114.1 (2C), 56.7, 55.4, 47.1, 30.7 (2C), 30.1 (2C), 26.2, 26.0 (2C), 25.1 (2C).

***N*-(5-(4-Methoxyphenyl)-1-phenyl-1*H*-imidazol-2-yl)cyclohexanecarboxamide (3.070)**



The title compound was prepared from 5-(4-methoxyphenyl)-1-phenyl-1*H*-imidazol-2-amine (200 mg, 0.75 mmol) cyclohexanecarboxylic acid (97 mg, 0.75 mmol) according to General Procedure B as a brown solid (58 mg, 20 %). HPLC – t_R 5.79 min > 97 % purity at 254 nm; LRMS $[M+H]^+$ 376.0 m/z ; HRMS $[M+H]^+$ 376.2020 m/z , found 376.2035 m/z ; 1H NMR (400 MHz, $CDCl_3$) δ_H 7.37 – 7.31 (m, 3H), 7.22 – 7.16 (m, 2H), 7.01 – 6.95 (m, 3H), 6.74 – 6.70 (m, 2H), 3.74 (s, 3H), 2.22 – 2.07 (m, 1H), 1.70 – 1.52 (m, 5H), 1.29 – 1.07 (m, 5H); 1H NMR (400 MHz, MeOD) δ_H 7.47 – 7.41 (m, 3H), 7.24 – 7.17 (m, 2H), 7.12 – 7.02 (m, 3H), 6.82 – 6.75 (m, 2H), 3.74 (s, 3H), 2.25 – 2.13 (m, 1H), 1.89 – 1.78 (m, 1H), 1.74 – 1.56 (m, 4H), 1.33 – 1.19 (m, 5H); ^{13}C NMR (101 MHz, MeOD) δ_C 160.9, 136.9, 135.2, 130.7 (2C), 130.2 (2C), 130.0, 129.1 (2C), 124.8, 123.0, 114.9 (2C), 55.7, 38.9, 30.2 (2C), 26.7, 26.5 (2C). Imidazole quaternary peaks not available.

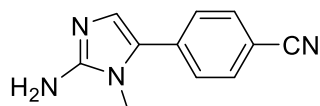
***N*-(1-Benzyl-5-(4-methoxyphenyl)-1*H*-imidazol-2-yl)cyclohexanecarboxamide (3.071)**



The title compound was prepared from 1-benzyl-5-(4-methoxyphenyl)-1*H*-imidazol-2-amine (200 mg, 0.71 mmol) and cyclohexanecarboxylic acid (91 mg, 0.71 mmol) according to General Procedure B as a brown solid (112 mg, 39 %) HPLC – t_R 6.00 min > 99 % purity at 254 nm; LRMS $[M+H]^+$ 390.0 m/z ; HRMS $[M+H]^+$ 389.2098 m/z , found 389.2138 m/z ; 1H NMR (400 MHz, $CDCl_3$) δ_H 7.24 – 7.16 (m, 5H), 6.92 – 6.86 (m, 4H), 6.76 (s, 1H), 5.14 (s, 2H), 3.81 (s, 3H), 2.32 – 2.24 (m, 1H), 1.81 – 1.67 (m, 4H), 1.65 – 1.57 (m, 1H), 1.46 – 1.33 (m, 2H), 1.28 – 1.15 (m, 3H); ^{13}C NMR (101 MHz, $CDCl_3$) δ_C 178.9, 160.0, 143.0, 137.1, 131.9, 130.7 (2C), 128.7 (2C), 127.5, 126.6 (2C), 121.8, 120.2, 114.3 (2C), 55.4, 47.4, 38.7, 29.6 (2C), 25.9 (2C), 25.7.

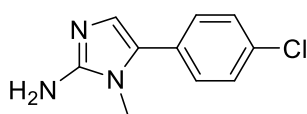
Analogue Series 6

4-(2-Amino-1-methyl-1*H*-imidazol-5-yl)benzonitrile (3.072)²



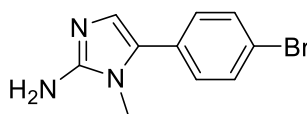
The known title compound was prepared from *N*-methylpyrimidin-2-amine (330 mg, 3.00 mmol) 4-(2-bromoacetyl)benzonitrile (907 mg, 4.05 mmol) according to General Procedure A as a yellow solid (605 mg, 90 %). HPLC – t_R 3.35 min > 99 % purity at 254 nm; LRMS $[M+H]^+$ 199.0 m/z ; 1H NMR (400 MHz, $CDCl_3$) δ_H 7.69 – 7.65 (m, 2H), 7.45 – 7.41 (m, 2H), 6.85 (s, 1H), 3.48 (s, 3H); ^{13}C NMR (101 MHz, $CDCl_3$) δ_C 150.8, 135.2, 132.8 (2C), 128.5, 127.3 (2C), 125.4, 119.0, 110.2, 31.2.²

5-(4-Chlorophenyl)-1-methyl-1*H*-imidazol-2-amine (3.073)²



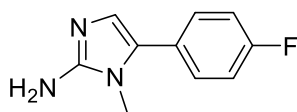
The known title compound was prepared from *N*-methylpyrimidin-2-amine (330 mg, 3.00 mmol) and 2-bromo-1-(4-chlorophenyl)ethan-1-one (944 mg, 4.05 mmol) according to General Procedure A as an orange solid (600 mg, 96 %). HPLC – t_R 4.27 min > 99 % purity at 254 nm; LRMS $[M+H]^+$ 208.0 m/z ; 1H NMR (400 MHz, $CDCl_3$) δ_H 7.32 – 7.28 (m, 2H), 7.19 – 7.17 (m, 2H), 6.62 (s, 1H), 3.33 (s, 3H). ² 1H NMR (400 MHz, MeOD) δ_H 7.44 – 7.40 (m, 2H), 7.38 – 7.35 (m, 2H), 6.63 (s, 1H), 3.40 (s, 3H); 1H NMR (400 MHz, MeOD) δ_H 7.45 – 7.34 (m, 4H), 6.63 (s, 1H), 3.40 (s, 3H); ^{13}C NMR (101 MHz, MeOD) δ_C 152.5, 134.0, 130.7, 130.2 (2C), 129.9 (2C), 129.5, 122.8, 30.8.²

5-(4-Bromophenyl)-1-methyl-1*H*-imidazol-2-amine (3.074)



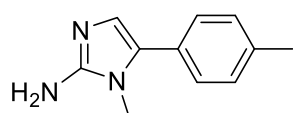
The title compound was prepared from *N*-methylpyrimidin-2-amine (330 mg, 3.00 mmol) and 2-bromo-1-(4-bromophenyl)ethan-1-one (1.12 g, 4.05 mmol) according to General Procedure A as an orange solid (605 mg, 80 %). HPLC – t_R 4.49 min > 95 % purity at 254 nm; LRMS $[M+H]^+$ 251.9 m/z .

5-(4-Fluorophenyl)-1-methyl-1*H*-imidazol-2-amine (3.075)²



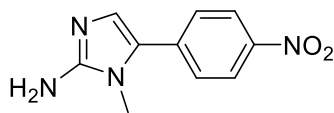
The known title compound was prepared from *N*-methylpyrimidin-2-amine (330 mg, 3.00 mmol) and 2-bromo-1-(4-fluorophenyl)ethan-1-one (879 mg, 4.05 mmol) according to General Procedure A as a yellow solid (440 mg, 76 %). HPLC – t_R 3.79 min > 99 % purity at 254 nm; LRMS $[M+H]^+$ 192.0 m/z ; 1H NMR (400 MHz, $CDCl_3$) δ_H 7.31 – 7.27 (m, 2H), 7.14 – 7.07 (m, 2H), 6.66 (s, 1H), 3.39 (s, 3H); ^{13}C NMR (101 MHz, $CDCl_3$) δ_C 162.4 (d, J_{C-F} = 247.3 Hz), 149.1, 130.0 (d, J_{C-F} = 8.1 Hz, 2C), 129.1, 126.7, 122.2, 115.9 (d, J_{C-F} = 21.7 Hz, 2C), 30.5.

1-Methyl-5-(*p*-tolyl)-1*H*-imidazol-2-amine (3.076)⁵⁸



The known title compound was prepared from *N*-methylpyrimidin-2-amine (330 mg, 3.00 mmol) and 2-bromo-1-(*p*-tolyl)ethan-1-one (863 mg, 4.05 mmol) according to General Procedure A as an orange solid (490 mg, 87 %). HPLC – t_R 4.25 min > 99 % purity at 254 nm; LRMS $[M+H]^+$ 188.0 m/z ; 1H NMR (400 MHz, $CDCl_3$) δ_H 7.23 – 7.16 (m, 4H), 6.66 (s, 1H), 3.39 (s, 3H), 2.37 (s, 3H); ^{13}C NMR (101 MHz, $CDCl_3$) δ_C 149.2, 137.1, 130.0, 129.5, 128.0, 127.9, 122.4, 30.5, 21.3.

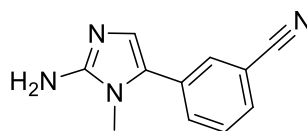
1-Methyl-5-(4-nitrophenyl)-1*H*-imidazol-2-amine NKM-0003 (3.077)²



The title compound was prepared from *N*-methylpyrimidin-2-amine (330 mg, 3.00 mmol) and 2-bromo-1-(4-nitrophenyl)ethan-1-one (988 mg, 4.05 mmol) according to General Procedure A as a red solid (653 mg, 99 %). HPLC – t_R 3.57 min

> 99 % purity at 254 nm; LRMS $[M+H]^+$ 219.0 m/z ; 1H NMR (400 MHz, $CDCl_3$) δ_H 8.21 – 8.18 (m, 2H), 7.44 – 7.41 (m, 2H), 6.79 (s, 1H), 3.42 (s, 3H); ^{13}C NMR (101 MHz, $CDCl_3$) δ_C 146.3, 136.7, 127.0 (2C), 126.0, 124.5, 124.4 (2C), 123.6, 31.1.

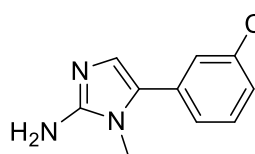
3-(2-Amino-1-methyl-1*H*-imidazol-5-yl)benzonitrile (3.078)



The title compound was prepared from *N*-methylpyrimidin-2-amine (330 mg, 3.00 mmol) and 3-(2-bromoacetyl)benzonitrile (907 mg, 4.05 mmol) according to General Procedure A as a light brown solid (477 mg, 80 %).

HPLC – t_R 3.35 min > 99 % purity at 254 nm; LRMS $[M+H]^+$ 199.0 m/z ; 1H NMR (400 MHz, $CDCl_3$) δ_H 7.61 – 7.56 (m, 3H), 7.55 – 7.50 (m, 1H), 6.79 (s, 1H), 3.46 (s, 3H); ^{13}C NMR (101 MHz, $CDCl_3$) δ_C 150.1, 143.5, 131.9, 131.8, 130.8, 130.7, 129.9, 123.3, 118.6, 113.3, 30.9.

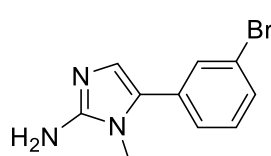
5-(3-Chlorophenyl)-1-methyl-1*H*-imidazol-2-amine (3.079)



The title compound was prepared from *N*-methylpyrimidin-2-amine (330 mg, 3.00 mmol) and 2-bromo-1-(3-chlorophenyl)ethan-1-one (946 mg, 4.05 mmol) according to General Procedure A as an orange solid (587 mg, 94 %).

HPLC – t_R 4.26 min > 99 % purity at 254 nm; LRMS $[M+H]^+$ 208.2 m/z ; 1H NMR (400 MHz, $CDCl_3$) δ_H 7.27 – 7.22 (m, 2H), 7.21 – 7.18 (m, 1H), 7.15 – 7.11 (m, 1H), 6.66 (s, 1H), 3.36 (s, 3H); ^{13}C NMR (101 MHz, $CDCl_3$) δ_C 150.0, 134.7, 132.6, 130.1, 128.7, 127.6, 127.2, 125.8, 123.8, 30.7.

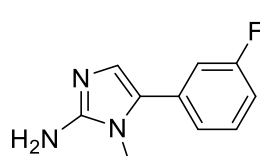
5-(3-Bromophenyl)-1-methyl-1*H*-imidazol-2-amine (3.080)



The title compound was prepared from *N*-methylpyrimidin-2-amine (330 mg, 3.00 mmol) and 2-bromo-1-(3-bromophenyl)ethan-1-one (1.12 g, 4.05 mmol) according to General Procedure A as a brown solid (754 mg, 99 %).

HPLC – t_R 4.40 min > 99 % purity at 254 nm; LRMS $[M+H]^+$ 252.1 m/z ; 1H NMR (400 MHz, $CDCl_3$) δ_H 7.47 – 7.42 (m, 2H), 7.28 – 7.21 (m, 2H), 6.70 (s, 1H), 4.81 (bs, 2H), 3.41 (s, 3H); ^{13}C NMR (101 MHz, $CDCl_3$) δ_C 149.8, 132.2, 130.7, 130.5, 130.4, 128.4, 126.5, 122.9, 121.5, 30.7.

5-(3-Fluorophenyl)-1-methyl-1*H*-imidazol-2-amine (3.081)

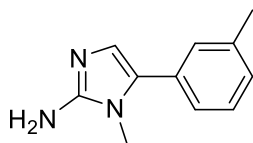


The title compound was prepared from *N*-methylpyrimidin-2-amine (330 mg, 3.00 mmol) and 2-bromo-1-(3-fluorophenyl)ethan-1-one (879 mg, 4.05 mmol) according to General Procedure A as an orange solid (570 mg, 99 %).

HPLC – t_R 3.75 min > 99 % purity at 254 nm; LRMS $[M+H]^+$ 192.2 m/z ; 1H NMR (400 MHz, $CDCl_3$) δ_H 7.37 – 7.33 (m, 1H), 7.12 – 7.08 (m, 1H), 7.04 – 6.97 (m, 2H), 6.72 (s, 1H), 3.43 (s, 3H); ^{13}C NMR (101 MHz, $CDCl_3$) δ_C 163.1 (d, J_{C-F} = 246.4 Hz), 149.7, 132.6 (d, J_{C-F} = 8.4 Hz), 130.5

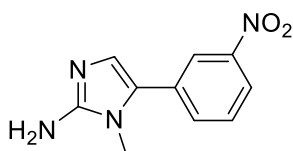
(d, J_{C-F} = 8.7 Hz), 128.9, 123.5 (d, J_{C-F} = 2.9 Hz), 122.6, 114.5 (d, J_{C-F} = 34.2 Hz), 114.3 (d, J_{C-F} = 33.1 Hz), 30.8.

1-Methyl-5-(*m*-tolyl)-1*H*-imidazol-2-amine (3.082)



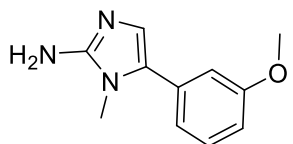
The title compound was prepared from *N*-methylpyrimidin-2-amine (330 mg, 3.00 mmol) and 2-bromo-1-(*m*-tolyl)ethan-1-one (863 mg, 4.05 mmol) according to General Procedure A as a brown solid (536 mg, 95 %). HPLC – t_R 4.18 min > 93 % purity at 254 nm; LRMS $[M+H]^+$ 188.2 m/z ; 1H NMR (400 MHz, $CDCl_3$) δ_H 7.32 – 7.27 (m, 1H), 7.17 – 7.11 (m, 3H), 6.69 (s, 1H), 3.43 (s, 3H), 2.38 (s, 3H); ^{13}C NMR (101 MHz, $CDCl_3$) δ_C 149.1, 138.6, 130.7, 130.3, 128.8, 128.7, 128.2, 125.1, 122.5, 30.6, 21.6.

1-Methyl-5-(3-nitrophenyl)-1*H*-imidazol-2-amine (3.083)



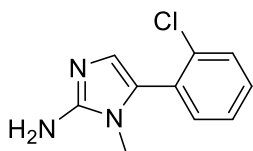
The title compound was prepared from *N*-methylpyrimidin-2-amine (330 mg, 3.00 mmol) and 2-bromo-1-(3-nitrophenyl)ethan-1-one (988 mg, 4.05 mmol) according to General Procedure A as a yellow solid (637 mg, 97 %). HPLC – t_R 3.59 min > 99 % purity at 254 nm; LRMS $[M+H]^+$ 219.0 m/z ; 1H NMR (400 MHz, $CDCl_3$) δ_H 8.19 – 8.12 (m, 2H), 7.69 – 7.65 (m, 1H), 7.60 – 7.55 (m, 1H), 6.85 (s, 1H), 3.50 (s, 3H); ^{13}C NMR (101 MHz, $CDCl_3$) δ_C 150.3, 148.8, 133.2, 132.4, 130.0, 127.8, 124.5, 121.9, 121.8, 31.1.

5-(3-Methoxyphenyl)-1-methyl-1*H*-imidazol-2-amine (3.084/ Ch 2, 2.005c)



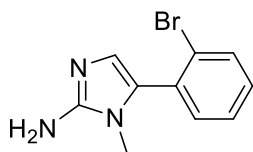
The title compound was prepared from 2-bromo-1-(3-methoxyphenyl)ethan-1-one (824.4 mg, 3.60 mmol) according to General Procedure A as an orange solid without further purification (484 mg, 88%). HPLC – t_R 4.17 min > 99% purity at 254 nm; LRMS $[M+H]^+$ 204.0 m/z ; 1H NMR (400 MHz, $CDCl_3$) δ_H 7.34 – 7.27 (m, 1H), 6.93 – 6.88 (m, 1H), 6.87 – 6.83 (m, 2H), 6.69 (s, 1H), 3.81 (s, 3H), 3.41 (s, 3H); ^{13}C NMR (101 MHz, $CDCl_3$) δ_C 159.8, 149.4, 131.9, 129.7, 122.5, 120.2, 113.6, 112.5, 104.9, 55.3, 30.5.

5-(2-Chlorophenyl)-1-methyl-1*H*-imidazol-2-amine (3.085)



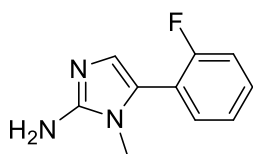
The title compound was prepared from *N*-methylpyrimidin-2-amine (330 mg, 3.00 mmol) and 2-bromo-1-(2-chlorophenyl)ethan-1-one (946 mg, 4.05 mmol) according to General Procedure A, heating to 150 °C for 25 min during the condensation step. The title compound was obtained as a brown solid (512 mg, 82 %). HPLC – t_R 4.02 min > 99 % purity at 254 nm; LRMS $[M+H]^+$ 208.1 m/z ; 1H NMR (400 MHz, MeOD) δ_H 7.78 – 7.66 (m, 1H), 7.45 – 7.25 (m, 3H), 7.18 – 7.12 (m, 1H), 2.91 (s, 3H); 1H NMR (400 MHz, $CDCl_3$) δ_H 7.47 – 7.43 (m, 1H), 7.35 – 7.27 (m, 3H), 6.64 (s, 1H), 5.03 (bs, 2H), 3.25 (s, 3H); ^{13}C NMR (101 MHz, $CDCl_3$) δ_C 148.9, 135.0, 133.0, 130.1, 130.0, 129.1, 127.1, 126.5, 121.2, 30.2.

5-(2-Bromophenyl)-1-methyl-1*H*-imidazol-2k-amine (3.086)



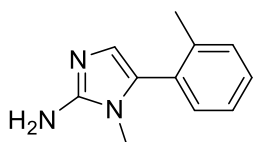
The title compound was prepared from *N*-methylpyrimidin-2-amine (330 mg, 3.00 mmol) and 2-bromo-1-(2-bromophenyl)ethan-1-one (1.12 g, 4.05 mmol) according to General Procedure A, heating to 150 °C for 25 min during the condensation step. The title compound was obtained as a brown solid (643 mg, 85 %). HPLC – t_R 4.08 min > 72 % purity at 254 nm; LRMS $[M+H]^+$ 252.1 m/z ; 1H NMR (400 MHz, $CDCl_3$) δ 7.58 (dd, J = 8.0, 1.2 Hz, 1H), 7.49 (dd, J = 7.8, 1.6 Hz, 1H), 7.31 – 7.26 (m, 1H), 7.14 – 7.09 (m, 1H), 7.06 (s, 1H), 2.93 (s, 3H); ^{13}C NMR (101 MHz, $CDCl_3$) δ_C 149.8, 134.1, 130.1, 129.9, 129.2, 127.9, 127.6, 121.0, 114.7, 30.0.

5-(2-Fluorophenyl)-1-methyl-1*H*-imidazol-2-amine (3.087)



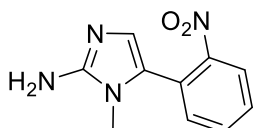
The title compound was prepared from *N*-methylpyrimidin-2-amine (330 mg, 3.00 mmol) and 2-bromo-1-(2-fluorophenyl)ethan-1-one (879 mg, 4.05 mmol) according to General Procedure A, heating to 150 °C for 25 min during the condensation step. The title compound was obtained as an orange solid (516 mg, 90 %). HPLC – t_R 3.64 min > 99 % purity at 254 nm; LRMS $[M+H]^+$ 192.2 m/z ; 1H NMR (400 MHz, $CDCl_3$) δ_H 7.34 – 7.27 (m, 2H), 7.18 – 7.09 (m, 2H), 6.70 (s, 1H), 3.29 (d, J = 2.0 Hz, 3H); ^{13}C NMR (101 MHz, $CDCl_3$) δ_C 159.7 (d, J_{C-F} = 247.0 Hz), 149.9, 131.4 (d, J_{C-F} = 3.0 Hz), 129.5 (d, J_{C-F} = 8.1 Hz), 124.4 (d, J_{C-F} = 3.6 Hz), 124.1 (d, J_{C-F} = 1.1 Hz), 123.6, 118.7 (d, J_{C-F} = 15.1 Hz), 115.9 (d, J_{C-F} = 22.1 Hz), 30.2 (d, J_{C-F} = 4.8 Hz).

1-Methyl-5-(*o*-tolyl)-1*H*-imidazol-2-amine (3.088)



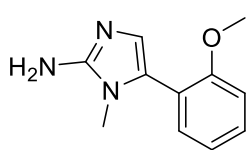
The title compound was prepared from *N*-methylpyrimidin-2-amine (330 mg, 3.00 mmol) and 2-bromo-1-(*o*-tolyl)ethan-1-one (863 g, 4.05 mmol) according to General Procedure A, heating to 150 °C for 25 min during the condensation step. The title compound was obtained as a brown solid (643 mg, 85 %). HPLC – t_R 4.21 min > 99 % purity at 254 nm; LRMS $[M+H]^+$ 188.2 m/z ; 1H NMR (400 MHz, $CDCl_3$) δ_H 7.30 – 7.26 (m, 1H), 7.26 – 7.15 (m, 4H), 6.64 (s, 1H), 3.02 (s, 3H), 2.33 (s, 3H).

1-Methyl-5-(2-nitrophenyl)-1*H*-imidazol-2-amine (3.089)



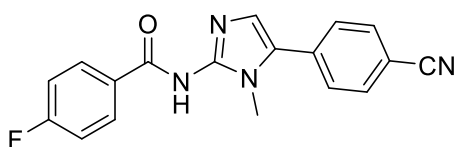
The title compound was prepared from *N*-methylpyrimidin-2-amine (330 mg, 3.00 mmol) and 2-bromo-1-(2-nitrophenyl)ethan-1-one (988 mg, 4.05 mmol) according to General Procedure A, heating to 150 °C for 25 min during the condensation step. The title compound was obtained an orange solid (591 mg, 90 %). HPLC – t_R 3.37 min > 95 % purity at 254 nm; LRMS $[M+H]^+$ 219.2 m/z .

5-(2-Methoxyphenyl)-1-methyl-1*H*-imidazol-2-amine (3.090/ Ch 2, 2.005d)



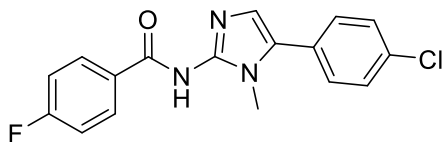
The title compound was prepared from 2-bromo-1-(2-methoxyphenyl)ethan-1-one (824 mg, 3.60 mmol) according to General Procedure A to give the product as an orange solid (482 mg, 87%). The product was used directly in the next step without further purification or characterization. HPLC - t_R 4.35 min > 77% purity at 254 nm; LRMS $[M+H]^+$ 204.0 m/z .

N-(5-(4-Cyanophenyl)-1-methyl-1*H*-imidazol-2-yl)-4-fluorobenzamide (3.091)



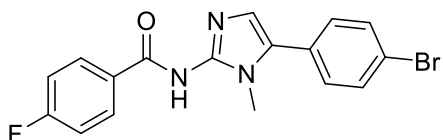
The title compound was prepared from 5-(4-cyanophenyl)-1-methyl-1*H*-imidazol-2-amine (150 mg, 0.76 mmol) and 4-fluorobenzoic acid (107 mg, 0.76 mmol) according to General Procedure B as an orange solid (150 mg, 61 %). HPLC - t_R 4.46 min > 99 % purity at 254 nm; LRMS $[M+H]^+$ 321.0 m/z ; HRMS $[M+H]^+$ 321.1146 m/z , found 321.1154 m/z ; 1H NMR (400 MHz, $CDCl_3$) δ_H 8.30 – 8.24 (m, 2H), 7.80 – 7.76 (m, 2H), 7.58 – 7.54 (m, 2H), 7.12 – 7.08 (m, 2H), 6.90 (s, 1H), 3.66 (s, 3H); ^{13}C NMR (101 MHz, $CDCl_3$) δ_C 171.9, 166.0, 164.9 (d, J_{C-F} = 251.3 Hz), 133.2, 132.7 (2C), 132.5, 130.8 (d, J_{C-F} = 9.0 Hz, 2C), 128.7 (2C), 128.3, 118.2, 115.3, 114.9 (d, J_{C-F} = 21.7 Hz, 2C), 111.9, 31.0.

N-(5-(4-Chlorophenyl)-1-methyl-1*H*-imidazol-2-yl)-4-fluorobenzamide (3.092)



The title compound was prepared from 5-(4-chlorophenyl)-1-methyl-1*H*-imidazol-2-amine (200 mg, 0.96 mmol) and 4-fluorobenzoic acid (135 mg, 0.96 mmol) according to General Procedure B as a yellow solid (195 mg, 62 %). HPLC - t_R 5.10 min > 99 % purity at 254 nm; LRMS $[M+H]^+$ 329.9 m/z ; HRMS $[M+H]^+$ 330.0804 m/z , found 330.0813 m/z ; 1H NMR (400 MHz, $CDCl_3$) δ_H 8.30 – 8.26 (m, 2H), 7.47 – 7.44 (m, 2H), 7.36 – 7.32 (m, 2H), 7.09 – 7.04 (m, 2H), 6.74 (s, 1H), 3.59 (s, 3H); ^{13}C NMR (101 MHz, $CDCl_3$) δ_C 173.4, 164.9 (d, J_{C-F} = 250.2 Hz), 151.1, 135.3, 134.2 (d, J_{C-F} = 2.5 Hz), 131.2 (d, J_{C-F} = 8.8 Hz, 2C), 130.1 (2C), 129.5 (2C), 127.9, 126.9, 114.9 (d, J_{C-F} = 21.5 Hz, 2C), 110.0, 30.5. M.p. 169.1-174.3 °C.

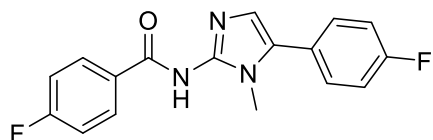
N-(5-(4-Bromophenyl)-1-methyl-1*H*-imidazol-2-yl)-4-fluorobenzamide (3.093)



The title compound was prepared from 5-(4-bromophenyl)-1-methyl-1*H*-imidazol-2-amine (200 mg, 0.79 mmol) and 4-fluorobenzoic acid (111 mg, 0.79 mmol) according to General Procedure B as an orange solid (203 mg, 68 %). HPLC - t_R 5.21 min > 99 % purity at 254 nm; LRMS $[M+H]^+$ 373.9 m/z ; HRMS $[M+H]^+$ 374.0299 m/z , found 374.0310 m/z ; 1H NMR (400 MHz, $CDCl_3$) δ_H 8.30 – 8.26 (m, 2H), 7.63 – 7.60 (m, 2H), 7.30 – 7.27 (m, 2H), 7.11 – 7.05 (m, 2H), 6.76 (s, 1H), 3.60 (s, 3H); ^{13}C NMR (101 MHz, $CDCl_3$) δ_C 173.5, 164.9 (d, J_{C-F} = 250.3 Hz), 151.2, 134.1 (d, J_{C-F} = 2.5

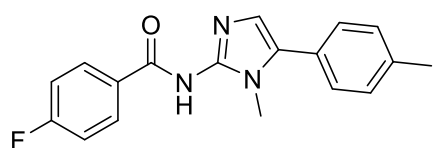
Hz), 132.5 (2C), 131.2 (d, J_{C-F} = 8.8 Hz, 2C), 130.3 (2C), 128.0, 127.3, 123.6, 114.9 (d, J_{C-F} = 21.6 Hz, 2C), 109.9, 30.5.

4-Fluoro-*N*-(5-(4-fluorophenyl)-1-methyl-1*H*-imidazol-2-yl)benzamide (3.094)



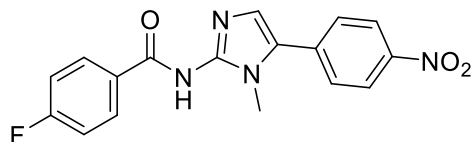
The title compound was prepared from 5-(4-fluorophenyl)-1-methyl-1*H*-imidazol-2-amine (200 mg, 1.05 mmol) and 4-fluorobenzoic acid (147 mg, 1.1 mmol) according to General Procedure B as a yellow solid (260 mg, 79 %). HPLC – t_R 4.72 min > 99 % purity at 254 nm; LRMS $[M+H]^+$ 314.0 m/z ; HRMS $[M+H]^+$ 314.1099 m/z , found 314.1106 m/z ; 1H NMR (400 MHz, $CDCl_3$) δ_H 8.30 – 8.25 (m, 2H), 7.39 – 7.35 (m, 2H), 7.20 – 7.14 (m, 2H), 7.07 – 7.02 (m, 2H), 6.71 (s, 1H), 3.57 (s, 3H); ^{13}C NMR (101 MHz, $CDCl_3$) δ_C 173.5, 164.8 (d, J_{C-F} = 250.0 Hz), 163.3 (d, J_{C-F} = 249.9 Hz), 151.0, 134.4, 131.1 (d, J_{C-F} = 8.8 Hz, 2C), 130.9 (d, J_{C-F} = 8.3 Hz, 2C), 127.9, 124.5 (d, J_{C-F} = 3.4 Hz, 2C), 116.3 (d, J_{C-F} = 21.9 Hz, 2C), 114.8 (d, J_{C-F} = 21.5 Hz, 2C), 109.6, 30.3. M.p. 198.8-202.7 °C.

4-Fluoro-*N*-(1-methyl-5-(*p*-tolyl)-1*H*-imidazol-2-yl)benzamide (3.095)



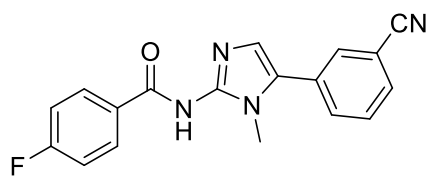
The title compound was prepared from 1-methyl-5-(*p*-tolyl)-1*H*-imidazol-2-amine (200 mg, 1.07 mmol) and 4-fluorobenzoic acid (149 mg, 1.07 mmol) according to General Procedure B as a yellow solid (256 mg, 77 %). HPLC – t_R 5.06 min > 99 % purity at 254 nm; LRMS $[M+H]^+$ 310.0 m/z ; HRMS $[M+H]^+$ 310.1350 m/z , found 310.1355 m/z ; 1H NMR (400 MHz, $CDCl_3$) δ_H 8.28 – 8.23 (m, 2H), 7.26 – 7.23 (m, 4H, signal overlapped with $CDCl_3$ peak), 7.06 – 7.01 (m, 2H), 6.67 (s, 1H), 3.57 (s, 3H), 2.39 (s, 3H); ^{13}C NMR (101 MHz, $CDCl_3$) δ_C 173.6, 164.8 (d, J_{C-F} = 249.8 Hz), 151.2, 139.3, 134.6 (d, J_{C-F} = 2.6 Hz), 131.1 (d, J_{C-F} = 8.8 Hz, 2C), 129.8 (2C), 129.0 (2C), 128.9, 125.4, 114.8 (d, J_{C-F} = 21.5 Hz, 2C), 108.7, 30.3, 21.4.

4-Fluoro-*N*-(1-methyl-5-(4-nitrophenyl)-1*H*-imidazol-2-yl)benzamide (3.096)



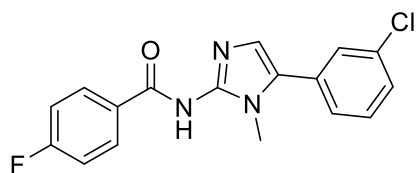
The title compound was prepared from 5-(4-nitrophenyl)-1-methyl-1*H*-imidazol-2-amine (200 mg, 0.92 mmol) and 4-fluorobenzoic acid (128mg, 0.92 mmol) according to General Procedure B as an orange solid (130 mg, 42 %). HPLC – t_R 4.69 min > 95 % purity at 254 nm; LRMS $[M+H]^+$ 341.0 m/z ; HRMS $[M+H]^+$ 341.1044 m/z , found 341.1053 m/z ; 1H NMR (400 MHz, DMSO) δ_H 10.81 (s, 1H), 8.28 – 8.23 (m, 2H), 8.20 – 8.09 (m, 3H), 7.82 (s, 2H), 7.29 – 7.26 (m, 2H), 7.23 – 7.17 (m, 2H), 2.26 (s, 3H).

***N*-(5-(4-Cyanophenyl)-1-methyl-1*H*-imidazol-2-yl)-4-fluorobenzamide (3.097)**



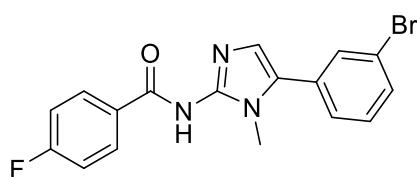
The title compound was prepared from 5-(3-cyanophenyl)-1-methyl-1*H*-imidazol-2-amine (200 mg, 1.01 mmol) and 4-fluorobenzoic acid (142 mg, 1.01 mmol) according to General Procedure B as a yellow solid (191 mg, 60 %). HPLC – t_R 4.48 min > 95 % purity at 254 nm; LRMS $[M+H]^+$ 321.0 m/z ; HRMS $[M+H]^+$ 321.1146 m/z , found 321.1151 m/z ; 1H NMR (400 MHz, $CDCl_3$) δ_H 8.11 – 8.05 (m, 2H), 7.78 – 7.72 (m, 2H), 7.03 – 6.97 (m, 4H), 6.85 (s, 1H), 3.50 (s, 3H); ^{13}C NMR (101 MHz, DMSO) δ_C 166.8, 164.6, 163.9 (d, J_{C-F} = 248.3 Hz), 132.7, 132.6, 130.8 (d, J_{C-F} = 9.0 Hz, 2C), 130.8, 130.8, 130.7, 130.1, 130.1, 130.0, 126.1, 118.4, 115.1 (d, J_{C-F} = 21.7 Hz, 2C), 38.2.

***N*-(5-(3-Chlorophenyl)-1-methyl-1*H*-imidazol-2-yl)-4-fluorobenzamide (3.098)**



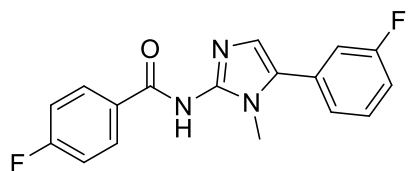
The title compound was prepared from 5-(3-chlorophenyl)-1-methyl-1*H*-imidazol-2-amine (200 mg, 0.96 mmol) and 4-fluorobenzoic acid (135 mg, 0.96 mmol) according to General Procedure B as a yellow solid (345 mg, 99 %). HPLC – t_R 5.08 min > 99 % purity at 254 nm; LRMS $[M+H]^+$ 329.9 m/z ; HRMS $[M+H]^+$ 330.0803 m/z , found 330.0804 m/z ; 1H NMR (400 MHz, $CDCl_3$) δ_H 8.31 – 8.25 (m, 2H), 7.44 – 7.40 (m, 3H), 7.31 – 7.28 (m, 1H), 7.10 – 7.04 (m, 2H), 6.78 (s, 1H), 3.61 (s, 3H); ^{13}C NMR (101 MHz, $CDCl_3$) δ_C 173.3, 164.9 (d, J_{C-F} = 250.3 Hz), 151.0, 135.2, 134.0 (d, J_{C-F} = 2.4 Hz), 131.2 (d, J_{C-F} = 8.8 Hz, 2C), 130.4, 130.2, 129.2, 128.8, 127.8, 126.9, 114.9 (d, J_{C-F} = 21.5 Hz, 2C), 110.6 (s), 30.7.

***N*-(5-(3-Bromophenyl)-1-methyl-1*H*-imidazol-2-yl)-4-fluorobenzamide (3.099)**



The title compound was prepared from 5-(3-bromophenyl)-1-methyl-1*H*-imidazol-2-amine (200 mg, 0.79 mmol) and 4-fluorobenzoic acid (111 mg, 0.79 mmol) according to General Procedure B as a yellow solid (145 mg, 37 %). HPLC – t_R 5.18 min > 99 % purity at 254 nm; LRMS $[M+H]^+$ 378.8 m/z ; HRMS $[M+H]^+$ 374.0299 m/z , found 374.0307 m/z ; 1H NMR (400 MHz, $CDCl_3$) δ_H 8.31 – 8.25 (m, 2H), 7.59 – 7.55 (m, 2H), 7.36 – 7.32 (m, 2H), 7.09 – 7.04 (m, 2H), 6.77 (s, 1H), 3.61 (s, 3H); ^{13}C NMR (101 MHz, $CDCl_3$) δ_C 173.2, 164.9 (d, J_{C-F} = 250.3 Hz), 150.9, 134.0 (d, J_{C-F} = 2.2 Hz), 132.1, 131.6, 131.2 (d, J_{C-F} = 8.8 Hz, 2C), 130.6, 130.5, 127.7, 127.3, 123.2, 114.9 (d, J_{C-F} = 21.5 Hz, 2C), 110.9, 30.6.

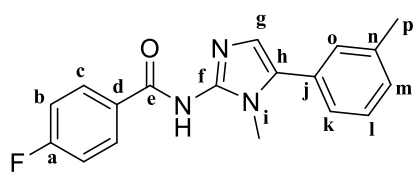
4-Fluoro-*N*-(5-(3-fluorophenyl)-1-methyl-1*H*-imidazol-2-yl)benzamide (3.100)



The title compound was prepared from 5-(3-fluorophenyl)-1-methyl-1*H*-imidazol-2-amine (200 mg, 1.05 mmol) and 4-fluorobenzoic acid (147 mg, 1.05 mmol) according to General

Procedure B as an orange solid (137 mg, 42 %). HPLC – t_R 4.74 min > 99 % purity at 254 nm; LRMS $[M+H]^+$ 314.0 m/z ; HRMS $[M+H]^+$ 314.1099 m/z , found 314.1106 m/z ; 1H NMR (400 MHz, $CDCl_3$) δ_H 8.31 – 8.26 (m, 2H), 7.47 – 7.41 (m, 1H), 7.20 – 7.04 (m, 5H), 6.78 (s, 1H), 3.61 (s, 3H); 1H NMR (400 MHz, $CDCl_3$) δ_H 8.34 – 8.23 (m, 2H), 7.47 – 7.41 (m, 1H), 7.21 – 7.03 (m, 5H), 6.78 (s, 1H), 3.61 (s, 3H); ^{13}C NMR (101 MHz, $CDCl_3$) δ_C 172.9, 164.9 (d, J_{C-F} = 250.3 Hz), 163.0 (d, J_{C-F} = 247.8 Hz), 150.6, 134.0 (d, J_{C-F} = 1.8 Hz), 131.1 (d, J_{C-F} = 8.8 Hz, 2C), 130.8 (d, J_{C-F} = 8.6 Hz), 130.5 (d, J_{C-F} = 8.4 Hz), 128.0, 124.4 (d, J_{C-F} = 3.0 Hz), 116.0 (d, J_{C-F} = 21.0 Hz), 115.7 (d, J_{C-F} = 22.6 Hz), 114.9 (d, J_{C-F} = 21.5 Hz, 2C), 111.1, 30.7.

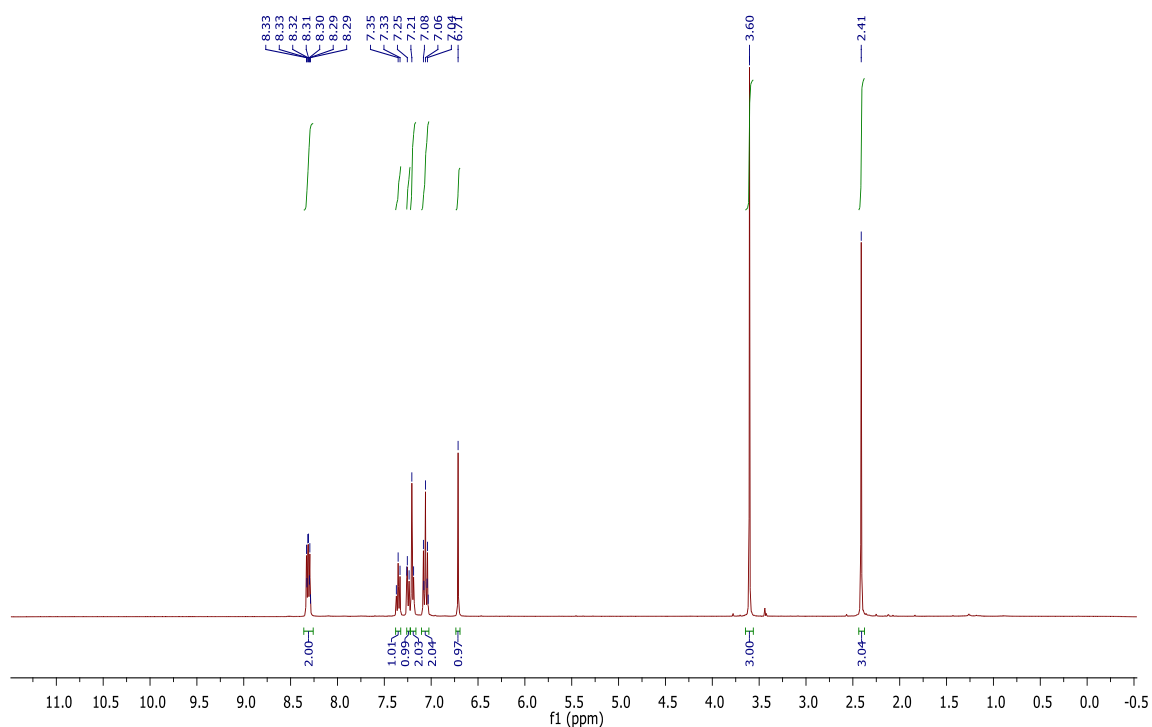
4-Fluoro-*N*-(1-methyl-5-(*m*-tolyl)-1*H*-imidazol-2-yl)benzamide (3.101)

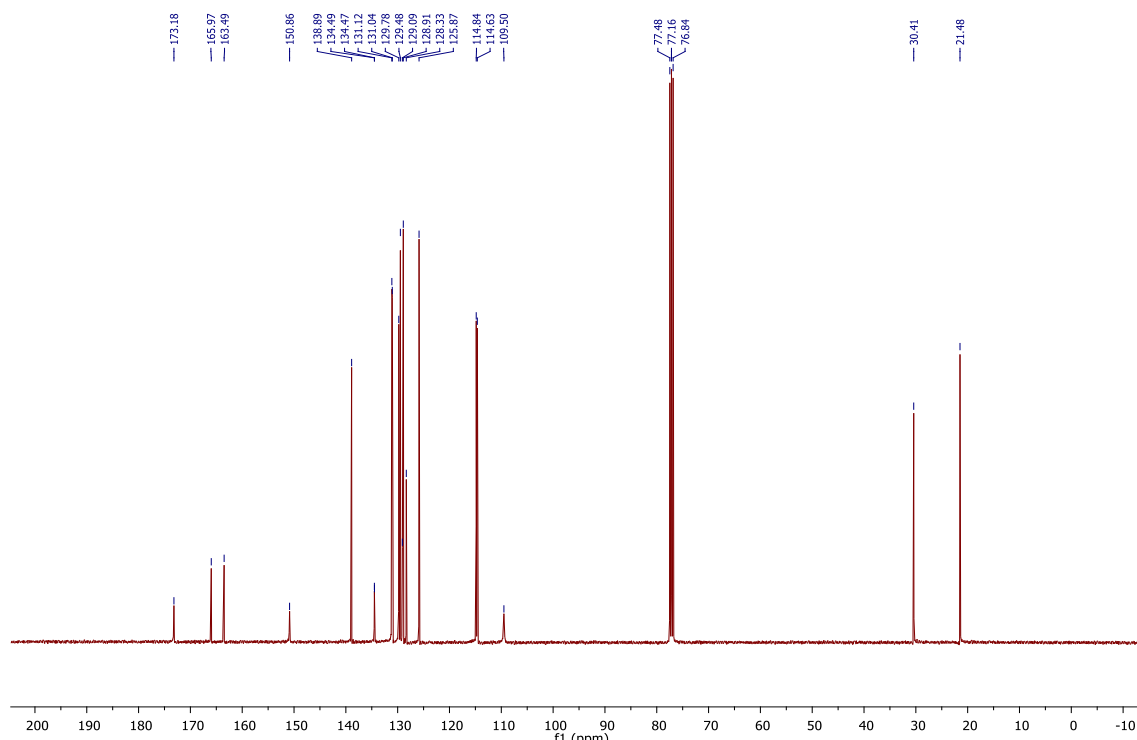


The title compound was prepared from 1-methyl-5-(*m*-tolyl)-1*H*-imidazol-2-amine (200 mg, 1.07 mmol) and 4-fluorobenzoic acid (149 mg, 1.07 mmol) according to General Procedure B as a yellow solid (248 mg, 74 %). HPLC – t_R 5.04 min > 99 % purity

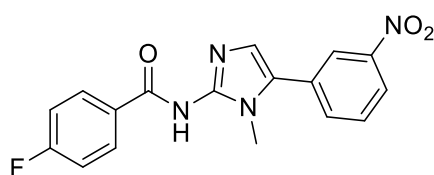
at 254 nm; LRMS $[M+H]^+$ 310.0 m/z ; HRMS $[M+H]^+$ 310.1350 m/z , found 310.1356 m/z ; 1H NMR (400 MHz, $CDCl_3$) δ_H 8.34 – 8.29 (m, 2H, Hc), 7.38 – 7.32 (m, 1H, Ho), 7.27 – 7.23 (m, 1H, Hk), 7.22 – 7.17 (m, 2H, Hl, Hm), 7.10 – 7.03 (m, 2H, Hb), 6.71 (s, 1H, Hg), 3.60 (s, 3H, Hi), 2.41 (s, 3H, Hp); ^{13}C NMR (101 MHz, $CDCl_3$) δ_C 173.2 (Cf), 164.7 (d, J_{C-F} = 249.7 Hz, Ca), 150.9 (Ch), 138.9 (Ce), 134.5 (d, J_{C-F} = 1.7 Hz, Cd), 131.1 (d, J_{C-F} = 8.8 Hz, 2C, Cc), 129.8 (Co), 129.5 (Cm), 129.1 (Cn), 128.9 (Cl), 128.3 (Cg), 125.9 (Ck), 114.7 (d, J_{C-F} = 21.5 Hz, 2C, Cb), 109.5 (Cj), 30.4 (Ci), 21.5 (Cp).

Example spectra for Series 6 (RHS investigation): 1H NMR (400 MHz, $CDCl_3$) and ^{13}C NMR (100 MHz, $CDCl_3$) spectrum of 4-Fluoro-*N*-(1-methyl-5-(*m*-tolyl)-1*H*-imidazol-2-yl)benzamide (3.101)



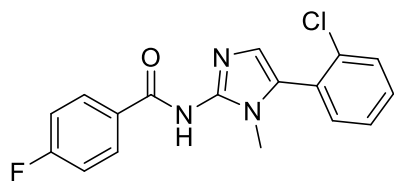


4-Fluoro-*N*-(1-methyl-5-(3-nitrophenyl)-1*H*-imidazol-2-yl)benzamide (3.102)



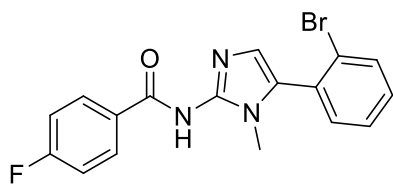
The title compound was prepared from 5-(3-nitrophenyl)-1-methyl-1*H*-imidazol-2-amine (200 mg, 0.92 mmol) and 4-fluorobenzoic acid (128 mg, 0.92 mmol) according to General Procedure B as a yellow solid (74 mg, 24 %). HPLC – t_R 4.67 min > 99 % purity at 254 nm; LRMS $[M+H]^+$ 340.9 m/z ; HRMS $[M+H]^+$ 341.1044 m/z , found 341.1049 m/z ; 1H NMR (400 MHz, DMSO) δ_H 12.56 (bs, 1H, NH), 8.41 – 8.04 (m, 6H), 7.79 (t, J = 8.0 Hz, 1H), 7.44 – 7.32 (m, 1H), 3.66 (bs, 3H).

***N*-(5-(2-Chlorophenyl)-1-methyl-1*H*-imidazol-2-yl)-4-fluorobenzamide (3.103)**



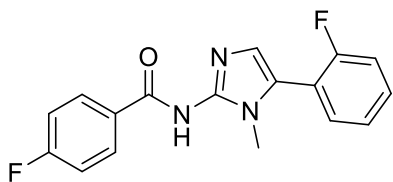
The title compound was prepared from 5-(2-chlorophenyl)-1-methyl-1*H*-imidazol-2-amine (200 mg, 0.96 mmol) and 4-fluorobenzoic acid (135 mg, 0.96 mmol) according to General Procedure B as a yellow solid (170 mg, 53 %). HPLC – t_R 4.97 min > 99 % purity at 254 nm; LRMS $[M+H]^+$ 329.9 m/z ; HRMS $[M+H]^+$ 330.0801 m/z , found 330.0804 m/z ; 1H NMR (400 MHz, $CDCl_3$) δ_H 8.32 – 8.27 (m, 2H), 7.54 – 7.50 (m, 1H), 7.45 – 7.34 (m, 3H), 7.08 – 7.02 (m, 2H), 6.74 (s, 1H), 3.44 (s, 3H). ^{13}C NMR (101 MHz, $CDCl_3$) δ_C 173.2, 164.7 (d, J_{C-F} = 249.8 Hz), 150.5, 135.4, 134.4, 133.0, 131.1, 131.1 (d, J_{C-F} = 8.8 Hz, 2C), 130.1, 127.5, 127.2, 125.7, 114.8 (d, J = 21.5 Hz, 2C), 111.1, 30.0.

***N*-(5-(2-Bromophenyl)-1-methyl-1*H*-imidazol-2-yl)-4-fluorobenzamide (3.104)**



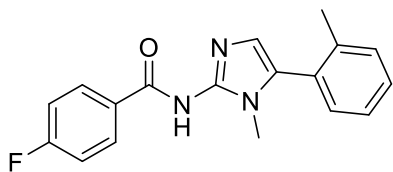
The title compound was prepared from 5-(2-bromophenyl)-1-methyl-1*H*-imidazol-2-amine (200 mg, 0.79 mmol) and 4-fluorobenzoic acid (111 mg, 0.79 mmol) according to General Procedure B as a yellow solid (55 mg, 14 %). HPLC – t_R 5.14 min > 99 % purity at 254 nm; LRMS $[M+H]^+$ 373.8 m/z ; HRMS $[M+H]^+$ 374.0299 m/z , found 374.0305 m/z ; 1H NMR (400 MHz, $CDCl_3$) δ_H 7.65 – 7.62 (m, 1H), 7.598– 7.55 (m, 2H), 7.37 – 7.33 (m, 2H), 7.20 – 7.09 (m, 4H), 3.62 (s, 3H); 1H NMR (400 MHz, MeOD) δ_H 7.75 – 7.29 (m, 6H), 7.28 – 7.03 (m, 3H), 3.51 (s, 3H); ^{13}C NMR (101 MHz, MeOD) δ_C 171.3, 165.1 (d, J_{C-F} = 250.8 Hz), 144.5, 134.4, 133.2 (d, J_{C-F} = 9.5 Hz, 2C), 132.3, 131.5, 131.5, 131.4, 129.7, 128.4, 128.0, 122.4, 116.1 (d, J_{C-F} = 22.2 Hz, 2C), 37.3.

4-Fluoro-*N*-(5-(2-fluorophenyl)-1-methyl-1*H*-imidazol-2-yl)benzamide (3.105)



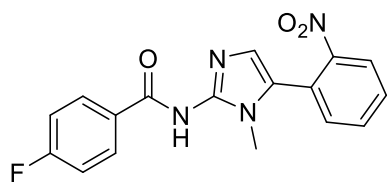
The title compound was prepared from 5-(2-fluorophenyl)-1-methyl-1*H*-imidazol-2-amine (200 mg, 1.05 mmol) and 4-fluorobenzoic acid (147 mg, 1.05 mmol) according to General Procedure B as a white solid (250 mg, 83 %). HPLC – t_R 4.72 min > 99 % purity at 254 nm; LRMS $[M+H]^+$ 314.0 m/z ; HRMS $[M+H]^+$ 314.1095 m/z , found 314.1099 m/z ; 1H NMR (400 MHz, $CDCl_3$) δ_H 8.32 – 8.26 (m, 2H), 7.51 – 7.45 (m, 1H), 7.40 – 7.34 (m, 1H), 7.29 – 7.26 (m, 1H), 7.25 – 7.20 (m, 1H), 7.09 (t, J = 8.3 Hz, 3H), 6.83 (s, 1H), 3.55 (s, 3H); ^{13}C NMR (101 MHz, $CDCl_3$) δ_C 173.3, 164.9 (d, J_{C-F} = 250.1 Hz), 160.4 (d, J_{C-F} = 249.4 Hz), 150.8, 134.2, 131.9 (d, J_{C-F} = 2.2 Hz), 131.6 (d, J_{C-F} = 8.2 Hz), 131.2 (d, J_{C-F} = 8.8 Hz, 2C), 124.8 (d, J_{C-F} = 3.7 Hz), 123.2, 116.4, 116.4 (d, J_{C-F} = 21.5 Hz), 114.9 (d, J_{C-F} = 21.5 Hz, 2C), 111.3, 30.4.

4-Fluoro-*N*-(1-methyl-5-(*o*-tolyl)-1*H*-imidazol-2-yl)benzamide (3.106)



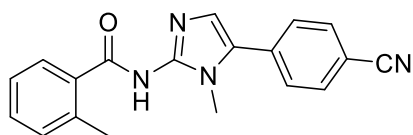
The title compound was prepared from 1-methyl-5-(*o*-tolyl)-1*H*-imidazol-2-amine (200 mg, 1.07 mmol) and 4-fluorobenzoic acid (149 mg, 1.07 mmol) according to General Procedure B as an orange solid (80 mg, 24 %). HPLC – t_R 4.93 min > 99 % purity at 254 nm; LRMS $[M+H]^+$ 310.0 m/z ; HRMS $[M+H]^+$ 310.1350 m/z , found 310.1344 m/z ; 1H NMR (400 MHz, $CDCl_3$) δ_H 8.32 – 8.27 (m, 2H), 7.35 – 7.27 (m, 3H), 7.12 – 7.06 (m, 3H), 6.70 (s, 1H), 3.38 (s, 3H), 2.24 (s, 3H); ^{13}C NMR (101 MHz, $CDCl_3$) δ_C 173.2, 164.9 (d, J_{C-F} = 250.0 Hz), 150.4, 138.7, 134.1 (d, J_{C-F} = 3.1 Hz), 131.6, 131.2 (d, J_{C-F} = 8.8 Hz, 2C), 130.7, 130.1, 127.8, 127.6, 126.3, 114.9 (d, J_{C-F} = 21.5 Hz, 2C), 109.9, 29.9, 20.0.

4-Fluoro-*N*-(1-methyl-5-(2-nitrophenyl)-1*H*-imidazol-2-yl)benzamide (3.107)



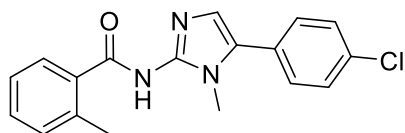
The title compound was prepared from 5-(2-nitrophenyl)-1-methyl-1*H*-imidazol-2-amine (200 mg, 0.92 mmol) and 4-fluorobenzoic acid (128 mg, 0.92 mmol) according to General Procedure B as a yellow solid (108 mg, 35 %). HPLC – t_R 4.59 min > 99 % purity at 254 nm; LRMS $[M+H]^+$ 340.9 m/z ; HRMS $[M+H]^+$ 341.1044 m/z , found 341.1045 m/z ; 1H NMR (400 MHz, $CDCl_3$) δ_H 8.30 – 8.26 (m, 2H), 8.15 (dd, J = 8.0, 1.3 Hz, 1H), 7.77 – 7.68 (m, 2H), 7.50 (dd, J = 7.4, 1.5 Hz, 1H), 7.10 – 7.04 (m, 2H), 6.72 (s, 1H), 3.41 (s, 3H); ^{13}C NMR (101 MHz, $CDCl_3$) δ_C 173.7, 164.9 (d, J_{C-F} = 250.1 Hz), 158.1, 151.0, 149.8, 134.3, 134.0, 133.5, 131.2 (d, J_{C-F} = 8.5 Hz, 2C), 125.1, 123.9, 123.0, 114.9 (d, J_{C-F} = 21.5 Hz, 2C), 110.5, 29.9.

N-(5-(4-Cyanophenyl)-1-methyl-1*H*-imidazol-2-yl)-2-methylbenzamide (3.108)



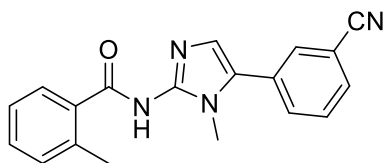
The title compound was prepared from 5-(4-cyanophenyl)-1-methyl-1*H*-imidazol-2-amine (200 mg, 1.01 mmol) and *o*-toluic acid (137 mg, 1.01 mmol) according to General Procedure B as a yellow solid (263 mg, 83 %). HPLC – t_R 4.47 min > 99 % purity at 254 nm; LRMS $[M+H]^+$ 317.0 m/z ; HRMS $[M+H]^+$ 317.1397 m/z , found 317.14 m/z ; 1H NMR (400 MHz, $CDCl_3$) δ_H 7.79 – 7.71 (m, 3H), 7.47 (d, J = 8.3 Hz, 2H), 7.40 – 7.36 (m, 1H), 7.26 (s, 2H), 6.68 (s, 1H), 3.61 (s, 3H), 2.56 (s, 3H); ^{13}C NMR (101 MHz, $CDCl_3$) δ_C 166.0, 137.9, 133.5, 132.9 (2C), 131.7, 131.0, 128.7 (2C), 128.5, 126.8, 126.0, 125.0, 118.8, 118.4, 112.3, 110.4, 38.8, 20.8.

N-(5-(4-Chlorophenyl)-1-methyl-1*H*-imidazol-2-yl)-2-methylbenzamide (3.109)



The title compound was prepared from 5-(4-chlorophenyl)-1-methyl-1*H*-imidazol-2-amine (200 mg, 0.96 mmol) and *o*-toluic acid (131 mg, 0.96 mmol) according to General Procedure B as a yellow solid (115 mg, 37 %). HPLC – t_R 5.12 min > 99 % purity at 254 nm; LRMS $[M+H]^+$ 326.0 m/z ; HRMS $[M+H]^+$ 326.1055 m/z , found 326.1062 m/z ; 1H NMR (400 MHz, $CDCl_3$) δ_H 7.78 (d, J = 7.3 Hz, 1H), 7.42 (d, J = 8.4 Hz, 2H), 7.36 – 7.27 (m, 3H), 7.25 – 7.21 (m, 2H), 6.51 (s, 1H), 3.55 (s, 3H), 2.57 (s, 3H); ^{13}C NMR (101 MHz, $CDCl_3$) δ_C 173.4, 146.1, 137.5, 136.6, 134.6, 131.4, 130.3, 130.0, 129.8 (2C), 129.3 (2C), 128.8, 127.7, 125.6, 117.6, 31.8, 20.9.

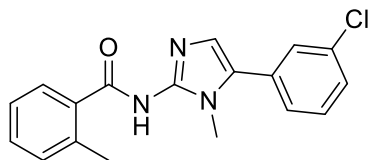
N-(5-(3-Cyanophenyl)-1-methyl-1*H*-imidazol-2-yl)-2-methylbenzamide (3.110)



The title compound was prepared from 5-(3-cyanophenyl)-1-methyl-1*H*-imidazol-2-amine (200 mg, 1.01 mmol) and *o*-toluic acid (137 mg, 1.01 mmol) according to General Procedure B as a yellow solid (181 mg, 57 %). HPLC – t_R 4.48 min > 99 % purity at 254 nm; LRMS $[M+H]^+$ 317.0 m/z ; HRMS $[M+H]^+$ 317.1401 m/z , found 317.1397 m/z ; 1H NMR (400 MHz,

CDCl₃) δ_H 7.80 – 7.77 (m, 1H), 7.72 – 7.68 (m, 2H), 7.64 – 7.57 (m, 2H), 7.37 – 7.32 (m, 2H), 7.25 – 7.22 (m, 1H), 6.81 (s, 1H), 3.60 (s, 3H), 2.58 (s, 3H); ¹³C NMR (101 MHz, CDCl₃) δ_C 165.9, 137.6, 132.5, 131.8, 131.7, 131.5, 130.8, 130.5, 130.0, 128.7, 125.8, 118.3, 113.6, 38.7, 20.9. Four quaternary carbons not visible, including imidazole quaternary carbons

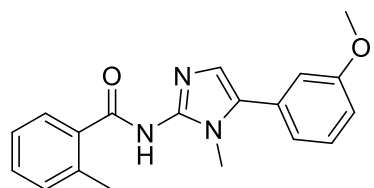
***N*-(5-(3-Chlorophenyl)-1-methyl-1*H*-imidazol-2-yl)-2-methylbenzamide (3.111)**



The title compound was prepared from 5-(3-chlorophenyl)-1-methyl-1*H*-imidazol-2-amine (200 mg, 0.96 mmol) and *o*-toluic acid (131 mg, 0.96 mmol) according to General Procedure B as a yellow solid (175 mg, 56 %). HPLC – t_R 5.11 min > 99 % purity at 254 nm; LRMS

[*M*+*H*]⁺ 326.0 *m/z*; HRMS [*M*+*H*]⁺ 326.1055 *m/z*, found 326.1057 *m/z*; ¹H NMR (400 MHz, CDCl₃) δ_H 7.72 – 7.68 (m, 1H), 7.32 – 7.25 (m, 4H), 7.20 – 7.15 (m, 3H), 6.44 (s, 1H), 3.49 (s, 3H), 2.49 (s, 3H); ¹H NMR (400 MHz, MeOD) δ 7.68 – 7.65 (m, 1H), 7.56 – 7.53 (m, 1H), 7.51 – 7.40 (m, 4H), 7.35 – 7.29 (m, 2H), 7.07 (s, 1H), 3.61 (s, 3H), 2.55 (s, 3H); ¹³C NMR (101 MHz, MeOD) δ_C 137.8, 136.7, 135.9, 132.8, 132.4, 132.1, 131.6, 131.5, 129.5, 129.5, 128.7, 128.0, 126.9, 32.0, 20.2. Imidazole and carbonyl quaternary carbons not visible.

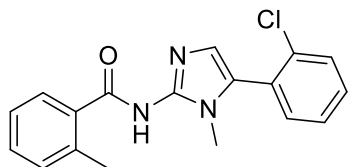
***N*-(5-(3-Methoxyphenyl)-1-methyl-1*H*-imidazol-2-yl)-2-methylbenzamide (3.112)**



The title compound was prepared from 5-(3-methoxyphenyl)-1-methyl-1*H*-imidazol-2-amine (200 mg, 0.98 mmol) and *o*-toluic acid (133 mg, 0.98 mmol) according to General Procedure B as a yellow solid (187 mg, 59 %). HPLC – t_R 4.89 min > 99 % purity at 254 nm;

LRMS [*M*+*H*]⁺ 322.0 *m/z*; HRMS [*M*+*H*]⁺ 322.1550 *m/z*, found 322.1551 *m/z*; ¹H NMR (400 MHz, CDCl₃) δ 7.73 – 7.70 (m, 1H), 7.29 – 7.22 (m, 2H), 7.18 – 7.12 (m, 2H), 6.88 – 6.80 (m, 3H), 6.47 (s, 1H), 3.76 (s, 3H), 2.50 (s, 3H); ¹³C NMR (101 MHz, CDCl₃) δ 173.85 (s), 160.0, 146.6, 137.4, 137.0, 131.3, 130.7, 130.5, 130.1, 130.0, 128.9, 125.6, 121.1, 116.4, 114.4, 114.0, 55.5, 31.7, 20.9.

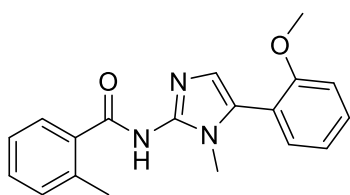
***N*-(5-(2-Chlorophenyl)-1-methyl-1*H*-imidazol-2-yl)-2-methylbenzamide (3.113)**



The title compound was prepared from 5-(2-chlorophenyl)-1-methyl-1*H*-imidazol-2-amine (200 mg, 0.96 mmol) and *o*-toluic acid (131 mg, 0.96 mmol) according to General Procedure B as a yellow solid (75 mg, 23 %). HPLC – t_R 5.01 min > 99 % purity at 254 nm; LRMS [*M*+*H*]⁺

326.0 *m/z*; HRMS [*M*+*H*]⁺ 326.1055 *m/z*, found 326.1058 *m/z*; ¹H NMR (400 MHz, CDCl₃) δ_H 7.89 – 7.85 (m, 1H), 7.55 – 7.52 (m, 1H), 7.44 – 7.39 (m, 2H), 7.38 – 7.36 (m, 2H), 7.33 – 7.28 (m, 2H), 7.25 – 7.20 (m, 2H), 6.77 (s, 1H), 3.43 (s, 3H), 2.63 (s, 3H); ¹³C NMR (101 MHz, CDCl₃) δ_C 163.6, 137.8, 135.5, 131.4, 131.3, 130.3, 129.2, 127.3, 125.7, 30.2, 21.2. Aromatic quaternary carbons not visible.

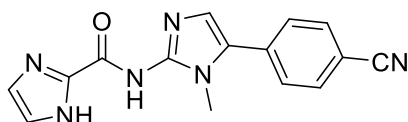
***N*-(5-(2-Methoxyphenyl)-1-methyl-1*H*-imidazol-2-yl)-2-methylbenzamide (3.114)**



The title compound was prepared from 5-(2-methoxyphenyl)-1-methyl-1*H*-imidazol-2-amine (200 mg, 0.98 mmol) and *o*-toluic acid (133 mg, 0.98 mmol) according to General Procedure B as a yellow solid (250 mg, 79 %). HPLC – t_R 4.91 min > 99 % purity at 254 nm; LRMS $[M+H]^+$ 322.0 m/z ; HRMS $[M+H]^+$ 322.1550 m/z , found

322.155 m/z ; 1H NMR (400 MHz, $CDCl_3$) δ_H 7.86 – 7.83 (m, 1H), 7.49 – 7.41 (m, 1H), 7.29 – 7.24 (m, 2H), 7.22 – 7.17 (m, 2H), 7.06 – 6.97 (m, 2H), 6.63 (s, 1H), 3.83 (s, 3H), 3.41 (s, 3H), 2.61 (s, 3H); ^{13}C NMR (101 MHz, $CDCl_3$) δ_C 175.9, 157.8, 148.3, 138.3, 137.3, 132.2, 131.1, 131.1, 129.6, 129.1, 126.8, 125.5, 120.9, 117.7, 113.1, 111.1, 55.5, 30.6, 21.2.

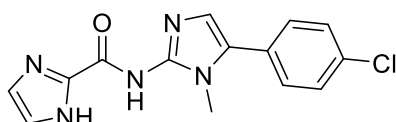
***N*-(5-(4-Cyanophenyl)-1-methyl-1*H*-imidazol-2-yl)-1*H*-imidazole-2-carboxamide (3.115)**



The title compound was prepared from 5-(4-cyanophenyl)-1-methyl-1*H*-imidazol-2-amine (200 mg, 1.02 mmol) and 1*H*-imidazole-2-carboxylic acid (114 mg, 1.02 mmol) according to

General Procedure C as a yellow solid (29 mg, 10 %). HPLC – t_R 4.00 min > 99 % purity at 254 nm; LRMS $[M+H]^+$ 293.0 m/z ; HRMS $[M+H]^+$ 293.1145 m/z , found 293.1144 m/z ; 1H NMR (400 MHz, MeOD) δ_H 7.89 – 7.86 (m, 2H), 7.77 – 7.73 (m, 2H), 7.37 (s, 2H), 7.18 (s, 1H), 3.70 (s, 3H); ^{13}C NMR (101 MHz, MeOD) δ 133.9 (2C), 127.2 (2C), 126.5, 126.5, 118.7, 111.8, 31.6. Aromatic and carbonyl quaternary carbons not available.

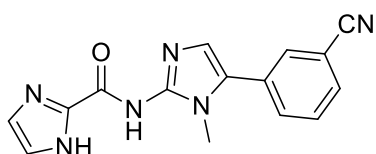
***N*-(5-(4-Chlorophenyl)-1-methyl-1*H*-imidazol-2-yl)-1*H*-imidazole-2-carboxamide (3.116)**



The title compound was prepared from 5-(4-chlorophenyl)-1-methyl-1*H*-imidazol-2-amine (200 mg, 0.97 mmol) and 1*H*-imidazole-2-carboxylic acid (108 mg, 0.97 mmol) according to

General Procedure C as a yellow solid (30 mg, 10 %). HPLC – t_R 4.74 min > 95 % purity at 254 nm; LRMS $[M+H]^+$ 302.0 m/z ; HRMS $[M+H]^+$ 302.0803 m/z , found 302.0803 m/z ; 1H NMR (400 MHz, $CDCl_3$) δ_H 7.47 – 7.43 (m, 2H), 7.36 – 7.32 (m, 2H), 7.22 – 7.16 (m, 2H), 6.83 (s, 1H), 3.60 (s, 3H); ^{13}C NMR (101 MHz, $CDCl_3$) δ_C 134.8, 129.8 (2C), 129.1 (2C), 126.9, 124.1, 30.6. Quaternary carbons not visible. M.p. 262.2-265.8 °C.

***N*-(5-(3-cyanophenyl)-1-methyl-1*H*-imidazol-2-yl)-1*H*-imidazole-2-carboxamide (3.117)**

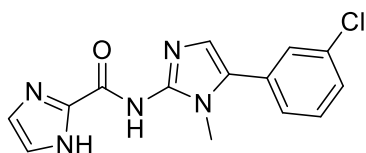


The title compound was prepared from 5-(3-cyanophenyl)-1-methyl-1*H*-imidazol-2-amine (200 mg, 1.02 mmol) and 1*H*-imidazole-2-carboxylic acid (114 mg, 1.02 mmol) according to General Procedure C as a yellow solid (58 mg, 20 %). HPLC – t_R 4.01 min > 99 % purity

at 254 nm; LRMS $[M+H]^+$ 293.0 m/z ; HRMS $[M+H]^+$ 293.1145 m/z , found 293.1148 m/z ; 1H NMR

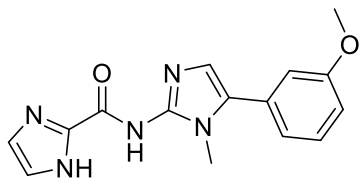
(400 MHz, CDCl₃) δ_{H} 7.69 – 7.62 (m, 3H), 7.59 – 7.54 (m, 1H), 7.17 (s, 2H), 6.96 (s, 1H), 3.57 (s, 3H); ¹³C NMR (101 MHz, CDCl₃) δ_{C} 132.8, 132.0, 131.8, 130.5, 130.0, 118.2, 113.3, 31.4. Quaternary Carbons not visible.

***N*-(5-(3-Chlorophenyl)-1-methyl-1*H*-imidazol-2-yl)-1*H*-imidazole-2-carboxamide (3.118)**



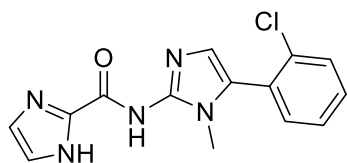
The title compound was prepared from 5-(2-chlorophenyl)-1-methyl-1*H*-imidazol-2-amine (200 mg, 0.97 mmol) and 1*H*-imidazole-2-carboxylic acid (108 mg, 0.97 mmol) according to General Procedure C as a yellow solid (85 mg, 29 %). HPLC – t_{R} 4.70 min > 99 % purity at 254 nm; LRMS [M+H]⁺ 302.0 m/z ; HRMS [M+H]⁺ 302.0803 m/z , found 302.0801 m/z ; ¹H NMR (400 MHz, CDCl₃) δ_{H} 7.31 – 7.28 (m, 3H), 7.21 – 7.14 (m, 3H), 6.85 (s, 1H), 3.50 (s, 3H); ¹H NMR (400 MHz, DMSO) δ_{H} 13.23 (bs, 1H, NH), 10.45 (bs, 1H, NH), 7.56 – 7.37 (m, 5H), 7.22 – 6.99 (m, 2H), 3.46 (s, 3H); ¹³C NMR (101 MHz, DMSO) δ_{C} 133.6, 131.7, 130.7, 127.6, 127.3, 126.4, 125.3, 31.1. Quaternary carbons not visible.

***N*-(5-(3-methoxyphenyl)-1-methyl-1*H*-imidazol-2-yl)-1*H*-imidazole-2-carboxamide (3.119)**



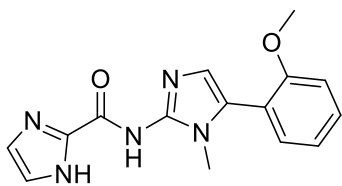
The title compound was prepared from 5-(3-methoxyphenyl)-1-methyl-1*H*-imidazol-2-amine (200 mg, 0.98 mmol) and 1*H*-imidazole-2-carboxylic acid (108 mg, 0.98 mmol) according to General Procedure C as a yellow solid (43 mg, 15 %). HPLC – t_{R} 4.39 min > 99 % purity at 254 nm; LRMS [M+H]⁺ 298.0 m/z ; HRMS [M+H]⁺ 298.1299 m/z , found 298.1294 m/z ; ¹H NMR (400 MHz, CDCl₃) δ_{H} 7.34 (t, J = 7.9 Hz, 1H), 7.19 (bs, 2H), 6.96 – 6.85 (m, 4H), 3.82 (s, 3H), 3.57 (s, 3H); ¹³C NMR (101 MHz, CDCl₃) δ_{C} 162.7, 160.0, 143.5, 130.6, 130.1, 129.9, 124.4, 121.2, 114.6, 114.3, 55.5, 31.1. Imidazole quaternary carbons not visible.

***N*-(5-(2-Chlorophenyl)-1-methyl-1*H*-imidazol-2-yl)-1*H*-imidazole-2-carboxamide (3.120)**



The title compound was prepared from 5-(2-chlorophenyl)-1-methyl-1*H*-imidazol-2-amine (200 mg, 0.97 mmol) and 1*H*-imidazole-2-carboxylic acid (108 mg, 0.97 mmol) according to General Procedure C as a yellow solid (50 mg, 17 %). HPLC – t_{R} 4.47 min > 99 % purity at 254 nm; LRMS [M+H]⁺ 302.0 m/z ; HRMS [M+H]⁺ 302.0803 m/z , found 302.0802 m/z ; ¹H NMR (400 MHz, CDCl₃) δ_{H} 7.52 (m, 1H), 7.44 – 7.40 (m, 1H), 7.38 – 7.34 (m, 2H), 7.21 (s, 2H), 6.85 (s, 1H), 3.46 (s, 3H); ¹H NMR (400 MHz, DMSO) δ_{H} 13.21 (bs, 1H), 10.41 (bs, 1H), 7.61 – 7.38 (m, 6H), 6.89 (s, 1H), 3.23 (s, 3H); ¹³C NMR (101 MHz, DMSO) δ_{C} 133.6, 132.9, 130.8, 129.8, 128.5, 127.5, 106.8, 30.5. Quaternary carbons not visible.

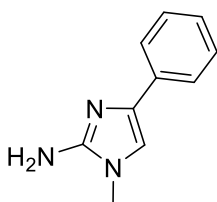
***N*-(5-(2-Methoxyphenyl)-1-methyl-1*H*-imidazol-2-yl)-1*H*-imidazole-2-carboxamide (3.121)**



The title compound was prepared from 5-(2-methoxyphenyl)-1-methyl-1*H*-imidazol-2-amine (300 mg, 1.47 mmol) and 1*H*-imidazole-2-carboxylic acid (165 mg, 1.47 mmol) according to General Procedure C as a yellow solid (50 mg, 11 %). HPLC – t_R 4.33 min > 99 % purity at 254 nm; LRMS $[M+H]^+$ 298.0 m/z ; HRMS $[M+H]^+$ 298.1296 m/z , found 298.1299 m/z ; 1H NMR (400 MHz, $CDCl_3$) δ_H 7.46 – 7.40 (m, 1H), 7.27 – 7.24 (m, 1H), 7.17 (s, 2H), 7.04 – 6.96 (m, 2H), 6.75 (s, 1H), 3.80 (s, 3H), 3.45 (s, 3H); ^{13}C NMR (101 MHz, $CDCl_3$) δ_C 164.0, 157.8, 148.5, 147.8, 144.5, 132.3, 131.2, 127.2, 123.4, 121.0, 117.5, 111.1, 106.7, 55.5, 30.8.

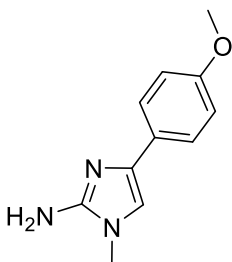
Analogue Series 7-8

1-Methyl-4-phenyl-1*H*-imidazol-2-amine (3.126)⁵⁹



To obtain the known title compound 2-phenylacetaldehyde (2.0 g, 16.7 mmol) was dissolved in 1,4-dioxane (2 mL) at 0 °C and bromine (0.7 mL) dropwise over 15 min. The mixture was left to stir at 0 °C for 10 mins then heated to room temperature and was left to stir for a further 10 min. The mixture was concentrated *in vacuo* to obtain 2-bromo-2-phenylacetaldehyde as a brown solid.^{15, 16} The 2-bromo-2-phenylacetamide (810 mg, 4.05 mmol) was taken directly and added to *N*-methylpyrimidin-2-amine (330 mg, 3 mmol) following General Procedure A, heating to 150°C during the condensation step. The title compound was obtained as a brown solid (500 mg, 96 %). HPLC – t_R 3.59 min > 90 % purity at 254 nm; LRMS $[M+H]^+$ 174.0 m/z ; 1H NMR (400 MHz, MeOD) δ_H 7.65 – 7.61 (m, 2H), 7.57 – 7.53 (m, 3H), 7.23 (s, 1H), 2.93 (s, 3H).

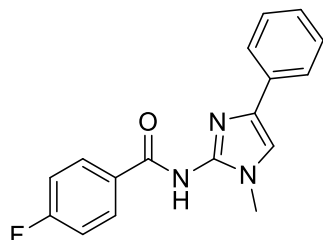
4-(4-Methoxyphenyl)-1-methyl-1*H*-imidazol-2-amine (3.127)³



To a solution of 2-(4-methoxyphenyl)acetaldehyde (2 g, 13.3 mmol), 4M HCl in dioxane (15 mL) and DCM (15 mL) was added bromine (0.8 mL) in DCM (15 mL) dropwise at 0°C over 1 h. The mixture was stirred for a further 30 min at 0°C. The mixture was then diluted with DCM and washed with $NaHCO_3$, $Na_2S_2O_3$ and brine. The organic layers were collected, dried over $MgSO_4$, filtered and concentrated *in vacuo* to obtain 2-bromo-2-(4-methoxyphenyl)acetaldehyde as a brown oil. The 2-bromo-2-(4-methoxyphenyl)acetaldehyde (924 mg, 4.05 mmol) was used directly with to *N*-methylpyrimidin-2-amine (330 mg, 3 mmol) following General Procedure A, heating to 150°C during the condensation step. The known title compound was obtained as an orange solid (596 mg, 97 %). HPLC – t_R 3.87 min > 99 % purity at 254 nm; LRMS $[M+H]^+$ 204.0 m/z ; 1H NMR (400 MHz, $CDCl_3$) δ_H 7.56 (d, J = 8.6 Hz, 2H), 6.87 (d, J = 8.6 Hz, 2H), 6.69 (s, 1H), 3.81 (s, 3H), 3.44 (s,

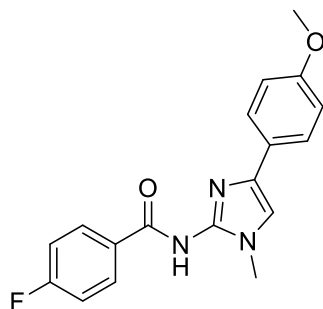
3H); ^{13}C NMR (101 MHz, CDCl_3) δ_{C} 158.5, 148.0, 136.5, 127.1, 125.7 (2C), 114.1 (2C), 111.2, 55.4, 31.8. Acquired data is consistent with the literature.³

4-Fluoro-*N*-(1-methyl-4-phenyl-1*H*-imidazol-2-yl)benzamide (3.128)



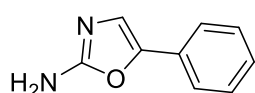
The title compound was prepared from 1-methyl-4-phenyl-1*H*-imidazol-2-amine (220 mg, 1.73 mmol) and 4-fluorobenzoic acid (179 mg, 1.27 mmol) according to General Procedure B as a yellow solid (200 mg, 53 %). HPLC – t_{R} 4.54 min > 99 % purity at 254 nm; LRMS $[\text{M}+\text{H}]^+$ 296.0 m/z ; HRMS $[\text{M}+\text{H}]^+$ 296.1194 m/z , found 296.1197 m/z ; ^1H NMR (400 MHz, CDCl_3) δ_{H} 8.29 – 8.24 (m, 2H), 7.51 – 7.46 (m, 2H), 7.41 – 7.35 (m, 2H), 7.32 – 7.27 (m, 1H), 7.11 – 7.05 (m, 2H), 6.79 (s, 1H), 3.61 (s, 3H); ^{13}C NMR (101 MHz, CDCl_3) δ_{C} 172.9, 164.9 (d, $J_{\text{C-F}}$ = 250.4 Hz), 150.0, 133.8 (d, $J_{\text{C-F}}$ = 2.5 Hz), 131.1 (d, $J_{\text{C-F}}$ = 8.9 Hz, 2C), 129.2, 128.6, 128.2, 126.9, 124.2, 114.9 (d, $J_{\text{C-F}}$ = 21.5 Hz, 2C), 111.4, 32.0.

4-Fluoro-*N*-(4-(4-methoxyphenyl)-1-methyl-1*H*-imidazol-2-yl)benzamide (3.129)



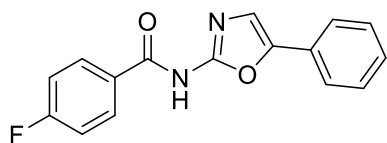
The title compound was prepared from 4-(4-methoxyphenyl)-1-methyl-1*H*-imidazol-2-amine (200 mg, 0.98 mmol) and 4-fluorobenzoic acid (140 mg, 0.98 mmol) according to General Procedure B as a yellow solid (155 mg, 49 %). HPLC – t_{R} 4.72 min > 99 % purity at 254 nm; LRMS $[\text{M}+\text{H}]^+$ 326.0 m/z ; HRMS $[\text{M}+\text{H}]^+$ 326.1299 m/z , found 326.1304 m/z ; ^1H NMR (400 MHz, CDCl_3) δ_{H} 8.33 – 8.26 (m, 2H), 7.46 – 7.40 (m, 2H), 7.12 – 7.07 (m, 2H), 6.97 – 6.93 (m, 2H), 6.69 (s, 1H), 3.84 (s, 3H), 3.67 (s, 3H); ^{13}C NMR (101 MHz, CDCl_3) δ_{C} 159.9, 131.1 (d, $J_{\text{C-F}}$ = 8.7 Hz, 2C), 125.8 (2C), 120.9, 114.9 (d, $J_{\text{C-F}}$ = 21.4 Hz, 2C), 114.8 (2C), 55.6, 31.8. Aromatic quaternary carbons not visible.

5-Phenyloxazol-2-amine (3.130)¹⁷



To obtain the known title compound 2-bromo-2-phenylacetaldehyde (500 mg, 2.5 mol) and urea (300 mg, 5 mmol) in DMF (3.5 mL) were heated to 160°C for 10 min using a microwave reactor. Upon reaction completion the mixture was diluted with water and concentrated *in vacuo*. The solid that had formed was filtered with water and dried via suction filtration to obtain the title compound as an orange solid. (385 mg, 96 %).¹⁸ HPLC – t_{R} 3.36 min > 99 % purity at 254 nm; LRMS $[\text{M}+\text{H}]^+$ 161.1 m/z ; ^1H NMR (400 MHz, CDCl_3) δ_{H} 8.35 – 6.51 (m, 6H).

4-Fluoro-*N*-(5-phenyloxazol-2-yl)benzamide (3.131)

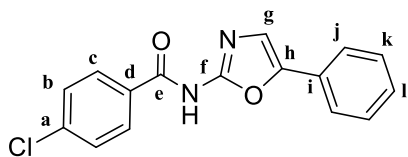


To a solution of DCM/DMF (10:0.1) and 4-fluorobenzoic acid (700 mg, 5 mmol) at 0°C was added oxalyl chloride (0.9 mL) dropwise.

The solution was heated to room temperature and left to stir for 5 h.

Upon reaction completion in which the solution had cleared and bubbling had ceased the mixture was concentrated *in vacuo* using toluene as an azeotrope. The converted 4-fluorobenzoyl chloride was added to a solution of 5-phenyloxazol-2-amine (200 mg, 1.24 mmol), DIPEA (2.5 eq) and DCM. The solution was heated to reflux and left to stir for 15 h. Upon reaction completion the mixture was concentrated, diluted with EtOAc and washed with brine. The organic layers were collected, dried over MgSO₄, filtered and concentrated. The crude material was subsequently purified via column chromatography (EtOAc: Petroleum spirits; 1:1) to obtain the title compound as a solid. (266 mg, 76 %). HPLC – *t_R* 5.68 min > 99 % purity at 254 nm; LRMS [M+H]⁺ 283.0 *m/z*; HRMS [M+H]⁺ 283.0877 *m/z*, found 283.0879 *m/z*; ¹H NMR (400 MHz, CDCl₃) δ_H 8.29 – 8.07 (m, 2H), 7.79 – 7.32 (m, 5H), 7.23 – 7.05 (m, 3H); ¹³C NMR (101 MHz, CDCl₃) δ_C 132.9 (d, *J*_{C-F} = 9.6 Hz, 2C), 129.1 (2C), 128.6, 124.1 (2C), 115.8 (d, *J*_{C-F} = 22.0 Hz, 2C). Quaternary carbons not visible.

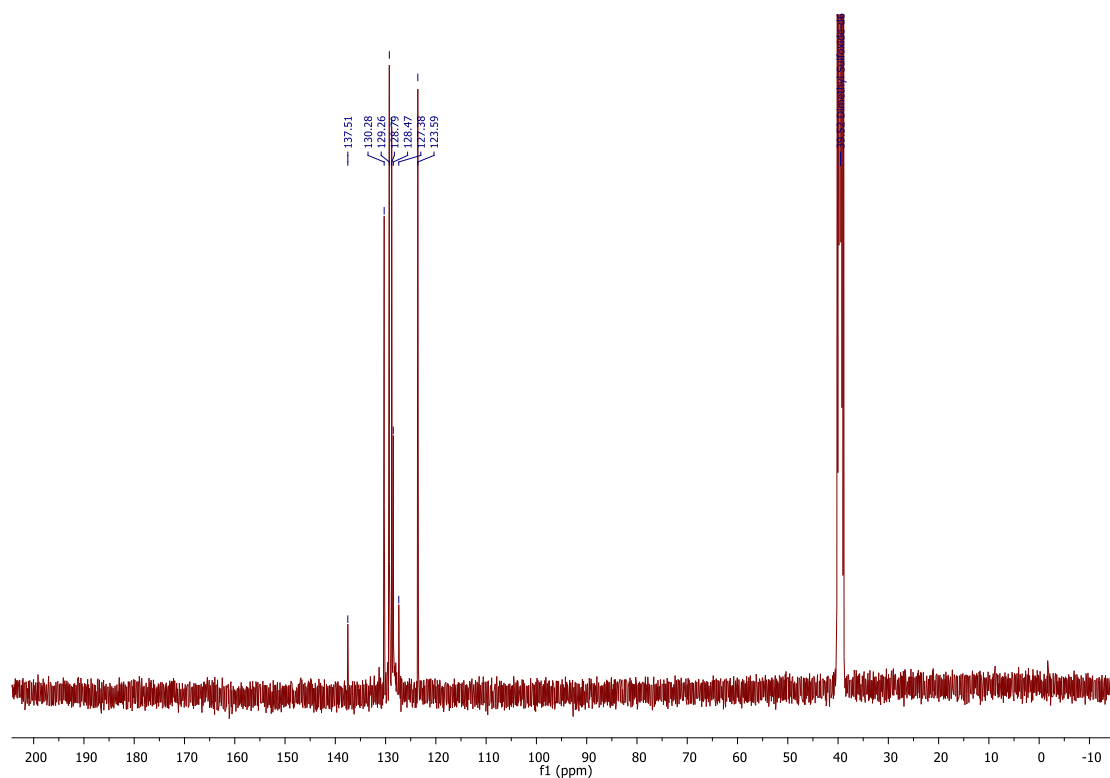
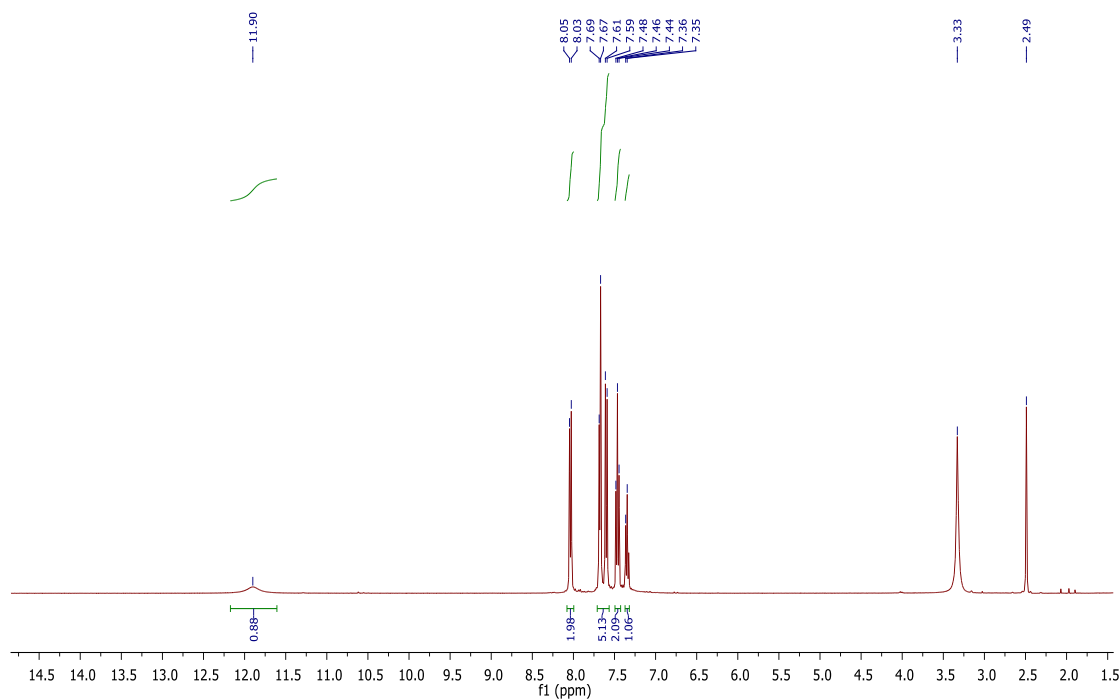
4-Chloro-*N*-(5-phenyloxazol-2-yl)benzamide (3.134)



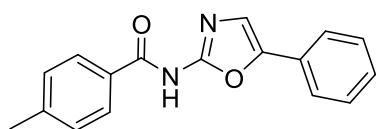
The title compound was obtained using 5-phenyloxazol-2-amine (100 mg, 0.63 mmol) and 4-chlorobenzoic acid (98 mg, 0.63 mmol) following General Procedure B, to afford the title compound as a brown (80 mg, 43 %). HPLC – *t_R* 6.02 min > 99 %

purity at 254 nm; LRMS [M+H]⁺ 299.0 *m/z*; HRMS [M+H]⁺ 299.0582 *m/z*, found 299.0588 *m/z*; ¹H NMR (401 MHz, DMSO) δ_H 11.90 (s, 1H, NH), 8.04 (d, *J* = 8.5 Hz, 2H, Hc), 7.70 – 7.57 (m, 5H, Hb, Hj, Hl), 7.50 – 7.42 (m, 2H, Hk), 7.35 m, (1H, Hg); ¹³C NMR (101 MHz, DMSO) δ_C 137.5 (Ce), 130.3 (2C, Ck), 129.3 (2C, Cb), 128.8 (2C, Cc), 128.5 (Cl), 127.4 (Cg), 123.6 (2C, Cj). Aromatic quaternary carbons not visible.

Example spectra for Series 7-8 (additive SAR, oxazole core): ¹H NMR (400 MHz, DMSO) and ¹³C NMR (100 MHz, DMSO) spectrum of 4-Chloro-*N*-(5-phenyloxazol-2-yl)benzamide (3.134)



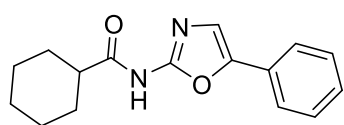
4-Methyl-*N*-(5-phenyloxazol-2-yl)benzamide (3.135)



The title compound was obtained using 5-phenyloxazol-2-amine (100 mg, 0.63 mmol) following General Procedure D. The converted acid halide concentrated *in vacuo* and taken up in DCM and added dropwise to a mixture of *p*-toluic acid (87 mg, 0.63 mmol) and DIPEA (2.5 eq) in DCM at 0°C. The

mixture was heated to reflux and stirred over 12 h. Upon reaction completion the mixture was concentrated *in vacuo*, diluted with EtOAc and washed with brine. The organic layers were collected, dried over MgSO₄, filtered and concentrated *in vacuo*. The crude material was purified via column chromatography (eluent: EtOAc: Petroleum ether, 1:1) to afford the title compound as an orange solid (65 mg, 37 %). HPLC – *t_R* 5.27 min > 99 % purity at 254 nm; LRMS [M+H]⁺ 279.0 *m/z*; HRMS [M+H]⁺ 279.1128 *m/z*, found 279.1134 *m/z*; ¹H NMR (400 MHz, DMSO) δ_H 11.57 (bs, 1H, NH), 7.91 (d, *J* = 7.9 Hz, 2H), 7.71 – 7.60 (m, 3H), 7.51 – 7.43 (m, 2H), 7.40 – 7.28 (m, 3H), 2.38 (s, 3H); ¹³C NMR (101 MHz, DMSO) δ_C 167.6, 143.0, 129.3 (2C), 129.3 (2C), 128.4, 128.3 (2C), 127.5, 123.6(2C), 21.2. Quaternary aromatic carbon not visible.

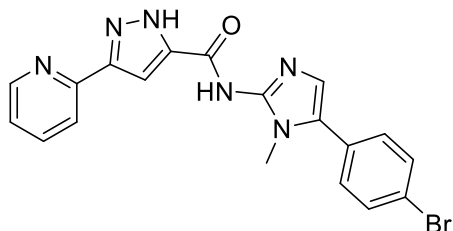
***N*-(5-Phenyloxazol-2-yl)cyclohexanecarboxamide (3.136)**



The title compound was obtained using cyclohexanecarboxylic acid (100 mg, 0.78 mmol) which was converted into its acid chloride equivalent following General Procedure D. Upon reaction completion the acid halide was concentrated *in vacuo*, taken up in DCM and added dropwise to a mixture of 5-phenyloxazol-2-amine (125 mg, 0.78 mmol), DIPEA (2.5 eq) and DCM at 0°C. The mixture was heated to 50°C and stirred over 12 h. Upon reaction completion the mixture was concentrated, washed with EtOAc and brine. The organic layers were dried over MgSO₄, filtered and concentrated. The crude mixture was purified via column chromatography (eluent: EtOAc: Petroleum ether, 1:1) to afford the title compound as an orange solid (44 mg, 21 %). HPLC – *t_R* 5.60 min > 99 % purity at 254 nm; LRMS [M+H]⁺ 271.1 *m/z*; HRMS [M+H]⁺ 271.1441 *m/z*, found 271.1444 *m/z*; ¹H NMR (400 MHz, MeOD) δ_H 7.68 – 7.62 (m, 2H), 7.46 – 7.39 (m, 2H), 7.35 – 7.29 (m, 2H), 2.54 – 2.34 (m, 1H), 1.96 – 1.69 (m, 5H), 1.61 – 1.47 (m, 2H), 1.43 – 1.24 (m, 3H); ¹³C NMR (101 MHz, MeOD) δ_C 176.2, 154.4, 148.7, 130.0 (2C), 129.3, 129.0, 124.7 (2C), 122.2, 46.4, 30.4 (2C), 26.8, 26.6 (2C).

Analogue Series 9

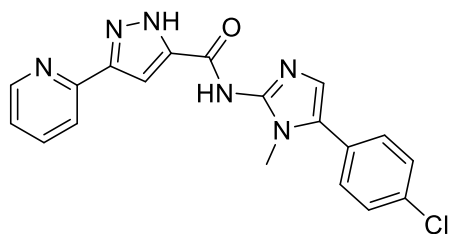
***N*-(5-(4-bromophenyl)-1-methyl-1*H*-imidazol-2-yl)-3-(pyridin-2-yl)-1*H*-pyrazole-5-carboxamide (3.137)**



The title compound was obtained using 5-(4-bromophenyl)-1-methyl-1*H*-imidazol-2-amine (250 mg, 1.0 mmol) and 3-(pyridin-2-yl)-1*H*-pyrazole-5-carboxylic acid (189 mg, 1.0 mmol) following General Procedure C, affording the title compound as a yellow solid (85 mg, 20 %). HPLC – *t_R* 4.54 min > 99 % purity at 254 nm; LRMS [M+H]⁺ 425.1 *m/z*; HRMS [M+H]⁺ 423.0563 *m/z*, found 423.0563 *m/z*; ¹H NMR (400 MHz, DMSO) δ 8.63 (d, *J* = 4.2 Hz, 1H), 8.02 – 7.86 (m, 2H), 7.73 – 7.68 (m, 2H), 7.57 – 7.50 (m, 2H), 7.44 – 7.34 (m, 2H), 7.15 (s, 1H), 3.57 (s, 3H). NH peaks too broad, not visible;

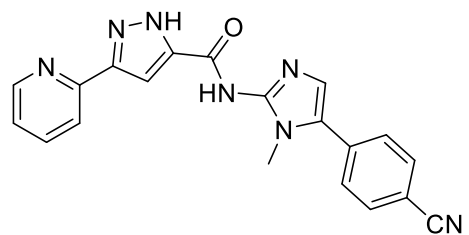
^{13}C NMR (101 MHz, DMSO) δ_{C} 149.3, 137.2, 131.8 (2C), 130.1 (2C), 128.0, 127.3, 123.0, 121.6, 119.9, 106.9, 104.7, 31.0. Aromatic quaternary carbons not visible.

***N*-(5-(4-Chlorophenyl)-1-methyl-1*H*-imidazol-2-yl)-3-(pyridin-2-yl)-1*H*-pyrazole-5-carboxamide (3.138)**



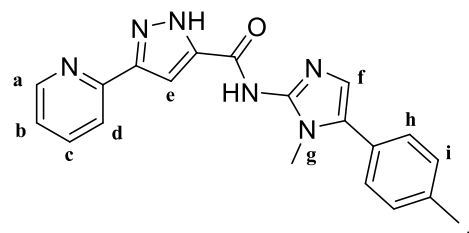
The title compound was obtained using 5-(4-chlorophenyl)-1-methyl-1*H*-imidazol-2-amine (100 mg, 0.48 mmol) and 3-(pyridin-2-yl)-1*H*-pyrazole-5-carboxylic acid (91 mg, 0.48 mmol) following General Procedure C to afford the title compound as a light pink solid (100 mg, 55 %). HPLC – t_{R} 4.45 min > 99 % purity at 254 nm; LRMS $[\text{M}+\text{H}]^+$ 379.1 m/z ; HRMS $[\text{M}+\text{H}]^+$ 379.1069 m/z , found 379.1078 m/z ; ^1H NMR (400 MHz, DMSO) δ 8.59 – 8.52 (m, 1H), 8.09 – 7.75 (m, 3H), 7.56 – 7.48 (m, 3H), 7.35 – 7.22 (m, 2H), 7.03 (s, 1H), 3.50 (s, 3H). N-H too broad, not visible. M.p. 276.3–278.8 °C.

***N*-(5-(4-cyanophenyl)-1-methyl-1*H*-imidazol-2-yl)-3-(pyridin-2-yl)-1*H*-pyrazole-5-carboxamide (3.140)**



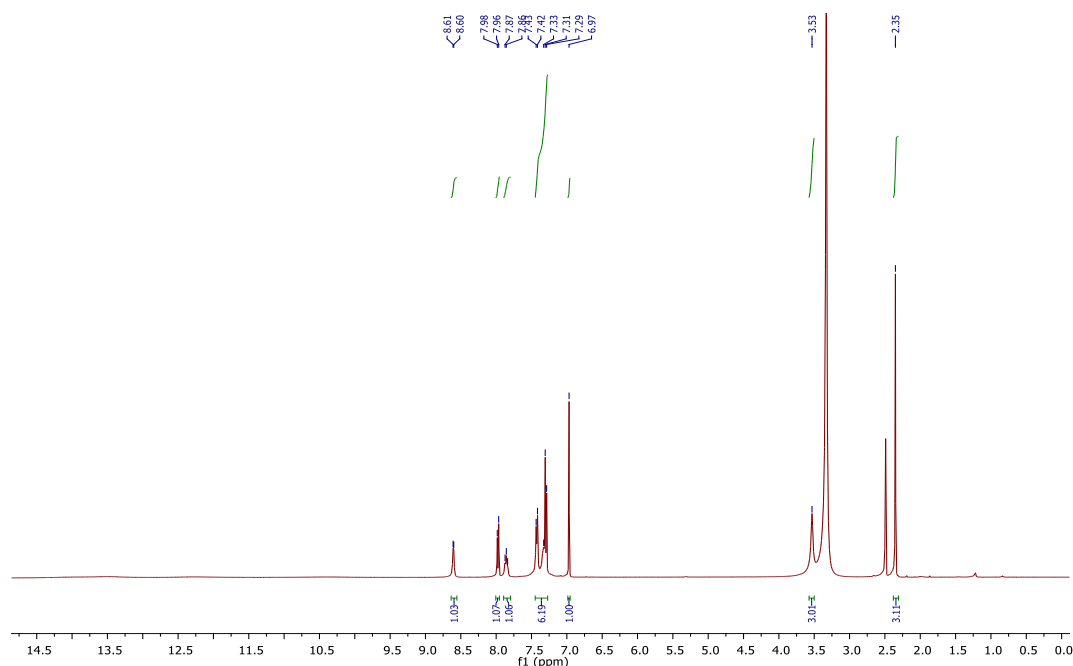
The title compound was obtained using 4-(2-amino-1-methyl-1*H*-imidazol-5-yl)benzonitrile (200 mg, 1.0 mmol) and 3-(pyridin-2-yl)-1*H*-pyrazole-5-carboxylic acid (189 mg, 1.0 mmol) following General Procedure C, affording the title compound as a white solid (92 mg, 25 %). HPLC – t_{R} 3.97 min > 99 % purity at 254 nm; LRMS $[\text{M}+\text{H}]^+$ 370.1 m/z ; HRMS $[\text{M}+\text{H}]^+$ 370.1411 m/z , found 370.1412 m/z ; ^1H NMR (400 MHz, DMSO) δ 8.62 (d, J = 4.2 Hz, 1H), 8.01 – 7.76 (m, 6H), 7.42 – 7.28 (m, 3H), 3.60 (s, 3H). N-H peaks too broad, not visible.

***N*-(1-methyl-5-(*p*-tolyl)-1*H*-imidazol-2-yl)-3-(pyridin-2-yl)-1*H*-pyrazole-5-carboxamide (3.141)**

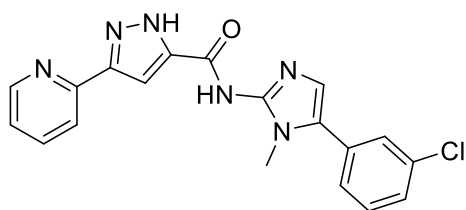


The title compound was obtained using 1-methyl-5-(*p*-tolyl)-1*H*-imidazol-2-amine (187 mg, 1.0 mmol) and 3-(pyridin-2-yl)-1*H*-pyrazole-5-carboxylic acid (189 mg, 1.0 mmol) following General Procedure C, affording the title compound as a white solid (125 mg, 25 %). HPLC – t_{R} 4.34 min > 99 % purity at 254 nm; LRMS $[\text{M}+\text{H}]^+$ 359.2 m/z ; HRMS $[\text{M}+\text{H}]^+$ 359.1615 m/z , found 359.1620 m/z ; ^1H NMR (400 MHz, DMSO) δ_{H} 8.60 (d, J = 3.9 Hz, 1H, Ha), 7.97 (d, J = 7.9 Hz, 1H, Hd), 7.86 (t, J = 7.2 Hz, 1H, Hc), 7.45 – 7.27 (m, 6H, Hb, He, Hh, Hi), 6.97 (s, 1H, Hf), 3.53 (s, 3H, Hg), 2.35 (s, 3H, Hj); ^1H NMR (400 MHz, MeOD) δ_{H} 8.66 (bs, 1H), 8.07 – 7.93 (m, 2H), 7.48 – 7.38 (m, 6H), 7.02 (s, 1H), 3.68 (s, 3H), 2.48 (s, 3H). N-H peaks not visible

Example spectra for Series 9 (Pyridine pyrazole hit 2.002 SAR investigation): ¹H NMR (400 MHz, DMSO) spectrum of *N*-(1-methyl-5-(*p*-tolyl)-1*H*-imidazol-2-yl)-3-(pyridin-2-yl)-1*H*-pyrazole-5-carboxamide (3.141)

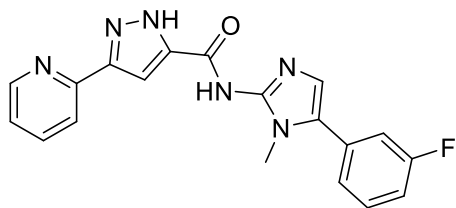


***N*-(5-(3-Chlorophenyl)-1-methyl-1*H*-imidazol-2-yl)-3-(pyridin-2-yl)-1*H*-pyrazole-5-carboxamide (3.142)**



The title compound was obtained following General Procedure C using 3-(pyridin-2-yl)-1*H*-pyrazole-5-carboxylic acid (100 mg, 0.50 mmol), 5-(3-chlorophenyl)-1-methyl-1*H*-imidazol-2-amine (100 mg, 0.48 mmol) and PyBop (250 mg, 0.5 mmol). The title compound was obtained as a white solid (20 mg, 11 %). HPLC – *t*_R 4.42 min > 99 % purity at 254 nm; LRMS [M+H]⁺ 379.1 *m/z*; HRMS [M+H]⁺ 379.1069 *m/z*, found 379.1075 *m/z*; ¹H NMR (400 MHz, DMSO) δ_H 8.61 – 8.58 (m, 1H), 7.96 (d, *J* = 7.9 Hz, 1H), 7.89 – 7.81 (m, 1H), 7.61 (bs, 1H), 7.53 – 7.30 (m, 5H), 7.11 (s, 1H). *N*-Me peak eclipsed by solvent peak, NH peaks not visible.

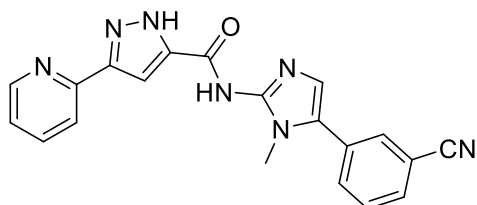
***N*-(5-(3-fluorophenyl)-1-methyl-1*H*-imidazol-2-yl)-3-(pyridin-2-yl)-1*H*-pyrazole-5-carboxamide (3.143)**



The title compound was obtained using 5-(3-fluorophenyl)-1-methyl-1*H*-imidazol-2-amine (191 mg, 1.0 mmol) and 3-(pyridin-2-yl)-1*H*-pyrazole-5-carboxylic acid (189 mg, 1.0 mmol) following General Procedure C, affording the title compound as a white solid (87 mg, 24 %). HPLC – *t*_R 4.15 min > 99 % purity at 254 nm; LRMS [M+H]⁺ 363.1 *m/z*; HRMS [M+H]⁺ 363.1364 *m/z*, found 363.1368 *m/z*; ¹H NMR (400 MHz, DMSO) δ_H 8.64

(d, $J = 4.7$ Hz, 1H), 8.00 (d, $J = 7.9$ Hz, 1H), 7.92 – 7.86 (m, 1H), 7.59 – 7.25 (m, 6H), 7.14 (s, 1H), 3.60 (s, 3H). NH peaks not visible.

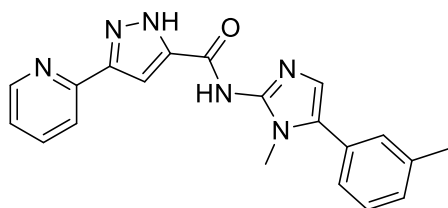
***N*-(5-(3-cyanophenyl)-1-methyl-1*H*-imidazol-2-yl)-3-(pyridin-2-yl)-1*H*-pyrazole-5-carboxamide (3.144)**



The title compound was obtained using 3-(2-amino-1-methyl-1*H*-imidazol-5-yl)benzonitrile (200 mg, 1.0 mmol) and 3-(pyridin-2-yl)-1*H*-pyrazole-5-carboxylic acid (189 mg, 1.0 mmol) following General Procedure C, affording the title compound as a red solid (40 mg, 11 %). HPLC – t_R

3.95 min > 99 % purity at 254 nm; LRMS $[M+H]^+$ 370.0 m/z ; HRMS $[M+H]^+$ 370.1411 m/z , found 370.1416 m/z ; 1H NMR (400 MHz, DMSO) δ_H 8.60 (d, $J = 4.4$ Hz, 1H), 8.05 (s, 1H), 7.97 (d, $J = 7.9$ Hz, 1H), 7.92 – 7.83 (m, 3H), 7.68 (t, $J = 7.8$ Hz, 1H), 7.37 – 7.31 (m, 2H), 7.18 (s, 1H), 3.57 (s, 3H). NH peaks not visible.

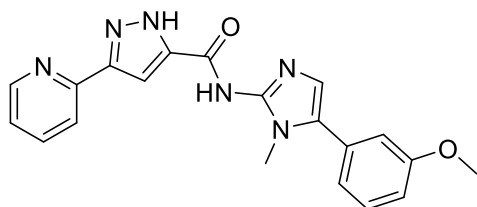
***N*-(1-methyl-5-(*m*-tolyl)-1*H*-imidazol-2-yl)-3-(pyridin-2-yl)-1*H*-pyrazole-5-carboxamide (3.145)**



The title compound was obtained using 1-methyl-5-(*m*-tolyl)-1*H*-imidazol-2-amine (187 mg, 1.0 mmol) and 3-(pyridin-2-yl)-1*H*-pyrazole-5-carboxylic acid (189 mg, 1.0 mmol) following General Procedure C, affording the title compound as a white fluffy solid. (106 mg, 30 %). HPLC – t_R 4.33 min >

99 % purity at 254 nm; LRMS $[M+H]^+$ 359.2 m/z ; HRMS $[M+H]^+$ 359.1615 m/z , found 359.1622 m/z ; 1H NMR (400 MHz, MeOD) δ_H 8.60 (s, 1H), 8.10 – 7.83 (m, 2H), 7.48 – 7.20 (m, 6H), 7.11 – 6.87 (m, 1H), 3.63 (s, 3H), 2.43 (s, 3H); 1H NMR (400 MHz, DMSO) δ_H 8.57 (bs, 1H), 8.03 – 7.76 (m, 2H), 7.53 – 7.07 (m, 6H), 6.96 (s, 1H), 2.33 (s, 3H). *N*-Me peak eclipsed by solvent peak.

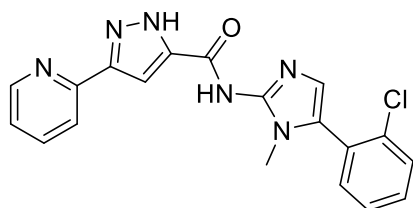
***N*-(5-(3-methoxyphenyl)-1-methyl-1*H*-imidazol-2-yl)-3-(pyridin-2-yl)-1*H*-pyrazole-5-carboxamide (3.146)**



The title compound was obtained using 5-(3-methoxyphenyl)-1-methyl-1*H*-imidazol-2-amine (200 mg, 1.0 mmol) and 3-(pyridin-2-yl)-1*H*-pyrazole-5-carboxylic acid (189 mg, 1.0 mmol) following General Procedure C, affording the title compound as a solid. (120 mg, 32 %)

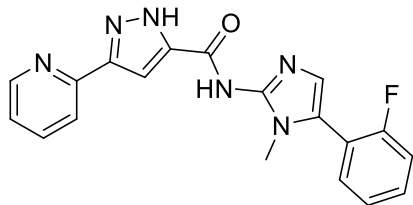
HPLC – t_R 4.18 min > 99 % purity at 254 nm; LRMS $[M+H]^+$ 375.2 m/z ; HRMS $[M+H]^+$ 375.1564 m/z , found 375.1570 m/z ; 1H NMR (400 MHz, MeOD) δ_H 8.65 (s, 1H), 8.13 – 7.91 (m, 2H), 7.52 – 7.35 (m, 3H), 7.20 – 7.03 (m, 4H), 3.91 (s, 3H), 3.69 (s, 3H).

***N*-(5-(2-chlorophenyl)-1-methyl-1*H*-imidazol-2-yl)-3-(pyridin-2-yl)-1*H*-pyrazole-5-carboxamide (3.147)**



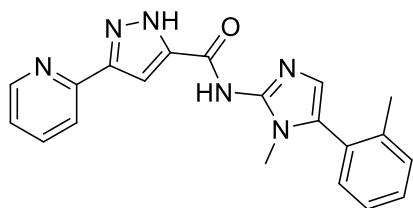
The title compound was obtained following General Procedure C using 3-(pyridin-2-yl)-1*H*-pyrazole-5-carboxylic acid (100 mg, 0.5 mmol), 5-(2-chlorophenyl)-1-methyl-1*H*-imidazol-2-amine (100 mg, 0.48 mmol) and PyBop (250 mg, 0.5 mmol). The title compound was obtained as a white solid (35 mg, 20 %). HPLC – t_R 4.27 min > 95 % purity at 254 nm; LRMS $[M+H]^+$ 379.1 m/z ; HRMS $[M+H]^+$ 379.1069 m/z , found 379.1074 m/z ; 1H NMR (400 MHz, MeOD) δ_H 8.67 – 8.54 (m, 1H), 8.11 – 8.02 (m, 1H), 7.92 – 7.88 (m, 1H), 7.66 – 7.35 (m, 6H), 7.00 (s, 1H), 3.48 (s, 3H).

***N*-(5-(2-fluorophenyl)-1-methyl-1*H*-imidazol-2-yl)-3-(pyridin-2-yl)-1*H*-pyrazole-5-carboxamide (3.148)**



The title compound was obtained using 5-(2-fluorophenyl)-1-methyl-1*H*-imidazol-2-amine (191 mg, 1.0 mmol) and 3-(pyridin-2-yl)-1*H*-pyrazole-5-carboxylic acid (189 mg, 1.0 mmol) following General Procedure C, affording the title compound as a white solid (54 mg, 15 %). HPLC – t_R 4.08 min > 99 % purity at 254 nm; LRMS $[M+H]^+$ 363.1 m/z ; HRMS $[M+H]^+$ 363.1364 m/z , found 363.1169 m/z ; 1H NMR (400 MHz, DMSO) δ_H 8.63 (d, J = 3.2 Hz, 1H), 7.99 (d, J = 7.9 Hz, 1H), 7.92 – 7.86 (m, 1H), 7.57 – 7.51 (m, 2H), 7.43 – 7.33 (m, 4H), 7.04 (s, 1H). N-Me eclipsed by solvent peak, N-H peaks too broad, not visible

***N*-(1-methyl-5-(*o*-tolyl)-1*H*-imidazol-2-yl)-3-(pyridin-2-yl)-1*H*-pyrazole-5-carboxamide (3.149)**



The title compound was obtained using 1-methyl-5-(*o*-tolyl)-1*H*-imidazol-2-amine (187 mg, 1.0 mmol) and 3-(pyridin-2-yl)-1*H*-pyrazole-5-carboxylic acid (189 mg, 1.0 mmol) following General Procedure C, affording the title compound as a white solid. (72 mg, 20 %). HPLC – t_R 4.19 min > 99 % purity at 254 nm; LRMS $[M+H]^+$ 359.1 m/z ; HRMS $[M+H]^+$ 359.1615 m/z , found 359.1622 m/z ; 1H NMR (400 MHz, MeOD) δ_H 8.62 – 8.60 (m, 1H), 8.01 – 7.97 (m, 1H), 7.90 (td, J = 7.7, 1.7 Hz, 1H), 7.45 – 7.32 (m, 6H), 6.90 (s, 1H), 3.40 (s, 3H), 2.28 (s, 3H); ^{13}C NMR (101 MHz, MeOD) δ_C 150.3, 147.5, 139.8, 138.6, 132.5, 131.5, 130.9, 127.2, 124.3, 121.6, 107.9, 105.8, 30.5, 20.0. Aromatic quaternary carbons not visible excluding tolyl group.

3.24 Chapter 3 References

1. Chen M-H, Chuang S-H, Chen Y-J, Chang L-H, Li T-H, Chen C-H, et al. Novel tubulin inhibitors and methods of using the same. WO 2012092471 A2, 2012.
2. Ermolat'ev DS, Van der Eycken EV. A Divergent Synthesis of Substituted 2-Aminoimidazoles from 2-Aminopyrimidines. *J Org Chem*. 2008;73(17):6691-6697.
3. Ermolat'ev DS, Babaev EV, Van der Eycken EV. Efficient One-Pot, Two-Step, Microwave-Assisted Procedure for the Synthesis of Polysubstituted 2-Aminoimidazoles. *Org Lett*. 2006;8(25):5781-5784.
4. Richter J, Bischof J, Zaja M, Kohlhof H, Othersen O, Vitt D, et al. Difluoro-dioxolo-benzoimidazol-benzamides As Potent Inhibitors of CK1 δ and ϵ with Nanomolar Inhibitory Activity on Cancer Cell Proliferation. *J Med Chem*.. 2014;57(19):7933-7946.
5. Mowbray CE, Braillard S, Speed W, Glossop PA, Whitlock GA, Gibson KR, et al. Novel Amino-pyrazole Ureas with Potent In Vitro and In Vivo Antileishmanial Activity. *J Med Chem*. 2015;58(24):9615-9624.
6. Shin JY, Wang Y-L, Yamada SA, Hung ST, Fayer MD. Imidazole and 1-Methylimidazole Hydrogen Bonding and Nonhydrogen Bonding Liquid Dynamics: Ultrafast IR Experiments. *J Phys Chem B*. 2019;123(9):2094-2105.
7. Huang X, Xu S, Tan Q, Gao M, Li M, Xu B. A copper-mediated tandem reaction through isocyanide insertion into N-H bonds: efficient access to unsymmetrical tetrasubstituted ureas. *Chem Commun*. 2014;50(12):1465-1468.
8. Treu M, Karner T, Reiser U. Preparation of substituted indolinones with antiproliferative activity. WO 2010012747 A1, 2010.
9. Li Y, Shen M, Zhang Z, Luo J, Pan X, Lu X, et al. Design, Synthesis, and Biological Evaluation of 3-(1H-1,2,3-Triazol-1-yl)benzamide Derivatives as Potent Pan Bcr-Abl Inhibitors Including the Threonine315 \rightarrow Isoleucine315 Mutant. *J Med Chem*.. 2012;55(22):10033-10046.
10. De Keersmaecker S, De Vos D, Ermolatev D, Steenackers H, Van der Eycken E, Vanderleyden J, et al. Compounds, compositions and methods for controlling biofilms. US 20130029981 A1, 2013.
11. Ermolat'ev DS, Svidritsky EP, Babaev EV, Van der Eycken E. Microwave-assisted synthesis of substituted 2-amino-1H-imidazoles from imidazo[1,2-a]pyrimidines. *Tetrahedron Lett*. 2009;50(37):5218-5220.
12. Zhou Q, Du F, Shi Y, Fang T. Synthesis and analysis of 1-methyl-4-phenyl-1H-imidazol-2-amine. *J Chem Res*. 2018;42(12):608-610.
13. Guo P, Wang Z, Li G, Liu Y, Xie Y, Wang Q. First Discovery of Polycarpine, Polycarpaurines A and C, and Their Derivatives as Novel Antiviral and Antiphytopathogenic Fungus Agents. *J Agric Food Chem*. 2016;64(21):4264-4272.

14. Beesu M, Caruso G, Salyer ACD, Shukla NM, Khetani KK, Smith LJ, et al. Identification of a Human Toll-Like Receptor (TLR) 8-Specific Agonist and a Functional Pan-TLR Inhibitor in 2-Aminoimidazoles. *J Med Chem*. 2016;59(7):3311-3330.
15. Trabanco-Suarez AA, Tresadern GJ, Vega Ramiro, JA; Cid-Nunez JM. Imidazo[1,2-a]pyridine derivatives and their use as positive allosteric modulators of mGluR2 receptors. WO 2009062676 A2, 2009.
16. Guo P, Yan S, Hu Z, Zhuang W, Xiong Y, Zhang L, et al. Efficient Preparation of Alkaloids Polycarpine and Polycarpaurines A and C. *J Heterocycl Chem*. 2017;54(1):121-124.
17. Alifanov VL, Babaev EV. Novel and Efficient Synthesis of 2-Aminooxazoles from Pyrimidin-2(1H)-one. *Synthesis*. 2007;2007(02):263-270.
18. Koch P, Laufer S. Unexpected Reaction of 2-Alkylsulfanylimidazoles to Imidazol-2-ones: Pyridinylimidazol-2-ones as Novel Potent p38 α Mitogen-Activated Protein Kinase Inhibitors. *J Med Chem*. 2010;53(12):4798-4802.
19. Ding J, Cao F-D, Geng Y-R, Tian Y, Li P, Li X-F, et al. Synthesis and in vitro anti-epileptic activities of novel [1,2,4]-triazolo[1,5-a]pyrimidin-7(4H)-one derivatives. *J Asian Nat Prod Res*. 2019;21(12):1190-1204.
20. Atkinson AJ, Wang J, Zhang Z, Gold A, Jung D, Zeng D, et al. Grafting of bioactive 2-aminoimidazole into active layer makes commercial RO/NF membranes anti-biofouling. *J Memb Sci*. 2018;556:85-97.
21. Shilatifard A, Liang K, Smith ER. Therapeutic targeting of interleukin-1 receptor-associated kinase 4 (IRAK4) in cancers characterized by rearrangements in the mixed lineage leukemia gene (MLL-r). US 20170305901 A1, 2017.
22. Lezama-Dávila CM, Isaac-Márquez AP, Kapadia G, Owens K, Oghumu S, Beverley S, et al. Leishmanicidal activity of two naphthoquinones against *Leishmania donovani*. *Biol Pharm Bull*. 2012;35(10):1761-1764.
23. Álvarez-Velilla R, Gutiérrez-Corbo MDC, Punzón C, Pérez-Pertejo MY, Balaña-Fouce R, Fresno M, et al. A chronic bioluminescent model of experimental visceral leishmaniasis for accelerating drug discovery. *PLoS Negl Trop Dis*. 2019;13(2):e0007133.
24. Zahid MS, Johnson M, Varma D, Ainslie K. Infecting THP-1 Macrophages with *Leishmania donovani* (Ds-Red-lux) and evaluating by Luciferase assay. [Unpublished data] Eshelman School of Pharmacy, University of North Carolina at Chapel Hill; 2019.
25. Stockert JC, Horobin RW, Colombo LL, Blázquez-Castro A. Tetrazolium salts and formazan products in Cell Biology: Viability assessment, fluorescence imaging, and labeling perspectives. *Acta Histochem*. 2018;120(3):159-167.
26. Chiu H-C, Kulp SK, Soni S, Wang D, Gunn JS, Schlesinger LS, et al. Eradication of Intracellular *Salmonella enterica* Serovar Typhimurium with a Small-Molecule, Host Cell-Directed Agent. *Antimicrob Agents Chemother*. 2009;53(12):5236-5244.

27. Lipinski CA, Lombardo F, Dominy BW, Feeney PJ. Experimental and computational approaches to estimate solubility and permeability in drug discovery and development settings IPII of original article: S0169-409X(96)00423-1. The article was originally published in *Adv Drug Deliv Rev* 23 (1997) 3–25.1. *Adv Drug Deliv Rev*. 2001;46(1):3-26.
28. Veber DF, Johnson SR, Cheng H-Y, Smith BR, Ward KW, Kopple KD. Molecular Properties That Influence the Oral Bioavailability of Drug Candidates. *J Med Chem*. 2002;45(12):2615-2623.
29. Lovering F, Bikker J, Humblet C. Escape from Flatland: Increasing Saturation as an Approach to Improving Clinical Success. *J Med Chem*. 2009;52(21):6752-6756.
30. Paloque L, Vidal N, Casanova M, Dumètre A, Verhaeghe P, Parzy D, et al. A new, rapid and sensitive bioluminescence assay for drug screening on *Leishmania*. *J Microbiol Methods*. 2013;95(3):320-323.
31. De Rycker M, Hallyburton I, Thomas J, Campbell L, Wyllie S, Joshi D, et al. Comparison of a High-Throughput High-Content Intracellular *Leishmania donovani* Assay with an Axenic Amastigote Assay. *Antimicrob Agents Chemother*. 2013;57(7):2913-2922.
32. Paape D, Bell AS, Heal WP, Hutton JA, Leatherbarrow RJ, Tate EW, et al. Using a Non-Image-Based Medium-Throughput Assay for Screening Compounds Targeting *N*-myristoylation in Intracellular *Leishmania* Amastigotes. *PLoS Negl Trop Dis*. 2014;8(12):e3363.
33. Van den Kerkhof M, Mabile D, Chatelain E, Mowbray CE, Braillard S, Hendrickx S, et al. In vitro and in vivo pharmacodynamics of three novel antileishmanial lead series. *Int J Parasitol Drugs Drug Resist*. 2018;8(1):81-86.
34. Gupta S, Yardley V, Vishwakarma P, Shivahare R, Sharma B, Launay D, et al. Nitroimidazoxazole compound DNDI-VL-2098: an orally effective preclinical drug candidate for the treatment of visceral leishmaniasis. *J Antimicrob Chemother*. 2014;70(2):518-527.
35. Lamotte S, Aulner N, Späth GF, Prina E. Discovery of novel hit compounds with broad activity against visceral and cutaneous *Leishmania* species by comparative phenotypic screening. *Sci Rep*. 2019;9(1):438.
36. DNDi. NTD Drug Discovery Booster Hit-to-lead [Internet]. [cited 2020 August 4]. Available from: <https://www.dndi.org/diseases-projects/open-innovation/drug-discovery-booster/>.
37. Dagley MJ, Saunders EC, Simpson KJ, McConville MJ. High-content assay for measuring intracellular growth of *Leishmania* in human macrophages. *Assay Drug Dev Technol*. 2015;13(7):389-401.
38. Duffy S, Sykes ML, Jones AJ, Shelper TB, Simpson M, Lang R, et al. Screening the Medicines for Malaria Venture Pathogen Box across Multiple Pathogens Reclassifies Starting Points for Open-Source Drug Discovery. *Antimicrob Agents Chemother*. 2017;61(9) e00379-17.

39. Phan T-N, Baek K-H, Lee N, Byun SY, Shum D, No JH. In Vitro and in Vivo Activity of mTOR Kinase and PI3K Inhibitors Against *Leishmania donovani* and *Trypanosoma brucei*. *Molecules*. 2020;25(8):1980.
40. Thermo Fisher Scientific. DRAQ5™ Fluorescent Probe Solution [Internet]. [cited 2020 August 4]. Available from: <https://www.thermofisher.com/order/catalog/product/62251#/62251>.
41. Saunders E, McConville M. 1 year milestones –Investigating the mode of action and antiparasite drugs. [Unpublished data] The Bio21 Institute of Molecular Science and Biotechnology, Department of Biochemistry and Molecular Biology, The University of Melbourne; 2018
42. De Muylder G, Ang KKH, Chen S, Arkin MR, Engel JC, McKerrow JH. A Screen against *Leishmania* Intracellular Amastigotes: Comparison to a Promastigote Screen and Identification of a Host Cell-Specific Hit. *PLoS Negl Trop Dis*. 2011;5(7):e1253.
43. Goyard S, Segawa H, Gordon J, Showalter M, Duncan R, Turco SJ, et al. An in vitro system for developmental and genetic studies of *Leishmania donovani* phosphoglycans. *Mol Biochem Parasitol*. 2003;130(1):31-42.
44. Hendrickx S, Van Bockstal L, Caljon G, Maes L. In-depth comparison of cell-based methodological approaches to determine drug susceptibility of visceral *Leishmania* isolates. *PLoS Negl Trop Dis*. 2019;13(12):e0007885.
45. Jain SK, Sahu R, Walker LA, Tekwani BL. A parasite rescue and transformation assay for antileishmanial screening against intracellular *Leishmania donovani* amastigotes in THP1 human acute monocytic leukemia cell line. *J Vis Exp*. 2012(70):4054.
46. Verma JK, Rastogi R, Mukhopadhyay A. *Leishmania donovani* resides in modified early endosomes by upregulating Rab5a expression via the downregulation of miR-494. *PLoS Pathog*. 2017;13(6):e1006459.
47. Yang Z, Mosser DM, Zhang X. Activation of the MAPK, ERK, following *Leishmania amazonensis* infection of macrophages. *J Immunol*. 2007;178(2):1077-1085.
48. Ryckmans T, Edwards MP, Horne VA, Correia AM, Owen DR, Thompson LR, et al. Rapid assessment of a novel series of selective CB2 agonists using parallel synthesis protocols: A Lipophilic Efficiency (LipE) analysis. *Bioorg Med Chem Lett*. 2009;19(15):4406-4409.
49. Murray CW, Erlanson DA, Hopkins AL, Keserü GM, Leeson PD, Rees DC, et al. Validity of ligand efficiency metrics. *ACS Med Chem Lett*. 2014;5(6):616-618.
50. Marroquin LD, Hynes J, Dykens JA, Jamieson JD, Will Y. Circumventing the Crabtree effect: replacing media glucose with galactose increases susceptibility of HepG2 cells to mitochondrial toxicants. *Toxicol Sci*. 2007;97(2):539-547.
51. Shum D et al. HepG2 Crabtree Cytotoxicity screening Standard Operating Procedure. [Unpublished data] Institut Pasteur Korea, Seongnam, South Korea; 2021.

52. Bevan CD, Lloyd RS. A High-Throughput Screening Method for the Determination of Aqueous Drug Solubility Using Laser Nephelometry in Microtiter Plates. *Anal Chem.* 2000;72(8):1781-1787.
53. Lombardo F, Shalaeva MY, Tupper KA, Gao F. ElogDoct: A Tool for Lipophilicity Determination in Drug Discovery. 2. Basic and Neutral Compounds. *J Med Chem.* 2001;44(15):2490-2497.
54. Ring BJ, Chien JY, Adkison KK, Jones HM, Rowland M, Jones RD, et al. PhRMA CPCDC initiative on predictive models of human pharmacokinetics, part 3: Comparative assessment of prediction methods of human clearance. *J Pharm Sci.* 2011;100(10):4090-4110.
55. Obach RS. Prediction of human clearance of twenty-nine drugs from hepatic microsomal intrinsic clearance data: An examination of in vitro half-life approach and nonspecific binding to microsomes. *Drug Metab Dispos.* 1999;27(11):1350-1359.
56. Li F, Chen L, Kang Q, Cai J, Zhu G. Regioselective N-alkylation with alcohols for the preparation of 2-(N-alkylamino)quinazolines and 2-(N-alkylamino)pyrimidines. *New J Chem.* 2013;37(3):624-631.
57. Soh CH, Chui WK, Lam Y. An Efficient and Expeditious Synthesis of Di- and Monosubstituted 2-Aminoimidazoles. *J Comb Chem.* 2008;10(1):118-122.
58. Steenackers HPL, Ermolat'ev DS, Savaliya B, De Weerd A, De Coster D, Shah A, et al. Structure–Activity Relationship of 4(5)-Aryl-2-amino-1H-imidazoles, N1-Substituted 2-Aminoimidazoles and Imidazo[1,2-a]pyrimidinium Salts as Inhibitors of Biofilm Formation by *Salmonella Typhimurium* and *Pseudomonas aeruginosa*. *J Med Chem.* 2011;54(2):472-484.
59. Zhou Q, Du F, Shi Y, Fang T, Chen G. Synthesis and Analysis of 1-Methyl-4-Phenyl-1H-Imidazol-2-Amine. *J Chem Res.* 2018;42(12):608-610.

Chapter 4: Exploration of new scaffolds for parallel hit-to-lead investigations

4.01 New Compound Class Investigation

As our initial chemotype has produced quite a library of analogues, during the waiting period between biological assessments, we decided to focus our attention toward other chemotypes for parallel hit-to-lead investigations. Once again, we sourced our antileishmanial hits from Pena *et al.* choosing four potential candidates (**Figure 4.01**).¹ Outlined in Chapter 1, these candidates were chosen based on their potent antileishmanial activity and low toxicity within the phenotypic screen. Briefly, the low molecular weight (< 500 Da), appropriate Log P range and the number of hydrogen bond donors and acceptors all fit within Lipinski's Rule of Five, suggesting drug-like properties.² The low polar surface area and number of rotatable bonds (<10) also align with Veber's rule, another guideline for drug-likeness.³ These collective properties were quite attractive starting points for a medicinal chemistry hit-to-lead campaign. Based on the small molecular weight and low to mid ranging Log P (<500 Da, <5 respectively) it could also be possible to add a variety of larger substituents to the scaffolds if needed, whilst still abiding by these guidelines on oral drug-likeness. The low IFI (promiscuity index) was also an attractive property, where the low IFI values suggest that selectivity issues may not arise majorly in the future. Excluding **4.001**, the chosen hits show higher antiparasitic activity in the MAC (intramacrophage) orthogonal assay than they do in the simple primary fluorescent intensity assay (FLINT) readout. This seemed promising to us, as the increased potency observed within the more biologically relevant intramacrophage assay suggested true activity.

Potency within the orthogonal intramacrophage assay conveyed that these chosen compounds seemed to have a real ability to cross the various physiological barriers; namely macrophage, phagolysosomal and leishmanial membranes, to exert inhibitory effects against the parasite. The compound mode of action and biological target is not yet known, therefore the binding site/s referred to within this chapter are more of a presumed concept used to help define SAR pathway of these scaffolds. Our aims for these scaffolds were to confirm the true activity within the hit, determine any key interactions with the putative binding site/s using a small library of analogues and gain further insights on the chemical modifications needed to improve antileishmanial potency. Future work involving a more optimized lead compound may allow for the elucidation of the compound's mode of action and/or target biological site.

Each one of the hits was individually resynthesized to confirm activity. Various synthetic pathways were established and optimized to obtain these hits, which is discussed below. The relative synthetic ease in accessing most of these hits was another key desirable feature endorsing these hits for potential hit-to-lead campaigns. As a result, a small number of analogues were also synthesized per hit, only

allowing for simple modifications to the relevant scaffold. Making use of these newly devised synthetic pathways, these small sets of analogues aimed to confirm whether certain chemical moieties were necessary for activity and begin to form potential SAR pathways around each compound class. After the resynthesis of each hit, confirming activity was necessary to decide on whether to pursue an individual series further or to set aside for the time being.

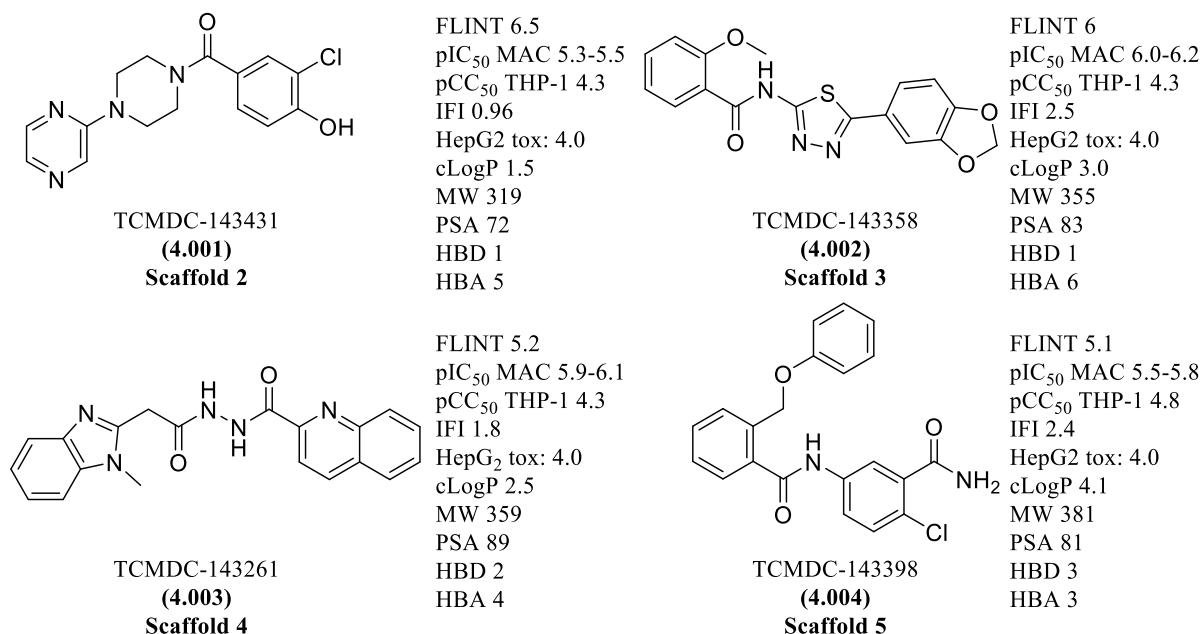


Figure 4.01: Chosen hits resynthesized for new hit-to-lead investigation

4.02 Scaffold 2 Exploration

To obtain the phenyl pyrazinyl methanone hit compound **4.001** and related analogues, a synthetically simple pathway was devised, following **Scheme 4.01**. The readily available 2-(piperazin-1-yl)pyrazine/ piperazine related compound underwent amide coupling with the chosen benzoic acids, achieved in good yield.^{4,5} Room temperature was initially trialled, but increasing the temperature saw an improved ability for efficiently pushing the reaction to completion and thus achieving hit **4.001** in high yield. The use of EDCI/ HOBt coupling agents is commonly used within medicinal chemistry, though for interested readers, the mechanism has been included in the Appendix

Scheme 4.01: Synthetic pathway for hit compound **4.001**



Reaction conditions: i) 3-chloro-4-hydroxybenzoic acid, DIPEA, HOBt, EDCI, ACN, 50°C

The structure of the hit was confirmed with LCMS and ^1H NMR analysis. The ^1H NMR spectrum of hit **4.001** is depicted in **Figure 4.02**, where each proton signal can be observed excluding the OH proton, which has presumably broadened out and is not visible. Based on structurally close analogues **4.009**, **4.010** and **4.034** discussed below, the OH peak of hit **4.001** is expected as a downfield singlet at approximately 10.0-11.0 ppm. The complete characterisation of each compound is reported in the Experimental section of this chapter. Key peaks used to confirm the formation of **4.001** include the aliphatic peaks of the piperazine are observed as overlapping broad singlets at 3.72 and 3.65 ppm (peaks G and H of **Figure 4.02**) along with all aromatic peaks present and accounted for within the aromatic region. The doublet centred at 7.06 ppm, which is the most upfield signal within the aromatic region (F) most likely belongs to the proton *ortho* to the electron donating hydroxy group causing a shielding effect. Furthermore, key peaks correlating to the starting materials, namely the carboxylic acid OH and piperazine NH (**4.000**) were not observed. This indicated the amide coupling of **Scheme 4.01** occurred successfully. According to the literature these peaks were expected as a broad singlet downfield at approximately 12.79 ppm and as an upfield singlet at approximately 1.88 ppm respectively.^{6, 7} The complete peak assignment for this spectrum and the corresponding ^{13}C NMR spectrum for **4.001** is also depicted in the Experimental section along with other sets of spectra for key example analogues/ hits within Chapter 4.

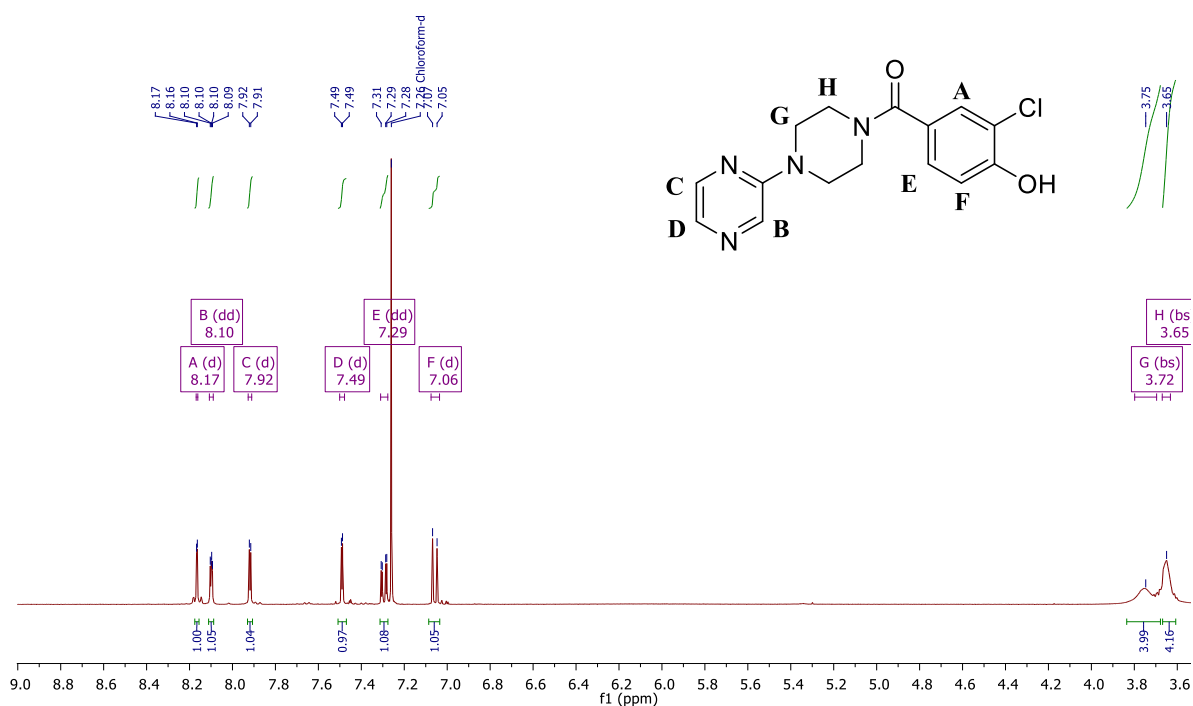


Figure 4.02: ^1H NMR spectrum of hit **4.001** performed in CDCl_3 confirming the correct structure of the hit

Initially, we decided to keep the analogues surrounding **4.001** to a small number as the reconfirmation of the hit was the higher priority. The initial analogues were kept simple, exploring the necessity of the 3-chloro and 4-hydroxy RHS substituents by removing them (**4.005-4.006**) and swapping their positions

(**4.007**). Removing the 3-chloro (**4.005**) would remove the electron withdrawing effect around the ring and cause a loss of lipophilicity and molecular refractivity in this chemical space. This would determine whether such properties were required to maintain activity. Removing the 4-hydroxy substituent (**4.006**) would remove the electron donating ability into the aromatic ring, as well as potential hydrogen bonding interactions (donating and accepting) with the putative binding site.

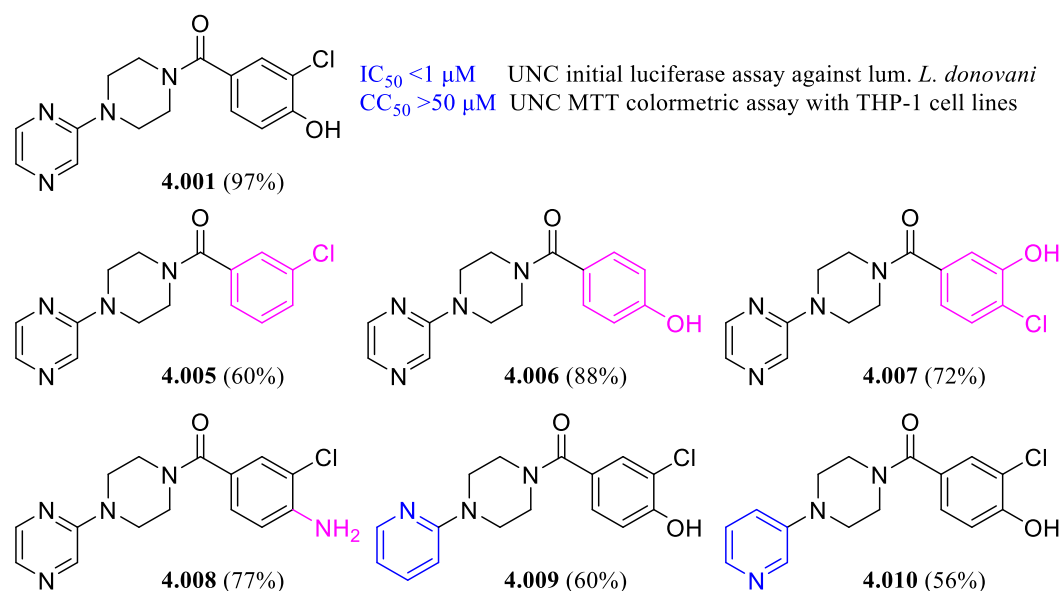


Figure 4.03: Initial analogues surrounding phenyl pyrazinyl methanone compound class (Scaffold 2) including yields from Scheme 4.01 and biological activity of hit **4.001**

Compound **4.007** was devised in order to understand whether the potential interactions made by the 3-chloro and 4-hydroxyl substituents were flexible or distant dependant within the binding site. Additionally, the 4-hydroxy was replaced with another electron donating substituent, also capable of forming hydrogen bond interactions with the binding site/s (**4.008**). This was undertaken in order to define whether such properties were required at this position. Finally, the pyrazine was replaced with 2-[N] and 3-[N] pyridines (**4.009-10**) to evaluate the heteroatom requirements of the LHS aromatic ring, and whether the change in electronics and orientation around this ring still allowed for a continued fit and interactions within the putative binding site/s. To obtain the analogues listed above in **Figure 4.03**, **Scheme 4.01** was followed, acquiring each compound successfully in high yield. The individual yields for each compound are also listed in **Figure 4.03**.

The antileishmanial activity of these compounds was initially assessed using the luciferase assay against a strain of *L. donovani* expressing firefly luciferase and a red fluorescent protein, LUC and DsRed2. The cytotoxicity of these compounds was explored using uninfected THP-1 cell lines in a colorimetric MTT assay.^{8, 9, 10-12} These assays were performed by our collaborators of the Ainslie group at the University of North Carolina and have been previously described in Chapter 3. These methods are also

outlined in the Experimental section of this chapter. Orthogonal intracellular assays performed by Bio21 and IPK were used to confirm activity. These assays employ fluorescent staining and high content imaging of the assay plates to determine the number of parasites within host macrophages. These assays have also been previously detailed in Chapter 3. Preliminary results from UNC first assessed the hit **4.001** alone to confirm the activity of this hit. This original hit was initially found to have potent antileishmanial activity ($MIC_{50} < 1 \mu M$, half minimum inhibitory concentration 50%) and low host cell cytotoxicity ($> 50 \mu M$). This was undertaken using a concentration range of 1-50 μM . Further testing using both the same concentration and lower concentration range (0.1-10 μM) to get a more accurate IC_{50} value was required along with evaluating the remaining analogues. During this time, further analogues around this compound class were synthesized as we had believed potent activity was established around the hit **4.001**.

The next set of analogues synthesized are listed in **Figure 4.04**, where most of the compounds were obtained following **Scheme 4.01** in moderate to high yield. The individual yields for each analogue are also summarized in **Figure 4.04**. To acquire analogues **4.016-4.018**, **4.021**, extra synthetic steps were required, which is also indicated in **Figure 4.04**. Their synthetic pathways are detailed below in **Schemes 4.02-4.04**. Analogues **4.011-4.018** focused on altering the RHS benzyl substituents to further probe the chemical space requirements. Compound **4.011** was synthesized to probe whether a more electronegative halogen was preferred over the *meta*-chloro at this position of the ring. Introduction of the fluoro atom would allow for increased hydrogen bonding accepting ability as well as decrease molecular refractivity at this site. Analogue **4.012** was devised in order to investigate whether the loss of H-donating ability was unfavorable, and if this interaction was key to maintaining antileishmanial activity. Analogue **4.013** was designed to explore whether these RHS benzyl substitutions were required at all, attempting to understand if specific interactions at these positions exist. Repositioning the hydroxy (**4.014**) would probe whether any H-bonding interactions formed with the binding site were distant dependant and could form stronger or weaker interactions depending on the position around the ring. Analogue **4.015** focused on the addition of a second chloro group to probe whether increased electron withdrawing ability was favoured for this system, and whether increased interactions could be formed with the binding site/s. Analogue **4.016** possesses a methylamine substituent in place of the hydroxyl group. This analogue was designed to probe whether the substituted electron donating amine substituent was preferred. This substituent would maintain hydrogen bonding ability though introducing a small protecting group would probe whether small lipophilic groups were preferred.

Compounds **4.017-4.018** were the final analogues aimed at investigating the RHS benzyl substitution. These analogues were devised in order to probe whether an aromatic group at this position of the chemical space was tolerated within the putative binding site/s. This functionality would probe whether an increase in lipophilicity and steric bulk was favourable, and whether any additional interactions such as pi-pi stacking could be made with the putative binding site/s. Finally, analogues **4.019-4.021** focused

on altering the LHS pyrazine ring in order to gauge the more favoured position of the heteroatoms, as well as decipher whether these heteroatoms were required at all.

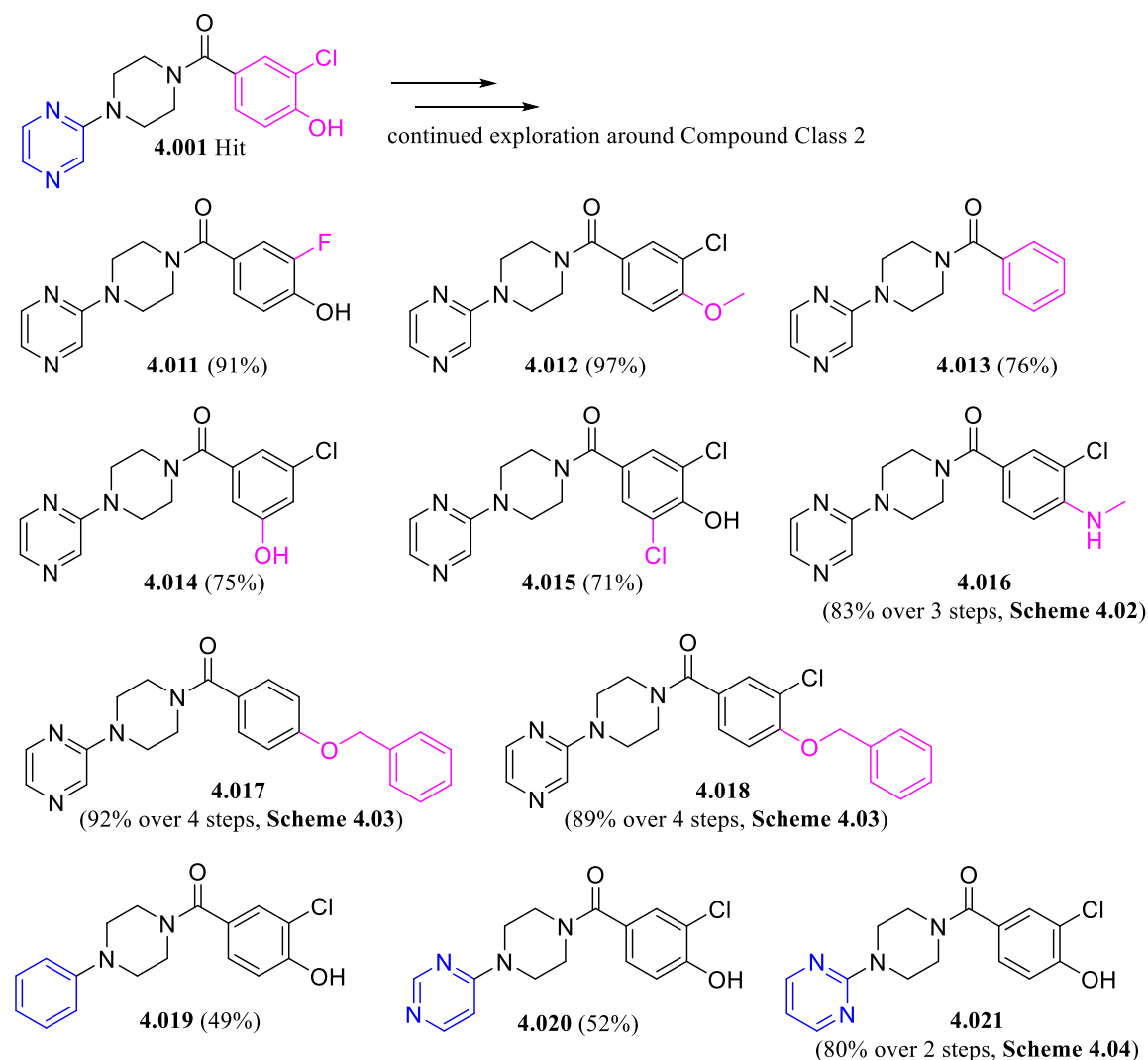
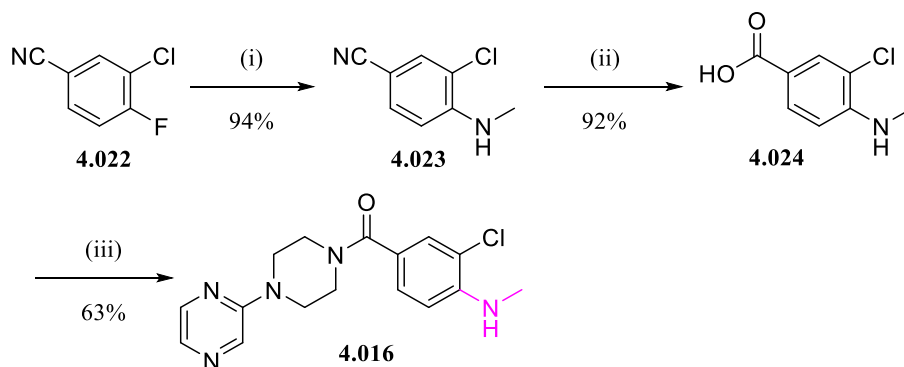


Figure 4.04: Further exploration of analogues surrounding hit **4.001** and their respective yields utilizing **Scheme 4.01** or **Schemes 4.02-4.04** where appropriate

As summarized in **Figure 4.04**, most of the analogues (**4.011-4.015**, **4.019-4.020**) followed the simple synthetic route described in **Scheme 4.01**, whilst the remaining set of analogues required extra synthetic steps to obtain the desired compounds, discussed below.

To attain analogue **4.016**, which possesses the methylamine group in place of the hydroxyl substituent, **Scheme 4.02** was devised. This pathway begins with the nucleophilic aromatic substitution of **4.022** to form 3-chloro-4-(methylamino)benzonitrile (**4.023**).¹³ Subsequent nitrile hydrolysis under basic conditions occurs leading to carboxylic acid formation (**4.024**).¹³ Compound **4.024** can then undergo amide coupling with the readily available 2-(piperazin-1-yl)pyrazine to successfully acquire the desired analogue **4.016**.⁵ Each step of **Scheme 4.02** was accomplished successfully in moderate to high yield, obtaining the desired analogue with synthetic ease.

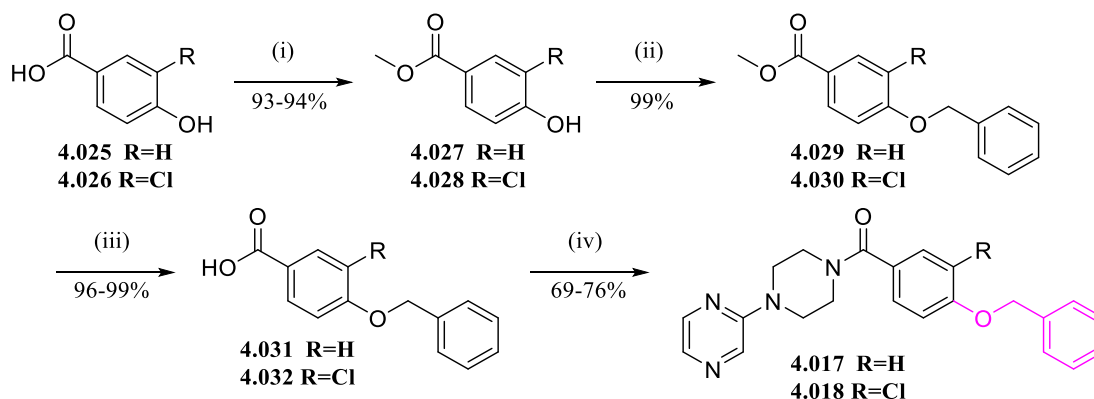
Scheme 4.02: Synthetic pathway for analogue 4.016



Reaction conditions: i) MeNH₂ in H₂O, THF, 65 °C, ii) NaOH, H₂O, reflux, iii) 2-(piperazin-1-yl)pyrazine, DIPEA, HOBT, EDCI, ACN, 50°C

Compounds **4.017-4.018** were the final analogues synthesized to investigate the RHS benzyl substitution. **Scheme 4.03** was utilized to obtain these compounds and was modelled off the initial benzyl substitutions used for analogues **2.052-2.054** of **Scheme 2.05**, Chapter 2. The hydroxybenzoic acids (**4.025-4.026**) underwent Fischer esterification to form the corresponding methyl esters (**4.027-4.028**).^{14, 15} This was followed by subsequent benzylation to form the benzyl ether (**4.029-4.030**) and saponification to remove the methyl ester, freeing up the carboxylic acid intermediates (**4.031-4.032**) for amide coupling with the 2-(piperazin-1-yl)pyrazine to successfully obtain analogues **4.017-4.018**.^{5, 16, 17} Each step was achieved successfully in overall high yields.

Scheme 4.03: Synthetic pathway for analogue 4.017 and 4.018

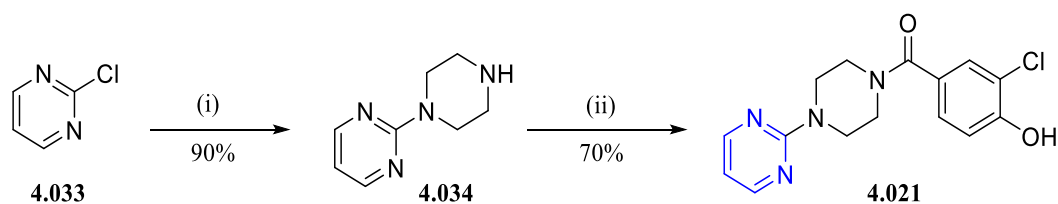


Reaction conditions: i) H₂SO₄, MeOH, reflux, ii) benzylbromide, K₂CO₃, ACN, 60 °C, iii) NaOH, MeOH/ H₂O (1:2), 65 °C, iv) 2-(piperazin-1-yl)pyrazine, DIPEA, HOBT, EDCI, ACN, 50°C

To target analogues altering the LHS aromatic ring of Scaffold 2, compounds **4.019-4.020** also followed **Scheme 4.01**, as mentioned in **Figure 4.04**. However, to obtain analogue **4.021** an extra synthetic step was required following **Scheme 4.04** to install the pyrimidine ring in place of the pyrazine. Altering the positions of the heteroatoms around the LHS ring would gauge which arrangement of heteroatoms was preferred. **Scheme 4.04** begins with 2-chloropyrimidine (**4.033**), which underwent nucleophilic

substitution with piperazine to form the piperinylpyrimidine building block (**4.034**).¹⁸ Subsequent amide coupling occurred to successfully producing analogue **4.021**.⁵

Scheme 4.04: Synthetic pathway for analogue 4.021



Reaction conditions: i) piperazine, K₂CO₃, H₂O, reflux, ii) 3-chloro-4-hydroxybenzoic acid, DIPEA, HOBt, EDCI, ACN, 50°C

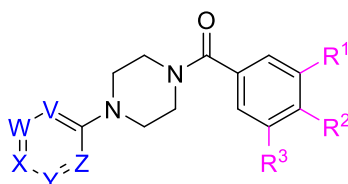
4.03 Scaffold 2 Biological results

The hit **4.001** was re-evaluated using the same luciferase assay against luminescence expressing *L. donovani* along with the complete library around Scaffold 2. The luciferase assay was undertaken at a lower concentration (0.1–10 μ M) in order to attain a more accurate IC₅₀ value for hit **4.001**. Upon reassessment, it was found that the hit **4.001** and the vast majority of analogues designed around this scaffold were completely ineffective against *L. donovani*. Only **4.018** was found to have some modest activity (15 μ M) within the luciferase assay. After consulting with our biologists, it was difficult to say exactly why hit **4.001** reported different IC₅₀ values between the initial screen and reassessment. They suggest this may be due to differences in infectivity of the THP-1 cells based on the passage number of cells or of *Leishmania*. Another possibility is that the parasites may not have been at the optimum growth phase during infection, which could have led to *Leishmania* overgrowth and over-infection of the host cell. This can cause THP-1 cell detachment and decreased luminescence, potentially causing the initial false positive. However, these are merely plausible suggestions and the exact cause remains unknown. Further study into the biological variability between screens may be required, though this is outside the scope of this thesis. Nonetheless, this library was confirmed inactive by the orthogonal high content screening assay performed by IPK. Previously described in Chapter 3, this assay employs an intracellular imaging assay, where infected THP-1 macrophages are treated with the investigational compounds over a 72-hour period before applying fluorescent stains to the assay plate. High content imaging of the assay plates is able to define the boundaries of the macrophage and parasites within.

Using this assay, no significant activity against *L. donovani* was reported for analogue **4.018**, suggesting another potential false positive. In an effort to quickly gauge and narrow down any true antileishmanial activity, the Bio21 biological high content screening was performed at a high one-point concentration (50 μ M) for this library. This was described previously in Chapter 3. Control compounds miltefosine and amphotericin B were also employed within the high one-point drug concentration HTS, strong antileishmanial activity was demonstrated by the control drugs, though an IC₅₀ value could not be

generated, since only one concentration was used. Their methods employ a similar intracellular imaging assay to IPK, where the *L. donovani* amastigote infected macrophages are treated with the compounds of interest over a 72-hour period, before fluorescent staining and high content imaging allow for the ability to identify the number of parasites within viable macrophage host cells. Each biological method has been detailed in Chapters 2 and 3, as well as outlined in the Experimental section.

Table 4.01: Complete summary of biological results for Scaffold 2. The hit 4.001 is highlighted in blue.



	Structure								HCS intracellular assay against <i>L. donovani</i>				Luciferase /MTT assay	
I.D	LHS					RHS			Bio21 ^{ab}		IPK ^{cd}		UNC ^{ef}	
	V	W	X	Y	Z	R ¹	R ²	R ³	IC ₅₀ (μM)	CC ₅₀ (μM)	IC ₅₀ (μM)	CC ₅₀ (μM)	IC ₅₀ (μM)	CC ₅₀ (μM)
4.001 HIT	N	CH	CH	N	CH	Cl	OH	H	>50	>50	>100	>100	>10 ^g	>50 ^g
4.005	N	CH	CH	N	CH	Cl	H	H	>50	>50	>100	>100	>50	>50
4.006	N	CH	CH	N	CH	H	OH	H	>50	>50	>100	>100	>50	>50
4.007	N	CH	CH	N	CH	OH	Cl	H	>50	>50	>100	>100	>20	>50
4.008	N	CH	CH	N	CH	Cl	NH ₂	H	>50	>50	>100	>100	>20	>50
4.009	N	CH	CH	CH	CH	Cl	OH	H	>50	>50	>100	>100	>50	>50
4.010	CH	CH	CH	N	CH	Cl	OH	H	>50	>50	>100	>100	>20	>50
4.011	N	CH	CH	N	CH	F	OH	H	>50	>50	>100	>100	>50	>50
4.012	N	CH	CH	N	CH	Cl	OMe	H	>50	>50	>100	>100	>50	>50
4.013	N	CH	CH	N	CH	H	H	H	>50	>50	>100	>100	>50	>50
4.014	N	CH	CH	N	CH	Cl	H	OH	>50	>50	>100	>100	>50	>50
4.015	N	CH	CH	N	CH	Cl	OH	Cl	>50	>50	>100	>100	>50	>50
4.016	N	CH	CH	N	CH	Cl	NHMe	H	>50	>50	>100	>100	>20	>50
4.017	N	CH	CH	N	CH	H	OBnz	H	>50	>50	>100	>100	>50	>50
4.018	N	CH	CH	N	CH	Cl	OBnz	H	>50	>50	86	50	15	>50
4.019	CH	CH	CH	CH	CH	Cl	OH	H	>50	>50	>100	>100	>20	>50
4.020	N	CH	N	CH	CH	Cl	OH	H	>50	>50	>100	>100	>20	>50
4.021	N	CH	CH	CH	N	Cl	OH	H	>50	>50	>100	>100	>20	>50

a= anti *L. donovani* activity and toxicity measured in THP-1 transformed macrophage host cell lines using a one-point concentration (50 μM) to assess any form of antileishmanial activity. Experiment performed in duplicate wells in one experiment, n=1.

b= control compounds for Bio21 intramacrophage *L. donovani* assay. Miltefosine IC₅₀=0.62 ± 0.16 μM, CC₅₀> 100 μM, Amphotericin B IC₅₀= 1.0 ± 0.74 μM, CC₅₀= 55 ± 19 μM.

c= anti *L. donovani* activity and toxicity measured in THP-1 transformed macrophage host cell lines using a top concentration of 100 μM (2x serial dilution 10-point curve). Experiment performed in duplicate wells in one experiment, n=1.

d= control compounds for IPK intramacrophage *L. donovani* assay. Miltefosine IC₅₀= 1.7 μM, CC₅₀ >100 μM, Amphotericin B IC₅₀= 0.83 μM, CC₅₀ > 100 μM.

e= anti *L. donovani* activity measured in THP-1 transformed macrophage host cell lines using luminescent expressing *L. donovani*. Experiment performed in triplicate wells in one experiment, n=1 using a concentration range of 1-50 μM. DMSO was used as sole control against which the percent *L. donovani* viability is calculated

f= host cell toxicity measured in MTT assay with uninfected macrophage host cells. Experiment performed in triplicate wells in one experiment, n=1 using a concentration range of 1-50 μM. DMSO was used as sole control against which the percent cell viability is calculated

g= this compound was initially found active at a higher concentration and retested here, at lower concentration to achieve a more accurate IC₅₀ (concentration range: 0.1-10 μM)

Each compound within this library was also found to be completely inactive within this high concentration one-point assay. Our biological testing strategy had initially planned to perform the initial one-point concentration assay to narrow down potential compounds of interest which showed any form of antileishmanial activity at this concentration, then repeat the assay using the usual 10-point dilution curve with a concentration range of 0.2-100 μ M. However, seeing as there was no antileishmanial behaviour at such a high concentration associated with this library, no further assessment was required. It seemed that the hit **4.001** may have been a false positive, as it exhibited no activity towards *L. donovani* inhibition in all intramacrophage assays. No solubility issues were reported by our collaborators during these biological assessments, therefore the inability to remain in solution to allow for cell permeation was not to blame here. It may be that it has a bimodal mechanism of action and was not able to exert antileishmanial behaviour within these assays, as such a window for activity may indeed exist. Nevertheless, seeing as not a single analogue was found to have any form of activity across all biological assays, regardless of how small the modification to the hit, further exploration around this scaffold was ceased. This would allow us to spend more time on a compound class with more obvious and buildable SAR with the aims of achieving a less complicated antileishmanial lead candidate with true potency.

4.04 Scaffold 3 Exploration

In parallel to the investigation surrounding TCMDC-143431 (**4.001**), we also began explorations surrounding the phenyl thiadiazolebenzamide compound class (Scaffold 3), starting with resynthesizing the hit TCMDC-143358 (**4.002**) which is re-illustrated in **Figure 4.05**.

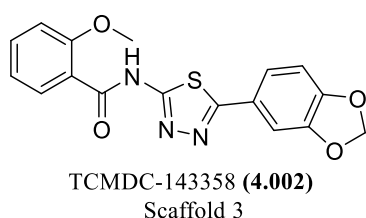


Figure 4.05: Structure of hit 4.002

In order to precure this compound, **Scheme 4.05** was devised. Beginning with 3,4-dihydroxybenzaldehyde (**4.035**), this starting reagent was first converted successfully to the benzodioxole carbaldehyde intermediate (**4.036**) using diiodomethane.¹⁹ Following the literature, dibromomethane and dichloromethane were also individually trialed in place of diiodomethane using similar conditions outlined in step i of **Scheme 4.05**.^{20, 21, 22} However, no reaction occurred as confirmed by LCMS and ¹H NMR analysis, thus the use of diiodomethane was endorsed for any future analogues employing step i of **Scheme 4.05** since it allowed for reaction completion to occur cleanly, also confirmed by ¹H NMR analysis, which is shown below in **Figure 4.06**. In **Figure 4.06**, peak E was the key signal used to identify the formation of **4.036**. This singlet indicated the presence of the aliphatic

methylene of the desired benzo[d][1,3]dioxole ring, where the high chemical shift was due to the adjacent O atoms, deshielding the protons of the methylene. The most downfield signal, peak A was assigned to the aldehyde proton, where the effects of magnetic anisotropy (non-uniform magnetic field) of this π system caused deshielding and high a chemical shift.²³ Finally, all aromatic peaks were accounted for, indicating the desired **4.036** had formed successfully. This spectrum is consistent with the literature reported for this known compound.²⁴

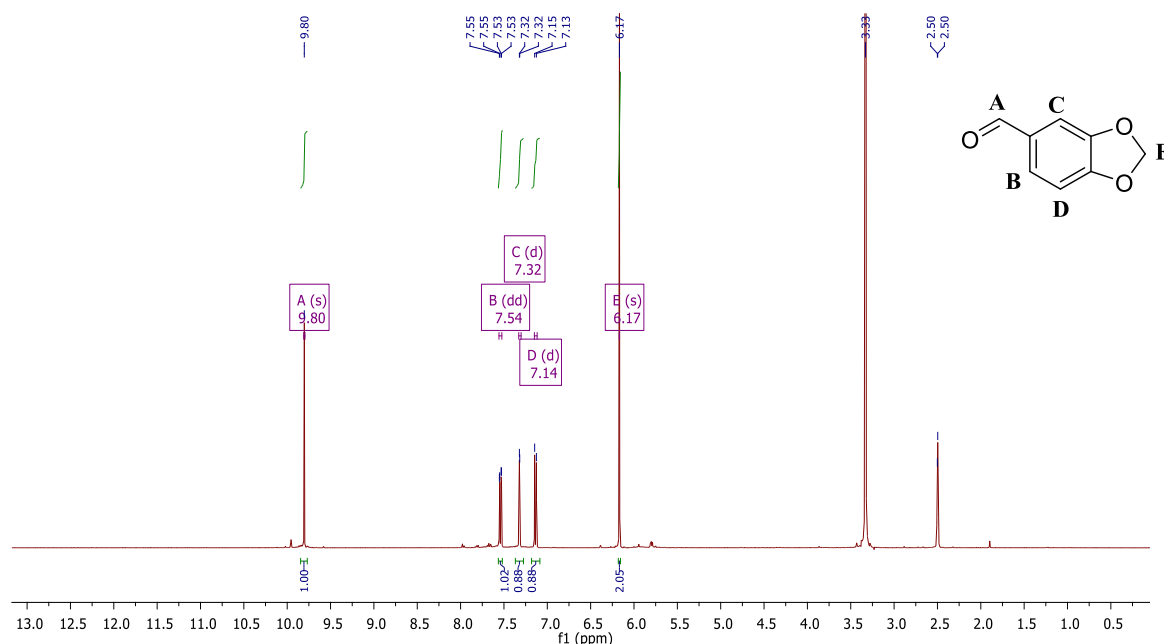
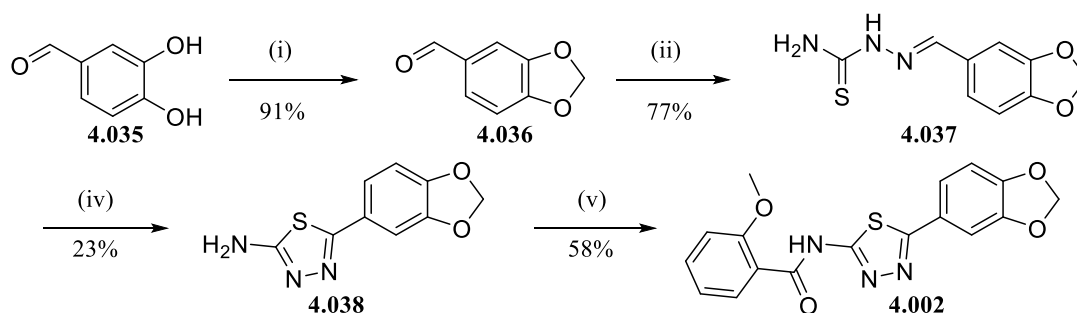


Figure 4.06: ^1H NMR spectrum of intermediate **4.036** performed in DMSO, confirming the correct structure of this intermediate

After the confirmed formation of compound **4.036**, the carbaldehyde functional group was used to install the 1,3-benzodioxol-5-ylmethylideneamino thiourea (**4.037**) which underwent subsequent intramolecular cyclization to form the five membered thiadiazole amine (**4.038**).^{25, 26} A low yield was observed during this step, if continued exploration around this scaffold was required this step would require further optimization. Finally, the amine underwent amide bond formation with 2-methoxybenzoyl chloride to obtain the hit (**4.002**).

Scheme 4.05: Synthetic pathway to obtain TCMDC-143358 (4.002**) and analogue **4.039****



Reaction conditions: i) Diiodomethane, K_2CO_3 , DMF, reflux 110°C , ii) thiosemicarbazide, AcOH, EtOH, iii) $\text{FeCl}_3 \cdot 6\text{H}_2\text{O}$, EtOH, reflux, iv) 2-methoxybenzoyl chloride, DIPEA, DCM

Using LCMS and ^1H NMR analysis the hit **4.002** was confirmed. The ^1H NMR spectrum of **4.002** is depicted below in **Figure 4.07**, where each proton peak of the structure is observed. The key signals confirming the formation of **4.002** included the downfield amide N-H singlet correlating to peak A, which is observed at 11.27 ppm. The deshielding effect is caused by the hydrogen bonding and proximity of the proton to the π system of the carbonyl group, overall contributing to the downfield chemical shift.²³ The loss of the previously observed broad singlet at 7.31 ppm (Chapter 4 Experimental section), corresponding to the NH_2 of starting material **4.038** further indicates the amide bond formation was successful. Other signals that confirm the formation of **4.002** include the aliphatic singlets I and J at chemical shifts 6.04 and 4.13 ppm respectively, signifying the presence of the methylene of the RHS benzo[*d*][1,3]dioxole ring and the methyl of the LHS *ortho*-methoxy group respectively. The presence of all aromatic protons further indicates the amide bond formation between the amine **4.038** and acid chloride building blocks was successful, and the desired hit was formed. The complete ^1H NMR and ^{13}C NMR spectra along with the peak assignments for **4.002** are included the Experimental section of this chapter.

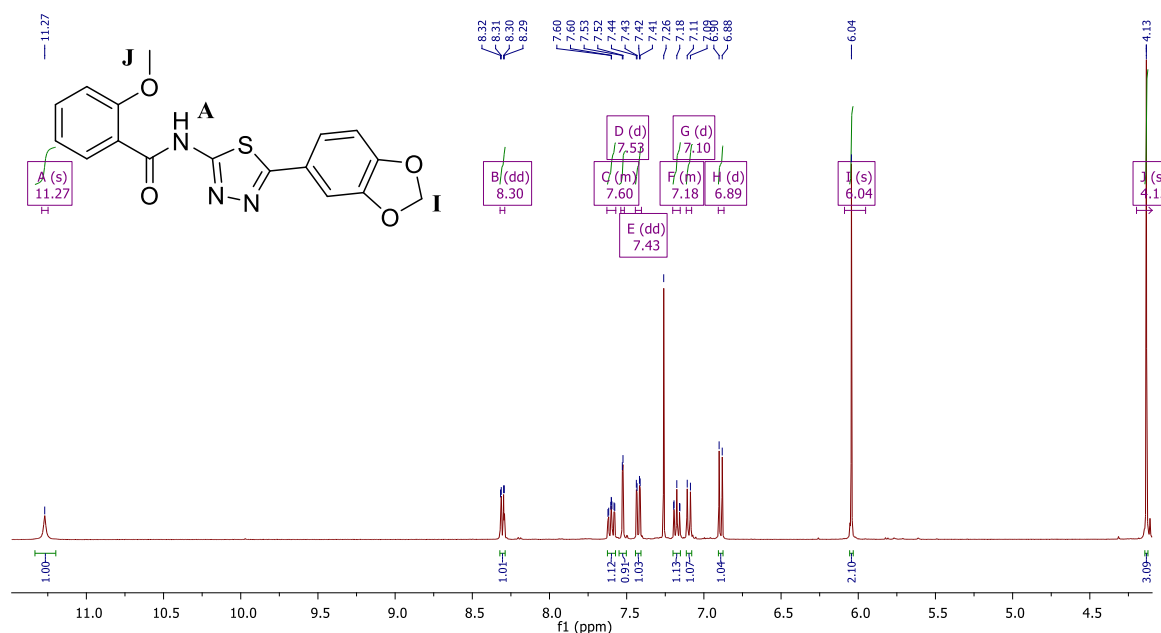


Figure 4.07: ^1H NMR spectrum of hit **4.002** performed in CDCl_3 confirming the correct structure of the hit

In the process of developing the synthetic pathway of hit **4.002**, analogue **4.039** depicted in **Figure 4.08** was also synthesized following **Scheme 4.05** as a model to further validate the pathway. This analogue would assess whether the dioxole RHS was required to maintain activity, and if the bare aromatic ring still allowed for key interactions to be made with the putative binding site/s. After the false positive result seen with the hit **4.001**, we were cautious around building a large library too quickly. No further analogues were synthesized around Scaffold 3 pending biological results.

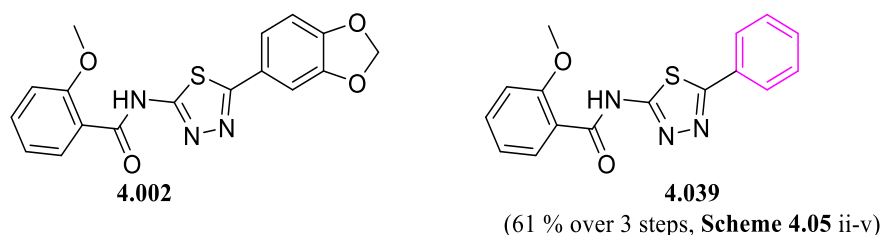


Figure 4.08: Initial exploration surrounding the benzodioxol thiadiazol methoxybenzamide hit **4.002**

4.05 Scaffold 3 Biological Results

These compounds underwent the same biological testing conditions against *L. donovani* as described above, in Section 4.04. Similar to the previous scaffold above, this phenyl thiadiazolebenzamide class (Class 3) was determined inactive against *L. donovani* across all the assays employed. The hit **4.002** may also be another false positive from the original HTS. Once again, no solubility issues around these compounds was reported, therefore the issue of a potentially potent compound being unable to exert its effect due to poor solubility and thus poor permeability is not relevant here. Rather than expending further effort around this scaffold, further studies around Scaffold 3 were paused. Investigations moved on to focus on other compound classes, looking for more obvious activity to build a clear SAR pathway.

Table 4.02: Complete summary of biological results for Scaffold 3, hit 4.002 outlined in blue.

I.D	HCS intracellular assay against <i>L. donovani</i>				Luciferase /MTT assay	
	Bio21 ^{ab}		IPK ^{cd}		UNC ^{ef}	
	IC ₅₀ (μM)	CC ₅₀ (μM)	IC ₅₀ (μM)	CC ₅₀ (μM)	IC ₅₀ (μM)	CC ₅₀ (μM)
4.002 Hit	>50	>50	>100	>100	>50	>50
4.039	>50	>50	>100	>100	>50	>50

a= anti *L. donovani* activity and toxicity measured in THP-1 transformed macrophage host cell lines using a one-point concentration (50 μM) to assess any form of antileishmanial activity. Experiment performed in duplicate wells in one experiment, n=1.

b= control compounds for Bio21 intramacrophage *L. donovani* assay. Miltefosine IC₅₀=0.62 ±0.16 μM, CC₅₀> 100 μM, Amphotericin B IC₅₀= 1.0 ±0.74 μM, CC₅₀= 55 ± 19 μM.

c= anti *L. donovani* activity and toxicity measured in THP-1 transformed macrophage host cell lines using a top concentration of 100 μM (2x serial dilution 10-point curve). Experiment performed in duplicate wells in one experiment, n=1.

d= control compounds for IPK intramacrophage *L. donovani* assay. Miltefosine IC₅₀= 1.7 μM, CC₅₀ >100 μM, Amphotericin B IC₅₀= 0.83 μM, CC₅₀ > 100 μM.

e= anti *L. donovani* activity measured in THP-1 transformed macrophage host cell lines using luminescent expressing *L. donovani*. Experiment performed in triplicate wells in one experiment, n=1 using a concentration range of 1-50 μM. DMSO was used as sole control against which the percent *L. donovani* viability is calculated

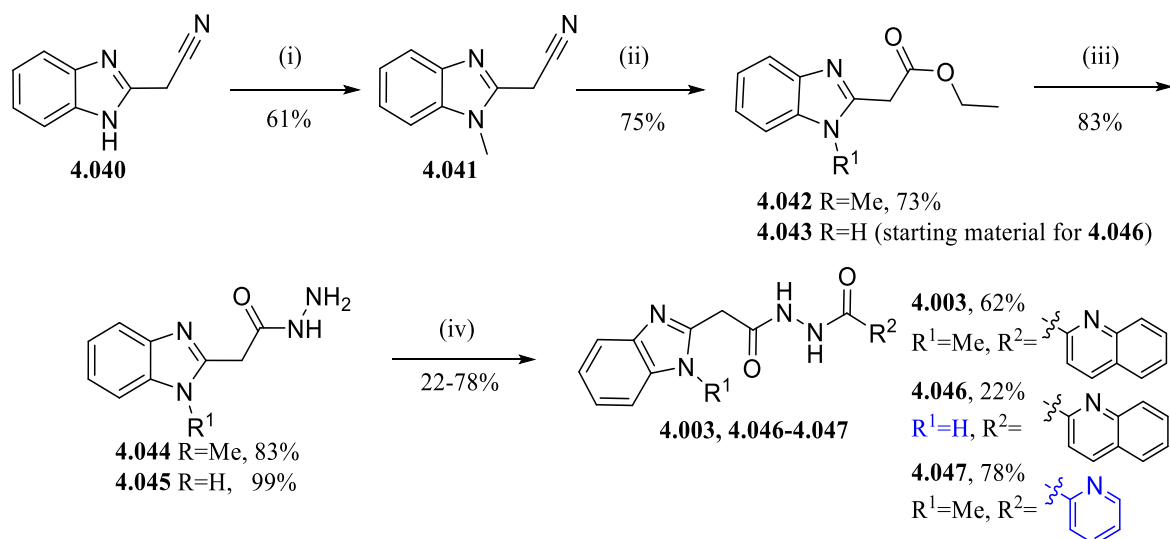
f= host cell toxicity measured in MTT assay with uninfected macrophage host cells. Experiment performed in triplicate wells in one experiment, n=1 using a concentration range of 1-50 μM. DMSO was used as sole control against which the percent cell viability is calculated

4.06 Scaffold 4 Exploration

Exploration surrounding the benzimidazole quinoline carbohydrazide hit TCMDC-143261 (**4.003**) was also pursued in parallel to the above compound classes. The study around this compound class began with the resynthesis of hit **4.003**, which is described below in Scheme 4.06. The synthetic route started with the benzimidazole acetonitrile (**4.040**), which underwent *N*-methylation to form the methylbenzimidazol-2-yl acetonitrile (**4.041**).²⁷ Following Innes *et al.*, the nitrile group (**4.041**) was

then transformed into the ethyl ester (**4.042**), using acetyl chloride and ethanol.²⁸ Following Akhtar *et al.* the formation of the ester (**4.042**) allowed for the installation of the hydrazide (**4.044**) using hydrazine hydrate.²⁹ The hydrazide then underwent amide coupling with quinaldic acid using conditions taken from the literature to successfully form the desired hit **4.003** in moderate yield.

Scheme 4.06: Synthetic pathway to obtain hit 4.003 and analogues 4.046-4.047



Reaction conditions: i) dimethylsulfate, NaOH, H₂O, 30°C, ii) acetyl chloride, EtOH, reflux, iii) hydrazine hydrate, EtOH, reflux, iv) quinaldic acid or picolinic acid, DIPEA, HOBt, EDCI, ACN/THF, 50°C

The hit **4.003** was confirmed with LCMS and ¹H NMR analysis. The ¹H NMR spectrum is depicted in **Figure 4.09**, where all proton signals are clearly observed using DMSO as the solvent. All aromatic peaks are present, suggesting that the amide coupling of the hydrazide **4.044** and quinaldic acid was successful. The most downfield of the aromatic signals (C) most likely belongs to the proton *para* to the nitrogen of the quinoline, where the heteroatom causes a downfield shift via a resonance effect. Other obvious handles were the aliphatic peaks, where the *N*-methyl singlet and methylene singlet that appear at 3.81 (J) and 4.02 (I) ppm respectively. Finally, the broader downfield singlets at 10.73 and 10.54 ppm, indicate both the N-H peaks of the hydrazide (A and B). The deshielding effect that occurs in the hydrogen bond causes these peaks to appear downfield and have a high chemical shift. Additionally, the proximity to the carbonyl group which is a π system that causes magnetic anisotropy and further deshielding of the N-H protons.²³ The presence of both downfield N-H peaks along with the loss of the broad singlet corresponding to the hydrazide **4.044** NH₂, previously observed at 4.33 ppm further indicated successful amide bond formation had occurred and the desired **4.003** was obtained. The complete spectrum and assignment of **4.003** is depicted in the Experimental section along with the ¹³C NMR spectrum and assignment.

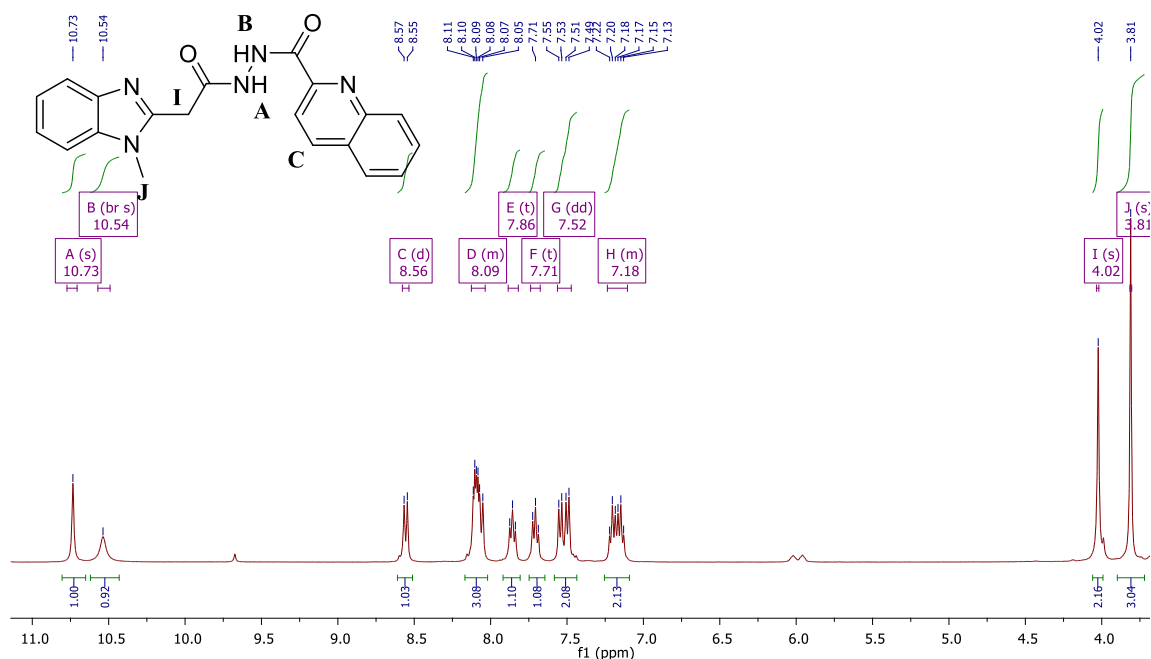


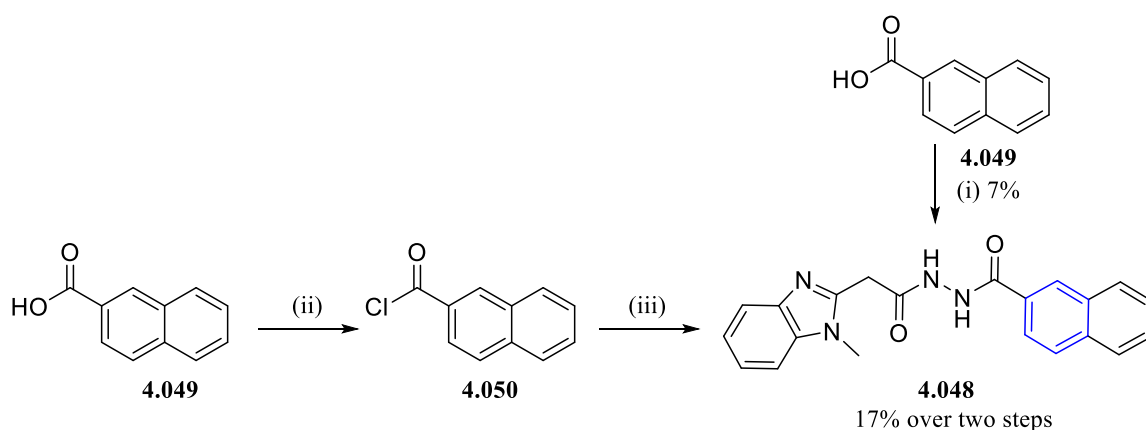
Figure 4.09: ^1H NMR spectrum of hit **4.003** performed in DMSO confirming the correct structure of the hit

A small number of analogues were synthesized surrounding **4.003**, utilizing the above synthetic pathway described in **Scheme 4.06**. The number of analogues devised was kept low, as confirming the true antileishmanial properties within the hit was a higher priority. Once again structural alterations around the scaffold were relatively simple, to confirm whether certain chemical moieties were required to maintain activity in comparison to the hit. This would help build an SAR pathway for any future studies. Compound **4.046** was synthesized to determine if the *N*-methyl group was required to maintain activity and was obtained starting with the readily available benzimidazole ethyl ester **4.043**, which was converted into the hydrazide (**4.045**) in excellent yield. This was followed by subsequent amide coupling to acquire analogue **4.046** in decreased yield. This was not an issue as a sufficient amount of the compound was obtained for all biological methods routinely employed. However, if future studies were to proceed around this compound class, this final step would require optimization. Analogue **4.047** was also synthesized following **Scheme 4.06** using picolinic acid and the hydrazide intermediate **4.044** in the final step to procure the desired analogue in high yield. Analogue **4.047** was designed to investigate whether the quinoline was key to maintain activity. This would also probe whether a decrease in molecular refractivity, lipophilicity, and the potential change in orientation and decreased ability for potential pi-pi stacking would still allow for appropriate fit and maintain key interactions with the binding site/s.

Compound **4.048** was the final analogue synthesized around this compound class focused on substituting the quinoline functionality with a naphthyl group, thereby removing the heteroatom and modifying the electronics of the aromatic system, potentially altering the orientation and pi-pi stacking interactions. To obtain this compound, **Scheme 4.06** was originally trialled using 2-naphthoic acid at

step (iv), where low reactivity and consumption of the starting materials was observed by TLC and LCMS analysis. Despite attempts to drive the reaction forward, i.e increased heat (from 50 to 80°C), longer reaction time (from 12 hours to 72 hours), increased equivalency of coupling reagents, change in solvent (DMF, to increase solubility), a low yield (<10%) was achieved. To further optimize the final step of **Scheme 4.06**, analogue **4.048** trialled an alternate final step, highlighted below in **Scheme 4.07**. Simply, the naphthoic acid (**4.049**) was first converted into the more reactive naphthoyl chloride (**4.050**) which underwent amide bond formation with the acetohydrazide **4.044** to form the final product **4.048**.³⁰ The analogue was formed successfully and was an improvement over the traditional amide coupling route above, however this alternate end route supplied still somewhat low yield. Nonetheless it may be a viable alternative for some unreactive intermediates entering the final steps of **Scheme 4.06**. Further optimization would be required for future analogues targeting this compound class, as the hydrazide proved difficult to utilize synthetically. Overall, this was not really an issue at this stage as the above analogues listed in **Scheme 4.06** had already been successfully acquired with enough sample for biological testing. In addition, the hydrazide functional group might be viewed as a potential structural alert capable of causing issues such as hepatotoxicity. Future work exploring bioisosteric replacement of the hydrazide may be useful strategy towards avoiding any potential issues with toxicity.^{31, 32}

Scheme 4.07: Alternate final step of scheme 4.06 used to synthesize analogue 4.048



Reaction conditions: i) acetohydrazide (**4.044**), DIPEA, HOBt, EDCI, ACN/THF, 50°C, ii) (COCl)₂ DMF, DCM, 0°C- rt, iii) 2-(1-methyl-1*H*-benzo[*d*]imidazol-2-yl)acetohydrazide (**4.044**), Et₃N, DCM

At this preliminary explorative stage, confirming biological activity against *L. donovani* was a higher priority over optimizing this pathway. Synthesis around this scaffold was paused as we were still cautious about synthesizing a library around a false positive compound class, as seen with Scaffolds 2 and 3, as discussed above.

4.07 Scaffold 4 Biological Results

Compounds were assessed using the bioassays previously described above. Their antileishmanial activity is reported in **Table 4.03**. As some activity was observed within this small library, the majority of analogues underwent the Bio21 bioassay examination outlined in Section **4.02**, where compounds first were subjected to a high one-point concentration HTS at 50 μM . As activity was observed against *L. donovani* from this primary assay, retesting occurred using the orthogonal and more routine assay, using the same method excluding the 10-point dilution curve with a top concentration of 100 μM performed by Bio21.

Table 4.03: Complete summary of biological results for Scaffold 4, hit **4.003** is outlined in blue.

I.D	HCS intracellular assay against <i>L. donovani</i>				Luciferase /MTT assay	
	Bio21 ^{ab}		IPK ^{cd}		UNC ^{ef}	
	IC ₅₀ (μM)	CC ₅₀ (μM)	IC ₅₀ (μM)	CC ₅₀ (μM)	IC ₅₀ (μM)	CC ₅₀ (μM)
4.003 Hit	6.3	>100	6.3	>100	5.9	>50
4.046	4.8	>100	36	>100	23	>50
4.047	>50 ^g	>50 ^g	48	>100	>20	50
4.048	>100 [§]	>100 [§]	>100	>100	>20	>50

anti *L. donovani* activity and toxicity measured in THP-1 transformed macrophage host cell lines using a top concentration of 100 μM (2x serial dilution 10-point curve). Experiment performed in duplicate wells in one experiment, n=1.

b= control compounds for Bio21 intramacrophage *L. donovani* assay. Average (\pm standard deviation) from experimental replicates; Miltefosine IC₅₀= 0.50 \pm 0.0077 μM , CC₅₀> 40 μM , Amphotericin B IC₅₀= 1.3 \pm 0.32 μM , CC₅₀> 60 μM .

c= anti *L. donovani* activity and toxicity measured in THP-1 transformed macrophage host cell lines using a top concentration of 100 μM (2x serial dilution 10-point curve). Experiment performed in duplicate wells in one experiment, n=1.

d= control compounds for IPK intramacrophage *L. donovani* assay. Miltefosine IC₅₀= 1.7 μM , CC₅₀>100 μM , Amphotericin B IC₅₀= 0.83 μM , CC₅₀> 100 μM .

e= anti *L. donovani* activity measured in THP-1 transformed macrophage host cell lines using luminescent expressing *L. donovani*. Experiment performed in triplicate wells in one experiment, n=1 using a concentration range of 1-50 μM . DMSO was used as sole control against which the percent *L. donovani* viability is calculated

f= host cell toxicity measured in MTT assay with uninfected macrophage host cells. Experiment performed in triplicate wells in one experiment, n=1 using a concentration range of 1-50 μM . DMSO was used as sole control against which the percent cell viability is calculated

g= anti *L. donovani* activity and toxicity measured in THP-1 transformed macrophage host cell lines using a one-point concentration (50 μM) to assess any form of antileishmanial activity. Experiment performed in duplicate wells in one experiment, n=1.

§= poor solubility observed in media up to 800 μM during Bio21 assay

The hit **4.003** was confirmed active and selective against *L. donovani*, with clear consistency across all assays employed. It was highly encouraging to see that a clear SAR story was visible within this set of analogues. The loss of the *N*-methyl (**4.046**) saw a decrease in activity across 2 out of 3 independent assays carried out by each of our collaborators. Even though Bio21 reported maintained activity for analogue **4.046**, we still were following the guidelines set in Chapter 3, therefore it was decided that the *N*-methyl was required to deliver true antiparasitic activity. Slightly elongating the *N*-methyl to an *N*-ethyl or replacing the benzimidazole with a benzoxazole and other bioisosteres is encouraged to understand key functionalities required to maintain antileishmanial activity at the portion of the chemical space. It was apparent that altering the quinoline, by either removing the nitrogen to give a naphthyl ring (**4.048**) or removing the fused 6-membered ring, leaving the pyridine (**4.047**) was unfavourable. A complete loss of activity across all assays was observed, advising that the quinoline in

this chemical space is required to maintain activity and allow for specific fit and interactions to be made with the binding site. The loss of the fused 6-membered ring may have caused a loss in pi-pi stacking and poor fit within the binding site, decreasing size and lipophilicity dramatically. Repositioning the nitrogen of the quinoline around the fused rings, as well as altering ring size (for example 6 +5 membered fused rings) would be encouraged to further understand the preferences of this scaffold around this portion of the chemical space. Solubility issues were reported in the Bio21 assay for compound **4.048** only, which was initially thought to have hindered activity. However, since solubility issues with **4.048** were not echoed by the other bioassays employed, it seems that this compound may be inactive due to the analogue's modification itself rather than solubility issues alone. Solubility issues were not observed within the rest of this series. Despite the negative SAR observed from the small set of analogues, this was not an undesirable discovery and it was enjoyable to see a clear SAR story forming.

The dose response curves of hit **4.003** reported by Bio21 are depicted in **Figure 4.10a-b**, which serve as a further visual demonstration of the activity and selectivity of the hit **4.003** against *L. donovani*. **Figure 4.10a** was used to report the IC₅₀ against *L. donovani* and **Figure 4.10b** was used to determine the CC₅₀ and cytotoxicity against the THP-1 transformed host macrophages. These curves are used as representatives to depict the consistent potency of **4.003** reported by each of our collaborators. Depicted in **Figure 4.10a**, hit **4.003** is shown to clearly reduce parasite burden, where an increase in compound concentration correlated to a decrease in the percentage of infection within viable host macrophage cells. A host cell is considered infected when ≥ 3 parasites per host macrophage are detected. Furthermore, **Figure 4.10b** depicts that the hit **4.003** exerted activity against the parasite only, as no cytotoxicity against the host macrophage was observed.

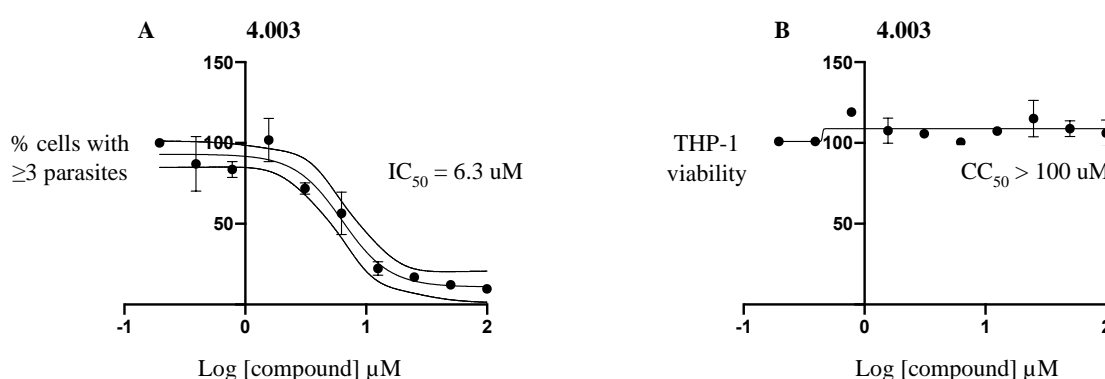


Figure 4.10a-b: Dose response curves of hit **4.003** reported by Bio21, a) measuring compound concentration (x axis) against % of infection within host macrophages (y axis) to determine the antileishmanial activity (IC₅₀) of **4.003**, b) measuring compound concentration (x axis) against the viability of the THP-1 transformed macrophages (y axis) to determine the cytotoxicity against the host cell (CC₅₀)

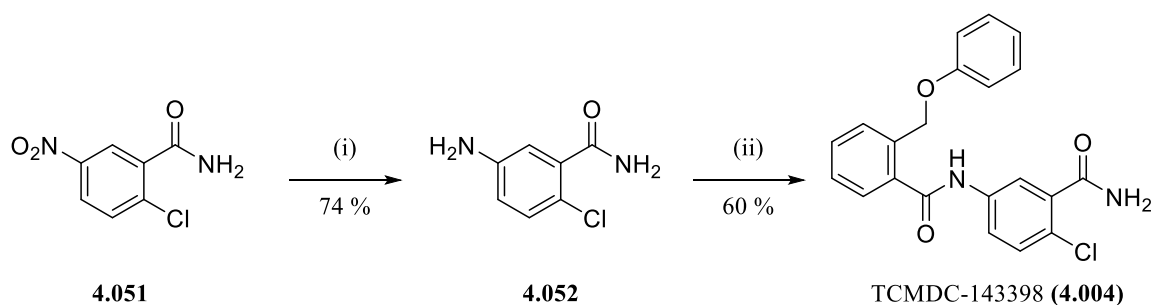
In addition to the fact that the hit **4.003** was reported to have consistent antileishmanial behaviour across all biological assays employed, the surrounding analogues of Scaffold 4 also gave more obvious and

consistent SAR. Therefore, it was decided that this compound class would be continued. Further investigations around the chemical space were favourable.

4.08 Scaffold 5 Exploration

The final compound class explored within this body of work was completed in parallel to the above classes. Investigations around *N*-(3-carbamoyl-4-phenyl)-2-(phenoxyethyl)benzamide scaffold began with the resynthesis of hit TCMDC-143398 (**4.004**). The synthesis of this hit followed **Scheme 4.08**, beginning with the reduction of the the nitro benzamide (**4.051**) via hydrogenation to obtain the 5-amino-2-chlorobenzamide (**4.052**). Platinum was employed as the catalyst to ensure the halogen would not be displaced.³³⁻³⁷ Using the free amine of compound **4.052**, amide coupling was employed to attain the target hit (**4.004**) in reasonable yield.⁵

Scheme 4.08: Synthetic pathway to obtain TCMDC-143398 (**4.004**), and related analogues



Reaction conditions: i) Pt-C, H₂ MeOH, ii) 2-(phenoxyethyl)benzoic acid, DIPEA, HOBt, EDCI, ACN, 50°C

The hit ¹H NMR spectrum of **4.004** is depicted in **Figure 4.11**. This analysis was undertaken in DMSO and all proton signals of the compound are observed. The aromatic peaks are all present within the aromatic region indicating the success of the amide coupling step in **Scheme 4.08**. Moreover, the downfield singlet at 10.61 ppm which correlates to the central N-H amide, along with the loss of the amine **4.052** NH₂ singlet within the aliphatic region further implies successful amide bond formation. This central amide N-H signal at peak A was found dramatically more downfield than the terminal amide, due to the deshielding effects of the surrounding π systems, namely the electron withdrawing carbonyl and its position adjacent to the aromatic ring. The multiplet centred at 6.88 ppm, corresponding to the overlapping protons (F) which are shifted upfield via resonance donating effect of the ether. Other key signals indicating the formation of **4.004** include the presence of the methylene peak at 5.26 ppm (peak G). In this spectrum the terminal amide is observed as two 1H singlets within the aromatic region, most likely within the overlapping multiplets of peak D centred at 7.50 ppm, **Figure 4.11**. This pattern was expected and has been observed throughout the literature.³⁸⁻⁴³ The rigid framework of the primary amide can lead to hindered rotation around the carbonyl-nitrogen bond and non-equivalent amide protons are observed in different magnetic environments.^{42, 43} Additionally, a crystal structure of

the hit **4.004** confirming the identity of the compound was obtained and is discussed in Chapter 5. The complete ^1H and ^{13}C NMR spectra and assignment of hit **4.004** is included in the Experimental section of this chapter.

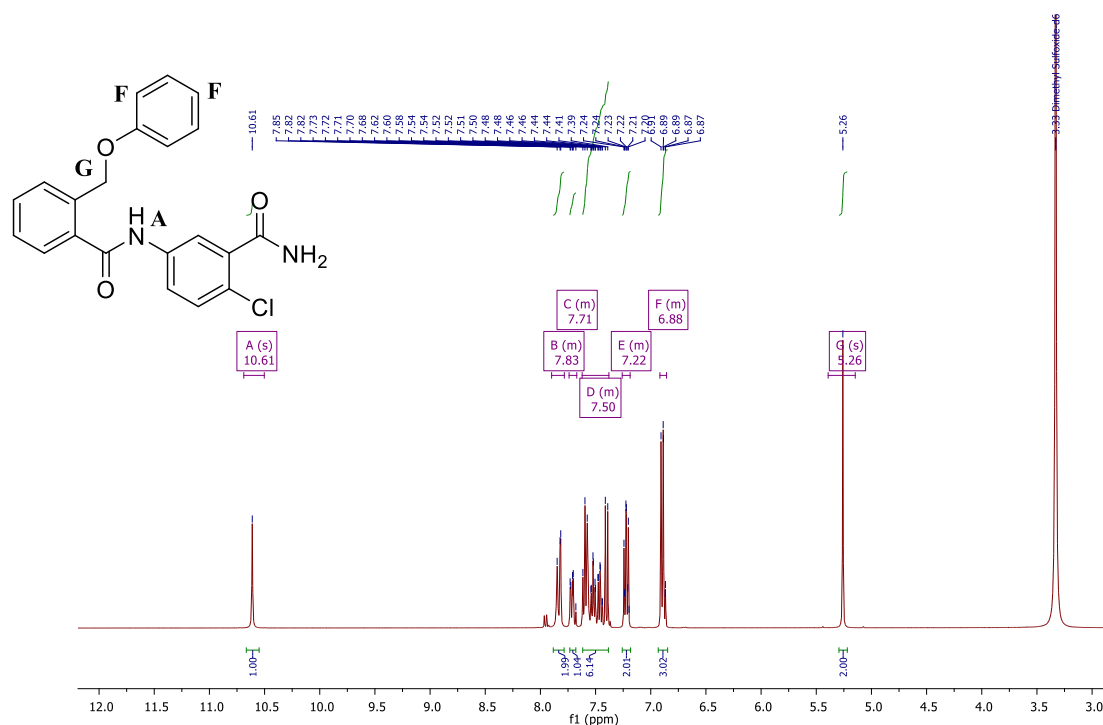


Figure 4.11: ^1H NMR spectrum of hit performed in DMSO confirming all protons are present and the amide coupling of step ii of Scheme 4.08 was successful

After resynthesis of the hit TCMDC-143398 (**4.004**), several analogues surrounding the hit were also synthesized (**Figure 4.12**), keeping the changes simple to ascertain which structural moieties of Scaffold 5 were required to maintain activity. Only a small number of analogues were made, as priority fell to confirming the activity of the hit. Of the analogues that were synthesized, analogue **4.053** and **4.054** focused on exploring the necessity of the RHS benzamide ring substituents, removing the halogen and replacing the terminal amide with an ester respectively. The ester bioisosteric substitution would share the same resonance as an amide, where the oxygen lone pair of electrons delocalizes into the antibonding orbital of the carbonyl group. This bioisostere would give an insight into hydrogen bonding ability requirements, as esters are weak hydrogen bond acceptors and don't possess hydrogen bond donating ability. Analogue **4.055** focused on altering the phenyl ether connection, to study the change in position of methylene and oxygen groups, therefore altering rotatable bond position, flexibility and allow for the benzyloxy group to change its orientation. This modification may also alter any specific or distant dependant hydrogen bonding interactions that exist between the oxygen atom and the binding site. Analogue **4.056** was also devised to investigate the chemical space around the ether by removing the methylene and provide a more rigid link between the aromatic rings, decreasing the number of rotatable bonds, changing the shape and orientation of the scaffold and potential fit within the binding

site. These analogues were obtained following **Scheme 4.08**, with some synthetic modifications required for achieving compounds **4.053** and **4.054** which is depicted below in **Schemes 4.09-10**. Overall, step ii of **Scheme 4.08** remained consistent, achieving the analogues of **Figure 4.12** successfully in somewhat moderate yield. The steric bulk of the *ortho*-phenoxyethyl benzoic acid may be a hindrance during amide coupling. The deactivating 4-chloro group may also be cause for the decreased yield and lower reactivity. Synthesis of compound **4.053**, which does not contain this 4-chloro group was able to achieve a higher yield during amide coupling than the remainder of analogues in **Figure 4.12**. If exploration of this scaffold was continued, further optimization of **Scheme 4.08** would be trialled.

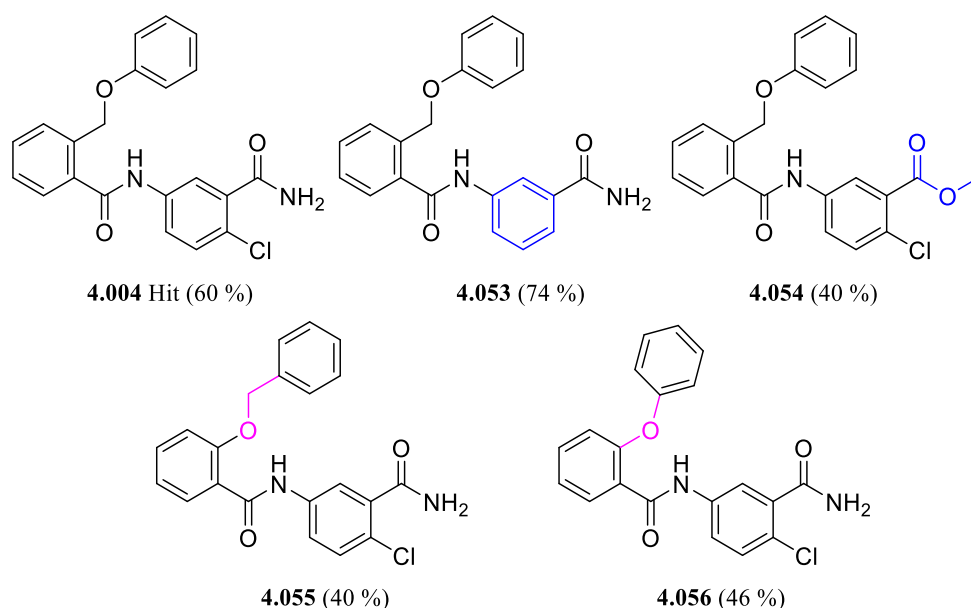
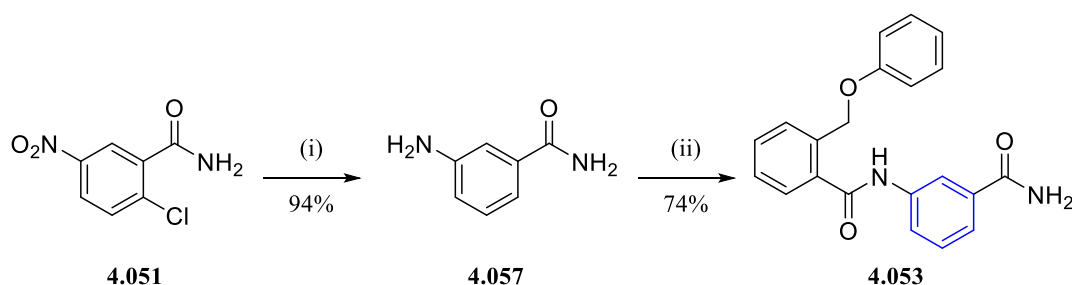


Figure 4.12: Initial exploration of analogues surrounding TCMDC-143398 (**4.004**) and their respective yields of step ii of **Scheme 4.08**.

To obtain analogue **4.053**, a modified pathway, **Scheme 4.09** as devised. The amino building block **4.051** was required to undergo amide coupling in the final step. This building block was acquired by simultaneously reducing the nitro group and removing the chloro group of **4.057** using a palladium catalyst.^{36, 37, 44, 45} Once obtained in excellent yield, the amine building block **4.057** subsequently underwent amide coupling to successfully afford analogue **4.053**.⁵

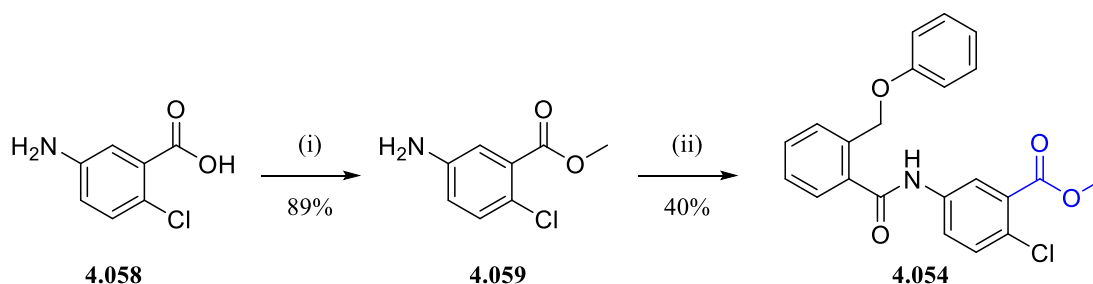
Scheme 4.09: Synthetic pathway to obtain analogue **4.053** (loss of 4-chloro substituent)



Reaction conditions: i) Pd/C, H₂ MeOH, ii) 2-(phenoxyethyl)benzoic acid, DIPEA, HOBt, EDCI, ACN, 50°C

To obtain analogue **4.054**, another amine building block intermediate required synthesis. Following **Scheme 4.10**, the 5-amino-2-chlorobenzoic acid (**4.058**) underwent Fischer esterification to obtain the methylated ester (**4.059**) in high yield.⁴⁶ Once formed, the methyl 5-amino-2-chlorobenzoate building block could then undergo subsequent amide coupling to successfully obtain analogue **4.054**.⁵

Scheme 4.10: Synthetic pathway to obtain analogue **4.054** (substitution of terminal amide with methyl ester)



Reaction conditions: i) H₂SO₄, MeOH, reflux, ii) 2-(phenoxyethyl)benzoic acid, DIPEA, HOBt, EDCI, ACN, 50°C

4.09 Scaffold 5 Biological Results

The antileishmanial activity of the initial *N*-(3-carbamoylphenyl)-2-(phenoxyethyl)benzamide analogues was assessed along with their cytotoxicity against the host macrophages. Following the guidelines outlined in Chapter 3 (2 out of 3 convergent results) the hit **4.004** was confirmed active and selective against *L. donovani*. Strong negative SAR was observed in the surrounding analogues. This is not such a bad thing, as it provides a clear outline of which modifications to avoid. The unanimous inactivity of **4.053**, signifies that the 4-chloro substituent is required to maintain activity, suggesting a possible key interaction between the halogen and the putative binding site. Future exploration substituting the 4-chloro with other groups altering the electronegativity and size or repositioning this group around the ring are encouraged. The substitution of the terminal amide with a methyl ester (**4.054**) also demonstrated unanimous inactivity, suggesting that the amine group of the terminal amide may also provide key hydrogen bonding interactions with the binding site. At this stage, ability to form H-bond interactions, both donating and accepting seems to be required at this portion of the chemical space.

Further substitution of the terminal amide with similar carbonyl groups would be encouraged in order to confirm the type of interactions required at this position. Repositioning this functionality around the ring would also be interesting, to gauge whether these interactions are preferred at other positions. Altering the ether chain in compounds **4.055** and **4.056** was also found to be detrimental to antileishmanial activity. By altering the position of the oxygen atom and methylene within the ether chain (**4.055**) a complete loss of activity was observed. This modification from the phenoxyethyl to

the benzyloxy meant altering the position of the rotatable bond to be adjacent to the bare aromatic ring, which may be able to alter its orientation within the putative binding site. This potential change in orientation may have moved the phenyl from fitting in the correct position, possibly preventing some possible key interactions with the binding site. Repositioning the oxygen of the ether chain may have also altered possible H-bonding interactions where it could act as an H-bond acceptor. This interaction may be distant dependant with the putative binding site. As we do not know the structure or identity of the putative binding site at this stage, we can only speculate. More analogues would be also required to further confirm this negative SAR.

Finally, the loss of the methylene chain in compound **4.056** also reduced the number of rotatable bonds and changed the size, orientation and fit of the scaffold, where the compound may not be able to reach a specific portion of the binding site. Discussed in Chapter 5, further investigations were undertaken to study whether the complete removal of the ether was preferred, devising analogues possessing only a carbon-carbon chain at this portion of the chemical space. Shortening and elongating the chain slightly to further understand what orientation and interactions were required at this position was also explored and is detailed further in Chapter 5.

Table 4.04: Complete summary of biological results for Scaffold 5 initial analogues, hit **4.004** outlined in blue

I.D	HCS intracellular assay against <i>L. donovani</i>				Luciferase /MTT assay	
	Bio21 ^a		IPK ^{de}		UNC ^{fg}	
	IC ₅₀ (μM)	CC ₅₀ (μM)	IC ₅₀ (μM)	CC ₅₀ (μM)	IC ₅₀ (μM)	CC ₅₀ (μM)
4.004 Hit^b	4.9	>100 ⁱ	21	>100	3.2	>50
4.053^c	>100 ⁱ	>100 ⁱ	>100	>100	>50	>50
4.054	>50 ^h	>50 ^h	>100	>100	>20	>50
4.055^b	>100 ⁱ	>100 ⁱ	>100	>100	>20	34.0
4.056	>50 ^h	>50 ^h	>100	>100	>20	>50

anti *L. donovani* activity and toxicity measured in THP-1 transformed macrophage host cell lines using a top concentration of 100 μM (2x serial dilution 10-point curve). Experiment performed in duplicate wells in one experiment, n=1.

b= control compounds for Bio21 intramacrophage *L. donovani* assay. Average (± standard deviation) from experimental replicates; Miltefosine IC₅₀= 0.50 ± 0.0077 μM, CC₅₀> 40 μM, Amphotericin B IC₅₀= 1.3 ± 0.32 μM, CC₅₀= 63 ± 3.6 μM.

c= control compounds for Bio21 intramacrophage *L. donovani* assay. Miltefosine IC₅₀= 0.53 μM, CC₅₀= 33 μM, Amphotericin B IC₅₀= 0.72 μM, CC₅₀> 100 μM.

d= anti *L. donovani* activity and toxicity measured in THP-1 transformed macrophage host cell lines using a top concentration of 100 μM (2x serial dilution 10-point curve). Experiment performed in duplicate wells in one experiment, n=1.

e= control compounds for IPK intramacrophage *L. donovani* assay. Miltefosine IC₅₀= 1.7 μM, CC₅₀>100 μM, Amphotericin B IC₅₀= 0.83 μM, CC₅₀> 100 μM.

f= anti *L. donovani* activity measured in THP-1 transformed macrophage host cell lines using luminescent expressing *L. donovani*. Experiment performed in triplicate wells in one experiment, n=1 using a concentration range of 1-50 μM. DMSO was used as sole control against which the percent *L. donovani* viability is calculated

g= host cell toxicity measured in MTT assay with uninfected macrophage host cells. Experiment performed in triplicate wells in one experiment, n=1 using a concentration range of 1-50 μM. DMSO was used as sole control against which the percent cell viability is calculated

h= anti *L. donovani* activity and toxicity measured in THP-1 transformed macrophage host cell lines using a one-point concentration (50 μM) to assess any form of antileishmanial activity. Experiment performed in duplicate wells in one experiment, n=1.

i= no inhibition detected within DRC at the top concentration tested (100 μM).

Within this series, no solubility issues were reported across all bioassays employed. This was favourable, as we wished to avoid the confusion associated with poor solubility as seen in some previous

leads of Scaffold 1. Avoiding poor solubility within a scaffold meant avoiding the uncertainty of whether analogue inactivity was due to its structural modification or inability to dissolve into the solution and permeate the cell, or both.

The dose response curves of hit **4.004** reported by Bio21 are also depicted in **Figure 4.13a-b**, which were used to ascertain the IC_{50} and CC_{50} values respectively. Similar to the above **Figure 4.10a-b**, here the **Figure 4.13a** is shown to decrease the percentage of infection within host macrophage cells when the concentration of compound **4.004** is increased. The potency against *L. donovani* is shown to be selective for the parasite only and displays no real cytotoxic behaviour against the transformed THP-1 host macrophage, observed in **Figure 4.13b**.

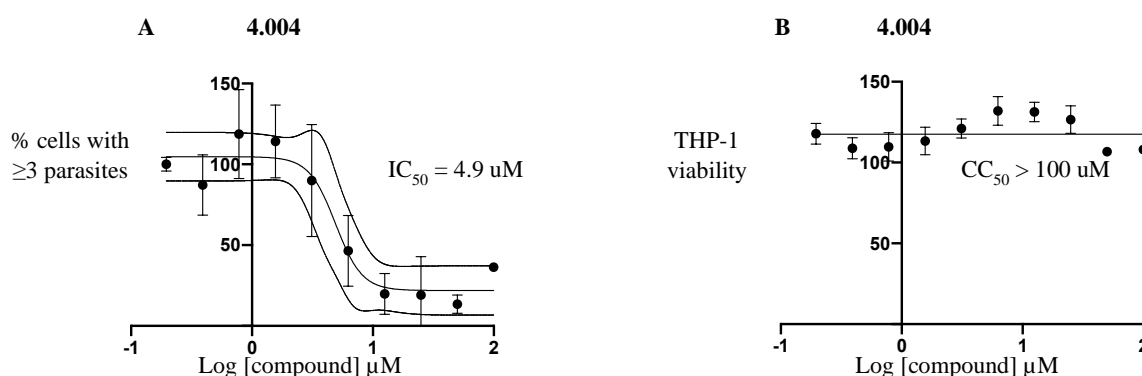


Figure 4.13a-b: Dose response curves of hit **4.004** reported by Bio21, a) measuring compound concentration (x axis) against % of infection within host macrophages (y axis) to determine the antileishmanial activity (IC_{50}) of **4.004**, b) measuring compound concentration (x axis) against the viability of the THP-1 transformed macrophages (y axis) to determine the cytotoxicity against the host cell (CC_{50})

As the hit **4.004** was confirmed as active, and the surrounding analogues of Scaffold 5 also gave more obvious and consistent SAR, it was decided that this compound class would be continued. Further investigations around the chemical space were favourable.

4.10 Summary and Future work

The search for new investigative compound classes to be used against *L. donovani* yielded mixed, yet interesting results. Outlined in the resynthesis of the phenyl pyrazinyl methanone hit (**4.001**), once again we demonstrated the difficulties of targeting *Leishmania* and the absolute need to confirm true activity against this kinetoplastid. The initial bio-evaluation of hit **4.001** was found active within the luciferase assay, though when performed at lower concentrations in the same assay to achieve a more accurate inhibitory value, the hit **4.001** was found to be inactive. Inactivity of the hit was confirmed across the HCS assays performed, suggesting this compound to be a false positive. The entire library surrounding this compound class was also found inactive, regardless of how small the analogue modification. This supported the notion that this compound class may be inactive against *L. donovani* and/or the mode of

action may be difficult to understand. Overall, it seemed pursuing this class may not be worthwhile, since we were after a series with a clear SAR story, in order to develop a more optimized lead candidate. Similarly, the benzodioxol thiadiazol methoxybenzamide hit (**4.002**) and analogue was found inactive and a likely false positive against *L. donovani*. These scaffolds may indeed hold some activity against *L. donovani*, however since no clear SAR pathway was elucidated and their biological targets remain unknown, we were cautious about spending the remaining time on this project focused on difficult and confusing compound classes. Therefore, these classes were set aside for the meantime, in an effort to focus on a compound class with a clear SAR pathway, and more obvious activity. Fortunately, true activity was confirmed unanimously across all bioassays employed for the benzimidazole quinoline carbohydrazide hit (**4.003**). The small series surrounding the hit gave negative SAR, which already suggests that there are certain functionalities of this scaffold that are required to maintain activity, namely the *N*-methyl of the benzimidazole ring and the RHS quinoline ring. Continued investigation around this compound class was favourable, due to the successful activity confirmation and obvious SAR in surrounding analogues. Therefore, it was decided that continued study around hit **4.003** would occur in a parallel project led by fellow PhD student Rebecca Zheng. This promising scaffold and synthetic access to altering various portions of the chemical space merited its own project, where additional time could be spent focused on exploration around altering **4.003**. In addition to altering the quinoline, bioisosteres of the benzimidazole and hydrazide functionalities would be explored.

Exemplary analogues of the current/ future work to be carried out for this series are depicted below in **Figure 4.14**. Exemplary analogues **4.060-4.061** aim to explore bioisosteres of the benzimidazole portion of the scaffold, altering the heteroatoms around the imidazole ring. Exemplary analogue **4.062** also involves a modification to the benzimidazole ring, via a non-fused 6+5 aromatic system to probe whether this arrangement is preferred. Exemplary analogues **4.063-4.065** were devised to alter the hydrazide functionality, with the amide and urea substitutions respectively. This would give an insight into the necessity of the hydrazide and explore any viable isosteric replacement. This is desired to avoid any possible hepatotoxicity *in vivo* mediated by the bioactivation of the hydrazide structural alert via cytochrome P450 or monoamine oxidase enzymes.⁴⁷⁻⁴⁹ Other examples of analogues planned for this scaffold include altering the quinoline by changing the fused ring system, depicted in examples **4.066-4.069**, which possesses a 5+6 fused aromatic ring system as well as introduce heteroatoms within the ring. This would gauge whether altering size, orientation was allowed as well as discover if any additional interactions could be made with the heteroatom and putative binding site. Finally repositioning the nitrogen atom of the quinoline (**4.070**) and adding a second nitrogen around the fused rings (**4.071**) was devised to understand where the heteroatom was preferred. Overall, there is a large opportunity for synthetic modification and improvement around this scaffold, making it an excellent target for a continued hit-to-lead medicinal chemistry campaign.

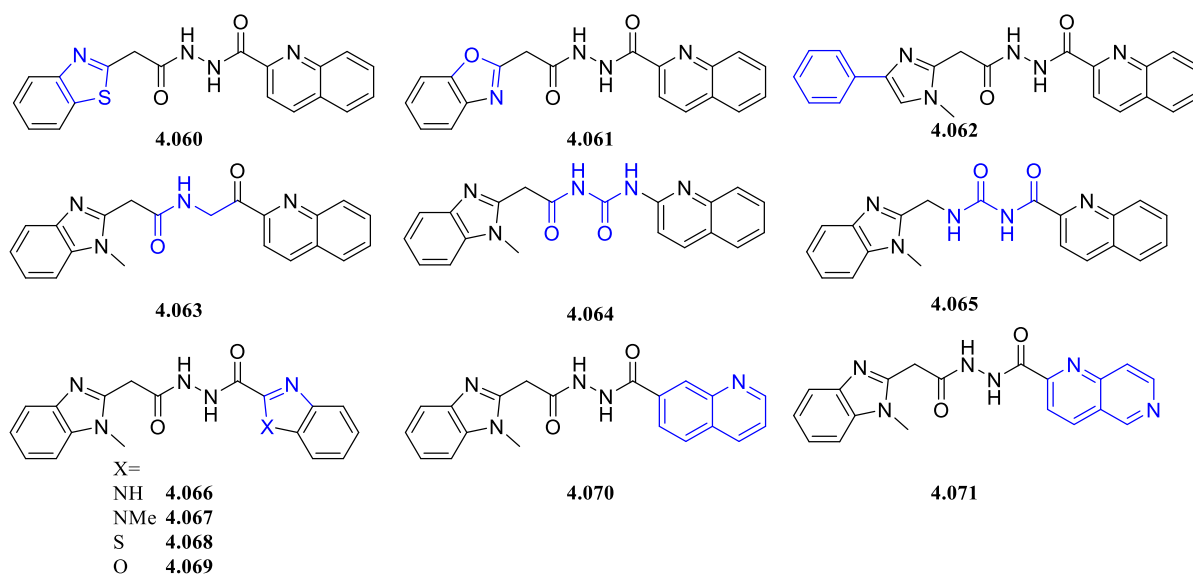


Figure 4.14: Examples of analogues as future work for Scaffold 4

The *N*-(3-carbamoylphenyl)-2-(phenoxy)methylbenzamide hit (**4.004**) and related analogues belonged to the final compound class explored within this chapter. The hit **4.004** was also successfully confirmed to have true antileishmanial activity and selectivity for the parasite. Similar to aforementioned series around **4.003**, the initial analogues surrounding **4.004** also gave negative SAR. This was not considered problematic as it outlined the required functionalities for activity maintenance. The confirmed activity and selectivity of **4.004** for *L. donovani* as well synthetic access to the various analogues made this compound class preferable for continued study. Additionally, no obvious toxicophores are incorporated within this scaffold.⁵⁰ The further investigation around **4.004** is detailed in Chapter 5 and the focal chemical space targeted is briefly summarized in **Figure 4.15**. Another reason as to why this scaffold seemed promising, was the abundant chemical space available to explore and modify. The continued primary SAR study would involve the synthesis of analogues targeting the 4-chloro and terminal amide functionalities. As seen with analogue **4.053**, the loss of the 4-chloro was unfavourable, giving a loss of antileishmanial activity. Further investigations substituting this group for other functionalities altering the sterics and electronics, as well as repositioning this group around the benzamide ring were explored to confirm whether the 4-chloro was favourable at this position. As seen with compound **4.054**, the substitution of the amine of the terminal amide with a methyl ester was unfavourable. Further confirmation as to whether both hydrogen bonding and donating ability is required at this position of the ring is explored in Chapter 5. Compounds **4.055** and **4.056** targeted changes to the ether chain, which suggested swapping the oxygen atom position or removing the methylene were unfavourable. Further exploration into the ether chain is discussed in Chapter 5, confirming whether the chain length, atoms required and subsequent change in orientation were key to maintaining activity. Finally, additional functional groups were added to the methoxyphenyl ring to gauge whether further interactions between the binding site and compound could occur. Additions to this ring would include

functionalities with varying electronic, hydrophobicity, hydrogen bonding ability and molecular refractivity, as outlined initially in Chapter 1, **Table 1.06**.

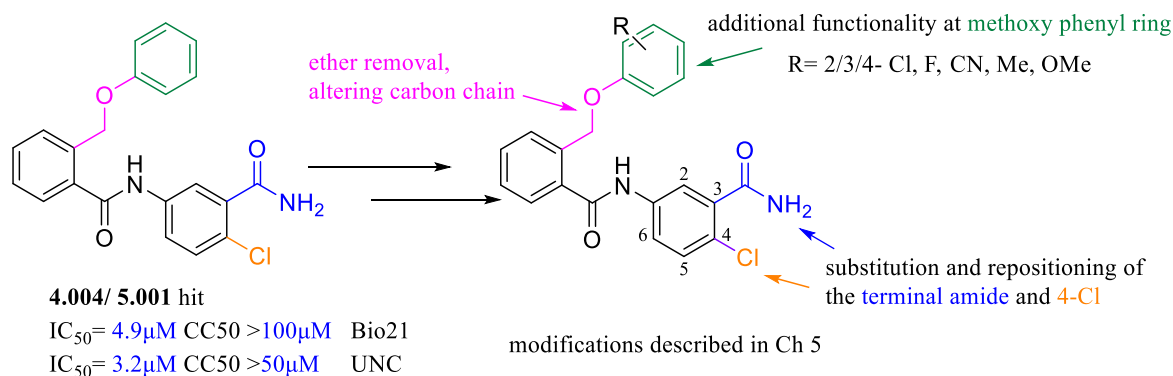


Figure 4.15: Highlights of the key portions of chemical space targeted in the library surrounding 4.004, detailed in Chapter 5

Overall, exploring these various scaffolds was a good exercise to take on. Various chemistry was able to be applied to achieve the various hits and their surrounding analogues. Our first scaffold, the phenyl imidazole benzamide compound class (Scaffold 1) and its SAR pathway was originally difficult to interpret. This search for new scaffolds whilst waiting for and then deciphering the Scaffold 1 SAR led to more divergence seen with the false positive hits **4.001-2**. Undertaking this exercise gave us more affirmation to the fact that targeting *Leishmania* intracellularly is indeed a difficult task. It might be wondered whether lack of confirmation of bioactivity was unexpected. Actually, this is not so uncommon in either target-based or phenotypic HTS. The reasons can be many, from active impurities (including heavy metal contamination) to incorrect structure.

Anecdotally, from conversations with collaborators, it seems that this problem is particularly prevalent amongst phenotypic antiparasitic HTS hits and underscores the importance of aiming as an initial priority to confirm activity in a small focused set that includes the originally reported hit. As discussed in Chapter 1, Lamotte *et al.* re-examined the potency of various antileishmanial hits sourced from the same LeishBox as our own hits. The structural identity of all hits was not disclosed, however they described many of these initial screening hits to possess weaker efficacy against *L. donovani* than originally reported by GSK, whilst some hits were found completely inactive.⁵¹ This was indeed the case for hits **4.001-2**, which gave more validation that activity against *L. donovani* from one source may not be confirmed in others. Spending more effort to corroborate true potency in more than one independent bioassay/ set of orthogonal assays was a reoccurring lesson, which may even act as a cautionary tale, encouraging others to practise when targeting this parasite using compounds taken from phenotypic screens. Fortunately, our search for new compound classes to target *L. donovani* was successful, as hits **4.003-4** were confirmed active with low host cell cytotoxicity and no reported solubility issues. Analogues surrounding both series provided negative SAR, which was a positive

attribute to us, suggesting clear SAR stories forming. Due to the efforts of this hit search and verification we now have two more active hit-to-lead campaigns focused on novel compound classes targeting *Leishmania donovani*.

4.11 Chapter 4 Experimental

Biological Experimental

Bio21 Methodology

Biological methods were previously described in detail, please refer to previous chapters, experimental section (2 and 3). These assays were carried out as previously reported with minor adjustments.⁵²

IPK Methodology

Parasite and cell culture along with the intracellular assay were performed according to Phan *et al.* with small modifications.⁵³ These methods were previously described in detail, please refer to Chapter 3, Experimental section.

UNC Methodology

Infecting THP-1 Macrophages with *Leishmania donovani* (Ds-Red-lux) and evaluating by Luciferase assay¹²

Parasites: *L. donovani* LV82 expressing firefly luciferase and a red fluorescent protein, LUC and DsRed2 promastigotes (Ds-Red-Lux) promastigotes were provided by Dr. Abhay Satoskar, Department of Pathology, The Wexner Medical Centre, The Ohio State University. Ds-Red-lux *L. donovani* promastigotes were routinely cultured at 26 °C in M199 medium (Catalogue number 10-060, Corning) supplemented with, 7.6 mM hemin, 0.1, 10% (v/v) heat-inactivated fetal bovine serum (FBS) and antibiotic cocktail (50 U/ml penicillin, 50 µg/ml streptomycin).

Generation of the red-shifted lux *L. donovani* strain was undertaken based on the methods described by Lezama-Davila *et al.*⁹

***In vitro* luciferase assay**

The assay and conditions were adapted from methods as previously described by Álvarez-Velilla *et al.* which employed *L. infantum* rather than *L. donovani* which was utilised within these studies.⁸ This has been previously described in detail, please refer to Chapter 3, Experimental section.

Cell viability analysis: MTT assay

These assay conditions are similar to that reported by Chiu *et al*, as directed by our colleagues at UNC.¹¹ This has been previously described in detail, please refer to Chapter 3, Experimental section.

General Chemistry

General chemistry, solvents and machines employed followed the same description detailed in Chapter 2, Experimental

Synthesis

General Procedure A Amide coupling^{4, 5}

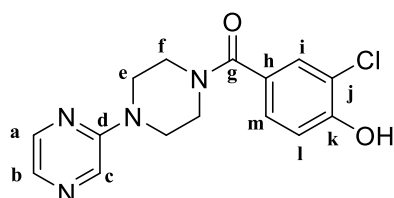
To a solution of the appropriate amine (1.3 equiv) and DIPEA (1.0-2.0 equiv) in ACN (5 mL) was added the appropriate benzoic acid (1.0 equiv). The mixture was stirred for 10 min before adding HOBt (2.5 equiv) and EDCI. HCl (1.0 equiv). The solution was stirred at 50°C over 12 h after which the reaction was reduced *in vacuo*. The reaction mixture was diluted with DCM and washed with citric acid/water followed by ammonia/water. The organic layer was dried with MgSO₄, filtered and reduced *in vacuo*. The crude material was subsequently purified via column chromatography (CHCl₃; MeOH; NH₄OH; 94:5:1).

General Procedure B Hydrogenation^{33, 45}

To a solution of the appropriate nitrobenzamide (2 mmol) in MeOH (5 mL) was added Pt-C. The mixture was degassed and backfilled with nitrogen before put under hydrogen. The mixture stirred at room temperature over 12 h. Upon reaction completion the solution was filtered through celite and the filtrate concentrated *in vacuo*. The crude product was diluted with diethyl ether and filtered via suction filtration. The filtrate was concentrated to afford to give the desired compound.

Scaffold 2 Compounds

(3-Chloro-4-hydroxyphenyl)(4-(pyrazin-2-yl)piperazin-1-yl)methanone (4.001)

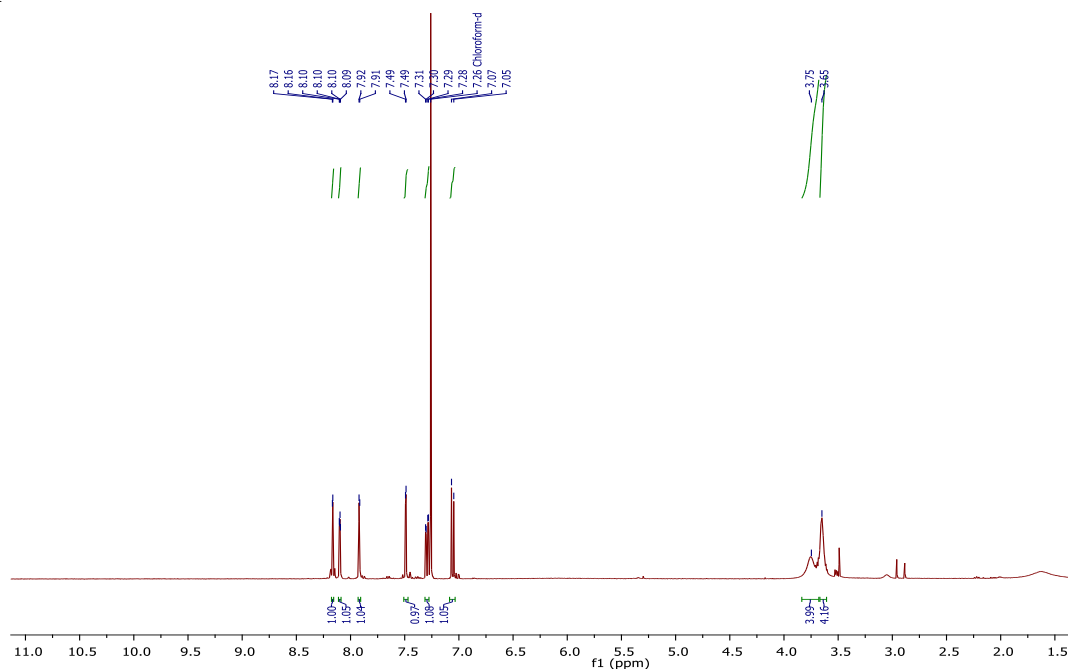


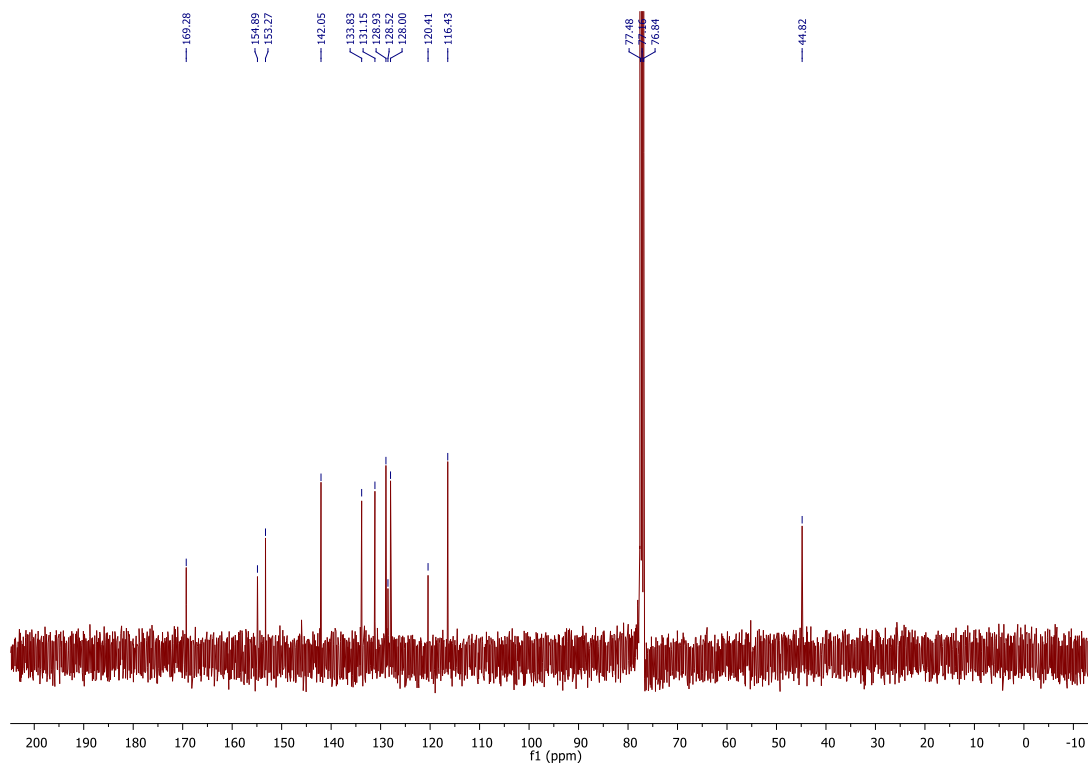
The title compound was obtained using 2-(piperazin-1-yl)pyrazine (2.13 mg, 1.3 mmol), 3-chloro-4-hydroxybenzoic acid (150 mg, 0.87 mmol), DIPEA (0.3 mL) which were dissolved in DMF (3 mL) and left to stir at room temperature for 10 min. To the solution HOBt (175 mg, 1.30 mmol) and EDCI. HCl (248 mg, 1.6 mmol)

was added and the solution was left to stir for 15 h. Upon reaction completion the solution was concentrated *in vacuo*, diluted with EtOAc and washed with brine. The organic layers were collected, dried with MgSO₄, filtered and concentrated.⁵ The crude material was subsequently purified via

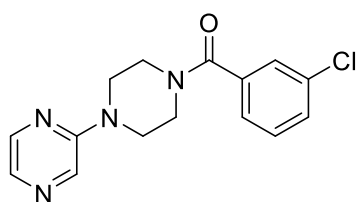
column chromatography (EtOAc: Petroleum spirits; 1:1) to obtain the title compound as an off white solid (270 mg, 97 %). HPLC – t_R 4.24 min > 99 % purity at 254 nm; LRMS $[M+H]^+$ 319.0 m/z ; HRMS $[M+H]^+$ 319.0956 m/z , found 319.0958 m/z ; 1H NMR (400 MHz, $CDCl_3$) δ_H 8.17 (d, J = 1.5 Hz, 1H, Hi), 8.10 (dd, J = 2.6, 1.5 Hz, 1H, Hc), 7.92 (d, J = 2.6 Hz, 1H, Ha), 7.49 (d, J = 2.0 Hz, 1H, Hb), 7.29 (dd, J = 8.4, 2.0 Hz, 1H, Hm), 7.06 (d, J = 8.4 Hz, 1H, Hl), 3.81 – 3.68 (m, 4H, He), 3.67– 3.63 (m, 4H, Hf); ^{13}C NMR (101 MHz, $CDCl_3$) δ_C 169.3 (Cg), 154.9 (Ck), 153.3 (Cd), 142.1 (Ca), 133.8 (Cc), 131.2 (Cb), 128.9 (Ci), 128.5 (Ch), 128.0 (Cm), 120.4 (Cj), 116.4 (Cl), 44.8 (br s, 4C, Ce,Cf). Aliphatic peaks overlap to form a broad singlet, this is evident throughout this scaffold series of analogues. M.p. 213.6-216.4 °C.

Example spectra for Scaffold 2: 1H (400 MHz, $CDCl_3$) and ^{13}C NMR (100 MHz, $CDCl_3$) spectrum of (3-Chloro-4-hydroxyphenyl)(4-(pyrazin-2-yl)piperazin-1-yl)methanone (4.001). Solvent impurity peaks present in 1H NMR spectrum



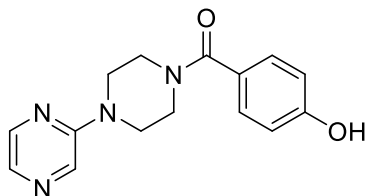


(3-Chlorophenyl)(4-(pyrazin-2-yl)piperazin-1-yl)methanone (4.005)



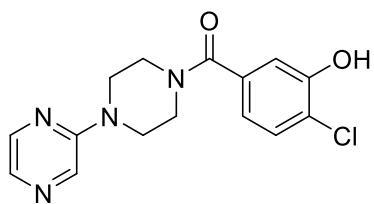
The title compound was obtained using 2-(piperazin-1-yl)pyrazine (215 mg, 1.3 mmol) and 3-chlorobenzoic acid (135 mg, 0.87 mmol) following General procedure A, affording the title compound as an off white solid (157 mg, 60 %). HPLC – t_R 4.962 min > 99 % purity at 254 nm; LRMS $[M+H]^+$ 303.0 m/z ; HRMS $[M+H]^+$ 303.1007 m/z , found 303.1011 m/z ; 1H NMR (400 MHz, $CDCl_3$) δ 8.15 (d, J = 1.3 Hz, 1H), 8.07 (dd, J = 2.5, 1.5 Hz, 1H), 7.90 (d, J = 2.6 Hz, 1H), 7.43 – 7.28 (m, 4H), 3.91 – 3.51 (m, 8H); ^{13}C NMR (101 MHz, $CDCl_3$) δ_C 169.2, 154.8, 142.0, 137.2, 134.9, 133.9, 131.2, 130.3, 130.2, 127.5, 125.3, 44.8 (br s, 4C).

(4-Hydroxyphenyl)(4-(pyrazin-2-yl)piperazin-1-yl)methanone (4.006)



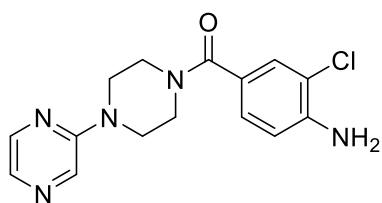
The title compound was obtained using 2-(piperazin-1-yl)pyrazine (400 mg, 2.44 mmol) and 4-hydroxybenzoic acid (224 mg, 1.63 mmol) following General procedure A, affording the title compound as a yellow solid (407 mg, 88 %). HPLC – t_R 3.79 min > 99 % purity at 254 nm; LRMS $[M+H]^+$ 285.9 m/z ; HRMS $[M+H]^+$ 285.1346 m/z , found 285.1354 m/z ; 1H NMR (400 MHz, $CDCl_3$) δ_H 8.11 – 8.02 (m, 1H), 7.82 (d, J = 2.5 Hz, 1H), 7.25 – 7.17 (m, 2H), 6.78 – 6.69 (m, 2H), 3.85 – 3.41 (m, 8H); ^{13}C NMR (101 MHz, $CDCl_3$) δ_C 171.7, 159.1, 154.9, 142.3, 133.2, 130.7, 129.4 (2C), 125.8, 115.8 (2C), 44.7 (br s, 4C).

(4-Chloro-3-hydroxyphenyl)(4-(pyrazin-2-yl)piperazin-1-yl)methanone (4.007)



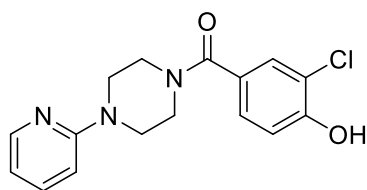
The title compound was obtained using 2-(piperazin-1-yl)pyrimidine (426 mg, 2.6 mmol) and 4-chloro-3-hydroxybenzoic acid (300 mg, 1.74 mmol) following General procedure A, affording the title compound as a solid (400 mg, 72 %) HPLC – t_R 4.49 min > 99 % purity at 254 nm; LRMS $[M+H]^+$ 318.9 m/z ; HRMS $[M+H]^+$ 319.0956 m/z , found 319.0956 m/z ; 1H NMR (400 MHz, $CDCl_3$) δ_H 8.22 (dd, J = 2.6, 1.4 Hz, 1H), 8.18 (d, J = 1.4 Hz, 1H), 7.90 (d, J = 2.7 Hz, 1H), 7.40 (d, J = 8.1 Hz, 1H), 7.12 (d, J = 1.9 Hz, 1H), 6.95 (dd, J = 8.2, 1.9 Hz, 1H), 3.88 – 3.60 (m, 8H); ^{13}C NMR (101 MHz, $CDCl_3$) δ_C 169.6, 154.9, 152.5, 142.0, 135.5, 134.0, 131.2, 129.9, 122.3, 119.7, 115.6, 44.8 (br s, 4C).

(4-Amino-3-chlorophenyl)(4-(pyrazin-2-yl)piperazin-1-yl)methanone (4.008)



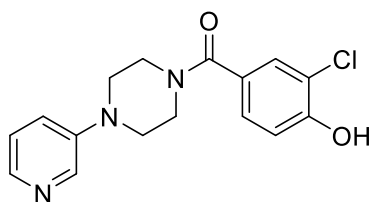
The title compound was obtained using 2-(piperazin-1-yl)pyrimidine (348 mg, 2.0 mmol) and 4-amino-3-chlorobenzoic acid (280 mg, 1.6 mmol) following General procedure A, affording the title compound as a yellow solid (390 mg, 77 %). HPLC – t_R 4.34 min > 99 % purity at 254 nm; LRMS $[M+H]^+$ 318.0 m/z ; HRMS $[M+H]^+$ 318.1116 m/z , found 318.1109 m/z ; 1H NMR (400 MHz, $CDCl_3$) δ_H 8.17 (br s, 1H), 8.11 (dd, J = 2.3, 1.4 Hz, 1H), 7.91 (d, J = 2.4 Hz, 1H), 7.42 (d, J = 1.9 Hz, 1H), 7.21 (dd, J = 8.2, 1.9 Hz, 1H), 6.77 (d, J = 8.2 Hz, 1H), 3.79 – 3.74 (m, 4H), 3.68 – 3.61 (m, 4H); ^{13}C NMR (101 MHz, $CDCl_3$) δ_C 169.9, 155.0, 145.0, 142.1, 133.4, 130.9, 129.5, 127.7, 125.4, 118.8, 115.1, 44.8 (br s, 4C).

(3-Chloro-4-hydroxyphenyl)(4-(pyridin-2-yl)piperazin-1-yl)methanone (4.009)



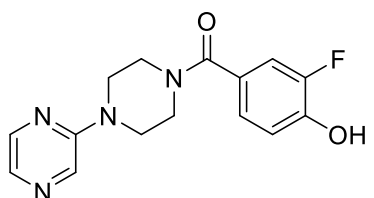
The title compound was obtained using 1-(pyridin-2-yl)piperazine (0.3 mL, 2.6 mmol) and 3-chloro-4-hydroxybenzoic acid (302 mg, 1.76 mmol) according to General procedure A, affording the title compound as an off white solid (334 mg, 60 %). HPLC – t_R 3.55 min > 99 % purity at 254 nm; LRMS $[M+H]^+$ 318.0 m/z ; HRMS $[M+H]^+$ 318.1000 m/z , found 318.1004 m/z ; 1H NMR (400 MHz, DMSO) δ_H 10.66 (br s, 1H), 8.11 (ddd, J = 4.9, 1.9, 0.6 Hz, 1H), 7.56 – 7.51 (m, 1H), 7.43 (d, J = 2.0 Hz, 1H), 7.25 (dd, J = 8.3, 2.1 Hz, 1H), 7.01 (d, J = 8.3 Hz, 1H), 6.82 (d, J = 8.6 Hz, 1H), 6.67 – 6.63 (m, 1H), 3.62 – 3.48 (m, 8H); ^{13}C NMR (101 MHz, DMSO) δ_C 167.9, 158.7, 154.4, 147.5, 137.6, 129.2, 127.5, 127.3, 119.5, 116.2, 113.3, 107.2, 44.6(4C).

(3-Chloro-4-hydroxyphenyl)(4-(pyridin-3-yl)piperazin-1-yl)methanone (4.010)



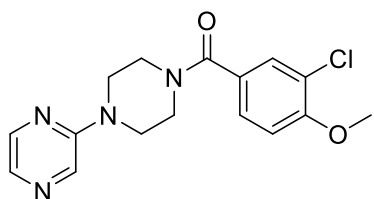
The title compound was obtained using using 1-(pyridin-3-yl)piperazine (300 mg, 1.3 mmol) and 3-chloro-4-hydroxybenzoic acid (218 mg, 1.3 mmol) following General procedure A, affording the title compound as a light brown solid (230 mg, 56 %). HPLC – t_R 3.55 min > 99 % purity at 254 nm; LRMS $[M+H]^+$ 318.0 m/z ; HRMS $[M+H]^+$ 318.1004 m/z , found 318.1008 m/z ; 1H NMR (400 MHz, DMSO) δ 10.66 (s, 1H), 8.28 (s, 1H), 7.98 (d, J = 4.0 Hz, 1H), 7.40 (d, J = 2.0 Hz, 1H), 7.34 – 7.29 (m, 1H), 7.25 – 7.18 (m, 2H), 6.99 (d, J = 8.3 Hz, 1H), 3.59 (br s, 4H), 3.20 (br s, 4H); ^{13}C NMR (101 MHz, DMSO) δ_C 167.9, 154.4, 146.4, 140.1, 138.1, 129.2, 127.5, 127.2, 123.5, 122.2, 119.5, 116.2, 47.7 (br s, 4C).

(3-Fluoro-4-hydroxyphenyl)(4-(pyrazin-2-yl)piperazin-1-yl)methanone (4.011)

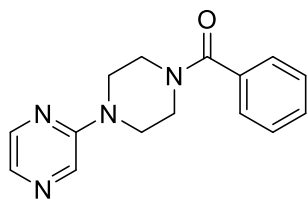


The title compound was obtained using 2-(piperazin-1-yl)pyrazine (400 mg, 2.44 mmol) and 3-fluoro-4-hydroxybenzoic acid (253 mg, 1.63 mmol) following General procedure A, affording the title compound as a light brown solid (450 mg, 91 %). HPLC – t_R 3.91 min > 99 % purity at 254 nm; LRMS $[M+H]^+$ 303.0 m/z ; HRMS $[M+H]^+$ 303.2152 m/z , found 303.1258 m/z ; 1H NMR (400 MHz, DMSO) δ_H 10.39 (br s, 1H), 8.33 (d, J = 1.3 Hz, 1H), 8.11 (dd, J = 2.6, 1.5 Hz, 1H), 7.87 (d, J = 2.6 Hz, 1H), 7.27 (dd, J = 11.6, 2.0 Hz, 1H), 7.17 – 7.09 (m, 1H), 7.01 (t, J = 8.5 Hz, 1H), 3.62 (br s, 8H); ^{13}C NMR (101 MHz, DMSO) δ_C 168.2, 154.4, 150.4 (d, J_{C-F} = 242.2 Hz), 146.6 (d, J_{C-F} = 11.9 Hz), 141.4, 132.7, 131.4, 126.4 (d, J_{C-F} = 5.5 Hz), 124.2 (d, J_{C-F} = 3.3 Hz), 117.4 (d, J_{C-F} = 3.2 Hz), 115.7 (d, J_{C-F} = 19.5 Hz), 43.9 (br s, 4C).

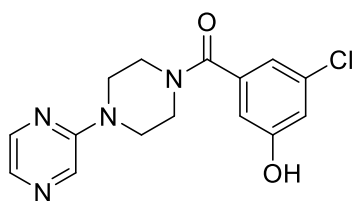
(3-Chloro-4-methoxyphenyl)(4-(pyrazin-2-yl)piperazin-1-yl)methanone (4.012)



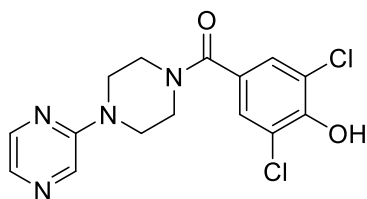
The title compound was obtained using 2-(piperazin-1-yl)pyrazine (400 mg, 2.44 mmol) and 3-chloro-4-methoxybenzoic acid (303 mg, 1.63 mmol) following General procedure A, affording the title compound as a white solid (530 mg, 97 %). HPLC – t_R 5.10 min > 99 % purity at 254 nm; LRMS $[M+H]^+$ 330.0 m/z ; HRMS $[M+H]^+$ 333.1133 m/z , found 333.1118 m/z ; 1H NMR (400 MHz, DMSO) δ_H 8.32 (d, J = 1.4 Hz, 1H), 8.09 (dd, J = 2.6, 1.5 Hz, 1H), 7.86 (d, J = 2.6 Hz, 1H), 7.52 (d, J = 2.0 Hz, 1H), 7.42 (dd, J = 8.5, 2.1 Hz, 1H), 7.21 (d, J = 8.5 Hz, 1H), 3.90 (s, 1H), 3.62 (br s, 8H); ^{13}C NMR (101 MHz, DMSO) δ_C 167.7, 155.5, 154.4, 141.4, 132.7, 131.4, 128.9, 128.6, 127.6, 120.9, 112.5, 56.3, 43.8 (br s, 4C).

Phenyl(4-(pyrazin-2-yl)piperazin-1-yl)methanone (4.013)

The title compound was obtained using 2-(piperazin-1-yl)pyrazine (215 mg, 1.3 mmol) and benzoic acid (106 mg, 0.87 mmol) following General procedure A, affording the title compound as a yellow solid (178 mg, 76 %). HPLC – t_R 4.374 min > 99 % purity at 254 nm; LRMS $[M+H]^+$ 269.0 m/z ; HRMS $[M+H]^+$ 269.1400 m/z , found 269.1397 m/z ; 1H NMR (400 MHz, MeOD) δ_H 8.25 (d, J = 1.5 Hz, 1H), 8.13 (dd, J = 2.7, 1.5 Hz, 1H), 7.83 (d, J = 2.7 Hz, 1H), 7.54 – 7.46 (m, 5H), 3.95 – 3.57 (m, 8H); ^{13}C NMR (101 MHz, MeOD) δ_C 172.2, 156.0, 143.0, 136.2, 133.4, 131.7, 131.0, 129.5 (2C), 127.9 (2C), 45.4 (2C), 45.0 (2C).

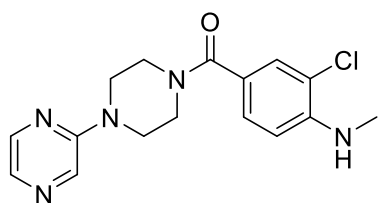
(3-Chloro-5-hydroxyphenyl)(4-(pyrazin-2-yl)piperazin-1-yl)methanone (4.014)

The title compound was obtained using 2-(piperazin-1-yl)pyrazine (400 mg, 2.44 mmol) and 3-chloro-5-hydroxybenzoic acid (280 mg, 1.63 mmol) following General procedure A, affording the title compound as a white solid (390 mg, 75 %). HPLC – t_R 4.66 min > 95 % purity at 254 nm; LRMS $[M+H]^+$ 318.9 m/z ; HRMS $[M+H]^+$ 319.0956 m/z , found 319.0962 m/z ; 1H NMR (400 MHz, DMSO) δ_H 10.32 (br s, 1H), 8.33 (d, J = 1.4 Hz, 1H), 8.10 (dd, J = 2.6, 1.5 Hz, 1H), 7.87 (d, J = 2.6 Hz, 1H), 6.91 – 6.88 (m, 2H), 6.76 – 6.74 (m, 1H), 3.74 – 3.39 (m, 8H); ^{13}C NMR (101 MHz, DMSO) δ_C 167.6, 158.6, 154.4, 141.4, 138.6, 133.6, 132.8, 131.4, 117.0, 116.3, 112.7, 44.7, 44.4.

(3,5-Dichloro-4-hydroxyphenyl)(4-(pyrazin-2-yl)piperazin-1-yl)methanone (4.015)

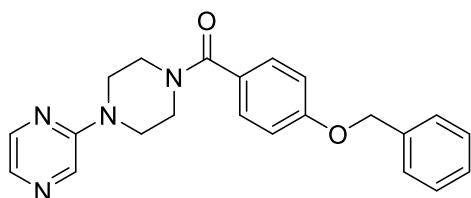
The title compound was obtained using 2-(piperazin-1-yl)pyrazine (400 mg, 2.44 mmol) and 3,5-dichloro-4-hydroxybenzoic acid (337 mg, 1.63 mmol) following General procedure A. Upon reaction completion the solution was concentrated *in vacuo*, diluted with EtOAc and washed with brine. The organic layers were collected, dried over $MgSO_4$, filtered and concentrated. The crude product was diluted with DCM and filtered via affording the title compound as light pink solid (407 mg, 71 %). HPLC – t_R 4.60 min > 99 % purity at 254 nm; LRMS $[M+H]^+$ 352.9 m/z ; HRMS $[M+H]^+$ 353.0567 m/z , found 353.0576 m/z ; 1H NMR (400 MHz, DMSO) δ_H 10.60 (br s, 1H), 8.32 (d, J = 1.4 Hz, 1H), 8.09 (dd, J = 2.6, 1.5 Hz, 1H), 7.86 (d, J = 2.6 Hz, 1H), 7.46 (s, 2H), 3.69 – 3.51 (m, 8H); ^{13}C NMR (101 MHz, DMSO) δ_C 166.7, 154.4, 150.5, 141.4, 132.7, 131.4, 127.9, 127.6 (2C), 122.1 (2C), 43.8 (br s, 4C).

(3-Chloro-4-(methylamino)phenyl)(4-(pyrazin-2-yl)piperazin-1-yl)methanone (4.016)



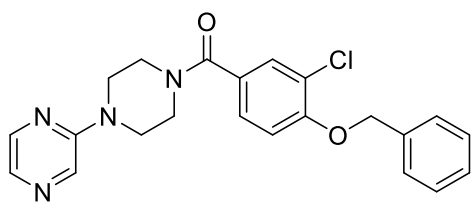
The title compound was obtained using 2-(piperazin-1-yl)pyrimidine (200 mg, 1.2 mmol) and 3-chloro-4-(methylamino)benzoic acid (225 mg, 1.2 mmol) following General procedure A, affording the title compound as a pale yellow solid (250 mg, 63 %). HPLC – t_R 4.87 min > 99 % purity at 254 nm; LRMS $[M+H]^+$ 332.0 m/z ; HRMS $[M+H]^+$ 332.1273 m/z , found 332.1279 m/z ; 1H NMR (400 MHz, $CDCl_3$) δ 8.15 (s, 1H), 8.09 – 8.07 (m, 1H), 7.90 (d, J = 2.2 Hz, 1H), 7.43 (d, J = 2.0 Hz, 1H), 7.31 (dd, J = 8.4, 2.0 Hz, 1H), 6.62 (d, J = 8.4 Hz, 1H), 3.79 – 3.73 (m, 4H), 3.66 – 3.61 (m, 4H), 2.94 (s, 3H); ^{13}C NMR (101 MHz, $CDCl_3$) δ_C 170.2, 154.9, 146.7, 142.0, 133.7, 131.2, 129.1, 128.1, 123.2, 118.6, 109.7, 44.8 (br s, 4C), 30.3.

(4-(Benzyloxy)phenyl)(4-(pyrazin-2-yl)piperazin-1-yl)methanone (4.017)



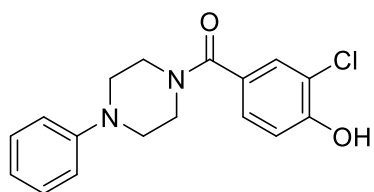
The title compound was obtained using 2-(piperazin-1-yl)pyrazine (508 mg, 3.1 mmol) and 4-(benzyloxy)benzoic acid (500 mg, 2.07 mmol) following General procedure A, affording the title compound as a white solid (586 mg, 76 %). HPLC – t_R 5.96 min > 99 % purity at 254 nm; LRMS $[M+H]^+$ 375.0 m/z ; HRMS $[M+H]^+$ 375.1816 m/z , found 375.1822 m/z ; 1H NMR (400 MHz, $CDCl_3$) δ_H 8.15 (d, J = 0.9 Hz, 1H), 8.08 (dd, J = 2.6, 1.5 Hz, 1H), 7.90 (d, J = 2.6 Hz, 1H), 7.46 – 7.33 (m, 7H), 7.03 – 6.99 (m, 2H), 5.11 (s, 2H), 3.84 – 3.60 (m, 8H); ^{13}C NMR (101 MHz, $CDCl_3$) δ_C 170.7, 160.4, 154.9, 141.9, 136.6, 133.9, 131.3, 129.4 (2C), 128.8 (2C), 128.7, 128.3, 127.6 (2C), 114.9 (2C), 70.3, 44.8 (br s, 4C).

(4-(Benzyloxy)-3-chlorophenyl)(4-(pyrazin-2-yl)piperazin-1-yl)methanone (4.018)



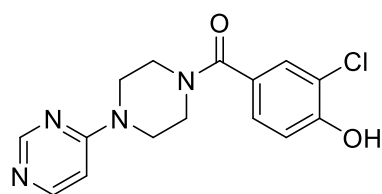
The title compound was obtained using 2-(piperazin-1-yl)pyrazine (469 mg, 2.90 mmol) and 4-(benzyloxy)-2-chlorobenzoic acid (500 mg, 1.91 mmol) following General procedure A, affording the title compound as a yellow solid (536 mg, 69 %). HPLC – t_R 6.32 min > 99 % purity at 254 nm; LRMS $[M+H]^+$ 409.0 m/z ; HRMS $[M+H]^+$ 409.1426 m/z , found 409.1432 m/z ; 1H NMR (400 MHz, MeOD) δ_H 8.17 (d, J = 1.0 Hz, 1H), 8.08 (dd, J = 2.6, 1.5 Hz, 1H), 7.80 (d, J = 2.6 Hz, 1H), 7.52 (t, J = 3.0 Hz, 1H), 7.48 – 7.42 (m, 2H), 7.40 – 7.26 (m, 3H), 7.16 (dd, J = 8.4, 4.2 Hz, 1H), 5.18 (s, 2H), 3.61 (br s, 8H); 1H NMR (400 MHz, $CDCl_3$) δ_H 8.15 (d, J = 1.2 Hz, 1H), 8.10 – 8.07 (m, 1H), 7.91 (d, J = 2.6 Hz, 1H), 7.54 – 7.24 (m, 7H), 7.01 – 6.96 (m, 1H), 5.21 (s, 2H), 3.81 – 3.58 (m, 8H); ^{13}C NMR (101 MHz, $CDCl_3$) δ_C 169.4, 155.8, 154.8, 142.0, 136.0, 133.6, 131.0, 129.8, 128.8 (2C), 128.4, 128.3, 127.3, 127.2 (2C), 123.6, 113.7, 71.0, 44.7 (4C).

(3-Chloro-4-hydroxyphenyl)(4-phenylpiperazin-1-yl)methanone (4.019)



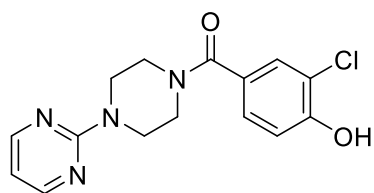
The title compound was obtained using 1-phenylpiperazine (0.3 mL) and 3-chloro-4-hydroxybenzoic acid (282 mg, 1.63 mmol) following General procedure A, affording the title compound as a white solid (250 mg, 49 %). HPLC – t_R 4.81 min > 99 % purity at 254 nm; LRMS $[M+H]^+$ 317.0 m/z ; HRMS $[M+H]^+$ 317.1051 m/z , found 317.1058 m/z ; 1H NMR (400 MHz, MeOD) δ_H 7.43 (d, J = 2.1 Hz, 1H), 7.26 – 7.21 (m, 3H), 6.99 – 6.92 (m, 3H), 6.88 – 6.84 (m, 1H), 3.64 (br s, 4H), 3.14 (br s, 4H); ^{13}C NMR (101 MHz, MeOD) δ_C 171.0 (2C), 156.1, 152.1, 130.4, 130.0 (2C), 128.3, 128.0, 121.7, 121.5, 117.7, 117.3, 50.6 (br s, 4C).

(3-Chloro-4-hydroxyphenyl)(4-(pyrimidin-4-yl)piperazin-1-yl)methanone (4.020)



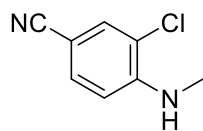
The title compound was obtained using 4-(piperazin-1-yl)pyrimidine (100 mg, 0.61 mmol) and 3-chloro-4-hydroxybenzoic acid (120 mg, 0.69 mmol) following General procedure A, affording the title compound as a white solid (100 mg, 52 %). HPLC – t_R 3.30 min > 99 % purity at 254 nm; LRMS $[M+H]^+$ 318.9 m/z ; HRMS $[M+H]^+$ 319.0956 m/z , found 319.0963 m/z ; 1H NMR (400 MHz, MeOD) δ_H 8.49 (s, 1H), 8.17 (d, J = 6.4 Hz, 1H), 7.49 (d, J = 2.1 Hz, 1H), 7.29 (dd, J = 8.4, 2.1 Hz, 1H), 6.99 (d, J = 8.4 Hz, 1H), 6.82 (dd, J = 6.4, 1.1 Hz, 1H), 3.85 – 3.68 (m, 8H); ^{13}C NMR (101 MHz, MeOD) δ_C 171.7, 162.9, 158.7, 156.8, 155.8, 130.7, 128.6, 128.1, 122.0, 117.5, 104.7, 44.6 (br s, 4C).

(3-Chloro-4-hydroxyphenyl)(4-(pyrimidin-2-yl)piperazin-1-yl)methanone (4.021)



The title compound was obtained using 2-(piperazin-1-yl)pyrimidine (328 mg, 2 mmol) and 3-chloro-4-hydroxybenzoic acid (173 mg, 1.0 mmol) following General procedure A, affording the title compound as a white solid (300 mg, 94 %). HPLC – t_R 4.27 min > 99 % purity at 254 nm; LRMS $[M+H]^+$ 319.0 m/z ; HRMS $[M+H]^+$ 319.0956 m/z , found 319.0963 m/z ; 1H NMR (400 MHz, DMSO) δ_H 10.68 (s, 1H), 8.37 (d, J = 4.7 Hz, 2H), 7.44 (d, J = 2.0 Hz, 1H), 7.26 (dd, J = 8.3, 2.0 Hz, 1H), 7.02 (d, J = 8.3 Hz, 1H), 6.65 (t, J = 4.7 Hz, 1H), 3.77 (br s, 4H), 3.56 (br s, 4H); ^{13}C NMR (101 MHz, DMSO) δ_C 167, 160.9, 157.7 (2C), 154.2, 129.0, 127.3, 127.1, 119.3, 116.0, 110.2, 43.0 (br s, 4C).

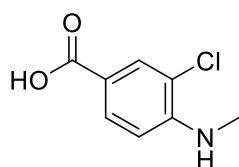
3-Chloro-4-(methylamino)benzonitrile (4.023)⁵⁴



A solution of 3-chloro-4-fluorobenzonitrile (1.0 g, 6.5 mmol), methylamine (1 mL) in MeOH (16 mL) and DIPEA was reacted in the microwave at 120°C for 15 min. The mixture was ethyl acetate and water. The organic layers were collected, dried

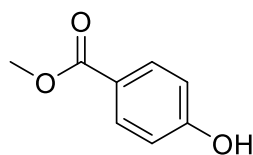
over MgSO_4 concentrated *in vacuo* to give 3-chloro-4-methylaminobenzonitrile to be used directly in the next step (1.02 g, 94 %).¹³ LRMS $[\text{M}+\text{H}]^+$ 167.0 m/z ; ^1H NMR (400 MHz, DMSO) δ_{H} 7.71 (d, J = 1.9 Hz, 1H), 7.57 – 7.54 (m, 1H), 6.70 (d, J = 8.6 Hz, 1H), 6.55 – 6.48 (m, 1H), 2.80 (d, J = 4.8 Hz, 3H); ^{13}C NMR (101 MHz, DMSO) δ_{C} 148.6, 132.7, 132.1, 119.2, 117.2, 110.4, 96.4, 29.5. Acquired data is consistent with the literature.⁵⁴

3-Chloro-4-(methylamino)benzoic acid (4.024)⁵⁵



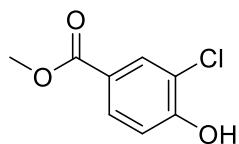
A suspension of 3-chloro-4-methylaminobenzonitrile (900 mg, 5.4 mmol) in 2M aqueous NaOH solution (30 mL) was heated to reflux for 3 h. The mixture was cooled to room temperature and the solution was acidified with 2M aqueous HCl solution. The resulting solid was collected by suction filtration to give the known title compound as a solid (920 mg, 92 %).¹³ HPLC – t_{R} 4.53 min > 99 % purity at 254 nm; LRMS $[\text{M}+\text{H}]^+$ 185.0 m/z ; ^1H NMR (400 MHz, DMSO) δ 12.39 (bs, 1H), 7.75 – 7.72 (m, 2H), 6.69 – 6.65 (m, 1H), 6.30 – 6.24 (m, 1H), 2.82 (d, J = 4.8 Hz, 3H); ^{13}C NMR (101 MHz, DMSO) δ_{C} 166.6, 148.6, 130.1, 130.0, 117.7, 116.8, 109.6, 29.6.

Methyl 4-hydroxybenzoate (4.027/ 2.048c-Chapter 2)⁵⁶



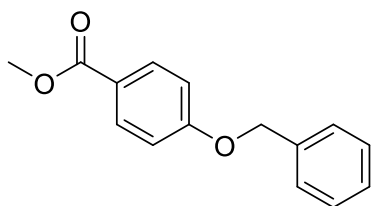
To a solution of 4-hydroxybenzoic acid (5.00 g, 36.0 mmol) in MeOH (5 mL), 1 drop of H_2SO_4 was added. The reaction mixture was then heated to reflux for 12 h then reduced *in vacuo*. Upon reaction completion the pH was neutralized with base (NaOH 1M/ Na_2CO_3) to give a solid. The product was filtered and dried. The organic layer was collected, dried over MgSO_4 , filtered and reduced *in vacuo* to afford the desired product as a white solid (5.17 g, 94%). HPLC – t_{R} 4.18 min > 99% purity at 254 nm; LRMS $[\text{M}-\text{H}]^-$ 150.9 m/z ; ^1H NMR (400 MHz, CDCl_3) δ_{H} 7.99 – 7.93 (m, 2H), 6.89 – 6.84 (m, 2H), 3.89 (s, 3H); ^{13}C NMR (101 MHz, CDCl_3) δ_{C} 167.5, 160.3, 132.1 (2C), 122.6, 115.4 (2C), 52.2. Acquired data is consistent with the literature.⁵⁶

Methyl 3-chloro-4-hydroxybenzoate (4.028)⁵⁷



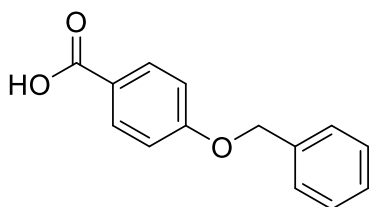
To a solution of 3-chloro-4-hydroxybenzoic acid (1.0 g, 5.81 mmol) dissolved in MeOH (10 mL) was added 3 drops of H_2SO_4 . The mixture was heated to reflux for 48 h. Upon reaction completion the mixture was concentrated *in vacuo*, diluted with DCM and washed with brine. The organic layers were combined and collected, dried over MgSO_4 , filter and concentrated *in vacuo* to afford the known title compound as an off-white solid without further purification (1.0 g, 93 %).⁵ HPLC – t_{R} 4.72 min > 99 % purity at 254 nm; LRMS $[\text{M}+\text{H}]^+$ 186.9 m/z ; ^1H NMR (400 MHz, MeOD) δ_{H} 7.95 (dd, J = 5.6, 2.1 Hz, 1H), 7.80 (dd, J = 8.5, 2.1 Hz, 1H), 6.97 (d, J = 8.5 Hz, 1H), 3.88 (s, 3H); ^{13}C NMR (101 MHz, MeOD) δ_{C} 167.5, 159.0, 132.6, 130.8, 123.5, 121.8, 117.2, 52.5.⁵⁷

Methyl 4-(benzyloxy)benzoate (4.029 /2.049c Chapter 2)⁵⁸



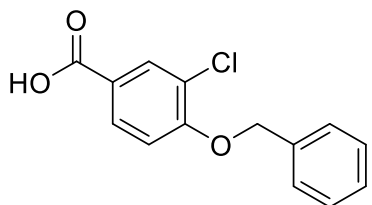
To a solution of methyl 4-hydroxybenzoate (5.00 g, 33.0 mmol), benzyl bromide (4.3 mL, 36.0 mmol) in ACN (5 mL) was added potassium carbonate (9.10 g, 66.0 mmol). The reaction was heated to reflux over 12 h then reduced *in vacuo*. The crude material was diluted with EtOAc and washed with brine, dried with MgSO₄, filtered and concentrated *in vacuo* to afford the desired product as a white solid (7.9 g, 99%). HPLC - t_R 7.04 min > 99% purity at 254 nm; LRMS [M+H]⁺ 242.9 m/z ; ¹H NMR (400 MHz, DMSO-*d*₆) δ_H 7.95 – 7.89 (m, 2H), 7.50 – 7.31 (m, 5H), 7.19 – 7.07 (m, 2H), 5.20 (s, 2H), 3.82 (s, 3H); ¹³C NMR (101 MHz, DMSO) δ_C 166.1, 162.4, 136.7, 131.4 (2C), 128.7 (2C), 128.2, 128.0 (2C), 122.3, 115.0 (2C), 69.8, 52.0. Acquired data is consistent with the literature.⁵⁸

4-(Benzyloxy)benzoic acid (4.031/ 2.050c Chapter 2)⁵⁹



To a solution of the methyl 4-(benzyloxy)benzoate (6.00 g, 25.0 mmol) in MeOH (5 mL) and water (10 mL) was added NaOH (4.90 g, 123 mmol). The reaction mixture was heated to 65°C for 3 h then reduced *in vacuo*. The mixture was acidified to pH 2 using 2N HCl. To the suspension EtOAc was added and washed with water. The organic layer was dried over MgSO₄, filtered and the solvent was removed *in vacuo* to afford the desired product as a white solid (5.7 g, 99%). HPLC - t_R 6.06 min > 99% purity at 254 nm; LRMS [M+H]⁺ 228.9 m/z ; ¹H NMR (400 MHz, CDCl₃) δ_H 7.76 – 7.68 (m, 2H), 7.48 – 7.31 (m, 6H), 7.25 – 7.20 (m, 1H), 5.13 (s, 2H); ¹H NMR (400 MHz, DMSO) δ_H 7.59 – 7.54 (m, 2H), 7.16 – 7.00 (m, 5H), 6.76 – 6.72 (m, 2H), 4.85 (s, 2H); ¹³C NMR (101 MHz, DMSO) δ_C 167.7, 161.5, 136.8, 131.3 (2C), 128.6 (2C), 128.1, 127.9 (2C), 125.3, 114.5 (2C), 69.5. Acquired data is consistent with the literature.⁵⁹

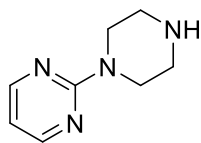
4-(Benzyloxy)-3-chlorobenzoic acid (4.032)⁶⁰



To a solution of methyl 3-chloro-4-hydroxybenzoate (1.0g, 5.35 mmol), K₂CO₃ in ACN (10 mL) was added bromobenzene (0.7 mL, 5.88 mmol). The mixture was heated to reflux over 12 h. Upon reaction completion the mixture was concentrated *in vacuo*, then washed with EtOAc and brine. The organic layers were collected and dried over MgSO₄, filtered and concentrated to give methyl 4-(benzyloxy)-3-chlorobenzoate (**4.030**). To this compound was added MeOH and H₂O (1:2), followed by NaOH (4.92 equiv). The solution was heated to 65°C for 3 h. Upon reaction completion the solution was quenched with 1M HCl, then washed with EtOAc and brine. The organic layers were collected and dried over MgSO₄, filtered and concentrated *in vacuo* to afford the known title compound as a white solid (1.35 g, 96 %). HPLC - t_R 6.19 min > 99 % purity at 254 nm; ¹H NMR (400 MHz, DMSO) δ 12.92 (br s, 1H), 7.91 – 7.82 (m, 2H), 7.46 – 7.26 (m, 6H), 5.25 (s, 2H);

^{13}C NMR (101 MHz, DMSO) δ_{C} 165.9, 157.0, 136.0, 130.7, 129.9, 128.5 (2C), 128.2, 128.1, 127.5 (2C), 121.5, 113.8, 70.3.

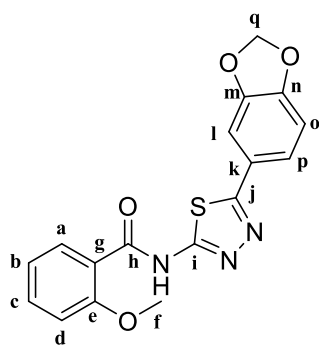
2-(Piperazin-1-yl)pyrimidine (4.034)^{18, 61}



To a stirred solution of piperazine (1.93 g, 22.5 mmol) and K_2CO_3 in H_2O (8 mL) was slowly added 2-chloropyrimidine (1.03 g, 9 mmol) at 50-60°C. The mixture was stirred at 60-65°C for 1 h. Upon reaction completion the mixture was cooled and filtered. The filtrate was extracted with chloroform, the organic layers collected and dried over MgSO_4 , filtered and concentrated to afford the known title compound as a yellow solid (1.20 g, 80 %).¹⁸ HPLC – t_{R} 1.77 min > 99 % purity at 254 nm; LRMS $[\text{M}+\text{H}]^+$ 165.1 m/z ; ^1H NMR (400 MHz, CDCl_3) δ_{H} 8.30 (d, $J = 4.7$ Hz, 2H), 6.47 (t, $J = 4.7$ Hz, 1H), 3.81 – 3.77 (m, 4H), 2.95 – 2.91 (m, 4H); ^{13}C NMR (101 MHz, CDCl_3) δ_{C} 162.0, 157.8 (2C), 109.9, 46.2 (2C), 45.0 (2C).⁶¹

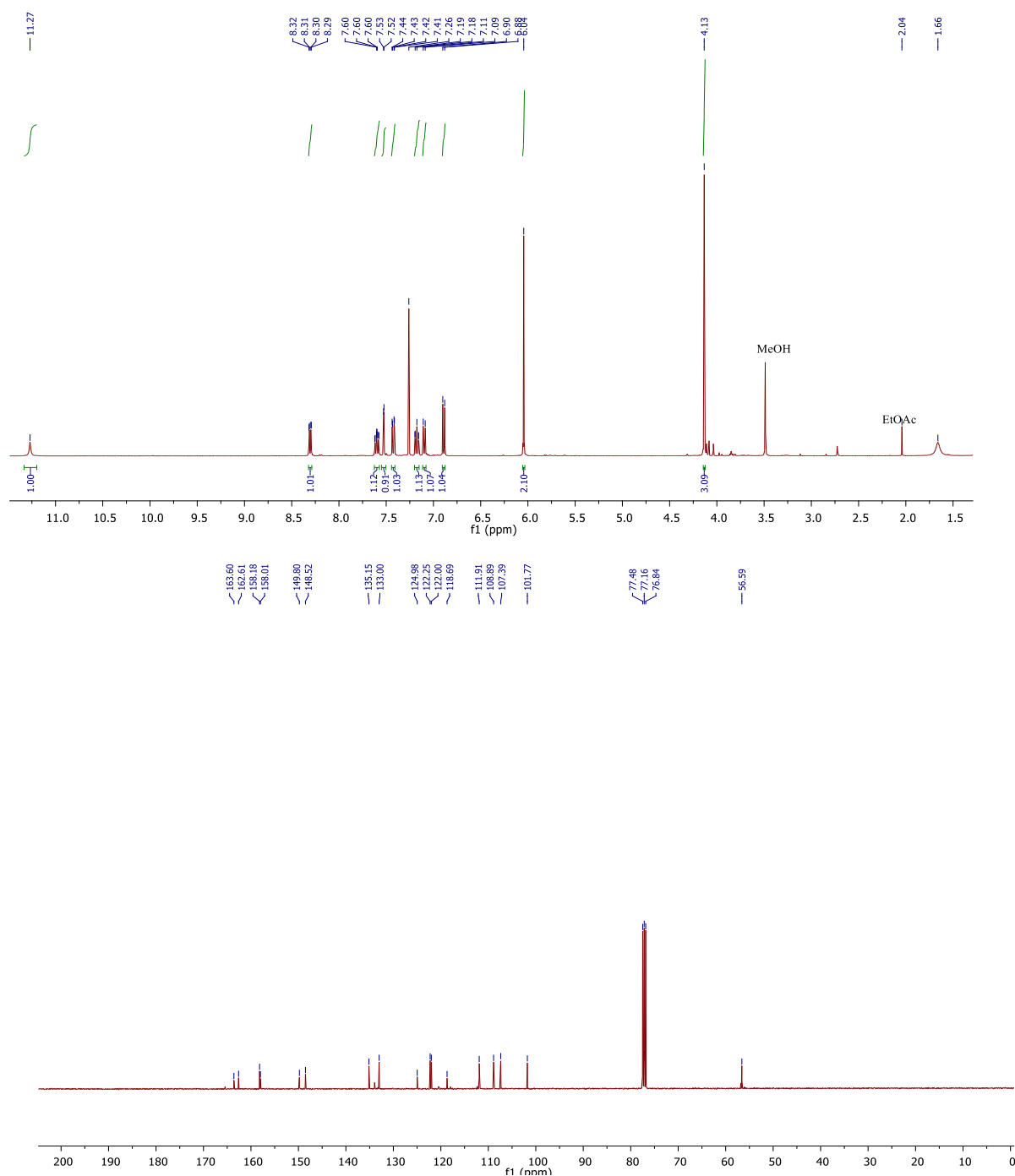
Scaffold 3 Compounds

N-(5-(benzo[*d*][1,3]dioxol-5-yl)-1,3,4-thiadiazol-2-yl)-2-methoxybenzamide (4.002)

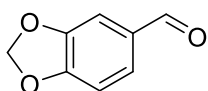


To a solution of 5-(benzo[*d*][1,3]dioxol-5-yl)-1,3,4-thiadiazol-2-amine (87 mg, 0.39 mmol) and DIPEA (0.4 mL) in DCM (5 mL) was added 2-methoxybenzoyl chloride (1 equiv.) slowly. The solution was stirred at room temp over 12 h. Upon reaction completion the mixture was concentrated, diluted with EtOAc, washed with brine. The mixture was extracted with EtOAc, the organic layers were collected, dried over MgSO_4 , filtered and concentrated, followed by column chromatography ($\text{CHCl}_3/\text{MeOH}/\text{NH}_4\text{OH}$: 94%, 5%, 1% eluent) to afford the title compound as an off white solid (80 mg, 58 %). HPLC – t_{R} 6.40 min > 99 % purity at 254 nm; LRMS $[\text{M}+\text{H}]^+$ 356.1 m/z ; HRMS $[\text{M}+\text{H}]^+$ 356.0700 m/z , found 356.0712 m/z ; ^1H NMR (400 MHz, CDCl_3) δ_{H} 11.27 (s, 1H, NH), 8.30 (dd, $J = 7.9, 1.8$ Hz, 1H, Ha), 7.62 – 7.58 (m, 1H, Hc), 7.53 (d, $J = 1.7$ Hz, 1H, Hl), 7.43 (dd, $J = 8.1, 1.8$ Hz, 1H, Hp), 7.20 – 7.16 (m, 1H, Hb), 7.10 (d, $J = 8.3$ Hz, 1H, Hd), 6.89 (d, $J = 8.1$ Hz, 1H, Ho), 6.04 (s, 2H, Hq), 4.13 (s, 3H, Hf), solvent impurity peaks are present within the spectrum (aliphatic region); ^{13}C NMR (101 MHz, CDCl_3) δ_{C} 163.6 (Ci), 162.6 (Cj), 158.2 (Ch), 158.0 (Ce), 149.8 (Cm/n), 148.5 (Cm/n), 135.2 (Ca/c), 133.0 (Ca/c), 125.0 (Ck), 122.3 (Cb), 122.0 (Cp), 118.7 (Cg), 111.9 (Cd), 108.9 (Cl), 107.4 (Co), 101.8 (Cq), 56.6 (Cf).

Example spectra for Scaffold 3: ^1H (400 MHz, CDCl_3) and ^{13}C NMR (100 MHz, CDCl_3) spectrum of *N*-(5-(benzo[*d*][1,3]dioxol-5-yl)-1,3,4-thiadiazol-2-yl)-2-methoxybenzamide (4.002). Solvent impurity peaks present within ^1H NMR spectrum (aliphatic region)



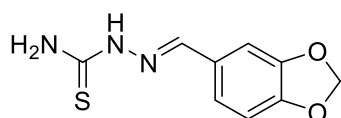
Benzo[*d*][1,3]dioxole-5-carbaldehyde (4.036)^{19, 24}



To a solution of 3,4-dihydroxybenzaldehyde (1.0 g, 7.3 mmol) in DMF (10 mL) was added K_2CO_3 (1.5 g) and diiodomethane (0.87 mL). The reaction mixture was refluxed for 2 h at 110°C . Upon reaction completion the mixture was cooled to room temperature, filtered through a celite pad and washed with DCM. The filtrate was diluted with water and extracted with DCM. The organic layers were collected, dried over MgSO_4 and concentrated

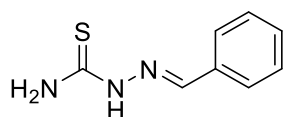
in vacuo to afford the known title compound as a pale brown solid (1.0 g, 91 % yield). ¹⁹ ¹H NMR (400 MHz, DMSO) δ_H 9.80 (s, 1H), 7.54 (dd, *J* = 8.0, 1.6 Hz, 1H), 7.32 (d, *J* = 1.6 Hz, 1H), 7.14 (d, *J* = 8.0 Hz, 1H), 6.17 (s, 2H); ¹³C NMR (101 MHz, DMSO) δ_C 190.9, 152.7, 148.3, 131.5, 128.5, 108.5, 106.3, 102.3. Acquired data is consistent with the literature.²⁴

2-(Benzo[*d*][1,3]dioxol-5-ylmethylene)hydrazine-1-carbothioamide (4.037)⁶²



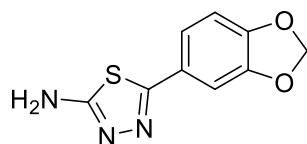
Benzo[*d*][1,3]dioxole-5-carbaldehyde (824 mg, 5.5 mmol) was reacted with thiosemicarbazide (1.0 eq) in ethanol (10 mL) with catalytic amounts of acetic acid at room temperature over 12 h. Upon reaction completion the mixture was filtered and the solid was washed with petroleum ether.²⁵ The white solid was collected and taken to the next step with out further purification (940 mg, 77 %). HPLC – *t*_R 4.24 min > 99 % purity at 254 nm; LRMS [M+H]⁺ 224.2 *m/z*; ¹H NMR (400 MHz, DMSO) δ_H 11.30 (s, 1H), 8.10 (s, 1H), 8.01 (s, 1H), 7.94 (s, 1H), 7.64 (d, *J* = 1.5 Hz, 1H), 7.07 (dd, *J* = 8.1, 1.6 Hz, 1H), 6.92 (d, *J* = 8.0 Hz, 1H), 6.06 (s, 2H). Acquired data is consistent with the literature.⁶²

2-Benzylidenehydrazine-1-carbothioamide (4.037b)⁶³



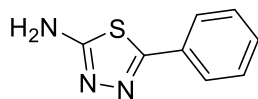
Benzaldehyde (1 mL, 9 mmol) was reacted with thiosemicarbazide (1.0 eq) in ethanol (10 mL) with catalytic amounts of acetic acid at room temperature over 12 h. Upon reaction completion the mixture was filtered and the solid was washed with petroleum ether. The white solid was collected and taken to the next step with out further purification (1.0 g, 62 %). HPLC – *t*_R 4.02 min > 99 % purity at 254 nm; LRMS [M+H]⁺ 180.1 *m/z*; ¹H NMR (400 MHz, DMSO) δ_H 11.43 (s, 1H), 8.20 (s, 1H, NH₂), 8.05 (s, 1H, NH), 7.99 (s, 1H, NH₂), 7.82 – 7.77 (m, 2H), 7.42 – 7.38 (m, 3H); ¹³C NMR (101 MHz, DMSO) δ_C 178.0, 142.3, 134.2, 129.8, 128.6 (2C), 127.3 (2C). Acquired data is consistent with the literature.⁶³

5-(Benzo[*d*][1,3]dioxol-5-yl)-1,3,4-thiadiazol-2-amine (4.038)⁶⁴



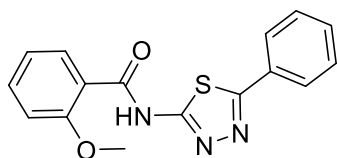
To a solution of 2-(Benzo[*d*][1,3]dioxol-5-ylmethylene)hydrazine-1-carbothioamide (448 mg, 2 mmol) in EtOH (5 mL) was added iron(III) chloride hexahydrate (2.0 equiv.) The mixture was heated to reflux over 12 h. Upon reaction completion the mixture was cooled and filtered with DCM. The filtrate was diluted with water and extracted with DCM.²⁶ The organic layers were collected, dried over MgSO₄ and concentrated *in vacuo* to afford the known title compound as a pale yellow solid (100 mg, 23 %). HPLC – *t*_R 3.75 min > 99 % purity at 254 nm; LRMS [M+H]⁺ 222.1 *m/z*; ¹H NMR (400 MHz, DMSO) δ_H 7.31 (br s, 3H), 7.18 (d, *J* = 8.0 Hz, 1H), 6.97 (d, *J* = 8.1 Hz, 1H), 6.07 (s, 2H).

5-Phenyl-1,3,4-thiadiazol-2-amine (4.038b)^{26, 65}



To a solution of 2-benzylidenehydrazine-1-carbothioamide (180 mg, 1 mmol) in EtOH (5 mL) was added iron(III) chloride hexahydrate (2.0 equiv.) The mixture was heated to reflux over 12 h. Upon reaction completion the mixture was cooled and filtered with DCM. The filtrate was diluted with water and extracted with DCM.²⁶ The organic layers were collected, dried over MgSO₄ and concentrated *in vacuo* to afford the known title compound as a pale yellow solid (110 mg, 62 %). HPLC – *t*_R 3.56 min > 95 % purity at 254 nm; LRMS [M+H]⁺ 178.1 *m/z*; ¹H NMR (400 MHz, DMSO) δ_H 7.77 – 7.73 (m, 2H), 7.50 – 7.41 (m, 3H), 7.41 (s, 2H, NH₂); ¹³C NMR (101 MHz, DMSO) δ_C 168.5, 156.4, 131.0, 129.5, 129.1 (2C), 126.3 (2C). Acquired data is consistent with the literature.⁶⁵

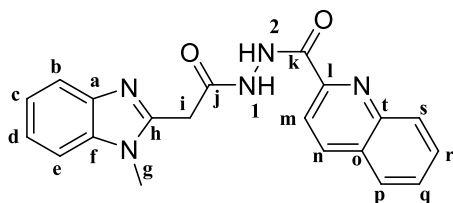
2-Methoxy-*N*-(5-phenyl-1,3,4-thiadiazol-2-yl)benzamide (4.039)



To a solution of 5-phenyl-1,3,4-thiadiazol-2-amine (100 mg, 0.56 mmol) and DIPEA (0.4 mL) in DCM (5 mL) was added 2-methoxybenzoyl chloride (1 equiv.) slowly. The solution was stirred at room temp over 12 h. Upon reaction completion the mixture was concentrated, diluted with EtOAc, washed with brine. The mixture was extracted with EtOAc, the organic layers were collected, dried over MgSO₄, filtered and concentrated, followed by column chromatography (CHCl₃/ MeOH/ NH₄OH: 94%, 5%, 1% eluent) to afford the title compound as an off white solid (102 mg, 59 %). HPLC – *t*_R 6.44 min > 95 % purity at 254 nm; LRMS [M+H]⁺ 312.1 *m/z*; HRMS [M+H]⁺ 312.0801 *m/z*, found 312.0811 *m/z*; ¹H NMR (400 MHz, CDCl₃) δ_H 11.30 (s, 1H, NH), 8.30 (dd, *J* = 7.9, 1.8 Hz, 1H), 7.99 – 7.95 (m, 2H), 7.61 – 7.56 (m, 1H), 7.49 – 7.45 (m, 3H), 7.18 – 7.14 (m, 1H), 7.08 (d, *J* = 8.3 Hz, 1H), 4.12 (s, 3H); ¹³C NMR (101 MHz, CDCl₃) δ_C 163.9, 162.6, 158.5, 158.2, 135.2, 133.0, 130.8, 130.6, 129.2 (2C), 127.4 (2C), 122.0, 118.6, 111.9, 56.6.

Scaffold 4 Compounds

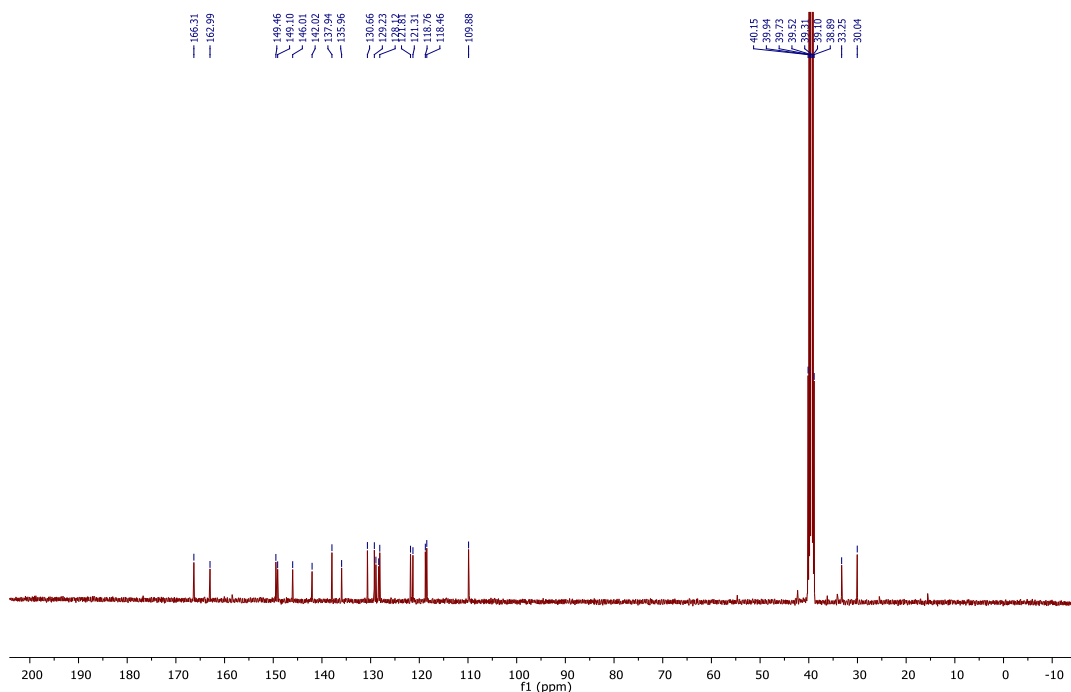
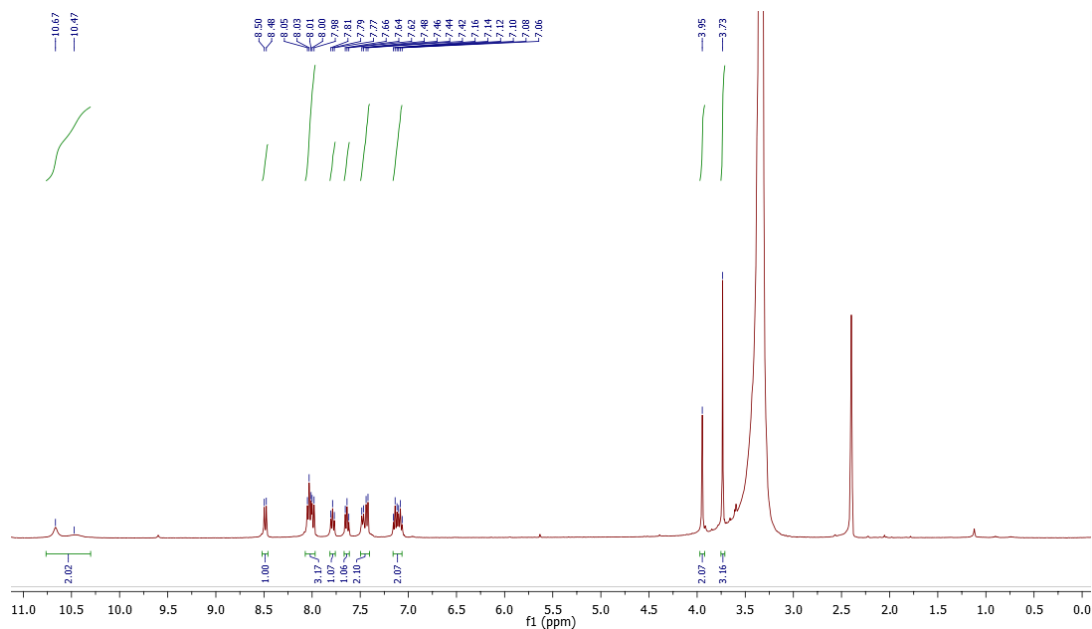
N'-(2-(1-Methyl-1*H*-benzo[d]imidazol-2-yl)acetyl)quinoline-2-carbohydrazide (4.003)



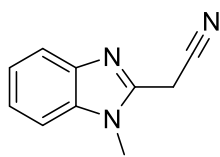
The title compound was obtained using 2-(1-methyl-1*H*-benzo[d]imidazol-2-yl)acetohydrazide (150 mg, 0.74 mmol) and quinaldic acid (140 mg, 0.81 mmol) following General procedure A, affording the title compound as a white solid (163 mg, 62 %). HPLC – *t*_R 4.41 min > 99 % purity at 254 nm; LRMS [M+H]⁺ 360.0 *m/z*; HRMS [M+H]⁺ 360.1455 *m/z*, found 360.1461 *m/z*; ¹H NMR (400 MHz, DMSO) δ_H 10.78 – 10.32 (m, 2H, two overlapping broad singlets, NH H1, NH H2), 8.49 (d, *J* = 8.5 Hz, 1H, Hn), 8.10 – 7.94 (m, 3H, Hp, Hr, Hs), 7.84 – 7.75 (m, 1H, Hb), 7.69 – 7.60 (m, 1H, He), 7.51 – 7.35 (m, 2H, Hm, Hq), 7.23 – 7.03 (m, 2H, Hc, Hd), 3.95 (s, 2H, Hi), 3.73 (s, 3H, Hg); ¹³C NMR (101 MHz, DMSO) δ_C 166.3 (Cj), 163.0 (Ck),

149.5 (Ch), 149.1 (Cl), 146.0 (Ct), 142.0 (Ca), 137.9 (Cn), 136.0 (Cf), 130.7 (Cr), 129.2 (Cs), 128.9 (Co/Cp/Cq), 128.3 (Co/Cp/Cq), 128.1 (Co/Cp/Cq), 121.8 (Cc/Cd), 121.3 (Cc/Cd), 118.8 (Cm), 118.5 (Cb), 109.9 (Ce), 33.3 (Ci), 30.0 (Cg).

Example spectra for Scaffold 4: ^1H (400 MHz, DMSO) and ^{13}C NMR (100 MHz, DMSO) for *N'*-(2-(1-Methyl-1*H*-benzo[*d*]imidazol-2-yl)acetyl)quinoline-2-carbohydrazide (4.003)

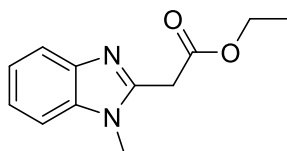


2-(1-Methyl-1H-benzo[d]imidazol-2-yl)acetonitrile (4.041)^{27, 66}



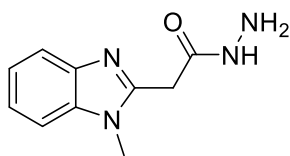
To a solution of 1H-benzimidazole-2-acetonitrile (1.0 g, 6.4 mmol) and NaOH (1.1 eq) in water (5 mL) was added dimethylsulfate (1.2 eq) dropwise. The mixture was heated to 30°C for 1h. Upon reaction completion the mixture was cooled, and the precipitate formed was filtered via suction filtration, washed with water, dried and collected.¹⁹ The known title compound was obtained as a light brown solid (665 mg, 61 %). HPLC – t_R 2.26 min > 99 % purity at 254 nm; LRMS $[M+H]^+$ 172.1 m/z ; 1H NMR (400 MHz, DMSO) δ_H 7.63 – 7.60 (m, 1H), 7.55 – 7.52 (m, 1H), 7.28 – 7.18 (m, J = 7.8, 7.2, 3.6 Hz, 2H), 4.52 (s, 2H), 3.75 (s, 3H); 1H NMR (400 MHz, $CDCl_3$) δ_H 7.78 – 7.75 (m, 1H), 7.37 – 7.29 (m, 3H), 4.11 (s, 2H), 3.88 (s, 3H); ^{13}C NMR (101 MHz, $CDCl_3$) δ_C 143.3, 142.2, 136.2, 123.7, 123.0, 120.2, 114.2, 109.6, 30.5, 18.2. Acquired data is consistent with the literature.⁶⁶

Ethyl 2-(1-methyl-1H-benzo[d]imidazol-2-yl)acetate (4.042)⁶⁷



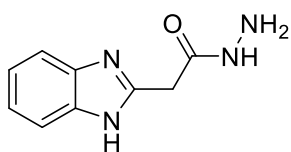
To a solution of 2-(1-Methyl-1H-benzo[d]imidazol-2-yl)acetonitrile (500 mg, 2.9 mmol) in EtOH (8 mL) was added acetyl chloride (1 mL, 14 mmol) dropwise at 0°C. The mixture was heated to reflux for 2 h, cooled to room temperature and concentrated *in vacuo*. The hydrochloric salt was dissolved in water and neutralized with $NaHCO_3$ solution.²⁸ The solution was extracted with DCM, the organic layers collected and dried over $MgSO_4$, filtered and concentrated to give the known title compound as a solid (476 mg, 75%). HPLC – t_R 3.27 min > 99 % purity at 254 nm; LRMS $[M+H]^+$ 219.0 m/z ; 1H NMR (400 MHz, $CDCl_3$) δ_H 7.75 – 7.72 (m, 1H), 7.35 – 7.26 (m, 3H), 4.21 (q, J = 7.2 Hz, 2H), 4.04 (s, 2H), 3.78 (s, 3H), 1.27 (t, J = 7.1 Hz, 3H); ^{13}C NMR (101 MHz, $CDCl_3$) δ_C 168.3, 147.9, 142.5, 136.1, 122.8, 122.2, 119.7, 109.4, 61.8, 34.6, 30.3, 14.2.

2-(1-Methyl-1H-benzo[d]imidazol-2-yl)acetohydrazide (4.044)



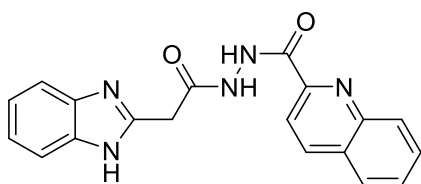
To a solution of ethyl 2-(1-methyl-1H-benzo[d]imidazol-2-yl)acetate (300 mg, 1.4 mmol) in EtOH (5 mL) was added hydrazine hydrate (0.5 mL) and heated to reflux for 16 h. Upon reaction completion, the mixture was cooled to room temperature, diluted with water and concentrated *in vacuo*. The solid was washed with water, filtered via suction filtration and dried to give the title compound as a white solid (234 mg, 83 %).²⁹ LRMS $[M+H]^+$ 205.2 m/z ; 1H NMR (400 MHz, MeOD) δ_H 7.61 – 7.58 (m, 1H), 7.51 – 7.49 (m, 1H), 7.33 – 7.24 (m, 2H), 3.93 (s, 2H), 3.86 (s, 3H); 1H NMR (400 MHz, DMSO) δ_H 9.39 (s, 1H), 7.58 – 7.45 (m, 2H), 7.31 – 7.08 (m, 2H), 4.32 (br s, 2H), 3.80 (s, 2H), 3.77 (s, 3H); ^{13}C NMR (101 MHz, DMSO) δ_C 166.4, 149.9, 141.2, 135.6, 122.0, 121.6, 118.1, 110.0, 32.9, 30.1.

2-(1*H*-Benzo[*d*]imidazol-2-yl)acetohydrazide (4.045)^{29,68}



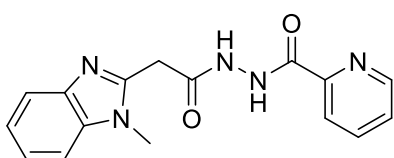
A solution of ethyl 2-(1*H*-benzo[*d*]imidazol-2-yl)acetate (150 mg, 0.74 mmol) and hydrazine hydrate (0.37 mL) in EtOH was refluxed over 16 h. Upon reaction completion the mixture was cooled to room temperature, diluted with water and concentrated *in vacuo*. The solid formed was washed and dried via suction filtration to obtain the known title compound as a yellow solid (140 mg, 99 %). HPLC – *t*_R 1.58 min > 99 % purity at 254 nm; LRMS [M+H]⁺ 191.0 *m/z*; ¹H NMR (400 MHz, MeOD) δ 7.54 – 7.50 (m, 2H), 7.23 – 7.19 (m, 2H), 3.82 (s, 2H).⁶⁸

N'-(2-(1*H*-Benzo[*d*]imidazol-2-yl)acetyl)quinoline-2-carbohydrazide (4.046)



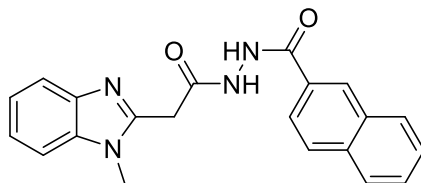
The title compound was obtained using 2-(1*H*-benzo[*d*]imidazol-2-yl)acetohydrazide (300 mg, 1.6 mmol) and quinaldic acid (230 mg, 1.2 mmol) following General procedure A, affording the title compound as a white solid (88 mg, 22 %). HPLC – *t*_R 4.24 min > 99 % purity at 254 nm; LRMS [M+H]⁺ 346.0 *m/z*; HRMS [M+H]⁺ 346.1299 *m/z*, found 346.1305 *m/z*; ¹H NMR (400 MHz, DMSO) δ 12.32 (br s, 1H), 10.75 (br s, 2H), 8.60 (d, *J* = 8.6 Hz, 1H), 8.16 – 8.10 (m, 3H), 7.92 – 7.87 (m, 1H), 7.78 – 7.73 (m, 1H), 7.52 (br s, 2H), 7.21 – 7.13 (m, 2H), 3.92 (s, 2H); ¹³C NMR (101 MHz, DMSO) δ_C 166.5, 162.9, 149.1, 148.6, 146.0, 138.0, 130.7, 129.3, 129.0, 128.4, 128.2, 118.8, 34.6. Aromatic quaternary carbons not observed.

N'-(2-(1-Methyl-1*H*-benzo[*d*]imidazol-2-yl)acetyl)picolinohydrazide (4.047)



The title compound was obtained using 2-(1-methyl-1*H*-benzo[*d*]imidazol-2-yl)acetohydrazide (200 mg, 1.5 mmol) and picolinic acid (180 mg, 1.5 mmol) following General procedure A, affording the title compound as a white solid (237 mg, 78 %). HPLC – *t*_R 3.34 min > 99 % purity at 254 nm; LRMS [M+H]⁺ 310.1 *m/z*; HRMS [M+H]⁺ 310.1299 *m/z*, found 310.1305 *m/z*; ¹H NMR (400 MHz, DMSO) δ 10.57 (br s, 1H), 10.47 (br s, 1H), 8.65 (d, *J* = 4.3 Hz, 1H), 8.03 – 7.98 (m, 2H), 7.64 – 7.60 (m, 1H), 7.52 (dd, *J* = 18.4, 7.8 Hz, 2H), 7.24 – 7.13 (m, 2H), 4.00 (s, 2H), 3.80 (s, 3H); ¹³C NMR (101 MHz, DMSO) δ_C 166.1, 162.8, 149.5, 149.0, 148.6, 142.0, 137.8, 136.0, 127.0, 122.3, 121.8, 121.3, 118.5, 109.9, 33.2, 30.0.

N'-(2-(1-Methyl-1*H*-benzo[*d*]imidazol-2-yl)acetyl)-2-naphthohydrazide (4.048)

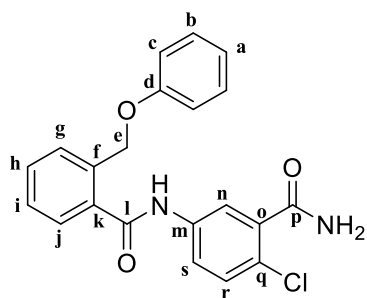


To a solution of 2-(1-methyl-1*H*-benzo[*d*]imidazol-2-yl)acetohydrazide (100 mg, 0.49 mmol) and Et₃N (0.4 mL) in DCM (5 mL) was added 2-naphthoyl chloride (1 equiv.) slowly. The solution was stirred at room temp over 12 h. Upon reaction completion the mixture was concentrated, diluted with EtOAc, washed with brine. The mixture was

extracted with EtOAc, the organic layers were collected, dried over MgSO₄, filtered and concentrated, followed by column chromatography (CHCl₃/ MeOH/ NH₄OH: 94%, 5%, 1% eluent) to afford the title compound as a white powder (30 mg, 17 %). HPLC – *t*_R 4.57 min > 99 % purity at 254 nm; LRMS [M+H]⁺ 359.2 *m/z*; HRMS [M+H]⁺ 359.1503 *m/z*, found 359.1516 *m/z*; ¹H NMR (400 MHz, DMSO) δ 10.54 (br s, 1H), 8.50 (s, 1H), 8.05 – 7.97 (m, 3H), 7.94 (dd, *J* = 8.6, 1.2 Hz, 1H), 7.66 – 7.51 (m, 4H), 7.26 – 7.16 (m, 2H), 4.05 (s, 2H), 3.85 (s, 3H); ¹³C NMR (101 MHz, DMSO) δ_C 166.6, 165.5, 149.6, 142.0, 135.9, 134.3, 132.0, 129.8, 128.9, 128.0, 128.0, 127.8, 127.6, 126.8, 124.0, 121.8, 121.3, 118.4, 109.9, 33.3, 30.0.

Scaffold 5 Compounds

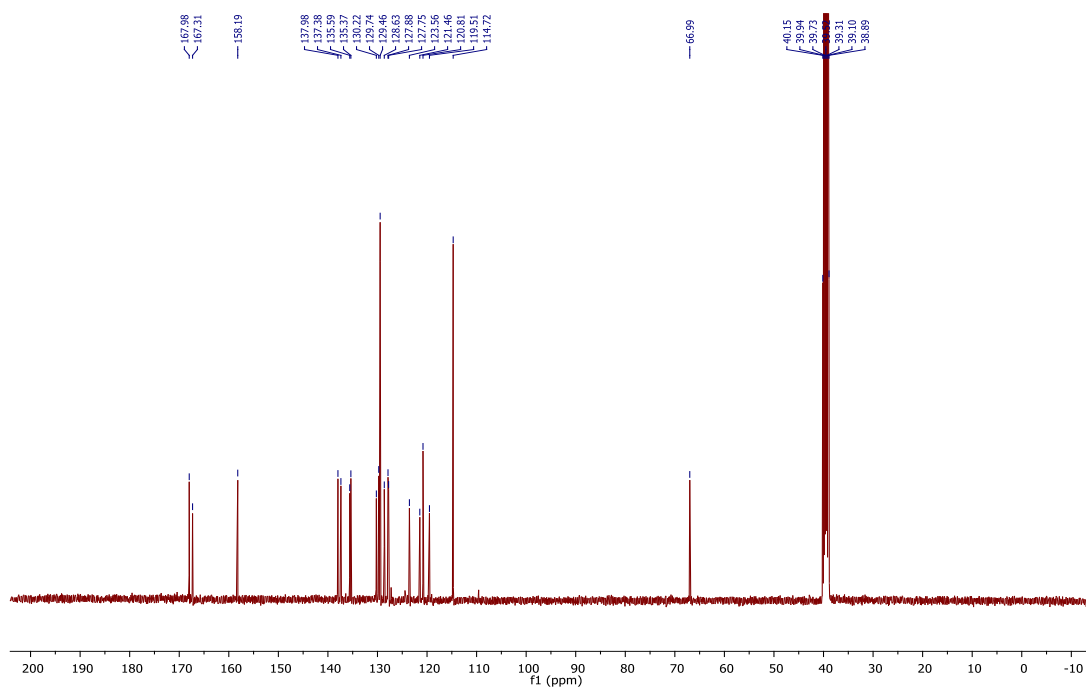
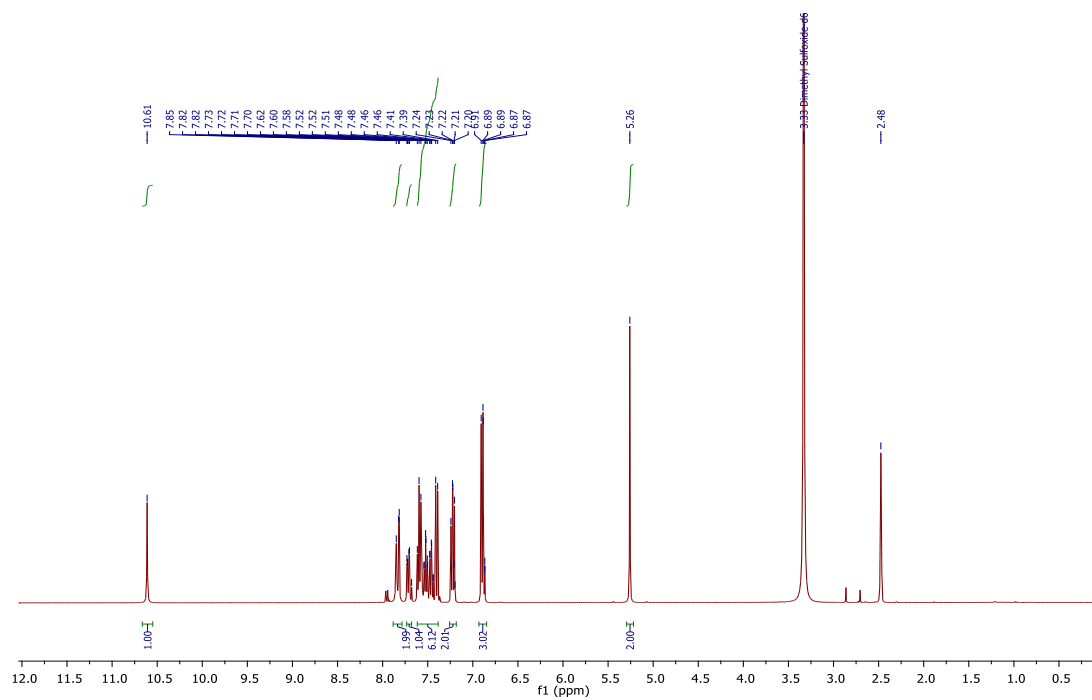
N-(3-Carbamoyl-4-chlorophenyl)-2-(phenoxyethyl)benzamide (4.004)

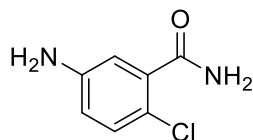


The title compound was obtained using 5-amino-2-chlorobenzamide (150 mg, 0.88 mmol) and 2-(phenoxyethyl)benzoic acid (200 mg, 0.88 mmol) in DMF (3 mL) following General procedure A. The title compound was afforded as an off white solid (200 mg, 60 %). HPLC – *t*_R 5.63 min > 95 % purity at 254 nm; LRMS [M+H]⁺ 380.9 *m/z*; HRMS [M+H]⁺ 381.1 *m/z*, found 381.1001 *m/z*; ¹H NMR (400 MHz,

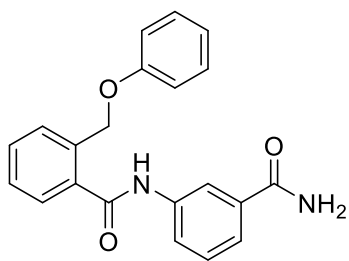
DMSO) δ_H 10.61 (s, 1H, NH), 7.86 – 7.81 (m, 2H, H_j, NH of NH₂), 7.74 – 7.68 (m, 1H, H_n), 7.62 – 7.39 (m, 6H, H_{g,h,i,r,s}, NH of NH₂), 7.25 – 7.19 (m, 2H, H_b), 6.92 – 6.86 (m, 3H, H_a, H_c), 5.26 (s, 2H, H_e); ¹³C NMR (101 MHz, DMSO) δ_C 168.0 (Cl), 167.3 (C_p), 158.2 (C_d), 138.0 (C_k), 137.4 (C_m), 135.6 (C_o), 135.4 (C_f), 130.2 (C_h), 129.7 (C_r), 129.5 (2C, C_b), 128.6 (C_{g/i/j/q}), 127.9 (C_{g/i/j/q}), 127.8 (C_{g/i/j/q}), 123.6 (C_{g/i/j/q}), 121.5 (C_s), 120.8 (C_a), 119.5 (C_n), 114.7 (2C, C_c), 67.0 (C_e). M.p. 126.4–139.7 °C.

Example spectra for Scaffold 5: ^1H (400 MHz, DMSO) and ^{13}C NMR (100 MHz, DMSO) for *N*-(3-Carbamoyl-4-chlorophenyl)-2-(phenoxyethyl)benzamide (4.004)

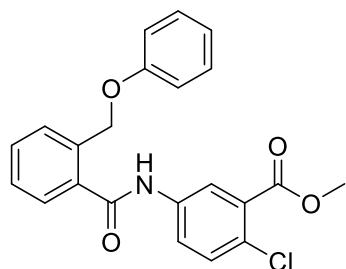


5-Amino-2-chlorobenzamide (4.052)⁶⁹

To obtain the known title compound 2-chloro-5-nitrobenzamide (1.0 g, 5 mmol) was used following General procedure B. The title compound was afforded as an pale yellow solid (629 mg, 74 %). HPLC – t_R 1.376 min > 95 % purity at 254 nm; LRMS $[M+H]^+$ 171.0 m/z ; 1H NMR (400 MHz, MeOD) δ_H 7.13 (d, J = 8.6 Hz, 1H), 6.82 (d, J = 2.8 Hz, 1H), 6.72 (dd, J = 8.6, 2.8 Hz, 1H).⁶⁹

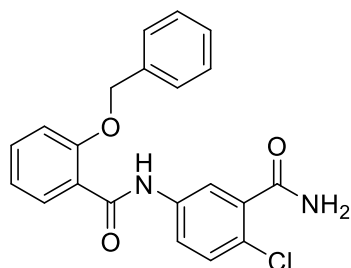
N-(3-Carbamoylphenyl)-2-(phenoxymethyl)benzamide (4.053)

The title compound was obtained using 3-aminobenzamide (100 mg, 0.73 mmol) and 2-(phenyloxymethyl)benzoic acid (166 mg, 0.73 mmol) following General procedure A. The title compound was afforded as an off white solid (188 mg, 74 %). HPLC – t_R 5.50 min > 99 % purity at 254 nm; LRMS $[M+H]^+$ 347.0 m/z ; HRMS $[M+H]^+$ 347.1390 m/z , found 347.1393 m/z ; 1H NMR (400 MHz, $CDCl_3$) δ_H 7.94 – 7.91 (m, 1H), 7.77 (d, J = 7.4 Hz, 1H), 7.61 – 7.46 (m, 5H), 7.37 – 7.28 (m, 3H), 7.02 – 6.98 (m, 3H), 5.24 (s, 2H); 1H NMR (400 MHz, MeOD) δ_H 8.12 – 8.10 (s, 1H), 7.90 – 7.86 (m, 1H), 7.83 – 7.79 (m, 1H), 7.76 – 7.73 (m, 1H), 7.66 – 7.60 (m, 2H), 7.57 – 7.41 (m, 4H), 7.27 – 7.16 (m, 1H), 6.94 – 6.86 (m, 2H), 5.32 (s, 2H); ^{13}C NMR (101 MHz, MeOD) δ_C 172.2, 170.6, 160.0, 140.1, 137.1, 137.1, 135.9, 131.5, 130.4 (2C), 130.0, 129.9, 129.1, 128.7, 125.1, 124.5, 122.1, 121.0, 115.9 (2C), 68.9.

Methyl 2-chloro-5-(2-(phenoxymethyl)benzamido)benzoate (4.054)

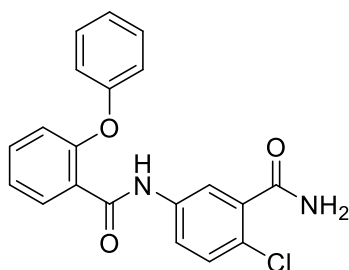
The title compound was obtained using methyl 5-amino-2-chlorobenzoate (400 mg, 2.16 mmol) and 2-(phenyloxymethyl)benzoic acid (493 mg, 2.16 mmol) following General procedure A. The title compound was afforded as an off white solid (341 mg, 40 %). HPLC – t_R 6.89 min > 99 % purity at 254 nm; LRMS $[M+H]^+$ 395.9 m/z ; HRMS $[M+H]^+$ 396.0997 m/z , found 396.1011 m/z ; 1H NMR (400 MHz, $CDCl_3$) δ_H 8.68 (s, 1H), 7.88 (d, J = 2.6 Hz, 1H), 7.83 – 7.78 (m, 1H), 7.56 – 7.47 (m, 3H), 7.36 – 7.27 (m, 3H), 7.04 – 7.00 (m, 3H), 5.21 (s, 2H), 3.86 (s, 3H); 1H NMR (400 MHz, DMSO) δ_H 10.71 (s, 1H), 8.26 (d, J = 2.5 Hz, 1H), 7.93 – 7.81 (m, 1H), 7.65 – 7.41 (m, 5H), 7.32 – 7.21 (m, 2H), 6.98 – 6.88 (m, 3H), 5.28 (s, 2H), 3.86 (s, 3H); ^{13}C NMR (101 MHz, DMSO) δ_C 167.5, 165.3, 158.2, 138.2, 132.1, 131.1, 130.4, 130.3, 129.9, 129.6, 129.5 (2C), 128.7, 127.6, 125.8, 124.1, 121.8, 120.8, 114.7 (2C), 67.1, 52.6.

2-(Benzyloxy)-N-(3-carbamoyl-4-chlorophenyl)benzamide (4.055)



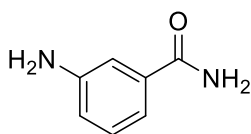
The title compound was obtained using 5-amino-2-chlorobenzamide (112 mg, 0.66 mmol) and 2-(benzyloxy)benzoic acid (150 mg, 0.66 mmol) following General procedure A. The title compound was afforded as an off white solid (100 mg, 40 %). HPLC – t_R 5.97 min > 99 % purity at 254 nm; LRMS $[M+H]^+$ 381.0 m/z ; HRMS $[M+H]^+$ 318.1016 m/z , found 318.1109 m/z ; 1H NMR (400 MHz, DMSO) δ_H 10.37 (s, 1H), 7.86 (s, 1H), 7.73 – 7.58 (m, 4H), 7.56 – 7.51 (m, 3H), 7.43 – 7.28 (m, 5H), 7.13 – 7.08 (m, 1H), 5.25 (s, 2H); ^{13}C NMR (101 MHz, DMSO) δ_C 168.0, 164.6, 155.7, 137.8, 137.5, 136.5, 132.3, 129.8, 129.8, 128.5 (2C), 128.1, 127.8 (2C), 124.8, 123.3, 120.9, 120.9, 119.0, 113.4, 70.1.

N-(3-Carbamoyl-4-chlorophenyl)-2-phenoxybenzamide (4.056)



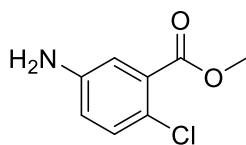
The title compound was obtained using 5-amino-2-chlorobenzamide (200 mg, 1.2 mmol) and 2-phenoxybenzoic acid (251 mg, 1.2 mmol) following General procedure A. The title compound was afforded as an off white solid (200 mg, 46 %). HPLC – t_R 5.62 min > 99 % purity at 254 nm; LRMS $[M+H]^+$ 366.9 m/z ; HRMS $[M+H]^+$ 367.0844 m/z , found 367.0847 m/z ; 1H NMR (400 MHz, DMSO) δ_H 10.53 (s, 1H), 7.87 (s, 1H), 7.79 (d, J = 2.5 Hz, 1H), 7.69 (dd, J = 8.8, 2.6 Hz, 1H), 7.65 (dd, J = 7.6, 1.7 Hz, 1H), 7.58 (br s, 1H), 7.53 – 7.48 (m, 1H), 7.42 – 7.36 (m, 3H), 7.30 – 7.25 (m, 1H), 7.16 – 7.12 (m, 1H), 7.07 – 7.03 (m, 2H), 6.96 (d, J = 7.7 Hz, 1H); ^{13}C NMR (101 MHz, DMSO) δ_C 168.4, 165.2, 156.9, 154.1, 138.3, 137.9, 132.4, 130.5 (2C), 130.3, 130.0, 129.1, 124.2, 124.0, 124.0, 121.7, 119.7, 119.4, 119.3 (2C).

3-Aminobenzamide (4.057)⁷⁰



To a solution of 2-chloro-5-nitrobenzamide (250 mg, 1.3 mmol) in MeOH (5 mL) was added Pd/C. The mixture was degassed and backfilled with nitrogen before put under hydrogen. The mixture stirred at room temperature over 12 h. Upon reaction completion the solution was filtered through celite and the filtrate concentrated *in vacuo* to afford the known title compound as a brown solid (167 mg, 94 %) without further purification.⁴⁵ HPLC – t_R 1.21 min > 99 % purity at 254 nm; LRMS $[M+H]^+$ 137.0 m/z ; 1H NMR (400 MHz, MeOD) δ_H 7.24 – 7.08 (m, 3H), 6.96 – 6.82 (m, 1H); ^{13}C NMR (101 MHz, MeOD) δ_C 173.1, 149.3, 135.8, 130.2, 119.6, 117.8, 115.1.

Methyl 5-amino-2-chlorobenzoate (4.059)^{46, 71}



To a solution of 5-amino-2-chlorobenzoic acid (800 mg, 4.7 mmol) in MeOH (5 mL) was added a 3 drops of H₂SO₄. The mixture was heated to reflux over 18 h. Upon reaction completion the solution was concentrated *in vacuo*, diluted with DCM, washed and washed with brine. The organic layers were collected, dried over MgSO₄, filtered and concentrated *in vacuo* to afford the known title compound. (778 mg, 89 %). HPLC – *t*_R 3.39 min > 99 % purity at 254 nm; LRMS [M+H]⁺ 186.0 *m/z*; ¹H NMR (400 MHz, DMSO) δ_H 7.11 (d, *J* = 8.6 Hz, 1H), 6.95 (d, *J* = 2.8 Hz, 1H), 6.69 (dd, *J* = 8.6, 2.8 Hz, 1H), 4.37 (br s, 2H), 3.75 (s, 3H); ¹H NMR (400 MHz, CDCl₃) δ_H 7.05 (dd, *J* = 9.7, 5.5 Hz, 1H), 7.01 (d, *J* = 2.8 Hz, 1H), 6.61 (dd, *J* = 8.6, 2.9 Hz, 1H), 3.98 (s, 2H), 3.79 (s, 3H); ¹³C NMR (101 MHz, CDCl₃) δ_C 166.4, 144.4, 131.8, 130.6, 122.9, 119.6, 117.8, 52.5.^{46, 71}

4.12 Chapter 4 References

1. Peña I, Pilar Manzano M, Cantizani J, Kessler A, Alonso-Padilla J, Bardera AI, et al. New Compound Sets Identified from High Throughput Phenotypic Screening Against Three Kinetoplastid Parasites: An Open Resource. *Sci Rep*. 2015;5:8771.
2. Lipinski CA, Lombardo F, Dominy BW, Feeney PJ. Experimental and computational approaches to estimate solubility and permeability in drug discovery and development settings IPII of original article: S0169-409X(96)00423-1. The article was originally published in *Adv Drug Deliv Rev* 23 (1997) 3–25.1. *Adv Drug Deliv Rev*. 2001;46(1):3-26.
3. Veber DF, Johnson SR, Cheng H-Y, Smith BR, Ward KW, Kopple KD. Molecular Properties That Influence the Oral Bioavailability of Drug Candidates. *J Med Chem*. 2002;45(12):2615-2623.
4. Takasugi H, Terasawa T, Inoue Y, Nakamura H, Nagayoshi A, Ohtake H, et al. Benzamide compounds as apo b secretion inhibitors. WO 2002028835 A1, 2002.
5. Bursavich MG, Gilbert AM, Stock JR. Piperazine metabotropic glutamate receptor 5 (MGLUR5) negative allosteric modulators for anxiety/depression. WO 2009143404 A1, 2009.
6. Derkach LG, Novikova NS, Gorecka E. Banana-shaped liquid crystals based on 2,7-dihydroxynaphthalene derivatives. *Russ J Gen Chem*. 2015;85(3):577-583.
7. Reilly SW, Mach RH. Pd-Catalyzed Synthesis of Piperazine Scaffolds Under Aerobic and Solvent-Free Conditions. *Org Lett*. 2016;18(20):5272-5275.
8. Álvarez-Velilla R, Gutiérrez-Corbo MDC, Punzón C, Pérez-Pertejo MY, Balaña-Fouce R, Fresno M, et al. A chronic bioluminescent model of experimental visceral leishmaniasis for accelerating drug discovery. *PLoS Negl Trop Dis*. 2019;13(2):e0007133.
9. Lezama-Dávila CM, Isaac-Márquez AP, Kapadia G, Owens K, Oghumu S, Beverley S, et al. Leishmanicidal activity of two naphthoquinones against *Leishmania donovani*. *Biol Pharm Bull*. 2012;35(10):1761-1764.

10. Stockert JC, Horobin RW, Colombo LL, Blázquez-Castro A. Tetrazolium salts and formazan products in Cell Biology: Viability assessment, fluorescence imaging, and labeling perspectives. *Acta Histochem.* 2018;120(3):159-167.
11. Chiu H-C, Kulp SK, Soni S, Wang D, Gunn JS, Schlesinger LS, et al. Eradication of Intracellular *Salmonella enterica* Serovar Typhimurium with a Small-Molecule, Host Cell-Directed Agent. *Antimicrob Agents Chemother.* 2009;53(12):5236-5244.
12. Zahid MS, Johnson M, Varma D, Ainslie K. Infecting THP-1 Macrophages with *Leishmania donovani* (Ds-Red-lux) and evaluating by Luciferase assay. [Unpublished data]. Eshelman School of Pharmacy, University of North Carolina at Chapel Hill; 2019.
13. Do S, Goldsmith R, Heffron T, Kolesnikov A, Staben S, Olivero AG et al. Benzopyran and benzoxepin PI3K inhibitor compounds and methods of use. US 20090247567 A1, 2009.
14. Segal M, Avinery R, Buzhor M, Shaharabani R, Harnoy AJ, Tirosh E, et al. Molecular Precision and Enzymatic Degradation: From Readily to Undegradable Polymeric Micelles by Minor Structural Changes. *J Am Chem Soc.* 2017;139(2):803-810.
15. Ramkumar SG, Rose KAA, Ramakrishnan S. Direct synthesis of terminally “clickable” linear and hyperbranched polyesters. *J Polym Sci A Polym Chem.* 2010;48(14):3200-3208.
16. Huang S-T, Hsei IJ, Chen C. Synthesis and anticancer evaluation of bis(benzimidazoles), bis(benzoxazoles), and benzothiazoles. *Bioorg Med Chem.* 2006;14(17):6106-6119.
17. Albrecht BK, Audia JE, Cook A, Gagnon A, Harmange J-C, Naveschuk CG. Modulators of Methyl Modifying Enzymes, Compositions and Uses thereof. WO 2013075083 A1, 2013.
18. Wang B, Shi Y, Zhan Y, Zhang L, Zhang Y, Wang L, et al. Synthesis and Biological Activity of Novel Furan/Thiophene and Piperazine-Containing (Bis)1,2,4-triazole Mannich Bases. *Chin J Chem.* 2015;33(10):1124-1134.
19. Potter GA, Huxley P. Preparation of 4,6-diphenylpyrid-2-ones as anticancer drugs. WO 2009146910 A1, 2009.
20. Oslob J, Anderson R, Aubele D, Evanchik M, Fox JC, Kane B et al. Pyrimidinedione compounds against cardiac conditions. WO 2014205223 A1, 2014.
21. Wang F, Wang X, Zhang M-X, Yang Y-H, Zhu H-L. Synthesis, biological evaluation and molecular modeling of 1H-benzo[d]imidazole derivatives as novel anti-tubulin polymerization agents. *RSC Adv.* 2015;5(91):74425-74437.
22. Wang T, Dong S, Chen X, Qian K, Wang H, Quan H, et al. Design, synthesis, biological evaluation, homology modeling and docking studies of (E)-3-(benzo[d][1,3]dioxol-5-ylmethylene) pyrrolidin-2-one derivatives as potent anticonvulsant agents. *Bioorg Med Chem Lett.* 2018;28(8):1324-1329.
23. Field LD, Sternhell S, Kalman JR. Chapter 5 Nuclear Magnetic Resonance (NMR) Spectroscopy. In: *Organic Structures from Spectra*. Fourth ed: John Wiley & Sons Ltd; 2008.p 33-64

24. Lagerblom K, Kesiväli J, Parviainen A, Mannisto J, Repo T. Selective Aerobic Oxidation of Alcohols with NO_3^- Activated Nitroxyl Radical/Manganese Catalyst System. *ChemCatChem*. 2018;10(13):2908-2914.
25. De Monte C, Carradori S, Secci D, D'Ascenzio M, Guglielmi P, Mollica A, et al. Synthesis and pharmacological screening of a large library of 1,3,4-thiadiazolines as innovative therapeutic tools for the treatment of prostate cancer and melanoma. *Eur J Med Chem*. 2015;105:245-262.
26. Darehkordi A, Zarezadeh Abarqouei B, Rahmani F. Cyclization–oxidation of Benzyldenehydrazinecarbothioamides by $\text{FeCl}_3 \cdot 6\text{H}_2\text{O}$ or $\text{ZnCl}_2 \cdot 6\text{H}_2\text{O}$ Catalysts and Synthesis of New 1,3,4-Thiadiazolo-[3,2- α]Pyrimidines. *J Heterocycl Chem*. 2017;54(3):1872-1879.
27. Gryshchenko AA, Tarnavskiy SS, Levchenko KV, Bdzhola VG, Volynets GP, Golub AG, et al. Design, synthesis and biological evaluation of 5-amino-4-(1H-benzoimidazol-2-yl)-phenyl-1,2-dihydro-pyrrol-3-ones as inhibitors of protein kinase FGFR1. *Bioorg Med Chem*. 2016;24(9):2053-2059.
28. Innes D, Perkins MV, Liepa AJ, Francis CL. *N,N*-Dialkyl-*N'*-Chlorosulfonyl Chloroformamidines in Heterocyclic Synthesis. Part XIV. Synthesis and reactivity of the new benzo[4,5]imidazo[1,2-b][1,2,6]thiadiazine ring system. *Aust J Chem*. 2018;71(1):58-69.
29. Akhtar MJ, Siddiqui AA, Khan AA, Ali Z, Dewangan RP, Pasha S, et al. Design, synthesis, docking and QSAR study of substituted benzimidazole linked oxadiazole as cytotoxic agents, EGFR and erbB2 receptor inhibitors. *Eur J Med Chem*. 2017;126:853-869.
30. Shinkai H, Ito T, Iida T, Kitao Y, Yamada H, Uchida I. 4-Aminoquinolines: Novel Nociceptin Antagonists with Analgesic Activity. *J Med Chem*. 2000;43(24):4667-4677.
31. Edwards PJ, Sturino C. Managing the Liabilities Arising from Structural Alerts: A Safe Philosophy for Medicinal Chemists. *Curr Med Chem*. 2011;18(20):3116-3135.
32. Smith GF. Designing Drugs to Avoid Toxicity. In: Lawton G, Witty DR, editors. *Progress in Medicinal Chemistry*. 50: Elsevier; 2011. p. 1-47.
33. McClelland BW, Davis RS, Palovich MR, Widdowson KL, Werner ML, Burman M, et al. Comparison of *N,N'*-diarylsquaramides and *N,N'*-diarylureas as antagonists of the CXCR2 chemokine receptor. *Bioorg Med Chem Lett*. 2007;17(6):1713-1717.
34. Palovich MR, Widdowson KL. Il-8 receptor antagonists. WO 2002067919 A1, 2002.
35. Allen JM, Butlin RJ, Green C, Mccoull W, Robb GR, Wood JM. Benzothiazoles as ghrelin receptor modulators. WO 2009047558 A1, 2009.
36. Cellier PP, Spindler J-F, Taillefer M, Cristau H-J. Pd/C-catalyzed room-temperature hydrodehalogenation of aryl halides with hydrazine hydrochloride. *Tetrahedron Lett*. 2003;44(38):7191-7195.
37. Xia C, Xu J, Wu W, Liang X. Pd/C-catalyzed hydrodehalogenation of aromatic halides in aqueous solutions at room temperature under normal pressure. *Catal Commun*. 2004;5(8):383-386.

38. Reed KL, Gupton JT, Solarz TL. A Mild and Convenient Oxidation of Aryl Nitriles to Aryl Amides by Aqueous Sodium Perborate. *Synth Commun.* 1990;20(4):563-571.
39. Van Baelen G, Maes BUW. Study of the microwave-assisted hydrolysis of nitriles and esters and the implementation of this system in rapid microwave-assisted Pd-catalyzed amination. *Tetrahedron.* 2008;64(23):5604-5619.
40. Von Dreele PH, Brewster AI, Bovey FA, Scheraga HA, Fenger MF, Du Vigneaud V. Nuclear Magnetic Resonance Studies of Lysine-Vasopressin: Structural Constraints. *Proc Natl Acad Sci U S A.* 1971;68(12):3088-3091.
41. Ishimoto B, Tonan K, Ikawa S-i. Intramolecular hydrogen bonding of the C-terminal NH₂ groups of small peptide amides in solution. *Spectrochim Acta A Mol Biomol Spectrosc.* 1999;55(11):2321-2327.
42. Gorobets NY, Yermolayev SA, Gurley T, Gurinov AA, Tolstoy PM, Shenderovich IG, et al. Difference between ¹H NMR signals of primary amide protons as a simple spectral index of the amide intramolecular hydrogen bond strength. *J Phys Org Chem.* 2012;25(4):287-295.
43. Stewart WE, Siddall TH. Nuclear magnetic resonance studies of amides. *Chem Revs.* 1970;70(5):517-551.
44. Lori F, Keri G, Chafouleas J, De Forni D, Solinas A, Varga Z et al. Novel 4,6-disubstituted Aminopyrimidine Derivatives. WO 2014031937 A1, 2014.
45. Buckman B; Nicholas JB, Beigelman L, Serebryany V, Stoycheva AD, Thrailkill T et al. Cyclic peptide inhibitors of hepatitis c virus replication. WO 2011038293 A1, 2011.
46. He L, Zhang L, Liu X, Li X, Zheng M, Li H, et al. Discovering Potent Inhibitors Against the β -Hydroxyacyl-Acyl Carrier Protein Dehydratase (FabZ) of *Helicobacter pylori*: Structure-Based Design, Synthesis, Bioassay, and Crystal Structure Determination. *J Med Chem.* 2009;52(8):2465-2481.
47. Hu D. Bioactivation of Structural Alerts [Internet]. Drug-Hunter.com 2019 [cited 2020 September 17]. Available from: <https://drughunter.com/bioactivation-of-structural-alerts/>.
48. Kalgutkar AS, Soglia JR. Minimising the potential for metabolic activation in drug discovery. *Expert Opin Drug Metab Toxicol.* 2005;1(1):91-142.
49. Amit S. Kalgutkar IG, R. Scott Obach, Christopher L. Shaffer, Ernesto Callegari, Kirk R. Henne, Abdul E. Mutlib, Deepak K. Dalvie, Jae S. Lee, Yasuhiro Nakai, John P. O'Donnell, Jason Boer and Shawn P. Harriman. A Comprehensive Listing of Bioactivation Pathways of Organic Functional Groups. *Curr Drug Metab.* 2005;6(3):161 - 225.
50. Hevener KE, Pesavento R, Ren J, Lee H, Ratia K, Johnson ME. Chapter Twelve - Hit-to-Lead: Hit Validation and Assessment. In: Lesburg CA, editor. *Methods in Enzymology.* 610: Academic Press; 2018. p. 265-309.

51. Lamotte S, Aulner N, Späth GF, Prina E. Discovery of novel hit compounds with broad activity against visceral and cutaneous *Leishmania* species by comparative phenotypic screening. *Sci Rep*. 2019;9(1):438.
52. Dagley MJ, Saunders EC, Simpson KJ, McConville MJ. High-content assay for measuring intracellular growth of *Leishmania* in human macrophages. *Assay Drug Dev Technol*. 2015;13(7):389-401.
53. Phan T-N, Baek K-H, Lee N, Byun SY, Shum D, No JH. In Vitro and in Vivo Activity of mTOR Kinase and PI3K Inhibitors Against *Leishmania donovani* and *Trypanosoma brucei*. *Molecules*. 2020;25(8):1980.
54. Claiborne AK, Gwaltney SL, Hasvold LA, Li Q, Li T, Lin N-H et al. Farnesyltransferase inhibitors. US 20020115640 A1, 2002.
55. Martinelli JE, Chaykovsky M. Aromatic chlorination of p-aminobenzoic acid derivatives. Improved syntheses of mono- and dichloromethotrexate. *J Org Chem*. 1980;45(3):527-529.
56. Ding A, Zhang Y, Chen Y, Rios R, Hu J, Guo H. Visible light induced oxidative hydroxylation of boronic acids. *Tetrahedron Lett*. 2019;60(9):660-663.
57. Hadida-Ruah SS; Binch HM, Deninno MP, Fanning LTD, Frieman BA, Grootenhuis PDJ et al. Morpholine-spirocyclic piperidine amides as modulators of ion channels. WO 2012125613 A1, 2012.
58. Orlowska E, Roller A, Wiesinger H, Pignitter M, Jirsa F, Krachler R, et al. Benzoic hydroxamate-based iron complexes as model compounds for humic substances: synthesis, characterization and algal growth experiments. *RSC Adv*. 2016;6(46):40238-40249.
59. Wang L-Y, Tsai H-Y, Lin H-C. Novel Supramolecular Side-Chain Banana-Shaped Liquid Crystalline Polymers Containing Covalent- and Hydrogen-Bonded Bent Cores. *Macromolecules*. 2010;43(3):1277-1288.
60. Lampe T, Alonso-Alija C, Bauser M, Beck H, Rosentreter U, Sandner P et al. Substituted 4-benzyloxy-benzoic acid amide derivatives. WO 2007017092 A1. 2007.
61. Yoo KH, Choi HS, Kim DC, Shin KJ, Kim DJ, Song YS, et al. Synthesis of Heteroaryl piperazines and Heteroaryl bipiperidines with a Restricted Side Chain and Their Affinities for 5-HT_{1A} Receptor. *Arch Pharm (Weinheim)*. 2003;336(4-5):208-215.
62. de Melos JLR, Torres-Santos EC, Faiões VdS, de Nigris Del Cistia C, Sant'Anna CMR, Rodrigues-Santos CE, et al. Novel 3,4-methylenedioxy-6-X-benzaldehyde-thiosemicarbazones: Synthesis and antileishmanial effects against *Leishmania amazonensis*. *Eur J Med Chem*. 2015;103:409-417.
63. El-Atawy MA, Omar AZ, Hagar M, Shashira EM. Transalkylation reaction: green, catalyst-free synthesis of thiosemicarbazones and solving the NMR conflict between their acyclic structure and intramolecular cycloaddition products. *Green Chem Lett Rev*. 2019;12(3):364-376.

64. Feng H, Ying X, Peng Y, Van der Eycken EV, Liu C, Zhao S, et al. FeCl₃-promoted synthesis of 1,3,4-thiadiazoles under combined microwave and ultrasound irradiation in water. *Monatsh Chem.* 2013;144(5):681-686.
65. Guan P, Sun Fe, Hou X, Wang F, Yi F, Xu W, et al. Design, synthesis and preliminary bioactivity studies of 1,3,4-thiadiazole hydroxamic acid derivatives as novel histone deacetylase inhibitors. *Bioorg Med Chem.* 2012;20(12):3865-3872.
66. Schulze V, Eis K, Wortmann L, Kosemund D, Prien O, Siemeister G, et al. Thiazolidinones for use as inhibitors of polo-like kinase (PLK) . WO 2006082107 A1, 2006.
67. Chapman DD, Elwood JK, Heseltine DW, Hess HM, Kurtz DW. Annulation of pyridinium rings onto nitrogen heterocycles. *J Org Chem.* 1977;42(14):2474-2480.
68. Shi X. Substituted hydrazide compounds and application thereof . EP 2468730 A1, 2010.
69. Coulter TS, Taylor S, Murfin S, Thammalaksa V, Aicher B, Jaekel S, et al. Novel use of pyrazolopyrimidines. WO 2006066937 A2, 2006.
70. Sharma S, Yamini, Das P. Hydrogenation of nitroarenes to anilines in a flow reactor using polystyrene supported rhodium in a catalyst-cartridge (Cart-Rh@PS). *New J Chem.* 2019;43(4):1764-1769.
71. Kazmierski WM, Aquino CJ, Bifulco N, Boros EE, Chauder BA, Chong PY, et al. Piperidine derivatives as CCR5 antagonists. WO 2004054974 A2, 2004

Chapter 5: Final Scaffold, *N*-(3-carbamoylphenyl)-2-(phenoxyethyl)benzamide exploration

5.01 Properties of hit 5.001

The final main chapter of this body of work details the continued hit-to-lead SAR campaign around the chosen *N*-(3-carbamoylphenyl)-2-(phenoxyethyl)benzamide compound class (Scaffold 5). The chosen hit is renamed here as **5.001** for convenience (previously labelled **4.004** in Chapter 4). The hit was chosen from the available compounds listed in the GSK HTS due to its potent antileishmanial activity and low toxicity, which are listed in **Figure 5.01**.¹ Furthermore, this compound was not being studied by other private or academic groups as confirmed by GSK. This left ample room for exploration and modifications to the scaffold without any competitive issues arising with independent groups. The antileishmanial activity of the hit was initially observed to be higher within the orthogonal intramacrophage bioassay (MAC) initially reported by GSK over their initial fluorescent intensity bioassay (FLINT).

As previously detailed in Chapter 4, increased activity observed within the more biologically relevant intramacrophage assay suggested a true ability of the compound to cross the various physiological membranes, as well as survive within the acidic phagolysosomal environment of the macrophage to reach the parasite and exert inhibitory activity. The antileishmanial activity of the hit was confirmed with the intramacrophage assays employed by our own independent collaborators and is summarized in **Figure 5.01**. Hit validation included corroboration using the low throughput luciferase assay with intracellular bioluminescent *L. donovani* performed by UNC as well as the high content imaging intracellular assay by Bio21. Furthermore, the selectivity for the parasite over the macrophage was confirmed using the same intramacrophage assay performed by Bio21 along with the colorimetric MTT assay performed by UNC. No cytotoxicity was observed within the uninfected transformed THP-1 macrophages in the latter bioassay. A small set of analogues built around **5.001** also gave clear and consistent results across all the biological assays employed, as discussed in Chapter 4. The validation of the hit was highly significant, as not all the potential antileishmanial hits we had investigated from this same GSK HTS list were reconfirmed, and/or had conflicting results between our independent biological collaborators. Moreover, through personal communications with our collaborators from IPK, they related to us that confirmed potent antileishmanial compounds at low micromolar levels within the intramacrophage assay against *L. donovani* are extremely rare. This gave our validated hits an even greater sense of value.

The hit **5.001** was also chosen due to its drug-like properties summarised in **Figure 5.01**. These properties have also been previously detailed in Chapter 1 and 4. Briefly, the low IFI suggests low promiscuity with this compound predicting selectivity for the desired putative binding site/s and that

issues with selectivity may not arise in the future. At time of writing, the binding site and mechanism of action of the compound has yet to be elucidated. The physicochemical properties of the compound satisfy several guidelines for drug-likeness. The low molecular weight (< 500 Da), good Log P value (< 5) and number of hydrogen bond donors and acceptors appease Lipinski's Rule of Five. In addition to the low molecular weight, the low polar surface area and number of rotatable bonds also satisfy Veber's rule, another predictive guideline for drug-likeness and oral bioavailability.^{2,3} Of course, these "rules" do not guarantee oral bioavailability or drug-likeness and were consulted as mere predictive tools to help guide us. Overall, this compound class proved promising to us, and further investigations around the chemical space were proceeded with enthusiasm.

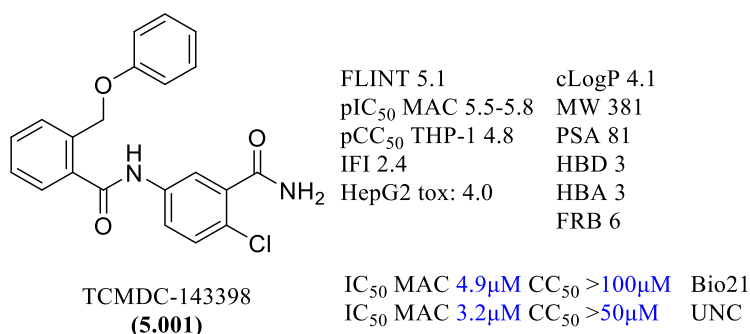


Figure 5.01 Summary of hit 5.001 biological and physicochemical properties

The chemical identity of the hit **5.001** was confirmed using X-ray crystallography performed by Prof Jonathan White, Melbourne University. Crystals were obtained via vapour diffusion, which were used to generate the crystal structure of compound **5.001** as an ethanol solvate.⁴ Depicted below in **Figure 5.02**, compound **5.001** is shown to have two intramolecular hydrogen bonding interactions with the ethanol molecule to the oxygen atom of the central amide (O2) and hydrogen atom of the terminal amide of N2. This hydrogen bonding gives a somewhat restricted confirmation of the compound. The crystal data, refinement parameter and other descriptors are listed in the Appendix section.

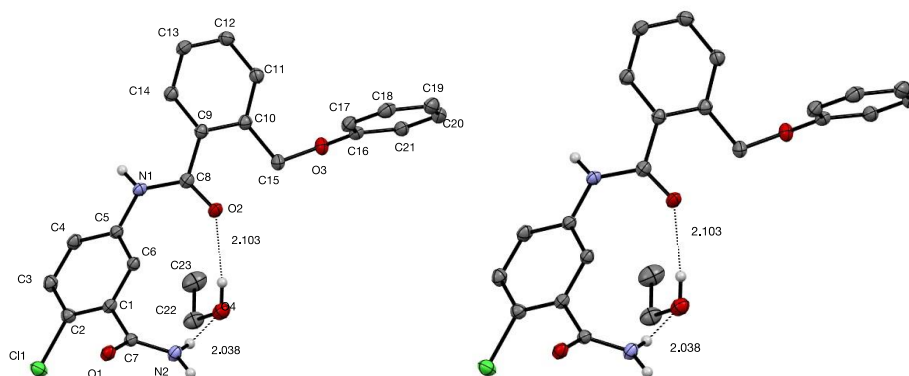


Figure 5.02 Crystal structure of compound 5.001 as an ethanol solvate

A small set of analogues have already been synthesized around compound **5.001**, which was detailed in Chapter 4. Their structures have been summarized in **Figure 5.03**. This initial set were each found unanimously inactive against *L. donovani* within the bioassays employed by each of our collaborators. Based on this early set, compound **4.053** and **4.054** suggest the 4-chloro and amine group of the terminal amide are required to maintain activity respectively. Whilst compounds **4.055** and **4.056** suggest swapping the oxygen and methylene positions within the ether chain as well as removing the methylene were also unfavourable. Continued investigation was undertaken in order to confirm whether isosteric replacements and repositioning these functionalities was possible to further confirm the negative SAR discovered in Chapter 4.

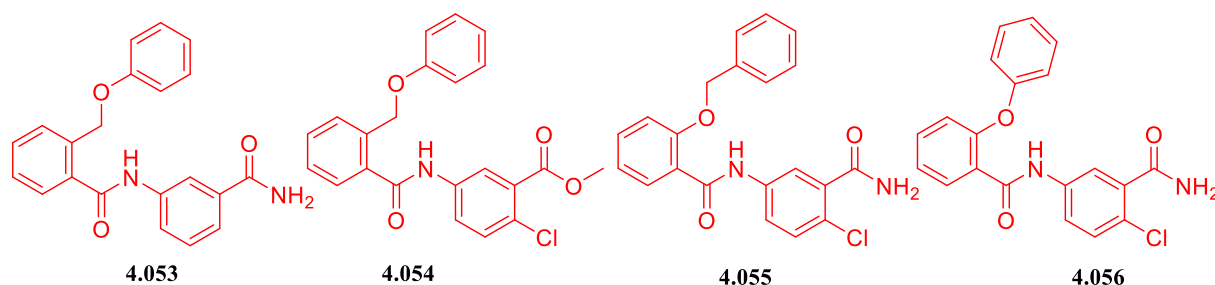


Figure 5.03 Summary of initial set of analogues around compound **5.001** discussed in Chapter 4

The primary SAR exploration described within this chapter focused on modifying three main sections of the chemical space, namely probing the functionalities around the benzamide ring (Section **5.02**), altering the ether chain (Section **5.04**) and additions to the phenoxymethyl ring (Section **5.06**). These sections of the scaffold were targeted as they were the most easily synthetically accessible whilst still allowing us to study a large majority of the compound class, making efficient use of the allotted time remaining on this project. These modifications are summarized below in **Figure 5.04**.

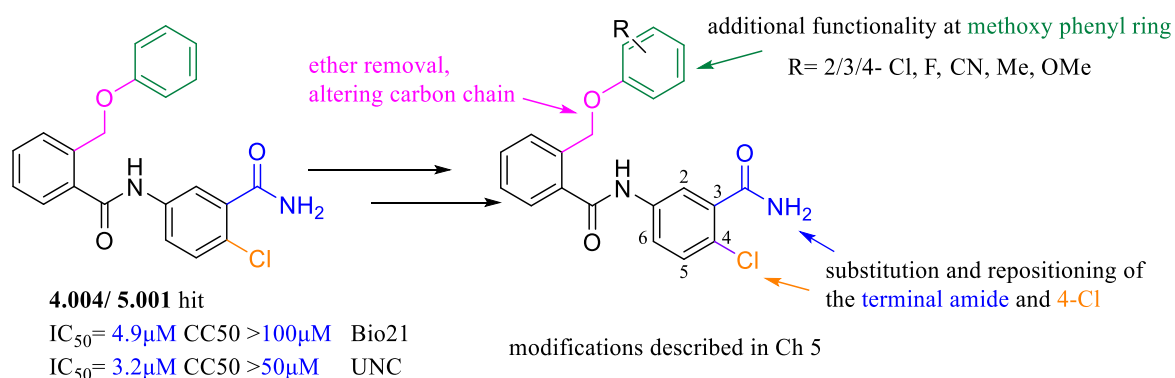


Figure 5.04 Summary of exploration around the carbamoyl phenoxymethyl benzamide scaffold

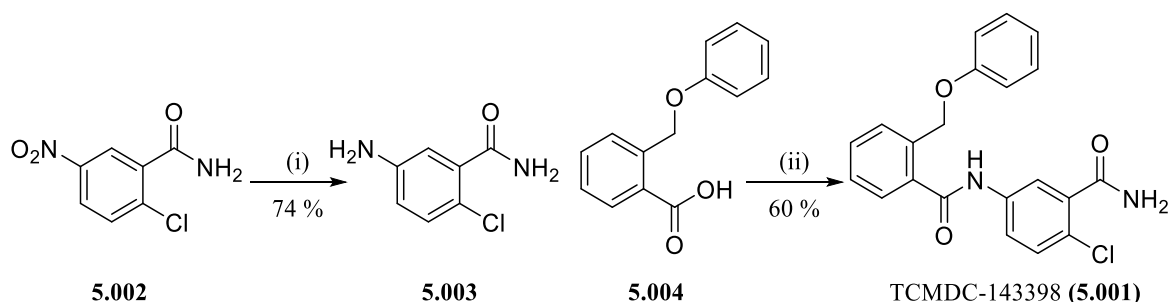
5.02 Targeting the benzamide ring

Several analogues were synthesized targeting modifications of the benzamide ring. As mentioned, the analogues devised included isosteric substitution of the terminal amide, removal of the terminal amide and repositioning this functionality around the ring. Similarly, substitution of chloro group *ortho* to the primary amide and *para* to the benzanilide core, removal and repositioning of the halogen were also investigated along. These modifications were undertaken in order to confirm whether these functional groups were most favourable in their original positions or whether they were preferred at other positions, possibly allowing for closer and/or stronger interactions with the putative binding site/s. Removal of these groups would also confirm whether their presence was key to maintaining antileishmanial activity.

5.02.1 Optimization of the nitro reduction step (Step i of Scheme 5.01)

Synthetic access to hit **5.001** and the surrounding *N*-(3-carbamoylphenyl)-2-(phenoxyethyl)benzamide compound class was previously developed in Chapter 4, restated here in **Scheme 5.01**. This synthetic pathway involved reduction of the nitro group (**5.002**) to obtain the amine intermediate (**5.003**) followed by subsequent amide coupling with 2-(phenoxyethyl)benzoic acid (**5.004**) to acquire the desired analogues.^{5, 6, 7} Continued exploration of this scaffold meant that this pathway would be significantly utilized in order to swiftly obtain a range of analogues. Therefore, attempts to optimize this synthetic pathway was undertaken, aiming to achieve improved yield and efficiency at each step.

Scheme 5.01 Initial synthetic pathway to obtain hit **5.001** and surrounding analogues



Reaction conditions: i) Pt/C, H₂ MeOH, ii) DIPEA, HOBT, EDCI, ACN/THF, 50°C

Taken from the literature, several conditions were trialled in an attempt to improve the efficiency and product yield of the reduction step which converts the nitro group to the amine (**5.003**).⁸⁻¹¹ These conditions employed reducing agents which did not require such anhydrous conditions as needed within the hydrogenation reaction and avoided the direct use of hydrogen gas. This would allow for an easier scale up of reagents used, also decreasing the risk associated with the hydrogenation process using palladium and/or platinum on carbon and hydrogen gas.¹² Other reducing agents such as sodium

dithionite, tin_(II) chloride dihydrate and iron powder were each studied for their efficiency within this system, aiming to replace the hydrogenation conditions originally employing platinum on carbon/ H₂ gas. These trials and outcomes are summarized below in **Table 5.01**.

Table 5.01 Trial conditions and outcomes to improve nitro to amine reduction step

Trial #	Conditions⁸⁻¹¹	Outcome
1	Na ₂ S ₂ O ₄ , EtOH, H ₂ O, THF (1:1:1), rt >12h	After 12-24 h, TLC/ LCMS analysis indicated reaction had still not reached completion. Large amount of starting material (5.002) still present.
2	SnCl ₂ .2H ₂ O, DMF, rt >12h	After 12-24 h, TLC/ LCMS analysis indicated reaction had still not reached completion. Large amount of starting material (5.002) still present. Reaction did not proceed cleanly. Other by-products were formed during this reaction, as suggested by TLC/LCMS analysis. This was not investigated further.
3	SnCl ₂ .2H ₂ O, EtOH, reflux, >12h	After 12h the majority of desired 5-amino-2-chlorobenzamide had formed. After washing steps, organic concentrate required further purification via column chromatography. The desired compound (5.003) was obtained at 85% yield.
4	Fe, NH ₄ Cl, H ₂ O, MeOH (1:1), 70°C, 2h	Reaction occurred quickly with no starting material present after 2 h, indicating complete conversion. After filtration through celite to remove the iron and washing steps, the desired compound (5.003) was obtained at high yield without the need for further purification. The desired compound (5.003) was obtained at 94% yield.

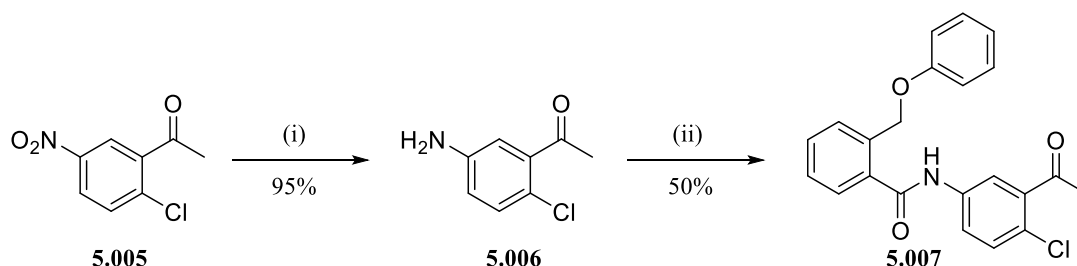
The reaction conditions of Trials 1-2 were unable to reach complete conversion of the nitro starting reagent (**5.002**) to the amine intermediate (**5.003**). After 12-24 hours, there was evidence of amine conversion, however a large majority of starting material remained as indicated by TLC and LCMS analysis. An increase in reaction run time and reducing agent may have improved the conversion ratio however this was not ideal and suggested an inefficient system. An increase in temperature is likely to have improved the outcome. This somewhat is evidenced by Trial 3, which was a large improvement over the previous Trial 2.

Following other methods taken from the literature, Trial 3 occurred by increasing temperature under reflux conditions and restricting the solvent employed to only the polar protic ethanol. The same reducing agent, tin_(II) chloride dihydrate was used in both Trials 2 and 3.⁸ The conditions of Trial 3 allowed for the nitro reduction to progress further within the same 12 hours, allowing for reaction completion, successfully achieving the amine intermediate (**5.003**). However, the most favourable conditions by far were accomplished in Trial 4, using iron as the reducing agent under slightly acidic conditions, once against favouring polar protic solvents (namely, methanol and water) at an increased temperature.¹¹ These somewhat harsher conditions were highly favourable and allowed for efficient reaction completion within 2 hours.

Trial 4 was also occurred quite cleanly which was highly favourable. Unlike Trial 3, this final study did not require further purification techniques after the usual filtration and washing steps, achieving the 5-amino-2-chlorobenzamide (**5.003**) at high yield and >95% purity by HPLC analysis. Overall, the conditions of Trial 4 obtained the desired compound **5.003** efficiently and with synthetic ease. Therefore, this method was further employed for continued nitro reductions using similar reagents. This is observed in **Schemes 5.02-5.05** where the reduced amine intermediates (**5.006**, **5.010**, **5.014**, **5.017**, **5.020**) were obtained in high yields.

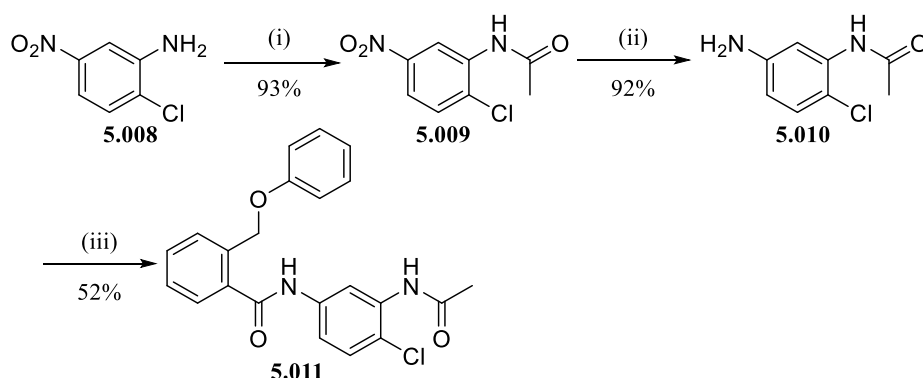
Beginning with **Scheme 5.02**, the synthetic pathway mirrors that of **Scheme 5.01**, following reduction of the nitro group followed by amide coupling to reach analogue **5.007**.^{6, 7, 11} However, the conditions of step i are now updated to involve the optimized nitro reduction using iron and ammonium chloride, replacing the previous hydrogenation conditions. The nitro group of the nitrophenylethanone (**5.005**) was successfully reduced to the amine intermediate (**5.006**) in high yield. Subsequent amide coupling procured analogue **5.007** in more moderate yield. This analogue would help confirm whether the amine group of the terminal amide was required to maintain activity, probing whether the potential hydrogen bonding interactions that could form between the amine and the putative binding site/s were essential for exerting potency.

Scheme 5.02: Modified synthetic pathway to reach analogue 5.007



Reaction conditions: i) Fe, NH₄Cl, H₂O, MeOH (1:1), 70°C ii) 2-(phenoxyethyl)benzoic acid, DIPEA, HOBt, EDCI, ACN/THF, 50°C

Scheme 5.03: Synthetic pathway to reach analogue 5.011



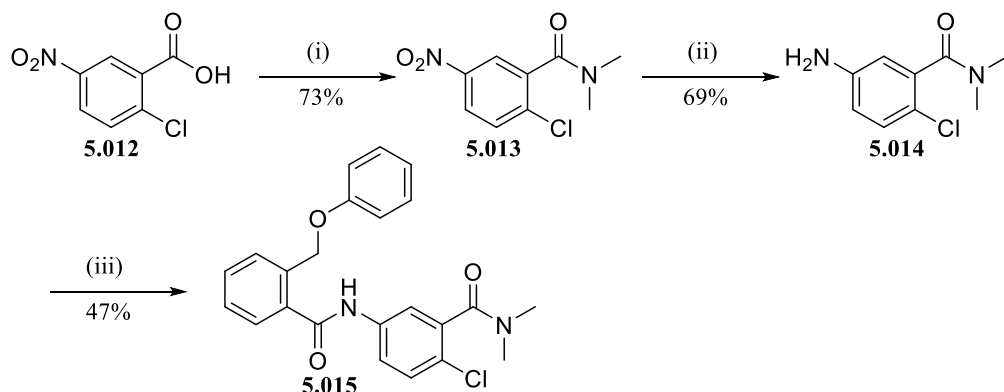
Reaction conditions: i) Acetyl chloride, DCE, DIPEA, 45°C, ii) Fe, NH₄Cl, H₂O, MeOH (1:1), 70°C iii) 2-(phenoxyethyl)benzoic acid, DIPEA, HOBt, EDCI, ACN/THF, 50°C

Continued use of the optimized nitro reduction step was also involved in **Scheme 5.03**, starting with 2-chloro-5-nitrobenzoic acid (**5.008**), which underwent amide bond formation to obtain the acetamide intermediate (**5.009**).¹³ The nitro group was then reduced to the amine intermediate in high yield (**5.010**) using the optimized protocol discussed above.¹¹ Finally, amide coupling occurred to obtain the reversed acetamide analogue (**5.011**).^{6, 7} This analogue was devised to investigate whether the reverse amide in relation to the original terminal amide (**5.001**) was tolerated, or whether possible specific hydrogen bonding interactions with the putative binding site existed, where the initial amide formation was required.

To investigate whether both hydrogen atoms of the terminal amide were required to form potential key interactions with the putative binding site/s and maintain activity, analogues **5.015** and **5.018** were devised. These analogues had small methyl groups installed onto the amine to decrease the hydrogen bond donating ability of the amino group. The methyl groups are still quite small, without being too intrusive by increasing steric bulk, significantly altering lipophilic or electronic effects onto the system.

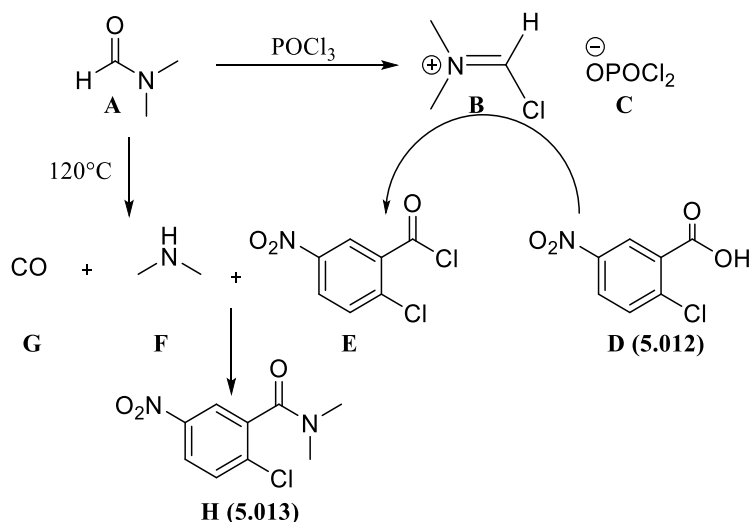
To acquire the tertiary amide analogue (**5.015**), the synthetic **Scheme 5.04** was followed. This began with coupling 2-chloro-5-nitrobenzoic acid (**5.012/D**) and DMF (**A**) using phosphoryl chloride (POCl₃) as the promoter. Bi *et al* suggest DMF and POCl₃ react to form a Vilsmeier reagent (**B**) which could act as the chlorinating agent to the carboxylic acid. Their proposed mechanism is depicted below in **Scheme 5.05**. Bi *et al* also suggest transformation of the carboxylic to the acid chloride (**E**) may also occurred through POCl₃ chlorination. At high temperatures and/or in an acidic environment DMF decomposes to dimethylamine (**F**) and carbon monoxide (**G**). The dimethyl amine (**F**) can then react with the acid halide to form the tertiary amide intermediate **5.013**.¹⁴ After **5.013** was obtained, continuing with **Scheme 5.04**, the reduction of the nitro group occurred using previously optimized conditions, to obtain the amine intermediate (**5.014**). The amine **5.014** would then undergo amide coupling to procure the tertiary amide analogue (**5.015**).^{6, 7, 11}

Scheme 5.04: Synthetic pathway to reach analogue 5.015



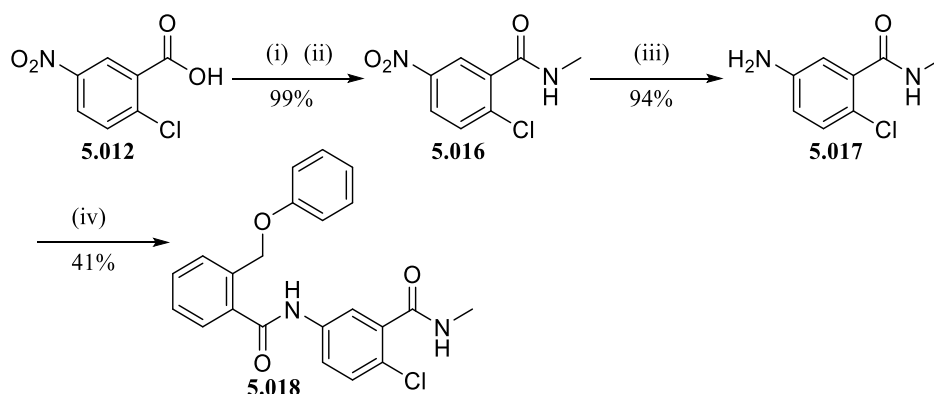
Reaction conditions: i) POCl₃, DMF, 120°C, ii) Fe, NH₄Cl, H₂O, MeOH (1:1), 70°C iv) 2-(benzyloxy)benzoic acid, DIPEA, HOBT, EDCI, ACN/THF, 50°C

Scheme 5.05 Mechanism of POCl₃ promoted synthesis of tertiary amide by coupling carboxylic acid and *N,N*-disubstituted formamide proposed by Bi *et al.*¹⁴



To acquire analogue **5.018**, the synthetic **Scheme 5.06** was followed. This pathway began with the 2-chloro-5-nitrobenzoic acid (**5.012**), which was converted into its acid chloride equivalent and directly underwent amide bond formation to successfully form the *N*-methyl nitrobenzamide intermediate (**5.016**).¹⁵ Reduction of the nitro group occurred to successfully form the amine building block (**5.017**) in high yield. The amine intermediate **5.017** was used for subsequent amide coupling to give the desired analogue **5.018**.^{6, 7, 11}

Scheme 5.06: Synthetic pathway to reach analogue 5.018



Reaction conditions: i) (COCl)₂, DCM, DMF, 0°C, ii) methylamine hydrochloride, Et₃N, DCM, iii) Fe, NH₄Cl, H₂O, MeOH (1:1), 70°C iv) 2-(benzyloxy)benzoic acid, DIPEA, HOBT, EDCI, DMF, 50-70°C

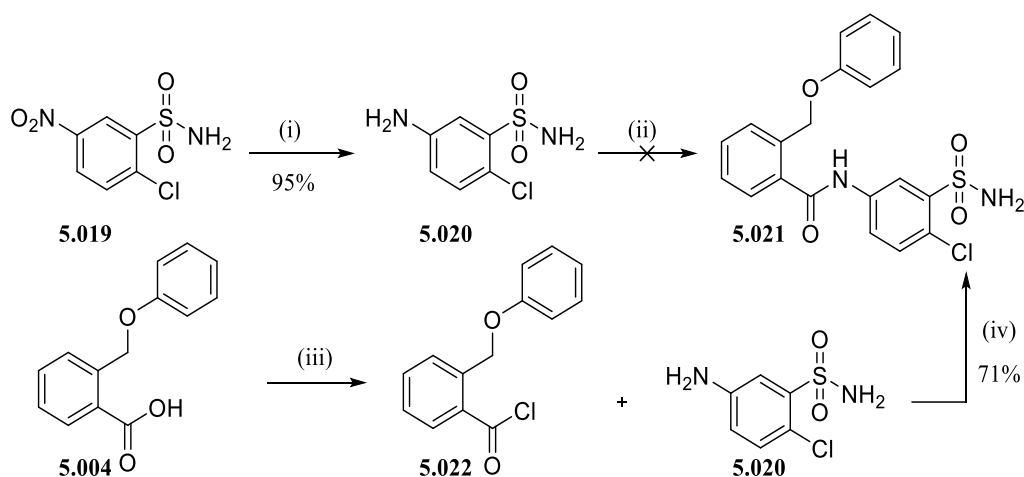
5.02.2 Optimization of the amide bond formation step

Optimization of the final amide bond formation step was required. Though I had already acquired sufficient amounts of each previous analogue synthesized for a range of biological testing, the majority of the analogue yields remained somewhat low and the reaction methods could be improved.

These initial coupling conditions required long reaction times (>72 h) for the formation of analogues **5.007** and **5.015** to reach completion. Furthermore, analogue **5.018** was unable to reach completion within this time, despite the efforts at increasing reactivity. The solvent was altered to DMF and fast stirring was employed to ensure reagent solubility. The reaction temperature was increased, and more time was allotted to the carboxylic acid-coupling agent complex formation before the addition of the amine **5.017**. After 72 h, LCMS analysis observed that though the desired analogue **5.018** had formed, both the amine **5.017** and benzoic acid **5.004** had not been completely consumed to form the amide bond. In addition to the slow reaction rate, in some instances the reaction did not occur cleanly causing difficulties during the purification steps. This was particularly evident for **5.015**, which contributed to a decreased product yield.

The formation of these *N*-(3-carbamoylphenyl)-2-(phenoxyethyl)benzamide analogues seem to be somewhat challenging as they are derived from sterically hindered carboxylic acids, where the bulky phenoxyethyl of compound **5.004** or similar group is required at the *ortho* position. The withdrawing effect of the ring attached carbonyl group of the terminal amide may also cause electron deficiency with the aromatic amine and cause decreased reactivity within this system.^{16, 17} As we aimed to explore this scaffold further, optimization of this step was undertaken in order to improve reactivity and efficiency of the amide formation. Furthermore, the coupling conditions previously utilized in **Scheme 5.01** and outlined below in **Schemes 5.07** (step ii), was found ineffective in reaching the desired analogues **5.021**. This gave us greater incentive to improve amide formation conditions, which are also depicted in **Scheme 5.07** (steps iii-iv).

Scheme 5.07 Synthetic pathways trialled to obtain analogue **5.021**



Reaction conditions: i) Fe, NH₄Cl, H₂O, MeOH (1:1), 70°C, ii) DIPEA, HOBT, EDCI, ACN/THF, 50°C, iv) 2-(phenoxyethyl)benzoic acid, DIPEA, HOBT, EDCI, DMF 50-70°C, iii) (COCl)₂, DCM, DMF, 0°C- rt, iv) Et₃N, THF, 0°C-rt

The synthetic pathway of **Scheme 5.07** begins with the nitrobenzenesulfonamide (**5.019**), which was reduced to the amine intermediate (**5.020**) and underwent amide coupling following the previous conditions with coupling agents HOBt and EDCI.^{6, 7, 11} After monitoring over 72 hours via LCMS analysis, the reaction was unable to meet fruition, despite the efforts to improve reactivity. As with the formation of **5.018**, a change in solvent, increased temperature and rapid stirring was applied in an attempt to push the reaction forward. Increased time for the activation of the benzoic acid **5.004** via the coupling reagents was also allowed. However, the desired analogue **5.021** had not formed and most of the starting material remained unreacted. As stated above, the 2-phenoxyethylbenzoic acid was already somewhat hindered due to the steric bulk of the phenoxyethyl functionality *ortho* to the carboxylic acid site, and may be further reducing the ability of the carboxylic acid to be activated by the coupling agents and/or for the carboxylic acid-EDCI/HOBt complex to interact with the amine. This hindrance is likely to have decreased reactivity throughout formation of the analogues formed for this series. In this instance the withdrawing nature of the sulfonamide functionality may further decrease reactivity of the system.^{16, 18}

Rather than spending more time altering amide coupling conditions to push this reaction forward, the carboxylic acid (**5.004**) was directly converted into an acid chloride intermediate (**5.022**) using oxalyl chloride as the chlorinating agent.^{19, 20} This was undertaken in order to increase reactivity of the carbonyl group (**Scheme 5.07 iii-iv**) where the chloro acts as an improved leaving group.²¹ The more reactive acid chloride intermediate (**5.022**) underwent amide bond formation directly with the amine intermediate (**5.020**), where the nucleophilic amine attacked the carbonyl carbon of the acid chloride intermediate, and the chloro leaving group was removed, forming the desired amide bond.²²⁻²⁵ Via LCMS and ¹H NMR analysis the reaction was able to reach completion quickly (under 12 h) obtaining the desired analogue **5.021** effectively in comparison to the previous amide coupling conditions. The ¹H NMR spectra of this analogue is depicted below in **Figure 5.05**, where all aromatic proton peak integrals are observed, indicating that the amide bond formation was successful. As seen previously observed in the spectra for hit **5.001/ 4.004** in **Figure 4.11**, Chapter 4, the most upfield aromatic signal centred at 6.91 ppm corresponds to the overlapping protons of multiplet F. These protons are shifted upfield due to the electron donating effect of the ether via resonance, directed at the *ortho* and *para* positions. Another key signal present is the singlet at 5.31 ppm, corresponding to the methylene (G). This analysis was undertaken in deuterated methanol, therefore the N-H peaks are not present due to solvent exchange.

Overall, this method was found to be much more successful and efficient and would replace the previous coupling conditions used as the final steps the remaining analogues to be synthesized. This method was further validated in **Schemes 5.08** and **5.09** below, achieving the desired final analogues in a more efficient manner.

Finally, analogue **5.021** contains a sulfonamide, a bioisostere of the terminal amide, which aims to probe whether additional hydrogen bonding abilities may be favourable to interacting with the putative binding site/s. The sulfonamide function group has also been reported to increase water solubility, which may help with solubilization within our *in vitro* studies, possibly helping avoid the compound crashing out of solution during biological assessments.²⁶

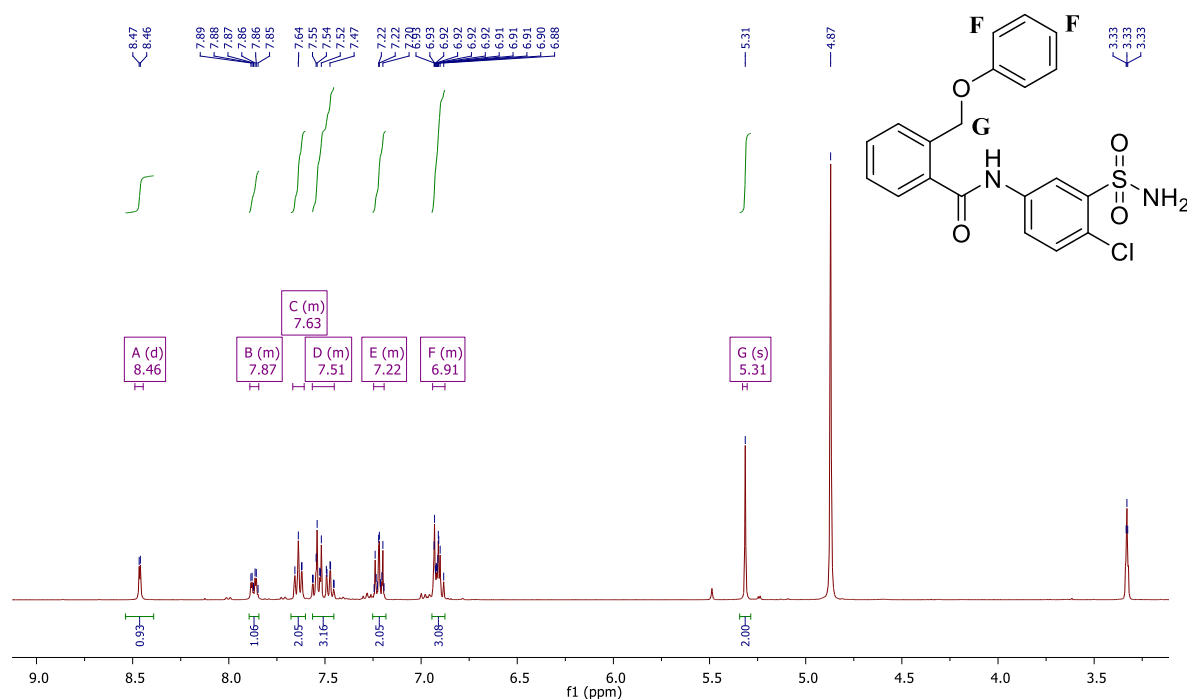


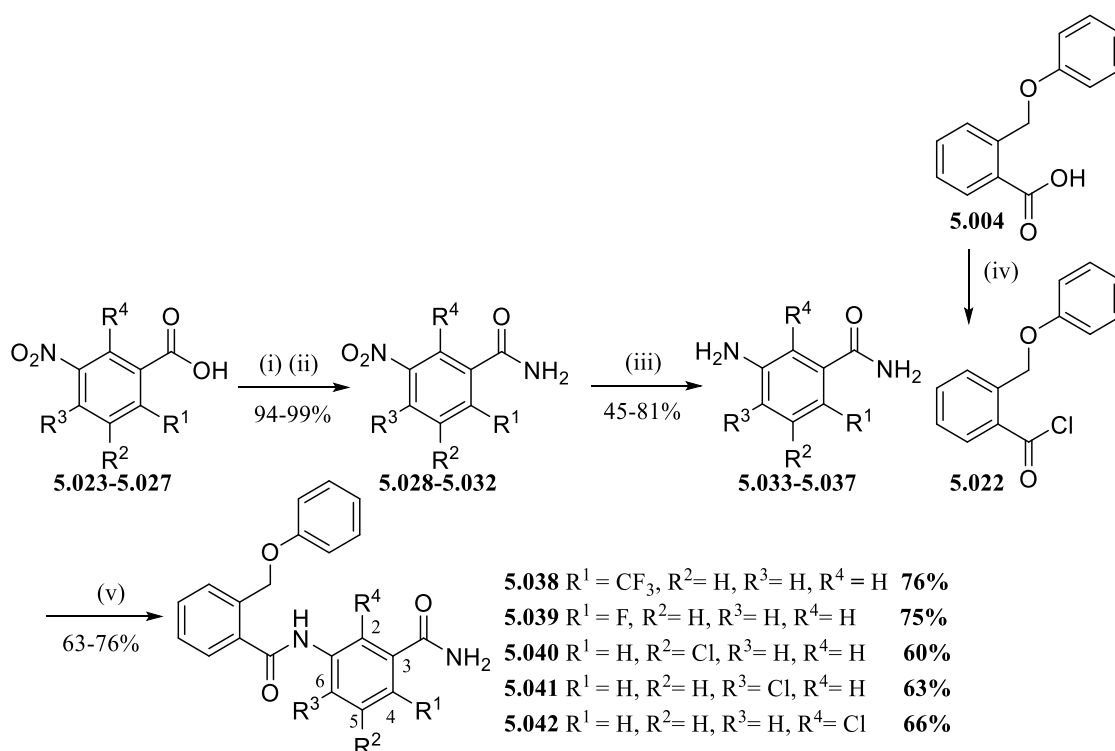
Figure 5.05 ¹H NMR spectra confirming the successful formation of analogue **5.021**. This analysis was undertaken using MeOD as the solvent

Continued synthesis of analogues targeting the benzamide ring, continued chloro modifications

Optimization of the nitro reduction and amide formation steps allowed for a more streamlined approach to further analogues. Further exploration around the functionalities of the terminal benzamide ring was continued, replacing the 4-chloro with the trifluoromethyl isostere (**5.038**). This substitution would determine whether a similar electron withdrawing functionality was preferred instead of the single halogen atom, keeping the molecular refractivity, inductive effect and Van der Waals radius similar. A future change to consider not yet accomplished would be to investigate a cyano isosteric replacement of the chloro, which would also have comparable effects on electronics, though would increase hydrophilicity. The 4-fluoro substituent was also substituted in compound **5.039**. This would give an insight into whether a more significant decrease in molecular refractivity and increase in electronegativity was preferred at this position.²⁷⁻²⁹ Synthesis of both **5.038-5.039** was preferable in measuring whether increasing electronegativity would increase activity, as the electronegativity of the trifluoromethyl is approximately halfway between the chlorine and fluorine.³⁰

Analogues **5.040-5.042** focus on repositioning the chloro group around the benzamide ring whilst keeping both amide functionalities in the same position. This was devised to study whether possible interactions with the chloro group and the putative binding site were still maintained at different positions around the ring. This would probe whether the chloro could be tolerated around the ring, or even form stronger interactions with the binding site. These analogues were all obtained followed the streamlined synthetic pathway depicted in **Scheme 5.08**. The various the carboxylic acid functionality of the nitrobenzoic acids (**5.023-5.027**) were converted into acid chlorides using oxalyl chloride, before immediate transformation to the terminal amide (**5.028-5.032**), acquired in high yield.³¹ The nitro group was then reduced into the amine intermediates (**5.033-5.037**) using iron powder under slightly acidic conditions.¹¹ The 2-phenoxyethyl benzoic acid was converted into the acid chloride (**5.022**) to undergo nucleophilic coupling with the previously formed amine intermediates (**5.033-5.037**) to successfully obtain the desired analogues (**5.038-5.042**) in relatively good yield.^{19, 20, 22-24} Amide bond formation for these analogues occurred without issue, reaching reaction completion quickly, where most of the amine (**5.033-5.037**) and acid chloride (**5.022**) were consumed via TLC and LCMS analysis. Purification of these analogues also occurred with ease to obtain the desired analogues (**5.038-5.042**) in greater efficiency following this improved synthetic method.

Scheme 5.08 Completely optimized synthetic route to form carbamoyl phenoxyethyl benzamide analogues exploring the benzamide ring, specifically chloro modifications



Reaction conditions: i) $(COCl)_2$, DCM, DMF, 0°C- rt, ii) NH_4OH , EtOAc, 0°C- rt, iii) Fe, NH_4Cl , H_2O , MeOH (1:1), 70°C, iv) $(COCl)_2$, DCM, DMF, 0°C- rt, v) Et_3N , THF, 0°C- rt

The ^1H NMR analysis of several of the terminal amide containing compounds synthesized throughout this chapter depicted an expected pattern first observed in Chapter 4. The primary amide protons were observed as two inequivalent, separate broad singlets with an integration of 1H each, rather than one broad peak with an integration of 2H. As mentioned in Chapter 4, the NH protons of the primary amide resonate at different magnetic environments due to the hindered rotation around the carbonyl-nitrogen bond amide bond.^{32,33} All compounds depicting this pattern have been reported within the Experimental section of this chapter and was most evident in some of the smaller intermediates, such as **5.030** and **5.037**. As expected, since less protons appear within the aromatic region it is much easier to identify this NH_2 peak separation, as seen in **Figure 5.06a-b**.

The ^1H NMR spectrum of intermediate **5.030** is depicted in **Figure 5.06 a**, where the two separate broad signals assigned to the NH_2 terminal amide are clearly visible at 8.40 ppm (peak C) and 7.85 ppm (peak E). These hallmark broad singlets of the magnetically inequivalent primary amide protons are also evident in **Figure 5.06 b**, assessing intermediate **5.037**. Two separate broad singlets are clearly observed at 7.68 and 7.38 ppm corresponding to the terminal amide proton peaks A and B respectively. In comparison, the primary amine protons (F) are equivalent and observed to give rise to one broad singlet at 5.43 ppm. These compounds are known entities which have been previously described in the literature.^{34, 35}

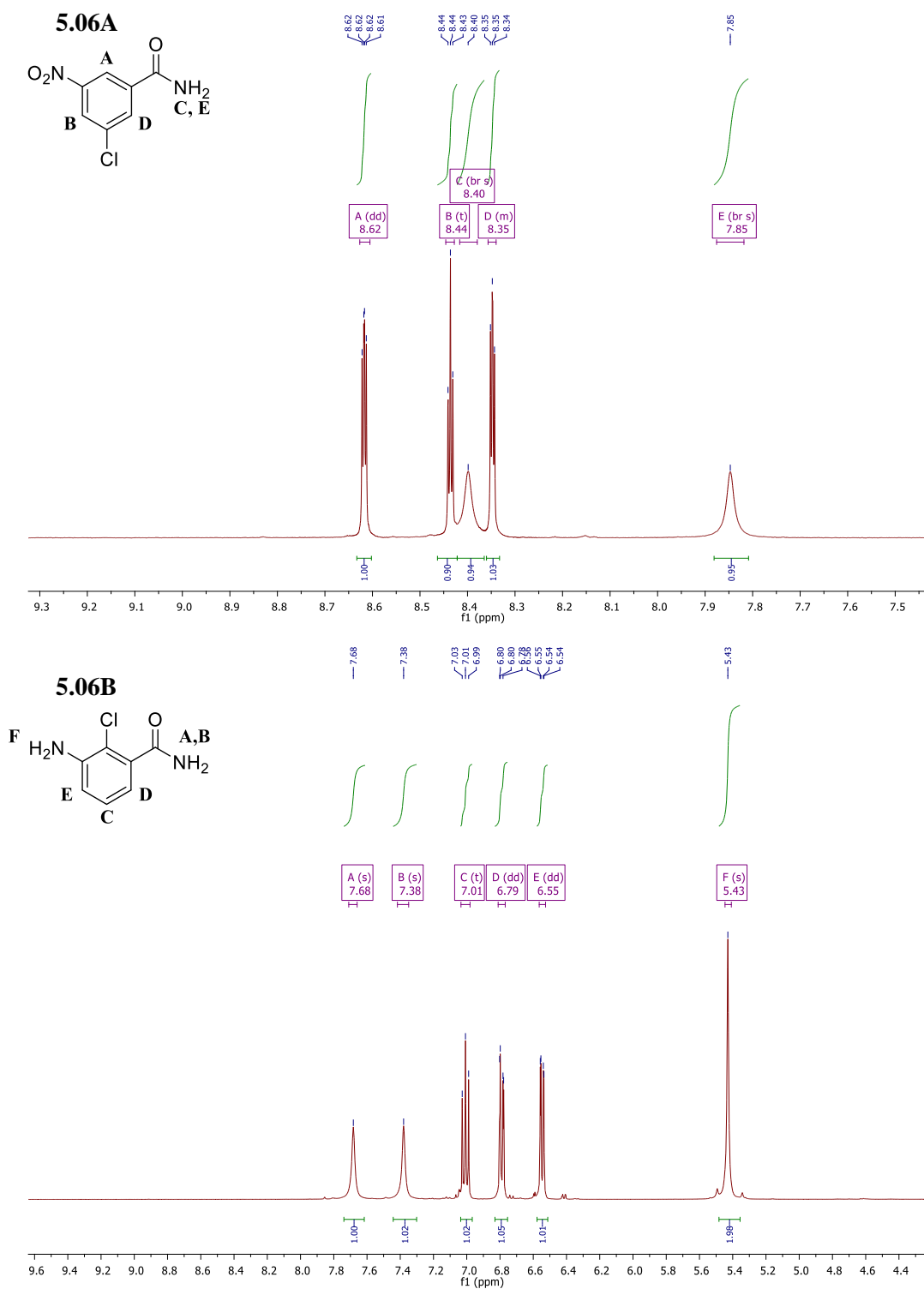


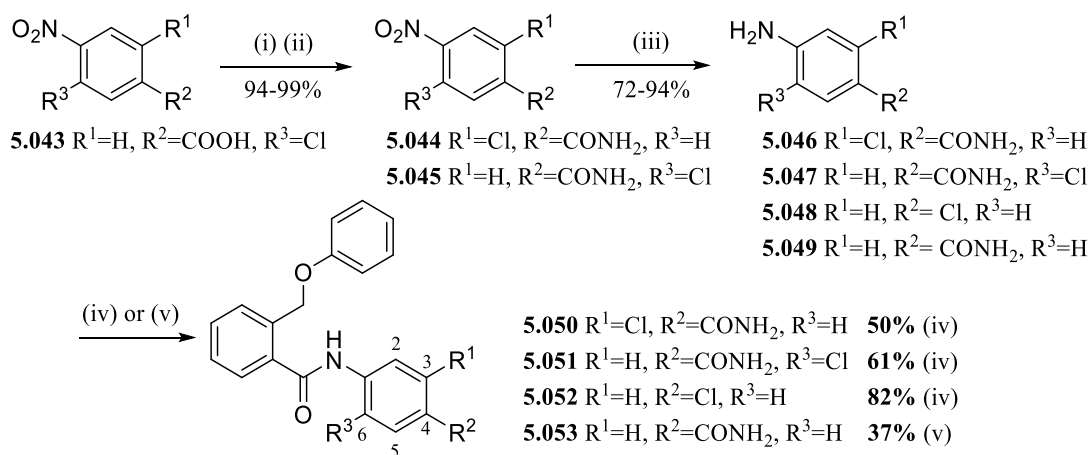
Figure 5.06a (top) ¹H NMR spectra of intermediate 5.030 in DMSO solvent and 5.07b (bottom) ¹H NMR spectra of intermediate 5.037. Both illustrate the separate broad singlets assigned to the NH₂ terminal amide.

5.02.3 Continued synthesis of analogues targeting the benzamide ring, terminal amide and chloro modifications

The optimized synthetic pathway shown in **Scheme 5.09** was utilized to form analogues focused on altering the terminal amide and chloro functional groups simultaneously. The first analogue of this set, **5.050** reversed the original positions of the terminal amide and chloro functionalities. This was undertaken in order to surmise whether these positions were preferable for binding or whether the original positions were required to maintain activity. Analogue **5.051** was also synthesized, possessing the terminal amide at the 3-position, whilst the chloro was moved to the 6-position of the ring, *ortho* to the central amide and *para* to the terminal amide. This analogue was synthesized more so for serendipitous activity. This analogue would be compared to the above analogues **5.041** and **5.050**, where the former shares the repositioned chloro to the 6-position, *ortho* to the central amide and *para* to the terminal amide, whilst the latter shares the repositioned terminal amide to the 4-position, *para* to the central amide and *meta* to the chloro substituent.

Overall compound **5.051** would discern whether both these repositioned functionalities are preferred at these altered positions, and give an insight into the benzamide system, if this proximity between the functionalities is favoured. Analogue **5.052** removed the terminal amide completely, which would confirm whether the terminal amide was required to maintain activity, and whether its potential hydrogen bonding abilities with the binding site/s are necessary interactions required to allow for antileishmanial activity. Finally, compound **5.053** repositioned the terminal amide to the 4-position and removed the chloro group concurrently. This compound would be compared to compounds **5.050-5.051** which also possessed the terminal amide at the 4-position and could gauge whether the chloro was required to maintain activity whilst the terminal amide was positioned *para* to the central amide. This compound would also be directly compared to the previous analogue **4.053** of Chapter 4, which also removed the chloro substituent though maintained the terminal amide at the original 3-position which was found inactive. This would give an insight into whether the loss of activity was due to the loss of the chloro from **4.053**, or whether the benzamide can still maintain some activity at the 4 position over the 3, determining whether the chloro is required at all.

Scheme 5.09 Completely optimized synthetic route to form carbamoyl phenoxyethyl benzamide analogues exploring the benzamide ring, specifically terminal amide and chloro modifications



Reaction conditions: i) $(COCl)_2$, DCM, DMF, $0^\circ C$ - rt, ii) NH_4OH , EtOAc, $0^\circ C$ - rt, iii) Fe, NH_4Cl , H_2O , MeOH (1:1), $70^\circ C$, iv) (2-(phenoxyethyl)benzoyl chloride (**5.022**), Et_3N , THF, $0^\circ C$ - rt or v) 2-(phenoxyethyl)benzoic acid, DIPEA, HOBt, EDCI, DMF, $50^\circ C$ (used for the synthesis of **5.053** only)

These analogues were obtained following **Scheme 5.09**, which employs the improved steps discussed above. This scheme has been depicted to display the complete yields of all intermediates and the continued success of all the aforementioned optimization efforts. Briefly, the nitrobenzoic acid (**5.043**) were converted to their acid chloride equivalent followed by immediate conversion to the terminal amide (**5.044-5.045**, where **5.044** was readily available).³¹ This was followed by subsequent reduction of the nitro group to the amine building blocks (**5.046-5.047**).¹¹ Aromatic amines (**5.046-5.047**) along with the readily available 4-chloroaniline (**5.048**) were reacted with the converted benzoyl chloride (**5.022**) to successfully obtain the analogues **5.050-5.052** in moderate to high yield.²²⁻²⁴ Analogue **5.053** employed step v of **Scheme 5.09**, the previous amide coupling conditions used.^{6, 7} These conditions were utilized as this analogue was synthesized before the optimization of the amide bond formation step, performed in parallel to **5.018** and other previously discussed analogues via synthesis stations capable of performing several individual, simultaneous reactions at one time. This was undertaken in order to efficiently obtain a larger number of devised compounds within the allotted time remaining.

Similar to the formation of **5.018**, the reaction solvent was altered to DMF with fast stirring in order to improve solubility. Increased reaction time and temperature were also applied in order to increase reactivity of the starting reagents. After 72 h, the desired compound **5.053** had formed, as confirmed by TLC and LCMS analysis, though the starting compounds **5.015** and **5.004** were unable to undergo complete consumption to form the desired amide bond, contributing to the lower product yield. Nonetheless, enough product was obtained for the array of *in vitro* biological tests we employed for anti-leishmanial activity confirmation. The low product yield of **5.053** obtained, and decreased reactivity of the starting reagents helps illustrate here the improvement of the amide formation step via

nucleophilic substitution with the acid halide over the direct use of the benzoic acid and coupling agents. If compound **5.053** required resynthesis, the optimized acid chloride method outlined in step iv of **Scheme 5.09** would be utilized. This was also the case for compounds **5.056**, **5.085** and **5.087**, which are discussed in later sections of this chapter. These compounds also utilized conditions listed in step v of **Scheme 5.09**, which generally observed low reactivity and decreased yield. As with **5.053**, any required resynthesis of these compounds would also employ the optimized pathway following step iv of **Scheme 5.09**.

5.03 Biological results of analogues targeting benzamide modifications

Compounds targeting the modifications around the benzamide ring underwent biological testing against *L. donovani* using the high throughput imaging intramacrophage assays performed by Bio21 and IPK. Detailed in Chapters 2-4, these assays use THP-1 transformed macrophages infected with *L. donovani* parasites. The investigative compounds are added to the assay plate and incubated for 72 hours. Subsequent fluorescent staining and high content imaging occurred, where the number of amastigotes within macrophages was made visible and counted to discern the efficacy of the compounds used. The cytotoxicity of the host cell was also determined using the simultaneous staining of the host macrophages.^{36,37} The luciferase assay performed by UNC was also utilized to determine compound potency. This assay employed *L. donovani* expressing firefly luciferase and a red fluorescent protein, and measured the level of luminescence of *L. donovani* amastigotes within THP-1 transformed macrophages.³⁸⁻⁴⁰ Toxicity of compounds was measured separately in uninfected macrophages, using the colorimetric MTT assay. This measures the ability of NAD(P)H-dependant cellular oxidoreductase enzymes to reduce the tetrazolium dye to formazan, which is purple in colour. This assessment of metabolic ability correlates the number of viable cells present, and thus the level of toxicity of the investigative compounds against the host cells.^{41, 42} As set out in Chapter 3, to manage any issues with conflicting activity and/or toxicity values between these independent assays, convergent results in 2 out of 3 independent assays would be considered reliable. As discussed throughout this body of work, targeting *Leishmania* in drug discovery is considered difficult and some deviations are expected when working with such a large library of analogues.

5.03.1 Biological results and SAR discussion around analogues with terminal amide substitution

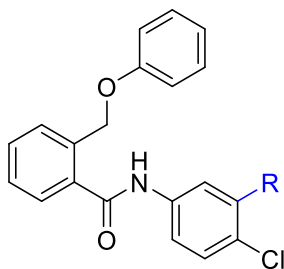
Analogues possessing modifications to the terminal amide underwent biological assessment against *L. donovani* amastigotes. Depicted below, **Table 5.02** summarizes the biological results of these compounds compared to the original hit **5.001**, which was previously confirmed to have potent antileishmanial activity. The ester isosteric substitution (**4.054**) was also included for a comprehensive

view of all the terminal amide substitutions made within this hit-to-lead campaign so far. Solubility issues were not reported by any of our collaborators during the range of bioassays performed.

Based on **Table 5.02**, the substitutions to this functionality were found unanimously unfavourable, suggested the terminal amide to be a necessity to maintaining antileishmanial activity. It was confirmed that the terminal amide was required to maintain activity, where the complete removal of this functionality correlated to complete inactivity against *L. donovani*, as seen in compound **5.052**. As seen in chapter 4, the ester bioisosteric replacement of compound **4.054** was found inactive against *L. donovani* causing a complete loss of activity. The loss of hydrogen bond donating ability seemed to be a key factor to activity loss. The complete loss the hydrogen bond donating ability at the terminal amide was further investigated using the acetyl group substitution (**5.007**) and demethylated tertiary amine (**5.015**). A significant decrease of potency compared to the original hit **5.001** was observed across all assays in both **5.007** and a complete loss of activity was witnessed in the demethylated amine analogue (**5.015**). This suggested hydrogen bond donating ability may be a key requirement at this position. However, the monosubstituted amide (**5.018**) was also found inactive, which may suggest any decrease in hydrogen bonding ability in unfavourable. The insertion of the methyl may even block some specific hydrogen bonding interactions, and that both hydrogen atoms may be involved in key interactions between the investigate compound and binding site/s. However, this did not seem to be the case for the bioisosteric replacement with sulfonamide (**5.021**), where the carbonyl moiety was substituted for the SO₂ group. This functionality also possessed the primary amine capable of similar interactions as the original terminal amide, along with an increased hydrogen bond accepting ability due to the second S=O bond.²⁶ Based on the previous loss of activity observed with the loss of hydrogen bond donating groups, it was expected that analogue **5.021** would maintain some activity. Yet, this analogue was also found completely inactive against *L. donovani*. It may be that specific hydrogen bonding interactions (both donating and accepting) occurs with the binding site and cannot be obstructed by other groups.

At this stage, the rationale is not completely understood, though it is known that a terminal amide is required in its original position and orientation. This was further confirmed with compound **5.011**, which reversed the amide, where the amine group was attached the aromatic ring instead of the carbonyl. This was found to give a significant loss in activity within the majority of bioassays, excluding the UNC luciferase. Following the “2 out of 3” guideline, this modification was determined to be unfavourable, and suggests the potential hydrogen bonding interactions with the binding site/s are quite specific, requiring both the C=O and the NH₂ in their original positions and orientation to achieve potency. Despite this negative SAR obtained, this was good news to us, as it defined clearly what the scaffold required and could not completely modify. Additionally, no cytotoxicity was observed within **Table 5.02** analogues, suggesting no selectivity against the host cell.

Table 5.02: Complete biological results of analogues possessing terminal amide substitutions, hit 5.001 outlined in blue



I.D	R	HCS intracellular assay against <i>L. donovani</i>				Luciferase /MTT assay	
		Bio21 ^a		IPK ^{ef}		UNC ^{gh}	
		IC ₅₀ (μM)	CC ₅₀ (μM)	IC ₅₀ (μM)	CC ₅₀ (μM)	IC ₅₀ (μM)	CC ₅₀ (μM)
5.001 (hit) ^b	CONH ₂	4.9	>100 ^h	21	>100 ^j	3.2	>50
4.054	COOCH ₃	>50 ⁱ	>50 ⁱ	>100 ^j	>100 ^j	>20	>50
5.007 ^c	COCH ₃	>100 ^j	>100 ^j	63	75	27	>50
5.011 ^c	NHCOCH ₃	>100 ^j	>100 ^j	97	71	6.1	>50
5.015 ^d	CON(CH ₃) ₂	>100 ^j	>100 ^j	>100 ^j	>100 ^j	>50	>50
5.018 ^c	CONHCH ₃	>100 ^j	>100 ^j	96	75	>50	>50
5.021 ^d	SO ₂ NH ₂	>100 ^j	>100 ^j	73	90	>50	>50
5.052 ^d	H	>100 ^j	>100 ^j	>100	>100 ^j	>50	>50

a= anti *L. donovani* activity and toxicity measured in THP-1 transformed macrophage host cell lines using a top concentration of 100 μM (2x serial dilution 10-point curve). Experiment performed in duplicate wells in one experiment, n=1.

b= control compounds for Bio21 intramacrophage *L. donovani* assay. Miltefosine IC₅₀= 0.50 μM, CC₅₀ = 40 μM, Amphotericin B IC₅₀= 1.1 μM, CC₅₀= 66 μM.

c= control compounds for Bio21 intramacrophage *L. donovani* assay. Miltefosine IC₅₀= 0.52 μM, CC₅₀ >100 μM, Amphotericin B IC₅₀= 2.6 μM, CC₅₀= 26 μM.

d= control compounds for Bio21 intramacrophage *L. donovani* assay. Average (± standard deviation) from experimental replicates; Miltefosine IC₅₀= 0.83 μM, CC₅₀ >100 μM, Amphotericin B IC₅₀= 0.61 ± 0.079 μM, CC₅₀ > 40 μM.

e= anti *L. donovani* activity and toxicity measured in THP-1 transformed macrophage host cell lines using a top concentration of 100 μM (2x serial dilution 10-point curve)

f= control compounds for IPK intramacrophage *L. donovani* assay. Miltefosine IC₅₀= 1.7 μM, CC₅₀ >100 μM, Amphotericin B IC₅₀= 0.83 μM, CC₅₀ > 100 μM.

g= anti *L. donovani* activity measured in THP-1 transformed macrophage host cell lines using luminescent expressing *L. donovani*. Experiment performed in triplicate wells in one experiment, n=1 using a concentration range of 1-50 μM. DMSO was used as sole control against which the percent *L. donovani* viability is calculated

h= host cell toxicity measured in MTT assay with uninfected macrophage host cells. Experiment performed in triplicate wells in one experiment, n=1 using a concentration range of 1-50 μM. DMSO was used as sole control against which the percent cell viability is calculated

i = anti *L. donovani* activity and toxicity measured in THP-1 transformed macrophage host cell lines using a one-point concentration (50 μM) to assess any form of antileishmanial activity. Experiment performed in duplicate wells in one experiment, n=1.

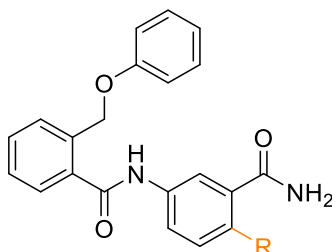
j= no inhibition detected within DRC at the top concentration tested (100 μM).

5.03.2 Biological results and SAR discussion around analogues 4-chloro substitution

The small set of analogues investigating substitution of the 4-chloro group were also found to be undesirable in comparison to the original hit **5.001**, shown in **Table 5.03**. Complete removal of the chloro group had previously been confirmed to give a loss of activity, observed with analogue **4.053**. This suggested that the 4-chloro was required at this position. The substitution of the chloro atom with the fluoro in compound **5.039** gave low antileishmanial activity. This suggested a significant increase in electronegativity and decrease in molecular refractivity was an unfavourable modification, though did not give a total loss of activity. The trifluoromethyl substitution (**5.038**) unanimously gave a

complete loss of activity. This substitution was closer in molecular refractivity and electronegativity to the original chloro group, though it may be that the increased electron withdrawing ability which is causing greater electron deficiency to the aromatic system, which may be potentially unfavourable for this system.^{17, 27-30} Another suggestion may be that the decrease in activity may be due to the an indirect geometrical effect around the primary amide. The hit **4.001** possesses a chloro group *ortho* to the primary amide, which can cause the amide to take on a greater “twisted” orientation out of plane in relation to the core, discouraging a planar confirmation. This is evidenced by the reported crystal structures of 2-chlorobenzamide and the unsubstituted benzamide within the Cambridge Crystallography Data Centre (CCDC) using the database deposit numbers 1127043 and 1118065 respectively.⁴³⁻⁴⁷ This “twisted” orientation of terminal amide, caused by the *ortho*-chloro group is also observed with the crystal structure of hit **5.001** within **Figure 5.02**, as an ethanol solvate. The removal of this chloro group (**4.053**) may not have allowed for the primary amide to take on the same “twisted” orientation suggested for **5.001**, thus possibly hindering the ability of the primary amide to reach and interact with the putative binding site. This may also be the case when the chloro is substituted for fluoro atoms (**5.038-5.039**), where the fluoro may form an intramolecular hydrogen bridge with the primary amide proton rather than inducing the same orientation as **5.001**.^{48, 49} However, further investigation understanding the orientation of the scaffold is still required to confirm this hypothesis.⁴⁴ The CCDC deposition number of related benzamides and anilides are listed within the Appendix of this thesis.

Table 5.03: Complete biological results of analogues possessing 4-chloro substitutions hit 5.001 outlined in blue



I.D	R	HCS intracellular assay against <i>L. donovani</i>				Luciferase /MTT assay	
		Bio21 ^a		IPK ^{ef}		UNC ^{gh}	
		IC ₅₀ (μM)	CC ₅₀ (μM)	IC ₅₀ (μM)	CC ₅₀ (μM)	IC ₅₀ (μM)	CC ₅₀ (μM)
5.001 (hit)^b	Cl	4.9	>100 ⁱ	21	>100 ⁱ	3.2	>50
4.053^c	H	>100 ⁱ	>100 ⁱ	>100 ⁱ	>100 ⁱ	>50	>50
5.038^d	CF ₃	>100 ⁱ	>100 ⁱ	>100 ⁱ	>100 ⁱ	>50	>50
5.039^d	F	22	>100 ⁱ	>100	>100 ⁱ	22	>50

a= anti *L. donovani* activity and toxicity measured in THP-1 transformed macrophage host cell lines using a top concentration of 100 μM (2x serial dilution 10-point curve). Experiment performed in duplicate wells in one experiment, n=1.

b= control compounds for Bio21 intramacrophage *L. donovani* assay. Miltefosine IC₅₀= 0.50 μM, CC₅₀ = 40 μM, Amphotericin B IC₅₀= 1.1 μM, CC₅₀= 66 μM.

c= control compounds for Bio21 intramacrophage *L. donovani* assay. Miltefosine IC₅₀= 0.53 μM, CC₅₀ = 33 μM, Amphotericin B IC₅₀= 0.72 μM, CC₅₀> 100 μM.

d= control compounds for Bio21 intramacrophage *L. donovani* assay. Average (± standard deviation) from experimental replicates; Miltefosine IC₅₀= 0.83 μM, CC₅₀ >100 μM, Amphotericin B IC₅₀= 0.61 ± 0.079 μM, CC₅₀ > 40 μM.

e= anti *L. donovani* activity and toxicity measured in THP-1 transformed macrophage host cell lines using a top concentration of 100 μM (2x serial dilution 10-point curve)

f= control compounds for IPK intramacrophage *L. donovani* assay. Miltefosine IC₅₀= 1.7 µM, CC₅₀ >100 µM, Amphotericin B IC₅₀= 0.83 µM, CC₅₀ > 100 µM.

g= anti *L. donovani* activity measured in THP-1 transformed macrophage host cell lines using luminescent expressing *L. donovani*. Experiment performed in triplicate wells in one experiment, n=1 using a concentration range of 1-50 µM. DMSO was used as sole control against which the percent *L. donovani* viability is calculated

h= host cell toxicity measured in MTT assay with uninfected macrophage host cells. Experiment performed in triplicate wells in one experiment, n=1 using a concentration range of 1-50 µM. DMSO was used as sole control against which the percent cell viability is calculated

i= no inhibition detected within DRC at the top concentration tested (100 µM).

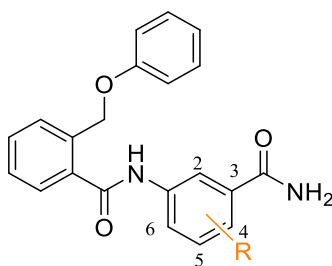
Overall, from this negative SAR so far, we can surmise that the single chloro atom was required at the 4-position of the benzamide ring, where loss of this group, increased electronegativity and possible change in orientation was to be avoided. No solubility or toxicity issues were observed within this set of analogues. This was also good news to us, as there was no question as to whether inability to remain in solution, preventing cell permeation was causing the inactivity. Furthermore, there was no question as to whether any antileishmanial activity was due to true interactions with *L. donovani* or toxicity against the whole host cell, causing consequent activity against the parasite.

5.03.4 Biological results and SAR discussion around analogues repositioning the chloro substituent

Based on the previous SAR, it is proposed that the chloro group at the 4-position of the benzamide ring (**5.001**) is required to maintain antileishmanial activity. Repositioning this substituent around the benzamide ring whilst preserving the terminal amide at the 3-position was undertaken in order to surmise whether the chloro group was preferred at other positions of the ring and could still maintain the same interactions with the putative binding site. However, biological assessment of these analogues, highlighted in **Table 5.04**, found that moving the chloro group to the 2-, 5- or 6- positions of the benzamide ring (**5.040**, **5.041** and **5.042** respectively) was completely unfavourable, unanimously causing a complete loss of activity against *L. donovani* across all assays employed. Continuing with the hypothesis introduced earlier, the loss of activity observed here may not have solely been due to altering a direct interaction between the chloro substituent and the putative binding site but rather could be an indirect geometrical effect. As stated above, when the chloro substituent is position *ortho* to the terminal amide, planarity is discouraged, causing the amide to “twist” out of plane in relation to the core.⁴³⁻⁴⁷ When the chloro was repositioned to the 6-position (**5.041**) it may induce the anilide core to twist out of plane, whilst the primary amide is unable to form the same potential orientation as **5.001**, overall hindering the ability to interact with the putative binding site in the same manner. This is evidenced by several reported crystal structures listed by the CCDC, including 2-chlorobenzamide, *N*-(2-chlorophenyl)benzamide and 4-chlorobenzamide. The CCDC deposit number of related benzamides and anilides are listed in the Appendix.^{43, 44, 50-55} In regard to compound **5.042**, it is uncertain whether the chloro group would induce a change in orientation in the anilide and/or primary amide. It may also be likely that the chloro group is acting as a steric hindrance rather than a “twist”, blocking potential interactions with the putative receptor and the scaffold and causing inactivity. This SAR interpretation

requires further investigation with a fuller set of analogues to further understand the potential geometrical influence involved in maintaining activity. Based on this SAR at this point, it can simply be stated that the chloro substituent was required at the 4-position, when the terminal amide was at the 3-position to maintain potency. Furthermore, the loss of the electron withdrawing group at the *para/ortho* position to the acetanilide may have further decreased the acidity of the acetanilide N-H proton and its willingness to undergo hydrogen bonding with the putative binding site. If this potential interaction is required to maintain activity, repositioning the electron withdrawing group to *meta* to the acetanilide core should be avoided. Once again, no issues with solubility or cytotoxicity were reported for this set of analogues.

Table 5.04: Complete biological results of analogues repositioning the 4-chloro group only, hit 5.001 outlined in blue



I.D	R	HCS intracellular assay against <i>L. donovani</i>				Luciferase /MTT assay	
		Bio21 ^a		IPK ^d		UNC ^{fg}	
		IC ₅₀ (μM)	CC ₅₀ (μM)	IC ₅₀ (μM)	CC ₅₀ (μM)	IC ₅₀ (μM)	CC ₅₀ (μM)
5.001 (hit)^{be}	4-Cl	4.9	>100 ^h	21	>100 ^h	3.2	>50
5.040^{ce}	5-Cl	>100 ^h	>100 ^h	92	75	>40	>50
5.041^{cf}	6-Cl	>100 ^h	>20	>100 ^h	>100 ^h	>50	>50
5.042^{cf}	2-Cl	>100	>100 ^h	>100 ^h	>100 ^h	>50	>50

a= anti *L. donovani* activity and toxicity measured in THP-1 transformed macrophage host cell lines using a top concentration of 100 μM (2x serial dilution 10-point curve). Experiment performed in duplicate wells in one experiment, n=1.

b= control compounds for Bio21 intramacrophage *L. donovani* assay. Miltefosine IC₅₀= 0.50 μM, CC₅₀ = 40 μM, Amphotericin B IC₅₀= 1.1 μM, CC₅₀= 66 μM.

c= control compounds for Bio21 intramacrophage *L. donovani* assay. Average (± standard deviation) from experimental replicates; Miltefosine IC₅₀= 0.83 μM, CC₅₀ >100 μM, Amphotericin B IC₅₀= 0.61 ± 0.079 μM, CC₅₀ > 40 μM.

d= anti *L. donovani* activity and toxicity measured in THP-1 transformed macrophage host cell lines using a top concentration of 100 μM (2x serial dilution 10-point curve)

e= control compounds for IPK intramacrophage *L. donovani* assay. Miltefosine IC₅₀= 1.7 μM, CC₅₀ >100 μM, Amphotericin B IC₅₀= 0.83 μM, CC₅₀ > 100 μM.

f= control compounds for IPK intramacrophage *L. donovani* assay. Miltefosine IC₅₀= 2.3 μM, CC₅₀ >100 μM, Amphotericin B IC₅₀= 0.45 μM, CC₅₀ > 100 μM.

g= anti *L. donovani* activity measured in THP-1 transformed macrophage host cell lines using luminescent expressing *L. donovani*. Experiment performed in triplicate wells in one experiment, n=1 using a concentration range of 1-50 μM. DMSO was used as sole control against which the percent *L. donovani* viability is calculated

h= host cell toxicity measured in MTT assay with uninfected macrophage host cells. Experiment performed in triplicate wells in one

experiment, n=1 using a concentration range of 1-50 μM. DMSO was used as sole control against which the percent cell viability is calculated

i= no inhibition detected within DRC at the top concentration tested (100 μM).

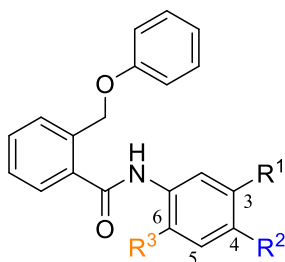
5.03.5 Biological results and SAR discussion around analogues repositioning both the terminal amide and chloro substituents

The final set of analogues belonging to the investigation around the benzamide ring was assessed for activity against *L. donovani* and the results are summarized in **Table 5.05**. It was found that swapping the terminal amide and chloro positions seen with compound **5.050**, where the amide was moved to the 4-position and the chloro to the 3-position, was highly unfavourable and should be avoided. It may be that when the chloro is repositioned to the 3-position, it may sterically hinder interactions made between the primary amide and putative binding site. However, unlike compound **5.050** and the previous SAR of **Table 5.04**, compound **5.051** (chloro at 6-position, terminal amide at 4-position) defied the original conclusion that the terminal amide and chloro groups should be fixed at the 3- and 4- positions respectively in order to exert potent antileishmanial behaviour.

Compound **5.051** was found to be truly active, reporting converging values across all bioassays and was determined to have close but not superior activity to the hit **5.001** in the majority of assays (significant improvement in IPK intramacrophage assay only). This was somewhat unexpected as close analogues **5.041** (chloro at 6-position, terminal amide at 3- position) and **5.050** (chloro at 3-position, terminal amide at 4-position) were found completely inactive. The maintained potency of **5.051**, suggested the 6-chloro was tolerated, so long as the terminal amide was also moved in closer proximity to it (4-position). Following our previous hypothesis, it may be that moving the chloro to the 6-position, may cause the now *ortho* benzanilide core to change orientation out of plane in relation to the benzamide ring, whereas the primary amide at the 4-position is no longer *ortho* to the chloro and therefore may not be subjugate to this exact same change in orientation as **5.001**.⁵¹⁻⁵⁴ It is plausible that by repositioning the primary amide to the 4-position, it is able to reach and interact with the putative binding site in a similar manner as the original hit **5.001**, where the primary amide is at the 3-position, though orientated out of plane due to the *ortho* chloro substituent. The potential simultaneous change in orientation of the anilide core coupled with the terminal amide at the 4-position may allow for similar interactions with the putative binding site to occur and exert anti-leishmanial activity. Alternatively, if the binding interactions were due to individual effects by substituents rather than a geometric change, the activity of **5.051** may be due the ability of the 6-chloro group to still be able to interact with the binding site, when moved from the 4- to 6-position around the benzamide ring, but requires the amide to be in closer proximity to allow for a potential synergistic interaction with the binding site. Whereas moving the chloro to the 3-position and terminal amide to the 4-position, in compound **5.050**, the chloro may have been too far away or could be blocking the terminal amide to allow for this potential specific interaction to occur. As with compound **5.041** the substituents may have been too far apart to allow for this hypothesized dual interaction, or not allowed for specific orientation of either the anilide core and/or the primary amide to take place and interact with the putative binding site/s. Future studies are

encouraged, where the 6-chloro remains and the terminal amide is moved to the 5-position, *ortho* to the chloro to test out this substituent proximity hypothesis as well as our suggestions around the geometric effect. Loss of the chloro group whilst maintaining the terminal amide at the 4-position was also discovered to be an unfavourable modification, as seen in compound **5.053**. It may be that both the change in orientation of the anilide core via the 6-chloro and the primary amide at the 4-position were required to specific interactions with the putative binding site/s. Due to COVID-19 delays, compound **5.053** has yet to be tested by UNC against *L. donovani*. This was not an issue as the current results reported by Bio21 and IPK seem to clearly demonstrate that this compound is truly inactive and the loss of the chloro substituent observed in both **5.053** and previously in **4.053** seemed to correlate to a loss in activity. Furthermore, it seemed that the terminal amide was only tolerated at the 4-position when the 6-chloro was present, where **5.050** was also inactive.

Table 5.05: Complete biological results of analogues altering both the terminal amide and chloro substituents of the benzamide ring, hit 5.001 outlined in blue



I.D	R ¹	R ²	R ³	HCS intracellular assay against <i>L. donovani</i>				Luciferase/MTT assay	
				Bio21 ^a		IPK ^f		UNC ^{jk}	
				IC ₅₀ (μM)	CC ₅₀ (μM)	IC ₅₀ (μM)	CC ₅₀ (μM)	IC ₅₀ (μM)	CC ₅₀ (μM)
5.001 (hit) ^{bg}	CONH ₂	Cl	H	4.9	>100 ^l	21	>100 ^l	3.2	>50
5.041 ^{ch}	CONH ₂	H	Cl	>100 ^l	>20	>100 ^l	>100 ^l	>50	>50
5.050 ^{dg}	Cl	CONH ₂	H	>100 ^l	>100 ^l	>100 ^l	>100 ^l	>50	>50
5.051 ^{ch}	H	CONH ₂	Cl	5.3	>100 ^l	8.5	>100 ^l	3.4	>50
5.053 ^{ei}	H	CONH ₂	H	>100	>100	>100	>100 ^l	-	-

a= anti *L. donovani* activity and toxicity measured in THP-1 transformed macrophage host cell lines using a top concentration of 100 μM (2x serial dilution 10-point curve). Experiment performed in duplicate wells in one experiment, n=1.

b= control compounds for Bio21 intramacrophage *L. donovani* assay. Miltefosine IC₅₀= 0.50 μM, CC₅₀ = 40 μM, Amphotericin B IC₅₀= 1.1 μM, CC₅₀= 66 μM.

c= control compounds for Bio21 intramacrophage *L. donovani* assay. Average (± standard deviation) from experimental replicates; Miltefosine IC₅₀= 0.83 μM, CC₅₀ >100 μM, Amphotericin B IC₅₀= 0.61 ± 0.079 μM, CC₅₀ > 40 μM.

d= control compounds for Bio21 intramacrophage *L. donovani* assay. Miltefosine IC₅₀= 0.52 μM, CC₅₀ >10 μM, Amphotericin B IC₅₀= 2.6 μM, CC₅₀= 26 μM.

e= control compounds for Bio21 *L. donovani* intramacrophage assay. Average from experimental replicates; Miltefosine IC₅₀ = 0.39 ± 0.55 μM, CC₅₀ > 20 μM, Amphotericin B IC₅₀= 0.12 ± 0.055 μM, CC₅₀ = 6.0 ± 1.8 μM

f= anti *L. donovani* activity and toxicity measured in THP-1 transformed macrophage host cell lines using a top concentration of 100 μM (2x serial dilution 10-point curve)

g= control compounds for IPK intramacrophage *L. donovani* assay. Miltefosine IC₅₀= 1.7 μM, CC₅₀ >100 μM, Amphotericin B IC₅₀= 0.83 μM, CC₅₀ > 100 μM.

h= control compounds for IPK intramacrophage *L. donovani* assay. Miltefosine IC₅₀= 2.3 μM, CC₅₀ >100 μM, Amphotericin B IC₅₀= 0.45 μM, CC₅₀ > 100 μM.

i= control compounds for IPK intramacrophage *L. donovani* assay. Miltefosine IC₅₀= 1.1 μM, CC₅₀ >100 μM, Amphotericin B IC₅₀= 0.26 μM, CC₅₀ > 100 μM.

j= anti *L. donovani* activity measured in THP-1 transformed macrophage host cell lines using luminescent expressing *L. donovani*. Experiment performed in triplicate wells in one experiment, n=1 using a concentration range of 1-50 μM. DMSO was used as sole control against which the percent *L. donovani* viability is calculated

k= host cell toxicity measured in MTT assay with uninfected macrophage host cells. Experiment performed in triplicate wells in one experiment, n=1 using a concentration range of 1-50 μM. DMSO was used as sole control against which the percent cell viability is calculated

l= no inhibition detected within DRC at the top concentration tested (100 μM).

- not tested

No cytotoxicity was observed throughout the benzamide altering investigation, suggesting no selectivity issues or harmful mode of action against the host macrophages. Furthermore, no solubility issues were reported by any of our biological collaborators for this complete set of analogues. This was gratifying to us as there was no need to question whether poor compound activity was due to the inability to solubilize into solution and then permeate the cell. Activity/inactivity of these investigative compounds was simply due to the structural modification. Overall, a somewhat clear SAR story was forming around this scaffold, as we now had a more informed idea of structural modifications to avoid, the key requirements of this system needed to maintain activity, along with a second potential lead compound to further investigate (**5.051**). To further understand whether activity is maintained by a geometric effect, a fuller set of analogues focusing on rearranging the chloro and primary amide substituents to potentially alter compound orientation is required to begin to confirm this hypothesis. Molecular modelling may also be required to further understand the SAR and potential geometric effect around this scaffold.

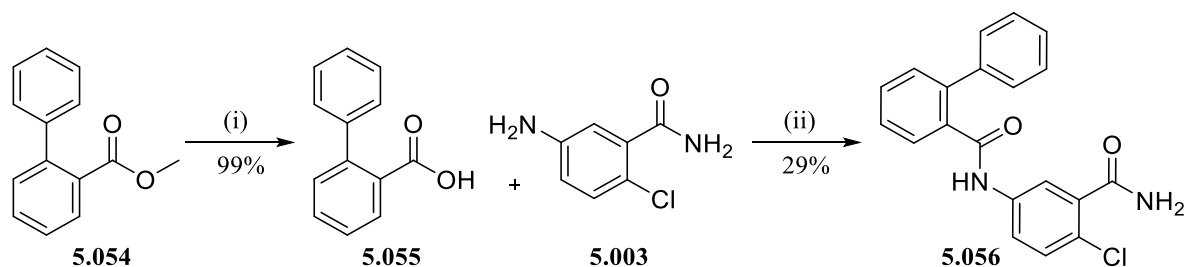
5.04 Targeting the ether linkage

In parallel to studying modifications around the benzamide ring, the ether linkage was also explored in order to further understand the requirements of this chemical space. Previous investigations outlined in Chapter 4 found reversing the methylene and oxygen groups (**4.055**) gave a complete loss in activity. This altered the position of the rotatable bonds, thereby potentially changing the orientation of the adjacent bare phenyl ring and causing a poor fit within the putative binding site/s, where a possible inability to form key interactions may have caused an inability to exert antileishmanial activity. Furthermore, reversing the oxygen and methylene groups may have prevented both groups from forming any specific or distant dependant interactions, such as hydrogen bonding interactions between the oxygen and the binding site. Based on the SAR from **4.055**, the original orientation and more rigid phenoxyethyl is required to maintain activity. Analogue **4.056** focused on removing the methylene group from the chain, causing a rigidity between the aromatic rings and again potentially altering the position of the phenoxy ring. This change to the ether linkage was also found unfavourable, suggesting this change to size and orientation may have also caused a poor fit within the putative binding sites/s. These analogues were previously summarized above in **Figure 5.03**. To confirm whether changes the ether linker could be tolerated or were just overall completely unfavourable to this scaffold, exploration

around this chemical space was continued. Analogues possessing modifications to the ether linker causing changes to hydrogen bonding ability, rigidity, orientation or overall fit within the binding site were devised and discussed below.

Removal of the entire ether linker (both methylene and oxygen atom) was devised using compound **5.056**, in order to confirm if this portion of the chemical space was required at all. This compound would probe whether the more rigid biphenyl system could be tolerated, altering the size and the orientation of the scaffold and consequent fit within the binding site, and measuring whether key interactions could still be formed. Compound **5.056** was obtained following **Scheme 5.10**, where the biphenyl carboxylate (**5.054**) was demethylated under basic conditions to obtain the biphenyl carboxylic acid (**5.055**).⁵⁶ The carboxylic acid was then free for direct amide coupling with 5-amino-2-chlorobenzamide (**5.003**), obtaining the biphenyl carboxamide analogue **5.056**.^{6, 7} The rigidity of the biphenyl functionality may have caused further steric hindrance and poor reactivity of the carboxylic acid, where starting materials were unable to be completely consumed to produce the desired compound. This is the likely cause for the low yield obtained. As mentioned above, this pathway was undertaken before the optimization of the amide bond formation step. As I had obtained sufficient product amount to undergo biological testing, the low yield was not an issue, however if more compound was required, the acid halide conversion pathway, depicted in both **Schemes 5.08-5.09** would be employed over **Scheme 5.10**.

Scheme 5.10 Synthetic route used to obtain analogue **5.056**

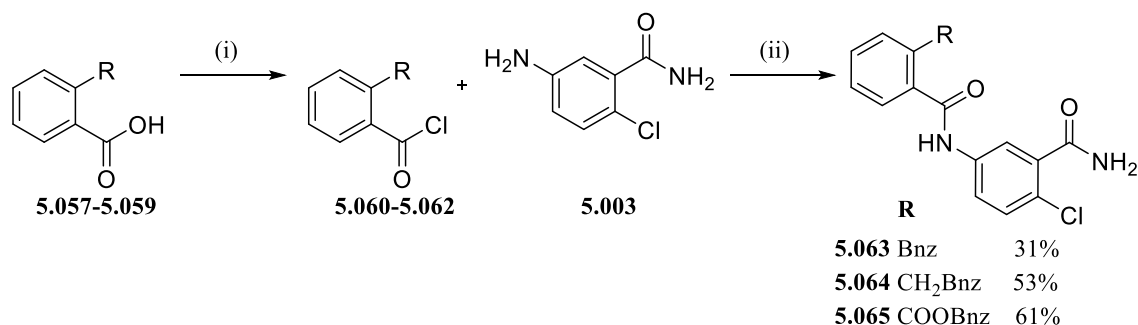


Reaction conditions: i) NaOH 10% aq solution, reflux, ii) DIPEA, EDCI, HOBt, DMF, 50°C

Analogues **5.063** and **5.064** were developed, following **Scheme 5.11**, in order to investigate whether the oxygen atom and any potential hydrogen bond accepting abilities were required to maintain activity. Compound **5.063** removed the oxygen atom leaving only the methylene substituent present, potentially altering the orientation of the adjoining phenyl ring. Compound **5.064** substitutes a second methylene group in place of the oxygen atom, adding to the number of rotatable bonds and flexibility of the system. This would help confirm whether increased flexibility of the carbon-carbon chain would still allow for the same interactions to be made with the putative binding site. The final compound **5.065** (**Scheme 5.11**) synthesized for this series focused on inserting an ester within this chemical space. This would gauge whether further hydrogen bonding interactions could be made with the binding site. The methylene group was also repositioned to be adjacent to the unsubstituted phenyl ring, due to ease of

synthetic access to this analogue. Repositioning the rotatable bond could again potentially alter flexibility and orientation of the system, possibly changing the position of the phenyl ring. The synthetic pathway used to obtain these compounds employed the use of the preferred conversion of the carboxylic acid (**5.057-5.059**) to the acid chloride (**5.060-5.062**) in order to increase reactivity of the hindered acid. This acid chloride was then able to undergo amide bond formation, reacting with the amine **5.003** to provide the desired analogues (**5.063-5.065**) in sufficient yield.^{19, 20, 22-24}

Scheme 5.11 Synthetic route employed to obtain remaining analogues modifying the ether linkage



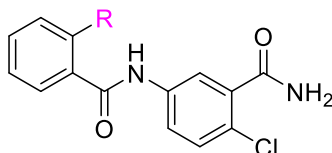
Reaction conditions: i) (COCl)₂, DCM, DMF, 0°C- rt, ii) Et₃N, THF, 0°C- rt

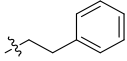
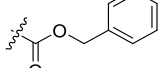
5.05 Biological results of analogues modifying the ether linkage

Biological analysis of analogues exploring the ether linkage are summarized in **Table 5.06**, which includes the hit **5.001** and previous analogues **4.055-4.056** from Chapter 4, for a direct comparison within this series. As discussed, **4.055-4.056** have already been reported as unanimously inactive, where reversing the methylene and oxygen of the ether linkage (**4.055**) as well as removal of the methylene (**4.056**) should be avoided. The changes to flexibility and orientation of the scaffold is unfavourable and does not seem to enable the required interactions with the binding site to exert antileishmanial activity. Removing both the ether linkage completely (both oxygen and methylene groups **5.056**) was also found give a loss of activity.

Further testing by UNC for compound **5.056** has been delayed due to COVID-19, however the current results from Bio21 and IPK along with the surrounding SAR have already demonstrated that this analogue does indeed hold poor antileishmanial potency. Based on analogue **5.063**, only the methylene is required to maintain potency. This analogue suggests the rotational bond is required adjacent to the phenyl ring, whilst the oxygen atom any hydrogen bonding ability are not required at this portion of the chemical space. Removal of this atom causes a slight change in orientation and overall size of the scaffold seems to be a better fit within the binding site, reporting superior potency over the hit **5.001** in two out of three of the bioassays employed. However, it is difficult to truly gauge the level of potency of **5.063** in comparison to the hit **5.001**, even though 2 out of 3 assays report superior activity to hit **5.001**. The majority of IC₅₀ values reported share a closer overall value of >5 μM for compound **5.063**

(Bio21 IC₅₀= 7.4 and IPK IC₅₀= 11 µM, and values are within <5 µM of each other). Whilst the original hit **5.001** reported 2 out of 3 IC₅₀ values at <5 µM (Bio21 IC₅₀= 4.9, UNC IC₅₀=3.2, values are within <5 µM of each other). Since the biological assays employed are all equal, where one is not superior to another, it is difficult to judge true superior potency. At this stage, we can simply conclude that both **5.001** and **5.063** both hold true antileishmanial activity and will both be pursued as leads for future SAR studies. The fit and flexibility of this chemical space seems highly specific, as an increase in the number of rotatable bonds and flexibility was unfavourable, observed with analogue **5.064**, substituting the oxygen atom with another methylene group. This carbon-carbon chain gave a unanimous loss of activity within all bioassays employed testing our investigative compounds against intramacrophage *L. donovani*. It seems only one methylene group is needed as the linker between aromatic rings, where increasing flexibility or rigidity is unfavourable, and seems to cause poor fit within the binding site. Finally, inserting an ester into the chain was also found unfavourable. No extra hydrogen bonding interactions were able to be made in this arrangement. This increase in steric hindrance around this portion of chemical space, again potentially altering the overall size, orientation and fit of the scaffold within the binding site seems to be highly unfavourable. Adding carbonyl groups to this portion of the chemical space should generally be avoided. Exploring modifications around the original ether linkage was a success, as we have achieved a better understanding of the requirements around this chemical space. The methylene alone (**5.063**) and methylene plus oxygen (**5.001**) in the original arrangement are the only functionalities tolerated at this stage. Both compounds would be considered leads for future SAR studies.



5.064^{df}		>100 _m	>100 ^m	>100	>100 ^m	>50	>50
5.065^{dg}		>100	>100	>100 ^m	>100 ^m	>50	>50

a= anti *L. donovani* activity and toxicity measured in THP-1 transformed macrophage host cell lines using a top concentration of 100 μ M (2x serial dilution 10-point curve). Experiment performed in duplicate wells in one experiment, n=1.

b= control compounds for Bio21 intramacrophage *L. donovani* assay. Average (\pm standard deviation) from experimental replicates; Miltefosine IC₅₀= 0.50 \pm 0.0077 μ M, CC₅₀> 40 μ M, Amphotericin B IC₅₀= 1.3 \pm 0.32 μ M, CC₅₀> 60 μ M.

c=control compounds for Bio21 *L. donovani* intramacrophage assay. Average from experimental replicates; Miltefosine IC₅₀ = 0.39 \pm 0.55 μ M, CC₅₀ > 20 μ M, Amphotericin B IC₅₀= 0.12 \pm 0.055 μ M, CC₅₀ = 6.0 \pm 1.8 μ M

d= control compounds for Bio21 intramacrophage *L. donovani* assay. Average (\pm standard deviation) from experimental replicates; Miltefosine IC₅₀= 0.83 μ M, CC₅₀ >100 μ M, Amphotericin B IC₅₀= 0.61 \pm 0.079 μ M, CC₅₀ > 40 μ M.

e= anti *L. donovani* activity and toxicity measured in THP-1 transformed macrophage host cell lines using a top concentration of 100 μ M (2x serial dilution 10-point curve)

f= control compounds for IPK intramacrophage *L. donovani* assay. Miltefosine IC₅₀= 1.7 μ M, CC₅₀ >100 μ M, Amphotericin B IC₅₀= 0.83 μ M, CC₅₀> 100 μ M.

g= control compounds for IPK intramacrophage *L. donovani* assay. Miltefosine IC₅₀= 2.3 μ M, CC₅₀ >100 μ M, Amphotericin B IC₅₀= 0.45 μ M, CC₅₀ > 100 μ M.

h= control compounds for IPK intramacrophage *L. donovani* assay. Miltefosine IC₅₀= 1.1 μ M, CC₅₀ >100 μ M, Amphotericin B IC₅₀= 0.26 μ M, CC₅₀ > 100 μ M.

j= anti *L. donovani* activity measured in THP-1 transformed macrophage host cell lines using luminescent expressing *L. donovani*. Experiment performed in triplicate wells in one experiment, n=1 using a concentration range of 1-50 μ M. DMSO was used as sole control against which the percent *L. donovani* viability is calculated

k= host cell toxicity measured in MTT assay with uninfected macrophage host cells. Experiment performed in triplicate wells in one experiment, n=1 using a concentration range of 1-50 μ M. DMSO was used as sole control against which the percent cell viability is calculated

l= anti *L. donovani* activity and toxicity measured in THP-1 transformed macrophage host cell lines using a one-point concentration (50 μ M) to assess any form of antileishmanial activity. Experiment performed in duplicate wells in one experiment, n=1.

m= no inhibition detected within DRC at the top concentration tested (100 μ M).

- not tested

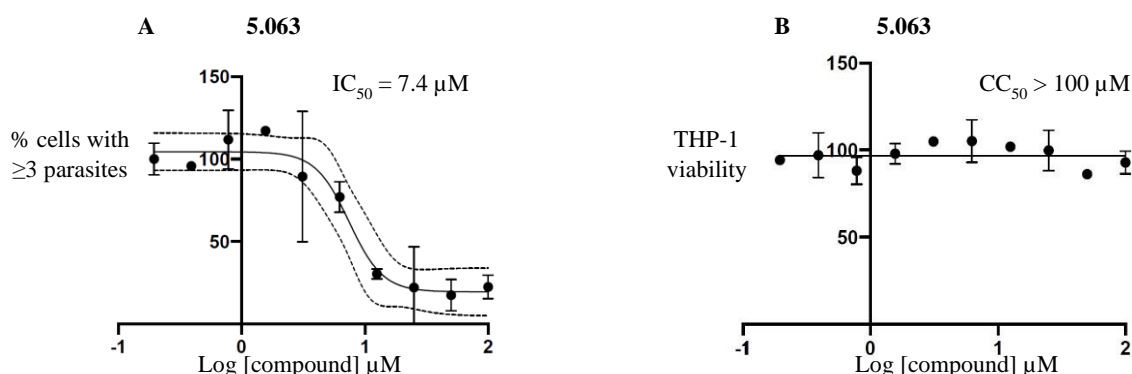


Figure 5.07a-b: Dose response curves of 5.063 reported by Bio21, a) measuring compound concentration (x axis) against % of infection within host macrophages (y axis) to determine the antileishmanial activity (IC₅₀) of 5.063, b) measuring compound concentration (x axis) against the viability of the THP-1 transformed macrophages (y axis) to determine the cytotoxicity against the host cell (CC₅₀)

The dose response curves of 5.063 reported by Bio21 are depicted in **Figure 5.07a-b**, which serve visual demonstration of the activity and selectivity of 5.063 against *L. donovani* within THP-1 macrophages. These curves are used as representatives to depict the consistent potency of 5.063 reported by each of our collaborators. **Figure 5.07a** was used to report the IC₅₀ against *L. donovani* and depicts the reduction of parasite burden, where an increase in compound concentration correlated to a decrease in the percentage of infection within viable host macrophage cells. A host cell is considered infected when ≥ 3 parasites per host macrophage are detected. **Figure 5.07b** was used to determine the CC₅₀ and

cytotoxicity against the THP-1 transformed host macrophages. From this graph it is clear that **5.063** exerted activity against the parasite only, as no cytotoxicity against the host macrophage was observed.

5.06 Additions to the phenoxy ring

The final study around the *N*-(3-carbamoylphenyl)-2-(phoxymethyl)benzamide compound class within this chapter, focused on the addition of various small functional groups (Cl, F, CN, Me, OMe) around the phoxymethyl ring. This would probe whether any stronger interactions could be made with the putative binding site/s or if these additions could push the overall compound out of its original fit within the putative binding pocket. The groups chosen would each possess differing electronics (σ), sterics (Molar refractivity/ MR), hydrophobicity (Π) and hydrogen bonding ability, gauging not only if extra interactions could be made, but also what sorts of interactions were preferred. **Table 5.07**, a derivative of **Table 1.06** listed in Chapter 1, summarizes the effects each of the substituents chosen for this final series to the phenyl ring, and can be directly compared to the H atom (unsubstituted ring). The chloro group aims to probe the effect on the phenyl ring and overall scaffold when increased hydrophobicity (positive Π value), electron withdrawing ability (positive σ value) as well as increase atom size (increased MR) is introduced around the ring. The electronegative fluoro aims to explore a change in electronics and increased hydrogen bonding ability whilst keeping size and hydrophobicity largely unchanged. The cyano group also aims to probe whether a stronger increase in electron withdrawing ability was tolerated around the ring, along with increasing sterics, hydrogen bonding ability though allowing for increased hydrophilicity (negative Π value). The methyl group on the other hand would be used to gauge whether electron donating ability (negative σ value) was more favourable for this system, as well as increasing size and hydrophobicity. Finally, the methoxy group would introduce play a more neutral role in relation to hydrophobicity, though increase sterics, hydrogen bond accepting ability and alter electronics, depending on its position (*ortho/para* directing, donating, *meta* directing, withdrawing).

Table 5.07: Parameters used to probe steric, electronic, and hydrophobic properties of some key aryl substituents used for this study^{57, 58}

Substituent	Π	HBA	HBD	MR	Electronics	
					σ_m	σ_p
H	0	0	0	1.03	0	0
Cl	0.71	0	0	6.03	0.37	0.23
F	0.14	1	0	0.92	0.34	0.06
CN	-0.57	1	0	6.33	0.56	0.66
CH ₃	0.56	0	0	5.65	-0.07	-0.17
OCH ₃	-0.02	1	0	7.87	0.12	-0.27

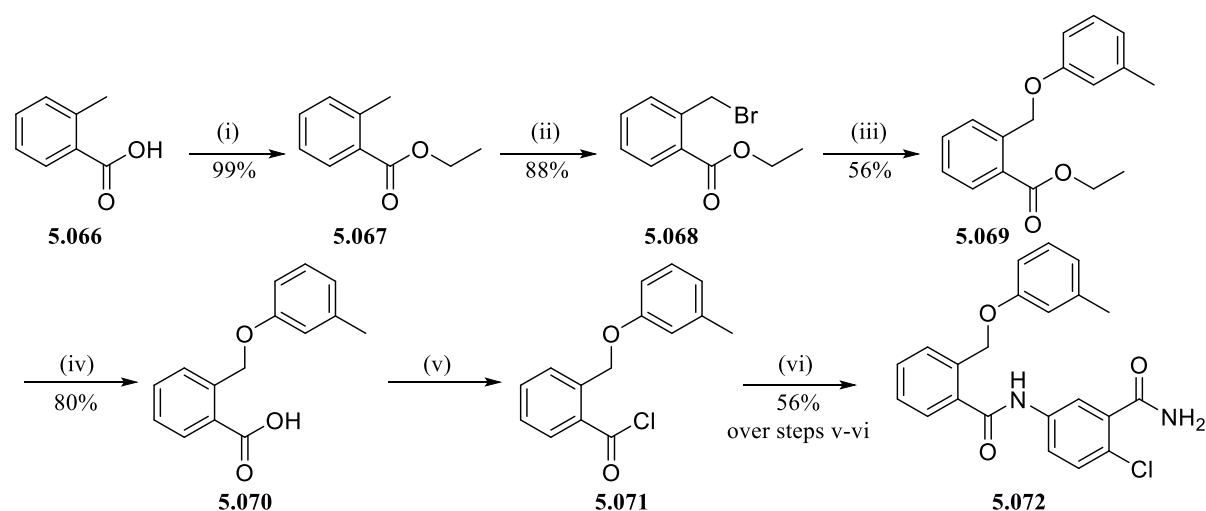
It should be noted that the all changes to the molecular refractivity are still quite small overall, larger groups such as a phenyl ring would drastically increase steric bulk in comparison. For a primary

investigation, smaller functional groups were considered, avoiding bulkier, more intrusive functionalities, potentially more likely to cause poor fit within the putative binding site/s. Once a better understanding of which groups were tolerated, future work may build up at adding larger functionalities within this chemical space. Each group would be added individually to the *ortho*, *meta* and *para* positions of the phenoxyethyl ring to understand whether these properties were tolerated, and where they are best tolerated.

5.06.1 Synthesis for phenoxyethyl modified analogues

Various synthetic pathways were devised to acquire this list series of analogues, starting with trialling various conditions within the synthetic route described in **Scheme 5.12**.

Scheme 5.12: Synthetic pathway to obtain analogue **5.072**



Reaction conditions: i) H_2SO_4 , EtOH, reflux ii) NBS, AIBN, ACN, 90°C , 15 min, microwave irradiation, iii) *m*-cresol, K_2CO_3 , KI, DMF, r/t, iv) NaOH, H_2O , EtOH, reflux, v) $(\text{COCl})_2$, DMF, DCM, 0°C - rt, vi) 5-amino-2-chlorobenzamide (**5.003**), Et_3N , THF, 0°C - rt

This pathway began with the esterification of the readily available *o*-toluic acid (**5.066**).⁵⁹ This was followed by allylic bromination using the Wohl-Ziegler reaction, employing *N*-bromosuccinimide (NBS) and AIBN as the radical initiator under microwave irradiation for 15 min to push the reaction forward, achieving the brominated intermediate **5.068** quickly (within 15 minutes) and efficiently.⁶⁰

Table 5.08 Summary of conditions trialled for the allylic bromination step (ii) of Scheme 5.12

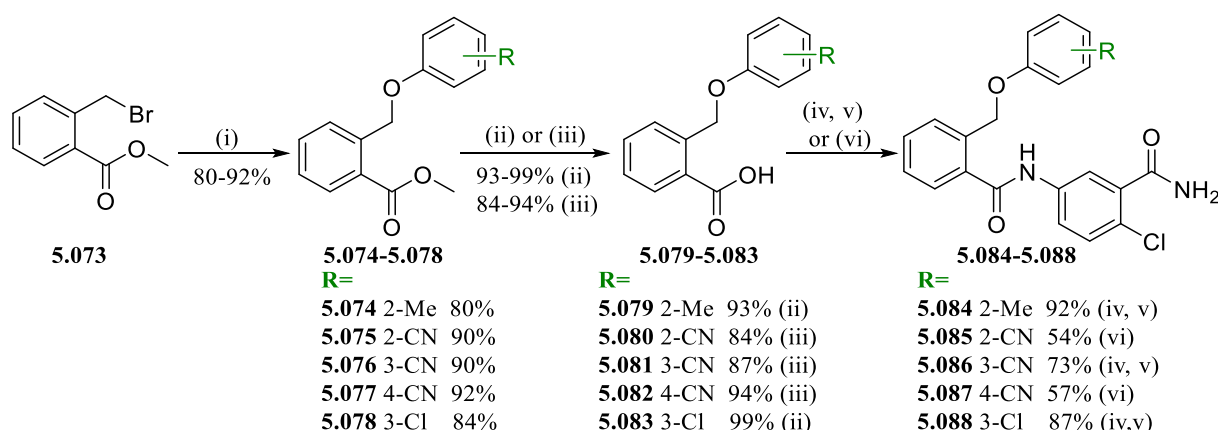
Trial #	Conditions ⁶⁰⁻⁶²	Outcome
1	NBS, AIBN, ACN, 90°C , 15 min, microwave irradiation ⁶⁰	Reaction complete within 15 minutes confirmed with LCMS and ^1H NMR analysis. Reaction conditions were favoured, due to success with fast reaction speed, and decreased toxicity compared to Trials #2-3.
2	NBS, benzoyl peroxide, CCl_4 , 80°C 4h, cooled to rt over 12h ⁶²	Reaction completion was achieved, compound 5.068 was formed after 12 h, confirmed by LCMS analysis. Despite

3	NBS, benzoyl peroxide, CCl ₄ , 0°C- reflux, 3.5 h, cooled to rt over 12 h ⁶¹	reaction success, conditions were not favoured due to increased toxicity and other hazards due to solvent and radical initiator, as well as slower reaction time. Conditions were abandoned in favour of Trial #1.
----------	----------------------------------------------------------------------------------------------------	--------------------------------------------------------------------------------------------------------------------------------------------------------------------------------------------------------------------

Summarized in **Table 5.08**, more traditional conditions of the Wohl-Ziegler reaction were also trialled in parallel, employing benzoyl peroxide as the radical initiator and carbon tetrachloride (CCl₄) as the non-polar inert solvent (Trials #2-3). Following these conditions, the reaction was able to successfully meet fruition and intermediate **5.068** was successfully obtained, indicated via LCMS analysis.⁶¹⁻⁶⁴ Despite the success of Trials #2-3, the reagents required were unfavourable for constant use or reaction scale up. The use of the solvent CCl₄ increased risk of toxicity and was also not easily available. Additionally, there was an increased risk of fire or explosion associated with benzoyl peroxide over AIBN. Finally, the longer reaction time required made these reaction conditions less favourable for use.^{65, 66} Of course, precautions were taken when using these chemicals, such as keeping temperatures well under the melting point of benzoyl peroxide to avoid explosive decomposition. Overall, the more efficient and less toxic reaction conditions of Trial #1 were still preferable and would be used for any further allylic bromination reactions for this system.

The following step in **Scheme 5.12** involved the brominated aromatic ester (**5.068**), which underwent Williamson etherification under basic conditions, where the primary alkyl bromide underwent S_N2 nucleophilic substitution with the selected deprotonated phenol to successfully form the phenoxymethyl intermediate (**5.069**).⁶⁷⁻⁷⁰ The *m*-cresol reagent was first used to trial this scheme, simply due to availability. Subsequent deprotection of the ethyl ester (**5.069**) occurred under basic conditions to achieve the free carboxylic acid (**5.070**) which was then converted into the acid chloride (**5.071**) to increase reactivity for the final nucleophilic substitution with the amino benzamide (**5.003**) to obtain the desired analogue **5.072** in moderate yield.^{19, 20, 22-24, 56} This synthetic scheme was further refined to decrease the number of steps involved and conditions were further optimized to improve analogue output speed. Attempts at a more refined pathway is depicted in **Scheme 5.13**.

Scheme 5.13: Synthetic route used to obtain analogues 5.084-5.088



Reaction conditions: i) substituted phenol, K_2CO_3 , KI, DMF, r/t or substituted phenol, K_2CO_3 , KI, ACN, $70^\circ C$, ii) NaOH, H_2O , EtOH, reflux or iii) LiOH, H_2O , MeOH, THF, rt, iv) $(COCl)_2$, DMF, DCM, $0^\circ C$ - rt, v) 5-amino-2-chlorobenzamide (**5.003**), Et_3N , THF, $0^\circ C$ - rt, or vi) 5-amino-2-chlorobenzamide, HOBt, EDCI, DMF, $50^\circ C$

Scheme 5.13 began with the commercially available compound **5.073**, which removed the need to perform the esterification and bromination steps of **Scheme 5.12**. Starting material **5.073** underwent S_N2 nucleophilic substitution (Williamson etherification) with the various substituted phenols to form the phenoxymethylbenzoates (**5.074-5.078**).⁶⁷⁻⁶⁹ Alternative conditions suggested by the literature were also trialled in parallel, summarized in **Table 5.09**.^{19, 70-73} Modifications to the nucleophilic reaction conditions included altering the temperature, aprotic solvent and base used. Only aprotic solvents were considered, since S_N2 reactions favour this type of solvent.²⁵

Table 5.09: Trial conditions and outcomes for S_N2 nucleophilic substitution of step i, Scheme 5.13

R	Trial	Conditions ^{19, 67, 70-73}	Outcome
2-Me	#1	<i>o</i> -cresol (1 eq), K_2CO_3 (5 eq), KI (0.1 eq), DMF, rt	Reaction completed within 12h, presence of desired compound 5.074 indicated by TLC/LCMS analysis, confirmed by 1H NMR analysis. Did not require further purification after filtration steps. High product yield obtained for Trials #1 and #2, 78% and 80% respectively.
	#2	<i>o</i> -cresol (1 eq), K_2CO_3 (5eq), KI (0.1eq), ACN $70^\circ C$	
	#3	<i>o</i> -cresol (1 eq), K_2CO_3 (5 eq), KI (0.1 eq), acetone, reflux	Reaction was completed within 24h, indicated by TLC/LCMS analysis. Extra time was required for the majority of 5.074 to form. Purification techniques were required after filtration steps. Yield obtained was 70%.
2-CN	#1	2-cyanophenol (1 eq), K_2CO_3 (5 eq), KI (0.1 eq) DMF, rt	All trials saw reaction completion within 12h, presence of desired compound 5.075 indicated by TLC/LCMS analysis, confirmed by 1H NMR analysis. Did not require further purification after filtration steps. High product yield obtained for all trials: Trial #1: 87%, Trial #2: 90%, Trial #3: 85%
	#2	2-cyanophenol (1 eq), K_2CO_3 (5 eq), KI (0.1 eq) ACN $70^\circ C$	
	#3	2-cyanophenol (1 eq), Cs_2CO_3 (2 eq), acetone, reflux	

3-CN	#1	3-cyanophenol (1 eq), K ₂ CO ₃ (5 eq), KI (0.1 eq) DMF, rt	Reaction completed within 12h, presence of desired compound 5.076 indicated by TLC/LCMS analysis, confirmed by ¹ H NMR analysis. Did not require further purification after filtration steps. High product yield obtained in Trials #1 and #2: 85 and 90% respectively.
	#2	3-cyanophenol (1 eq), K ₂ CO ₃ (5 eq), KI (0.1 eq) ACN 70°C	
	#3	3- cyanophenol (1 eq), Cs ₂ CO ₃ (2 eq), acetone, reflux	The majority of 5.076 was formed within 12h, indicated by TLC/LCMS analysis. Further purification was required after filtration steps. Product yield obtained was 70%
4-CN	#1	4-cyanophenol (1 eq), K ₂ CO ₃ (5eq), KI (0.1 eq), DMF, rt	All trials saw reaction completion within 12h, presence of desired compound 5.077 indicated by TLC/LCMS analysis, confirmed by ¹ H NMR analysis. Reaction occurred cleanly, observed with LCMS/ ¹ H NMR and did not require further purification after filtration steps. High product yield obtained for all trials, Trial #1: 92%, Trial #2: 88%, Trial #3: 86%
	#2	4-cyanophenol (1 eq), K ₂ CO ₃ (5eq), KI (0.1 eq), ACN 70°C	
	#3	4-cyanophenol (1 eq), Cs ₂ CO ₃ (2 eq), acetone, reflux	
3-Cl	#1	3-chlorophenol (1 eq), K ₂ CO ₃ (5 eq), KI (0.1 eq) DMF, rt	All trials saw reaction completion within 12h, presence of desired compound 5.078 indicated by TLC/LCMS analysis, confirmed by ¹ H NMR analysis. Reaction proceeded cleanly, observed with LCMS/ ¹ H NMR and did not require further purification after filtration steps. High product yield obtained for all trials, Trial #1: 80%, Trial #2: 84%, Trial #3: 76%
	#2	3-chlorophenol (1 eq), K ₂ CO ₃ (5 eq), KI (0.1 eq) ACN 70°C	
	#3	3-chlorophenol (1 eq), Cs ₂ CO ₃ (2 eq), acetone, reflux	

Despite changes to the solvent and temperature (Trials #2 in particular) or changes to the base (Trials #3 for R=CN, Cl), the outcome and product yield remained quite similar, as summarized in **Table 5.09**. Most of trials proceeded quite cleanly and efficiency, where all the starting reagents were used up within the reaction and no side products were visible by ¹H NMR analysis. Further purification techniques such as crystallization or column chromatography were also not required for the majority of cases. The product yield generally remained close between the trials, where conditions of #1 and #2 with all substituted phenols (R= 2-Me, 2/3/4-CN, 3-Cl) were found the most favourable overall. Either of these conditions was encouraged for further use, leaning towards conditions of Trials #2, which seemed to perform best overall, though with only marginal improvement. Despite this, this was a good activity to undertake, as I now had several immediate “backup” options, if certain compounds gave inactivity or poor yield for this step. The next step of **Scheme 5.13** involved the demethylation of the various phenoxyethylbenzoates (**5.074-5.078**). Two experimental conditions suggested by the literature were trialled in parallel to determine which gave superior yields and should be used for later compounds following **Scheme 5.13** or a similar pathway.^{19, 56, 74} Benson *et al.* described mild basic conditions to demethylate cyano-substituted phenoxyethyl benzoate compounds very close in structure to **5.075-5.077**. Therefore these suggested conditions were trialled for our cyano-compounds **5.075-5.077**, using lithium hydroxide (LiOH) (5 eq) in a mixture of protic and aprotic solvents (water, methanol and

THF).¹⁹ These conditions were also found effective, allowing for efficient deprotection, providing the desired carboxylic acids **5.080-5.082** in high yield (84-94%). Compounds **5.079** (*ortho*-methyl) and **5.083** (*meta*-chloro) were acquired in high yield (92-99% respectively) using NaOH (10% in aq solution) as the base under reflux conditions.⁵⁶ Both conditions were found effective for deesterification, with the harsher conditions (NaOH aq, reflux) slightly more favourable overall. These conditions would be used for future demethylation steps following **Scheme 5.13**, or a similar pathway. However, trialling both methods was a positive exercise, as I had found a mild alternative for future compounds that may be susceptible to heat.

In hindsight, this exercise also could have been more cohesive by trialling both conditions for all benzoates used to confirm superiority, as done in the previous step. Though, since all desired carboxylic acids were obtained in high yield, this was not a large issue and it was decided to move on to the next step, focusing on obtaining the final analogues for biological testing, using the remaining time on this project efficiently.

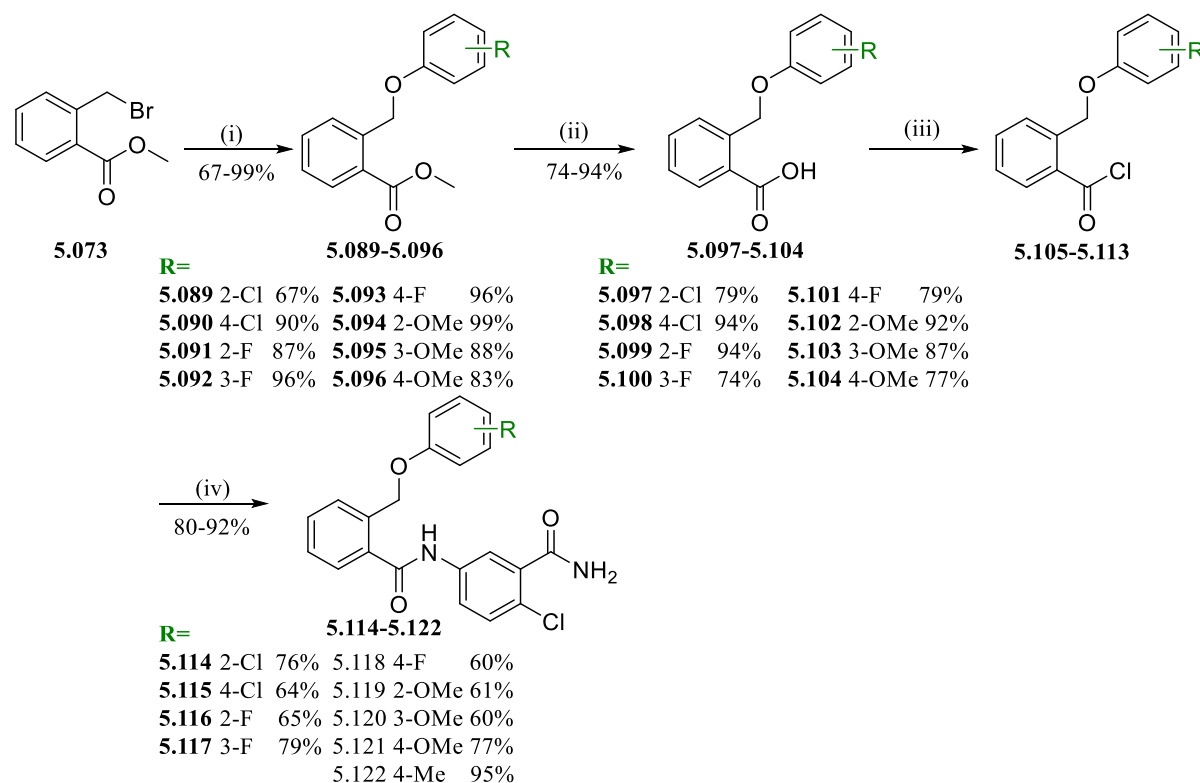
To obtain analogues **5.085** and **5.087** (*ortho* and *para*-cyano respectively), the carboxylic acids (**5.080**, **5.082**) were used directly under amide coupling conditions with coupling reagents (EDCI, HOBt) and reacted with the amino benzamide (**5.003**) to obtain the desired analogues in moderate yield respectively (54- 57%).^{6, 7} These analogues along with **5.072** were also synthesized during the time period where the amide formation steps were being altered and optimized (Sections **5.02**), hence the difference in methods. At this time, analogues **5.085** and **5.087** employed the direct amide coupling conditions listed in step vi of **Scheme 5.13**, to confirm whether these conditions were at all preferable since these analogues possessed modifications distant to the reacting carboxylic acid and amine groups and may not further impact coupling ability. The formation of both analogues was observed by LCMS and TLC analysis to reach reaction completion without the low reactivity issues that were observed in the previous analogues following these conditions (**5.018**, **5.053**). The desired analogues **5.085** and **5.087** were formed, where most of the starting materials had been consumed in favour of the amide bond formation. In the case of the formation of compound **5.085**, some of the amine **5.003** still remained when the reaction was stopped. If this reaction was repeated following step v, a simple increase of benzoic acid **5.080** reagent equivalency would have improved the reaction yield by allowing for further consumption of the amine **5.003**. The later analogues **5.084**, **5.086** and **5.088** were synthesized after the efforts around optimising the amide formation step were made. Therefore, they all involve the initial conversion of the carboxylic acid (**5.079**, **5.081**, **5.083**) to the acid chloride intermediate (step vi) using oxalyl chloride, followed by direct use in the nucleophilic substitution (step v) with the amino benzamide (**5.003**).^{19, 20, 22-24} The desired analogues were obtained in improved yield (73- 87%). In comparison to the analogues **5.085**, **5.087** formed using step vi, the formation of **5.079**, **5.081**, **5.083** all occurred more efficiently, requiring less reaction time and proceeded more cleanly and selectively,

allowing for ease of purification and an overall increase in product yield, further endorsing the optimized amide bond formation conditions of step vi.

5.06.2 Refined synthetic pathway for phoxymethyl modified analogues

After further refinement around reaction conditions of **Schemes 5.12-5.13**, a more streamlined approach to producing substituted phoxymethyl analogues was achieved. The final synthetic pathway is depicted in **Scheme 5.14**, a derivative of the previous schemes, following a similar routine with refined conditions. The final selection of substituted phenol groups underwent nucleophilic substitution (Williamson etherification) with the bromomethylbenzoate (**5.073**).^{67-69, 71, 72} The newly formed substituted phoxymethylbenzoate intermediates (**5.089-5.096**) underwent subsequent demethylation to form the benzoic acids (**5.097-5.104**).⁵⁶ The benzoic acid was then free to be transformed into the acyl chloride (**5.105-5.113**) via oxalyl chloride as the chlorinating agent.^{19, 20} As with the previous use of the acid halide/amide formation step, the more reactive acyl chloride underwent amide bond formation with the amine **5.003**, obtaining the desired amide analogues (**5.114-5.122**).²²⁻²⁵ The 2-((*p*-tolylloxy)methyl)benzoic acid was readily available and thus only steps iii-iv were required in the formation of analogue **5.122**, which was obtained in high yield. Several example ¹H and ¹³C NMR spectra of analogues from this chapter have been included in the Experimental section.

Scheme 5.14: Refined synthetic pathway to obtain the substituted phoxymethyl analogues 5.114-5.122



Reaction conditions: i) substituted phenol, K₂CO₃, KI, DMF, r/t or ACN, 70°C, ii) NaOH, H₂O, EtOH, reflux, iii) (COCl)₂, DMF, DCM, 0°C- rt, iv) 5-amino-2-chlorobenzamide (**5.003**), Et₃N, THF, 0°C- rt

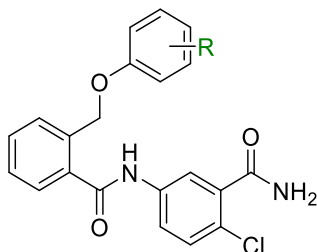
5.07 Biological results of analogues modifying the phenoxy ring

The final series of analogues underwent biological assessment against *L. donovani* and are listed in **Table 5.10**, with hit **5.001** as a comparison. For ease of assessment, compounds were ordered by function group addition over assigned compound I.D number for an easier interpretation of the SAR. Due COVID-19 related delays, not all compounds were able to be assessed by UNC. Overall, most of substitutions positioned the *meta* and *para* positions were found to be unfavourable in all biological assays employed. This suggested adding functional groups to these positions did not allow any extra favourable interactions with the target and may have also caused poor fit within the putative binding site, regardless of changes to sterics, electronics, hydrophobicity and hydrogen bonding ability to the phenoxymethyl chemical space. This excludes two potential exceptions, **5.115** (*para*-chloro) and **5.117** (*meta*-fluoro) which were observed to exert moderate antileishmanial activity within the Bio21 intramacrophage assay only. Even though **5.115** and **5.117** were not at all an improvement to the original unsubstituted phenoxymethyl hit **5.001**, a complete loss of activity was not reported within this assay screen, suggesting the larger, electron withdrawing chloro to be merely tolerated at the *para*-position only, and the smaller, increasingly electronegative fluoro group to be tolerated at the *meta*-position.

Due to COVID-19 related delays, these compounds yet to undergo antileishmanial and cytotoxic assessment using the luciferase and MTT assays performed by UNC. Therefore, a decision has not been made as to whether true antileishmanial activity does exist for these compounds, as I cannot yet exercise our “two out of three” guidelines. It may be that these analogues do possess some antileishmanial activity, but at this stage no IC₅₀ values close or superior to hit **5.001** have been reported, regardless of the pending result from UNC. Based on the current results, **5.115** and **5.117** would not be considered as leads or compounds of interest. Analogue **5.085** (*ortho*-cyano), as with the rest of the cyano substitutions (**5.086**, **5.087**) was reported to give an overall loss of activity, suggesting a strongly electron withdrawing, more hydrophilic group was not tolerated within this chemical space. The *ortho*-chloro (**5.114**) was also found unfavourable in 2 out of 3 of the bioassays employed. Though potency was observed within the UNC luciferase assay, this was not reflected by either HCS based experiments. Based on this, it would seem the chloro group, which possessed similar molecular refractivity to the cyano groups and some electron withdrawing ability as an *ortho* director, was unfavourable around the ring. However, sterics could not be completely to blame for loss of activity. The similar sized methyl (**5.084**) and methoxy groups (**5.119**) at the *ortho* position, with electron donating ability at the *ortho/para* position were able to exert antiparasitic activity, more so with **5.119**, which gave superior potency in comparison to the lead **5.001** in 2 out of 3 assays, despite the pending UNC assessment. Additionally, no cytotoxicity was observed against the host cell, making **5.119** an ideal new lead compound. The increased ability for hydrogen bonding interaction, without strong ring-deactivating at the *ortho* position may be the ideal properties for this position. Analogue **5.116** (*ortho*-fluoro) was also

found to be highly potent at the same position within the Bio21 assay only. Though they do not share similar sterics, the decreased electron withdrawing ability (weakly deactivating) at the *ortho* position and increase hydrogen bonding ability may also be the cause for the antileishmanial activity observed within this assay. However, this same high level of potency was not mirrored within the IPK assay, though since a complete loss of activity was not observed with this assay, it does suggest that this analogue may be least tolerated within the putative binding site/s. Assessment with the pending UNC assay is required to make a final decision on the true level of antileishmanial activity of analogue **5.116**, as well as confirm whether hydrogen bonding ability and/or more electron donating, or neutral group is required at the *ortho* position. From these substitutions, a clearer SAR pathway has been unearthed, where it seems substitution at the *para* and *meta* positions are generally unfavourable and should be avoided. Substitutions at the *ortho* position using sterically bulkier, deactivating groups are also not tolerated (chloro, cyano). Electron donating groups at this position (methyl, methoxy) were found to be tolerated. Furthermore, it seems functionalities with hydrogen bonding ability seem to be favoured at this position (methoxy, fluoro). This suggests an extra hydrogen bonding interaction with the binding site may occur at this position. Overall, not only has an SAR pathway been identified, but an additional new lead (**5.119**, *ortho*-methoxy) has been identified for further SAR investigation, along with another compound of interest (**5.116**, *ortho*-fluoro), with even greater potency, though overall activity confirmation is still pending.

Table 5.10 Biological results of analogues with phenoxyethyl modifications, hit 5.001 outlined in blue



I.D	R	HCS intracellular assay against <i>L. donovani</i>				Luciferase /MTT assay	
		Bio21 ^a		IPK ^e		UNC ^{ij}	
		IC ₅₀ (μM)	CC ₅₀ (μM)	IC ₅₀ (μM)	CC ₅₀ (μM)	IC ₅₀ (μM)	CC ₅₀ (μM)
5.001 (hit)^{bf}	H	4.9	>100 ^k	21	>100 ^k	3.2	>50
5.114^{cg}	2-Cl	>100 ^k	>100 ^k	>100	>100	6.5	>50
5.088^{cg}	3-Cl	>100 ^k	>100 ^k	>100	>100 ^k	>50	>50
5.115^{cg}	4-Cl	15	>100	92	>100 ^k	>50	>50
5.116^{ch}	2-F	0.57	>100 ^k	35	>100 ^k	-	-
5.117^{cg}	3-F	12	>100 ^k	62	>100 ^k	-	-
5.118^{cg}	4-F	>50	>100 ^k	>100	>100 ^k	-	-
5.085^{cg}	2-CN	>100 ^k	>100 ^k	>100	>100 ^k	-	-
5.086^{cg}	3-CN	>100 ^k	>100 ^k	>100	>100 ^k	-	-
5.087^{cg}	4-CN	>100 ^k	>100 ^k	>100	>100 ^k	-	-
5.084^{cg}	2-Me	15	>100 ^k	15	>100 ^k	5.6	>50
5.072^{cf}	3-Me	>50	>100	>100	>100 ^k	22	>50
5.122^{cg}	4-Me	>100 ^k	>100 ^k	>100	>100	-	-

5.119^{dg}	2-OMe	3.8	>100 ^k	7.2	>100 ^k	-	-
5.120^{cg}	3-OMe	>100 ^{k§}	>100 ^{k§}	>100 ^k	>100 ^k	-	-
5.121^{cg}	4-OMe	>100 ^{k§}	>100 [§]	>100	>100	-	-

a= anti *L. donovani* activity and toxicity measured in THP-1 transformed macrophage host cell lines using a top concentration of 100 µM (2x serial dilution 10-point curve). Experiment performed in duplicate wells in one experiment, n=1.

b= control compounds for Bio21 intramacrophage *L. donovani* assay. Miltefosine IC₅₀= 0.50 µM, CC₅₀ = 40 µM, Amphotericin B IC₅₀= 0.72 µM, CC₅₀>100 µM.

c= control compounds for Bio21 intramacrophage *L. donovani* assay. Miltefosine IC₅₀= 0.53 µM, CC₅₀ = 33 µM, Amphotericin B IC₅₀= 1.1 µM, CC₅₀= 66 µM.

d= control compounds for Bio21 intramacrophage *L. donovani* assay. Average (± standard deviation) from experimental replicates; Miltefosine IC₅₀= 0.83 µM, CC₅₀ >100 µM, Amphotericin B IC₅₀= 0.61 ± 0.079 µM, CC₅₀ > 40 µM.

e= anti *L. donovani* activity and toxicity measured in THP-1 transformed macrophage host cell lines using a top concentration of 100 µM (2x serial dilution 10-point curve)

f= control compounds for IPK intramacrophage *L. donovani* assay. Miltefosine IC₅₀= 1.7 µM, CC₅₀ >100 µM, Amphotericin B IC₅₀= 0.83 µM, CC₅₀ > 100 µM.

g= control compounds for IPK intramacrophage *L. donovani* assay. Miltefosine IC₅₀= 2.3 µM, CC₅₀ >100 µM, Amphotericin B IC₅₀= 0.45 µM, CC₅₀ > 100 µM.

h= control compounds for IPK intramacrophage *L. donovani* assay. Miltefosine IC₅₀= 1.1 µM, CC₅₀ >100 µM, Amphotericin B IC₅₀= 0.26 µM, CC₅₀ > 100 µM.

i= anti *L. donovani* activity measured in THP-1 transformed macrophage host cell lines using luminescent expressing *L. donovani*. Experiment performed in triplicate wells in one experiment, n=1 using a concentration range of 1-50 µM. DMSO was used as sole control against which the percent *L. donovani* viability is calculated

j= host cell toxicity measured in MTT assay with uninfected macrophage host cells. Experiment performed in triplicate wells in one experiment, n=1 using a concentration range of 1-50 µM. DMSO was used as sole control against which the percent cell viability is calculated

k= no inhibition detected within DRC at the top concentration tested (100 µM).

- not tested

§= poor solubility observed in media up to 800 µM during Bio21 assay

Analogues **5.120-5.121** were the only compounds from this series which displayed poor solubility, reported within the Bio21 HCS assay only. The poor solubility observed may have barred complete permeability within host cells, contributing to the inactivity reported within this assay. Overall, complications with solubility were not reported for the large remaining set of analogues from this series across all assays performed. Additionally, cytotoxic behaviour against the host macrophages was not observed. This suggests that the mode of action for this scaffold is not detrimental to the host cell and is selective for the parasite alone. The compounds of interest **5.116** and **5.119** underwent further physicochemical and metabolic studies, discussed in later sections (**5.09**). The dose response curves of both compounds of interest, reported by Bio21 are depicted below in **Figures 5.08-5.09**.

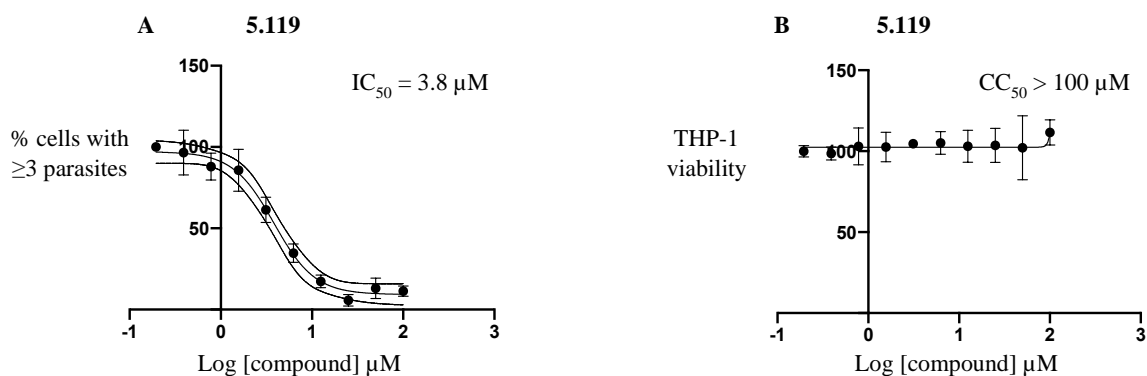


Figure 5.08a-b: Dose response curves of 5.116 reported by Bio21, a) measuring compound concentration (x axis) against % of infection within host macrophages (y axis) to determine the antileishmanial activity (IC_{50}) of 5.116, b) measuring compound concentration (x axis) against the viability of the THP-1 transformed macrophages (y axis) to determine the cytotoxicity against the host cell (CC_{50})

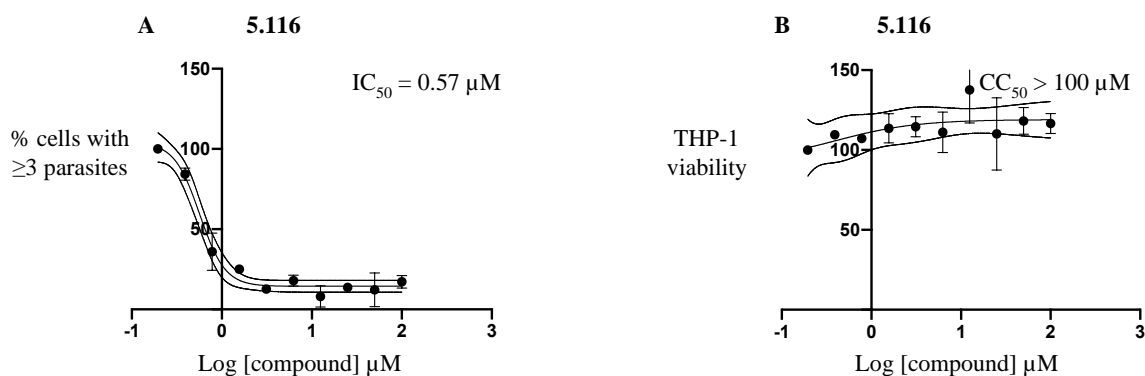


Figure 5.09a-b: Dose response curves of 5.119 reported by Bio21, a) measuring compound concentration (x axis) against % of infection within host macrophages (y axis) to determine the antileishmanial activity (IC_{50}) of 5.119, b) measuring compound concentration (x axis) against the viability of the THP-1 transformed macrophages (y axis) to determine the cytotoxicity against the host cell (CC_{50})

Similar to the above **Figure 5.07a-b**, here the **Figure 5.08a, 5.09a** is shown to decrease the percentage of infection within host macrophage cells when the concentration of compound is increased. Both compounds are depicted to be selective for the parasite only and displays no real cytotoxic behaviour against the transformed THP-1 host macrophage, observed in **Figure 5.08b, 5.09b**.

5.08 Summary of final scaffold

The investigations described in Chapters 4 and 5 have provided some clear SAR around this chosen scaffold, highlighted in **Figure 5.10**. Probing the substituents of the benzamide ring found that removal of either the terminal amide at the 3-position (**5.052**) or the 4-chloro (**4.053**) gave a complete loss of activity. Modifications to the terminal amide at the 3-position, such as bioisosteric replacement (**4.054**, **5.021**), removal of the amine group (**5.007**), reversal of the amide (**5.011**) as well as *N*-methylation of the amine (**5.015**, **5.018**) were all found to be unfavourable. The terminal amide was found to be required at the 3-position, where the amine group of the amide remains unsubstituted, suggesting both

H atoms to be required for H-bonding interactions with the binding site. Substitution of the 4-chloro with electronegative substituents (trifluoromethyl **5.039** and fluoro **5.040**) was also found to be unfavourable, dictating that the weaker electronegative atom is required at this position. Repositioning the chloro and terminal amide groups was generally not well tolerated (**5.025**, **5.041**, **5.042**, **5.050**). However, moving the terminal amide to the 4-position was highly favourable only when the chloro was repositioned to the 6-position. Analogue **5.051** has been chosen as a current lead for future SAR investigations around this scaffold. Further investigation would be required to understand whether these functionalities are required to be in proximity of one another to cause a potential synergistic interaction with the binding site.

Modifications to the ether linkage found that the only the initial arrangement of hit **5.001**, as well as removal of the O atom (**5.063**) were favourable, where a sole methylene group gave favourable flexibility and influenced orientation to fit well and allow interactions with the putative binding site. The analogue **5.063** has also been selected as a lead for further SAR investigation involving this scaffold. Removal of the methylene group (**4.056**, **5.056**) as well as increasing flexibility and potential changes to orientation with the substitution of another methylene group in place of the O atom (**5.064**) all gave a loss of activity. Based on studies around the ether chemical space has also revealed hydrogen bonding interactions are not required to maintain activity.

The final study for this body of work focused on adding functionalities around the phenoxymethyl ring in order to probe for any additional interactions that could be made with the binding site. It was found that adding stronger electron withdrawing groups around the ring was highly unfavourable, where compounds **5.085-5.087** gave a complete loss of activity. Overall, substitutions at the *meta* and *para* positions were generally found unfavourable, where at best, decreased, more moderate activity was observed in analogues **5.115** and **5.117** (*para*-chloro and *meta*-fluoro respectively, IC₅₀ of 12-15µM). Substitutions to the *ortho* position were the most tolerated, using electron donating groups (methoxy, methyl), or weakly deactivating *ortho* directors (fluoro). At this stage, it would seem superior activity was observed in these group which also possessed hydrogen bonding ability, where analogue **5.119** (*ortho*-methoxy) gave superior potency to the hit **5.001** and has also been selected for continued investigations as a new lead. Substituted aniline could be explored to further gauge whether electron donating functionalities with hydrogen bonding abilities were preferred. Analogue **5.116** (*ortho*-fluoro) is a current compound of interest and potential new lead, as it too demonstrated vastly superior antileishmanial activity, though this was reported within the Bio21 assay alone. Further confirmation is required from the UNC assay and retesting by Bio21 before it can be confidently considered as lead-like. This would also allow us to confirm whether hydrogen bonding ability and weak electron withdrawing abilities are tolerated at this position.

Overall, each of our new leads, along with the vast majority of analogues surrounding this scaffold have not reported issues with solubility nor host cell cytotoxicity. This was excellent news, as the reasons for potency or lack thereof, are not questionable. Poor compound activity is therefore derived solely from the structural modification rather than questioning whether inability to solubilize and permeate the cell. Additionally, since non-cytotoxic values were unanimously reported, any strong antileishmanial activity is viewed as selective for the parasites. At this stage, it would seem the mode of action, whether incorporating the host cell or not, is not harmful toward the macrophages. Therefore, activity is not due to detriment against the host cell, causing overall damage to both parasite and host, but rather selective targeting of the parasite alone. These were excellent qualities to confirm within this final scaffold.

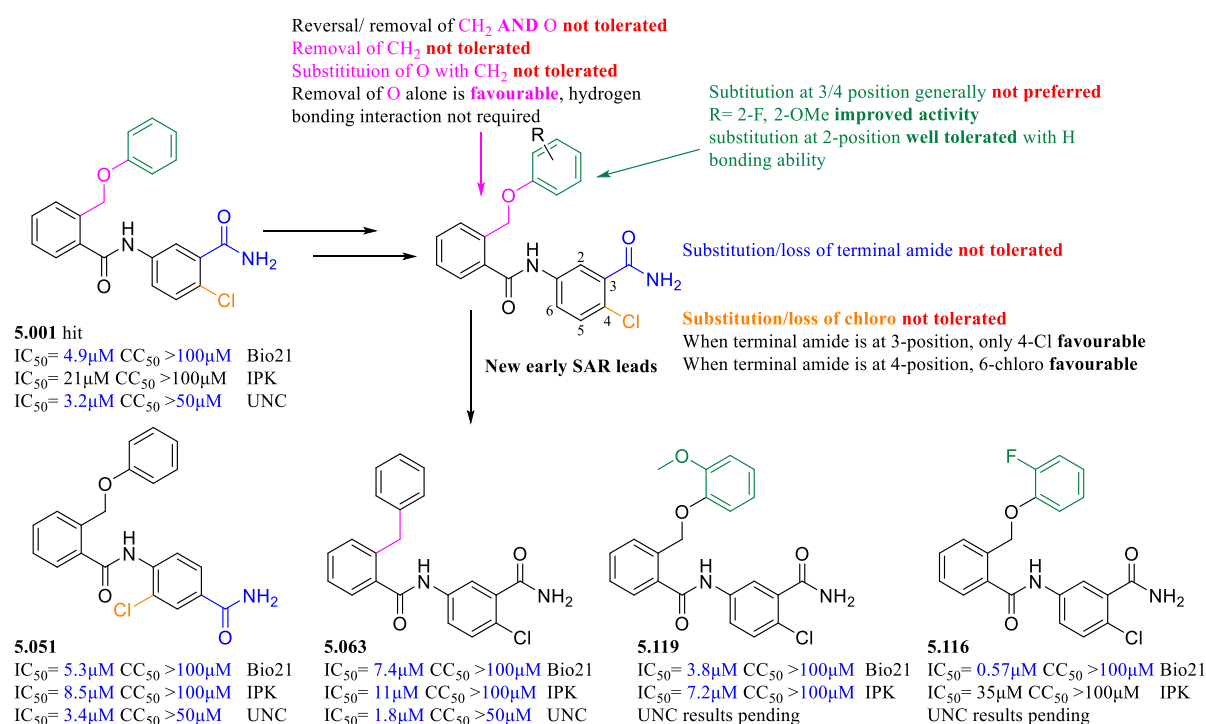
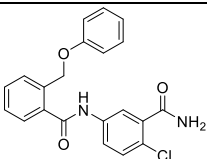
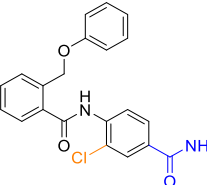
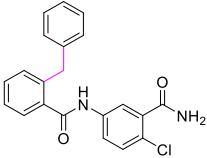
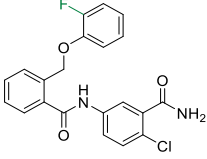
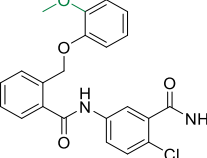


Figure 5.10 Summary of SAR exploration around final scaffold, carbamoyl phenoxymethyl benzamide

5.09 Physicochemical and metabolic assessment of lead compounds

The hit, new leads and compounds of interest also underwent physicochemical and metabolic evaluation to understand whether their modifications allowed for improved theoretical “drug-likeness” and stability for this final scaffold. **Table 5.11** and **5.12** summarizes the predicated physicochemical properties and microsomal stability, using both human and mouse microsomes respectively. The methods used to derive these properties has been previously described in the Experimental Section.

Table 5.11: Summary of physicochemical properties of key compounds for final scaffold (Scaffold 5)

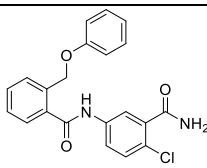
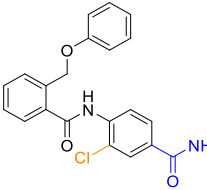
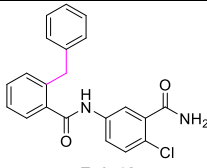
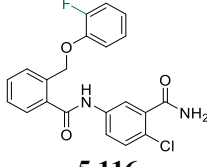
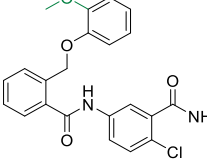
ID/ Structure							Solubility (µg/mL) ^b	
	MW ^a	PSA (Å ²) ^a	FRB ^a	HBD ^a	HBA ^a	cLogD _{at} pH 7.4 ^s	pH 2.0	pH 6.5
 5.001	381	81	6.0	2.0	3.0	4.1	25-50	25-50
 5.051	381	81	6.0	2.0	3.0	4.1	12.5-25	12.5-25
 5.063	365	72	5.0	2.0	2.0	4.6	12.5-25	12.5-25
 5.116	399	81	6.0	2.0	3.0	4.2	12.5-25	12.5-25
 5.119	411	91	7.0	2.0	4.0	3.9	12.5-25	12.5-25

a= Calculated using ChemAxon JChem software, b=kinetic solubility determined by Nephelometry (Sol_{pH}).

As shown in the table above, like the initial hit **5.001**, the newly discovered leads listed all possess physicochemical properties that indicate drug-likeness. This includes low molecular weight (<500 Da) and moderate LogD (<5). The number of Hydrogen bond donors and acceptors remains under 5 and 10 respectively, all adhering to Lipinski's Rule of Five.² Additionally, the low polar surface area (<140 Å²) and moderate number of rotatable bonds (<10 required) follow Veber's rule, another indicator of drug-likeness. The surface area of **5.119** is the most ideal of the current leads, since its value is greater than 90, this indicates decreased ability to permeate the blood brain barrier.³ Such penetration is not required for an antileishmanial, since parasites do not target this organ. The solubility of the hit **5.001** remains superior to the remaining key analogues listed in **Table 5.11**, suggesting the original arrangement is still preferred. Overall, the solubility of the remaining analogues was still sufficient for the *in vitro* assessments undertaken, though maintaining solubility levels similar to the hit **5.001** should be kept in mind for future work. The metabolic stability of future analogues is another key property to improve,

based on the analogues summarised below in **Table 5.12**. In comparison to the hit **5.001**, repositioning the terminal amide and chloro functionalities to the 4- and 6-positions respectively (**5.051**), was the only compound to give any improvement to metabolic stability. The reduced microsomal degradation of **5.051** relative to the original hit was reflected in a longer microsomal half-life ($T_{1/2} = 53$ min from 44 min) as well as decreased intrinsic clearance (**5.051** $Cl_{int\ in\ vitro} = 33$ $\mu\text{L}/\text{min}/\text{mg}$ protein, from 39 $\mu\text{L}/\text{min}/\text{mg}$ protein) and hepatic extraction ratio ($E_H = 0.56$ from 0.61). This improvement was observed in human microsomes alone. Even though the eventual drug candidate is targeted for use in humans, *in vivo* testing is a prerequisite, and favourable stability in mice is needed. Despite this, most of the physicochemical and metabolic properties of **5.051** still satisfy the criteria set out in **Table 1.07** of Chapter 1 and may still be considered for early lead optimization. Removal of the ether oxygen (**5.063**) and additions to the phenoxymethyl ring (**5.116**, **5.119**) were found to be unfavourable modifications, decreasing stability. If found tolerable within the putative binding site/s, future investigations could focus on examining whether the terminal amide could be protected, or whether a trifluoromethoxy group could replace the methoxy of **5.119** to further enhance stability, where the more electron deficient ring could kinetically slow down metabolism at these metabolic “soft spots”.⁷⁵⁻⁷⁸ Introducing electron withdrawing groups around the benzamide ring could also be investigated, keeping the terminal amide and chloro in their preferred positions. As seen already, substitution of the chloro group with more electronegative groups was unfavourable to potency, therefore additions to this ring may be explored. Other strategies could involve steric shielding at these metabolic sites, if a sterically bulky group was tolerated within these chemical spaces, this could help interfere with metabolic activation, incumbering the metabolically susceptible sites. However, the metabolic pathway for this scaffold has yet to be elucidated, we have not confirmed which enzymes and metabolic sites of the scaffold are involved. This remains outside the scope of this thesis. Once metabolomic assessments have been undertaken, greater insight into how to improve such properties will assist in continued development. Overall, the physicochemical properties of the key compounds were found favourable, whereas the metabolic stability and solubility, though not completely troubling, still had room for improvement. Original hit **5.001** and listed leads of **Table 5.11-5.12** would all undergo continuous hit-to-lead SAR studies, aimed to improve antileishmanial activity as well as physicochemical and metabolic properties in order to develop a superior lead candidate for *in vivo* studies, and further assessment for drug candidacy.

Table 5.12: Summary of metabolic properties of key compounds for final scaffold (Scaffold 5)

ID/ Structure	Species	T _{1/2} (min)	Cl _{int} <i>in vitro</i> (μL/min/ mg protein)	Microsome- predicted E _H	Clearance classification ^a
 5.001	Human	44	39	0.61	Intermediate
	Mouse	17	100	0.68	Intermediate
 5.051^b	Human	53	33	0.56	Intermediate
	Mouse	13	131	NA	NA
 5.063	Human	17	100	0.80	High
	Mouse	8.0	228	0.83	High
 5.116	Human	35	50	0.66	Intermediate
	Mouse	12	145	0.76	High
 5.119	Human	17	104	0.80	High
	Mouse	8.0	215	0.82	High

a= The E_H was used to classify compounds as low (< 0.3), intermediate (0.3 - 0.7), high (0.7 - 0.95) or very high (> 0.95) extraction compounds

b= Apparent non-NADPH mediated degradation (>30% degradation) was observed in mouse metabolism control samples. Putative degradation products were looked for but not detected. Predicted *in vivo* clearance parameters are therefore not reported.

NA= not applicable

5.10 Further studies with lead compound

Briefly, the hit **5.001** and lead compound **5.063** underwent further toxicity assessment via cytotoxicity and mitotoxicity profiling, undertaken using the Crabtree effect assay by IPK. As outlined in Chapter 3, to gauge whether compounds exerted toxicity against mitochondria, they were assessed against HepG2 cells in both glucose and galactose media. Under glucose conditions, the cells utilize ATP from glycolysis whereas under galactose conditions, ATP is utilized from oxidative phosphorylation and is therefore mitochondria dependant. The impact of the compounds, at increasing concentrations can be

directly compared between conditions to determine whether mitotoxicity was observed.^{79, 80} No clear mitochondrial toxicity or cytotoxicity was observed for both compounds in HepG2 cells, which is encouraging for future optimization and development potential. The dose response curves and CC₅₀ values are listed within the Appendix. Further mitochondrial toxicity assessment will be required for the next generation of optimized analogues.

The new lead compounds **5.051** and **5.063** were also subjected to an *in vivo* proof of concept study using VL mouse models, with BALB/c mice infected with *L. donovani* amastigotes. This was undertaken by our collaborators at IPK following the methods described by Phan *et al.*³⁷ Compounds were dosed at 100 mg/kg, via bolus intraperitoneal injection, with the aim increasing the potential for an observable therapeutic window *in vivo*. Some problematic toxicity was observed, and compounds **5.051** and **5.063** were found to be lethal at this dose. Clearly, improvements in pharmacokinetic properties and potency would be necessary before resubmitting the next generation of optimized analogues for efficacy studies *in vivo*.

5.11 Future work

Future work pertaining to our final scaffold should first involve combining the ideal modifications of our current leads, in an additive SAR campaign. This would allow us to assess whether both modifications were able to work synergistically together, giving a better fit or stronger interaction within the putative binding site. A continued SAR investigation around this scaffold is encouraged, focusing on the currently unexplored aromatic ring which joins the central amide and ether linkage moieties. Addition of various functionalities, including small groups employed in Section **5.06** (Cl, CN, F, Me, OMe) as well as larger aromatic rings may be installed around the free positions of this middle ring. Substituting the phenoxymethyl ring for a heteroatomic system such as pyridine could be trialled. Further investigation around the benzamide ring is also required to understand whether the SAR observed in Section **5.03** was based on individual substituents or an overall geometric effect. A fuller set of analogues repositioning the chloro and primary substituents is required to attain a better understanding of this chemical space. Further studies into the scaffold's metabolism are required, so that any "soft spots" can be modified to slow down the rate of metabolism. This could involve studies into whether additional electron withdrawing groups (e.g fluoro, trifluoromethyl) can be tolerated at the free positions of the benzamide ring. Though these groups were unfavourable in place of the chloro group, an addition of the electronegative functionalities at a free position instead of a substitution removing the chloro may be tolerated. Substitution of the *ortho*-methoxy of new lead **5.119** with a trifluoromethoxy or trifluoromethyl group may also assist in increasing metabolic stability. However, further studies around the metabolic pathway of our current scaffold are first required to guide further modifications aimed at improving metabolism whilst maintaining potency. These suggested compounds that could be studied for future work are summarized below in **Figure 5.11**.

Overall, this scaffold is quite promising as the hit and current leads possess potent antileishmanial activity selective for the parasite alone. Despite the difficulties around targeting *L. donovani* within the harsh macrophage environment, success was achieved in understanding the SAR around this scaffold and improving antileishmanial activity whilst maintaining low host cell cytotoxicity, accomplished with our new lead compounds and confirmed with the array of biological assays employed by our various collaborators. The lack of issues with solubility or cytotoxicity have made interpretations of the SAR much easier in comparison to our previous antileishmanial hit-to-lead campaigns described within this body of work, encouraging future exploration around this scaffold, using the established synthetic pathways described above. Overall, this initial hit-to-lead study can be used to guide future work around this scaffold, using the current promising leads to develop a more optimized candidate for the leishmaniasis pipeline.

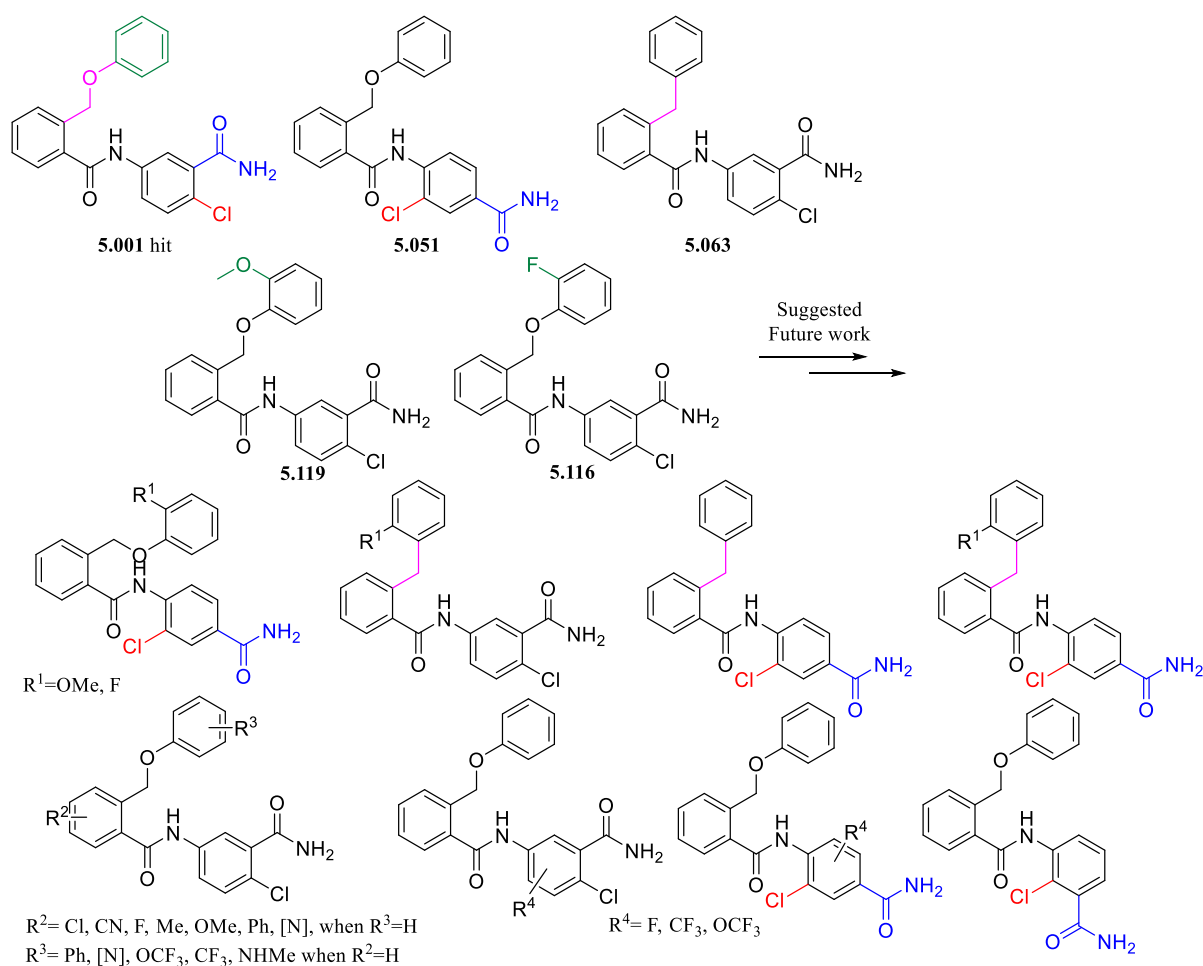


Figure 5.11: Suggested structures for future work around this scaffold

5.12 Chapter 5 Experimental

Biological methods

Bio21 Methodology

Biological methods were previously described in detail, please refer to previous chapters, experimental section (2 and 3). These assays were carried out as previously reported with minor adjustments.³⁶

IPK Methodology

Parasite and cell culture along with the intracellular assay were performed according to Phan *et al.* with small modifications.³⁷ These methods were previously described in detail, please refer to Chapter 3, Experimental section.

UNC Methodology

Infecting THP-1 Macrophages with *Leishmania donovani* (Ds-Red-lux) and evaluating by Luciferase assay⁴⁰

Parasites: *L. donovani* LV82 expressing firefly luciferase and a red fluorescent protein, LUC and DsRed2 promastigotes (Ds-Red-Lux) promastigotes were provided by Dr. Abhay Satoskar, Department of Pathology, The Wexner Medical Centre, The Ohio State University. Ds-Red-lux *L. donovani* promastigotes were routinely cultured at 26 °C in M199 medium (Catalogue number 10-060, Corning) supplemented with, 7.6 mM hemin, 0.1, 10% (v/v) heat-inactivated fetal bovine serum (FBS) and antibiotic cocktail (50 U/ml penicillin, 50 µg/ml streptomycin).

Generation of the red-shifted lux *L. donovani* strain was undertaken based on the methods described by Lezama-Davila *et al.*³⁹

***In vitro* luciferase assay**

The assay and conditions were adapted from methods as previously described by Álvarez-Velilla *et al.* which employed *L. infantum* rather than *L. donovani* which was utilised within these studies.³⁸ This has been previously described in detail, please refer to Chapter 3, Experimental section.

Cell viability analysis: MTT assay

These assay conditions are similar to that reported by Chiu *et al.*, as directed by our colleagues at UNC.⁴² This has been previously described in detail, please refer to Chapter 3, Experimental section.

Physicochemical and *in vitro* Metabolic Experimental

Calculated physicochemical parameters using ChemAxon JChem software

A range of physicochemical properties evaluating likely oral absorption characteristics and drug-likeness were calculated using the ChemAxon chemistry cartridge via JChem for Excel software (version 16.4.11). A brief description of each parameter is provided below:

MW (< 500): Molecular Weight

PSA_{pH 7.4} (< 140 Å²): Polar surface area also inversely correlates with membrane permeability.

FRB (≤ 10): Number of freely rotating bonds represents the flexibility of a molecule's conformation.

HBD (< 5) & HBA (< 10): Number of hydrogen bond donors and acceptors gives an indication of the hydrogen bonding capacity, which is inversely related to membrane permeability.

cLogP/cLogD_{pH} (< 5): Calculated partition coefficients reflect the lipophilic character of the neutral structure, while distribution coefficients reflect the partitioning properties of the ionised molecule at a specific pH.

Kinetic Solubility Estimation using Nephelometry

Compound in DMSO was spiked into either pH 6.5 phosphate buffer or 0.01M HCl (approx. pH 2.0) with the final DMSO concentration being 1%. After 30 minutes had elapsed, samples were analysed via Nephelometry to determine a solubility range.⁸¹

Distribution Coefficient Estimation using Chromatography

Partition coefficient values (LogD) of the test compounds were estimated at pH 7.4 by correlation of their chromatographic retention properties against the characteristics of a series of standard compounds with known partition coefficient values. The method employed is gradient HPLC based derivation of the method originally developed by Lombardo *et al.*⁸²

In vitro Metabolic Stability

Incubation:

The metabolic stability assay was performed by incubating each test compound in liver microsomes at 37 °C and a protein concentration of 0.4 mg/mL. The metabolic reaction was initiated by the addition of an NADPH-regenerating system and quenched at various over a 60 min incubation period by the addition of ACN containing diazepam as internal standard. Control samples (containing no NADPH) were included (and quenched at 2, 30 and 60 min) to monitor for potential degradation in the absence of cofactor. The human liver microsomes used in this experiment were supplied by XenoTech, lot # 1410230. The mouse liver microsomes used in this experiment were supplied by XenoTech, lot #

1910002 (for our compounds tested in 2020) and lot #1510256 (for our compounds tested in 2018, 2019). Microsomal incubations were performed at a substrate concentration of 0.5-1 μ M.

Data analysis:

Species scaling factors from Ring *et al.* were used to convert the *in vitro* CL_{int} (μ L/min/mg) to an *in vivo* CL_{int} (mL/min/kg).⁸³ Hepatic blood clearance and the corresponding hepatic extraction ratio (E_H) were calculated using the well stirred model of hepatic extraction in each species, according to the "in vitro T_{1/2}" approach described by Obach *et al.*⁸⁴ The E_H was then used to classify compounds as low (< 0.3), intermediate (0.3 - 0.7), high (0.7 - 0.95) or very high (> 0.95) extraction compounds. Predicted *in vivo* clearance values have not been corrected for microsomal or plasma protein binding. Species scaling calculations are based on two assumptions: 1) NADPH-dependent oxidative metabolism predominates over other metabolic routes (*i.e.* direct conjugative metabolism, reduction, hydrolysis, *etc.*), and; 2) rates of metabolism and enzyme activities *in vitro* are truly reflective of those that exist *in vivo*. If significant non-NADPH-mediated degradation is observed in microsome control samples, then assumption (1) is invalid and predicted clearance parameters are therefore not reported.

General Chemistry

General chemistry, solvents and machines employed followed the same description detailed in Chapter 2, Experimental

General Procedure A: Reduction¹¹

A mixture of the appropriate nitrobenzene (5.0 mmol), ammonium chloride (1.27 g, 24 mmol) and iron powder (1.5 g, 18 mmol) was dissolved in water and MeOH (1:2). The slurry was stirred at 70°C for 2 h, monitored by TLC. Upon reaction completion the mixture was cooled to room temperature and filtered through a pad of celite. The filtrate was concentrated *in vacuo*, taken up in EtOAc and washed with brine. The organic layers were collected, dried over MgSO₄, filtered and concentrated. DCM was added in order to form a precipitate, filtered via suction filtration where the desired product could be collected.

General Procedure B: Amide coupling^{6,7}

To a solution of the appropriate amine (1.0-1.3 equiv) and DIPEA (1.0-2.0 equiv) in ACN (5 mL) was added the appropriate benzoic acid (1.0-1.5 equiv). The mixture was stirred for 10 min before adding HOBt (2.5 equiv) and EDCI. HCl (1 equiv). The solution was stirred at 50°C, over 12 h after which the reaction was reduced *in vacuo*. The reaction mixture was diluted with DCM and washed with citric acid/water followed by ammonia/water. The organic layer was dried with MgSO₄, filtered and reduced *in vacuo*. The crude material was subsequently purified via column chromatography (CHCl₃; MeOH; NH₄OH; 94:5:1).

General Procedure C Amide formation via acid chloride^{19, 20, 22-24}

To a solution of the appropriate carboxylic acid (1 eq) dissolved in DCM (10 mL) was added oxalyl chloride (1 eq) dropwise at 0°C, followed by 5 drops of DMF. The mixture was heated to room temperature and stirred until bubbling ceased and solution cleared. The reaction was monitored by TLC analysis. Upon reaction completion the mixture was concentrated *in vacuo* using toluene as an azeotrope. The crude can then be used directly in the next reaction. A mixture of the appropriate amine (1 eq) and Et₃N (1 eq) dissolved in THF as cooled to 0°C. The converted acid chloride was taken up in THF and added to the mixture dropwise. The reaction mixture was heated to room temperature and left to stir for 12 h. The reaction was monitored via TLC and LCMS analysis. Upon reaction completion the crude mixture was concentrated *in vacuo*, diluted with EtOAc and washed with brine. The organic layers were collected, dried over MgSO₄, filtered and concentrated *in vacuo*. The crude product is diluted with a small volume of DCM in order to crash out the desired product followed by subsequent suction filtration. If the solid remains impure, subsequent purification via column chromatography was employed (EtOAc/ Petroleum ether, 1:1).

General Procedure D Ether formation^{67, 68, 71, 72}

To a solution of the appropriate alkyl 2-(bromomethyl)benzoate (1 eq) and substituted phenol (1 eq) was added K₂CO₃ (5 eq), KI (1 eq) and the mixture was dissolved in DMF and left to stir at rt over 12 h, or dissolved in ACN and heated up to 70°C over 12 h. Upon reaction completion the mixture was filtered and concentrated *in vacuo* to give the desired compound.

General Procedure E Alkyl deprotection⁵⁶

To the appropriate benzoate (1 eq) was added NaOH 10% aq solution and 10 mL of EtOH. The mixture was heated to 100°C and refluxed over 12 h. Upon reaction completion the mixture was concentrated, acidified with 2M HCl and the precipitate was filtered via suction filtration. The solid was collected, dissolved in DCM and dried over MgSO₄, filtered and concentrated to give the desired compound.

General Procedure F Terminal amide formation³¹

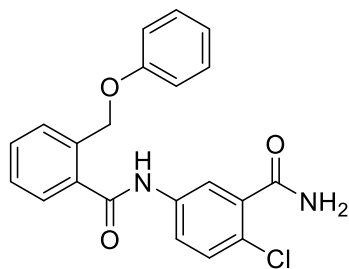
To a solution of the appropriate carboxylic acid (1 eq) dissolved in DCM (10 mL) was added oxalyl chloride (1 eq) at 0°C followed by DMF (5 drops). The solution was heated to room temperature and allowed to stir over night. The mixture was concentrated *in vacuo* and taken up in EtOAc. Ammonium hydroxide (10 mL) was added at 0°C heated to room temperature and stirred for 1 hour. Upon reaction completion the mixture was concentrated and diluted with EtOAc and washed with brine. The organic layers were collected, dried with MgSO₄, filtered and concentrated to afford the desired compound.³¹

General Procedure G Alternate Alkyl deprotection¹⁹

To a mixture of the appropriate benzoate (1 eq) in MeOH (5 mL), H₂O (5 mL) and THF (10 mL) was added Lithium hydroxide (5 eq). The mixture stirred at room temperature over 12 h. Upon reaction completion the solvent was removed *in vacuo*, acidified with 2M HCl and washed with EtOAc and brine. The organic layers were collected and dried over MgSO₄, filtered and concentrated to yield the desired compound.

Synthesis

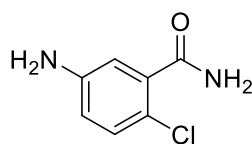
N-(3-Carbamoyl-4-chlorophenyl)-2-(phenoxymethyl)benzamide (4.004/5.001)



The title compound was obtained using 5-amino-2-chlorobenzamide (150 mg, 0.88 mmol) and 2-(phenoxymethyl)benzoic acid (200 mg, 0.88 mmol) in DMF (3 mL) following General Procedure A. The title compound was afforded as an off white solid (200 mg, 60 %). HPLC – t_R 5.63 min > 95 % purity at 254 nm; LRMS [M+H]⁺ 380.9 *m/z*; HRMS [M+H]⁺ 381.1000 *m/z*, found 381.1001 *m/z*; ¹H NMR (400 MHz,

DMSO) δ_H 10.61 (s, 1H), 7.86 – 7.81 (m, 2H), 7.74 – 7.68 (m, 1H), 7.62 – 7.39 (m, 6H), 7.25 – 7.19 (m, 2H), 6.92 – 6.86 (m, 3H), 5.26 (s, 2H); ¹³C NMR (101 MHz, DMSO) δ_C 168.0, 167.3, 158.2, 138.0, 137.4, 135.6, 135.4, 130.2, 129.7, 129.5 (2C), 128.6, 127.9, 127.8, 123.6, 121.5, 120.8, 119.5, 114.7 (2C), 67.0. M.p. 126.4-139.7 °C.

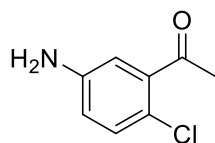
5-Amino-2-chlorobenzamide (5.003)⁸⁵



To obtain the known title compound 2-chloro-5-nitrobenzamide (1.0 g, 5 mmol) was used following General Procedure A. The title compound was afforded as a pale yellow solid (800 mg, 94 %). HPLC – t_R 1.376 min > 95 % purity at 254 nm; LRMS [M+H]⁺ 171.0 *m/z*; ¹H NMR (400 MHz, MeOD) δ_H 7.13 (d, *J* = 8.6

Hz, 1H), 6.82 (d, *J* = 2.8 Hz, 1H), 6.72 (dd, *J* = 8.6, 2.8 Hz, 1H). Acquired data is consistent with the literature.⁸⁵

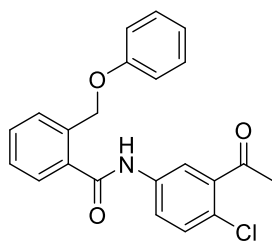
1-(5-Amino-2-chlorophenyl)ethan-1-one (5.006)¹¹



The known title compound was obtained using 1-(2-chloro-5-nitrophenyl)ethan-1-one (1.0 g, 5.0 mmol) following General Procedure A, affording the title compound as an orange solid (800 mg, 95 %). HPLC – t_R 2.86 min > 95 % purity at 254 nm; LRMS [M+H]⁺ 170.0 *m/z*; ¹H NMR (400 MHz, MeOD) δ_H 7.13 (d, *J* = 8.6 Hz,

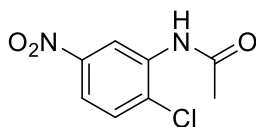
1H), 6.87 (d, *J* = 2.8 Hz, 1H), 6.76 (dd, *J* = 8.6, 2.8 Hz, 1H), 2.56 (s, 3H); ¹³C NMR (101 MHz, MeOD) δ_C 203.2, 148.6, 140.7, 132.0, 119.4, 118.9, 115.7, 30.7.

***N*-(3-Acetyl-4-chlorophenyl)-2-(phenoxyethyl)benzamide (5.007)**



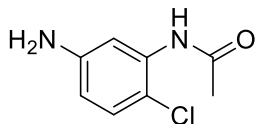
The title compound was obtained using 1-(5-amino-2-chlorophenyl)ethan-1-one (100 mg, 0.6 mmol) and 2-(phenoxyethyl)benzoic acid (137 mg, 0.60 mmol) following General Procedure B, affording the title compound as a yellow solid (113 mg, 50 %). HPLC – t_R 6.62 min > 99 % purity at 254 nm; LRMS $[M+H]^+$ 380.1 m/z ; HRMS $[M+H]^+$ 380.1048 m/z , found 380.1051 m/z ; 1H NMR (400 MHz, MeOD) δ_H 7.90 (d, J = 2.5 Hz, 1H), 7.76 – 7.71 (m, 1H), 7.65 – 7.60 (m, 2H), 7.57 – 7.51 (m, 1H), 7.49 – 7.41 (m, 2H), 7.23 – 7.19 (m, 2H), 6.93 – 6.89 (m, 3H), 5.30 (s, 2H), 2.58 (s, 3H); ^{13}C NMR (101 MHz, MeOD) δ_C 201.8, 170.5, 160.0, 140.5, 139.2, 137.1, 137.0, 132.0, 131.6, 130.4 (2C), 130.0, 129.2, 128.7, 126.6, 124.9, 122.1, 122.0, 115.9 (2C), 68.9, 30.6.

***N*-(2-Chloro-5-nitrophenyl)acetamide (5.009)^{13, 86}**



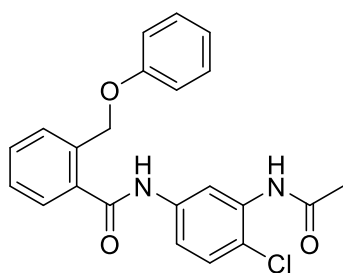
To a solution of 2-chloro-5-nitroaniline (2.0 g, 12 mmol) in 1,2-dichloroethane (20 mL) was added DIPEA (2.2 mL) followed by acetyl chloride (1.8 mL, 25.5 mmol). The reaction mixture was warmed to 45°C for 6 h. A precipitate was formed. The organics were dissolved in DCM and washed with saturated sodium bicarbonate.¹³ The organic layers were dried over $MgSO_4$, filtered and concentrated to give the known title compound as an off-white solid (2.4 g, 93 %). HPLC – t_R 4.12 min > 99 % purity at 254 nm; LRMS $[M+H]^+$ 215.0 m/z ; 1H NMR (400 MHz, DMSO) δ_H 9.87 (s, 1H, NH), 8.75 (d, J = 2.7 Hz, 1H), 7.99 (dd, J = 8.9, 2.8 Hz, 1H), 7.80 (d, J = 8.9 Hz, 1H), 2.18 (s, 3H); ^{13}C NMR (101 MHz, DMSO) δ_C 169.4, 146.2, 136.1, 131.8, 130.6, 120.0, 119.2, 23.5.

***N*-(5-Amino-2-chlorophenyl)acetamide (5.010)⁸⁷**



The known title compound was obtained using *N*-(2-chloro-5-nitrophenyl)acetamide (1.0 g, 4.7 mmol) following General Procedure A, affording the title compound as a yellow solid (800 mg, 92 %). HPLC – t_R 1.79 min > 99 % purity at 254 nm; LRMS $[M+H]^+$ 185.1 m/z ; 1H NMR (400 MHz, DMSO) δ_H 9.13 (s, 1H, NH), 7.03 (d, J = 8.6 Hz, 1H), 6.97 (s, 1H), 6.35 (dd, J = 8.6, 2.5 Hz, 1H), 5.25 (s, 2H, NH₂), 2.04 (s, 3H); ^{13}C NMR (101 MHz, DMSO) δ_C 168.3, 148.0, 135.1, 129.1, 112.0, 111.7, 110.9, 23.4. Acquired data is consistent with the literature.⁸⁷

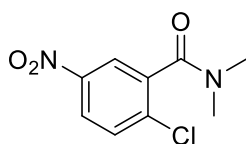
***N*-(3-Acetamido-4-chlorophenyl)-2-(phenoxyethyl)benzamide (5.011)**



The title compound was obtained using *N*-(5-amino-2-chlorophenyl)acetamide (100 mg, 0.54 mmol) and 2-(phenoxyethyl)benzoic acid (110 mg, 0.54 mmol) following General Procedure B, to afford the title compound as a white solid (50 mg, 52 %). HPLC – t_R 5.98 min > 99 % purity at 254 nm; LRMS $[M+H]^+$ 395.1 m/z ; HRMS $[M+H]^+$ 395.1157 m/z , found 395.1153 m/z ; 1H NMR (400

MHz, DMSO) δ 10.57 (s, 1H, NH), 9.49 (s, 1H, NH), 8.09 (s, 1H), 7.62 – 7.39 (m, 6H), 7.26 – 7.20 (m, 2H), 6.93 – 6.87 (m, 3H), 5.26 (s, 2H), 2.08 (s, 3H); ^{13}C NMR (101 MHz, DMSO) δ_C 168.5, 167.2, 158.2, 138.3, 135.7, 135.3, 135.0, 130.1, 129.4 (2C), 129.2, 128.5, 127.8, 121.0, 121.0, 120.8, 117.7, 117.6, 114.7 (2C), 67.0, 23.2.

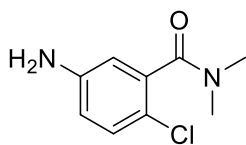
2-chloro-*N,N*-dimethyl-5-nitrobenzamide (5.013)¹⁴



A mixture of 2-chloro-5-nitrobenzoic acid (600 mg, 3.0 mmol), POCl₃ (0.28 mL, 3.0 mmol) and DMF (20 mL) was heated to 120°C in a sealed tube for 1 h. The mixture was cooled to room temperature and sodium carbonate was added.

The mixture was extracted with EtOAc, the organic layers were collected, dried over MgSO₄ over 12 h. The solution was filtered and concentrated *in vacuo*. The oil residue was then freeze dried to obtain the known title compound as an off-white powder (500 mg, 73 %). HPLC – t_R 4.02 min > 99 % purity at 254 nm; LRMS $[M+H]^+$ 229.0 m/z ; 1H NMR (400 MHz, CDCl₃) δ_H 8.21 – 8.17 (m, 2H), 7.60 (dt, J = 2.6, 1.0 Hz, 1H), 3.17 (s, 3H), 2.90 (s, 3H); ^{13}C NMR (101 MHz, CDCl₃) δ_C 166.1, 146.9, 137.9, 137.5, 130.9, 124.9, 123.4, 38.2, 35.0. Acquired data is consistent with the literature.¹⁴

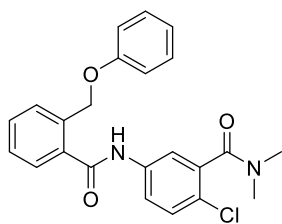
5-amino-2-chloro-*N,N*-dimethylbenzamide (5.014)



The known title compound was obtained using 2-chloro-*N,N*-dimethyl-5-nitrobenzamide (500 mg, 2.2 mmol) following General Procedure A, affording the title compound as a solid (300 mg, 69 %). LRMS $[M+H]^+$ 199.0 m/z ; 1H

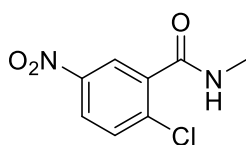
NMR (400 MHz, MeOD) δ_H 7.14 (d, J = 8.7 Hz, 1H), 6.73 (dd, J = 8.7, 2.7 Hz, 1H), 6.61 (d, J = 2.7 Hz, 1H), 3.11 (s, 3H), 2.92 (s, 3H); ^{13}C NMR (101 MHz, MeOD) δ_C 171.3, 148.8, 137.4, 131.0, 118.2, 118.0, 114.2, 38.6, 34.9.

2-Chloro-*N,N*-dimethyl-5-(2-(phenoxyethyl)benzamido)benzamide (5.015)



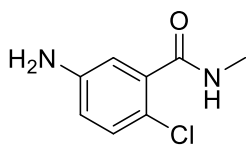
The title compound was obtained using 2-(phenoxyethyl)benzoic acid (228 mg, 1.0 mmol) and 4-amino-2-chlorobenzamide (200 mg, 1.0 mmol) following General Procedure B. The title compound was produced as a yellow solid (191 mg, 47 %). HPLC – t_R 6.01 min > 99 % purity at 254 nm; LR MS $[M+H]^+$ 409.0 m/z ; HRMS $[M+H]^+$ 409.1313 m/z , found 409.1314 m/z ; 1H NMR (400 MHz, MeOD) δ_H 7.71 – 7.60 (m, 4H), 7.57 – 7.42 (m, 3H), 7.24 – 7.19 (m, 2H), 6.95 – 6.87 (m, 3H), 5.30 (s, 2H), 3.12 (s, 3H), 2.88 (s, 3H); ^{13}C NMR (101 MHz, MeOD) δ_C 170.4, 170.2, 160.0, 139.5, 137.4, 137.0, 136.9, 131.6, 131.0, 130.4 (2C), 130.1, 129.2, 128.6, 125.8, 123.4, 122.1, 120.3, 115.9 (2C), 68.9, 38.6, 35.0.

2-Chloro-*N*-methyl-5-nitrobenzamide (5.016)^{15, 88}



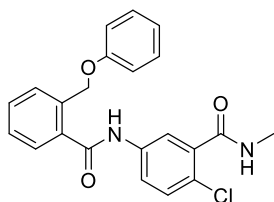
To a mixture of 2-chloro-5-nitrobenzoic acid (1.0 g, 5 mmol) in DCM (10 mL) was added oxalyl chloride (0.54 mL) at 0°C followed by the addition of DMF (5 drops). The mixture was heated to room temperature and heated for 2 h. Upon reaction completion, the mixture was concentrated *in vacuo*. The residue (500 mg, 2.3 mmol) was taken up in DCM and added to methylamine hydrochloride (213 mg, 3.1 mmol) DCM (10 mL) and triethylamine (0.84 mL, 6.0 mmol) was stirred for 72 h. Upon reaction completion the mixture was diluted with EtOAc and washed with brine, 1M HCl and aqueous sodium carbonate solution. The organic layers were collected, dried over MgSO₄, filtered and concentrated to give the title compound as a pale yellow solid (485 mg, 99%).¹⁵ HPLC – t_R 3.15 min > 99 % purity at 254 nm; LRMS $[M+H]^+$ 215.0 m/z ; 1H NMR (400 MHz, MeOD) δ_H 8.34 – 8.29 (m, 2H), 7.76 (dd, J = 8.6, 0.5 Hz, 1H), 2.96 (s, 3H); ^{13}C NMR (101 MHz, MeOD) δ_C 168.2, 147.9, 138.9, 138.8, 132.5, 126.6, 124.9, 26.8.

5-Amino-2-chloro-*N*-methylbenzamide (5.017)⁸⁸



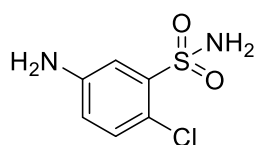
The known title compound was obtained using 2-chloro-*N*-methyl-5-nitrobenzamide (500 mg, 2.3 mmol) following General Procedure A, affording the title compound as a yellow solid (400 mg, 94 %). HPLC – t_R 1.60 min > 99 % purity at 254 nm; LRMS $[M+H]^+$ 185.1 m/z ; 1H NMR (400 MHz, CDCl₃) δ_H 7.12 (d, J = 8.6 Hz, 1H), 6.99 (d, J = 2.9 Hz, 1H), 6.64 (dd, J = 8.6, 2.9 Hz, 1H), 6.35 (bs, 1H), 3.49 (bs, 2H), 2.99 (d, J = 4.9 Hz, 3H); ^{13}C NMR (101 MHz, CDCl₃) δ_C 167.3, 145.6, 135.3, 131.0, 119.1, 118.0, 116.6, 26.9. Acquired data is consistent with the literature.⁸⁸

2-Chloro-*N*-methyl-5-(2-(phenoxy)methyl)benzamido)benzamide (5.018)



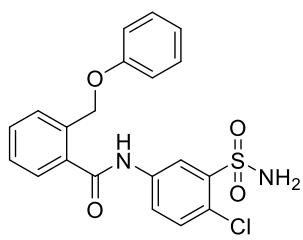
The title compound was obtained using 5-amino-2-chloro-*N*-methylbenzamide (100 mg, 0.54 mmol) and 2-(phenoxy)methylbenzoic acid (185 mg, 0.81 mmol) following General Procedure B, to afford the title compound as a white solid (88 mg, 41 %). HPLC – t_R 5.71 min > 99 % purity at 254 nm; LRMS $[M+H]^+$ 395.0 m/z ; HRMS $[M+H]^+$ 395.1157 m/z , found 395.1158 m/z ; 1H NMR (400 MHz, DMSO) δ 10.64 (s, 1H), 8.37 – 8.33 (m, 1H), 7.85 (d, J = 2.5 Hz, 1H), 7.71 (dd, J = 8.8, 2.5 Hz, 1H), 7.65 – 7.60 (m, 2H), 7.58 – 7.42 (m, 3H), 7.28 – 7.23 (m, 2H), 6.94 – 6.89 (m, 3H), 5.28 (s, 2H), 2.76 (d, J = 4.6 Hz, 3H); ^{13}C NMR (101 MHz, DMSO) δ_C 167.3, 166.5, 158.2, 138.0, 137.3, 135.6, 135.4, 130.3, 129.8, 129.5 (2C), 128.7, 127.9, 127.8, 123.8, 121.6, 120.8, 119.6, 114.7 (2C), 67.0, 25.9.

5-Amino-2-chlorobenzenesulfonamide (5.020)⁸⁹



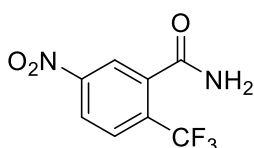
The known title compound was obtained using 2-chloro-5-nitrobenzenesulfonamide (1.0 g, 4.2 mmol) following General Procedure A, affording the title compound as a yellow solid (820 mg, 95 %). HPLC – t_R 1.61 min > 99 % purity at 254 nm; LRMS $[M+H]^+$ 207.0 m/z ; 1H NMR (401 MHz, DMSO) δ 7.23 (s, 2H), 7.10 (d, J = 2.8 Hz, 1H), 7.05 (d, J = 8.5 Hz, 1H), 6.59 (dd, J = 8.5, 2.8 Hz, 1H), 5.60 (s, 2H); 1H NMR (400 MHz, MeOD) δ_H 7.39 (d, J = 2.8 Hz, 1H), 7.23 (d, J = 8.6 Hz, 1H), 6.83 (dd, J = 8.6, 2.8 Hz, 1H); ^{13}C NMR (101 MHz, MeOD) δ_C 148.9, 141.9, 132.9, 119.9, 118.5, 116.0.⁸⁹

N-(4-Chloro-3-sulfamoylphenyl)-2-(phenoxy)methylbenzamide (5.021)



The title compound was obtained using 2-(phenoxy)methylbenzoic acid (200 mg, 0.88 mmol) and 5-amino-2-chlorobenzenesulfonamide (181 mg, 0.88 mmol) following General Procedure C. The title compound was produced as a white solid (260 mg, 71 %). HPLC – t_R 5.76 min > 99 % purity at 254 nm; LRMS $[M+H]^+$ 416.9 m/z ; HRMS $[M+H]^+$ 417.0670 m/z , found 417.0665 m/z ; 1H NMR (400 MHz, MeOD) δ_H 8.46 (d, J = 2.5 Hz, 1H), 7.89 – 7.85 (m, 1H), 7.66 – 7.61 (m, 2H), 7.57 – 7.44 (m, 3H), 7.24 – 7.19 (m, 2H), 6.95 – 6.87 (m, 3H), 5.31 (s, 2H); ^{13}C NMR (101 MHz, MeOD) δ_C 170.5, 160.0, 142.3, 139.2, 137.2, 136.8, 132.9, 131.6, 130.5 (2C), 130.0, 129.1, 128.7, 126.9, 125.7, 122.2, 122.1, 115.9 (2C), 68.9.

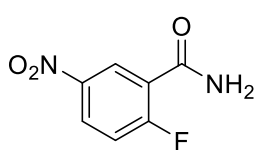
5-Nitro-2-(trifluoromethyl)benzamide (5.028)



The title compound was obtained following General Procedure F using 5-nitro-2-(trifluoromethyl)benzoic acid (1.0 g, 4.3 mmol) to form the acid halide intermediate. The solution was concentrated *in vacuo*, taken up in EtOAc and cooled to 0°C. Ammonium hydroxide (10 mL) was added dropwise to the

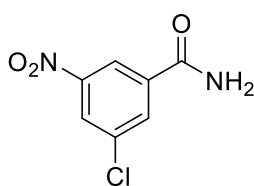
solution and allowed to stir for 1 h. Upon completion the reaction mixture was washed with brine and the organic layers were dried over MgSO_4 , filtered and concentrated to give the title compound as a yellow solid. (950 mg, 94 %). HPLC – t_R 3.06 min > 99 % purity at 254 nm; LRMS $[\text{M}+\text{H}]^+$ 233.0 m/z ; ^1H NMR (400 MHz, DMSO) δ_H 8.45 – 8.42 (m, 1H), 8.32 – 8.30 (m, 1H), 8.21 (bs, 1H, NH), 8.12 (d, J = 8.7 Hz, 1H), 7.90 (bs, 1H, NH); ^1H NMR (400 MHz, MeOD) δ_H 8.50 – 8.46 (m, 1H), 8.42 (d, J = 2.2 Hz, 1H), 8.08 (d, J = 8.7 Hz, 1H); ^{13}C NMR (101 MHz, MeOD) δ_C 170.5, 151.2, 139.2 – 138.9 (m, expected q but peaks too undefined, C-F), 133.4 (q, $J_{\text{C-F}}$ = 33.0 Hz), 129.7 (q, $J_{\text{C-F}}$ = 4.9 Hz), 125.7, 124.4, 124.2 (q, $J_{\text{C-F}}$ = 273.9 Hz).

2-Fluoro-5-nitrobenzamide (5.029)



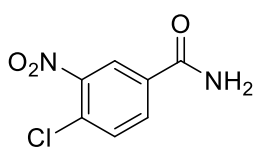
The title compound was obtained following General Procedure F using 2-fluoro-5-nitrobenzoic acid (1.0 g, 5.4 mmol) to form the acid halide intermediate. The solution was concentrated *in vacuo*, taken up in EtOAc and cooled to 0°C. Ammonium hydroxide (10 mL) was added dropwise to the solution and allowed to stir for 1 h. Upon completion the reaction mixture was washed with brine and the organic layers were dried over MgSO_4 , filtered and concentrated to give the title compound as a fluffy yellow solid (990 mg, 99 %).³¹ HPLC – t_R 2.74 min > 99 % purity at 254 nm; LRMS $[\text{M}+\text{H}]^+$ 185.1 m/z ; ^1H NMR (400 MHz, DMSO) δ 8.47 – 8.44 (m, 1H), 8.42 – 8.38 (m, 1H), 8.02 (br s, 1H, NH), 7.93 (br s, 1H, NH), 7.61 (t, J = 9.3 Hz, 1H). ^1H NMR (400 MHz, MeOD) δ_H 8.69 (dd, J = 6.1, 2.9 Hz, 1H), 8.49 – 8.44 (m, 1H), 7.51 (t, J = 9.4 Hz, 1H); ^{13}C NMR (101 MHz, MeOD) δ_C 166.2, 164.7 (d, $J_{\text{C-F}}$ = 260.1 Hz), 145.8, 129.4 (d, $J_{\text{C-F}}$ = 11.1 Hz), 127.6 (d, $J_{\text{C-F}}$ = 4.6 Hz), 125.2 (d, $J_{\text{C-F}}$ = 16.2 Hz), 119.0 (d, $J_{\text{C-F}}$ = 26.3 Hz).

3-Chloro-5-nitrobenzamide (5.030)⁹⁰



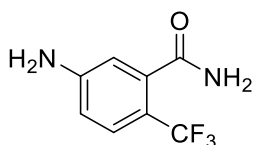
A solution of 3-chloro-5-nitrobenzoic acid (1.0 g, 5.0 mmol) in DCM (20 mL) was cooled to 0°C. Oxalyl chloride (0.60 mL) was added dropwise followed by the addition of DMF (5 drops) following General Procedure F. The mixture was heated to room temperature and stirred over 12 h. Upon reaction completion the mixture was concentrated. The residue was taken up in EtOAc and added to concentrated ammonium hydroxide (10 mL). The mixture was stirred for 30 min. The phases were separated and washed with brine. The organic layers were collected, dried over MgSO_4 , filtered and concentrated *in vacuo* to give the title compound as a yellow solid (800 mg, 80 %). HPLC – t_R 3.96 min > 99 % purity at 254 nm; LRMS $[\text{M}+\text{H}]^+$ 201.0 m/z ; ^1H NMR (400 MHz, DMSO) δ 8.63 – 8.61 (m, 1H), 8.45 – 8.43 (m, 1H), 8.40 (bs, 1H, NH₂), 8.35 – 8.34 (m, 1H), 7.85 (s, 1H, NH₂); ^{13}C NMR (101 MHz, DMSO) δ_C 164.4, 148.7, 137.2, 134.3, 133.4, 125.8, 121.1.

4-Chloro-3-nitrobenzamide (5.031)⁹¹



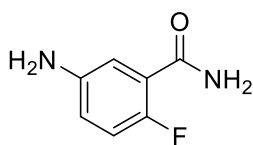
The known title compound was obtained following General Procedure F using 4-chloro-3-nitrobenzoic acid (1.0 g, 5.0 mmol) to afford 4-chloro-3-nitrobenzamide which was used directly in the next step (990 mg, 99%).³¹ HPLC – t_R 3.90 min > 99 % purity at 254 nm; LRMS $[M+H]^+$ 201.1 m/z ; 1H NMR (400 MHz, MeOD) δ_H 8.45 (d, J = 1.9 Hz, 1H), 8.13 (dd, J = 8.4, 2.0 Hz, 1H), 7.79 (d, J = 8.4 Hz, 1H); ^{13}C NMR (101 MHz, MeOD) δ_C 168.6, 149.4, 135.4, 133.2, 133.2, 130.5, 125.8

5-Amino-2-(trifluoromethyl)benzamide (5.033)



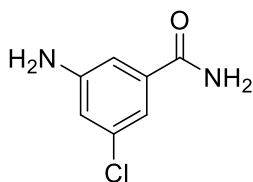
The title compound was obtained using 5-nitro-2-(trifluoromethyl)benzamide (760 mg, 3.3 mmol) following General Procedure A. The title compound was obtained as a yellow solid (300 mg, 45 %). HPLC – t_R 2.29 min > 99 % purity at 254 nm; LRMS $[M+H]^+$ 205.1 m/z ; 1H NMR (400 MHz, MeOD) δ_H 7.44 – 7.41 (m, 1H), 6.80 – 6.76 (m, 2H); ^{13}C NMR (101 MHz, MeOD) δ_C 174.2, 152.9, 138.18 – 138.07 (m, q expected, too undefined), 128.74 (q, J_{C-F} = 4.9 Hz), 126.0 (q, J_{C-F} = 270.6 Hz), 115.4 (q, J_{C-F} = 32.2 Hz), 115.1, 114.1.

5-Amino-2-fluorobenzamide (5.034)⁹²



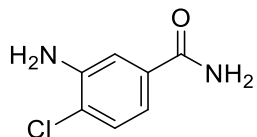
The title compound was obtained using 2-fluoro-5-nitrobenzamide (800 mg, 4.4 mmol) following General Procedure A. The title compound was obtained as a yellow solid (400 mg, 59 %). HPLC – t_R 1.22 min > 99 % purity at 254 nm; LRMS $[M+H]^+$ 155.1 m/z ; 1H NMR (400 MHz, MeOD) δ_H 7.19 – 7.15 (m, 1H), 7.01 – 6.95 (m, 1H), 6.90 – 6.85 (m, 1H); ^{13}C NMR (101 MHz, MeOD) δ_C 168.9 (d, J_{C-F} = 2.0 Hz), 154.8 (d, J_{C-F} = 238.7 Hz), 145.7 (d, J_{C-F} = 2.0 Hz), 122.8 (d, J_{C-F} = 13.9 Hz), 120.7 (d, J_{C-F} = 8.2 Hz), 117.5 (d, J_{C-F} = 25.1 Hz), 117.1 (d, J_{C-F} = 1.7 Hz).

3-Amino-5-chlorobenzamide (5.035)



The title compound was obtained using *N*-(2-chloro-5-nitrophenyl)acetamide (800 mg, 4.0 mmol) following General Procedure A, affording the title compound as an orange solid (600 mg, 88 %). HPLC – t_R 1.92 min > 99 % purity at 254 nm; LRMS $[M+H]^+$ 171.0 m/z ; 1H NMR (400 MHz, MeOD) δ_H 7.08 – 7.06 (m, 1H), 7.05 – 7.02 (m, 1H), 6.84 – 6.82 (m, 1H); ^{13}C NMR (101 MHz, MeOD) δ_C 171.7, 151.2, 137.4, 135.9, 118.1, 116.7, 113.2.

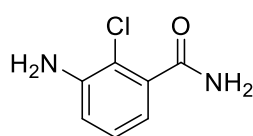
3-Amino-4-chlorobenzamide (5.036)⁹³



The title compound was obtained using 4-chloro-3-nitrobenzamide (990 mg, 4.93 mmol) following General Procedure A. The title compound was obtained

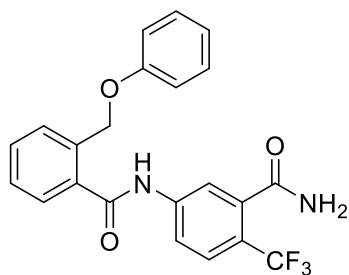
as an orange solid (687 mg, 82 %). HPLC – t_R 2.62 min > 92 % purity at 254 nm; LRMS $[M+H]^+$ 171.1 m/z ; 1H NMR (400 MHz, MeOD) δ 7.31 (d, J = 2.1 Hz, 1H), 7.27 (d, J = 8.3 Hz, 1H), 7.09 (dd, J = 8.3, 2.1 Hz, 1H); 1H NMR (400 MHz, DMSO) δ 7.83 – 7.78 (m, 1H), 7.28 (d, J = 2.0 Hz, 1H), 7.24 – 7.21 (m, 2H), 7.00 (dd, J = 8.2, 2.0 Hz, 1H), 5.46 (s, 2H); ^{13}C NMR (101 MHz, MeOD) δ_C 172.1, 145.7, 134.7, 130.2, 123.1, 117.8, 116.0.

3-Amino-2-chlorobenzamide (5.032/ 5.037)³⁵



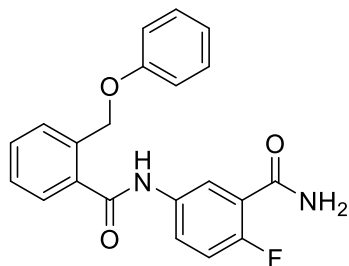
The known title compound was obtained following General Procedure F using 2-chloro-3-nitrobenzoic acid (1.0 g, 5.0 mmol) to afford the 2-chloro-3-nitrobenzamide intermediate. The intermediate was directly used following General Procedure A to afford the title compound as a solid. (584 mg, 69 %). HPLC – t_R 1.45 min > 95 % purity at 254 nm; LRMS $[M+H]^+$ 171.0 m/z ; 1H NMR (400 MHz, DMSO) δ 7.68 (s, 1H, NH benzamide), 7.38 (s, 1H, NH benzamide), 7.03 – 6.98 (m, 1H), 6.79 (dd, J = 8.1, 1.5 Hz, 1H), 6.55 (dd, J = 7.4, 1.5 Hz, 1H), 5.43 (s, 2H, NH₂); ^{13}C NMR (101 MHz, DMSO) δ 168.9, 145.0, 137.9, 126.9, 115.3, 115.2, 113.4.

N-(3-Carbamoyl-4-(trifluoromethyl)phenyl)-2-(phenoxyethyl)benzamide (5.038)



To obtain the title compound 5-amino-2-(trifluoromethyl)benzamide (250 mg, 1.2 mmol) and 2-(phenoxyethyl)benzoic acid (279 mg, 1.2 mmol) were used following General Procedure C. The title compound was obtained as a white solid (380 mg, 76 %). HPLC – t_R 5.75 min > 99 % purity at 254 nm; LRMS $[M+H]^+$ 415.1 m/z ; HRMS $[M+H]^+$ 415.1264 m/z , found 415.1275 m/z ; 1H NMR (400 MHz, DMSO) δ_H 10.89 (s, 1H), 8.00 – 7.90 (m, 3H), 7.73 (d, J = 8.5 Hz, 1H), 7.67 – 7.48 (m, 5H), 7.28 – 7.23 (m, 2H), 6.98 – 6.87 (m, 3H), 5.31 (s, 2H); ^{19}F NMR (376 MHz, CDCl₃) δ_F -58.47; ^{13}C NMR (101 MHz, DMSO) δ_C 168.9, 167.8, 158.2, 142.4, 137.9 – 137.7 (m, peaks too undefined, q expected), 135.5, 135.4, 130.4, 129.5 (2C), 128.7, 127.9, 127.8, 127.1 (q, J_{C-F} = 4.8 Hz), 127.9 – 119.7 (m, peaks too undefined, q expected), 120.9, 120.7 – 119.6 (m, peaks too undefined, q expected), 119.4, 118.5, 114.8 (2C), 67.0.

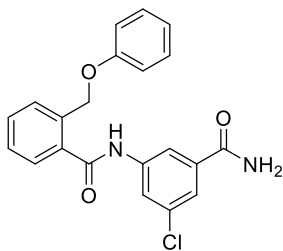
N-(3-Carbamoyl-4-fluorophenyl)-2-(phenoxyethyl)benzamide (5.039)



To obtain the title compound 5-amino-2-fluorobenzamide (300 mg, 2.0 mmol) and 2-(phenoxyethyl)benzoic acid (456 mg, 2.0 mmol) were used following General Procedure C. The title compound was obtained as an off white solid (545 mg, 75 %). HPLC – t_R 5.45 min > 99 % purity at 254 nm; LRMS $[M+H]^+$ 365.1 m/z ; HRMS $[M+H]^+$ 365.1296 m/z , found 365.1310 m/z ; 1H NMR (400 MHz, MeOD) δ_H 8.05 (dd, J = 6.5, 2.8 Hz, 1H), 7.88 – 7.83 (m, 1H), 7.67 – 7.62 (m, 2H), 7.57 – 7.46 (m, 2H), 7.25 – 7.16 (m, 3H), 6.96

– 6.88 (m, 3H), 5.32 (s, 2H). ^{13}C NMR (101 MHz, MeOD) δ_{C} 170.5, 168.1 (d, $J_{\text{C-F}} = 1.8$ Hz), 160.0, 158.1 (d, $J_{\text{C-F}} = 247.5$ Hz), 137.1, 137.0, 136.4 (d, $J_{\text{C-F}} = 2.9$ Hz), 131.5, 130.4 (2C), 130.0, 129.2, 128.7, 126.6 (d, $J_{\text{C-F}} = 8.8$ Hz), 123.8 (d, $J = 1.6$ Hz), 123.5 (d, $J_{\text{C-F}} = 14.6$ Hz), 122.1, 117.5 (d, $J_{\text{C-F}} = 24.9$ Hz), 116.0 (2C), 68.9.

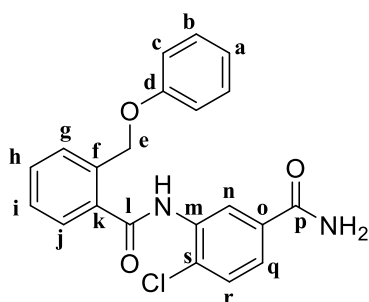
***N*-(3-Carbamoyl-5-chlorophenyl)-2-(phenoxyethyl)benzamide (5.040)**



The title compound was obtained first by converting (phenoxyethyl)benzoic acid (200 mg, 0.88 mmol) into an acid halide following General Procedure C. The acid chloride was then added to a mixture of 3-amino-5-chlorobenzamide (207 mg, 1.2 mmol) following General Procedure C to afford the title compound as a white solid (200 mg, 60 %). HPLC – t_{R} 5.89 min > 99 % purity at 254 nm; LRMS $[\text{M}+\text{H}]^+$ 380.9

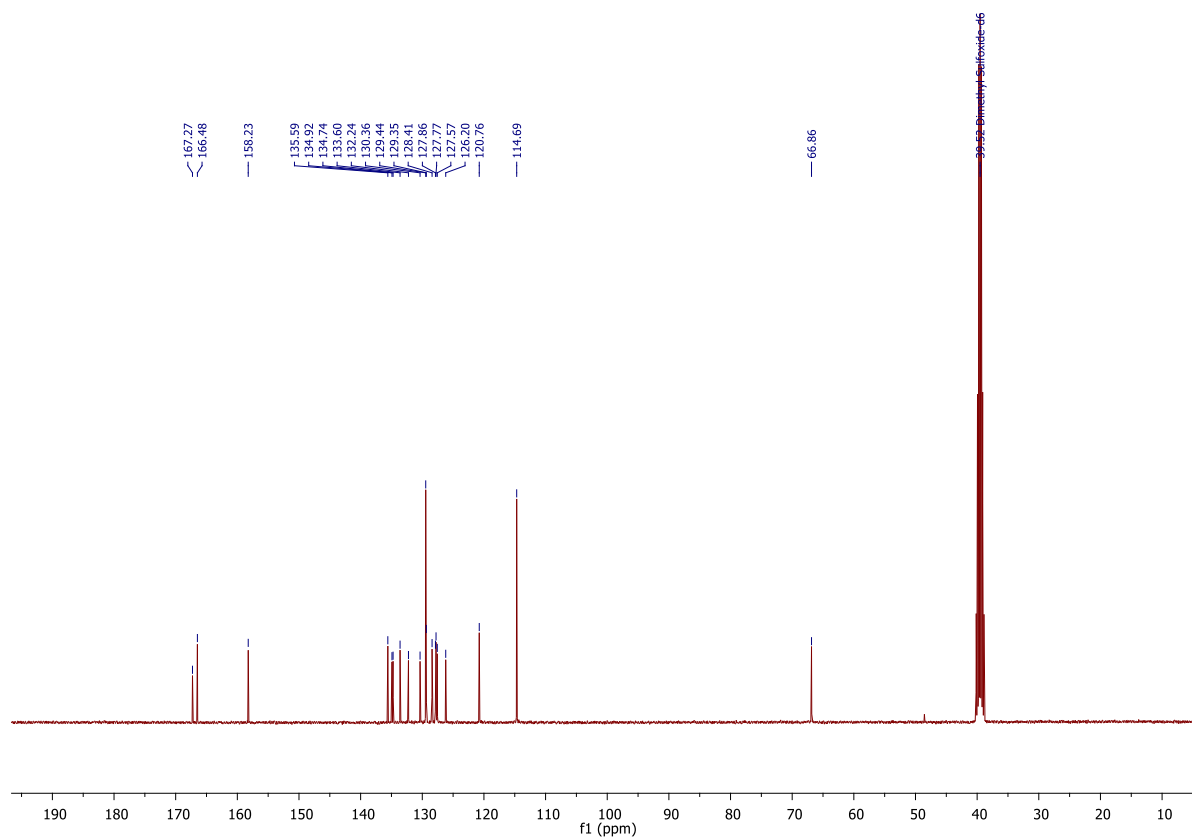
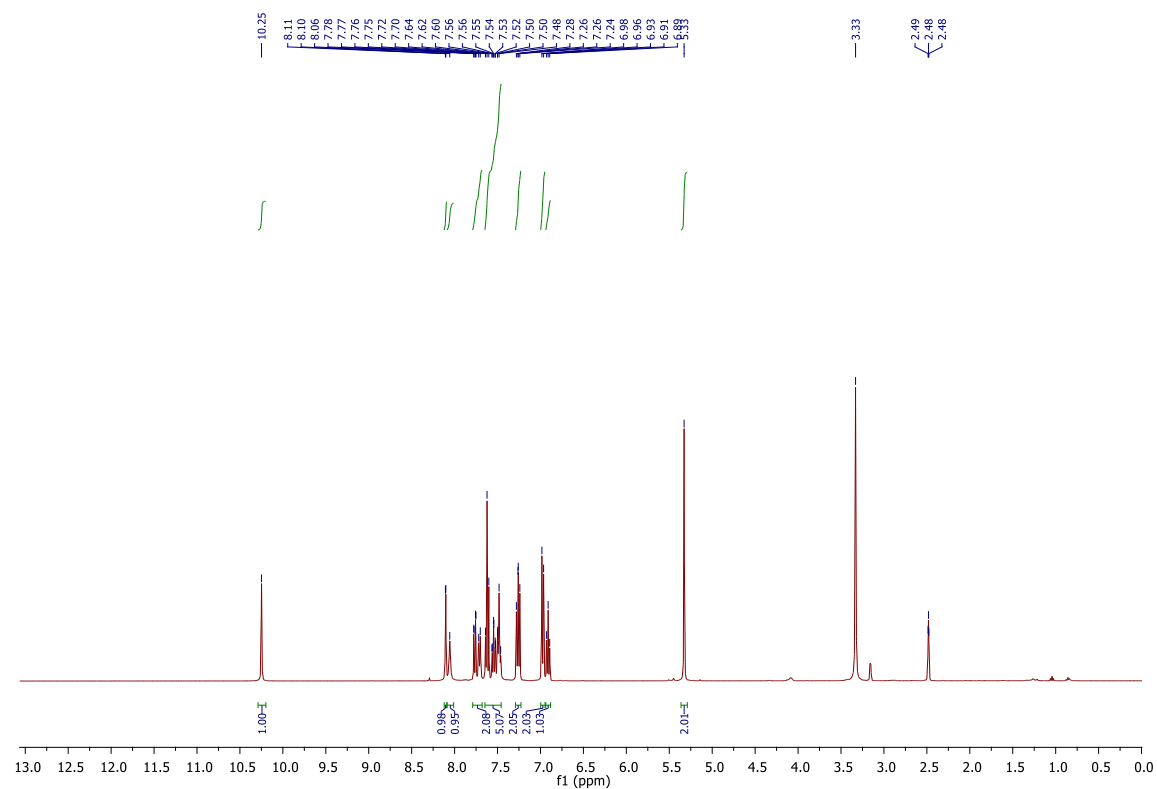
m/z ; HRMS $[\text{M}+\text{H}]^+$ 381.1000 m/z , found 381.1007 m/z ; ^1H NMR (400 MHz, MeOD) δ_{H} 7.99 – 7.96 (m, 2H), 7.67 – 7.61 (m, 3H), 7.55 (td, $J = 7.5, 1.4$ Hz, 1H), 7.48 (td, $J = 7.5, 1.1$ Hz, 1H), 7.24 – 7.19 (m, 2H), 6.95 – 6.88 (m, 3H), 5.32 (s, 2H); ^1H NMR (400 MHz, DMSO) δ_{H} 10.69 (s, 1H), 8.10 – 7.94 (m, 3H), 7.63 – 7.58 (m, 3H), 7.55 – 7.43 (m, 3H), 7.24 – 7.18 (m, 2H), 6.91 – 6.85 (m, 3H), 5.26 (s, 2H); ^{13}C NMR (101 MHz, DMSO) δ_{C} 167.5, 166.4, 158.2, 140.5, 136.7, 135.5, 135.4, 132.8, 130.3, 129.4 (2C), 128.5, 127.8, 127.8, 121.9, 121.7, 120.8, 118.1, 114.7 (2C), 67.0.

***N*-(5-Carbamoyl-2-chlorophenyl)-2-(phenoxyethyl)benzamide (5.041)**

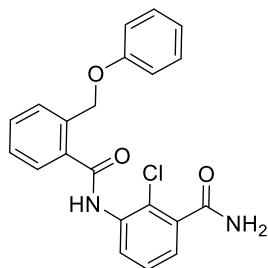


To obtain the title compound 3-amino-4-chlorobenzamide (225 mg, 1.3 mmol) and 2-(phenoxyethyl)benzoic acid (300 eq, 1.3 mmol) were used following General Procedure C. The title compound was obtained as a pale yellow solid (312 mg, 63 %). HPLC – t_{R} 5.72 min > 99 % purity at 254 nm; LRMS $[\text{M}+\text{H}]^+$ 381.1 m/z ; HRMS $[\text{M}+\text{H}]^+$ 381.1000 m/z , found 381.1010 m/z ; ^1H NMR (400 MHz, DMSO) δ_{H} 10.25 (s, 1H, NH), 8.10 (d, $J = 2.0$ Hz, 1H, Hn), 8.06 (br s, 1H, NH of NH₂), 7.78 – 7.69 (m, 2H, Hj,q), 7.65 – 7.45 (m, 5H, Hg,h,i,r, NH of NH₂), 7.29 – 7.22 (m, 2H, Hb), 7.00 – 6.95 (m, 2H, Hc), 6.93 – 6.88 (m, 1H, Ha), 5.33 (s, 2H, He); ^{13}C NMR (101 MHz, DMSO) δ_{C} 167.3 (Cl), 166.5 (Cp), 158.2 (Cd), 135.6 (Ck), 134.9 (Cm), 134.7 (Co), 133.6 (Cf), 132.2 (Ch), 130.4 (Cr), 129.4 (2C, Cb), 129.4 (Cs), 128.4 (Cg/i/j), 127.9 (Cg/j/i), 127.8 (Cg/j/i), 127.6 (Cq), 126.2 (Cn), 120.8 (Ca), 114.7 (2C, Cc), 66.9 (Ce).

Example spectra for *N*-(5-Carbamoyl-2-chlorophenyl)-2-(phenoxyethyl)benzamide (5.041): ^1H (400 MHz, DMSO) and ^{13}C NMR (100 MHz, DMSO)

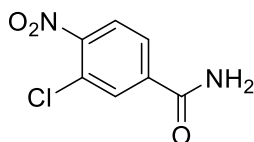


***N*-(3-Carbamoyl-2-chlorophenyl)-2-(phenoxyethyl)benzamide (5.042)**



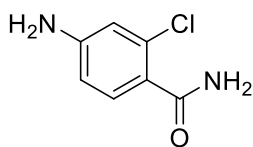
To obtain the title compound 3-amino-2-chlorobenzamide (225 mg, 1.3 mmol) and 2-(phenoxyethyl)benzoic acid (300 mg, 1.3 mmol) were used following General Procedure C. The title compound was obtained as a solid. (325 mg, 66 %). HPLC – t_R 5.40 min > 99 % purity at 254 nm; LRMS $[M+H]^+$ 381.1 m/z ; HRMS $[M+H]^+$ 381.1000 m/z , found 381.1007 m/z ; 1H NMR (400 MHz, DMSO) δ_H 10.17 (s, 1H), 7.90 (s, 1H), 7.71 – 7.45 (m, 6H), 7.36 (t, J = 7.7 Hz, 1H), 7.31 – 7.24 (m, 3H), 7.00 – 6.90 (m, 3H), 5.32 (s, 2H); ^{13}C NMR (101 MHz, DMSO) δ_C 168.0, 167.3, 158.3, 138.4, 135.4, 135.2, 135.2, 130.2, 129.5 (2C), 128.5, 128.4, 127.8, 127.8, 126.8, 125.6, 125.6, 120.8, 114.6 (2C), 66.9.

3-Chloro-4-nitrobenzamide (5.045)⁹⁴



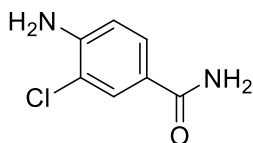
The known title compound was obtained following General Procedure F using 3-chloro-4-nitrobenzoic acid (1.0 g, 5.0 mmol) to form the acid halide intermediate. The solution was concentrated *in vacuo*, taken up in EtOAc and cooled to 0°C. Ammonium hydroxide (10 mL) was added dropwise to the solution and allowed to stir for 1 h. Upon completion the reaction mixture was washed with brine and the organic layers were dried over MgSO₄, filtered and concentrated to give the title compound as a solid. (980 mg, 98 %).¹³¹ HPLC – t_R 3.85 min > 99 % purity at 254 nm; LRMS $[M+H]^+$ 198.9 m/z ; 1H NMR (400 MHz, MeOD) δ_H 8.15 (d, J = 1.5 Hz, 1H), 8.04 – 7.97 (m, 2H); 1H NMR (400 MHz, DMSO) δ_H 8.23 – 7.96 (m, 3H), 6.67 (bs, 2H); ^{13}C NMR (101 MHz, DMSO) δ_C 164.9, 148.9, 138.9, 130.4, 127.6, 125.7, 124.9.

4-Amino-2-chlorobenzamide (5.046)⁹⁵



The known title compound was obtained using 2-chloro-4-nitrobenzamide (1.0 g, 5.0 mmol) following General Procedure A, affording the title compound as a pale orange solid (800 mg, 94 %). HPLC – t_R 1.46 min > 99 % purity at 254 nm; LRMS $[M+H]^+$ 171.0 m/z ; 1H NMR (400 MHz, MeOD) δ_H 7.38 (d, J = 8.4 Hz, 1H), 6.70 (d, J = 2.2 Hz, 1H), 6.59 (dd, J = 8.5, 2.2 Hz, 1H); ^{13}C NMR (101 MHz, MeOD) δ_H 172.4, 153.1, 133.5, 132.2, 123.0, 116.0, 113.5.

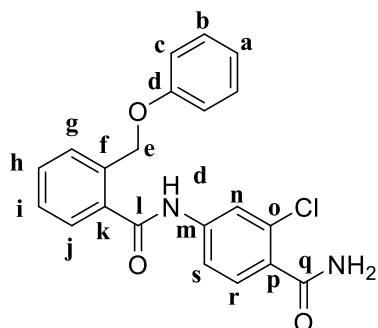
4-Amino-3-chlorobenzamide (5.047)⁹⁶



The known title compound obtained following General Procedure A using 3-chloro-4-nitrobenzamide (250 mg, 1.3 mmol). The title compound was obtained as a solid (160 mg, 72 %). HPLC – t_R 2.46 min > 99 % purity at 254 nm; LRMS $[M+H]^+$ 171.1 m/z ; 1H NMR (400 MHz, MeOD) δ_H 7.83 (dd, J = 10.4, 2.1 Hz, 1H), 7.61

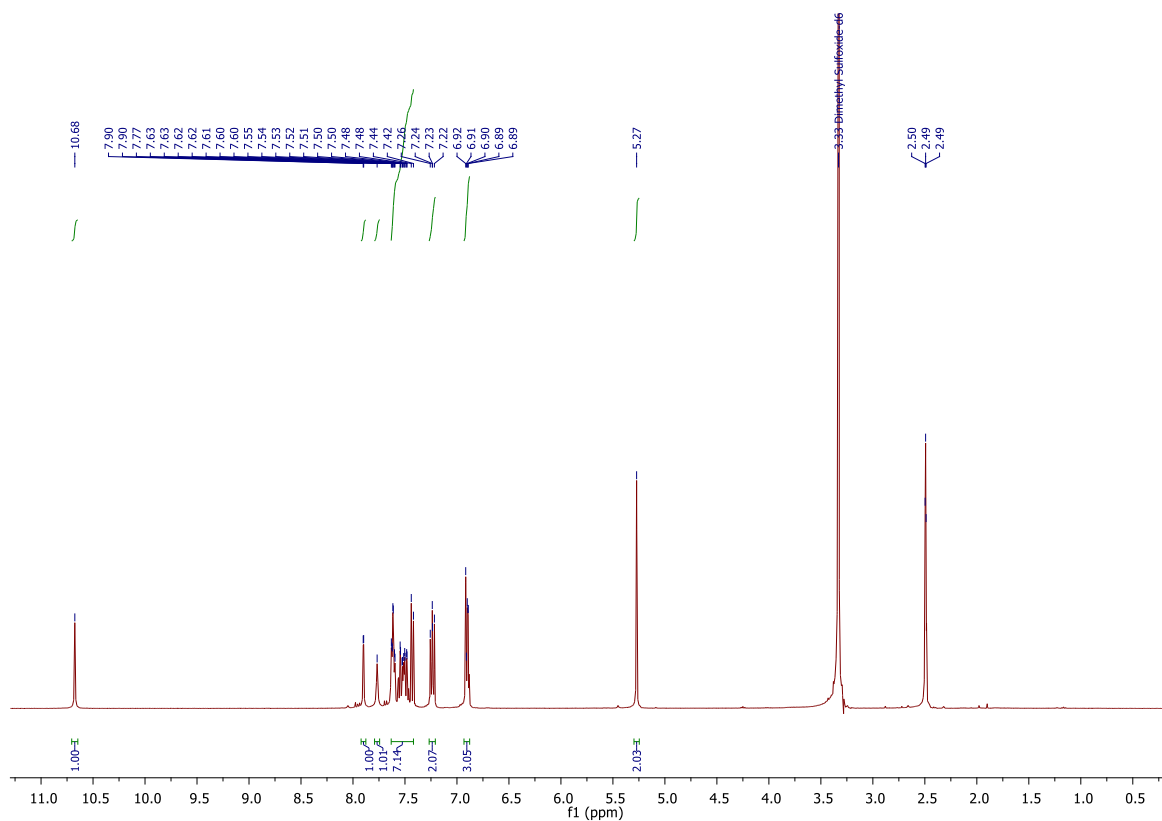
(dd, $J = 8.5, 2.1$ Hz, 1H), 6.82 (dd, $J = 8.4, 4.2$ Hz, 1H); ^{13}C NMR (101 MHz, MeOD) δ_{C} 171.4, 149.2, 130.3, 128.7, 123.4, 118.7, 115.5

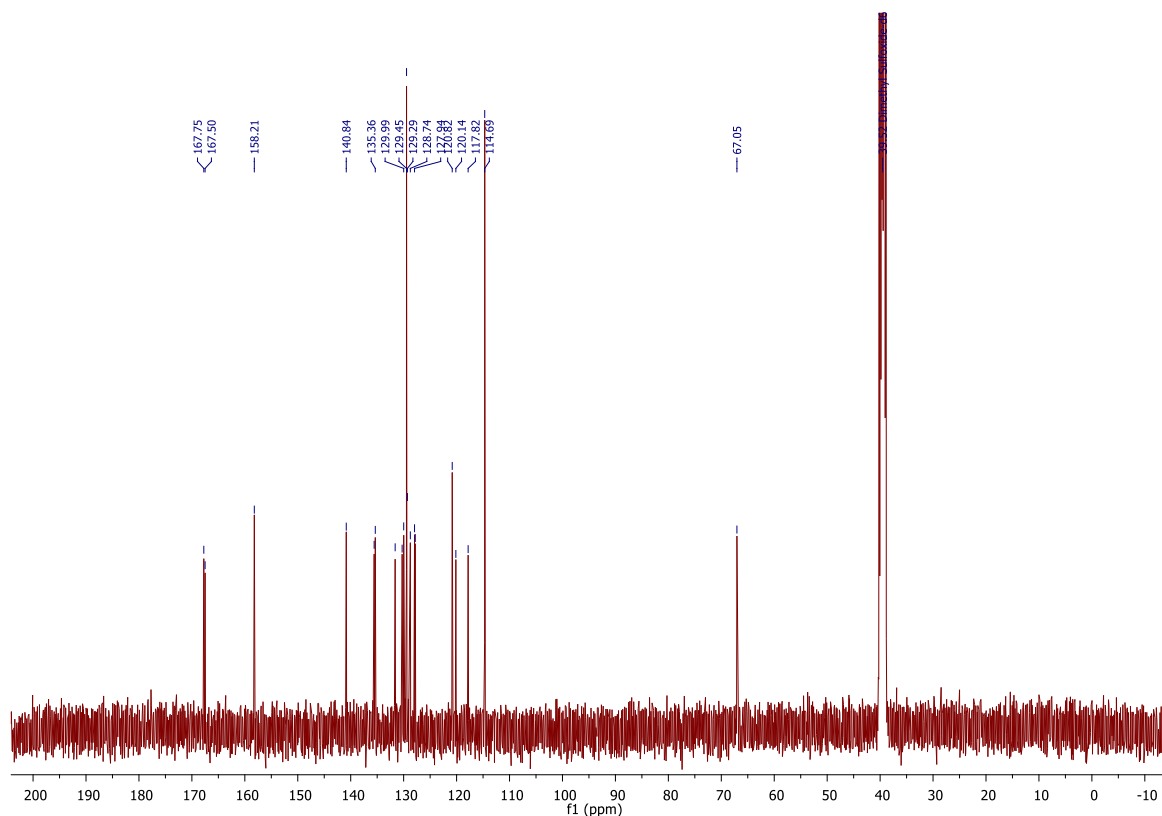
***N*-(4-carbamoyl-3-chlorophenyl)-2-(phenoxyethyl)benzamide (5.050)**



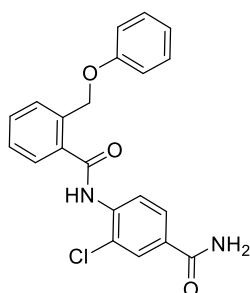
The title compound was obtained using 2-(phenoxyethyl)benzoic acid (200 mg, 0.88 mmol) and 4-amino-2-chlorobenzamide (181 mg, 0.88 mmol) following General Procedure C. The title compound was produced as a white solid (166 mg, 50 %). HPLC – t_{R} 5.64 min > 99 % purity at 254 nm; LRMS $[\text{M}+\text{H}]^+$ 381.0 m/z ; HRMS $[\text{M}+\text{H}]^+$ 381.1000 m/z , found 381.1013 m/z ; ^1H NMR (400 MHz, DMSO) δ_{H} 10.68 (s, 1H, NH), 7.90 (d, $J = 1.7$ Hz, 1H, Hr), 7.77 (br s, 1H, NH of NH_2), 7.64 – 7.41 (m, 7H, Hg,h,i,j,n,s NH of NH_2), 7.26 – 7.21 (m, 2H, Hb), 6.93 – 6.88 (m, 3H, Ha,c), 5.27 (s, 2H, He); ^{13}C NMR (101 MHz, DMSO) δ_{C} 167.8 (Cl), 167.5 (Cq), 158.2 (Cd), 140.8 (Ck), 135.6 (Cm), 135.4 (Co), 131.6 (Cf), 130.3 (Ch/p), 130.0 (Ch/p), 129.5 (2C, Cb), 129.3 (Cg/i/j), 128.7 (Cg/i/j), 127.9 (Cg/i/j), 127.8 (Cr), 120.8 (Ca/n), 120.1 (Ca/n), 117.8 (Cs), 114.7 (2C, Cc), 67.1 (Ce).

Example spectra for *N*-(4-carbamoyl-3-chlorophenyl)-2-(phenoxyethyl)benzamide (5.050): ^1H (400 MHz, DMSO) and ^{13}C NMR (100 MHz, DMSO)



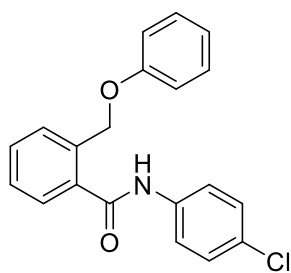


***N*-(4-Carbamoyl-2-chlorophenyl)-2-(phenoxyethyl)benzamide (5.051)**



To obtain the title compound 4-amino-3-chlorobenzamide (225 mg, 1.3 mmol) and 2-(phenoxyethyl)benzoic acid (300 mg, 1.3 mmol) were used following General Procedure C. The title compound was obtained as a yellow solid (300 mg, 61 %). HPLC – t_R 5.50 min > 99 % purity at 254 nm; LRMS $[M+H]^+$ 381.1 m/z , $[M+Na]^+$ 403.1; HRMS $[M+H]^+$ 381.1000 m/z , found 381.1014 m/z ; 1H NMR (400 MHz, DMSO) δ_H 10.63 (s, 1H), 7.88 – 7.81 (m, 2H), 7.73 (dd, J = 8.8, 2.5 Hz, 1H), 7.64 – 7.40 (m, 6H), 7.27 – 7.20 (m, 2H), 6.94 – 6.88 (m, 3H), 5.28 (s, 2H); ^{13}C NMR (101 MHz, DMSO) δ_C 168.0, 167.3, 158.2, 138.0, 137.4, 135.6, 135.4, 130.2, 129.7, 129.5 (2C), 128.6, 127.9, 127.7, 123.6, 121.5, 120.8, 119.5, 114.7 (2C), 67.0. M.p. 127.1–134.4°C.

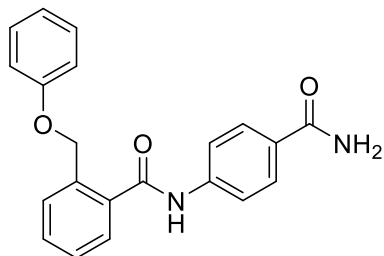
***N*-(4-Chlorophenyl)-2-(phenoxyethyl)benzamide (5.052)**



The title compound was obtained using 2-(phenoxyethyl)benzoic acid (300 mg, 1.3 mmol) and 4-chloroaniline (168 mg, 1.3 mmol) following General Procedure C. The title compound was produced as a white solid (359 mg, 82 %). HPLC – t_R 6.79 min > 99 % purity at 254 nm; LRMS $[M+H]^+$ 338.1 m/z ; HRMS $[M+H]^+$ 338.0942 m/z , found 338.0944 m/z ; 1H NMR (400 MHz, MeOD) δ_H 7.66 – 7.60 (m, 4H, Hg,j,n), 7.53 (td, J = 7.5, 1.4 Hz, 1H, Hh), 7.46 (td, J = 7.5, 1.0 Hz, 1H, Hi), 7.34 – 7.29 (m, 2H, Ho), 7.25 – 7.19 (m, 2H, Hb), 6.95 – 6.88 (m, 3H, Ha,c), 5.30 (s, 2H, He); ^{13}C NMR (101 MHz, MeOD) δ_C 176.7 (Cl), 167.7 (Cd),

147.6 (Ck), 145.3 (Cm), 144.8 (Cf), 139.5 (Cp), 138.9 (2C, Cb), 138.0 (Ch), 137.9 (2C, Co), 137.3, (Cg/i/j), 137.2 (Cg/i/j), 136.7, 130.8, 130.2, 124.2 (2C), 76.5.

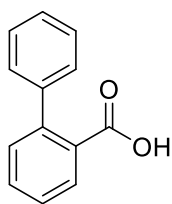
***N*-(4-Carbamoylphenyl)-2-(phenoxymethyl)benzamide (5.053)**



The title compound was obtained following General Procedure B using 2-(phenoxymethyl)benzoic acid (228 mg, 1.0 mmol) and 4-aminobenzamide (136 mg, 1.0 mmol). The title compound was obtained as a white solid (128 mg, 37 %). HPLC – t_R 5.05 min > 99 % purity at 254 nm; LRMS $[M+H]^+$ 347.1 m/z ; HRMS $[M+H]^+$ 347.1390 m/z , found 347.1399 m/z ; 1H NMR (400 MHz, DMSO) δ

10.55 (s, 1H), 7.83 – 7.75 (m, 3H), 7.69 (d, J = 8.6 Hz, 2H), 7.54 (d, J = 8.4 Hz, 2H), 7.48 – 7.38 (m, 2H), 7.19 – 7.11 (m, 3H), 6.86 – 6.79 (m, 3H), 5.20 (s, 2H); ^{13}C NMR (101 MHz, DMSO) δ_C 167.5, 167.5, 158.3, 141.9, 135.9, 135.4, 130.2, 129.5 (2C), 129.1, 128.7, 128.3, 128.0, 127.9, 120.9, 119.0, 114.8 (2C), 67.1.

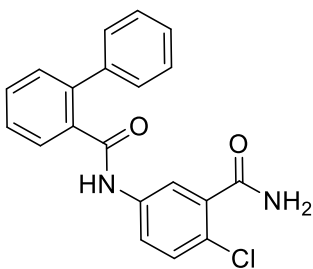
[1,1'-Biphenyl]-2-carboxylic acid (5.055)⁹⁷



The known title compound was obtained using methyl [1,1'-biphenyl]-2-carboxylate (540 mg, 2.5 mmol) following General Procedure E. The title compound was obtained as a white solid. (495 mg, 99 %). HPLC – t_R 4.78 min > 96 % purity at 254 nm; LRMS $[M+H]^+$ 199.1 m/z ; 1H NMR (400 MHz, $CDCl_3$) δ_H 7.95 (dd, J = 7.8, 1.2 Hz, 1H), 7.56 (td, J = 7.6, 1.4 Hz, 1H), 7.45 – 7.32 (m, 7H); ^{13}C NMR (101 MHz, $CDCl_3$) δ_C 172.9,

143.5, 141.2, 132.2, 131.3, 130.8, 129.5, 128.6 (2C), 128.2 (2C), 127.5, 127.3.⁹⁷

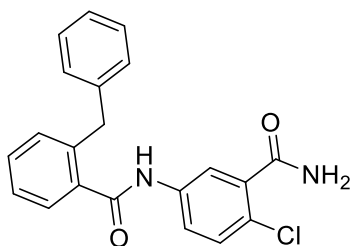
***N*-(3-Carbamoyl-4-chlorophenyl)-[1,1'-biphenyl]-2-carboxamide (5.056)**



The title compound was obtained following General Procedure B using [1,1'-biphenyl]-2-carboxylic acid (100 mg, 0.5 mmol) and 5-amino-2-chlorobenzamide (90 mg, 0.5 mmol). The title compound was afforded as a white solid (51 mg, 29 %). HPLC – t_R 4.81 min > 99 % purity at 254 nm; LRMS $[M+H]^+$ 351.1 m/z ; HRMS $[M+H]^+$ 351.0895 m/z , found 351.0899 m/z ; 1H NMR (400 MHz, MeOD) δ 7.65 – 7.55 (m, 3H), 7.53 –

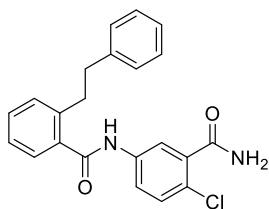
7.28 (m, 9H); ^{13}C NMR (101 MHz, MeOD) δ_C 171.9, 171.4, 141.5, 141.5, 138.7, 137.6, 137.5, 131.5, 131.4, 131.3, 129.7 (2C), 129.5 (2C), 128.9, 128.6, 128.5, 126.5, 123.6, 121.4.

2-Benzyl-*N*-(3-carbamoyl-4-chlorophenyl)benzamide (5.063)



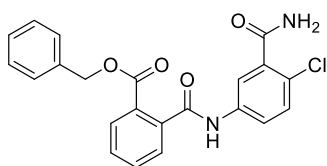
The title compound was obtained using 2-benzylbenzoic acid (300 mg, 1.4 mmol) and 5-amino-2-chlorobenzamide (240 mg, 1.4 mmol) following General Procedure C. The title compound was produced as a white solid (160 mg, 31 %). HPLC – t_R 5.49 min > 99 % purity at 254 nm; LRMS $[M+H]^+$ 365.1 m/z ; HRMS $[M+H]^+$ 365.1051 m/z , found 365.1059 m/z ; 1H NMR (400 MHz, MeOD) δ_H 7.77 (d, J = 2.5 Hz, 1H), 7.63 (dd, J = 8.7, 2.6 Hz, 1H), 7.50 – 7.41 (m, 3H), 7.37 – 7.31 (m, 2H), 7.22 – 7.10 (m, 5H), 4.21 (s, 2H); ^{13}C NMR (101 MHz, MeOD) δ_C 172.0 171.3, 142.0, 140.7, 138.8, 138.0, 137.5, 131.9, 131.4 (2C), 130.1 (2C), 129.4 (2C), 128.4, 127.5, 127.1, 126.6, 124.0, 121.8, 39.9.

N-(3-Carbamoyl-4-chlorophenyl)-2-phenethylbenzamide (5.064)



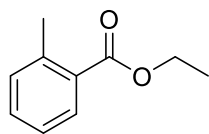
The title compound was obtained using 2-bibenzylcarboxylic acid (300 mg, 1.3 mmol) following General Procedure C. The title compound was obtained as a solid. (261 mg, 53 %). HPLC – t_R 5.84 min > 99 % purity at 254 nm; LRMS $[M+H]^+$ 379.1 m/z ; HRMS $[M+H]^+$ 379.1208 m/z , found 379.1218 m/z ; 1H NMR (400 MHz, MeOD) δ_H 7.91 (d, J = 2.5 Hz, 1H), 7.76 (dd, J = 8.7, 2.6 Hz, 1H), 7.50 – 7.39 (m, 3H), 7.35 – 7.29 (m, 2H), 7.23 – 7.18 (m, 2H), 7.16 – 7.10 (m, 3H), 3.13 – 3.08 (m, 2H), 2.94 – 2.90 (m, 2H); ^{13}C NMR (101 MHz, MeOD) δ_C 172.0, 171.3, 142.9, 141.1, 139.1, 137.7, 137.7, 131.5, 131.5, 131.3, 129.5 (2C), 129.3 (2C), 128.3, 127.2, 127.0, 126.6, 123.8, 121.6, 39.0, 36.7.

Benzyl 2-((3-carbamoyl-4-chlorophenyl)carbamoyl)benzoate (5.065)



To obtain the title compound 5-amino-2-chlorobenzamide (200 mg, 1.2 mmol) and 2-((benzyloxy)carbonyl)benzoic acid (300 mg, 1.2 mmol) were used following General Procedure C. The title compound was obtained as an orange solid (300 mg, 61 %). HPLC – t_R 5.22 min > 99 % purity at 254 nm; LRMS $[M+Na]^+$ 431.0 m/z ; HRMS $[M+H]^+$ 409.0950 m/z , found 409.0955 m/z ; 1H NMR (400 MHz, DMSO) δ_H 10.65 (s, 1H), 7.94 – 7.88 (m, 2H), 7.81 (d, J = 2.5 Hz, 1H), 7.75 – 7.60 (m, 5H), 7.43 (d, J = 8.7 Hz, 1H), 7.38 – 7.34 (m, 2H), 7.31 – 7.26 (m, 3H), 5.25 (s, 2H); ^{13}C NMR (101 MHz, DMSO) δ_C 168.0, 167.0, 165.9, 138.2, 138.1, 137.4, 135.5, 132.2, 129.9, 129.7, 129.5, 128.9, 128.3 (2C), 128.0, 128.0 (2C), 127.9, 123.3, 121.1, 119.2, 66.7.

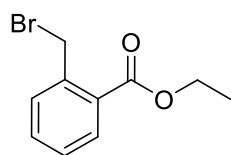
Ethyl 2-methylbenzoate (5.067)⁹⁸



A catalytic amount of H₂SO₄ was added to a mixture of 2-methylbenzoic acid (1.0 g, 7.3 mmol) and EtOH (10 mL). The mixture was heated to reflux overnight. The reaction mixture was cooled, neutralized with Na₂CO₃ and extracted with DCM.

The organic layers were collected, dried over MgSO₄ filtered and concentrated *in vacuo* to afford the known title compound as an oil. (1.15 mL, 99 %). HPLC – *t*_R 5.95 min > 99 % purity at 254 nm; ¹H NMR (401 MHz, CDCl₃) δ_H 7.93 – 7.90 (m, 1H), 7.39 – 7.34 (m, 1H), 7.25 – 7.19 (m, 2H), 4.35 (q, *J* = 7.1 Hz, 2H), 2.61 (s, 3H), 1.38 (t, *J* = 7.1 Hz, 3H); ¹³C NMR (101 MHz, CDCl₃) δ_C 167.8, 140.1, 131.9, 131.7, 130.6, 130.1, 125.8, 60.8, 21.8, 14.4. Acquired data is consistent with the literature.⁹⁸

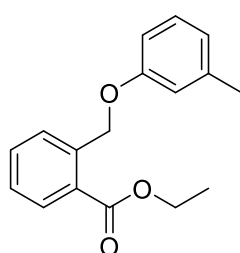
Ethyl 2-(bromomethyl)benzoate (5.068)⁶⁰



To a solution of ethyl 2-methylbenzoate (1.9 mL) in ACN (5 mL) was added NBS (2.35 g, 14 mmol) and AIBN (100 mg, 0.61 mmol). The closed vial was evacuated and backfilled with nitrogen. The mixture was heated to 90°C using microwave

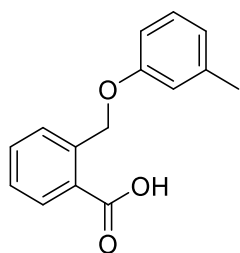
irradiation over 15 min. The mixture was cooled and concentrated *in vacuo*, filtered with DCM via suction filtration to remove the NBS and the filtrate was collected and concentrated. The crude material was purified via column chromatography (eluent: Petroleum ether: Ethyl acetate, 90:30) to afford the known title compound as an oil (1.7 mL, 88 %).⁶⁰ LRMS [M+H]⁺ 244.1 *m/z*; ¹H NMR (400 MHz, CDCl₃) δ_H 7.94 – 7.89 (m, 1H), 7.41 – 7.36 (m, 1H), 7.26 – 7.21 (m, 2H), 4.36 (q, *J* = 7.1 Hz, 2H), 2.60 (s, 3H), 1.39 (t, *J* = 7.1 Hz, 3H); ¹³C NMR (101 MHz, MeOD) δ_C 169.3, 140.9, 133.0, 132.6, 131.3, 129.6, 126.8, 61.9, 21.7, 14.6. Acquired data is consistent with the literature.⁶⁰

Ethyl 2-((*m*-tolylloxy)methyl)benzoate (5.069)⁹⁹



To a solution of ethyl 2-(bromomethyl)benzoate (1.1 mL) was added *m*-cresol (0.7 mL) following General Procedure D to afford the title compound as a white solid. The known title compound was used directly in the next step without further purification or complete characterization. (1.0 g, 56 %). LRMS [M+H]⁺ 271.1 *m/z*, [M+Na]⁺ 293.1 *m/z*.

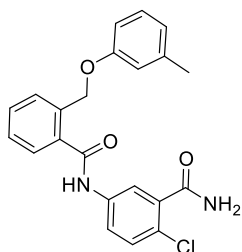
2-((*m*-Tolylloxy)methyl)benzoic acid (5.070)¹⁰⁰



To obtain the title compound ethyl 2-((*m*-tolylloxy)methyl)benzoate (1.0 g, 3.7 mmol) was refluxed in 10 % NaOH aq solution following General Procedure E. The known title compound was obtained as a white solid (711 mg, 79 %). LRMS [M+H]⁺ 244.0 *m/z*, [M+Na]⁺ 265.1 *m/z*; ¹H NMR (400 MHz, MeOD) δ_H 8.03 (dd, *J* = 7.8, 1.3 Hz, 1H), 7.76 – 7.71 (m, 1H), 7.58 (td, *J* = 7.6, 1.4 Hz, 1H), 7.44 – 7.39 (m, 1H), 7.15 (t, *J* = 7.9 Hz, 1H), 6.84 – 6.81 (m, 1H), 6.79 – 6.75 (m,

2H), 5.46 (s, 2H), 2.32 (s, 3H); ^{13}C NMR (101 MHz, MeOD) δ_{C} 170.5, 160.3, 140.8, 140.6, 133.3, 131.9, 130.2, 130.2, 128.7, 128.4, 122.7, 116.6, 112.8, 69.2, 21.5.

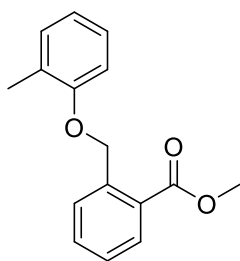
***N*-(3-Carbamoyl-4-chlorophenyl)-2-((*m*-tolylloxy)methyl)benzamide (5.072)**



To obtain the title compound 5-amino-2-chlorobenzamide (120 mg, 0.7 mmol) and 2-((*m*-tolylloxy)methyl)benzoic acid (170 mg, 0.7 mmol) were used following General Procedure C. The title compound was obtained as a pale-yellow solid (155 mg, 56 %). HPLC – t_{R} 5.80 min > 99 % purity at 254 nm; LRMS $[\text{M}+\text{H}]^+$ 395.1 m/z ; HRMS $[\text{M}+\text{H}]^+$ 395.1157 m/z , found 395.1170 m/z ;

^1H NMR (400 MHz, MeOD) δ_{H} 7.85 (d, $J = 2.5$ Hz, 1H), 7.70 (dd, $J = 8.7, 2.5$ Hz, 1H), 7.65 – 7.60 (m, 2H), 7.53 (dt, $J = 7.6, 3.8$ Hz, 1H), 7.49 – 7.45 (m, 1H), 7.42 (d, $J = 8.7$ Hz, 1H), 7.11 – 7.06 (m, 1H), 6.75 – 6.71 (m, 3H), 5.28 (s, 2H), 2.25 (s, 3H); ^{13}C NMR (101 MHz, MeOD) δ_{C} 171.9, 170.6, 160.0, 140.6, 138.9, 137.5, 137.1, 137.1, 131.6, 131.4, 130.2, 130.1, 129.2, 128.7, 126.7, 124.0, 122.9, 121.8, 116.7, 112.8, 68.9, 21.5.

Methyl 2-((*o*-tolylloxy)methyl)benzoate (5.074)¹⁰¹

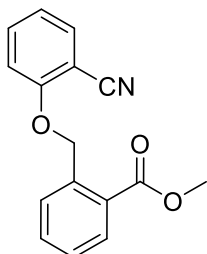


The title compound was obtained following General Procedure D using *o*-cresol (0.10 mL, 1.0 mmol) and methyl 2-(bromomethyl)benzoate (227 mg, 1.0 mmol).

The known title compound was obtained as a solid (205 mg, 80 %). HPLC – t_{R} 6.99 min > 99 % purity at 254 nm; LRMS $[\text{M}+\text{H}]^+$ 257.1 m/z ; ^1H NMR (400 MHz, MeOD) δ_{H} 7.99 (dd, $J = 7.7, 1.2$ Hz, 1H), 7.76 (d, $J = 7.7$ Hz, 1H), 7.60 (td, $J = 7.6, 1.2$ Hz, 1H), 7.44 (t, $J = 7.5$ Hz, 1H), 7.18 – 7.10 (m, 2H), 6.93 –

6.83 (m, 2H), 5.45 (s, 2H), 3.87 (s, 3H), 2.27 (s, 3H); ^1H NMR (400 MHz, CDCl_3) δ_{H} 8.03 (d, $J = 7.6$ Hz, 1H), 7.82 (d, $J = 8.1$ Hz, 1H), 7.60 – 7.51 (m, 1H), 7.40 – 7.31 (m, 2H), 7.19 – 7.11 (m, 1H), 7.00 – 6.85 (m, 2H), 5.50 (s, 2H), 3.90 (s, 3H), 2.34 (s, 3H); ^{13}C NMR (101 MHz, CDCl_3) δ_{C} 167.6, 156.9, 140.3, 132.8, 130.9, 130.8, 127.8, 127.3, 127.3, 127.0, 127.0, 120.7, 111.7, 68.2, 52.2, 16.6

Methyl 2-((2-cyanophenoxy)methyl)benzoate (5.075)¹⁰²

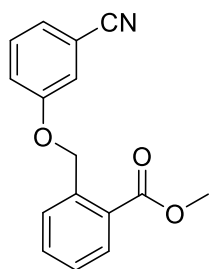


The title compound was obtained following General Procedure D using 2-cyanophenol (119 mg, 1.0 mmol) and methyl 2-(bromomethyl)benzoate (227 mg, 1.0 mmol). The known title compound was obtained as a solid (241 mg, 90 %).

HPLC – t_{R} 6.13 min > 90 % purity at 254 nm; LRMS $[\text{M}-\text{H}]^-$ 266.1 m/z ; ^1H NMR (400 MHz, DMSO) δ_{H} 7.95 – 7.93 (m, 1H), 7.77 – 7.65 (m, 4H), 7.51 (td, $J = 7.7, 1.6$ Hz, 1H), 7.28 (d, $J = 8.4$ Hz, 1H), 7.12 (td, $J = 7.6, 0.8$ Hz, 1H), 5.57 (s, 2H),

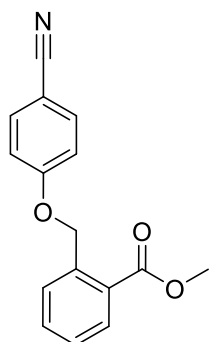
3.82 (s, 3H); ^{13}C NMR (101 MHz, DMSO) δ_{C} 167.0, 160.0, 137.0, 135.3, 133.9, 132.7, 130.6, 128.9, 128.6, 128.6, 121.6, 116.4, 113.5, 100.8, 68.8, 52.4. Acquired data is consistent with the literature.¹⁰²

Methyl 2-((3-cyanophenoxy)methyl)benzoate (5.076)



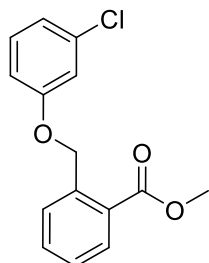
The title compound was obtained following General Procedure D using 3-cyanophenol (119 mg, 1.0 mmol) and methyl 2-(bromomethyl)benzoate (227 mg, 1.0 mmol). The title compound was obtained as a solid (241 mg, 90 %). LRMS $[M-H]^-$ 266.1 m/z ; 1H NMR (400 MHz, DMSO) δ_H 7.94 (s, 1H), 7.90 (d, $J = 7.6$ Hz, 1H), 7.64 – 7.58 (m, 2H), 7.51 – 7.44 (m, 2H), 7.42 – 7.38 (m, 1H), 7.34 – 7.29 (m, 1H), 5.45 (s, 2H), 3.78 (s, 3H).

Methyl 2-((4-cyanophenoxy)methyl)benzoate (5.077)

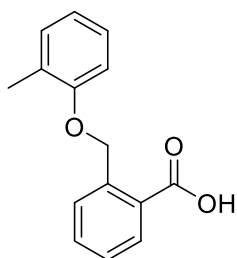


The title compound was obtained following General Procedure D using 4-cyanophenol (119 mg, 1.0 mmol) and methyl 2-(bromomethyl)benzoate (227 mg, 1.0 mmol). The title compound was obtained as a solid (245 mg, 92 %). HPLC – t_R 6.26 min > 99 % purity at 254 nm; LRMS $[M+H]^+$ 268.1 m/z , $[M+Na]^+$ 290.1 m/z ; 1H NMR (400 MHz, MeOD) δ_H 8.04 (dd, $J = 7.8, 1.2$ Hz, 1H), 7.73 – 7.69 (m, 3H), 7.63 (td, $J = 7.6, 1.3$ Hz, 1H), 7.51 – 7.46 (m, 1H), 7.19 – 7.15 (m, 2H), 5.59 (s, 2H), 3.91 (s, 3H); ^{13}C NMR (101 MHz, MeOD) δ_C 168.9, 163.7, 139.2, 135.3 (2C), 133.7, 131.8, 129.9, 129.2, 129.1, 120.0, 116.9 (2C), 105.1, 69.7, 52.6.

Methyl 2-((3-chlorophenoxy)methyl)benzoate (5.078)⁶⁸

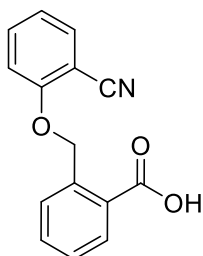


The known title compound was obtained following General Procedure D using 3-chlorophenol (387 mg, 3.0 mmol) and methyl 2-(bromomethyl)benzoate (681 mg, 3.0 mmol). The title compound was obtained as a white solid (700 mg, 84 %). HPLC – t_R 7.05 min > 99 % purity at 254 nm; LRMS $[M-H]^-$ 275.1 m/z ; 1H NMR (400 MHz, DMSO) δ_H 7.90 (d, $J = 7.6$ Hz, 1H), 7.65 – 7.60 (m, 2H), 7.50 – 7.45 (m, 1H), 7.31 (t, $J = 8.2$ Hz, 1H), 7.06 (t, $J = 2.2$ Hz, 1H), 7.00 (dd, $J = 7.9, 1.2$ Hz, 1H), 6.95 (dd, $J = 8.2, 2.2$ Hz, 1H), 5.42 (s, 2H), 3.80 (s, 3H); 1H NMR (400 MHz, MeOD) δ_H 8.01 (dd, $J = 7.8, 1.2$ Hz, 1H), 7.73 – 7.69 (m, 1H), 7.62 (td, $J = 7.6, 1.3$ Hz, 1H), 7.49 – 7.44 (m, 1H), 7.29 (t, $J = 8.2$ Hz, 1H), 7.03 (t, $J = 2.2$ Hz, 1H), 7.00 – 6.91 (m, 2H), 5.47 (s, 2H), 3.90 (s, 3H); ^{13}C NMR (101 MHz, MeOD) δ_C 169.0, 161.0, 139.7, 135.9, 133.5, 131.7, 131.6, 129.9, 129.1, 128.8, 122.1, 116.3, 114.4, 69.6, 52.7.⁶⁸

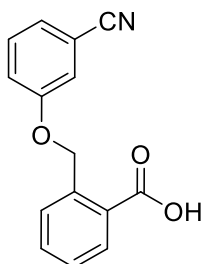
2-((*o*-Tolyloxy)methyl)benzoic acid (5.079)^{103, 104}

The known title compound was obtained following General Procedure E using methyl 2-((*o*-tolyloxy)methyl)benzoate (200 mg, 0.78 mmol) to afford the title compound as a white solid.¹⁰³ (175 mg, 93 %). HPLC – t_R 6.11 min > 99 % purity at 254 nm; LRMS $[M+H]^+$ 243.1 m/z , $[M+Na]^+$ 265.1 m/z ; 1H NMR (400 MHz, $CDCl_3$) δ 8.19 (d, J = 7.7 Hz, 1H), 7.89 (d, J = 7.8 Hz, 1H), 7.65 (t, J = 7.5 Hz, 1H), 7.44 (t, J = 7.6 Hz, 1H), 7.21 – 7.13 (m, 2H), 6.93 – 6.86 (m, 2H), 5.57 (s, 2H), 2.37 (s, 3H); ^{13}C NMR (101 MHz, $CDCl_3$) δ_C 172.3, 156.9, 141.3, 133.8, 131.8, 130.9, 127.4, 127.3, 127.1, 127.0, 126.4, 120.9, 111.9, 68.2, 16.6. Acquired data is consistent with the literature.^{103,}

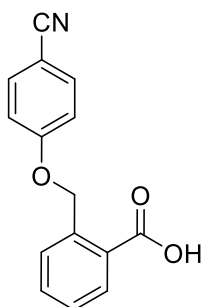
104

2-((2-Cyanophenoxy)methyl)benzoic acid (5.080)

The title compound was obtained following General Procedure G using methyl 2-((2-cyanophenoxy)methyl)benzoate (200 mg, 0.76 mmol). The title compound was obtained as a white solid (163 mg, 84 %). HPLC – t_R 4.72 min > 99 % purity at 254 nm; LRMS $[M+H]^+$ 255.1 m/z ; 1H NMR (400 MHz, MeOD) δ_H 8.06 (dd, J = 7.8, 1.2 Hz, 1H), 7.96 (d, J = 7.8 Hz, 1H), 7.84 (dd, J = 7.7, 1.8 Hz, 1H), 7.58 (td, J = 7.7, 1.3 Hz, 1H), 7.53 – 7.47 (m, 1H), 7.41 (t, J = 7.3 Hz, 1H), 7.14 (d, J = 8.3 Hz, 1H), 7.05 – 7.01 (m, 1H), 5.60 (s, 2H).

2-((3-Cyanophenoxy)methyl)benzoic acid (5.081)

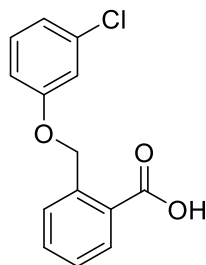
The title compound was obtained following General Procedure G using methyl 2-((3-cyanophenoxy)methyl)benzoate (200 mg, 0.76 mmol). The title compound was obtained as a white solid (169 mg, 87 %). HPLC – t_R 5.07 min > 85 % purity at 254 nm; 1H NMR (400 MHz, DMSO) δ_H 12.98 (bs, 1H), 8.00 – 7.88 (m, 1H), 7.76 – 7.03 (m, 7H), 5.49 (s, 2H); ^{13}C NMR (101 MHz, DMSO) δ_C 168.3, 167.2, 158.6, 138.1, 132.5, 132.3, 130.7, 130.0, 129.7, 128.2, 128.0, 122.1, 119.8, 115.0, 68.0.

2-((4-Cyanophenoxy)methyl)benzoic acid (5.082)

The title compound was obtained following General Procedure G using methyl 2-((4-cyanophenoxy)methyl)benzoate (200 mg, 0.76 mmol). The title compound was obtained as a white solid (170 mg, 88 %). HPLC – t_R 5.04 min > 99 % purity at 254 nm; LRMS $[M+H]^+$ 255.1 m/z ; 1H NMR (400 MHz, MeOD) δ 8.06 (dd, J = 7.8, 1.2 Hz, 1H), 8.02 – 7.98 (m, 2H), 7.71 (d, J = 7.4 Hz, 1H), 7.60 (td, J = 7.6, 1.3 Hz, 1H), 7.47 – 7.42 (m, 1H), 7.09 – 7.05 (m, 2H), 5.58 (s, 2H); 1H NMR (400 MHz, DMSO) δ_H 12.96 (bs, 1H, OH), 8.13 – 8.04 (m, 3H), 7.82 – 7.73 (m, 2H), 7.63 (t, J

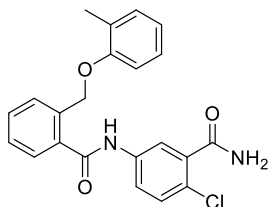
= 6.6 Hz, 1H), 7.23 (d, J = 8.7 Hz, 2H), 5.69 (s, 2H); ^{13}C NMR (101 MHz, DMSO) δ_{C} 168.0, 166.9, 161.9, 137.6, 132.1, 131.4 (2C), 130.5, 129.6, 128.1, 127.9, 123.3, 114.5 (2C), 67.9.

2-((3-Chlorophenoxy)methyl)benzoic acid (5.083)⁵⁶



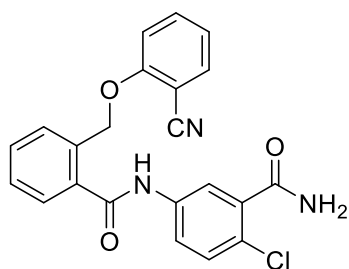
The known title compound was obtained following General Procedure E using methyl 2-((3-chlorophenoxy)methyl)benzoate (700 mg, 2.5 mmol). The title compound was obtained as an off white solid (647 mg, 99%). HPLC – t_{R} 6.19 min > 99 % purity at 254 nm; ^1H NMR (400 MHz, DMSO) δ_{H} 13.07 (bs, 1H), 7.93 (d, J = 7.6 Hz, 1H), 7.65 – 7.55 (m, 2H), 7.49 – 7.41 (m, 1H), 7.31 (t, J = 8.1 Hz, 1H), 7.08 – 6.90 (m, 3H), 5.46 (s, 2H); ^{13}C NMR (101 MHz, DMSO) δ_{C} 168.1, 159.3, 137.6, 133.7, 132.0, 130.9, 130.4, 129.8, 128.1, 127.8, 120.7, 114.8, 113.7, 68.0. Acquired data is consistent with the literature.⁵⁶

N-(3-Carbamoyl-4-chlorophenyl)-2-((*o*-tolylloxy)methyl)benzamide (5.084)



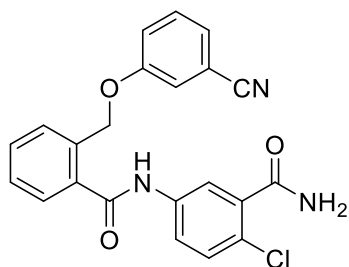
To obtain the title compound 5-amino-2-chlorobenzamide (212 mg, 1.2 mmol) and 2-((*o*-tolylloxy)methyl)benzoic acid (300 mg, 1.2 mmol) were used following General Procedure C. The title compound was obtained as a yellow solid (436 mg, 92 %). HPLC – t_{R} 5.86 min > 99 % purity at 254 nm; LRMS $[\text{M}+\text{H}]^+$ 395.1 m/z , $[\text{M}+\text{Na}]^+$ 417.1 m/z ; HRMS $[\text{M}+\text{H}]^+$ 395.1157 m/z , found 395.1178 m/z ; ^1H NMR (400 MHz, MeOD) δ_{H} 7.85 (d, J = 2.5 Hz, 1H), 7.71 – 7.63 (m, 3H), 7.56 (td, J = 7.5, 1.3 Hz, 1H), 7.51 – 7.46 (m, 1H), 7.42 (d, J = 8.7 Hz, 1H), 7.12 – 7.06 (m, 2H), 6.93 (d, J = 8.0 Hz, 1H), 6.84 – 6.79 (m, 1H), 5.33 (s, 2H), 2.15 (s, 3H); ^{13}C NMR (101 MHz, MeOD) δ_{C} 171.9, 170.5, 158.0, 139.0, 137.6, 137.4, 136.8, 131.7, 131.6, 131.4, 130.0, 129.1, 128.8, 127.9, 127.8, 126.6, 123.9, 121.7, 121.7, 112.4, 68.8, 16.4.

N-(3-Carbamoyl-4-chlorophenyl)-2-((3-cyanophenoxy)methyl)benzamide (5.085)



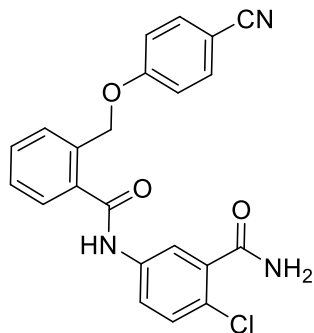
To obtain the title compound 5-amino-2-chlorobenzamide (101 mg, 0.59 mmol) and 2-((2-cyanophenoxy)methyl)benzoic acid (150 mg, 0.59 mmol) were used following General Procedure B. The title compound was obtained as a white solid. (129 mg, 54 %). HPLC – t_{R} 5.29 min > 95 % purity at 254 nm; LRMS $[\text{M}+\text{H}]^+$ 406.1 m/z ; HRMS $[\text{M}+\text{H}]^+$ 406.0953 m/z , found 406.0953 m/z ; ^1H NMR (400 MHz, MeOD) δ_{H} 7.92 – 7.84 (m, 1H), 7.77 – 7.67 (m, 3H), 7.64 – 7.39 (m, 5H), 7.24 (d, J = 8.3 Hz, 1H), 7.09 – 7.03 (m, 1H), 5.50 (s, 2H); ^{13}C NMR (101 MHz, MeOD) δ_{C} 170.1, 161.7, 139.0, 137.4, 136.6, 136.1, 135.9, 134.9, 131.9, 131.4, 130.0, 129.6, 128.9, 126.8, 124.1, 122.4, 121.9, 117.2, 114.1, 102.7, 69.6.

***N*-(3-Carbamoyl-4-chlorophenyl)-2-((3-cyanophenoxy)methyl)benzamide (5.086)**



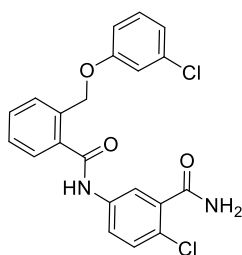
To obtain the title compound 5-amino-2-chlorobenzamide (101 mg, 0.59 mmol) and 2-((3-cyanophenoxy)methyl)benzoic acid (150 mg, 0.59 mmol) were used following General Procedure C. The title compound was obtained as a white solid. (174 mg, 73 %). HPLC – t_R 5.04 min > 99 % purity at 254 nm; LRMS $[M+H]^+$ 406.1 m/z ; HRMS $[M+H]^+$ 406.0953 m/z , found 406.0958 m/z ; 1H NMR (400 MHz, DMSO) δ_H 10.62 (s, 1H), 7.85 – 7.79 (m, 2H), 7.72 (dd, J = 8.7, 2.5 Hz, 1H), 7.65 – 7.34 (m, 9H), 7.27 – 7.22 (m, 1H), 5.36 (s, 2H); ^{13}C NMR (101 MHz, DMSO) δ_C 167.9, 167.2, 158.3, 137.9, 137.4, 135.7, 134.6, 130.9, 130.3, 129.7, 128.9, 128.2, 127.9, 124.8, 123.6, 121.4, 120.5, 119.5, 118.5, 117.7, 112.2, 67.6.

***N*-(3-Carbamoyl-4-chlorophenyl)-2-((4-cyanophenoxy)methyl)benzamide (5.087)**

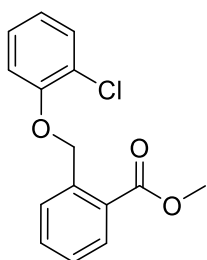


To obtain the title compound 5-amino-2-chlorobenzamide (101 mg, 0.59 mmol) and 2-((4-cyanophenoxy)methyl)benzoic acid (150 mg, 0.59 mmol) were used following General Procedure B. The title compound was obtained as a white solid. (136 mg, 57 %). HPLC – t_R 5.27 min > 99 % purity at 254 nm; LRMS $[M+H]^+$ 406.0 m/z ; HRMS $[M+H]^+$ 406.0953 m/z , found 406.0959 m/z ; 1H NMR (400 MHz, DMSO) δ_H 10.64 (s, 1H), 7.93 – 7.80 (m, 2H), 7.77 – 7.69 (m, 3H), 7.67 – 7.48 (m, 5H), 7.45 – 7.41 (m, 1H), 7.13 – 7.06 (m, 2H), 5.40 (s, 2H); ^{13}C NMR (101 MHz, DMSO) δ_C 168.0, 167.2, 161.7, 137.9, 137.4, 135.6, 134.4, 134.2 (2C), 130.4, 129.8, 128.9, 128.3, 127.9, 123.6, 121.5, 119.6, 119.0, 115.8 (2C), 103.1, 67.6.

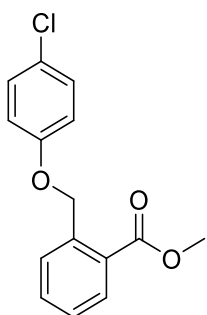
***N*-(3-Carbamoyl-4-chlorophenyl)-2-((3-chlorophenoxy)methyl)benzamide (5.088)**



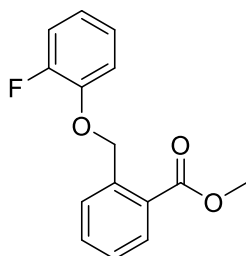
To obtain the title compound 5-amino-2-chlorobenzamide (195 mg, 1.1 mmol) and 2-((3-chlorophenoxy)methyl)benzoic acid (300 mg, 1.1 mmol) were used following General Procedure C. The title compound was obtained as a pale brown solid (398 mg, 87 %). HPLC – t_R 5.93 min > 99 % purity at 254 nm; LRMS $[M+H]^+$ 417.1 m/z ; HRMS $[M+H]^+$ 415.0611 m/z , found 415.0616 m/z ; 1H NMR (400 MHz, DMSO) δ_H 10.62 (s, 1H), 7.87 – 7.80 (m, 2H), 7.73 (dd, J = 8.7, 2.5 Hz, 1H), 7.63 – 7.46 (m, 5H), 7.41 (d, J = 8.7 Hz, 1H), 7.25 (t, J = 8.1 Hz, 1H), 7.01 – 6.94 (m, 2H), 6.88 (dd, J = 8.1, 2.1 Hz, 1H), 5.30 (s, 2H); ^{13}C NMR (101 MHz, DMSO) δ_C 167.9, 167.2, 159.1, 137.9, 137.3, 135.6, 134.8, 133.6, 130.8, 130.2, 129.7, 128.7, 128.0, 127.8, 123.6, 121.4, 120.8, 119.5, 114.8, 113.8, 67.5.

Methyl 2-((2-chlorophenoxy)methyl)benzoate (5.089)²⁰

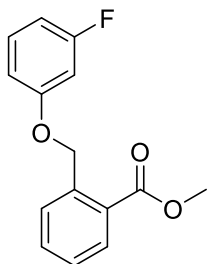
The title compound was obtained following General Procedure D using 2-chlorophenol (0.3 mL) and methyl 2-(bromomethyl)benzoate (684 mg, 3.0 mmol). The title compound was obtained as a white solid (556 mg, 67 %). The compound was used directly in the next step without further purification and characterization. HPLC – t_R 6.89 min > 75 % purity at 254 nm; LRMS $[M+Na]^+$ 299.0 m/z .

Methyl 2-((4-chlorophenoxy)methyl)benzoate (5.090)²⁰

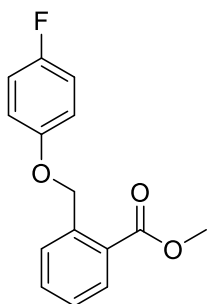
The title compound was obtained following General Procedure D using 4-chlorophenol (387 mg, 3.0 mmol) and methyl 2-(bromomethyl)benzoate (681 mg, 3.0 mmol). The title compound was obtained as a beige solid (745 mg, 90 %). HPLC – t_R 7.02 min > 95 % purity at 254 nm; LRMS $[M-H]^-$ 275.0 m/z ; 1H NMR (400 MHz, DMSO) δ 7.95 (s, 1H), 7.89 (d, J = 7.6 Hz, 1H), 7.64 – 7.58 (m, 2H), 7.34 – 7.29 (m, 2H), 7.02 – 6.96 (m, 2H), 5.39 (s, 2H), 3.79 (s, 3H); ^{13}C NMR (101 MHz, DMSO) δ_C 166.8, 157.1, 137.7, 132.3, 130.1, 129.2 (2C), 128.6, 128.2, 127.9, 124.5, 116.4 (2C), 67.9, 52.1.

Methyl 2-((2-fluorophenoxy)methyl)benzoate (5.091)

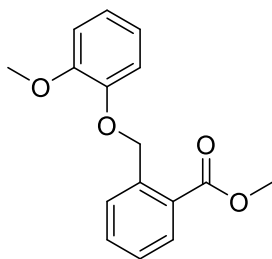
The title compound was obtained following General Procedure D 2-fluorophenol (448 mg, 4.0 mmol) and methyl 2-(bromomethyl)benzoate (916 mg, 4.0 mmol) to obtain methyl 2-((2-fluorophenoxy)methyl)benzoate. The benzoate intermediate (900 mg, 87 %). This compound was used directly in the next step. LRMS $[M+H]^+$ 261.1 m/z , $[M+Na]^+$ 283.1 m/z .

Methyl 2-((3-fluorophenoxy)methyl)benzoate (5.092)

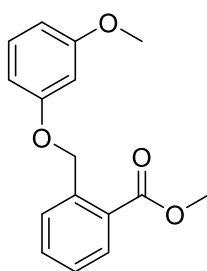
The title compound was obtained following General Procedure D 3-fluorophenol (448 mg, 4.0 mmol) and methyl 2-(bromomethyl)benzoate (916 mg, 4.0 mmol) to obtain methyl 2-((3-fluorophenoxy)methyl)benzoate (1.0 g, 96 %). This compound was used directly in the next step. LRMS $[M+H]^+$ 261.1 m/z , $[M+Na]^+$ 283.0 m/z .

Methyl 2-((4-fluorophenoxy)methyl)benzoate (5.093)

The title compound was obtained following General Procedure D 4-fluorophenol (448 mg, 4.0 mmol) and methyl 2-(bromomethyl)benzoate (916 mg, 4.0 mmol). The title compound was obtained as a white solid (1.0 g, 96 %). HPLC – t_R 6.59 min > 86 % purity at 254 nm; LRMS $[M+H]^+$ 261.1 m/z ; 1H NMR (400 MHz, MeOD) δ_H 8.05 – 8.01 (m, 1H), 7.74 (d, J = 7.8 Hz, 1H), 7.63 (td, J = 7.6, 1.3 Hz, 1H), 7.50 – 7.45 (m, 1H), 7.09 – 6.99 (m, 4H), 5.45 (s, 2H), 3.92 (s, 3H); ^{13}C NMR (101 MHz, MeOD) δ_C 169.0, 158.8 (d, J_{C-F} = 237.1 Hz), 156.3 (d, J_{C-F} = 2.0 Hz), 140.2, 133.5, 131.6, 129.7, 129.0, 128.7, 117.1 (d, J_{C-F} = 8.0 Hz, 2C), 116.7 (d, J_{C-F} = 23.3 Hz, 2C), 69.9, 52.6.

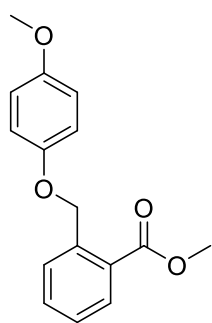
Methyl 2-((2-methoxyphenoxy)methyl)benzoate (5.094)

The title compound was obtained following General Procedure D using methyl 2-(bromomethyl)benzoate (1.14 g, 5.0 mmol) and 2-methoxyphenol (1 eq) to achieve 2-((2-methoxyphenoxy)methyl)benzoate which was used directly in the next step (1.35 g, 99%). HPLC – t_R 6.19 min > 80 % purity at 254 nm; LRMS $[M+Na]^+$ 295.1 m/z ; 1H NMR (400 MHz, DMSO) δ_H 7.90 (dd, J = 7.8, 1.2 Hz, 1H), 7.68 (dd, J = 7.6, 0.6 Hz, 1H), 7.63 (td, J = 7.5, 1.3 Hz, 1H), 7.46 (td, J = 7.7, 1.4 Hz, 1H), 7.01 – 6.83 (m, 4H), 5.38 (s, 2H), 3.80 (s, 3H), 3.77 (s, 3H); ^{13}C NMR (101 MHz, DMSO) δ_C 166.8, 149.2, 147.7, 138.4, 132.4, 130.1, 128.4, 128.0, 127.7, 121.3, 120.7, 113.8, 112.4, 68.2, 55.6, 52.0.

Methyl 2-((3-methoxyphenoxy)methyl)benzoate (5.095)

The title compound was obtained following General Procedure D 3-methoxyphenol (1 eq) and methyl 2-(bromomethyl)benzoate (912 mg, 4.0 mmol). The title compound was obtained as a white solid. (957 mg, 88 %). HPLC – t_R 6.49 min > 75 % purity at 254 nm; LRMS $[M+H]^+$ 273.1 m/z ; 1H NMR (400 MHz, DMSO) δ_H 7.61 (dd, J = 7.8, 0.9 Hz, 1H), 7.38 – 7.31 (m, 2H), 7.18 (td, J = 7.7, 1.7 Hz, 1H), 6.93 – 6.87 (m, 1H), 6.28 – 6.23 (m, 3H), 5.10 (s, 2H), 3.52 (s, 3H), 3.43 (s, 3H).

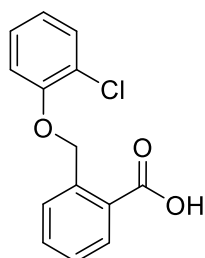
Methyl 2-((4-methoxyphenoxy)methyl)benzoate (5.096)²⁰



55.3, 52.0.

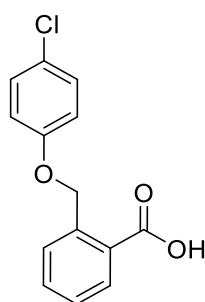
The known title compound was obtained following General Procedure D using 4-methoxyphenol (248 mg, 2.0 mmol) and methyl 2-(bromomethyl)benzoate (454 mg, 2.0 mmol). The title compound was obtained as a white solid (450 mg, 83%). LRMS $[M+H]^+$ 273.1 m/z ; 1H NMR (400 MHz, DMSO) δ_H 7.85 (dd, $J = 7.8$, 1.1 Hz, 1H), 7.64 – 7.55 (m, 2H), 7.41 (td, $J = 7.7$, 1.5 Hz, 1H), 6.88 – 6.80 (m, 4H), 5.30 (s, 2H), 3.77 (s, 3H), 3.65 (s, 3H); ^{13}C NMR (101 MHz, DMSO) δ_C 166.9, 153.5, 152.2, 138.4, 132.2, 130.0, 128.5, 128.0, 127.6, 115.6 (2C), 114.6 (2C), 68.0,

2-((2-Chlorophenoxy)methyl)benzoic acid (5.097)⁵⁶



The known title compound was obtained following General Procedure E using methyl 2-((3-chlorophenoxy)methyl)benzoate (556 mg, 2.0 mmol). The title compound was obtained as a white solid (414 mg, 79 %). The compound was used directly in the next step without further purification and characterization. HPLC – t_R 6.10 min > 99 % purity at 254 nm; LRMS $[M+Na]^+$ 285.0 m/z

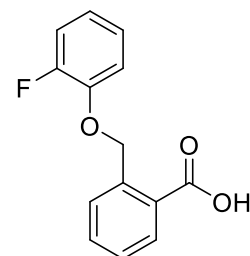
2-((4-Chlorophenoxy)methyl)benzoic acid (5.098)^{56, 100}



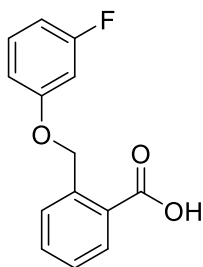
literature.^{56, 100}

The known title compound was obtained following General Procedure E using methyl 2-((4-chlorophenoxy)methyl)benzoate (700 mg, 2.5 mmol). The title compound was obtained as a white solid (618 mg, 94 %). LRMS $[M-H]^-$ 261.0 m/z ; 1H NMR (400 MHz, DMSO) δ_H 13.09 (bs, 1H), 7.94 – 7.89 (m, 1H), 7.64 – 7.56 (m, 2H), 7.50 – 7.42 (m, 1H), 7.33 (d, $J = 8.8$ Hz, 2H), 7.02 – 6.97 (m, 2H), 5.44 (s, 2H); ^{13}C NMR (101 MHz, DMSO) δ_C 168.1, 157.2, 137.9, 132.1, 130.5, 129.3 (2C), 128.2, 127.9, 127.7, 124.5, 116.5 (2C), 68.0. Acquired data is consistent with the

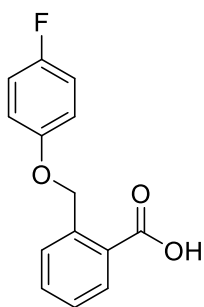
2-((2-Fluorophenoxy)methyl)benzoic acid (5.099)



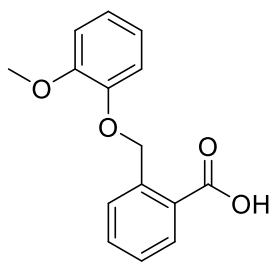
The title compound was obtained following General Procedure E using methyl 2-((2-fluorophenoxy)methyl)benzoate (900 mg, 3.46 mmol). The title compound was obtained as a yellow solid (800 mg, 94 %). HPLC – t_R 5.69 min > 99 % purity at 254 nm; LRMS $[M+H]^+$ 247.1 m/z ; 1H NMR (400 MHz, MeOD) δ_H 7.93 (dd, $J = 7.8$, 1.2 Hz, 1H), 7.65 (d, $J = 7.8$ Hz, 1H), 7.48 (td, $J = 7.6$, 1.3 Hz, 1H), 7.33 – 7.28 (m, 1H), 7.04 – 6.92 (m, 3H), 6.84 – 6.78 (m, 1H), 5.43 (s, 2H); ^{13}C NMR (101 MHz, MeOD) δ_C 170.2, 154.2 (d, $J_{C-F} = 244.4$ Hz), 148.1 (d, $J_{C-F} = 10.6$ Hz), 140.3, 133.5, 132.0, 129.9, 128.6, 125.6 (d, $J_{C-F} = 3.9$ Hz), 122.5 (d, $J_{C-F} = 6.8$ Hz), 117.1, 116.9, 116.6, 70.4.

2-((3-Fluorophenoxy)methyl)benzoic acid (5.100)¹⁰⁵

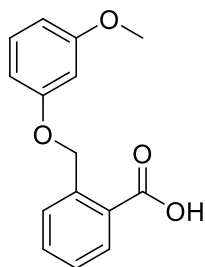
The known title compound was obtained following General Procedure E using 2-((3-fluorophenoxy)methyl)benzoate (1.0 g, 3.85 mmol). The title compound was obtained as a yellow solid (700 mg, 74 %). HPLC – t_R 5.46 min > 91 % purity at 254 nm; LRMS $[M+H]^+$ 247.1 m/z ; 1H NMR (400 MHz, MeOD) δ_H 7.83 (dd, J = 7.8, 1.2 Hz, 1H), 7.49 (d, J = 7.7 Hz, 1H), 7.38 (td, J = 7.7, 1.3 Hz, 1H), 7.22 (t, J = 7.5 Hz, 1H), 7.07 (td, J = 8.3, 7.0 Hz, 1H), 6.60 (dd, J = 8.3, 2.2 Hz, 1H), 6.56 – 6.44 (m, 2H), 5.27 (s, 2H); ^{13}C NMR (101 MHz, MeOD) δ_C 170.3, 165.0 (d, J_{C-F} = 243.7 Hz), 161.7 (d, J_{C-F} = 11.0 Hz), 140.0, 133.4, 132.0, 131.5 (d, J_{C-F} = 10.1 Hz), 130.2, 128.8, 128.6, 111.8 (d, J_{C-F} = 2.8 Hz), 108.5 (d, J_{C-F} = 21.5 Hz), 103.4 (d, J_{C-F} = 25.1 Hz), 69.6.¹⁰⁵

2-((4-Fluorophenoxy)methyl)benzoic acid (5.101)¹⁰⁶

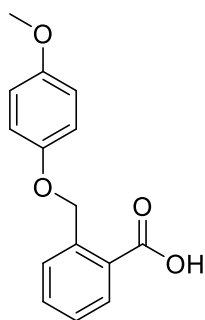
The known title compound was obtained following General Procedure E using methyl 2-((4-fluorophenoxy)methyl)benzoate (1.0 g, 3.85 mmol). The title compound was obtained as a white solid (740 mg, 79 %). HPLC – t_R 5.78 min > 99 % purity at 254 nm; LRMS $[M+H]^+$ 247.1 m/z ; 1H NMR (400 MHz, $CDCl_3$) δ_H 8.18 (dd, J = 7.8, 1.2 Hz, 1H), 7.80 (d, J = 7.7 Hz, 1H), 7.63 (td, J = 7.7, 1.2 Hz, 1H), 7.44 (t, J = 7.5 Hz, 1H), 7.01 – 6.92 (m, 4H), 5.52 (s, 2H); ^{13}C NMR (101 MHz, $CDCl_3$) δ_C 172.7, 157.6 (d, J_{C-F} = 238.6 Hz), 154.9 (d, J_{C-F} = 2.1 Hz), 140.7, 133.9, 131.9, 127.6, 127.6, 126.5, 116.2 (d, J_{C-F} = 2.4 Hz, 2C), 116.0 (d, J_{C-F} = 17.6 Hz, 2C), 69.0.

2-((2-Methoxyphenoxy)methyl)benzoic acid (5.102)¹⁰⁴

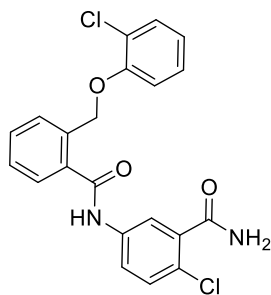
The known title compound was obtained following General Procedure E using 2-((2-methoxyphenoxy)methyl)benzoate (1.35 g, 4.95 mmol). The title compound was obtained as a white solid (1.18 g, 92 % over two steps). HPLC – t_R 5.39 min > 99 % purity at 254 nm; LRMS $[M+H]^+$ 259.1 m/z , $[M+Na]^+$ 281.1 m/z ; 1H NMR (400 MHz, MeOD) δ_H 7.90 (dd, J = 7.7, 1.3 Hz, 1H), 7.70 (d, J = 7.4 Hz, 1H), 7.48 (td, J = 7.6, 1.3 Hz, 1H), 7.37 – 7.32 (m, 1H), 7.00 – 6.81 (m, 4H), 5.48 (s, 2H), 3.86 (s, 3H); ^{13}C NMR (101 MHz, MeOD) δ 172.6, 151.1, 149.7, 139.5, 133.3, 132.2, 131.0, 128.4, 128.2, 122.6, 122.2, 115.4, 113.7, 70.3, 56.6.¹⁰⁴

2-((3-Methoxyphenoxy)methyl)benzoic acid (5.103)¹⁰⁴

The known title compound was obtained following General Procedure E using methyl 2-((3-methoxyphenoxy)methyl)benzoate (957 mg, 3.3 mmol). The title compound was obtained as a white solid (740 mg, 87 %). HPLC – t_R 5.68 min > 99 % purity at 254 nm; LRMS $[M+H]^+$ 259.0 m/z ; 1H NMR (400 MHz, MeOD) δ_H 8.03 (dd, J = 7.8, 1.3 Hz, 1H), 7.72 (d, J = 7.8 Hz, 1H), 7.57 (td, J = 7.6, 1.4 Hz, 1H), 7.43 – 7.39 (m, 1H), 7.19 – 7.14 (m, 1H), 6.58 – 6.51 (m, 3H), 5.46 (s, 2H), 3.77 (s, 3H); 1H NMR (400 MHz, DMSO) δ_H 13.09 (bs, 1H), 7.92 (dd, J = 7.7, 0.8 Hz, 1H), 7.66 – 7.56 (m, 2H), 7.46 – 7.42 (m, 1H), 7.21 – 7.16 (m, 1H), 6.57 – 6.51 (m, 3H), 5.42 (s, 2H), 3.72 (s, 3H); ^{13}C NMR (101 MHz, DMSO) δ_C 168.1, 160.5, 159.6, 138.2, 132.0, 130.4, 130.0, 129.5, 128.0, 127.6, 106.8, 106.5, 101.1, 67.5, 55.0.¹⁰⁴

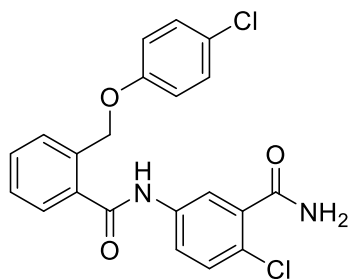
2-((4-Methoxyphenoxy)methyl)benzoic acid (5.104)¹⁰⁴

The known title compound was obtained following General Procedure E using methyl 2-((4-methoxyphenoxy)methyl)benzoate (400 mg, 1.5 mmol). The title compound was obtained as a white solid (300 mg, 77 %). HPLC – t_R 5.58 min > 90 % purity at 254 nm; LRMS $[M-H]^-$ 257.1 m/z ; 1H NMR (400 MHz, MeOD) δ_H 8.01 (d, J = 7.8 Hz, 1H), 7.72 (d, J = 7.8 Hz, 1H), 7.56 (td, J = 7.7, 1.2 Hz, 1H), 7.40 (t, J = 7.3 Hz, 1H), 6.94 – 6.89 (m, 2H), 6.87 – 6.82 (m, 2H), 5.42 (s, 2H), 3.75 (s, 3H); 1H NMR (400 MHz, DMSO) δ_H 7.91 (d, J = 7.2 Hz, 1H), 7.64 (d, J = 7.5 Hz, 1H), 7.61 – 7.56 (m, J = 10.7, 4.2 Hz, 1H), 7.43 (t, J = 7.4 Hz, 1H), 6.92 – 6.84 (m, 4H), 5.37 (s, 2H), 3.69 (s, 3H); ^{13}C NMR (101 MHz, DMSO) δ_C 168.1, 153.5, 152.4, 138.6, 132.0, 130.3, 129.4, 127.8, 127.5, 115.7 (2C), 114.7 (2C), 68.1, 55.4.¹⁰⁴

N-(3-Carbamoyl-4-chlorophenyl)-2-((2-chlorophenoxy)methyl)benzamide (5.114)

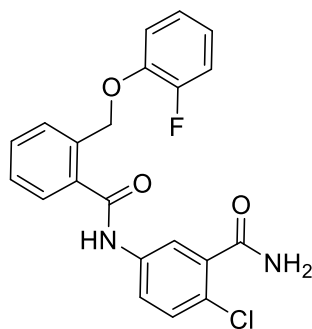
To obtain the title compound 5-amino-2-chlorobenzamide (98 mg, 0.6 mmol) and 2-((2-chlorophenoxy)methyl)benzoic acid (150 mg, 0.6 mmol) were used following General Procedure C. The title compound was obtained as a white solid. (190 mg, 76 %). HPLC – t_R 5.81 min > 99 % purity at 254 nm; LRMS $[M+H]^+$ 415.0 m/z ; HRMS $[M+H]^+$ 415.0611 m/z , found 415.0615 m/z ; 1H NMR (400 MHz, MeOD) δ_H 7.89 (d, J = 2.5 Hz, 1H), 7.75 – 7.69 (m, 2H), 7.68 – 7.63 (m, 1H), 7.57 (td, J = 7.6, 1.4 Hz, 1H), 7.50 (td, J = 7.5, 1.0 Hz, 1H), 7.43 (d, J = 8.7 Hz, 1H), 7.33 (dd, J = 7.9, 1.6 Hz, 1H), 7.25 – 7.19 (m, 1H), 7.12 (dd, J = 8.3, 1.3 Hz, 1H), 6.91 (td, J = 7.7, 1.4 Hz, 1H), 5.41 (s, 2H); 1H NMR (400 MHz, DMSO) δ_H 10.63 (s, 1H), 7.84 (d, J = 2.3 Hz, 2H), 7.77 – 7.35 (m, 8H), 7.29 – 7.23 (m, 1H), 7.19 – 7.13 (m, 1H), 6.93 (td, J = 7.7, 1.3 Hz, 1H), 5.39 (s, 2H); ^{13}C NMR (101 MHz, DMSO) δ_C 168.0, 167.1, 153.5, 138.0, 137.3, 135.3, 135.0, 130.4, 129.9, 129.7, 128.5, 128.2, 128.0, 128.0, 123.5, 121.7, 121.5, 121.5, 119.6, 114.1, 67.7.

***N*-(3-Carbamoyl-4-chlorophenyl)-2-((4-chlorophenoxy)methyl)benzamide (5.115)**



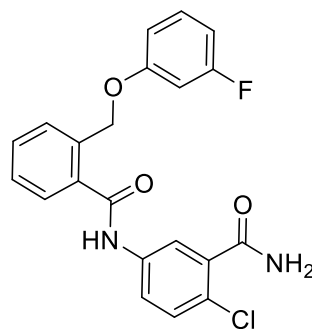
To obtain the title compound 5-amino-2-chlorobenzamide (195 mg, 1.1 mmol) and 2-((4-chlorophenoxy)methyl)benzoic acid (300 mg, 1.1 mmol) were used following General Procedure C. The title compound was obtained as a yellow solid (290 mg, 64 %). HPLC – t_R 5.93 min > 99 % purity at 254 nm; LRMS $[M+H]^+$ 415.0 m/z ; HRMS $[M+H]^+$ 415.0611 m/z , found 415.0617 m/z ; 1H NMR (400 MHz, MeOD) δ_H 7.88 (d, J = 2.5 Hz, 1H), 7.72 (dd, J = 8.7, 2.5 Hz, 1H), 7.66–7.62 (m, 2H), 7.56 (td, J = 7.5, 1.5 Hz, 1H), 7.50 (td, J = 7.5, 1.2 Hz, 1H), 7.45 (d, J = 8.7 Hz, 1H), 7.25–7.20 (m, 2H), 6.95–6.91 (m, 2H), 5.32 (s, 2H); ^{13}C NMR (101 MHz, MeOD) δ_C 171.9, 170.4, 158.8, 139.0, 137.6, 137.0, 136.7, 131.6, 131.4, 130.3 (2C), 130.0, 129.3, 128.7, 127.0, 126.6, 123.9, 121.7, 117.5 (2C), 69.3.

***N*-(3-Carbamoyl-4-chlorophenyl)-2-((2-fluorophenoxy)methyl)benzamide (5.116)**



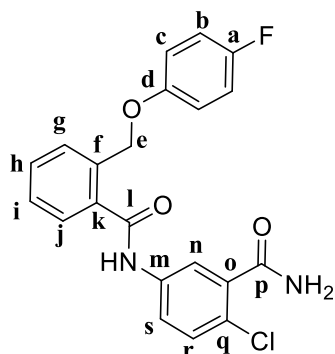
To obtain the title compound 5-amino-2-chlorobenzamide (70 mg, 0.41 mmol) and 2-((2-fluorophenoxy)methyl)benzoic acid (100 mg, 0.41 mmol) were used following General Procedure C. The title compound was obtained as a white solid. (107 mg, 65 %). HPLC – t_R 5.18 min > 99 % purity at 254 nm; LRMS $[M+H]^+$ 399.1 m/z ; HRMS $[M+H]^+$ 399.0906 m/z , found 399.0907 m/z ; 1H NMR (400 MHz, DMSO) δ_H 10.60 (s, 1H), 7.89–7.77 (m, 2H), 7.68 (dd, J = 8.8, 2.5 Hz, 1H), 7.62–7.36 (m, 6H), 7.21–6.99 (m, 3H), 6.92–6.84 (m, 1H), 5.31 (s, 2H); ^{13}C NMR (101 MHz, DMSO) δ_C 168.1, 167.3, 152.0 (d, J_{C-F} = 243.8 Hz), 146.2 (d, J_{C-F} = 10.4 Hz), 138.0, 137.4, 135.6, 135.0, 130.5, 129.8, 128.9, 128.2, 128.0, 124.8 (d, J_{C-F} = 3.8 Hz), 123.7, 121.7, 121.5 (d, J_{C-F} = 7.0 Hz), 119.7, 116.1 (d, J_{C-F} = 17.8 Hz), 115.5 (d, J_{C-F} = 1.0 Hz), 68.1.

***N*-(3-Carbamoyl-4-chlorophenyl)-2-((3-fluorophenoxy)methyl)benzamide (5.117)**



To obtain the title compound 5-amino-2-chlorobenzamide (70 mg, 0.41 mmol) and 2-((3-fluorophenoxy)methyl)benzoic acid (100 mg, 0.41 mmol) were used following General Procedure C. The title compound was obtained as a white solid. (130 mg, 79 %). HPLC – t_R 5.30 min > 99 % purity at 254 nm; LRMS $[M+H]^+$ 399.1 m/z ; HRMS $[M+H]^+$ 399.0906 m/z , found 399.0894 m/z ; 1H NMR (400 MHz, DMSO) δ_H 10.63 (s, 1H), 7.89–7.81 (m, 2H), 7.76–7.69 (m, 1H), 7.63–7.46 (m, 5H), 7.42 (d, J = 8.7 Hz, 1H), 7.31–7.21 (m, 1H), 6.82–6.69 (m, 3H), 5.30 (s, 2H); ^{19}F NMR (376 MHz, DMSO) δ_F -111.59 (s); ^{13}C NMR (101 MHz, DMSO) δ_C 168.0, 167.3, 162.9 (d, J_{C-F} = 243.1 Hz), 159.7 (d, J_{C-F} = 11.0 Hz), 138.0, 137.4, 135.6, 134.9, 130.7 (d, J_{C-F} = 10.2 Hz), 130.3, 129.7, 128.8, 128.1, 127.8, 123.6, 121.5, 119.6, 111.1 (d, J_{C-F} = 2.7 Hz), 107.5 (d, J_{C-F} = 21.1 Hz), 102.3 (d, J_{C-F} = 24.8 Hz), 67.5.

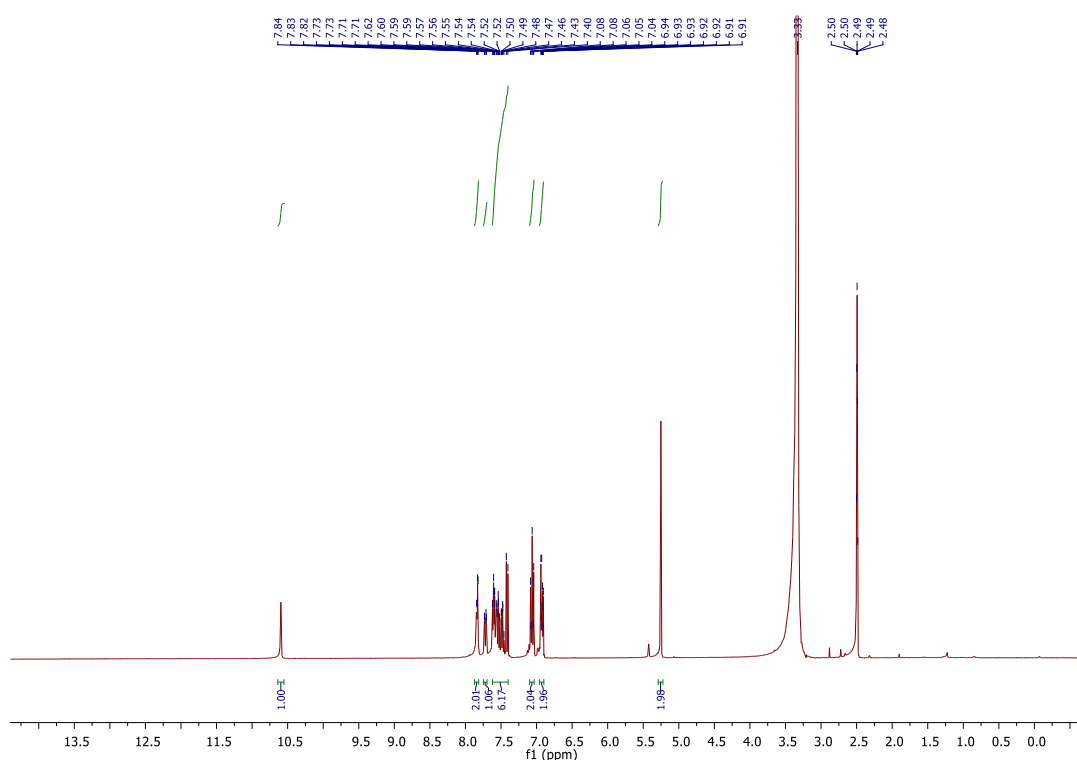
***N*-(3-Carbamoyl-4-chlorophenyl)-2-((4-fluorophenoxy)methyl)benzamide (5.118)**

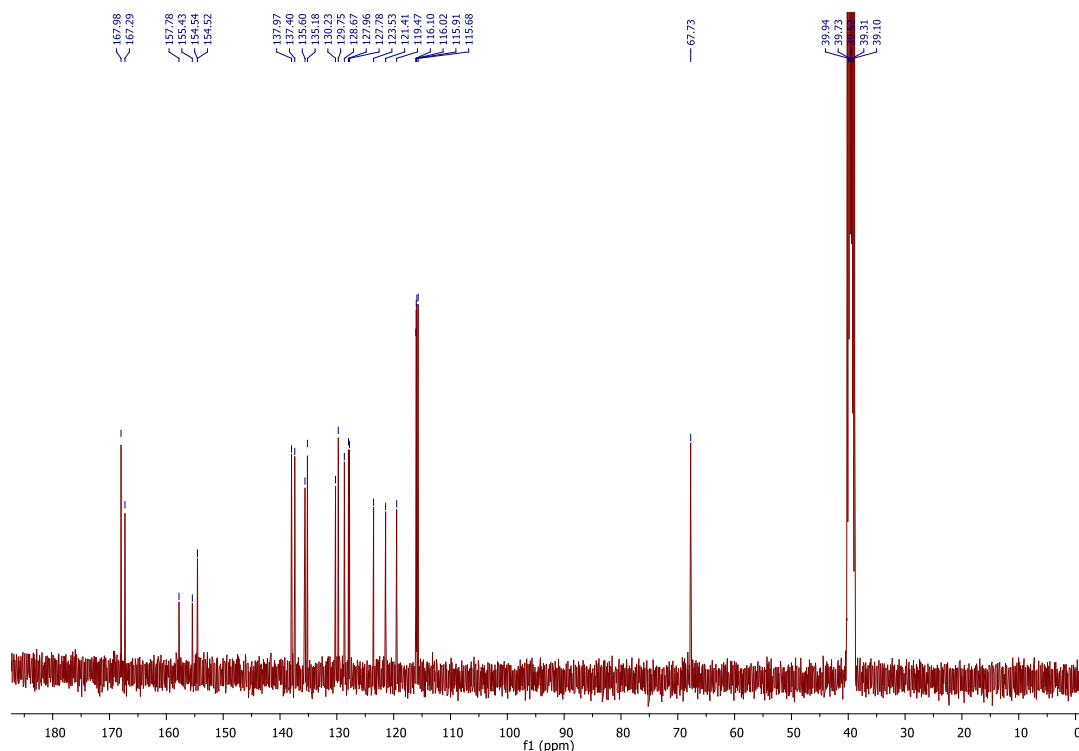


To obtain the title compound 5-amino-2-chlorobenzamide (70 mg, 0.41 mmol) and 2-((4-fluorophenoxy)methyl)benzoic acid (100 mg, 0.41 mmol) were used following General Procedure C. The title compound was obtained as a fluffy white solid. (95 mg, 60 %). HPLC – t_R 5.23 min > 99 % purity at 254 nm; LRMS $[M+H]^+$ 399.1 m/z ; HRMS $[M+H]^+$ 399.0906 m/z , found 399.0912 m/z ; 1H NMR (400 MHz, MeOD) δ_H 7.87 (d, $J = 2.4$ Hz, 1H), 7.74 – 7.60 (m, 3H), 7.57 – 7.39 (m, 3H), 7.01 – 6.89 (m, 4H), 5.28 (s, 2H); 1H NMR (400 MHz, DMSO) δ_H 10.60 (s, 1H,

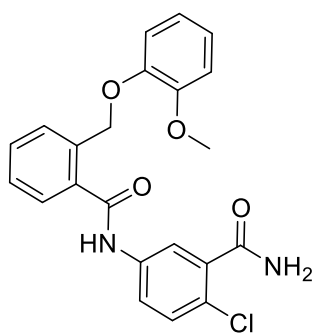
NH), 7.86 – 7.80 (m, 2H, Hn, NH of NH₂), 7.72 (dd, $J = 8.7, 2.5$ Hz, 1H, Hj), 7.64 – 7.40 (m, 6H, Hg,h,i,r,s NH of NH₂), 7.10 – 7.02 (m, 2H, Hb), 6.96– 6.90 (m, 2H, Hc), 5.25 (s, 2H, He); ^{13}C NMR (101 MHz, DMSO) δ_C 168.0 (Cl), 167.3 (Cp), 156.6 (d, $J = 236.2$ Hz, Ca), 154.5 (d, $J_{C-F} = 1.8$ Hz, Cd), 138.0 (Ck), 137.4 (Cm), 135.6 (Co), 135.2 (Cf), 130.2 (Ch), 129.8 (Cr), 128.7 (Cg/i/j/q), 128.0 (Cg/i/j/q), 127.8 (Cg/i/j/q), 123.5 (Cg/i/j/q), 121.4 (Cs), 119.5 (Cn), 116.1 (d, $J_{C-F} = 8.2$ Hz, 2C, Cc), 115.8 (d, $J_{C-F} = 23.0$ Hz, 2C, Cb), 67.7 (Ce).

Example spectra for *N*-(3-Carbamoyl-4-chlorophenyl)-2-((4-fluorophenoxy)methyl)benzamide (5.118): 1H (400 MHz, DMSO) and ^{13}C NMR (100 MHz, DMSO)





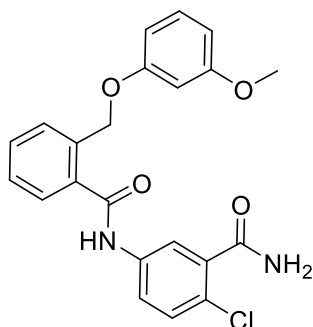
***N*-(3-Carbamoyl-4-chlorophenyl)-2-((2-methoxyphenoxy)methyl)benzamide (5.119)**



To obtain the title compound 5-amino-2-chlorobenzamide (100 mg, 0.6 mmol) and 2-((2-methoxyphenoxy)methyl)benzoic acid (150 mg, 0.6 mmol) were used following General Procedure C. The title compound was obtained as a white solid. (150 mg, 61 %). HPLC – t_R 5.35 min > 99 % purity at 254 nm; LRMS $[M+H]^+$ 411.1 m/z ; HRMS $[M+H]^+$ 411.1106 m/z , found 411.1105 m/z ; 1H NMR (400 MHz, MeOD) δ_H 7.84 (d, J = 2.5 Hz, 1H), 7.70 (dd, J = 8.7, 2.6 Hz, 1H), 7.64 – 7.58 (m, 2H), 7.53 – 7.37 (m, 3H), 7.01 – 6.94 (m, 1H), 6.92 – 6.86 (m, 2H), 6.86 – 6.79 (m, 1H), 5.29 (s, 2H), 3.66 (s, 3H); ^{13}C NMR (101 MHz, MeOD) δ_C 171.9, 170.3, 151.2, 149.1, 139.0, 137.5, 137.3, 136.6, 131.6, 131.4, 130.7, 129.4, 128.9, 126.6, 123.9, 123.1, 122.0, 121.7, 115.9, 113.3, 70.2, 56.2.

***N*-(3-Carbamoyl-4-chlorophenyl)-2-((3-methoxyphenoxy)methyl)benzamide (5.120)**

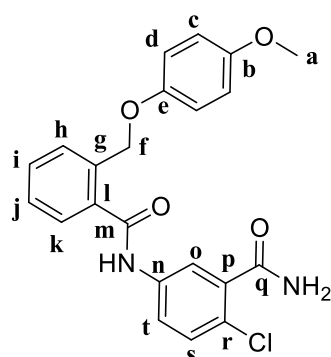
To obtain the title compound 5-amino-2-chlorobenzamide (100 mg, 0.6 mmol) and 2-((3-methoxyphenoxy)methyl)benzoic acid (150 mg, 0.6 mmol) were used following General Procedure C.



The title compound was obtained as a white solid. (143 mg, 58 %). HPLC – t_R 5.50 min > 99 % purity at 254 nm; LRMS $[M+H]^+$ 411.1 m/z ; HRMS $[M+H]^+$ 411.1106 m/z , found 411.1085 m/z ; 1H NMR (400 MHz, MeOD) δ_H 7.86 (d, J = 2.5 Hz, 1H), 7.71 (dd, J = 8.7, 2.5 Hz, 1H), 7.65 – 7.60 (m, 2H), 7.56 – 7.41 (m, 3H), 7.11 (t, J = 8.2 Hz, 1H), 6.54 – 6.46 (m, 3H), 5.29 (s, 2H), 3.70 (s, 3H); ^{13}C NMR (101 MHz, MeOD) δ_C 171.9, 170.6,

162.3, 161.2, 139.0, 137.5, 137.1, 137.0, 131.6, 131.4, 130.9, 130.1, 129.2, 128.7, 126.6, 124.0, 121.7, 108.1, 107.9, 102.4, 69.0, 55.7.

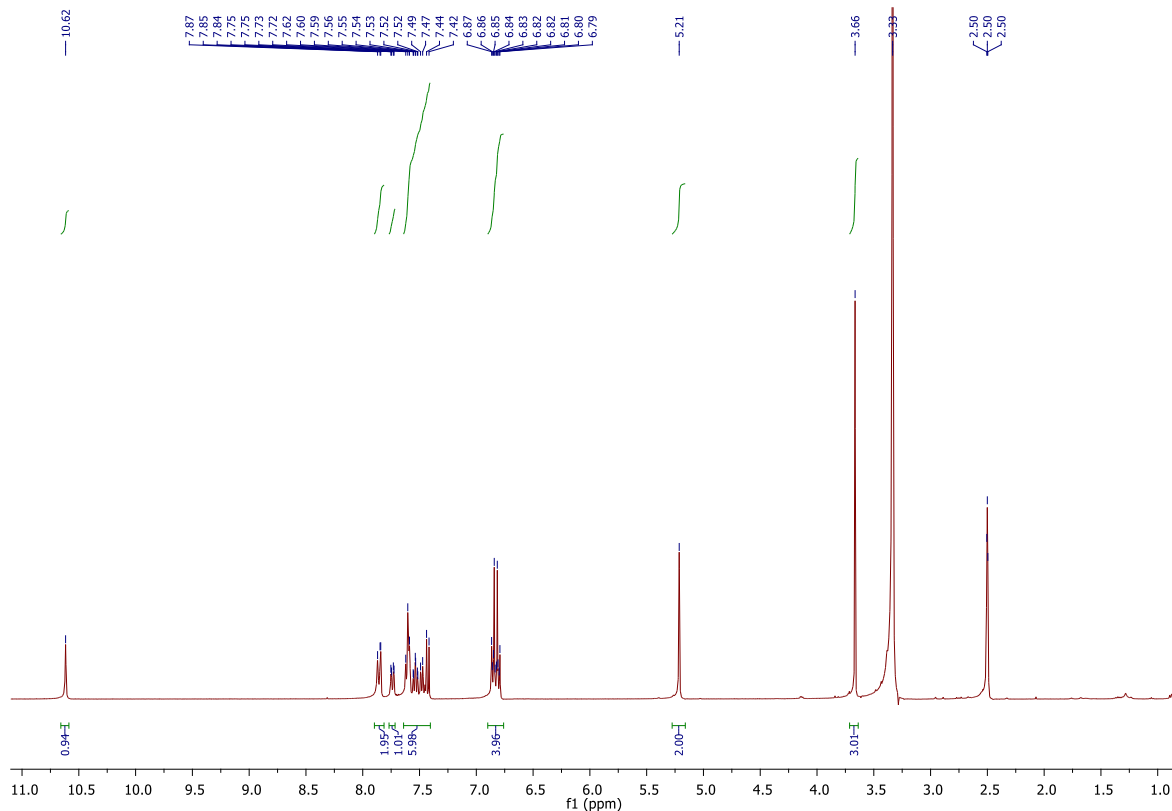
***N*-(3-Carbamoyl-4-chlorophenyl)-2-((4-methoxyphenoxy)methyl)benzamide (5.121)**

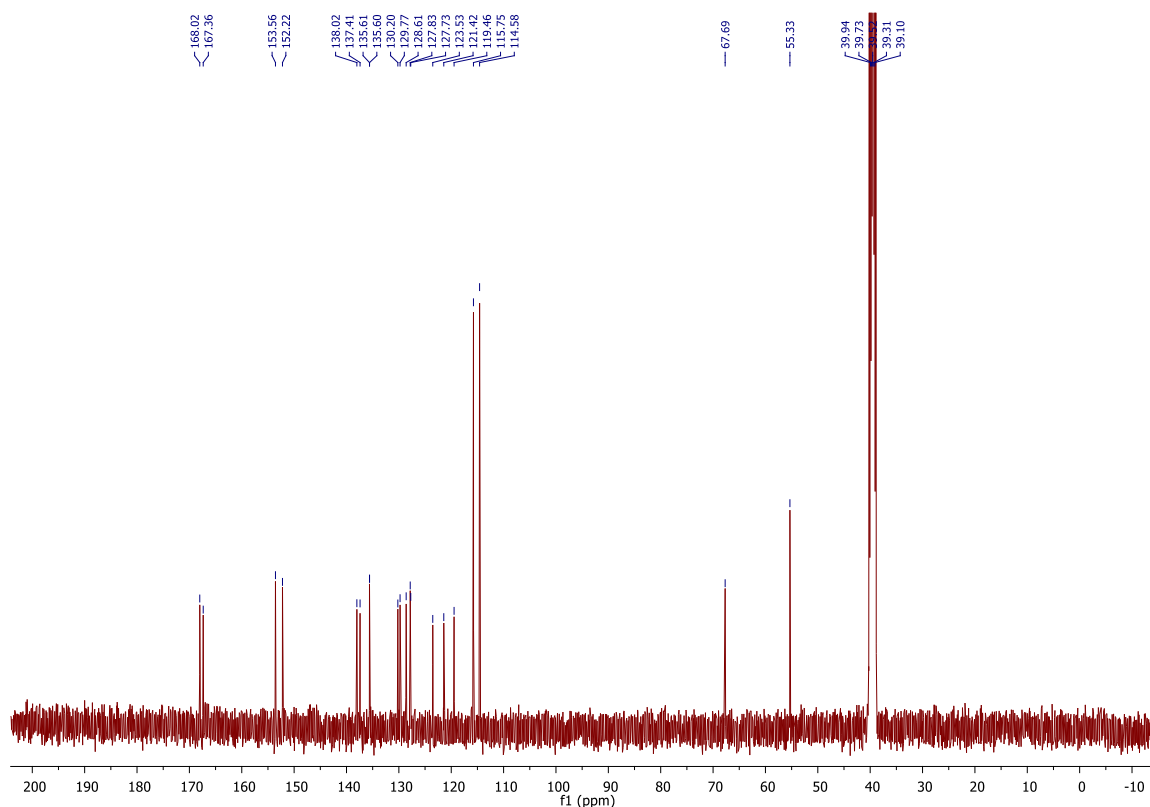


To obtain the title compound 5-amino-2-chlorobenzamide (100 mg, 0.6 mmol) and 2-((4-methoxyphenoxy)methyl)benzoic acid (150 mg, 0.6 mmol) were used following General Procedure C. The title compound was obtained as a white solid. (190 mg, 77 %). HPLC – t_R 5.41 min > 99 % purity at 254 nm; LRMS $[M+H]^+$ 411.1 m/z ; HRMS $[M+H]^+$ 411.1106 m/z , found 411.1101 m/z ; 1H NMR (400 MHz, DMSO) δ_H 10.62 (s, 1H, NH), 7.88–7.83 (m, 2H, Ho, NH of NH₂), 7.74 (dd, J = 8.7, 2.4 Hz, 1H, Hk), 7.63–7.41 (m, 6H, Hh,i,j,s,t NH of NH₂), 6.91–6.77 (m, 4H, Hc,d),

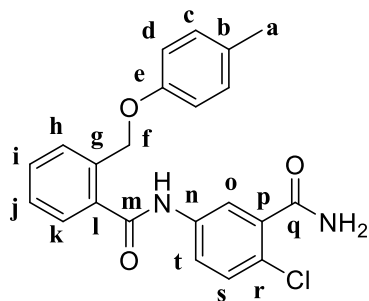
5.21 (s, 2H, Hf), 3.66 (s, 3H, Ha); ^{13}C NMR (101 MHz, DMSO) δ_C 168.0 (Cm), 167.4 (Cq), 153.6 (Cb/Ce), 152.2 (Cb/Ce), 138.0 (Cl), 137.4 (Cn), 135.6 (Cp), 135.6 (Cg), 130.2 (Ci), 129.8 (Cs), 128.6 (Ch/j/k/r), 127.8 (Ch/j/k/r), 127.7 (Ch/j/k/r), 123.5 (Ch/j/k/r), 121.4 (Ct), 119.5 (Co), 115.8 (2C, Cd), 114.6 (2C, Cc), 67.7 (Cf), 55.3 (Ca).

Example spectra for *N*-(3-Carbamoyl-4-chlorophenyl)-2-((4-methoxyphenoxy)methyl)benzamide (5.121): 1H (400 MHz, DMSO) and ^{13}C NMR (100 MHz, DMSO)





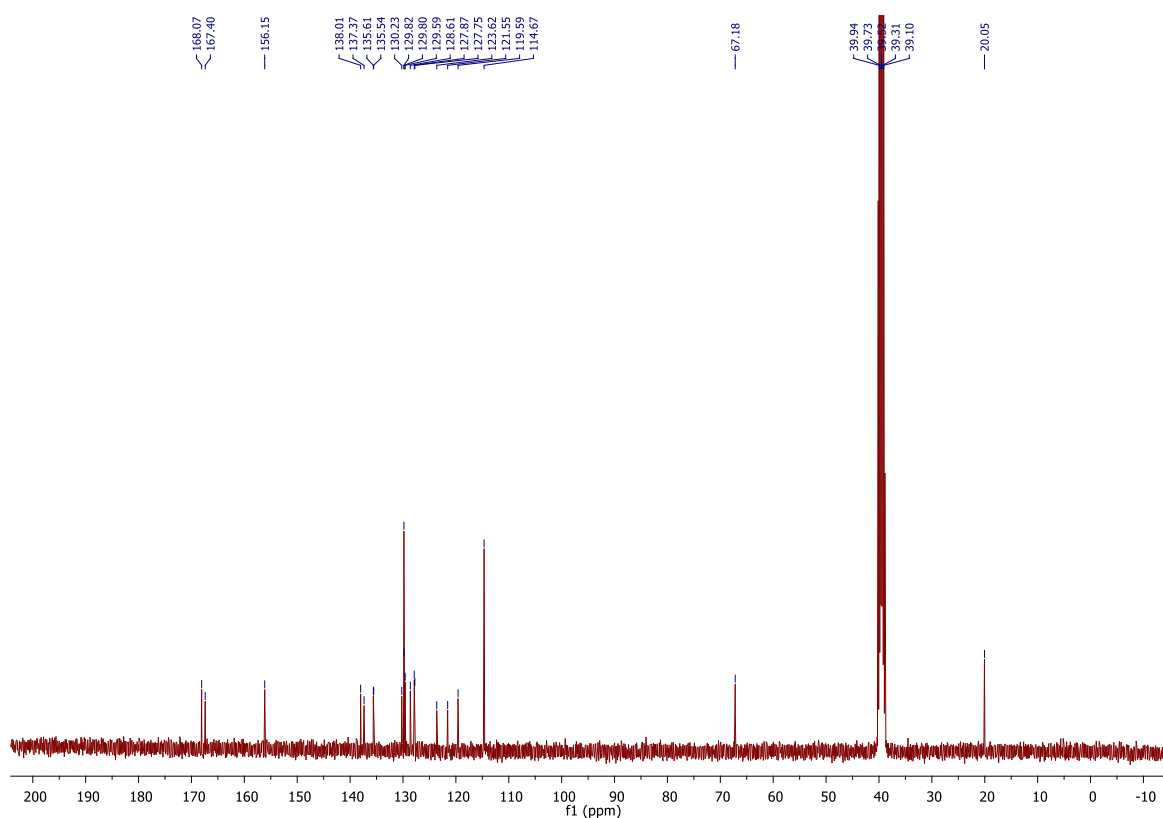
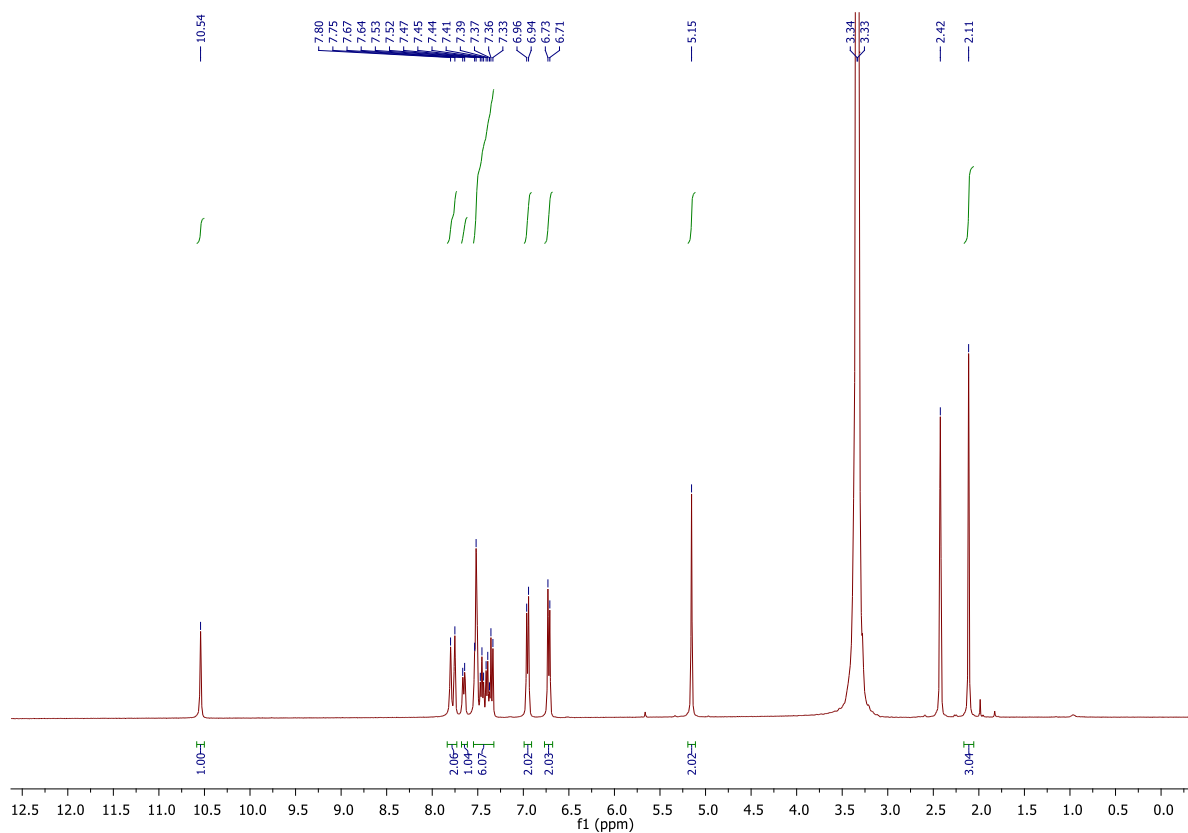
***N*-(3-Carbamoyl-4-chlorophenyl)-2-((*p*-tolylloxy)methyl)benzamide (5.122)**



To obtain the title compound 5-amino-2-chlorobenzamide (212 mg, 1.2 mmol) and 2-((*p*-tolylloxy)methyl)benzoic acid (300 mg, 1.2 mmol) were used following General Procedure C. The title compound was obtained as a yellow solid (450 mg, 95 %). HPLC – t_R 5.83 min > 99 % purity at 254 nm; LRMS $[M+H]^+$ 395.1 m/z , $[M+Na]^+$ 417.1 m/z ; HRMS $[M+H]^+$ 395.1157 m/z , found 395.117 m/z ; 1H NMR (400 MHz, DMSO) δ_H 10.54 (s, 1H, NH), 7.78 (d*, J = 18.9 Hz, 2H,

*two overlapping br s, Ho, NH of NH_2), 7.65 (d, J = 8.4 Hz, 1H, Hk), 7.55 – 7.32 (m, 6H, Hh,i,j,s,t NH of NH_2), 6.95 (d, J = 8.2 Hz, 2H, Hc), 6.72 (d, J = 8.3 Hz, 2H, Hd), 5.15 (s, 2H, Hf), 2.11 (s, 3H, Ha); ^{13}C NMR (101 MHz, DMSO) δ_C 168.1 (Cm), 167.4 (Cq), 156.2 (Ce), 138.0 (Cl), 137.4 (Cn) 135.6 (Cp), 135.5 (Cg), 130.2 (Ci), 129.8 (2C, Cc), 129.8 (Cb/s), 129.6 (Cb/s), 128.6 (Ch/j/k/r), 127.9 (Ch/j/k/r), 127.8 (Ch/j/k/r), 123.6 (Ch/j/k/r), 121.6 (Ct), 119.6 (Co), 114.7 (2C, Cd), 67.2 (Cf), 20.1 (Ca).

Example spectra for *N*-(3-Carbamoyl-4-chlorophenyl)-2-(*p*-tolylloxy)methylbenzamide (5.122): ^1H (400 MHz, DMSO) and ^{13}C NMR (100 MHz, DMSO)



5.13 Chapter 5 Reference

1. Peña I, Pilar Manzano M, Cantizani J, Kessler A, Alonso-Padilla J, Bardera AI, et al. New Compound Sets Identified from High Throughput Phenotypic Screening Against Three Kinetoplastid Parasites: An Open Resource. *Sci Rep*. 2015;5:8771.
2. Lipinski CA, Lombardo F, Dominy BW, Feeney PJ. Experimental and computational approaches to estimate solubility and permeability in drug discovery and development settings 1PII of original article: S0169-409X(96)00423-1. The article was originally published in *Adv Drug Deliv Rev* 23 (1997) 3–25.1. *Adv Drug Deliv Rev*. 2001;46(1):3-26.
3. Veber DF, Johnson SR, Cheng H-Y, Smith BR, Ward KW, Kopple KD. Molecular Properties That Influence the Oral Bioavailability of Drug Candidates. *J Med Chem*. 2002;45(12):2615-2623.
4. Staples RJ. Getting Crystals Your Crystallographer Will Treasure. Michigan State University, Department of Chemistry 2020. 1-19. Originated at Harvard University, Department of Chemistry and Chemical Biology, 1998-2006, taken in part from the lecture given at MIT, 1998 Getting Crystals Your Crystallographer Will Treasure
5. Buckman B; Nicholas JB, Beigelman L, Serebryany V, Stoycheva AD, Thrailkill T et al. Cyclic peptide inhibitors of hepatitis c virus replication. WO 2011038293 A1, 2011.
6. Hui X, Desrivot J, Bories C, Loiseau PM, Franck X, Hocquemiller R, et al. Synthesis and antiprotozoal activity of some new synthetic substituted quinoxalines. *Bioorg Med Chem Lett*. 2006;16(4):815-820.
7. Bursavich MG, Gilbert AM, Stock JR. Piperazine metabotropic glutamate receptor 5 (MGLUR5) negative allosteric modulators for anxiety/depression. WO 2009143404 A1, 2009.
8. Frackenpohl J, Heinemann I, Müller T, Zeiss H-J, Busch M, Willms L, et al. Fluoroalkyl-substituted 2-amidobenzimidazoles. US 20110218103 A1, 2011.
9. Arienti KL, Axe FU, Breitenbucher JG, Huang L, Lee A, McClure KJ. 2-phenyl benzimidazoles and imidazo-[4,5]-pyridines as CDSI/CHK2-inhibitors and adjuvants to chemotherapy or radiation therapy in the treatment of cancer. WO 2003032984 A1, 2003.
10. Lagu B, Wachter M, Rupert K, Meng P. Phospholipase C inhibitors for use in treating inflammatory disorders. WO 2004087685 A2, 2004.
11. Ungashe S, Wei Z, Basak A, Charvat TT, Chen W, Jin J, et al. Preparation of aryl and heteroaryl sulfonamides as CCR2 antagonists. US 20110118248 A1, 2011.
12. Chandra T, Zebrowski J. Hazards associated with laboratory scale hydrogenations. *J Chem Health Saf*. 2016;23(4):16-25.
13. Breslin HJ, Chatterjee S, Diebold JL, Dorsey BD, Dunn D, Gingrich DE, et al. Pyrrolotriazines as ALK and JAK2. WO 2010071885 A1, 2010.

14. Bi X, Li J, Shi E, Li Y, Liu Y, Wang H, et al. POCl₃ promoted metal-free synthesis of tertiary amides by coupling of carboxylic acids and *N,N*-disubstituted formamides. *Phosphorus Sulfur Silicon Relat Elem.* 2019;194(3):236-240.
15. Bhatt R, Gong B, Hong F, Jenkins SA, Klein JP, Kumar AM, et al. 6-Phenyl-*n*-phenyl-(1,3,5)-triazine-2,4-diamine derivatives and related compounds with lysophosphatidic acid acyltransferase beta (LPAAT-beta) inhibitory activity for use in the treatment of cancer. WO 2003037346 A1, 2003.
16. Zhu Y-P, Sergeyev S, Franck P, Orru RVA, Maes BUW. Amine Activation: Synthesis of *N*-(Hetero)arylamides from Isothioureas and Carboxylic Acids. *Org Lett.* 2016;18(18):4602-4605.
17. Hunt I. Substituent Effects [Internet]. University of Calgary [cited 2020 September 29]. Available from: <http://www.chem.ucalgary.ca/courses/350/Carey5th/useful/subeff.html>.
18. Wilden JD. The Sulfonamide Motif as a Synthetic Tool. *J Chem Res.* 2010;34(10):541-548.
19. Benson GM, Bleicher K, Feng S, Grether U, Kuhn B, Martin RE, et al. New benzimidazole derivatives. US 20110077273 A1, 2010.
20. Shinkai H, Ito T, Iida T, Kitao Y, Yamada H, Uchida I. 4-Aminoquinolines: Novel Nociceptin Antagonists with Analgesic Activity. *J Med Chem.* 2000;43(24):4667-4677.
21. Hunt I. Chapter 20: Carboxylic Acid Derivatives. Nucleophilic Acyl Substitution. [Internet] University of Calgary [cited 2020 September 29]. Available from: <http://www.chem.ucalgary.ca/courses/350/Carey5th/Ch20/ch20-1-3.html>.
22. Wang J, Li F, Pei W, Yang M, Wu Y, Ma D, et al. Selective cleavage of the *N*-propargyl group from sulfonamides and amides under ruthenium catalysis. *Tetrahedron Lett.* 2018;59(20):1902-1905.
23. Gao Y, Mao Y, Zhang B, Zhan Y, Huo Y. Regioselective nitration of anilines with Fe(NO₃)₃·9H₂O as a promoter and a nitro source. *Org Biomol Chem.* 2018;16(21):3881-3884.
24. Youn SW, Ko TY, Kim YH, Kim YA. Pd(II)/Cu(II)-Catalyzed Regio- and Stereoselective Synthesis of (E)-3-Arylmethyleneisoindolin-1-ones Using Air as the Terminal Oxidant. *Org Lett.* 2018;20(24):7869-7874.
25. Jonathan Clayden, Greeves N and Stuart Warren. Chapter 15- Nucleophilic Substitution at Saturated Carbon. In: Jonathan Clayden, Greeves N and Stuart Warren, editor. *Organic Chemistry*. 2nd ed. Oxford University Press UK. 2012. p. 328-359
26. Kumari S, Carmona AV, Tiwari AK, Trippier PC. Amide Bond Bioisosteres: Strategies, Synthesis, and Successes. *J Med Chem.* 2020; 63(21):12290-12358.
27. Mitsos C. Isosteres in Medicinal Chemistry. [Internet] 2006 [cited 2020 September 30]. Available from: https://www.scripps.edu/baran/images/grpmtgpdf/Mitsos_Feb_06.pdf.
28. Patani GA, LaVoie EJ. Bioisosterism: A Rational Approach in Drug Design. *Chem Rev.* 1996;96(8):3147-3176.
29. Wermuth CG. *The Practice of Medicinal Chemistry*. 3rd ed. Wermuth CG, editor: Academic Press, Elsevier; 2008.

30. True JE, Thomas TD, Winter RW, Gard GL. Electronegativities from Core-Ionization Energies: Electronegativities of SF₅ and CF₃. *Inorg Chem*. 2003;42(14):4437-4441.
31. Callahan JF, Li T, Wan Z, Yan H. Dual pharmacophores-PDE4-muscarinic antagonistics. WO 2009100169 A1, 2009.
32. Stewart WE, Siddall TH. Nuclear magnetic resonance studies of amides. *Chem Rev*. 1970;70(5):517-51.
33. Gorobets NY, Yermolayev SA, Gurley T, Gurinov AA, Tolstoy PM, Shenderovich IG, et al. Difference between ¹H NMR signals of primary amide protons as a simple spectral index of the amide intramolecular hydrogen bond strength. *J Phys Org Chem*. 2012;25(4):287-295.
34. Piskov VB, Kasperovich VP, Yakovleva LM. Synthesis of Δ^2 -imidazolines in ethylene glycol. *Chem Heterocycl Compd (N Y)*. 1976;12(8):917-923.
35. Hilpert K, Hubler F, Kimmerlin T, Murphy M, Renneberg D, Stamm S. Heterocyclic amide derivatives as P2X₇ receptor antagonists. WO 2013014587 A1, 2013.
36. Dagley MJ, Saunders EC, Simpson KJ, McConville MJ. High-content assay for measuring intracellular growth of *Leishmania* in human macrophages. *Assay Drug Dev Technol*. 2015;13(7):389-401.
37. Phan T-N, Baek K-H, Lee N, Byun SY, Shum D, No JH. In Vitro and in Vivo Activity of mTOR Kinase and PI3K Inhibitors Against *Leishmania donovani* and *Trypanosoma brucei*. *Molecules*. 2020;25(8):1980.
38. Álvarez-Velilla R, Gutiérrez-Corbo MDC, Punzón C, Pérez-Pertejo MY, Balaña-Fouce R, Fresno M, et al. A chronic bioluminescent model of experimental visceral leishmaniasis for accelerating drug discovery. *PLoS Negl Trop Dis*. 2019;13(2):e0007133.
39. Lezama-Dávila CM, Isaac-Márquez AP, Kapadia G, Owens K, Oghumu S, Beverley S, et al. Leishmanicidal activity of two naphthoquinones against *Leishmania donovani*. *Biol Pharm Bull*. 2012;35(10):1761-1764.
40. Zahid MS, Johnson M, Varma D, Ainslie K. Infecting THP-1 Macrophages with *Leishmania donovani* (Ds-Red-lux) and evaluating by Luciferase assay. [Unpublished data] Eshelman School of Pharmacy, University of North Carolina at Chapel Hill; 2019.
41. Stockert JC, Horobin RW, Colombo LL, Blázquez-Castro A. Tetrazolium salts and formazan products in Cell Biology: Viability assessment, fluorescence imaging, and labeling perspectives. *Acta Histochem*. 2018;120(3):159-167.
42. Chiu H-C, Kulp SK, Soni S, Wang D, Gunn JS, Schlesinger LS, et al. Eradication of Intracellular *Salmonella enterica* Serovar Typhimurium with a Small-Molecule, Host Cell-Directed Agent. *Antimicrob Agents Chemother*. 2009;53(12):5236-5244.
43. Cockcroft JK, Buanz ABM, Ntantou A, Price LS, Tocher DA, Vickers M, et al. Polymorphism in 2-Chlorobenzamide: Run of the Mill or Not? *Cryst Growth Des*. 2016;16(11):6144-6147.

44. The Cambridge Crystallographic Data Centre [Internet]. 2021. [cited 2021 January 16]. Available from: <https://www.ccdc.cam.ac.uk/>.
45. Kato Y, Takaki Y, Sakurai K. Polymorphism and disordered structures of o-chlorobenzamide. *Acta Crystallogr B Struct Sci Cryst Eng Mater*. 1974;30(11):2683-2687.
46. Fomulu SL, Hendi MS, Davis RE, Wheeler KA. Structural Studies of Enantiomers, Racemates, and Quasiracemates. *N*-(2-Chlorobenzoyl)methylbenzylamine and *N*-(2-Bromobenzoyl)methylbenzylamine. *Cryst Growth Des*. 2002;2(6):645-651.
47. Penfold BR, White JCB. The crystal and molecular structure of benzamide. *Acta Crystallogr*. 1959;12(2):130-135.
48. Krishnakumar V, Murugeswari K, Surumbarkuzhali N. Molecular structure, intramolecular hydrogen bonding and vibrational spectral investigation of 2-fluoro benzamide – A DFT approach. *Spectrochim Acta A Mol Biomol Spectrosc*. 2013;114:410-420.
49. Yoshihiro K, Kiichi S. The Crystal Structure of o-Fluorobenzamide. *Bull Chem Soc Jpn*. 1982;55(5):1643-1644.
50. Gowda BT, Sowmya BP, Kozisek J, Tokarcik M, Fuess H. *N*-(2-Chlorophenyl)benzamide. *Acta Crystallogr E Crystallogr Commun*. 2007;63(6):o2906.
51. Taiichi H, Kazuaki N, Yoshito T, Kiichi S. The Crystal Structure of the β Form of *p*-Chlorobenzamide. *Bull Chem Soc Jpn*. 1980;53(3):801-802.
52. Taniguchi T, Nakata K, Takaki Y, Sakurai K. The crystal structures of the [alpha] form of *p*-chlorobenzamide at room temperature and -120°C. *Acta Crystallogr B Struct Sci Cryst Eng Mater*. 1978;34(8):2574-2578.
53. Rodrigues VZ, Kuckova L, Gowda BT, Kozisek J. 4-Chloro-*N*-phenylbenzamide. *Acta Crystallogr Sect E Struct Rep Online*. 2011;67(12):o3171.
54. Gowda BT, Foro S, Sowmya BP, Fuess H. 2-Chloro-*N*-(3,5-dimethylphenyl)benzamide. *Acta Crystallogr E Crystallogr Commun*. 2009;65(3):o444.
55. Rodrigues VZ, Herich P, Gowda BT, Kozisek J. 3-Chloro-*N*-phenylbenzamide. *Acta Crystallogr Sect E Struct Rep Online*. 2011;67(12):o3329.
56. Naporra F, Gobleder S, Wittmann H-J, Spindler J, Bodensteiner M, Bernhardt G, et al. Dibenzo[b,f][1,4]oxazepines and dibenzo[b,e]oxepines: Influence of the chlorine substitution pattern on the pharmacology at the H1R, H4R, 5-HT2AR and other selected GPCRs. *Pharmacol Res*. 2016;113:610-625.
57. Corwin H, Leo A, Hoekman D. Exploring QSAR: Hydrophobic, Electronic, and Steric Constants. Washington DC: American Chemical Society; 1995.
58. Corwin Hansch AL, David Hoekman. Exploring QSAR: Fundamentals and Applications in Chemistry and Biology. Washington DC: American Chemical Society; 1995.

59. Segal M, Avinery R, Buzhor M, Shaharabani R, Harnoy AJ, Tirosh E, et al. Molecular Precision and Enzymatic Degradation: From Readily to Undegradable Polymeric Micelles by Minor Structural Changes. *J Am Chem Soc.* 2017;139(2):803-810.
60. Andersson H, Demaegdt H, Vauquelin G, Lindeberg G, Karlén A, Hallberg M. Ligands to the (IRAP)/AT4 receptor encompassing a 4-hydroxydiphenylmethane scaffold replacing Tyr2. *Bioorg Med Chem.* 2008;16(14):6924-6935.
61. Fernandes PB, Mailman RB, Nichols DE. Method of administration of dopamine receptor agonists. WO2006012640 A2, 2006.
62. Roberts RS, Gomez SS, Buil Albero MA. New pyrazole derivatives having CRTH2 antagonistic behaviour. WO2012069175 A1, 2010.
63. Djerassi C. Brominations with *N*-Bromosuccinimide and Related Compounds. The Wohl-Ziegler Reaction. *Chem Rev.* 1948;43(2):271-317.
64. Shimojo H, Moriyama K, Togo H. A One-Pot, Transition-Metal-Free Procedure for C–O, C–S, and C–N Bond Formation at the Benzylic Position of Methylarenes. *Synthesis.* 2015;47(09):1280-1290.
65. Thermo Fisher Scientific. Safety Data Sheet: Dibenzyl peroxide. Regulatory Affairs, Thermo Fischer Scientific; 2018. p1-8.
66. Thermo Fisher Scientific. Safety Data Sheet: Carbon tetrachloride. Regulatory Affairs, Thermo Fischer Scientific; 2018. p1-8.
67. Zhou Z, Yang S. A kind of preparation method of adjacent hydroxyl olopatadine. CN 104031020 B, 2014.
68. Martz KE, Dorn A, Baur B, Schattel V, Goettert MI, Mayer-Wrangowski SC, et al. Targeting the Hinge Glycine Flip and the Activation Loop: Novel Approach to Potent p38 α Inhibitors. *J Med Chem.* 2012;55(17):7862-7874.
69. Wang Z. Williamson Ether Synthesis. *Comprehensive Organic Name Reactions and Reagents.* Wang Z, editor. Jon Wiley & Sons, Inc. 2010 p. 3026-3030. doi [10.1002/9780470638859.conrr673](https://doi.org/10.1002/9780470638859.conrr673)
70. Dudler T, Farouz F, Fowler K, Hawthorn N, Huang D, Judkins A, et al. Substituted phenyl acetic acids as DP-2 antagonists. WO 2007143745 A2, 2007.
71. Li L. Benzoic acid derivatives as modulators of ppar alpha and gamma. WO 2004000295 A1, 2003.
72. Potapov VV, Fetisova NA, Nikitina AV, Ivachtchenko AV. A convenient synthesis of heterocyclic compounds containing 11-oxo-6,11,12,13-tetrahydrodibenzo[b,g][1,5]oxazone fragment. *Mendeleev Commun.* 2009;19(5):287-289.
73. Baur B, Storch K, Martz KE, Goettert MI, Richters A, Rauh D, et al. Metabolically Stable Dibenzo[b,e]oxepin-11(6H)-ones as Highly Selective p38 MAP Kinase Inhibitors: Optimizing Anti-Cytokine Activity in Human Whole Blood. *J Medicinal Chem.* 2013;56(21):8561-8578.

74. Albrecht BK, Audia JE, Cook A, Gagnon A, Harmange J-C, Naveschuk CG. Modulators of methyl modifying enzymes., compositions and uses thereof. WO 2013075083 A1. 2013.
75. Barnes-Seeman D, Jain M, Bell L, Ferreira S, Cohen S, Chen X-H, et al. Metabolically Stable tert-Butyl Replacement. ACS Med Chem Lett. 2013;4(6):514-516.
76. Meanwell N. Tools for the Medicinal Chemist Tools for the Medicinal Chemist- Symposium 2017; July 20-21; Monash Institute of Pharmaceutical Sciences, Melbourne 2017.
77. Stepan AF, Mascitti V, Beaumont K, Kalgutkar AS. Metabolism-guided drug design. MedChemComm. 2013;4(4):631-652.
78. Lazzara PR, Moore TW. Scaffold-hopping as a strategy to address metabolic liabilities of aromatic compounds. RSC Med Chem. 2020;11(1):18-29.
79. Marroquin LD, Hynes J, Dykens JA, Jamieson JD, Will Y. Circumventing the Crabtree effect: replacing media glucose with galactose increases susceptibility of HepG2 cells to mitochondrial toxicants. Toxicol Sci. 2007;97(2):539-547.
80. Shum D et al. HepG2 Crabtree Cytotoxicity screening Standard Operating Procedure. [Unpublished data] Institut Pasteur Korea, Seongnam, South Korea; 2021.
81. Bevan CD, Lloyd RS. A High-Throughput Screening Method for the Determination of Aqueous Drug Solubility Using Laser Nephelometry in Microtiter Plates. Anal Chem. 2000;72(8):1781-1787.
82. Lombardo F, Shalaeva MY, Tupper KA, Gao F. ElogDoct: A Tool for Lipophilicity Determination in Drug Discovery. 2. Basic and Neutral Compounds. J Med Chem. 2001;44(15):2490-2497.
83. Ring BJ, Chien JY, Adkison KK, Jones HM, Rowland M, Jones RD, et al. PhRMA CPCDC initiative on predictive models of human pharmacokinetics, part 3: Comparative assesment of prediction methods of human clearance. J Pharm Sci. 2011;100(10):4090-4110.
84. Obach RS. Prediction of human clearance of twenty-nine drugs from hepatic microsomal intrinsic clearance data: An examination of in vitro half-life approach and nonspecific binding to microsomes. Drug Metab Dispos. 1999;27(11):1350-1359.
85. Coulter TS, Taylor S, Murfin S, Thammalaksa V, Aicher B, Jaekel S, et al. Preparation of pyrazolopyrimidines as inhibitors of kinase activity. WO 2006066937 A2, 2006.
86. Sriramoju V, Kurva S, Madabhushi S. New method for the preparation of *N*-chloroamines by oxidative *N*-halogenation of amines using oxone-KCl. Synth Commun. 2018;48(6):699-704.
87. Nirogi R, Shinde AK, Kambhampati RS, Jayarajan P, Bhyrapuneni G, Jasti V. Preparation of aryl sulfonamide amine compounds and their use as 5-HT6 ligands. WO 2010032258 A1, 2010.
88. Martin TP, Eckelbarger JD, Ross R, Dekorver KA, Heemstra RJ, Knueppel DI, et al. Molecules having pesticidal utility, and intermediates, compositions, and processes, related thereto. WO 2016168058 A1, 2016.

89. Pan L, Jiang Y, Liu Z, Liu X-H, Liu Z, Wang G, et al. Synthesis and evaluation of novel monosubstituted sulfonylurea derivatives as antituberculosis agents. *Eur J Med Chem.* 2012;50:18-26.
90. Ball SJ, Parnell EW. Anti-coccidial Activity of Halogenonitrobenzamides. *Nature.* 1963;199(4893):612.
91. Jamatia R, Gupta A, Pal AK. Ru-Ferrite-Decorated Graphene (RuFG): A Sustainable and Efficient Catalyst for Conversion of Aromatic Aldehydes and Nitriles to Primary Amides in Aqueous Medium. *ACS Sustain Chem Eng.* 2017;5(9):7604-7612.
92. Thomson SA. Carboxamides as modulators of sodium channels. WO 2020146682 A1, 2020.
93. Georgiou C, McNae I, Wear M, Ioannidis H, Michel J, Walkinshaw M. Pushing the Limits of Detection of Weak Binding Using Fragment-Based Drug Discovery: Identification of New Cyclophilin Binders. *J Mol Biol.* 2017;429(16):2556-2570.
94. Mohamed K, Venugopala Katharigatta N, Mohana R, Gopal Krishna R. Synthesis, Antibacterial Activity of 2,4-Disubstituted Oxazoles and Thiazoles as Bioisosteres. *Lett Drug Des Discov.* 2009;6(1):21-28.
95. Lori F, Kéri G, Chafouleas J, Forni DD, Solinas A, Varga Z, et al. Preparation of novel 4,6-disubstituted aminopyrimidine derivatives as CDK9 inhibitors. WO 2014031937 A1, 2014.
96. Saggar S, Sisko J, Tucker T, Tynebor R, Su D-S, Anthony N. HIV reverse transcriptase inhibitors. US 20070021442 A1, 2007.
97. Mousseau JJ, Vallée F, Lorion MM, Charette AB. Umpolung Direct Arylation Reactions: Facile Process Requiring Only Catalytic Palladium and Substoichiometric Amount of Silver Salts. *J Am Chem Soc.* 2010;132(41):14412-14414.
98. Shang R, Fu Y, Li J-B, Zhang S-L, Guo Q-X, Liu L. Synthesis of Aromatic Esters via Pd-Catalyzed Decarboxylative Coupling of Potassium Oxalate Monoesters with Aryl Bromides and Chlorides. *J Am Chem Soc.* 2009;131(16):5738-5739.
99. Naveena CS, Boja P, Kumari NS. Synthesis, characterization and antimicrobial activity of some disubstituted 1,3,4-oxadiazoles carrying 2-(aryloxymethyl)phenyl moiety. *Eur J Med Chem.* 2010;45(11):4708-4719.
100. Naveena CS, Poojary B, Arulmoli T, Manjunatha K, Prabhu A, Kumari NS. Synthesis and evaluation of biological and nonlinear optical properties of some novel 2,4-disubstituted [1,3]-thiazoles carrying 2-(aryloxymethyl)-phenyl moiety. *Med Chem Res.* 2013;22(4):1925-1937.
101. Isloor AM, Sankappa Rai U, Shetty P, Gerber T, Hosten E, Betz R. Methyl 2-[(2-methylphenoxy)methyl]benzoate. *Acta Crystallogr Sect E Struct Rep Online.* 2012;68(3):o728.
102. Kalugin VE, Shestopalov AM. A convenient synthesis of benzofuro[3,2-c]isoquinolines and naphtho[1',2':4,5]furo[3,2-c]isoquinolines. *Tetrahedron Lett.* 2011;52(14):1557-1560.
103. Channamata Shankara Naveena BP, Chikkanna Chandrashekhara and Nalilu Suchetha Kumari. Synthesis and Biological Evaluation of Some [1,2,4]Triazolo[3,4-b][1,3,4]Thiadiazoles and [1,2,4]Triazolo[3,4-b][1,3,4]Thiadiazines. *Lett Drug Des Discov.* 2011;8(2):189-200.

104. Scoccia J, Castro MJ, Faraoni MB, Bouzat C, Martín VS, Gerbino DC. Iron(II) promoted direct synthesis of dibenzo[b,e]oxepin-11(6H)-one derivatives with biological activity. A short synthesis of doxepin. *Tetrahedron*. 2017;73(20):2913-2922.
105. Laufer SA, Ahrens GM, Karcher SC, Hering JS, Niess R. Design, Synthesis, and Biological Evaluation of Phenylamino-Substituted 6,11-Dihydro-dibenzo[b,e]oxepin-11-ones and Dibenzo[a,d]cycloheptan-5-ones: Novel p38 MAP Kinase Inhibitors. *J Med Chem*. 2006;49(26):7912-7915.
106. Müller J, Limban C, Stadelmann B, Missir AV, Chirita IC, Chifiriuc MC, et al. Thioureides of 2-(phenoxymethyl)benzoic acid 4-R substituted: A novel class of anti-parasitic compounds. *Parasitol Int*. 2009;58(2):128-135.

Epilogue

The main objectives of this project, as outlined in **Chapter 1**, were to confirm the antileishmanial properties of the chosen hits summarized in **Figure 1**, and to synthesize novel compounds based on these chosen hit compound classes. Compounds were biologically assessed against the clinically relevant *L. donovani* amastigotes using intramacrophage assays performed by our independent collaborators to determine the antileishmanial properties of our novel compounds. We aimed to investigate and develop a first-generation SAR profile around these novel scaffolds.

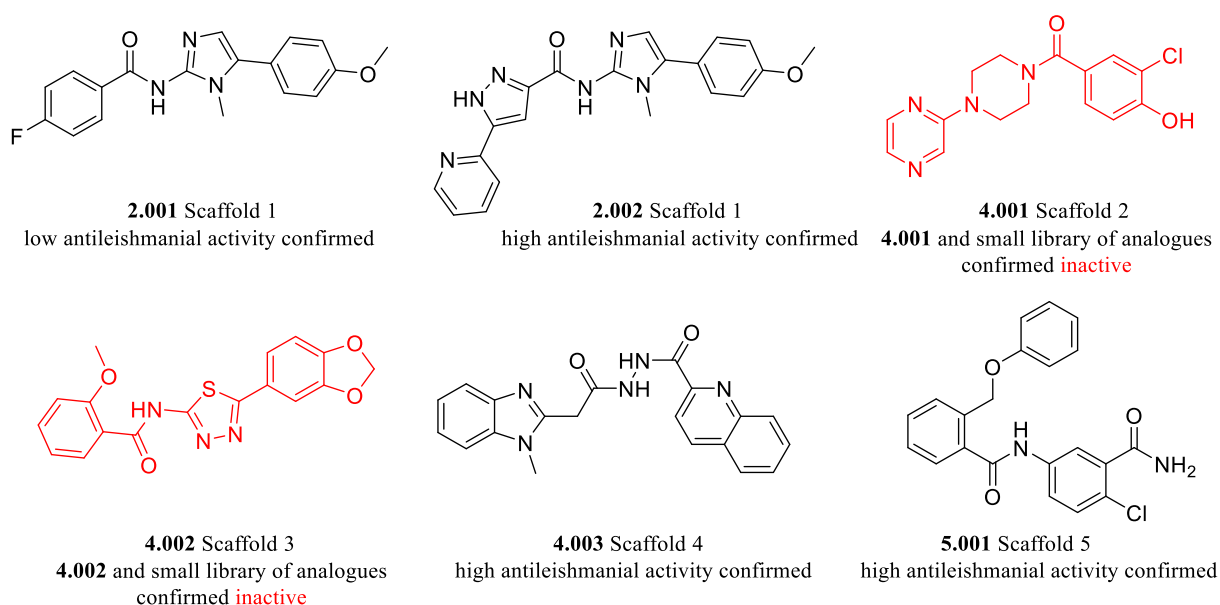


Figure 1: Summary of initial hit compounds chosen for optimization

Studies involving Scaffold 1 were the largest focus of this PhD project, particularly around investigating the chemical space around hit **2.001**. Even though the hit **2.001** was confirmed to exhibit significantly weaker antileishmanial activity than originally reported, the large medicinal chemistry efforts around this structure gave rise to an extensive SAR profile of this compound class, further leading to the development of the new early lead compounds summarized in **Figure 2**. These new lead compounds demonstrated strong inhibition of *L. donovani*, whilst maintaining selectivity for the parasite (**Figure 2**). Various investigations around the structure of hit **2.001** confirmed that the amide and 5-membered heteroaromatic core were required to maintain activity, however bioisosteric replacement of the imidazole with an oxazole core was preferable, when the arrangement of heteroatoms remained constant. Numerous modifications to the LHS aromatic ring found that including somewhat larger, more lipophilic, non-hydrogen bonding substituents, namely bromo, chloro and methyl substituents were favoured over the *para*-fluoro group. Substituting the bromo and chloro functionalities around the RHS aromatic ring was also preferable. The initial *para*-fluoro substituent (LHS) and *para*-methoxy substituent (RHS) were confirmed as non-essential functionalities. Replacing the LHS 6-membered

aromatic ring with the 5-membered imidazole ring also accomplished strong parasitic inhibition also improved parasite inhibition when simultaneous changes to the RHS region of the scaffold were made, namely substituting chloro groups at the *meta* and *para*-positions of the RHS aromatic ring. These structural modifications also allowed for superior solubility and metabolic stability *in vitro* in comparison to the initial hit **2.001**.

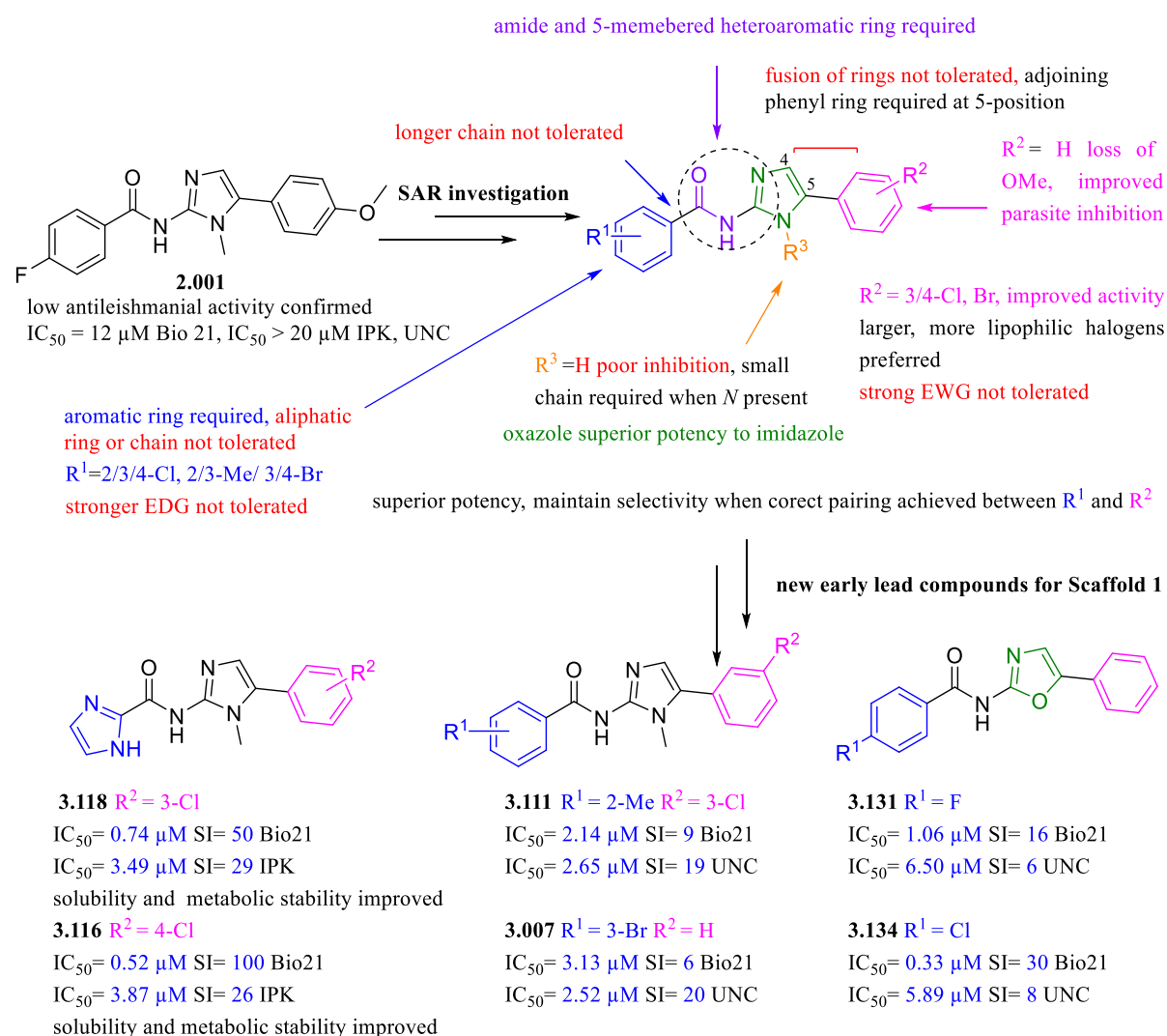


Figure 2: Summary of SAR profile around hit 2.001, Scaffold 1 and the early lead compounds developed

Studies around the chemical space of hit **2.002** also contributed to the primary SAR profile around Scaffold 1 and are summarized in **Figure 3**. Loss of the pyridine ring and structural changes to the amide and imidazole ring functionalities were confirmed to cause a loss of antileishmanial activity. As with the hit **2.001**, removal of the *para*-methoxy substituent at the RHS region of the scaffold was found to maintain high antileishmanial activity, suggesting this functionality was not required to interact with the putative binding site/s. This modification also improved microsomal stability and aqueous solubility over the initial hit **2.002**. Substitution of halogen groups at the *para*-position demonstrated improved antileishmanial activity over **2.002**. Including the chloro group at the *para*-position also improved

metabolic stability over the hit **2.002**. Incorporating methyl substituents around the RHS phenyl ring was found to be the most consistent improvement to **2.002**. In particular, the *ortho*-methyl substituent demonstrated the strongest parasitic inhibition within our entire analogue library. Selectivity toward the parasite over the host cell was also maintained.

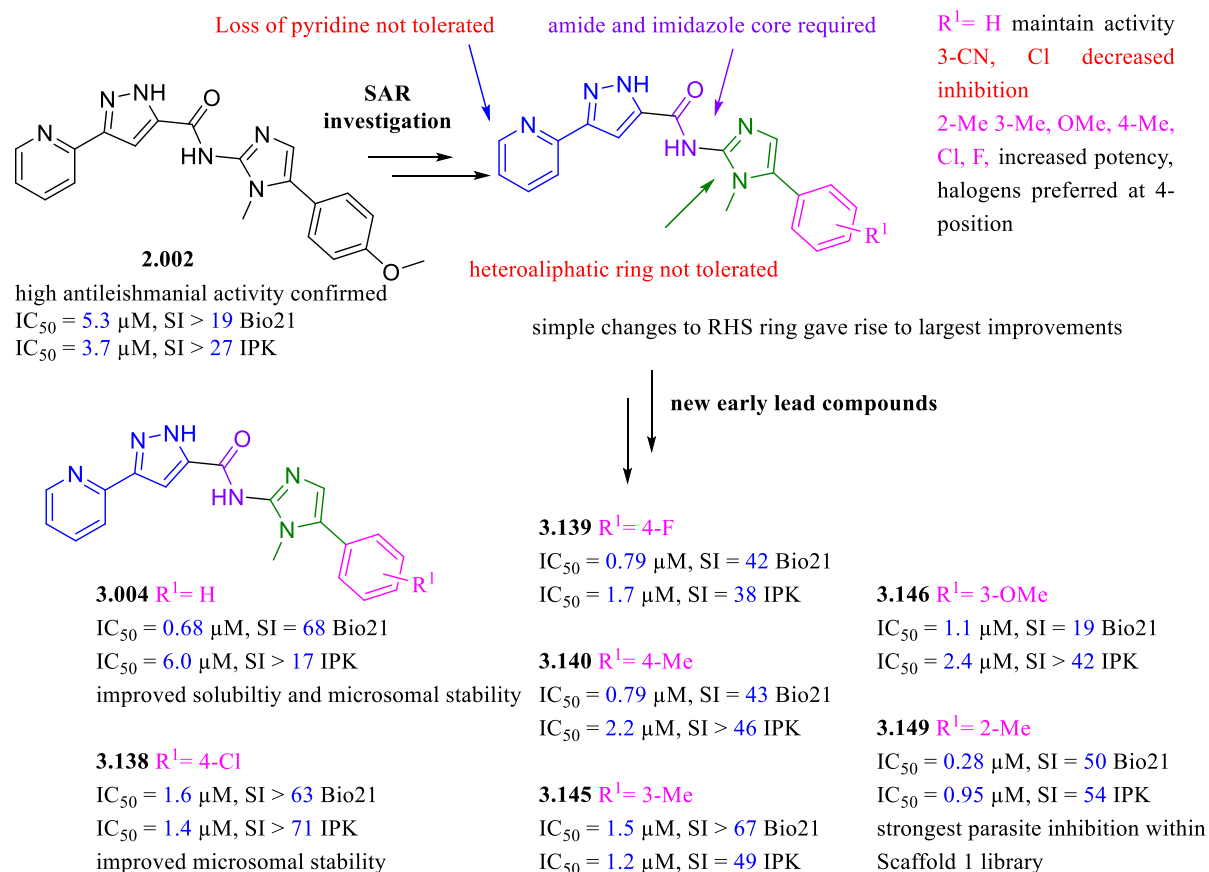


Figure 3: Summary of SAR profile around hit 2.002, Scaffold 1 and the early lead compounds developed

In addition to accomplishing our aim of generating a first-generation SAR profile around Scaffold 1, we have now achieved new early lead SAR compounds which have significantly improved potency against *L. donovani*, targeting the parasite selectively. By following the guidelines for early lead compounds outlined in Chapter 1, **Table 1.07**, we have achieved new lead compounds which also maintained drug-like properties, where the physicochemical properties of each hit adhere to the guidelines for oral availability and drug-likeness, outlined in Chapter 1. These new lead compounds also achieved improvements to *in vitro* metabolic stability in comparison to the original hits. Using our newly developed early lead compounds, further SAR investigations around this compound class guided by our established SAR profile may help optimize a stronger lead candidate for visceral leishmaniasis treatment.

In parallel to the studies around Scaffold 1, small analogue libraries around Scaffolds 2 to 5 (**Figure 1**) were developed in addition to reconfirming the respective hits **4.001-4.003**, **5.001**. The hits **4.001**, **4.002**

and the relevant small libraries of analogues surrounding Scaffold 2 and 3 respectively, were confirmed to demonstrate no activity against *L. donovani*, suggesting these initial hits to be false positives. Further investigations around Scaffold 2 and 3 were therefore discontinued.

The hit **4.003** (Scaffold 4) was confirmed to possess high antileishmanial activity and selectivity for the parasite over the host cell. Brief SAR studies around the hit **4.003** are summarized in **Figure 4**, suggesting that the quinoline ring was required to maintain antileishmanial activity, and loss of the *N*-methyl group within the benzimidazole ring was unfavourable. Continued studies around Scaffold 4 would continue within a parallel project at the Monash Institute of Pharmaceutical Sciences, with a particular focus on bioisosteric replacement of the hydrazide functionality.

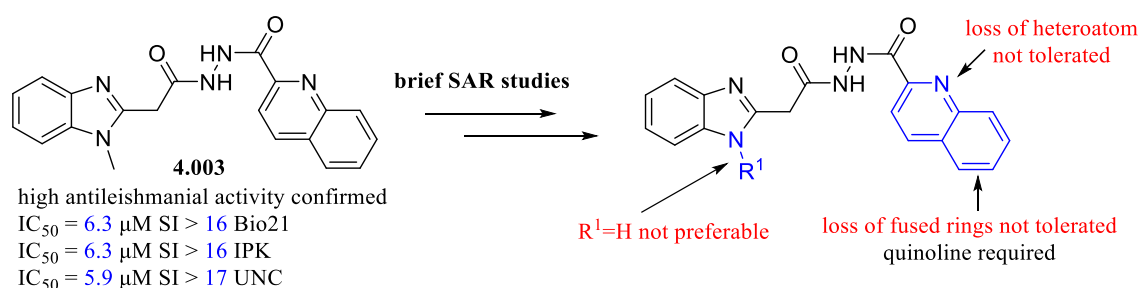


Figure 4: Summary of brief SAR studies around hit 4.003

The hit **5.001** of Scaffold 5 was confirmed to exert high antileishmanial activity and selectivity for the parasite over the host macrophages. A primary SAR profile was developed around Scaffold 5, which is summarized in **Figure 5**. Our studies confirmed that the terminal amide and chloro functionalities were required to maintain antileishmanial activity. Repositioning these substituents was only tolerated when the terminal amide was substituted at the 4-position, and the chloro group was also simultaneously repositioned to the 6-position. The loss of the O atom of the ether linkage was not required to maintaining antileishmanial activity, however removal of the methylene group or extending the carbon-carbon chain were highly unfavourable within the putative binding site/s. Addition of various functional groups around the phenoxy ring was only favourable at the *ortho*-position. The addition of the methoxy and fluoro substituents at the *ortho*-position were confirmed to exert high antileishmanial activity, whilst maintaining selectivity for the parasite over the host cell. By studying the various structural attributes of Scaffold 5, we have accomplished another primary SAR profile around a novel chemical class and have achieved new early lead compounds, which possess high antileishmanial activity and selectivity for the parasite over the host cell. Additionally, each of these new leads continues to maintain the desired physicochemical properties outlined in **Table 1.07**, Chapter 1, following guidelines for drug-likeness. These new early lead compounds and the established primary SAR profile will help guide further studies around Scaffold 5, to develop a more optimized candidate to be used against *L. donovani*.

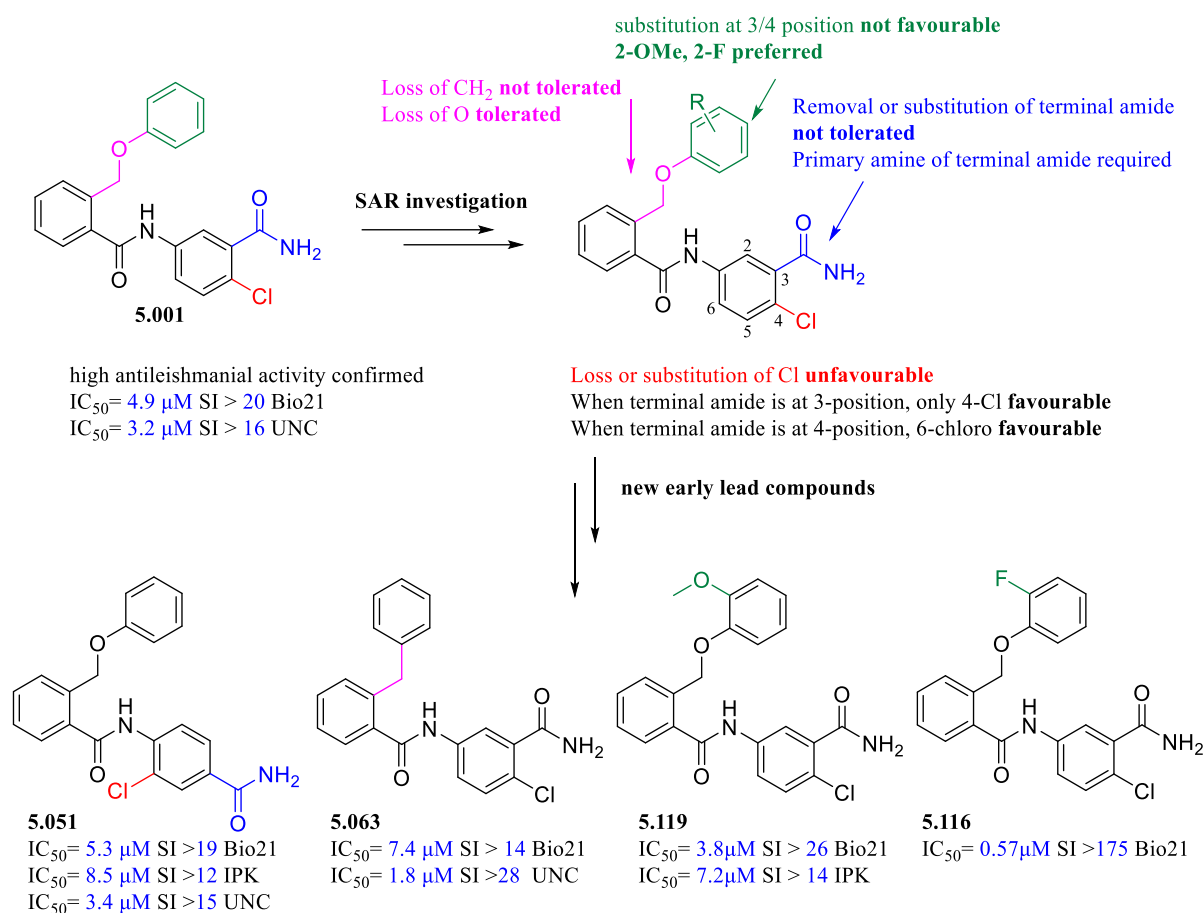


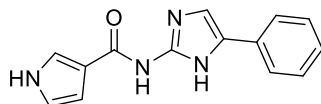
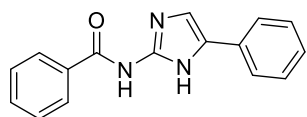
Figure 5: Summary of SAR profile around hit 5.001, Scaffold 1 and the early lead compounds developed

Overall, the work described in this thesis was a large collaborative effort undertaken in the pursuit for better antileishmanial agents. As discussed, we have accomplished our initial aims and hypothesis of developing a primary SAR profile around more than one of our initial hit compounds of **Figure 1** and achieved new early lead compounds which demonstrate strong antileishmanial activity and low cytotoxicity against the mammalian host cells. These primary SAR profiles and new lead compounds will help guide the optimization of the next generation of analogues, with the overall aim of developing a new chemical entity to treat visceral leishmaniasis.

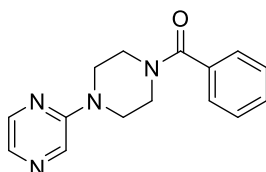
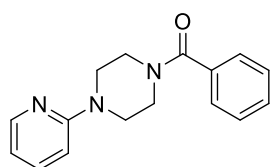
Appendix

Chapter 1 Appendix

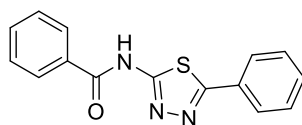
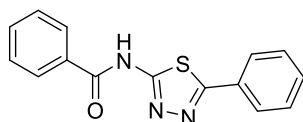
Appendix 1: Structures used for Substructure search around scaffolds of interest



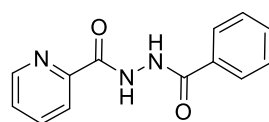
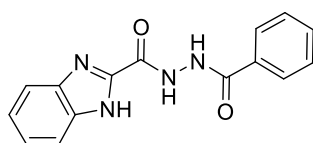
Scaffold 1



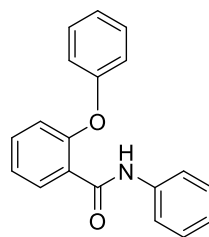
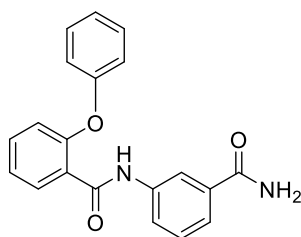
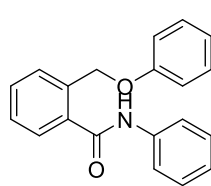
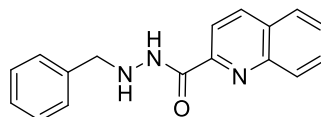
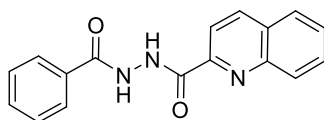
Scaffold 2



Scaffold 3



Scaffold 4



Scaffold 5

Chapter 2 Appendix

Appendix 2: Cell health studies using HepG2 and HepaRG cell lines using HCS GSH, ROS, MMP & ATP Assay

Compound **2.015** HepG2

Assay Summary	
Incubation time:	48h
Concentrations (µM):	0.04, 0.1, 0.4, 1, 4, 10, 40, 100
Replicates per concentration:	3
Cell model:	HepG2
Certified on:	2018-09-14

Data Summary

Cell Health Parameter	↑↓	MEC (µM)	AC ₅₀ (µM)	First Signal	
				MEC	AC ₅₀
Cell count	↓	1.63	19.2		
Nuclear size	↑	4.34	52.4		
DNA structure	↑	4.18	53.0		
Mitochondrial mass	↑	5.10	>40 †		
Mitochondrial membrane potential	↑	8.97	>40 †		
Oxidative stress	↑	1.38	>40 †		
Glutathione content	↑	61.8	92.3		
Cellular ATP	↓	0.606	2.21	•	•

MEC Minimum effective concentration that significantly crosses vehicle control threshold.

AC₅₀ The concentration at which 50% maximum effect is observed for each cell health parameter.

† An AC₅₀ was calculated, but is greater than the maximum surviving concentration.

↑↓ Direction of response.

NR No response observed.

NS Fit not statistically significant.

ER Early response observed (the compound responded at the lowest concentration tested).

First Signal The cell health feature which responds at the lowest observed dose (marked by •).

Cell Health Parameter Summary

MEC

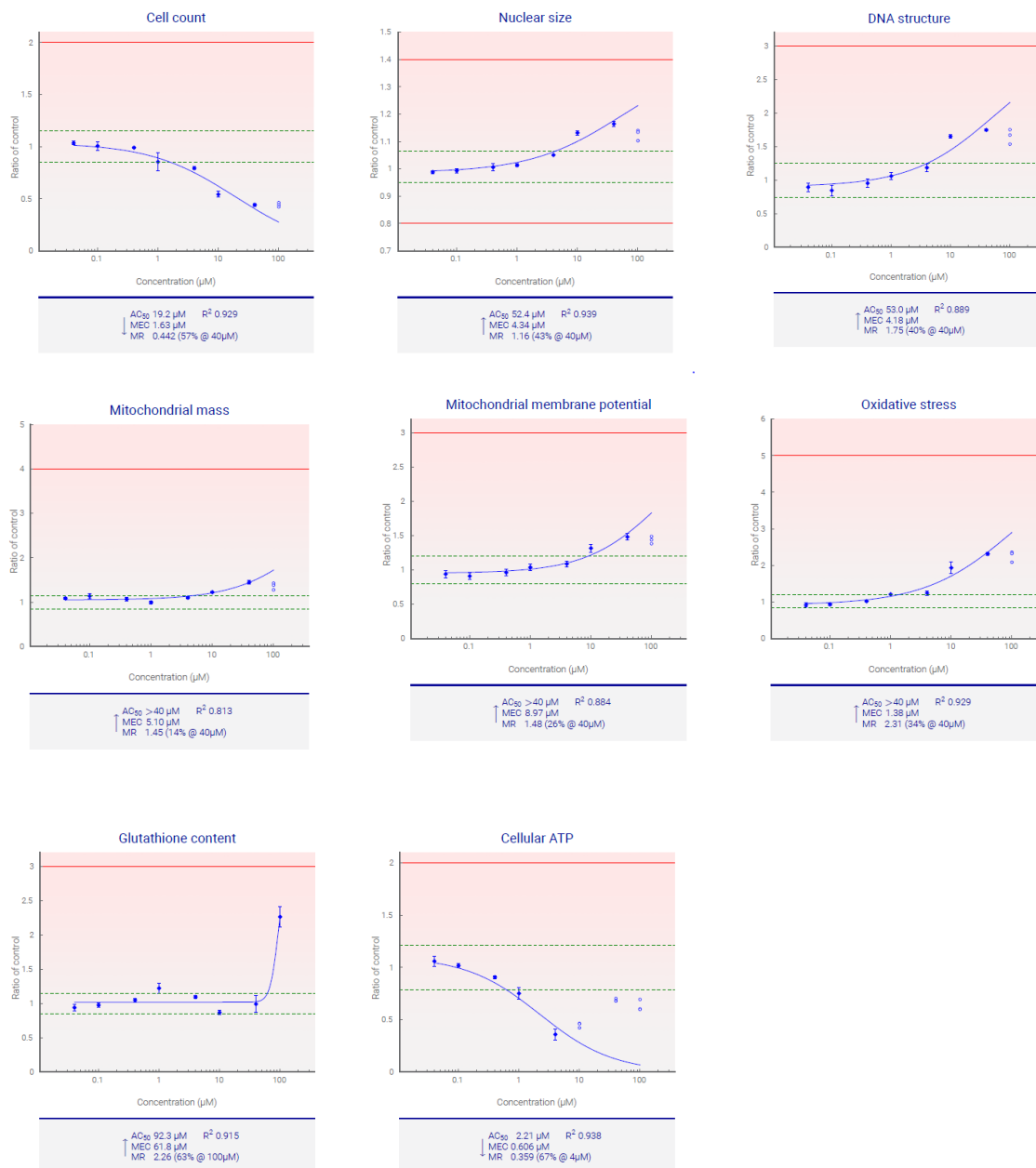
The lowest MEC response indicates compound **2.015** has resulted in a decrease in ATP (indicating a decrease in metabolically active cells); please refer to graphical representation for more information.

Other cell health parameters which respond are a loss of total cells per well (indicating toxicity due to necrosis, apoptosis or a reduction in cellular proliferation), an increase in nuclear size (indicating necrosis or G2 cell cycle arrest), an increase in DNA structure (indicating chromosomal instability and DNA fragmentation), an increase in mitochondrial mass (indicating an adaptive response to cellular energy demands), an increase in mitochondrial potential (implying adaption to cellular energy requirements), an increase in ROS (indicating an increase in toxic superoxide intermediates) and increased GSH content (indicating an adaptive cellular response to oxidative stress); please refer to graphical representation for more information.

AC₅₀

The lowest AC₅₀ response indicates compound **2.015** has resulted in a decrease in ATP (indicating a decrease in metabolically active cells); please refer to graphical representation for more information.

Other cell health parameters which respond are a loss of total cells per well (indicating toxicity due to necrosis, apoptosis or a reduction in cellular proliferation), an increase in nuclear size (indicating necrosis or G2 cell cycle arrest), an increase in DNA structure (indicating chromosomal instability and DNA fragmentation), an increase in mitochondrial mass (indicating an adaptive response to cellular energy demands), an increase in mitochondrial potential (implying adaption to cellular energy requirements), an increase in ROS (indicating an increase in toxic superoxide intermediates) and increased GSH content (indicating an adaptive cellular response to oxidative stress); please refer to graphical representation for more information.



Legend

Green dashed lines Significant cut-off from vehicle control (used to calculate the MEC).

Filled blue diamonds Mean data points for each concentration (plus or minus standard deviation).

Blue x Data points excluded from plot due to precipitate in well.

Open blue circles Data points excluded from plot due to data plateau, or other reasons. Points lying outside y-axis limits are annotated with small arrows.

Open blue squares Data points excluded from plot due to cell loss or nuclear size.

Red solid lines Historical maximum and minimum responses, used to calculate AC₅₀.

NS Fit not statistically significant.

MR Maximum response (ratio of control).

Compound **2.015** HepaRG

Assay Summary	
Incubation time:	48h
Concentrations (µM):	0.04, 0.1, 0.4, 1, 4, 10, 40, 100
Replicates per concentration:	3
Cell model:	HepaRG
Certified on:	2018-09-24

Data Summary

Cell Health Parameter	↑↓	MEC (µM)	AC ₅₀ (µM)	First Signal	
				MEC	AC ₅₀
Cell count		NR	NR		
Nuclear size		NR	NR		
DNA structure		NR	NR		
Mitochondrial mass		NR	NR		
Mitochondrial membrane potential		NR	NR		
Oxidative stress		NR	NR		
Glutathione content	↑	0.173	19.3	•	•
Cellular ATP		NR	NR		

MEC Minimum effective concentration that significantly crosses vehicle control threshold.
AC₅₀ The concentration at which 50% maximum effect is observed for each cell health parameter.
↑ An AC₅₀ was calculated, but is greater than the maximum surviving concentration.
↑↓ Direction of response.
NR No response observed.
NS Fit not statistically significant.
ER Early response observed (the compound responded at the lowest concentration tested).
First Signal The cell health feature which responds at the lowest observed dose (marked by •).

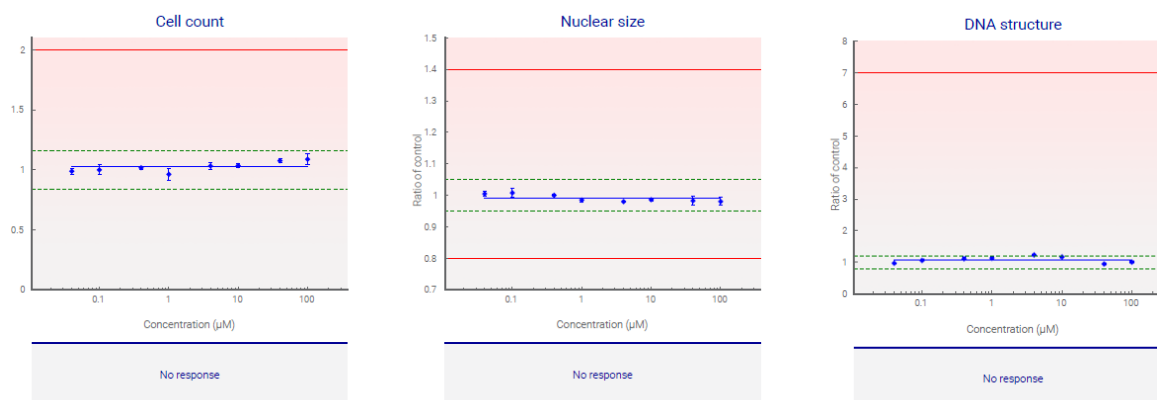
Cell Health Parameter Summary

MEC

The lowest MEC response indicates compound **2.015** has resulted in increased GSH content (indicating an adaptive cellular response to oxidative stress); please refer to graphical representation for more information.

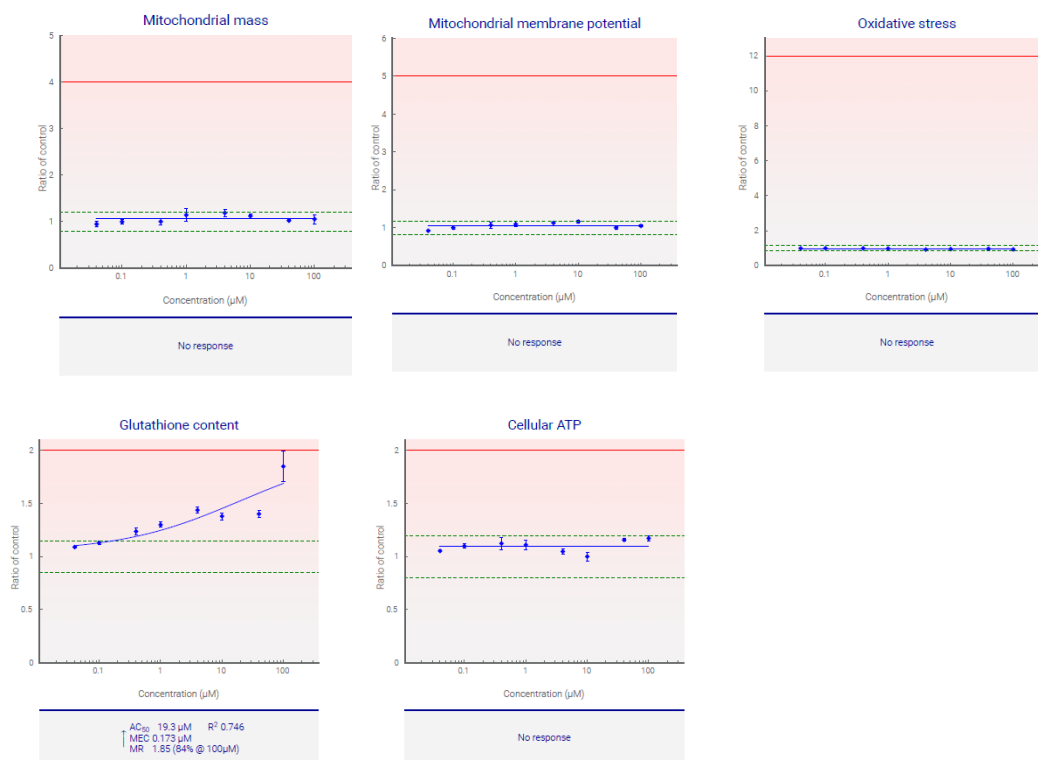
AC₅₀

The lowest AC₅₀ response indicates compound **2.015** has resulted in increased GSH content (indicating an adaptive cellular response to oxidative stress); please refer to graphical representation for more information.



Legend

Green dashed lines Significant cut-off from vehicle control (used to calculate the MEC).
Filled blue diamonds Mean data points for each concentration (plus or minus standard deviation).
Blue x Data points excluded from plot due to precipitate in well.
Open blue circles Data points excluded from plot due to data plateau, or other reasons. Points lying outside y-axis limits are annotated with small arrows.
Open blue squares Data points excluded from plot due to cell loss or nuclear size.
Red solid lines Historical maximum and minimum responses, used to calculate AC₅₀.
NS Fit not statistically significant.
MR Maximum response (ratio of control).



Legend

Green dashed lines: Significant cut-off from vehicle control (used to calculate the MEC).

Filled blue diamonds: Mean data points for each concentration (plus or minus standard deviation).

Blue x: Data points excluded from plot due to precipitate in well.

Open blue circles: Data points excluded from plot due to data plateau, or other reasons. Points lying outside y-axis limits are annotated with small arrows.

Open blue squares: Data points excluded from plot due to cell loss or nuclear size.

Red solid lines: Historical maximum and minimum responses, used to calculate AC₅₀.

NS: Fit not statistically significant.

MR: Maximum response (ratio of control).

Compound 2.018 HepG2

Assay Summary

Incubation time:	48h
Concentrations (μM):	0.04, 0.1, 0.4, 1, 4, 10, 40, 100
Replicates per concentration:	3
Cell model:	HepG2
Certified on:	2018-09-14

Data Summary

Cell Health Parameter	↑↓	MEC (μM)	AC ₅₀ (μM)	First Signal	
				MEC	AC ₅₀
Cell count	↓	1.38	25.0		
Nuclear size	↑	3.33	59.0		
DNA structure	↑	0.886	33.4		
Mitochondrial mass	↑	21.6	>100 †		
Mitochondrial membrane potential	↑	3.43	>100 †		
Oxidative stress	↑	0.909	89.2		
Glutathione content		NR	NR		
Cellular ATP	↓	0.643	2.41	•	•

MEC: Minimum effective concentration that significantly crosses vehicle control threshold.

AC₅₀: The concentration at which 50% maximum effect is observed for each cell health parameter.

†: An AC₅₀ was calculated, but is greater than the maximum surviving concentration.

↑↓: Direction of response.

NR: No response observed.

NS: Fit not statistically significant.

ER: Early response observed (the compound responded at the lowest concentration tested).

First Signal: The cell health feature which responds at the lowest observed dose (marked by •).

Cell Health Parameter Summary MEC

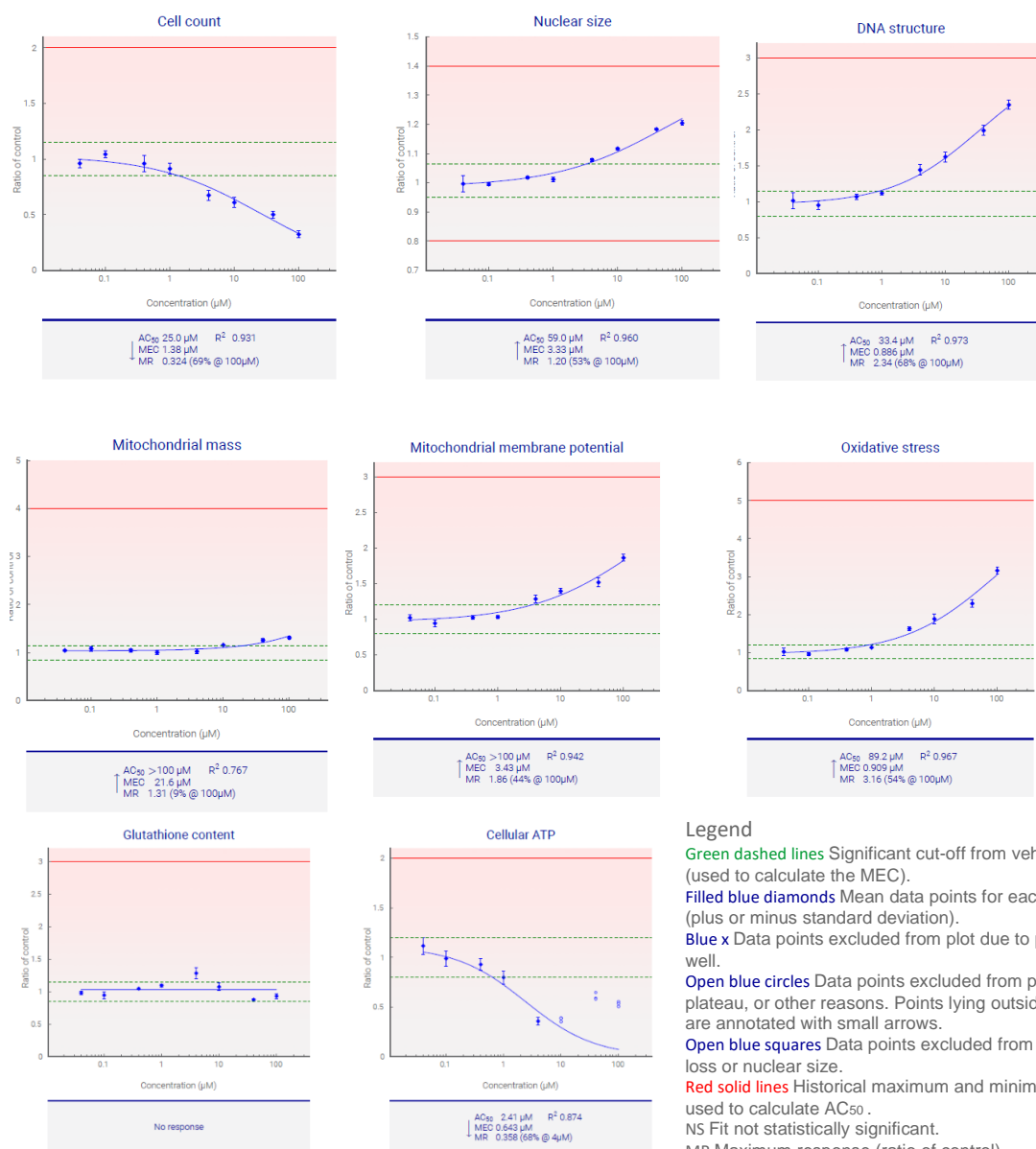
The lowest MEC response indicates compound **2.018** has resulted in a decrease in ATP (indicating a decrease in metabolically active cells); please refer to graphical representation for more information.

Other cell health parameters which respond are a loss of total cells per well (indicating toxicity due to necrosis, apoptosis or a reduction in cellular proliferation), an increase in nuclear size (indicating necrosis or G2 cell cycle arrest), an increase in DNA structure (indicating chromosomal instability and DNA fragmentation), an increase in mitochondrial mass (indicating an adaptive response to cellular energy demands), an increase in mitochondrial potential (implying adaption to cellular energy requirements) and an increase in ROS (indicating an increase in toxic superoxide intermediates); please refer to graphical representation for more information.

AC50

The lowest AC50 response indicates compound **2.018** has resulted in a decrease in ATP (indicating a decrease in metabolically active cells); please refer to graphical representation for more information.

Other cell health parameters which respond are a loss of total cells per well (indicating toxicity due to necrosis, apoptosis or a reduction in cellular proliferation), an increase in nuclear size (indicating necrosis or G2 cell cycle arrest), an increase in DNA structure (indicating chromosomal instability and DNA fragmentation), an increase in mitochondrial mass (indicating an adaptive response to cellular energy demands), an increase in mitochondrial potential (implying adaption to cellular energy requirements) and an increase in ROS (indicating an increase in toxic superoxide intermediates); please refer to graphical representation for more information.



Compound **2.018** HepaRG

Assay Summary	
Incubation time:	48h
Concentrations (µM):	0.04, 0.1, 0.4, 1, 4, 10, 40, 100
Replicates per concentration:	3
Cell model:	HepaRG
Certified on:	2018-09-24

Data Summary

Cell Health Parameter	↑↓	MEC (µM)	AC ₅₀ (µM)	First Signal	
				MEC	AC ₅₀
Cell count		NR	NR		
Nuclear size		NR	NR		
DNA structure		NR	NR		
Mitochondrial mass	↑	26.5 (NS)	>100 † (NS)	•	
Mitochondrial membrane potential		NR	NR		
Oxidative stress	↓	64.4	>100 †		•
Glutathione content		NR	NR		
Cellular ATP	↑	64.6	>100 †		•

MEC Minimum effective concentration that significantly crosses vehicle control threshold.
AC₅₀ The concentration at which 50% maximum effect is observed for each cell health parameter.
† An AC₅₀ was calculated, but is greater than the maximum surviving concentration.
↑↓ Direction of response.
NR No response observed.
NS Fit not statistically significant.
ER Early response observed (the compound responded at the lowest concentration tested).
First Signal The cell health feature which responds at the lowest observed dose (marked by •).

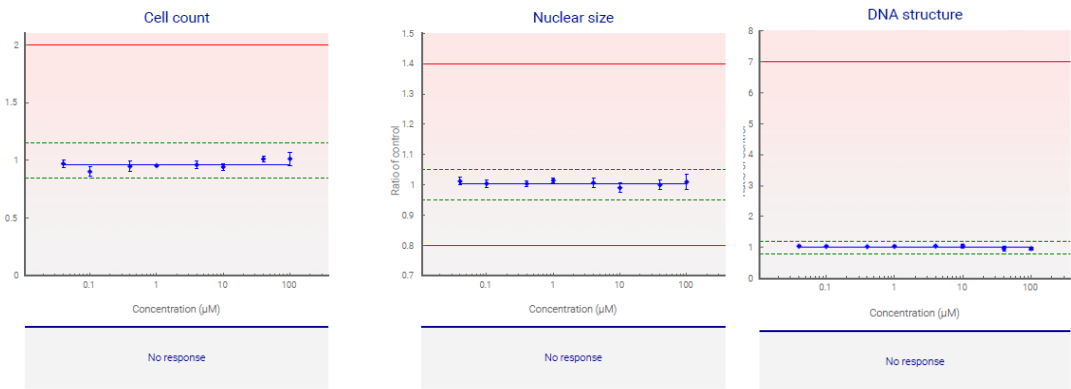
Cell Health Parameter Summary

MEC

The lowest MEC response indicates compound **2.018** has resulted in an increase in mitochondrial mass (indicating an adaptive response to cellular energy demands); please refer to graphical representation for more information. Other cell health parameters which respond are a decrease in ROS and an increase in ATP; please refer to graphical representation for more information.

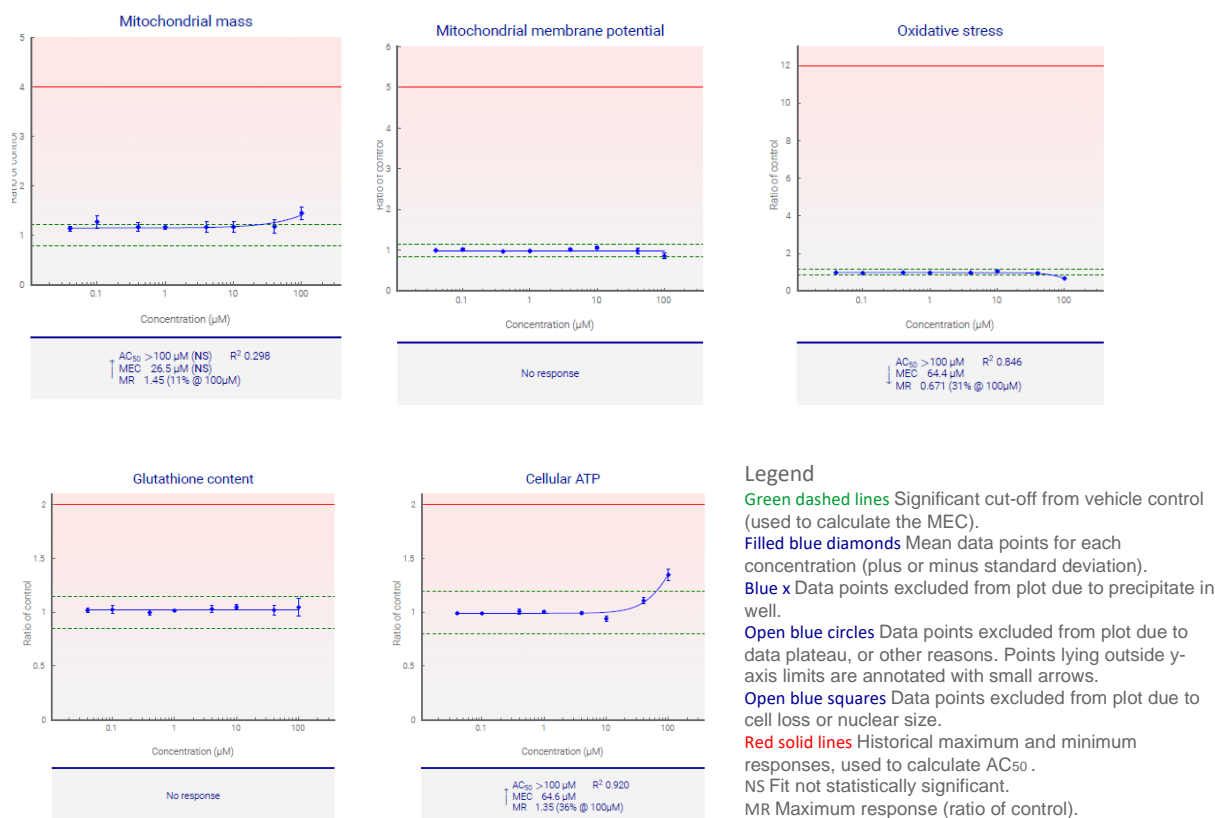
AC50

The lowest AC50 response indicates compound **2.018** has resulted in a decrease in ROS and an increase in ATP; please refer to graphical representation for more information



Legend

Green dashed lines Significant cut-off from vehicle control (used to calculate the MEC).
Filled blue diamonds Mean data points for each concentration (plus or minus standard deviation).
Blue x Data points excluded from plot due to precipitate in well.
Open blue circles Data points excluded from plot due to data plateau, or other reasons. Points lying outside y-axis limits are annotated with small arrows.
Open blue squares Data points excluded from plot due to cell loss or nuclear size.
Red solid lines Historical maximum and minimum responses, used to calculate AC₅₀.
NS Fit not statistically significant.
MR Maximum response (ratio of control).



Compound 2.024 HepG2

Assay Summary

Incubation time:	48h
Concentrations (μM):	0.04, 0.1, 0.4, 1, 4, 10, 40, 100
Replicates per concentration:	3
Cell model:	HepG2
Certified on:	2018-09-14

Data Summary

Cell Health Parameter	$\uparrow\downarrow$	MEC (μM)	AC ₅₀ (μM)	First Signal	
				MEC	AC ₅₀
Cell count	\downarrow	11.9	54.2		
Nuclear size	\uparrow	16.1	>100 \dagger		
DNA structure	\uparrow	7.22	62.6		
Mitochondrial mass		NR	NR		
Mitochondrial membrane potential	\uparrow	16.3	>100 \dagger		
Oxidative stress	\uparrow	4.45	>100 \dagger		
Glutathione content		NR	NR		
Cellular ATP	\downarrow	0.825	9.31	•	•

MEC Minimum effective concentration that significantly crosses vehicle control threshold.
AC₅₀ The concentration at which 50% maximum effect is observed for each cell health parameter.
 \dagger An AC₅₀ was calculated, but is greater than the maximum surviving concentration.
 $\uparrow\downarrow$ Direction of response.
NR No response observed.
NS Fit not statistically significant.
ER Early response observed (the compound responded at the lowest concentration tested).
First Signal The cell health feature which responds at the lowest observed dose (marked by •).

Cell Health Parameter Summary

MEC

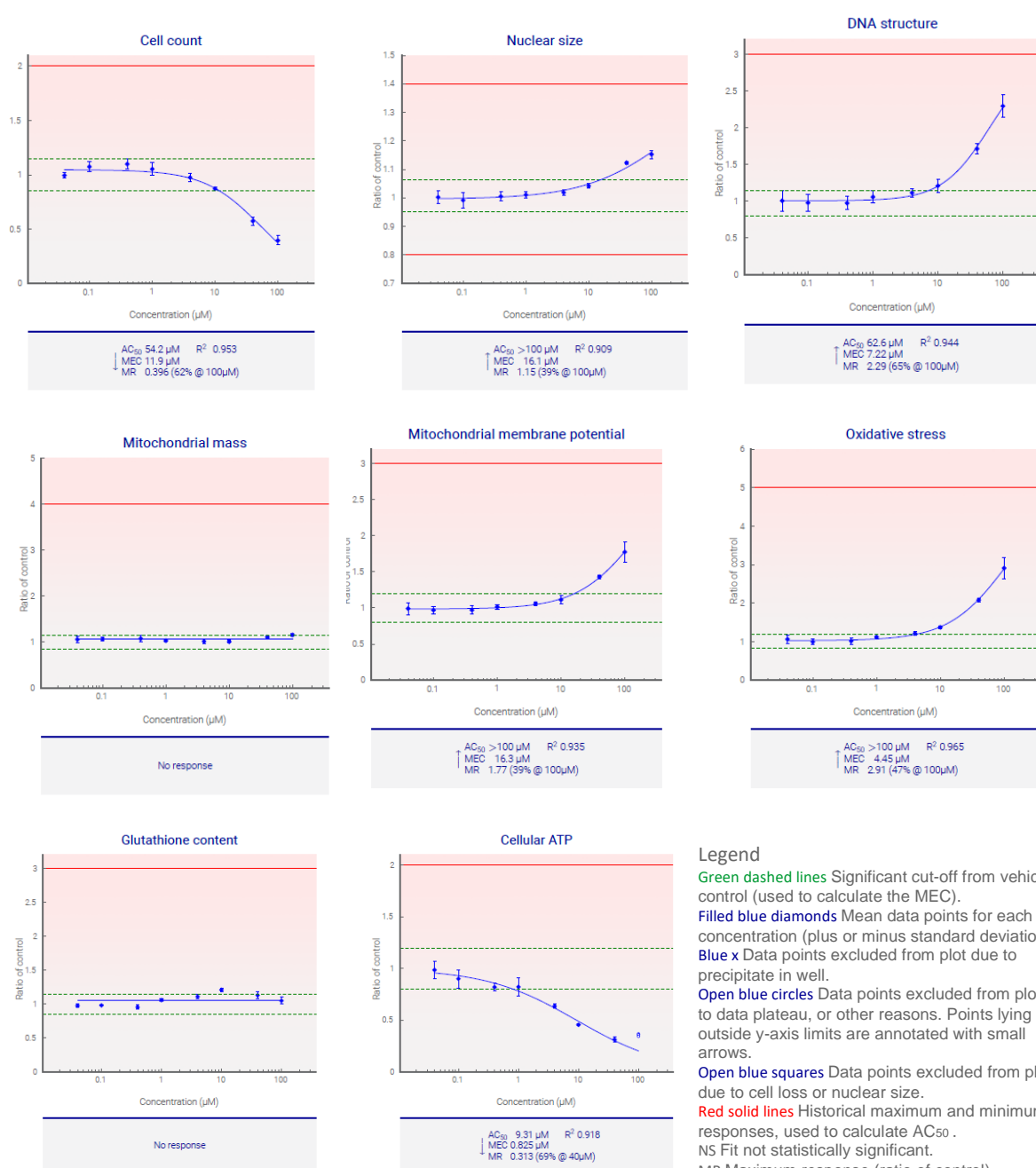
The lowest MEC response indicates compound **2.024** has resulted in a decrease in ATP (indicating a decrease in metabolically active cells); please refer to graphical representation for more information.

Other cell health parameters which respond are a loss of total cells per well (indicating toxicity due to necrosis, apoptosis or a reduction in cellular proliferation), an increase in nuclear size (indicating necrosis or G2 cell cycle arrest), an increase in DNA structure (indicating chromosomal instability and DNA fragmentation), an increase in mitochondrial potential (implying adaption to cellular energy requirements) and an increase in ROS (indicating an increase in toxic superoxide intermediates); please refer to graphical representation for more information.

AC50

The lowest AC50 response indicates compound **2.024** has resulted in a decrease in ATP (indicating a decrease in metabolically active cells); please refer to graphical representation for more information.

Other cell health parameters which respond are a loss of total cells per well (indicating toxicity due to necrosis, apoptosis or a reduction in cellular proliferation), an increase in nuclear size (indicating necrosis or G2 cell cycle arrest), an increase in DNA structure (indicating chromosomal instability and DNA fragmentation), an increase in mitochondrial potential (implying adaption to cellular energy requirements) and an increase in ROS (indicating an increase in toxic superoxide intermediates); please refer to graphical representation for more information.



Compound **2.024** HepaRG

Assay Summary	
Incubation time:	48h
Concentrations (µM):	0.04, 0.1, 0.4, 1, 4, 10, 40, 100
Replicates per concentration:	3
Cell model:	HepaRG
Certified on:	2018-09-24

Data Summary

Cell Health Parameter	↑↓	MEC (µM)	AC ₅₀ (µM)	First Signal	
				MEC	AC ₅₀
Cell count		NR	NR		
Nuclear size		NR	NR		
DNA structure		NR	NR		
Mitochondrial mass		NR	NR		
Mitochondrial membrane potential		NR	NR		
Oxidative stress		NR	NR		
Glutathione content	↑	45.9	>100 †	•	•
Cellular ATP		NR	NR		

MEC Minimum effective concentration that significantly crosses vehicle control threshold.
AC₅₀ The concentration at which 50% maximum effect is observed for each cell health parameter.
† An AC₅₀ was calculated, but is greater than the maximum surviving concentration.
↑↓ Direction of response.
NR No response observed.
NS Fit not statistically significant.
ER Early response observed (the compound responded at the lowest concentration tested).
First Signal The cell health feature which responds at the lowest observed dose (marked by •).

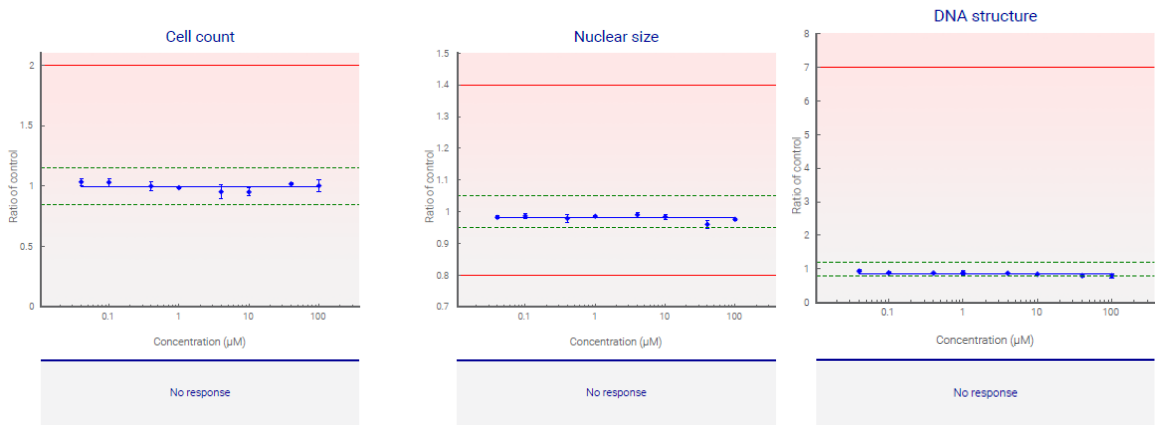
Cell Health Parameter Summary

MEC

The lowest MEC response indicates compound **2.024** has resulted in increased GSH content (indicating an adaptive cellular response to oxidative stress); please refer to graphical representation for more information.

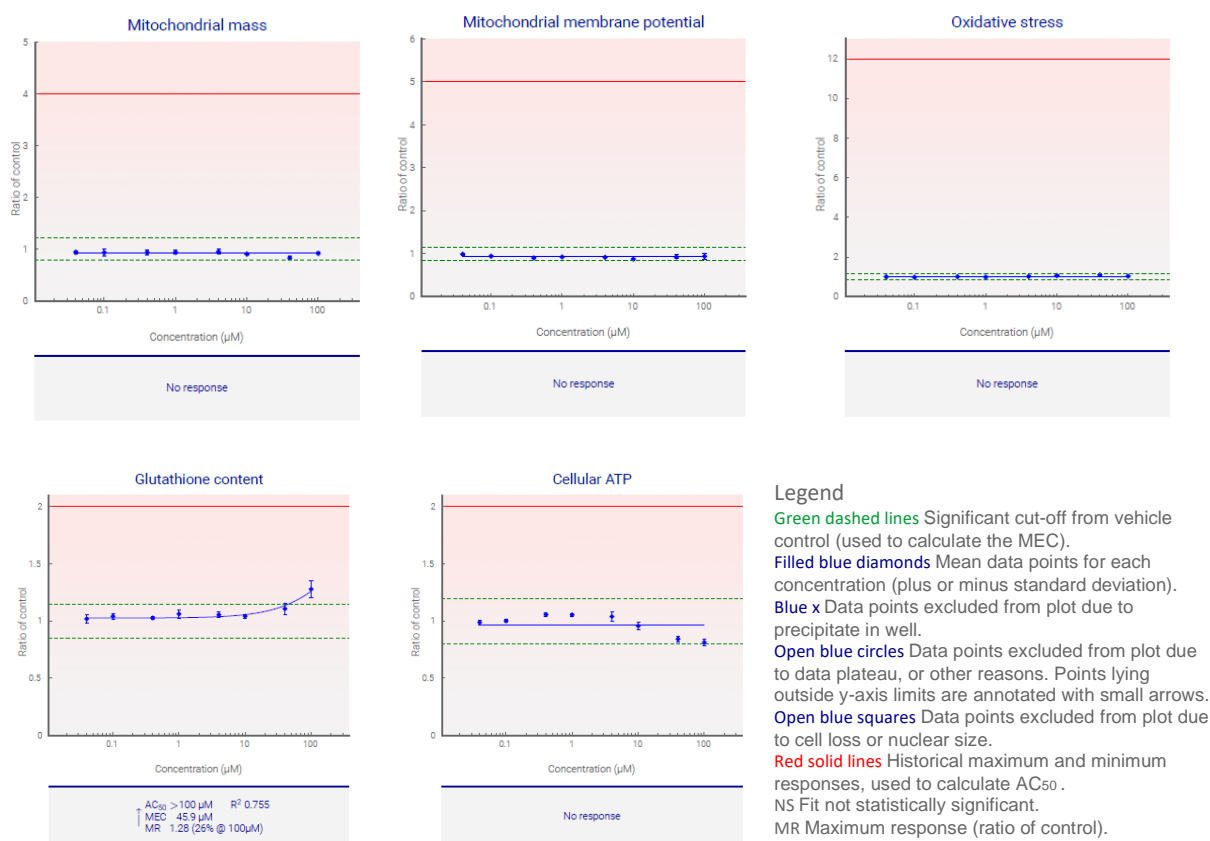
AC50

The lowest AC50 response indicates compound **2.024** has resulted in increased GSH content (indicating an adaptive cellular response to oxidative stress); please refer to graphical representation for more information.



Legend

Green dashed lines Significant cut-off from vehicle control (used to calculate the MEC).
Filled blue diamonds Mean data points for each concentration (plus or minus standard deviation).
Blue x Data points excluded from plot due to precipitate in well.
Open blue circles Data points excluded from plot due to data plateau, or other reasons. Points lying outside y-axis limits are annotated with small arrows.
Open blue squares Data points excluded from plot due to cell loss or nuclear size.
Red solid lines Historical maximum and minimum responses, used to calculate AC₅₀.
NS Fit not statistically significant.
MR Maximum response (ratio of control).



Compound 2.037 HepG2

Assay Summary

Incubation time:	48h
Concentrations (μM):	0.04, 0.1, 0.4, 1, 4, 10, 40, 100
Replicates per concentration:	3
Cell model:	HepG2
Certified on:	2018-09-14

Data Summary

Cell Health Parameter	↑↓	MEC (μM)	AC ₅₀ (μM)	First Signal	
				MEC	AC ₅₀
Cell count	↓	10.8	45.4		
Nuclear size	↑	29.8	>100 †		
DNA structure	↑	21.6	>100 †		
Mitochondrial mass		NR	NR		
Mitochondrial membrane potential	↑	26.0	>100 †		
Oxidative stress	↑	11.5	93.3		
Glutathione content	↑	14.5	>40 †		
Cellular ATP	↓	5.68	33.0	•	•

MEC Minimum effective concentration that significantly crosses vehicle control threshold.
AC₅₀ The concentration at which 50% maximum effect is observed for each cell health parameter.
† An AC₅₀ was calculated, but is greater than the maximum surviving concentration.
↑, ↓ Direction of response.
NR No response observed.
NS Fit not statistically significant.
ER Early response observed (the compound responded at the lowest concentration tested).
First Signal The cell health feature which responds at the lowest observed dose (marked by •).

Cell Health Parameter Summary

MEC

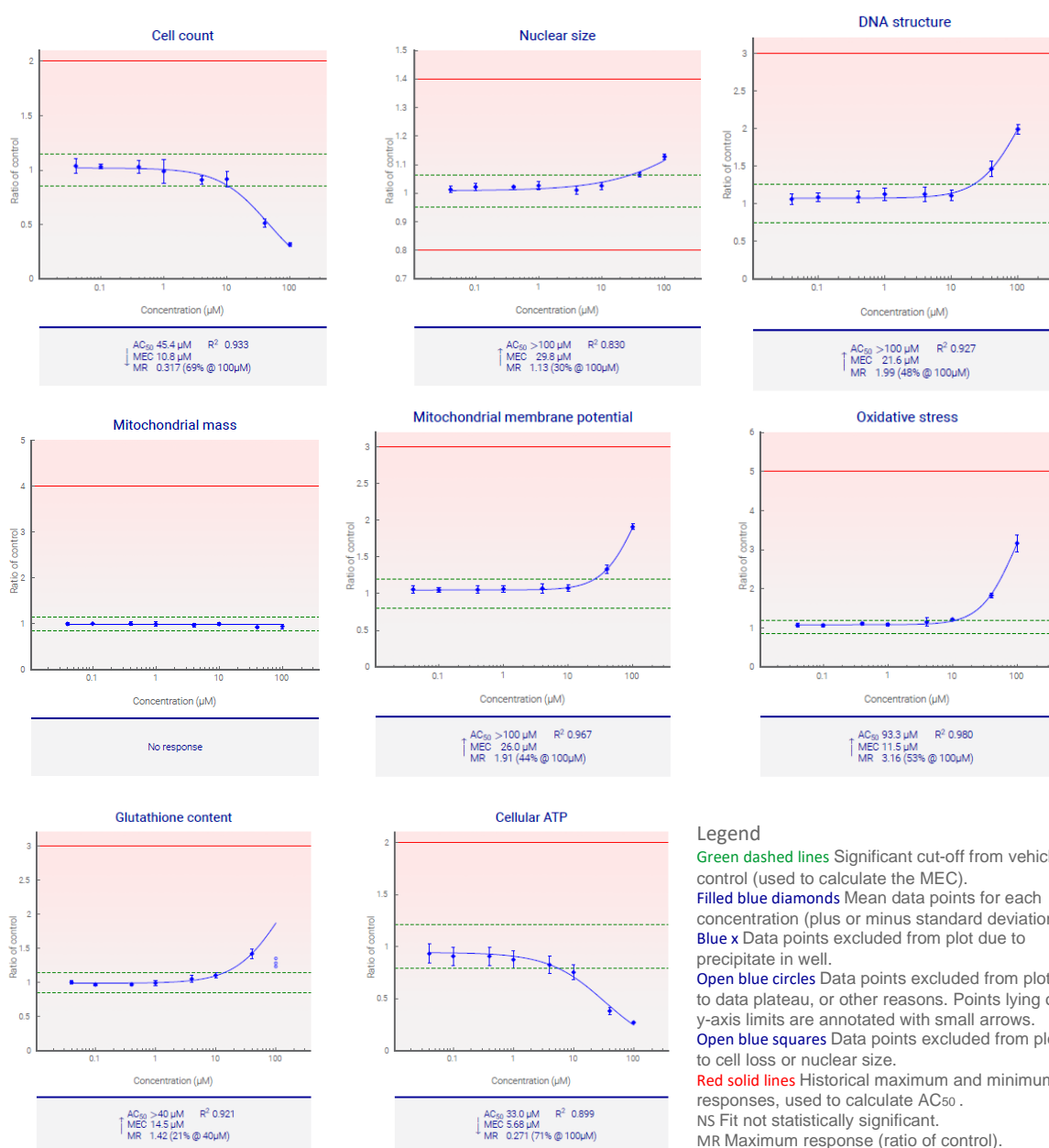
The lowest MEC response indicates compound **2.037** has resulted in a decrease in ATP (indicating a decrease in metabolically active cells); please refer to graphical representation for more information.

Other cell health parameters which respond are a loss of total cells per well (indicating toxicity due to necrosis, apoptosis or a reduction in cellular proliferation), an increase in nuclear size (indicating necrosis or G2 cell cycle arrest), an increase in DNA structure (indicating chromosomal instability and DNA fragmentation), an increase in mitochondrial potential (implying adaption to cellular energy requirements), an increase in ROS (indicating an increase in toxic superoxide intermediates) and increased GSH content (indicating an adaptive cellular response to oxidative stress); please refer to graphical representation for more information.

AC50

The lowest AC50 response indicates compound **2.037** has resulted in a decrease in ATP (indicating a decrease in metabolically active cells); please refer to graphical representation for more information.

Other cell health parameters which respond are a loss of total cells per well (indicating toxicity due to necrosis, apoptosis or a reduction in cellular proliferation), an increase in nuclear size (indicating necrosis or G2 cell cycle arrest), an increase in DNA structure (indicating chromosomal instability and DNA fragmentation), an increase in mitochondrial potential (implying adaption to cellular energy requirements), an increase in ROS (indicating an increase in toxic superoxide intermediates) and increased GSH content (indicating an adaptive cellular response to oxidative stress); please refer to graphical representation for more information.



Compound **2.037** HepaRG

Assay Summary	
Incubation time:	48h
Concentrations (µM):	0.04, 0.1, 0.4, 1, 4, 10, 40, 100
Replicates per concentration:	3
Cell model:	HepaRG
Certified on:	2018-09-24

Data Summary

Cell Health Parameter	↑↓	MEC (µM)	AC ₅₀ (µM)	First Signal	
				MEC	AC ₅₀
Cell count		NR	NR		
Nuclear size		NR	NR		
DNA structure		NR	NR		
Mitochondrial mass		NR	NR		
Mitochondrial membrane potential		NR	NR		
Oxidative stress		NR	NR		
Glutathione content	↑	14.7 (NS)	>100 ‡ (NS)	•	
Cellular ATP		NR	NR		

MEC Minimum effective concentration that significantly crosses vehicle control threshold.
AC₅₀ The concentration at which 50% maximum effect is observed for each cell health parameter.
‡ An AC₅₀ was calculated, but is greater than the maximum surviving concentration.
↑↓ Direction of response.
NR No response observed.
NS Fit not statistically significant.
ER Early response observed (the compound responded at the lowest concentration tested).
First Signal The cell health feature which responds at the lowest observed dose (marked by •).

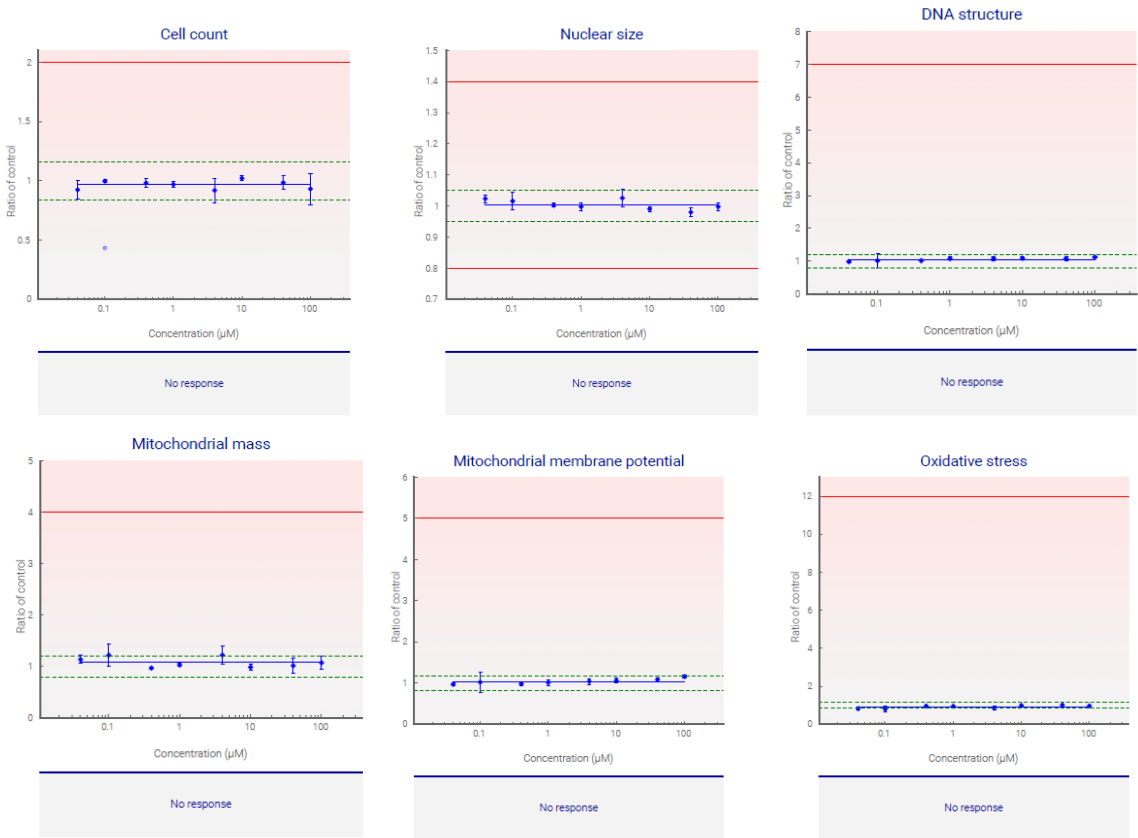
Cell Health Parameter Summary

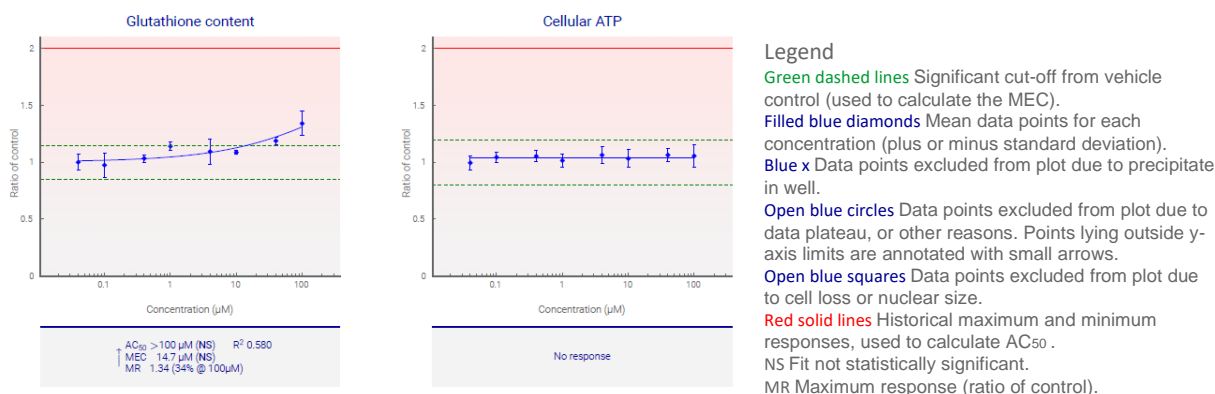
MEC

The lowest MEC response indicates compound **2.037** has resulted in increased GSH content (indicating an adaptive cellular response to oxidative stress); please refer to graphical representation for more information.

AC50

No significant response was observed at any of the cell health parameters measured, for the concentration range tested. Please refer to graphical representation for more information.





Compound 2.042 HepG2

Assay Summary

Incubation time:	48h
Concentrations (μM):	0.04, 0.1, 0.4, 1, 4, 10, 40, 100
Replicates per concentration:	3
Cell model:	HepG2
Certified on:	2018-10-01

Data Summary

Cell Health Parameter	↑↓	MEC (μM)	AC ₅₀ (μM)	First Signal	
				MEC	AC ₅₀
Cell count	↓	3.40 (NS)	>100 † (NS)	•	
Nuclear size		NR	NR		
DNA structure	↑	44.0 (NS)	>100 † (NS)		
Mitochondrial mass		NR	NR		
Mitochondrial membrane potential	↑	70.7	>100 †		
Oxidative stress	↑	17.2	>100 †		
Glutathione content	↑	18.7	>100 †		
Cellular ATP	↓	61.0	99.2		•

MEC Minimum effective concentration that significantly crosses vehicle control threshold.
 AC₅₀ The concentration at which 50% maximum effect is observed for each cell health parameter.
 † An AC₅₀ was calculated, but is greater than the maximum surviving concentration.
 ↑↓ Direction of response.
 NR No response observed.
 NS Fit not statistically significant.
 ER Early response observed (the compound responded at the lowest concentration tested).
 First Signal The cell health feature which responds at the lowest observed dose (marked by •).

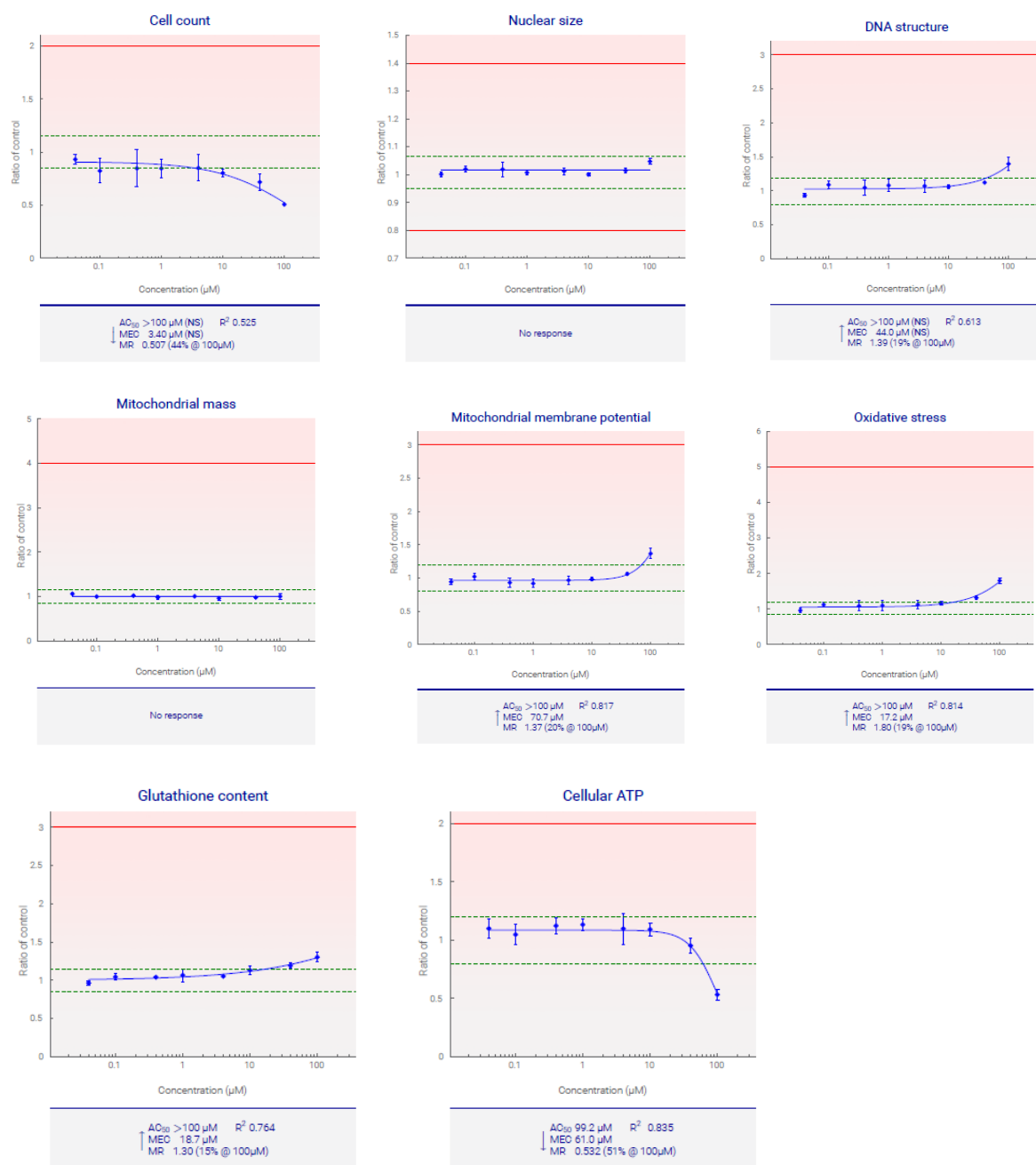
Cell Health Parameter Summary

MEC

The lowest MEC response indicates compound **2.042** has resulted in a loss of total cells per well (indicating toxicity due to necrosis, apoptosis or a reduction in cellular proliferation); please refer to graphical representation for more information. Other cell health parameters which respond are an increase in DNA structure (indicating chromosomal instability and DNA fragmentation), an increase in mitochondrial potential (implying adaption to cellular energy requirements), an increase in ROS (indicating an increase in toxic superoxide intermediates), increased GSH content (indicating an adaptive cellular response to oxidative stress) and a decrease in ATP (indicating a decrease in metabolically active cells); please refer to graphical representation for more information.

AC50

The lowest AC50 response indicates compound **2.042** has resulted in a decrease in ATP (indicating a decrease in metabolically active cells); please refer to graphical representation for more information. Other cell health parameters which respond are an increase in mitochondrial potential (implying adaption to cellular energy requirements), an increase in ROS (indicating an increase in toxic superoxide intermediates) and increased GSH content (indicating an adaptive cellular response to oxidative stress); please refer to graphical representation for more information.



Legend

Green dashed lines Significant cut-off from vehicle control (used to calculate the MEC).

Filled blue diamonds Mean data points for each concentration (plus or minus standard deviation).

Blue x Data points excluded from plot due to precipitate in well.

Open blue circles Data points excluded from plot due to data plateau, or other reasons. Points lying outside y-axis limits are annotated with small arrows.

Open blue squares Data points excluded from plot due to cell loss or nuclear size.

Red solid lines Historical maximum and minimum responses, used to calculate AC₅₀.

NS Fit not statistically significant.

MR Maximum response (ratio of control).

Compound **2.042** HepaRG

Assay Summary

Incubation time:	48h
Concentrations (µM):	0.04, 0.1, 0.4, 1, 4, 10, 40, 100
Replicates per concentration:	3
Cell model:	HepaRG
Certified on:	2018-10-04

Data Summary

Cell Health Parameter	↑↓	MEC (µM)	AC ₅₀ (µM)	First Signal	
				MEC	AC ₅₀
Cell count		NR	NR		
Nuclear size		NR	NR		
DNA structure		NR	NR		
Mitochondrial mass		NR	NR		
Mitochondrial membrane potential		NR	NR		
Oxidative stress		NR	NR		
Glutathione content	↑	1.10	17.5	•	•
Cellular ATP	↑	16.0	>40 †		

MEC Minimum effective concentration that significantly crosses vehicle control threshold.

AC₅₀ The concentration at which 50% maximum effect is observed for each cell health parameter.

† An AC₅₀ was calculated, but is greater than the maximum surviving concentration.

↑↓ Direction of response.

NR No response observed.

NS Fit not statistically significant.

ER Early response observed (the compound responded at the lowest concentration tested).

First Signal The cell health feature which responds at the lowest observed dose (marked by •).

Cell Health Parameter Summary

MEC

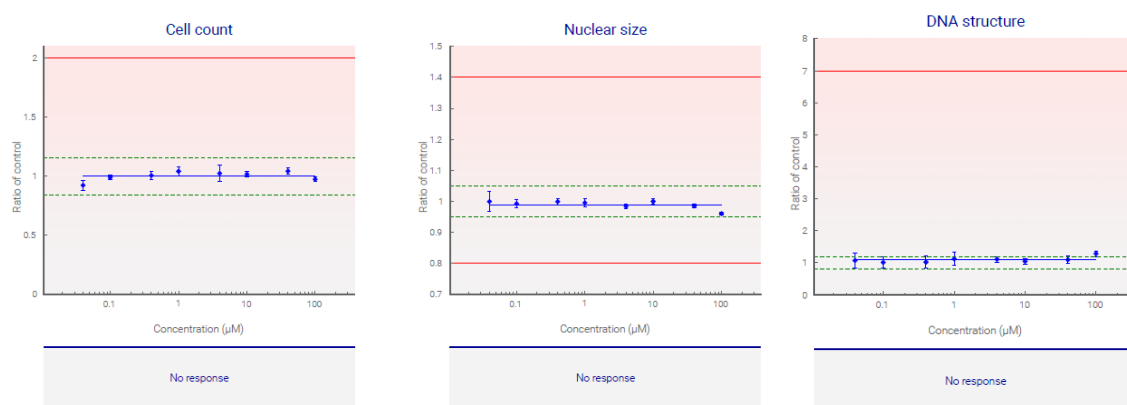
The lowest MEC response indicates compound **2.042** has resulted in increased GSH content (indicating an adaptive cellular response to oxidative stress); please refer to graphical representation for more information.

Other cell health parameters which respond are an increase in ATP; please refer to graphical representation for more information.

AC₅₀

The lowest AC₅₀ response indicates compound **2.042** has resulted in increased GSH content (indicating an adaptive cellular response to oxidative stress); please refer to graphical representation for more information.

Other cell health parameters which respond are an increase in ATP; please refer to graphical representation for more information.



Legend

Green dashed lines Significant cut-off from vehicle control (used to calculate the MEC).

Filled blue diamonds Mean data points for each concentration (plus or minus standard deviation).

Blue x Data points excluded from plot due to precipitate in well.

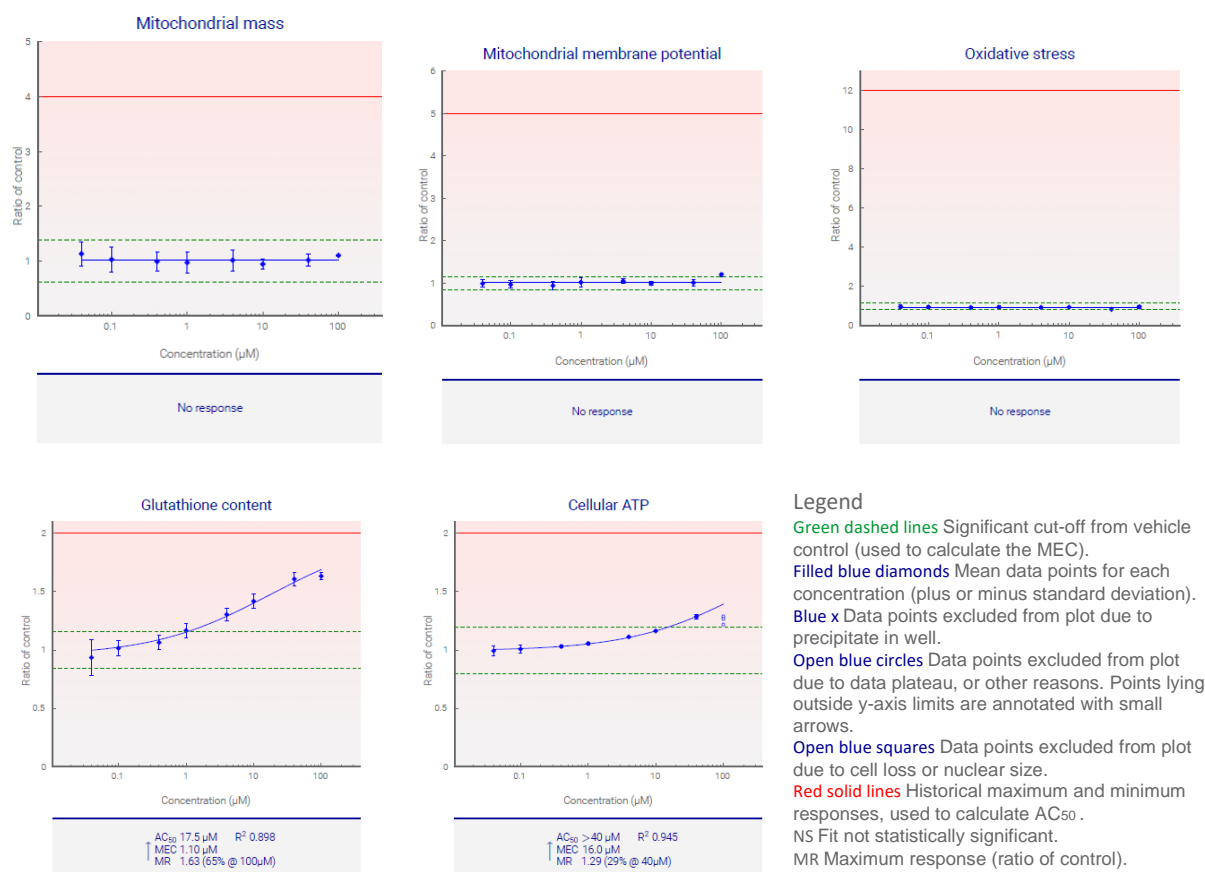
Open blue circles Data points excluded from plot due to data plateau, or other reasons. Points lying outside y-axis limits are annotated with small arrows.

Open blue squares Data points excluded from plot due to cell loss or nuclear size.

Red solid lines Historical maximum and minimum responses, used to calculate AC₅₀.

NS Fit not statistically significant.

MR Maximum response (ratio of control).



Compound 2.059 HepG2

Assay Summary

Incubation time: 48h
Concentrations (μM): 0.04, 0.1, 0.4, 1, 4, 10, 40, 100
Replicates per concentration: 3
Cell model: HepG2
Certified on: 2018-09-14

Data Summary

Cell Health Parameter	↑↓	MEC (μM)	AC ₅₀ (μM)	First Signal MEC AC ₅₀
Cell count	↓	0.773	24.9	•
Nuclear size	↑	5.19	>100 †	
DNA structure	↑	9.99	>100 †	
Mitochondrial mass	↑	7.38	>40 †	
Mitochondrial membrane potential	↑	9.15	>100 †	
Oxidative stress	↑	3.39	>100 †	
Glutathione content	↓	20.7	56.1	
Cellular ATP	↓	0.906	2.24	•

MEC Minimum effective concentration that significantly crosses vehicle control threshold.
AC₅₀ The concentration at which 50% maximum effect is observed for each cell health parameter.
† An AC₅₀ was calculated, but is greater than the maximum surviving concentration.
↑↓ Direction of response.
NR No response observed.
NS Fit not statistically significant.
ER Early response observed (the compound responded at the lowest concentration tested).
First Signal The cell health feature which responds at the lowest observed dose (marked by •).

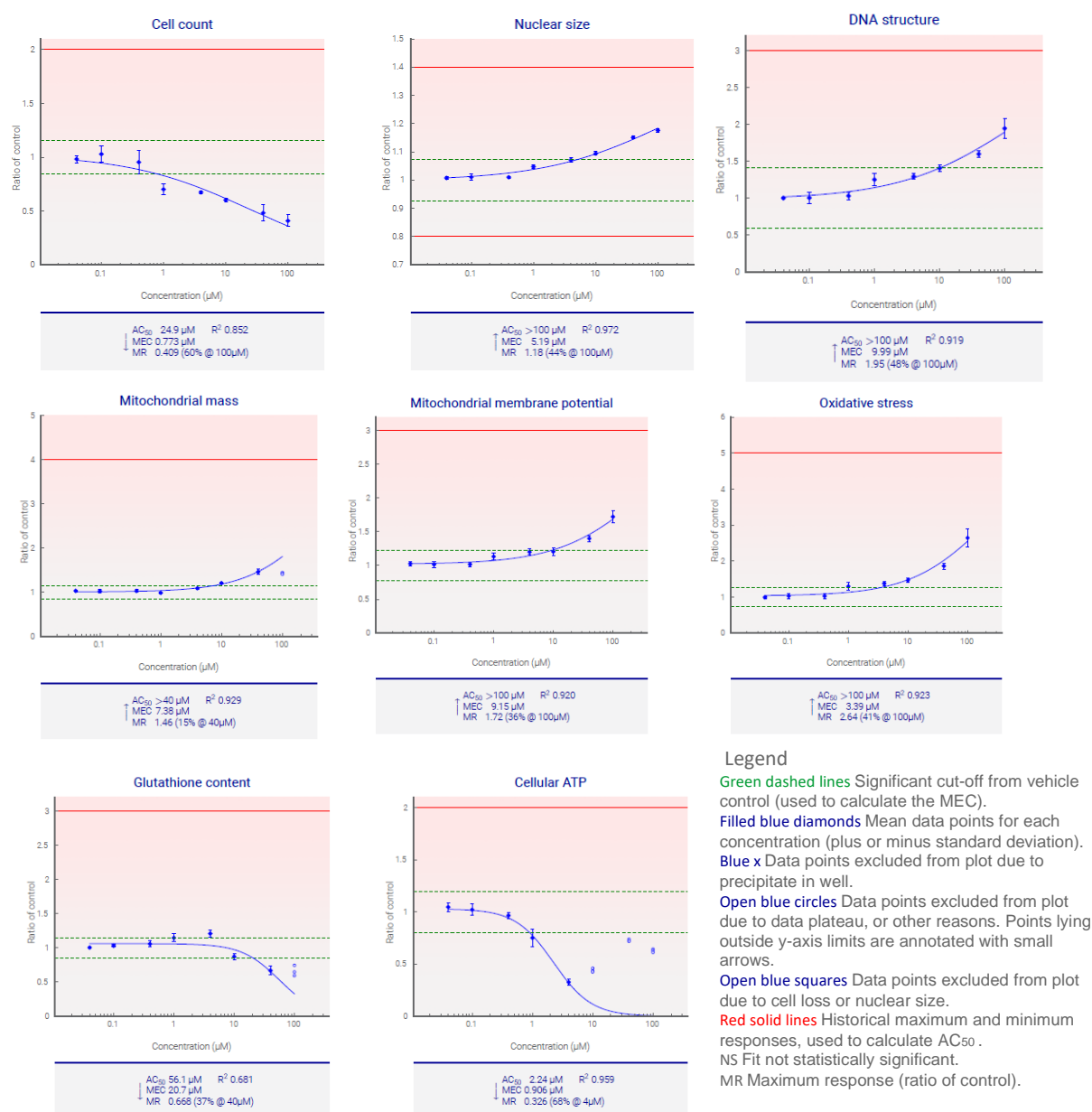
Cell Health Parameter Summary

MEC

The lowest MEC response indicates compound **2.059** has resulted in a loss of total cells per well (indicating toxicity due to necrosis, apoptosis or a reduction in cellular proliferation); please refer to graphical representation for more information. Other cell health parameters which respond are an increase in nuclear size (indicating necrosis or G2 cell cycle arrest), an increase in DNA structure (indicating chromosomal instability and DNA fragmentation), an increase in mitochondrial mass (indicating an adaptive response to cellular energy demands), an increase in mitochondrial potential (implying adaption to cellular energy requirements), an increase in ROS (indicating an increase in toxic superoxide intermediates), a decrease in GSH content (indicating that the available GSH cellular pool is depleted) and a decrease in ATP (indicating a decrease in metabolically active cells); please refer to graphical representation for more information.

AC₅₀

The lowest AC₅₀ response indicates compound **2.059** has resulted in a decrease in ATP (indicating a decrease in metabolically active cells); please refer to graphical representation for more information. Other cell health parameters which respond are a loss of total cells per well (indicating toxicity due to necrosis, apoptosis or a reduction in cellular proliferation), an increase in nuclear size (indicating necrosis or G2 cell cycle arrest), an increase in DNA structure (indicating chromosomal instability and DNA fragmentation), an increase in mitochondrial mass (indicating an adaptive response to cellular energy demands), an increase in mitochondrial potential (implying adaption to cellular energy requirements), an increase in ROS (indicating an increase in toxic superoxide intermediates) and a decrease in GSH content (indicating that the available GSH cellular pool is depleted); please refer to graphical representation for more information.



Compound **2.059** HepaRG

Assay Summary	
Incubation time:	48h
Concentrations (µM):	0.04, 0.1, 0.4, 1, 4, 10, 40, 100
Replicates per concentration:	3
Cell model:	HepaRG
Certified on:	2018-09-24

Data Summary

Cell Health Parameter	↑↓	MEC (µM)	AC ₅₀ (µM)	First Signal	
				MEC	AC ₅₀
Cell count		NR	NR		
Nuclear size		NR	NR		
DNA structure		NR	NR		
Mitochondrial mass		NR	NR		
Mitochondrial membrane potential		NR	NR		
Oxidative stress		NR	NR		
Glutathione content		NR	NR		
Cellular ATP		NR	NR		

MEC Minimum effective concentration that significantly crosses vehicle control threshold.
AC₅₀ The concentration at which 50% maximum effect is observed for each cell health parameter.
† An AC₅₀ was calculated, but is greater than the maximum surviving concentration.
↑↓ Direction of response.
NR No response observed.
NS Fit not statistically significant.
ER Early response observed (the compound responded at the lowest concentration tested).
First Signal The cell health feature which responds at the lowest observed dose (marked by ●).

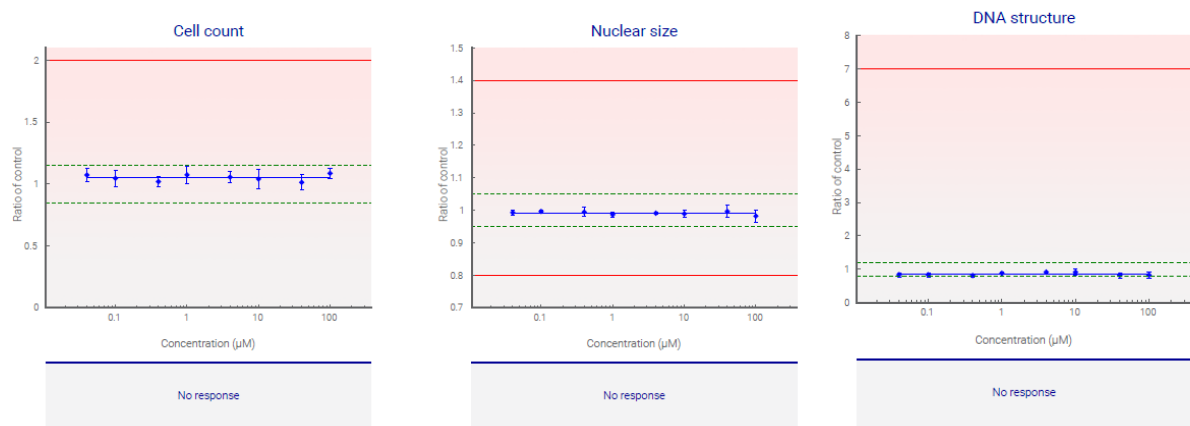
Cell Health Parameter Summary

MEC

No significant response was observed at any of the cell health parameters measured, for the concentration range tested. Please refer to graphical representation for more information.

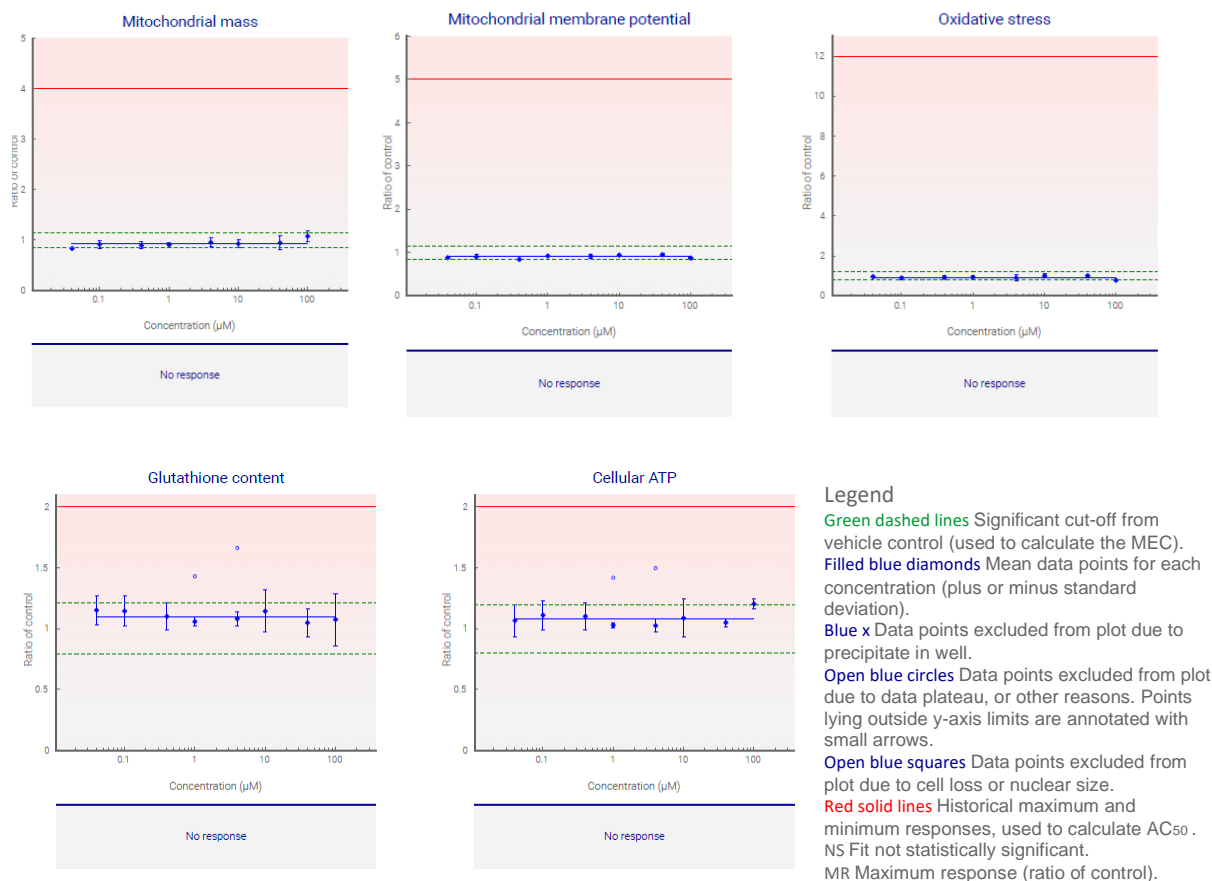
AC₅₀

No significant response was observed at any of the cell health parameters measured, for the concentration range tested. Please refer to graphical representation for more information.



Legend

Green dashed lines Significant cut-off from vehicle control (used to calculate the MEC).
Filled blue diamonds Mean data points for each concentration (plus or minus standard deviation).
Blue x Data points excluded from plot due to precipitate in well.
Open blue circles Data points excluded from plot due to data plateau, or other reasons. Points lying outside y-axis limits are annotated with small arrows.
Open blue squares Data points excluded from plot due to cell loss or nuclear size.
Red solid lines Historical maximum and minimum responses, used to calculate AC₅₀.
NS Fit not statistically significant.
MR Maximum response (ratio of control).



Control compounds: Rotenone **HepG2**

Assay Summary	
Incubation time:	48h
Concentrations (μM):	0.04, 0.1, 0.4, 1, 4, 10, 40, 100
Replicates per concentration:	3
Cell model:	HepG2
Certified on:	2018-09-14

Data Summary

Cell Health Parameter	↑↓	MEC (μM)	AC ₅₀ (μM)	First Signal MEC AC ₅₀
Cell count	↓	<0.04	0.180	•
Nuclear size		NR	NR	
DNA structure	↑	<0.04	0.129	•
Mitochondrial mass		NR	NR	
Mitochondrial membrane potential	↑	<0.04	0.628	•
Oxidative stress	↑	<0.04	0.321	•
Glutathione content		NR	NR	
Cellular ATP	↓	<0.04	<0.04	• ER

MEC Minimum effective concentration that significantly crosses vehicle control threshold.
AC₅₀ The concentration at which 50% maximum effect is observed for each cell health parameter.
† An AC₅₀ was calculated, but is greater than the maximum surviving concentration.
↑↓ Direction of response.
NR No response observed.
NS Fit not statistically significant.
ER Early response observed (the compound responded at the lowest concentration tested).
First Signal The cell health feature which responds at the lowest observed dose (marked by •).

Cell Health Parameter Summary

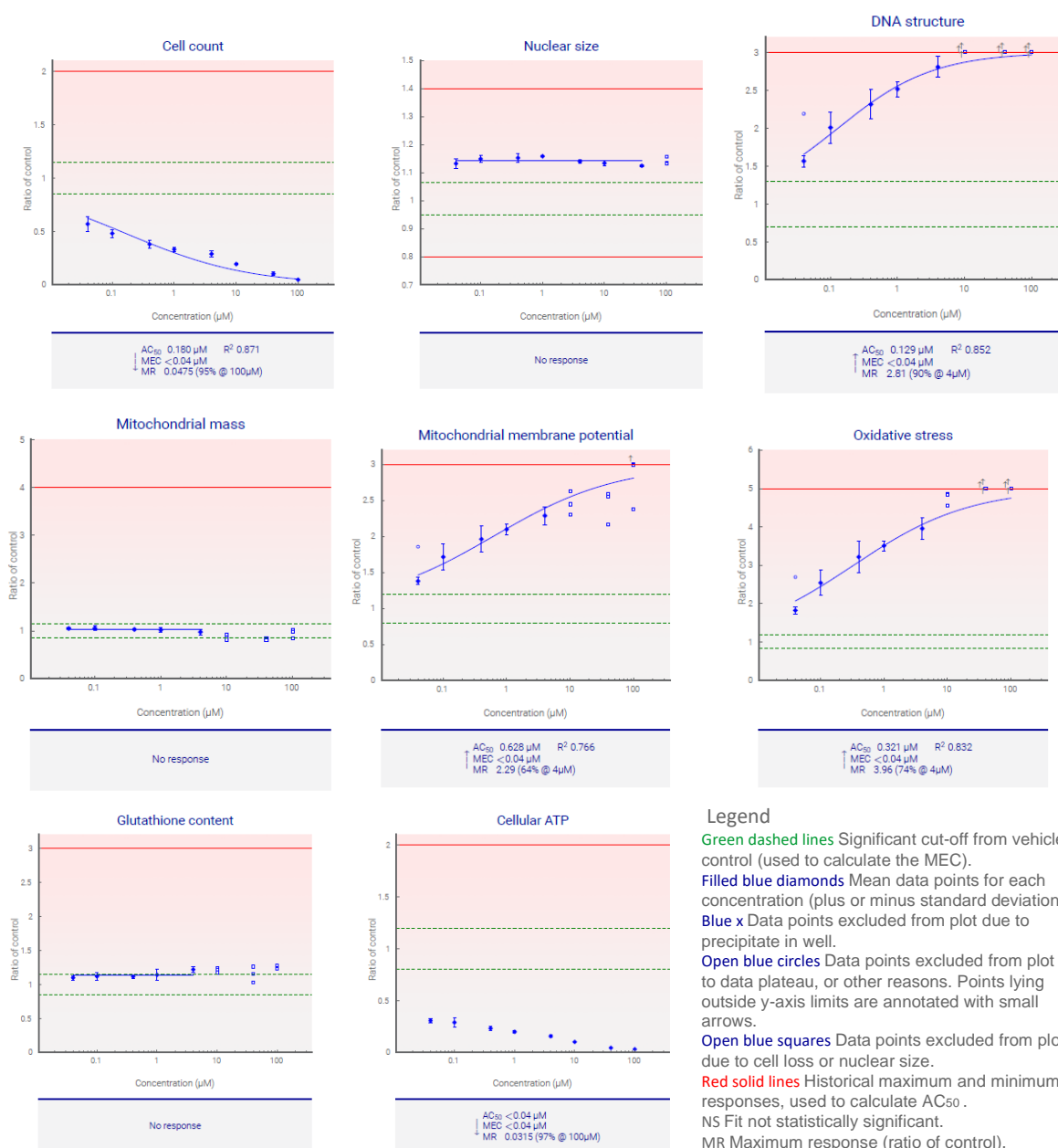
MEC

The lowest MEC response indicates compound rotenone has resulted in a loss of total cells per well (indicating toxicity due to necrosis, apoptosis or a reduction in cellular proliferation), an increase in DNA structure (indicating chromosomal instability and DNA fragmentation), an increase in mitochondrial potential (implying adaption to cellular energy requirements), an increase in ROS (indicating an increase in toxic superoxide intermediates) and a decrease in ATP (indicating a decrease in metabolically active cells); please refer to graphical representation for more information.

AC50

The lowest AC50 response indicates compound rotenone has resulted in a decrease in ATP (indicating a decrease in metabolically active cells); please refer to graphical representation for more information.

Other cell health parameters which respond are a loss of total cells per well (indicating toxicity due to necrosis, apoptosis or a reduction in cellular proliferation), an increase in DNA structure (indicating chromosomal instability and DNA fragmentation), an increase in mitochondrial potential (implying adaption to cellular energy requirements) and an increase in ROS (indicating an increase in toxic superoxide intermediates); please refer to graphical representation for more information.



Control compounds: Rotenone **HepaRG**

Assay Summary	
Incubation time:	48h
Concentrations (µM):	0.04, 0.1, 0.4, 1, 4, 10, 40, 100
Replicates per concentration:	3
Cell model:	HepaRG
Certified on:	2018-09-24

Data Summary

Cell Health Parameter	↑↓	MEC (µM)	AC ₅₀ (µM)	First Signal	
				MEC	AC ₅₀
Cell count	↓	2.14	9.34		
Nuclear size	↓	9.13	34.0		
DNA structure	↑	0.0846	30.8	●	
Mitochondrial mass	↑	6.66	31.3		
Mitochondrial membrane potential	↑	0.147	>10 †		
Oxidative stress	↑	0.150	29.5		
Glutathione content	↑	0.135	0.336		●
Cellular ATP	↓	0.605	2.71		

MEC Minimum effective concentration that significantly crosses vehicle control threshold.
AC₅₀ The concentration at which 50% maximum effect is observed for each cell health parameter.
† An AC₅₀ was calculated, but is greater than the maximum surviving concentration.
↑↓ Direction of response.
NR No response observed.
NS Fit not statistically significant.
ER Early response observed (the compound responded at the lowest concentration tested).
First Signal The cell health feature which responds at the lowest observed dose (marked by ●).

Cell Health Parameter Summary

MEC

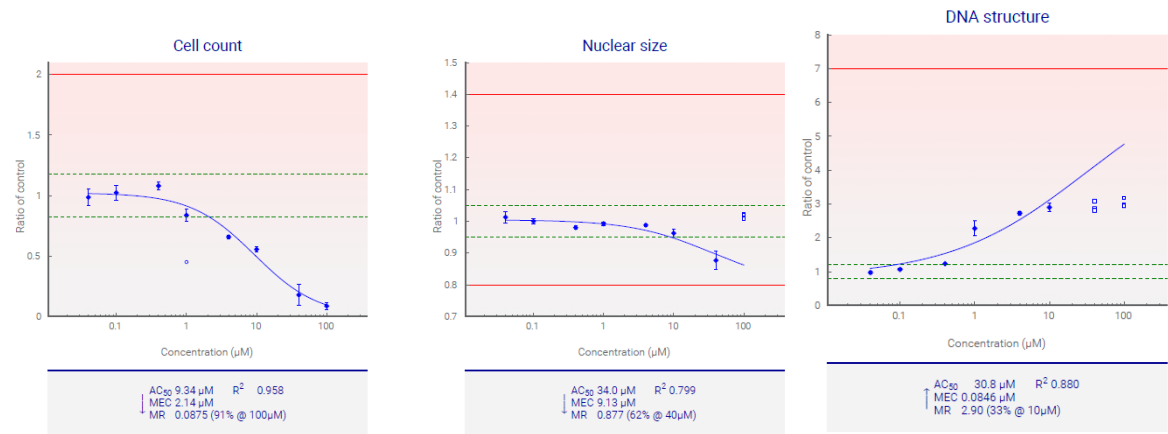
The lowest MEC response indicates compound rotenone has resulted in an increase in DNA structure (indicating chromosomal instability and DNA fragmentation); please refer to graphical representation for more information.

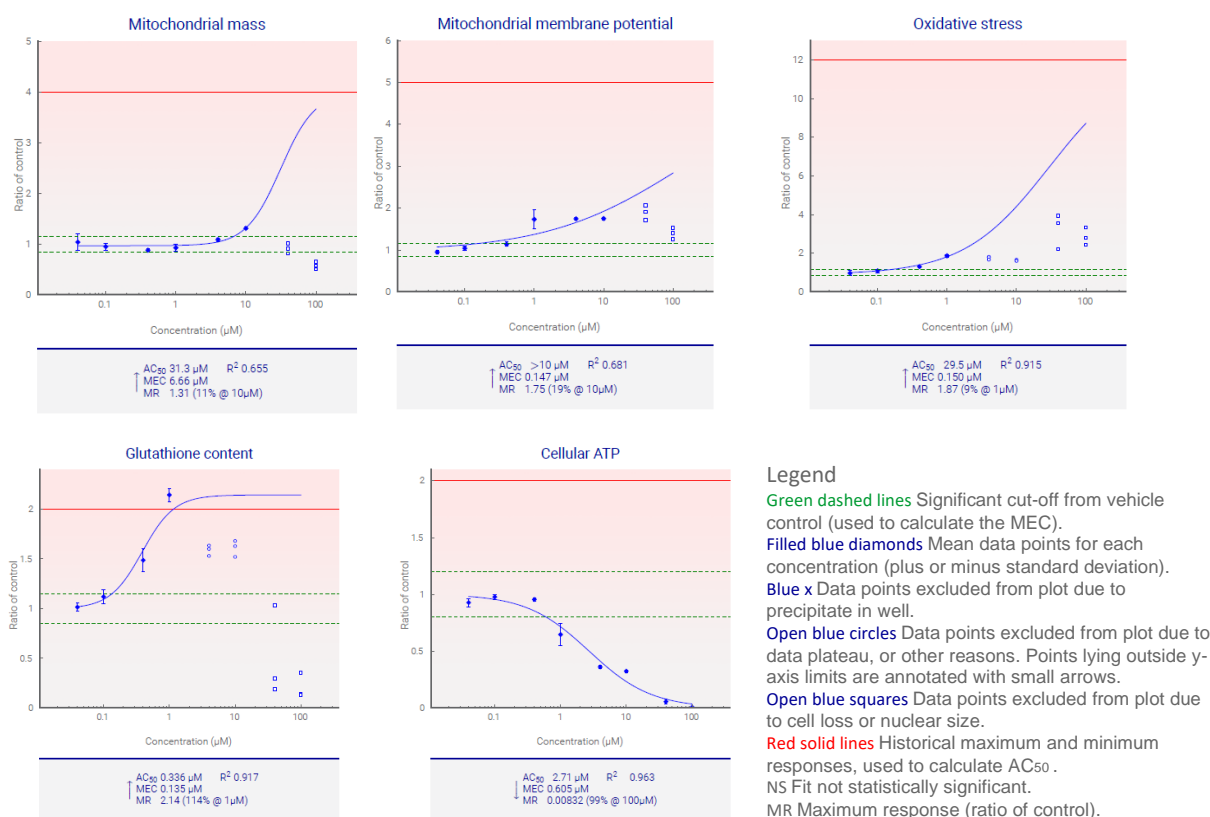
Other cell health parameters which respond are a loss of total cells per well (indicating toxicity due to necrosis, apoptosis or a reduction in cellular proliferation), a decrease in nuclear size (indicating DNA fragmentation), an increase in mitochondrial mass (indicating an adaptive response to cellular energy demands), an increase in mitochondrial potential (implying adaption to cellular energy requirements), an increase in ROS (indicating an increase in toxic superoxide intermediates), increased GSH content (indicating an adaptive cellular response to oxidative stress) and a decrease in ATP (indicating a decrease in metabolically active cells); please refer to graphical representation for more information.

AC50

The lowest AC50 response indicates compound rotenone has resulted in increased GSH content (indicating an adaptive cellular response to oxidative stress); please refer to graphical representation for more information.

Other cell health parameters which respond are a loss of total cells per well (indicating toxicity due to necrosis, apoptosis or a reduction in cellular proliferation), a decrease in nuclear size (indicating DNA fragmentation), an increase in DNA structure (indicating chromosomal instability and DNA fragmentation), an increase in mitochondrial mass (indicating an adaptive response to cellular energy demands), an increase in mitochondrial potential (implying adaption to cellular energy requirements), an increase in ROS (indicating an increase in toxic superoxide intermediates) and a decrease in ATP (indicating a decrease in metabolically active cells); please refer to graphical representation for more information.





Control compounds: L-buthionine-sulfoximine **HepG2**

Assay Summary

Incubation time:	48h
Concentrations (µM):	0.4, 1, 4, 10, 40, 100, 400, 1000
Replicates per concentration:	3
Cell model:	HepG2
Certified on:	2018-09-14

Data Summary

Cell Health Parameter	↑↓	MEC (µM)	AC ₅₀ (µM)	First Signal	
				MEC	AC ₅₀
Cell count		NR	NR		
Nuclear size		NR	NR		
DNA structure		NR	NR		
Mitochondrial mass		NR	NR		
Mitochondrial membrane potential		NR	NR		
Oxidative stress		NR	NR		
Glutathione content	↓	0.935	10.2	•	•
Cellular ATP	↓	26.9	459		

MEC Minimum effective concentration that significantly crosses vehicle control threshold.
 AC₅₀ The concentration at which 50% maximum effect is observed for each cell health parameter.
 † An AC₅₀ was calculated, but is greater than the maximum surviving concentration.
 ↑↓ Direction of response.
 NR No response observed.
 NS Fit not statistically significant.
 ER Early response observed (the compound responded at the lowest concentration tested).
 First Signal The cell health feature which responds at the lowest observed dose (marked by •).

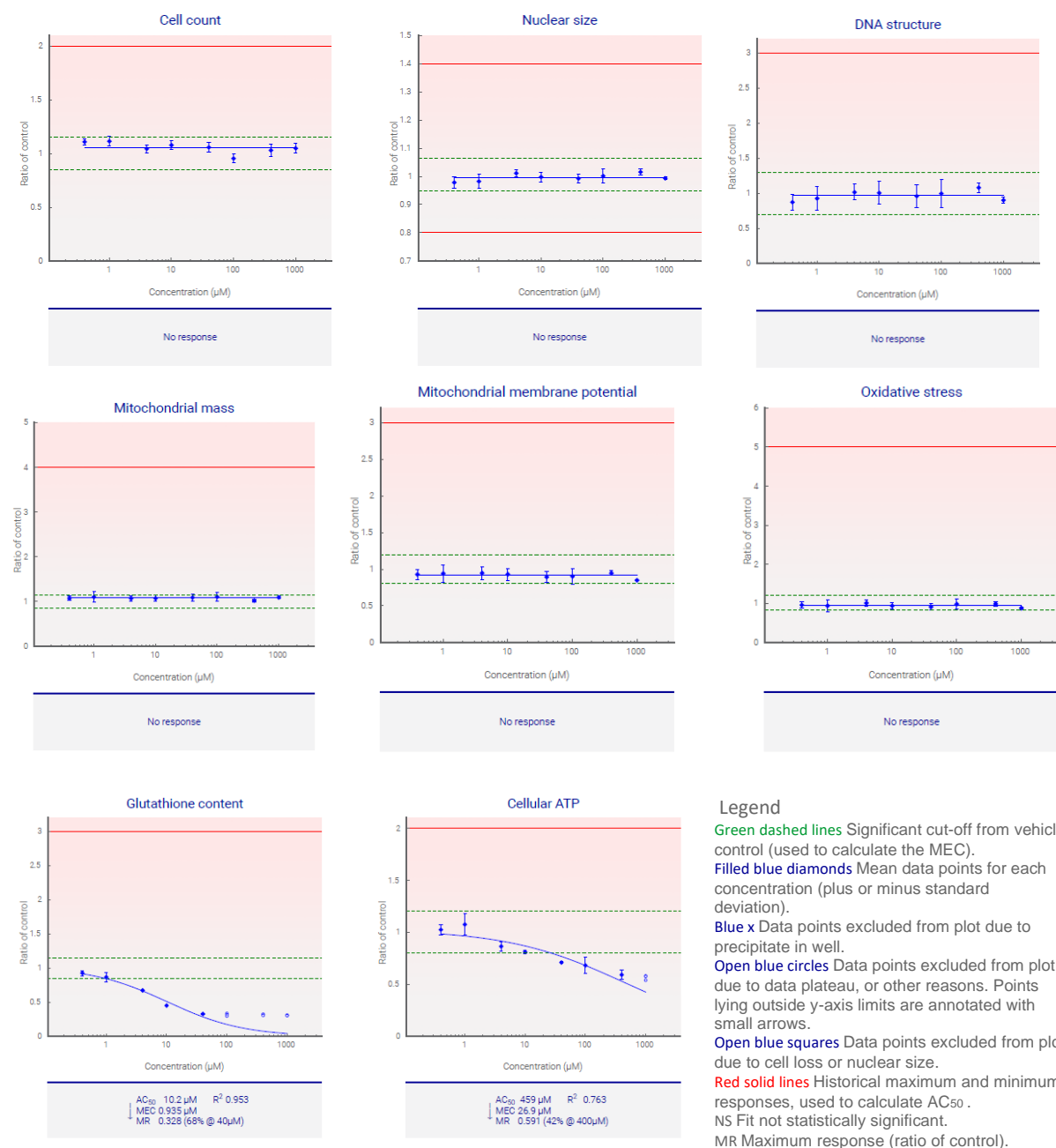
Cell Health Parameter Summary

MEC

The lowest MEC response indicates compound L-buthionine-sulfoximine has resulted in a decrease in GSH content (indicating that the available GSH cellular pool is depleted); please refer to graphical representation for more information. Other cell health parameters which respond are a decrease in ATP (indicating a decrease in metabolically active cells); please refer to graphical representation for more information.

AC50

The lowest AC50 response indicates compound L-buthionine-sulfoximine has resulted in a decrease in GSH content (indicating that the available GSH cellular pool is depleted); please refer to graphical representation for more information. Other cell health parameters which respond are a decrease in ATP (indicating a decrease in metabolically active cells); please refer to graphical representation for more information.



Control compounds: L-buthionine-sulfoximine **HepaRG**

Assay Summary	
Incubation time:	48h
Concentrations (µM):	0.4, 1, 4, 10, 40, 100, 400, 1000
Replicates per concentration:	3
Cell model:	HepaRG
Certified on:	2018-09-24

Data Summary

Cell Health Parameter	↑↓	MEC (µM)	AC ₅₀ (µM)	First Signal	
				MEC	AC ₅₀
Cell count		NR	NR		
Nuclear size		NR	NR		
DNA structure		NR	NR		
Mitochondrial mass		NR	NR		
Mitochondrial membrane potential		NR	NR		
Oxidative stress		NR	NR		
Glutathione content	↓	90.1	719	•	•
Cellular ATP		NR	NR		

MEC Minimum effective concentration that significantly crosses vehicle control threshold.
AC₅₀ The concentration at which 50% maximum effect is observed for each cell health parameter.
† An AC₅₀ was calculated, but is greater than the maximum surviving concentration.
↑↓ Direction of response.
NR No response observed.
NS Fit not statistically significant.
ER Early response observed (the compound responded at the lowest concentration tested).
First Signal The cell health feature which responds at the lowest observed dose (marked by •).

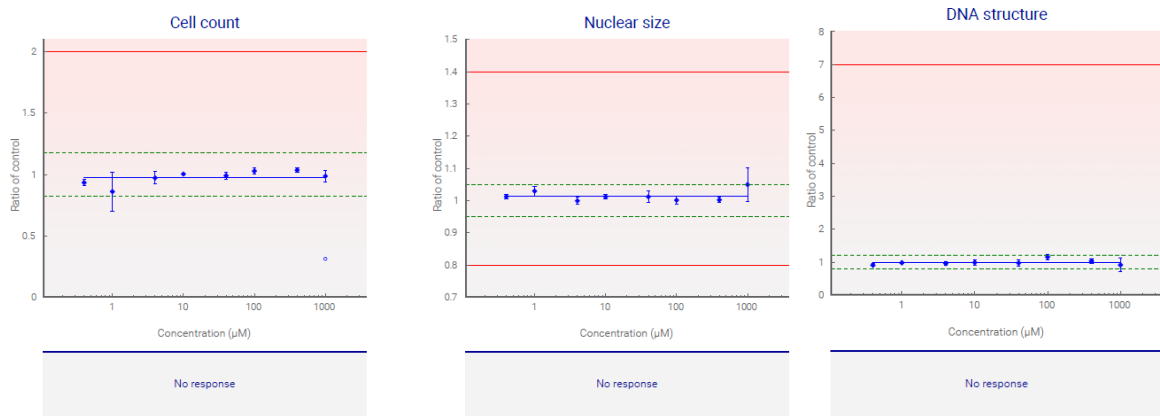
Cell Health Parameter Summary

MEC

The lowest MEC response indicates compound L-buthionine-sulfoximine has resulted in a decrease in GSH content (indicating that the available GSH cellular pool is depleted); please refer to graphical representation for more information.

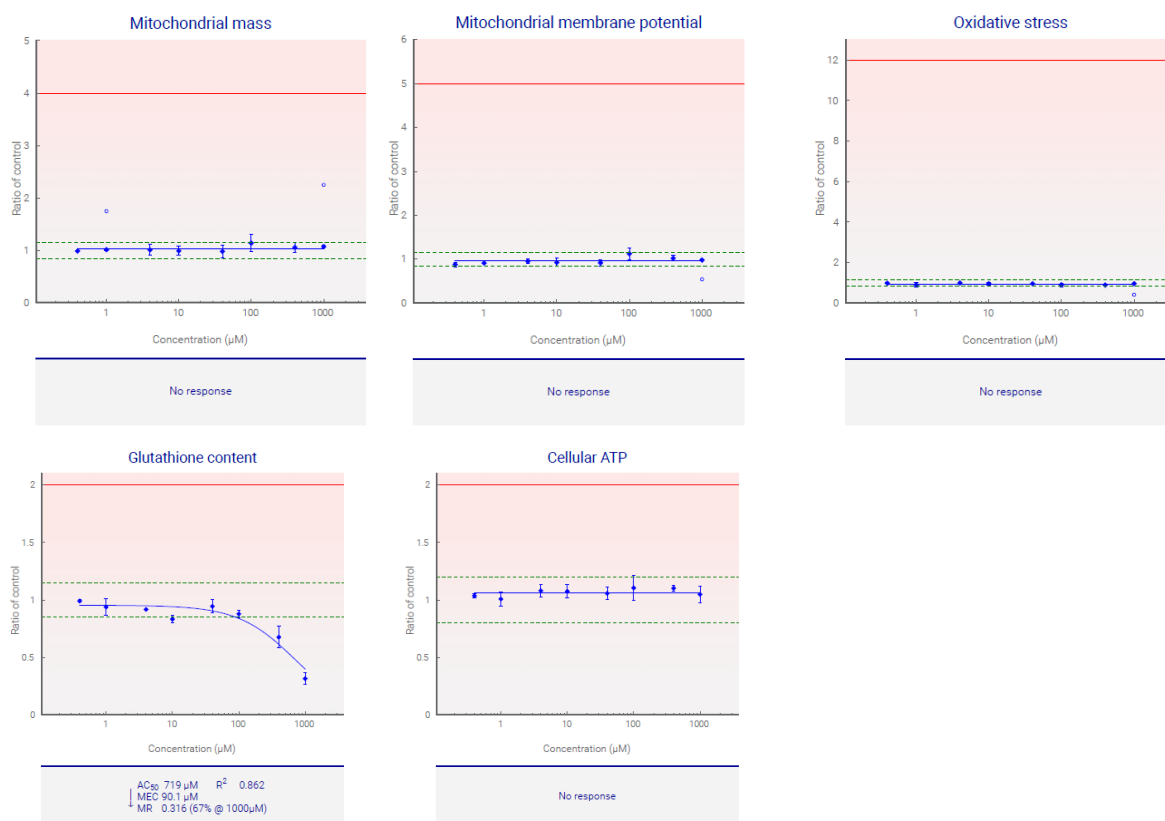
AC₅₀

The lowest AC₅₀ response indicates compound L-buthionine-sulfoximine has resulted in a decrease in GSH content (indicating that the available GSH cellular pool is depleted); please refer to graphical representation for more information.



Legend

Green dashed lines Significant cut-off from vehicle control (used to calculate the MEC).
Filled blue diamonds Mean data points for each concentration (plus or minus standard deviation).
Blue x Data points excluded from plot due to precipitate in well.
Open blue circles Data points excluded from plot due to data plateau, or other reasons. Points lying outside y-axis limits are annotated with small arrows.
Open blue squares Data points excluded from plot due to cell loss or nuclear size.
Red solid lines Historical maximum and minimum responses, used to calculate AC₅₀.
NS Fit not statistically significant.
MR Maximum response (ratio of control).



Legend

Green dashed lines Significant cut-off from vehicle control (used to calculate the MEC).

Filled blue diamonds Mean data points for each concentration (plus or minus standard deviation).

Blue x Data points excluded from plot due to precipitate in well.

Open blue circles Data points excluded from plot due to data plateau, or other reasons. Points lying outside y-axis limits are annotated with small arrows.

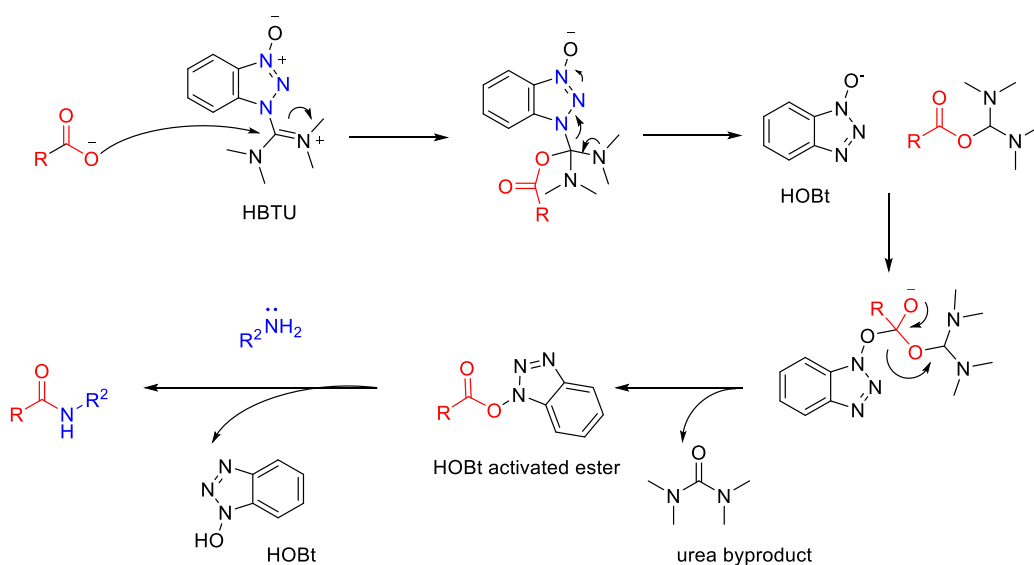
Open blue squares Data points excluded from plot due to cell loss or nuclear size.

Red solid lines Historical maximum and minimum responses, used to calculate AC₅₀.

NS Fit not statistically significant.

MR Maximum response (ratio of control).

Appendix 2.b HBTU amide coupling mechanism⁵



Chapter 3 Appendix

Appendix 3 Cytotoxicity and Mitotoxicity profiling by IPK of compounds of interest

Assay description:

Aim: To identify cytotoxicity and mitotoxicity of compounds using the Crabtree effect assay adapted using methods outlined by Marroquin *et al.* and unpublished proprietary methods by IPK.^{1, 2}

Screening Info.: Reformatted as 384-well format (1 plate)

DRCs starting at 100 μ M; two-fold serial dilution; 10-points in 0.5 % DMSO (v/v)

Cell Conditioning (metabolic switch):

1. Glucose Condition: HepG2 cells maintained in glucose media, utilizing ATP from glycolysis

2. Galactose Condition: HepG2 cells maintained in galactose media for one passage and seeded in the same media, utilizing ATP from oxidative phosphorylation.

Experimental Controls:

High control: 0.5 % DMSO, IC₁₀₀ low control: 200 μ M Chlorpromazine (0.5 % v/v DMSO)

Endpoint Read-out:

-Hoechst nuclei staining: Cell viability assessment via cell count

-Alamar blue staining: Metabolic activity measurement via fluorescence readout

Reference Compounds used:

1. Chlorpromazine: moderate cytotoxicity; used as low control IC₁₀₀ (200 μ M)
2. Tacrine: moderate cytotoxicity
3. Benznidazole: no cytotoxicity (in low conc.)
4. Praziquantel: no cytotoxicity (in low conc.)
5. FCCP: mitochondrial toxicity; mitochondrial oxidative phosphorylation uncoupler
6. Rotenone: mitochondrial toxicity; inhibitor of mitochondrial electron transport

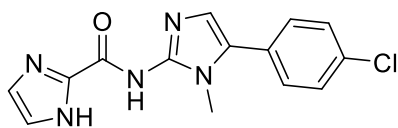
Data Analysis:

- Selectivity index (SI) was calculated by dividing the value of cytotoxic concentration at 50 % (CC₅₀) of a compound in Glucose condition by that of the compound in Galactose condition.

* Note: This Crabtree effect assay may not detect compounds inhibiting fatty acid oxidation as mitochondrial toxicants.^{3, 4}

Cell viability measures whether compound is overall cytotoxic to the HepG2 cells. Metabolic stability measures whether compounds cause toxicity to the mitochondria. This is measured by the impact of the compound against cells under galactose conditions. Under these conditions, cells utilize ATP from oxidative phosphorylation, which occurs in the mitochondria. If compounds were found to be toxic to the mitochondria, it would be reflected under these conditions. Under glucose conditions, cells are able to use ATP from glycolysis rather than rely on mitochondria.

Appendix Table 3a: Summary of toxicity of **3.116**

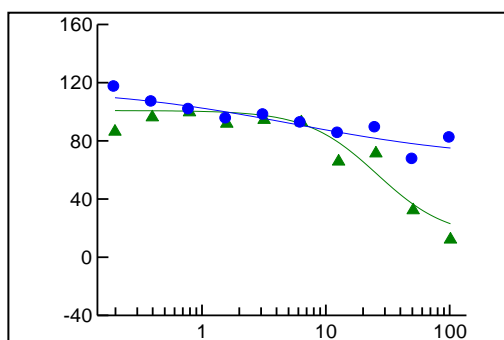


		Glucose condition	Galactose condition	SI (glu/galac)
Cell viability	CC ₅₀ (μM)	PI	PI	NA
	CC (Y=50) (μM)	32	28	1.1
Metabolic activity	CC ₅₀ (μM)	PI	PI	NA
	CC (Y=50) μM	>100	>100	>1.0

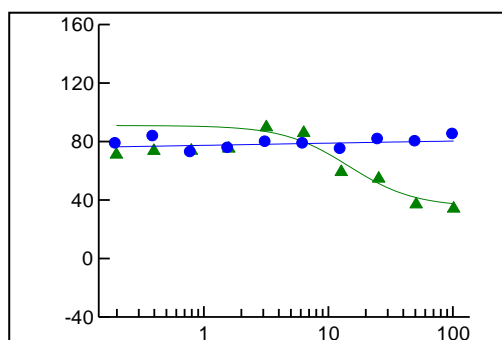
CC₅₀= cytotoxic concentration at 50 % , CC (Y=50)= normalised CC₅₀ from graph, PI= partial inhibition

Appendix 3 Figure 3a: Dose response curves of **5.001** measuring the cytotoxic concentration (CC₅₀) in glucose (left) and galactose (right) conditions

Glucose condition 3.116



Galactose condition 3.116



X axis: Concentration (μM)

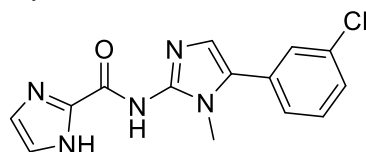
Y axis: Ratio (%)

● Cell ratio by Hoechst staining

▲ Metabolic activity ratio by Alamar blue staining

No mitochondrial toxicity or cytotoxicity observed overall when HepG2 were subjected to **3.116**.

Appendix Table 3b: Summary of toxicity of **3.118**

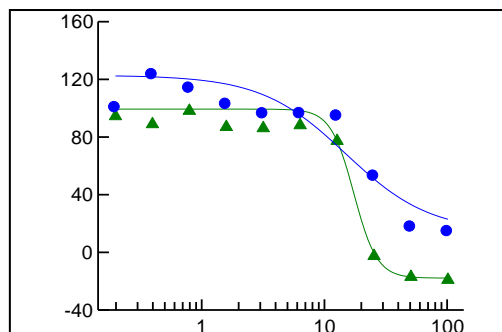


		Glucose condition	Galactose condition	SI (glu/galac)
Cell viability	CC ₅₀ (μM)	17	PI	NA
	CC (Y=50) (μM)	16	19	0.84
Metabolic activity	CC ₅₀ (μM)	PI	PI	NA
	CC (Y=50) μM	26	30	0.87

CC₅₀= cytotoxic concentration at 50 % , CC (Y=50)= normalised CC₅₀ from graph, PI= partial inhibition

Appendix 3 Figure 3b: Dose response curves of **5.063** measuring the cytotoxic concentration (CC_{50}) in glucose (left) and galactose (right) conditions

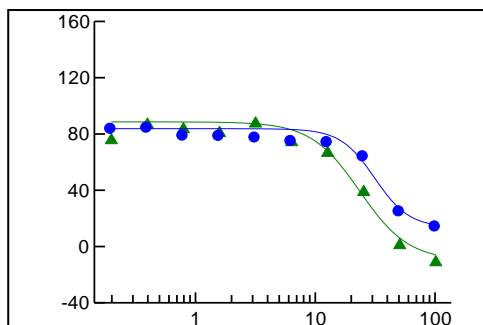
Glucose condition 3.118



X axis: Concentration (μM)

Y axis: Ratio (%)

Galactose condition 3.118



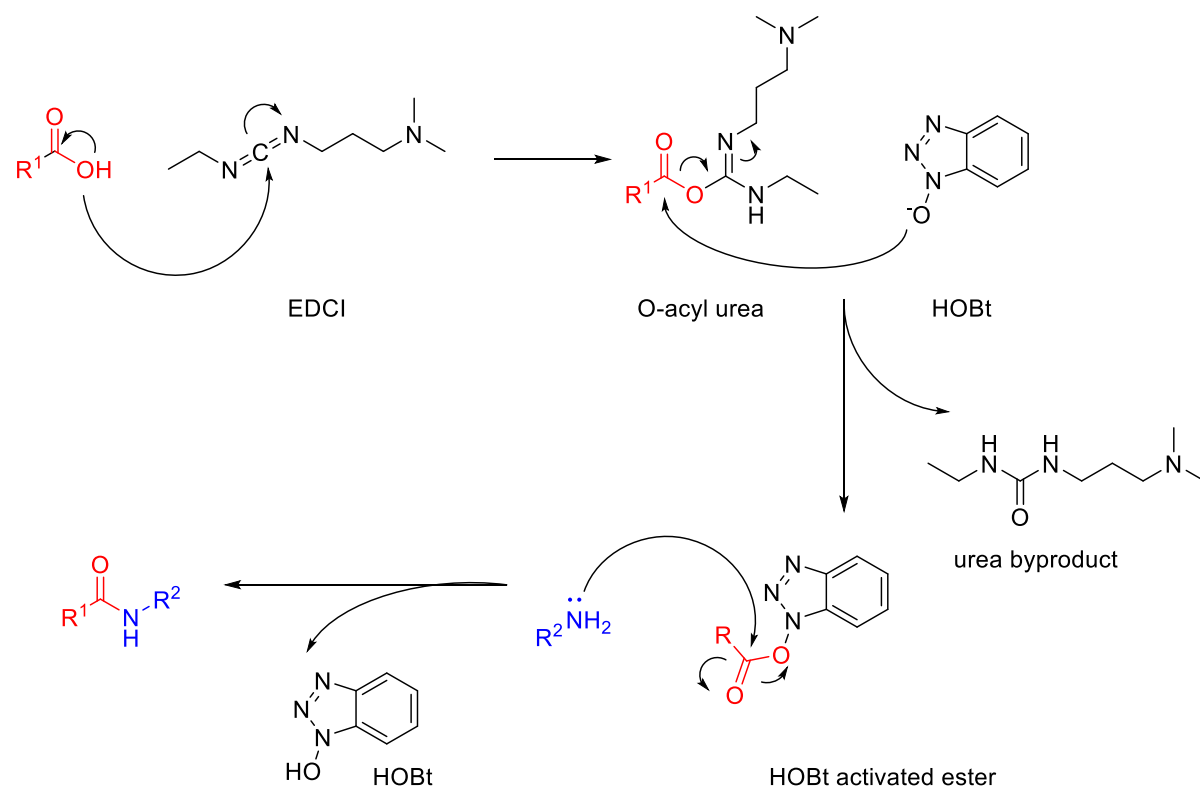
● Cell ratio by Hoechst staining

▲ Metabolic activity ratio by Alamar blue staining

No significant mitochondrial toxicity was observed when HepG2 were subjected to **3.118**. Cytotoxicity was observed at high concentrations only.

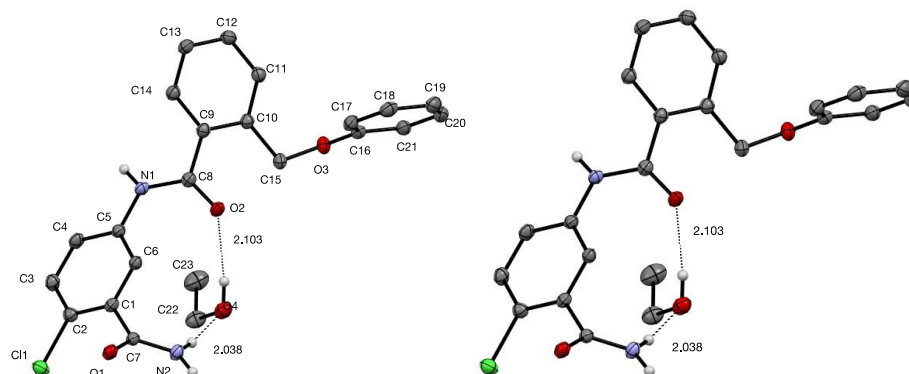
Chapter 4 Appendix

EDCI HOBt amide coupling mechanism⁶



Chapter 5 Appendix

Appendix 5.1: Crystal Structure, crystal data and structure refinement for compound 5.001



Appendix Table 5a. Crystal data and structure refinement for compound **5.001**.

Empirical formula	C23 H23 Cl N2 O4
Formula weight	426.88
Temperature	100.00(10) K
Wavelength	1.54184 Å
Crystal system	Orthorhombic
Space group	P b c a
Unit cell dimensions	a = 12.41730(10) Å $\square = 90^\circ$ b = 17.7648(2) Å $\square = 90^\circ$ c = 18.12950(10) Å $\square = 90^\circ$
Volume	3999.20(6) Å ³
Z	8
Density (calculated)	1.418 Mg/m ³
Absorption coefficient	1.977 mm ⁻¹
F(000)	1792
Crystal size	0.426 x 0.090 x 0.035 mm ³
Theta range for data collection	4.979 to 77.332°
Index ranges	-15 ≤ h ≤ 15, -21 ≤ k ≤ 21, -22 ≤ l ≤ 20
Reflections collected	52700
Independent reflections	4208 [R(int) = 0.0671]
Completeness to theta = 67.684°	100.0 %
Absorption correction	Gaussian
Max. and min. transmission	1.000 and 0.390
Refinement method	Full-matrix least-squares on F ²
Data / restraints / parameters	4208 / 7 / 297
Goodness-of-fit on F ²	1.071
Final R indices [I > 2σ(I)]	R1 = 0.0401, wR2 = 0.1092
R indices (all data)	R1 = 0.0427, wR2 = 0.1115
Extinction coefficient	n/a
Largest diff. peak and hole	0.285 and -0.500 e.Å ⁻³

Appendix Table 5b. Atomic coordinates ($\times 10^4$) and equivalent isotropic displacement parameters ($\text{\AA}^2 \times 10^3$) for **5.001**. $U(\text{eq})$ is defined as one third of the trace of the orthogonalized U^{ij} tensor.

	x	y	z	U(eq)
C(1)	1523(1)	4558(1)	3375(1)	17(1)
C(2)	1353(1)	3927(1)	2936(1)	19(1)
C(3)	2010(1)	3781(1)	2333(1)	21(1)
C(4)	2853(1)	4260(1)	2172(1)	20(1)
C(5)	3058(1)	4885(1)	2613(1)	17(1)
C(6)	2374(1)	5041(1)	3206(1)	17(1)
C(7)	843(1)	4739(1)	4040(1)	17(1)
C(8)	4505(1)	5793(1)	2898(1)	18(1)
C(9)	5386(1)	6241(1)	2541(1)	18(1)
C(10)	6360(1)	6388(1)	2913(1)	18(1)
C(11)	7142(1)	6814(1)	2552(1)	21(1)
C(12)	6968(1)	7100(1)	1848(1)	22(1)
C(13)	6006(1)	6960(1)	1489(1)	22(1)
C(14)	5219(1)	6530(1)	1832(1)	19(1)
C(15)	6585(1)	6061(1)	3671(1)	21(1)
C(16)	7616(1)	6991(1)	4317(1)	19(1)
C(17)	6820(1)	7536(1)	4239(1)	22(1)
C(18)	6928(1)	8222(1)	4603(1)	25(1)
C(19)	7816(2)	8367(1)	5041(1)	27(1)
C(20)	8604(1)	7818(1)	5120(1)	26(1)
C(21)	8512(1)	7132(1)	4761(1)	22(1)
C(22)	4008(2)	3937(1)	4295(1)	29(1)
C(23)	4982(2)	3954(1)	3837(1)	41(1)
C(22A)	4468(11)	4049(6)	4534(8)	31(2)
C(23A)	4982(2)	3954(1)	3837(1)	41(1)
N(1)	3948(1)	5342(1)	2428(1)	18(1)
N(2)	1379(1)	4798(1)	4670(1)	20(1)
O(1)	-149(1)	4832(1)	3984(1)	20(1)
O(2)	4308(1)	5842(1)	3564(1)	21(1)
O(3)	7595(1)	6299(1)	3977(1)	21(1)
O(4)	3720(1)	4654(1)	4613(1)	26(1)
Cl(1)	351(1)	3275(1)	3148(1)	24(1)

Appendix Table 5c. Bond lengths [\AA] and angles [$^\circ$] for **5.001**.

C(1)-C(2)	1.390(2)
C(1)-C(6)	1.394(2)
C(1)-C(7)	1.5068(19)
C(2)-C(3)	1.390(2)
C(2)-Cl(1)	1.7418(15)
C(3)-C(4)	1.379(2)
C(3)-H(3)	0.9300
C(4)-C(5)	1.391(2)
C(4)-H(4)	0.9300
C(5)-C(6)	1.3979(19)

C(5)-N(1)	1.4111(19)
C(6)-H(6)	0.9300
C(7)-O(1)	1.2473(19)
C(7)-N(2)	1.3262(19)
C(8)-O(2)	1.2340(18)
C(8)-N(1)	1.3586(19)
C(8)-C(9)	1.499(2)
C(9)-C(14)	1.400(2)
C(9)-C(10)	1.410(2)
C(10)-C(11)	1.394(2)
C(10)-C(15)	1.518(2)
C(11)-C(12)	1.390(2)
C(11)-H(11)	0.9300
C(12)-C(13)	1.383(2)
C(12)-H(12)	0.9300
C(13)-C(14)	1.388(2)
C(13)-H(13)	0.9300
C(14)-H(14)	0.9300
C(15)-O(3)	1.4343(17)
C(15)-H(15A)	0.9700
C(15)-H(15B)	0.9700
C(16)-O(3)	1.3759(19)
C(16)-C(17)	1.390(2)
C(16)-C(21)	1.397(2)
C(17)-C(18)	1.394(2)
C(17)-H(17)	0.9300
C(18)-C(19)	1.383(2)
C(18)-H(18)	0.9300
C(19)-C(20)	1.389(3)
C(19)-H(19)	0.9300
C(20)-C(21)	1.387(2)
C(20)-H(20)	0.9300
C(21)-H(21)	0.9300
C(22)-O(4)	1.443(2)
C(22)-C(23)	1.467(3)
C(22)-H(22A)	0.9700
C(22)-H(22B)	0.9700
C(23)-H(23A)	0.9600
C(23)-H(23B)	0.9600
C(23)-H(23C)	0.9600
C(22A)-C(23A)	1.426(12)
C(22A)-O(4)	1.428(5)
C(22A)-H(22C)	0.9700
C(22A)-H(22D)	0.9700
C(23A)-H(23D)	0.9600
C(23A)-H(23E)	0.9600
C(23A)-H(23F)	0.9600
N(1)-H(1)	0.87(2)
N(2)-H(2A)	0.91(2)
N(2)-H(2B)	0.89(2)
O(4)-H(4A)	0.83(3)

C(2)-C(1)-C(6)	119.06(13)
C(2)-C(1)-C(7)	122.92(13)
C(6)-C(1)-C(7)	118.01(13)
C(3)-C(2)-C(1)	120.72(14)
C(3)-C(2)-Cl(1)	117.92(12)
C(1)-C(2)-Cl(1)	121.30(11)
C(4)-C(3)-C(2)	119.80(14)
C(4)-C(3)-H(3)	120.1
C(2)-C(3)-H(3)	120.1
C(3)-C(4)-C(5)	120.63(13)
C(3)-C(4)-H(4)	119.7
C(5)-C(4)-H(4)	119.7
C(4)-C(5)-C(6)	119.24(13)
C(4)-C(5)-N(1)	117.81(13)
C(6)-C(5)-N(1)	122.94(13)
C(1)-C(6)-C(5)	120.49(13)
C(1)-C(6)-H(6)	119.8
C(5)-C(6)-H(6)	119.8
O(1)-C(7)-N(2)	123.66(13)
O(1)-C(7)-C(1)	121.15(12)
N(2)-C(7)-C(1)	115.19(13)
O(2)-C(8)-N(1)	123.60(14)
O(2)-C(8)-C(9)	121.95(13)
N(1)-C(8)-C(9)	114.45(12)
C(14)-C(9)-C(10)	119.84(13)
C(14)-C(9)-C(8)	118.86(13)
C(10)-C(9)-C(8)	121.28(13)
C(11)-C(10)-C(9)	118.29(13)
C(11)-C(10)-C(15)	120.36(13)
C(9)-C(10)-C(15)	121.27(13)
C(12)-C(11)-C(10)	121.45(14)
C(12)-C(11)-H(11)	119.3
C(10)-C(11)-H(11)	119.3
C(13)-C(12)-C(11)	120.04(14)
C(13)-C(12)-H(12)	120.0
C(11)-C(12)-H(12)	120.0
C(12)-C(13)-C(14)	119.72(14)
C(12)-C(13)-H(13)	120.1
C(14)-C(13)-H(13)	120.1
C(13)-C(14)-C(9)	120.65(14)
C(13)-C(14)-H(14)	119.7
C(9)-C(14)-H(14)	119.7
O(3)-C(15)-C(10)	113.45(12)
O(3)-C(15)-H(15A)	108.9
C(10)-C(15)-H(15A)	108.9
O(3)-C(15)-H(15B)	108.9
C(10)-C(15)-H(15B)	108.9
H(15A)-C(15)-H(15B)	107.7
O(3)-C(16)-C(17)	124.29(13)
O(3)-C(16)-C(21)	115.65(13)
C(17)-C(16)-C(21)	120.06(14)
C(16)-C(17)-C(18)	119.48(14)

C(16)-C(17)-H(17)	120.3
C(18)-C(17)-H(17)	120.3
C(19)-C(18)-C(17)	120.76(16)
C(19)-C(18)-H(18)	119.6
C(17)-C(18)-H(18)	119.6
C(18)-C(19)-C(20)	119.44(15)
C(18)-C(19)-H(19)	120.3
C(20)-C(19)-H(19)	120.3
C(21)-C(20)-C(19)	120.67(15)
C(21)-C(20)-H(20)	119.7
C(19)-C(20)-H(20)	119.7
C(20)-C(21)-C(16)	119.59(15)
C(20)-C(21)-H(21)	120.2
C(16)-C(21)-H(21)	120.2
O(4)-C(22)-C(23)	114.32(18)
O(4)-C(22)-H(22A)	108.7
C(23)-C(22)-H(22A)	108.7
O(4)-C(22)-H(22B)	108.7
C(23)-C(22)-H(22B)	108.7
H(22A)-C(22)-H(22B)	107.6
C(22)-C(23)-H(23A)	109.5
C(22)-C(23)-H(23B)	109.5
H(23A)-C(23)-H(23B)	109.5
C(22)-C(23)-H(23C)	109.5
H(23A)-C(23)-H(23C)	109.5
H(23B)-C(23)-H(23C)	109.5
C(23A)-C(22A)-O(4)	117.9(8)
C(23A)-C(22A)-H(22C)	107.8
O(4)-C(22A)-H(22C)	107.8
C(23A)-C(22A)-H(22D)	107.8
O(4)-C(22A)-H(22D)	107.8
H(22C)-C(22A)-H(22D)	107.2
C(22A)-C(23A)-H(23D)	109.5
C(22A)-C(23A)-H(23E)	109.5
H(23D)-C(23A)-H(23E)	109.5
C(22A)-C(23A)-H(23F)	109.5
H(23D)-C(23A)-H(23F)	109.5
H(23E)-C(23A)-H(23F)	109.5
C(8)-N(1)-C(5)	126.13(12)
C(8)-N(1)-H(1)	120.4(15)
C(5)-N(1)-H(1)	112.4(15)
C(7)-N(2)-H(2A)	120.8(14)
C(7)-N(2)-H(2B)	121.3(14)
H(2A)-N(2)-H(2B)	118(2)
C(16)-O(3)-C(15)	116.89(12)
C(22A)-O(4)-H(4A)	108.3(19)
C(22)-O(4)-H(4A)	110.8(18)

Appendix Table 5d. Anisotropic displacement parameters ($\text{\AA}^2 \times 10^3$) for **5.001**. The anisotropic displacement factor exponent takes the form: $-2\pi^2 [h^2 a^{*2} U^{11} + \dots + 2 h k a^* b^* U^{12}]$

	U ¹¹	U ²²	U ³³	U ²³	U ¹³	U ¹²
C(1)	17(1)	21(1)	13(1)	1(1)	0(1)	2(1)
C(2)	17(1)	21(1)	19(1)	1(1)	0(1)	0(1)
C(3)	23(1)	21(1)	20(1)	-5(1)	1(1)	0(1)
C(4)	21(1)	24(1)	15(1)	-3(1)	3(1)	1(1)
C(5)	16(1)	20(1)	15(1)	2(1)	0(1)	0(1)
C(6)	18(1)	19(1)	13(1)	-1(1)	0(1)	0(1)
C(7)	19(1)	17(1)	14(1)	1(1)	1(1)	-1(1)
C(8)	18(1)	21(1)	16(1)	0(1)	0(1)	2(1)
C(9)	20(1)	18(1)	16(1)	-2(1)	2(1)	0(1)
C(10)	20(1)	18(1)	17(1)	-2(1)	0(1)	0(1)
C(11)	20(1)	21(1)	21(1)	-2(1)	0(1)	-3(1)
C(12)	24(1)	22(1)	21(1)	0(1)	5(1)	-5(1)
C(13)	27(1)	24(1)	15(1)	2(1)	1(1)	-1(1)
C(14)	20(1)	22(1)	16(1)	-1(1)	0(1)	0(1)
C(15)	21(1)	23(1)	20(1)	0(1)	-4(1)	-4(1)
C(16)	21(1)	23(1)	14(1)	1(1)	1(1)	-3(1)
C(17)	24(1)	27(1)	16(1)	1(1)	-1(1)	1(1)
C(18)	31(1)	25(1)	18(1)	1(1)	5(1)	2(1)
C(19)	36(1)	26(1)	19(1)	-4(1)	5(1)	-6(1)
C(20)	27(1)	33(1)	18(1)	-1(1)	-1(1)	-9(1)
C(21)	20(1)	28(1)	19(1)	3(1)	-1(1)	-3(1)
C(22)	31(1)	29(1)	28(1)	5(1)	3(1)	6(1)
C(23)	48(1)	39(1)	34(1)	5(1)	7(1)	9(1)
C(22A)	31(3)	31(3)	31(3)	3(3)	-1(3)	5(3)
C(23A)	48(1)	39(1)	34(1)	5(1)	7(1)	9(1)
N(1)	18(1)	22(1)	13(1)	-1(1)	3(1)	-2(1)
N(2)	18(1)	28(1)	14(1)	-1(1)	1(1)	1(1)
O(1)	16(1)	29(1)	16(1)	1(1)	1(1)	1(1)
O(2)	21(1)	29(1)	14(1)	-2(1)	2(1)	-4(1)
O(3)	20(1)	23(1)	21(1)	-2(1)	-5(1)	0(1)
O(4)	25(1)	31(1)	21(1)	2(1)	2(1)	2(1)
Cl(1)	24(1)	22(1)	27(1)	-2(1)	5(1)	-5(1)

Appendix Table 5e. Hydrogen coordinates ($\times 10^4$) and isotropic displacement parameters ($\text{\AA}^2 \times 10^3$) for **5.001**.

	x	y	z	U(eq)
H(3)	1883	3362	2038	25
H(4)	3289	4163	1766	24
H(6)	2487	5470	3489	20
H(11)	7794	6909	2786	25
H(12)	7499	7385	1619	27
H(13)	5887	7153	1019	26
H(14)	4574	6433	1589	23

H(15A)	6010	6209	4004	25
H(15B)	6580	5516	3637	25
H(17)	6219	7442	3946	26
H(18)	6398	8588	4551	30
H(19)	7885	8827	5280	32
H(20)	9200	7911	5418	31
H(21)	9045	6767	4815	26
H(22A)	3412	3759	3997	35
H(22B)	4115	3577	4691	35
H(23A)	5121	3460	3646	61
H(23B)	4878	4298	3435	61
H(23C)	5583	4116	4130	61
H(22C)	5026	4114	4904	37
H(22D)	4093	3585	4650	37
H(23D)	5461	3531	3859	61
H(23E)	4446	3869	3464	61
H(23F)	5383	4400	3719	61
H(1)	4204(19)	5239(13)	1994(13)	32(5)
H(2A)	1031(18)	4922(12)	5097(13)	31(5)
H(2B)	2086(19)	4722(12)	4691(12)	33(6)
H(4A)	3920(20)	5007(15)	4342(15)	47(7)

Appendix Table 5f. Torsion angles [°] for **5.001**.

C(6)-C(1)-C(2)-C(3)	-0.7(2)
C(7)-C(1)-C(2)-C(3)	-179.26(14)
C(6)-C(1)-C(2)-Cl(1)	176.44(11)
C(7)-C(1)-C(2)-Cl(1)	-2.1(2)
C(1)-C(2)-C(3)-C(4)	1.0(2)
Cl(1)-C(2)-C(3)-C(4)	-176.19(12)
C(2)-C(3)-C(4)-C(5)	0.5(2)
C(3)-C(4)-C(5)-C(6)	-2.4(2)
C(3)-C(4)-C(5)-N(1)	178.52(14)
C(2)-C(1)-C(6)-C(5)	-1.2(2)
C(7)-C(1)-C(6)-C(5)	177.42(13)
C(4)-C(5)-C(6)-C(1)	2.8(2)
N(1)-C(5)-C(6)-C(1)	-178.23(13)
C(2)-C(1)-C(7)-O(1)	-58.9(2)
C(6)-C(1)-C(7)-O(1)	122.52(15)
C(2)-C(1)-C(7)-N(2)	121.93(15)
C(6)-C(1)-C(7)-N(2)	-56.66(18)
O(2)-C(8)-C(9)-C(14)	-142.23(15)
N(1)-C(8)-C(9)-C(14)	37.3(2)
O(2)-C(8)-C(9)-C(10)	36.2(2)
N(1)-C(8)-C(9)-C(10)	-144.26(14)
C(14)-C(9)-C(10)-C(11)	-1.0(2)
C(8)-C(9)-C(10)-C(11)	-179.43(14)
C(14)-C(9)-C(10)-C(15)	-177.81(14)
C(8)-C(9)-C(10)-C(15)	3.8(2)
C(9)-C(10)-C(11)-C(12)	1.1(2)
C(15)-C(10)-C(11)-C(12)	177.97(14)
C(10)-C(11)-C(12)-C(13)	-0.4(2)

C(11)-C(12)-C(13)-C(14)	-0.4(2)
C(12)-C(13)-C(14)-C(9)	0.5(2)
C(10)-C(9)-C(14)-C(13)	0.2(2)
C(8)-C(9)-C(14)-C(13)	178.68(14)
C(11)-C(10)-C(15)-O(3)	5.8(2)
C(9)-C(10)-C(15)-O(3)	-177.41(13)
O(3)-C(16)-C(17)-C(18)	-179.33(13)
C(21)-C(16)-C(17)-C(18)	0.4(2)
C(16)-C(17)-C(18)-C(19)	-0.1(2)
C(17)-C(18)-C(19)-C(20)	-0.3(2)
C(18)-C(19)-C(20)-C(21)	0.5(2)
C(19)-C(20)-C(21)-C(16)	-0.3(2)
O(3)-C(16)-C(21)-C(20)	179.54(13)
C(17)-C(16)-C(21)-C(20)	-0.2(2)
O(2)-C(8)-N(1)-C(5)	2.0(2)
C(9)-C(8)-N(1)-C(5)	-177.49(13)
C(4)-C(5)-N(1)-C(8)	-155.21(15)
C(6)-C(5)-N(1)-C(8)	25.8(2)
C(17)-C(16)-O(3)-C(15)	-15.3(2)
C(21)-C(16)-O(3)-C(15)	165.01(12)
C(10)-C(15)-O(3)-C(16)	82.01(15)

Appendix Table 5g. Hydrogen bonds for **5.001** [Å and °].

D-H...A	d(D-H)	d(H...A)	d(D...A)	<(DHA)
C(4)-H(4)...O(1)#1	0.93	2.65	3.4037(18)	138.6
C(6)-H(6)...O(2)	0.93	2.36	2.8655(18)	113.9
C(15)-H(15A)...O(2)	0.97	2.35	2.8611(18)	112.1
C(17)-H(17)...Cl(1)#2	0.93	2.84	3.5925(16)	138.4
N(1)-H(1)...O(1)#1	0.87(2)	2.08(2)	2.9393(16)	171(2)
N(2)-H(2A)...O(1)#3	0.91(2)	2.04(2)	2.9518(17)	176(2)
N(2)-H(2B)...O(4)	0.89(2)	2.04(2)	2.9205(18)	172(2)
O(4)-H(4A)...O(2)	0.83(3)	2.10(3)	2.9331(16)	173(3)

Symmetry transformations used to generate equivalent atoms:

#1 $x+1/2, y, -z+1/2$ #2 $-x+1/2, y+1/2, z$ #3 $-x, -y+1, -z+1$

Appendix 5.2 CCDC deposit numbers for relevant compounds of Chapter 5, Section 5.03

Appendix Table 5h: CCDC deposit numbers for relevant benzamides and anilides of Section 5.03

Compound name	CCDC deposit number
benzamide	1118065
2-chlorobenzamide	1127043
3-chlorobenzamide	1215611
4-chlorobenzamide	1229369, 1229371, 1229370
2-fluorobenzamide	1110591
<i>N</i> -(2-chlorophenyl)benzamide	651441
2-chloro- <i>N</i> -phenylbenzamide	200386
3-chloro- <i>N</i> -phenylbenzamide	858418
4-chloro- <i>N</i> -phenylbenzamide	858298, 1059364
2-chloro- <i>N</i> -(3,5-di-methyl-phen-yl)benzamide	722857

Appendix 5.3 Cytotoxicity and Mitotoxicity profiling by IPK of compounds of interest

Assay description:

Aim: To identify cytotoxicity and mitotoxicity of compounds using the Crabtree effect assay adapted using methods outlined by Marroquin *et al.* and unpublished methods by IPK.^{1,2}

Screening Info.: Reformatted as 384-well format (1 plate)

DRCs starting at 100 μ M; two-fold serial dilution; 10-points in 0.5 % DMSO (v/v)

Cell Conditioning (metabolic switch):

1. Glucose Condition: HepG2 cells maintained in glucose media, utilizing ATP from glycolysis
2. Galactose Condition: HepG2 cells maintained in galactose media for one passage and seeded in the same media, utilizing ATP from oxidative phosphorylation.

Experimental Controls:

High control: 0.5 % DMSO, IC₁₀₀ low control: 200 μ M Chlorpromazine (0.5 % v/v DMSO)

Endpoint Read-out:

- Hoechst nuclei staining: Cell viability assessment via cell count
- Alamar blue staining: Metabolic activity measurement via fluorescence readout

Reference Compounds used:

1. Chlorpromazine: moderate cytotoxicity; used as low control IC₁₀₀ (200 μ M)
2. Tacrine: moderate cytotoxicity
3. Benznidazole: no cytotoxicity (in low conc.)
4. Praziquantel: no cytotoxicity (in low conc.)
5. FCCP: mitochondrial toxicity; mitochondrial oxidative phosphorylation uncoupler
6. Rotenone: mitochondrial toxicity; inhibitor of mitochondrial electron transport

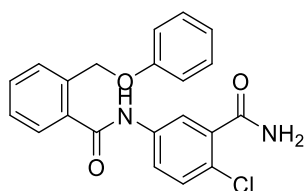
Data Analysis:

- Selectivity index (SI) was calculated by dividing the value of cytotoxic concentration at 50 % (CC₅₀) of a compound in Glucose condition by that of the compound in Galactose condition.

* Note: This Crabtree effect assay may not detect compounds inhibiting fatty acid oxidation as mitochondrial toxicants.^{3,4}

Cell viability measures whether compound is overall cytotoxic to the HepG2 cells. Metabolic stability measures whether compounds cause toxicity to the mitochondria. This is measured by the impact of the compound against cells under galactose conditions. Under these conditions, cells utilize ATP from oxidative phosphorylation, which occurs in the mitochondria. If compounds were found to be toxic to the mitochondria, it would be reflected under these conditions. Under glucose conditions, cells are able to use ATP from glycolysis rather than rely on mitochondria.

Appendix Table 5i: Summary of toxicity of **5.001**



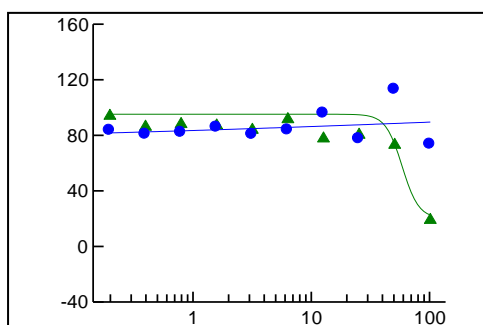
5.001

		Glucose condition	Galactose condition	SI (glu/galact)
Cell viability	CC ₅₀ (μM)	PI	PI	NA
	CC (Y=50) (μM)	62	32	1.9
Metabolic activity	CC ₅₀ (μM)	PI	PI	NA
	CC (Y=50) μM	>100	73	>1.4

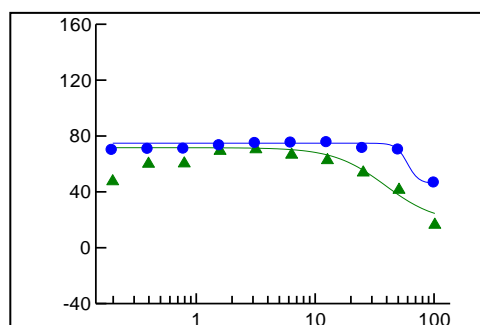
CC₅₀= cytotoxic concentration at 50 % , CC (Y=50)= normalised CC₅₀ from graph, PI= partial inhibition

Appendix 5 Figure a: Dose response curves of **5.001** measuring the cytotoxic concentration (CC₅₀) in glucose (left) and galactose (right) conditions

Glucose condition 5.001



Galactose condition 5.001



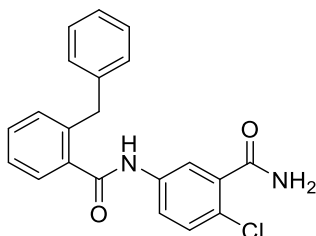
X axis: Concentration (μM)

Y axis: Ratio (%)

● Cell ratio by Hoechst staining
▲ Metabolic activity ratio by Alamar blue staining

No mitochondrial toxicity or cytotoxicity observed overall when HepG2 were subjected to **5.001**.

Appendix Table 5j: Summary of toxicity of **5.063**



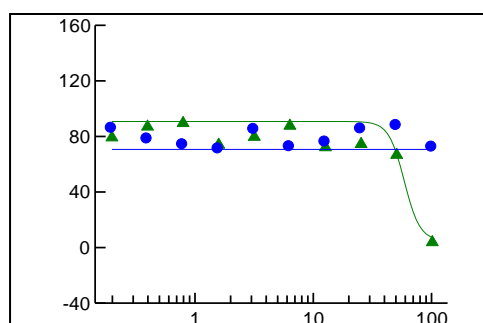
5.063

		Glucose condition	Galactose condition	SI (glu/galac)
Cell viability	CC ₅₀ (μM)	58	PI	NA
	CC (Y=50) (μM)	57	33	1.7
Metabolic activity	CC ₅₀ (μM)	PI	PI	NA
	CC (Y=50) μM	>100	>100	NA

CC₅₀= cytotoxic concentration at 50 % , CC (Y=50)= normalised CC₅₀ from graph, PI= partial inhibition

Appendix 5 Figure b: Dose response curves of **5.063** measuring the cytotoxic concentration (CC₅₀) in glucose (left) and galactose (right) conditions

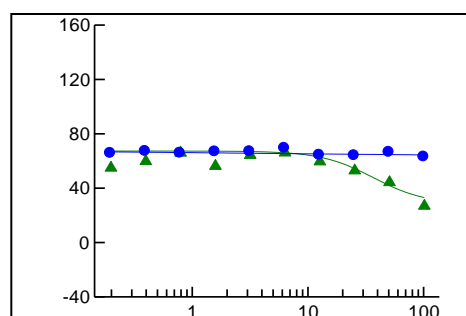
Glucose condition 5.063



X axis: Concentration (μM)

Y axis: Ratio (%)

Galactose condition 5.063



● Cell ratio by Hoechst staining

▲ Metabolic activity ratio by Alamar blue staining

No mitochondrial toxicity or cytotoxicity observed overall when HepG2 were subjected to **5.063**.

References

1. Marroquin LD, Hynes J, Dykens JA, Jamieson JD, Will Y. Circumventing the Crabtree effect: replacing media glucose with galactose increases susceptibility of HepG2 cells to mitochondrial toxicants. *Toxicol Sci.* 2007;97(2):539-47.
2. Shum D et al. HepG2 Crabtree Cytotoxicity screening Standard Operating Procedure. [Unpublished data] Institut Pasteur Korea, Seongnam, South Korea; 2021.
3. Kamalian L, Chadwick AE, Bayliss M, French NS, Monshouwer M, Snoeys J, et al. The utility of HepG2 cells to identify direct mitochondrial dysfunction in the absence of cell death. *Toxicol In Vitro.* 2015;29(4):732-40.
4. Eakins J, Bauch C, Woodhouse H, Park B, Bevan S, Dilworth C, et al. A combined in vitro approach to improve the prediction of mitochondrial toxicants. *Toxicol In Vitro.* 2016;34:161-70.
5. Pedersen SL, Tofteng AP, Malik L, Jensen KJ. Microwave heating in solid-phase peptide synthesis. *Chemical Society Reviews.* 2012;41(5):1826-1844.
6. Stephanou AS, Roberts GA, Cooper LP, Clarke DJ, Thomson AR, MacKay CL, et al. Dissection of the DNA Mimicry of the Bacteriophage T7 Ocr Protein using Chemical Modification. *J Mol Biol.* 2009;391(3):565-576.